Zoosystematics and Evolution

100 (**3**) 2024

PENSOFT

MUSEUM FÜR NATURKUNDE BERLIN

Zoosystematics and Evolution
A Bulletin of Zoology since 1898

Zoosystematics and Evolution

2024. Volume 100. 3 Issue

ISSN: 1435-1935 (print), 1860-0743 (online)
Abbreviated keys title: Zoosyst. Evol.

In Focus

The cover picture shows female habitus of *Spiracme lendli* (Kulczyński, 1897), comb. nov.

See paper of **Gallé-Szpisjak N, Gallé R, Szabó K, Szűts T:** On the identity and placement of *Xysticus lendli* Kulczyński, 1897 (Araneae, Thomisidae): an integrative approach

Cover design
Pensoft

Zoosystematics and Evolution
A Bulletin of Zoology since 1898

Content of volume **100** (**3**) 2024

Abstract & Indexing Information

Biological Abstracts® (Thompson ISI)
BIOSIS Previews® (Thompson ISI)
Cambridge Scientific Abstracts (CSA/CIG)
Web of Science® (Thompson ISI)
Zoological Record™ (Thompson ISI)

Zoosystematics and Evolution
A Bulletin of Zoology since 1898

Content of volume **100** (**3**) 2024

Zoosystematics and Evolution
A Bulletin of Zoology since 1898

Content of volume **100** (**3**) 2024

Zoosyst. Evol. 100 (3) 2024, 769–778 | DOI 10.3897/zse.100.126069

PENSOFT

für Natur MUSEUM FÜR NATURKUNDE BERLIN

Addition to the known diversity of Chinese freshwater mussels: integrative description of a new species of *Postolata* Dai et al., 2023 (Bivalvia, Unionidae, Gonideinae)

Lili Liu[1*], Liping Zhang[1*], Kaiyu Hou[1], Liyang Ning[1], Ruiwen Wu[1]

1 *School of Life Science, Shanxi Normal University, Taiyuan 030031, China*

https://zoobank.org/354401E7-E9A4-45FD-83DA-876BB4A09650

Corresponding author: Ruiwen Wu (wurw@sxnu.edu.cn)

Academic editor: Matthias Glaubrecht ♦ **Received** 24 April 2024 ♦ **Accepted** 30 May 2024 ♦ **Published** 13 June 2024

Abstract

In this study, we present a new species of freshwater mussel in the genus *Postolata* Dai et al., 2023, from Guangxi Province, China, by integrating morphological, anatomical, and molecular data. *Postolata longjiangensis* Liu & Wu, **sp. nov.** is distinguished from its congener (i.e., *Postolata guangxiensis*) by its shell shape, beak position, surface sculpture, nacre color, and hinge structure. Molecular species delimitation results based on the mitochondrial COI gene support the separation of *Postolata longjiangensis* Liu & Wu, **sp. nov.** from its congener. The multi-locus (COI + 16S rRNA + 28S rRNA) phylogeny reveals that this species forms the sister lineage to *Postolata guangxiensis* in the tribe Gonideini.

Key Words

China, cryptic species, freshwater mussels, integrative taxonomy, multi-locus phylogeny, *Postolata*

Introduction

Freshwater mussels (order Unionida) are renowned for their distinctive life cycle, characterized by a parasitic phase primarily reliant on fish hosts and an uncommon doubly mitochondrial inheritance (Barnhart et al. 2008; Modesto et al. 2018; Guerra et al. 2019). They are globally distributed in freshwater habitats, with the highest levels of diversity observed in East Asia and North America (Zieritz et al. 2018; Graf and Cummings 2023). This group plays crucial ecological roles, with certain mussel species simultaneously fulfilling the criteria of indicator, umbrella, and flagship species (Howard and Cuffey 2006; Vaughn et al. 2008; Vaughn 2018). Unfortunately, freshwater mussels have become one of the most imperiled faunas worldwide, with an increasing number of species at risk of extinction (Lydeard et al. 2004; Haag and Williams 2014; Ferreira-Rodríguez et al. 2019). Consequently, the urgency of describing their diversity and systematics is highlighted by the growing research efforts and conservation attention dedicated to this group (Lopes-Lima et al. 2017a, 2017b; Do et al. 2018; Huang et al. 2019; Liu et al. 2022).

The Guangxi Zhuang Autonomous Region (hereinafter referred to as Guangxi), located in southern China and sharing a border with Vietnam, plays a significant role within the Indo-Burma biodiversity hotspot situated in the Chinese region (Tordoff et al. 2012). In recent years, new species of freshwater mussels such as *Postolata guangxiensis* Dai et al., 2023, *Pseudocuneopsis yangshuoensis* Wu & Liu, 2023 and *Pseudocuneopsis wuana* Liu & Wu, 2023 have been discovered in Guangxi (Dai et al. 2023; Wu et al. 2023b; Liu et al. 2023). It suggests that the unique habitats and geographical flora of this region may harbor previously undescribed species, while still underestimating the level of species diversity.

* These authors contributed equally to this work.

The freshwater mussel genus *Postolata* Dai et al., 2023 belongs to the tribe Gonideini in the subfamily Gonideinae (Dai et al. 2023; Wu et al. 2024). It was recently established as a monotypic genus comprising only one species, namely *Postolata guangxiensis* Dai et al., 2023, which is endemic to Guangxi province in China.

In this study, another new species of *Postolata*, also from Guangxi, is diagnosed and described. We employ an integrative taxonomic approach that incorporates morphological, anatomical, and molecular phylogeny to identify and differentiate this species.

Materials and methods

Specimen collection, identification, and anatomical observations

In April 2024, six freshwater mussel specimens were collected from a rural streamlet at an altitude of approximately 150.18 m in Hechi City, Guangxi Province, China (24.530716°N, 108.5762°E; Fig. 1). Meanwhile, two specimens of *Postolata guangxiensis* were collected from the type locality (Luoqing River, Guangxi Province; Fig. 1). All specimens were deposited as vouchers at the Museum of Zoology, Shanxi Normal University (**SXNU**), China (voucher numbers SXNU_24040701–SXNU_24040706 for *Postolata longjiangensis* sp. nov.; voucher numbers SXNU_PG_22102301 and SXNU_PG_22102303 for *Postolata guangxiensis*).

The conchological and anatomical features of all individuals were visually examined with the naked eye and under a stereoscopic microscope (CX31-12C03, Olympus Corporation, Japan), including shell shape, umbo position and sculpture, shell surface sculpture, hinge structure, muscle attachment, and papillae in the incurrent and excurrent apertures (Figs 2, 3). The anatomical features of the soft body were described according to Williams et al. (2008).

DNA extraction, amplification, and sequencing

According to the manufacturer's instructions, a small piece of foot tissue was excised for DNA extraction using the TIANamp Marine Animals DNA Kit (Tiangen Biotech, Beijing, China). Three gene fragments, i.e., the mitochondrial cytochrome *c* oxidase subunit I (COI) and 16S ribosomal RNA (16S rRNA), and the nuclear gene of 28S ribosomal RNA (28S rRNA), were sequenced based on our previous studies (Wu et al. 2024). PCR amplification was implemented in a 25-μL volume using the following thermal cycling conditions: 3.5 min at 94 °C, followed by 35 cycles of 94 °C for 30 sec, 50 °C for 30 sec, 72 °C for 1 min, and a final extension of 72 °C for 5 min. The amplified PCR products were purified and sequenced by Sangon Biotech (Shanghai). All newly obtained sequences in this study have been submitted to GenBank.

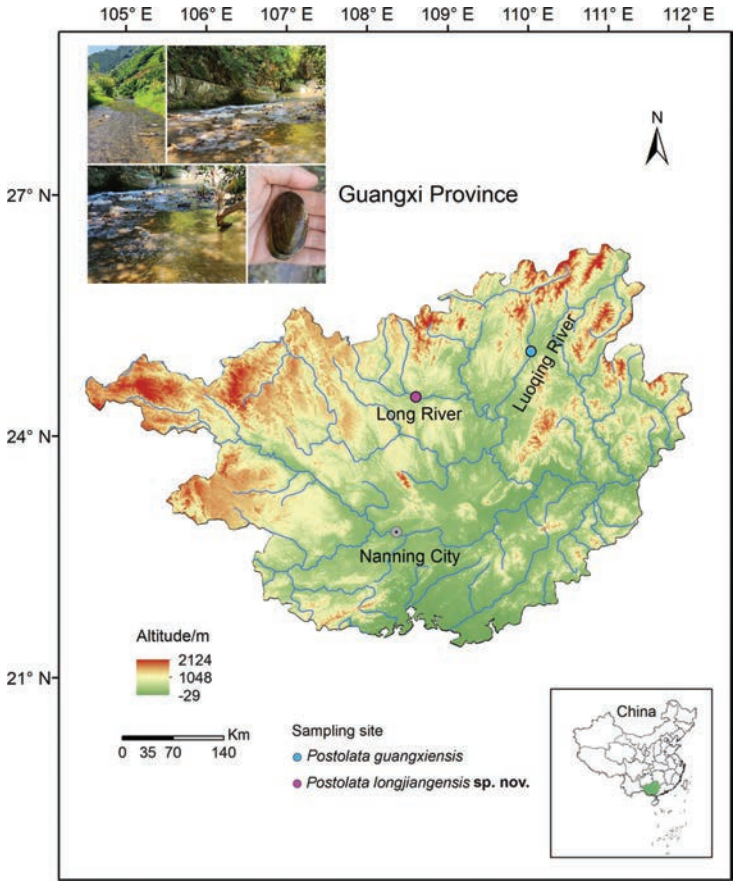

Figure 1. Map (Guangxi Province) of sampling localities of *Postolata* species and habitat of *Postolata longjiangensis* sp. nov.

Alignments, partitioning strategies, and model selection

In this study, we constructed two datasets. First, a DNA barcoding (COI) dataset for molecular species delimitation was compiled (Table 1). We downloaded the COI sequences of eight species in the tribe Gonideini, as well as all published COI sequences of *Postolata guangxiensis*, along with COI sequences from the new species described in this study. Two species from the tribe Lamprotulini, i.e., *Lamprotula caveata* (Heude, 1877) and *Lamprotula leaii* (Gray, 1833), were selected as outgroups. Second, a three-gene dataset for phylogenetic analysis was prepared (Table 2). This dataset contains species from all eight recognized tribes in the subfamily Gonideinae. In addition, *Margaritifera dahurica* (Middendorff, 1850) and *M. margaritifera* (Linnaeus, 1758) from the family Margaritiferidae were selected as outgroups.

The molecular data analyses and phylogenetic reconstruction were consistent with the methods used in our previous studies (Wu et al. 2023a; Wu et al. 2024). Protein-coding genes (COI) were aligned by built-in MACSE with invertebrate mitochondrial codon modes implemented in PhyloSuite v1.2.3 (Zhang et al. 2020). Ribosomal genes (16S rRNA and 28S rRNA) were aligned using MAFFT v7.2 (Katoh and Standley 2013) with the L-INS-i algorithm. Ambiguous alignment areas were trimmed by Gblocks (Castresana 2000), the parameter ribosomal gene block with a minimum length was set to 2 base pairs (bp), and the allowed gap position was selected with half; the minimum length of the protein-coding gene block was set to 3 bp, and the allowed gap position was also selected with half.

For the barcoding dataset, the COI sequence fragment length was 510 bp after alignment and trimming. For the three-gene dataset, COI, 16S, and 28S sequences were aligned and trimmed to lengths of 624 bp, 471 bp, and 751 bp, respectively. Sequences of the multi-gene dataset were concatenated using Phylosuite v1.2.3.

The three-gene dataset was analyzed with partition schemes based on the genes and codons. PartitionFinder (Lanfear et al. 2017) was used to select the models for Bayesian inference (BI) analyses. ModelFinder (Kalyaanamoorthy et al. 2017) was used to select the maximum likelihood (ML) analysis models in IQ-TREE (Minh et al. 2020). The selection of best-fit models was based on the corrected Akaike Information Criterion (AICc). Substitution models assigned to each partition by PartitionFinder and ModelFinder are listed in Suppl. material 1.

Neighbor-joining clustering and phylogenetic analyses

We used an integrative approach that combined molecular and morphological analyses for species delimitation and diagnosis. Based on the COI dataset, the NJ tree was constructed using the uncorrected *p*-distance model in MEGA 7.0 (Kumar et al. 2016) with 1000 bootstrap replicates. Intraspecific and interspecific genetic distances were calculated based on the COI barcoding dataset using the uncorrected *p*-distance model in MEGA 7.0.

Table 1. List of COI sequences used in this study.

Species	GenBank accession number
Postolata guangxiensis Dai et al., 2023	OP009379
Postolata guangxiensis Dai et al., 2023	OP009380
Postolata guangxiensis Dai et al., 2023	OP009381
Postolata guangxiensis Dai et al., 2023	OP009382
Postolata guangxiensis Dai et al., 2023	OP009383
Postolata guangxiensis Dai et al., 2023	OP009384
Postolata guangxiensis Dai et al., 2023	OP009385
Postolata longjiangensis **Liu & Wu, sp. nov. 1***	PP713224
Postolata longjiangensis **Liu & Wu, sp. nov. 2***	PP713225
Postolata longjiangensis **Liu & Wu, sp. nov. 3***	PP713226
Postolata longjiangensis **Liu & Wu, sp. nov. 4***	PP713227
Postolata longjiangensis **Liu & Wu, sp. nov. 5***	PP713228
Postolata longjiangensis **Liu & Wu, sp. nov. 6***	PP713229
Obovalis omiensis (Heimburg, 1884)	LC518997
Sinosolenaia carinata (Heude, 1877)	MG742248
Sinosolenaia oleivora (Heude, 1877)	MG742249
Ptychorhynchus pfisteri (Heude, 1874)	MG742247
Gonidea angulata (Lea, 1838)	DQ272372
Leguminaia anatolica Gürlek et al., 2021	MZ511008
Leguminaia saulcyi (Bourguignat, 1852)	MZ510997
Inversidens rentianensis Wu & Wu, 2021	OR826138
Lamprotula caveata (Heude, 1877)	KJ434503
Lamprotula leaii (Gray, 1833)	MF072503

*Sequences from this study.

For the multi-locus dataset, the IQ-TREE web server (http://iqtree.cibiv.univie.ac.at/) performed maximum likelihood (ML) phylogenetic analysis using the ultrafast bootstrapping algorithm with 1000 repetitions. Bayesian inference (BI) phylogenetic analyses were carried out in MrBayes v2.01 (Ronquist et al. 2012) with generated models in PartitionFinder (Lanfear et al. 2017). Four independent Markov Chain Monte Carlo (MCMC) models were run simultaneously for ten million generations, and sampling was conducted every 1000 generations with a burn-in of 25%. The process terminated when the average standard deviation of the splitting frequency fell below 0.01. Ultimately, the constructed phylogenetic trees were implemented in the online iTOL (https://itol.embl.de/itol.cgi) to realize editing and visualization (Letunic and Bork 2007).

Results

Systematics

Family Unionidae Rafinesque, 1820
Subfamily Gonideinae Ortmann, 1916
Tribe Gonideini Ortmann, 1916

Genus *Postolata* Dai, Huang, Guo & Wu, 2023

Type species. *Postolata guangxiensis* Dai et al., 2023.

Table 2. Sequences from the three-gene dataset used for molecular analyses and corresponding GenBank numbers.

Family	Subfamily	Tribe	Taxa	COI	16S	28S
Unionidae	Gonideinae	Gonideini	*Ptychorhynchus pfisteri* (Heude, 1874)	MG463034	KY067440	MG595562
			Obovalis omiensis (Heimburg, 1884)	LC518995	LC223994	LC519064
			Postolata longjiangensis **Liu & Wu, sp. nov. 1***	PP713224	PP717959	PP717965
			Postolata longjiangensis **Liu & Wu, sp. nov. 2***	PP713225	PP717960	PP717966
			Postolata longjiangensis **Liu & Wu, sp. nov. 3***	PP713226	PP717961	PP717967
			Postolata longjiangensis **Liu & Wu, sp. nov. 4***	PP713227	PP717962	PP717968
			Postolata longjiangensis **Liu & Wu, sp. nov. 5***	PP713228	PP717963	PP717969
			Postolata longjiangensis **Liu & Wu, sp. nov. 6***	PP713229	PP717964	PP717970
			Postolata guangxiensis Dai et al., 2023 1	OP009379	OP020466	OP020470
			Postolata guangxiensis Dai et al., 2023 2	OP009380	OP020467	OP020470
			Postolata guangxiensis Dai et al., 2023 3	OP009381	OP020468	OP020470
			Postolata guangxiensis Dai et al., 2023 4	OP009382	OP020469	OP020471
			Postolata guangxiensis Dai et al., 2023 5	OP009383	OP020467	OP020472
			Postolata guangxiensis Dai et al., 2023 6	OP009384	OP020468	OP020470
			Postolata guangxiensis Dai et al., 2023 7	OP009385	OP020469	OP020471
			Parvasolenaia rivularis (Heude, 1877)	KX966393	KX966393	MG595632
			Koreosolenaia sitgyensis Lee et al., 2020	GQ451872	GQ451859	MT020817
			Sinosolenaia carinata (Heude, 1877)	KX822669	MK683025	KX822626
			Gonidea angulata (Lea, 1838)	DQ272371	KF011258	AF400691
			Microcondylaea bonellii (Férussac, 1827)	KX822652	KP218021	KX822609
		Pseudodontini	*Bineurus loeiensis* Konopleva et al., 2021	KX865879	KX865650	KX865750
			Bineurus anodontinum (Rochebrune, 1882)	MW603662	MZ684076	MZ684018
			Thaiconcha callifera (Martens, 1860)	KX865862	KX865633	KX865734
			Pseudodon mekongi (Bolotov et al., 2020)	KX865861	KX865632	KX865733
			Pseudodon vondembuschianus (Lea, 1840)	KP795029	KP795052	MZ684028
			Pilsbryoconcha exilis (Lea, 1838)	KX051291	KX865646	KX822613
			Indopseudodon kayinensis (Bolotov et al., 2020)	MZ678754	MZ684081	MZ684033
			Indopseudodon bogani (Bolotov et al., 2017)	MF352218	MF352292	MF352350
		Schepmaniini	*Schepmania* sp. 5973	MZ678755	MZ684082	MZ684035
		Lamprotulini	*Lamprotula caveata* (Heude, 1877)	KX822646	NC_030336	KX822603
			Lamprotula leaii (Gray, 1833)	NC_023346	NC_023346	MG595524
			Potomida littoralis (Cuvier, 1798)	JN243905	NC_030073	JN243883
		Contradentini	*Yaukthwa inlenensis* Konopleva et al., 2019	KX865927	KX865681	KX865798
			Yaukthwa paiensis Konopleva et al., 2019	MH345972	MH346012	MH345992
			Yaukthwa elongatula Bolotov et al., 2019	MK372408	MK372456	MK372486
			Lens contradens (Lea, 1838)	MG581991	MT993693	MT993745
			Lens eximius (Lea, 1856)	KX865941	KX865689	KX865812
			Physunio superbus (Lea, 1843)	MG582020	MT993689	MT993741
			Trapezoideus foliaceus (Gould, 1843)	MH345985	MH346025	MH346005
		Rectidentini	*Hyriopsis bialata* Simpson, 1900	KX051274	MT993644	MT993697
			Hyriopsis desowitzi Brandt, 1974	KX822644	MT993679	KX822601
			Rectidens sumatrensis (Dunker, 1852)	KX051314	MW242818	KX822620
			Ensidens sagittarius (Lea, 1856)	KX865950	KX865696	KX865821
		Ctenodesmini	*Khairuloconcha lunbawangorum* Zieritz et al., 2021	MN900790	MZ684078	MN902294
			Khairuloconcha sahanae Zieritz et al., 2021	MZ678752	MZ684079	MZ684024
		Chamberlainiini	*Chamberlainia somsakpanhai* Kongim et al., 2023	KX822635	MK994770	KX822592
Margaritiferidae			*Margaritifera dahurica* (Middendorff, 1850)	KJ161516	KJ943526	KT343747
			Margaritifera margaritifera (Linnaeus, 1758)	KX550089	KX550091	KX550093

*Sequences from this study.

***Postolata longjiangensis* Liu & Wu, sp. nov.**

https://zoobank.org/615D6E27-0FF5-4A62-8287-817768787DD0

Fig. 2

Type materials. ***Holotype*** (Fig. 2E): SXNU_24040702 (length 53.06 mm, height 27.11 mm, width 17.28 mm); Long River, Hechi City, Guangxi Province, China. ***Paratypes*** (Fig. 2A–D, F): five specimens, SXNU_24040703, SXNU_24040705, SXNU_24040706, SXNU_24040704, and SXNU_24040701. Same collection location as the holotype.

Morphological diagnosis. *Postolata longjiangensis* sp. nov. can be distinguished from *Postolata guangxiensis* by the shell shape, beak position, surface sculpture, nacre color, and hinge structure (Table 3). Diagnostic characteristics: shell elongated, irregularly rectangular; the umbo situated at 1/4 of the shell length; epidermis brown with greenish tinge; nacre blue-white; and hinge tooth weaker than that of *Postolata guangxiensis*.

Molecular diagnosis. *Postolata longjiangensis* sp. nov. and *Postolata guangxiensis* formed a closely related group within the tribe Gonideini. The sequences of

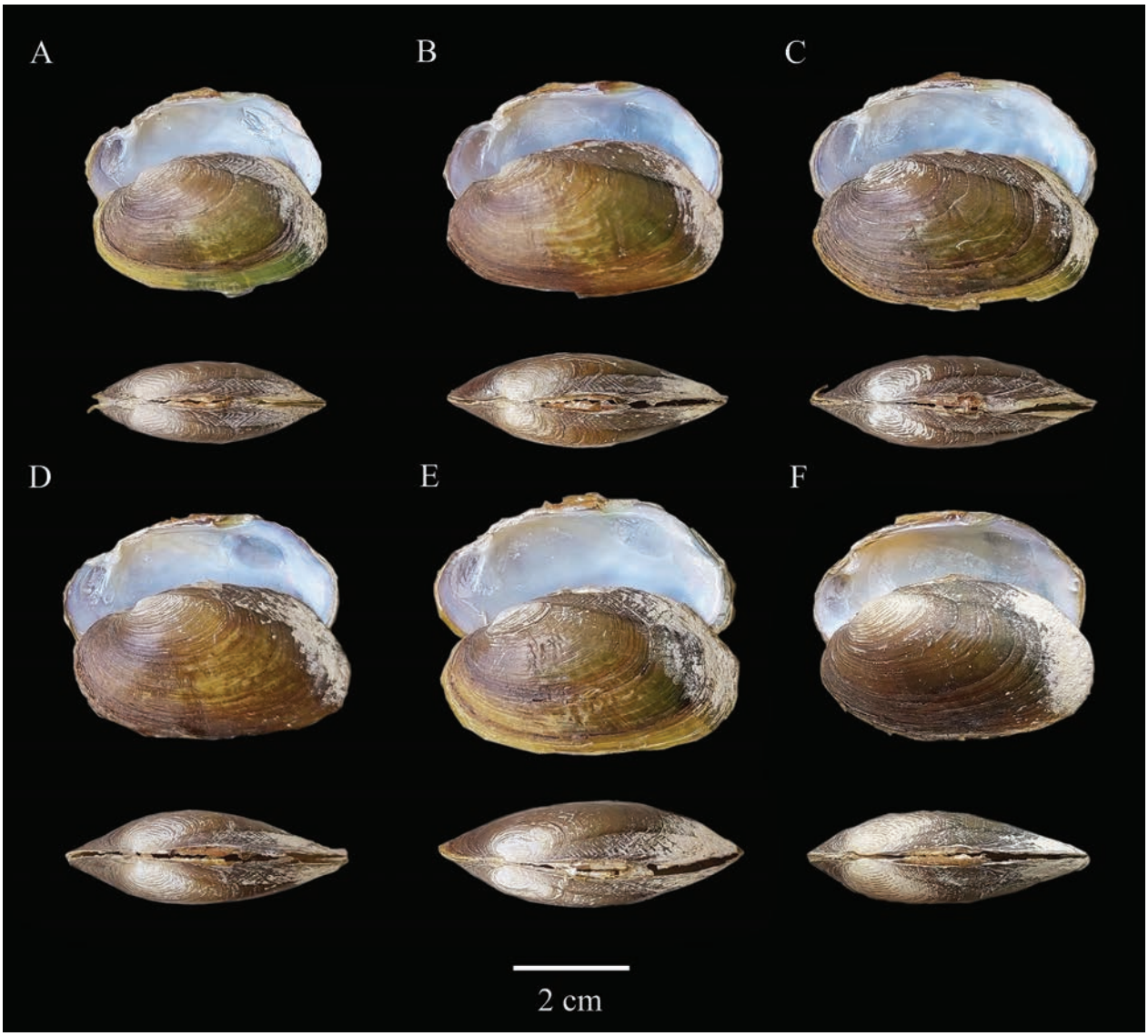

Figure 2. Shells of *Postolata longjiangensis* sp. nov. **A.** Paratype: SXNU_24040703; **B.** paratype: SXNU_24040705; **C.** Paratype: SXNU_24040706; **D.** Paratype: SXNU_24040704; **E.** Holotype: SXNU_24040702; and **F.** Paratype: SXNU_24040701.

Postolata longjiangensis sp. nov. revealed a well-supported lineage that is distinct from its congener (Fig. 4). The genetic distance between the new species and *Postolata guangxiensis* is 8.13% based on the COI barcoding sequences.

Description. Shell elongated, irregularly rectangular, slightly thickened, moderately inflated; anterior margin rounded and short; ventral margin nearly straight; posterior margin wide and long; posterior slope significantly prominent; dorsal margin nearly straight, with an upward tilt angle; umbo located at 1/4 of the shell length and sculptured with wavy ridges; epidermis brown with greenish tinge; shell surface sculptured with fine concentric growth lines (Fig. 2; Table 3). Anterior adductor muscle attachment oblong, little deep, and smooth; posterior adductor muscle attachment round to oval, shallow, and smooth; anterior retractor muscle attachment completely integrated with anterior adductor muscle attachment; posterior retractor muscle attachment irregularly round and fused with the posterior adductor muscle attachment; mantle muscle attachment obvious. Hinge weakly developed; anterior tooth extremely small, posterior tooth small, thin, and pyramidal in the left valve; anterior tooth upright pyramidal; posterior tooth degenerate and merge into the lateral teeth in the right valve; there is one short lateral tooth of both shells; nacre-bule-white (Fig. 2; Table 3). Papillae in the incurrent aperture short and cylindrical, arranged in two rows; papillae in the excurrent aperture weakly developed, sparsely arranged in one row; and the pigmentation of the incurrent and excurrent aperture significant; the size of inner gills exceeds that of outer gills; labial palps medium-thick, flat elliptical (Fig. 3; Table 3).

Etymology. This species' name is dedicated to its collection location, the Long River in Hechi City, Guangxi Province, China. For the common name, we recommend "Longjiang Rear-wide Mussel" (English) and "Long Jiang Hou Ju Bang" (龙江后矩蚌) (Chinese).

Distribution. Long River at Hechi City, Guangxi Province, China.

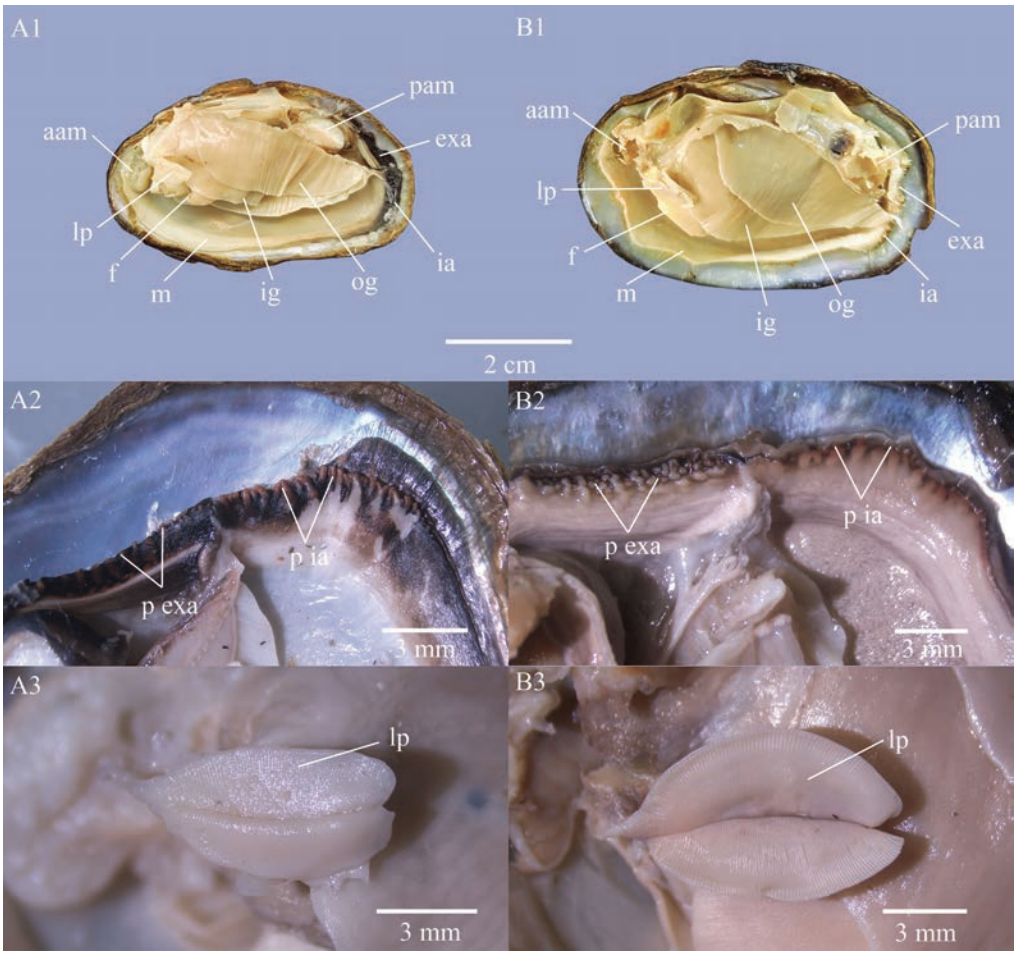

Figure 3. Anatomical features of *Postolata longjiangensis* sp. nov. and *Postolata guangxiensis*; **A1–3.** *Postolata longjiangensis* sp. nov.; **B1–3.** *Postolata guangxiensis*. Abbreviations: aam, anterior adductor muscle; pam, posterior adductor muscle; exa, excurrent aperture; ia, incurrent aperture; f, foot; ig, inner gill; og, outer gill; lp, labial palps; m, mantle; p ia, papillae in incurrent aperture; p exa, papillae of excurrent aperture.

Table 3. Conchological and soft-body characteristics of *Postolata longjiangensis* sp. nov. and *Postolata guangxiensis*.

Features	***Postolata longjiangensis* sp. nov.**	***Postolata guangxiensis***
Length (mm)	41.14–49.93	49.22–57.76
Width (mm)	13.82–17.28	19.95–21.42
Height (mm)	22.89–27.63	33.47–39.34
Shell shape	Elongated, irregularly rectangular	Irregularly rectangular
Shell thickness	Slightly thick	Moderately thick
Umbo position and sculpture	1/4 of shell length; umbo sculptured with wavy ridges	1/3 of shell length; umbo often eroded
Surface sculpture	Epidermis is brown with a bit green; shell surface sculptured with fine concentric growth lines	Epidermis is black-brown; shell surface sculptured with fine concentric growth lines; there is one sulcus near the posterior dorsal margin
Nacre colour	Blue-white	Milky-white
Posterior slope	Significantly prominent	Insignificant
Dorsal margin	Nearly straight, with an upward tilt angle	Slightly curved downwards
Hinge	Weakly developed	Well developed
Pseudocardinal teeth of the left valve	Anterior tooth extremely small, posterior tooth small, thin, and pyramidal	Anterior tooth small, posterior tooth thick and pyramidal
Pseudocardinal teeth of the right valve	Anterior tooth upright pyramidal, posterior tooth degenerate and merge into the lateral teeth	Anterior tooth well-developed, posterior tooth reduced
Lateral teeth	One tooth on both valves, nearly straight	One tooth on both valves, small and short
Incurrent aperture	Papillae is short cylindrical, arranged in two rows; and pigmentation is significant	Papillae is distinctly short cylindrical, arranged in one to two rows
Excurrent aperture	Papillae is weakly developed, sparsely arranged in one row; and pigmentation is significant	Papillae is short and dense; pigmentation unnoticeable
Labial palps	Medium-thick, flat elliptical	Medium-thick, elliptical

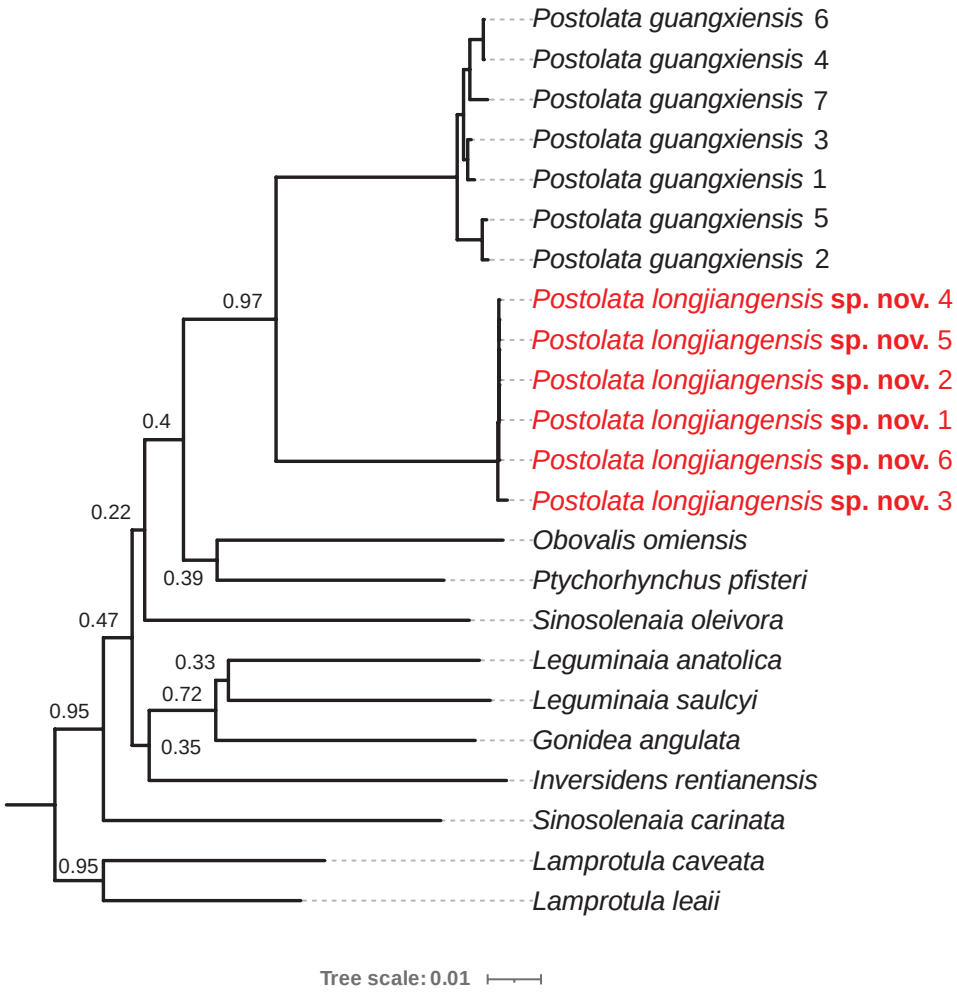

Figure 4. Neighbor-joining tree generated from 23 COI sequences (12 taxa) based on the uncorrected *p*-distance model. The numbers at the nodes indicate bootstrap supports (BS). The red fonts represent the species defined in this study.

Phylogenetic analyses

Multilocus phylogenies that were reconstructed using Bayesian inference (BI) and maximum likelihood (ML) analyses produced consistent topologies (Fig. 5). Both BI and ML analyses indicated that *Postolata longjiangensis* sp. nov. formed the sister lineage to *Postolata guangxiensis* in the tribe Gonideini with high support values (BS/PP = 96/0.96) (Fig. 5).

All eight recognized tribes in the subfamily Gonideinae formed monophyletic groups with the following relationships: ((Gonideini + (((Contradentini + Rectidentini) + Ctenodesmini) + (Lamprotulini + Chamberlainiini)) + (Pseudodontini + Schepmaniini)) (Fig. 5).

Discussion

We integrated comprehensive molecular evidence, shell morphology, and soft-body anatomy into the identification and classification of the new species from Guangxi, namely *Postolata longjiangensis* sp. nov. The topology of our phylogenetic tree (Fig. 5) basically corresponds to those generated in previous studies, except for some nodes (Wu et al. 2024). In our phylogenetic tree, the six individuals of *P. longjiangensis* occupy a single branch that shares a sister-group relationship with *Postolata guangxiensis* in the tribe Gonideini (Fig. 5). The long branch of *P. longjiangensis* unequivocally indicates its distinct (species-level) divergence from congeneric species (uncorrected *p*-distance = 8.13%; Fig. 4).

In addition to the molecular phylogenetic evidence, *Postolata longjiangensis* and *Postolata guangxiensis* also display significant disparities in both shell morphology and soft-body anatomy (Table 3). The shell thickness of *P. longjiangensis* is relatively lower compared to that of *P. guangxiensis*, and the hinge is weakly developed, with only one prominent pseudocardinal tooth. The morphological characteristics of the apertures and labial palps also differ significantly (Fig. 3). The convergence of shell and anatomical features in freshwater mussels is an important factor contributing to the difficulty in species definition (Inoue et al. 2013; Lopes-Lima et al. 2024). However, both species of *Postolata* possess inter-specific diagnostic features in terms of both shell morphology and anatomy.

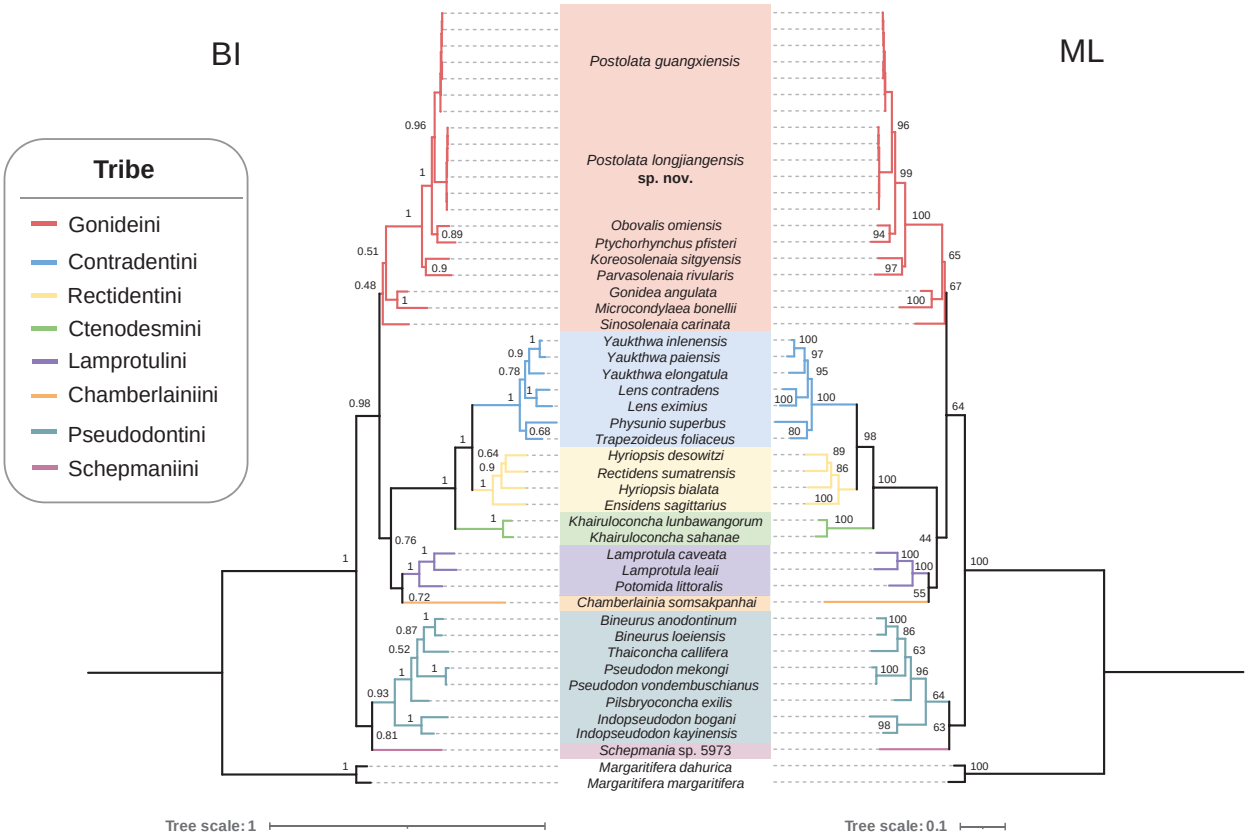

Figure 5. Bayesian inference (BI) and maximum likelihood (ML) trees reconstructed from the three-gene dataset (COI + 16S rRNA + 28S rRNA). Numbers at the nodes indicate the statistical support values for posterior probability (PP) and bootstrap support (BS). Color-coded clades and shadows represent eight tribes in the subfamily Gonideinae.

The southern region of Guangxi, situated in the Indo-Burma hotspot area, has garnered significant attention and conservation efforts for its rich biodiversity (Tordoff et al. 2012). However, there remains a dearth of research on freshwater mussels in this area, including accurate species distribution, precise classification, and population dynamics (Zieritz et al. 2018; Liu et al. 2022). This knowledge gap severely impedes the progress of mussel conservation in this region. The construction and planning of hydraulic projects for large rivers in recent years have led to the emergence of small rivers and tributaries as vital habitats for aquatic life (Jiang et al. 2011; Sabo et al. 2012; Xie 2017). The type locality of *Postolata guangxiensis* is a small tributary of the Luoqing River, characterized by good water quality and a silt bottom, with numerous residential structures in close proximity (Dai et al. 2023). It is interesting that *Postolata longjiangensis* was discovered 100 km away in the Long River and shares a similar habitat type (Fig. 1). The river habitats housing endemic mussel species are highly vulnerable and require immediate attention and protection due to the impacts of urbanization and human activities. Therefore, we advocate for the implementation of in situ conservation measures for select endemic and endangered freshwater mussels through the establishment of nature reserves. Additionally, comprehensive research on artificial breeding techniques and their practical application is imperative to facilitate the recovery of this critically endangered species.

Acknowledgements

This work was funded by the National Natural Science Foundation of China (No. 32200370), the Basic Research Program of Shanxi Province, China (No. 20210302124253), the Research Project Supported by the Shanxi Scholarship Council of China (2024-088), and the Innovation and Entrepreneurship Training Program for college students in Shanxi Province (2023DXCM-31).

References

Barnhart MC, Haag WR, Roston WN (2008) Adaptations to host infection and larval parasitism in Unionoida. Journal of the North American Benthological Society 27(2): 370–394. https://doi.org/10.1899/07-093.1

Castresana J (2000) Selection of conserved blocks from multiple alignments for their use in phylogenetic analysis. Molecular Biology and Evolution 17(4): 540–552. https://doi.org/10.1093/oxfordjournals.molbev.a026334

Dai YT, Huang XC, Wu CHZ, Chen ZGL, Guo L, Shu FY, Ouyang S, Wu XP (2023) Multilocus and mitogenomic phylogenetic analyses

reveal a new genus and species of freshwater mussel (Bivalvia: Unionidae) from Guangxi, China. Invertebrate Systematics 37(2): 152–166. https://doi.org/10.1071/IS22048

Do VT, Tuan LQ, Bogan AE (2018) Freshwater mussels (Bivalvia: Unionida) of Vietnam: Diversity, distribution, and conservation status. Freshwater Mollusk Biology and Conservation 21(1): 1–18. https://doi.org/10.31931/fmbc.v21i1.2018.1-18

Ferreira-Rodríguez N, Akiyama YB, Aksenova OV, Araujo R, Christopher Barnhart M, Bespalaya YV, Bogan AE, Bolotov IN, Budha PB, Clavijo C, Clearwater SJ, Darrigran G, Do VT, Douda K, Froufe E, Gumpinger C, Henrikson L, Humphrey CL, Johnson NA, Klishko O, Vaughn CC (2019) Research priorities for freshwater mussel conservation assessment. Biological Conservation 231: 77–87. https://doi.org/10.1016/j.biocon.2019.01.002

Graf DL, Cummings KS (2023) The MUSSEL project database. http://www.mussel-project.net/

Guerra D, Lopes-Lima M, Froufe E, Gan HM, Ondina P, Amaro R, Klunzinger MW, Callil C, Prié V, Bogan AE, Stewart DT, Breton S (2019) Variability of mitochondrial ORFans hints at possible differences in the system of doubly uniparental inheritance of mitochondria among families of freshwater mussels (Bivalvia: Unionida). BMC Evolutionary Biology 19(1): 229. https://doi.org/10.1186/s12862-019-1554-5

Haag WR, Williams JD (2014) Biodiversity on the brink: An assessment of conservation strategies for North American freshwater mussels. Hydrobiologia 735(1): 45–60. https://doi.org/10.1007/s10750-013-1524-7

Howard JK, Cuffey KM (2006) The functional role of native freshwater mussels in the fluvial benthic environment. Freshwater Biology 51(3): 460–474. https://doi.org/10.1111/j.1365-2427.2005.01507.x

Huang XC, Su JH, Ouyang JX, Ouyang S, Zhou CH, Wu XP (2019) Towards a global phylogeny of freshwater mussels (Bivalivia: Unionida): Species delimitation of Chinese taxa, mitochondrial phylogenomics, and diversification patterns. Molecular Phylogenetics and Evolution 130: 45–59. https://doi.org/10.1016/j.ympev.2018.09.019

Inoue K, Hayes DM, Harris JL, Christian AD (2013) Phylogenetic and morphometric analyses reveal ecophenotypic plasticity in freshwater mussels *Obovaria jacksoniana* and *Villosa arkansasensis* (Bivalvia: Unionidae). Ecology and Evolution 3(8): 2670–2683. https://doi.org/10.1002/ece3.649

Jiang X, Xiong J, Xie Z, Chen Y (2011) Longitudinal patterns of macroinvertebrate functional feeding groups in a Chinese river system: A test for river continuum concept (RCC). Quaternary International 244(2): 289–295. https://doi.org/10.1016/j.quaint.2010.08.015

Kalyaanamoorthy S, Minh BQ, Wong TKF, von Haeseler A, Jermiin LS (2017) ModelFider: Fast model selection for accurate phylogenetic estimates. Nature Methods 14(6): 587–589. https://doi.org/10.1038/nmeth.4285

Katoh K, Standley DM (2013) MAFFT multiple sequence alignment software version 7: Improvements in performance and usability. Molecular Biology and Evolution 30(4): 772–780. https://doi.org/10.1093/molbev/mst010

Kumar S, Stecher G, Tamura K (2016) MEGA7: Molecular evolutionary genetics analysis Version 7.0 for bigger datasets. Molecular Biology and Evolution 33(7): 1870–1874. https://doi.org/10.1093/molbev/msw054

Lanfear R, Frandsen PB, Wright AM, Senfeld T, Calcott B (2017) PartitionFinder 2: New methods for selecting partitioned models of evolution for molecular and morphological phylogenetic analyses. Molecular Biology and Evolution 34(3): 772–773. https://doi.org/10.1093/molbev/msw260

Letunic I, Bork P (2007) Interactive tree of life (iTOL): An online tool for phylogenetic tree display and annotation. Bioinformatics (Oxford, England) 23(1): 127–128. https://doi.org/10.1093/bioinformatics/btl529

Liu XJ, Liu YY, Wu RW, Zanatta DT, Lopes-Lima M, Gonçalves DV, Bogan AE, Ouyang S, Wu XP (2022) Systematics, distribution, biology, and conservation of freshwater mussels (Bivalvia: Unionida) in China. Aquatic Conservation 32(5): 859–895. https://doi.org/10.1002/aqc.3799

Liu L, Zhang L, Jin D, Wang H, Liu X, Wu R (2023) Molecular and morphological evidence reveals a hidden new taxon in the endemic genus *Pseudocuneopsis* (Bivalvia, Unionidae) from China. ZooKeys 1179: 219–229. https://doi.org/10.3897/zookeys.1179.109817

Lopes-Lima M, Froufe E, Do VT, Ghamizi M, Mock KE, Kebapçi U, Klishko O, Kovitvadhi S, Kovitvadhi U, Paulo OS, Pfeiffer JM III, Raley M, Riccardi N, Şereflişan H, Sousa R, Teixeira A, Varandas S, Wu X, Zanatta DT, Zieritz A, Bogan AE (2017a) Phylogeny of the most species-rich freshwater bivalve family (Bivalvia: Unionida: Unionidae): Defining modern subfamilies and tribes. Molecular Phylogenetics and Evolution 106: 174–191. https://doi.org/10.1016/j.ympev.2016.08.021

Lopes-Lima M, Sousa R, Geist J, Aldridge DC, Araujo R, Bergengren J, Bespalaya Y, Bódis E, Burlakova L, Van Damme D, Douda K, Froufe E, Georgiev D, Gumpinger C, Karatayev A, Kebapçi Ü, Killeen I, Lajtner J, Larsen BM, Lauceri R, Legakis A, Lois S, Lundberg S, Moorkens E, Motte G, Nagel K-O, Ondina P, Outeiro A, Paunovic M, Prié V, von Proschwitz T, Riccardi N, Rudzīte M, Rudzītis M, Scheder C, Seddon M, Şereflişan H, Simić V, Sokolova S, Stoeckl K, Taskinen J, Teixeira A, Thielen F, Trichkova T, Varandas S, Vicentini H, Zajac K, Zajac T, Zogaris S (2017b) Conservation status of freshwater mussels in Europe: State of the art and future challenges. Biological Reviews of the Cambridge Philosophical Society 92(1): 572–607. https://doi.org/10.1111/brv.12244

Lopes-Lima M, Geist J, Egg S, Beran L, Bikashvili A, Van Bocxlaer B, Bogan AE, Bolotov IN, Chelpanovskaya OA, Douda K, Fernandes V, Gomes-dos-Santos A, Gonçalves DV, Gürlek ME, Johnson NA, Karaouzas I, Kebapçı Ü, Kondakov AV, Kuehn R, Lajtner J, Mumladze L, Nagel K-O, Neubert E, Österling M, Pfeiffer J, Prié V, Riccardi N, Sell J, Schneider LD, Shumka S, Sîrbu I, Skujienė G, Smith CH, Sousa R, Stöckl K, Taskinen J, Teixeira A, Todorov M, Trichkova T, Urbańska M, Välilä S, Varandas S, Veríssimo J, Vikhrev IV, Woschitz G, Zając K, Zając T, Zanatta D, Zieritz A, Zogaris S, Froufe E (2024) Integrative phylogenetic, phylogeographic and morphological characterisation of the *Unio crassus* species complex reveals cryptic diversity with important conservation implications. Molecular Phylogenetics and Evolution 195: 108046. https://doi.org/10.1016/j.ympev.2024.108046

Lydeard C, Cowie RH, Ponder WF, Bogan AE, Bouchet P, Clark SA, Cummings KS, Frest TJ, Gargominy O, Herbert DG, Hershler R, Perez KE, Roth B, Seddon M, Strong EE, Thompson FG (2004) The global decline of nonmarine mollusks. Bioscience 54(4): 321–330. https://doi.org/10.1641/0006-3568(2004)054[0321:TGDONM]2.0.CO;2

Minh BQ, Schmidt HA, Chernomor O, Schrempf D, Woodhams MD, von Haeseler A, Lanfear R (2020) IQTREE 2: New models and efficient methods for phylogenetic inference in the genomic era.

Molecular Biology and Evolution 37(5): 1530–1534. https://doi.org/10.1093/molbev/msaa015

Modesto V, Ilarri M, Souza AT, Lopes-Lima M, Douda K, Clavero M, Sousa R (2018) Fish and mussels: Importance of fish for freshwater mussel conservation. Fish and Fisheries 19(2): 244–259. https://doi.org/10.1111/faf.12252

Ronquist F, Teslenko M, van der Mark P, Ayres DL, Darling A, Höhna S, Larget B, Liu L, Suchard MA, Huelsenbeck JP (2012) MrBayes 3.2: Efficient Bayesian phylogenetic inference and model choice across a large model space. Systematic Biology 61(3): 539–542. https://doi.org/10.1093/sysbio/sys029

Sabo JL, Bestgen K, Graf W, Sinha T, Wohl EE (2012) Dams in the Cadillac Desert: Downstream effects in a geomorphic context. Annals of the New York Academy of Sciences 1249(1): 227–246. https://doi.org/10.1111/j.1749-6632.2011.06411.x

Tordoff AW, Baltzer MC, Fellowes JR, Pilgrim JD, Langhammer PF (2012) Key biodiversity areas in the Indo-Burma hotspot: Process, progress and future directions. Journal of Threatened Taxa 4(8): 2779–2787. https://doi.org/10.11609/JoTT.o3000.2779-87

Vaughn CC (2018) Ecosystem services provided by freshwater mussels. Hydrobiologia 810(1): 15–27. https://doi.org/10.1007/s10750-017-3139-x

Vaughn CC, Nichols SJ, Spooner DE (2008) Community and foodweb ecology of freshwater mussels. Journal of the North American Benthological Society 27(2): 409–423. https://doi.org/10.1899/07-058.1

Williams JD, Bogan A, Garner JT (2008) Freshwater mussels of Alabama and the Mobile Basin in Georgia, Mississippi and Tennessee. University of Alabama Press, Tuscaloosa.

Wu RW, Liu LL, Liu XJ, Ye YY, Wu XP, Xie ZC, Liu ZY, Li ZF (2023a) Towards a systematic revision of the superfamily Cyrenoidea (Bivalvia: Imparidentia): species delimitation, multi-locus phylogeny and mitochondrial phylogenomics. Invertebrate Systematics 37(9): 607–622. https://doi.org/10.1071/IS23015

Wu RW, Liu LL, Zhang LP, Jia JL, Jin DD, Wu XP, Liu XJ (2023b) New species of the genus *Pseudocuneopsis* Huang, Dai, Chen & Wu, 2022 (Bivalvia, Unionidae) from Guangxi Province, China. ZooKeys 1166: 261–270. https://doi.org/10.3897/zookeys.1166.104150

Wu RW, Zhang LP, Liu LL, Jia JL, Liu XJ (2024) Unraveling the Phylogenetic Relationships and Taxonomic Status of a Puzzling Freshwater Mussel Genus *Inversidens* (Bivalvia, Unionidae) through Multilocus Phylogeny and Mitochondrial Phylogenomics. Journal of Zoological Systematics and Evolutionary Research 1499508: 1–18. https://doi.org/10.1155/2024/1499508

Xie P (2017) Biodiversity crisis in the Yangtze River: The culprit was dams, followed by overfishing. Hupo Kexue 29(6): 1279–1299. https://doi.org/10.18307/2017.0601

Zhang D, Gao F, Jakovlić I, Zhou H, Zhang J, Li WX, Wang GT (2020) PhyloSuite: An integrated and scalable desktop platform for streamlined molecular sequence data management and evolutionary phylogenetics studies. Molecular Ecology Resources 20(1): 348–355. https://doi.org/10.1111/1755-0998.13096

Zieritz A, Bogan AE, Froufe E, Klishko O, Kondo T, Kovitvadhi U, Kovitvadhi S, Lee JH, Lopes-Lima M, Pfeiffer JM, Sousa R, Do TV, Vikhrev I, Zanatta DT (2018) Diversity, biogeography and conservation of freshwater mussels (Bivalvia: Unionida) in East and Southeast Asia. Hydrobiologia 810(1): 29–44. https://doi.org/10.1007/s10750-017-3104-8

Supplementary material 1

Partitioning schemes and best-fit models identified from PartitionFinder and ModelFinder for three-locus dataset

Authors: Lili Liu, Liping Zhang, Kaiyu Hou, Liyang Ning, Ruiwen Wu

Data type: xlsx

Link: https://doi.org/10.3897/zse.100.126069.suppl1

Zoosyst. Evol. 100 (3) 2024, 779–789 | DOI 10.3897/zse.100.117952

PENSOFT

für Natur MUSEUM FÜR NATURKUNDE BERLIN

A new species of velvet worm of the genus *Oroperipatus* (Onychophora, Peripatidae) from western Amazonia

Jorge L. Montalvo-Salazar[1], M. Lorena Bejarano[2], Alfredo Valarezo[2], Diego F. Cisneros-Heredia[1,3,4]

1 *Universidad San Francisco de Quito USFQ, Colegio de Ciencias Biológicas y Ambientales, Instituto de Biodiversidad Tropical IBIOTROP, Laboratorio de Zoología Terrestre, Museo de Zoología, Quito 170901, Ecuador*

2 *Universidad San Francisco de Quito USFQ, Colegio Politécnico de Ciencias e Ingenierías, Departamento de Ingeniería Mecánica, Instituto de Energía y Materiales, Quito, Ecuador*

3 *Universidad San Francisco de Quito USFQ, Estación de Biodiversidad Tiputini, Orellana, Quito, Ecuador*

4 *Instituto Nacional de Biodiversidad, Quito, Ecuador*

https://zoobank.org/D477CDCE-B280-4EBC-AC4F-B8377DF1A274

Corresponding authors: Jorge L. Montalvo-Salazar (jorgemontalvo2000@gmail.com); Diego F. Cisneros-Heredia (diego.cisnerosheredia@gmail.com)

Academic editor: Pavel Stoev ♦ **Received** 29 December 2023 ♦ **Accepted** 7 May 2024 ♦ **Published** 14 June 2024

Abstract

The diversity of Neotropical velvet worms (Onychophora, Neopatida) is significantly underestimated, particularly within the Andean clade represented by the genus *Oroperipatus*, the last species of which was described more than 70 years ago. Here, we describe a new species of *Oroperipatus* from the Amazonian lowlands of Ecuador, bringing the total number of described species on mainland Ecuador to seven and in western Amazonia to three. The new species, *Oroperipatus tiputini* **sp. nov.**, can be distinguished from its congenerics by the following combination of characters: two variations of primary papillae alternated between dorsal plicae; four scale ranks in the apical piece of primary papillae; reduced fifth spinous pad of legs IV and V; four supraocular papillae; occasionally reduced anterior papilla; males with two crural tubercles per leg in the first pregenital pair and a single crural tubercle per leg in the next pair; and some accessory papillae with one lateral rudimentary apical piece. We also discuss novel morphological similarities and differences with other Neopatida genera, as revealed by scanning electron microscopy (SEM).

Key Words

Andean peripatids, Ecuador, Neopatida, new species, taxonomy, Tiputini Biodiversity Station, Yasuni

Introduction

Onychophorans, commonly known as velvet worms, possess a soft, elongated body covered by a lightly sclerotised cuticle, multiple locomotor limbs, and a pair of anterior slime papillae that expel a sticky slime used to immobilise their prey (Mayer et al. 2015). Members of the phylum Onychophora are found in tropical and subtropical regions around the world, with about 230 described species divided into two families: Peripatidae, with a pantropical distribution (Neotropics, Antilles, west Africa, and southeast Asia), and Peripatopsidae, with a circum-Antarctic distribution (Chile, South Africa, New Guinea, Australia, and New Zealand) (Monge-Nájera 1995; Oliveira et al. 2012; Giribet et al. 2018). Neotropical peripatids form the clade Neopatida and are divided into two lineages: the "Andean peripatids", represented by species of the genus *Oroperipatus* Cockerell, 1908, and the "Caribbean peripatids", comprising all other neopatid genera (Giribet et al. 2018; Costa and Giribet 2021).

Oroperipatus is characterised by four or more foot papillae and a nephridial tubercle on legs IV and V inserted in a complete third spinous pad (Bouvier 1905; Clark 1913; Costa et al. 2021). While knowledge of the diversity of Caribbean peripatids has significantly increased (e.g., Morera-Brenes and Nájera 2010; Costa et al. 2018; Barquero González et al. 2020; Costa and Giribet 2021), the most recent descriptions of *Oroperipatus* species date

back over 70 years (du Bois-Reymond Marcus 1952). Currently, twenty species of *Oroperipatus* are known from México, Panama, Colombia, Ecuador, Peru, Bolivia, and Brazil, with a wide altitudinal range from the Pacific coast to the high Andes and the Amazonian lowlands (Bouvier 1905, Fuhrmann 1915; Clark and Zetek 1946; Sampaio-Costa et al. 2009; Oliveira 2023). In South America, only two described species have been reported from the lowlands of western Amazonia: *Oroperipatus bluntschlii* (Fuhrmann, 1915), from the area of the Samiria and Lagartococha rivers, Loreto, Peru, and *O. weyrauchi* (Bois-Reymond Marcus, 1952), from Yúrac, River Aguaytía, Ucayali, Peru (Fuhrmann 1915; du Bois-Reymond Marcus 1952; Icochea and Ramírez 1996). In this contribution, we are pleased to describe a new species of *Oroperipatus* from the northern Amazonian lowlands of Ecuador.

Methods

We conducted fieldwork at the Tiputini Biodiversity Station (TBS), situated approximately 280 km ESE of Quito, in the Orellana province, Republic of Ecuador. Established in 1994 by Universidad San Francisco de Quito (USFQ), TBS is a research station spanning 744 hectares of undisturbed lowland evergreen rainforest on the northern bank of the Tiputini River, within the Yasuni Biosphere Reserve – one of the planet's most biodiverse regions (Cisneros-Heredia 2003, 2006; Bass et al. 2010; Blake et al. 2012; Ryder and Sillett 2016; Romo et al. 2017). The station encompasses various habitats, including Terra Firme Forest, Várzea Forest, small areas of Igapo Forest, palm swamps, and natural gaps. Mean annual precipitation ranges between 2700 and 3100 mm, with a relatively aseasonal climate characterised by peak rainfall from April to August and drier conditions from November to March and August (Cisneros-Heredia 2003, 2006; Blake et al. 2012; Ryder and Sillett 2016; Romo et al. 2017).

Opportunistic collections were conducted at night on trails at TBS in April–July 2001, June 2017, May–June 2018, April–May 2019, May–June 2022 and June 2023. Specimens were collected by hand, placed in plastic bags with leaf litter for transportation to the laboratory, photographed alive, and then euthanised and preserved in 75% ethanol. Additionally, we examined specimens deposited by previous researchers at the Museo de Zoología, Universidad San Francisco of Quito, Ecuador (ZSFQ). All specimens of the type series are deposited at ZSFQ. Jaws are preserved in glycerol in microvials alongside their respective specimens. Information for comparative diagnoses was obtained from the original descriptions and the comprehensive revision by Bouvier (1905).

Description, character definition, and terminology adhere to standards proposed by Oliveira et al. (2010, 2012). We followed the definition of antennal tip by Oliveira et al. (2010) due to the undetected chemoreceptors (see Remarks). The concept of diagnosis is used as proposed by the ICZN (1999). Specimens were examined using an Olympus SZX16 stereomicroscope. To facilitate jaw extraction and minimise mouth damage, specimens were rehydrated using gradually lowered ethanol concentrations (from 75% to 10%) and warm water for five hours. Jaws were then placed on a slide with gel alcohol and observed under an Olympus CX22 optic microscope. All measurements were taken in preserved specimens under a stereomicroscope with a Truper digital vernier calliper (0.05 mm accuracy, rounded to the nearest 0.1 mm) and reported as a mean ± standard deviation (range, sample size). Specimens were studied and photographed using an Olympus SZX16 stereomicroscope with an Olympus DP73 digital camera attached. Photographs shown in Fig. 3 were obtained by photograph stacking using CombineZP 1.0 software and then adjusted for brightness and contrast to highlight taxonomically important structures with Adobe Photoshop CC 2020 software (Adobe Systems, USA). Raw photographs are available at http://doi.org/10.5281/zenodo.10864497. Photographs in other figures were not adjusted. Descriptions of colouration in life are based on digital in-situ photographs.

We used scanning electron microscopy (SEM) to study the morphology of the tegument. One male paratype (ZSFQ-i8004) preserved in 75% ethanol was dissected to extract samples of its dorsal tegument, legs, antenna, and genital pad. Images were captured using a JEOL JSM-IT300L SEM at 15 kV with a working distance of 13 mm, operated under low vacuum conditions (30 Pa) and a high probe current of 40 nA. Samples were carefully dried by natural convection on a petri dish using a fluorescent lamp for 20 minutes. This method was chosen due to the lack of a critical point dryer. Samples were gold-coated for 1 minute and electrically grounded to the stage using carbon tape.

We conducted this research under research permits (006-2015-FAU-DPAP-MA, 001-16 IC-FLO-FAU-DNB/MA, 018-2017-IC-FAU-DNB/MAE, 019-2018-IC-FAU-DNB/MAE, and MAAE-ARSFC-2022-2204) issued by the Ministry of Environment of Ecuador.

Results

***Oroperipatus tiputini* sp. nov.**

https://zoobank.org/F37273EE-10A9-49D7-A332-8B354F12DCBC

Figs 1–5

Material examined. ***Holotype*.** Ecuador • ♀, province of Orellana, Tiputini Biodiversity Station; -0.637, -76.152; 220 m elevation; 6 Jun. 2022; Pedro Peñaherrera-R., Roberto J. León-E., and Diego F. Cisneros-Heredia leg.; ZSFQ-i8249

***Paratypes*.** Ecuador • 1 ♂, same locality data as holotype; 22 May 2018; Diego F. Cisneros-Heredia, Francisco Velásquez, and Juan Pablo Jordán leg.; ZSFQ-i5151; • 1 ♂, same locality data as holotype; 21 May 2019; Francisco Velásquez and Diego F. Cisneros-Heredia leg.; ZSFQ-i8004, • 1 ♂, same locality data as holotype; 13 Apr.

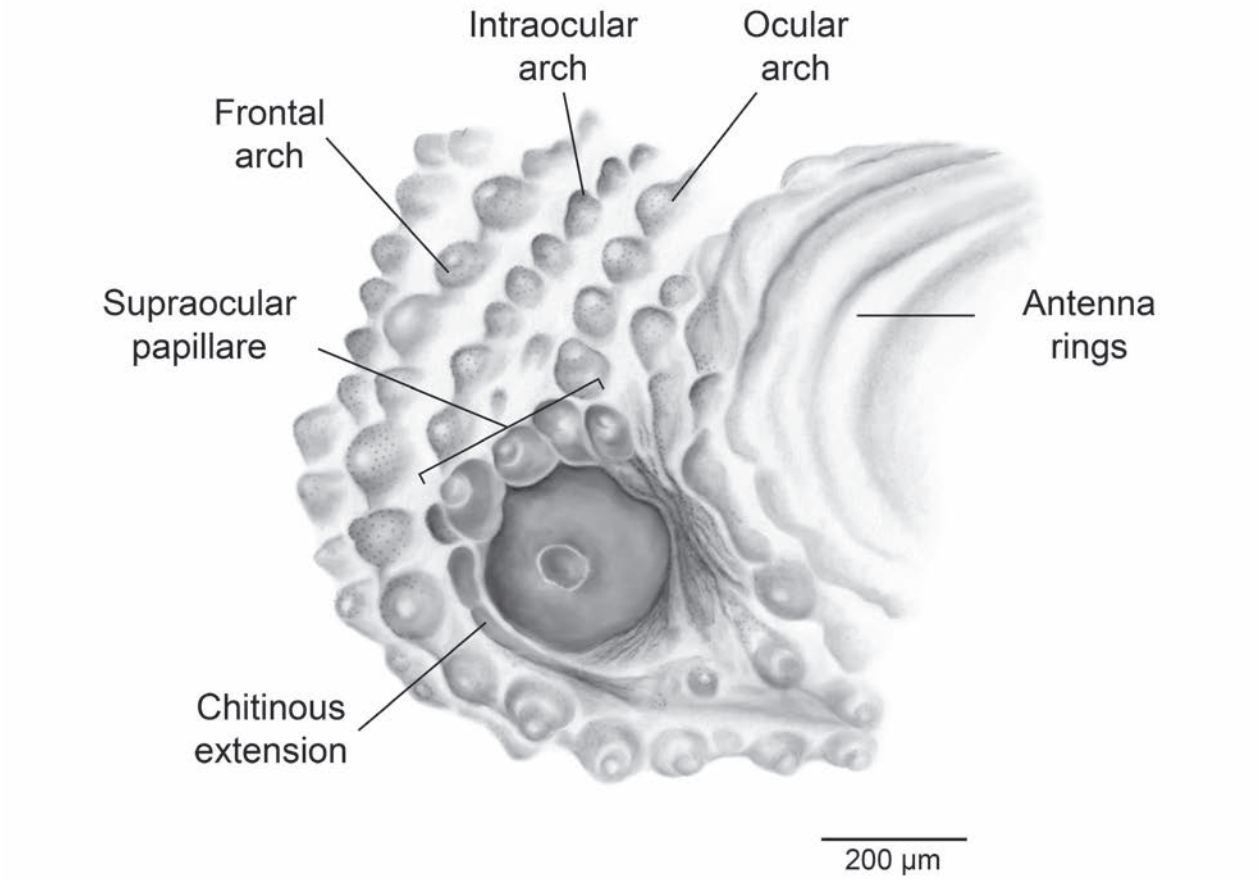

Figure 1. Illustration of the head morphology around the eye of *Oroperipatus tiputini* sp. nov. showing four supraocular papillae, the chitinous extension, and frontal, intraocular, and ocular arches.

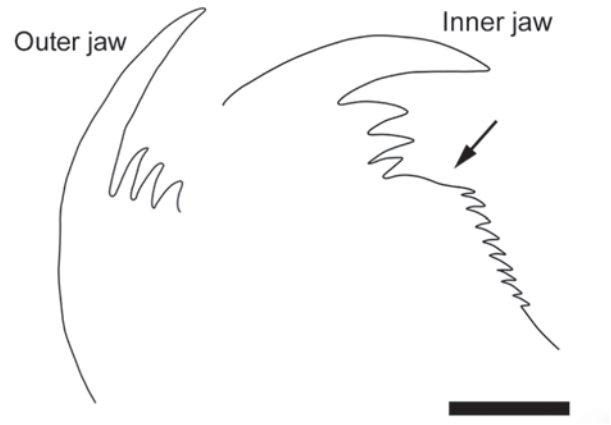

Figure 2. Drawing of the outer and inner jaws of *Oroperipatus tiputini* sp. nov.; the black arrow points to the diastema. Scale bar: 0.2 mm.

2021; K. Faloon leg.; ZSFQ-8250; • 1 ♂, same locality data as holotype; 30 Jun. 2023; Montalvo, J. leg. ZSFQ-i17992• 1 ♂, same locality data as holotype; 8 Jun. 2022; Pedro Peñaherrera-R., Roberto J. León-E., and Diego F. Cisneros-Heredia leg.; on the root of a Ceiba tree; ZSFQ-i8270; 1 ♀ and 1 juvenile, same locality data as holotype; 7 Jun. 2017; Diego F. Cisneros-Heredia leg.; ZSFQ-i5143, ZSFQ-i17793; • 1 juvenile, same data as holotype; ZSFQ-i17794; • 1 ♀, same locality data as holotype; 25 May 2022; Diego F. Cisneros-Heredia, Paula Leoro and María Sol Salazar leg.; ZSFQ-i8248. • 1 juvenile, same locality data as holotype; 30 Jul. 2001; Diego F. Cisneros-Heredia leg.; ZSFQ-i5149.

Type locality. Tiputini Biodiversity Station (-0.637, -76.152, 220 m elevation), provincia de Orellana, República del Ecuador.

Diagnosis. *Oroperipatus tiputini* sp. nov. differs from all other congeneric species by having two size variations of primary papillae alternated between dorsal plicae (Figs 3A, 4C), apical piece of primary papillae with four scale ranks (Fig. 4B), reduced fifth spinous pad of legs IV and V (Fig. 3B), four foot papillae, four supraocular papillae, and occasionally the anterior papilla reduced (Fig. 1); some accessory papillae with one lateral rudimentary apical piece (Fig. 4C); males with two crural tubercles per leg in first pregenital pair and a single crural tubercle per leg in the next pair (Fig. 3C).

Oroperipatus tiputini sp. nov. is most similar to *O. lankesteri* by having dorsal plica alternation, two variations of primary papillae alternated between dorsal plicae, two to three accessory teeth in outer jaw, one to two accessory teeth in inner jaw, reduced fifth spinous pad of legs IV and V, and seven rings on tip of antenna. However, *O. tiputini* sp. nov. is distinguished from *O. lankesteri* (characters in

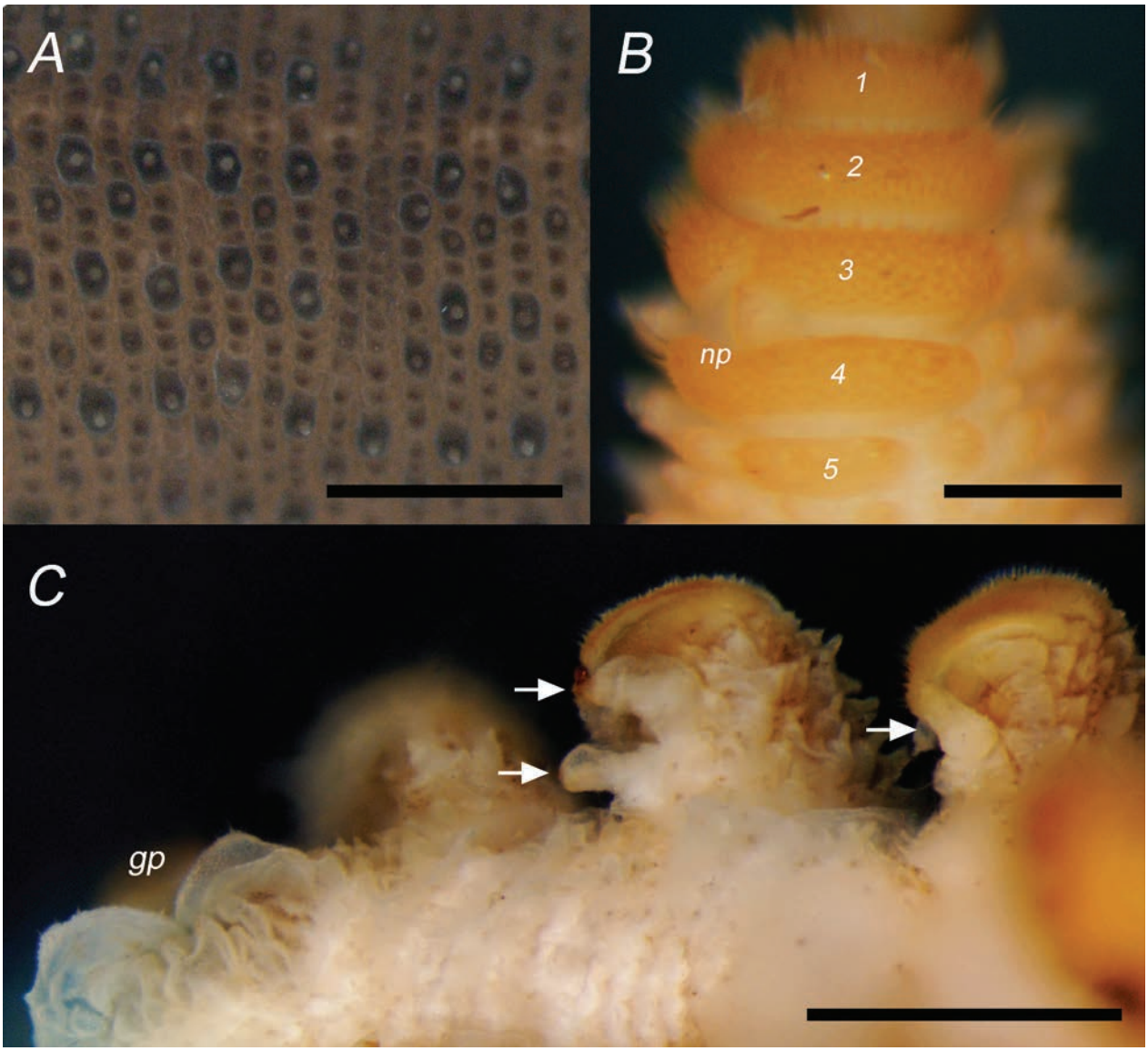

Figure 3. Tegument and leg morphology of *Oroperipatus tiputini* sp. nov. **A.** Dorsal integument. **B.** Ventral detail of the right V leg showing five spinous pads and a nephridial tubercle (np) indented at the third spinous pad. **C.** Genital pad (gp) and pregenital legs of the right side showing the crural tubercules pointed by white arrows. Scale bars: 1 mm (**A**); 0.2 mm (**B**); 0.4 mm (**C**).

parentheses) by having a well-developed diastema (short diastema), absence of distal foot papillae, and always presenting two anterior and posterior foot papillae (five to seven foot papillae with distal papillae); third spinous pad divided into two unequal fragments by nephridial tubercle (nephridial tubercle at posterior edge of third spinous pad without dividing it); a smaller frontal organ (size as five to six papillae); four supraocular papillae (two); and one to three accessory papillae between primary papillae (uniformly three accessory papillae). *Oroperipatus tiputini* sp. nov. differs from *O. ecuadoriensis* (characters in parentheses), a species similar to *O. lankesteri*, by having reduced fifth spinous pad in IV and V pairs of legs (same width as other spinous pads), two variations of primary papillae (three), hyaline organs inconspicuous (conspicuous), incomplete plicae in every segment (some segments without incomplete plicae), four foot papillae (five to six), a smaller frontal organ (size as five to six papillae), and accessory papillae more abundant (rare on dorsum and more abundant on flanks). *Oroperipatus tiputini* sp. nov can be differentiated from *O. weyrauchi* and *O. bluntschlii*, the other two described species from the Amazonian lowlands (characters of *O. weyrauchi* and *O. bluntschlii* in parentheses) by having two pair of crural tubercles in pregenital pair of legs (one pair in *O. weyrauchi*), legs with more number of transverse leg rings (17–18 in *O. tiputini* vs. 14 in *O. weyrauchi*), four foot papillae (some legs with five in *O. weyrauchi* and *O. bluntschlii*), two types of primary papillae (primary papillae greatly varies in size with all intergradations to accessory papillae), diastema well-developed (short diastema in *O. bluntschlii*), five spinous pad (sixth vestigial spinous pad in *O. bluntschlii*), and biggest primary papillae disposed on large plicae (biggest primary papillae in all segments).

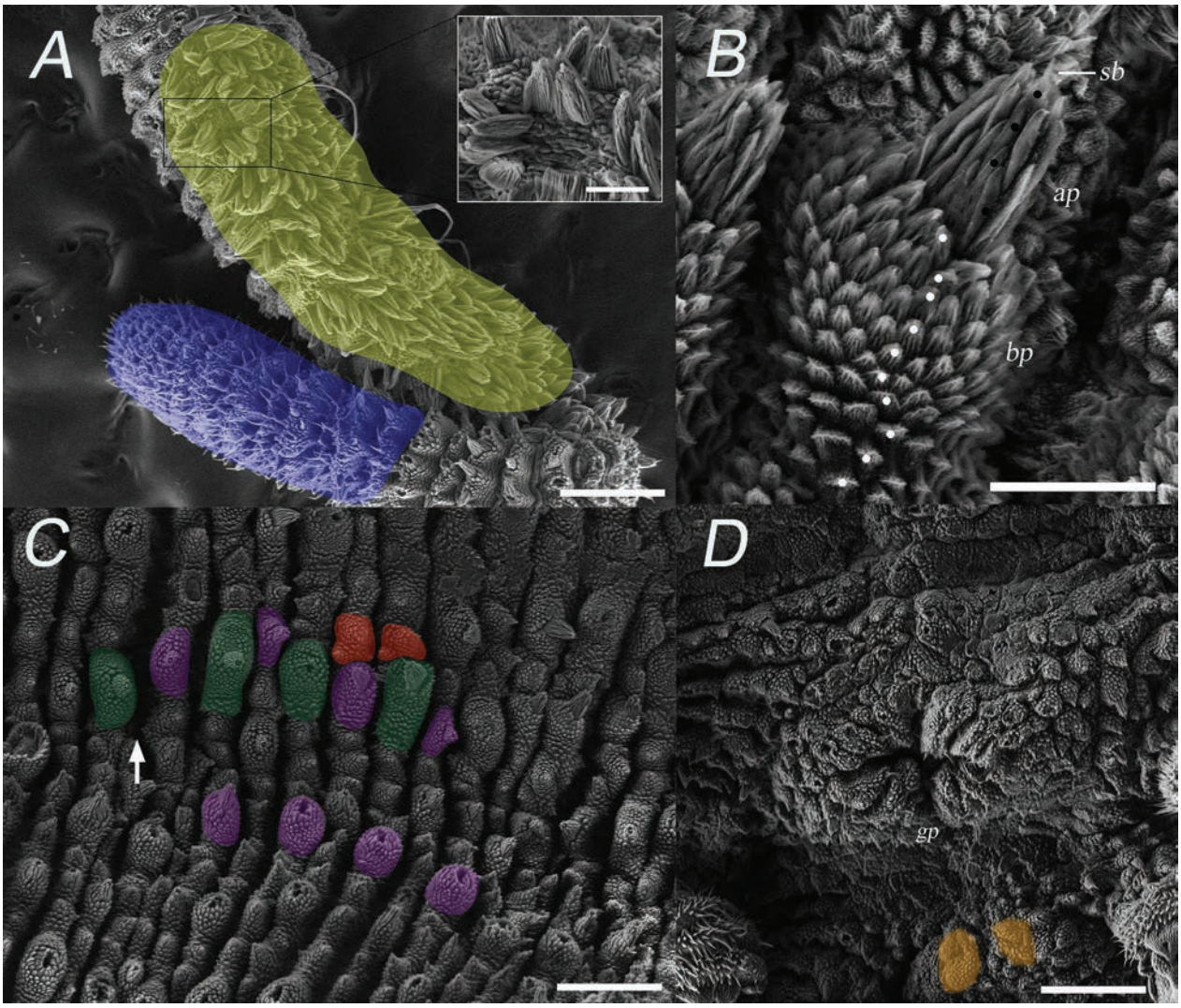

Figure 4. Antenna, dorsal integument, and genital pad morphology of *Oroperipatus tiputini* sp. nov. under a scanning electron microscope. **A.** Antenna: in blue, the antennal tip, and in yellow, the sensory field of the antenna; insert in **A**: spindle-shaped papillae in detail. **B.** Primary papilla with 10 scale ranks in the basal piece (bp), four scale ranks in the apical piece (ap), and the sensory bristle (sb). **C.** Dorso-lateral integument: in green, the biggest primary papillae; in purple, the smallest primary papillae (or secondary papillae); and in red, the accessory papillae that possess rudimentary apical pieces; the arrow points to the incomplete plica. **D.** Posterior region in ventral view showing the opening of the genital pad (gp) and, in orange, the anal glands. Scale bars: 200 µm (**A, C**, **D**), 50 µm (**B** and insert in **A**).

Description. ***Head.*** Antennal rings 40 to 52. Antennal tip with 14 antennal rings alternated type I and type II sensillum; smallest rings only with type II sensillum (Fig. 4A). Antennal chemoreceptors not detected. Ventrally, from ring 17 to base of the antenna, spindle-shaped papillae form sensory field of antenna (Fig. 4A). Slightly wrinkled eyes laterally behind base of antennae. Ocular and frontal arches with large primary papillae and intraocular arch formed by smaller primary papillae and accessory papillae. Intraocular arch interrupted, with a chitinous extension under eye (Fig. 1). A frontal organ located ventral behind base of antennae and equivalent in size to four to five anterior dermal papillae. Mouth with seven pairs of lobes or internal lips (although in some specimens is difficult to distinguish most posterior pair) and unpaired lip. One to three accessory teeth in outer jaw and two or three accessory teeth in inner jaw with deep diastema, followed by seven to nine denticles (Fig. 2).

Dorsal integument. Plicae per segment 12, alternating between large and narrow, ten complete plicae and two incomplete plicae and irregular above base of legs; seven plicae overpass between legs to venter. Dorsomedian furrow continuously and flanked by one to three accessory papillae on both sides. Two variations of primary papillae, ovoid. Biggest primary papillae on the large plicae, while smallest primary papillae (or secondary papillae) on every plica. Primary papillae separated by one to three accessory papillae, more frequently by three (Figs 3A, 4C). Primary dermal papillae cylindrical. Apical pieces with four scale ranks. Basal pieces with ten scale rank in largest primary papillae and nine in smallest primary dermal papillae. Scales of apical pieces elongated, three

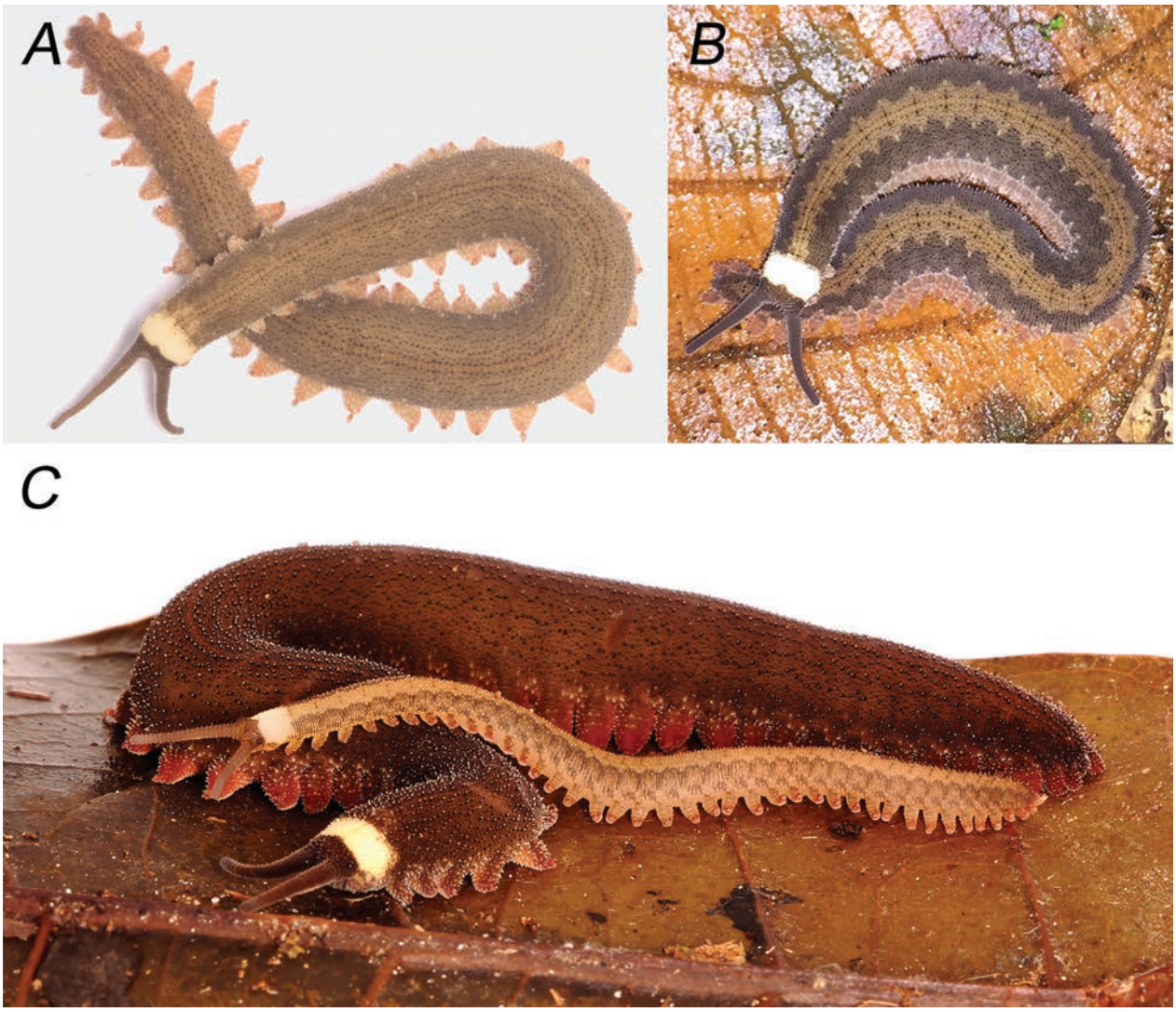

Figure 5. A–C. Colour variation in the life of *Oroperipatus tiputini* sp. nov. **A.** Adult male paratype, ZSFQ-i8270; **B.** Adult male paratype, ZSFQ-i5151; **C.** Adult female holotype (ZSFQ-i8248) and youngling paratype (ZSFQ-17794) a few days after being born. All photographs were taken at the Tiputini Biodiversity Station. Photographs by Pedro Peñaherrera R. (**A, C**) and Diego F. Cisneros-Heredia (**B**).

times larger and half wider than scales of basal pieces (Fig. 4B).

Ventral integument. Visible ventral organs. Preventral organs inconspicuous.

Legs. Transverse rings 17 to 18. Pairs of legs IV and V with four first spinous pads of the same size and fifth one reduced. Proximal margin of third spinous pad indented by nephridial tubercle and separate not completely into two unequal segments (Fig. 3B). Three spinous pads on last pair of legs plus one vestigial, four spinous pads on penultimate pair of legs, and four spinous pads on first pair of legs. Last pair of legs not rotated and used for walking. Eversible coxal vesicle present but not seen in all legs. Two anterior foot papillae and two posterior foot papillae. Two bristles on distal and proximal setiform ridges. Females with 37–40 pairs of legs and males with 34–36 pairs of legs.

Posterior region. Genital opening of females and males cruciform (Fig. 4D). Crural tubercles on four pregenital legs of the male: two crural tubercles per leg in first pregenital pair, and a single crural tubercle per leg in the next pair (Fig. 3C). Concolorous slit-like anal glands in males.

Colouration. One adult male (ZSFQ-i8270) was brown with faded rhomboids (Fig. 5A); two adult males and one adult female (i5151, i17992, 8248; Fig. 5B) were brown with orange diamonds; an adult female (ZSFQ-i8249, holotype) was completely plain dark orange and the youngling it gave birth was yellowish with diamond-shaped dorsal patterns (ZSFQ-i17794; Fig. 5C). All specimens, juveniles and adults, have a very conspicuous anterior white band with a heart-shaped border along midline (Fig. 3). All specimens show head and antennae darker than dorsum, and orange or brown legs. Preserved specimens show high depigmentation, with background colouration changing from pale orange or brown to white and dorsal patterns lost or blurred.

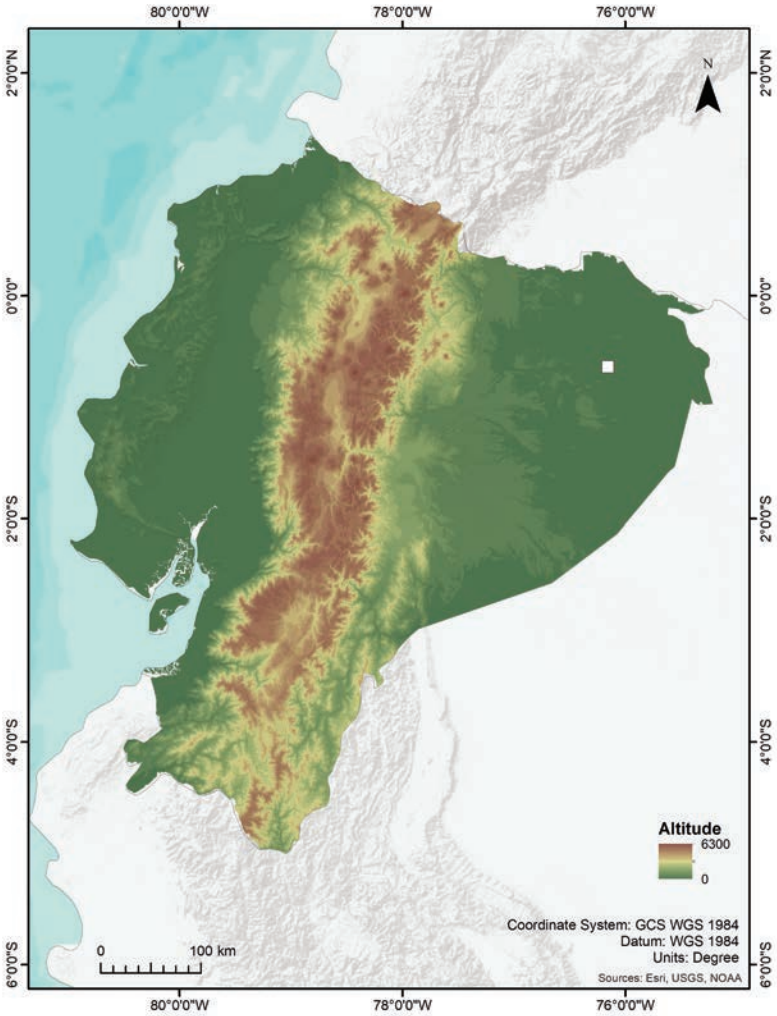

Figure 6. Map of Ecuador showing the location of the Tiputini Biodiversity Station (white square), type locality of *Oroperipatus tiputini* sp. nov., in the Amazonian lowlands.

Measurements. ***Holotype in preservative (in mm):*** Length: 48.1, width: 3.15, number of pairs of legs: 40.

All preserved specimens (in mm): Length of females: 52.6 ± 11.0 (46–65.3, n = 3), width of females: 4.7 ± 1.6 (3.2–6.3, n = 3); length of males: 32.5 ± 6.9 (22.7–39.8, n = 5), width of males: 3.4 ± 0.9 (2.0–4.3, n = 5); length of juveniles: 30.1 ± 4.4 (25.5–34.3, n = 3), width of juveniles: 2.9 ± 0.4 (2.5–3.3, n = 3); number of pairs of legs in females: 37–40, number of pairs of legs in males: 34–37.

Etymology. The specific epithet is used as a name in apposition in reference to the type locality of the new species, Tiputini Biodiversity Station (TBS). We present this new species in recognition of the hard work done to protect Amazonian biodiversity by TBS's management, research, and field team at one of the most important research stations in western Amazonia (Bass et al. 2010).

Distribution and natural history. The species is currently known only from the type locality, Tiputini Biodiversity Station, in the northern Amazonian lowlands of Ecuador (Fig. 4). Most individuals of *O. tiputini* sp. nov. have been found in old-growth, closed-canopy Terra Firme forests, on the leaves and stems of small forbs at less than 70 cm above ground, in leaf litter, and on buttress roots. One specimen (ZSFQ-i8250) was found inside a bromeliad. Most specimens were found active at night (19h00–23h00), except for a male individual active on a tree trunk, 1.5 m above the floor in old-growth Várzea forest, at 16h00. Individuals have been found singly or in pairs. In captivity, the female holotype (ZSFQ-i8248) gave birth to a single youngling (ZSFQ-i17794) (Fig. 5C), staying together for three days until euthanised; during that time, the juvenile remained surrounded by the mother or on her back. One adult male (ZSFQ-i17992) was caught using a baiting net at 1 m height in the vegetation during the day.

Remarks. One male specimen (ZSFQ-i5151) exhibited a different number of legs on each side, with 35 on the right and 36 on the left. The new species undergoes ontogenic colour changes, as shown by the uniform dorsal colouration of the adult female holotype compared with the rhomboid pattern over a yellowish background of its youngling. Juveniles display brighter colours (lighter yellow and rhomboid pattern), which darken with age, and the rhomboid pattern fades in males or is lost in females.

We encountered challenges with two characters in our SEM images. Spindle-shaped papillae appeared notably flattened (Fig. 4A), a condition not previously reported in Onychophora. Additionally, antennal chemoreceptors were not detected, a feature only reported in *Mongeperipatus*. We think these characters were affected by the SEM preparation method.

During our examination, technical limitations prevented a thorough review of certain structures, notably the interpedal structures. However, as these structures are not described for any other *Oroperipatus* species and a comparative analysis was unfeasible, we deemed them non-essential for the purposes of our study aimed at describing a new species.

Discussion

The description of *Oroperipatus tiputini* sp. nov. brings the total number of described velvet worm species from mainland Ecuador to seven. This species is the first described from the Amazonian lowlands of Ecuador and the third from western Amazonia. Most velvet worm species from Ecuador are known only from their type localities, and, in some cases, their taxonomy is unclear and requires further revision (Table 1) (Oliveira 2023). Morphologically, *O. tiputini* sp. nov. is more similar to *O. lankesteri* than to *O. weyrauchi* or *O. bluntschli*, despite the last two being the only congeners inhabiting the Amazon basin. The morphological similarities between *O. tiputini* sp. nov. and *O. lankesteri* could indicate an evolutionary relationship; however, without additional data, proposing any phylogenetic hypothesis would be premature. *Oroperipatus lankesteri* is known solely from its type locality, Paramba, in the northern Pacific lowlands of Ecuador (Table 1). While *O. tiputini* sp. nov. is easily diagnosed from *O. weyrauchi* and *O. bluntschlii*, it is important to note that the descriptions of both species lack certain important characters and others are only presented in figures, making interpretation difficult. The author of these descriptions emphasised characters such as pigmentation, leg number, and dentition, which can be variable. The holotype of *O. bluntschli* was fixed with formaldehyde (Fuhrmann 1915), likely causing deformation of its tegument. The number of leg pairs in onychophorans is related to the length of the individual; however, this variability is low in many species (Monge-Najera, 1994). Therefore, it could be useful for distinguishing certain species if length-related correlations are accounted for (Monge-Nájera 1994). The male reported for *O. weyrauchi* had a length (in 75% ethanol) of 35 mm (du Bois-Reymond Marcus 1952), which falls within the range of *O. tiputini* sp. nov. Thus, the number of leg pairs could be comparable, with *O. weyrauchi* having more leg pairs (40) than *O. tiputini* sp. nov. (34–37). Moreover, the female of *O. weyrauchi*, which was 10 mm longer than the male, had fewer leg pairs (38) than the male, while females of *O. tiputini* sp. nov. have a higher number of leg pairs than males.

Table 1. Described species of *Oroperipatus* (Onychophora, Peripatidae) currently known from mainland Ecuador.

Species	Author	Known distribution	Sources
Oroperipatus quitensis	Schmarda, 1871	Described from the unspecific locality "Aequatorial-Hochland" (= Equatorial highlands), subsequently reported from the valley of Quito, northern Andean highlands[1]	Schmarda (1871); Bouvier (1905); Correoso Rodríguez (2011)
Oroperipatus corradoi	Camerano, 1898	Surroundings of Quito, northern Andean highlands, but also reported from Guayaquil, Balzar and River Giron on the western Andean slopes of Ecuador, and from localities in Panama and Venezuela	Camerano (1898); Bouvier (1905); Clark (1914a, 1914b); Brues (1925); Clark and Zetek (1946); Ribera (1977)
Oroperipatus cameranoi	Bouvier, 1899	Sigsig and Cuenca, southern Andean highlands	Camerano (1897); Bouvier (1905)
Oroperipatus lankesteri	Bouvier, 1899	Paramba, northern Pacific lowlands[2]	Bouvier (1899, 1905)
Oroperipatus ecuadoriensis	Bouvier, 1902	Bulim (nowadays Pulún), northern Pacific lowlands[3]	Bouvier (1902, 1905)
Oroperipatus belli	Bouvier, 1904	Durán, southern Pacific lowlands	Bouvier (1904, 1905)
Oroperipatus tiputini sp. nov.	Montalvo-Salazar & Cisneros-Heredia, 2023	Tiputini Biodiversity Station, northern Amazonian lowlands	This paper

[1] We consider the record of *O. quitensis* from the northern Amazonian lowlands of Ecuador presented by Read (1988) to be in error and correspond to a different, unidentified species.

[2] See Reyes-Puig et al. (2020) for details about the location of Paramba.

[3] See Paynter (1993) for details about the location of Bulim or Pulún.

The rhomboid pattern on the dorsum of *O. tiputini* sp. nov. has been reported in *O. weyrauchii* (du Bois-Reymond, 1952). Field observations suggest this dorsal pattern with some colour variations could be widespread in described and undescribed species from the Ecuadorian and Peruvian Amazonia. The colouration ontogenic changes evidenced in *O. tiputini* sp. nov. are apparently responsible for the significant colour variation observed in the new species. It would be the first case of drastic colour ontogenic changes reported in Onychophora. It has been reported that there are variable intraspecific colourations within the same brood in some species of Peripatopsidae (Ruhberg & Daniels, 2013), and three stages of pigmentation in juveniles of the *Peripatoides novaezealandiae* complex have been distinguished, getting more pigmented and lustred between 25 and >50 days after birth (Pripnow and Rhuberg 2003). Ontogenetic colour changes have been reported in several species of terrestrial arthropods and are related mainly to anti-depredation mimicry and aposematism (Booth 1990).

Oroperipatus tiputini sp. nov. presents four scale ranks in the apical pieces of the primary papillae. The number of scale ranks in the apical pieces varies interspecifically from four to five in *Oroperipatus*, a characteristic that helps differentiate it from most *Epiperipatus* (except for *E. adenocryptus*; Oliveira et al 2011) and *Macroperipatus*, which has three or fewer scale ranks (Read 1988; Chagas-Júnior and Costa 2014). Read (1988) reported that *Oroperipatus* was divided into two groups based on the shape of the primary papillae.*Oroperipatus tiputini* sp. nov. is more closely related to what Read (1988) identified as *Oroperipatus quitensis*, although it probably belongs to an undescribed species given its conical-shaped apical piece and Amazonian locality. In contrast, *O. corradoi* and *O. eisenii* present spherical apical pieces. The number of scale ranks in the basal piece of the dermal papilla shows intraspecific variation and lacks taxonomic relevance. Currently, no additional SEM characters can be used to compare *O. tiputini* sp. nov. with other species of Andean peripatids. It is necessary to explore the morphological diversity of *Oroperipatus* due to its usefulness in onychophoran taxonomy (Oliveira et al. 2012; Barquero González et al. 2020).

The arrangement of antennal sensilla in *O. tiputini* sp. nov. does not differ from that in other species of Neotropical peripatids. The spindle-shaped papilla presents two scale ranks, as seen in other known peripatid species (Oliveira et al. 2012). The shape of the gonopore opening resembles that of other Andean species, such as *O. quitensis* and *O. eisenii* (Bouvier 1905; Contreras-Félix et al. 2018), and does not vary between sexes, as is the case in *Eoperipatus* and *Principapillatus* (Oliveira et al. 2012, 2013).

There are some morphological similarities between *Oroperipatus tiputini* sp. nov. and *Mongeperipatus* in characters otherwise considered restricted to *Mongeperipatus*, including the absence of hyaline organs, the presence of four scale ranks in the apical piece (although it varies from four to seven in *Mongeperipatus*), and the alternation between the largest and mid-sized primary papillae in the dorsal plicae. Also, *Oroperipatus tiputini* sp. nov. shares with *Mongeperipatus keköldi* the absence of antennal chemoreceptors and the presence of accessory papillae with lateral apical rudimentary pieces. Currently, it is unknown whether these characteristics are present in other species of *Oroperipatus*, due to the poor SEM exploration of Andean peripatids. These morphological similarities are likely the result of convergence, as phylogenetic analyses have placed *Mongeperipatus* in the Caribbean peripatid clade (Barquero González et al. 2020).

Acknowledgments

We express our gratitude to Emilia Peñaherrera-Romero for her constant support and companionship at the Tiputini Biodiversity Station and the Laboratory of Terrestrial Zoology of Universidad San Francisco de Quito; to all the students of the course of Tropical Ecology that accompanied us to the Tiputini Biodiversity Station; to all the management, administrative and field staff of the Tiputini Biodiversity Station for their support during fieldwork along the years, especially David Romo, Consuelo Barriga, Gonzalo Rivas, Catalina Ulloa, Jaime Guerra, Tomi Sugahara, Zoila Rivera, Carla Larrea, Mayer Rodríguez, Ramiro Sanmiguel, and José Macanilla; to David Torres and Melannie Nuñez for their help in the translation and interpretation of articles written in French and German; to Kelly Swing for providing photographs of living specimens and sharing natural history information; to Krutskaya Yépez for her support during scanning electron microscopy; to Giovanni Ramón and Margarita Lopez, curators of the invertebrate collection at the Museo de Zoología, Universidad San Francisco de Quito, for their constant support; to two anonymous reviewers for their valuable comments on the manuscript; and to Biodiversity Heritage Library BHL, Internet Archive, Google Books, the library system of Universidad San Francisco de Quito, and Sci-Hub for making important literature available. We acknowledge the role of Sci-Hub in providing free access to important literature that otherwise would be behind paywalls, recognising both its contribution to facilitating research and the complex ongoing debates regarding scholarly publishing practices and access (Greshake 2017; Himmelstein et al. 2018). The work by Jorge L. Montalvo-Salazar was supported by Diego Montalvo, Wilma Salazar, María Paz Rueda, Giovani Ramón, and Galilea Pérez. The work by Diego F. Cisneros-Heredia was supported by María Elena Heredia, Laura Heredia, Jonathan Guillemot, David Romo, and Consuelo Barriga. Universidad San Francisco de Quito USFQ supported this work through research grants awarded to Diego F. Cisneros-Heredia by the office of the Dean of Research, the College of Biological and Environmental Sciences, and the Tiputini Biodiversity Station; and through research, outreach, and operative funds assigned to the Institute of Tropical Biodiversity (IBIOTROP).

References

Barquero González JP, Sánchez-Vargas S, Morera-Brenes B (2020) A new giant velvet worm from Costa Rica suggests absence of the genus *Peripatus* (Onychophora, Peripatidae) in Central America. Revista de Biología Tropical 68. https://doi.org/10.15517/rbt.v68i1.37675

Bass MS, Finer M, Jenkins CN, Kreft H, Cisneros-Heredia DF, McCracken SF, Pitman NCA, English PH, Swing K, Villa G, Fiore AD, Voigt CC, Kunz TH (2010) Global Conservation Significance of Ecuador's Yasuní National Park. PLoS One 5: e8767. https://doi.org/10.1371/journal.pone.0008767

Blake JG, Mosquera D, Loiselle BA, Swing K, Guerra J, Romo D (2012) Temporal activity patterns of terrestrial mammals in lowland rainforest of eastern Ecuador. Ecotropica (Bonn) 18: 137–146.

du Bois-Reymond Marcus E (1952) On South American Malacopoda. Boletins da Faculdade de Philosophia, Sciencias e Letras, Universidade de São Paulo. Zoologia 17: 189–209. https://doi.org/10.11606/issn.2526-4877.bsffclzoologia.1952.125190

Boot CL (1990) Evolutionary significance of ontogenetic colour change in animals. Biological Journal of the Linnean Society. Linnean Society of London 40(2): 125–163. https://doi.org/10.1111/j.1095-8312.1990.tb01973.x

Bouvier EL (1899) Nouvelles observations sur les Péripates américains. Comptes Rendus Hebdomadaires des Séances de l'Académie des Sciences 129: 1029–1031. https://doi.org/10.5962/bhl.part.26693

Bouvier EL (1902) Le Peripatus ecuadoriensis. Bulletin de la Société Philomathique de Paris 4: 53–62. https://doi.org/10.5962/bhl.part.19238

Bouvier EL (1904) *Peripatus belli* (espéce nouvelle de l'Equateur). Bulletin du Muséum National d'Histoire Naturelle 10: 56–57.

Bouvier EL (1905) Monographie des Onychophores. Annales des Sciences Naturelles. Zoologie 2: 1–383.

Brues CT (1925) Notes on Neotropical Onycophora. Psyche (Cambridge, Massachusetts) 32: 159–165. https://doi.org/10.1155/1925/79079

Camerano L (1897) Sul *Peripatus quitensis* Schmarda. Atti della Reale Accademia della Scienze di Torino 32: 395–398.

Camerano L (1898) Viaggio del Dr. Enrico Festa nella Repubblica dell'Ecuador e regioni vicine. VII. Onicofori. Bollettino dei Musei di Zoologia ed Anatomia comparata della R. Università di Torino 13: 1–3. https://doi.org/10.5962/bhl.part.16811

Chagas-Júnior A, Costa CS (2014) *Macroperipatus ohausi*: Redescription and taxonomic notes on its status (Onychophora, Peripatidae). Revista de Biología Tropical 62: 977–985. https://doi.org/10.15517/rbt.v62i3.11643

Cisneros-Heredia DF (2003) Herpetofauna de la Estación de Biodiversidad Tiputini, Amazonía Ecuatoriana. In: Memorias del I Congreso de Ecología y Ambiente, Ecuador país megadiverso. Universidad San Francisco de Quito USFQ, Quito, 21.

Cisneros-Heredia DF (2006) Turtles of the Tiputini Biodiversity Station with remarks on the diversity and distribution of the Testudines from Ecuador. Biota Neotropica 6. https://doi.org/10.1590/S1676-06032006000100011

Clark AH (1913) A revision of the American species of *Peripatus*. Proceedings of the Biological Society of Washington 16: 15–20.

Clark AH (1914a) Notes on Some Specimens of a Species of Onychophore (*Oroperipatus corradoi*) New to the Fauna of Panama. Smithsonian Miscellaneous Collections 63: 1–2.

Clark AH (1914b) On some onychophores (*Peripatus*) from the Republic of. Panama. Zoologischer Anzeiger 45: 145–146.

Clark AH, Zetek J (1946) The onychophores of Panama and the Canal Zone. Proceedings of the United States National Museum 96: 205–213. https://doi.org/10.5479/si.00963801.96-3197.205

Cockerell TDA (1908) Monographie des Onychophores. By E. L. Bouvier. Extracted from Annales de Sciences Naturelles, Zoologie (1907), pp. 383 + 318, Pls. XIII. Science 27: 619–621. https://doi.org/10.1126/science.27.694.619

Contreras-Félix GA, Montiel-Parra G, Cupul-Magaña FG, Pérez TM (2018) Redescription of the velvet worm Oroperipatus eisenii (Onychophora, Peripatidae), through DNA sequencing, scanning electron microscopy and new collection records from Western Mexico. Revista Mexicana de Biodiversidad 89. https://doi.org/10.22201/ib.20078706e.2018.4.2586

Correoso Rodríguez M (2011) Nueva localidad de *Oroperipatus quitensis* (Peripatidae-Onychophora) en el Ecuador, consideraciones biogeográficas. Revista Geoespacial 8: 23–33.

Costa CS, Giribet G (2021) Panamanian velvet worms in the genus *Epiperipatus*, with notes on their taxonomy and distribution and the description of a new species (Onychophora, Peripatidae). Invertebrate Biology 12. https://doi.org/10.1111/ivb.12336

Costa CS, Chagas-Junior A, Pinto-da-Rocha R (2018) Redescription of *Epiperipatus edwardsii*, and descriptions of five new species of Epiperipatus from Brazil (Onychophora, Peripatidae). Zoologia 35: e23366. https://doi.org/10.3897/zoologia.35.e23366

Costa CS, Giribet G, Pinto-Da-Rocha R (2021) Morphological and molecular phylogeny of *Epiperipatus* (Onychophora: Peripatidae): a combined approach. Zoological Journal of the Linnean Society 192(3): 763–793. https://doi.org/10.1093/zoolinnean/zlaa100

Fuhrmann O (1915) Über eine neue Peripatus-Art vom Oberlauf des Amazonas. Abhandlungen der Senckenbergischen Naturforschenden Gesellschaft 36: 275–283.

Greshake B (2017) Looking into Pandora's Box: The Content of Sci-Hub and its Usage. F1000 Research 6: 541. https://doi.org/10.12688/f1000research.11366.1

Giribet G, Buckman-Young RS, Costa CS, Baker CM, Benavides LR, Branstetter MG, Daniels SR, Pinto-da-Rocha R (2018) The 'Peripatos' in Eurogondwana? – Lack of evidence that southeast Asian onychophorans walked through Europe. Invertebrate Systematics 32: 842. https://doi.org/10.1071/IS18007

Himmelstein DS, Romero AR, Levernier JG, Munro TA, McLaughlin SR, Greshake B, Greene CS (2018) Sci-Hub provides access to nearly all scholarly literature. eLife 7: e32822. https://doi.org/10.7554/eLife.32822

Icochea J, Ramírez Ri (1996) Nota sobre los Onychophora del Perú. Revista Peruana de Entomología 39: 17–18.

ICZN (1999) International Code of Zoological Nomenclature. 4th edition. International Trust for Zoological Nomenclature, London. https://www.iczn.org/the-code/the-code-online/

Mayer G, Franke FA, Treffkorn S, Gross V, de Sena Oliveira I (2015) Onychophora. In: Wanninger A (Ed.) Evolutionary Developmental Biology of Invertebrates 3: Ecdysozoa I: Non-Tetraconata. Springer, Vienna, 53–98. https://doi.org/10.1007/978-3-7091-1865-8_4

Monge-Nájera J (1994) Reproductive trends, habitat type and body characteristics in velvet worms (Onychophora). Revista de Biología Tropical 42: 611–622.

Monge-Nájera J (1995) Phylogeny, biogeography and reproductive trends in the Onychophora. Zoological Journal of the Linnean Society 114: 21–60. https://doi.org/10.1006/zjls.1995.0015

Morera-Brenes B, Nájera JM (2010) A new giant species of placented worm and the mechanism by which onychophorans weave their nets (Onychophora, Peripatidae). Revista de Biología Tropical 58: 1127–1142. https://doi.org/10.15517/rbt.v58i4.5398

Oliveira IDS (2023) An updated world checklist of velvet worms (Onychophora) with notes on nomenclature and status of names. ZooKeys 1184: 133–260. https://doi.org/10.3897/zookeys.1184.107286

Oliveira IDS, Wieloch AH, Mayer G (2010) Revised taxonomy and redescription of two species of the Peripatidae (Onychophora) from Brazil: A step towards consistent terminology of morphological characters. Zootaxa 2493: 16–34. https://doi.org/10.11646/zootaxa.2493.1.2

Oliveira I de S, Schaffer S, Kvartalnov PV, Galoyan EA, Palko IV, Weck-Heimann A, Geissler P, Ruhberg H, Mayer G (2013) A new species of *Eoperipatus* (Onychophora) from Vietnam reveals novel morphological characters for the South-East Asian Peripatidae. Zoologischer Anzeiger 252: 495–510. https://doi.org/10.1016/j.jcz.2013.01.001

Oliveira IDS, Franke FA, Hering L, Schaffer S, Rowell DM, Weck-Heimann A, Monge-Nájera J, Morera-Brenes B, Mayer G (2012) Unexplored Character Diversity in Onychophora (Velvet Worms): A Comparative Study of Three Peripatid Species. PLoS ONE 7: e51220. https://doi.org/10.1371/journal.pone.0051220

Paynter RA (1993) Ornithological gazetteer of Ecuador. 2nd ed. Museum of Comparative Zoology, Harvard University, Cambridge, Mass., 268 pp. https://doi.org/10.5962/bhl.title.14626

Pripnow B, Ruhberg H (2003) Peripatopsidae (Onychophora) from New Zealand – observations on selected morphs of the '*Peripatoides novaezealandiae*-complex' in culture: Morphological and reproductive aspects. African Invertebrates 44: 103–114. https://hdl.handle.net/10520/EJC84511

Read VMSTJ (1988) The application of scanning electron microscopy to the systematics of the neotropical Peripatidae (Onychophora). Zoological Journal of the Linnean Society 93: 187–223. https://doi.org/10.1111/j.1096-3642.1988.tb01361.x

Reyes-Puig C, Wake DB, Kotharambath R, Streicher JW, Koch C, Cisneros-Heredia DF, Yánez-Muñoz MH, Ron S (2020) Two extremely rare new species of fossorial salamanders of the genus *Oedipina* (Plethodontidae) from northwestern Ecuador. PeerJ 8: e9934. https://doi.org/10.7717/peerj.9934

Ribera C (1977) Sobre *Peripatus corradoi* L. Camerano 1898. Miscel·lània. Zoològica 4: 57–59.

Romo D, Mosquera D, Swing K, di Fiore A, Blake JG, Loiselle BA, Ryder TB, de la Torre S, Erwin TL, Pitman NCA, Cisneros-Heredia D, Voigt CC, Burnham RJ, Alvarez H, Vinueza G, Abondano L, Alvarez S, Bruna EM, Durães R, Ellis K, Fernández E, Ghanem SJ, Guerra J, Hidalgo J, Jenkins CN, Link A, Maehr E, Paniagua F, Porter A, Rodríguez M, Schmidtt C, Seales L, Snowdon C, Stocks G, Tori WP, Widmer J, Yépez P, Zamorano L (2017) Los secretos del Yasuní: Avances en investigación en la Estación de Biodiversidad Tiputini, Universidad San Francisco de Quito USFQ. USFQ PRESS, Quito, 356 pp.

Ruhberg H, Daniels SR (2013) Morphological assessment supports the recognition of four novel species in the widely distributed velvet worm *Peripatopsis moseleyi* sensu lato (Onychophora, Peripatopsidae). Invertebrate Systematics 27(2): 131–145. https://doi.org/10.1071/IS12069

Ryder TB, Sillett TS (2016) Climate, demography and lek stability in an Amazonian bird. Proceedings. Biological Sciences 283: 20152314. https://doi.org/10.1098/rspb.2015.2314

Sampaio-Costa C, Chagas-Junior A, Baptista RLC (2009) Brazilian species of Onychophora with notes on their taxonomy and distribution. Zoologia 26: 553–561. https://doi.org/10.1590/S1984-46702009005000004

Schmarda LK (1871) 2 Zoologie. Volume 1. Wilhelm Braumüller K. K. Hof- und Universitätsbuchhändler, Vienna, 372 pp.

Zoosyst. Evol. 100 (3) 2024, 791–802 | DOI 10.3897/zse.100.125246

PENSOFT

MUSEUM FÜR NATURKUNDE BERLIN

Population genetic structure and demographic history of the East Asian wolf spider *Pardosa astrigera*

Dan Fu[1], Lijuan Liu[1], Ying Cheng[1], Haodong Chen[1], Yufa Luo[1]

1 *Key Laboratory of Wetland Biodiversity of the Jianhu Basin of Shaoxing, School of Life and Environmental Sciences, Shaoxing University, Shaoxing 312000, China*

https://zoobank.org/2DC3026A-5A4B-411A-851F-4107F7AF9B87

Corresponding author: Yufa Luo (lyf223@126.com)

Academic editor: Danilo Harms ♦ **Received** 12 April 2024 ♦ **Accepted** 27 May 2024 ♦ **Published** 14 June 2024

Abstract

The wolf spider *Pardosa astrigera* L. Koch, 1878, an important biological control agent for pests in agriculture, is widely distributed in various ecosystems across East Asia. This study used mitochondrial DNA and aimed to provide an in-depth understanding of population genetic structure and evolutionary history throughout the species. Mitochondrial gene sequences from 107 samples of *P. astrigera* from 25 East Asian populations were used for genetic analyses. Our data revealed an asymmetric phylogeographic distribution in two sympatric lineages (1–2) of *P. astrigera* in continental East Asia. The spatio-temporal pattern of two mitotypes of *P. astrigera* in this region gives strong support for a Northeast Asian origin during the late Pleistocene (~1.69 million years ago) and the population expansion time of ~74,340 (58,832–104,236) years ago (during the last glacial period) and dual colonization around East Asia from two directions: from North to South and from East to West. Our phylogeographic results suggested that Pleistocene climate oscillations with subsequent fragmentation events and secondary contacts were the major impact factors of the diversification, geographic distribution, and expansion patterns of *P. astrigera*, and human activities and ballooning probably accelerated its recent dispersal.

Key Words

Last glacial period, late Pleistocene diversification, Lycosidae, mtDNA, phylogeography

Introduction

Pardosa astrigera (Araneae: Lycosidae), a wandering spider, inhabits a relatively arid-cold environment. It is a common species in various ecosystems of the temperate and subtropical regions of East Asia and possesses strong environmental adaptability, high dispersal potentiality, and rapid population diversification (Lida et al. 2016; Li et al. 2020). This spider can prey on a variety of pests in agriculture and forestry and has strong hunger tolerance and high fertility, as well as long-term population stability and substantially large populations (Li et al. 2020). Therefore, *P. astrigera* plays a vital role in pest control. It is widespread in East Asian regions such as China, Korea, Japan, and Russia (Far East) (Song et al. 1999; World Spider Catalog 2024). This wolf spider is a dominant species in various ecosystems across Korea (Kim and Yoo 1997) and most parts of China, except Fujiang, Guangdong, and Hainan provinces (Song et al. 1999). Previous morphological studies suggested that *P. astrigera* was likely a species complex (Schenkel 1963). Recent investigations have considered the morphological variations among the different geographical populations to be intraspecific (Yin et al. 1997; Chang et al. 2007). Studies on the population genetic structure of *P. astrigera* can estimate genetic diversity and gene flow among its different populations and infer the ancestral populations and the phylogeographic pattern. Such information is essential for effectively protecting and utilizing the natural predators of pests in agriculture and forestry.

The phylogeography of *P. astrigera* distributed in local regions of China was investigated using nuclear ITS2 gene sequences, and two major lineages were observed (Chang et al. 2007). However, for the ancient spider

species with an extensive geographic range, the information concerning genetic structure, spatio-temporal evolution patterns, and demographic history across the whole distribution range in East Asia was still unclear, and the following questions concerning this widespread species have not been investigated: 1) genetic relationships among the East Asian populations based on mitochondrial genes; 2) allopatric divergence among the East Asian regions; and 3) origin and dispersal across East Asia. These questions will provide a better understanding of the *P. astrigera* population history in East Asia.

Because of the haploid maternal inheritance of mitochondrial genes and their high mutation rate and abundance in cells, they are widely used as molecular markers to analyze the population genetic structure and phylogeography of broadly distributed animal species (Avise 2000). To assess the mtDNA population genetic structure and potential dispersal routes of *P. astrigera*, we studied its genetic structure and phylogeography using mitochondrial *COI*, 16S, and *NADH1* genes. We recently collected individuals of the spider from China and augmented our sampling with sequences from GenBank covering nearly the entire geographic range of *P. astrigera*. The current data set covers 25 distinct localities (21 from China, three from South Korea, and one from Japan) around East Asia. It thus offers a more holistic insight into *P. astrigera* matriline history than have prior studies.

Materials and methods

Sampling, sequencing, and sequence analyses

We collected 19 samples of *P. astrigera* from 6 provinces of China (Suppl. material 1: table S1) and sequenced 3 mitochondrial genes (*COI*, 16S, and *NADH1*) using three primer pairs (Suppl. material 1: table S2) according to the procedures of Luo and Li (2022). Additional sequences of the species from Korea, Japan and 14 provinces of China were taken from Chang et al. (2007), Li et al. (2011), and GenBank (Suppl. material 1: table S1). The mtDNA sequences of 107 colonists from 25 geographic sites in East Asia were used for genetic analyses (Fig. 1a; Suppl. material 1: table S1). BioEdit was used to check the quality of the DNA sequences (Hall 1999). Sequence alignments were done with MAFFT v7 (Katoh and Standley 2013). Unique haplotypes were identified using DnaSP v5 (Librado and Rozas 2009). The data matrix is available from the authors and will be submitted to the Dryad database (online at http://datadryad.org/).

Phylogeny and haplotype network reconstruction

A matrix combining the sequences of the *COI*, 16S, and *NADH1* markers was constructed and used to obtain the phylogenetic relationships of 107 *P. astrigera* individuals using the Bayesian inference (BI) and maximum likelihood (ML) approaches. *Pardosa laura* was used as an outgroup. Bayesian analysis was performed in MrBayes V3.2.1 (Ronquist and Huelsenbeck 2003). We used jModelTest to select the best-fit evolutionary model for each codon base or gene partition (Posada 2008) with the Bayesian information criterion (Suppl. material 1: table S3). The Markov chain Monte Carlo (MCMC) simulation was run for 15 million generations and sampled every 1,000 generations, and unlinked parameters among partitions were used in the chain runs. Tracer v1.5 was employed to check effective sample size (ESS) values (>200) for each parameter (Rambaut and Drummond 2009), and a 50% majority rule consensus tree was computed after discarding the first 25% of sampled trees as burn-in. The ML tree was reconstructed using IQ-Tree v1.6.12 (Nguyen et al. 2015) as implemented in the W-IQ-Tree web server (Trifinopoulos et al. 2016). The substitution model for each codon base or gene partition was automatically selected, and an ultrafast bootstrap with 1,000 iterations was conducted to estimate nodal support across the topology (Minh et al. 2013; Kalyaanamoorthy et al. 2017; Hoang et al. 2018). To compare genetic connections between geographic populations, three haplotype networks were inferred in PopART (Leigh and Bryant 2015) using unrooted minimum-spanning trees (Bandelt et al. 1999) based on the separate mtDNA gene sequences. Based on climate, geographical divisions, distributional data for the *P. astrigera* species from the literature (Song et al. 1999; World Spider Catalog 2024), and information from our samples. We delimited 6 areas, including Northwest China (Qinghai+Gansu, China); Northeast Asia (Neimenggu+Heilongjiang, China+Korea+Japan); East China (Jiangsu+Shandong+Zhejiang, China); Southwest China (Yunnan+Guizhou, China); Central China (Hubei+Hunan+Anhui, China); and North China (Hebei+Henan+Shanxi+Sanxi, China).

Genetic diversity and distance calculation

We defined six populations from the sampled regions for the haplotype network reconstruction above. Population genetic diversity was inferred from the *COI*, 16S, and *NADH1* sequences. Estimations of genetic diversity (number of haplotypes, nh; nucleotide diversity, π; haplotype diversity, h) from each population were performed in DnaSP 5.10.01 (Librado and Rozas 2009). Genetic distances among haplotypes and overall mean distances of *P. astrigera* populations were estimated using MEGA v5 (Tamura et al. 2011).

Estimations of divergence time and mtDNA substitution rate

Divergence times and mtDNA substitution rates were inferred based on the combined *COI*, 16S, and *NADH1* sequences. They were implemented in BEAST v1.6.1 (Drummond and Rambaut 2007).

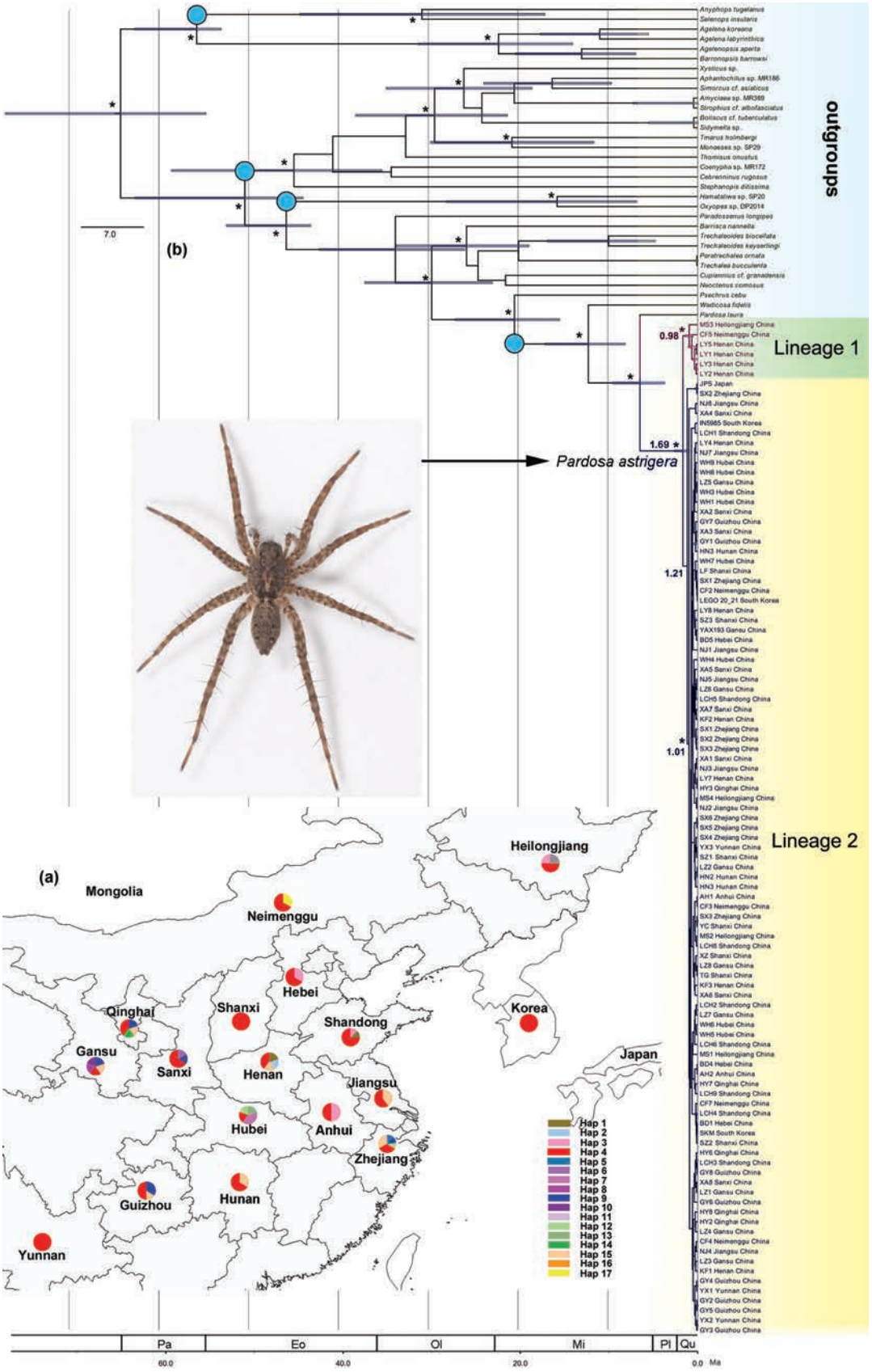

Figure 1. a. Sampling regions of the East Asian wolf spider *Pardosa astrigera* and the haplotype distribution of the *16S* gene. Detailed sampling information is presented in Suppl. material 1: table S1 in the Supplemental materials; **b.** Time-tree of the species *Pardosa astrigera* based on the combined mitochondrial *COI*, *16S*, and *NADH1* sequences. Blue dots mark the four fossil calibration nodes. Numbers at nodes indicate the main divergence times of the haplotypes of the species. "*" indicates stable branches with Bayesian support >0.90.

First, a test was run to determine if a molecular clock model was appropriate based on the harmonic mean (HM) of the likelihood values of the MCMC samples (Newton and Raftery 1994) and a more accurate stepping-stone (SS) sampling method (Xie et al. 2011) in MrBayes v3.2.1. We found that the total data sets did not conform to a strict molecular clock ($P<0.001$) and that a relaxed molecular clock method was more suitable for estimating divergence time. Therefore, we estimated divergence times using the uncorrelated lognormal relaxed molecular clock model. The tree prior was set to the birth-death and Yule speciation process models. We repeated the analysis with birth-death and Yule prior to assess the sensitivity of our results to tree-prior specification. According to the marginal likelihood estimated using stepping-stone sampling, the birth-death model outperformed the Yule model. Hence, subsequent analyses focused on the chronogram resulting from the birth-death prior. jModelTest (Posada 2008) was used to select the best-fitting substitution model for each gene or codon base partition under the Bayesian information criterion (Suppl. material 1: table S4). To obtain reliable results, we ran five independent MCMC tree searches for 300 million generations and sampled every 1,000 generations. The convergence of MCMC chains was assessed in TRACER v1.5 (Rambaut and Drummond 2009). TreeAnnotator v1.6.1 (in the BEAST package) was used to produce a maximum clade credibility (MCC) tree with median heights after discarding 25% of the trees as burn-in. We dated the tree of all sampled *P. astrigera* haplotypes from East Asia. For the molecular clock analysis, we used the minimum ages based on fossils of Lycosidae (15 million years ago, Ma; Iturralde-Vinent and MacPhee 1996), Oxyopidae (43 Ma; Wunderlich 2004a; Magalhaes et al. 2020), Thomisidae (43 Ma; Wunderlich 2004b; Magalhaes et al. 2020), and Selenopidae (53 Ma; Penney 2006; Magalhaes et al. 2020) as calibration points (Suppl. material 1: table S4; Renner 2005; Donoghue and Benton 2007). The outgroups include the Agelenidae, Thomisidae, Oxyopidae, Psechridae, Trechaleidae, Selenopidae, and some Lycosidae species (Suppl. material 1: table S4). Their gene sequences were available from GenBank (Suppl. material 1: table S1).

Demographic analysis

To test for range expansions, Fu's FS, Tajima's D, and the mismatch distribution were calculated (Tajima 1989; Fu 1997; Jaeger et al. 2005; Smith and Farrell 2005) in Arlequin v3.5 (Excoffier and Lischer 2010), with 10,000 permutations to test for significance. A significant, large negative value for Fu's FS, a significant value for Tajima's D, or an unimodal shape of the mismatch distribution indicates population expansion (Slatkin and Hudson 1991; Rogers and Harpending 1992; Aris-Brosou and Excoffier 1996; Tajima 1996; Fu 1997).

We used a mean substitution rate (V) to infer the expansion time of *P. astrigera*. The value of V was estimated from the above mitochondrial molecular clock analysis. The generation time in East Asia for *P. astrigera* is 6 months (Chen et al. 2010; Yang et al. 2018). Therefore, the substitution rate per generation was given as $v = 0.5V$. Once v was estimated, the coalescence time in generations (t) was obtained by the relationship $t = \tau/(2 \times 2\,mv)$ (Rogers and Harpending 1992; Harpending et al. 1993; Rogers 1995), where m was the concatenated *COI*, 16S, and *NADH1* sequence length, and the value of τ was calculated using Arlequin v3.5.

Bayesian skyline plots (BSPs) reconstruct historical population sizes from mtDNA genealogies (Drummond and Rambaut 2007). BSPs were implemented in BEAST v1.6.1. The substitution rate (2.58%) of the combined mitochondrial gene sequences was estimated from the mitochondrial molecular clock analysis. The substitution models were selected using jModelTest (Suppl. material 1: table S4). For Bayesian skyline coalescent tree priors, we chose the piecewise-linear skyline model. Otherwise, default parameters were used. The chain was run for 10 million steps under an uncorrelated lognormal relaxed clock model and sampled every 1,000 steps. The result of the Bayesian skyline plot was checked and analyzed using Tracer v1.5 with a burn-in of 10%.

The expansion history of *P. astrigera* was increasingly estimated using Bayesian binary MCMC analyses (BBM, a method considered the most general and complex model in biogeographical reconstruction; Sanmartín et al. 2001). BBM was implemented in RASP v3.0 (Yu et al. 2014) using a maximum of two areas per node. The 10,000 trees obtained from the BEAST analysis were input into RASP. The 1,000 random trees were used for the biogeographical reconstruction (BBM). The MCC tree produced in the BEAST analysis was used as the input tree. Based on the dated chronogram for *P. astrigera*, we pruned the tree to remove outgroups. We divided the range into the same six biogeographical areas as above.

Results

Sequences

The 96, 81, and 76 sequences were obtained for the *COI*, 16S, and *NADH1* genes from all samples of *P. astrigera*, respectively. The aligned data of the sequences from *P. astrigera* had lengths of 932 base pairs (bp) for *COI*, 574 bp for 16S, and 584 bp for *NADH1*. In total, 62, 17, and 38 haplotypes were found for the *COI*, 16S, and *NADH1* gene sequences, respectively. Among the 62 unique *COI* haplotypes, Hap20 dominated in 8.3% of the samples, Hap39 in 6.3%, and each of Hap3, Hap15, and Hap52 in 4.2%; among the 17 unique *16S* haplotypes, Hap4 dominated in 55.6% of the samples, Hap15 in 14.8%, and Hap9 in 7.4%; and among the 38 unique *NADH1* haplotypes, Hap13 dominated in 36.8% of the samples, Hap22 in 6.6%, and Hap1 in 5.3%. The concatenated mitochondrial genes comprised 2,090 bp. All sequences are deposited in GenBank (for accession numbers, see Suppl. material 1: table S1).

Molecular phylogeny

In the dated phylogenetic tree, *P. astrigera* is composed of the two lineages (1–2; Fig. 1b). Lineage 1 consists of the sample (CF5) from Neimonggu, China, the four samples (LY1–3 and LY5) from Henan, China, and the sample (MS3) from Heilongjiang province of China, and the lineage spiders occur on a clade of the ML tree (Suppl. material 1: fig. S1b); and Lineage 2 consists of all other individuals of *P. astrigera* across continental East Asia, and the lineage samples cluster together in a clade of the BI tree (Suppl. material 1: fig. S1a). The BI and ML trees (Suppl. material 1: fig. S1) indicated five sister groups (2a–e). The samples in Group 2a are from Neimenggu, Shanxi, and Zhejiang provinces of China and South Korea; Group 2b from Heilongjiang and Zhejiang provinces of China and Japan; Group 2c from Shandong, Gansu, and Hubei provinces of China; Group 2d from Sanxi and Zhejiang provinces of China; and Group 2e from Neimenggu, Hebei, Shandong, and Shanxi provinces of China and South Korea. However, the relevance of these groups is not clear in the molecular phylogeny.

Haplotype network

The haplotype network analyses based on both 16S and *NADH1* genes revealed clear genetic structuring among the East Asian populations of *P. astrigera* (Fig. 2a, b); in contrast, those based on the *COI* gene showed a complex and intricate haplotype connection pattern (Fig. 2c). In 16S and *NADH1* networks, all studied individuals clustered into two lineages (1–2; Fig. 2a, b). Lineage 1 comprises three haplotypes from Neimenggu and Henan regions in China; Lineage 2 is composed of the 35 and 14 haplotypes from all analyzed regions, with one (Hap13) and two (Hap4 and Hap15) universal haplotypes occurring at the center of a star-like cluster of rare haplotypes in the *NADH1* and 16S networks, respectively (Fig. 2a, b). The *COI* network structure consists of 62 haplotypes with Hap20 at the center, indicating that the wolf spider has complex population genetic relationships and a high gene flow among populations (Fig. 2c).

Genetic diversity

Northeast Asia and North China populations exhibited higher genetic diversity than the other four regional populations based on *COI* and *NADH1* genes (Table 1). The genetic diversity of the East China population was higher than that of the Central China population based on the two protein-coding genes (Table 1). Among all analyzed populations, the population of Southwest China had the lowest genetic diversity based on *COI* and 16S genes, whereas Northwest China had the lowest genetic diversity based on the *NADH1* gene (Table 1).

Haplotype divergence times and population expansion time

Based on fossil calibrations (Suppl. material 1: table S5), the estimated initial haplotype divergence of *P. astrigera* started at ~1.69 Ma (95% credibility interval, CI: 0.95–2.66 Ma; Fig. 1b). Diversification of the five haplotypes (Lineage 1) from Heilongjiang, Neimenggu, and Henan provinces of China occurred ~0.98 Ma (95% CI: 0.50–1.44 Ma; Fig. 1b). The two haplotypes from Jiangsu and Zhejiang provinces of China diverged from the other haplotypes of Lineage 2 at ~1.21 Ma (95% CI: 0.62–1.95 Ma; Fig. 1b). The mean substitution rate (*V*) of the concatenated mtDNA sequences for the species was estimated to be 0.0129 (95% CI: 0.0092–0.0163) per million years, equivalent to a divergence rate of 2.58% (1.84%–3.26%) per million years. The τ value was inferred from the mitochondrial allele frequencies and linkage disequilibrium to be 2.244. Using the values of *V* and τ, the estimated generation time since expansion for the *P. astrigera* populations in East Asia was approximately 74,340 (58,832–104,236) years ago.

Table 1. Summary of genetic diversity in *P. astrigera* from East Asia based on mtDNA sequences. The number of haplotypes (nh), nucleotide diversity (π), haplotype diversity (h), Fu's FS, and Tajima's D are shown. Northeast Asia (Neimenggu+Heilongjiang, China+Korea+Japan); Northwest China (Qinghai+Gansu, China); North China (Hebei+Henan+Shanxi+Sanxi, China); Central China (Hubei+Hunan+Anhui, China); East China (Jiangsu+Shandong+Zhejiang, China); and Southwest China (Yunnan+Guizhou, China).

Population	COI						16S						NADH1					
	ni	nh	π	h	Fu's FS	Tajima's D	ni	nh	π	h	Fu's FS	Tajima's D	ni	nh	π	h	Fu's FS	Tajima's D
Northeast Asia	10	9	0.014 ± 0.003	0.978 ± 0.054	-3.323	-0.90274**	9	4	0.004 ± 0.001	0.694 ± 0.147	-0.722	-0.84257**	9	8	0.010 ± 0.002	0.972 ± 0.064	-4.093	-0.95811**
Northwest China	11	10	0.007 ± 0.002	0.982 ± 0.046	-6.904	-1.69129**	10	6	0.005 ± 0.001	0.889 ± 0.075	-2.781	-0.78138**	10	6	0.005 ± 0.001	0.778 ± 0.137	-2.521	-1.57285**
North China	27	23	0.010 ± 0.001	0.986 ± 0.015	-21.022	-1.39856**	19	7	0.003 ± 0.001	0.544 ± 0.136	-4.179	-1.20300**	19	11	0.009 ± 0.002	0.895 ± 0.057	-3.876	-1.45647**
Central China	13	10	0.009 ± 0.002	0.923 ± 0.069	-4.517	-1.20786**	10	6	0.004 ± 0.001	0.844 ± 0.103	-3.412	-1.38818**	9	6	0.005 ± 0.002	0.833 ± 0.127	-2.495	-1.79752*
East China	23	21	0.011 ± 0.001	0.992 ± 0.015	-18.844	-1.51301**	22	7	0.003 ± 0.001	0.671 ± 0.094	-3.870	-1.46068**	18	11	0.005 ± 0.001	0.856 ± 0.079	-7.230	-2.05890*
Southwest China	12	7	0.006 ± 0.002	0.879 ± 0.075	-1.828	-1.25306**	11	3	0.002 ± 0.001	0.473 ± 0.162	-0.659	-0.77815**	10	7	0.006 ± 0.002	0.867 ± 0.107	-3.347	-1.68719**
Total (East Asia)	96	58	0.010 ± 0.001	0.979 ± 0.006	-72.764	-1.58133**	81	17	0.003 ± 0.000	0.668 ± 0.054	-15.586	-1.85939*	76	38	0.007 ± 0.001	0.860 ± 0.039	-45.933	-2.39099*

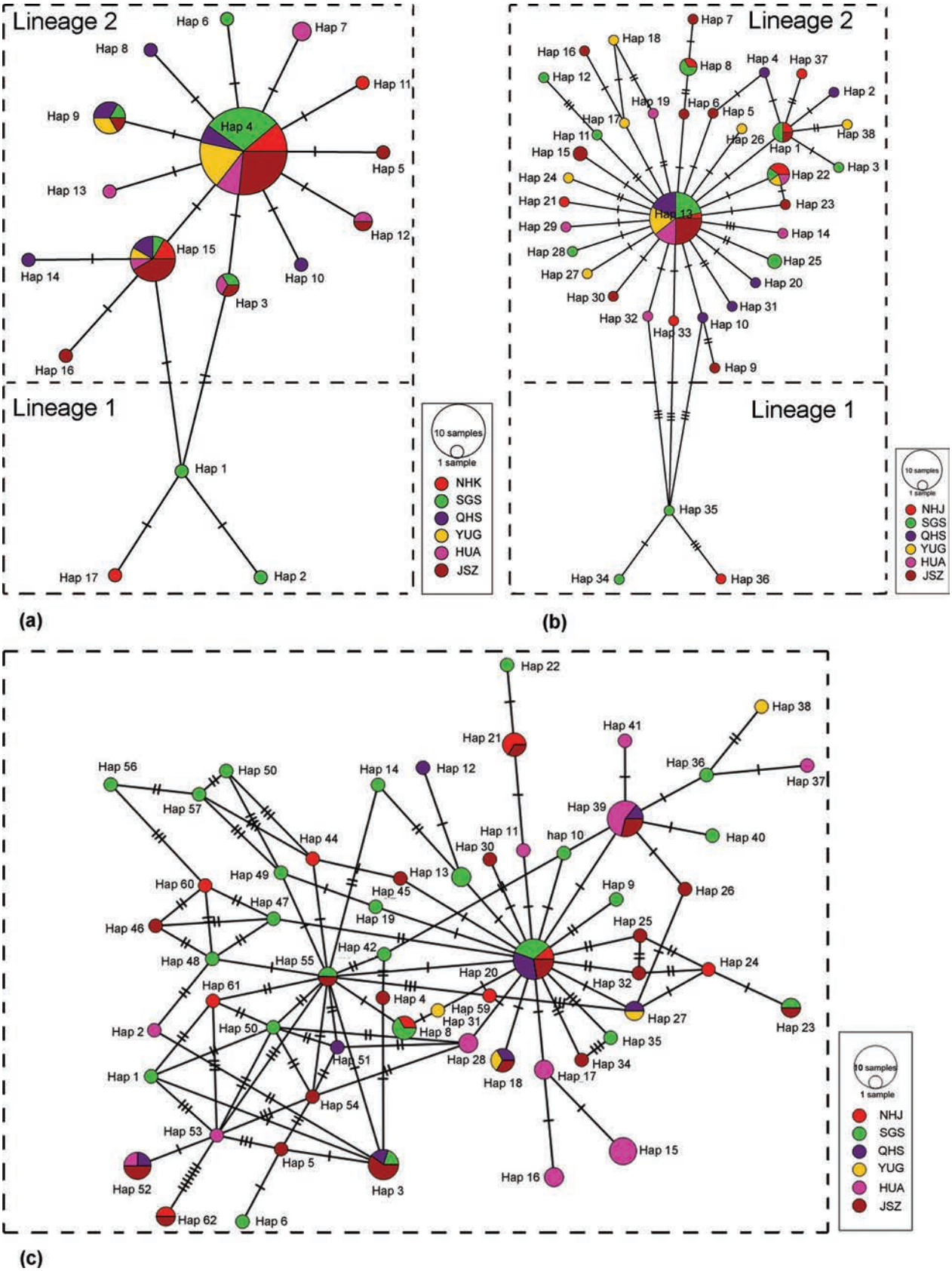

Figure 2. a. *16S* haplotype network of the *Pardosa astrigera* spiders; **b.** Network from *NADH1*; **c.** Network from *COI*: NHJ, Northeast Asia (Neimenggu+Heilongjiang, China+Korea+Japan); SGS, North China (Hebei+Henan+Shanxi+Sanxi, China); QHS, Northwest China (Qinghai+Gansu, China); YUG, Southwest China (Yunnan+Guizhou, China); HUA, Central China (Hubei+Hunan+Anhui, China); JSZ, East China (Jiangsu+Shandong+Zhejiang, China).

Demographic history

The neutrality test of mitochondrial genes showed all six separate populations, and the total population had negative values of Fu's FS/Tajima's D or significantly negative values of Tajima's D (Table 1). These values indicate historical population size expansions, genetic hitchhiking, and/or selection (Tajima 1989; Fu 1997). The 16S and *NADH1* network structures in which one or two universal haplotypes occurred at the center of a star-like cluster of rare haplotypes indicated rapid demographic expansion of the *P. astrigera* population in East Asia (Fig. 2a, b). The unimodal mismatch distribution and its strong bias toward low divergence values, as distinguished by 0- and 1-nucleotide changes, illustrated relatively recent expansion from a small number of ancestors (Rogers and Harpending 1992) or a range expansion with high levels of migration between neighboring demes (Ray et al. 2003; Excoffier 2004; Fig. 3a–c). The BSP analyses revealed that the East Asian *P. astrigera* adequate population size underwent four stages: 1) a gradual growth since ~50,000 years ago; 2) a slight fall between 8,000 and 1,800 years ago; 3) a sharp decrease from 1,800 to 600 years ago; and 4) a rapid rise after ~600 years ago (Fig. 3d).

The possible ancestral ranges and dispersal pathways of *P. astrigera* in East Asia were inferred by the BBM analyses (Fig. 4a). The most likely ancestral area of this spider was Northeast Asia, and it possibly dispersed from North China and East China to Northwest China or Southwest China via Central China (Fig. 4b). These results were further supported by the genetic diversity estimations (Table 1) because ancestral populations possess higher genetic diversity than derived populations (Savolainen et al. 2002).

Discussion

Genetic variations of *P. astrigera*

Previous studies suggested that *P. astrigera* was a species complex that showed high intraspecific and interspecific morphological variations (Schenkel 1963; Yin et al. 1997; World Spider Catalog, 2024). Our analyses of the mitochondrial *COI*, 16S, and *NADH1* data also found the largest genetic distance (*p*-distance) among the *P. astrigera* haplotypes was 0.033 for *COI*, 0.013 for 16S, and 0.030 for *NADH1*, and the largest overall mean distance (*p*-distance) among the six populations was 0.014 for *COI*, 0.005 for *16S*, and 0.010 for *NADH1* (Suppl. material 1: table S6). Our DNA data indicated that the wolf spider has a rich genetic diversity, and the six divided geographical populations showed obvious genetic variations (Table 1). Moreover, in the study of Chang et al. (2007),

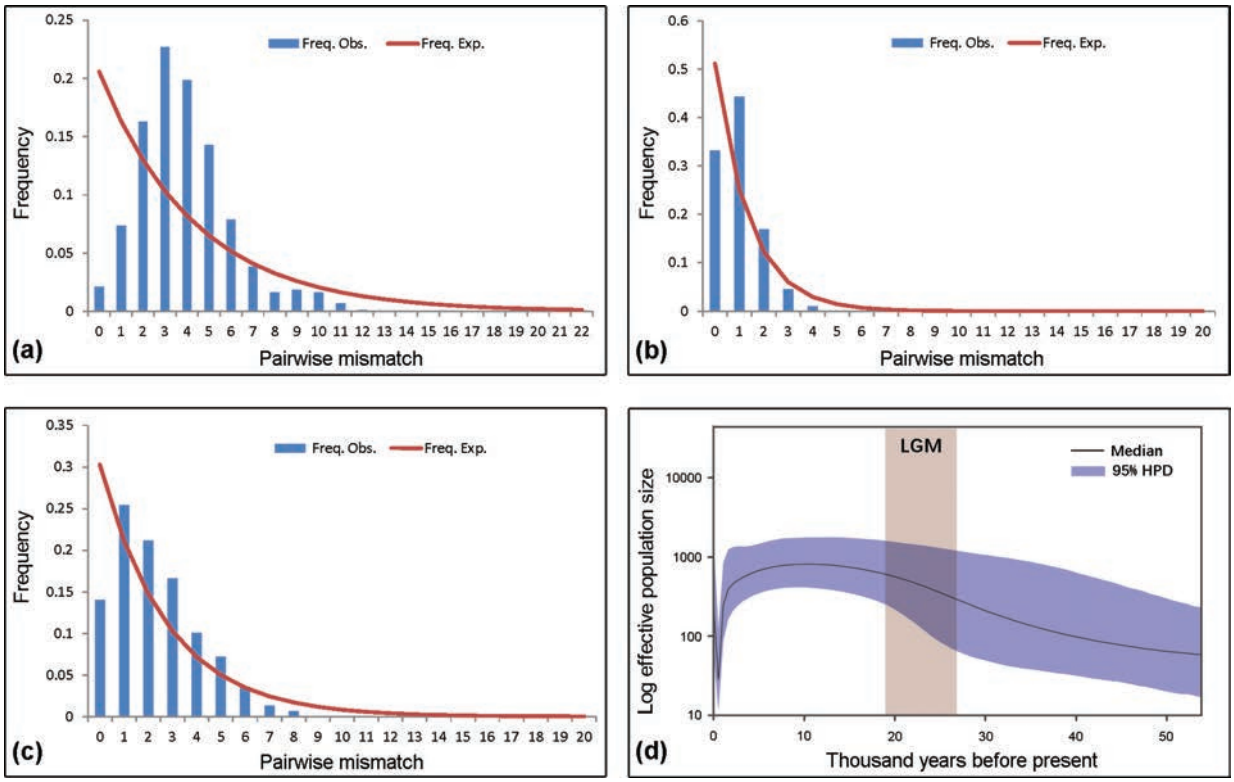

Figure 3. Mismatch distributions of *Pardosa astrigera* from the whole sample based on the *COI* sequences (**a**) and based on the *16S* sequences (**b**) and the *NADH1* sequences (**c**) independently. Bayesian skyline plots from the whole sample (**d**); middle lines represent median estimates of the effective population size, and shaded areas represent 95% of the highest posterior densities (95% HPD). The effective population size is presented on a logarithmic scale. The LGM represents the last glacial maximum.

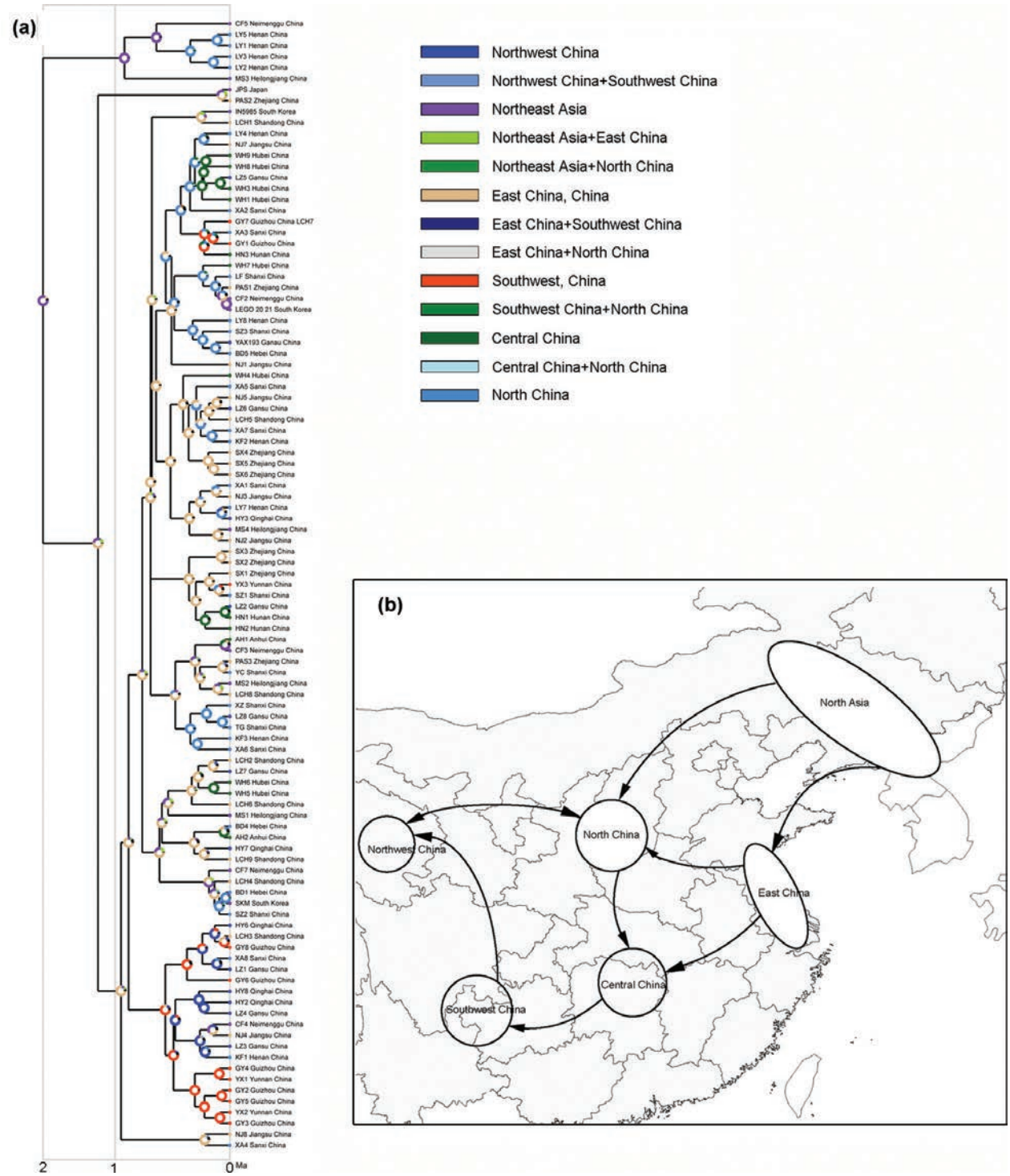

Figure 4. a. Biogeographical reconstruction of *P. astrigera*; **b.** Probable dispersion routes in East Asia. Northeast Asia (Neimenggu+Heilongjiang, China+Korea+Japan); North China (Hebei+Henan+Shanxi+Sanxi, China); Northwest China (Qinghai+Gansu, China); Southwest China (Yunnan+Guizhou, China); Central China (Hubei+Hunan+Anhui, China); East China (Jiangsu+Shandong+Zhejiang, China).

two phenotypes (types A and B distinguished by the shape and length of the median apophysis in palpus) of the *P. astrigera* males were recognized in China, and they differed genetically in the presence (type A corresponding to Lineage 1 of this study) or absence (type B corresponding to Lineage 2) of common insertions and deletions in the nuclear ITS2 gene. Therefore, our mtDNA data also supported the two differentiated phenotypes.

The evolutionary potential of species under environmental stress depends on levels of genetic diversity (Black et al. 1992; Gurdebeke et al. 2003). High genetic diversity is an important factor in adaptation to environmental changes. The wolf spider, *P. astrigera*, is widespread in East Asia. As a major natural predator of pests in various semi-arid land ecosystems such as farmland, forests, vegetable fields, tea gardens, and fruit orchards,

it has a wide distribution, a large population size, strong adaptability, and a complex mechanism for protecting offspring (spiderlings clustering on the abdomen and back of mothers after hatching and dispersing after one molt). Therefore, this wolf spider seems to be highly resistant to environmental changes and has the genetic basis to become a dominant and widespread species.

Haplotype relationships and mitochondrial genes

The complex haplotype relationships among populations of *P. astrigera* and the high frequency of gene flow within regions were revealed by the *COI* haplotype network analyses. However, the inferred 16S and *NADH1* networks show clear haplotype relationships and a lower degree of divergence than that obtained using *COI*. These findings can be explained by the importance of *COI* in cells and strong natural selection (Arnold 2012). The haplotype network structure revealed by the mitochondrial 16S or *NADH1* analyses is consistent with that by nuclear ITS2 analyses (Chang et al. 2007), and we found a similar mutation rate of 16S to ITS2 in *P. astrigera*.

Both haplotype networks inferred from 16S and *NADH1* are composed of two lineages (1–2). Combined with the results of the biogeographical reconstruction (BBM), we speculated that the Lineage 1 spiders were the ancestors of *P. astrigera*. The main haplotypes (Hap 4 and Hap 15 for 16S; Hap 13 for *NADH1*) at the center of Lineage 2 of each haplotype network were identified in all populations. Therefore, we proposed them as the ancestral haplotypes within the lineage. Further, the number of mutation steps suggested that the other haplotypes of Lineage 2 might have derived from the main haplotypes over different time periods.

Phylogeographical pattern and historical demography

Our mtDNA data support that *P. astrigera* comprises two sympatric lineages (1–2). Lineage 1 has a limited geographic distribution north of the Qinling Mountains (Mts) of China, including the sample (CF5) from Neimonggu province of China, the four samples (LY1-3 and LY5) from Henan of China, and the sample (MS3) from Heilongjiang of China; in contrast, Lineage 2 is present across the entire ranges of the species in continental East Asia. This population structure pattern supports the hypothesis that intraspecific phylogeography involves common lineages that are widespread, plus related lineages that are confined to one or a few nearby locales (Avise 2000). The two lineages of *P. astrigera* early split ~1.69 (0.95–2.66) Ma, diversified since the late Pleistocene in East Asia, and exist sympatrically at multiple locations. The results suggest that the Pleistocene glaciation is probably a major driving factor in its genetic differentiation. One haplotype (Hap 13) of *NADH1* and two (Hap 4 and Hap 15 of 16S) occurred in all six sampled populations across continental East Asia, indicating recent frequent dispersal of the wolf spider, probably with human activities. *Pardosa astrigera* is a dominant species and has strong environmental adaptability in various open ecosystems such as farmland, grassland, urban regions, and hills with human activity. Moreover, continental East Asia has a dense population. Therefore, human movements and trades can change the geographic distribution range of *P. astrigera* and accelerate its dispersal across the East Asian region. Additionally, ballooning is likely another driver for the frequent and/or long-distant dispersal of *P. astrigera* across East Asia. Dispersal by ballooning on silken threads is a well-known behavior in wolf spiders (Matthew 1982; Postiglioni et al. 2017).

Analyses of the mtDNA population genetics revealed that *P. astrigera* may have undergone a recent demographic expansion in East Asia. Our estimation of the population expansion time [~74,340 (58,832–104,236) years ago] of the spider based on fossil calibrations is during the last glaciation. The time is earlier than that (28,000 years ago) inferred by Chang et al. (2007) using a calibration assuming a rate of 2.3% sequence divergence per million years for arthropod mtDNA. Our estimated divergence rate (2.58%) was comparable to those estimated by Papadopoulou et al. (2010), who, through an extensive survey of tenebrionid beetles, obtained a divergence rate of 2.69% per million years for their concatenated *COI* and 16S sequences.

Lycosidae spiders occur globally, with many species reported to have widespread distributions and inhabit various ecosystems (Song et al. 1999; World Spider Catalog, 2024). The wolf spider *P. astrigera* lives mainly in the East Asian regions (Song et al. 1999; World Spider Catalog 2024; Fig. 1a; Suppl. material 1: table S1). Our analyses provide novel insights into the diversification of *P. astrigera* in continental East Asia during the Cenozoic. This spider is thought to originate most likely in Northeast Asia around the Pliocene and possibly dispersed in the major directions from North to South and from East to West. Our findings indicated that the pattern of genetic diversity within populations seems predominantly determined by historical factors but is modified by contemporary aspects.

Impacts of the Pleistocene glaciation on the evolution of *P. astrigera*

Many species experience retreats, expansions, and diversification in response to cold-warm climatic oscillations during the Pleistocene gracial periods (Hewitt 2000, 2004; Ding et al. 2011). They often retracted to their southern range or refugia during the cold glaciation periods and expanded their distribution ranges during the warm interglacial periods, and thus their glacial refugia are often located at the south and postglacial expansions are often northward (Fu and Wen 2023). These

evolutionary patterns resulted in a genetic diversity pattern of "southern richness to northern purity" (Hewitt 2000). That was, however, not supported by the present study, which found the Northeast Asian *P. astrigera* population had the highest genetic diversity among the six divided geographic populations from continental East Asia. Moreover, the ancestral area reconstruction of this species suggests its ancestors inhabited Northeast Asia and subsequently dispersed southwestward. Therefore, the Northeast Asian regions were probably the glacial refugia of *P. astrigera.* The refugia affected the phylogeography and genetic structure of the species. That is similar to the results of González-Trujillo et al. (2016), who studied the Pleistocene refugia of *Pardosa sierra* on the Baja California Peninsula. On continental East Asia, the Pleistocene glacial-interglacial climatic cycle plays a crucial role in some species (Fu and Wen 2023). Pleistocene climatic fluctuations have also been shown to influence the distribution patterns of European and North American lycosids (Muster and Berendonk 2006; Ivanov et al. 2023). These results and our findings suggested that similar interglacial dynamics shaped the modern boreal fauna of the wolf spiders in the Holarctic region, and secondary contacts were likely to be common among the allopatric cold-adapted species.

The spiders of *P. astrigera* started during the mid-Pleistocene, resulting in Lineage 1 and Lineage 2, and subsequently both the two lineages rapidly diversified. Therefore, the mid-Pleistocene glaciation is an important driver for the diversification of this spider. The population expansion of *P. astrigera* began during the last glaciation. We speculated that the co-existence of Lineage 1 and Lineage 2 occurred before the last glacial epoch. The last glaciation triggered the expansion of the Lineage 2 populations into the south of the Qinling Mts, whereas the Lineage 1 populations were likely blocked by the Qinling Mts. Thus, multiple glaciations during the Pleistocene affected the arid-cold distribution and diversification of *P. astrigera* in East Asia.

Future directions

This study has allowed understanding of the matrilineage structure of the wolf spider *P. astrigera* and generated hypotheses regarding its origin and dispersal using the mitochondrial *COI*, 16S, and *NADH1* loci. However, while mtDNA data have proven highly useful in phylogeographic analyses, there are several shortcomings to this approach (e.g., Avise 2000). There is a potential mismatch between the dispersal histories of males and females and a likely mismatch between a species tree and any single gene tree. In this paper, we summarize available *COI*, 16S, and *NADH1* data, add new data analyses of patterns across East Asia, and discuss hypotheses on the dispersal history of *P. astrigera*. Robustly testing the historical expansion hypotheses and gaining a deeper understanding of the population structure of this spider will require DNA data from the whole genome, using methods such as RAD-seq. Such data will tease apart male and female dispersal, testing the "female-based" dispersal hypotheses proposed here. They will also allow testing of the "independent lineages" hypothesis through precise measures of genetic isolation and gene flow unavailable to several marker studies. Sampling is the process of choosing a subset of a target population that will serve as its representative. In this paper, the total sampling specimens for some regions are on the low side. However, we hope our study can aid in strategic resampling, reflecting known lineage divergences.

Acknowledgements

The manuscript benefited greatly from comments by Danilo Harms (Hamburg, Germany), Yanfeng Tong (Shen-yang, China) and one anonymous referees. We thank Li Tan, Xuanxuan Chi, Jun Wang, and Zhaojun Bao (Shaoxing, China) for their help in collecting the material and laboratory work. This study was supported by the National Natural Sciences Foundation of China (NSFC-32170463, 31860602, 31660611) and the Zhejiang Provincial Natural Science Foundation of China (LTGN24C140006).

References

Aris-Brosou S, Excoffier L (1996) The impact of population expansion and mutation rate heterogeneity on DNA sequence polymorphism. Molecular Biology and Evolution 13(3): 494–504. https://doi.org/10.1093/oxfordjournals.molbev.a025610

Arnold S (2012) The power of life: Cytochrome c oxidase takes center stage in metabolic control, cell signalling and survival. Mitochondrion 12(1): 46–56. https://doi.org/10.1016/j.mito.2011.05.003

Avise JC (2000) Phylogeography: the History and Formation of Species. Harvard University Press, Cambridge, 447 pp. https://doi.org/10.17129/botsci.1619

Bandelt H, Forster P, Röhl A (1999) Median-joining networks for inferring intraspecific phylogenies. Molecular Biology and Evolution 16(1): 37–48. https://doi.org/10.1093/oxfordjournals.molbev.a026036

Black WC, Duteau NM, Puterka GJ, Nichols JR, Pettorini JM (1992) Use of the random amplified polymorphic DNA polymerase chain reaction (RAPD-PCR) to detect DNA polymorphism in Aphids (Homoptera: Aphididae). Bulletin of Entomological Research 82(2): 151–159. https://doi.org/10.1017/S0007485300051671

Chang J, Song DX, Zhou KY (2007) Incongruous nuclear and mitochondrial phylogeographic patterns in two sympatric lineages of the wolf spider *Pardosa astrigera* (Araneae: Lycosidae) from China. Molecular Phylogenetics and Evolution 42(1): 104–121. https://doi.org/10.1016/j.ympev.2006.06.013

Chen ZQ, Jiao XG, Wu J, Chen J, Liu FX (2010) Effects of copulation temperature on female reproductive output and longevity in the wolf spider *Pardosa astrigera* (Araneae: Lycosidae). Journal of Thermal Biology 35(3): 125–128. https://doi.org/10.1016/j.jtherbio.2010.01.002

Ding L, Gan XN, He SP, Zhao EM (2011) A phylogeographic, demographic and historical analysis of the short-tailed pit viper (*Gloydius brevicaudus*): Evidence for early divergence and late expansion during the Pleistocene. Molecular Ecology 20(9): 1905–1922. https://doi.org/10.1111/j.1365-294X.2011.05060.x

Donoghue PCJ, Benton MJ (2007) Rocks and clocks: Calibrating the tree of life using fossils and molecules. Trends in Ecology & Evolution 22(8): 424–431. https://doi.org/10.1016/j.tree.2007.05.005

Drummond AJ, Rambaut A (2007) Beast: Bayesian evolutionary analysis by sampling trees. BMC Evolutionary Biology 7(1): 214–221. https://doi.org/10.1186/1471-2148-7-214

Excoffier L (2004) Patterns of DNA sequence diversity and genetic structure after a range expansion: Lessons from the infinite island model. Molecular Ecology 13(4): 853–864. https://doi.org/10.1046/j.1365-294X.2003.02004.x

Excoffier L, Lischer HEL (2010) Arlequin suite ver 3.5: A new series of programs to perform population genetics analyses under Linux and Windows. Molecular Ecology Resources 10(3): 564–567. https://doi.org/10.1111/j.1755-0998.2010.02847.x

Fu YX (1997) Statistical tests of neutrality of mutations against population growth, hitchhiking, and background selection. Genetics 147(2): 915–925. https://doi.org/10.1093/genetics/147.2.915

Fu J, Wen L (2023) Impacts of Quaternary glaciation, geological history and geography on animal species history in continental East Asia: A phylogeographic review. Molecular Ecology 32(16): 4497–4514. https://doi.org/10.1111/mec.17053

González-Trujillo R, Correa-Ramírez MM, Ruiz-Sanchez E, Salinas EM, Jiménez ML, León FJG (2016) Pleistocene refugia and their effects on the phylogeography and genetic structure of the wolf spider *Pardosa* sierra (Araneae: Lycosidae) on the Baja California Peninsula. The Journal of Arachnology 44(3): 367–379. https://doi.org/10.1636/R15-84.1

Gurdebeke S, Maelfait JP, Backeljau T (2003) Contrasting allozyme and RAPD variation in spider populations from patchy forest habitats. Genetica 119(1): 27–34. https://doi.org/10.1023/A:1024497407583

Hall TA (1999) BioEdit: A user-friendly biological sequence alignment editor and analysis program for windows 95/98/NT. Nucleic Acids Symposium Series 41: 95–98. https://doi.org/10.1021/bk-1999-0734.ch008

Harpending HC, Sherry ST, Rogers AR, Stoneking M (1993) The genetic structure of ancient human populations. Current Anthropology 34(4): 483–496. https://doi.org/10.1086/204195

Hewitt GM (2000) The genetic legacy of the quaternary ice ages. Nature 405(6789): 907–913. https://doi.org/10.1038/35016000

Hewitt GM (2004) Genetic consequences of climatic oscillations in the Quaternary. Philosophical Transactions of the Royal Society of London. Series B, Biological Sciences 359(1442): 183–195. https://doi.org/10.1098/rstb.2003.1388

Hoang DT, Chernomor O, Von Haeseler A, Minh BQ, Vinh LS (2018) UFBoot2: Improving the ultrafast bootstrap approximation. Molecular Biology and Evolution 35(2): 518–522. https://doi.org/10.1093/molbev/msx281

Iturralde-Vinent MA, MacPhee RDE (1996) Age and paleogeographical origin of dominican amber. Science 273(5283): 1850–1852. https://doi.org/10.1126/science.273.5283.1850

Ivanov V, Blagoev G, Danflous S, Gajdoš P, Høye TT, Lee KM, Marusik Y, Mielec CL, Muster C, Pétillon J, Spelda J, Mutanen M (2023) Across mountains and ocean: Species delimitation and historical connectivity in Holarctic and Arctic-Alpine wolf spiders (Lycosidae, *Pardosa*). Insect Systematics and Diversity 7(5): 1–14. https://doi.org/10.1093/isd/ixad018

Jaeger JR, Riddle BR, Bradford DF (2005) Cryptic neogene vicariance and Quaternary dispersal of the redspotted toad (*Bufo punctatus*): Insights on the evolution of North American warm desert biotas. Molecular Ecology 14(10): 3033–3048. https://doi.org/10.1111/j.1365-294X.2005.02645.x

Kalyaanamoorthy S, Minh BQ, Wong TK, Von Haeseler A, Jermiin LS (2017) ModelFinder: Fast model selection for accurate phylogenetic estimates. Nature Methods 14(6): 587–589. https://doi.org/10.1038/nmeth.4285

Katoh K, Standley DM (2013) MAFFT multiple sequence alignment software version 7: Improvements in performance and usability. Molecular Biology and Evolution 30(4): 772–780. https://doi.org/10.1093/molbev/mst010

Kim JP, Yoo JS (1997) Korean spiders of the genus *Pardosa* C. L. Koch, 1848 (Araneae: Lycosidae). Korean Arachnology 13: 31–45.

Leigh JW, Bryant D (2015) PopART: Full-feature software for haplotype network construction. Methods in Ecology and Evolution 6(9): 1110–1116. https://doi.org/10.1111/2041-210X.12410

Li R, Yan XZ, Li SC (2011) Population genetic structure of *Pardosa astrigera* based on molecular evidence from mtDNA. Acta Zootaxonomica Sinica 36(2): 341–346. https://doi.org/10.1111/j.1749-4877.2010.00232.x

Li M, Luo FZ, Liu J, Yuan ML (2020) Biological and ecological characteristics of *Pardosa astrigera*: Status and prospect. Caoye Kexue 37(6): 1183–1193. https://doi.org/10.11829/j.issn.1001-0629.2019-0497

Librado P, Rozas J (2009) DnaSP v5: A software for comprehensive analysis of DNA polymorphism data. Bioinformatics 25(11): 1451–1452. https://doi.org/10.1093/bioinformatics/btp187

Lida H, Kohno K, Takeda M (2016) Seasonal fluctuations in offspring body size in the wolf spider, *Pardosa astrigera* (Araneae: Lycosidae). Applied Entomology and Zoology 51(1): 1–7. https://doi.org/10.1007/s13355-015-0381-4

Luo YF, Li SQ (2022) The stepwise Indian-Eurasian collision and uplift of the Himalayan-Tibetan Plateau drove the diversification of high-elevation *Scytodes* spiders. Cladistics 38(5): 582–594. https://doi.org/10.1111/cla.12512

Magalhaes IL, Azevedo GH, Michalik P, Ramírez MJ (2020) The fossil record of spiders revisited: Implications for calibrating trees and evidence for a major faunal turnover since the Mesozoic. Biological Reviews of the Cambridge Philosophical Society 95(1): 184–217. https://doi.org/10.1111/brv.12559

Matthew HG (1982) Ballooning frequency and habitat predictability in two wolf spider species (Lycosidae: *Pardosa*). The Florida Entomologist 65(1): 83–89. https://doi.org/10.2307/3494147

Minh BQ, Nguyen MA, Von Haeseler A (2013) Ultrafast approximation for phylogenetic bootstrap. Molecular Biology and Evolution 30(5): 1188–1195. https://doi.org/10.1093/molbev/mst024

Muster C, Berendonk TU (2006) Divergence and diversity: Lessons from an arctic-alpine distribution (*Pardosa saltuaria* group, Lycosidae). Molecular Ecology 15(10): 2921–2933. https://doi.org/10.1111/j.1365-294X.2006.02989.x

Newton MA, Raftery AE (1994) Approximate Bayesian inference with the weighted likelihood bootstrap. Journal of the Royal Statistical Society. Series B, Statistical Methodology 56(1): 3–48. https://doi.org/10.1111/j.2517-6161.1994.tb01956.x

Nguyen LT, Schmidt HA, Von Haeseler A, Minh BQ (2015) IQ-TREE: A fast and effective stochastic algorithm for estimating maximum-likelihood phylogenies. Molecular Biology and Evolution 32(1): 268–274. https://doi.org/10.1093/molbev/msu300

Papadopoulou A, Anastasiou I, Vogler AP (2010) Revisiting the insect mitochondrial molecular clock: The mid-Aegean trench calibration. Molecular Biology and Evolution 27(7): 1659–1672. https://doi.org/10.1093/molbev/msq051

Penney D (2006) The oldest fossil pholcid and selenopid spiders (Araneae) in Lowermost Eocene amber from the Paris Basin, France. The Journal of Arachnology 34(3): 592–598. https://doi.org/10.1636/H05-61.1

Posada D (2008) jModelTest: Phylogenetic model averaging. Molecular Biology and Evolution 25(7): 1253–1256. https://doi.org/10.1093/molbev/msn083

Postiglioni R, Aisenberg A, Carlozzi A, Bidegaray-Batista L (2017) The dark side of ballooning: Nocturnal aerial dispersal in wolf spiders from the South American Coastline. Arachnology 17(6): 312–316. https://doi.org/10.13156/arac.2017.17.6.312

Rambaut A, Drummond AJ (2009) Tracer v1.5. http://beast.bio.ed.ac.uk/Tracer

Ray N, Currat M, Excoffier L (2003) Intra-deme molecular diversity in spatially expanding populations. Molecular Biology and Evolution 20(1): 76–86. https://doi.org/10.1093/molbev/msg009

Renner SS (2005) Relaxed molecular clocks for dating historical plant dispersal events. Trends in Plant Science 10(11): 550–558. https://doi.org/10.1016/j.tplants.2005.09.010

Rogers AR (1995) Genetic evidence for a Pleistocene population explosion. Evolution; International Journal of Organic Evolution 49(4): 608–615. https://doi.org/10.2307/2410314

Rogers AR, Harpending H (1992) Population growth makes waves in the distribution of pairwise genetic differences. Molecular Biology and Evolution 9: 552–569. https://doi.org/10.1093/oxfordjournals.molbev.a040727

Ronquist F, Huelsenbeck JP (2003) MrBayes 3: Bayesian phylogenetic inference under mixed models. Bioinformatics 19(12): 1572–1574. https://doi.org/10.1093/bioinformatics/btg180

Sanmartín I, Enghoff H, Ronquist F (2001) Patterns of animal dispersal, vicariance and diversification in the Holarctic. Biological Journal of the Linnean Society, Linnean Society of London 73(4): 345–390. https://doi.org/10.1006/bijl.2001.0542

Savolainen P, Zhang Y, Luo J, Lundeberg J, Leitner T (2002) Genetic evidence for an east Asian origin of domestic dogs. Science 298(5598): 1610–1613. https://doi.org/10.1126/science.1073906

Schenkel E (1963) Ostasiatische Spinnen aus dem Meseum d'Histotorie Naturelle de Pairs. Mémoires du Muséum National d'Histoire Naturelle de Paris (A, Zoology) 25: 1–481.

Slatkin M, Hudson RR (1991) Pairwise comparisons of mitochondrial DNA sequences in stable and exponentially growing populations. Genetics 129(2): 555–562. https://doi.org/10.1093/genetics/129.2.555

Smith CI, Farrell BD (2005) Range expansions in the flightless longhorn cactus beetles, *Moneilema gigas* and *Moneilema armatum*, in response to Pleistocene climate changes. Molecular Ecology 14(4): 1025–1044. https://doi.org/10.1111/j.1365-294X.2005.02472.x

Song DX, Zhu MS, Chen J (1999) The Spiders of China. Hebei Science and Technology Publishing House, Shijiazhuang, China.

Tajima F (1989) Statistical method for testing the neutral mutation hypothesis by DNA polymorphism. Genetics 123(3): 585–595. https://doi.org/10.1093/genetics/123.3.585

Tajima F (1996) The amount of DNA polymorphism maintained in a finite population when the neutral mutation rate varies among sites. Genetics 143(3): 1457–1465. https://doi.org/10.1093/genetics/143.3.1457

Tamura K, Peterson D, Peterson N, Stecher G, Nei M, Kumar S (2011) MEGA5: Molecular evolutionary genetics analysis using maximum likelihood, evolutionary distance, and maximum parsimony methods. Molecular Biology and Evolution 28(10): 2731–2739. https://doi.org/10.1093/molbev/msr121

Trifinopoulos J, Nguyen LT, Von Haeseler A, Minh BQ (2016) W-IQ-TREE: A fast online phylogenetic tool for maximum likelihood analysis. Nucleic Acids Research 44(W1): 232–235. https://doi.org/10.1093/nar/gkw256

World Spider Catalog (2024) World Spider Catalog. Version 25.0. Natural History Museum Bern. http://wsc.nmbe.ch [accessed on March 10, 2024]

Wunderlich J (2004a) Fossil spiders (Araneae) of the family Oxyopidae in Baltic and Dominican amber. Beiträge zur Araneologie 3: 1554–1556.

Wunderlich J (2004b) Fossil crab spiders (Araneae: Thomisidae) in Baltic and Dominican amber. Beiträge zur Araneologie 3: 1747–1760.

Xie W, Lewis PO, Fan Y, Kuo L, Chen MH (2011) Improving marginal likelihood estimation for Bayesian phylogenetic model selection. Systematic Biology 60(2): 150–160. https://doi.org/10.1093/sysbio/syq085

Yang J, Wu Q, Xiao R, Zhao J, Chen J, Jiao X (2018) Seasonal variations in body melanism and size of the wolf spider *Pardosa astrigera* (Araneae: Lycosidae). Ecology and Evolution 8(8): 4352–4359. https://doi.org/10.1002/ece3.3988

Yin CM, Peng XJ, Bao YH, Wang JF (1997) The Wolf Spiders of China. Hunan Normal University Publishing House, Changsha, China.

Yu Y, Harris AJ, Blair C, He XJ (2014) RASP (reconstruct ancestral state in phylogenies) 3.0. http://mnh.scu.edu.cn/soft/blog/RASP

Supplementary material 1

Supplemental materials and datasets

Authors: Dan Fu, Lijuan Liu, Ying Cheng, Haodong Chen, Yufa Luo

Data type: zip

Link: https://doi.org/10.3897/zse.100.125246.suppl1

Zoosyst. Evol. 100 (3) 2024, 803–820 | DOI 10.3897/zse.100.120207

PENSOFT

für Natur MUSEUM FÜR NATURKUNDE BERLIN

Exploring the diversity of *Eutimesius* Roewer, 1913: new species and records from Colombia and Venezuela (Opiliones, Gonyleptoidea, Stygnidae)

Osvaldo Villarreal[1,2,3], Daniela Ahumada-C.[4], Gabriel R. Navas-S.[5]

1 *Centro de Ecología, Instituto Venezolano de Investigaciones Científicas (IVIC), km 11 carretera Panamericana, Altos de Pipe, edo. Miranda 1204-A, Venezuela*

2 *Instituto y Museo del Instituto de Zoología Agrícola, Facultad de Agronomía, Universidad Central de Venezuela, Apartado 4579, Maracay 2101, Aragua, Venezuela*

3 *Departamento de Invertebrados, Museu Nacional/UFRJ, Quinta da Boa Vista, São Cristóvão, 20.940-040, Rio de Janeiro – RJ, Brazil*

4 *Grupo de Investigación Biología Descriptiva y Aplicada, Programa de Biología, Universidad de Cartagena, Zaragocilla Cra. 50 #24-120, Cartagena de Indias, Bolívar, Colombia*

5 *Grupo de Investigación Hidrobiología, Programa de Biología, Universidad de Cartagena, Zaragocilla Cra. 50 #24-120, Cartagena de Indias, Bolívar, Colombia*

https://zoobank.org/55DBF63A-85CF-42C0-8218-15F310FB177A

Corresponding author: Osvaldo Villarreal (osvaldovillarreal@gmail.com)

Academic editor: Danilo Harms ♦ **Received** 4 February 2024 ♦ **Accepted** 10 May 2024 ♦ **Published** 17 June 2024

Abstract

This study contributes taxonomic information on the genus *Eutimesius* Roewer, 1913. Three new species are described: the sympatric species *E. aroa* **sp. nov.** and *E. guaichia* **sp. nov.** from Yaracuy state and *E. canoabo* **sp. nov.** from Carabobo state in Venezuela. The male of *E. ephippiatus* (Roewer, 1915) is described for the first time. Remarks are made on the distribution of *E. ornatus*, and a complimentary description of male genitalia is provided for *E. simoni* Roewer, 1913. New departmental records are added for *E. ephippiatus* and *E. simoni*. An updated distribution map and a key to the identification of the males of the species in the genus are presented.

Key Words

Harvestmen, Heterostygninae, Laniatores, Neotropics

Introduction

The family Stygnidae is a group of primarily mid-sized harvestmen with 114 species (Kury et al. 2023), most diverse in Brazil (61 species), Venezuela (26 species), and Colombia (13 species); however, it occurs in other Andean and Caribbean countries (Pinto-da-Rocha 1997; Kury 2003). A systematic revision of the family, including a hypothesis of its relationship, was published over two decades ago (Pinto-da-Rocha 1997), dividing the group into three subfamilies: Nomoclastinae (now considered a separate family) and the rest of the species arranged in a symmetrical topology containing two subfamilies, Heterostygninae and Stygninae (except for *Gaibulus* Roewer, 1943) (Pinto-da-Rocha 1997).

The genus *Eutimesius* Roewer, 1913 belongs to the subfamily Heterostygninae and is characterized by the presence of white, dry spots on the dorsal scutum. These dry spots bear a resemblance to those documented by Kury in DaSilva and Gnaspini (2010) for certain Gonyleptidae species. Within the context of our study, we opt for the term ‘Dry Spots’ instead of ‘Dry Mark,’ as employed in the aforementioned research. Notably, these spots exhibit a tendency to diminish in visibility or become nearly imperceptible upon contact with alcohol, mirroring what has been previously documented in Gonyleptidae species.

The five species currently included within the genus were originally classified under at least five different genera: *Eutimesius*; *Dichobunistygnus* Roewer, 1915; *Hoplostygnus* Roewer, 1915; *Metaphareus* Roewer, 1912; and *Xanthostygnus* Mello-Leitão, 1949. Pinto-da-Rocha (1997) synonymized four of these genera and restructured the group into *Eutimesius*, defined at the time as four species distributed in Colombia and Venezuela. Since the comprehensive taxonomic revision of the family (Pinto-da-Rocha 1997), the genus *Eutimesius* has experienced minimal modifications within its classification. Notably, the taxonomy remained relatively stable until the inclusion of a unique species, *Eutimesius punctatus* (Roewer, 1913), which was incorporated into its taxonomic framework from the genus *Metaphareus* by Villarreal et al. (2019a).

Most of the species within the genus are restricted to the northern Andes of Colombia and Venezuela (Pinto-da-Rocha 1997; Villarreal et al. 2019a). In the Colombian Andes, two species have been recorded: *Eutimesius ephippiatus* (Roewer, 1915) from the department of Quindío (see Kury 2003 for details) and *Eutimesius ornatus* (Roewer, 1943) from the department of Cundinamarca. In Venezuela, only two species have also been recorded: *Eutimesius albicinctus* (Roewer, 1915) and *E. punctatus* (Roewer, 1913) from Mérida State, both in the Andean region of this country (Villarreal et al. 2019a). Additionally, a female of "*E. ornatus*" has been recorded in Táchira State (Pinto-da-Rocha 1997); however, the identity of this record is here discussed.

Only the type species of the genus occurs outside the Andes: *Eutimesius simoni* Roewer, 1913, which inhabits the Amazonas basin and has been recorded from Brazil, Colombia, Ecuador, and Peru. In Colombia, *E. simoni* is known to occur in the department of Putumayo (Pinto-da-Rocha 1997).

Despite the relatively low number of described species in this genus, recent unpublished surveys suggest a significantly greater diversity, with at least seven undescribed species (OV unpublished data) known exclusively in the Venezuelan Andean cloud forests exhibiting high levels of endemism.

This paper describes three new species: two sympatric species from Yaracuy State and one from Carabobo State in Venezuela. Additionally, the description of the previously unknown male of *E. ephippiatus*, remarks on the distribution of *E. ornatus*, and a complimentary description of male genitalia for *E. simoni* also report new departamental records of *E. ephippiatus* and *E. simoni* in Colombia.

Materials and methods

All measurements are in millimeters and were taken with a stereomicroscope, referring to the maximum length and width. Setiferous tubercles (i = small, I = large) on pedipalps are given in proximal to distal order. For color descriptions, we used the standard names of the 267 color centroids of the NBS/IBCC color system as named in Centore (2016). The description pattern follows Villarreal et al. (2021); the nomenclature of tubercle rows in the legs follows Da Silva and Gnaspini (2010) and Hara et al. (2010); the integumentary ornamentation follows Da Silva and Gnaspini (2010); and the nomenclature of dry spots on the DS follows Kury in DaSilva and Gnaspini (2010). The terminology for chaetotaxy of penis lamina parva and malleus follows Kury and Villarreal (2015), and the terminology for dorsal scutum outline types follows Kury and Medrano (2016). The term "genital bauplan as Heterostygninae," as employed in diagnosis or descriptions, adheres to the definition provided by Villarreal et al. (2019b). We refer to intercoxal tubercles as those fused tubercles that connect two coxae of the legs on their ventral side. The pictures were taken with a Canon digital camera coupled to a stereoscopic microscope Wild M7A, a Nikon COOLPIX P1000 with tripod, and an Olympus OMD Mark II attached to a stereoscopic microscope and microscope AmScope. The multiple images of each species at different focal planes were combined with CombineZP Suite software (Hadley 2015) to increase the depth of field and were posteriorly edited in Photoshop CC 2017 software. The drawings were made with Inkscape 1.3.2. Genital features were studied following the protocol described by Acosta et al. (2007). The first-order administrative divisions of Colombia (departments) and Venezuela (states) are underlined. Maps were made using ESRI ArcGIS® 10.1 software.

Abbreviations: **AL** – maximum abdominal scutum length; **AW** – maximum abdominal scutum width; **BaCh** – basichelicerite length; **br** – broken; **CL** – carapace length; **ClPp** – pedipalp claw; **CoPp** – pedipalpal coxa; **CW** – maximum carapace width; **DS** – dorsal scutum; **DSW** – dorsal scutum width; **DSL** – dorsal scutum length; **FeL** – femur length; **FePp** – pedipalpal femur; **IOD** – interocular distance; **LP** – lamina parva; **MS** – macrosetae of penis; **PeTr** – pedipalpal trochanter; **Pp** – pedipalps; **PaPp** – pedipalpal patella; **TaPp** – pedipalpal tarsus; **TiPp** – pedipalpal tibia; **TiL** – tibia length.

Depositories (curators): **IAvH** – Instituto Alexander von Humboldt, Villa de Leyva, Colombia (Jhon Neita Moreno); **ICN-Ao** – Instituto de Ciencias Naturales of the Universidad Nacional de Colombia, Bogotá, Colombia (Eduardo Flórez); **MPUJ_ENT –** Colección entomólogica, Museo Javeriano de Historia Natural (Giovanny Fagua); and **MIZA** – Museo del Instituto de Zoología Agrícola "Francisco Fernández Yépez", Maracay, Venezuela (Quintín Arias).

Results

Taxonomic accounts

Family Stygnidae Simon, 1879
Subfamily Heterostygninae Roewer, 1913

Genus *Eutimesius* Roewer, 1913

Included species. *Eutimesius albicinctus* (Roewer, 1915); *Eutimesius aroa* sp. nov.; *Eutimesius canoabo* sp. nov.; *Eutimesius ephippiatus* (Roewer, 1915); *Eutimesius guaichia* sp. nov.; *Eutimesius ornatus* (Rower, 1943); *Eutimesius punctatatus* (Roewer, 1913); *Eutimesius simoni* Roewer, 1913.

Diagnosis. Heterostygninae with white, dry spot on the dorsal scutum. Carapace with interocular monticle or spine, and scutal area III with two acute paramedian spines. Genital "bauplan" as Heterostygninae, LP with distal cleft, and long basal "neck." MS-B ventrally positioned (Fig. 1) when compared to *Innoxius*.

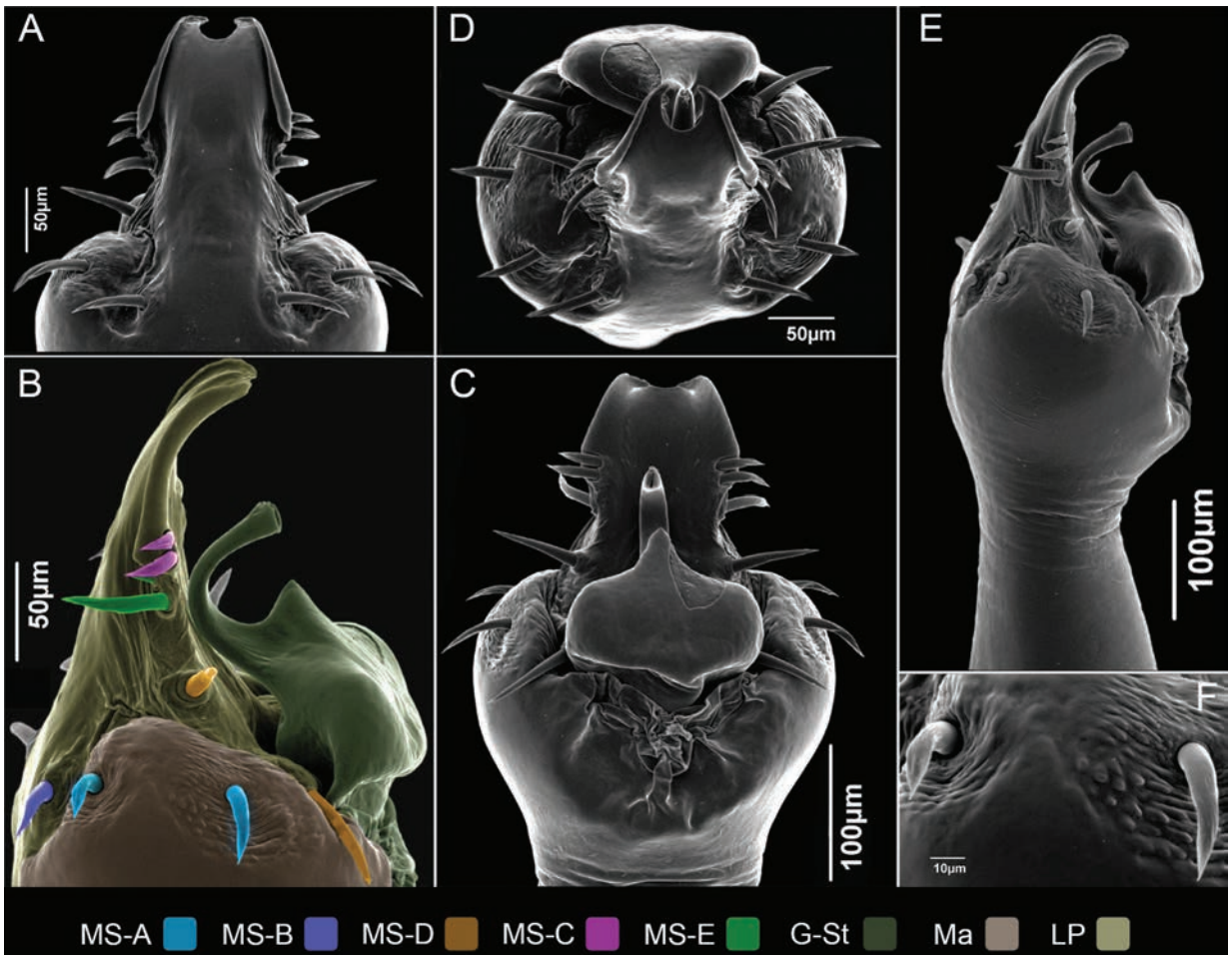

Figure 1. *Eutimesius* sp., male (IAvH 3000054 - undescribed species from Norte de Santander, Colombia), showing the genital bauplan in the genus. Penis: **A.** Ventral view; **B, E.** Lateral views; **C.** Dorsal view; **D.** Apical view; **F.** MS-A, detail in lateral view. Abbreviations: GSt = gland, stylus; LP = lamina parva; Ma = malleus; MS = macrosetae of penis.

Distribution (Fig. 2). So far, species of the genus (except the Amazonic *E. simoni*) are primarily known to be distributed in the Andes, specifically in the Cordillera Oriental of Colombia (WWF ecoregion, Cordillera Oriental montane forests, NT0118; and Northern Andean páramo, NT1006) and in the Cordillera de Mérida of Venezuela (WWF ecoregion, Venezuelan Andes montane forests, NT0175). The records of *Eutimesius aroa* sp. nov., *Eutimesius canoabo* sp. nov., and *Eutimesius guaichia* sp. nov. represent the first occurrences of the genus—considered until now an Andean component—in the Venezuelan Coastal Range (WWF ecoregion, Cordillera de la Costa montane forests, NT0117) and the first records outside the Cordillera de Mérida in this country. Records of Heterostygninae in the Coast Range refer primarily to the genera *Stygnoplus* Simon, 1879, and *Stenostygnellus* Roewer, 1913.

Natural history (Fig. 3). Opiliones exhibit diverse microhabitat preferences within forest ecosystems. Within the family Stygnidae, species demonstrate foraging locations within the understory, utilizing both arboreal substrates such as tree trunks

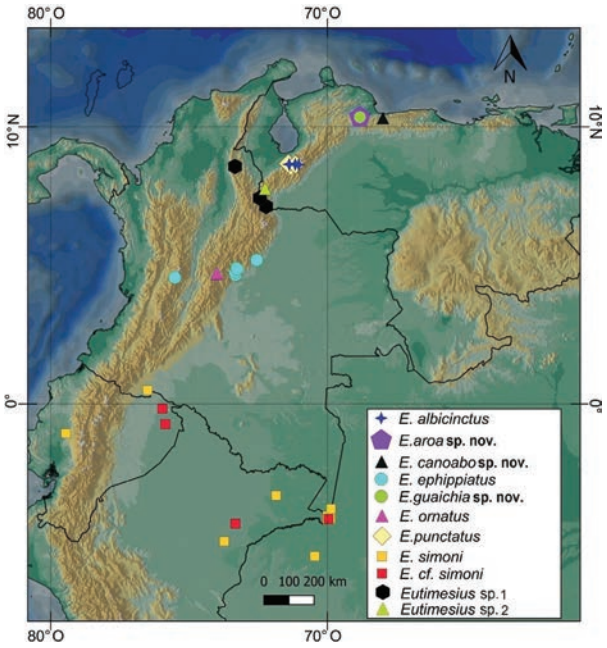

Figure 2. Map showing the distribution of *Eutimesius*.

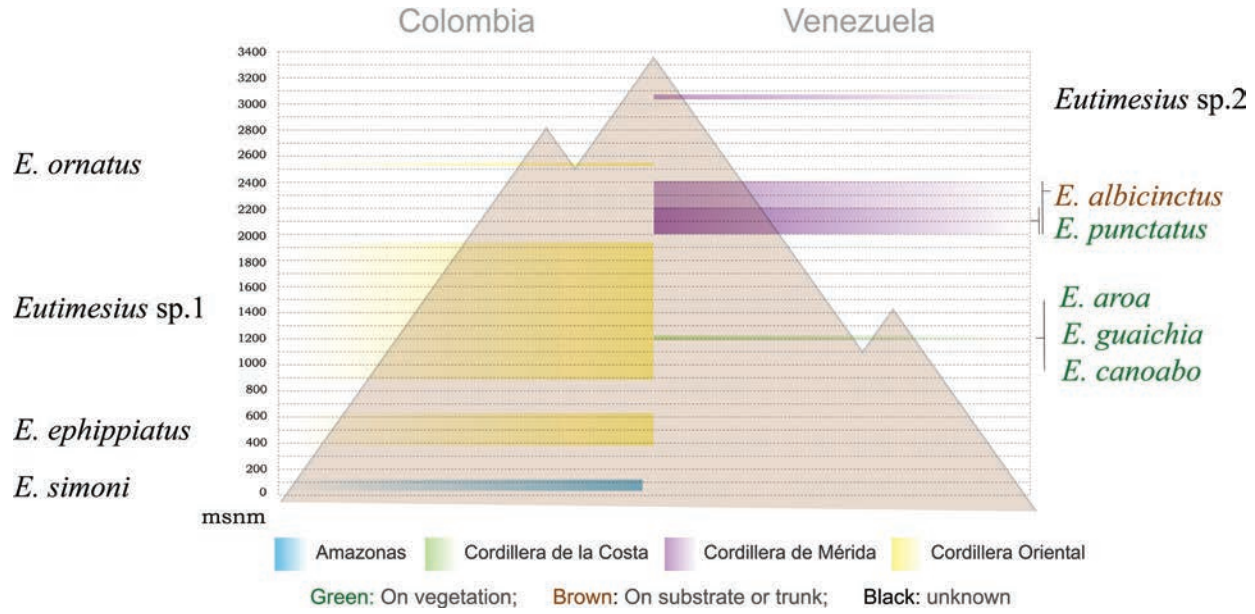

Figure 3. Schematic diagram illustrating the known altitudinal range for species of *Eutimesius*, their biogeographic area of occurrence, the country, and the microhabitat used if known.

and ground-level leaf litter. Villarreal et al. (2019b) documented *E. punctatus* utilizing the upper vegetation, such as small trees and shrubs, positioned well above the forest floor at heights of 1.5–3 meters, for foraging and oviposition. Additionally, at least one species of *Stenostygnellus* has been reported to deposit its eggs between the leaf and stem of certain palms (Villarreal and Machado 2011). The three species described here were consistently collected at heights between 1.5 and 2 meters above ground, exclusively within shrubby vegetation or small trees. A preference for microhabitat was suggested for species within this genus (Villarreal et al. 2019b).

The altitudinal range occupied by species of this genus is extensive, ranging from low elevations in the Amazon to heights reaching 3,050 meters in the Venezuelan Andes. However, the majority of species are found above 1,000 meters, typically in cloud forest habitats. Only *E. simoni* has been recorded in lowland areas between 70 and 110 meters in altitude, which is characteristic of the Amazonian region. *E. ephippiatus* occurs at the foothills of the Andes between 500 and 1,000 meters. All other species occur above 1,000 meters in altitude. The highest altitude record corresponds to a single female from Táchira state in Venezuela, misidentified as *E. ornatus* (Pinto-da-Rocha 1997), reaching 3,050 m.

Key to males of *Eutimesius* species

1 Paramedian spines of the area III fused (Fig. 13) ..... *E. simoni*
– Paramedian spines of the area III separated (Figs 5A, 7 A) 2
2 DS yellowish background with conspicuous dark circular spots on the scutal areas (Villarreal et al. 2019b: figs 1–4) ..... *E. punctatus*
– DS generally dark brown; rarely yellow, but in no case with that pattern of dark circular spots on the scutal areas (Figs 4, B, 6A, C) 3
3 Tibia IV with a conspicuous prodorsal subdistal spine (Fig. 7F) ..... *E. canoabo* sp. nov.
– Tibia IV without a conspicuous prodorsal subdistal spine (Figs 5F, G, F) 4
4 Scutal areas II–III divided (Figs 9, 10A, B); chelicerae, pedipalp and sometimes legs with intense green coloration 5
– Scutal areas II–III entire (Figs 4, 5A, B, 11, 12 A, B); no intense green coloring on the chelicerae, pedipalps, or legs (Figs 4, 11) 6
5 Lateral margins of DS and inner margin of eyes without white dry spots (Pinto-da-Rocha, 1997: figs 57, 58); femora III greenish ..... *E. ornatus*
– Lateral margins of DS and inner margin of eyes with white dry spots, eyes completely encircled by white dry spots (Figs 9, 10A, B); femora III not greenish ..... *E. ephippiatus*
6 Femur IV slightly curved and distally widened, with long and wide ventrodistal spines; patella IV as wide as long, with two distal very large dorsal tubercles; and tibia IV swollen, about two times as long as wide (Fig. 12F, G) ..... *E. guaichia* sp. nov.
– Femur IV almost straight, with small ventrodistal tubercles; patella IV longer than wide, and tibia IV cylindrical and not swollen, between 5.5 and 9.6 times longer than wide 7

7 Pattern of small, white dry spots forming a lateral line on the margins of the DS and delineating the border of both halves of the scutal area I (Pinto-da-Rocha, 1997: figs 49, 50); tubercles of the pro and retroventral rows of the femora IV confined to the distal portion (Pinto-da-Rocha, 1997: fig. 53)..... *E. albicinctus*

– Pattern of dry white spots not forming a lateral line on the DS margins; at most, they are only present in the anterior region of the carapace and do not delineate the border of both halves of the I area; instead, they are mainly confined to the lateral portions of the area I (Figs 4A, B, 5 A, B); pro and retroventral rows of the femora IV complete..... ..... *E. aroa* sp. nov.

Eutimesius aroa Villarreal & Ahumada-C., sp. nov.

https://zoobank.org/C957434C-5804-4610-88B7-8966D3A24FF7

Figs 4, 5, 14A–C, 2

Type material. Venezuela • ♂ ***holotype***; Yaracuy, Road Cocorote – Aroa, sector Las Cumaraguas; (10.3520°N, 68.8298°W); 1,200 m a.s.l.; 09 Mar. 2008; (Villarreal O., Escalona H., Jayaro Y., Viera E. leg.) (MIZA 0105934). ***Paratypes*** • 1 ♀, 1 ♂; same as the holotype; (MIZA 0105936).

Diagnosis. It is distinguishable from all other species in the genus by the pattern of dry white spots, occupying

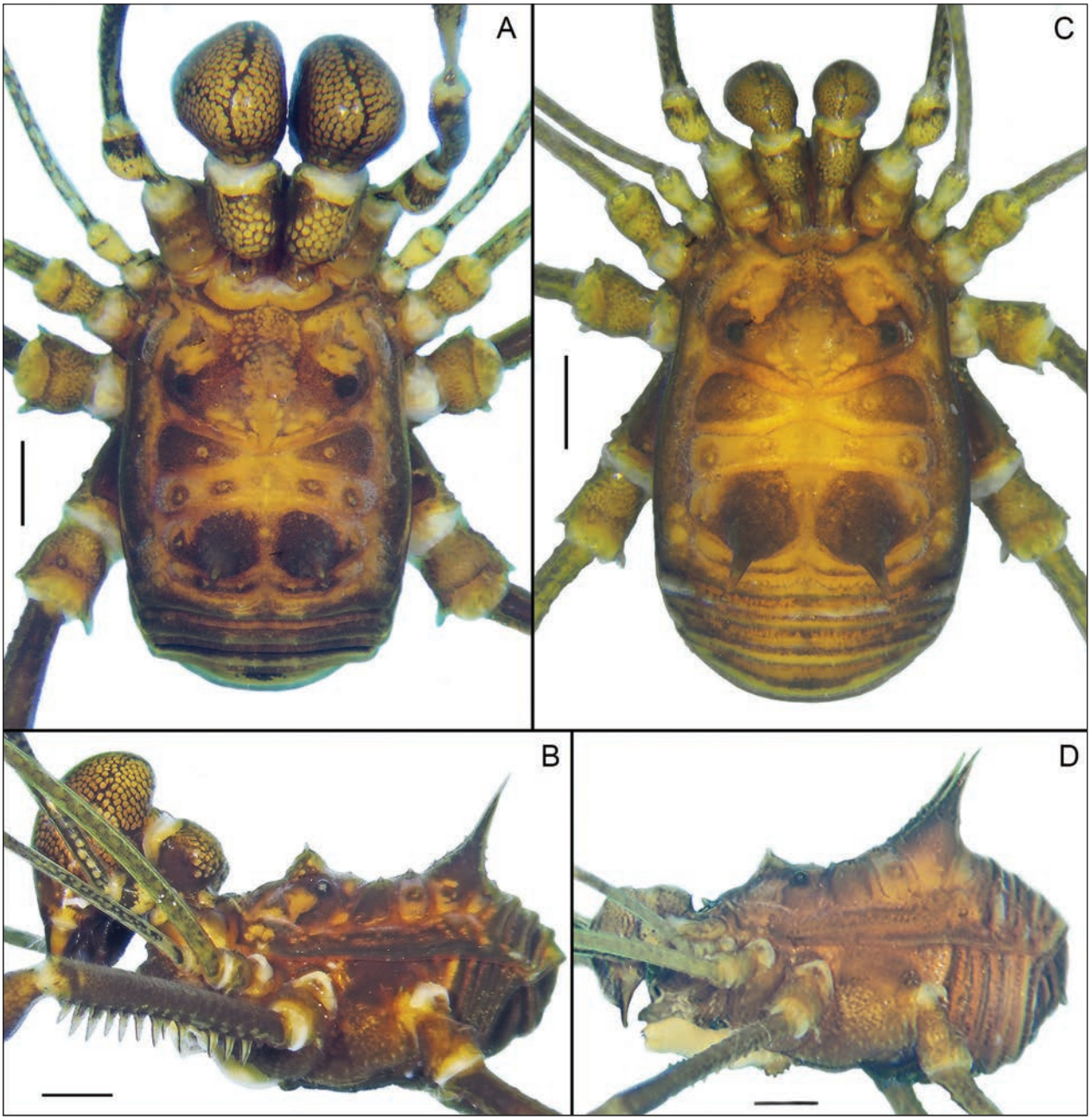

Figure 4. *Eutimesius aroa* sp. nov., **A, B.** Male habitus, dorsal and lateral views (MIZA 0105934); **C, D.** Female habitus, dorsal view (MIZA 0105936); **C.** Male habitus, lateral view (MIZA 0105934). Scale bars: 1 mm.

the anterolateral zone of the carapace, lateral areas of the II and III areas, and part of the lateral margins of the dorsal shield (Figs 4 A, C, 5 A, B), and by the ornamentation of the male femur IV, with large tubercles on both complete ventral rows (Fig. 5 G).

Etymology. The species is named in reference to the Sierra de Aroa, the mountain range in which it inhabits. Aroa is a Chibcha word believed to have a meaning associated with the jaguar, or "tigre." Noun in apposition.

Description. Male. ***Measurements.*** DSL 4.0; DSW 3.5; AL 1.9; AW 2.7; IOD 2.0; pedipalp: CoPp 0.8, TrPp 1.1, FePp 3.8, PaPp 1.8, TiPp 2.4, TaPp 2.2, ClPp 1.8; total 13.9; leg IV: FeL 7.2, TiL 3.9. ***Dorsum*** (Figs 4A, C, 5A, B). DS outline Epsilon type. Anterior margin of DS with 1–2 anterolateral tubercles. Anteromedial process of the cheliceral sockets shorter than lateral processes. Eyes separated into two small smooth mounds, placed posteriorly on the carapace. Interocular region with small granules in the posterior zone and one central elevated mound that terminates in two short spines. Lateral margins smooth. Mesotergum divided into four areas, III–IV partially fused: I divided medially into two triangular halves, with one conspicuous tubercle on each side; II entire, with four conspicuous tubercles; III with a lateral pair of large tubercles; one pair of paramedian large spines with granulated base; IV with some granules and one row of four tubercles, two each side. Posterior margin and free tergites with a pair of paramedian acute granules. ***Venter*** (Figs 4C, 5B). Coxa I with four distal tubercles and a medial row of six tubercles; II with a median row of seven-eight tubercules and a posterior row of two-three small tubercles; III with six intercoxal tubercles, five distal, two anterior, six medial, five posterior tubercles; IV with eight intercoxal tubercles, six anterior tubercles, nine medial tubercles, and about 12 posterior tubercles not aligned. Genital operculum with scattered granules. Stigmatic area with two anterior tubercles, a medial row of four tubercles, and a posterior row of minute granules on the posterior border. Free sternites with a row of small granules. ***Chelicerae*** (Fig. 5A–C). Segment I smooth with well-defined bulla, with one or two ectoproximal tubercles and one ectodistal tubercle. Segment II swollen, fixed finger with a proximal wide laminar tooth, followed by two very small denticles and three decreasing medial teeth; mobile finger with one subproximal large truncated tooth,one medial pyramidal tooth, and two small subdistal teeth. ***Pedipalps*** (Fig. 5D, E). Coxa with a group of eight ventral tubercles and three-four dorsal tubercles. Trochanter with a large ventral tubercle and two-three dorsal tubercles. Femur with a ventral row of six small tubercles and dorsally smooth. Patella smooth, distally swollen. Tibia dorsal smooth, ventrally with a row of minute granules; mesal IIiIi; ectal IiIiI. Tarsus dorsally smooth, ventrally with two rows of minute granules, mesal IiIiIi; ectal iIiiIii. ***Legs*** (Fig. 5F–I). Coxae I–II with two dorsal tubercles; III–IV connected by four–five intercoxal tubercles; IV with one dorsodistal large tubercle and scattered small granules and tubercles. Trochanter I dorsally smooth, ventrally with three tubercles; II with two dorsal, one retrodistal, and three ventral tubercles; III with one prolateral, two-four dorsal, one retrodorsal large, and five ventral tubercles; IV with one prolateral, one dorsal, and some minute dorsal granules; one retrolateral large tubercle; and eight ventral tubercles. Femora I–II with longitudinal rows of minute granules; III and IV with the one proventral and one retroventral row of large and spaced apart tubercles; and with two dorsoapical tubercles. Patella III–IV each with one large proventral tubercle; IV

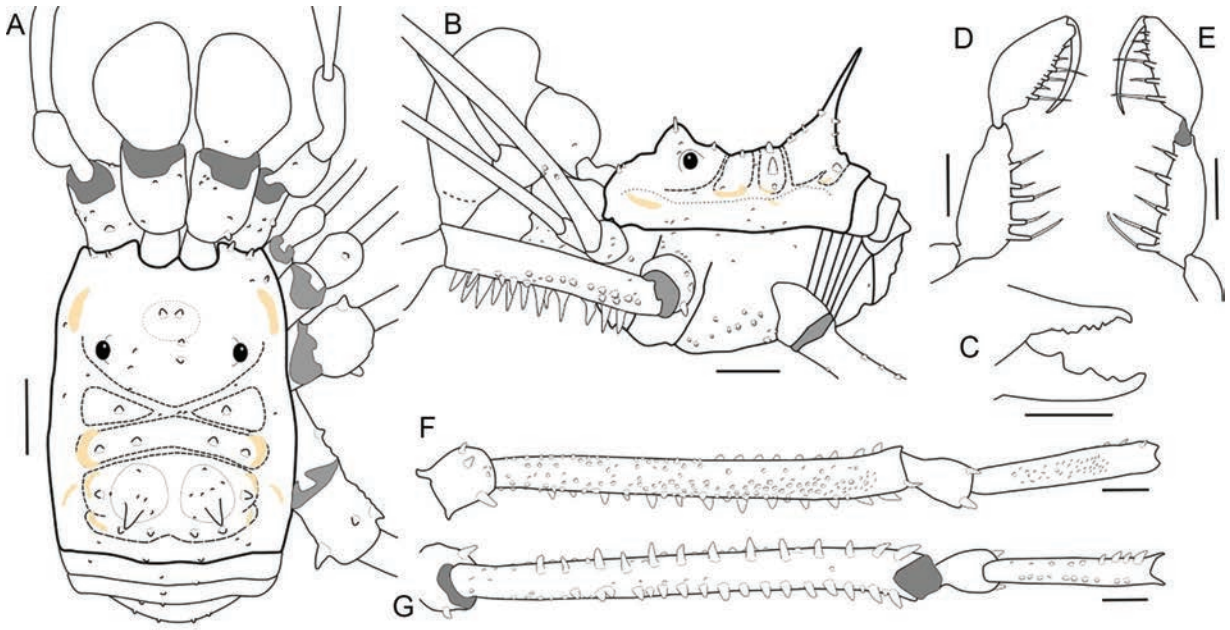

Figure 5. *Eutimesius aroa* sp. nov., male (MIZA 0105934): **A.** Habitus, dorsal view; **B.** Ditto, lateral view; **C.** Right chelicera, frontal view; **D.** Right pedipalp, tibia, and tarsus, ectal view; **E.** Ditto, mesal view; **F.** Right leg IV, dorsal view; **G.** Ditto, ventral view. Scale bars: 1 mm.

with pro and retrodorsal distal large tubercles and with sparse minute granules. Tibia III, with the tubercles of the distal portion of the proventral row enlarged and all the retroventral row with large tubercles increasing in size distally; IV with similar pattern but more conspicuous. Basitarsus I slightly swollen. Tarsal process and scopula present. Tarsal claws III and IV opposites and pectinated. Tarsal counts: 7(3)/19(br)-22(3)/8/9. ***Penis*** (Fig. 14A–C). Heterostygninae general pattern, as described in Villarreal et al. (2019b). Truncus with the malleus swollen. *Lamina parva* (LP) with a shallow neck and a deep distal cleft. MS-A1-A2 located on the malleus, one pair laterally and one pair more ventrally; MS-B pair ventrally located on the LP; two pairs of MS-C located medially on the LP, dorsally to the neck; MS-D1 large, located slightly proximal to MS-E; MS-D2 basally located, near the base of the gland; MS-E with only one pair of short setae. Gland globose, with short and dorsally curved stylus with small dorsal process. ***Color*** (Fig. 4A, C). DS mottled on background brilliant yellow (83). Spots on the carapace moderate brown (58); area I, bases of tubercles of area II; tubercles of area III and margins of DS; free tergites and coxae I–IV dorsally dark grayish brown (62) and blackish red (21). Trochanters I–IV and chelicerae reticulated in the same colors as DS. Femora I–II reticulated dark grayish olive (111) on background moderate yellow green (120); III and IV dark grayish olive (111).

Female. ***Measurements*****.** Dorsal scutum length 4.1; dorsal scutum width 3.4; abdominal scutum length 1.8; abdominal scutum width 2.8; interocular distance 1.7; pedipalp: coxa 0.6, trochanter 0.8, femur 3.9, patella 1.6, tibia 2.0, tarsus 2.2, claw 1.7; total 12.8; leg IV: femur 7.3, tibia 3.9. ***Description*** (Fig. 4B). Similar to male, except by abdominal scutum Eta type; chelicerae not swollen; ornamentation of leg IV conspicuously less developed; basitarsus I not swollen.

Distribution. Venezuela, Yaracuy. Only known from the type locality (Fig. 2).

Eutimesius canoabo **Villarreal & Ahumada-C., sp. nov.**

https://zoobank.org/D9A7D2ED-CF81-4446-B721-B4402141826B

Figs 6–8, 14D–F, 2

Type material. Venezuela • ♂ ***holotype***; Carabobo, El Santuario, Posada Ecológica Casa María, near Canoabo, (10.3132°N, 68.2232°W); 1,220 m a.s.l.; 19 Mar. 2008; (Villarreal O., Pereira M.P. leg.); on vegetation abbott 1.5–2 m above the ground (MIZA 0105945). ***Paratypes*** • 2 ♀, 1 ♂; same as the holotype; (MIZA 0105946).

Diagnosis. It is distinguishable from all other species in the genus by the pattern of dry white spots, occupying lateral zones of the scutal areas II and III, the medial zone of the scutal areas I and II, dispersal spots on the medial zone of the carapace, and part of the lateral margins of the dorsal scutum (Figs 6A, B, 7A, 8A); and by the ornamentation of the male femur IV, with large tubercles on both complete ventral rows (Fig. 7G).

Etymology. Canoabo is an indigenous word of Arawako origin that means “village next to fresh water.” The species name refers to the type locality, a forest near Canoabo, a town and river of the Cordillera de la Costa in Carabobo State, Venezuela.

Description. Male. ***Measurements*****.** DSL 3.4; DSW 3.1; AL 1.8; AW 3.1; IOD 1.9; pedipalp: CoPp 0.5, TrPp 0.9, FePp 3.3, PaPp 1.5, TiPp 1.2, TaPp 1.1, ClPp 1.1; total 9.6; leg IV: FeL 7.4, TiL 3.6. ***Dorsum*** (Figs 6A, 7A, 8A, C). DS outline Epsilon type. Anterior margin of DS with two anterolateral tubercles. Anteromedial process of the cheliceral sockets shorter than lateral processes. Eyes separated into two small smooth mounds, placed posteriorly on the carapace. Interocular region with one central elevated mound with small granules that terminates in four short spines. Lateral margins smooth. Mesotergum divided into four areas, III–IV fused: I divided medially into two triangular halves, with one conspicuous tubercle on each side; II entire, with four conspicuous tubercles; III–IV with a lateral pair of large tubercles; one pair of paramedian large spines with granulated base, with two posterior tubercles. Posterior margin and free tergites smooth, with a pair of paramedian acute granules. ***Venter*** (Figs 6B, 7B). Coxa I with a cluster of three mesal granules and about 7–8 dispersed granules; II with five intercoxal tubercles, with a median row of eight tubercles and two distal tubercles; III with five-six intercoxal tubercles, 14–15 six tubercles, medially aligned and distally irregularly distributed; IV with seven anterior tubercles and about 18–19 posterior tubercles not aligned. Genital operculum with scattered granules. Stigmatic area with a posterior row of minute granules on the posterior border. Free sternites with a row of small granules. ***Chelicerae*** (Figs 6A, B, 7A–C). Segment I smooth with well-defined bulla, with three or four ectoproximal tubercles and one ectodistal tubercle. Segment II swollen, fixed finger with a proximal wide laminar tooth, followed by one medial tooth and one small denticle subdistal; mobile finger with one subproximal large truncated tooth,one medial pyramidal tooth, and two small subdistal teeth. ***Pedipalps*** (Fig. 7D, E). Coxa with a group of about nine ventral tubercles and three dorsal tubercles. Trochanter with two ventral tubercles and two dorsal tubercles. Femur with a ventroectal row of six-eight small granules and one-two ventromesal granules, and dorsally with a row of minute granules. Patella smooth, distally swollen. Tibia dorsal smooth, ventrally with some proximal minute granules; mesal IIiIi; ectal IIiIii. Tarsus dorsally smooth, ventrally with two rows of minute granules, mesal IiIiIi; ectal iiIiiiIii. ***Legs*** (Fig. 7F, G). Coxae I–II with two dorsal tubercles; III–IV connected by one intercoxal tubercle; IV with four dorsodistal tubercles and scattered small lateral granules and tubercles. Trochanter I dorsally smooth, ventrally with three tubercles; II with one dorsal and three ventral tubercles; III with one retrolateral and five ventral tubercles; IV with one prolateral and one retrolateral tubercle and seven ventral tubercles. Femora I–II smooth; III with longitudinal rows of tubercles and granules, the ventrodistal larger,

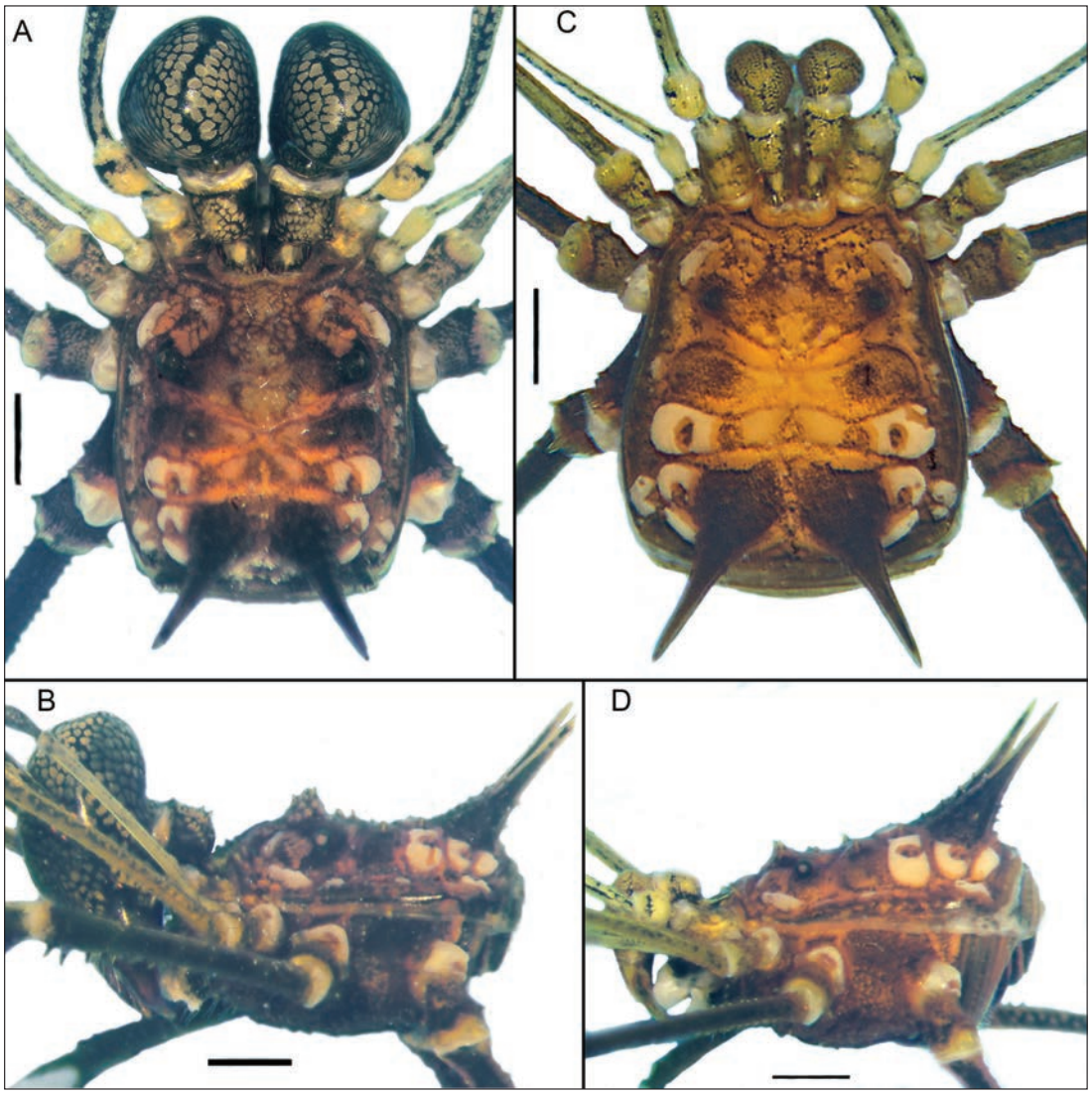

Figure 6. *Eutimesius canoabo* sp. nov., **A, B.** Male habitus, dorsal and lateral views (MIZA 0105945); **C, D.** Female habitus, dorsal view (MIZA 0105946). Scale bars: 1 mm.

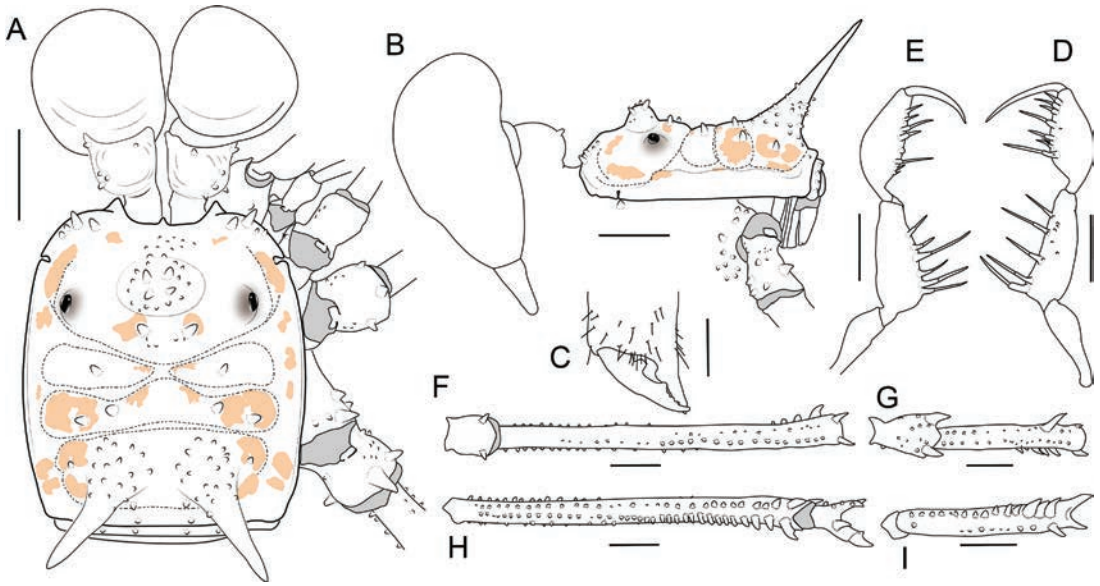

Figure 7. *Eutimesius canoabo* sp. nov., male (MIZA 0105945): **A.** Habitus, dorsal view; **B.** Ditto, lateral view; **C.** Right chelicera, frontal view; **D.** Right pedipalp, tibia, and tarsus, ectal view; **E.** Ditto, mesal view; **F.** Right leg IV, dorsal view; **G.** Ditto, ventral view. Scale bars: 1 mm.

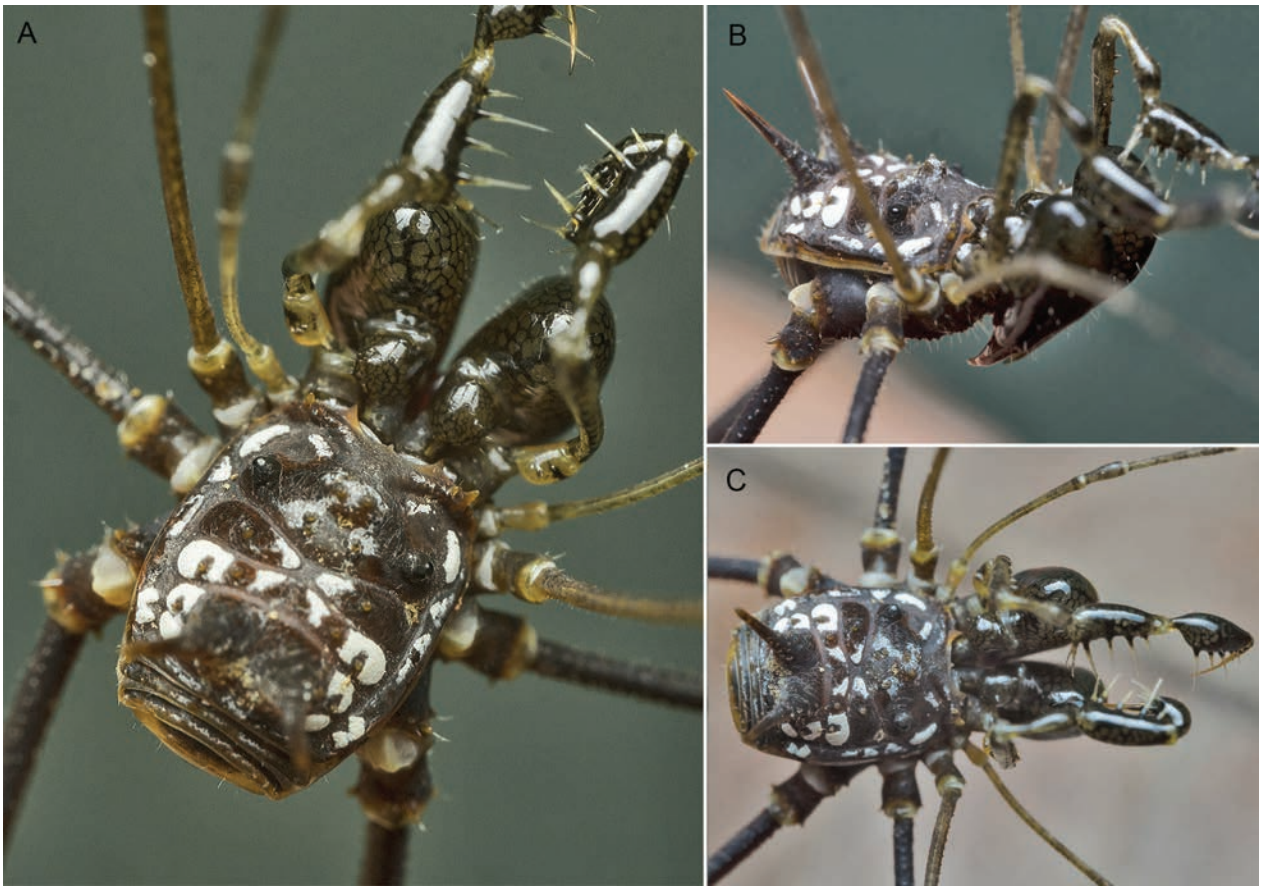

Figure 8. *Eutimesius canoabo* sp. nov. **A–C.** From Carabobo State, Venezuela.

and one retrodorsal distal large tubercle; IV with the one proventral and one retroventral rows of tubercles increasing in size distally, and with two dorsoapical tubercles. Patella III dorsally granulated and with a proventral tubercle; IV with one large ventral tubercle; and pro and retrodorsal distal large tubercles and with sparse minute granules. Tibia III slightly increased distally, with two rows of ventral granules in the distal portion; IV with the proventral row of tubercles increasing in size distally; and retrovental row of tubercles, with the distal-most tubercle larger than the others. Basitarsus I slightly swollen. Tarsal process and scopula present. Tarsal claws III and IV opposites and pectinated. Tarsal counts: 7(2)-7(3)/19(3)-18(3)/8/9-10. ***Penis*** (Fig. 14D–F). Heterostygninae general pattern, as described in Villarreal et al. (2019b). Truncus with the malleus swollen. *Lamina parva* (LP) with a shallow neck and a deep distal cleft. MS-A1-A2 located on the malleus, one pair laterally and one pair more ventrally, with duplication in the more ventral on the left side; MS-B pair ventrally located, distally to the MS-A; two pairs of MS-C located medially on the LP, dorsally to the neck; MS-D1 located slightly proximal to between MS-E and MS-C; MS-D2 basally located, near the base of the gland; MS-E with only one pair of short setae visible. Gland globose, with short and dorsally curved stylus with inconspicuous dorsal process. ***Color*** (Figs 6, 8). DS mottled on dark yellowish brown (78). Spots on the carapace Brilliant orange (49); tubercles of area I–IV; margins of DS; margins of free tergites; and edge of coxae I–IV; dorsally light olive brown (94). Trochanters I–IV, with the same colors as DS. Femora I–II reticulated dark yellowish brown (78) on a background of light olive brown (94); III–IV with the same colors as DS. Chelicerae reticulated in the same colors as DS.

Female. ***Measurements*****.** Dorsal scutum length 3.9; dorsal scutum width 3.5; abdominal scutum length 1.9; abdominal scutum width 2.9; interocular distance 1.5; pedipalp: coxa 0.8, trochanter 0.7, femur 2.8, patella 1.2, tibia 1.8, tarsus 1.6, claw 1.3; total 10.2; leg IV: femur 8.0, tibia 3.4. ***Description*** (Fig. 6C, D). Similar to male, except by abdominal scutum Epsilon type; chelicerae not swollen; interocular projection lower and slightly forward; ornamentation of leg IV conspicuously less developed; basitarsus I not swollen. Chelicerae and legs lighter.

Distribution. Venezuela, Yaracuy. Only known from the type locality (Fig. 2).

Eutimesius ephippiatus (Roewer, 1915)

Figs 9, 10, 14G–I, 2

Dichobunistygnus ephippiatus Roewer C-F, (1915): 105, figs 57a–b.
Eutimesius ephippiatus: Pinto-da-Rocha (1997): 187, figs 54–56.

Material examined. Colombia • 1 ♂, 1 ♀; Boyacá (New department record), Santa María, sendero Hyca Quye, 5.5 km NW from Santa María, forest edge roadside; (4.89811°N, 73.29344°W); Ago. 2016; (Rodríguez, C. leg.)

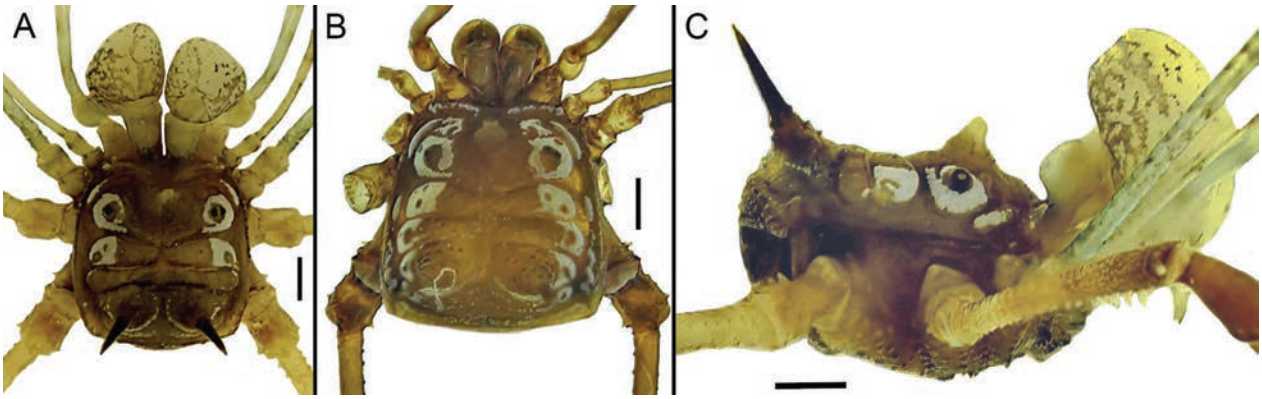

Figure 9. *Eutimesius ephippiatus*: **A.** Male habitus, dorsal view (ICN-Ao-1492); **B.** Female habitus, dorsal view (ICN-Ao-18); **C.** Male habitus, lateral view (ICN-Ao-1492). Scale bars: 1 mm.

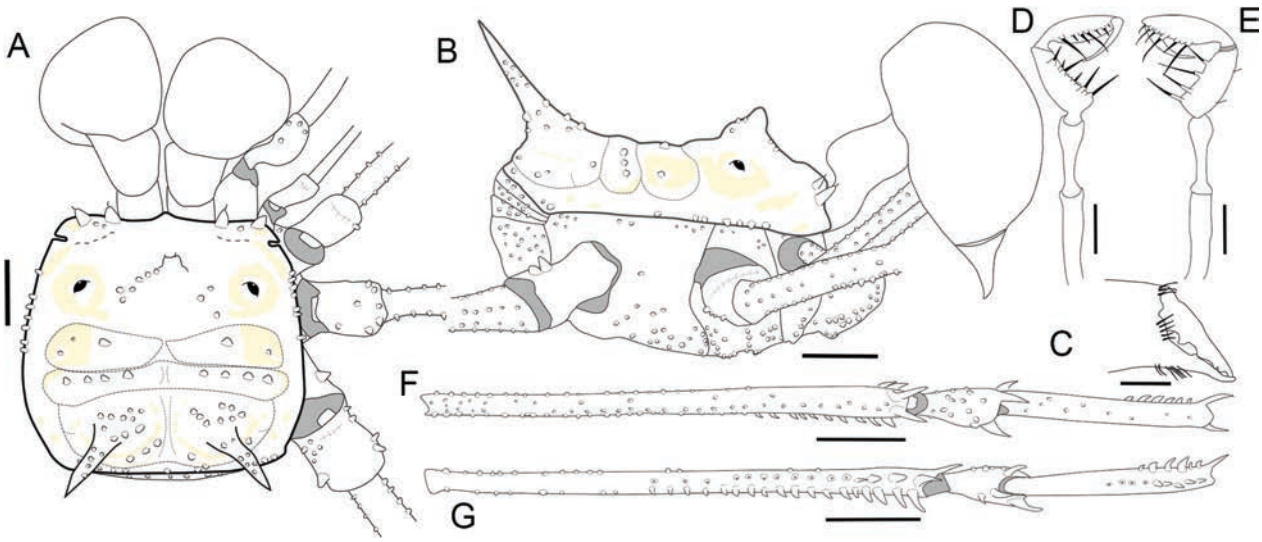

Figure 10. *Eutimesius ephippiatus* male (ICN-Ao-18): **A.** Habitus, dorsal view; **B.** Ditto, lateral view; **C.** Right chelicera, frontal view; **D.** Right pedipalp, tibia, and tarsus, ectal view; **E.** Ditto, mesal view; **F.** Right leg IV, dorsal view; **G.** Ditto, ventral view. Scale bars: 1 mm.

(MPUJ_ENT 004 8876). • 1 ♂, Boyacá, Santa María, Quebrada La Argentina, forest edge, 0.5 km SSW from Santa María; (4.85673°N, 73.26375°W); manual capture; 850 m a.s.l.; Ago-Sep. 2015; (Guzmán, K. leg.) (MPUJ_ENT 0039466). • 1 ♀; Casanare (new department record), Agua Azul; [5.1866°N, 72.5558°W]; 14 Oct. 1978; (La Rotta, C. leg.) (ICN-Ao-18). • 1 ♀; Cundinamarca, Ubalá, Ubalá B., Inspección San Pedro de Jágua, left bank of the Rio Zaquea; [4.7133°N, 73.3016°W]; 500 m a.s.l.; manual capture; Apr. 1998; (Rodríguez, V., Sierra, S., Flórez, E., Varón, A. leg.) (ICN-Ao-1491). • 1 ♂; Cundinamarca, Ubalá, Ubalá B., Inspección Mambita, Vda. Boca de Monte, surroundings Boca de Monte school; (4.7430°N, 73.3016°W); 1,000 m a.s.l.; manual capture; Apr. 1998; (Rodríguez, V., Sierra, S., Flórez, E., Varón, A. leg.) (ICN-Ao-1492). • 1 ♀; Cundinamarca, Ubalá, Ubalá B., Inspección San Pedro de Jágua, Vda. Soya, left bank of the Rio Zaquea; (4.7133°N, 73.3392°W); 500 m a.s.l.; manual capture; Apr. 1998; (Rodríguez, V., Sierra, S., Flórez, E., Varón, A. leg.) (ICN-Ao-1511).

Diagnosis. It is distinguishable from all other species in the genus by the pattern of dry white spots that encircled completely the eyes (Figs 9, 10A, B), and the proximal half of femora and tibiae IV without tubercles or with only minute granules (Figs 10F, G).

Complementary description. Male. ***Measurements.*** DSL: 1.4; DSW: 2.8; AL: 1.7; AW: 3.0; IOD: 1.6; pedipalp: CoPp 0.7, TrPp 0.7, FePp 2.9, PaPp 1.3, TiPp 1.5, TaPp 1.3, ClPp 0.8; total 9.2; Leg IV: FeL 7.6, TiL 2.6. ***Dorsum*** (Figs 9A, C, 10A, B). DS outline Epsilon type. Anterior margin of DS with four anterolateral large tubercles. Anteromedial and lateral process of the cheliceral sockets short. Eyes separated into two small smooth mounds, placed slightly posteriorly on the carapace. Interocular region with small granules and one central elevated and irregular mound that terminates in two short tubercles. Lateral margins with a row of seven tubercles. Mesotergum divided into four areas, III–IV mostly fused: I divided medially into two oval halves, with one conspicuous tubercle on each side and some lateral granules; two entire, with seven-eight conspicuous tubercles; III/IV with one pair of paramedian very large spines projected backward (three times the length of the interocular eminence); and granulated, posterior region with

a row of small granules. Posterior margin smooth, free tergites with a row of small granules. Anal operculum and sternites with small granules. ***Venter*** (Figs 9C, 10B). Coxa I with three distal tubercles and a medial row of five tubercles; II with three distal tubercles, a median row of nine tubercles, and a posterior row of three-five small tubercles; III with three distal tubercles, three-five anterior, eight medial, and five posterior tubercles; IV with four intercoxal tubercles, one median row with eight tubercles aligned, some scattered anterior tubercles, and about eight-ten posterior tubercles aligned. Genital operculum and stigmatic area with scattered granules. Free sternites with a row of small granules. ***Chelicerae*** (Figs 9A, C, 10A–C). Segment I smooth with well-defined bulla with tiny granules. Segment II swollen. Fixed finger with one medial tooth, mobile finger with one sub-proximal large tooth, one medial large tooth and two small subdistal teeth. ***Pedipalps*** (Figs 9A, 10A, D, F). Coxa with some granules. Trochanter with three dorsodistal tubercles and one dorsal tubercle in the medial position, ventrally with some minute granules. Femur and patella dorsally and ventrally, with some scattered granules. Patella distally swollen. Tibia dorsal with some minute granules, ventrally with a row of minute granules, mesal IIII, ectal IIiIiI. Tarsus dorsally and ventrally smooth; mesal IiIiIi, ectal IiiIiii. ***Legs*** (Figs 9A, C, 10A, B, F, G). Coxae I–III unarmed, IV with one large prodorsal tubercle in medial position. Trochanter II with one dorsodistal tubercle, III–IV ventrally granulated, III with one row of 4–5 dorsodistal tubercles and one row of four proventral tubercles, IV with 4–5 prodorsal tubercles (the two distalmost larger), one large retrodorsal sub-distal tubercle, and a group of small prodorsal proximal tubercles. Femora I–II with longitudinal rows of granules dorsally and ventrally, III with one prodorsal distal conical tubercle and ventral row of conical tubercles increasing in size distally, IV with one prolateral and one retrolateral row of small tubercles, dorsally with two distal conical tubercles, and ventrally with two longitudinal rows of conical tubercles increasing in size distally. Patellae III–IV granulated, IV dorsally tuberculated, with one retrodorsal distal conical tubercle, one retroventral row of tubercles (the distalmost larger), two conical ventral tubercles in medial portion (the distalmost larger), and one proventral conical tubercle in distal portion. Tibia III with some granules, IV with one large retrodorsal distal tubercle and some scattered granules and small tubercles, two ventral rows of tubercles. Tarsal claws III and IV opposites and pectinated. Tarsal counts:7(3)-7(3)/17-19 /9-10/9-9. ***Penis*** (Fig. 14G–I). Heterostygninae general pattern. Malleus swollen. LP with a shallow neck and a deep distal cleft. MS-A located on the malleus, two pair dorsally and one pair more ventrally; MS-B pair located ventrally; MS-C pair located medially on the LP, distally to the neck; MS-D1 large, located sligthly proximal to MS-E; MS-D2 located basally, near the base of the glans; MS-E apparently with only one pair of setae visible. Glans globose, with short and dorsally curved stylus with small dorsal process. ***Color*** (Fig. 9 A, C). DS, and free tergites Dark orange yellow (72). Spots on carapace and mesotergum Vivid orange yellow (66). Pair of paramedian spines in area III Brownish black (65). Free sternites Dark yellowish brown (78). Chelicerae reticulated and pedipalps Light greenish yellow (101). Coxae I–IV and trochanters I–IV brilliant yellow (83), Femora I–II reticulated light greenish yellow (101), and III and VI brilliant yellow (83).

Female. ***Measurements*****.** DSL: 1.2–1.5; DSW: 2.5–3.2; AL: 1.5–2.2; AW: 2.9–3.5; IOD: 1.3–1.7; pedipalp: CoPp 0.4–0.8, TrPp 0.5–0.6, FePp 1.9–2.6, PaPp 1.0–1.4, TiPp 0.8–1.4, TaPp 0.8–1.3, ClPp 0.7–0-9, total 4.3–8.0; Leg IV: FeL 6.2–8.2, TiL 3.4–4.1. ***Description of female*** (Fig. 9B). Similar to male, except by abdominal scutum wider posteriorly; spots on area II, anterior and lateral margins; chelicerae not swollen; ornamentation of leg IV conspicuously less developed; basitarsus I not swollen. Chelicerae dark yellow (88), pedipalps, trochanters I–III, and femora I–III strong yellow (84), Trochanter IV strong yellowish brown (74), and femur IV strong yellow (84).

Distribution. Colombia, Casanare, Cundinamarca, Quindio (Fig. 2).

Eutimesius guaichia Villarreal & Ahumada-C., sp. nov.

https://zoobank.org/DCF81C07-BF22-4862-B864-F852AB35F806

Figs 11, 12, 14 J–L, 2

Type material. ***Holotype*****.** Venezuela • ♂, Yaracuy, road Cocorote - Aroa, sector Las Cumaraguas; (10.3520°N, 68.8298°W); 1,200 m a.s.l.; 09 Mar. 2008; (Villarreal O., Escalona H., Jayaro Y., Viera E. leg.) (MIZA 0105935). ***Paratype*****.** • 1 ♀, same as the holotype (MIZA 0105935).

Diagnosis. It can be distinguished from other congeneric species by the pattern of dry white spots occupying the anterolateral zone of the carapace, the posterior zone of the eyes, and the lateroposterior corner of the DS (Figs 11A, B, 12A, B) and by the shape and ornamentation of the leg IV of the males: femur with a subdistal dorsal group of conspicuous tubercles, patella inflated, dorsal face densely tuberculated with two large curve distal spines like horns, and tibia swollen, dorsally almost smooth, with the prolateral face densely tuberculated, with the retrolateral row with numerous contiguous large tubercles and the retrodorsal row with distal tubercles larger (Fig. 12F, G).

Etymology. The species is named after Guaichía, another name given to María Lionza, a female deity belonging to Venezuelan spiritism, which originates from the state of Yaracuy, where the species inhabits. The myth of María Lionza has been interpreted as a symbol of the biological and cultural mestizaje, or intermixing, that characterizes Venezuela. It expresses the Indigenous, European, and African roots that comprise the cultural diversity of Venezuela. This is a noun in apposition.

Description. Male. ***Measurements*****.** DSL: 4.4; DSW: 3.7; AL: 1.8; AW: 3.0; IOD: 2.4; pedipalp: CoPp 0.7, TrPp 0.9, FePp 3.3, PaPp 1.3, TiPp 1.8, TaPp 1.7, ClPp 1.3,

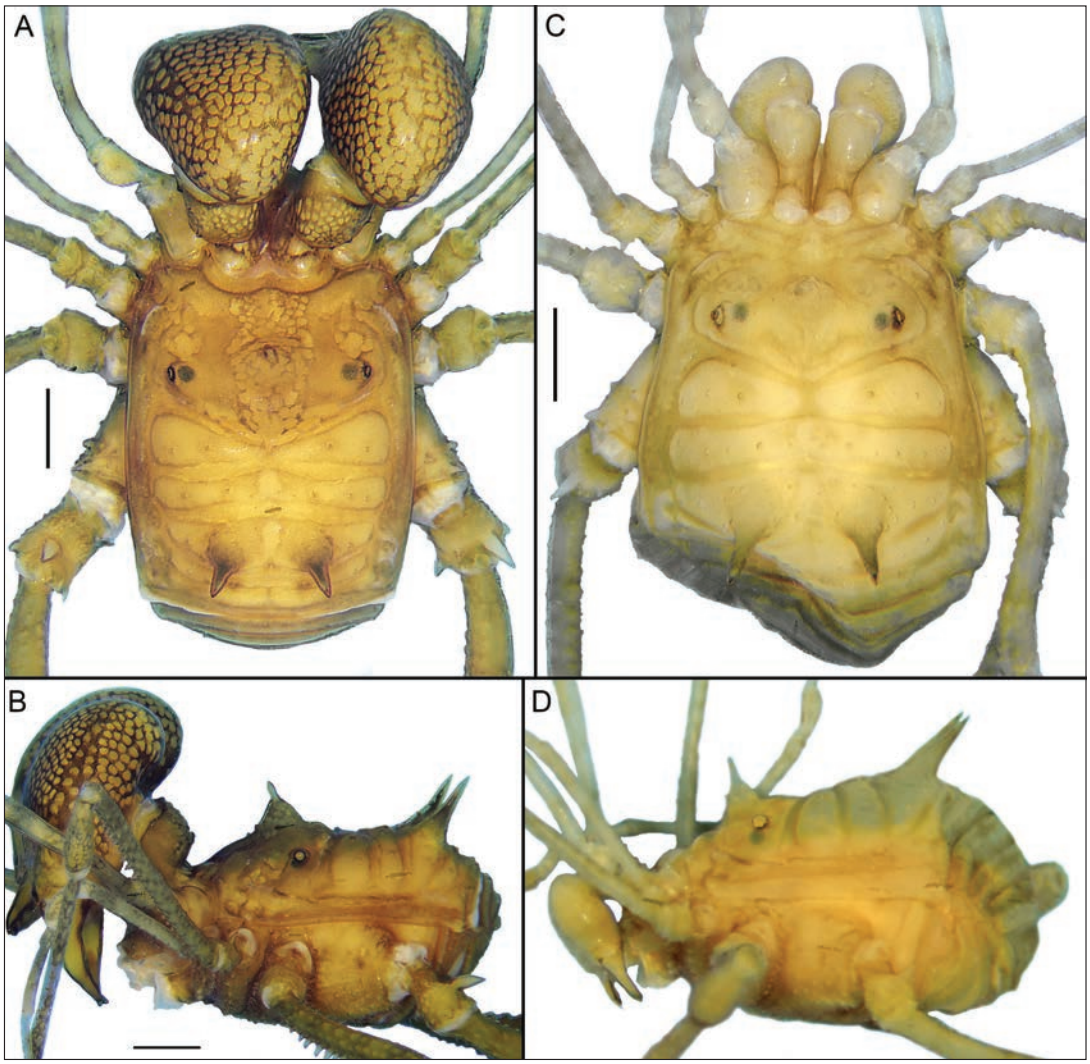

Figure 11. *Eutimesius guaichia* sp. nov., **A, B.** Male habitus, dorsal and lateral views (MIZA 0105935); **C, D.** Female habitus, dorsal and lateral views (MIZA 0105935). Scale bars: 1 mm.

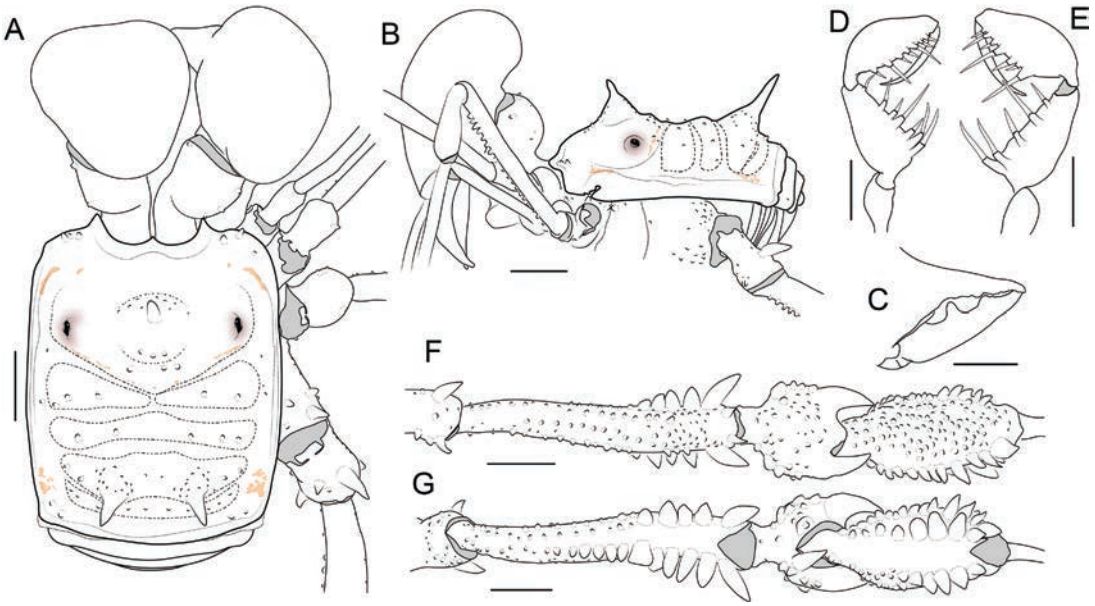

Figure 12. *Eutimesius guaichia* sp. nov., male (MIZA 0105935): **A.** Habitus, dorsal view; **B.** Ditto, lateral view; **C.** Right chelicera, frontal view; **D.** Right pedipalp, tibia, and tarsus, ectal view; **E.** Ditto, mesal view; **F.** Right leg IV, dorsal view; **G.** Ditto, ventral view. Scale bars: 1 mm.

total 11.0; Leg IV: FeL 4.2, TiL 2.7. ***Dorsum*** (Figs 11A, B, 12A, B). DS outline Epsilon type. Anterior margin of DS with two anterolateral tubercles on each side. Anteromedial process of the cheliceral sockets shorter than lateral processes. Eyes separated into two small smooth mounds, placed slightly posterior on the carapace. Interocular region with some anteromedial granules, with one central elevated eminence that terminates in one spine. Lateral margins smooth. Mesotergum divided into four well-delimited areas: I divided medially into two triangular halves, with three tubercles on each side; II entire, with 3–4 conspicuous tubercles; III with a lateral pair of tubercles; one pair of paramedian large spines with granulated base; IV with a row of 10 tubercles. Posterior margin and free tergites with a row of granules. ***Venter*** (Figs 11B, 12B). Coxa I with three distal tubercles and some tubercles irregularly distributed; II with three clearly separate rows of tubercles/granules, six anterior, eight medial and larger, and four posterodistal; III with six intercoxal tubercles, one mesodistal wide tubercle, and three rows of granules; IV with eight intercoxal tubercles and densely tuberculated, the distal larger; the prolateral face anteriorly smooth; and posteriorly with seven conspicuous tubercles. Genital operculum with scattered granules. Stigmatic area with scattered granules in the anterior zone and with two rows of granules on the posterior zone. Free sternites with a row of small granules. ***Chelicerae*** (Fig. 11A, B, 12A–C). Segment I smooth with well-defined bulla, with two or three small ectal tubercles and one mesodistal small tubercle. Segment II very swollen; fixed finger irregularly dentated; mobile finger with one medial large tooth and one subdistal tooth; the apical part finely serrated. ***Pedipalps*** (Figs 11A, 12D, E). Coxa with a group of 6–7 ventral tubercles and one dorsal tubercle. Trochanter with two ventral tubercles and one dorsal tubercle. Femur with one ventroproximal tubercle and dorsally smooth. Patella smooth, distally swollen. Tibia dorsal smooth, ventrally with a group of small granules; mesal IIiIi; ectal IIiIiIi. Tarsus dorsally smooth, ventrally with two rows of minute granules, mesal IiiIiIi; ectal iIiiIii. ***Legs*** (Figs 11A, B, 12F, G). Coxae I with two dorsal tubercles; II with one tubercle; III–IV connected by two-three intercoxal tubercles; IV with one dorsodistal large tubercle and scattered tubercles. Trochanter I with one dorsal granule, ventrally with four tubercles; II with one large dorsal, two retrolateral and ventrally tuberculated; III with one large prolateral distal, three dorsal, two retrodorsal, and ventrally tuberculated; IV with one prolateral large and some granules, two dorsal, the prodorsal very large, one retrolateral distal, and densely tuberculated ventrally. Femora I–II with longitudinal rows of minute granules; III with the proventral y retroventral rows of large tubercles; and with two dorsoapical tubercles, the retrolateral large; IV curved and distally swollen, all the rows with large tubercles; the ventral rows with very large tubercles, especially the distal ones; and some dorsodistal tubercles. Patella III dorsally smooth, only with one prodistal tubercle, and ventrally with some minute granules and two distal tubercles, the proventral larger; IV with a petiolate base and circular shape in dorsal view, prolateral, dorsal, and retrolateral faces densely tuberculated, with two very large distal spiniform tubercles, and ventrally with two large curved tubercles, the proventral larger. Tibia III cylindrical and smooth, with only a retroventral row of about seven granules; IV enlarged, all rows with large tubercles, especially in the distal portion, and on proventral, rostroventral, and retrolateral rows. Basitarsus I slightly swollen. Tarsal process and scopula present. Tarsal claws III and IV opposite and pectinated. Tarsal counts: 6(3)/16(3)/8/9. ***Penis*** (Fig. 14J–L). Heterostygninae general pattern. Malleus swollen. *Lamina parva* (LP) almost as wide as it is long; the distal half triangular, with a well-marked neck and a circular distal cleft. MS-A1–2 located on malleus, one pair laterally and one pairs more ventrally; MS-B pair ventrally located on the truncus, supernumerary and asymmetric; two pairs of MS-C located medially on the LP, dorsally to the neck; MS-D1 and MS-D2 similar in size; MS-D1 located slightly proximal to MS-E; and MS-D2 basally located, near the base of glans; MS-E as one pair of short setae and one pair of large setae. Glans globose and wide, with a dorsally curved stylus with small triangular dorsal process. ***Color*** (Fig. 15A, B). DS background Brilliant orange yellow (67), carapace reticulated, lateral margins and spines of area III Dark orange yellow (72), abdominal scutum, and coxa I–IV dorsally Light greenish yellow (101), areas II and III with a medial zone lighter than lateral regions. Pale greenish yellow (104). Chelicerae reticulated dark olive (108) on background moderate greenish yellow (102). Legs reticulated dark grayish olive (111) on background moderate yellow green (120) to moderate greenish yellow (102).

Female. *Measurements*. DSL: 4.3; DSW: 3.8; AL: 2.1; AW: 3.1; IOD: 1.8; pedipalp: CoPp 0.7, TrPp 0.5, FePp 2.9, PaPp 1.4, TiPp 1.7, TaPp 1.8, ClPp 1.2, total 10.2; Leg IV: FeL 4.7, TiL 3.0. ***Description*** (Fig. 11C, D). Similar to male, except by the shape of DS, Eta (Fig. 11C), chelicerae not swollen. The mesotergal areas slightly larger in comparison to males. Basitarsus I not swollen. Legs III and IV without developed secondary sexual characteristics, only rows of granules or small tubercles. The female displays the same color pattern as the males, yet the hues are lighter in tone.

Distribution. Venezuela, Yaracuy. Only known for the type locality (Fig. 2).

Eutimesius ornatus (Roewer, 1943)

Fig. 2

Bunistygnellus ornatus Roewer, C.-F. (1943): 37, figs 37–37a.

Eutimesius ornatus: Pinto-da-Rocha (1997): 187, figs 57–64, 461–462, 597.

Remarks. *Eutimesius ornatus* (Roewer, 1943) was described from Bogotá, Colombia (Roewer 1943), and

recorded from Venezuela on a female specimen from the northeastern region of San Cristóbal in Táchira state (Pinto-da-Rocha 1997). However, this particular specimen exhibits clear discrepancies when compared to the male holotype (MCR-3862, SMFD, Pinto-da-Rocha 1997: figs 57, 58, 61, 63, 64), specifically in the pattern of white, dry spots and the size and shape of the spines in area III. While the pattern of white dry spots has displayed stability or minimal intraspecific variation in the specimens examined by us, for example, females with larger spots (Figs 5A, B, 9A, B), the pronounced aforementioned differences observed between the male and female of *E. ornatus* as depicted by Pinto-da-Rocha (1997), coupled with the geographical distance between both disjunct populations, raise the question regarding the identity of the female from Venezuela. *E. ornatus*", Therefore, we propose that the female from Venezuela represents an undescribed species distinct from *E. ornatus*.

Eutimesius simoni Roewer, 1913

Figs 13, 14 M–O, 2

Eutimesius simoni Roewer, C.-F. (1913): 453, figs 178.

Xanthostygnus fractus Mello-Leitão, C.F. (1949): 32.

Xanthostygnus fractus Mello-Leitão, 1949 is a junior subjective synonym of *Eutimesius simoni* Roewer, 1913 in Pinto-da-Rocha (1997): 190.

Eutimesius miles Henriksen, K.L. (1932): 293, fig. 10.

Eutimesius miles Sørensen, 1932, is a junior subjective synonym of *Eutimesius simoni* Roewer, 1913, in Pinto-da-Rocha (1997): 190.

Material examined. Colombia • 1 ♂; Amazonas (New department record), Leticia, Km 11 vía a Tarapacá; [4.1209°S, 69.9508°W]; (Animal systematics [students leg.]) (ICN-Ao-196). • 1 ♂; Amazonas, Leticia, Km 11 vía a Tarapacá; [4.1195°S, 69.9522°W]; 110 m a.s.l.; pitfall; 27 Oct. 2002; (Animal systematics II leg.) (ICN-Ao-512). • 1 ♂; Amazonas, Leticia, Km 11 vía a Tarapacá; [4.1195°S, 69.9522°W]; 11 Nov. 2001; (Students and Flórez, E. leg.) (ICN-Ao-328). • 1 ♀; Amazonas, Leticia, Km 11 vía a Tarapacá, Quebrada Yahuarcaca, Finca El Agape; [4.1348°S, 69.9436°W]; 100 m a.s.l.; pitfall; Mar. 2009; (Mojica, J.I. leg.) (ICN-Ao-641). • 1 ♀; Amazonas, Leticia, Monifue Amena; [4°6'54.45"S, 69°55'39.82"W]; 70 m a.s.l.; 06 Oct. 2005; (Hernandéz, C., Lozano, M., Otero, T. leg.) (MPUJ_ENT 0094626). • 1 ♂; Leticia, Monifue Amena; [4°6'54.45"S, 69°55'39.82"W]; 70 m a.s.l.; Oct 2005; (Cortes, Hernández, Lozano, Otero leg.) (MPUJ_ENT 0094638). • 1 ♀; Amazonas, Leticia, Monifue Amena; [4°6'54.45"S, 69°55'39.82"W]; 70 m a.s.l.; manual collection; 24 Mar. 2004; (Galindo, A. leg.) (MPUJ_ENT 0094635). • 1 ♀; Amazonas, Leticia, Monifue Amena; [4°6'54.45"S, 69°55'39.82"W]; 70 m a.s.l.; 06 Oct. 2005; (Trejos, C. et al. leg.) (MPUJ_ENT 0094636) • 1 ♀; Amazonas, Leticia, Monifue Amena; [4°6'54.45"S, 69°55'39.82"W]; 70 m a.s.l.; 30 Oct. 2005; (Rodríguez, G. et al. leg.) (MPUJ_ENT 0094623). • 1 ♀; Amazonas, Leticia, Monilla Amena; [4°6'54.45"S, 69°55'39.82"W]; 70 m a.s.l.; vegetation shake; 24 Mar. 2004; (Rodríguez, D. leg.) (MPUJ_ENT 0094643). • 1 ♀; Amazonas, Leticia, Monilla Amena, Várzea; [4°6'54.45"S, 69°55'39.82"W]; 70 m a.s.l.; vegetation shake; 05 Oct. 2005; (Escobar, L., Morales, A. leg.) (MPUJ_ENT 0094628) • 1 ♂; Amazonas, Leticia, Monifue Amena, Várzea; [4°6'54.45"S, 69°55'39.82"W]; 70 m a.s.l.; manual collection; 05 Oct. 2005; (Ardilla, Corredor, Echeverri leg.) (MPUJ_ENT 0094634). • 1 ♀; Amazonas, Leticia, Monifue Amena; [4°6'54.45"S, 69°55'39.82"W]; 70 m a.s.l.; vegetation shake; 04 Oct. 2005; (Ardila, Corredor, Echeverri leg.) (MPUJ_ENT 0094642). • 1 ♂; Amazonas, Leticia, Monifue Amena; [4°6'54.45"S, 69°55'39.82"W]; 70 m a.s.l.; vegetation shake; 24 Mar. 2004; (Moreno, N., Uribe, D. leg.) (MPUJ_ENT 0094630). • 1 ♂; Amazonas, Leticia, Monifue Amena, Várzea; [4°6'54.45"S, 69°55'39.82"W]; 70 m a.s.l.; vegetation shake; 30 Sep. 2004; (Salcedo, A., Charry, E., Jaramillo leg.) (MPUJ_ENT 0094637). • 1 ♀; Amazonas, Leticia, Comunidad Monilla Amena; [3°47'34.75"S, 69°52'13.88"W]; 70 m a.s.l.; vegetation shake; (Díaz, A., Arango, S., Sánchez, F. leg.) (MPUJ_ENT 0094625).

Diagnosis. Can be distinguished from all other species of the genus by the fusion of the paired spines of scutal area III (Fig. 13).

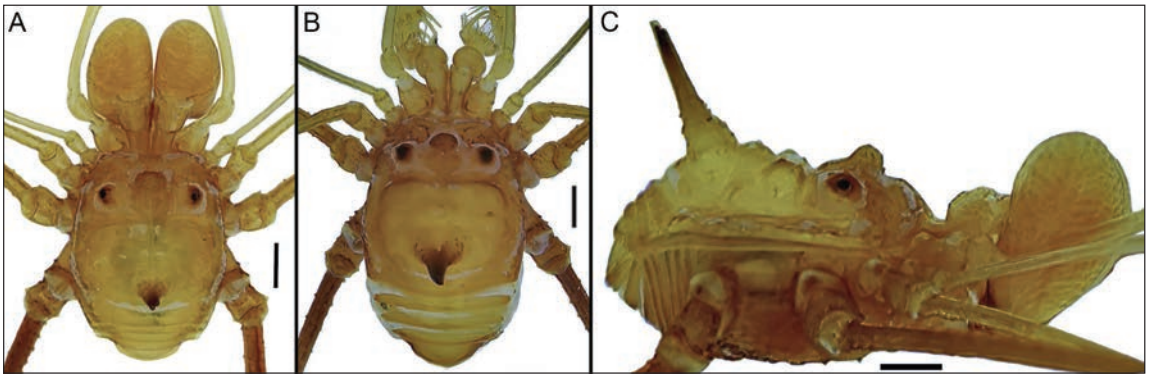

Figure 13. *Eutimesius simoni*: **A.** Male habitus, dorsal view (ICN-Ao-328); **B.** Female habitus, dorsal view (ICN-Ao-641); **C.** Male habitus, lateral view (ICN-Ao-328). Scale bars: 1 mm.

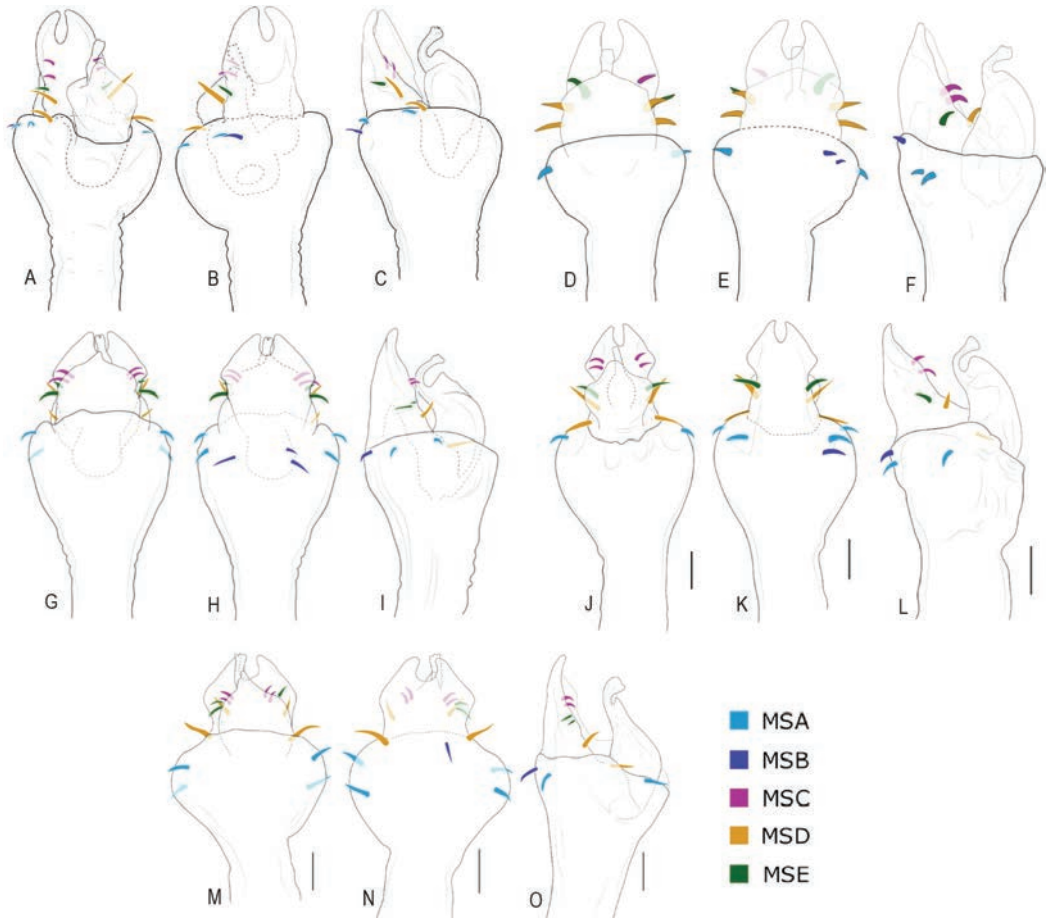

Figure 14. *Eutimesius* spp., penis, distal portion in dorsal, ventral, and lateral view: **A–C.** *E. aroa* sp. nov., (MIZA 0105934); **D–F.** *E. canoabo* sp. nov., (MIZA 0105945); **G–I.** *E. ephippiatus*, (ICN-Ao-1492); **J–L.** *E. guaichia* sp. nov., (MIZA 0105935); **M–O.** *E. simoni*, (ICN-Ao-328). **A–I.** Unscaled.

Complementary description. Male. ***Measurements.*** Males (ICN-Ao-196, ICN-Ao-328, ICN-Ao-512). DSL: 1.3–1.5; DSW: 2.2–2.5; AL: 1.8–2.4; AW: 2.6–2.7; IOD: 1.2–1.5; pedipalp: CoPp 0.6–0.7, TrPp 0.4–0.6, FePp 2.7–3.0, PaPp 1.3–1.6, TiPp 1.2–1.4, TaPp 0.9–1.2, ClPp: 0.5–0.7, total 6.8–8.5; Leg IV: FeL 7.8–8.9, TiL 4.1–4.9. Female (ICN-Ao-641). DSL: 2.5; DSW: 2.9; AL: 1.2; AW: 2.4; IOD: 1.3; pedipalp: CoPp 0.6, TrPp 0.4, FePp 2.6, PaPp 1.3, TiPp 1.2, TaPp 0.9, ClPp 0.6, total 6.5; Leg IV: FeL 8.7, TiL 5.1. ***Penis*** (Fig. 14M–O). Heterostygninae general pattern. Malleus swollen. LP with a neck and a wide circular distal cleft. MS-A1-A2 located on malleus; MS-B pair ventrally located, near the base of LP on the malleus; two pairs of MS-C located dorsomedially on LP, distally to the neck; MS-D1 large, located slightly proximal to MS-E; MS-D2 basally located, near glans basis; MS-E with two pairs of short setae. Glans bulbous, with short and dorsally curved stylus with small dorsal process.

Remarks. Subtle variations were observed in the shape of the LP, which presents less pronounced and rounded lateral projections (instead of acute), a wider neck, and the MS-A, which are separated from each other, with one pair positioned almost ventrally and the other almost dorsally (Fig. 14M–O). Additionally, slight variations in leg coloration and the pattern of dry spots were observed in individuals potentially identified as *E. simoni*, which were evaluated solely through photographs of live specimens (Fig. 15). Due to these variations and limitations in the material study, we have included these records on the map (Fig. 2) as *Eutimesius* cf. *simoni*, leaving open the possibility that more than one species may be involved in the Amazonian populations.

Distribution. Brazil, Amazonas; Colombia, Amazonas; Ecuador, Napo, and Los Ríos; Peru, Loreto (Fig. 15). The species was originally documented in Puerto Asis but erroneously attributed to the Department of Guainia (Pinto-da-Rocha 1997). We hereby correct this misattribution and reassign it to its accurate department, Putumayo.

Discussion

Within Heterostygninae, at least four genera share a similar genital morphology, namely *Eutimesius* and *Innoxius* Pinto-da-Rocha, 1997, from the Andean region; *Minax* Pinto-da-Rocha, 1997; and *Yapacana* Pinto-da-Rocha, 1997, from the Amazon. The latter two can be distinguished from *Eutimesius* by the reduction and shape of

Figure 15. *Eutimesius* cf. *simoni*: **A.** From Puerto Montúfar, Sucumbíos, Ecuador; **B–D.** From Iquitos, Maynas, Peru; **E.** From Leticia, Amazonas, Colombia; **F.** From Parque Nacional Yasuní Tipu Tini, Napo, Ecuador. Photographs by: Mark Silverstein (**A**), Jiri Hodecek (**B**), Martin Cejka (**C**), Phill Kahler (**D**), Traveler Dan (**E**), and Cinthya Villegas (**F**).

the LP and the widening of the malleus in the former, and by the increase in the number of MS-A and the loss of the dorsal process of the stylus in *Minax*. Meanwhile, *Innoxius* is separated from *Eutimesius* solely by somatic characters, including the DS shape, the ornamentation of scutal areas, and the presence of white dry spots (Pinto-da-Rocha 1997; Villarreal et al. 2019a). However, the position of the MS-B, which is ventral in *Eutimesius* (Figs 1, 14) and tends to be lateral in *Innoxius*, is suggested here as a putative character that could help distinguish the two Andean genera.

The monophyly of *Eutimesius* was demonstrated by Pinto-da-Rocha (1997) based on the three following characters: (1) cephalothorax with one wide median eminence, (2) cephalothorax with white spots, and (3) dorsal scute areas with white spots. To date, only three species of the genus have been included in phylogenetic analyses (Pinto-da-Rocha 1997). In that analysis, *E. simoni*

was identified as the sister species to *E. albicinctus*, with *E. ornatus* as the sister species to both.

Despite raising questions about intergeneric relationships in our work, we have chosen not to conduct a phylogenetic analysis in this study due to several key factors. Recent taxonomic changes and the reinterpretation of genital traits in the Stygnidae family have occurred independently of a phylogenetic analysis (e.g., Villarreal et al. 2019a, 2019b). In addition, since the proposal of a homology hypothesis for genital macrosetae (Kury and Villarreal 2015), many of the characters would require significant reinterpretation, necessitating a nearly complete reanalysis to create a new matrix, altering our focus primarily on the alpha taxonomy of a single genus. Additionally, we face challenges related to homologies in characters directly involving the study group, such as tegument coloration and dry spots. Lastly, it is important to note that we are aware of the existence of some new species that will be described in the near future.

Although the need for a complete phylogenetic analysis of the family is increasingly evident, this goes beyond the main objective of our present work and is part of future projects that involve a broader group of authors. In addition, due to the nature of the group studied, the lack of this analysis does not limit or affect the results obtained in this work.

Author contributions

All authors of this work contributed significantly to the project. OV designed and led the project, collecting Venezuelan species, diagnosing new species from Venezuela and Colombia, and working on the description, photography, and illustration of the new species. DAC visited Colombian collections, analyzed the material from this country, and generated the corresponding figures. DAC also contributed to the description of the new species and created the map. GRN provided the facilities for the project to be carried out, including funding for the visits to collections and laboratory facilities. All authors worked together on the writing of the article and agreed on the final version of the manuscript presented.

Acknowledgments

Claudia Medina, scientific manager of the collection at the Instituto Alexander von Humboldt, coordinated the loan of material to Adriano B. Kury. We would like to thank Adriano B. Kury for his invaluable assistance during our research in his laboratory (MNRJ), as well as for his outstanding coordination in arranging the loan of materials from the Instituto Alexander von Humboldt. To Eduardo Flórez, Daniela Martínez, and Sebastian Galvis for their collaboration during the visit of DAC and OV to the arachnological collection of ICN. To Julian Clavijo-Bustos for his collaboration during the visit of the DAC to the IAvH. To Giovanny Fagua and Alejandra Rodríguez for their collaboration during the visit of DAC to the entomological collection of MPUJ. We would like to express our gratitude to Adriano Kury, Amanda Mendes, and Ricardo Pinto-da-Rocha, who served as reviewers of the manuscript, providing comments that helped improve the final version. We are also deeply appreciative of Miguel Medrano and Pío Colmenares for taking the time to read and provide valuable feedback on an earlier version of the manuscript. To Cynthia Villegas, Jiri Hodecek, Martin Cejka, Mark Silverstein, and Dan Doucette for permitting us the use of the photographs in Figure 14. The SEM micrographs were taken in the SEM Lab of Marine Diversity of the MNRJ (financed by PETROBRAS) with the financial support of Programa de Posgraduação em Zoologia do Museu Nacional/UFRJ and Programa de Apoio à Pós-graduação (PROAP), with the assistance of Beatriz Cordeiro and Camila Simões. José Clavijo made contact and support possible with the Casa María in allowing the visit, and Norbert Flauer and the staff of the Posada Casa María, as well as Maria Paula Pereira, provided invaluable support in the field work. We thank Pío Colmenares (AMNH) for coordinating the donation of optical equipment and supplies to MIZA through the Cooperation Agreement between MIZA and AMNH. Idea Wild financed photographic equipment for OV in the framework of project ID. VILLVENE0122, which partially made this project possible. This work was partially supported by the Vicerectory of Research of the Universidad de Cartagena (Plan de Fortalecimiento Grupo de Investigación Hidrobiología).

References

Acosta LE, Pérez A, Tourinho AL (2007) Methods for taxonomic study. In: Pinto-da-Rocha R, Machado G, Giribet G (Eds) Harvestmen: The Biology of Opiliones. Harvard University Press, United states of America: 494–505.

Centore P (2016) sRGB Centroids for the ISCC-NBS Colour System. Self Published. 21–21.

DaSilva MB, Gnaspini P (2010) A systematic revision of Goniosomatinae (Arachnida: Opiliones: Gonyleptidae), with a cladistic analysis and biogeographical notes. Invertebrate Systematics 23(6) [“2009"]: 530–624. https://doi.org/10.1071/IS09022

Hadley A (2015) CombineZP. https://alan-hadley.software.informer.com/ [accessed on february 20, 2022]

Hara MR, Pinto-da-Rocha R, Kury AB (2010) Revision of *Nanopharreus*, a mysterious harvestman genus from Chile, with descriptions of three new species (Opiliones: Laniatores: Gonyleptidae). Zootaxa 3579(1): 37–66. https://doi.org/10.11646/zootaxa.3579.1.2

Henriksen KL (1932) Descriptiones *Laniatorum* (Arachnidorum Opilionum Subordinis). Opus posthumum recognovit et edidit Kai L. Henriksen. Nye samling af det Kongelige Danske Videnskabernes Selskabs skrifter 3(4): 197–422.

Kury AB (2003) Annotated catalogue of the Laniatores of the New World (Arachnida, Opiliones). Revista Ibérica de Aracnología 1: 1–337.

Kury AB, Medrano M (2016) Review of terminology for the outline of dorsal scutum in Laniatores (Arachnida, Opiliones). Zootaxa 4097(1): 130–134. https://doi.org/10.11646/zootaxa.4097.1.9

Kury AB, Villarreal MO (2015) The prickly blade mapped: Establishing homologies and a chaetotaxy for macrosetae of penis ventral plate in Gonyleptoidea (Arachnida, Opiliones, Laniatores). Zoological Journal of the Linnean Society 174(1): 1–46. https://doi.org/10.1111/zoj.12225

Kury AB, Mendes AC, Cardoso L, Kury MS, Granado A de A, Giribet G, Cruz-López JA, Longhorn SJ, Medrano M, Oliveira ABR de, Kury IS, Souza-Kury MA (2023) World Catalogue of Opiliones. WCO-Lite version 2.6. [may 20, 2024] https://wcolite.com/

Mello-Leitão CF (1949) Famílias, subfamília, espécies e gêneros novos de opiliões e notas de sinonimia. Boletim do Museu Nacional 94: 1–33.

Pinto-da-Rocha R (1997) Systematic review of the neotropical family Stygnidae (Opiliones: Laniatores, Gonyleptoidea). Arquivos de Zoologia 33(4): 163–342. https://doi.org/10.11606/issn.2176-7793.v33i4p163-342

Roewer C-F (1913) Die Familie der Gonyleptiden der Opiliones - Laniatores. Archiv für Naturgeschichte, Abteilung A 79(5): 257–472. [Part 2]

Roewer C-F (1915) 106 neue Opilioniden. Archiv für Naturgeschichte 81(3): 1–152.

Roewer C-F (1943) Über Gonyleptiden. Weitere Weberknechte (Arachn., Opil.) XI. Senckenbergiana 26(1–3): 12–68.

Villarreal O, Machado G (2011) First record of paternal care in the family Stygnidae (Opiliones: Laniatores). The Journal of Arachnology 39(3): 500–502. https://doi.org/10.1636/Hi11-29.1

Villarreal O, Ázara LND, Kury AB (2019a) Revalidation of *Obidosus* Roewer, 1913 and description of two new cave-dwelling species of *Protimesius* Roewer, 1913 from Brazil (Opiliones: Stygnidae). Journal of Natural History 53(15–16): 965–989. https://doi.org/10.1080/00222933.2019.1620893

Villarreal O, Sanchéz N, De Ascenção A (2019b) New generic assignment to the harvestman *Metaphareus punctatus* (Opiliones: Stygnidae) and observations about it reproductive behavior. Iheringia. Série Zoologia 109(1): 1–6. https://doi.org/10.1590/1678-4766e2019008

Villarreal O, Kury AB, Colmenares PA (2021) Contributions to the taxonomy of some Amazonian Stygnidae (Opiliones: Laniatores: Gonyleptoidea). Zootaxa 4984(1): 218–227. https://doi.org/10.11646/zootaxa.4984.1.17

Zoosyst. Evol. 100 (3) 2024, 821–840 | DOI 10.3897/zse.100.121512

PENSOFT

für Natur MUSEUM FÜR NATURKUNDE BERLIN

Integrative taxonomy of *Dicellophilus* Cook, 1896 (Chilopoda, Geophilomorpha, Mecistocephalidae) in Japan, with a description of a new species

Sho Tsukamoto[1], Katsuyuki Eguchi[1,2]

1 *Systematic Zoology Laboratory, Graduate School of Science, Tokyo Metropolitan University, Minami-osawa 1-1 Hachioji-shi, Tokyo 192-0397, Japan*

2 *Department of International Health and Medical Anthropology, Institute of Tropical Medicine, Nagasaki University, 1-12-4 Sakamoto, Nagasaki 852-8523, Japan*

https://zoobank.org/B0AF778B-E394-4C17-910D-FA2BDFB14A4F

Corresponding author: Sho Tsukamoto (esutukamoto153@gmail.com)

Academic editor: Pavel Stoev ♦ **Received** 23 February 2024 ♦ **Accepted** 7 May 2024 ♦ **Published** 19 June 2024

Abstract

The genus *Dicellophilus* Cook, 1896, is a peculiar genus from the point of view of distribution. *Dicellophilus* is distributed in three limited areas that are well separated from one another: central Europe (*D. carniolensis*), Honshu (*D. pulcher*), and the southwestern part of the USA (*D. anomalus* and *D. limatus*). In the present study, in a field survey conducted throughout Japan, specimens belonging to the genus *Dicellophilus* were collected from Tohoku to the Kansai region, Honshu. Morphological analysis, molecular phylogenetic analysis, and genetic distance among *Dicellophilus* in Japan and *D. carniolensis* revealed that specimens from Sendai-shi, Miyagi Pref., could be assigned to an undescribed species. This previously unrecognized species is herein described as *D. praetermissus* **sp. nov.** The new species can be distinguished from *D. carniolensis* and *D. limatus* by the number of pairs of legs (43 pairs in *D. carniolensis* and 45 in *D. limatus*, but 41 in *D. praetermissus* **sp. nov.**), from *D. anomalus* by the lack of a pair of setae on the posteromedian part of the clypeus and variable crenulation on the internal margin of the forcipular tarsungulum, and from *D. pulcher* based on the following combination of characteristics: both ends of the transverse suture not evidently convex forward; long rather than wide trochanteroprefemur; wide rather than long metasternite.

Key Words

Cryptic species, DNA barcoding, geophilomorph centipede, molecular, phylogeny

Introduction

The geophilomorph family Mecistocephalidae Bollman, 1893, is mainly distributed from temperate to tropical regions in both hemispheres, and species diversity is remarkably high in Japan (Uliana et al. 2007; Bonato 2011). To date, approximately 180 species are known worldwide, and 31 species have been recorded from Japan (Uliana et al. 2007; Tsukamoto et al. 2019, 2022). Therefore, approximately 20% of all known mecistocephalid species are distributed in Japan. Moreover, Japan is the richest with regard to the number of genera (nine out of 11 genera; Uliana et al. 2007; Tsukamoto et al. 2022).

Mecistocephalidae are morphologically characterized by a cephalic capsule and a forcipular segment that are evidently sclerotized and darker than the remaining trunk segments (Bonato et al. 2003, 2014; Uliana et al. 2007; Bonato 2011). In addition, the following three features characterize Mecistocephalidae: a mandible with a series of pectinate lamellae only; trunk sternites with an internal apodeme; and a mid-longitudinal sulcus (Bonato et al. 2003). Notably, the segment number of most species of Mecistocephalidae has no intraspecific variation, except for some species of the genus *Mecistocephalus* Newport, 1843, with a very high number of leg-bearing segments (Bonato et al. 2003, 2014; Uliana et al. 2007; Bonato 2011).

Among Mecistocephalidae, the genus *Dicellophilus* Cook, 1896, is a distinct genus from a morphological viewpoint, with the following diagnostic characteristics: a macropore near the center of the coxopleuron and a concave margin of the lateral side pieces of the labrum (Uliana et al. 2007; Bonato et al. 2010a). See table 2 of Bonato et al. (2010a) and table 1 of Dyachkov and Bonato (2022) for diagnostic characteristics of the genus *Dicellophilus*. To date, four valid species have been known in the genus *Dicellophilus*, namely, *D. carniolensis* (C.L. Koch, 1847), *D. pulcher* (Kishida, 1928), *D. anomalus* (Chamberlin, 1904), and *D. limatus* (Wood, 1862).

The distribution of *Dicellophilus* is limited to three areas that are well separated from one another: central Europe (*D. carniolensis*), Honshu of Japan (*D. pulcher*), and the southwestern part of the USA (*D. anomalus* and *D. limatus*) (Bonato et al. 2003, 2010a). All three distribution areas are located within a narrow latitudinal band, at approximately 35–45°N, and all species inhabit humid litter and soil in forests (Bonato et al. 2010a).

Bonato et al. (2010a) performed phylogenetic analyses of the genus *Dicellophilus* with a morphological dataset consisting of 30 characteristics and indicated that the two American species, viz., *D. anomalus* and *D. limatus*, were sister species, and *D. pulcher* formed a clade with the two American species. As far as extant species are concerned, *D. carniolensis* is thus the first diverged species in the genus *Dicellophilus*.

For a decade, the combination of morphological observation, molecular phylogenetic analyses, and DNA barcoding ("integrative taxonomy") has helped detect undescribed species and reveal the genetic structure of the taxa concerned (Dayrat 2005; Padial et al. 2010). For example, some studies using integrative approaches to scolopendromorphs and geophilomorphs have revealed the existence of many cryptic species under one validly named species or distinct morphospecies (Joshi and Karanth 2012; Siriwut et al. 2015, 2016; Tsukamoto et al. 2021b; Peretti et al. 2022; Bonato et al. 2023). Tsukamoto et al. (2022) also detected the existence of two species of the mecistocephalid genus *Nannarrup* Foddai, Bonato, Pereira & Minelli, 2003 by using an integrative approach.

Inspired by these previous studies, the present study aims to reveal the genetic diversity and confirm whether the morphospecies *D. pulcher* involves unnoticed and undescribed cryptic species by using an integrative taxonomic approach.

Materials and methods

Taxon sampling

Although our ongoing sampling efforts to taxonomically reveal the East Asian mecistocephalid faunas cover the whole of Japan and surrounding areas, the present study focused on Honshu (the largest island of mainland Japan), from which *D. pulcher* was described.

A total of 38 specimens morphologically identified as *Dicellophilus pulcher*, hitherto the only known Japanese species of the genus, were collected from Honshu from 2018 to 2021. The detailed collection sites of the examined specimens are shown in Fig. 1, Table 1, and the "Taxonomic account" section. The altitude data provided by AW3D of JAXA (https://www.eorc.jaxa.jp/ALOS/jp/index_j.htm) and the coastal line provided by the digital nation land information (https://nlftp.mlit.go.jp/index.html) were used to generate Fig. 1.

Each specimen was labeled with its unique specimen identification number in the form "TSYYYYMMDD-XX," where TS is an abbreviation of the first author's name, Tsukamoto Sho; YYYYMMDD designates the date on which the specimen was collected; and XX is the identification number assigned to each specimen collected on a particular date (e.g., TS20171010-01).

All of the type specimens of *Dicellophilus* designated in this paper were deposited at the Collection of Myriapoda, Department of Zoology, National Museum of Nature and Science, Tokyo (NSMT), and the Museum of Nature and Human Activities, Hyogo (MNHAH). The deposition site of each type specimen is shown in the "Taxonomic account" section. All non-type voucher specimens of *Dicellophilus pulcher* are managed by the first author.

Morphological examination

For dissected specimens, the cephalic capsule, maxillae, mandibles, forcipular segment, and leg-bearing segments were made transparent using lactic acid to examine the anatomy and produce images. Multi-focused images of these body parts were produced using Affinity Photo 1.10.4 (https://affinity.serif.com/ja-jp/photo/) from a series of source images taken using a Canon EOS Kiss X9 digital camera attached to a Nikon AZ100 microscope and improved using Adobe Photoshop Elements 10 and Affinity Designer 1.10.5 (https://affinity.serif.com/ja-jp/designer/). Then, the body parts were measured directly using an ocular micrometer attached to the microscope.

The morphological terminology used in this study is in accordance with Bonato et al. (2010b). Specimens with fully developed paired gonopods, that is, evidently biarticulated in males and touching one another in females, were determined to be adults, and those with incompletely developed paired gonopods were determined to be subadults. Specimens without gonopods were determined to be juveniles based on Uliana et al. (2007). In the present study, 23 adult specimens out of 38 collected were examined morphologically.

DNA sequencing

Genomic DNA was extracted from one or two legs of each specimen in accordance with the Chelex-TE-ProK protocol described by Satria et al. (2015), with incubation for 4–24 h.

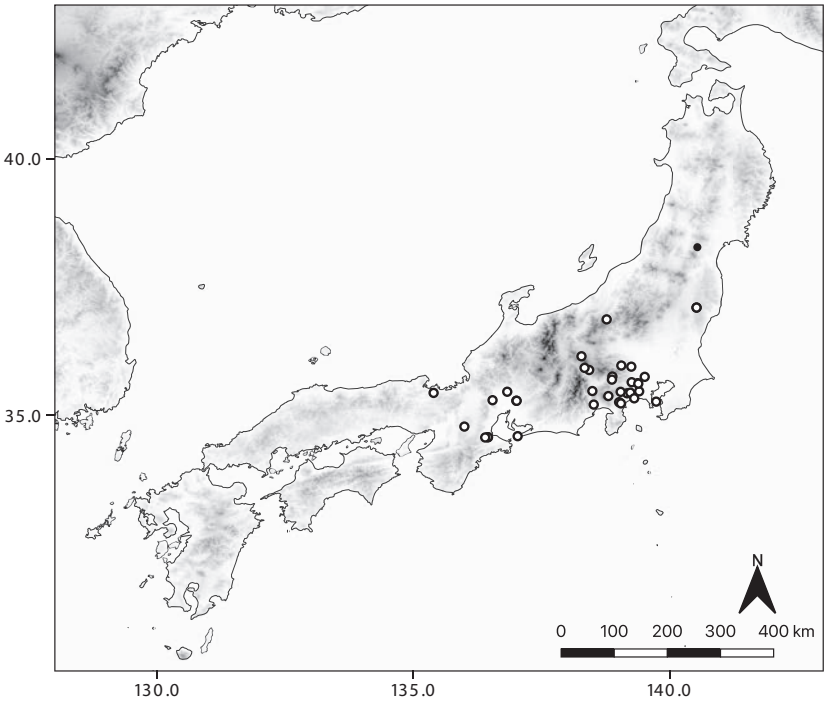

Figure 1. Map of the collection sites of specimens examined in the present study. White circle, *Dicellophilus pulcher*; black circle, *D. praetermissus* sp. nov.

PCR amplification was performed in a MiniAmp Thermal Cycler (Thermo Fisher Scientific, Waltham, Massachusetts, USA) in a 10.5-μL reaction volume containing 5 μL of 2× PCR buffer for KOD FX Neo, 2 μL of 2 mM dNTPs, 0.3 μL of 10 pmol/μL forward and reverse primers, 0.2 μL of 1.0 U/μL DNA polymerase KOD FX Neo (TOYOBO KFX-201X5), and 1.0 μL of DNA template. The sequences of primers for mitochondrial cytochrome *c* oxidase subunit I (*COI*), *16S rRNA* (*16S*), and nuclear *28S rRNA* (*28S*) genes are shown in Table 2. Each PCR product was screened by electrophoresis on a 2.0% agarose gel in 1× TAE.

The amplification conditions for mitochondrial *COI* were as follows: 98 °C for 2 min; 5 cycles of 98 °C for 10 s; 45 °C for 30 s; and 68 °C for 45 s; 40 cycles of 98 °C for 10 s; 48.5 °C for 30 s (annealing step); 68 °C for 45 s; and 68 °C for 7 min. If the target fragment of *COI* was not appropriately amplified, then the annealing temperature was changed from 48.5 °C to 50 °C. PCR was performed again by omitting the first five cycles of annealing and the extension step.

The amplification conditions for mitochondrial *16S* were as follows: 98 °C for 2 min; 35 cycles of 98 °C for 10 s; 45 °C for 30 s (annealing step); 68 °C for 45 s; and 68 °C for 7 min. If the target fragment of *16S* was not appropriately amplified, then the annealing temperature was changed from 45 °C to 48 °C. The number of annealing cycles was changed from 35 to 45.

The amplification conditions for nuclear *28S* were as follows: 98 °C for 2 min; 5 cycles of 98 °C for 10 s; 42 °C for 30 s; and 68 °C for 1 min; 30 cycles of 98 °C for 10 s; 50 °C for 30 s (annealing step); 68 °C for 1 min; and 68 °C for 7 min. If the target fragment of *28S* was not appropriately amplified, then the annealing temperature was changed from 50 °C to 48 °C. The number of annealing cycles was changed from 30 to 40–45 cycles. In addition, PCR was performed again by omitting the first five cycles of annealing and the extension step.

The amplified products were incubated at 37 °C for 4 min and at 80 °C for 1 min using ExoSAP-IT™ Express (Thermo Fisher Scientific) to remove any excess primers and nucleotides. All nucleotide sequences were determined by direct sequencing using the ABI PRISM BigDye™ Terminator Cycle Sequencing Kit ver. 3.1 (Thermo Fisher Scientific) or BrilliantDye™ Terminator Cycle Sequencing Kit v. 3.1 (Nimagen, B.V., Nijmegen, Netherlands) equipped with an ABI 3130xl automated sequencer (Thermo Fisher Scientific). The sequences were assembled using ChromasPro 1.7.6 (Technelysium Pty Ltd., Australia) and deposited onto the DDBJ, EMBL, and GenBank databases under the accession numbers LC815125– LC815233 (Table 1).

Molecular phylogenetic analyses

The sequences obtained using the abovementioned methods were used for phylogenetic analyses, together with the *COI*, *16S*, and *28S* sequences of *Dicellophilus carniolensis* (C.L. Koch, 1847) and *Nannarrup innuptus* Tsukamoto in Tsukamoto et al. (2022) obtained from GenBank as outgroups (Table 1). The datasets for *COI* (658 bp positions), *16S* (514 bp positions), and *28S* (971 bp positions) were concatenated to form the *COI* + *16S* + *28S* dataset for phylogenetic analyses.

Table 1. The list of specimens that were used in the phylogenetic analyses. Geographic coordinates enclosed by parentheses are secondary due to the lack of information in the labels.

Specimen ID	Geographic coordinate of collection sites	Sequence data (Accession no.)			Remarks
		COI	*16S*	*28S*	
***Dicellophilus pulcher* (Kishida, 1928)**					
TS20220518-01	35°16.45'N, 137°00.59'E (Aichi Pref.)	LC815129	LC815167	LC815205	Tomoki Sumino leg.
TS20210809-01	34°33.71'N, 136°27.33'E (Mie Pref.)	LC815130	LC815168	LC815206	Tomoki Sumino & Fukube Sumino leg.
TS20210809-02	34°33.71'N, 136°27.33'E (Mie Pref.)	LC815131	LC815169	LC815207	Tomoki Sumino & Fukube Sumino leg.
TS20220813-01	34°33.42'N, 136°24.13'E (Mie Pref.)	LC815132	LC815170	LC815208	Tomoki Sumino leg.
TS20230517-01	35°16.38'N, 137°00.96'E (Aichi Pref.)	LC815133	LC815171	LC815209	Tomoki Sumino leg.
TS20190413-01	35°25.15'N, 139°10.39'E (Kanagawa Pref.)	LC815134	LC815172	LC815210	Sho Tsukamoto leg.
TS20181214-01	35°37.02'N, 139°22.74'E (Tokyo Pref.)	LC815135	LC815173	–	Joe Kutsukake leg.
TS20180714-01	35°27.46'N, 139°24.51'E (Kanagawa Pref.)	LC815136	LC815174	–	Joe Kutsukake leg.
TS20191006-02	35°38.15'N, 139°15.71'E (Tokyo Pref.)	LC815137	LC815175	–	Sho Tsukamoto leg.
TS20200924-01	35°52.42'N, 138°25.96'E (Yamanashi Pref.)	LC815138	–	–	Joe Kutsukake leg.
TS20200927-01	35°54.95'N, 138°20.55'E (Yamanashi Pref.)	LC815139	LC815176	–	Koshi Kawamoto leg.
TS20201122-01	(35°25.62'N, 135°23.69'E) (Kyoto Pref.)	LC815140	LC815177	LC815211	Tatsumi Suguro leg.
TS20210322-01	35°15.40'N, 139°44.43'E (Kanagawa Pref.)	LC815141	LC815178	–	Ryo Miyata leg.
TS20210401-03	35°44.46'N, 139°31.01'E (Tokyo Pref.)	LC815142	LC815179	LC815212	Mayu Susukida leg.
TS20210411-08	35°26.84'N, 139°02.82'E (Kanagawa Pref.)	LC815143	LC815180	LC815213	Namiki Kikuchi leg.
TS20210424-07	35°25.88'N, 139°14.15'E (Kanagawa Pref.)	LC815144	LC815181	LC815214	Katsuyuki Eguchi leg.
TS20210504-01	35°21.91'N, 138°48.44'E (Shizuoka Pref.)	LC815145	LC815182	LC815215	A topotype of *D. pulcher*; Sho Tsukamoto leg.
TS20210418-01	34°34.94'N, 137°02.13'E (Aichi Pref.)	LC815146	LC815183	LC815216	Katsuyuki Eguchi leg.
TS20210522-01	35°44.78'N, 138°53.15'E (Yamanashi Pref.)	LC815147	LC815184	LC815217	Takahiro Yoshida leg.
TS20210530-02	35°41.19'N, 138°52.64'E (Yamanashi Pref.)	LC815148	LC815185	LC815218	Namiki Kikuchi leg.
TS20210722-01	35°57.71'N, 139°03.60'E (Saitama Pref.)	LC815149	LC815186	LC815219	Mayu Susukida leg.
TS20211004-01	(36°08.54'N, 138°16.92'E) (Nagano Pref.)	LC815150	LC815187	LC815220	Masaru Nonaka leg.
TS20211030-04	36°51.75'N, 138°46.43'E (Niigata Pref.)	LC815151	LC815188	LC815221	Katsuyuki Eguchi leg.
TS20211018-02	35°26.99'N, 136°49.95'E (Gifu Pref.)	LC815152	LC815189	LC815222	Katsuyuki Eguchi leg.
TS20210919-01	34°46.18'N, 135°59.73'E (Kyoto Pref.)	LC815153	LC815190	LC815223	Katsuyuki Eguchi leg.
TS20210711-15	35°17.08'N, 136°32.74'E (Gifu Pref.)	LC815154	LC815191	LC815224	Katsuyuki Eguchi leg.
TS20210819-01	35°36.51'N, 139°23.48'E (Tokyo Pref.)	LC815155	LC815192	LC815225	Katsuyuki Eguchi leg.
TS20210523-01	35°27.82'N, 138°29.66'E (Yamanashi Pref.)	LC815156	LC815193	LC815226	Katsuyuki Eguchi leg.
TS20210531-01	37°05.59'N, 140°31.72'E (Fukushima Pref.)	LC815157	LC815194	LC815227	Katsuyuki Eguchi leg.
TS20210523-03	35°11.94'N, 138°31.29'E (Shizuoka Pref.)	-	LC815195	LC815228	Katsuyuki Eguchi leg.
TS20210718-01	35°56.36'N, 139°15.30'E (Saitama Pref.)	LC815158	LC815196	LC815229	Katsuyuki Eguchi leg.
TS20210508-02	35°19.27'N, 139°18.72'E (Kanagawa Pref.)	LC815159	LC815197	LC815230	Katsuyuki Eguchi leg.
TS20210531-02	37°05.59'N, 140°31.72'E (Fukushima Pref.)	LC815160	LC815198	LC815231	Katsuyuki Eguchi leg.
TS20210728-01	35°14.75'N, 139°01.02'E (Kanagawa Pref.)	LC815161	LC815199	LC815232	Sho Tsukamoto leg.
TS20210728-02	35°13.32'N, 139°03.13'E (Kanagawa Pref.)	LC815162	LC815200	LC815233	Sho Tsukamoto leg.
***Dicellophilus praetermissus* sp. nov.**					
TS20201007-02	38°16.33'N, 140°32.69'E (Miyagi Pref.)	LC815125	LC815163	LC815201	Sho Tsukamoto leg.
TS20201007-03	38°16.33'N, 140°32.69'E (Miyagi Pref.)	LC815126	LC815164	LC815202	Sho Tsukamoto leg.
TS20201007-04	38°16.33'N, 140°32.69'E (Miyagi Pref.)	LC815127	LC815165	LC815203	Sho Tsukamoto leg.
TS20201007-05	38°16.33'N, 140°32.69'E (Miyagi Pref.)	LC815128	LC815166	LC815204	Sho Tsukamoto leg.
***Dicellophilus carniolensis* (Koch, 1847) (outgroup)**					
DNA102580/LBv792	No data	KF569305	HM453225	HM453285	Referred from Murienne et al. (2010), Bonato et al. (2014)
***Nannarrup innuptus* Tsukamoto in Tsukamoto et al. 2022 (outgroup)**					
TS20210503-09	34°51.39'N, 138°55.40'E (Shizuoka Pref.)	LC715530	LC715605	LC715680	Referred from Tsukamoto et al. (2022)

All sequences were aligned using MAFFT v. 7.475 (Katoh and Standley 2013). For *COI*, alignment was performed using the default setting. For *16S* and *28S*, secondary structure alignment was performed using the X-INS-i option.

Maximum-likelihood (ML) trees were created on the basis of the sequence dataset for each gene and concatenated using IQ-tree 1.6.12 (Nguyen et al. 2015). As an optimal substitution model in accordance with BIC, TNe + I + G4 was selected for the first codon position

Table 2. The list of primers used in the present study.

Genes	Primer name	Sequence (5' - 3')	Source
COI	LCO-CH	TTT CAA CAA AYC AYA AAG ACA TYG G	Tsukamoto et al. (2021a)
	HCO-CH	TAA ACT TCT GGR TGR CCR AAR AAT CA	
16S rRNA	16Sa	CGC CTG TTT ATC AAA AAC AT	Xiong and Kocher (1991)
	16Sbi	CTC CGG TTT GAA CTC AGA TCA	
28S rRNA	28S D1F	GGG ACT ACC CCC TGA ATT TAA GCA T	Boyer and Giribet (2007)
	28S rD4b	CCT TGG TCC GTG TTT CAA GAC	Edgecombe and Giribet (2006)

of *COI* in the concatenated dataset; TNe + G4 for the *COI* dataset; HKY + F was selected for the second codon position of *COI* in both datasets; TN + F + G4 was selected for the third codon position of *COI* in both datasets; HKY + F + I + G4 was selected for *16S* of both datasets; and TIM3e + G4 was selected for *28S* of both datasets. Ultrafast bootstrap analysis (UFBoot; Hoang et al. 2018) and the SH-like approximate likelihood ratio test (SH-aLRT; Guindon et al. 2010) were performed with 1,000 replicates.

Bayesian inference trees were created using ExaBayes 1.4.1 (Aberer et al. 2014) under the default substitution model "GTR + G." The Markov chain Monte Carlo method was used with random starting trees and performed once for each of the four chains (three hot and one cold) for 10,000,000 generations for each dataset except *COI*, but for 20,000,000 generations for the *COI* dataset. Trees were sampled every 500 generations, tuning parameters every 100 generations, and the first 25% of the trees were discarded as burn-in. Other parameters were set in accordance with the default settings. The effective sampling size of each parameter was confirmed to be 200 using Tracer 1.7.1 (Rambaut et al. 2018).

Calculation of the genetic distances

The aligned *COI* dataset used for phylogenetic analyses were also used to calculate genetic distances. Kimura two-parameter (K2P) distances were calculated using MEGA X (Kumar et al. 2018) with the setting "pairwise deletion."

Delimitation of "provisional" operational taxonomic units

The program "assemble species by automatic partitioning (ASAP)" was used to delimit "provisional" operational taxonomic units (POTUs). ASAP is a species delimitation program based on a hierarchical clustering algorithm that only uses pairwise genetic distances (Puillandre et al. 2021; available at https://bioinfo.mnhn.fr/abi/public/asap/). ASAP was performed for the *COI* sequence dataset of *Dicellophilus* (excluding the outgroup) under the "pairwise K2P distance" method.

Delimitation of putative species and provisional naming of each putative species

The present study preliminarily relied on the morphological information provided by Bonato et al. (2010a) as the basis for the monophyly of the genus *Dicellophilus*. Then, putative species were proposed. Except for the assumption of monophyly of the abovementioned genus, the following steps generally followed the workflow "DI-system" proposed by the first author in Tsukamoto (2023) for discriminating and labeling putative species: (I) sorting specimens, which are morphologically conferrable to *Dicellophilus*, into morphospecies; (II) confirming the monophyly of the morphospecies with the phylogenetic tree inferred by the sequence dataset of three gene markers, mitochondrial *COI* and *16S*, and nuclear *28S*; (III) calculating the genetic distance of *COI* between congeneric morphospecies, which are confirmed to be monophyletic, to define the intermorphospecific threshold; (IV) delimiting POTUs using ASAP (see above) and confirming the most conferrable hypotheses of species-level independence by considering the phylogenetic tree and the intermorphospecific threshold defined in step III. By steps III and IV, species hypotheses can be established from two viewpoints, viz., phylogeny and clustering based on DNA data. In step IV, putative species were recognized by considering three species delimitation principles: (1) each clade is regarded as an independent putative species if it diverges from all others with a minimum K2P distance higher than the intermorphospecific threshold; (2) a single putative species that satisfies (1) can contain inner lineage(s) diverging extremely from the others unless the maximum distance from the sister inner lineage exceeds the intermorphospecific threshold; (3) a single putative species that satisfies (2) cannot contain inner lineage(s) diverging extremely from the sister inner lineage with the minimum K2P distance exceeding the intermorphospecific threshold, and such a lineage must be further considered as a distinct species if it exists.

As mentioned above, the present study presupposes the monophyly of *Dicellophilus*, supported by the morphological evidence (Bonato et al. 2010a). This is because the possibility of a difference in evolutionary rate among genera is important for defining the intermorphospecific threshold in the "DI-system". "DI-system" is planned to be proposed formally in future studies.

Each putative species recognized by following the abovementioned steps was also labeled in accordance with the study of Tsukamoto (2023), with a unique, permanent, and citable identifier "DI," such as "0000-0003-3020-8454_XXXX," in which "0000-0003-3020-8454" shows the author's ORCID and "XXXX" shows a unique identification number given to each species in the author's life-long research. ORCIDs involved in the species identification codes were omitted except for section titles, figure legends, and tables to avoid redundancy.

Depending on the availability of the morphological information necessary to formally describe and name species in the conventional manner of Linnaean Taxonomy (The International Commission on Zoological Nomenclature 1999), the putative species labeled with the DI can be described and named (step V). In the present study, species discrimination (steps I–IV) and formal description and naming of the species (step V) were separated as two methodologically distinct phases.

Results

Molecular phylogenetic analyses

COI was successfully sequenced for 38 specimens, *16S* for 38 specimens, and *28S* for 33 specimens (Table 1). The ML tree based on the concatenated dataset (Fig. 2) and BI tree based on the same dataset (only show the posterior probability in Fig. 2) involving 39 specimens shows that the clade consisting of TS20201007-02, TS20201007-03, TS20201007-04, and TS20201007-05 from Miyagi Pref. (UFBoot = 100%, SH-aLRT = 100%, posterior probability (PP) = 1.00; hereafter referred to as "Clade A") is deeply separated from the clade consisting of all other *Dicellophilus* specimens collected in Japan and the European species *D. carniolensis* (UFBoot = 95.4%, SH-aLRT = 98%, PP = 1.00). The monophyly of the clade, which consists of the remaining *Dicellophilus* specimens from Japan, was strongly supported (UFBoot = 100%, SH-aLRT = 100%,

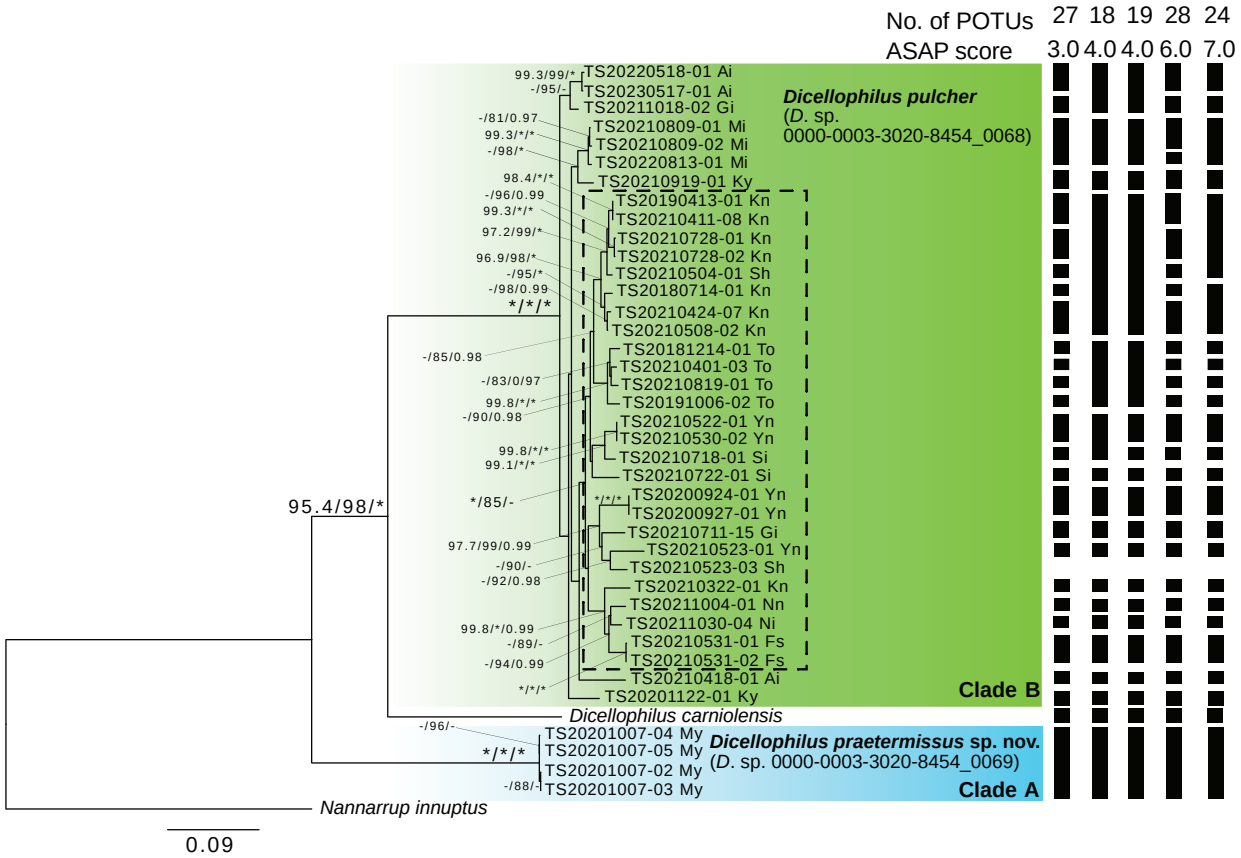

Figure 2. Maximum-likelihood tree of *Dicellophilus* based on the concatenated dataset of *COI*, *16S*, and *28S*, with the results of species delimitation by ASAP. Note that specimens whose *COI* sequence was not determined were included in the conferred species if they belonged to the same concerning clade to easily understand the result of species delimitation. Nodal values are obtained from the ultrafast bootstrap (UFBoot), SH-like approximate likelihood ratio test (SH-aLRT), and posterior probability (PP). The asterisk (*) indicates 100% in UFBoot, SH-aLRT, and 1.0 in PP. Hyphen (-) indicates lower than 95% in UFBoot, 80% in SH-aLRT, or 0.95 in PP. Nodal values are not shown when UFBoot, SH-aLRT, and PP values are <95%, <80%, and <0.95, respectively. The unit of evolutionary distance is the number of base substitutions per site. A broken square shows that the clade consisted of specimens from eastern Honshu. Abbreviations: Ai = Aichi Pref.; Fs = Fukushima Pref.; Gi = Gifu Pref.; Kn = Kanagawa Pref.; Ky = Kyoto Pref.; Mi = Mie Pref.; My = Miyagi Pref.; Ni = Niigata Pref.; Nn = Nagano Pref.; Sh = Shizuoka Pref.; Si = Saitama Pref.; To = Tokyo Pref.; Yn = Yamanashi Pref.

PP = 1.00; hereafter "Clade B"), and notably, specimens from Eastern Honshu (Fukushima Pref. to Shizuika Pref., and one specimen from Gifu Pref.) formed a clade with a high support value (UFBoot = 100%, SH-aLRT = 85%, PP = 0.91; enclosed by a broken square in Fig. 2). On the contrary, the monophyly of specimens from western Honshu (Gifu Pref. to Kyoto Pref.) was not supported.

The ML tree based on the *COI* dataset (Fig. 3) and the BI tree based on the same dataset (only PP shown in Fig. 3) involving 38 specimens also show Clade A (UFBoot = 99.6%, SH-aLRT = 100%, PP = 1.00). Although Clade A forms a further clade with *D. carniolensis* (UFBoot = 99.6%, SH-aLRT = 100%, PP = 1.00), Clade A is deeply separated from clade B (UFBoot = 90.8%, SH-aLRT = 95%, PP = 1.00). In addition, the monophyly of specimens from western Honshu in Clade B (Gifu Pref. to Kyoto Pref.) was moderately supported (UFBoot = 88.2%, SH-aLRT = 88%, PP = 0.98; enclosed by a broken square in Fig. 3), but that of eastern Honshu was not supported.

The ML tree based on the *16S* dataset (Fig. 4) and the BI tree based on the same dataset (only PP shown in Fig. 4) involving 38 specimens also show Clade A (UFBoot = 100%, SH-aLRT = 100%, PP = 1.00). Clade A is deeply separated from all other *Dicellophilus* specimens, but Clade B is not well supported (UFBoot = 78.2%, SH-aLRT = 63%, PP = 0.91). In addition, the phylogenetic relationship among Clade B and other *Dicellophilus* specimens was not clear due to low support values.

The ML tree based on the *28S* dataset (Fig. 5) and the BI tree based on the same dataset (only PP shown in Fig. 5) involving 33 specimens also show Clade A (UFBoot = 99.7%, SH-aLRT = 100%, PP = 1.00). Clade A is deeply separated from all other *Dicellophilus* specimens, and Clade B conforms to a further clade with *D. carniolensis*, like the topology of the concatenated dataset (UFBoot = 93.6%, SH-aLRT = 97%, PP = 0.99). However, the phylogenetic relationship among Clade B and other *Dicellophilus* specimens was not clear due to low support values.

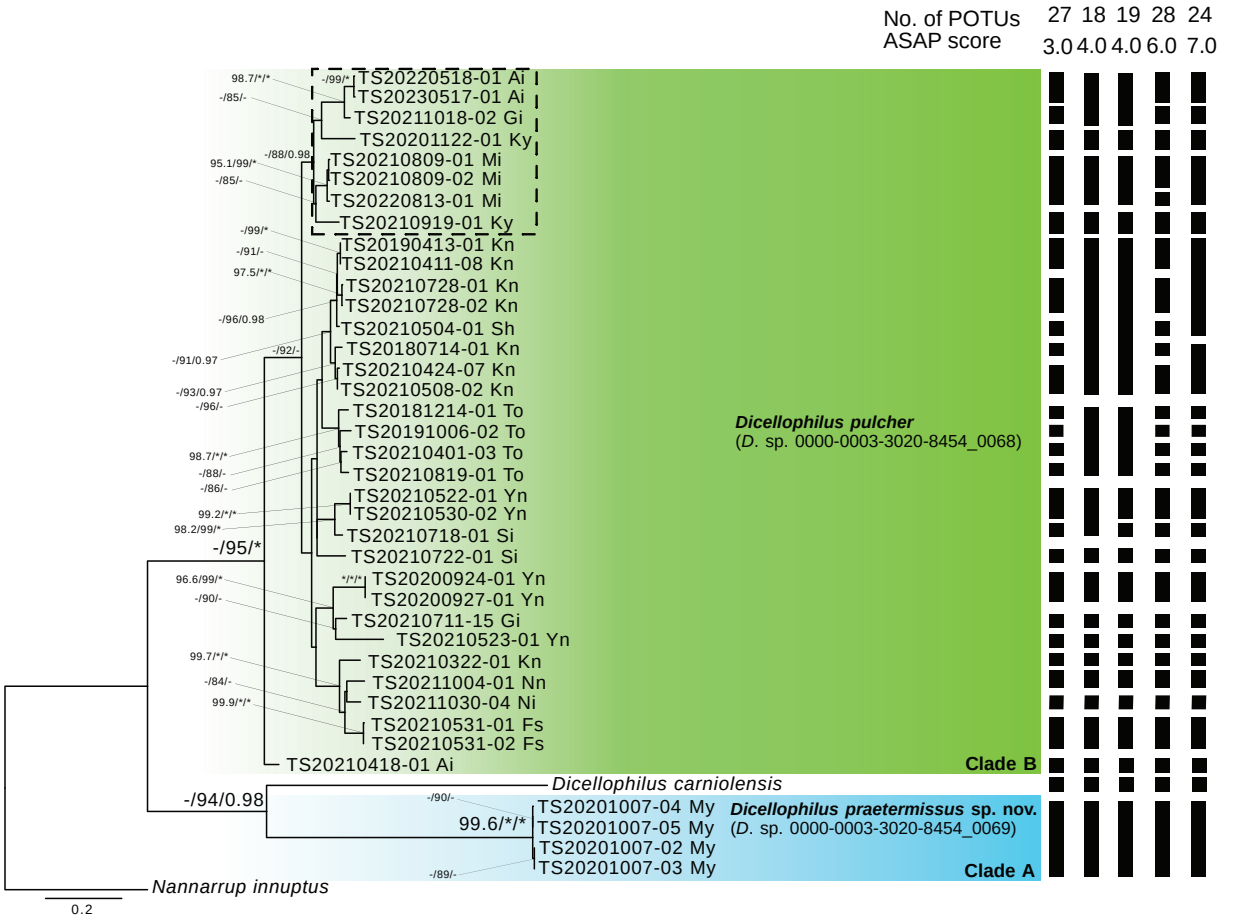

Figure 3. Maximum-likelihood tree of *Dicellophilus* based on the dataset of *COI*, with the results of species delimitation by ASAP. Nodal values are obtained from the ultrafast bootstrap (UFBoot), SH-like approximate likelihood ratio test (SH-aLRT), and posterior probability (PP). The asterisk (*) indicates 100% in UFBoot, SH-aLRT, and 1.0 in PP. Hyphen (-) indicates lower than 95% in UFBoot, 80% in SH-aLRT, or 0.95 in PP. Nodal values are not shown when UFBoot, SH-aLRT, and PP values are <95%, <80%, and <0.95, respectively. The unit of evolutionary distance is the number of base substitutions per site. A broken square shows that the clade consisted of specimens from eastern Honshu. Abbreviations: Ai = Aichi Pref.; Fs = Fukushima Pref.; Gi = Gifu Pref.; Kn = Kanagawa Pref.; Ky = Kyoto Pref.; Mi = Mie Pref.; My = Miyagi Pref.; Ni = Niigata Pref.; Nn = Nagano Pref.; Sh = Shizuoka Pref.; Si = Saitama Pref.; To = Tokyo Pref.; Yn = Yamanashi Pref.

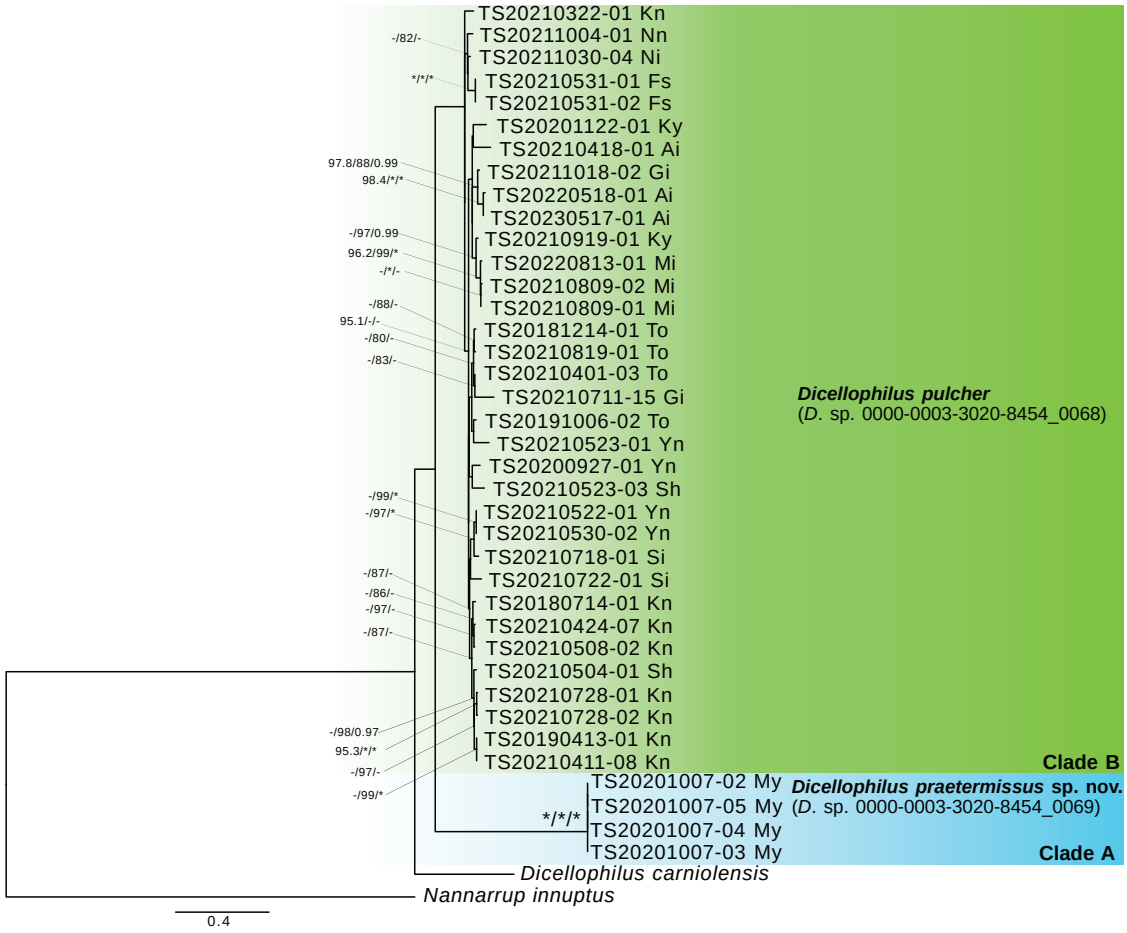

Figure 4. Maximum-likelihood tree of *Dicellophilus* based on the dataset of *16S*. Nodal values are obtained from the ultrafast bootstrap (UFBoot), SH-like approximate likelihood ratio test (SH-aLRT), and posterior probability (PP). The asterisk (*) indicates 100% in UFBoot, SH-aLRT, and 1.0 in PP. Hyphen (-) indicates lower than 95% in UFBoot, 80% in SH-aLRT, or 0.95 in PP. Nodal values are not shown when UFBoot, SH-aLRT, and PP values are <95%, <80%, and <0.95, respectively. The unit of evolutionary distance is the number of base substitutions per site. A broken square shows that the clade consisted of specimens from eastern Honshu. Abbreviations: Ai = Aichi Pref.; Fs = Fukushima Pref.; Gi = Gifu Pref.; Kn = Kanagawa Pref.; Ky = Kyoto Pref.; Mi = Mie Pref.; My = Miyagi Pref.; Ni = Niigata Pref.; Nn = Nagano Pref.; Sh = Shizuoka Pref.; Si = Saitama Pref.; To = Tokyo Pref.; Yn = Yamanashi Pref.

Although there is no consistency of phylogenetic relationship among Clades A, B, and *D. carniolensis* in four datasets, each topology shows that Clade A is a distinct lineage from other *Dicellophilus* specimens.

Intermorphospecific threshold and POTU delimitation of *Dicellophilus* specimens

The minimum K2P distance between congeneric morphospecies was 21% (*D. carniolensis* (accession no.: KF569305) vs. *D. pulcher* TS20230517-01 from Aichi Pref.). Thus, the intermorphospecific threshold induced by this dataset is 21%. However, the maximum K2P distance was 24% within *D. pulcher* (TS20191006-02 from Tokyo Pref. in Clade B vs. TS20201007-04 from Miyagi Pref. in Clade A).

The maximum K2P distance within Clade A was 0.6% (TS20201007-04 vs. TS20201007-02 and TS20201007-03), and that within Clade B was 15% (TS20210322-01 from Kanagawa Pref. vs. TS20210523-01 from Yamanashi Pref.).

The best five partitioning hypotheses inferred by the ASAP program are shown in Figs 2, 3, with the following ASAP scores: (1) 27 POTUs with a score of 3.0; (2) 18 POTUs with a score of 4.0; (3) 19 POTUs with a score of 4.0; (4) 28 POTUs with a score of 6.0; and (5) 24 POTUs with a score of 7.0.

Morphological examination of Japanese *Dicellophilus*

All 38 specimens of *D. pulcher* (a combination of Clades A and B) examined in steps I–IV have 41 pairs of legs and can be distinguished from *D. carniolensis* and *D. limatus* by the number of pairs of legs (43 pairs in *D. carniolensis* and 45 in *D. limatus*). Examined 23 adult specimens can also be distinguished from *D. anomalus*, which has 41 pairs of legs, by the lack of a pair of setae on the posteromedian part of the clypeus and variable crenulation on the internal margin of the forcipular tarsungulum (Bonato et al. 2010a).

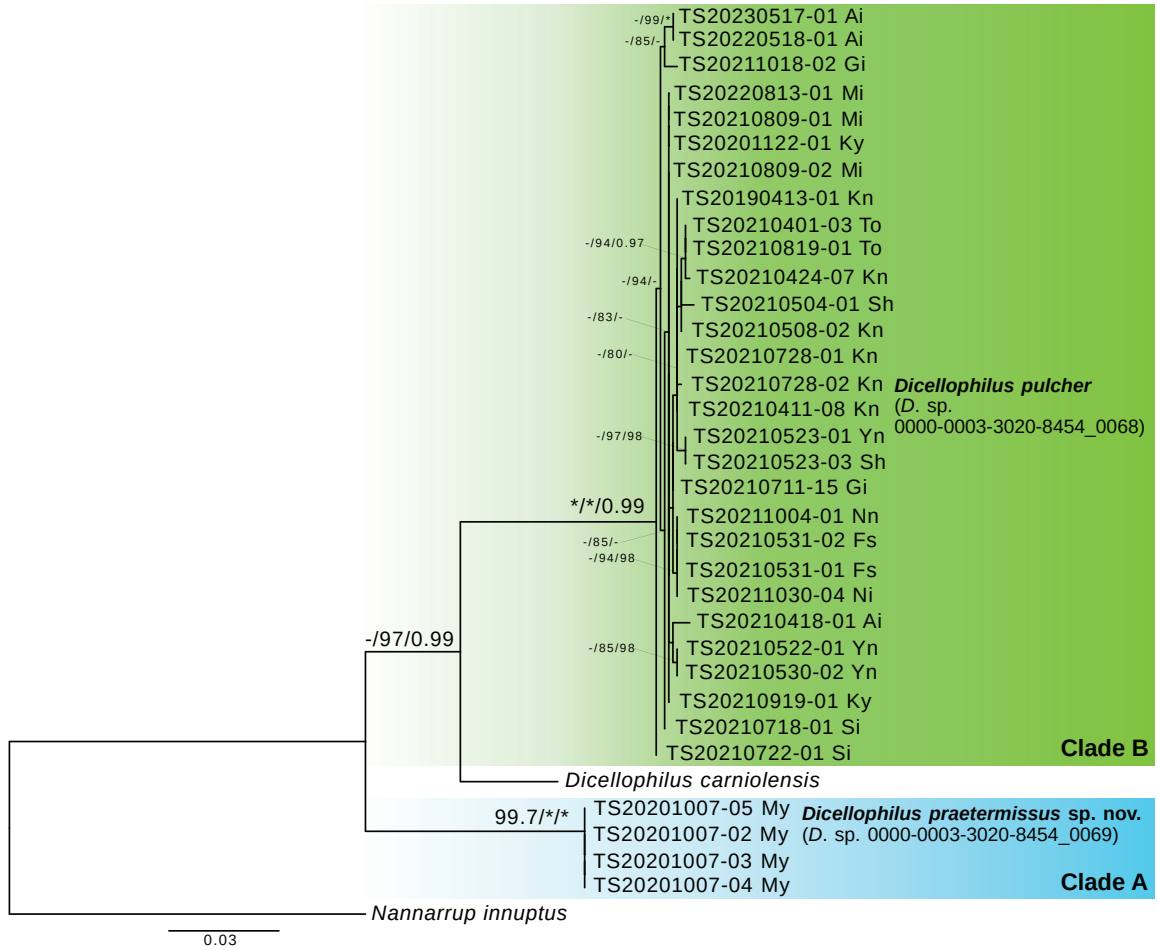

Figure 5. Maximum-likelihood tree of *Dicellophilus* based on the dataset of *28S*. Nodal values are obtained from the ultrafast bootstrap (UFBoot), SH-like approximate likelihood ratio test (SH-aLRT), and posterior probability (PP). The asterisk (*) indicates 100% in UFBoot, SH-aLRT, and 1.0 in PP. Hyphen (-) indicates lower than 95% in UFBoot, 80% in SH-aLRT, or 0.95 in PP. Nodal values are not shown when UFBoot, SH-aLRT, and PP values are <95%, <80%, and <0.95, respectively. The unit of evolutionary distance is the number of base substitutions per site. A broken square shows that the clade consisted of specimens from eastern Honshu. Abbreviations: Ai = Aichi Pref.; Fs = Fukushima Pref.; Gi = Gifu Pref.; Kn = Kanagawa Pref.; Ky = Kyoto Pref.; Mi = Mie Pref.; My = Miyagi Pref.; Ni = Niigata Pref.; Nn = Nagano Pref.; Sh = Shizuoka Pref.; Si = Saitama Pref.; To = Tokyo Pref.; Yn = Yamanashi Pref.

In addition, the 23 adult specimens, including a specimen from the type locality of *D. pulcher* (Subashiri, Oyama, Suntou-gun, Shizuoka Pref.), had the following diagnostic characteristics of *D. pulcher* (Uliana et al. 2007; Bonato et al. 2010a): trunk segments without dark patches; head 1.2–1.4 times as long as it is wide; cephalic plate with a markedly convex lateral margin; clypeus with densely scattered setae; palaclypeal suture evidently converging posteriorly; transverse suture uniformly rounded at center; mandible with 5–7 lamellae; forcipular tarsungulum with evident and variably spaced notches; and 41 pairs of legs.

On the other hand, four specimens of Clade A (TS20201007-02, TS20201007-03, TS20201007-04, and TS20201007-05) were morphologically different from the specimens of Clade B based on the following characteristics: both ends of transverse suture not evidently convex forward; long rather than wide trochanteroprefemur; wide rather than long metasternite (Table 3).

Taxonomic account

Family Mecistocephalidae Bollman, 1893
Genus *Dicellophilus* Cook, 1896

Dicellophilus praetermissus sp. nov.

https://zoobank.org/8A967E03-A5B0-4495-A0E9-6CE1298F3E3D

Figs 6–13

New Japanese name: Date-hirozujimukade

DI. *Dicellophilus* sp. 0000-0003-3020-8454_0069

Type material. ***Holotype*.** 1 adult male, Baba, Akiu-machi, Taihaku-ku, Sendai-shi, Miyagi Pref., Japan (38°16.33'N, 140°32.69'E), 7 October 2020, coll. Sho Tsukamoto (labeled as TS20201007-02), deposited at the Collection of Myriapoda, Department of Zoology, **NSMT**.

***Paratype*.** 1 adult male, Baba, Akiu-machi, Taihaku-ku, Sendai-shi, Miyagi Pref., Japan (38°16.33'N, 140°32.69'E), 7 October 2020, coll. Sho Tsukamoto

Table 3. Morphological comparison between *D. pulcher* and *D. praetermissus* sp. nov.

Putative species identification code	Species identified in the present study	Both ends of transverse suture	The width to length ratio of trochanteroprefemur	The width to length ratio of sternite of ULBS
Dicellophilus sp. 0000-0003-3020-8454_0068	*Dicellophilus pulcher* (Kishida, 1928)	evidently convex forward	1: 0.9–1.1	1: 1.0–1.3
Dicellophilus sp. 0000-0003-3020-8454_0069	*Dicellophilus praetermissus* sp. nov.	not evidently convex	1: 1.3–1.4	1: 0.66–1.0

Figure 6. Habitus of *Dicellophilus praetermissus* sp. nov., paratype (TS20201007-05). Photo by Joe Kutsukake.

(labeled as TS20201007-03), 1 adult female, Baba, Akiu-machi, Taihaku-ku, Sendai-shi, Miyagi Pref., Japan (38°16.33'N, 140°32.69'E), 7 October 2020, coll. Sho Tsukamoto (labeled as TS20201007-04), 1 adult male, Baba, Akiu-machi, Taihaku-ku, Sendai-shi, Miyagi Pref., Japan (38°16.33'N, 140°32.69'E), 7 October 2020, coll. Sho Tsukamoto (labeled as TS20201007-05), deposited at **MNHAH**.

Etymology. The species name is a masculine adjective derived from "overlooked" in Latin. Since the description by Kishida (1928) of *D. pulcher* (as *Mecistocephalus pulcher*), this new species has been overlooked for 90 years, despite documentation of its distribution as *Dicellophilus* in the Sendai-shi, Miyagi Pref. (Takakuwa 1940).

Diagnosis. Trunk segments without dark patches; head 1.4 times as long as wide; lateral margin of cephalic plate abruptly converged posteriorly; clypeus with densely scattered setae; palaclypeal suture evidently converging posteriorly; both ends of transverse suture uniformly rounded; mandible with 6 lamellae; forcipular trochanteroprefemur longer than wide, with one small distal denticle; forcipular tarsungulum with evident and variably spaced notches; metatergite subtrapezoidal; metasternite trapezoidal, wide rather than long; forty-one pairs of legs.

Description. ***General features*** (Fig. 6): Body about 50 mm long (holotype ca 52 mm), gradually attenuated posteriorly, almost uniformly pale yellow, with head and forcipular segment ocher.

Cephalic capsule (Fig. 7A, B): Cephalic plate ca 1.3–1.4× as long as wide; lateral margins markedly convex; posterior margin straight; areolate part visible only at anterior margin; scutes approximately isometric and up to 20 μm wide in 50 mm long specimen; both ends of transverse suture uniformly rounded or slightly convex forward; setae up to ca 300 μm long. Clypeus ca 2.3–2.5× as wide as long, with lateral margins complete, anterior part areolate, with scutes ca 30 μm wide in 50 mm long specimen, clypeal areas absent; clypeus with about 200 setae on most part except lateral and posterior margins; clypeal plagulae undivided by mid-longitudinal areolate stripe. Anterior and distolateral parts of pleurites areolate, without setae, non-areolate part extending forwards distinctly beyond labrum. Side-pieces of labrum not in contact, anterior margin not concave posteriorly but horizontally, divided into anterior and posterior alae by chitinous line, with longitudinal stripes on posterior alae, with medial tooth, and short fringe on posterior margin of side-pieces; mid-piece ca 6.2 times as long as wide, lateral margin concaved.

Antenna (Fig. 8A–H): Antenna with 14 articles, when stretched, ca 2.7–3.2× as long as head length. Intermediate articles longer than wide. Distal part of article areolate, remaining surface not areolate in article I–XIII. Article XIV ca 2.1–2.5× as long as wide, ca 1.1–1.5× as long as article XIII. Setae on articles VIII–XVI denser than articles I–VII. Setae gradually shorter from article VIII to XIV, up to ca 290 μm long on article I, up to ca 270 μm long on article VIII and < 75 μm long on article XIV. Article XIV with two types of sensilla; apical sensilla (arrows in Fig. 8G, H) ca 25 μm long, with wide flat ring at mid-length; club-like (arrowheads in Fig. 8G, H) sensilla ca 15 μm long, clustered in distal part of internal and external sides of article. Rows of spine-like basal sensilla (the 'sensilla microtrichoidea' of Ernst 1983, 1997, 2000) absent on antennal article VI and X. A few pointed sensilla, up to 7.5 μm long, on both dorso-external and ventro-internal position, close to distal margin of articles II, V, IX and XIII.

Figure 7. *Dicellophilus praetermissus* sp. nov., holotype (TS20201007-02) **A** cephalic plate, dorsal **B** clypeus, and clypeal pleurite, ventral. Scale bars: 0.5 mm.

Mandible (Fig. 9A): Five–six pectinate lamellae present; first lamellae with at least 4 elongated teeth. Anterior surface hairy.

First maxillae (Fig. 9B): Coxosternite medially divided but slightly, without setae, without projection on antero-external corners, non-areolate. Coxal projections well developed, with ca 20 setae along internal margin, distal lobe subtriangular. Telopodite uni-articulated and hyaline distally, with 5–6 setae. No lobes on either coxosternite or telopodites.

Second maxillae (Fig. 9B): Coxosternite medially undivided, without suture but areolated on isthmus, with 4+4 setae along anterior margin, with about 25 setae on isthmus, with about 15 setae on lateral margin and posterior corners, anterior margin concave, with metameric pores on posterior part. Telopodites tri-articulate, reaching medial projections and telopodites of first maxillae. Claw of telopodite present.

Forcipular segment (Fig. 10A–E): Tergite trapezoidal, ca 1.3–1.4× as wide as long, with lateral margins converging anteriorly, areolation mainly along two marginal lateral and anterior bands and two paramedian posterior areas, gradually fading into central non-areolate surface; ca 0.5–0.6× as wide as cephalic plate and ca 0.4–0.5× as wide as tergite 1; 3+2 setae of similar length arranged in an anterior row, and ca 20 setae of similar length arranged symmetrically in a posterior row. Mid-longitudinal sulcus of tergite not visible. Pleurite 1.8–1.9× as long as the tergite; dorsal ridge sclerotized; anterior tip (scapular point) well behind anterior margin of coxosternite, and only slightly projecting. Cerrus composed of a group of 10–20 setae on each side of anterodorsal surface of coxosternite, but no paramedian rows of setae. Exposed part of coxosternite ca 1.2× as wide as long; anterior margin with shallow medial concavity and with one pair of denticles; coxopleural sutures complete in entire ventrum, sinuous and diverging anteriorly; chitin-lines absent; condylar processes of forcipular coxosternite well developed. Trochanteroprefemur ca 1.3–1.4× as long as wide; with a pigmented tubercle at distal internal margin. Intermediate articles distinct, with a tubercle on femur and tibia. Tarsungulum with well-pigmented basal tubercle on dorsal surface; both external and internal margins uniformly curved, except for moderate mesal basal bulge; ungulum not distinctly flattened; internal margin of ungulum evidently crenulated, with variably spaced notches. Elongated poison calyx lodged inside intermediate forcipular articles.

Leg-bearing segments (Fig. 11A–D): Forty-one pairs of legs present. Metatergite 1 slightly wider than subsequent one, with two paramedian sulci visible on tergites of anterior half of body, with pretergite. No paratergites. Legs of first pair much smaller than following ones; claws simple, uniformly bent, with 2 accessory spines; posterior spine shorter than anterior spine; with a subsidiary spine near posterior spine (arrow in Fig. 11D). Metasternites slightly longer than wide. Sternal sulcus evident on segment II, but fading towards posterior segments, anteriorly not furcate. No ventral glandular pores on each metasternite.

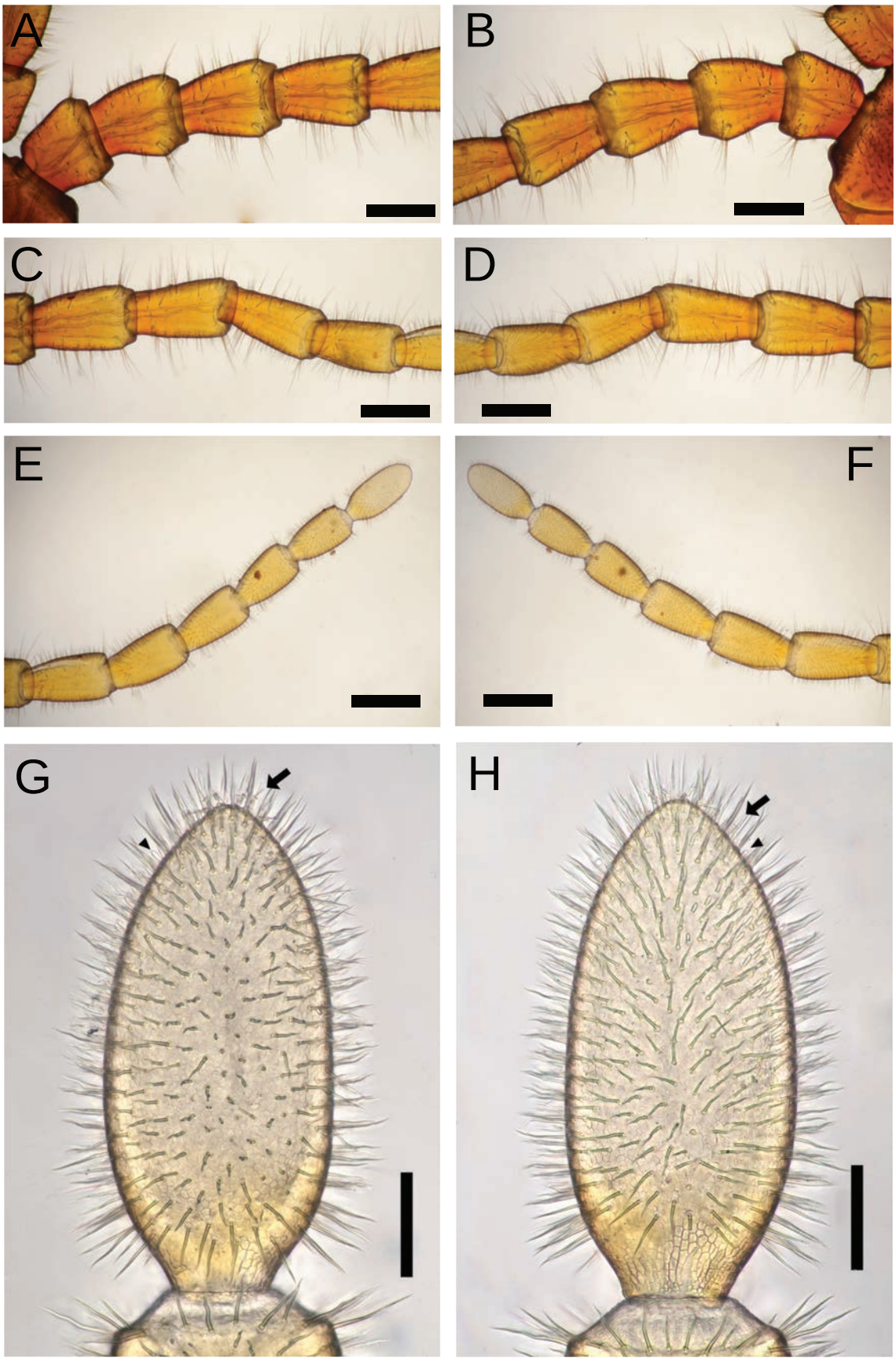

Figure 8. *Dicellophilus praetermissus* sp. nov. **A–F.** Holotype (TS20201007-02) **G, H.** Paratype (TS20201007-04) **A.** Antennal articles I–IV, dorsal; **B.** Antennal articles I–IV, ventral; **C.** Antennal articles V–VIII, dorsal; **D.** Antennal articles V–III, ventral; **E.** Antennal articles IX–XIV, dorsal; **F.** Antennal articles IX–XIV, ventral; **G.** Antennal article XIV, dorsal; **H.** Antennal article XIV, ventral. Arrows indicate apical sensillum; arrowheads indicate club-like sensillum. Scale bars: 0.5 mm (**A–F**); 0.1 mm (**G, H**).

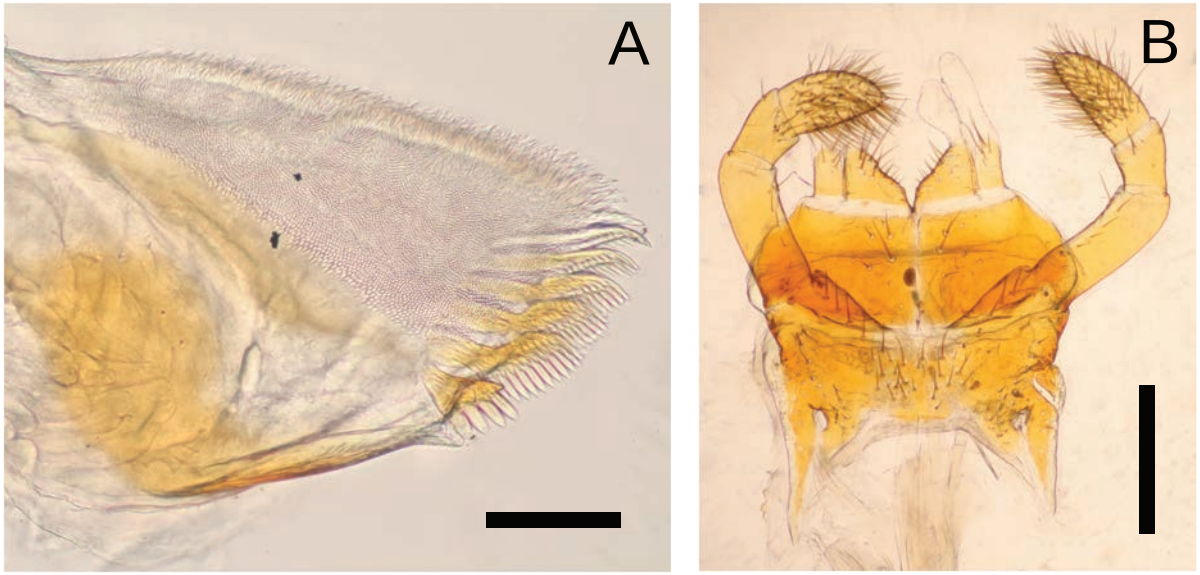

Figure 9. *Dicellophilus praetermissus* sp. nov., holotype (TS20201007-02) **A.** Left mandible, ventral; **B.** Maxillae complex, ventral. Scale bars: 0.1 mm (**A**); 0.5 mm (**B**).

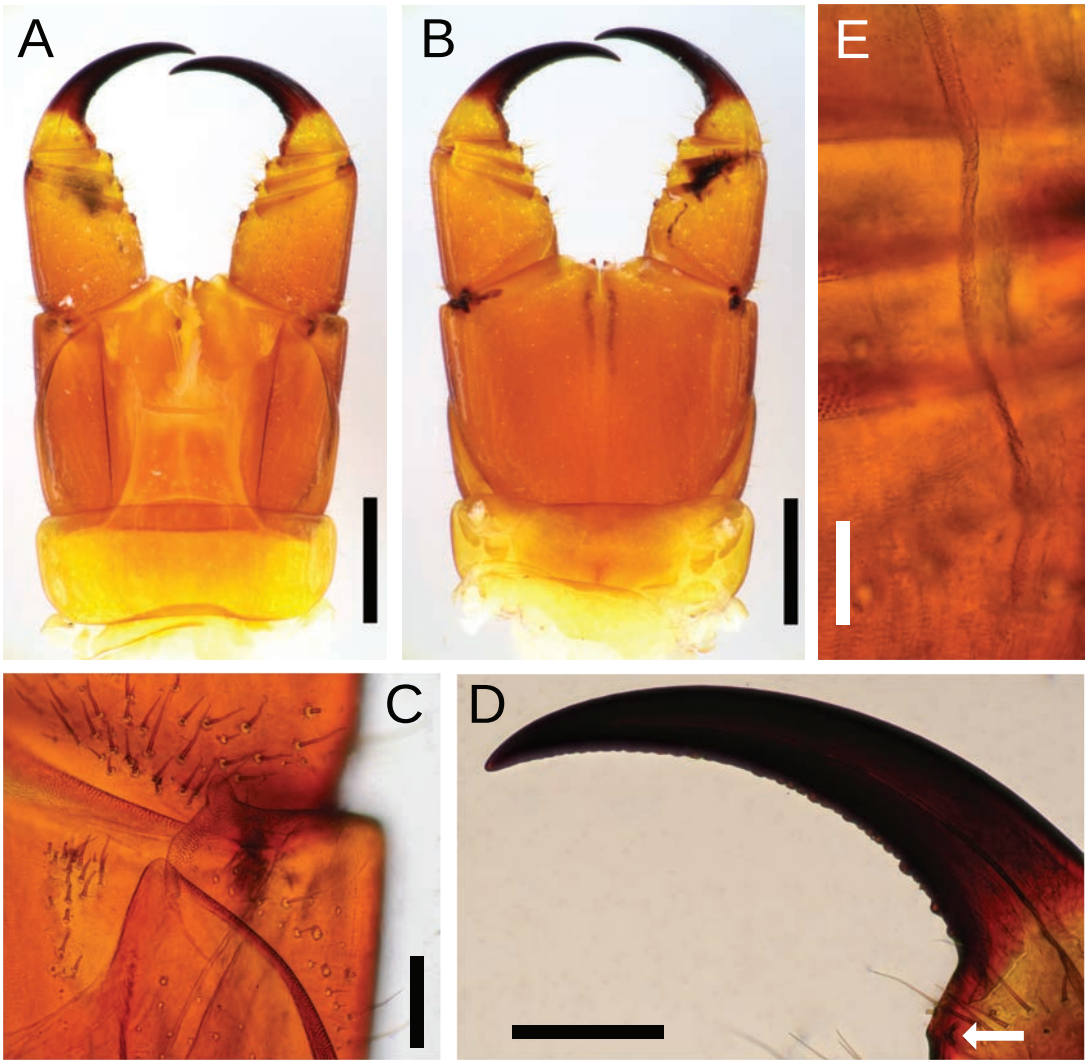

Figure 10. *Dicellophilus praetermissus* sp. nov., holotype (TS20201007-02). **A.** Forcipular segment, dorsal; **B.** Forcipular segment, ventral; **C.** Right condylar process of forcipular coxosternite, dorsal; **D.** Right forcipular tarsungulum, dorsal; **E.** Poison calyx, dorsal. The arrow indicates the basal tubercle of the forcipular tarsungulum. Scale bars: 0.5 mm (**A, B**); 0.2 mm (**C**); 0.3 mm (**D**); 0.1 mm (**E**).

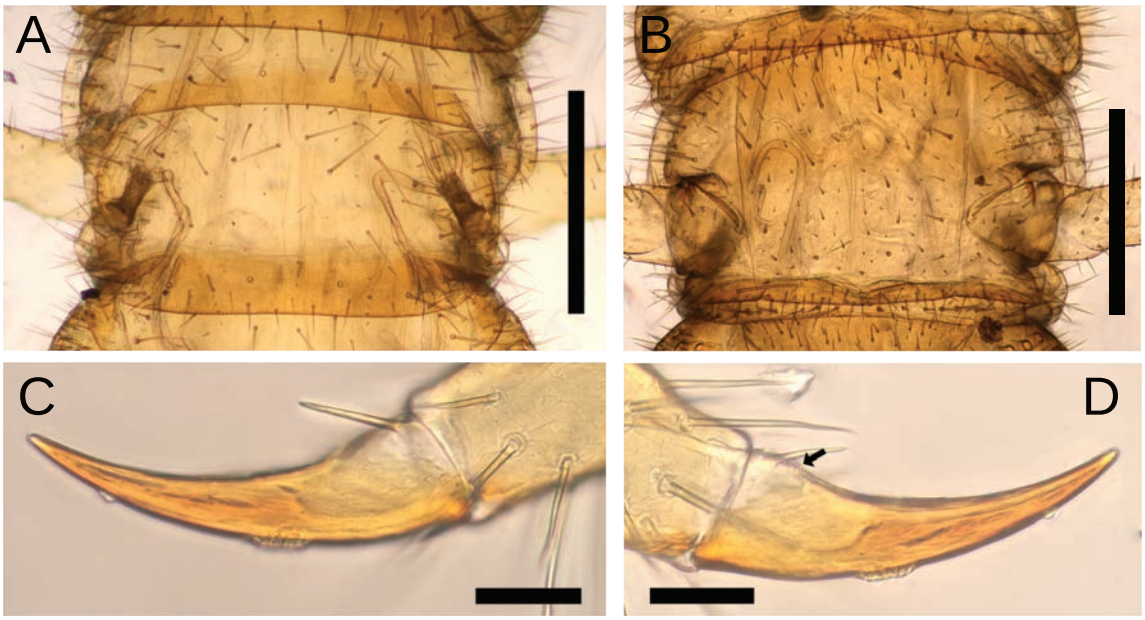

Figure 11. *Dicellophilus praetermissus* sp. nov., holotype (TS20201007-02). **A.** Tergite of leg-bearing segment 40, dorsal; **B.** Sternite of leg-bearing segment 40, ventral; **C.** Pretarsus of left leg 40, anterolateral. **D.** Pretarsus of left leg 2, posterolateral. The arrow indicates a subsidiary spine. Scale bars: 0.5 mm (**A, B**); 0.1 mm (**C, D**).

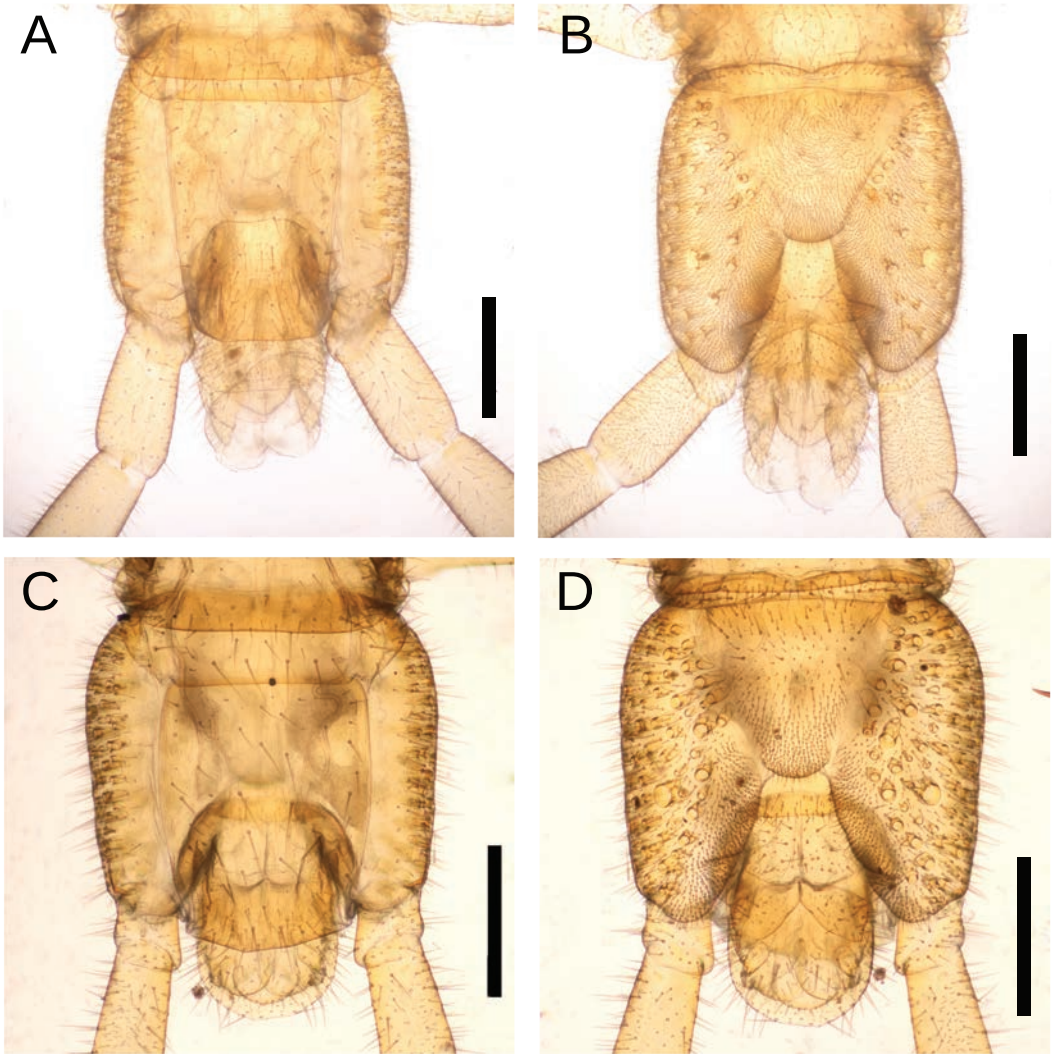

Figure 12. *Dicellophilus praetermissus* sp. nov. **A, B.** Holotype (TS20201007-02) **C, D.** Paratype (TS20201007-04) **A, C.** Ultimate leg-bearing segment and postpedal segment, dorsal; **B, D.** Ultimate leg-bearing segment and postpedal segment, ventral. Scale bars: 0.5 mm.

Figure 13. *Dicellophilus praetermissus* sp. nov., holotype (TS20201007-02). **A.** Left ultimate leg, dorsal; **B.** Left ultimate leg, ventral. Scale bars: 0.5 mm.

Ultimate leg-bearing segment (Figs 12A–D, 13A, B): Pretergite accompanied by pleurites. Metatergite subtrapezoidal, ca 1.2–1.5× as long as wide; lateral margins converging posteriorly. Coxopleuron ca 1.8–2.3× as long as metasternite; coxal organs of each coxopleuron opening through ca 70 independent pores, placed ventrally; distinctly larger pore (macropore) near center of the ventral side. Metasternite trapezoidal, ca 1.1–1.5× as wide as long, anteriorly ca 3.0–3.6× as wide as posteriorly; lateral margins converging backward straightly; setae almost arranged symmetrically, dense on posterior margin. In male holotype (TS20201004-02), telopodite ca 11.5× as long as wide, ca 1.6× as long, and ca 1.3× as wide as penultimate telopodite, with six articles; tarsus 2 ca 3.3× as long as wide and ca 1.1× as long as tarsus 1; setae arranged uniformly, < 200 μm long; pretarsus without claw. In female paratype (TS20201004-04), telopodite ca 13.5× as long as wide, ca 1.8× as long, and ca 1.3× as wide as penultimate telopodite, with six articles; tarsus 2 ca 5.2× as long as wide and ca 1.3× as long as tarsus 1; setae arranged uniformly, < 300 μm long; pretarsus without claw.

Male postpedal segments (Fig. 12A, B): Two gonopods, very widely separated from one another, conical in outline, bi-articulated with sutures, covered with setae. Anal pore present.

Female postpedal segments (Fig. 12C, D): Two gonopods basally touching, subtriangular, bi-articulated with sutures, covered with setae. Anal pore present.

Distribution. Only known from the type locality.

Remarks. *Dicellophilus praetermissus* sp. nov. most closely resembles *D. pulcher* but is distinguishable by the following combination of characteristics: both ends of transverse suture not evidently convex forward; the longer than wide trochanteroprefemur; the wide rather than long metasternite (Table 3).

The record of *D. latifrons* Takakuwa, 1934 (= *D. pulcher*) from Sendai, Miyagi Pref. (Takakuwa 1940) requires confirmation of its identification.

Dicellophilus pulcher (Kishida, 1928)

Figs 14–16

Mecistocephalus pulcher Kishida, 1928: Kishida 1928, 300.
Dicellophilus latifrons: Takakuwa 1934a, 707; Takakuwa 1934b, 355; Takakuwa 1934c, 878.
Dicellophilus japonicus: Verhoeff 1934, 32.
Tygarrup monoporus: Shinohara 1961, 212.
Dicellophilus pulcher: Uliana et al. 2007, 27; Bonato et al. 2010, 525.

DI. *Dicellophilus* sp. 0000-0003-3020-8454_0068

Material examined. See Table 1.

Diagnosis. Mainly based on Bonato et al. (2010a), Uliana et al. (2007), and the present study. Trunk segments without dark patches; head 1.2–1.4 times as long as wide (Fig. 14A, B); lateral margin of cephalic plate abruptly converged posteriorly; clypeus with densely scattered setae (Fig. 14B); paraclypeal suture evidently converging posteriorly (Fig. 14B); both ends of transverse suture convexed forward (Fig. 14A); mandible with 5–7 lamellae; forcipular trochanteroprefemur almost as long as wide, with one small distal denticle (Fig. 15A, B); forcipular tarsungulum with evident and variably spaced notches; metatergite subtrapezoidal (Fig. 16A); metasternite trapezoidal, longer than wide (Fig. 16B); forty-one pairs of legs.

Figure 14. *Dicellophilus pulcher* (TS20210504-01). **A.** Cephalic plate, dorsal; **B.** Clypeus, and clypeal pleurite, ventral. Scale bars: 0.5 mm.

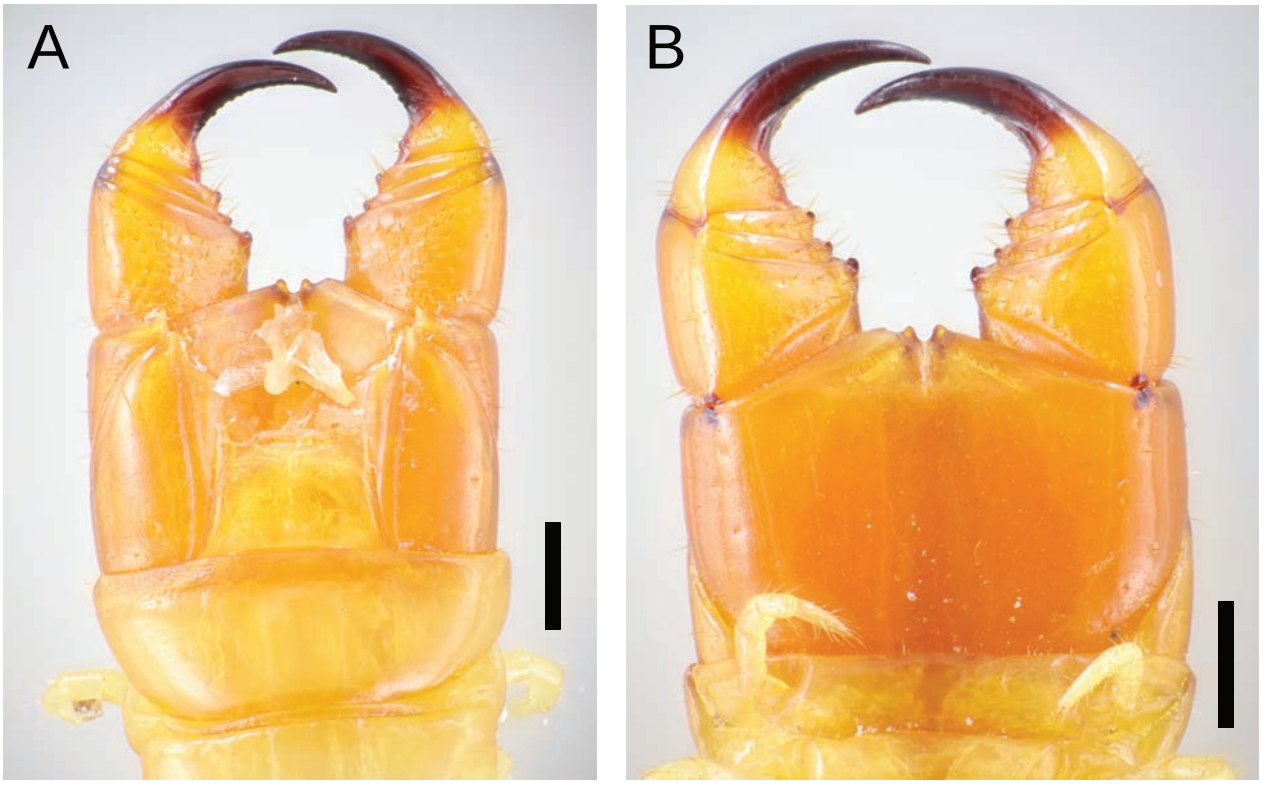

Figure 15. *Dicellophilus pulcher* (TS20210504-01). **A.** Forcipular segment, dorsal; **B.** Forcipular segment, ventral. Scale bars: 0.5 mm.

Type locality. The first section of the Subashiri trail of Mt. Fuji, Shizuoka Pref., Japan (Kishida 1928).

Distribution. Honshu (Fukushima Pref. to Hyogo Pref.).

Remarks. See remarks and the diagnosis of *D. praetermissus* sp. nov. for confirming how to distinguish *D. pulcher* from *D. praetermissus* sp. nov.

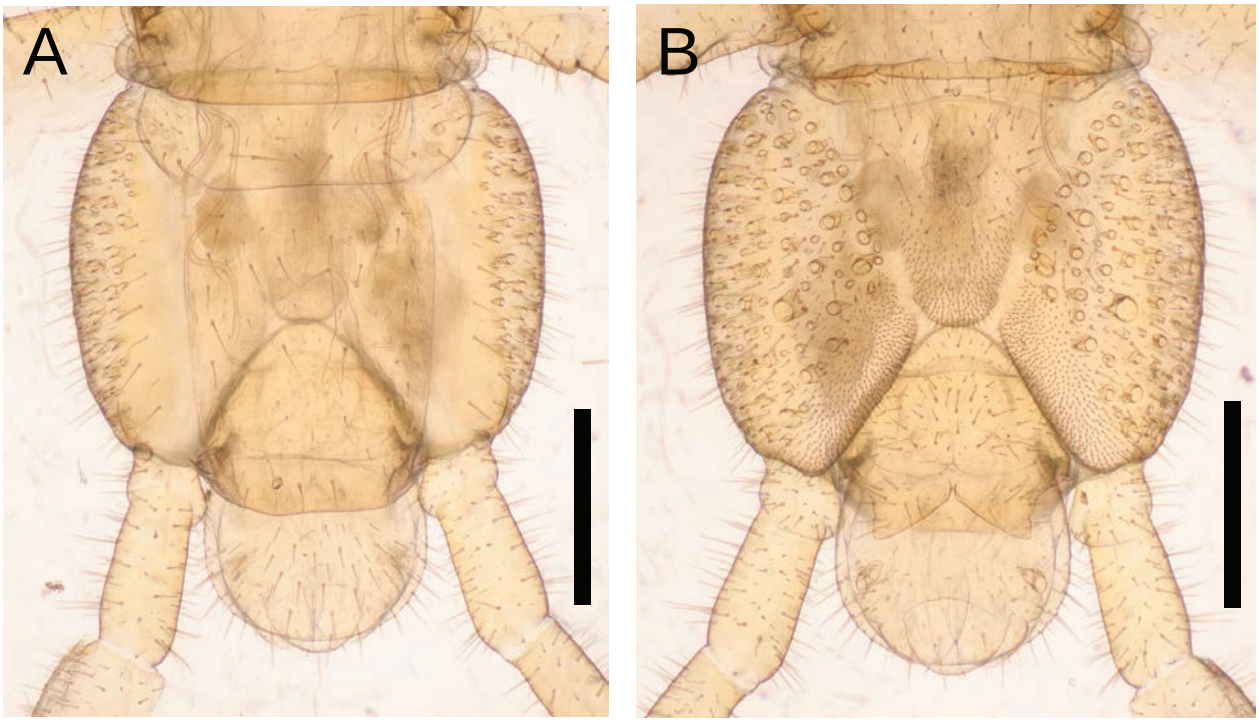

Figure 16. *Dicellophilus pulcher* (TS20210504-01). **A.** Ultimate leg-bearing segment and postpedal segment, dorsal; **B.** Ultimate leg-bearing segment and postpedal segment, ventral. Scale bars: 0.5 mm.

There are three junior synonyms under *D. pulcher*, which were synonymized by previous authors based on morphological examination (Takakuwa 1940; Shinohara 1983; Uliana et al. 2007): *D. latifrons* Takakuwa, 1934; *D. japonicus* Verhoeff, 1934; *Tygarrup monoporus* Shinohara, 1961. *Dicellophilus latifrons* Takakuwa, 1934, which was described in a key to Japanese and Taiwanese species of Mecistcephalidae by Takakuwa (1934a), was later described by Takakuwa (1934b, c) as a new species. Takakuwa (1934a) did not designate a type locality for *D. latifrons*, and Takakuwa (1934b, c) listed the localities: "Kaibara (Hyogo)" (= Tamba City, Hyogo Pref.), "Masudo (bei Tokyo)" (possibly misread of Masuko-mura, currently in Akiruno-shi, Tokyo Pref.), "Komono (Miye)" (= Komono-cho, Mie Pref.), "Ikao (Gumma)" (= Ikahocho, Shibukawa-shi, Gunma Pref.), "Ōta (Gumma)" (= Ota-shi, Gunma Pref.), "Odawara (Kanagawa)" and "Suwa (Nagano)" (annotated by Jonishi and Nakano 2022). Considering the geographic distribution of *D. latifrons* and *D. pulcher* sensu stricto, *D. latifrons* is a junior synonym of *D. pulcher*. *Dicellophilus japonicus* Verhoeff, 1934, was described based on a specimen from "Tokyo" (Verhoeff 1934) and later regarded as a junior synonym of *D. latifrons* based on the comparison of diagnostic characteristics (Takakuwa 1940; Shinohara 1983). Considering the geographic distribution of *D. japonicus* and *D. pulcher* and the phylogenetic analyses of the present study, including TS20181214-01, TS20191006-02, TS20210401-03, and TS20210819-01 from Tokyo Pref., it is not conflicting that *D. japonicus* is a junior synonym of *D. pulcher*. *Tygarrup monoporus* Shinohara, 1961, which is identical to the juvenile of *D. pulcher*, according to Uliana et al. (2007), was described based on the specimen from Manazuru-machi, Ashigarashimo-gun, Kanagawa Pref. (Shinohara 1961). Considering the geographic distribution of *T. monoporus* and *D. pulcher* and the phylogenetic analyses of the present study, including TS20210728-02, which was collected at a linear distance of approximately 13 km from the type locality and could be identified as *T. monoporus*, *T. monoporus* can also be regarded as a junior synonym of *D. pulcher*.

Discussion

Species hypothesis for Japanese *Dicellophilus*

No POTU delimitation hypotheses proposed by ASAP corresponded well to the principle in steps I–IV. This is because each of those hypotheses involves many POTUs, which were separated from each other with a K2P distance lower than the intermorphospecific threshold. Although Clade B could be divided into many more POTUs, such partitioning hypotheses can be rejected as oversplitting in accordance with the species delimitation criteria in step IV with the intermorphospecific threshold (21% in *COI*). Therefore, two putative species were recognized in the 38 *D. pulcher* specimens examined in steps I–IV, and they can be separately labeled as follows: *Dicellophilus* sp. 0000-0003-3020-8454_0068 (= Clade B; hereafter referred to as *D.* sp. 0068) and *D.* sp. 0000-0003-3020-8454_0069 (= Clade A; hereafter referred to as *D.* sp. 0069, Table 3, Figs 2–5).

Only one validly named species of *Dicellophilus* from Japan, *D. pulcher*, was described on the basis of a specimen from the Subashiri trail of Mt. Fuji, Shizuoka Pref. (Kishida 1928). *Dicellophilus* sp. 0068 involves a specimen

from the type locality (TS20210504-01) and shares the number of pairs of legs, the presence of macropores on the coxopleuron, and a wide forcipular trochanteroprefemur with the original description (including figures) of *D. pulcher*. Therefore, *D.* sp. 0068 is conferrable to *D. pulcher*. By contrast, *D.* sp. 0069 can be regarded as a new species based on morphological comparison with other congeners, including *D. pulcher*. This new species is described in the "Taxonomic account" section under the name *Dicellophilus praetermissus* sp. nov. (step V); see also the taxonomic discussion of junior synonyms of *D. pulcher*.

Oversplit of the number of POTUs by ASAP

As mentioned in the result section, many POTUs were divided from the *COI* dataset of *Dicellophilus* examined in the present study. When taking into account the overall genetic diversity of all examined specimens of *Dicellophilus*, i.e., *D. pulcher*, *D. carniolensis* and *D. praetermissus* sp. nov. (maximum genetic divergence in K2P: 24%), the genetic diversity within the morphospecies *D. pulcher* alone is quite high (15%).

Possibly, such an oversplit of POTU would have been caused by the algorithm ASAP and the quite high genetic divergence of *D. pulcher* in the dataset. According to Puillandre et al. (2021), ASAP is a hierarchical clustering algorithm. Each subgroup was separated depending on the average pairwise distance between subgroups and within the subgroup, sample size, and a coalescent mutation rate. Based on this algorithm, the distribution of genetic distances will affect the result of the number of species (= POTUs). In detail, when there is high genetic diversity within one morphospecies compared to the whole dataset, the morphospecies will be divided into several POTUs, in accordance with the possibility of panmixia (*p*-value).

POTUs are divided by the possibility of panmixia, so it can be expected that each POTU will be a biological species. However, each POTU within the morphospecies *D. pulcher* detected in the present study is not regarded as a species until morphological evidence is discovered.

Distribution of *Dicellophilus* in Japan

Dicellophilus specimens examined in Japan were collected from 34°33'N to 38°16'N on Honshu within a latitudinal band, which is congeners' distribution. The authors and their collaborators have collected *Dicellophilus* exclusively from Miyagi Pref. to Kyoto Pref. but not from other areas, despite a comprehensive field trip in Japan (Fig. 1). Therefore, the distribution of *Dicellophilus* in Japan should be restricted from Miyagi Pref. to Kyoto Pref. (see Remarks of *D. pulcher* in this paper; Takakuwa 1940; Uliana et al. 2007).

According to the molecular phylogenetic analyses of *Dicellophilus* specimens in Japan, it is possible that there are two large populations among *D. pulcher*, viz., specimens from Eastern Honshu (Fukushima Pref. to Shizuika Pref. and one specimen from Gifu Pref.) and those from western Honshu (Gifu Pref. to Kyoto Pref.), because the monophyly was supported by the phylogenetic analysis based on the concatenated and *COI* datasets, respectively. However, the boundary between two populations is still not clear due to the lack of field surveys in the central part of Honshu.

In field surveys conducted by the authors in Japan, *D. praetermissus* sp. nov. was collected only in Sendai-shi, Miyagi Pref. (the northern part of Honshu). It is also noteworthy that *D. pulcher* has yet to be collected from the northern part of Honshu (from Aomori Pref. to Miyagi Pref). This result of field surveys shows that the distribution of *D. praetermissus* sp. nov. may segregate from *D. pulcher*, but further field surveys are needed around Miyagi Pref.

Acknowledgments

We are grateful to Dr Masaru Nonaka (visiting researcher of Tokyo Metropolitan University), Dr Namiki Kikuchi (Toyohashi Museum of Natural History), Dr Takahiro Yoshida (assistant professor of Tokyo Metropolitan University), Mr Joe Kutsukake (Tokyo Metropolitan University), Mr Koshi Kawamoto (Tokyo Metropolitan University), Ms Mayu Susukida, Mr Ryo Miyata, Mr Tatsumi Suguro (Keio Yochisha Elementary School), Mr Tomoki Sumino, and Mr Fukube Sumino for collecting and providing *Dicellophilus* specimens. We are further grateful to Dr Namiki Kikuchi and Mr Joe Kutsukake for assisting in collecting and taking photographs of *Dicellophilus praetermissus* sp. nov., respectively. We thank two reviewers for providing valuable comments and suggestions. We also would like to thank Enago (www.enago.jp) for the English language review. This study was supported by the following funds: the Fund for the Promotion of Joint International Research (Fostering Joint International Research (B), JSPS KAKENHI, no. 22KK0087, leader: Katsuyuki Eguchi, FY2022–2025), Grant-in-Aid for Scientific Research (C) (JSPS KAKENHI, no 23K05299, Leader: Emiko Oguri, FY2023–2026), the Tokyo Metropolitan University Fund for TMU Strategic Research (leader: Noriaki Murakami, FY2020–FY2022), and the Asahi Glass Foundation (leader: Katsuyuki Eguchi, FY2017–FY2023).

References

Aberer AJ, Kobert K, Stamatakis A (2014) ExaBayes: Massively parallel Bayesian tree inference for the whole-genome era. Molecular Biology and Evolution 31(10): 2553–2556. https://doi.org/10.1093/molbev/msu236

Bonato L (2011) Order Geophilomorpha. In: Minelli A (Ed.) Treatise on Zoology— Anatomy, Taxonomy, Biology. The Myriapoda I, Brill, Leiden, 407–443.

Bonato L, Foddai D, Minelli A (2003) Evolutionary trends and patterns in centipede segment number based on a cladistic analysis of Mecistocephalidae (Chilopoda: Geophilomorpha). Systematic

Entomology 28(4): 539–579. https://doi.org/10.1046/j.1365-3113.2003.00217.x

Bonato L, Dányi L, Minelli A (2010a) Morphology and phylogeny of *Dicellophilus*, a centipede genus with a highly disjunct distribution (Chilopoda: Mecistocephalidae). Zoological Journal of the Linnean Society 158(3): 501–532. https://doi.org/10.1111/j.1096-3642.2009.00557.x

Bonato L, Edgecombe GD, Lewis JGE, Minelli A, Pereira LA, Shelley RM, Zapparoli M (2010b) A common terminology for the external anatomy of centipedes (Chilopoda). ZooKeys 69: 17–51. https://doi.org/10.3897/zookeys.69.737

Bonato L, Drago L, Murienne J (2014) Phylogeny of Geophilomorpha (Chilopoda) inferred from new morphological and molecular evidence. Cladistics 30(5): 485–507. https://doi.org/10.1111/cla.12060

Bonato L, Bortlin F, De Zen G, Decker P, Linder EN, Orlando M, Spelda J, Voigtländer K, Wesener T (2023) Towards elucidating species diversity of European inland *Strigamia* (Chilopoda: Geophilomorpha): a first reassessment integrating multiple lines of evidence. Zoological Journal of the Linnean Society 199(4): 945–966. https://doi.org/10.1093/zoolinnean/zlad070

Boyer SL, Giribet G (2007) A new model Gondwanan taxon: Systematics and biogeography of the harvestman family Pettalidae (Arachnida, Opiliones, Cyphophthalmi), with a taxonomic revision of genera from Australia and New Zealand. Cladistics 23(4): 337–361. https://doi.org/10.1111/j.1096-0031.2007.00149.x

Dayrat B (2005) Towards integrative taxonomy. Biological Journal of the Linnean Society. Linnean Society of London 85(3): 407–415. https://doi.org/10.1111/j.1095-8312.2005.00503.x

Dyachkov YuV, Bonato L (2022) Morphology and distribution of the Middle Asian centipede genus *Krateraspis* Lignau, 1929 (Chilopoda, Geophilomorpha, Mecistocephalidae). ZooKeys 1095: 143–164. https://doi.org/10.3897/zookeys.1095.80806

Edgecombe GD, Giribet G (2006) A century later – a total evidence re-evaluation of the phylogeny of scutigeromorph centipedes (Myriapoda, Chilopoda). Invertebrate Systematics 20(5): 503–525. https://doi.org/10.1071/IS05044

Ernst A (1983) Die Ultrastruktur der Sinneshaare auf den Antennen von *Geophilus longicornis* Leach (Myriapoda, Chilopoda). IV. Die Sensilla microtrichoidea. Zoologische Jahrbücher. Abteilung für Anatomie 109: 521–546.

Ernst A (1997) Sensilla microtrichoidea – mutmaßliche 'Stel-lungs-rezeptoren' an der Basis der Antennenglieder des Chilopoden Geophilus longicornis Leach. Verhandlungen der Deutschen Zoologischen Gesellschaft 90: 274.

Ernst A (2000) Structure and function of different cuticular sensilla in the centipede *Geophilus longicornis* Leach. Fragmenta Faunistica, Warszawa 43(Suppl.): 113–129.

Guindon S, Dufayard JF, Lefort V, Anisimova M, Hordijk W, Gascuel O (2010) New algorithms and methods to estimate maximum-likelihood phylogenies: Assessing the performance of PhyML 3.0. Systematic Biology 59(3): 307–321. https://doi.org/10.1093/sysbio/syq010

Hoang DT, Chernomor L, von Haeseler A, Minh BQ, Vinh LS (2018) UFBoot2: Improving the ultrafast bootstrap approximation. Molecular Biology and Evolution 35(2): 518–522. https://doi.org/10.1093/molbev/msx281

Jonishi T, Nakano T (2022) Correct Authorships, Synonymies, and Remarks on the Type Series of Fourteen Names of Centipedes Introduced by Yoshioki Takakuwa in 1934 and *Mecistocephalus takakuwai* (Chilopoda: Geophilomorpha and Scolopendromorpha). Species Diversity : An International Journal for Taxonomy, Systematics, Speciation, Biogeography, and Life History Research of Animals 27(1): 71–81. https://doi.org/10.12782/specdiv.27.71

Joshi J, Karanth KP (2012) Coalescent Method in Conjunction with Niche Modeling Reveals Cryptic Diversity among Centipedes in the Western Ghats of South India. PLoS ONE 7(8): e42225. https://doi.org/10.1371/journal.pone.0042225

Katoh K, Standley DM (2013) MAFFT multiple sequence alignment software version 7: Improvements in performance and usability. Molecular Biology and Evolution 30(4): 772–780. https://doi.org/10.1093/molbev/mst010

Kishida K (1928) Ch. 6. Chilopoda. In: Sengen Shrine (Ed.) Animals of Mt. Fuji. Kokinshoin, Tokyo, 290–303. [in Japanese]

Kumar S, Stecher G, Li M, Knyaz C, Tamura K (2018) MEGA X: Molecular evolutionary genetics analysis across computing platforms. Molecular Biology and Evolution 35(6): 1547–1549. https://doi.org/10.1093/molbev/msy096

Murienne J, Edgecombe GD, Giribet G (2010) Including secondary structure, fossils and molecular dating in the centipede tree of life. Molecular Phylogenetics and Evolution 57(1): 301–313. https://doi.org/10.1016/j.ympev.2010.06.022

Nguyen LT, Schmidt HA, von Haeseler A, Minh BQ (2015) IQ-TREE: A Fast and Effective Stochastic Algorithm for Estimating Maximum-Likelihood Phylogenies. Molecular Biology and Evolution 32(1): 268–274. https://doi.org/10.1093/molbev/msu300

Padial JM, Miralles A, De la Riva I, Vences M (2010) The integrative future of taxonomy. Frontiers in Zoology 7(1): 16. https://doi.org/10.1186/1742-9994-7-16

Peretti E, Cecchin C, Fusco G, Gregnanin L, Kos I, Bonato L (2022) Shedding light on species boundaries in small endogeic animals through an integrative approach: species delimitation in the centipede *Clinopodes carinthiacus* (Chilopoda: Geophilidae) in the south-eastern Alps. Zoological Journal of the Linnean Society 196(2): 902–923. https://doi.org/10.1093/zoolinnean/zlac008

Puillandre N, Brouillet S, Achaz G (2021) ASAP: Assemble species by automatic partitioning. Molecular Ecology Resources 21(2): 609–620. https://doi.org/10.1111/1755-0998.13281

Rambaut A, Drummond AJ, Xie D, Baele G, Suchard MA (2018) Posterior summarization in Bayesian phylogenetics using Tracer 1.7. Systematic Biology 67(5): 901–904. https://doi.org/10.1093/sysbio/syy032

Satria R, Kurushima H, Herwina H, Yamane S, Eguchi K (2015) The trap-jaw ant genus *Odontomachus* Latreille (Hymenoptera: Formicidae) from Sumatra, with a new species description. Zootaxa 4048(1): 1–36. https://doi.org/10.11646/zootaxa.4048.1.1

Shinohara K (1961) Taxonomical and morphological studies of Myriapoda VII. Two new species of Mecistocephalidae (Chilopoda). Zoological Magazine 70(7): 212–216. [in Japanese with English Resume]

Shinohara K (1983) Revision on the scientific names of Japanese myriapods. V. On the *Dicellophilus pulcher* (Kishida). Takakuwaia 15: 5–6.

Siriwut W, Edgecombe GD, Sutcharit C, Panha S (2015) The Centipede Genus Scolopendra in Mainland Southeast Asia: Molecular Phylogenetics, Geometric Morphometrics and External Morphology as Tools for Species Delimitation. PLoS ONE 10(8): e0135355. https://doi.org/10.1371/journal.pone.0135355

Siriwut W, Edgecombe GD, Sutcharit C, Tongkerd P, Panha S (2016) A taxonomic review of the centipede genus *Scolopendra* Linnaeus, 1758 (Scolopendromorpha, Scolopendridae) in mainland Southeast

Asia, with description of a new species from Laos. ZooKeys 590: 1–124. https://doi.org/10.3897/zookeys.590.7950

Takakuwa Y (1934a) The family Mecistocephalidae of Japan, I. Botany and Zoology 2(4): 706–712. [in Japanese]

Takakuwa Y (1934b) Neue japanische Mecistocephalidae. Annotationes Zoologicae Japonenses 14: 355–363.

Takakuwa Y (1934c) The family Mecistocephalidae of Japan, II. Botany and Zoology 2(5): 878–884. [in Japanese]

Takakuwa Y (1940) Fauna Nipponica 9 (8, 1). Geophilomorpha. Sanseido, Tokyo, 156 pp. [in Japanese]

The International Commission on Zoological Nomenclature (1999) International Code of Zoological Nomenclature. The International Trust for Zoological Nomenclature 1999, The Natural History Museum - Cromwell Road - London SW7 5BD – UK. https://code.iczn.org/authorship/article-51-citation-of-names-of-authors/?frame=1

Tsukamoto S (2023) Phylogenetic and Taxonomic Study of Japanese and Taiwanese Species of the Centipede Family Mecistocephalidae (Chilopoda: Geophilomorpha). PhD Thesis, Graduate School of Science, Tokyo Metropolitan University, Tokyo.

Tsukamoto S, Shimano S, Murakami T, Hiruta SF, Yamasaki T, Eguchi K (2019) A new species of the genus *Arrup* from a limestone cave in Akiyoshi-dai, Western Japan (Chilopoda, Geophilomorpha, Mecistocephalidae). ZooKeys 830: 33–51. https://doi.org/10.3897/zookeys.830.33060

Tsukamoto S, Nguyen AD, Eguchi K (2021a) Confirmation of the phylogenetic position of the unique geophilomorph genus *Vinaphilus* Tran, Tran & Bonato, 2019 (Chilopoda: Geophilomorpha: Gonibregmatidae) by molecular phylogenetic analyses, with two new species from the Central Highlands of Vietnam. Zoologischer Anzeiger 293: 74–88. https://doi.org/10.1016/j.jcz.2021.05.004

Tsukamoto S, Hiruta SF, Eguchi K, Liao J-R, Shimano S (2021b) A new amphibious species of the genus *Scolopendra* Linnaeus, 1758 (Scolopendromorpha, Scolopendridae) from the Ryukyu Archipelago and Taiwan. Zootaxa 4952(3): 465–494. https://doi.org/10.11646/zootaxa.4952.3.3

Tsukamoto S, Shimano S, Eguchi K (2022) Two new species of the dwarf centipede genus *Nannarrup* Foddai, Bonato, Pereira & Minelli, 2003 (Chilopoda, Geophilomorpha, Mecistocephalidae) from Japan. ZooKeys 1115: 117–150. https://doi.org/10.3897/zookeys.1115.83946

Uliana M, Bonato L, Minelli A (2007) The Mecistocephalidae of the Japanese and Taiwanese islands (Chilopoda: Geophilomorpha). Zootaxa 1396(1): 1–84. https://doi.org/10.11646/zootaxa.1396.1.1

Verhoeff KW (1934) Beiträge zur Systematik und Geographie der Chilopoden. Zoologische Jahrbücher. Abteilung für Systematik 66: 1–112.

Xiong B, Kocher TD (1991) Comparison of mitochondrial DNA sequences of seven morphospecies of black flies (Diptera: Simuliidae). Genome 34(2): 306–311. https://doi.org/10.1139/g91-050

Zoosyst. Evol. 100 (3) 2024, 841–850 | DOI 10.3897/zse.100.125409

PENSOFT

für Natur MUSEUM FÜR NATURKUNDE BERLIN

Integrative taxonomy of a new giant deep-sea caudofoveate from South China Sea cold seeps

Chong Chen[1*], Xu Liu[2*], Xinyu Gu[2], Jian-Wen Qiu[3], Jin Sun[2]

1 *X-STAR, Japan Agency for Marine-Earth Science and Technology (JAMSTEC), 2–15 Natsushima-cho, Yokosuka, Kanagawa 237-0061, Japan*

2 *Key Laboratory of Evolution & Marine Biodiversity (Ministry of Education) and Institute of Evolution & Marine Biodiversity, Ocean University of China, Qingdao 266003, China*

3 *Department of Biology, Hong Kong Baptist University, Hong Kong, China*

https://zoobank.org/8DFFEAA8-B091-46DE-B950-3F25D116CDEE

Corresponding author: Jin Sun (jin_sun@ouc.edu.cn)

Academic editor: Thomas von Rintelen ♦ **Received** 15 April 2024 ♦ **Accepted** 16 May 2024 ♦ **Published** 19 June 2024

Abstract

Caudofoveata is a class of worm-like molluscs (aplacophorans) that typically have an infaunal lifestyle, burrowing in soft bottoms in a wide range of marine habitats from shallow to deep waters. Here, we describe a very large new species of caudofoveate from South China Sea methane seeps growing up to 154 mm in length: *Chaetoderma shenloong* **sp. nov.** It is the first caudofoveate to be named from a chemosynthetic ecosystem and the first aplacophoran mollusc associated with seeps. Our new species stands out from other Pacific *Chaetoderma* species by its large size, a wide body relative to its length, a barely sclerotised radula, and the presence of isosceles-triangular sclerites. Phylogenetic reconstruction using the mitochondrial cytochrome *c* oxidase subunit I (COI) gene placed it within a paraphyletic clade comprising Chaetodermatidae and Limifossoridae, in line with a previous phylogenetic analysis. This also revealed that *C. shenloong* **sp. nov.** is conspecific with a *Chaetoderma* sp. whose whole genome was recently sequenced and assembled but remained undescribed until now. The most closely related species with an available COI sequence was *C. felderi*, the largest caudofoveate species recorded. Our discovery suggests caudofoveates may be present in other seeps globally but so far neglected; a potential example is *C. felderi* from the Gulf of Mexico, where seeps are abundant but whose exact habitat remains unclear.

Key Words

Aplacophora, Caudofoveata, chemosynthetic, F site, Haima, hydrocarbon seep, Jiaolong Ridge, new species

Introduction

Collectively known as the aplacophorans, shell-less worm-molluscs characterised by dense calcareous sclerites covering the body surface comprise two distinct lineages currently considered separate classes, including Solenogastres, which retains a foot groove, and the footless Caudofoveata (Salvini-Plawen 1975; Ponder et al. 2020). While solenogasters mostly live on cnidarians and are predominantly carnivorous, caudofoveates are infaunal and typically feed on detritus, diatoms, and foraminifera (Salvini-Plawen 1972; Salvini-Plawen 2003). Solenogasters are hermaphroditic and lack ctenidia, while caudofoveates are gonochoristic and possess a pair of ctenidia in the posterior mantle cavity.

Caudofoveata comprises about 140 species in three currently recognised families, including Chaetodermatidae Théel, 1875; Limifossoridae Salvini-Plawen, 1970; and Prochaetodermatidae Salvini-Plawen, 1972 (Mikkelsen et al. 2019). Important taxonomic characters include the radula, body form, and shape of the oral shield. Families and genera are primarily defined by radular characteristics, with

* These authors contributed equally to this paper.

chaetodermatids exhibiting a very reduced radula with just one pair of teeth attached to a cone and the other two families having multiple rows of teeth. Prochaetodermatids differ morphologically from limifossorids by the presence of central plates between the teeth as well as jaws. Chaetodermatidae is the largest family with over 80 species, but in the most complete molecular phylogeny of caudofoveates to date (Mikkelsen et al. 2019), Limifossoridae and Chaetodermatidae were nested together, suggesting paraphyly.

Within Chaetodermatidae, the three genera are also separated primarily by radula features (Salvini-Plawen 1984; Saito 2020), where the two denticles are separated in the most species-rich *Chaetoderma* Lovén, 1844, connected by a structure called the symphysis in *Falcidens* Salvini-Plawen, 1968, and completely lacking in *Furcillidens* Scheltema, 1998. Nevertheless, the distinction between *Chaetoderma* and *Falcidens* has been made less clear-cut by the finding that juvenile *Chaetoderma* specimens may exhibit radular characters close to those of *Falcidens* (Mikkelsen and Todt 2018) and that the two genera are paraphyletic and nested within each other in a recent molecular phylogeny (Mikkelsen et al. 2019).

Though both classes range widely from shallow to deep waters, the majority of the described species inhabit the upper continental shelf. Only Solenogastres has been recorded from deep-sea chemosynthetic ecosystems, with six described species in Simrothiellidae Salvini-Plawen, 1978, from east Pacific hydrothermal vents; these include four species of *Helicoradomenia* Scheltema & Kuzirian, 1991, plus *Sensilloherpia pholidota* Salvini-Plawen, 2008, and *Diptyaloherpia insolita* Salvini-Plawen, 2008 (Scheltema and Kuzirian 1991; Scheltema 2000; Salvini-Plawen 2008). No aplacophorans specific to cold seeps have been found to date, except an unnamed species provisionally assigned to *Chaetoderma* from methane seep sites in the South China Sea (He et al. 2023; Wang et al. 2024). Here, we collected caudofoveate specimens from the Haima cold seep in the South China Sea and characterised them using morphological and molecular methods. These revealed them to belong to a new species morphologically corresponding to a very large-sized *Chaetoderma*, which we describe herein.

Materials and methods

Sample collection

Caudofoveate molluscs were collected by the remotely operated vehicle (ROV) *Pioneer* using a push-corer equipped with a 60-cm-long tube from dark-coloured sediments around a population of the vesicomyid clam *Archivesica marissinica* (Chen, Okutani, Liang & Qiu, 2018) (originally described as *"Calyptogena" marissinica*) (Chen et al. 2018) within Site 01 of the Haima methane seep in the South China Sea, on-board R/V *Xiangyanghong 01* cruise XYH01-2022-06. Upon recovery on the research vessel, caudofoveates were picked out from the cores and placed in 99% ethanol or flash-frozen using liquid nitrogen and kept in a freezer at -80 °C.

Morphology

Specimens were photographed using a Canon EOS-5Ds R digital single-reflex lens camera equipped with an EF100mm f/2.8L Macro IS USM lens. For radula examinations, the radula was dissected out with the tissue around it and slowly dissolved using a 20% household bleach solution. Upon dissolution, the radula was washed in MilliQ water and then photographed using a Nikon Eclipse Ti2 slide microscope, where multiple photographs were stacked using Adobe Photoshop CC. To examine the spicules, the cuticle was dissected using fine tweezers and forceps under a dissecting binocular (Olympus SZX16). Sclerites were examined in six regions of the body (see Fig. 1A), including the peribuccal region, the foregut region, the midgut region, the midgut sac region, the prepallial region, and the pallial region (Saito and Salvini-Plawen 2014). The cuticle pieces were dissolved in a 20% household bleach solution for approximately four hours until the sclerites could be easily removed. The sclerites were washed in MilliQ water and then placed on slide glasses, cover-slipped, and examined under an Olympus BX53 compound microscope. Sclerite lengths were measured using the Olympus CellSens software. Additionally, scanning electron microscopy (SEM) was carried out for the primary spicule types of each body region using a LEO 1530 FE-SEM at Hong Kong Baptist University.

DNA amplification, sequencing, and phylogenetic analyses

We attempted to amplify the barcoding region of the mitochondrial cytochrome *c* oxidase subunit I gene (COI) using invertebrate universal primers (Folmer et al. 1994), but this was unsuccessful for all specimens. Previously, a long COI sequence covering the barcoding region (1085 bp) of a caudofoveate belonging to the same species collected from the Haima seep preserved in ethanol (designated as paratype 3 herein, see below) was published from Illumina sequencing (GenBank accession OQ749925) (He et al. 2023). Furthermore, the whole genome of a caudofoveate tentatively identified as '*Chaetoderma* sp.' from Jiaolong Ridge (also known as 'F site' or 'Formosa Ridge'), another South China Sea seep, had been published (Wang et al. 2024) on GenBank (BioProject PRJNA1009791, genome sequencing survey data SRX21498718). We used the MEGAHIT assembler (Li et al. 2015) to run an assembly of this draft genome downloaded from NCBI and used the BLAST tool with the Haima COI sequence to obtain the COI sequence from the Jiaolong Ridge individual sequenced by Wang et al. (2024).

To check the similarity of COI sequences among the studied individuals, a custom primer pair was specifically designed using the NCBI primer designing tool from avail-

able COI sequences of Caudofoveata. Our primer pairs Caudo_COI_F: TTAAGAGTATAGTGATTGCTCCTGC and Caudo_COI_R: AGGATTTGGAAACTGACTACTCCC, designed to amplify a 408-bp fragment, were used to sequence the COI gene in all study individuals from Haima. This primer pair lies within the barcoding region and can also be useful for use on other caudofoveates, with the primers aligning reasonably well with most available chaetodermatid and limifossorid sequences. The PCR amplification was done using the following protocol: 94 °C for 1 min for initial denaturation, followed by 94 °C for 45 s, 53 °C for 45 s, and 72 °C for 45 s. After 35 cycles, the reaction was held at 72 °C for 7 min. Successful PCR products confirmed using gel electrophoresis were sent to the Beijing Genomics Institute (Qingdao, China) for Sanger sequencing. Sequences were checked by eye before downstream analyses. Newly generated COI sequences were deposited in NCBI GenBank under the accession numbers PP664117–PP664119.

As the region amplified using our new primer set is significantly shorter than the Folmer et al. (1994) barcoding region, we only used the long COI sequences (one from Haima and one from Jiaolong Ridge) for phylogenetic reconstruction. We downloaded COI barcoding sequences of described caudofoveate species available on NCBI GenBank used in a previous phylogenetic reconstruction (Mikkelsen et al. 2019) and added our two long sequences to the analysis. Three solenogaster species were used as the outgroup, following the same study. All COI sequences were imported into Phylosuite v1.2.2 (Zhang et al. 2020) for phylogenetic analyses. The sequences were first aligned with MAFFT v7.313 (Katoh and Standley 2013) using the "L-INS-I" strategy to result in a 660 bp alignment. Then, trimAl v1.2 was used to remove spurious regions with the "automated1" option. This led to a final alignment of 594 bp. We note that the two sequences of Prochaetodermatidae caused a gap of about 50 bp in our pre-trimming alignment available on Figshare (see Chen et al. 2024). For now, we have included these sequences following a previous study (Mikkelsen et al. 2019), but this issue may require further investigation in the future by re-sequencing more prochaetodermatids. Partionfinder2 (Lanfear et al. 2016) was used to find the best-fit model for the alignment (GTR+I+G), and phylogenetic reconstruction was carried out using the maximum likelihood method in IQ-TREE2 (Minh et al. 2020), where we carried out 5000 bootstraps. The consensus tree was visualised using FigTree v1.3.1. The alignment files as well as the consensus tree output from IQ-TREE2 are available on Figshare (Chen et al. 2024). Pairwise Kimura-2-Parameter (K2P) distances between the COI sequences were calculated using MEGA X (Kumar et al. 2018).

Type repository

Type specimens are deposited in the Tropical Marine Biodiversity Collections of the South China Sea, Chinese Academy of Sciences, Guangzhou, China (TMBC).

Results

Taxonomy

Order Chaetodermatida Simroth, 1893
Family Chaetodermatidae Théel, 1875

Genus *Chaetoderma* Lovén, 1844

Type species. *Chaetoderma nitidulum* Lovén, 1844 (type by monotypy)

***Chaetoderma shenloong* sp. nov.**

https://zoobank.org/234D44D1-8542-43E6-BAD8-261CB5D8850F
Figs 1–4

'Caudofoveata Indet. 1' – He et al. (2023): 4, table 1, fig. 2i.
'*Chaetoderma* sp.' – Wang et al. (2024): 1, fig. 1.

Type locality. Inside dark-coloured mud around a vesicomyid clam colony, Haima methane seep (16°43.937'N, 110°27.681'E, depth 1385 m), South China Sea, taken using a push-corer by ROV *Pioneer*, R/V *Xiangyanghong 01* cruise XYH01-2022-06, September 20th, 2022.

Type specimens. ***Holotype*** (Fig. 1A, B), total length 154 mm, maximum width 20 mm, 99% ethanol, specimen with different parts of the body dissected and mounted on glass slides that are deposited together with the body, COI sequence PP664117 (TMBC031015). ***Paratype 1*** (Fig. 1C), total length 106 mm, maximum width 11 mm, 99% ethanol, COI sequence PP664118 (TMBC031016). ***Paratype 2*** (Figs 1D, 2A), total length 58 mm, maximum width 6 mm, 99% ethanol, COI sequence PP664119 (TMBC031017). ***Paratype 3*** (Fig. 5 inset), total length 115 mm, maximum width 8 mm, 99% ethanol (TMBC031018); a photograph of this specimen was published as fig. 2i of (He et al. 2023), COI sequence OQ836653. All type specimens were from a single sampling event at the type locality.

Diagnosis. A very large *Chaetoderma* reaching over 150 mm in body length, with a thick body up to 20 mm in width. Radula translucent with irregular sclerotisation in the median cone, a single pair of barely sclerotised teeth, and a dome-shaped membrane with circular lateral projections. Sclerites shaped like isosceles-triangles present between the foregut region and the midgut sac region.

Description. Animal (Fig. 1) up to 154 mm in length, rather chunky and broad cylindrical, up to 20 mm in width. Foregut region and midgut region separated by a deep groove ('neck'), situated approximately one-fourth to one-fifth from anterior of the body. Anterior of the neck typically slightly thicker than the posterior. Posterium (the posterior-most part of the body from prepallial to pallial regions) short at about the hindmost one-tenth of the body. The bulbous, dorsoterminal sense organ takes the form of an elongated dorsal-median groove (Fig. 1B). Oral shield (Fig. 2A) small, about one-third as wide as the

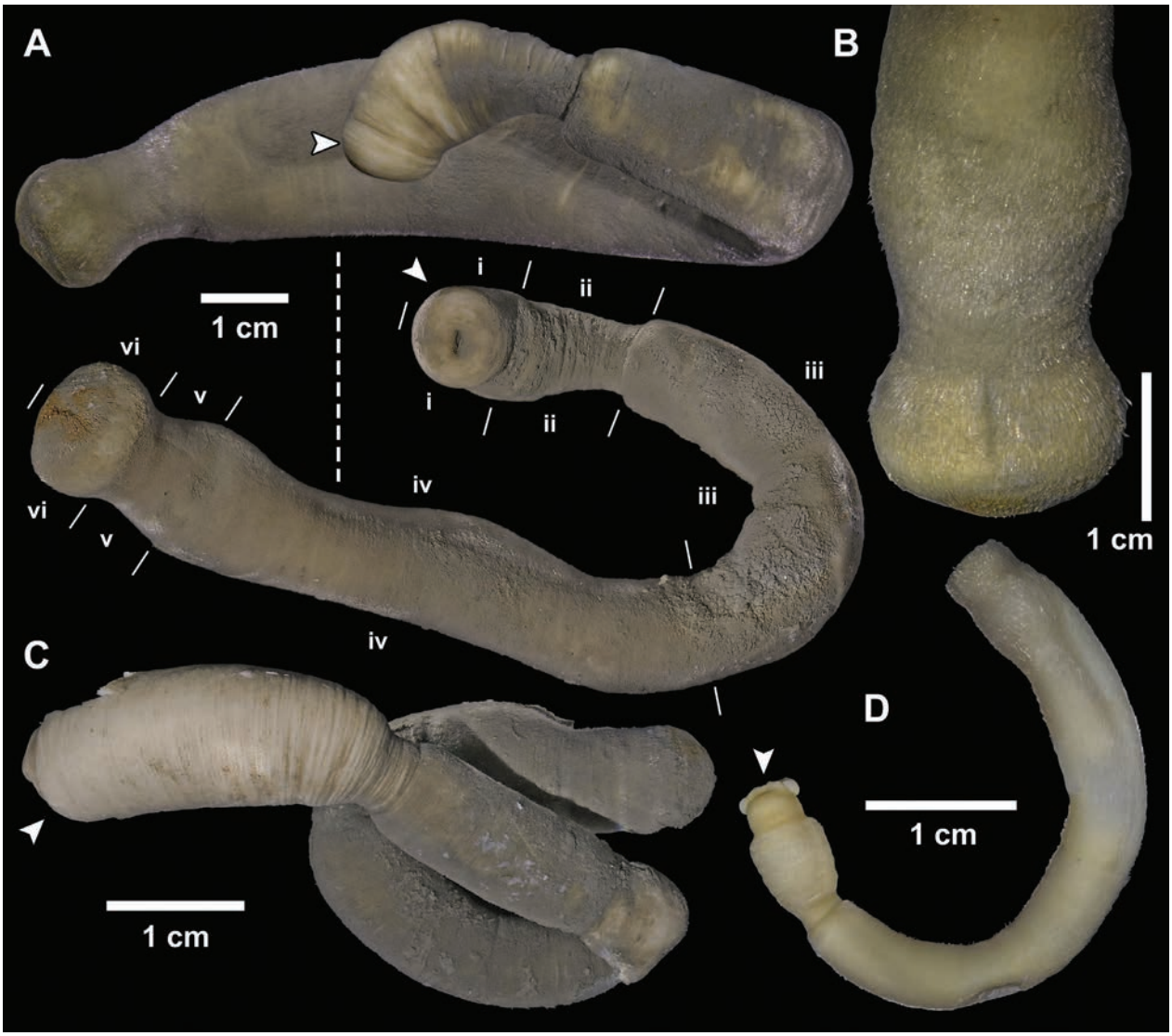

Figure 1. *Chaetoderma shenloong* sp. nov., photographs of preserved-type specimens. **A.** Holotype (TMBC031015), lowercase Roman numerals indicate the six body regions from where sclerites were examined: i) peribuccal region, ii) foregut region, iii) midgut region, iv) midgut sac region, v) prepallial region, and vi) pallial region; **B.** Holotype (TMBC031015), enlarged dorsal view of the prepallial and pallial regions; **C.** Paratype 1 (TMBC031016); **D.** Paratype 2 (TMBC031017). Arrowheads indicate the anterior end of the animal.

body, wider than high, with mouth opening at the centre. Colouration at different shades of yellowish white, with some variability across body regions and individuals. Dark mud accumulates between sclerites, resulting in a blackish appearance in fresh specimens before cleaning.

Radula (Fig. 2B, C) very small compared to the size of the body (190 by 125 μm in size), translucent, and barely sclerotised overall. Consisting of a single pair of barely sclerotised and sickle-shaped denticles about 35 μm in length, each denticle individually connected to the median cone by lateral connections. Median cone about 130 μm in length, irregularly and very weakly sclerotised in the distal 80% along the length and about one-third to half of the width. The dome-shaped membrane is extensive and surrounds the cone, with a circular lateral projection on either side near the base of each tooth.

Sclerites (Figs 3, 4) in the peribuccal region are of two types: the dominant type, small, lead-shaped or narrow teardrop-shaped cylindrical forms (Figs 3A, 4) without waist, basal margin flat in the middle and slightly curved to the side, narrowing to a sharp tip distally along the blade, blade 5–6 times as long as the base, lacking obvious sculpture, up to 107 by 18 μm in size. The second type lanceolate, flat, waist indistinct, basal margin almost flat, blade 5 times as long as base, the side facing outside ornamented by a median keel that weakens towards the base, sided by weak longitudinal grooves with thickened lateral margins, the side facing the body with only very weak longitudinal lines; up to 145 by 28 μm in size. The same two types also present in the foregut region (Figs 3B, 4), but larger, with the teardrop-shaped ones up to 146 by 23 μm and the lanceolate type up to 171 by 33 μm in size. In this region, a rare third type present, overall similar in morphology to the lanceolate type but with a flatter basal margin and a much wider base, with the blade being 2.5–3 times as

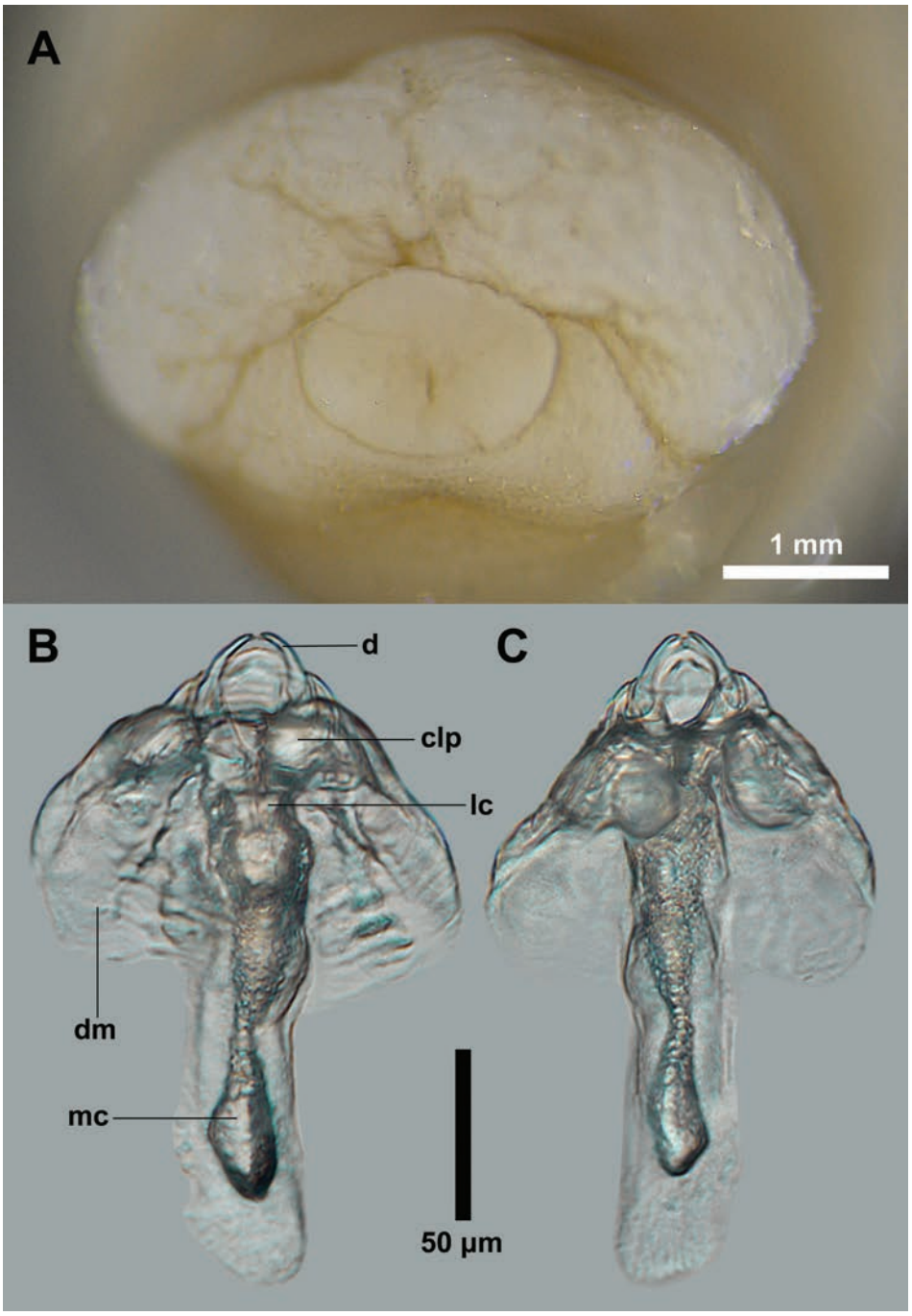

Figure 2. *Chaetoderma shenloong* sp. nov. **A.** Oral shield of paratype 2 (TMBC031017); radula: **B.** Dorsal view; **C.** Ventral view. Abbreviations: clp, circular lateral projection; d, denticles; dm, dome-shaped membrane; lc, lateral connections; mc, median cone.

long as the base, leading to an isosceles-triangle shape up to 149 by 53 µm in size.

The midgut region (Figs 3C, 4) has both lanceolate and isosceles-triangle types, but larger at up to 287 by 40 µm and up to 257 by 51 µm in size, respectively. Here, the lanceolate type more common than the isosceles-triangle type. The isosceles-triangle sclerites here narrower, with the blades being 4–5 times as long as the base. These two types also present in the midgut sac region (Figs 3D, 4) but larger, with the lanceolate type being up to 391 by 50 µm and the isosceles-triangle type up to 330 by 70 µm in size. Furthermore, an additional needle-type sclerite present from this region, cylindrical at the slanted base, lacking waist, blade 12–13 times as long as the base, straight-sided until the distal one-fourth, where it narrows and flattens to a sharp tip, the side facing outwards ornamented by weak to strong median keel sided by several weak longitudinal grooves, lateral margin slightly thickened, the side facing the body smooth except weak longitudinal grooves; up to 655 by 51 µm in size. In this region, needle-type sclerites rather rare.

The prepallial region (Figs 3E, 4) has lanceolate-type and needle-type sclerites, but even larger at up to 404 by 53 µm and 850 by 55 µm in size. The needle-type becoming more common in this region than the midgut sac region.

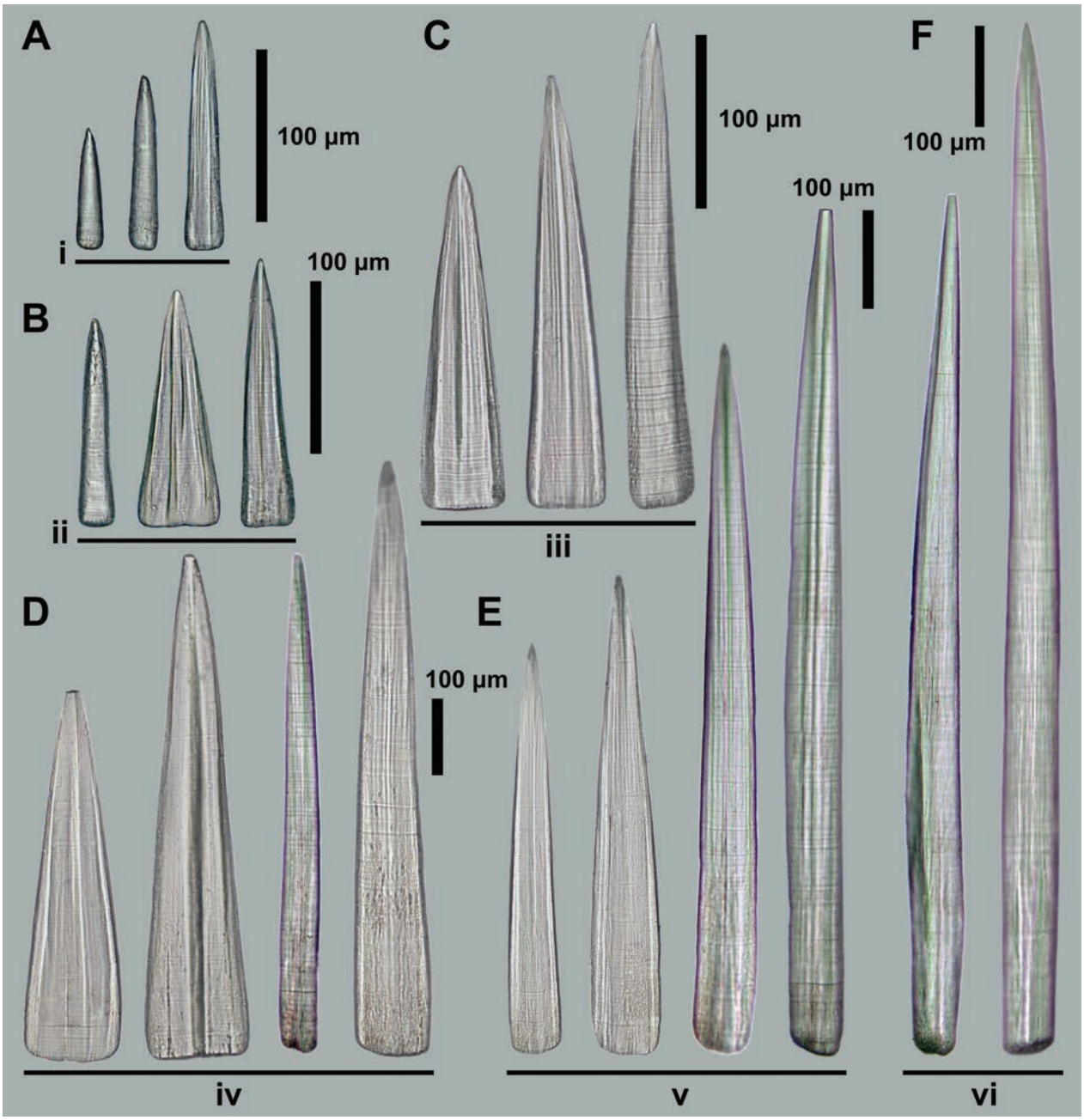

Figure 3. *Chaetoderma shenloong* sp. nov., light micrographs of representative sclerites from each body region. **A.** Peribuccal region (i); **B.** Foregut region (ii); **C.** Midgut region (iii); **D.** Midgut sac region (iv); **E.** Prepallial region (v); **F.** Pallial region (vi).

In the pallial region, only the needle-type sclerite present, where it reaches the longest dimensions across the whole animal at 1023 by 56 µm in size and also more slender, with the blade being 16–20 times as long as the base.

Etymology. From Mandarin Chinese, "*Shén"* (divine, deity) + "*Loong"* (dragon), referring to a group of mysterious and mystic dragons in Chinese mythology. Named in allusion to the long and giant body form of the new *Chaetoderma*, which carries many 'scales' on its body like dragons. A well-known Chinese saying is 'You shall never see the head and tail of "*Shén Loong"* at the same time,' used to refer to something or someone being highly elusive, like caudofoveates living deep inside sediments. Used as a noun in apposition.

Distribution. Haima and Jiaolong Ridge methane seep sites in the South China Sea (see molecular phylogeny section below). For a map of these sites, see He et al. (2023).

Remarks. The placement of this new species in *Chaetoderma* is supported by the overall body form, the oral shield morphology, and the radula. *Chaetoderma shenloong* sp. nov. is among the largest species known in the genus; the only species larger in size is *C. felderi* (Ivanov & Scheltema, 2007), trawled from between 610 and 850 m in the Gulf of Mexico, reaching a body length of 365 mm (Ivanov and Scheltema 2007; Mikkelsen et al. 2019). The body shape of *C. felderi* is much more elongated and only reaches 9 mm in width despite being much longer

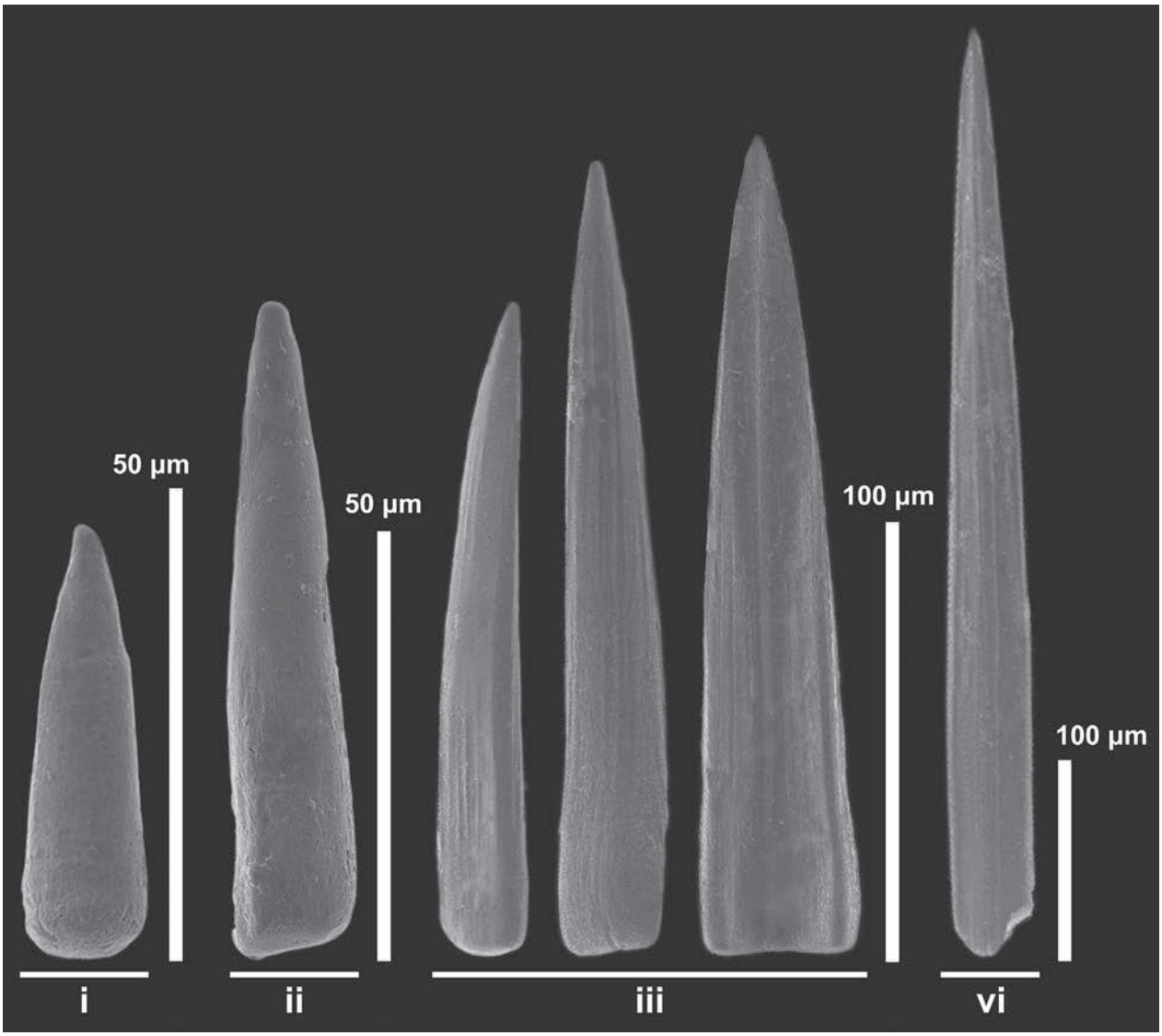

Figure 4. *Chaetoderma shenloong* sp. nov., scanning electron micrographs of representative sclerites from each section of the body. From left to right: the peribuccal region (i), the neck represented by the foregut region (ii), the trunk represented by the midgut region (iii), and the pallial region (vi).

(Ivanov and Scheltema 2007), making it easy to separate from *C. shenloong* sp. nov. morphologically. These two species are also the only species possessing isosceles-triangular sclerites, but their radulae are completely different, with those of *C. felderi* being much larger at about 690 µm in length with much more reduced teeth (Ivanov and Scheltema 2007). *Chaetoderma productum* Wirén, 1892, from the northeastern Atlantic is another species that may reach a similar length as *C. shenloong* sp. nov., but even at 150 mm in length, the width of *C. productum* is only about 3 mm (Wirén 1892), making it very distinctly different from *C. shenloong* sp. nov. No other described *Chaetoderma* species from the western Pacific are known to reach comparable sizes (Saito and Salvini-Plawen 2014), and even small specimens of *C. shenloong* sp. nov. would be distinct from them by the barely sclerotised radula and the presence of isoceles-triangular sclerites.

Molecular phylogeny and genetic distance

Our maximum likelihood phylogenetic reconstruction using the mitochondrial COI gene (Fig. 5) recovered a monophyletic and fully supported Prochaetodermatidae (bootstrap support, BS = 100) and a strongly supported clade consisting of Chaetodermatidae and Limifossoridae nested within each other (BS = 95). This condition was also recovered in a previous phylogeny (Mikkelsen et al. 2019) and is suggestive that these families may be paraphyletic. Furthermore, species assigned to the two chaetodermatid genera *Chaetoderma* and *Falcidens* did not form monophyletic clades but were scattered within the Chaetodermatidae/Limifossoridae clade, again agreeing with the same previous study. The two *Chaetoderma* sequences from South China Sea seeps, including paratype 3 of *C. shenloong* sp. nov. and the Jiaolong Ridge data recovered from a published genomic study (Wang

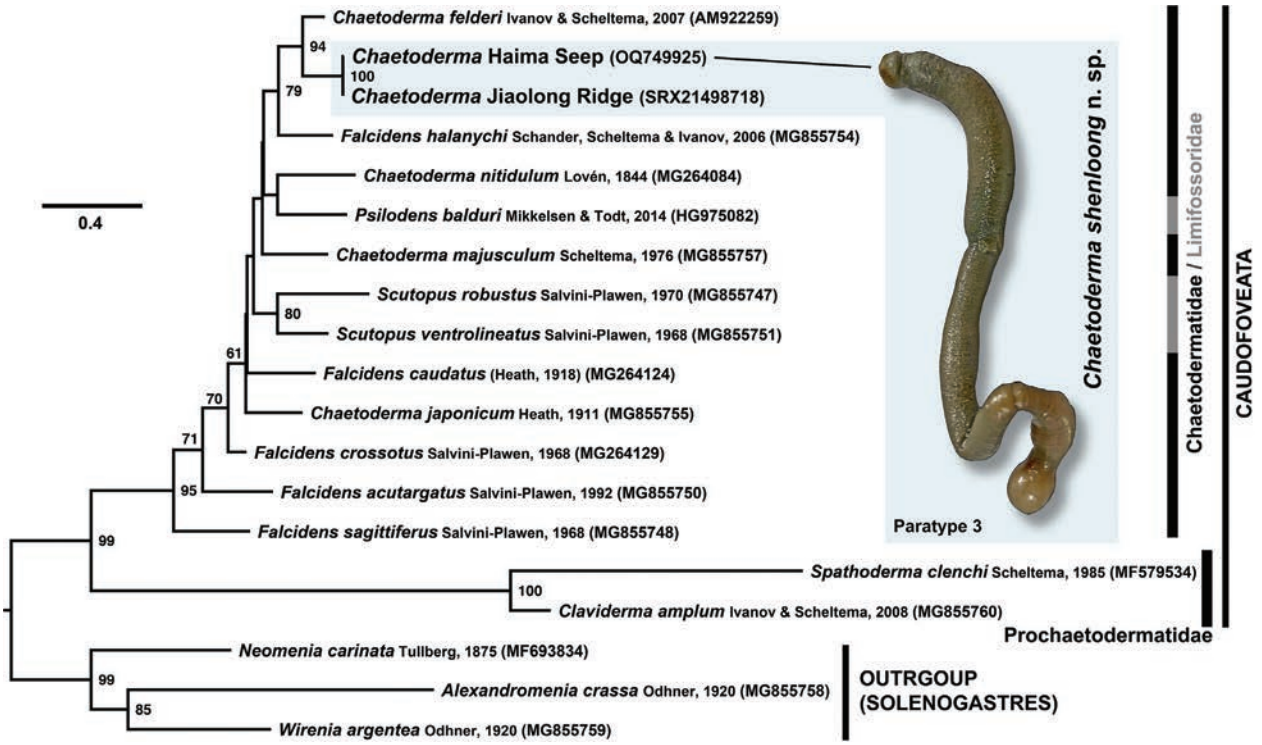

Figure 5. Maximum likelihood phylogenetic reconstruction of Caudofoveata carried out using a 594 bp alignment of the mitochondrial COI gene, with a photograph of paratype 3 (TMBC031018) when alive as an inset. Node values indicate bootstrap support; only those over 60 are shown.

et al. 2024), formed a fully supported clade (BP = 100). We interpret that these two both represent *C. shenloong* sp. nov., meaning the '*Chaetoderma* sp.' whose genome was recently sequenced (Wang et al. 2024) is the same as *C. shenloong* sp. nov. The sister species of *C. shenloong* sp. nov. in the tree was *C. felderi*, the two species forming a well-supported clade (BP = 94).

The K2P distance between the two COI sequences of *C. shenloong* sp. nov. used for phylogenetic reconstruction was 0.5% across 660 bp, supporting their conspecificity. From a 393-bp alignment of all five *C. shenloong* sp. nov. COI sequences (the holotype and three paratypes from Haima plus the Jiaolong Ridge sequence) obtained using our newly designed primers, the K2P distance was 0.3–0.8%. The K2P distance calculated across the 660-bp COI gene fragment between *C. shenloong* sp. nov. and *C. felderi* was 15.4–16.0%.

Discussion

Our phylogenetic reconstruction revealed a sister relationship between *Chaetoderma shenloong* sp. nov. and *C. felderi*, the two largest-bodied species thus far known across Caudofoveata, in a derived position within the class. Although the taxon sampling of our tree across the caudofoveate diversity is still limited, this plus the two species sharing the isosceles-triangular sclerite type are suggestive that they represent a lineage of deep-sea caudofoveates characterised by large body sizes. The distant geographic distribution between these two taxa (South China Sea vs. Gulf of Mexico) may mean many more deep-sea giant caudofoveates remain to be discovered in all oceans around the globe but have simply been overlooked, which is not surprising given the caudofoveates are severely understudied (Señarís et al. 2016; Mikkelsen et al. 2019; Ponder et al. 2020).

Chaetoderma shenloong sp. nov. is the first caudofoveate reported from chemosynthetic ecosystems (He et al. 2023; Wang et al. 2024) and also the first aplacophoran mollusc linked to deep-sea hydrocarbon seeps, with the only previous examples being solenogasters from hot vents (Scheltema and Kuzirian 1991; Scheltema 2000; Salvini-Plawen 2008). The atypical microhabitat of *C. shenloong* sp. nov., located tens of centimetres beneath the sediment surface in oxygen-depleted mud, poses challenges for its collection during standard surveys conducted by deep-submersibles. These surveys tend to focus on epifaunal communities, thereby generating a bias against infaunal species (Mizuno et al. 2022; Sigwart et al. 2023). Classical methods such as dredges or box corers can sample infauna more effectively, but targeting small-sized hotspots, such as specific parts of a seep, is challenging. These may explain why *C. shenloong* sp. nov. eluded earlier efforts to characterise seep communities in the South China Sea (Feng et al. 2018). Although the specific habitat of the other giant species, *C. felderi*, is unknown as it was

serendipitously dredged, the upper continental shelf above 1000 m of water depth in the Gulf of Mexico is known to harbour many dozens of hydrocarbon seep sites (Cordes et al. 2009). It is possible that *C. felderi* also inhabits reducing mud in such seeps. Our discovery of the magnificent seep caudofoveate *C. shenloong* sp. nov. warrants the search for such deep infaunal species in other chemosynthetic habitats worldwide.

Data availability

Specimens studied in the present study have been deposited in the Tropical Marine Biodiversity Collections of the South China Sea, Chinese Academy of Sciences, Guangzhou, China, under numbers TMBC031015–TMBC031018. New sequences generated in this study have been deposited in NCBI GenBank under accession numbers PP664117–PP664119. For phylogenetic analyses, the alignment file before and after trimming as well as the consensus tree output from IQ-TREE2 are available on Figshare (Chen et al. 2024) under the DOI: 10.6084/m9.figshare.25834315.

Author contributions

CC, J-WQ, and JS conceived and designed the study. JS collected the specimens at sea. CC, XL, and XG carried out dissections and light microscopy. XL carried out molecular work and scanning electron microscopy. CC drafted the original manuscript, which was critically revised and contributed to by all other authors.

Acknowledgements

We thank the captain and crew of R/V *Xiangyanghong 01* and the pilots of ROV *Pioneer* for their efforts to ensure successful sampling during the cruise XYH01-2022-06. Yixuan Li (Hong Kong Baptist University) is gratefully acknowledged for her help in specimen photography, and Yunlong Li (Ocean University of China) for his help in bioinformatics. This study was supported by the Natural Science Foundation of Shandong Province (ZR2023IQ014) and the Fundamental Research Funds for the Central Universities (202172002 and 202241002). Constructive comments from Franziska S. Bergmeier (The University of Alabama), Kevin M. Kocot (The University of Alabama), and Hiroshi Saito (National Science and Nature Museum, Tsukuba) improved an earlier version of this paper. We take this chance to express our deepest condolences for the recent passing of artist Akira Toriyama (1955–2024), whose characters *Shenron* (= *Shenlong* or *Shenloong*) in *Dragon Ball* and the dragon family in the *Dragon Quest* series in part inspired the specific epithet of our new species.

References

Chen C, Okutani T, Liang Q, Qiu J-W (2018) A noteworthy new species of the family Vesicomyidae from the South China Sea (Bivalvia: Glossoidea). Venus (Tokyo) 76: 29–37. https://doi.org/10.18941/venus.76.1-4_29

Chen C, Liu X, Gu X, Qiu J-W, Sun J (2024) Supplementary files for molecular analyses in: Integrative taxonomy of a new giant deep-sea caudofoveate from South China Sea cold seeps by Chong Chen, Xu Liu, Xinyu Gu, Jian-Wen Qiu, Jin Sun in Zoosystematics and Evolution. Figshare. https://doi.org/10.6084/m9.figshare.25834315

Cordes EE, Bergquist DC, Fisher CR (2009) Macro-ecology of Gulf of Mexico cold seeps. Annual Review of Marine Science 1(1): 143–168. https://doi.org/10.1146/annurev.marine.010908.163912

Feng D, Qiu J-W, Hu Y, Peckmann J, Guan H, Tong H, Chen C, Chen J, Gong S, Li N, Chen D (2018) Cold seep systems in the South China Sea: An overview. Journal of Asian Earth Sciences 168: 3–16. https://doi.org/10.1016/j.jseaes.2018.09.021

Folmer O, Black M, Hoeh W, Lutz R, Vrijenhoek R (1994) DNA primers for amplification of mitochondrial cytochrome *c* oxidase subunit I from diverse metazoan invertebrates. Molecular Marine Biology and Biotechnology 3: 294–299.

He X, Xu T, Chen C, Liu X, Li Y-X, Zhong Z, Gu X, Lin Y-T, Lan Y, Yan G, Sun Y, Qiu J-W, Qian P-Y, Sun J (2023) Same (sea) bed different dreams: Biological community structure of the Haima seep reveals distinct biogeographic affinities. The Innovation Geoscience 1(2): 100019. https://doi.org/10.59717/j.xinn-geo.2023.100019

Ivanov DL, Scheltema AH (2007) *Chaetoderma felderi* – a new giant caudofoveate species from the Gulf of Mexico (Mollusca: Aplacophora). Ruthenica 17: 7–12.

Katoh K, Standley DM (2013) MAFFT multiple sequence alignment software version 7: Improvements in performance and usability. Molecular Biology and Evolution 30(4): 772–780. https://doi.org/10.1093/molbev/mst010

Kumar S, Stecher G, Li M, Knyaz C, Tamura K (2018) MEGA X: Molecular evolutionary genetics analysis across computing platforms. Molecular Biology and Evolution 35(6): 1547–1549. https://doi.org/10.1093/molbev/msy096

Lanfear R, Frandsen PB, Wright AM, Senfeld T, Calcott B (2016) PartitionFinder 2: New methods for selecting partitioned models of evolution for molecular and morphological phylogenetic analyses. Molecular Biology and Evolution 34: 772–773. https://doi.org/10.1093/molbev/msw260

Li D, Liu C-M, Luo R, Sadakane K, Lam T-W (2015) MEGAHIT: An ultra-fast single-node solution for large and complex metagenomics assembly via succinct de Bruijn graph. Bioinformatics (Oxford, England) 31(10): 1674–1676. https://doi.org/10.1093/bioinformatics/btv033

Mikkelsen NT, Todt C (2018) One or many? Molecular versus morphological diversity in the aplacophoran *Chaetoderma nitidulum* Lovén, 1844 (Mollusca: Caudofoveata). The Journal of Molluscan Studies 84(2): 113–131. https://doi.org/10.1093/mollus/eyy009

Mikkelsen NT, Todt C, Kocot KM, Halanych KM, Willassen E (2019) Molecular phylogeny of Caudofoveata (Mollusca) challenges traditional views. Molecular Phylogenetics and Evolution 132: 138–150. https://doi.org/10.1016/j.ympev.2018.10.037

Minh BQ, Schmidt HA, Chernomor O, Schrempf D, Woodhams MD, von Haeseler A, Lanfear R (2020) IQ-TREE 2: New models and efficient methods for phylogenetic inference in the genomic era.

Molecular Biology and Evolution 37(5): 1530–1534. https://doi.org/10.1093/molbev/msaa015

Mizuno K, Nomaki H, Chen C, Seike K (2022) Deep-sea infauna with calcified exoskeletons imaged in situ using a new 3D acoustic coring system (A-core-2000). Scientific Reports 12(1): 12101. https://doi.org/10.1038/s41598-022-16356-3

Ponder WF, Lindberg DR, Ponder JM (2020) Biology and Evolution of the Mollusca, Volume 2. CRC Press, Boca Raton, FL, 892 pp. https://doi.org/10.1201/9781351115254

Saito H (2020) A new species of *Falcidens* (Mollusca: Caudofoveata: Chaetodermatidae) from the Pacific Coast of Japan. Bulletin of the National Museum of Nature and Science Series A 46: 79–87.

Saito H, Salvini-Plawen L (2014) Four new species of the aplacophoran class Caudofoveata (Mollusca) from the southern Sea of Japan. Journal of Natural History 48(45–48): 2965–2983. https://doi.org/10.1080/00222933.2014.959577

Salvini-Plawen Lv (1972) Zur Morphologie und Phylogenie der Mollusken: Die Beziehungen der Caudofoveata und der Solenogastres als Aculifera, als Mollusca und als Spiralia. Zeitschrift für Wissenschaftliche Zoologie 184: 205–394.

Salvini-Plawen Lv (1975) Mollusca, Caudofoveata. In: Sneli J-A, Sivertsen E, Brattstrøm H (Eds) Marine Invertebrates of Scandinavia No 4 Vol 4. Universitetsforlaget, Oslo, 1–55. https://doi.org/10.1163/9789004627192

Salvini-Plawen Lv (1984) Comments on *Chaetoderma* and *Crystallophrisson* (Mollusca, Caudofoveata). Zoologicheskii Zhurnal 63: 171–175.

Salvini-Plawen Lv (2003) On the phylogenetic significance of the aplacophoran Mollusca. Iberus: Revista de la Sociedad Espanola de Malacologia 21: 67–97.

Salvini-Plawen L (2008) Three new species of Simrothiellidae (Solenogastres) associated with the hot-vent biotope. The Journal of Molluscan Studies 74(3): 223–238. https://doi.org/10.1093/mollus/eyn010

Scheltema A (2000) Two new hydrothermal vent species, *Helicoradomenia bisquama* and *Helicoradomenia acredema*, from the eastern Pacific Ocean (Mollusca, Aplacophora). Argonauta 14: 15–25.

Scheltema A, Kuzirian AM (1991) *Helicoradomenia juani* gen *et* sp. nov., a Pacific hydrotermal vent aplacophora (Mollusca: Neomeniomorpha). The Veliger 34: 195–203.

Señarís MP, García-Álvarez O, Urgorri V (2016) Four new species of Chaetodermatidae (Mollusca, Caudofoveata) from bathyal bottoms of the NW Iberian Peninsula. Helgoland Marine Research 70(1): 28. https://doi.org/10.1186/s10152-016-0475-6

Sigwart JD, Brandt A, Di Franco D, Briones EE, Gerken S, Gooday AJ, Grimes CJ, Głuchowska K, Hoffmann S, Jażdżewska AM, Kamyab E, Kelch A, Knauber H, Kohlenbach K, Miguez-Salas O, Moreau C, Ogawa A, Poliseno A, Santín Muriel A, Tandberg AHS, Theising FI, Walter T, Wölfl A-C, Chen C (2023) Heterogeneity on the abyssal plains: A case study in the Bering Sea. Frontiers in Marine Science 9: 1037482. https://doi.org/10.3389/fmars.2022.1037482

Wang Y, Wang M, Li J, Zhang J, Zhang L (2024) A chromosome-level genome assembly of a deep-sea symbiotic Aplacophora mollusc *Chaetoderma* sp. Scientific Data 11(1): 133. https://doi.org/10.1038/s41597-024-02940-x

Wirén A (1892) Studien über die Solenogastren. II. *Chaetoderma productum*, *Neomenia*, *Proneomenia acuminata*. Kungliga Svenska Vetenskaps-Akademiens Handlingar 25: 1–99.

Zhang D, Gao F, Jakovlić I, Zou H, Zhang J, Li WX, Wang GT (2020) PhyloSuite: An integrated and scalable desktop platform for streamlined molecular sequence data management and evolutionary phylogenetics studies. Molecular Ecology Resources 20(1): 348–355. https://doi.org/10.1111/1755-0998.13096

Zoosyst. Evol. 100 (3) 2024, 851–862 | DOI 10.3897/zse.100.120224

PENSOFT

MUSEUM FÜR NATURKUNDE BERLIN

Hidden in the bamboo: A new parachuting frog (Rhacophoridae, *Rhacophorus*) from the borderlands of western China, with comments on the taxonomy of *R. rhodopus*

Ping-Shin Lee[1*], Ben Liu[1*], Meng Ouyang[1], Ren-Da Ai[2], Xiao-Long Liu[3], Yan-Hong He[2], Ping-Qian Huang[1], Ying-Chun Li[4], R. S. Naveen[5,6], Zhi-Yong Yuan[3], Jin-Min Chen[1]

1 *The Anhui Provincial Key Laboratory of Biodiversity Conservation and Ecological Security in the Yangtze River Basin, College of Life Sciences, Anhui Normal University, Wuhu 241000, Anhui, China*

2 *Key Laboratory for Conserving Wildlife with Small Populations in Yunnan, Southwest Forestry University, Kunming 650224, Yunnan, China*

3 *Key Laboratory of Freshwater Fish Reproduction and Development Ministry of Education, College of Life Science, Southwest University, Chongqing, 400715, China*

4 *Gaoligong Mountain Forest Ecosystem Observation and Research Station of Yunnan Province, Yunnan, China*

5 *Sálim Ali Centre for Ornithology and Natural History, Anaikatty, Coimbatore, Tamil Nadu, India*

6 *EDGE of Existence Programme, Conservation and Policy, Zoological Society of London, London, NW1 4RY, UK*

https://zoobank.org/2245A35B-E010-455D-82AC-DE9B327F4440

Corresponding authors: Jin-Min Chen (chenjinminkiz@126.com); Zhi-Yong Yuan (yuanzhiyongkiz@126.com)

Academic editor: Umilaela Arifin ♦ **Received** 4 February 2024 ♦ **Accepted** 3 June 2024 ♦ **Published** 21 June 2024

Abstract

The Gaoligong Mountains are characterized by large variations in elevation and topography, which support high levels of biodiversity and endemism that remain largely understudied. Herein, based on the integration of morphological comparisons and phylogenetic reconstruction, we describe a new species of *Rhacophorus* from the northern Gaoligong Mountains, Yunnan Province, China. The new species, *Rhacophorus dulongensis* **sp. nov.**, is morphologically distinguishable from its congeners based on the differences in body size, head length, tibia length, snout and tongue shape, toe webbing formula and coloration, ventral skin texture and coloration, dorsal pattern and coloration, body macroglands, iris coloration, and pattern of markings on flanks. Phylogenetically, it differs from its congeners by uncorrected *p*-distances of >4.8% for the 16S rRNA gene fragment. *Rhacophorus dulongensis* **sp. nov.** is likely to be found in Myanmar, considering its type locality lies close to the China-Myanmar border. The phylogenetic analysis revealed that the "widespread" species, *R. rhodopus*, is a species complex and a composite of five distinct lineages. The results revealed that *R. napoensis* is also found in Vietnam, making it a new country record for Vietnam. Interestingly, *R. dulongensis* **sp. nov.** likely breeds in bamboo, a hidden behavioral characteristic that makes them easy to overlook. Given the ongoing habitat loss and degradation in the region, further biological exploration is urgently needed in the Gaoligong Mountains as a biodiversity reservoir.

Key Words

Biodiversity hotspot, frog, Gaoligong Mountains, new record species, new species, systematics

* These authors contributed equally to this work.

Introduction

The Gaoligong Mountains, situated longitudinally along the border of China and Myanmar, are at the convergence of three key biodiversity hotspots: Indo-Burma, the Himalaya, and the Mountains of Southwest China (Myers et al. 2000). These mountains extend north-south in the western part of Yunnan Province, China, and are drained by the Irrawaddy River on the west and the Salween River on the east (Chaplin 2005). Due to its large variation in elevation, multiple latitudinal belts, and complex topography, which provided a wide range of neighboring climatic and structural niches, this region represents a classic example of a montane hotspot for biodiversity and endemicity (Ricketts et al. 2005). Recently, the rate of new species discovery from the Gaoligong Mountains has been high, including new primates (e.g., Geissmann et al. 2011; Fan et al. 2017; Hu et al. 2022; Li et al. 2024). Despite this, amphibians and reptiles in the northern Gaoligong Mountains have remained poorly studied because of difficulties in accessing the region previously (Liu et al. 2021; Wu et al. 2021), suggesting that our knowledge of the region's herpetofaunal diversity is incomplete.

Currently, the frog genus *Rhacophorus* Kuhl and Van Hasselt, 1822, contains 43 species, distributed widely across Asia, including India, Myanmar, Bangladesh, Laos, Thailand, Vietnam, Cambodia, Malaysia, Brunei, and Indonesia, as well as southern China (Jiang et al. 2019; Frost 2024). At present, the following eight species of *Rhacophorus* have been recorded from China: *R. bipunctatus* Ahl, 1927; *R. kio* Ohler & Delorme, 2006; *R. laoshan* Mo, Jiang, Xie, & Ohler, 2008; *R. napoensis* Li, Liu, Yu, & Sun, 2022; *R. orlovi* Ziegler & Köhler, 2001; *R. rhodopus* Liu & Hu, 1960; *R. translineatus* Wu, 1977; and *R. tuberculatus* (Anderson, 1871) (Che et al. 2020; Naveen et al. 2023; AmphibiaChina 2024). Recent studies suggest that the overall species richness of *Rhacophorus* is underestimated (Kropachev et al. 2022; Li et al. 2022). The reevaluations of the "widespread" species and the survey of unexplored areas are likely to reveal overlooked diversity.

During the recent herpetological surveys in Dulongjiang Village, northern Gaoligong Mountains, Yunnan Province, China, we collected unidentified specimens of a *Rhacophorus* population, which differed from other congeneric members by both morphological and molecular characteristics. As a result, we herein describe it as a new species.

Materials and methods

Sampling

During a field survey at Dulongjiang Village, Gongshan County, Nujiang Prefecture, Yunnan Province, China, in February 2022 (Fig. 1), two adult specimens (one male and one female) of *Rhacophorus* were collected and photographed. Sex was determined by the presence of internal vocal sac openings and the presence of eggs in the abdomen, as observed via external inspection. The specimens were then euthanized, fixed in 10% formalin, and subsequently stored in 75% ethanol for 24 hours. Liver tissues were taken and preserved in 95% alcohol. The procedures for DNA tissue sampling and specimen fixation follow the protocols detailed in Chen et al. (2021). Voucher specimens were deposited at Anhui Normal University (ANU), China. The protocols (No. SYDW-20130814-71) of the Animal Care and Ethics Committee were followed for the proper treatment of animals.

DNA extraction, PCR, and sequencing

Total genomic DNA was extracted from liver tissue stored in 95% ethanol using the standard phenol-chloroform extraction protocol (Sambrook et al. 1989). The partial sequences of the mitochondrial 16S rRNA gene from the new samples were amplified and sequenced using the primers in Yu et al. (2019). PCR amplification was performed in a 25 μl reaction volume with the following cycling conditions: initial denaturation step at 95 °C for 5 min, 35 cycles of denaturation at 95 °C for 1 min, annealing at 55°C for 1 min, extension at 72 °C for 1 min, and final extension at 72 °C for 10 min. PCR products were purified using the Gel Extraction Mini Kit (Watson BioTechnologies, Shanghai, China) and then sequenced in both directions using the BigDye Terminator Cycle Sequencing Kit on an ABI PRISM 3730 DNA Analyzer (Applied Biosystems, Foster City, CA, USA). Newly generated sequences were deposited in GenBank (Table 1).

Phylogenetic analyses

Newly obtained nucleotide sequences were first assembled and edited using DNASTAR LASERGENE 7.1. To obtain the phylogenetic relationships among *Rhacophorus*, homologous sequences of all *Rhacophorus* species available in the NCBI GenBank were downloaded (Table 1). Our final dataset included 37 described species of *Rhacophorus*. In cases of geographically widespread species, multiple samples from different localities were included. *Zhangixalus burmanus* and *Z. wui* were chosen as outgroups based on previous phylogenetic studies (Jiang et al. 2019). New sequences incorporated with the data retrieved from GenBank were aligned using MUSCLE 3.8 (Edgar 2004) and then inspected by eye for accuracy and trimmed to minimize missing characters in MEGA11 (Tamura et al. 2021). The aligned length of the complete 16S rRNA data matrix was 969 bps.

The phylogenetic reconstruction was performed using Bayesian (BI) analyses and maximum likelihood

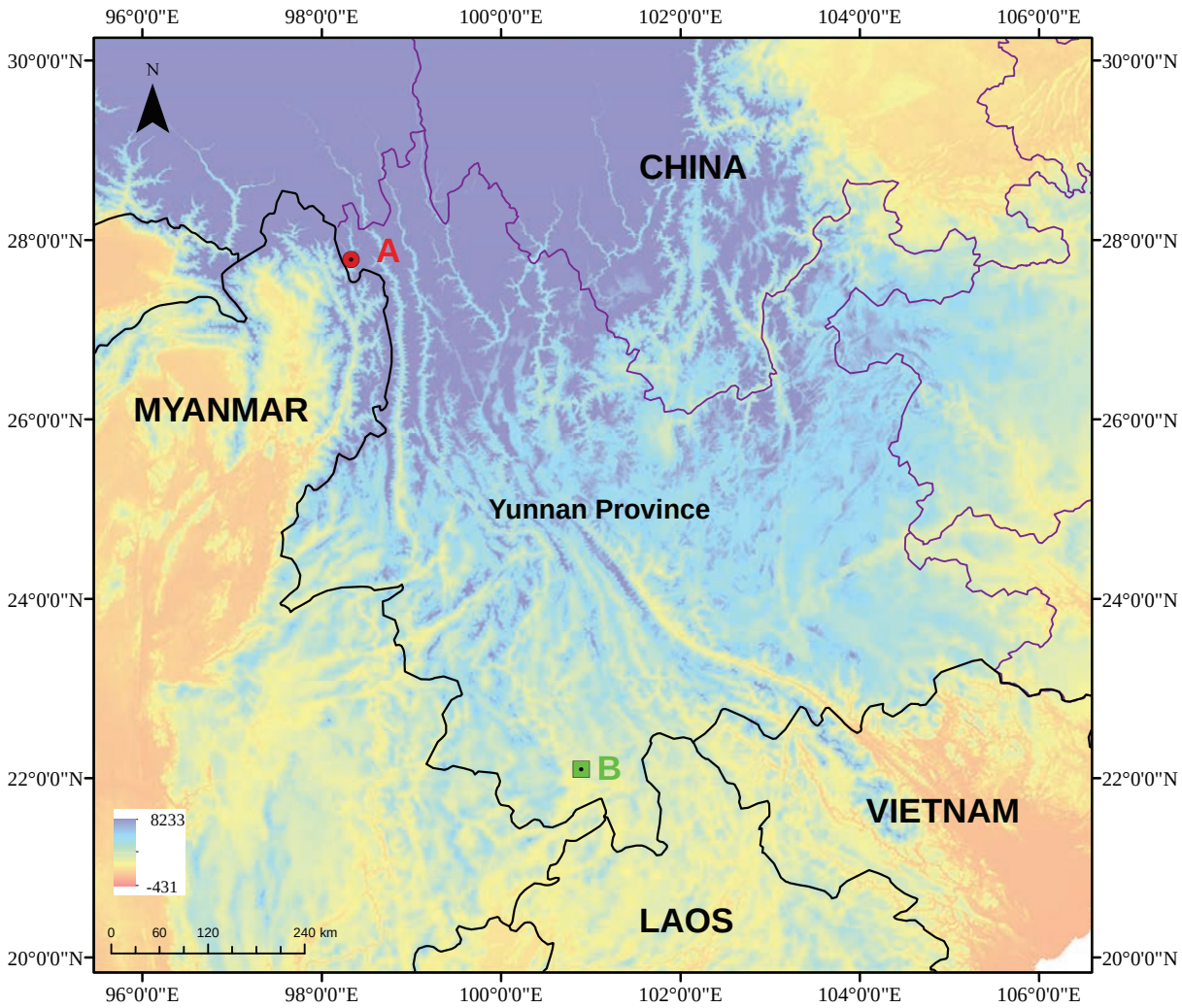

Figure 1. Map showing the collection site and type locality of *Rhacophorus dulongensis* sp. nov. (**A**; red circle) and *R. rhodopus* (**B**; green square).

(ML) methods for the 16S rRNA gene. The best-fit model of evolution for 16S rRNA was determined using the Bayesian Information Criterion (BIC) by jModelTest 2.1.7 (Darriba et al. 2012). The BI analyses were conducted in MrBayes 3.2 (Ronquist and Huelsenbeck 2003) with 30 million generations and sampled every 1000 generations. Convergence was assessed in Tracer 1.5 (Rambaut and Drummond 2009) based on having an average standard deviation of split frequencies less than 0.01 and ESS values greater than 200. We excluded the first 25% of trees before the log-likelihood scores stabilized as burn-in. The ML analyses were performed using RAxML-HPC BlackBox 8.2.10 (Stamatakis 2014) on the CIPRES Science Gateway (Miller et al. 2010). The analyses used the proportion of invariable sites estimated from the data and 1000 bootstrap pseudoreplicates under the GTR+gamma model. Nodes in the trees were considered well-supported when ML bootstrap support (BS) was ≥ 75% and Bayesian posterior probabilities (PP) were ≥ 0.95. Uncorrected pairwise distances (*p*-distances) between species were calculated in MEGA 11 (Tamura et al. 2021).

Morphology and morphometrics

Measurements were recorded to the nearest 0.1 mm with digital calipers by Renda Ai following Fei et al. (2009) and Li et al. (2022). The measurements taken were as follows: SVL (snout-vent length, the length from the tip of snout to vent); HL (head length, the length from the tip of snout to the posterior edge of the mandibular joint); HW (head width, the maximum distance between two sides of the head); SL (snout length, the length from the tip of snout to anterior border of eye); INS (internasal space, the distance between the inner edges of the left and right nostrils); IOS (interorbital space, the narrowest distance between the medial edges of the left and right upper eyelids); UEW (width of upper eyelid, the maximum width of upper eyelid); ED (diameter of eye, the diameter of the eye parallel to the body axis); TD (diameter of tympanum, the maximum diameter of tympanum); DNE (distance from nostril to eye, the length from the anterior border of the eye to the inner edge of the ipsilateral nostril); SN (distance from snout to nostril, the length from the tip of snout to the inner edge of the

Table 1. Information for samples used in the molecular phylogenetic analyses in this study. New sequences generated for the present study are PP574166–PP574167.

	Species	Voucher	Locality	GenBank No.
Ingroup				
1	*R. dulongjiang* sp. nov.	ANU010645	Dulongjiang Village, Yunnan, China	PP574166
2	*R. dulongjiang* sp. nov.	ANU010646	Dulongjiang Village, Yunnan, China	PP574167
3	*R. annamensis*	KIZ1196	Binh Thuan, Vietnam	JX219446
4	*R. baluensis*	FM235958	Tambunan District, Sabah, Malaysia	KC961089
5	*R. barisani*	UTAA-61235	Gunung Dempo, Provinsi Sumatera Selatan, Indonesia	KC701714
6	*R. bengkuluensis*	UTAA-62770	Kabupaten Lampung Barat, Lampung, Sumatra	KM212948
7	*R. bipunctatus*	CAS229913	Au Yin Gacamp, Kachin State, Myanmar	JX219445
8	*R. bipunctatus*	PUCZM/IX/SL612	Mizoram, India	MH087076
9	*R. borneensis*	BORN:22410	Maliau Basin, Sabah, Malaysia	AB781693
10	*R. calcadensis*	SDB.2011.291	Kadalar, Idukki, Kerala	KC571276
11	*R. calcaneus*	KIZ528	Bi Doup National Park, Lam Dong, Vietnam	JX219450
12	*R. catamitus*	ENS7657	Sumatra, Indonesia	JF748387
13	*R. edentulus*	MZB:Amp:30875	Gunung Katopasa, Sulawesi, Indonesia	MH751448
14	*R. exechopygus*	VNMN:4107	Gia Lai, Vietnam	LC010585
15	*R. gauni*	FMNH273928	Bintulu Division, Sarawak, Malaysia	JX219456
16	*R. georgii*	MZB:Amp:23395	Suaka Marga Satwa Nantu, Sulawesi, Indonesia	MH751453
17	*R. helenae*	NAP03164	Ba Ria-Vung Tau, Vietnam	KX139175
18	*R. hoabinhensis*	IEBRA.2016.18	Hoa Binh, Vietnam	LC331096
19	*R. indonesiensis*	MZB:Amp:23619	Birun Village, Jambi Province, Indonesia	AB983367
20	*R. kio*	KUHE:55167	Than Hoa, Vietnam	AB781697
21	*R. laoshan*	1705014	Guangxi, China	MW149528
22	*R. lateralis*	RBRL050709-35,36,37	Mudigere, India	AB530548
23	*R. malabaricus*	Release	Madikeri, India	AB530549
24	*R. margaritifer*	ENS16162	Tilu, Indonesia	KX398889
25	*R. modestus*	ENS16853	Samosir, Sumatra, Indonesia	KX398904
26	*R. monticola*	RMB1236	Mt. Lompo Batang, Sulawesi , Indonesia	AY326060
27	*R. napoensis*	GXNUYU000171	Napo, Guangxi, China	ON217796
28	*R. nigropalmatus*	Rao081204	Malaysia	JX219437
29	*R. norhayatii*	KUHEUNL	Endau Rompin, Johor, Malaysia	AB728191
30	*R. orlovi*	LJTR44	Maguan, Yunan, China	KC465840
31	*R. pardalis*	FMNH273245	Bintulu Division, Sarawak, Malaysia	JX219453
32	*R. poecilonotus*	ENS16480	Sibayak, Sumatra, Indonesia	KX398920
33	*R. pseudomalabaricus*	SDB.2011.1010	Kadalar, Kerala, India	KC593855
34	*R. reinwardtii*	ENS16179	Patuha, Java, Indonesia	KY886328
35	*R. rhodopus* (Lineage 1)	KIZYPX20553	Mengyang, Yunnan, China	MW133350
36	*R. rhodopus* (Lineage 2)	Loc08007018	Longchuan, Yunnan, China	JX219439
37	*R. rhodopus* (Lineage 2)	KIZ587	Longling, Yunnan, China	EF564577
38	*R. rhodopus* (Lineage 3)	L062456	Mêdog, Tibet, China	JX219442
39	*R. rhodopus* (Lineage 4)	SN030035	Hainan, China	EU215529
40	*R. rhodopus* (Lineage 4)	VNMN:4117	Gia Lai, Vietnam	LC010604
41	*R. rhodopus* (Lineage 5)	VNMN:4118	Bac Giang, Vietnam	LC010605
42	*R. robertingeri*	VNMN:4123	Gig Lai, Vietnam	LC010613
43	*R. rufipes*	FMNH272858	Bintulu Division, Sarawak, Malaysia	JX219455
44	*R. spelaeus*	IEBRA.2011.1	Khammouan, Laos	LC331095
45	*R. translineatus*	KIZ06648	Mêdog, Tibet, China	MW111521
46	*R. tuberculatus*	KIZ014154	Mêdog, Tibet, China	MW111522
Outgroup				
47	*Zhangixalus burmanus*	SCUM060614L	Mt. Gaoligong, Yunnan, China	EU215537
48	*Zhangixalus wui*	CIB097690	Lichuan, Hubei, China	JN688880

ipsilateral nostril); LAHL (length of lower arm and hand, the length from elbow joint to the tip of the third finger); HAL (hand length, from proximal end of outer palmar tubercle to tip of the third finger); TYE (distance from anterior margin of tympanum to posterior corner of eye); HLL (hindlimb length, measured as length of straightened hindlimb from groin to tip of fourth toe); THL (thigh length, the length from vent to knee); TIL (tibia length, the length from knee to ankle); TFL (length of the foot and tarsus, the length from the tibial tarsal joint to the tip of the fourth toe); FL (foot length, the length from the proximal end of the medial metatarsal process to the tip of the fourth toe). The description of webbing formula followed Guayasamin et al. (2006).

Results

Morphology

The two collected specimens were assigned to the genus *Rhacophorus* based on the following morphological characters: intercalary cartilage between terminal and penultimate phalanges of digits present, Y-shaped distal end of terminal phalanx, finger tips expanding into large disks bearing circum-marginal grooves, webbing exists between all fingers, skin not co-ossified with the skull, pupil horizontal, extensive dermal folds exist on the limbs, and dorsal color predominantly brown or green (Li et al. 2012; Jiang et al. 2019; AmphibiaChina 2024).

The samples of *Rhacophorus* collected in Dulongjiang Village, Gongshan County, Nujiang Prefecture, Yunnan Province were reliably differentiated from all known congeners based on the body size, head length, tibia length, snout and tongue shape, toe webbing formula and coloration, ventral skin texture and coloration, dorsal pattern and coloration, body macroglands, iris coloration, and pattern of markings on flanks, which supported the recognition of the new species.

Phylogenetics and genetic divergence

The BI and ML analyses resulted in essentially identical topologies (Fig. 2). Although the basal relationships within *Rhacophorus* were not well resolved, our analyses revealed two major clades, denoted A and B, within *Rhacophorus*. Clade A contained the majority of species of *Rhacophorus* and was widely distributed across Southeast Asia and southwestern China. Our new samples from Dulongjiang Village belong to Clade A, which strongly clustered into a lineage (BI = 1.00, ML = 100; Fig. 2) and clustered with *R. tuberculatus*, *R. orlovi*, and *R. spelaeus* from the eastern Himalayas, southwestern China, and northern Indochina with strong support (BI = 1.00, ML = 100; Fig. 2).

The putative new species from Dulongjiang Village showed obvious genetic divergence from other congeners. When compared with closely related recognized congeners, the minimum uncorrected genetic distance was 4.8% between the clade from Dulongjiang Village and *R. tuberculatus* (Table 2). These levels of pairwise divergence of the 16S rRNA gene obviously exceeded the accepted threshold of species-level genetic divergence in anurans (3.0%; Vences et al. 2005) and are greater than some known interspecific distances for *Rhacophorus* (Table 2). In addition, the analysis showed that *R. rhodopus* is not monophyletic and is a composite of five phylogenetically distinct lineages (Fig. 2). The sequence divergence in the 16S rRNA gene among the five lineages of *R. rhodopus* is 4.7–9.1% (Table 2). The samples of *R. rhodopus* from Bac Giang, Vietnam (Lineage 5; GenBank accession numbers: LC010605; Fig. 2) strongly clustered with *R. napoensis* with only 0.2% sequence divergence.

Taken together, our results indicated that the observed molecular divergence of the newly discovered population of *Rhacophorus* from Dulongjiang Village is concordant with stable differences in diagnostic morphological character, which distinguish it from all known congeners (see Comparisons). Thus, upon combining morphological and molecular lines of evidence, we herein describe this distinct lineage of *Rhacophorus* as a new species.

Taxonomic account

***Rhacophorus dulongensis* Chen, Lee & Yuan, sp. nov.**

https://zoobank.org/976AF923-DDF9-4E9A-BF72-0B2141DF493C

Figs 3, 4

Type materials. *Holotype*. ANU010645, adult male, collected from Dulongjiang Village, Gongshan County, Nujiang Prefecture, Yunnan Province, China (27.7838°N, 98.3248°E, 1620 m a.s.l.; Fig. 1) on 15 February 2022, by Renda Ai. ***Paratypes.*** ANU010646,

Table 2. Sequence divergences based on uncorrected *p*-distances (%) of 16S rRNA between the new species and its close congeners of *Rhacophorus* used in this study.

	Species	1	2	3	4	5	6	7	8	9	10	11	12	13	14	15
1	*R. dulongensis* sp. nov.															
2	*R. rhodopus* (Lineage 1)	15.0														
3	*R. rhodopus* (Lineage 2)	11.6	4.8													
4	*R. rhodopus* (Lineage 3)	13.6	8.2	6.0												
5	*R. rhodopus* (Lineage 4)	12.4	7.4	9.1	6.8											
6	*R. rhodopus* (Lineage 5)	10.5	8.1	7.7	4.7	6.5										
7	*R. napoensis*	12.9	7.7	6.6	7.1	6.8	0.2									
8	*R. tuberculatus*	4.8	13.8	10.7	12.0	11.0	9.3	12.0								
9	*R. orlovi*	7.5	14.1	11.8	13.3	13.5	11.2	12.8	7.7							
10	*R. spelaeus*	8.6	12.8	13.9	11.6	13.3	11.6	11.6	8.8	3.7						
11	*R. bipunctatus*	14.1	10.2	6.6	8.5	8.4	5.8	7.7	13.0	14.0	11.3					
12	*R. poecilonotus*	10.2	8.9	7.6	7.2	10.2	8.8	7.8	9.1	10.0	10.9	8.0				
13	*R. barisani*	9.5	8.4	7.5	6.7	9.4	8.4	7.3	8.8	9.3	10.2	7.5	2.2			
14	*R. bengkuluensis*	12.3	10.2	9.2	9.1	11.2	10.7	9.3	11.2	10.4	10.2	9.8	8.3	7.7		
15	*R. margaritifer*	11.8	9.7	9.1	8.3	10.7	10.7	9.3	11.0	11.2	10.9	10.1	6.4	6.6	4.3	

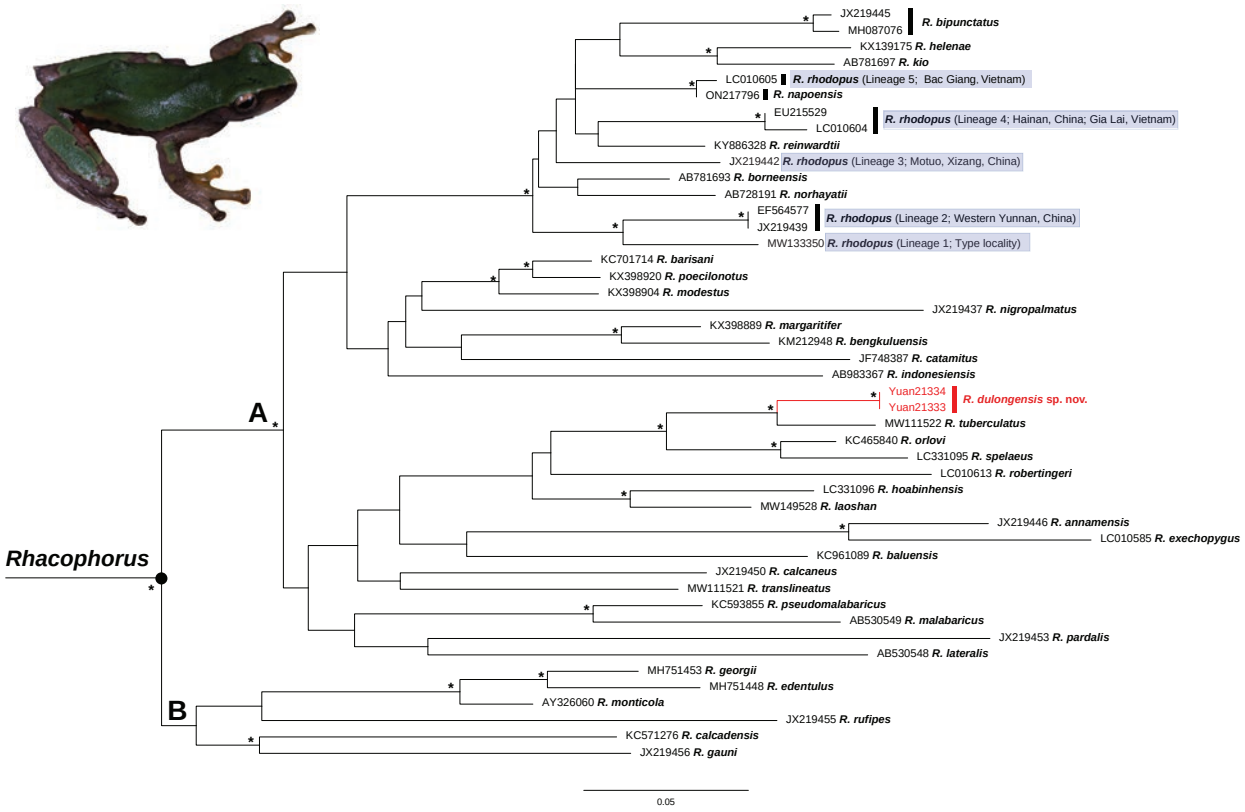

Figure 2. Phylogram of *Rhacophorus* inferred from a 16S rRNA mtDNA gene fragment. "*" denotes high support by bootstrap support values (BS > 75%) and Bayesian posterior probabilities (BPP > 0.95); nodes without any numbers or symbols represent low support values (BS < 75% and BPP < 0.95). Outgroup taxa are not shown. The inserted photo (acknowledgment to Renda Ai) shows *Rhacophorus dulongensis* sp. nov. Scale bars represent the number of substitutions per site. The new samples for the present study are indicated by the red font. *R. rhodopus* is framed by the purple shade.

adult female, collected at the same time as the holotype from the type locality by Renda Ai.

Etymology. The specific epithet "dulongensis" is given as a noun in apposition and refers to the name of the Dulongjiang Village, where the new species occurs. We suggest the English common name "Dulongjiang tree frog" and the Chinese common name "独龙江树蛙" (dú lóng jiāng shù wā).

Diagnosis. *Rhacophorus dulongensis* sp. nov. can be distinguished from its congeners by the following combination of morphological characters: (1) body size small (SVL 31.7 mm in male; 35.3 mm in female); (2) head length longer than head width; (3) tibia length shorter than half of snout-vent length; (4) third finger disk smaller in diameter than tympanum; (5) snout pointed without a distinct bulge; (6) the tibiotarsal articulation reaches the eye when hindlimb is stretched along the side of the body; (7) dorsal surface of body uniformly green, and dorsal surface of limbs brown with irregular green patches; (8) belly mostly yellowish, rough, and granular (9) large black warts present on ventral surface of thigh near vent; (10) webs between toes red and webbing formula on toes: $I1^{0}$-$1^{2/3}II1^{-}$-$2^{1/2}III1^{+}$-$2^{1/3}IV2^{1/3}$-$1^{1/3}V$; (11) black spots at axillary region absent; (12) vomerine teeth weakly developed; (13) iris darkgoldenrod; (14) maxillary teeth distinct; (15) tongue notably notched posteriorly.

Description of holotype. Adult male, body size small (SVL 31.7 mm); head length (HL 9.8 mm) longer than head width (HW 8.7 mm); snout pointed, protruding from the margin of the lower jaw, longer (SL 4.6 mm) than diameter of eye (ED 3.5 mm); canthus rostralis distinct; loreal region oblique; nostril small, closer to tip of snout than to eye; interorbital space (IOS 2.8 mm) longer than internasal space (INS 2.5 mm) and width of upper eyelid (UEW 2.1 mm); pupil horizontal and iris darkgoldenrod; pineal ocellus absent; tympanum rounded and distinct, diameter of tympanum (TD 1.7 mm) shorter than half of eye diameter (ED 3.5 mm), internasal space (INS 2.5 mm) and interorbital space (IOS 2.8 mm); supratympanic fold distinct; maxillary teeth distinct; vomerine teeth weak; internal single subgular vocal sac; vocal sac openings small, slit-like; tongue heart-shaped, attached anteriorly, with distinct notch at posterior end; choanae oval (Table 3).

Forelimbs thin, slender and not very long; length of lower arm and hand (LAHL 13.4 mm) shorter than half snout-vent length (SVL 31.7 mm); relative length of fingers: III>IV>II>I; tips of fingers expanded into discs; finger webbing formula: $I2^{+}$-$2^{1/3}II1^{+}$-$2^{2/3}III2^{1/3}$-$1^{2/3}IV$; subarticular tubercles distinct, blunt and round; third finger disk shorter than diameter of tympanum (TD 1.7 mm); supernumerary tubercles below the base of finger present;

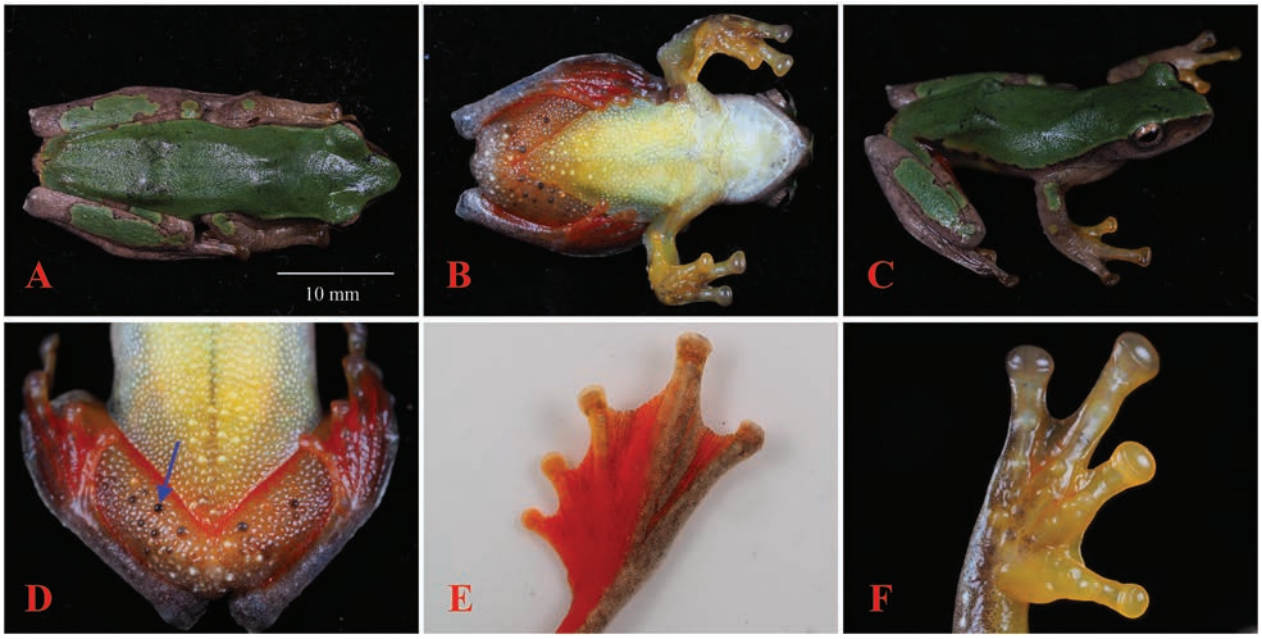

Figure 3. Holotype of *Rhacophorus dulongensis* sp. nov. (ANU010645) in life. **A.** Dorsal view; **B.** Ventral view; **C.** Dorso-lateral view; **D.** Ventral surface of the thigh and the cloacal region; **E.** Plantar view of the left foot; **F.** Thenar view of the right hand. The blue arrow in **D** points to large black warts. Photos by Renda Ai.

Table 3. Measurements of the type series of *Rhacophorus dulongensis* sp. nov. and *R. turpes* (all measurements are in mm). N/A indicates that data are lacking for that morphological index. Abbreviations are defined in the text.

Species	*R. dulongensis* **sp. nov.**		*R. turpes*	
	Holotype	**Paratype**	**Syntype**	**Paratype**
Voucher Nos.	**ANU010645**	**ANU010646**	**BMNH1940.6.1.30**	**BMNH1974.832**
Sex	Male	Female	Female	Female
SVL	31.7	35.3	37.4	35.8
HL	9.8	10.5	12.2	10.8
HW	8.7	8.8	9.7	9.8
SL	4.6	4.3	4.9	5.4
INS	2.5	2.3	2.8	3.1
IOS	2.8	3.2	4.3	4.1
UEW	2.1	2.3	2.4	2.0
ED	3.5	3.4	3.5	3.0
TD	1.7	1.9	2.4	2.8
SN	1.2	1.5	N/A	N/A
LAHL	13.4	13.8	N/A	N/A
HAL	7.9	8.5	9.2	8.6
TYE	0.6	0.8	1.1	1.2
HLL	49.1	48.9	N/A	N/A
THL	15.2	14	14.9	16.2
TIL	14.6	15.1	16.9	18.3
TFL	19.3	19.8	N/A	N/A
FL	13.1	12.6	10.8	10.4
DNE	2.7	3.2	2.7	3.3

nuptial pads absent; inner metacarpal tubercle distinct, large and oval (Fig. 3; Table 3).

Hindlimbs slender, relatively long, tibia length (TIL 14.6 mm) shorter than half of snout-vent length (SVL 31.7 mm) and thigh length (THL 15.2 mm); tibiotarsal articulation reaches the eye when hindlimb is stretched along the side of the body; heels overlapping when held at right angles to the body; relative length of toes:

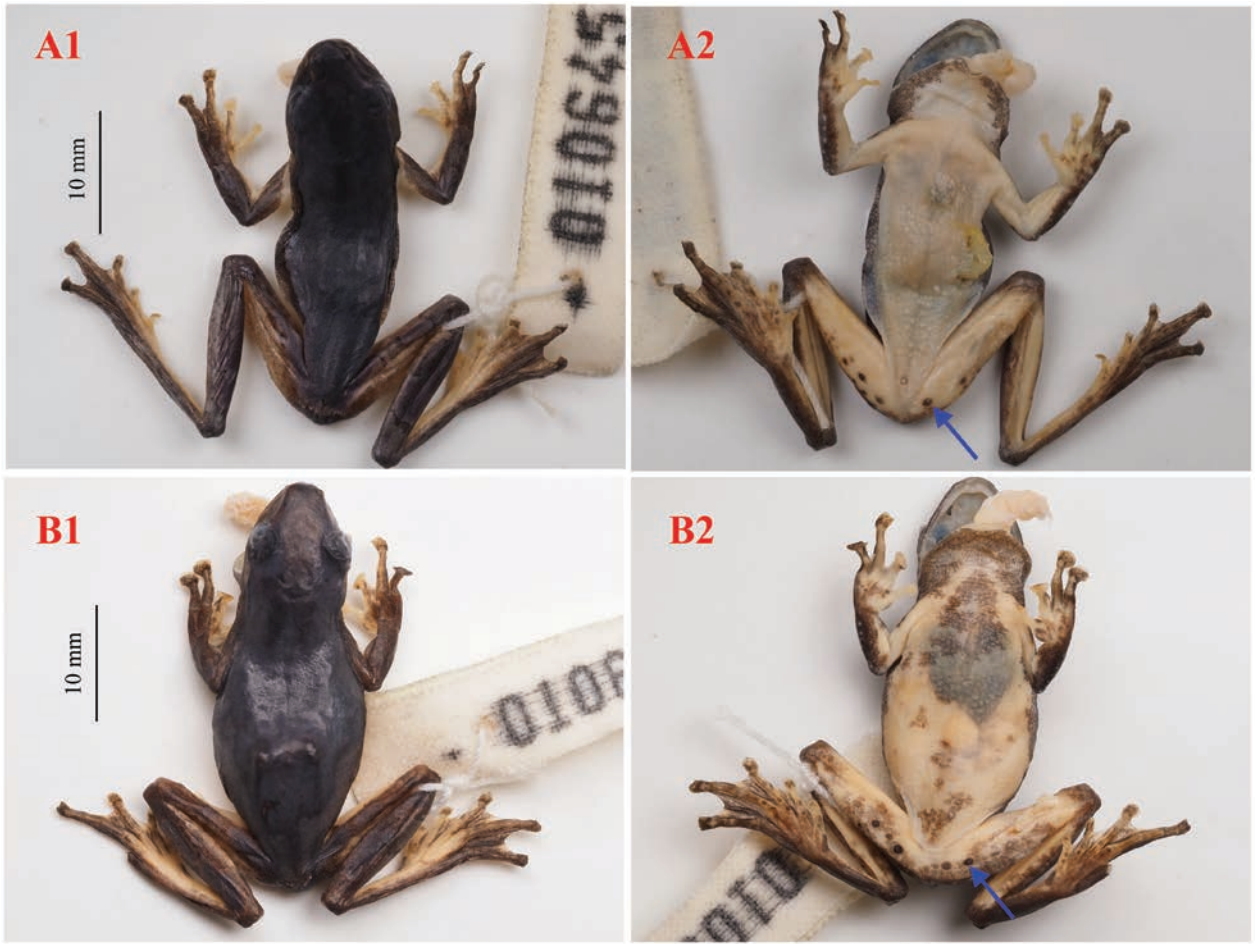

Figure 4. Type series of *Rhacophorus dulongensis* sp. nov. in preservation. **A.** ANU010645; **B.** ANU010645; **A1.** Dorsal view; **A2.** Ventral view; **B1.** Dorsal view; **B2.** Ventral view. The blue arrows in **A2** and **B2** point to large black warts. Photos by Renda Ai.

IV>V>III>II>I; tips of toes expanded into discs; subarticular tubercles on all toes round, distinct, and protuberant; entire web between toes; toes webbing formula: $I1^{0}$-$1^{2/3}II1^{-}$-$2^{1/2}III1^{+}$-$2^{1/3}IV2^{1/3}$-$1^{1/3}V$; inner metatarsal tubercle small; outer metatarsal tubercle absent (Fig. 3; Table 3).

The dorsal surface of body smooth and uniformly green; dorsal surface of limbs brown with irregular green patches; the skin of throat, chest, and ventral surface of tibia, foot, and tarsus smooth; black dusting present on the margin of the throat; the belly mostly yellowish and rough; large black warts present on ventral surface of thigh near vent; dermal fringe along the outer sides of limbs indistinct; webs between toes red; black spots at axillary region absent.

Color of holotype in preservative. Dorsal color darkened; ventral surface faded to creamy white; brown dusting present on ventral surfaces of throat. The patterns of dark spots and markings all over the body are the same as in life. Large black warts on the ventral surface of the thigh near the vent are more distinct (Figs 3, 4).

Male secondary sexual characteristics. Nuptial pad and lineae masculinae were not observed.

Morphological variation. The paratype matches the overall characters of the holotype (Table 3; Fig. 4). Female larger than male (SVL 35.3 mm in one female and 31.7 mm in one male). The male has small slit-like vocal sac openings. Dusting pattern on the belly, chest, throat, and ventral surfaces of limbs varies individually. Female has more distinct brown dusting on the venter than male (Figs 3, 4).

Distribution and ecology. *Rhacophorus dulongensis* sp. nov. is presently known only from its type locality, near Dulongjiang Village, Gongshan County, Nujiang Prefecture, Yunnan Province, China. Both individuals of the new species were found inside bamboo internodes along rocky streams in well-preserved montane evergreen broadleaf forest (Fig. 5). Vocal recordings and tadpoles of this new species were not collected.

Comparisons. *Rhacophorus dulongensis* sp. nov. is distinguishable from all other species of *Rhacophorus* by a combination of features of body size, head length, tibia length, snout and tongue shape, toe webbing formula and coloration, ventral skin texture and coloration, dorsal pattern and coloration, body macroglands, iris coloration, and pattern of markings on flanks (Tao et al. 2014; Fei et al. 2009; Li et al. 2012; Che et al. 2020; Li et al. 2022; Naveen et al. 2023).

In particular, *R. dulongensis* sp. nov. can be easily distinguished from its four morphologically and phylogenetically close congeners (*R. tuberculatus*, *R. orlovi*,

Figure 5. Habitat of *Rhacophorus dulongensis* sp. nov. at the type locality in Dulongjiang Village, Yunnan Province, China. **B, C.** show the native bamboo species, *Cephalostachyum virulentum*, where the new species inhabits. Photos by Ying-Chun Li.

R. spelaeus, and *R. turpes*; Figs 2, 6; Table 3). Specifically, it differs from *R. tuberculatus* by having green dorsum coloration in life (vs. uniform brown dorsum coloration), different webbing formula on toes ($I1^{0}$-$1^{2/3}II1^{-}$-$2^{1/2}III1^{+}$-$2^{1/3}IV2^{1/3}$-$1^{1/3}V$ vs. $I1^{1/2}$-$2^{1/2}II1^{1/3}$-$2^{1/2}III1^{+}$-$2^{1/3}IV2^{-}$-$1^{-}V$), as well as the absence of a prominent calcar at tibio-tarsal articulation (vs. presence) and the absence of dark stripes on the hindlimb (vs. presence).

R. dulongensis sp. nov. differs from *R. orlovi* by having smaller head (HL/SVL = 0.30–0.31 vs. HL/SVL = 0.38–0.41), different webbing formula on toes ($I1^{0}$-$1^{2/3}II1^{-}$-$2^{1/2}III1^{+}$-$2^{1/3}IV2^{1/3}$-$1^{1/3}V$ vs. $I1^{0}$-$2^{0}II1^{0}$-$2^{0}III1^{0}$-$2^{0}IV2^{0}$-$1^{0}V$), green dorsal coloration in life (vs. reddish brown), hindlimb without transverse stripes (vs. limbs with transverse stripes), as well as the presence of large black warts on the ventral surface of the thigh (vs. absence) and the absence of spotting on flanks (vs. presence).

R. dulongensis sp. nov. differs from *R. spelaeus* by having smaller body size in males (SVL 31.7 vs. 38.9–43.1 mm), different webbing formula on toes ($I1^{0}$-$1^{2/3}II1^{-}$-$2^{1/2}III1^{+}$-$2^{1/3}IV2^{1/3}$-$1^{1/3}V$ vs. I0-1II0-1/2III1-0V1/2-1/2V), green dorsal coloration in life (vs. grey-brown coloration in life), ventral surface of belly yellowish (vs. light gray), as well as the presence of vomerine teeth (vs. absence).

Specifically, *R. dulongensis* sp. nov. differs from *R. turpes* by having hindlimbs without dark stripes (vs. hindlimbs with dark stripes), by different webbing formula on toes ($I1^{0}$-$1^{2/3}II1^{-}$-$2^{1/2}III1^{+}$-$2^{1/3}IV2^{1/3}$-$1^{1/3}V$ vs. $I1^{1/3}$-$1^{1/2}II1^{1/2}$-$1^{2/3}III1^{0}$-$1^{1/2}IV2^{0}$-$1^{0}V$), vomerine teeth weak and small (vs. vomerine teeth distinct and large), dermal projection on the heel poorly developed (vs. well-developed), having a relatively longer foot length (FL/SVL ratio 0.36–0.41 in *R. dulongensis* sp. nov. vs. 0.29 in *R. turpes*), numerous and large black warts on ventral surface of thigh (vs. few and small in *R. turpes*), as well as the absence of small black spots in male (vs. presence in *R. turpes*) (Fig. 6).

In addition, *R. dulongensis* sp. nov. further differs from *R. rhodopus*, the notoriously "widespread" species of *Rhacophorus* in China and Indochina, by head length longer than head width (vs. head length almost equal to head width), third finger disk shorter than diameter of tympanum (vs. third finger disk longer than diameter of tympanum), tibia length shorter than half of snout-vent length (vs. tibia length about half of snout-vent length), as well as the absence of the black spots at axillary region (vs. presence), the absence of dermal calcars on vent (vs. present), and the absence of transverse stripes on hindlimb (vs. presence).

Among the species that are geographically close to *R. dulongensis* sp. nov., it distinctly differs from *R. bipunctatus* by having distinct tympanum (vs. indistinct), head length longer than head width (vs. head length almost equal to head width), as well as the absence of dermal calcars on heels (vs. presence), and the absence of black spots at axillary region (vs. presence). *R. dulongensis* sp. nov. differs from *R. translineatus* by having smaller body size (SVL 31.7 mm in male, 35.3 mm in female vs. 49.4–54.1 mm in males, 61.5–65.2 mm in females), different webbing formula on toes ($I1^{0}$-$1^{2/3}II1^{-}$-$2^{1/2}III1^{+}$-$2^{1/3}IV2^{1/3}$-$1^{1/3}V$ vs. I0-0II0-0III0-0-IV0-0V), as well as the absence of transverse dark brown lines on the back (vs. presence), and the absence of an appendage on the tip of snout (vs. presence). *R. dulongensis* sp. nov. differs from *R. subansiriensis* by having smaller body size in male (SVL 31.7 mm vs. 37.0–39.0 mm), head length longer than head width (vs. head length shorter than head width), as well as the absence of dark cross bands on limbs (vs. presence), and the absence of spots on flanks (vs. presence).

For the remaining congeners, *R. dulongensis* sp. nov. differs from *R. kio* by having smaller body size (SVL 31.7 mm in male, 35.3 mm in female vs. 58.0–79.1 mm in male, 82.6–88.9 mm in female), different webbing on toes (entirely webbed vs. fully webbed), red web (vs. web

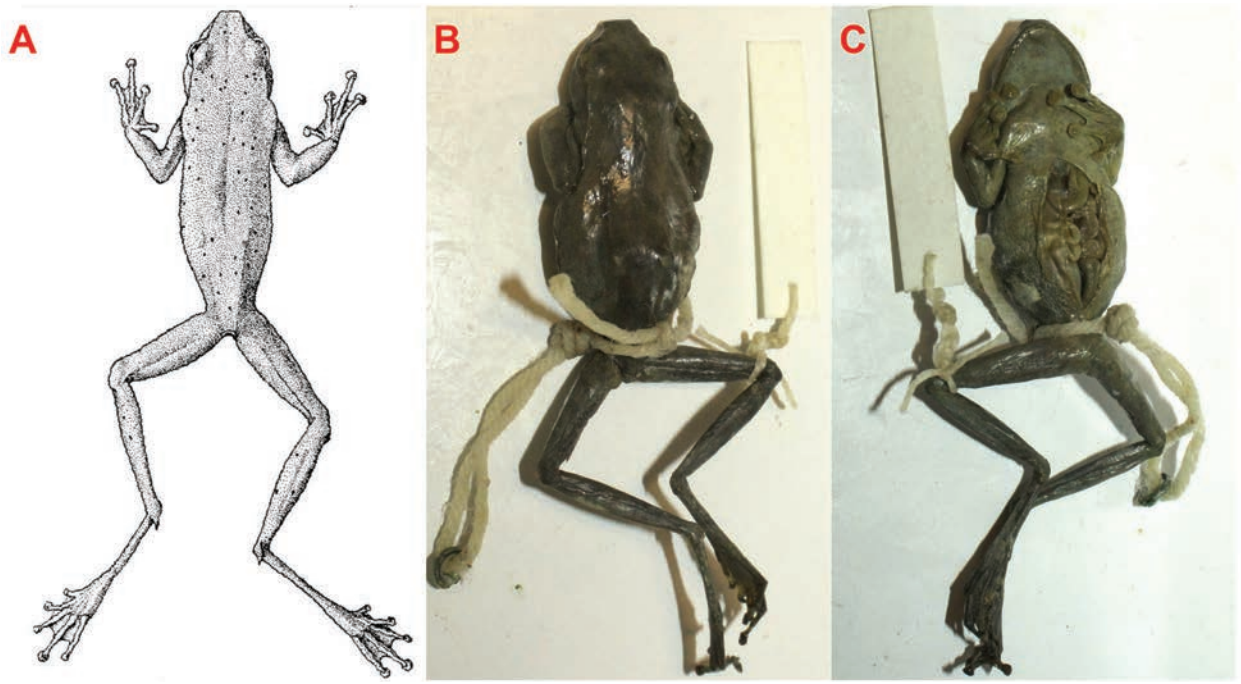

Figure 6. Type series of *Rhacophorus turpes*. **A.** The illustration of *R. turpes* in the original literature (Smith 1940); **B, C.** The syntype of *R. turpes* (BMNH1940.6.1.30) in the dorsal and ventral views, respectively (Photos by R. S. Naveen).

with black spot and orange yellow distal zone), as well as the absence of pointed dermal flap on heels (vs. presence), and the absence of black marking on flanks (vs. presence). *R. dulongensis* sp. nov. differs from *R. laoshan* by having fifth finger longer than third finger (vs. equal), different webbing formula on toes ($I1^{0}$-$1^{2/3}II1^{-}$-$2^{1/2}III1^{+}$-$2^{1/3}IV2^{1/3}$-$1^{1/3}V$ vs. I1-$2^{1/2}$II1-$2^{1/2}$III1-$2^{1/2}$IV2-1V), limbs without broad transverse stripes (vs. limbs with broad transverse stripes), and uniform green dorsum coloration in life (vs. chocolate brown dorsum coloration with wide dark cross-shaped mark). *R. dulongensis* sp. nov. differs from *R. napoensis* by having smaller body size in male (SVL 31.7 mm vs. 38.6–43.6 mm), head width shorter than head length (vs. head width longer than head length), the tibiotarsal articulation reaches the eye (vs. the tibiotarsal articulation reaches the snout), as well as the absence of a distinct bulge on the tip of snout (vs. presence), the absence of black spots at axillary region (vs. presence), and the absence of horizontal banding on dorsum and dorsal surface of limbs (vs. presence).

Lastly, *R. dulongensis* sp. nov. can be distinguished by its smaller body size in male (SVL 31.7 mm vs. 53.16 mm in *R. barisani*; 40.5–46.7 mm in *R. bengkuluensis*; 50.9 mm in *R. borneensis*; 60.0 mm in *R. helenae*; 49.9 mm in *R. larissae*; 64.7 mm in *R. norhayatiae*; 66.8 mm in *R. pseudomalabaricus*; over 58.0 mm in *R. reinwardtii*; 49.5–68.2 mm in *R. malabaricus*; 46.3 mm in *R. pardalis*; 45.9–46.4 mm in *R. exechopygus*); green dorsum coloration in life (vs. brown in *R. barisani*, *R. margaritifer* and *R. vanbanicus*; brown with darker cross bands in *R. bengkuluensis* and *R. catamitus*; yellowish grey with brown blotches in *R. hoabinhensis*; reddish brown with irregular dark brown blotches in *R. indonesiensis*; X-shaped blotch on the anterior part of the back in *R. monticola*; cream-colored in *R. marmoridorsum*; dark grey or brownish-grey in *R. calcadensis*; yellowish grey in *R. hoabinhensis*); head longer than head width (vs. head wider than long in *R. calcaneus*, *R. baluensis*, *R. trangdinhensis* and *R. viridimaculatus*); third finger disk shorter than diameter of tympanum (vs. third finger disk longer than diameter of tympanum in *R. calcaneus*, *R. annamensis*, *R. hoanglienensis*, *R. exechopygus*, *R. robertingeri* and *R. baluensis*); red webs between toes (vs. black webs in *R. borneensis*; proximally black and distally greenish webs in *R. helenae*; yellow webs in *R. edentulus*); tibiotarsal articulation reaches the eye (vs. tibiotarsal articulation reaches the tip of the snout in *R. nigropalmatus*; tibiotarsal articulation reaches beyond the tip of snout in *R. georgii*); absence of narrow dark cross-streaks on the limbs (vs. presence in *R. bifasciatus*); absence of a white streak on each side of body (vs. presence in *R. lateralis*); absence of a large triangular calcar heel (vs. presence in *R. robertingeri*).

Discussion

Our study further reveals the underestimation of species diversity and the taxonomic dispute in *Rhacophorus*. The discovery of *R. dulongensis* sp. nov. brings the total number of *Rhacophorus* species to 44 and the number of *Rhacophorus* known from China to 9. Besides, this study uncovers that the notoriously "widespread" species, *R. rhodopus*, is not monophyletic and is a composite of five phylogenetically distinct lineages (Fig. 2), as also revealed previously (e.g., Li et al. 2012; Li

et al. 2022). The divergence among the five lineages of *R. rhodopus* exceeds the threshold of species-level genetic divergence in anurans (3.0%; Vences et al. 2005) and is greater than some known interspecific distances for *Rhacophorus* (Table 2). Specifically, in addition to *R. rhodopus* from the type locality (Lineage 1), lineages 2–4 are likely to represent three new species (Fig. 2). Lineage 5 of *R. rhodopus* from northern Vietnam (Tao et al. 2014) is conspecific with *R. napoensis* with only 0.2% sequence divergence (Fig. 2; Table 2). *Rhacophorus napoensis* is currently only known from Baise City, Guangxi Province, China (Li et al. 2022; Frost 2024). Thus, our results revealed that *R. napoensis* is also found in Vietnam, making it a new country record for Vietnam, and we would formally correct the identity of LC010605 from Vietnam as *R. napoensis*. Detailed field investigations and more integrative studies, i.e., combining morphological, acoustic, and molecular data, are warranted to resolve these taxonomic disparities.

In addition, interestingly, both individuals of *R. dulongensis* sp. nov. were found inside the hollow internodes of the native bamboo species, *Cephalostachyum virulentum*. This behavior is a non-random event because its sister species, *R. tuberculatus*, has been reported to use bamboo internodes as breeding sites (Che et al. 2020). Moreover, this behavior has been reported in other genera of Rhacophoridae, such as *Raorchestes*. They usually enter the bamboo internodes through narrow openings and deposit eggs inside the bamboo. This elusive habit makes them easy to overlook (Seshadri and Bickford 2018; Che et al. 2020). However, the overharvesting of bamboo is threatening the survival of these bamboo nesting frogs (Seshadri et al. 2015). How this novel reproductive mode evolved is still unclear and needs further study.

Lastly, our study further highlights the lack of knowledge about the cryptic diversity in the Gaoligong Mountains. There was no previous record of the genus *Rhacophorus* from Dulongjiang Village (Yuan et al. 2022; AmphibiaChina 2024), where the new species was discovered in this study. Our finding and other recent discoveries (e.g., Yang et al. 2016; Chen et al. 2020; Liu et al. 2021; Wu et al. 2021) revealed that the increased expeditions to remote, previously unexplored areas largely contribute to the high discovery rate of new species in the Gaoligong Mountains. Besides, considering that the continuous forest habitats stretch across the international borders in this region, we expect that the new species found in this study may also occur in the adjacent regions of Myanmar. Further studies are needed to investigate the true extent of the occurrence of *R. dulongensis* sp. nov. Therefore, we propose that *R. dulongensis* sp. nov. be considered data deficient (DD) following the IUCN's Red List categories. With the increasing anthropogenic pressures and changing climatic conditions in the Gaoligong Mountains (Yang et al. 2019; Chen et al. 2020), focal biodiversity surveys and transboundary collaboration along the Chinese-Myanmar border are needed to detect more overlooked biodiversity and reinforce its value.

Acknowledgements

This work was supported by the National Natural Science Foundation of China (NSFC 31900323), and Anhui Provincial Key Laboratory of the Conservation and Exploitation of Biological Resources (692001) to J.M.C.; NSFC 32001222 to P.S.L.; the Fundamental Research Funds for the Central Universities (SWU-KR22014, SWU 5330500880), NSFC32170478, NSFC32370478; and the "Youth Top Talent Program of Chongqing" (CQYC 20220510893) to Z.Y.Y.

References

AmphibiaChina (2024) The database of Chinese amphibians. Kunming Institute of Zoology (CAS), Kunming, Yunnan, China. http://www.amphibiachina.org/ [Accessed on: 2024-1-31]

Chaplin G (2005) Physical geography of the Gaoligong Shan Area of southwest China in relation to biodiversity. Proceedings of the California Academy of Sciences 56: 527–556.

Che J, Jiang K, Yan F, Zhang Y (2020) Amphibians and Reptiles in Tibet-Diversity and Evolution [In Chinese with English abstracts and species descriptions]. Chinese Academy of Sciences, Science Press, Beijing, China, 385–393 pp.

Chen JM, Xu K, Poyarkov NK, Wang K, Yuan ZY, Hou M, Suwannapoom C, Wang J, Che J (2020) How little is known about "the little brown frogs": Description of three new species of the genus *Leptobrachella* (Anura, Megophryidae) from Yunnan Province, China. Zoological Research 41: 292. https://doi.org/10.24272/j.issn.2095-8137.2020.036

Chen JM, Jin JQ, Wu YH, Hou SB, Liu S, Che J (2021) Protocols for DNA Tissue Sampling and Specimen Fixation of Amphibians. Bio-101: e1010656. https://doi.org/10.21769/BioProtoc.1010656 [In Chinese]

Darriba D, Taboada GL, Doallo R, Posada D (2012) jModelTest 2: More models, new heuristics and parallel computing. Nature Methods 9(8): 772–772. https://doi.org/10.1038/nmeth.2109

Edgar RC (2004) MUSCLE: Multiple sequence alignment with high accuracy and high throughput. Nucleic Acids Research 32(5): 1792–1797. https://doi.org/10.1093/nar/gkh340

Fan PF, He K, Chen X, Ortiz A, Zhang B, Zhao C, Li YQ, Zhang HB, Kimock C, Wang WZ, Groves C, Turvey ST, Roos C, Helgen KM, Jiang XL (2017) Description of a new species of *Hoolock* gibbon (Primates, hylobatidae) based on integrative taxonomy. American Journal of Primatology 79(5): e22631. https://doi.org/10.1002/ajp.22631

Fei L, Hu SQ, Ye CY, Huang YZ (2009) Fauna Sinica. Amphibia Vol. 2 Anura. Science Press, Beijing. [In Chinese]

Frost DR (2024) Amphibian Species of the World: an Online Reference. Version 6.0. Electronic Database. American Museum of Natural History, New York. http://research.amnh.org/herpetology/amphibia/index.html [Accessed on: 2024-1-31]

Geissmann T, Lwin N, Aung SS, Aung TN, Aung ZM, Hla TH, Grindley M, Momberg F (2011) A new species of snub-nosed monkey, genus *Rhinopithecus* Milne-Edwards, 1872 (Primates, Colobinae), from northern Kachin state, northeastern Myanmar. American Journal of Primatology 73(1): 96–107. https://doi.org/10.1002/ajp.20894

Guayasamin JM, Bustamante MR, Almeida-Reinoso D, Funk WC (2006) Glass frogs (Centrolenidae) of Yanayacu Biological Station, Ecuador, with the description of a new species and comments on centrolenid systematics. Zoological Journal of the Linnean Society 147(4): 489–513. https://doi.org/10.1111/j.1096-3642.2006.00223.x

Hu T, Peng S, Zhou XX, Zheng YM, Cong YY, Hu GW (2022) Two new species of *Impatiens* (Balsaminaceae) from Gaoligong Mountains, Yunnan, China. Phytotaxa 566(3): 268–278. https://doi.org/10.11646/phytotaxa.566.3.2

Jiang DC, Jiang K, Ren JL, Wu J, Li JT (2019) Resurrection of the genus *Leptomantis*, with description of a new genus to the family Rhacophoridae (Amphibia, Anura). Asian Herpetological Research 10: 1–16. https://doi.org/10.16373/j.cnki.ahr.180058

Kropachev II, Evsyunin AA, Orlov NL, Nguyen TT (2022) A New Species of *Rhacophorus* Genus (Anura, Rhacophoridae, Rhacophorinae) from Lang Son Province, Northern Vietnam. Russian Journal of Herpetology 29(1): 35–46. https://doi.org/10.30906/1026-2296-2022-29-1-35-46

Li JT, Li Y, Murphy RW, Rao DQ, Zhang YP (2012) Phylogenetic resolution and systematics of the Asian tree frogs, *Rhacophorus* (Rhacophoridae, Amphibia). Zoologica Scripta 41(6): 557–570. https://doi.org/10.1111/j.1463-6409.2012.00557.x

Li J, Liu S, Yu G, Sun T (2022) A new species of *Rhacophorus* (Anura, Rhacophoridae) from Guangxi, China. ZooKeys 1117: 123–138. https://doi.org/10.3897/zookeys.1117.85787

Li Q, Li XY, Hu WQ, Song WY, He SW, Wang HJ, Hu ZC, Li MC, Onditi KO, Chen ZZ, Pu CZ, Xiong Y, Rao CH, Zhang FY, Zuo CS, Jiang XL (2024) Mammals of Gaoligong Mountain in China: Diversity, distribution, and conservation. Zoological Research. Diversity and Conservation 1(1): 3–19.

Liu XL, He YH, Wang YF, Beukema W, Hou S, Li YC, Che J, Yuan ZY (2021) A new frog species of the genus *Odorrana* (Anura, Ranidae) from Yunnan, China. Zootaxa 4908(2): 263–275. https://doi.org/10.11646/zootaxa.4908.2.7

Miller MA, Pfeiffer W, Schwartz T (2010) Creating the CIPRES Science Gateway for inference of large phylogenetic trees. 2010 gateway computing environments workshop (GCE). Ieee, New Orleans, 1–8. https://doi.org/10.1109/GCE.2010.5676129

Myers N, Mittermeier RA, Mittermeier CG, Da Fonseca GA, Kent J (2000) Biodiversity hotspots for conservation priorities. Nature 403(6772): 853–858. https://doi.org/10.1038/35002501

Naveen RS, Liu S, Chandramouli SR, Babu S, Karunakaran PV, Kumara HN (2023) Redescription of *Rhacophorus tuberculatus* (Anderson, 1871) and the validity of *Rhacophorus verrucopus* Huang, 1983. Herpetozoa (Wien) 36: 325–333. https://doi.org/10.3897/herpetozoa.36.e113656

Rambaut A, Drummond AJ (2009) Tracer v1.5. http://beast.bio.ed.ac.uk/Tracer

Ricketts TH, Dinerstein E, Boucher T, Wikramanayake E (2005) Pinpointing and preventing imminent extinctions. Proceedings of the National Academy of Sciences of the United States of America 102(51): 18497–18501. https://doi.org/10.1073/pnas.0509060102

Ronquist F, Huelsenbeck JP (2003) MrBayes 3: Bayesian phylogenetic inference under mixed models. Bioinformatics (Oxford, England) 19(12): 1572–1574. https://doi.org/10.1093/bioinformatics/btg180

Sambrook J, Fritsch E, Maniatis T (1989) Molecular cloning: a laboratory manual (2nd edition). Cold spring harbor laboratory press.

Seshadri KS, Bickford DP (2018) Faithful fathers and crooked cannibals: The adaptive significance of parental care in the bush frog *Raorchestes chalazodes*, Western Ghats, India. Behavioral Ecology and Sociobiology 72(1): 1–14. https://doi.org/10.1007/s00265-017-2420-3

Seshadri KS, Gururaja KV, Bickford DP (2015) Breeding in bamboo: A novel anuran reproductive strategy discovered in rhacophorid frogs of the Western Ghats, India. Biological Journal of the Linnean Society, Linnean Society of London 114(1): 1–11. https://doi.org/10.1111/bij.12388

Smith MA (1940) The amphibians and reptiles obtained by Mr. Ronald Kaulback in Upper Burma. Records of the Indian Museum 42: 465–486. https://doi.org/10.26515/rzsi/v42/i3/1940/162431

Stamatakis A (2014) RAxML version 8: A tool for phylogenetic analysis and post-analysis of large phylogenies. Bioinformatics (Oxford, England) 30(9): 1312–1313. https://doi.org/10.1093/bioinformatics/btu033

Tamura K, Stecher G, Kumar S (2021) MEGA11: Molecular Evolutionary Genetics Analysis Version 11. Molecular Biology and Evolution 38(7): 3022–3027. https://doi.org/10.1093/molbev/msab120

Tao NT, Matsui M, Eto K, Orlov NL (2014) A preliminary study of phylogenetic relationships and taxonomic problems of Vietnamese *Rhacophorus* (Anura, Rhacophoridae). Russian Journal of Herpetology 21: 274–280.

Vences M, Thomas M, Van der Meijden A, Chiari Y, Vieites DR (2005) Comparative performance of the 16S rRNA gene in DNA barcoding of amphibians. Frontiers in Zoology 2(1): 1–12. https://doi.org/10.1186/1742-9994-2-5

Wu YH, Liu XL, Gao W, Wang YF, Li YC, Zhou EE, Yuan ZY, Che J (2021) Description of a new species of Bush frog (Anura, Rhacophoridae, *Raorchestes*) from northwestern Yunnan, China. Zootaxa 4941(2): 239–258. https://doi.org/10.11646/zootaxa.4941.2.5

Yang J, Wang Y, Chen G, Rao D (2016) A new species of the genus *Leptolalax* (Anura, Megophryidae) from Mt. Gaoligongshan of western Yunnan Province, China. Zootaxa 4088(3): 379–394. https://doi.org/10.11646/zootaxa.4088.3.4

Yang Y, Ren G, Li W, Huang Z, Lin AK, Garber P, Ma C, Yi S, Momberg F, Gao Y, Wang X, Li G, Behie A, Xiao W (2019) Identifying transboundary conservation priorities in a biodiversity hotspot of China and Myanmar: Implications for data poor mountainous regions. Global Ecology and Conservation 20: e00732. https://doi.org/10.1016/j.gecco.2019.e00732

Yu GH, Hui H, Hou M, Wu ZJ, Rao DQ, Yang JX (2019) A new species of *Zhangixalus* (Anura, Rhacophoridae), previously confused with *Zhangixalus smaragdinus* (Blyth, 1852). Zootaxa 4711(2): 275–292. https://doi.org/10.11646/zootaxa.4711.2.3

Yuan ZY, Chen JM, Wu YH, Li XQ, Che J (2022) Revision of the list of amphibian species in Yunnan Province. Shengwu Duoyangxing 30(4): 21470. https://doi.org/10.17520/biods.2021470

Zoosyst. Evol. 100 (3) 2024, 863–876 | DOI 10.3897/zse.100.119945

PENSOFT

für Natur MUSEUM FÜR NATURKUNDE BERLIN

Base-substitution rates of nuclear and mitochondrial genes for polyclad flatworms

Daniel Cuadrado[1], Jorge Rodríguez[2,3], Annie Machordom[1], Carolina Noreña[1], Fernando Á. Fernández-Álvarez[4], Pat A. Hutchings[2,3], Jane E. Williamson[3]

1 *Department of Biodiversity and Evolutionary Biology, National Museum of Natural Science, MNCN (CSIC), Madrid 28006, Spain*

2 *Australian Museum Research Institute, Australian Museum, Sydney, NSW 2010, Australia*

3 *Marine Ecology Group, School of Natural Sciences, Wallumattagal Campus, Macquarie University, Sydney, NSW 2109, Australia*

4 *Institut de Ciències del Mar (ICM-CSIC), Passeig Marítim de la Barceloneta 37-49, 08003 Barcelona, Spain*

https://zoobank.org/653F388E-73B8-4CA4-BB1E-0C7262D170D7

Corresponding author: Daniel Cuadrado (cuadradopm@hotmail.com)

Academic editor: Pavel Stoev ♦ **Received** 31 January 2024 ♦ **Accepted** 27 May 2024 ♦ **Published** 1 July 2024

Abstract

The increase in the use of molecular methodologies in systematics has driven the necessity for a comprehensive understanding of the limitations of different genetic markers. Not every marker is optimal for all species, which has led to multiple approaches in the study of the taxonomy and phylogeny of polyclad flatworms. The present study evaluates base-substitution rates of nuclear ribosomal (*18S rDNA* and *28S rDNA*), mitochondrial ribosomal (*16S rDNA*), and protein-codifying (*cytb*, *cox1*) markers for this taxonomic group, with the main objective of assessing the robustness of these different markers for phylogenetic studies. Mutation rates and Ti/Tv ratios of the other markers were assessed for the first time. We estimated substitution rates and found *cytb* to be the most variable, while *18S rDNA* was the least variable among them. On the other hand, the transition to transversion (Ti/Tv) ratio of the different genes revealed differences between the markers, with a higher number of transitions in the nuclear gene *28S* and a higher number of transversions in the mitochondrial genes. Lastly, we identified that the third codon position of the studied protein-codifying genes was highly variable and that this position was saturated in the *cox1* marker but not in *cytb*. We conclude that it is important to assess the markers employed for different phylogenetic levels for future studies, particularly in the order Polycladida. We encourage the use of mitochondrial genes *cytb* and *16S* for phylogenetic studies at suborder, superfamily, and family levels and species delimitation in polyclads, in addition to the well-known *28S* and *cox1*.

Key Words

Acotylea, codon, Cotylea, entropy, flatworm, molecular, purines, pyrimidines, saturation

Introduction

Fast and reliable DNA sequencing has become a routinely used methodology in the description and barcoding of new species. In particular, a fragment of the mitochondrial gene cytochrome oxidase *c* subunit 1 (*cox1*) has become the most frequently used marker for molecular identification-based DNA barcoding (Hebert et al. 2003) in the majority of species across all taxa, incentivised by the Barcode of Life initiative (www.barcodeoflife.org) (Ratnasingham and Hebert 2007). Recent studies show, however, that genome-wide nucleotide substitution patterns in coding sequences have species-specific features and are variable among evolutionary lineages (Zou and Zhang 2021), leading to the question of the ubiquity of their use of particular nuclear and mitochondrial genes for systematics.

To address this issue, we investigated transition bias, which involves analysing the frequency and nature of nucleotide changes between purines and pyrimidines

across species genomes. This information is crucial for understanding the behaviour of different markers commonly employed in phylogenetic studies. Nucleotide changes between purines (adenine, A, and guanine, G) and pyrimidines (cytosine, C, and thymine, T) are known as transitions, whereas changes between a purine and a pyrimidine are coined transversions. Due to the disparity in the number of types of each possible nucleotide change (four types of transitions compared to eight types of transversions), the expected number of transitions relative to that of transversions (Ti/Tv ratio) would be 0.5 in DNA sequence evolution, assuming all types of nucleotide changes had equal rates of occurrence. However, Ti/Tv often exceeds 0.5 or even 1, a phenomenon known as transition bias (Nei and Kumar 2000; Yang 2006). Ti/Tv bias is commonly considered for estimating nucleotide substitution rates, inferring molecular phylogenies, and testing for natural selection (Kimura 1980; Tamura and Nei 1993; Yang et al. 1998) and has been extensively studied in model organisms such as the yeast *Saccharomyces cerevisiae* (Liu and Zhang 2019), the common fruit fly *Drosophila melanogaster* (Schrider et al. 2013), the flowering plant *Arabidopsis thaliana* (Ossowski et al. 2010), and the nematode *Caenorhabditis elegans* (Denver et al. 2009). These studies suggest that transitions are less deleterious and less likely to be purged by natural selection than transversions, which could be a reason why transitions are more commonly found. Furthermore, studies on genome error correction show that, due to the structure of the genetic code, transversions often lead to non-synonymous mutations compared to transitions, which usually lead to synonymous mutations, thereby potentially affecting the function and phenotype of the encoded proteins (Zhang 2000; Schrider et al. 2013). Therefore, while transitions are more frequent than transversions, especially at lower taxonomic levels, transversions are considered less informative and more difficult to interpret, potentially leading to homoplasy effects (evolutionary convergence) when comparing distantly related species in parsimony-based phylogenies (Broughton et al. 2000).

Understanding relationships among closely related taxa at a species level is essential for conserving biodiversity, maintaining ecosystem functioning, and understanding macroevolutionary processes (Oliver et al. 2015). External morphological characteristics are historically used as diagnostic features for species identification; however, contrasting results among morphological and molecular analyses appear across the entire animal kingdom, including nemerteans (Strand and Sundberg 2005), corals (Forsman et al. 2009), molluscs (Valdés et al. 2017; Fernández-Álvarez et al. 2020), polychaetes (Kupriyanova et al. 2023), fish (Park et al. 2020), insects (Selivon et al. 2005; Zhang et al. 2021), and also flatworms (Litvaitis et al. 2019).

Flatworms (order Polycladida) are free-living, carnivorous organisms that occur in a diversity of marine habitats, with over 800 species described worldwide (Tyler et al. 2006–2024). Exploring the diversity of polyclad species is critical, considering recent studies indicating the importance of the chemical and ecological roles of flatworms (Rawlinson and Stella 2012; Gammoudi et al. 2016; McNab et al. 2021, 2022; Tosetto et al. 2023). Traditionally, the taxonomy and phylogenetics of the order Polycladida have been based on morphological characteristics, where differences in tentacles, eyespots, ventral sucker, and genitalia are used to classify polyclads into different genera and families (Faubel 1983, 1984; Prudhoe 1985). External morphological characters are, however, not always an accurate reflection of the evolutionary relationships in flatworms. For example, different families of Leptoplanoidea (Acotylea) display very similar external morphologies but show different and distinguishable features internally and molecularly (Bahia 2016; Dittmann et al. 2019). Sometimes species with few morphological differences show large molecular discrepancies (Carrera-Parra et al. 2011), and the problem is exacerbated when different cryptic polyclad species live in sympatry, thereby complicating accurate identification and potentially resulting in the amalgamation of multiple species into a single one. It is therefore important to identify which molecular markers are best suited to resolving the evolutionary lineages of flatworms.

A variety of molecular markers have been used to date for the systematic analysis of polyclads. Resolution of deep nodes such as suborders (Cotylea and Acotylea) and assessment of differences in superfamilies and families have initially been based on the *28S rDNA* marker (Litvaitis and Newman 2001; Litvaitis et al. 2010; Rawlinson et al. 2011; Bahia et al. 2017; Cuadrado et al. 2021). Recent studies have, however, noted deficiencies in this marker (Dittmann et al. 2019; Litvaitis et al. 2019), because only a section of the phylogenetic tree topologies in Cotylea is consistently reconstructed. In the case of suborder Acotylea, despite recent studies (Oya and Kajihara 2020), there is a need for the inclusion of more taxa, additional genetic markers, complete markers, and/or searching for other alternatives to enhance understanding.

Other polyclad studies have used a range of different molecular markers, often employing specific primers due to performance issues with universal primers, such as *cox1*, the *16S* mitochondrial ribosomal subunit (*16S rDNA*), the mitochondrial cytochrome *b* (*cytb*), and the nuclear *18S rDNA* (Vella et al. 2016; Aguado et al. 2017; Tsunashima et al. 2017; Oya and Kajihara 2017, 2020; Oya et al. 2019; Tsuyuki et al. 2019, 2022; Cuadrado et al. 2021; Rodríguez et al. 2021), as well as complete mitochondrial genomes (Aguado et al. 2016; Kenny et al. 2019; Yonezawa et al. 2020) for both systematics and species delimitation.

This study evaluates the strength of support provided by *cox1*, *16S* rRNA, and *cytb* mitochondrial genes, as well as the *18S rDNA* and *28S rDNA* nuclear genes, on the phylogeny of the Polycladida through the study of nucleotide substitutions.

Materials and methods

Sampling sites and processing of materials

Polyclad flatworms were collected from different sites along the coasts of eastern Australia, the Iberian Peninsula, the Canary Islands, Cape Verde, Costa Rica, Cyprus, and Martinique Island (Table 2). This broad distribution range included representation of the majority of superfamilies across the order Polycladida, including Pseudocerotoidea Faubel, 1984; Prosthiostomoidea Bahia, Padula, & Schrödl, 2017 for the suborder Cotylea; Leptoplanoidea Faubel, 1984; Stylochoidea Poche, 1925; and Discoceloidea Laidlaw, 1903 for the Acotylea suborder. These species stem from a compilation of available biological material from recent studies (Noreña et al. 2014, 2015; Marquina et al. 2015a, 2015b; Aguado et al. 2017; Pérez-García et al. 2019; Cuadrado et al. 2021; Rodríguez et al. 2021; Soutullo et al. 2021), with the aim of achieving the greatest possible representativeness and sequencing of all available samples.

Flatworms were collected from under rocks in coastal environments, either by hand for intertidal and shallow individuals or using SCUBA in deeper areas, and placed in separate containers filled with seawater (specific information on species is available in the bibliography of Table 2). After being transported to a laboratory, a small piece of tissue (<1 g) was removed from the body margin of each individual using a sterile scalpel blade. The tissue of each animal was fixed in absolute ethanol and stored for DNA extraction. Each animal was then coaxed onto a piece of paper and transferred to a Petri dish containing clean, frozen seawater, where it was fixed with either 10% formalin or Bouin's liquid. Once the fixation process was complete, specimens were stored in 70% ethanol for species identification through morphological techniques, as per Rodríguez et al. (2021).

DNA extraction and amplification

Total genomic DNA was extracted from each tissue sample using an Isolate II Genomic DNA Kit (Meridian Bioscience®) following the manufacturer's protocol. Amplicons from two nuclear (*28S rDNA*, *18S rDNA*) and three mitochondrial (*16S* rRNA, *cox1*, and *cytb*) target genes from each polyclad species were sequenced. All polymerase chain reactions (PCRs) were performed using Taq DNA polymerase (Qiagen). The reaction mix included: H_2O – 10.92 µl; 10x buffer − 2 µl; 25 mM $MgCl_2$ − 4 µl; 0.5 mM dNTP − 1 µl; 10 µM primer – 0.25 µl /primer; Taq 5 U/µl − 0.08 µl; DNA – 1.5 µl. This gave a reaction volume of 20 µl.

Sequences of approximately 1100 base pairs (bp) (*28S*), 800 pb (*18S*), 500 bp (*16S*), 1000 bp (*cox1*), and 400 bp (*cytb*) were amplified using the primers listed in Table 1. The PCR consisted of an initial denaturation at 95 °C for 3 min, followed by 40 cycles of denaturation at 95 °C for 1 min, annealing at 47 °C (*cytb*), 49 °C (*cox1*), 59 °C (*28S rDNA*, *18S rDNA*, *16S* rRNA) for 30 sec, and extension at 72 °C for 1 min, with a final extension of 10 min at 72 °C.

The PCR products were observed using TBE gel electrophoresis in 1.5% agarose gel stained with SYBER Safe and visualised under UV light. PCR products were sent to Macrogen Korea for clean-up and sequencing. Lastly, the obtained forward and reverse sequences were combined using the programme Geneious Prime 2020.2.4 (http://www.geneious.com, Kearse et al. 2012) using the alignment-transition/transversion with the consensus sequence tool and manually curated.

The species with the highest possible number of correctly sequenced genes was selected to compare the analyses performed on the different markers. All sequences obtained in the present study have been deposited in the GenBank database under the accession numbers listed in Table 2.

Comparison of genetic markers

Alignments of each molecular marker were performed with the Clustal W algorithm (Larkin et al. 2007) using the programme Geneious Prime 2020.2.4. Ambiguously aligned and variable regions were recognised and excluded using the programme Gblocks version 0.91b

Table 1. Primers used in this study.

Gene	Primer name	Sequence	Reference
18S	*18S*F2	ACTTTGAACAAATTTGAGTGCTCA	Morgan et al. (2003)
	1800mod	GATCCTTCCGCAGGTTCACCTACG	Raupach et al. (2009)
28S	Platy*28S*_F	AGCCCAGCACCGAATCCT	Cuadrado et al. (2021)
	Platy*28S*_R	GCAAACCAAGTAGGGTGTCGC	Cuadrado et al. (2021)
16S	PLATYS*16S*F1	ACAACTGTTTATCAAAAACAT	Aguado et al. (2017)
	PLATYS*16S*R1	ACGCCGGTYTTAACTCAAATCA	Aguado et al. (2017)
cox1	HRpra2	AATAAGTATCATGTARACTDATRTCT	Tsunashima et al. (2017)
	HRprb2-2	GDGGVTTTGGDAATTGAYTAATACCTT	Tsunashima et al. (2017)
	Acotylea_COI_F	ACTTTATTCTACTAATCATAAGGATATAGG	Oya and Kajihara (2017)
	Acotylea_COI_R	CTTTCCTCTATAAAATGTTACTATTTGAGA	Oya and Kajihara (2017)
cytb	*cytb*424-444	CAGGAAACAGCTATGACCGGWTAYGTWYTWCCWTGRGGWCARAT	Jondelius et al. (2002)
	*cytb*876-847	TGTAAAACGACGGCCAGTGCRTAWGCRAAWARRAARTAYCAYTCWGG	Jondelius et al. (2002)

Table 2. List of species and sequences studied (material from previous studies, see table list of references).

Family	Species	*18S*	*28S*	*16S*	*cox1*	*cytb*	Locality	Reference
Discoceloidea								
Cryptocelidae	*Cryptocelis* sp.	MZ292810	MZ292829	MZ292858	MZ273073	PP856191	Galicia, Spain	Noreña et al. (2015)
Discocelidae	*Discocelis tigrina*	MZ292799	MK299370	-	-	PP856182		Cuadrado et al. (2021)
Leptoplanoidea								
Gnesiocerotidae	*Echinoplana celerrima*	MW376754	MW377507	MW376599	MW375911	MW392971	New South Wales, Australia	Rodríguez et al. (2021)
	Ceratoplana falconerae	MW376740	MW377493	MW376585	MW375897	MW392973	Victoria, Australia	Rodríguez et al. (2021)
	Parabolia megae	MW376744	MW377497	MW376589	MW375901	MW392974	New South Wales, Australia	Rodríguez et al. (2021)
Leptoplanidae	*Leptoplana* sp.	-	MZ292828	MZ292853	MZ273072	-	Cape Verde Island	Cuadrado et al. (2021)
	Parviplana geronimoi	MZ292807	-	MZ292855	-	-	Cádiz, Spain	Pérez-García et al. (2019)
Notoplanidae	*Notoplana australis*	MW376750	MW377503	MW376595	MW375907	MW392986	New South Wales, Australia	Rodríguez et al. (2021)
	Notoplana felis	MW376753	MW377506	MW376598	MW375910	MW392985	Victoria, Australia	Rodríguez et al. (2021)
Pleioplanidae	*Pleioplana atomata*	MZ292820	MZ292832	MZ292866	MZ273074	PP856198	Asturias, Spain	Marquina et al. (2015a)
	Pleioplana sp.	MZ292808	MZ292840	MZ292856	MZ273079	PP856189	Cádiz, Spain	This study
Pseudostylochidae	*Tripylocelis typica*	MW376752	MW377505	MW376597	MW375909	MW392983	New South Wales, Australia	Rodríguez et al. (2021)
Stylochoplanidae	*Stylochoplana clara*	MW376741	MW377494	MW376586	MW375898	MW392972	Victoria, Australia	Rodríguez et al. (2021)
Stylochoidea								
Callioplanidae	*Callioplana marginata*	MW376747	MW377500	MW376592	MW375904	MW392984	New South Wales, Australia	Rodríguez et al. (2021)
	Neostylochus ancorus	MW376748	MW377501	MW376593	MW375905	-	New South Wales, Australia	Rodríguez et al. (2021)
Latocestidae	*Eulatocestus australis*	MW376749	MW377502	MW376594	MW375906	-	New South Wales, Australia	Rodríguez et al. (2021)
	Latocestus plehni	MZ292806	MK299376	MZ292852	-	PP856187	Cape Verde Island	Cuadrado et al. (2021)
Planoceridae	*Paraplanocera marginata*	MW376745	MW377498	MW376590	MW375902	MW392981	New South Wales, Australia	Rodríguez et al. (2021)
	Paraplanocera sp.	MZ292818	MZ292833	MZ292868	MZ273075	PP856200	Cyprus	This study
	Planocera edmondsi	MW376755	MW377508	MW376600	MW375912	MW392979	Victoria, Australia	Rodríguez et al. (2021)
	Planocera pellucida	MZ292797	MK299355	-	-	PP856180	Canary Island, Spain	Cuadrado et al. (2021)
Idioplanidae	*Idioplana australiensis*	MW376746	MW377499	MW376591	MW375903	MW392980	New South Wales, Australia	Rodríguez et al. (2021)
Stylochidae	*Imogine fafai*	MZ292817	MZ292835	MZ292865	MF371138	PP856197	Asturias, Spain	Aguado et al. (2017)
	Leptostylochus victoriensis	MW376742	MW377495	MW376587	MW375899	MW392982	New South Wales, Australia	Rodríguez et al. (2021)
	Stylochus neapolitanus	MZ292800	MZ292841	MZ292846	MF371141	PP856183	Galicia, Spain	Aguado et al. (2017)
Boninioidea								
Boniniidae	*Boninia* sp.	MZ292819	MZ292834	MZ292869	-	PP856201	Costa Rica	Soutullo et al. (2021)
Cestoplanidae	*Cestoplana rubrocincta*	MW376751	MW377504	MW376596	MW375908	MW392977	New South Wales, Australia	Rodríguez et al. (2021)
Pericelidae	*Pericelis beyerleyana*	MZ292801	MK299374	MZ292847	-	PP856184	Martinique Island	Cuadrado et al. (2021)
	Pericelis cata	MZ292805	MK299352	MZ292851	-	-	Cape Verde Island	Cuadrado et al. (2021)
Prosthiostomoidea								
Prosthiostomidae	*Prosthiostomum amri*	MW376743	MW377496	MW376588	MW375900	MW392978	New South Wales, Australia	Rodríguez et al. (2021)
	Prosthiostomum siphunculus	MZ292816	MZ292836	MZ292864	MZ273080	PP856196	Almuñécar, Spain	Pérez-García et al. (2019)
	Prosthiostomum sp.	MZ292795	MZ292826	MZ292842	MZ273071	-	New South Wales, Australia	Rodriguez et al. (2021)
	Enchiridium magec	-	MK299349	MZ292844	-	PP856179	Canary Island, Spain	Cuadrado et al. (2021)
Pseudocerotoidea								

Family	Species	*18S*	*28S*	*16S*	*cox1*	*cytb*	Locality	Reference
Euryleptidae	*Eurylepta cornuta*	MZ292809	MZ292839	MZ292857	MF371139	PP856190	Galicia, Spain	Aguado et al. (2017)
	Eurylepta guayota	MZ292804	MK299372	MZ292850	-	PP856186	Martinique Island	Cuadrado et al. (2021)
	Prostheceraeus roseus	MZ292811	KY263688	MZ292859	MZ273078	PP856192	Galicia, Spain	Noreña et al. (2014)
Pseudocerotidae	*Phrikoceros sp.*	MZ292796	MZ292827	MZ292843	-	PP856178	Victoria, Australia	Rodriguez et al. (2021)
	Pseudoceros depiliktabub	MZ292813	MZ292837	MZ292861	-	PP856194	Lizard Island, Australia	Marquina et al. (2015b)
	Pseudoceros stimpsoni	MZ292812	MZ292838	MZ292860	MF371147	PP856193	Lizard Island, Australia	Aguado et al. (2017)
	Pseudoceros velutinus	MZ292798	MK299381	MZ292845	MZ273076	PP856181	Canary Island, Spain	Cuadrado et al. (2021)
	Pseudoceros rawlinsonae var. *galaxy*	-	MK299357	MZ292854	-	PP856188	Cape Verde Island	Cuadrado et al. (2021)
	Pseudobiceros flowersi	MZ292814	MZ292830	MZ292862	-	PP856195	Lizard Island, Australia	Marquina et al. (2015b)
	Pseudobiceros hymanae	MZ292815	MZ292831	MZ292863	-	-	Lizard Island, Australia	Marquina et al. (2015b)
	Pseudobiceros caribbensis	MZ292803	MK299378	MZ292849	MZ273077	PP856185	Martinique Island	Cuadrado et al. (2021)
	Thysanozoon alagoensis	MZ292802	MK299383	MZ292848	-	-	Martinique Island	Cuadrado et al. (2021)
	Thysanozoon brocchii	MW376738	MW377491	MW376583	-	MW392976	Victoria, Australia	Rodríguez et al. (2021)
	Yungia aurantiaca	-	MK299386	MZ292867	-	PP856199	Cádiz, Spain	Cuadrado et al. (2021)

(Castresana 2000) with relaxed parameters (smaller final blocks). This resulted in matrices of 521 bp (*cox1*), 500 bp (*16S rRNA*), 393 bp (*cytb*), 1047 bp (*28S rDNA*), and 859 bp (*18S rDNA*).

A supplementary entropy analysis was also performed with IQ-TREE version 1.6.12 (Trifinopoulos et al. 2016) to quantify the genetic variability across the length of the obtained sequences and assess the grade of conservation of each marker (entropy estimation by site).

The saturation rate of the substitutions of each genetic marker was quantified through a transition (Ti) and transversion (Tv) saturation graph using PAUP* Version 4.0a (Build 166) (Swofford 2003), as well as the distribution of variable sites and grade of genetic variability by site along the genes' matrices with an entropy analysis using DAMBE 5 (Xia 2013). Interspecific distances for each gene were calculated in Mega 6 (Tamura et al. 2013).

Maximum likelihood (ML) analysis was performed with IQ-TREE (Trifinopoulos et al. 2016). The optimal substitution model selected by the Bayesian information criterion (BIC) proposed by the ModelFinder (Kalyaanamoorthy et al. 2017) was GTR+F+I+G4 (*16S rDNA*, *cox1*), TIM+F+I+G4 (*cytb*), K2P+I (*18S rDNA*), and TIM3+F+I+G4 (*28S rDNA*). The consensus tree of 1000 standard bootstrap pseudo-replicates was selected and edited with iTOL version 4 (Letunic and Bork 2019). A node was considered well supported when the bootstrap value was 80% or greater. Phylogenies without outgroups have been analysed to avoid including inconsistencies since it was not possible to obtain a common outgroup for the five markers studied.

Results

Entropy estimation by site

Entropy analysis revealed genetic variability across the length of the obtained sequences and assessed the grade of conservation of each marker. The variable positions of each studied gene presented a continuous distribution, with substitutions unequally distributed in the nuclear genes. *18S rDNA* presented 58 out of 859 (6.75% of the alignment) variable positions (37 parsimonies informative, PIs), while *28S rDNA* presented 388 out of 1047 (37.0%) variable positions (306 PIs). *16S rDNA* presented 322 out of 500 (64.4%) variable positions (286 PIs), while *cytb* presented 234 out of 393 (59.54%) variable positions (218 PIs), and *cox1* presented 293 out of 521 (56.2%) variable positions (280 PIs) (Table 3, Fig. 1A).

Table 3. Genetic variability of the analysed sequences.

Gene	Average distance (%)	Min distance (%)	Max distance (%)	S	Cs	PIs
18S rDNA	1.37	0.00	3.14	859	58 (6.75%)	37
28S rDNA	11.21	0.00	18.71	1047	388 (37.0%)	306
16S rRNA	22.06	0.28	32.77	500	322 (64.4%)	286
cytb	26.86	0.00	34.40	393	234 (59.5%)	218
cox1	24.86	0.22	34.44	521	293 (56.2%)	280

The minimum distance was calculated as the minimum divergence of all sequences; the maximum distance was calculated as the maximum divergence of all sequences; Cs: number of constant sites; S: total number of sites in the matrix; and PIs: number of parsimony informative sites.

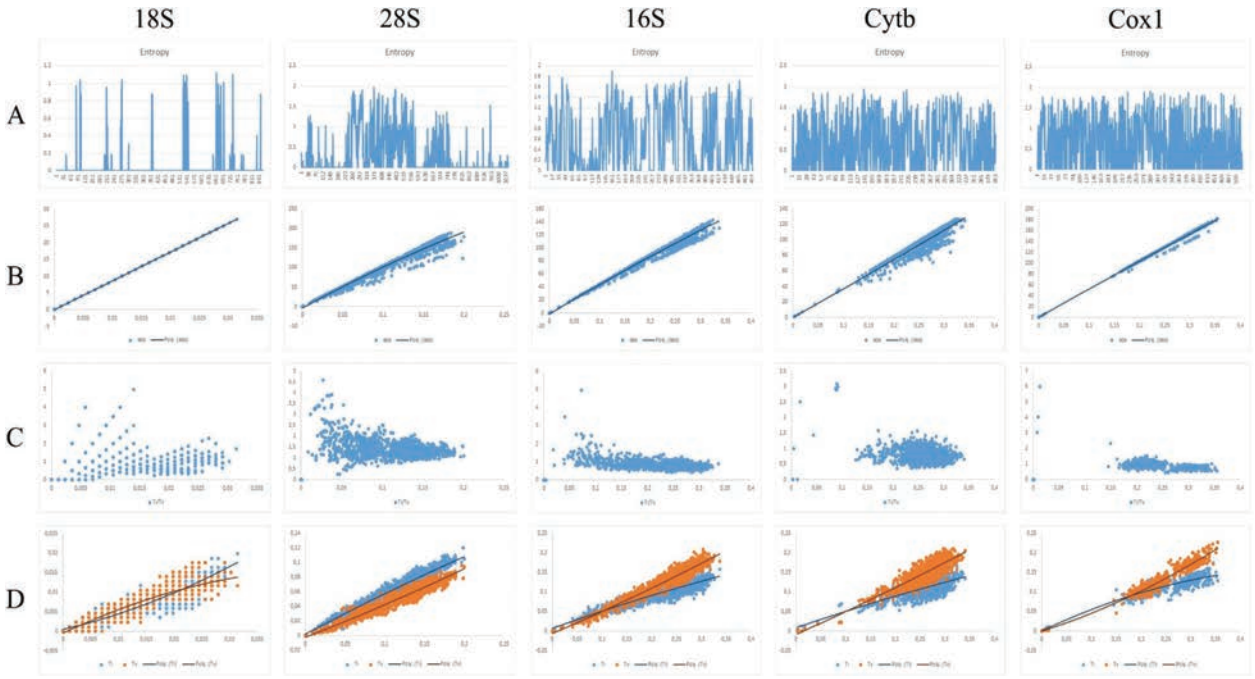

Figure 1. Genomic analysis of the studied genes. **A.** Entropy estimation by site: The X-axis indicates the number of sequenced positions, and the Y-axis indicates the number of variations of each position; **B.** Estimation of substitution rates in absolute values: The X-axis displays the pairwise genetic distance between sample pairs; the Y-axis indicates the number of mutations in absolute values; **C.** Estimation of Ti/Tv in pairwise sequence comparisons: The X-axis shows the pairwise genetic distance between sample pairs, and the Y-axis shows the Ti/Tv proportion; **D.** Estimation of transitions and transversions in pairwise sequence comparisons: The X-axis indicates the pairwise genetic distance between sample pairs, and the Y-axis indicates the proportion of transitions and transversions.

The variable sites of each codon position of the protein-codifying genes (*cytb* and *cox1*) were also assessed. The third codon position presented the highest values of interspecific maximum distances in both markers: 69.41% in *cytb* and 53.83% in *cox1*. On the other hand, the second codon position had the lowest values of maximum distances, with 16.66% in *cytb* and 13.42% in *cox1* (Table 4).

Table 4. Genetic variability of the analysed sequences of *cytb* and *cox1* by codon position.

Gene	Average distance (%)	Min distance (%)	Max distance (%)
cytb first codon position	20.38	0.00	30.58
cytb second codon position	8.88	0.00	16.66
cytb third codon position	51.71	0.00	69.41
cox1 first codon position	16.25	0.65	30.06
cox1 second codon position	5.51	0.00	13.42
cox1 third codon position	53.83	2.02	53.83

The minimum distance was calculated as the minimum divergence of all sequences; and the maximum distance was calculated as the maximum divergence of all sequences.

Estimate of substitution rate in absolute values

A total of 1485 (*18S rDNA*), 2556 (*28S rDNA*), 1653 (*16S rDNA*), 1176 (*cytb*), and 703 (*cox1*) pairwise comparisons from 43 (*18S rDNA*), 46 (*28S rDNA*), 45 (*16S rDNA*), 39 (*cytb*), and 30 (*cox1*) species were performed. Fig. 1B shows the number of substitutions in absolute values (abs) plotted against the pairwise distance between each sample. All cases presented a linear growth following these equations:

18S rDNA:

$$y = - 16.054x^2 + 858.37x – 8E-05$$

$$R^2 = 1.0000$$

28S rDNA:

$$y = - 760.97x^2 + 1123.5x – 3.5153$$

$$R^2 = 0.9743$$

16S rDNA:

$$y = - 114.54x^2 + 462.66x – 1.4178$$

$$R^2 = 0.9766$$

cytb:

$$y = 30.873x^2 + 366.5x + 0.3227$$

$$R^2 = 0.8436$$

cox1:

$$y = - 43.538x^2 + 524.81x + 0.1409$$

$$R^2 = 0.9901$$

The coefficient of determination (R^2) was close to 1 in most cases, indicating that all values were close to a linear progression except for the *cytb* mitochondrial gene ($R^2 = 0.84$).

Estimates of the transition/transversion ratio (Ti/Tv) in pairwise sequence comparisons

The estimated Ti/Tv ratios plotted against the estimated sequence distances showed the Ti/Tv ratio plotted against the pairwise distance between each sample (Fig. 1C). Two differentiated regions can be observed: the first was a region where the number of transitions and transversions randomly appeared with great variation. Due to the short distances between phylogenetic closely related species and the different numbers of transversions and transitions that each pair presented, the estimation showed disparate values depending on the selected samples, predominating the number of transitions, as they are the most probable among closely related species. As the distance between species pairs increased, a second region where the values stabilised around 1 (where 1 indicates the same number of transversions and transitions) appeared. While the value was slightly higher than 1 in most cases (indicating a greater number of transitions over transversions), starting from pairwise distances greater than 20%, the number of transversions increased compared to that of transitions in the case of the *16S rDNA* and *cox1* mitochondrial genes. Meanwhile, *28S rDNA* presented a Ti/Tv ratio between 1 and 2 at longer distances, indicating an overall higher number of transitions.

Estimates of transitions and transversions in pairwise sequence comparisons

Congruent with the results of the Ti/Tv ratio, the initial number of transitions was higher than that of transversions for all gene markers. However, the number of transversions was greater at higher distances across all markers, as observed in the graphs, except for *28S rDNA*, where transitions remained higher (Fig. 1D).

Differences among the three codon positions were evident (Fig. 2). The first codon position displayed maximum distances of 30.58% for *cytb* and 30.06% for *cox1*, compared to the maximum distances for the second codon position (16.66% and 13.42%, respectively) and those of the third codon position (69.41% and 70.94%).

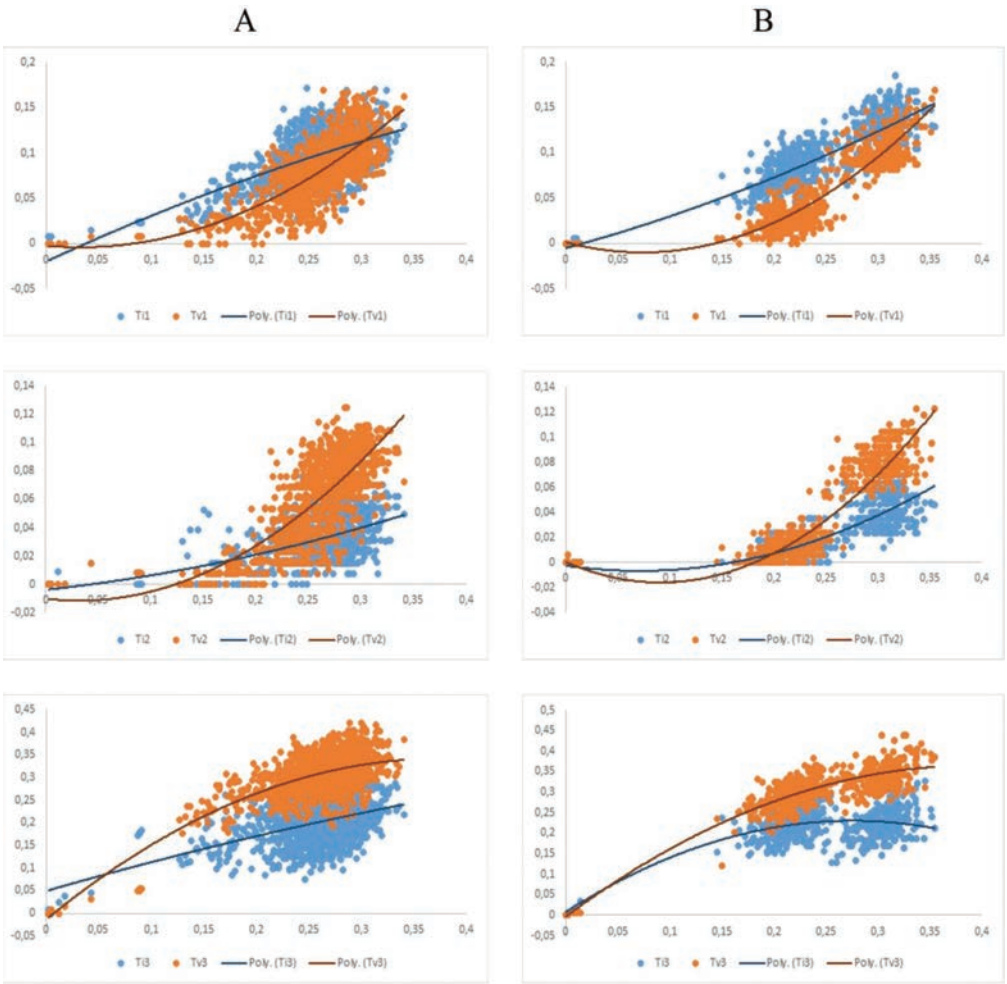

Figure 2. Estimation of transitions and transversions for each codon position (from top to bottom: first (1), second (2), and third (3) codon positions) in *cytb* (**A**) and *cox1* (**B**). The X-axis indicates the pairwise genetic distance between sample pairs, and the Y-axis indicates the proportion of transitions and transversions.

In both markers, the overall number of transversions was higher than that of transitions, apart from the first codon position, where the number of transitions was always higher than that of transversions. The second codon position displayed a lower mutation rate at shorter distances. Lastly, the third codon position presented a higher number of overall mutations (both transitions and transversions), with a higher proportion of transversions in both markers; however, a decrease in transition in the *cox1* gene was observed at pairwise distances higher than 25%.

Maximum-likelihood phylogenetic analyses

The matrices employed to analyse substitution ratios provided the following phylogenetic results through a maximum-likelihood analysis performed for each gene (Figs 3, 4). The results obtained for each marker are:

18S rDNA (Fig. 3): This marker showed the separation of the two suborders of Polycladida (Cotylea and Acotylea) with a bootstrap support (BS) of 97.

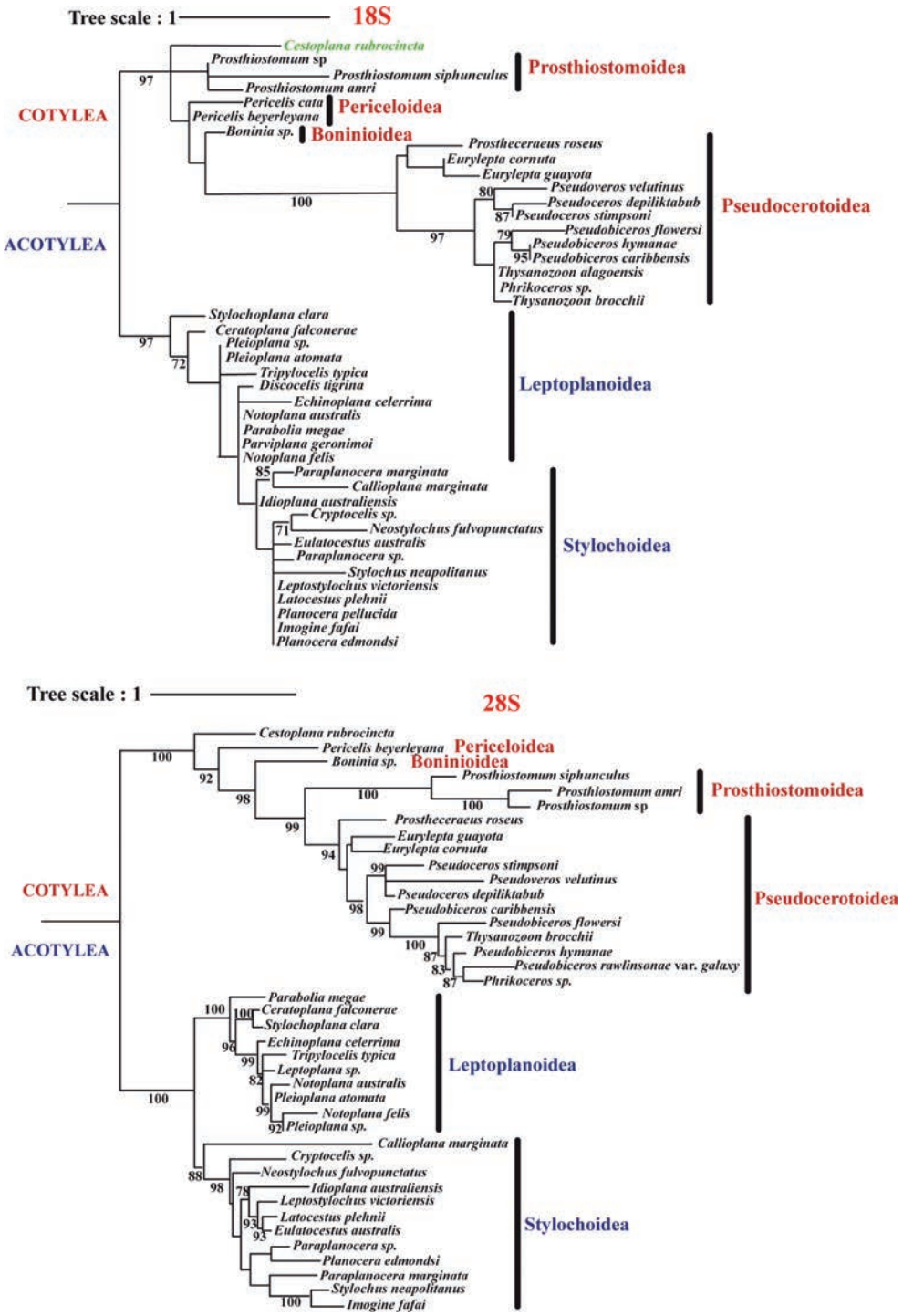

Figure 3. Maximum-likelihood phylogenetic analysis of nuclear gene markers (*18S* and *28S*).

The superfamily Pseudocerotidae (Cotylea) was highly supported (BS = 100), as were the genera *Pseudoceros* (BS = 80) and *Pseudobiceros* (BS = 79). The superfamilies and families of Acotylea appeared without strong support (BS < 70).

28S rDNA (Fig. 3): In this study, the two suborders were well supported (BS = 100). Within Cotylea, the four analysed superfamilies were well delimited and held: Periceloidea and Boninioidea produced two independent lineages, and Pseuderotoidea (BS = 94) and Prosthiostomoidea (BS = 100) were highly supported. Within the last superfamily Pseudocerotidae (including the genera *Pseudoceros*, *Pseudobiceros*, *Thysanozoon*, and *Phrikoceros*; BS = 98), an independent cluster for the family Eurylepidae was seen. Similarly, within the Acotylea suborder, the different superfamilies Leptoplanoidea and Stylochoidea showed high support values (BS = 100 and 88, respectively). Families such as Styochoplanidae (BS = 100), Leptoplanidae (BS = 99), Latocestidae (BS = 93), and Stylochidae (BS = 100) were also well supported.

16S rRNA (Fig. 4): This marker provided robust support for the suborders Cotylea and Acotylea and good resolution for the Cotylean superfamilies Periceloidea (BS = 100), Prosthiostomoidea (BS = 99), and Pseudocerotoidea (BS = 98). The two largest Cotylean superfamilies (Prosthiostomoidea and Pseudocerotoidea) were grouped in a clade with a bootstrap support of 95. Within Acotylea, the superfamily Stylochoidea was not supported (BS = 75), and the superfamily Leptoplanoidea did not form a monophyletic assemblage. As a result, at the family and genus levels, *16S rRNA* did not yield clear groups within the leptoplanoids.

cox1 (Fig. 4): This marker is considered the molecular "barcode" for the majority of species. In this study, support varied depending on the taxonomic level. At the suborder level, the support values were lower than those from other genes (BS = 77). At the next level, the mainly Cotylean and Acotylean superfamilies were recovered. The majority of families in both suborders did not form monophyletic clusters.

cytb (Fig. 4): Regarding the last of the studied markers, *cytb* separated the two suborders Cotylea and Acotylea (BS = 100). It also displayed high support for the Cotylean and Acotylean superfamilies. At family level, *cytb* provided good support in both suborders (Colylea: Eurylepidae BS = 86 and Pseudocerotidae BS = 99; Acotylea: Leptoplanidae BS = 98, Planoceridae BS = 77, Latocestidae BS = 82, and Stylochidae BS = 80), but the majority of Cotylean and Acotylean superfamilies were not recovered (Fig. 4).

All assessed markers placed *Cestoplana* within or as the sister lineage of Cotylea, but none showed an unequivocal phylogenetic or kinship relationship between *Cestoplana rubrocincta* and the other taxa.

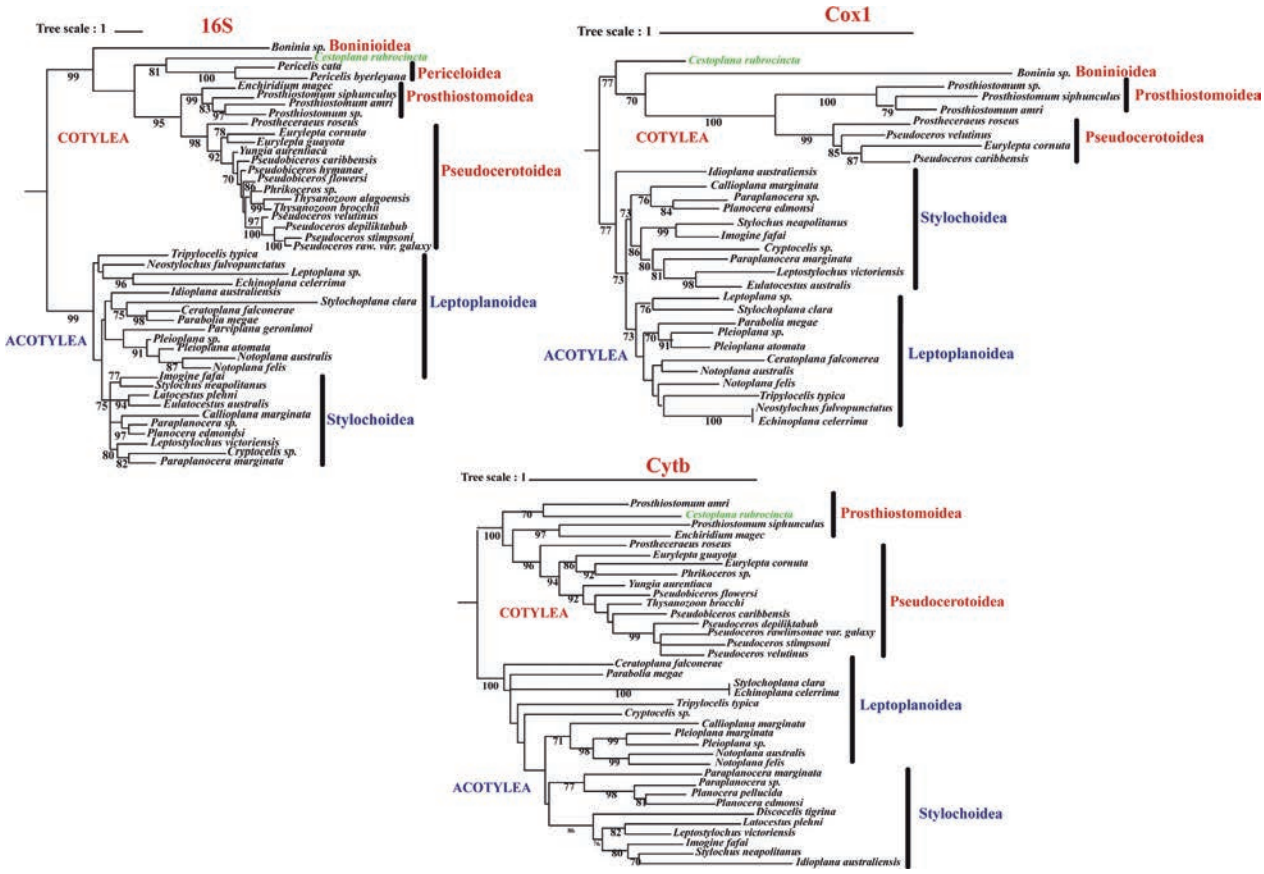

Figure 4. Maximum-likelihood phylogenetic analysis of mitochondrial gene markers (*16S*, *cox1*, and *cytb*).

Discussion

This study compares, for the first time, the substitutions of mitochondrial and nuclear molecular markers at the order level for polyclad flatworms, including representatives of all superfamilies within the suborders Cotylea and Acotylea.

Regarding entropy values, it is worth noting the small proportion of variable sites in the *18S rDNA* nuclear gene that denote low phylogenetic values in our analyses of the order compared to *28S rDNA*, which presented regions with clear variability alternating with conserved regions (Fig. 1A). This difference is made more apparent when compared to the studied mitochondrial markers (*16S rDNA*, *cox1*, and *cytb*), which all presented high variability and substitution rates. In addition, in the three mitochondrial markers, variability was present throughout the entire DNA sequence, which is possibly one of the reasons for the difficulty in creating generic primers for these species, especially in the case of *cox1*. In most invertebrate taxa, *cox1* sequencing is possible using universal primers such as those designed by Folmer and co-workers (Folmer et al. 1994) or, more recently, Lobo and colleagues (Lobo et al. 2013). For some taxonomic groups, however, these markers do not hybridise, and this appears to be the case for most Rhabditophora (Platyhelminthes), including those in the order Polycladida (mainly in the suborder Cotylea). In this situation, specific primers are frequently required (Aguado et al. 2017; Oya et al. 2019; Cuadrado et al. 2021).

The absolute values of substitution rates observed in our research reflect a linear increase in variability in all cases. A decrease in the absolute mutation rate was only observed in *cytb*, which may have been caused by a certain saturation in the signal of sequence substitution due to multiple recurrent changes since more than 80% of each sequence displayed variability. This saturation trend could lead to underestimating the variation in determinate terminal taxa. Therefore, it would be more advisable to use this marker for conducting phylogenetic analyses of closer groups, such as families or superfamilies.

The Ti/Tv ratio remained relatively stable for most cases, except for *28S rDNA*, which presented a higher number of transitions at all distances, and *cytb*, which displayed a higher number of transversions. In the case of the *28S* ribosomal gene, the elevated number of transitions is most likely due to a lack of conservation of the secondary structure of the RNA molecule (Rivas 2021), which may be required to preserve its function, with stem structures forming at transitions where needed.

In contrast, the overall increase in transversions in mitochondrial genes, particularly in *cytb*, could be the accumulation of substitutions when comparing variable sequences very distant from each other. All four types of transitions, as opposed to eight types of transversions, need to be considered in such situations. Previous studies have suggested that, compared with non-synonymous transversions, non-synonymous transitions are less deleterious because they tend not to cause radical changes in amino acid physicochemical properties such as charge, polarity, and size (e.g., Zhang 2000). However, our research shows a higher proportion of transitions were observed for the *28S rDNA* nuclear gene in comparison to the mitochondrial markers. Meanwhile, *18S rDNA* presented so few changes that it could hardly indicate a tendency in the analyses. Our results appear to validate the proposition made by Zou and Zhang (2021), who stated that the Ti/Tv ratio can be more or less than 1 (i.e., transversions or transitions being more prevalent) depending on the group studied. They attributed variations between interchangeable amino acids in protein-coding genes as a possible cause for this (e.g., variations in the genetic code of different taxa, differences in the functionality of generated proteins, etc.). In the case of the phylum Platyhelminthes, it is important to point out that the flatworm mitochondrial genetic code possesses four variations compared to the standard invertebrate mitochondrial code. For example, AAA codifies for asparagine (Asn) in flatworms, while in the standard mitochondrial code only AAT and AAC codify for this amino acid, which leads to fixating a transversion in this group. Likewise, the codons AGA and AGG translate to serine (Ser) in the flatworm mitochondrial genetic code instead of Arg, fixating two additional transversions, and UGA codifies for Trp rather than being a stop codon (Telford et al. 2000).

Different patterns of substitutions were also observed for the results of the *28S rDNA* nuclear gene (Fig. 1B) and those present in the mitochondrial genes when comparing transition and transversion rates. The number of transitions surpasses the number of transversions in the *28S rDNA*, while the mitochondrial markers show more transversions than transitions. The variations in the mitochondrial genetic code of flatworms mentioned earlier could lead to a higher chance of fixating transversions. Because of this, we suggest a more exhaustive study on this increase in transversions in the mitochondrial DNA of polyclads and its implications for Platyhelminthes more generally.

Conspicuous differences were observed when comparing all codon positions of each of the studied protein-codifying genes (*cytb* and *cox1*). Saturation of the transversions was observed in the third codon position of *cox1*. Such saturation has been reported previously for other taxonomic groups such as triclads (Alvarez-Presas et al. 2008), protists (Liu and Zhang 2019), insects (Schrider et al. 2013), plants (Ossowski et al. 2010), and nematodes (Denver et al. 2009). It is possible that the decrease in the signal of the number of transitions at distances higher than 25% observed in our research could lead to errors in phylogenetic analyses of polyclad flatworms when using the *cox1* genetic marker. A plausible solution to reduce this effect during future phylogenetic analyses would be to delete the third codon position from the alignment. The effectiveness of this, however, is beyond the scope of this study.

Based on the results obtained in the ML analysis (Figs 3, 4), the markers with the best clade support and agree-

ment with morphological relationships by histological analyses (Faubel 1983, 1984) were *28S rDNA* (nuclear) and the mitochondrial markers *16S rDNA* and *cytb*. *18S rDNA* did not offer strong support at any taxonomic level studied. Moreover, substantial differences in support existed within the effective and resolving markers: *28S rDNA* (nuclear) and *16S rDNA*/*cytb* (mitochondrial). The differences observed between mitochondrial and nuclear markers, along with their potential incongruences in phylogenetic analyses, have previously been documented in other taxa, including Anthozoa, Insecta, and mammals (Zadra et al. 2021; Fedorov et al. 2022; Quattrini et al. 2023).

28S rDNA resolved the majority of nodes well for the systematics of suborder, superfamily, family, and, in some cases, at the genus and species level in Cotylea. Nevertheless, the *28S rDNA* proved less effective in resolving deep nodes within Acotylea, resulting in the formation of paraphyletic nodes.

Within the mitochondrial markers, the best resolution level (>75 bootstrap support), compared to current phylogeny (Goodheart et al. 2023), was observed at the genus and species level. Both *16S rDNA* and *cytb* strengthened and delimited the genera, resolving specific clusters within Cotylea and Acotylea. The specific combinations presented in our analyses revealed differences, such as the relationship between *Cestoplana* and *Pericelis* within Cotylea or *Echinoplana* with *Leptoplana* in Acotylea, although these relationships were not recovered by *cytb*. This may be caused by the increased substitution rate present among distantly related taxa within the phylogenetic tree (resulting in decreased linear progression of R^2) and a more complex evolutionary history for these genes or taxa.

Conclusion

Among the tested markers, *cytb* presented a higher rate of variability and did not show saturation of transitions for any codon position. Moreover, this marker presented the highest range of distances (0% to 34.40%), with an average distance of 26.86% compared to that of *cox1* (highest range of distances: 0.22% to 34.44%, average distance: 24.86%).

The use of a common marker for the order Polycladida would allow direct phylogenetic comparison across studies. General primers for these mitochondrial genes often fail to hybridise, so we also recommend designing *de novo cox1*-specific primers for families within the suborder Cotylea and *cytb*-specific primers for those within Acotylea, taking into consideration third base positions. The *de novo* design markers will allow amplification of *cox1* and *cytb* sequences for certain groups of polyclad flatworms that previously could not be analysed due to the high number of substitutions across the whole sequence and the lack of conserved regions.

Thus, for polyclad flatworms, we conclude that for future studies at the order level, we encourage the use of mitochondrial genes *cytb* and *16S rDNA* and nuclear ribosomal genes *28S rDNA*. We also encourage the use of the *cox1* gene with the caution of analysing the third codon position to avoid errors in the analyses and resolution of deep nodes at a generic or specific level. Certainly, the most crucial aspect is to determine the specific research inquiry and taxonomic level (such as order, family, or genus) and consequently select the appropriate genes to better address the study. In the present study, we analysed five markers currently used in the resolution of phylogenies, kinship analysis, delimitation of species, etc. We look forward to future polyclad studies using our suggested approach so that we can continue advancing the systematics and origin of this taxon on a global scale. New sequencing techniques offer the possibility of incorporating additional molecular information if the selected genes accurately represent the evolutionary history of the species. Concatenating data from different suitable markers will further bolster support for the analysed clusters.

Our case study highlights the need to evaluate how well nuclear and mitochondrial genes perform within a specific taxonomic group level. We propose that the use of transition bias is a useful tool for distinguishing which markers may be more effective for any taxon and could help streamline success for future systematic studies. It would also make cross-study evaluation within a taxonomic group more effective. A more globally collaborative approach to molecular systematics would certainly facilitate the use of this approach.

Acknowledgements

We thank the Linnean Society of New South Wales for their funding via a Vickery Fund Research Grant. The authors thank the School of Natural Sciences at Macquarie University for their institutional and financial support, the Australian Museum Research Institute, and the members of the Marine Invertebrates and Malacology Departments for providing access to their facilities and laboratories and assisting in fieldwork. Thanks to Audrey Falconer, Leon Altoff, and the members of the Field Naturalists' Club of Victoria for their assistance in collecting samples and financial support through the FNCV Environment Fund. We extend our gratitude to the members of the Marine Ecology Group from Macquarie University (Justin McNab, Louise Tosetto, Patrick Burke, and Ryan Nevatte) for their help during fieldwork. F.Á.F.-Á. was supported by a Beatriu de Pinós fellowship from the Secretaria d'Universitats i Recerca del Departament de Recerca i Universitats of the Generalitat de Catalunya (Ref. BP 2021 00035). This research was also supported by the Spanish government through the 'Severo Ochoa Centre of Excellence' accreditation (CEX2019-000928-S). Lastly, J.R. expresses his gratitude to the Australian Government and Macquarie University for funding his livelihood and research through the International Research Training Programme (iRTP) Scholarship.

References

Aguado MT, Grande C, Gerth M, Bleidorn C, Noreña C (2016) Characterization of the complete mitochondrial genomes from Polycladida (Platyhelminthes) using next-generation sequencing. Gene 575(2): 199–205. https://doi.org/10.1016/j.gene.2015.08.054

Aguado MT, Noreña C, Alcaraz L, Marquina D, Brusa F, Almon B, Bleidorn C, Grande C (2017) Phylogeny of Polycladida (Platyhelminthes) based on mtDNA data. Organisms, Diversity & Evolution 17(4): 767–778. https://doi.org/10.1007/s13127-017-0344-4

Alvarez-Presas M, Baguna J, Riutort M (2008) Molecular phylogeny of land and freshwater planarians (Tricladida, Platyhelminthes): From freshwater to land and back. Molecular Phylogenetics and Evolution 47(2): 555–568. https://doi.org/10.1016/j.ympev.2008.01.032

Bahia J (2016) First records of polyclads (Platyhelminthes, Polycladida) associated with *Nodipecten nodosus* (Linnaeus 1758) aquaculture. Marine Biodiversity 46(4): 911–915. https://doi.org/10.1007/s12526-015-0425-6

Bahia J, Padula V, Schrödl M (2017) Polycladida phylogeny and evolution: Integrating evidence from *28S rDNA* and morphology. Organisms, Diversity & Evolution 17(3): 653–678. https://doi.org/10.1007/s13127-017-0327-5

Broughton RE, Stanley SE, Durrett RT (2000) Quantification of homoplasy for nucleotide transitions and transversions and a reexamination of assumptions in weighted phylogenetic analysis. Systematic Biology 49(4): 617–627. https://doi.org/10.1080/106351500750049734

Carrera-Parra LF, Fauchald K, Gambi C (2011) Revision of the taxonomic status of *Lysidice* (Polychaeta, Eunicidae) in the western Caribbean Sea with observation on species reproductive features and habitat preference. The Italian Journal of Zoology 78(Suppl. 1): 27–40. https://doi.org/10.1080/11250003.2011.593850

Castresana J (2000) Selection of conserved blocks from multiple alignments for their use in phylogenetic analysis. Molecular Biology and Evolution 17(4): 540–552. https://doi.org/10.1093/oxfordjournals.molbev.a026334

Cuadrado D, Rodríguez J, Moro L, Grande C, Noreña C (2021) Polycladida (Platyhelminthes, Rhabditophora) from Cape Verde and related regions of Macaronesia. European Journal of Taxonomy 736: 1–43. https://doi.org/10.5852/ejt.2021.736.1249

Denver DR, Dolan PC, Wilhelm LJ, Sung W, Lucas-Lledo JI, Howe DK, Lewis SC, Okamoto K, Thomas WK, Lynch M, Baer CF (2009) A genome-wide view of *Caenorhabditis elegans* base-substitution mutation processes. Proceedings of the National Academy of Sciences of the United States of America 106(38): 16310–16314. https://doi.org/10.1073/pnas.0904895106

Dittmann IL, Cuadrado D, Aguado MT, Noreña C, Egger B (2019) Polyclad phylogeny persists to be problematic. Organisms, Diversity & Evolution 19(4): 585–608. https://doi.org/10.1007/s13127-019-00415-1

Faubel A (1983) The Polycladida, Turbellaria; Proposal and establishment of a new system. Part I. The Acotylea. Mitteilungen aus dem Hamburgischen Zoologischen Museum und Institut 80: 17–121.

Faubel A (1984) The Polycladida, Turbellaria; Proposal and establishment of a new system. Part II. The Cotylea. Mitteilungen aus dem Hamburgischen Zoologischen Museum und Institut 81: 189–259.

Fedorov VB, Trucchi E, Goropashnaya AV, Chr Stenseth N (2022) Conflicting nuclear and mitogenome phylogenies reveal ancient mitochondrial replacement between two North American species of collared lemmings (*Dicrostonyx groenlandicus*, *D. hudsonius*). Molecular Phylogenetics and Evolution 168: 107399. https://doi.org/10.1016/j.ympev.2022.107399

Fernández-Álvarez FÁ, Braid HE, Nigmatullin CM, Bolstad KSR, Haimovici M, Sánchez P, Sajikumar KK, Ragesh N, Villanueva R (2020) Global biodiversity of the genus *Ommastrephes* d'Orbigny, 1834 (Ommastrephidae: Cephalopoda): an allopatric cryptic species complex. Zoological Journal of the Linnean Society 190(2): 460–482. https://doi.org/10.1093/zoolinnean/zlaa014

Folmer O, Black M, Hoeh W, Lutz R, Vrijenhoek R (1994) DNA primers for amplification of mitochondrial cytochrome c oxidase subunit I from diverse metazoan invertebrates. Molecular Marine Biology and Biotechnology 3: 294–299.

Forsman ZH, Barshis DJ, Hunter CL, Toonen RJ (2009) Shape-shifting corals: Molecular markers show morphology is evolutionarily plastic in *Porites*. BMC Evolutionary Biology 9(1): 1–9. https://doi.org/10.1186/1471-2148-9-45

Gammoudi M, Ahmed RB, Bouriga N, Ben-Attia M, Harrath AH (2016) Predation by the polyclad flatworm *Imogine mediterranea* on the cultivated mussel *Mytilus galloprovincialis* in Bizerta Lagoon (northern Tunisia). Aquaculture Research 1: 10. https://doi.org/10.1111/are.12995

Goodheart JA, Collins AG, Cummings MP, Egger B, Rawlinson KA (2023) A phylogenomic approach to resolving interrelationships of polyclad flatworms, with implications for life history evolution. Royal Society Open Science 10(3): 220939. https://doi.org/10.1098/rsos.220939

Hebert PDN, Cywinska A, Ball SL, deWaard JR (2003) Biological identifications through DNA barcodes. Proceedings. Biological Sciences 270(1512): 313–321. https://doi.org/10.1098/rspb.2002.2218

Jondelius U, Ruiz-Trillo I, Baguna J, Riutort M (2002) The Nemertodermatida are basal bilaterians and not members of the Platyhelminthes. Zoologica Scripta 31(2): 201–215. https://doi.org/10.1046/j.1463-6409.2002.00090.x

Kalyaanamoorthy S, Minh BQ, Wong TKF, von Haeseler A, Jermiin LS (2017) ModelFinder: Fast model selection for accurate phylogenetic estimates. Nature Methods 14(6): 587–589. https://doi.org/10.1038/nmeth.4285

Kearse M, Moir R, Wilson A, Stones-Havas S, Cheung M, Sturrock S, Buxton S, Cooper A, Markowitz S, Duran C, Thierer T, Ashton B, Meintjes P, Drummond A (2012) Geneious basic: An integrated and extendable desktop software platform for the organization and analysis of sequence data. Bioinformatics 28(12): 1647–1649. https://doi.org/10.1093/bioinformatics/bts199

Kenny NJ, Noreña C, Damborenea C, Grande C (2019) Probing recalcitrant problems in polyclad evolution and systematics with novel mitochondrial genome resources. Genomics 111(3): 343–355. https://doi.org/10.1016/j.ygeno.2018.02.009

Kimura M (1980) A simple method for estimating evolutionary rates of base substitutions through comparative studies of nucleotide sequences. Journal of Molecular Evolution 16(2): 111–120. https://doi.org/10.1007/BF01731581

Kupriyanova EK, ten Hove HA, Rouse GW (2023) Phylogenetic relationships of Serpulidae (Annelida, Polychaeta) inferred from morphology and molecular data: Re-classification of Serpulidae. Diversity 15(3): 398. https://doi.org/10.3390/d15030398

Larkin MA, Blackshields G, Brown NP, Chenna R, McGettigan PA, McWilliam H, Valentin F, Wallace IM, Wilm A, Lopez R, Thompson

JD, Gibson TJ, Higgins DG (2007) Clustal W and Clustal X version 2.0. Bioinformatics 23(21): 2947–2948. https://doi.org/10.1093/bioinformatics/btm404

Letunic I, Bork P (2019) Interactive Tree of Life (iTOL) v4: Recent updates and new developments. Nucleic Acids Research 47(W1): W256–W259. https://doi.org/10.1093/nar/gkz239

Litvaitis MK, Newman LJ (2001) A molecular framework for the phylogeny of the Pseudocerotidae (Platyhelminthes, Polycladida). Hydrobiologia 444(1–3): 177–182. https://doi.org/10.1023/A:1017503124908

Litvaitis MK, Bolaños DM, Quiroga SY (2010) When names are wrong and colours deceive: unravelling the species complex (Turbellaria: Polycladida). Journal of Natural History 44(13–14): 829–845. https://doi.org/10.1080/00222930903537074

Litvaitis MK, Bolaños DM, Quiroga SY (2019) Systematic congruence in Polycladida (Platyhelminthes, Rhabditophora): Are DNA and morphology telling the same story? Zoological Journal of the Linnean Society 186(4): 865–891. https://doi.org/10.1093/zoolinnean/zlz007

Liu H, Zhang J (2019) Yeast spontaneous mutation rate and spectrum vary with environment. Current Biology 29(10): 1584–1591. https://doi.org/10.1016/j.cub.2019.03.054

Lobo J, Costa PM, Teixeira MA, Ferreira MSG, Costa MH, Filipe O, Costa FO (2013) Enhanced primers for amplification of DNA barcodes from a broad range of marine metazoans. BMC Ecology 13: 34. https://doi.org/10.1186/1472-6785-13-34

Marquina D, Fernández-Álvarez FA, Noreña C (2015a) Five new records and one new species of Polycladida (Platyhelminthes) for the Cantabrian coast (North Atlantic) of the Iberian Peninsula. Journal of the Marine Biological Association of the United Kingdom 95(2): 311–322. https://doi.org/10.1017/S0025315414001106

Marquina D, Aguado MT, Noreña C (2015b) New records of Cotylea (Polycladida, Platyhelminthes) and one new species from Lizard Island (Australia), with remarks on the distribution of the *Pseudoceros* Lang, 1884 and *Pseudobiceros* Faubel, 1984 species of the Indo-Pacific marine region. Zootaxa 4019(1): 354–377. https://doi.org/10.11646/zootaxa.4019.1.14

McNab JM, Rodríguez J, Karuso P, Williamson JE (2021) Natural products in polyclad flatworms. Marine Drugs 19(2): 47. https://doi.org/10.3390/md19020047

McNab JM, Briggs MT, Williamson JE, Hoffmann P, Rodríguez J, Karuso P (2022) Structural characterization and spatial mapping of tetrodotoxins in Australian polyclads. Marine Drugs 20(12): 788. https://doi.org/10.3390/md20120788

Morgan J, DeJong R, Kazibwe F, Mkoji G, Loker E (2003) A newly-identified lineage of *Schistosoma*. International Journal for Parasitology 33(9): 977–985. https://doi.org/10.1016/S0020-7519(03)00132-2

Nei M, Kumar S (2000) Molecular evolution and phylogenetics. Oxford University Press, New York. https://doi.org/10.1093/oso/9780195135848.001.0001

Noreña C, Marquina D, Perez J, Almon B (2014) First records of Cotylea (Polycladida, Platyhelminthes) for the Atlantic coast of the Iberian Peninsula. ZooKeys 404: 1–22. https://doi.org/10.3897/zookeys.404.7122

Noreña C, Rodríguez J, Pérez J, Almon B (2015) New Acotylea (Polycladida, Platyhelminthes) from the east coast of the North Atlantic Ocean with special mention of the Iberian littoral. Zootaxa 4039(1): 157–172. https://doi.org/10.11646/zootaxa.4039.1.7

Oliver T, Isaac N, August T, Woodcock BW, David BR, Bullock JM (2015) Declining resilience of ecosystem functions under biodiversity loss. Nature Communications 6(1): 10122. https://doi.org/10.1038/ncomms10122

Ossowski S, Schneeberger K, Lucas-Lledo JI, Warthmann N, Clark RM, Shaw RG, Weigel D, Lynch M (2010) The rate and molecular spectrum of spontaneous mutations in *Arabidopsis thaliana*. Science 327(5961): 92–94. https://doi.org/10.1126/science.1180677

Oya Y, Kajihara H (2017) Description of a new *Notocomplana* species (Platyhelminthes: Acotylea), new combination and new records of Polycladida from the northeastern Sea of Japan, with a comparison of two different barcoding markers. Zootaxa 4282(3): 526–542. https://doi.org/10.11646/zootaxa.4282.3.6

Oya Y, Kajihara H (2020) Molecular Phylogenetic Analysis of Acotylea (Platyhelminthes: Polycladida). Zoological Science 37(3): 271–279. https://doi.org/10.2108/zs190136

Oya Y, Kimura T, Kajihara H (2019) Description of a new species of *Paraplehnia* (Polycladida, Stylochoidea) from Japan, with inference on the phylogenetic position of Plehniidae. ZooKeys 864: 1–13. https://doi.org/10.3897/zookeys.864.33955

Park JM, Powell NN, Gillings MR, Gaston TF, Williamson JE (2020) Phylogeny and form in fishes: Genetic and morphometric characteristics of dragonets (*Foetorepus* sp.) do not align. Acta Zoologica (Stockholm, Sweden) 101(2): 218–226. https://doi.org/10.1111/azo.12287

Pérez-García P, Noreña C, Cervera JL (2019) Two new acotylean flatworms (Polycladida) of two genera unrecorded in the Eastern Atlantic. Marine Biodiversity 49(3): 1187–1195. https://doi.org/10.1007/s12526-018-0900-y

Prudhoe S (1985) A monograph on Polyclad Turbellaria. London/Oxford: British Museum of Natural History and Oxford University Press.

Quattrini AM, Snyder KE, Purow-Ruderman R, Seiblitz IGL, Hoang J, Floerke N, Ramos NI, Wirshing HH, Rodriguez E, McFadden CS (2023) Mito-nuclear discordance within Anthozoa, with notes on unique properties of their mitochondrial genomes. Scientific Reports 13(1): 7443. https://doi.org/10.1038/s41598-023-34059-1

Ratnasingham S, Hebert PD (2007) Bold: The Barcode of Life Data System (www.barcodinglife.org). Molecular Ecology Notes 7(3): 355–364. https://doi.org/10.1111/j.1471-8286.2007.01678.x

Raupach MJ, Mayer C, Malyutina M, Wagele JW (2009) Multiple origins of deep-sea *Asellota* (Crustacea: Isopoda) from shallow waters revealed by molecular data. Proceedings of the Royal Society B, Biological Sciences 276(1658): 799–808. https://doi.org/10.1098/rspb.2008.1063

Rawlinson KA, Stella JS (2012) Discovery of the Corallivorous Polyclad flatworm, *Amakusaplana acroporae*, on the Great Barrier Reef, Australia – the first report from the wild. PLOS ONE 7(8): e42240. https://doi.org/10.1371/journal.pone.0042240

Rawlinson KA, Gillis JA, Billings Jr RE, Borneman EH (2011) Taxonomy and life history of the *Acropora*-eating flatworm *Amakusaplana acroporae* nov. sp. (Polycladida: Prosthiostomidae). Coral Reefs 30(3): 693. https://doi.org/10.1007/s00338-011-0745-3

Rivas E (2021) Evolutionary conservation of RNA sequence and structure. Wiley Interdisciplinary Reviews. RNA 12(5): e1649. https://doi.org/10.1002/wrna.1649

Rodríguez J, Hutchings P, Williamson JE (2021) Biodiversity of intertidal marine flatworms (Polycladida, Platyhelminthes) in southeastern Australia. Zootaxa 5024(1): 1–63. https://doi.org/10.11646/zootaxa.5024.1.1

Schrider DR, Houle D, Lynch M, Hahn MW (2013) Rates and genomic consequences of spontaneous mutational events in *Drosophila melanogaster*. Genetics 194(4): 937–954. https://doi.org/10.1534/genetics.113.151670

Selivon D, Perondini ALP, Morgante JS (2005) A genetic-morphological characterization of two cryptic species of the *Anastrepha fraterculus* complex (Diptera: Tephritidae). Annals of the Entomological Society of America 98(3): 367–381. https://doi.org/10.1603/0013-8746(2005)098[0367:AGCOTC]2.0.CO;2

Soutullo P, Cuadrado D, Noreña C (2021) First study of the Polycladida (Rhabditophora, Platyhelminthes) from the Pacific Coast of Costa Rica. Zootaxa 4964(2): 363–381. https://doi.org/10.11646/zootaxa.4964.2.7

Strand M, Sundberg P (2005) Delimiting species in the hoplonemertean genus *Tetrastemma* (phylum Nemertea): Morphology is not concordant with phylogeny as evidenced from mtDNA sequences. Biological Journal of the Linnean Society, Linnean Society of London 86(2): 201–212. https://doi.org/10.1111/j.1095-8312.2005.00535.x

Swofford DL (2003) PAUP*. Phylogenetic Analysis Using Parsimony (*and Other Methods). Version 4. Sinauer Associates, Sunderland, Massachusetts.

Tamura K, Nei M (1993) Estimation of the number of nucleotide substitutions in the control region of mitochondrial DNA in humans and chimpanzees. Molecular Biology and Evolution 10(3): 512–526.

Tamura K, Stecher G, Peterson D, Filipski A, Kumar S (2013) MEGA6: Molecular evolutionary genetics analysis version 6.0. Molecular Biology and Evolution 30(12): 2725–2729. https://doi.org/10.1093/molbev/mst197

Telford MJ, Herniou EA, Russell RB, Littlewood DTJ (2000) Changes in mitochondrial genetic codes as phylogenetic characters: Two examples from the flatworms. Proceedings of the National Academy of Sciences of the United States of America 97(21): 11359–11364. https://doi.org/10.1073/pnas.97.21.11359

Tosetto L, McNab JM, Hutchings PA, Rodríguez J, Williamson JE (2023) Fantastic flatworms and where to find them: Insights into intertidal polyclad flatworm distribution in southeastern Australian boulder beaches. Diversity 15(3): 393. https://doi.org/10.3390/d15030393

Trifinopoulos J, Nguyen LT, von Haeseler A, Minh BQ (2016) W-IQ-TREE: A fast online phylogenetic tool for maximum likelihood analysis. Nucleic Acids Research 44(W1): 232–235. https://doi.org/10.1093/nar/gkw256

Tsunashima T, Hagiya M, Yamada R, Koito T, Tsuyuk N, Izawa S, Kosoba K, Itoi S, Sugita H (2017) A molecular framework for the taxonomy and systematics of Japanese marine turbellarian flatworms (Platyhelminthes, Polycladida). Aquatic Biology 26: 159–167. https://doi.org/10.3354/ab00682

Tsuyuki A, Oya Y, Kajihara H (2019) A New Species of *Prosthiostomum* (Platyhelminthes: Polycladida) from Shirahama, Japan. Species Diversity : An International Journal for Taxonomy, Systematics, Speciation, Biogeography, and Life History Research of Animals 24(2): 137–143. https://doi.org/10.12782/specdiv.24.137

Tsuyuki A, Oya Y, Kajihara H (2022) Two new species of the marine flatworm *Pericelis* (Platyhelminthes: Polycladida) from southwestern Japan with an amendment of the generic diagnosis based on phylogenetic inference. Marine Biology Research. https://doi.org/10.1080/17451000.2022.2048669

Tyler S, Schilling S, Hooge M, Bush LF [comp.] (2006–2024) Turbellarian taxonomic database. Version 1.8. http://turbellaria.umaine.edu

Valdés A, Breslau E, Padula V, Schrödl M, Camacho Y, Malaquias MA, Alexander J, Bottomley M, Vital XG, Hooker Y, Gosliner TM (2017) Molecular and morphological systematics of *Dolabrifera* Gray, 1847 (Mollusca: Gastropoda: Heterobranchia: Aplysiomorpha). Zoological Journal of the Linnean Society 184(1): 31–65. https://doi.org/10.1093/zoolinnean/zlx099

Vella A, Vella N, Maslin M, Bichlmaier L (2016) First molecular barcoding and record of the Indo-Pacific punctuated flatworm *Maritigrella fuscopunctata* (Newman and Cannon 2000), (Polycladida: Euryleptidae) from the Mediterranean Sea. Journal of the Black Sea/Mediterranean Environment 22: 119–127.

Xia X (2013) DAMBE5: A comprehensive software package for data analysis in molecular biology and evolution. Molecular Biology and Evolution 30(7): 1720–1728. https://doi.org/10.1093/molbev/mst064

Yang Z (2006) Computational molecular evolution. Oxford: Oxford University Press. https://doi.org/10.1093/acprof:oso/9780198567028.001.0001

Yang Z, Nielsen R, Hasegawa M (1998) Models of amino acid substitution and applications to mitochondrial protein evolution. Molecular Biology and Evolution 15(12): 1600–1611. https://doi.org/10.1093/oxfordjournals.molbev.a025888

Yonezawa R, Itoi S, Igarashi Y, Yoshitake K, Oyama H, Kinoshita S, Suo R, Yokobori S, Sugita H, Asakawa S (2020) Characterization and phylogenetic position of two sympatric sister species of toxic flatworms *Planocera multitentaculata* and *Planocera reticulata* (Platyhelminthes: Acotylea). Mitochondrial DNA, Part B, Resources 5(3): 2352–2354. https://doi.org/10.1080/23802359.2020.1730255

Zadra N, Rizzoli A, Rota-Stabelli O (2021) Chronological Incongruences between Mitochondrial and Nuclear Phylogenies of Aedes Mosquitoes. Life 11(3): 181. https://doi.org/10.3390/life11030181

Zhang J (2000) Rates of conservative and radical nonsynonymous nucleotide substitutions in mammalian nuclear genes. Journal of Molecular Evolution 50(1): 56–68. https://doi.org/10.1007/s002399910007

Zhang YM, Egan SP, Driscoe AL, Ott JR (2021) One hundred and sixty years of taxonomic confusion resolved: (Hymenoptera: Cynipidae: Cynipini) gall wasps associated with live oaks in the USA. Zoological Journal of the Linnean Society 193(4): 1234–1255. https://doi.org/10.1093/zoolinnean/zlab001

Zou Z, Zhang J (2021) Are nonsynonymous transversions generally more deleterious than nonsynonymous transitions? Molecular Biology and Evolution 38(1): 181–191. https://doi.org/10.1093/molbev/msaa200

Zoosyst. Evol. 100 (3) 2024, 877–895 | DOI 10.3897/zse.100.120244

PENSOFT

für Natur MUSEUM FÜR NATURKUNDE BERLIN

Marine microturbellarians from Japan, with descriptions of two new species of *Reinhardorhynchus* (Platyhelminthes, Rhabdocoela, Koinocystididae)

Aoi Tsuyuki[1,2], Jhoe Reyes[3], Yuki Oya[4], Kevin C. Wakeman[5,6], Brian S. Leander[7], Niels W. L. Van Steenkiste[7,8]

1 *Faculty of Science, Hokkaido University, Sapporo, Hokkaido, 060-0810, Japan*
2 *Creative Research Institution, Hokkaido University, Sapporo, Hokkaido, 001-0021, Japan*
3 *Facultad de Ciencias de la Vida y de la Salud, Universidad Científica del Sur, Lima, Peru*
4 *College of Arts and Sciences, J. F. Oberlin University, 3758 Tokiwa, Machida, Tokyo, 194-0294, Japan*
5 *Institute for the Advancement of High Education, Hokkaido University, Sapporo, Hokkaido, Japan*
6 *Graduate School of Science, Hokkaido University, Sapporo, Hokkaido, 080-0810, Japan*
7 *Departments of Botany and Zoology, University of British Columbia, Vancouver, BC, V6T 1Z4, Canada*
8 *Hakai Institute, Heriot Bay, Quadra Island, BC, V0P 1H0, Canada*

https://zoobank.org/C025A8A6-116F-4BAF-94AA-6276BC84D2C8

Corresponding author: Jhoe Reyes (jreyesp@cientifica.edu.pe)

Academic editor: Pavel Stoev ♦ **Received** 5 February 2024 ♦ **Accepted** 1 April 2024 ♦ **Published** 3 July 2024

Abstract

Marine microturbellarians are an assemblage of meiofaunal flatworms abundant in sediments and on seaweeds around the world. The diversity and distribution of these animals in Japan are poorly understood. Here, we provide an overview of all recorded species in Japan and characterize two new species of the rhabdocoel genus *Reinhardorhynchus* based on morphological features and a molecular phylogeny inferred from 18S and 28S rDNA sequences. *Reinhardorhynchus ryukyuensis* **sp. nov.** can be distinguished from other species in the genus by the lack of an armed cirrus and by the presence of two larger opposing hooks and five smaller interconnected hooks in its male copulatory organ. *Reinhardorhynchus sagamianus* **sp. nov.** differs from its congeners because its male copulatory organ combines a bipartite cirrus armed with a belt of overlapping scale-like spines, an unarmed accessory cirrus, and two large distal accessory hooks. Our molecular phylogenetic analyses show that *R. ryukyuensis* **sp. nov.** and *R. sagamianus* **sp. nov.** form a clade with all the other species of *Reinhardorhynchus* for which DNA sequence data are available. Within this clade, *R. sagamianus* **sp. nov.** is in a clade that also includes *R. riegeri* and *R. anamariae*. The discovery of these new species highlights the importance of uncovering and documenting the hidden biodiversity along Japan's coastal margin.

Key Words

Distribution, flatworms, Japanese invertebrates, Kalyptorhynchia, marine meiofauna

Introduction

Microturbellarians are microscopic and mostly free-living flatworms that are common in marine meiofaunal communities around the globe (Schockaert et al. 2008; Armonies 2017; Fegley et al. 2020). They inhabit various types of interstitial substrates (e.g., algae and sediments) in intertidal and subtidal habitats and have also been recorded at depths of up to ~600 m (Artois et al. 2000; Aramayo 2018; Armonies 2023). Our understanding of the diversity and distribution of marine microturbellarians is mostly limited to regions where dedicated research has been conducted on these animals, including the coastal areas in Europe (e.g., Casu et al. 2014; Schockaert 2014; Gobert

et al. 2020; Armonies 2023), Brazil (e.g., Marcus 1950, 1951, 1952; Braccini et al. 2016), Cuba (e.g., Diez et al. 2018, 2023a, 2023b), or Canada (e.g., Van Steenkiste and Leander 2018a, 2018b; Stephenson et al. 2019). However, even in some of these well-studied areas, the diversity of marine microturbellarians can be significantly higher than initial studies have shown. For example, ecological estimations suggest the presence of ~200 species in Cuba (Diez et al. 2023b) and ~400 species on the island of Sylt (northern Germany, in the North Sea) (Armonies 2023).

For Japan, only scattered records of marine and brackish water microturbellarians are known from the literature. The first marine microturbellarians described from Japan were prolecithophorans (Tozawa 1918). Since the 1950's, new representatives of Macrostomorpha, Rhabdocoela, Proseriata, and Prolecithophora have been reported intermittently (Westblad 1955; Karling 1966; Tajika 1977, 1978, 1979, 1980, 1981a, 1981b, 1982a, 1982b, 1982c, 1983a, 1983b, 1983c, 1984; Ax 2008; Omi 2018, 2020; Takeda and Kajihara 2018). However, these studies are confined to a limited number of localities in Japan. With numerous islands and inlets bordering the Sea of Okhotsk, the Sea of Japan, the East China Sea, the Philippines Sea, and the Northwest Pacific Ocean, the coastal margin of Japan represents an important but poorly explored part of the wider Pacific Ocean. It is expected that the diversity of marine microturbellarians in Japan is far from being adequately described.

Here, we characterize two new species of Koinocystididae (Rhabdocoela) with morphological and molecular data. Their phylogenetic positions are determined based on analyses using 18S and 28S rDNA sequences. Additionally, we provide a concise overview of the marine and brackish microturbellarian diversity of Japan and highlight the importance of such research.

Materials and methods

Specimen collection and fixation

The specimens of *Reinhardorhynchus ryukyuensis* sp. nov. were collected by Niels Van Steenkiste and Kevin Wakeman at Onna, Okinawa, Japan (26°28'52.7"N, 127°50'18.8"E) in February 2019 from a coarse mixture of sand, coral fragments, and shell hash in seagrass meadows in a shallow intertidal bay. The specimens of *Reinhardorhynchus sagamianus* sp. nov. were collected by Aoi Tsuyuki and Yuki Oya at Sangashita beach, Hayama, Kanagawa (35°15'58.3"N, 139°34'19.64"E) in April and August 2023, from clean, coarse sandy sediments in the upper intertidal zone (Fig 1). The upper centimeters

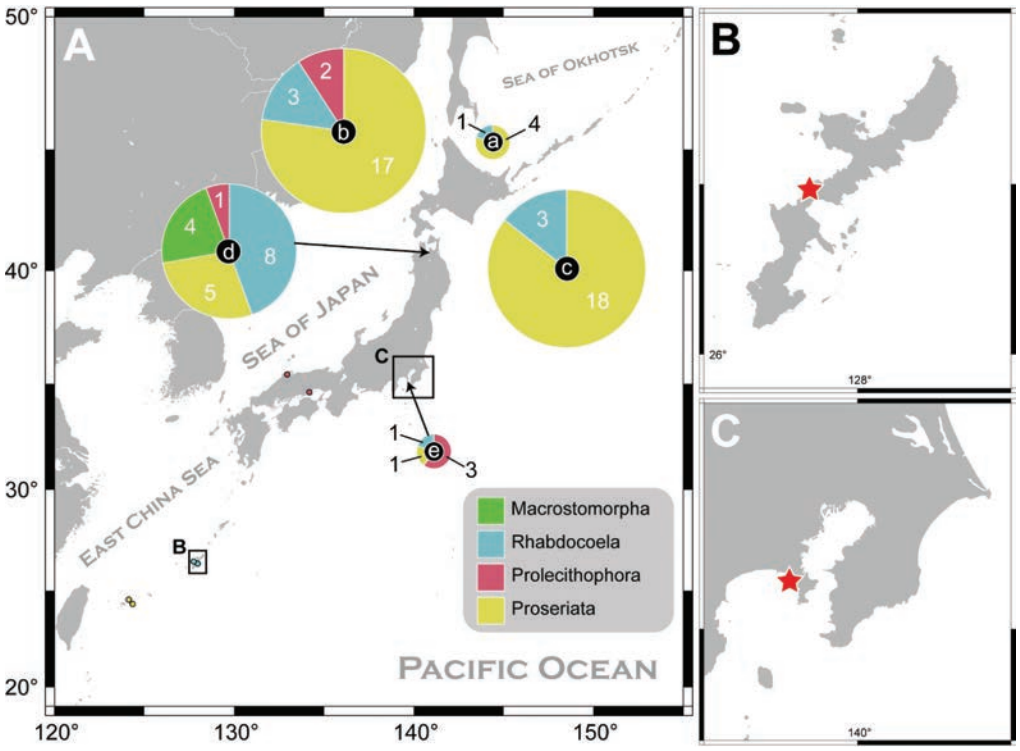

Figure 1. Records of marine microturbellarians in Japan. **A.** Map shows the documented occurrences of marine microturbellarians reported from Japan. The size and numbers within the pie chart represent the number of recorded species from a) the Okhotsk Sea coast of Hokkaido, b) the Sea of Japan coast of Hokkaido, c) the Pacific coast of Hokkaido, d) Mutsu Bay and the brackish water areas of Aomori, and e) the Pacific coast of Kanagawa. The small circles without numbers indicate single species from the Inland Sea, East China, and the Pacific coasts of Okinawa and Ishigaki Islands, respectively. **B.** Magnification of the area, including Okinawa, with a star designating the type locality of *Reinhardorhynchus ryukyuensis* n. sp. **C.** Magnification of the area, including Kanagawa, with a star designating the type locality of *R. sagamianus* sp. nov.

of sediment were collected using a shovel. Specimens of *R. ryukyuensis* sp. nov. were separated from sediments using the $MgCl_2$ decantation method (Schockaert 1996). Individual worms were isolated under a stereoscope and whole-mounted alive in seawater to be studied and photographed at the Okinawa Institute of Science and Technology (OIST) under a compound microscope (Zeiss Axioscope) equipped with DIC. Two specimens were whole-mounted in lactophenol to study the sclerotized parts of the male copulatory organ. Two additional specimens were frozen in 3 µl of filtered seawater for DNA extraction. The specimens of *R. sagamianus* sp. nov. were procured by meticulously rinsing the collected sandy substrate with seawater, employing a dip net with an approximately 1-mm mesh size. Subsequently, the specimens were pipetted into petri dishes to facilitate isolation, whole-mounted in seawater to observe morphological characters on two life specimens, mounted in Entellan New (Merck) to study the sclerotized structures, or fixed in 99.5% ethanol for DNA extraction.

Morphological observations

Measurements and descriptions were made based on squashed preparations. Measurements of the sclerotized structures such as hooks and spines, as well as for soft body tissues, are expressed in micrometers (µm) and were taken using ImageJ software (Schneider et al. 2012). The sclerotized structures in live and fixed specimens were photographed with a Nikon D5600 digital camera affixed to an Olympus BX51 light microscope and with an Olympus DP20 digital camera affixed to an Olympus BX21 compound microscope. Figures were created with Adobe Illustrator CC 23.0.3 (Adobe Systems Inc., USA). All the whole mounted specimens fixed in lactophenol and Entellan New were deposited at the National Museum of Nature and Science, Tokyo (NSMT). A comprehensive bibliographic compilation of historic records and distribution data of free-living microturbellarians from marine and brackish water environments in Japan was also conducted.

DNA extraction, polymerase chain reaction, and sequencing

Total genomic DNA was extracted using a DNeasy Blood & Tissue Kit (Qiagen) following the manufacturer's instructions. For phylogenetic inference, fragments of the 18S rDNA and 28S rDNA were PCR amplified using the primers and thermocycling conditions in Table 1. For the 18S and 28S rDNA of *R. sagamianus* sp. nov., 10-µl reaction volumes were used, each of which contained 1 µl of total DNA template, 1 µl of 10 × ExTaq buffer (Takara Bio), 2 mM of each dNTP, 1 µM of each primer, and 0.25 U of Takara Ex Taq DNA polymerase (5 U/µl; Takara Bio) in deionized water. For the 18S and 28S rDNA of *R. ryukyuensis* sp. nov., Illustra™ PuReTaq™ Ready-To-Go™ PCR beads (GE Healthcare) were suspended in a 25-µl volume of water, primers (0.2 µM), and DNA template (1.5 µl). Amplicons were visualized on 1.5% agarose gels stained with GelRed™ (Biotium) (*R. ryukyuensis* sp. nov.) or 1.0% agarose gels stained with FluoroDye DNA Fluorescent Loading Dye (SMOBIO) (*R. sagamianus* sp. nov.) and purified enzymatically using Illustra™ ExoProStar S (GE Healthcare) (*R. ryukyuensis* sp. nov.) or Exonuclease I and SAP (Takara Bio) (*R. sagamianus* sp. nov.). Amplicons of *R. ryukyuensis* sp. nov. were subsequently sequenced by Genewiz (Azenta Life Sciences) through standard Sanger DNA sequencing, while amplicons of *R. sagamianus* sp. nov. were sequenced with a BigDye Terminator Kit ver. 3.1 and a 3730 Genetic Analyzer (Life Technologies), using the amplification and internal sequencing primers shown in Table 1. Trace files were assembled into full sequences in either Geneious v11.0.15 (Kearse et al. 2012) or MEGA ver. 7.0 (Kumar et al. 2016) and subjected to a BLAST search on the NCBI website (http://blast.ncbi.nlm.nih.gov) to verify the specimens' taxonomic identity. Sequences were deposited in DDBJ/EMBL/GenBank, with accession numbers provided in Table 2.

Molecular phylogenetic analyses

For phylogenetic analyses, a concatenated dataset (3,264 bp) comprising partial 18S rDNA (1,642 bp) and 28S rDNA (1,622 bp) was prepared using DNA sequences of 24 koinocystidids in addition to the sequences of two individuals of *Reinhardorhynchus ryukyuensis* sp. nov. and one individual of *R. sagamianus* sp. nov. (Table 2). *Cystiplex axi* Karling, 1964, and *Cystiplex* sp. were included as outgroup taxa. Sequences were aligned using MAFFT ver. 7.472 (Katoh et al. 2019) with the L-INS-I strategy selected under the "Auto" option. Ambiguous sites were trimmed with Clipkit ver. 1.0 using the "kpic" option (Steenwyk et al. 2020). The optimal substitution models selected with PartitionFinder ver. 2.1.1. (Lanfear et al. 2016) were GTR+I+G for both the 18S and 28S rDNA partitions. A maximum likelihood (ML) analysis was performed using IQTree ver. 1.6 (Nguyen et al. 2015) under a partition model (Chernomor et al. 2016). Bayesian inference (BI) of the phylogeny was performed using MrBayes ver. 3.2.3 (Ronquist and Huelsenbeck 2003; Altekar et al. 2004) with two independent runs of Metropolis-coupled Markov chain Monte Carlo (MCMC), each consisting of four chains of 1,000,000 generations. All parameters (*statefreq*, *revmat*, *shape*, and *pinvar*) were unlinked between each position; trees were sampled every 100 generations. The first 25% of the trees were discarded as burn-in before a 50% majority-rule consensus tree was constructed based on the remaining 7,500 trees. Convergence was confirmed with the average standard deviation of split frequencies (0.008833), potential scale reduction factors for all parameters (0.999–1.006), and effective sample sizes for all parameters (≥322). Nodal support within the ML tree was assessed by analyses

Table 1. Primers and thermocycling conditions used in this study.

Primers	Primer name	Sequence (5'–3')	Application	Reference
R. ryukyuensis sp. nov.				
18S rDNA	TimA	AMCTGGTTGATCCTGCCAG	Amplification and sequencing	Norén and Jondelius (1999)
18S rDNA	TimB	TGATCCATCTGCAGGTTCACCT	Amplification and sequencing	Norén and Jondelius (1999)
18S rDNA	600F	GGTGCCAGCAGCCGCGGT	Sequencing	Norén and Jondelius (1999)
18S rDNA	600R	ACCGCGGCTGCTGGCACC	Sequencing	Norén and Jondelius (1999)
18S rDNA	1100F	CAGAGGTTCGAAGACGATC	Sequencing	Norén and Jondelius (1999)
18S rDNA	1100R	GATCGTCTTCGAACCTCTG	Sequencing	Norén and Jondelius (1999)
18S rDNA	18S7F	GCAATAACAGGTCTGTGATGC	Sequencing	Norén and Jondelius (1999)
18S rDNA	18S7FK	GCATCACAGACCTGTTATTGC	Sequencing	Norén and Jondelius (1999)
28S rDNA	LSU5	TAGGTCGACCCGCTGAAYTTA	Amplification and sequencing	Littlewood et al. (2000)
28S rDNA	LSUD6-3B	GCTGTTCACATGGAACCCTTCTC	Amplification and sequencing	Van Steenkiste et al. (2013)
28S rDNA	L300F	CAAGTACCGTGAGGGAAAGTTG	Sequencing	Littlewood et al. (2000)
28S rDNA	L300R	CAACTTTCCCTCACGGTACTTG	Sequencing	Littlewood et al. (2000)
28S rDNA	L1200F	CCCGAAAGATGGTGAACTATG	Sequencing	Littlewood et al. (2000)
28S rDNA	L1200R	GCATAGTTCACCATCTTTCGG	Sequencing	Littlewood et al. (2000)
R. sagamianus sp. nov.				
18S rDNA	hrms18S_F	ATCCTGCCAGTAGTCATATGC	Amplification and sequencing	Oya and Kajihara (2020)
18S rDNA	hrms18S_Fi1	GCCGCGGTAATTCCAG	Sequencing	Oya and Kajihara (2020)
18S rDNA	hrms18S_R	CTACGGAAACCTTGTTACGAC	Sequencing	Oya and Kajihara (2020)
18S rDNA	hrms18S_Ri1	CTTTAATATACGCTATTGGAGCTGG	Sequencing	Oya and Kajihara (2020)
18S rDNA	hrms18S_Ri2	CTATTTAGTGGCTAGAGTCTCGTTCG	Amplification and sequencing	Oya and Kajihara (2020)
28S rDNA	LSU5	TAGGTCGACCCGCTGAAYTTA	Amplification and sequencing	Littlewood et al. (2000)
28S rDNA	Rd4.8a	ACCTATTCTCAAACTTTAAATGG	Sequencing	Whiting (2002)
28S rDNA	rD5b	CCACAGCGCCAGTTCTGCTTAC	Sequencing	Whiting (2002)
28S rDNA	LSUD6-3B	GCTGTTCACATGGAACCCTTCTC	Amplification and sequencing	Van Steenkiste et al. (2013)
Thermocycling conditions				
R. ryukyuensis				
18S rDNA	95 °C for 3m, touch down in 9 cycles (94 °C for 30 s, 60 °C down to 56 °C for 30 s, 72 °C for 1 m 30 s), 31 cycles (94 °C for 30s, 55 °C for 30 s, 72 °C for 1 m 30 s), 72 °C for 5m			
28S rDNA	95 °C for 3m, touch down in 9 cycles (94 °C for 30 s, 60 °C down to 56 °C for 30 s, 72 °C for 1 m 30 s), 31 cycles (94 °C for 30 s, 55 °C for 30 s, 72 °C for 1 m 30 s), 72 °C for 5m			
R. sagamianus				
18S rDNA	94 °C for 1 m, 35 cycles (94 °C for 30 s, 50 °C for 30 s, 72 °C for 2 m), 72 °C for 7 m			
28S rDNA	94 °C for 1m, 35 cycles (94 °C for 30 s, 50 °C for 30 s, 72 °C for 1.5 m), 72 °C for 7 m			

of 1,000 pseudoreplicates of ultrafast bootstrap (UFBoot) (Minh et al. 2013) and SH-aLRT branch tests (Guindon et al. 2010). ML UFBoot values ≥95%, SH-aLRT values ≥85%, and posterior probability (PP) values ≥0.90 were considered to indicate clade support.

Abbreviations used in Figures

a: apicomplexan; br: brain; bs: bursal stalk; bu: bursa; cg: common gonopore; cds: spines of the distal part of the spiny belt; ciu: unarmed accessory cirrus; cia: armed cirrus; cm: circular muscles; cms: spines of the middle part of the spiny belt; cps: spines of the proximal part of the spiny belt; ed: ejaculatory duct; fa: female atrium; fd: female duct; fg: female glands; h: hook; i: intestine; ilm: inner layer of longitudinal muscles; lh: larger hooks; ma: male genital atrium; oe: oesophagus; olm: outer layer of longitudinal muscles; om: oblique muscles; ov: ovary; pg: prostate glands; ph: pharynx; pp: penis papilla; pr: proboscis; s: spine; sh: smaller hook; scl: sclerotized layer; sv: seminal vesicle; t: testis; u: uterus; vi: vitellaria.

Table 2. List of species and respective GenBank accession numbers used for the molecular phylogenetic analyses in this study.

Species	18S rDNA	28S rDNA
Itaipusa divae	MW081596	MW054455
Itaipusa biglandula	MW081601	MW054460
Itaipusa karlingi	MW081598	MW054457
Itaipusa novacaledonica	KJ887481	KJ887528
Itaipusa sp. 1	KJ887451	KJ887557
Koinogladius sinensis YTP1	MF443159	MF443174
Koinogladius sinensis YTP2	MF443160	MF443175
Koinogladius sinensis YTP3	MF443161	MF443176
Mesorhynchus terminostylis	AY775741	KJ887500
Reinhardorhynchus anamariae	MW081597	MW054456
Reinhardorhynchus hexacornutus	MW054464	MW054451
Reinhardorhynchus riegeri	MW081595	MW054454
Reinhardorhynchus riegeri (CU1272)	OR490859	OR490875
Reinhardorhynchus ryukyuensis sp. nov.	LC807766	LC807768
Reinhardorhynchus ryukyuensis sp. nov.	–	LC807769
Reinhardorhynchus sagamianus sp. nov.	LC807767	LC807770
Reinhardorhynchus tahitiensis A	MW054463	MW054452
Reinhardorhynchus tahitiensis B	MW054462	MW054453
Rhinolasius dillonicus	MW081602	MW054461
Sekerana stolci	–	KJ887537
Utelga heinckei	MW081600	MW054459
Utelga heinckei (QU4)	OR490861	OR490876
Utelga heinckei (QU43)	OR490862	–
Utelga heinckei (QU44)	OR490863	OR490877
Utelga pseudoheinckei	MW081599	MW054458
Koinocystididae sp. 1	KR339027	–
Outgroup		
Cystiplex axi	KJ887437	KJ887549
Cystiplex sp.	KJ887469	KJ887495

Results

Taxonomic Account

Rhabdocoela Ehrenberg, 1831
Kalyptorhynchia von Graff, 1905
Eukalyptorhynchia Meixner, 1928
Koinocystididae Meixner, 1924
Reinhardorhynchus Diez, Monnens, & Artois, 2021

Reinhardorhynchus ryukyuensis Van Steenkiste, Wakeman, & Leander, sp. nov.

https://zoobank.org/57D2EE7F-0934-4BB1-AF9A-84E1D0D804FB
Fig. 2

Material examined. ***Holotype:*** **Japan •1**; Okinawa Prefecture, Onna; 26°28'52.7"N, 127°50'18.8"E; Feb. 2019; coarse mixture of sand, coral fragments, and shell hash from an intertidal seagrass bed; Niels Van Steenkiste and Kevin Wakeman leg.; one individual worm in a single slide [Holotype: NSMT-Pl 6458];

Paratype: **Japan •1**; locality same as for holotype; Feb. 2019; Niels Van Steenkiste and Kevin Wakeman leg.; one individual worm in a single slide; [Paratype: NSMT-Pl 6459].

Other material. **Japan •1**; locality same as for holotype; Feb. 2019; Niels Van Steenkiste and Kevin Wakeman leg.; two genomic DNA extracts from two individuals stored at -20 °C; GenBank: LC807766 (18S rDNA; 1,760 bp), LC807768, LC807769 (28S rDNA; 1,675 bp).

Type locality. Japan, Okinawa Prefecture, Onna (26°28'52.7"N, 127°50'18.8"E).

Diagnosis. Species of *Reinhardorhynchus* with conjuncta-duplex type male copulatory organ composed of a proximal globular part, a weakly sclerotized cylindrical middle part, and a distal penis papilla. Sclerotized structures of the copulatory organ consist of two large, separate hooks at the transition between the middle part and penis papilla and a distal girdle of two semi-elliptical plates bearing five smaller hooks. One larger hook with collared striated base, 29–31 µm long, pointing proximally; the other larger hook straight, with striated base, 29–34 µm long, pointing distally. The smaller distal hooks are 9–17 µm long. Female system with bipartite female duct, muscular bursal stalk, large bursa, and pouch of female glands.

Description. ***General morphology.*** Animals are 840–1060 µm long ($\bar{x}$ = 935 µm; n = 4), transparent, and have two eyes (Fig. 2A, B). General organization and internal morphology are consistent with other species of *Reinhardorhynchus*, as described by Diez et al. (2021). The large,

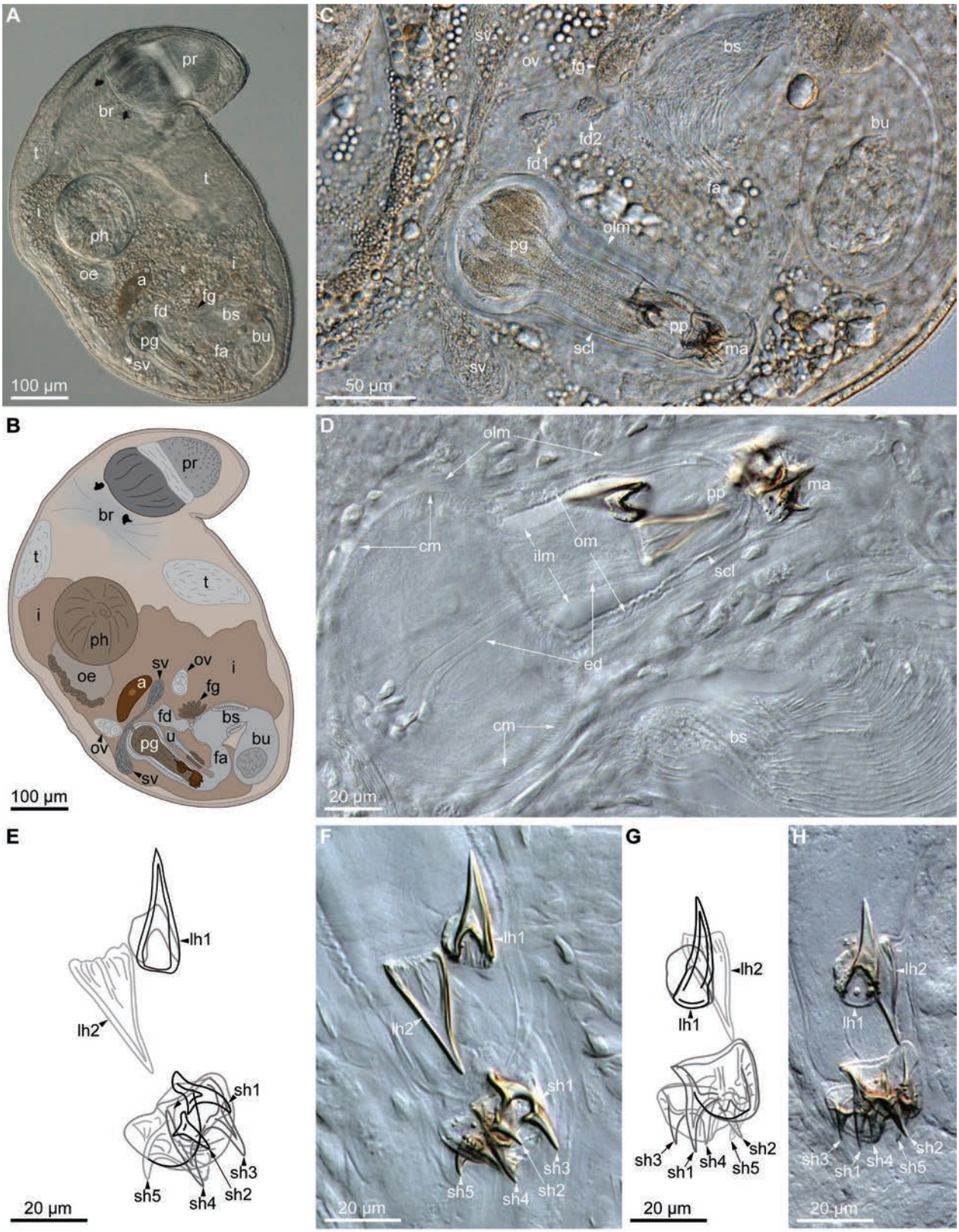

Figure 2. *Reinhardorhynchus ryukyuensis* sp. nov. **A, B.** Micrograph and drawing of a live animal. **C.** Detail of the atrial organs in a live specimen. **D.** Male copulatory organ in a whole-mounted specimen fixed in lactophenol. **E, F.** Drawing and micrograph of the sclerotized parts of the male copulatory organ in the holo/paratype. **G, H.** Drawing and micrograph of the sclerotized parts of the male copulatory organ in the holo/paratype.

typical koinocystidid proboscis (pr, Fig. 2A, B) is about 1/4 of the body length (215–233 µm; $\bar{x}$ = 224 µm; n = 3), with a well-developed juncture sphincter. Ciliated cellular epidermis with needle-like rhabdites is present all over the body.

The globular pharynx (ph, Fig. 2A, B) is at about 50% of the body length, followed by an intestine (i, Fig. 2A, B) that runs all the way to the posterior end. The oesophagus (oe, Fig. 2A, B) is visible as a clear, transparent zone bordered by oesophageal glands right behind the pharynx.

Male reproductive system. Paired testes are located in front of the pharynx (t, Fig. 2A, B). The conjuncta-duplex type male copulatory organ (165–195 µm; $\bar{x}$ = 180 µm; n = 4) is inverted-pear shaped and encompasses the prostate vesicle (pg, Fig. 2A–C). This prostate vesicle is composed of gland necks of prostate glands originating extracapsularly, extending into the middle part of the copulatory organ, and opening distally into the ejaculatory duct. The bulbous proximal part of the prostate vesicle is surrounded by circular muscles (cm, Fig. 2D), while the cylindrical middle part is surrounded by two layers of oblique muscles (om, Fig. 2D) and an inner layer of longitudinal muscles (ilm, Fig. 2D). The walls of the middle and distal parts of the copulatory organ are weakly sclerotized (scl, Fig. 2C, D) and distally form a penis papilla (pp, Fig. 2C, D), which enters into the male genital atrium (ma, Fig. 2C, D). The entire copulatory organ is encased in an outer layer of longitudinal muscles (olm, Fig. 2C, D). Paired seminal vesicles (sv, Fig. 2A–C) merge right before entering the copulatory organ proximally and form the ejaculatory duct (ed, Fig. 2D). The necks of the prostate glands and the ejaculatory duct run throughout the entire length of the copulatory organ and into the penis papilla.

The male copulatory organ is provided with sclerotized structures consisting of two larger separate hooks and a girdle of five smaller interconnected hooks (lh1–lh2, sh1–sh5, Fig. 2E–H). The two larger hooks are positioned at the transition of the cylindrical middle part to the penis papilla and point in opposite directions. The proximally pointing larger hook (lh1, Fig. 2E–H) measures 29–31 µm (n = 2) and is provided with a collared striated base. The distally pointing larger hook (lh2, Fig. 2E–H) is straight, measures 29–34 µm (n = 2), and has a striated base that seems to be continuous with the weakly sclerotized layer. The five distal, smaller hooks are connected by a complex sclerotized girdle surrounding the distal tip of the penis papilla. The smaller hooks sh1 (15–17 µm; n = 2) and sh2 (10–13 µm; n = 2), and sh3 (10–13 µm; n = 2) and sh4 (9–12 µm; n = 2) are each connected through a semi-elliptical base, respectively. The base of the smaller hook sh5 (10–12 µm; n = 2) seems to connect both semi-elliptical bases into an open girdle.

Female reproductive system. The female structures are located caudal to the pharynx and include paired ovaries (ov, Fig. 2B, C), a female duct (fd, Fig. 2B) consisting of two parts (fd1 and fd2, Fig. 2C), and a very muscular bursal stalk (bs, Fig. 2B–D) guarding the entrance to a large bursa (bu, Fig. 2B, C). At its proximal end, the female atrium (fa, Fig. 2B, C) receives the female duct, the bursal stalk, and a pouch of female glands (fg, Fig. 2B, C). The female duct is separated from the female atrium by a small sphincter. A uterus (u, Fig. 2B) is present between the male and female atria. Vitellaria and the common gonopore could not be observed in the live animals.

Etymology. Species epithet based on its occurrence on the Ryukyu Islands.

Distribution. Okinawa Islands, Japan.

Reinhardorhynchus sagamianus Tsuyuki, Reyes, Oya, & Van Steenkiste, sp. nov.

https://zoobank.org/B2534AFD-3461-4329-A62F-3C6AC8467FB2

Fig. 3

Material examined. ***Holotype:*** **Japan •1**; Kanagawa Prefecture, Hayama, Sangashita beach; (35°15'58.3"N, 139°34'19.6"E); 21 April 2023; sandy substrates; Aoi Tsuyuki and Yuki Oya leg.; one individual worm in a single slide; [Holotype: NSMT-Pl 6460].

Paratype: **Japan •1**; locality same as for holotype; 30 Aug 2023; Yuki Oya leg.; genomic DNA extract from one individual stored at -20 °C; GenBank: LC807767 (18S rDNA; 1,654 bp), LC807770 (28S rDNA; 1,667 bp); [Paratype: NSMT-DNA 56985].

Type locality. Japan, Kanagawa Prefecture, Hayama, Sangashita Beach (35°15'58.3"N, 139°34'19.6"E).

Diagnosis. Species of *Reinhardorhynchus* with a copulatory organ encompassing an armed cirrus, an unarmed accessory cirrus, and two distal hooks. Bipartite armed cirrus consisting of two sacs lined with a continuous ±295.2-µm-long sclerotized belt of overlapping scale-like spines. Larger sac with more spaced-out, triangular, ±20.1 µm-long spines on the proximal end of the belt. Spines gradually decrease in size distally as the belt runs towards and folds into the smaller sac, increasing in size (±6.1 to ±22.2 µm long) towards the proximal tip of the smaller sac, and decreasing in size again from the proximal to the distal tip of the smaller sac. Unarmed accessory cirrus as an elongated sac. The larger distal hook is slightly curved, ±111.5 µm long and ±43.5 µm wide at its base; its base is provided with a slightly curved, ±42.3 µm-long projection with a blunt distal tip forming a ~90° angle with the axis of the hook. The smaller hook is funnel-shaped, ±58.9 µm long and ±46.6 µm wide at its base.

Description. ***General morphology.*** Live mature specimens are 1500–1800 µm long (n = 2), with two eyes (Fig. 3A, B). The proboscis is 297–304 µm (n = 2) long in swimming animals and is characteristic for koinocystidids (Brunet 1972; Karling 1980; Diez et al. 2021). The pharynx (ph, Fig. 3A, B) is positioned near the body's midpoint and has an approximate diameter of 231–258 µm (n = 2) in the live specimens. The oesophagus is visible as a clear zone surrounded by oesophageal glands behind the pharynx. It empties into the intestine, which is situated in the posterior portion of the body. The male and female reproductive systems are mainly located in the third posterior region of the body.

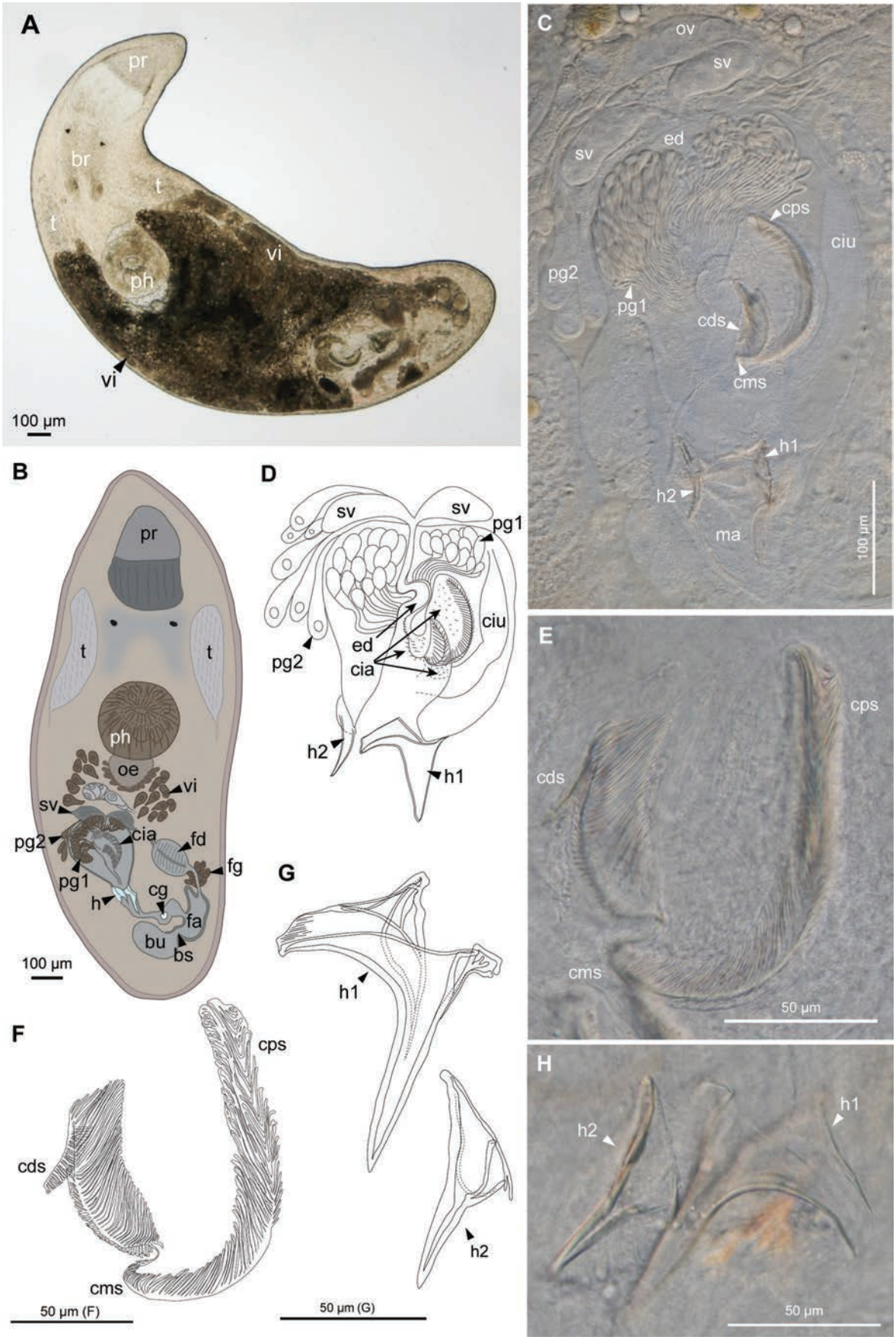

Figure 3. *Reinhardorhynchus sagamianus* n. sp., NSMT-DNA 56985 (paratype) (**A**) and NSMT-Pl 6460 (holotype) (**B**–**H**). **A, B.** Micrograph and drawing of live animals. **C.** Detail of the male copulatory organ in a live animal. **D, E.** Drawing and micrograph of the belt of overlapping spines in the armed cirrus of the male copulatory organ in a whole mounted specimen fixed in Entellan New. **F–H.** Drawings and micrograph of the distal hooks associated with the male copulatory organ in a whole mounted specimen fixed in Entellan New.

Male reproductive system. Paired testes anterior to the pharynx are on each side of the body (t, Fig. 3A, B). A pair of sac-like seminal vesicles (sv, Fig. 3B–D) fuse distally before entering the copulatory organ and forming an ejaculatory duct (ed; Fig. 3C, D). The piriform copulatory organ is 323–376 μm (n = 2) long and encompasses a proximal prostate vesicle, a bipartite armed cirrus, and an unarmed accessory cirrus. Distally, it bears two large hooks of varying shapes (h1, h2, Fig. 3D). The prostate vesicle consists of one type of intracapsular prostate gland (pg1; Fig. 3B–D) opening into the transition zone between the ejaculatory duct and armed cirrus through filiform ducts (Fig. 3B–D; Suppl. material 1). A second type of extracapsular prostate gland (pg2; Fig. 3B–D) enters the copulatory organ proximally. The armed cirrus bears small spines on its entire surface (cia, Fig. 3B–D; Suppl. materials 1, 2) and has two sacs of differing sizes, both of which are equipped with an interconnecting belt of overlapping, scale-like spines (Fig. 3B–F; Suppl. material 1). The spines of the proximal part of the spiny belt start in the larger sac. Here, the scale-like spines are triangular, more spaced out, and 20.1 μm long (cps, Fig. 3B–F). Gradually, these spines become less triangular, more overlapping, and decrease in size (8.8 μm long) until they reach the transition to the smaller sac, where they fold backwards and continue into the smaller sac (cms, Fig. 3C, E, F; Suppl. materials 1–3). From this fold, the spines gradually increase in size (from 6.1 to 22.2 μm long) towards the proximal tip of the smaller sac, where they fold again to continue along the distal side of this sac while gradually decreasing in size again (cds, Fig. 3C, E, F). The total length of this spiny belt is 295.2 μm. The unarmed accessory cirrus (ciu, Fig. 3C, D; Suppl. material 1) runs alongside the armed cirrus from the proximal end of the copulatory organ to the distal end of the armed cirrus. It appears as an elongated sac that narrows proximally. It is possible that this narrow proximal part of the unarmed accessory cirrus connects to the bundles of extracapsular prostate glands (pg2, Fig. 3C) visible around the copulatory organ and seminal vesicles, but this connection could not be established with certainty. The larger distal hook is 111.5 μm long and 43.5 μm wide at its base (h1, Fig. 3G, H; Suppl. material 1). One side of the base features a sturdy, slightly curved projection with a blunt distal tip. The projection itself is 42.3 μm long and forms an ~90° angle with the axis of the hook. The smaller distal hook is 58.9 μm long and has a 46.6 μm-wide base (h2, Fig. 3G, H).

Female reproductive system. The vitellaria (vi; Fig. 3A) extends from the rear end of the pharynx to the posterior body end. Paired ovaries with oocytes arranged in a single line are situated anterior to the copulatory organ (ov, Fig. 3B, C). The bursa (bu, Fig. 3B) opens into the female atrium through a muscular bursal stalk (bs, Fig. 3B). The female atrium also receives the female duct (fd, Fig. 3B), which consists of a narrow distal duct in which bundles of female glands (fg, Fig. 3B) discharge, and a wide, muscular proximal part that receives the oviducts.

Etymology. The species epithet *sagamianus* refers to the type locality, which is located in Sagami Bay.

Distribution. Kanawaga, Sangashita Beach, Japan.

Molecular phylogeny

The resulting ML and BI trees were congruent with each other in terms of topology, so only the ML tree is shown in Fig. 4. All of the examined koinocystidid species form a clade with full support. Within this clade, four major clades can be recognized: (1) a clade composed of *Utelga heinckei* (Attems, 1897), *Utelga pseudoheinckei* Karling, 1980, and *Parautelga* sp. (with full support); (2) a clade with *Koinogladius sinensis* (Wang & Lin, 2017) and *Rhinolasius dillonicus* Karling, 1980 (‘*sinensis*’ clade in Diez et al. (2021)) (PP = 1.00; SH-aLRT = 99.5%; UFBoot = 99%), (3) a clade composed of four representatives of *Itaipusa* (‘*divae*’ clade in Diez et al. (2021)) (with full support), and (4) a clade with several representatives of *Reinhardorhynchus*, *Itaipusa* sp. 1, and Koinocystididae sp. 1 (‘*riegeri*’ clade in Diez et al. (2021)) (PP = 0.82; SH-aLRT = 99.1%; UFBoot = 82%). Our two new species, *R. ryukyuensis* sp. nov. and *R. sagamianus* sp. nov., from Japan, are nested in the ‘*riegeri*’ clade. *Reinhardorhynchus ryukyuensis* sp. nov. is the sister taxon to a clade including *R. hexacornutus* Jouk, Diez, Reygel & Artois, 2021, *R. tahitiensis* Jouk, Diez, Yurduseven, Reygel & Artois, 2021, and an unidentified species of Koinocystididae, albeit with relatively low support (PP = 0.75; SH-aLRT = 99.3%; UFBoot = 54%). *Reinhardorhynchus sagamianus* sp. nov. is sister to a clade consisting of *R. riegeri* (Karling, 1978), *R. anamariae* Diez, Reygel & Artois, 2021, and *Itaipusa* sp. 1 with full support (Fig. 4).

Faunistic account

A total of 58 taxa of marine and brackish water microturbellarians that have been identified to species level have been recorded from the coastal areas of Japan, including the two new species of *Reinhardorhynchus* described in this study; four taxa were only identified up to genus level (Table 3). All these taxa belong to the Macrostomorpha, Rhabdocoela, Prolecithophora, and Proseriata. Nineteen species were found in brackish water habitats, all of which belong to genera that are either considered typical to these environments or euryhaline marine taxa. Most of the records are from Hokkaido (33 taxa) and the northern part of Honshu (18 taxa) (Table 3; Fig. 1). A few records are from locations in southern Honshu (Kanagawa, Okayama, and Shimane) and the Ryukyu Islands (Okinawa).

Discussion

Morphology

Koinocystididae is one of the most species-rich groups of kalyptorhynch rhabdocoels. Its representatives are found globally in marine sediments and on seaweeds; however, some species also occur in freshwater habitats. Most koinocystidids have a large proboscis with a sphincter at the

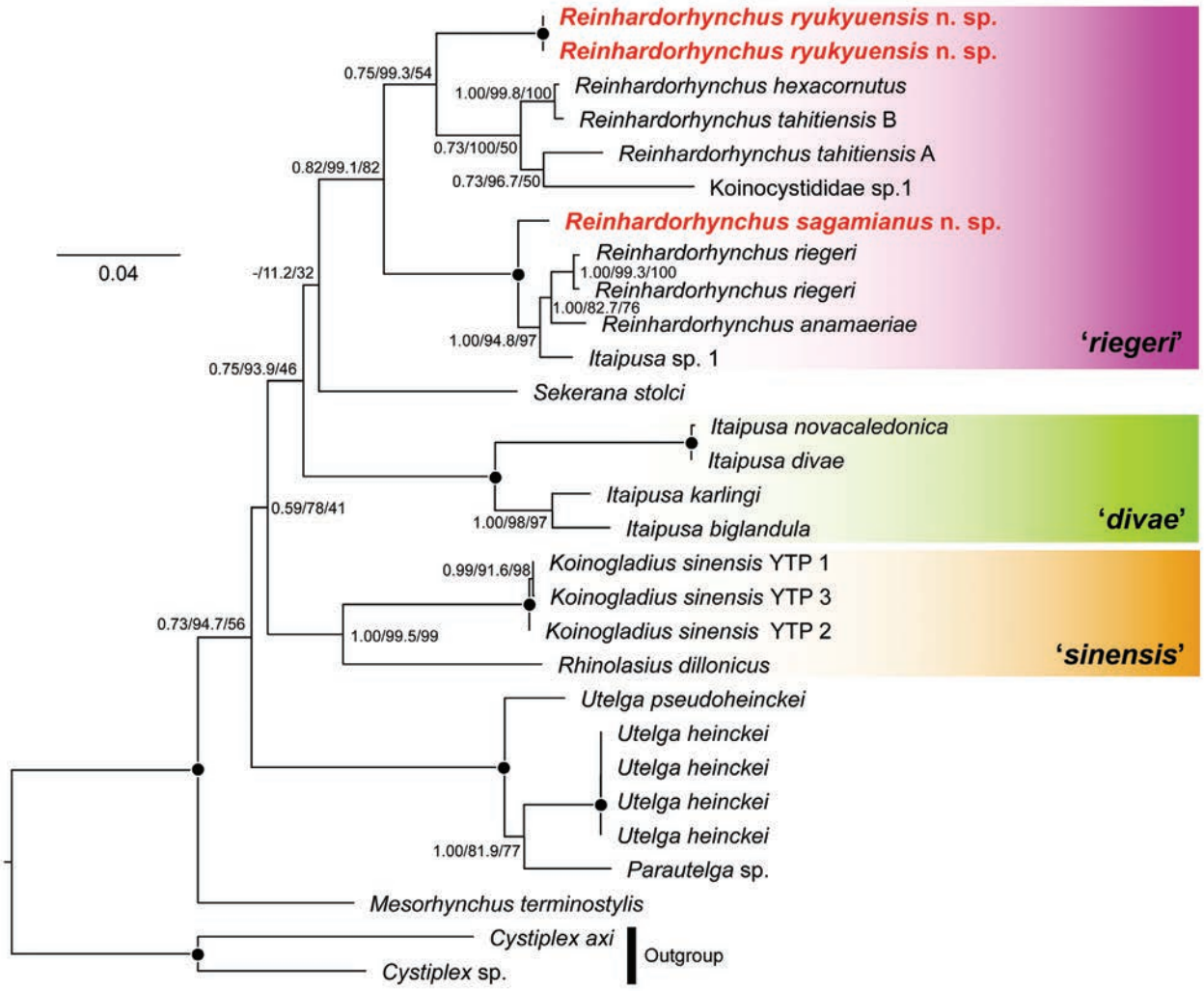

Figure 4. ML phylogenetic genetic tree based on a concatenated dataset of partial 18S and 28S rDNA sequences. Branch support values are indicated next to the nodes as posterior possibilities/SH-aLRT values/UFBoot values. Black dots indicate the maximum values for all support measures.

base of the cone and complex atrial organs with sclerotized structures and a copulatory bursa (Brunet 1972; Karling 1980; Diez et al. 2021). The two new koinocystidid species from Japan exhibit the characteristics described for the recently proposed genus *Reinhardorhynchus*. At present, this genus accommodates sixteen species, half of which were newly described by Diez et al. (2021). Representatives of *Reinhardorhynchus* all have large accessory hooks or spikes associated with the male copulatory organ, in contrast to species of *Itaipusa*, which lack such accessory structures (Karling 1978, 1980; Diez et al. 2021).

The new species of *Reinhardorhynchus* from Okinawa, *R. ryukyuensis* sp. nov., has a unique combination of features. Firstly, *R. ryukyuensis* sp. nov. has no armed cirrus in its male copulatory organ. However, the presence of a short, unarmed cirrus cannot be excluded, as the exact ending of the prostate glands and ejaculatory duct in the tip of the penis papilla could not be observed. In all other known species of *Reinhardorhynchus*, except for *R. scoticus* (Karling, 1954), the male copulatory organ possesses one (*R. hexacornutus* Jouk, Diez, Reygel & Artois, 2021, *R. renei* (Reygel, Willems & Artois, 2011)), two (*R. riegeri* (Karling, 1978), *R. unicornis* Diez, Aguirre, Reygel, & Artois, 2021, *R. variodentatus* (Karling, Mack-Fira, & Doerjes, 1972)) or three (*R. pacificus* Diez, Reygel & Artois, 2021) armed cirri provided with fields of spines, or a single cirrus armed with belts/rows of overlapping spines (*R. anamariae* Diez, Reygel & Artois, 2021, *R. beatrizae* Diez, Aguirre, Reygel & Artois, 2021, *R. bispina* (Karling, 1980), *R. curvicirrus* (Karling, 1980), *R. evelinae* (Marcus, 1954), *R. riae* Diez, Reygel & Artois, 2021, *R. ruffinjonesi* (Karling, 1978), *R. soror* Diez, Reygel & Artois, 2021, *R. tahitiensis* Jouk, Diez, Yurduseven, Reygel, & Artois, 2021) (Karling et al. 1972; Karling 1980; Reygel et al. 2011; Diez et al. 2021). *Reinhardorhynchus ryukyuensis* sp. nov. differs from *R. scoticus* because it has a girdle of five smaller interconnected hooks around the distal tip of the penis papilla rather than a circular plate with fine needle-like spines as in *R. scoticus*, and because it has two larger separate hooks instead of three to five

foldable hooks at the base of the penis papilla (Karling 1954, 1963; Ax 2008). Secondly, the configuration of the larger and smaller hooks in *R. ryukyuensis* sp. nov. markedly deviates from the sclerotized hooks and spines found in other species of *Reinhardorhynchus*. The complex arrangement of the five smaller hooks on a girdle composed of two semi-elliptical plates surrounding the penis papilla is unique among representatives of the genus. Another species, *R. riae*, also has sclerotized structures associated with a pseudocuticular penis papilla, but in this species, these structures consist of two flattened hooks with a broad and rounded distal end (Diez et al. 2021). In addition, *R. riae* also has a cirrus armed with two spinous rows. The above-mentioned differences make it easy to distinguish *R. ryukyuensis* sp. nov. from its congeners and thus warrant the description of a new species.

The new species of *Reinhardorhynchus* from Kanagawa, *R. sagamianus* sp. nov., is also unique among its congeners because it is the only species with the combination of a bipartite armed cirrus with a belt of spines, an unarmed accessory cirrus, and two distal accessory hooks associated with the male copulatory organ. Only three other species of *Reinhardorhynchus*, *R. riegeri*, *R. unicornis*, and *R. variodentatus*, possess two cirri and one (*R. unicornis*) or two (*R. riegeri* and *R. variodentatus*) accessory hooks in their male copulatory organ. However, in these three species, both the cirri are provided with spines. Eight other species of *Reinhardorhynchus*, *R. anamariae*, *R. beatrizae*, *R. bispina*, *R. curvicirrus*, *R. riae*, *R. ruffinjonesi*, *R. soror*, and *R. tahitiensis*, possess a single cirrus armed with belts or rows of spines and two distal hooks (Karling 1978, 1980; Diez et al. 2021). One species, *R. evelinae*, has a single cirrus with hooked denticles and two or three rows of spines in combination with three distal spines (Marcus 1954). Apart from the lack of an unarmed accessory cirrus in all these species, other noticeable differences in the morphology of the male copulatory organ are present when compared to *R. sagamianus* sp. nov. The two distal hooks in *R. riae* and *R. tahitiensis* are symmetrical and have broad and rounded distal ends. In addition, these two species have multiple spinous belts – two in *R. riae* and four in *R. tahitiensis* (Diez et al. 2021) – and are, therefore, very distinct from *R. sagamianus* sp. nov. and the other six species mentioned above. The morphology of the spiny cirrus belt, including its overall length and shape and the shape and size of the individual spines, is unique in every species of *Reinhardorhynchus* with such a belt. In *R. bispina*, these spines are mostly uniform in size, whereas in *R. anamariae*, *R. beatrizae*, *R. curvicirrus*, *R. ruffinjonesi*, *R. sagamianus* sp. nov., and *R. soror*, there are clear sections with a gradual increase or decrease in the size of the spines (Karling 1978, 1980; Diez et al. 2021). In *R. soror* and *R. ruffinjonesi*, a row of larger hook- or claw-shaped spines is also present in the belt (Diez et al. 2021). Another unique feature of the new species from Kanagawa is the fact that the armed cirrus has two sacs, which results in the unique curved and twisted contour of the spinous belt as it spans the different compartments of the cirrus. While described as a "fold in the cirrus wall," the configuration of the armed cirrus in *R. curvicirrus* also implies the presence of a blind sac (Karling 1980). A small "spiny diverticulum" as part of the armed cirrus has also been described for *R. ruffinjonesi* (Karling 1978; Diez et al. 2021). Finally, only *R. beatrizae* and *R. soror* share the presence of a projection on the base of one of the distal hooks with *R. sagamianus* sp. nov. In *R. sagamianus* sp. nov., this projection has a blunt, angled distal tip and is oriented at a ~90° angle to the main axis of the larger distal hook. In *R. beatrizae*, this projection is more funnel-shaped, distally more pointed, and at an angle of more than 100° to the main axis of the hook (Diez et al. 2021). In *R. soror*, the tip of the largest hook is noticeably curved compared to *R. sagamianus* sp. nov., which has a straight tip. Also, there are two projections on the base of the largest hook of *R. soror*: one long straight, funnel-shaped projection with a blunt tip making an angle of 90° to the main axis of the hook, and one shorter, more or less square and folded projection (Diez et al. 2021). These characteristics are clearly different from *R. sagamianus* sp. nov.

Molecular phylogeny

The interrelationships of the Koinocystididae have been extensively discussed by Diez et al. (2021) based on the results of molecular phylogenetic analyses inferred from 18S and 28S rDNA sequences. Our reconstructed tree is congruent with these results and shows that the new species *R. ryukyuensis* sp. nov. and *R. sagamianus* sp. nov. form a clade with five other species of *Reinhardorhynchus* and the unidentified taxa *Itaipusa* sp. 1 and Koinocystididae sp. 1 with high support ('*riegeri*' clade in Fig. 4). With 12 out of 18 species of *Reinhardorhynchus* still lacking from the analyses, the molecular phylogenetic interrelationships within the *'riegeri'* clade are difficult to interpret within the context of character evolution. *Reinhardorhynchus ryukyuensis* sp. nov., *R. hexacornutus*, and *R. tahitiensis* belong to the same clade and have a clearly different morphology from other species of *Reinhardorhynchus*. For example, the lack of an armed cirrus, the presence of two large separate hooks, and a distal girdle of five smaller hooks in the male copulatory organ are unique features of *R. ryukyuensis* sp. nov. However, it does share this relatively large number of hooks with *R. hexacornutus*, which has six separate hooks associated with the male copulatory organ; moreover, these six hooks are also organized in two groups (4+2) (Diez et al. 2021). In all other species of *Reinhardorhynchus*, the number of hooks or spines not associated with a cirrus is either one, two, or three, except for *R. scoticus*, which has five separate sclerotized structures associated with its copulatory organ. The male copulatory organ of *R. tahitiensis* has an armed cirrus with four rows of spines that vary in size and two similar, blunt accessory hooks. *Reinhardorhynchus sagamianus* sp. nov. forms a clade with *R. anamariae*, *R. riegeri*, and *Itaipusa* sp. 1. The first three

Table 3. Species of free-living microturbellarians from marine (M) and brackish water (B) habitats in Japan and territories claimed by Japan, including their geographical distributions and reference literature.

Taxonomic idenitity			Locality in Japan	Prefecture in Japan	Reference	Distribution outside of Japan
Identitified species						
Macrostomorpha	**Macrostomidae**	*Macrostomum flexum* Ax, 2008 (B)	Jusan Lake	Aomori	Ax (2008)	–
		Macrostomum guttulatum Ax, 2008 (B)	Jusan Lake, Noheji River, Obuchi Pond	Aomori	Ax (2008)	–
		Macrostomum semicirculatum Ax, 2008 (B)	Takase River, Obuchi Pond, Takahoko Pond	Aomori	Ax (2008)	–
		Macrostomum uncinatum Ax, 2008 (B)	Takase River	Aomori	Ax (2008)	–
Rhabdocoela	**Koinocystididae**	*Reinhardorhynchus ryukyuensis* sp. nov. (M)	Onna (26°28'52.7"N, 127°50'18.8"E)	Okinawa	This study	–
		Reinhardorhynchus sagamianus sp. nov. (M)	Hayama (35°1'58"N, 139°3'19.4"E)	Kanagawa	This study	–
		Utelga monodon Ax, 2008 (B)	Obuchi pond, Takase River	Aomori	Ax (2008)	–
	Polycystididae	*Palladia nigrescens* (Evdonin, 1971) Evdonin, 1977 (B)	Kominato River, Obuchi Pond, Takase River	Aomori	Ax (2008)	Posyet, Russia (Evdonin 1971, 1977)
		Phonorhynchoides japonicus Ax, 2008 (B)	Takase River	Aomori	Ax (2008)	–
	Cheliplanidae	*Cheliplana setosa* Evdonin, 1971 (B)	Takase River	Aomori	Ax (2008); Gobert et al. (2021)†	Posyet, Russia (Evdonin 1977), British Columbia, Canada (Gobert et al. 2021); California, USA (Karling 1983); Asturias, Spain (Noreña et al. 2007)
		Cheliplana terminalis Brunet, 1968 (M)	Igei (26°27'17.9"N, 127°52'27.5"E)	Okinawa	Van Steenkiste et al. (2023)	Port Lincoln, Australia (Gobert et al. 2021); Southern France (Brunet 1968; Gobert et al. 2021); Blanes, Spain (Gobert et al. 2021); Djezira, Somalia (Schockaert 1982); Mombasa, Kenya (Jouk and De Vocht 1989); Santiago de Cuba, Cuba (Diez et al. 2019)
		Freddius tricaudatus Takeda & Kajihara, 2018 (M)	Akkeshi (43°01'16"N, 144°50'13"E)	Hokkaido	Takeda and Kajihara (2018)	–
	Schizorhynchidae	*Proschizorhynchella caudociliata* Takeda & Kajihara, 2018 (M)	Mukawa (42°33'25"N, 141°55'42"E)	Hokkaido	Takeda and Kajihara (2018)	–
		Proschizorhynchella magnoliae Takeda & Kajihara, 2018 (M)	Akkeshi (43°01'16"N, 144°50'13"E)	Hokkaido	Takeda and Kajihara (2018)	–
		Proschizorhynchella shibazakii Takeda & Kajihara, 2018 (M)	Oshoro (43°12'33"N, 140°51'31"E)	Hokkaido	Takeda and Kajihara (2018)	–
		Proschizorhynchella shuttlecock Takeda & Kajihara, 2018 (M)	Obira (44°03'03"N, 141°39'46"E), Soya (45°29'16"N, 141°58'05"E)	Hokkaido	Takeda and Kajihara (2018)	–
		Proschizorhynchella pacificus (Evdonin, 1969) (M)	Kunashiri	Hokkaido‡	Evdonin (1969)	–
Rhabdocoela	**Provorticidae**	*Pogaina japonica* Ax, 2008 (B)	Takase River, Obuchi Pond, Noheji River, Takahoko Pond	Aomori	Ax (2008)	–
		Pogaina scypha Ax, 2008 (B)	Obuchi Pond	Aomori	Ax (2008)	–
	Trigonostomidae	*Trigonostomum vanmecheleni* Artois et al., 2013 (M)	Otaru (43°13'31.2"N, 141°01'04.0"E)	Hokkaido	Van Steenkiste et al. (2023)	Venice, Italy (Artois et al. 2013); Guangdong, China (Hu et al. 2019); Santiago de Cuba (Diez et al. 2023a)
		Ptychopera japonica Ax, 2008 (B)	Takase River, Obuchi Pond	Aomori	Ax (2008)	British Columbia, Canada (Van Steenkiste and Leander 2018a)
	Promesostomidae	*Promesostoma teshirogii* Ax, 1992 (B)	Takase River, Jusan Lake, Takahoko Pond	Aomori	Ax (1992)	–
Prolecithophora	**Plagiostomidae**	*Vorticeros lobatum* Tozawa, 1918 (M)	Misaki	Kanagawa	Tozawa (1918)	–

Taxonomic idenitity			Locality in Japan	Prefecture in Japan	Reference	Distribution outside of Japan
Prolecithophora	**Plagiostomidae**	*Vorticeros ijimai* Tozawa, 1918 (M)	1) Misaki; 2) Ushimado	1)Kanagawa; 2) Okayama	Tozawa (1918)	–
		Plagiostomum lobatum kurilense Kulinitch, 1979 (M)	Rishiri Island	Hokkaido	Omi (2018)	–
	Pseudostomidae	?*Allostoma durum* (Fuhrmann 1896) (M)	Misaki	Kanagawa	Westblad (1955); Omi (2020)	Concarneau, France (Fuhrmann 1896); Isle of Man, UK (Graff 1913; Westblad 1955); Plymouth, UK (Graff 1913); Trieste, Italy (Graff 1913); Sevastopol, Ukraine (Graff 1913); Falkland Islands, UK (Westblad 1952); Gullmarn, Sweden (Westblad 1955); Vestland, Norway (Karling 1940; Westblad 1955); Istria, Croatia (Westblad 1955)
		Cylindrostoma monotrochum (Graff, 1882) Westblad, 1955 (M)	Wakkanai, Rishiri Island (from Kelps)	Hokkaido	Omi (2018)	Kınalıada, Turkey (Ax 1959); Adriatic Sea, Italy (Graff 1882, 1913; Ritter-Zahony 1908); Sevastopol, Ukraine (Graff 1913); Devon, UK (Westblad 1955); Ilha de São Sebastião, Brazil (Marcus 1951); Hawaii, USA (Karling et al. 1972); California, USA (Karling 1962); Bermuda (Karling 1978).
		Enterostomula densissimabursa Omi, 2020 (B)	Shinji Lake, Nakaumi	Shimane	Omi (2020)	–
	Multipeniatidae	*Multipeniata kho* Nasonov, 1927 (B)	Jusan Lake, Kominato River, Takahoko Pond, Takase River	Aomori	Ax (2008)	Posyet, Russia (Nasonov 1927)
		Japanoplana insolita Ax, 1994 (B)	Kominato River, Takase River	Aomori	Ax (1994; 2008)	–
Proseriata	**Monocelididae**	*Minona pelvivaginalis* Tajika, 1982 (M)	Rumoi, Raigishi, Setana	Hokkaido	Tajika (1982b)	–
		Tajikina juliae (Tajika, 1982) (M)	Onbetsu, Akkeshi	Hokkaido	Tajika (1982b)	–
		Monocelis tenella japonica Tajika, 1982 (M)	Oshoro	Hokkaido	Tajika (1982b)	–
		Monocelis colpotriplicis Tajika, 1982 (M)	Oshoro, Abuta, Shakubetsu, Akkeshi, Habomai, Abashiri, Saruru	Hokkaido	Tajika (1982b)	–
		Minona dolichovesicula Tajika, 1982 (M)	Muroran, Habomai, Nemuro	Hokkaido	Ax (2008)	–
		Duplominona filiformis Ax, 2008 (B)	Takase River	Aomori	Ax (2008)	–
		Duplominona japonica Ax, 2008 (B)	Jusan Lake	Aomori	Ax (2008)	–
		Archilina japonica Ax, 2008 (B)	Noheji River, Takase River	Aomori	Ax (2008)	–
		Minona minuta Ax, 2008 (B)	Obuchi pond	Aomori	Ax (2008)	–
	Nematoplanidae	*Ezoplana oxygona* Tajika, 1982 (M)	1) Cape Erimo, Harutachi; 2) Yaeyama Islands	1)Hokkaido; 2) Okinawa	Tajika (1982a)	–
		Ezoplana masacoae Tajika, 1982 (M)	1) Raigishi, Kameda Peninnsula, Hidaka, Abashiri; 2) Joga-Shima Island; 3) Hateruma Island	1)Hokkaido; 2) Kanagawa; 3) Okinawa	Tajika (1982a)	–
	Coelogynoporidae	*Ezona habomaiensis* Tajika, 1980 (M)	Habomai	Hokkaido	Tajika (1980)	–
		Coelogynopora coniuncta Tajika, 1978 (M)	Oshoro, Hakodate, Akkeshi	Hokkaido	Tajika (1978)	–
		Ezona pinnigera Tajika, 1980 (M)	Oshoro, Cape Aikappu, Raigishi, Habomai	Hokkaido	Tajika (1980)	–
		Invenusta paracnida (Karling, 1966) (M)	Akkeshi, Ishikari, Harutachi, Erimo, Habomai, Saruru	Hokkaido	Tajika (1981b)	Alaska, USA (Ax and Armonies 1990); Washington, USA (Ax and Sopott-Ehlers 1979; Ehlers and Sopott-Ehlers 1987); California, USA (Karling 1966)
		Coelogynopora birostrata Tajika, 1978 (M)	Oshoro, Hakodate, Akkeshi, Okushiri Island	Hokkaido	Tajika (1978)	–
		Pseudovannuccia hirutai (Tajika, 1981) (M)	1) Oshoro, Tomamae, Rebun Island, Rishiri Island, Muroran, Abuta, Akkeshi; 2) Ishigaki Island	1)Hokkaido, 2) Okinawa	Tajika (1981b)	–

Taxonomic idenitity			Locality in Japan	Prefecture in Japan	Reference	Distribution outside of Japan
Proseriata	**Coelogynoporidae**	*Vannuccia tripapillosa* Tajika, 1977 (M)	Oshoro, Akkeshi, Rebun Island, Cape Erimo	Hokkaido	Tajika (1977)	–
		Coelogynopora alata Tajika, 1981 (M)	Okushiri Island, Muroran, Harutachi	Hokkaido	Tajika (1981b)	–
	Otoplanidae	*Archotoplana abutaensis* Tajika, 1983 (M)	Abuta	Hokkaido	Tajika (1983b)	–
		Zygotoplana ezoensis Tajika, 1983 (M)	Ishikari	Hokkaido	Tajika (1983b)	–
		Archotoplana yamadai Tajika, 1983 (M)	Ishikari	Hokkaido	Tajika (1983b)	–
		Polyrhabdoplana perforata Tajika, 1983 (M)	Muroran	Hokkaido	Tajika (1983c)	–
		Notocaryoplana geminofollicularis Tajika, 1983 (M)	Ishikari, Raigishi, Muroran, Samani, Akkeshi, Habomai, Abashiri, Sawaki	Hokkaido	Tajika (1983a)	–
		Itaspiella macrostilifera Tajika, 1984 (M)	Muroran, Raigishi	Hokkaido	Tajika (1984)	–
	Nematoplanidae	*Nematoplana ciliovesiculae* Tajika, 1979 (M)	Raigishi	Hokkaido	Tajika (1979)	–
		Nematoplana pullolineata Tajika, 1979 (M)	Toya	Hokkaido	Tajika (1979)	–
	Archimonocelididae	*Tajikacelis itoi* (Tajika, 1981) Curini-Galletti & Schockaert, 2021 (M)	Uchikabuto, Satokabuto (Oshoro)	Hokkaido	Tajika (1981a)	–
Unidentified species						
Macrostomorpha	**Macrostomidae**	*Bradburia* sp.[§] (M)	Kataya Port, Miura Peninnsula (35°08'31.24"N, 139°40'14.50"E)	Kanagawa	Kobayashi (2009)	
		Macrostomum sp. (M)	Hanami Beach, Noto Peninnsula (37°17'19.09"N, 137°0'00.76"E)	Ishikawa	Kobayashiw (2009)	
Rhabdocoela	**Koinocystididae**	*Parautelga* sp. (M)	Igei (26°27'17.9"N, 127°52'27.5"E)	Okinawa	Van Steenkiste et al. (2023)	
	Schizorhynchidae	*Carcharodorhynchus* sp. (M)	Onna (26°29'05.1"N, 127°50'25.6"E)	Okinawa	Van Steenkiste et al. (2023)	

The numbers in each locality correspond to the numbers assigned in each prefecture.

[†]Gobert et al. (2021) considered the specimens from Japan to belong to a different species of *Cheliplana*, most likely *C. hawaiiensis* Gobert, Reygel, Van Steenkiste & Artois, 2021, although *C. evdonini* Karling, 1983 was also considered.

[‡]Kunashir Island is claimed by both Japan and Russia.

[§]The genus *Bradburia* is currently considered as incertae sedis by Brand et al. (2022).

species in this clade all have the combination of at least one armed cirrus and two large, heteromorphic accessory hooks (Diez et al. 2021; this study). In addition, *R. sagamianus* sp. nov. and *R. anamariae* both have a conspicuous belt consisting of overlapping lamellar spines of varying sizes in the armed cirrus. It is possible that other species of *Reinhardorhynchus* with such a combination of characters, including *R. beatrizae*, *R. curvicirrus*, *R. ruffinjonesi*, and *R. soror*, also gather in this clade, but further analyses with more dense taxon sampling are needed to confirm its synapomorphic traits.

Marine microturbellarians in Japan

Most of the species recorded in Japan have been accurately identified except for a prolecithophoran that most likely belongs to the species *Allostoma durum* (Fuhrmann, 1896) and four unidentified species of Macrostomorpha (*Bradburia*, *Macrostomum*) and Rhabdocoela (*Carcharodorhynchus*, *Parautelga*), respectively (Table 3). The putative representative of *Allostoma durum* lacks a specified collection locality in Japan based on our literature survey (Westblad 1955; Omi 2020). The four unidentified species await further description. Some microturbellarians found in Japan, including specimens likely belonging to Plagiostomidae (*Vorticeros*, unidentified genus) and Cylindrostomidae (unidentified genus) collected from Rishiri Island (Hokkaido), are not listed in Table 3 because the individuals were immature (Omi 2018). Resampling will be required for an accurate identification.

Macrostomorphs, rhabdocoels, prolecithophorans, and proseriates are the most commonly encountered microturbellarians in marine and brackish water environments around the world. It is, therefore, not surprising that all microturbellarians collected in Japan so far belong to these groups (Table 3). Other marine taxa of free-living microturbellarians, including catenulids and gnosonesimids, are rarely encountered, and while they seem to have widespread distributions, they have not yet been found in Japan. Most recorded species were collected in Hokkaido and northern Honshu as a result of the research activities conducted in these areas over the years (Evdonin 1969; Tajika 1978, 1981b, 1982a, 1982b, 1983b, 1983c; Ax 1994, 2008; Omi 2018; Takeda and Kajihara 2018; Van Steenkiste et al. 2023). Japan extends from 20° to 45° north latitude and consists of more than 14,000 islands and almost 30,000 km of coastline. This results in a wide variety of marine habitats and climatic conditions, from seasonal sea ice along the northern coasts of Hokkaido to tropical coral reefs around the atolls and islands of the Ryukyu and Ogasawara Islands. Undoubtedly, rich communities of microturbellarians are also present in these diverse but unexplored marine areas of Japan.

Only nine out of 58 species of marine or brackish water microturbellarians from Japan have also been collected in other parts of the world (Table 3). Our overview indicates that some of these species might be confined to the regional seas around Japan (*Palladia nigrescens* (Evdonin, 1971), *Multipeniata kho* Nasonov, 1927) or the Northern Pacific (*Ptychopera japonica* Ax, 2008, *Invenusta paracnida* (Karling, 1966)), while others have widespread distributions (*Cheliplana setosa* Evdonin, 1971, *Cheliplana terminalis* Brunet, 1968, *Trigonostomum vanmecheleni* Artois, Schockaert, Beenaerts & Reygel, 2013, *Allostoma durum* (Fuhrmann, 1896), *Cylindrostoma monotrochum* (von Graff, 1882)). The fact that 49 species have only been recorded from Japan does not necessarily indicate a high degree of endemism for microturbellarians in the marine areas of Japan, but rather exemplifies how little species discovery and exploration has been done in the surrounding coastal areas of the Russian Far East, the Korean peninsula, Eastern China, and the Philippines.

The scarcity of researchers focusing on various meiofaunal groups, such as microturbellarians, has been recognized as a significant challenge that needs urgent attention (Schockaert et al. 2008; Balsamo et al. 2020). Marine microturbellarians play crucial roles in the trophic dynamics of coastal marine environments (Urban-Malinga 2011; Leasi et al. 2016, 2018; Schratzberger and Ingels 2018; Martínez et al. 2019; Balsamo et al. 2020). Hence, understanding their diversity and interactions with other organisms, including prokaryotes, protists, and other micro-invertebrates, is essential for evaluating their impact on marine ecosystems along the Japanese coasts. Microturbellarians also establish symbiotic relationships with other micro-organisms. The rhabdocoel representatives of *Pogaina*, of which two species have been recorded from Japan (Table 3), are known to practice kleptoplasty by sequestering plastids from diatom prey cells (Van Steenkiste et al. 2019). Recent studies identified single-celled parasites in microturbellarians from Japan and other parts of the world as apicomplexans belonging to the genus *Rhytidocystis* (Holt et al. 2022; Van Steenkiste et al. 2023). An apicomplexan cell was also observed inside the intestine of *R. ryukyuensis* sp. nov., which was collected in the same location as *Carcharodorhynchus* sp. (Table 3), one of the host taxa in the study of Van Steenkiste et al. (2023). It is therefore likely that the apicomplexan in *R. ryukyuensis* sp. nov. also belongs to the genus *Rhytidocystis*. The effects of these interactions on the flatworm hosts and their symbionts or parasites are still largely unknown. Understanding these complex ecological relationships is crucial for addressing the challenges in environmental management and conservation in the region (Zeppilli et al. 2015).

Acknowledgements

This work was funded by the Universidad Cientifica del Sur (JR), the Tula Foundation's Hakai Institute (NWLVS and BSL), and the Natural Sciences and Engineering Research Council of Canada (NSERC 2019-03986 to BSL). We thank Dr. Yander Diez and Dr. Julian Smith III for critically reviewing previous versions of the manuscript.

References

Altekar G, Dwarkadas S, Huelsenbeck JP, Ronquist F (2004) Parallel Metropolis coupled Markov chain Monte Carlo for Bayesian phylogenetic inference. Bioinformatics (Oxford, England) 20(3): 407–415. https://doi.org/10.1093/bioinformatics/btg427

Aramayo V (2018) Diversidad, densidad y distribución vertical de la meiofauna bentónica en sedimentos fangosos frente a Perú central (12°S). Boletín Instituto Del Mar Del Perú 33(1): 90–97. http://biblioimarpe.imarpe.gob.pe/handle/123456789/3260

Armonies W (2017) Long-term change of meiofaunal species composition in a sandy beach, with description of 7 new species of Platyhelminthes. Helgoland Marine Research 71(1): 12. https://doi.org/10.1186/s10152-017-0492-0

Armonies W (2023) Platyhelminth fauna of the Island of Sylt: A meta-analysis of distributional patterns and description of 19 new species. Marine Biodiversity 53(1): 17. https://doi.org/10.1007/s12526-022-01309-w

Artois T, Vermin W, Schockaert E (2000) Rhabdocoela (Platyhelminthes) from the Weddell Sea (Antarctica) with the description of eight new species. Belgian Journal of Zoology 130: 103–110.

Artois T, Schockaert E, Beenaerts N, Reygel P (2013) *Trigonostomum vanmecheleni* sp. nov., a new species of Trigonostomidae (Rhabdocoela, Dalytyphloplanida) from the channels of Venice (Italy), with a discussion on the *T. lilliei* species group. The Italian Journal of Zoology 80(1): 46–51. https://doi.org/10.1080/11250003.2012.754058Ax

Ax P (1959) Zur Systematik, Ökologie und Tiergeographie der Turbellarienfauna in den ponto-kaspischen Brackwassermeeren. Zoologische Jahrbucher. Abteilung fur Systematik, Ökologie und Geographie der Tiere 87: 43–184.

Ax P (1994) *Japanoplana insolita* n. sp. – Eine neue Organisation der Lithophora (Seriata, Plathelminthes) aus Japan. Meiofauna Marina 9: 7–23.

Ax P (2008) Plathelminthes aus Brackgewässern der Nordhalbkugel. Akademie Der Wissenschaften Und Der Literatur 1: 1–696.

Ax P, Armonies W (1990) Brackish water Platyhelminthes from Alaska as evidence for the existence of a boreal brackish water community with circumpolar distribution. Meiofauna Marina 6: 7–109.

Ax P, Sopott-Ehlers B (1979) Turbellaria Proseriata von der Pazifikkiiste der USA (Washington). II. Coelogynoporidae. Zoologica Scripta 8(1–4): 25–35. https://doi.org/10.1111/j.1463-6409.1979.tb00617.x

Balsamo M, Artois T, Smith JPS III, Todaro MA, Guidi L, Leander BS, Van Steenkiste NWL (2020) The curious and neglected soft-bodied meiofauna: Rouphozoa (Gastrotricha and Platyhelminthes). Hydrobiologia 847(12): 2613–2644. https://doi.org/10.1007/s10750-020-04287-x

Braccini JAL, Amaral SV, Leal-Zanchet AM (2016) Microturbellarians (Platyhelminthes and Acoelomorpha) in Brazil: Invisible organisms? Brazilian Journal of Biology 76(2): 476–494. https://doi.org/10.1590/1519-6984.21514

Brand JN, Viktorin G, Wiberg RAW, Beisel C, Schärer L (2022) Large-scale phylogenomics of the genus *Macrostomum* (Platyhelminthes) reveals cryptic diversity and novel sexual traits. Molecular Phylogenetics and Evolution 166: 107296. https://doi.org/10.1016/j.ympev.2021.107296

Brunet M (1968) Turbellariés Karkinorhynchidae de la région de Marseille. Les genres *Cheliplana* et *Cheliplanilla*. Cahiers de Biologie Marine 9: 421–440.

Brunet M (1972) Koinocystididae de la région de Marseille (Turbellaria, Kalyptorhynchia). Zoologica Scripta 1(3): 157–174. https://doi.org/10.1111/j.1463-6409.1972.tb00673.x

Casu M, Scarpa F, Delogu V, Cossu P, Lai T, Sanna D, Curini-Galletti M (2014) Biodiversity patterns in interstitial marine microturbellaria: A case study within the genus Parotoplana (Platyhelminthes, Rhabditophora) with the description of four new species. Journal of Zoological Systematics and Evolutionary Research 52(3): 190–202. https://doi.org/10.1111/jzs.12058

Chernomor O, von Haeseler A, Minh BQ (2016) Terrace Aware Data Structure for Phylogenomic Inference from Supermatrices. Systematic Biology 65(6): 997–1008. https://doi.org/10.1093/sysbio/syw037

Diez YL, Hernández CS, Reygel P, Roosen P, Artois T (2018) First record of Polycystididae (Platyhelminthes, Kalyptorhynchia) from Cuba, with the description of a new genus and five new species, and remarks and the description of one new species from Panama. Zootaxa 4514(1): 107–125. https://doi.org/10.11646/zootaxa.4514.1.9

Diez YL, Reygel P, Artois T (2019) Schizorhynchia (Platyhelminthes, Rhabdocoela) from eastern Cuba, with the description of fifteen new species. Zootaxa 4646(1): 1–30. https://doi.org/10.11646/zootaxa.4646.1.1

Diez YL, Monnens M, Aguirre RI, Yurduseven R, Jouk P, Van Steenkiste NWL, Leander BS, Schockaert E, Reygel P, Smeets K, Artois T (2021) Taxonomy and phylogeny of Koinocystididae (Platyhelminthes, Kalyptorhynchia), with the description of three new genera and twelve new species. Zootaxa 4948(4): 451–500. https://doi.org/10.11646/zootaxa.4948.4.1

Diez YL, Monnens M, Wuyts A, Brendonck L, Reygel P, Schmidt-Rhaesa A, Artois T (2023a) Taxonomy and phylogeny of Dalytyphloplanida Willems et al., 2006 (Platyhelminthes, Rhabdocoela), with the description of a new family, a new genus, and sixteen new species from Cuba and Panama. Organisms, Diversity & Evolution 23(4): 631–681. https://doi.org/10.1007/s13127-023-00623-w

Diez YL, Sanjuan C, Bosch C, Catalá A, Monnens M, Curini-Galletti M, Artois T (2023b) Diversity of free-living flatworms (Platyhelminthes) in Cuba. Biological Journal of the Linnean Society. Linnean Society of London 140(3): 1–11. https://doi.org/10.1093/biolinnean/blad041

Ehlers U, Sopott-Ehlers B (1987) Zum Protonephridialsystem von *Invenusta paracnida* (Plathelminthes, Proseriata). Meiofauna Marina 3: 377–390.

Evdonin LA (1969) A new representative of the interstitial Kalyptorhynchia (Turbellaria, Neorhabdocoela, Kaluptorhynchia) of Kunashir island. Vestnik Leningradskogo Universiteta Serija Biologii 15: 7–14. [in Russian]

Evdonin LA (1971) The interstitial Kalyptorhynchia (Turbellaria, Neorhabdocoela) from the Bay of Great Peter of the Sea of Japan Akademiia Nauk SSSR Zoologicheskiy Institut. Issledovaniia Fauny Morey 8(16): 55–71. [in Russian]

Evdonin LA (1977) Monograph of the Turbellaria Kalyptorhynchia in the fauna of the USSR and adjacent areas. Akademiia Nauk SSSR Zoologicheskiy Institut, Fauna SSSR, 115. Turbellaria 1(Part 1): 1–400.

Fegley SR, Smith JPS III, Johnson D, Schirmer A, Jones-Boggs J, Edmonds A, Bursey J (2020) Nourished, Exposed Beaches Exhibit Altered Sediment Structure and Meiofaunal Communities. Diversity 12(6): 245. https://doi.org/10.3390/d12060245

Fuhrmann MO (1896) Note faunique sur les Turbellariés rhabdocoeles de la Baie de Concarneau. Comptes rendus des séances de la Société de Biologie 48: 1011–1013.

Gobert S, Monnens M, Eerdekens L, Schockaert E, Reygel P, Artois T (2020) Schizorhynchia Meixner, 1928 (Platyhelminthes, Rhabdocoela) of the Iberian Peninsula, with a description of four new species from Portugal. European Journal of Taxonomy 595(595): 1–17. https://doi.org/10.5852/ejt.2020.595

Gobert S, Diez YL, Monnens M, Reygel P, Van Steenkiste NWL, Leander BS, Artois T (2021) A revision of the genus *Cheliplana* de Beauchamp, 1927 (Rhabdocoela, Schizorhynchia), with the description of six new species. Zootaxa 4970(3): 453–494. https://doi.org/10.11646/zootaxa.4970.3.2

Guindon S, Dufayard J-F, Lefort V, Anisimova M, Hordijk W, Gascuel O (2010) New Algorithms and Methods to Estimate Maximum-Likelihood Phylogenies: Assessing the Performance of PhyML 3.0. Systematic Biology 59(3): 307–321. https://doi.org/10.1093/sysbio/syq010

Holt CC, Boscaro V, Van Steenkiste NWL, Herranz M, Mathur V, Irwin NAT, Buckholtz G, Leander BS, Keeling PJ (2022) Microscopic marine invertebrates are reservoirs for cryptic and diverse protists and fungi. Microbiome 10(1): 161. https://doi.org/10.1186/s40168-022-01363-3

Hu X-Z, Chen Y-S, Zhong L-H, Xie Y-H, Feng W-T, Zhang Y, Wang A-T (2019) Two new species of Rhabdocoela (Polycystididae and Trigonostomidae) from China. Zootaxa 4695(4): 351–366. https://doi.org/10.11646/zootaxa.4695.4.3

Jouk PEH, De Vocht AJP (1989) Kalyptorhynchia (Plathelminthes, Rhabdocoela) from the Kenyan Coast, with descriptions of four new species. Tropical Zoology 2(2): 145–157. https://doi.org/10.1080/03946975.1989.10539435

Karling TG (1940) Zur Morphologie und Systematik der Alloeocoela Cumulata und Rhabdocoela Lecithophora (Turbellaria). Acta Zoologica Fennica 26: 1–260.

Karling TG (1954) Einige marine Vertreter der Kalyptorhynchien-Familie Koinocystididae. Arkiv för Zoologi 7(8): 165–183.

Karling TG (1962) Marine Turbellaria from the Pacific coast of North America. II. Pseudostomidae and Cylindrostomidae. Arkiv för Zoologi 15: 181–209.

Karling TG (1963) Die Turbellarien ostfennoskandiens. V. Neorhabdocoela. 3. Kalyptorhynchia. Societas pro Fauna et Flora Fennica Fauna Fennica 17: 5–59.

Karling TG (1966) Marine Turbellaria from the Pacific Coast of North America. IV. Coelogynoporidae and Monocelididae. Arkiv för Zoologi 18(22): 493–528.

Karling TG (1978) Anatomy and Systematics of Marine Turbellaria from Bermuda. Zoologica Scripta 7(1–4): 225–248. https://doi.org/10.1111/j.1463-6409.1978.tb00605.x

Karling TG (1980) Revision of Koinocystididae (Turbellaria). Zoologica Scripta 9(1–4): 241–269. https://doi.org/10.1111/j.1463-6409.1980.tb00666.x

Karling TG (1983) Structural and Systematic Studies on Turbellaria Schizorhynchia (Platyhelminthes). Zoologica Scripta 12(2): 77–89. https://doi.org/10.1111/j.1463-6409.1983.tb00552.x

Karling TG, Mack-Fira V, Dorjes J (1972) First Report on Marine Microturbellarians from Hawaii. Zoologica Scripta 1(5): 251–269. https://doi.org/10.1111/j.1463-6409.1972.tb00575.x

Katoh K, Rozewicki J, Yamada KD (2019) MAFFT online service: Multiple sequence alignment, interactive sequence choice and visualization. Briefings in Bioinformatics 20(4): 1160–1166. https://doi.org/10.1093/bib/bbx108

Kearse M, Moir R, Wilson A, Stones-Havas S, Cheung M, Sturrock S, Buxton S, Cooper A, Markowitz S, Duran C, Thierer T, Ashton B, Meintjes P, Drummond AA (2012) Geneious Basic: An integrated and extendable desktop software platform for the organization and analysis of sequence data. Bioinformatics (Oxford, England) 28(12): 1647–1649. https://doi.org/10.1093/bioinformatics/bts199

Kobayashi K (2009) Umiushi-Tsushin 64: 4–5. [Marine flatworms in Macrostomidae found by a sea water ice method.] [in Japanese]

Kumar S, Stecher G, Tamura K (2016) MEGA7: Molecular Evolutionary Genetics Analysis Version 7.0 for Bigger Datasets. Molecular Biology and Evolution 33(7): 1870–1874. https://doi.org/10.1093/molbev/msw054

Lanfear R, Frandsen PB, Wright AM, Senfeld T, Calcott B (2016) PartitionFinder 2: New Methods for Selecting Partitioned Models of Evolution for Molecular and Morphological Phylogenetic Analyses. Molecular Biology and Evolution 34(3): 772–773. https://doi.org/10.1093/molbev/msw260

Leasi F, Gaynus C, Mahardini A, Moore TN, Norenburg JL, Barber PH (2016) Spatial and ecological distribution of neglected microinvertebrate communities across endangered ecosystems: Meiofauna in Bali (Indonesia). Marine Ecology (Berlin) 37(5): 970–987. https://doi.org/10.1111/maec.12305

Leasi F, Sevigny JL, Laflamme EM, Artois T, Curini-Galletti M, de Jesus Navarrete A, Di Domenico M, Goetz F, Hall JA, Hochberg R, Jörger KM, Jondelius U, Todaro MA, Wirshing HH, Norenburg JL, Thomas WK (2018) Biodiversity estimates and ecological interpretations of meiofaunal communities are biased by the taxonomic approach. Communications Biology 1(1): 112. https://doi.org/10.1038/s42003-018-0119-2

Littlewood DTJ, Curini-Galletti M, Herniou EA (2000) The Interrelationships of Proseriata (Platyhelminthes, Seriata) Tested with Molecules and Morphology. Molecular Phylogenetics and Evolution 16(3): 449–466. https://doi.org/10.1006/mpev.2000.0802

Marcus E (1950) Turbellaria Brasileiros (8). Boletins Da Faculdade de Filosofia, Ciencias e Letras Da Universidade de Sao Paulo. Zoologia 15: 5–191. https://doi.org/10.11606/issn.2526-4877.bsffclzoologia.1950.125192

Marcus E (1951) Turbellaria Brasileiros (9). Boletins Da Faculdade de Filosofia, Ciencias e Letras Da Universidade de Sao Paulo. Zoologia 15: 5–215. https://doi.org/10.11606/issn.2526-4877.bsffclzoologia.1951.125221

Marcus E (1952) Turbellaria Brasileiros (10). Boletins Da Faculdade de Filosofia, Ciencias e Letras Da Universidade de Sao Paulo. Zoologia 17: 5–157. https://doi.org/10.11606/issn.2526-4877.bsffclzoologia.1952.125189

Marcus E (1954) Turbellaria Brasileiros (11). Papéis Avulsos. 11: 419–489. https://doi.org/10.11606/issn.2526-4877.bsffclzoologia.1946.125301

Martínez A, Di Domenico M, Leasi F, Curini-Galletti M, Todaro MA, Zotto MD, Gobert S, Tom A, Norenburg J, Jörger KM, Núñez J, Fontaneto D, Worsaae K (2019) Patterns of diversity and ende-

mism of soft-bodied meiofauna in an oceanic island, Lanzarote, Canary Islands. Marine Biodiversity 49(5): 2033–2055. https://doi.org/10.1007/s12526-019-01007-0

Minh BQ, Nguyen MAT, von Haeseler A (2013) Ultrafast Approximation for Phylogenetic Bootstrap. Molecular Biology and Evolution 30(5): 1188–1195. https://doi.org/10.1093/molbev/mst024

Nasonov NV (1927) Uber eine neue Familie Multipeniatidae (Alloecoela) aus dem Japanischen Meer mit einem aberranten Bau der Fortpflanzungsorgane. Bulletin de l'Académie des Sciences de l'URSS, VI série, 21(5): 865–874.

Nguyen L-T, Schmidt HA, von Haeseler A, Minh BQ (2015) IQ-TREE: A Fast and Effective Stochastic Algorithm for Estimating Maximum-Likelihood Phylogenies. Molecular Biology and Evolution 32(1): 268–274. https://doi.org/10.1093/molbev/msu300

Norén M, Jondelius U (1999) Phylogeny of the Prolecithophora (Platyhelminthes) Inferred from 18S rDNA sequences. Cladistics 15(2): 103–112. https://doi.org/10.1111/j.1096-0031.1999.tb00252.x

Noreña C, Damborenea C, Faubel A, Brusa F (2007) Composition of meiobenthonic Platyhelminthes from brackish environments of the Galician and Cantabrian coasts of Spain with the description of a new species of *Djeziraia* (Polycystididae, Kalyptorhynchia). Journal of Natural History 41(29–32): 1989–2005. https://doi.org/10.1080/00222930701526055

Omi N (2018) First Record of *Cylindrostoma monotrochum* (Graff, 1882) (Platyhelminthes, Cylindrostomidae) from Rishiri Island and Wakkanai, Japan. Rishiri Studies, 37, 01–05.

Omi N (2020) A novel *Enterostomula* (Platyhelminthes, Prolecithophora) species from two brackish lakes in Japan. Biodiversity Data Journal 8: e47161. https://doi.org/10.3897/BDJ.8.e47161

Oya Y, Kajihara H (2020) Molecular Phylogenetic Analysis of Acotylea (Platyhelminthes, Polycladida). Zoological Science 37(3): 271. https://doi.org/10.2108/zs190136

Reygel PC, Willems WR, Artois TJ (2011) Koinocystididae and Gnathorhynchidae (Platyhelminthes, Rhabdocoela, Kalyptorhynchia) from the Galapagos, with the description of three new species. Zootaxa 40(3096): 27–40. https://doi.org/10.11646/zootaxa.3096.1.3

Ronquist F, Huelsenbeck JP (2003) MrBayes 3: Bayesian phylogenetic inference under mixed models. Bioinformatics (Oxford, England) 19(12): 1572–1574. https://doi.org/10.1093/bioinformatics/btg180

Schneider CA, Rasband WS, Eliceiri KW (2012) NIH Image to ImageJ: 25 years of image analysis. Nature Methods 9(7): 671–675. https://doi.org/10.1038/nmeth.2089

Schockaert ER (1982) Turbellaria from Somalia. Monitore Zoologico Italiano. Supplemento 17(2): 81–96. https://doi.org/10.1080/03749444.1982.10736660

Schockaert ER (1996) The Importance of Turbellarians in Ecosystems. In: Hall GS (Ed.) Methods for the Examination of Organismal Diversity in Soils and Sediments. CAB International, Wallingford, 211–225.

Schockaert ER (2014) Marine Macrostomorpha (Platyhelminthes, Rhabditophora) from the Algarve (Southern Portugal). Zootaxa 3872(5): 577–590. https://doi.org/10.11646/zootaxa.3872.5.8

Schockaert ER, Hooge M, Sluys R, Schilling S, Tyler S, Artois T (2008) Global diversity of free living flatworms (Platyhelminthes, "Turbellaria") in freshwater. Hydrobiologia 595(1): 41–48. https://doi.org/10.1007/s10750-007-9002-8

Schratzberger M, Ingels J (2018) Meiofauna matters: The roles of meiofauna in benthic ecosystems. Journal of Experimental Marine Biology and Ecology 502: 12–25. https://doi.org/10.1016/j.jembe.2017.01.007

Steenwyk JL, Buida TJ, Li Y, Shen X-X, Rokas A (2020) ClipKIT: A multiple sequence alignment trimming software for accurate phylogenomic inference. PLoS Biology 18(12): e3001007. https://doi.org/10.1371/journal.pbio.3001007

Stephenson I, Van Steenkiste NWL, Leander BS (2019) Molecular phylogeny of neodalyellid flatworms (Rhabdocoela), including three new species from British Columbia. Journal of Zoological Systematics and Evolutionary Research 57(1): 41–56. https://doi.org/10.1111/jzs.12243

Tajika K-I (1977) Eine neue Art der Gattung *Vannuccia* Marcus, 1948 (Proseriata, Coelogynoporidae) aus Hokkaido, Japan. Journal of the Faculty of Science, Hokkaido University. Series 6, Zoology 21(1): 31–43.

Tajika K-I (1978) Zwei neue Arten der Gattung *Coelogynopora* Steinböck, 1924 (Turbellaria, Proseriata) aus Hokkaido, Japan. Journal of the Faculty of Science, Hokkaido University. Series 6, Zoology 21(3): 295–316.

Tajika K-I (1979) Marine Turbellarien aus Hokkaido, Japan 3. *Nematoplana* Meixner, 1938 (Proseriata, Nematoplanidae). Journal of the Faculty of Science, Hokkaido University. Series 6, Zoology 22(1): 69–87.

Tajika K-I (1980) Eine neue Gattung der Familie Coelogynoporidae (Turbellaria, Proseriata) aus Hokkaido, Japan. Annotationes Zoologicae Japonenses 53(1): 18–36.

Tajika K-I (1981a) Eine neue Art der Gattung *Archimonocelis* (Turbellaria: Proseriata: Monocelididae) aus Hokkaido, Japan. Proceedings of the Japanese Society of Systematic Zoology 21: 1–9.

Tajika K-I (1981b) Marine Turbellarien aus Hokkaido, Japan V. Coelogynoporidae (Proseriata). Journal of the Faculty of Science, Hokkaido University. Series 6, Zoology 22(4): 451–473.

Tajika K-I (1982a) Eine neue Gattung der Familie Nematoplanidae (Turbellaria, Proseriata) aus Hokkaido, Japan. Annotationes Zoologicae Japonenses 55(1): 9–25.

Tajika K-I (1982b) Marine Turbellarien aus Hokkaido, Japan. IX. Monocelididae (Proseriata). Bulletin of the Liberal Arts & Science Course. Nihon University School of Medicine 10: 9–34.

Tajika K-I (1982c) Proseriate Turbellarians from the Yaeyama Islands, Southwestern Japan. I, Coelogynoporidae and Nematoplanidae. Proceedings of the Japanese Society of Systematic Zoology 46: 109–116.

Tajika K-I (1983a) Zur Kenntnis der Gattung *Notocaryoplana* Steinböck, 1935 (Turbellaria, Proseriata, Otoplanidae). Bulletin of the National Science Museum, Tokyo, Series A 9(3): 97–104.

Tajika K-I (1983b) Zwei neue interstitielle Turbellarien der Gattung *Archotoplana* (Proseriata, Otoplanidae) aus Hokkaido, Japan. Journal of the Faculty of Science, Hokkaido University. Series 6, Zoology 23(2): 179–194.

Tajika K-I (1983c) Zwei neue Otoplaniden (Turbellaria, Proseriata) aus Hokkaido, Japan. Annotationes Zoologicae Japonenses 56(2): 100–110.

Tajika K-I (1984) Eine neue Art der Gattung *Itaspiella* Ax, 1956 (Turbellaria, Proseriata, Otoplanidae) aus Hokkaido, Japan. Bulletin of the Liberal Arts & Science Course. Nihon University School of Medicine 12: 25–33.

Takeda N, Kajihara H (2018) A New Genus and Five New Species of Kalyptorhynchia (Platyhelminthes, Rhabdocoela) Discovered in Northern Japan. Species Diversity: An International Journal for Tax-

onomy, Systematics, Speciation, Biogeography, and Life History Research of Animals 23(1): 1–11. https://doi.org/10.12782/specdiv.23.1

Tozawa T (1918) *Vorticeros ijimai* and *Vorticeros lobatum* spp. n. from Misaki. Dobutsugaku Zasshi [Zoological Magazine] 30(77–80): 111–115; 196–199.

Urban-Malinga B (2011) Free-living interstitial Plathelminthes of the Baltic Sea: Diversity and abundance. Polish Journal of Ecology 59(3): 623–630.

Van Steenkiste NWL, Leander BS (2018a) Molecular phylogeny of Trigonostomine turbellarians (Platyhelminthes, Rhabdocoela, Trigonostomidae), including four new species from the Northeast Pacific Ocean. Zoological Journal of the Linnean Society 182(2): 237–257. https://doi.org/10.1093/zoolinnean/zlx046

Van Steenkiste NWL, Leander BS (2018b) Species diversity of eukalyptorhynch flatworms (Platyhelminthes, Rhabdocoela) from the coastal margin of British Columbia: Polycystididae, Koinocystididae, and Gnathorhynchidae. Marine Biology Research 14(9–10): 899–923. https://doi.org/10.1080/17451000.2019.1575514

Van Steenkiste N, Tessens B, Willems W, Backeljau T, Jondelius U, Artois T (2013) A Comprehensive Molecular Phylogeny of Dalytyphloplanida (Platyhelminthes, Rhabdocoela) Reveals Multiple Escapes from the Marine Environment and Origins of Symbiotic Relationships. PLoS One 8(3): e59917. https://doi.org/10.1371/journal.pone.0059917

Van Steenkiste NWL, Stephenson I, Herranz M, Husnik F, Keeling PJ, Leander BS (2019) A new case of kleptoplasty in animals: Marine flatworms steal functional plastids from diatoms. Science Advances 5(7): eaaw4337. https://doi.org/10.1126/sciadv.aaw4337

Van Steenkiste NWL, Wakeman KC, Söderström B, Leander BS (2023) Patterns of host-parasite associations between marine meiofaunal flatworms (Platyhelminthes) and rhytidocystids (Apicomplexa). Scientific Reports 13(1): 21050. https://doi.org/10.1038/s41598-023-48233-y

von Graff L (1882) Monographie der Turbellarien. I. Rhabdocoelida. Leipzig: Verlag von Wilhelm Engelmann.

von Graff L (1913) Das Tierreich •••: 35. [Turbellaria II. Rhabdocoelida. Berlin: Verlag von R. Friedländer und Sohn.]

von Ritter-Záhony R (1908) Beitrag zur Anatomie von *Allostoma monotrochum* Graff. Mitteilungen des Naturwissenschaftlichen Vereines für Steiermark 44(1907): 147–155.

Westblad E (1952) Turbellaria (exc. Kalyptorhynchia) of the Swedish South Polar Expedition 1901–1903. Further Zoological Results of the Swedish Antarctic Expedition 1901–03 4(8): 1–55.

Westblad E (1955) Marine "Alloeocoels" (Turbellaria) from North Atlantic and Mediterranean coasts. I. Arkiv för Zoologi 7(24): 491–526.

Whiting MF (2002) Mecoptera is paraphyletic: Multiple genes and phylogeny of Mecoptera and Siphonaptera. Zoologica Scripta 31(1): 93–104. https://doi.org/10.1046/j.0300-3256.2001.00095.x

Zeppilli D, Sarrazin J, Leduc D, Arbizu PM, Fontaneto D, Fontanier C, Gooday AJ, Kristensen RM, Ivanenko VN, Sørensen MV, Vanreusel A, Thébault J, Mea M, Allio N, Andro T, Arvigo A, Castrec J, Danielo M, Foulon V, Fumeron R, Hermabessiere L, Hulot V, James T, Langonne-Augen R, Le Bot T, Long M, Mahabror D, Morel Q, Pantalos M, Pouplard E, Raimondeau L, Rio-Cabello A, Seite S, Traisnel G, Urvoy K, Van Der Stegen T, Weyand M, Fernandes D (2015) Is the meiofauna a good indicator for climate change and anthropogenic impacts? Marine Biodiversity 45(3): 505–535. https://doi.org/10.1007/s12526-015-0359-z

Supplementary material 1

Reinhardorhynchus sagamianus sp. nov – detail of the male copulatory organ in a live animal

Authors: Aoi Tsuyuki, Jhoe Reyes, Yuki Oya, Kevin C. Wakeman, Brian S. Leander, Niels W. L. Van Steenkiste

Data type: mov

Link: https://doi.org/10.3897/zse.100.120244.suppl1

Supplementary material 2

Reinhardorhynchus sagamianus sp. nov – detail of the male copulatory organ in a live animal

Authors: Aoi Tsuyuki, Jhoe Reyes, Yuki Oya, Kevin C. Wakeman, Brian S. Leander, Niels W. L. Van Steenkiste

Data type: mov

Link: https://doi.org/10.3897/zse.100.120244.suppl2

Supplementary material 3

Reinhardorhynchus sagamianus sp. nov – detail of the male copulatory organ in a live animal

Authors: Aoi Tsuyuki, Jhoe Reyes, Yuki Oya, Kevin C. Wakeman, Brian S. Leander, Niels W. L. Van Steenkiste

Data type: mov

Link: https://doi.org/10.3897/zse.100.120244.suppl3

Zoosyst. Evol. 100 (3) 2024, 897–911 | DOI 10.3897/zse.100.125798

PENSOFT

für Natur MUSEUM FÜR NATURKUNDE BERLIN

Revalidated after having been described more than a century ago: *Calamaria berezowskii* Günther, 1896 (Squamata, Colubridae) from Sichuan, Southwestern China

Ya-Ting Liang[1,2,3], Zi-Dan Huang[1,2,3], Li Ding[4], Gernot Vogel[5], Natalia B. Ananjeva[6], Nikolai L. Orlov[6], Sheng-Chao Shi[7], Zheng-Jun Wu[1,2,3], Ze-Ning Chen[1,2,3]

1 *Key Laboratory of Ecology of Rare and Endangered Species and Environmental Protection (Guangxi Normal University), Ministry of Education, Guilin 541006, Guangxi, China*
2 *Guangxi Key Laboratory of Rare and Endangered Animal Ecology, Guangxi Normal University, Guilin 541006, Guangxi, China*
3 *School of Life Sciences, Guangxi Normal University, Guilin 541006, Guangxi, China*
4 *Chengdu Institute of Biology, Chinese Academy of Sciences, Chengdu 610041, Sichuan, China*
5 *Society for Southeast Asian Herpetology, D-69115 Heidelberg, Germany*
6 *Division of Herpetology, Zoological Institute, Russian Academy of Sciences, St. Petersburg 199034, Russia*
7 *Hubei Engineering Research Center for Protection and Utilization of Special Biological Resources in the Hanjiang River Basin, School of Life Science, Jianghan University, Wuhan 430056, China*

https://zoobank.org/453CA1DC-07E7-40E8-9979-243C9B948373

Corresponding authors: Natalia B. Ananjeva (nananjeva09@gmail.com); Ze-Ning Chen (chenzn@gxnu.edu.cn)

Academic editor: Justin Bernstein ♦ **Received** 19 April 2024 ♦ **Accepted** 9 June 2024 ♦ **Published** 5 July 2024

Abstract

The reed snakes of the genus *Calamaria* Boie, 1827 are one of the largest groups of Asian snakes, distributed from northeast India to the Maluku Islands of east Indonesia. Recent research on the genus in China has revealed that the species diversity of the group was underestimated. In this study, morphological comparisons and mitochondrial DNA analysis revealed that a junior synonym of *C. pavimentata* Duméril, Bibron & Duméril, 1854 — *Calamaria berezowskii* Günther, 1896 is valid, hence we redescribed and recovered the validity of *C. berezowskii*. This species can be distinguished from other congeners by the combination of the following characters: four supralabials; one preocular; rostral shield width larger than height; mental not touching anterior chin shields; eye diameter less than the distance from eye to mouth edge; less than 1/2 of the posterior chin shield meets in the midline; dorsal scales reduced to six rows at tail; indistinct light ring present in the nuchal region or a more or less distinct yellowish collar. Phylogenetically, this species is sister to *C. pavimentata*, with significant genetic differences (0.190) on mitochondrial gene Cyt *b*.

Key Words

Calamaria berezowskii, Colubridae, morphology, phylogenetics, taxonomy

Introduction

Calamaria Boie, 1827 is the largest group of the colubrid subfamily Calamariinae (Reed Snakes), containing more than 68 species (Uetz et al. 2023). In mainland Southeast Asia and China, 20 species of *Calamaria* are known at present, including *C. lumbricoidea* Boie, 1827; *C. albiventer* (Gray, 1834); *C. schlegeli* Duméril, Bibron & Duméril, 1854; *C. pavimentata* Duméril, Bibron & Duméril, 1854; *C. lovii* Boulenger, 1887; *C. septentrionalis* Boulenger, 1890; *C. prakkei* Lidth De Jeude, 1893; *C. buchi* Marx & Inger, 1955; *C. yunnanensis* Chernov, 1962 (Yeung et al. 2022; Uetz et al. 2023); *C. thanhi* Ziegler & Quyet, 2005; *C. gialaiensis* Ziegler, Nguyen & Nguyen, 2009; *C. sangi* Nguyen, Koch et Ziegler, 2009; *C. abramovi* Orlov, 2009; *C. concolor* Orlov, Nguyen, Nguyen, Ananjeva &

Ho, 2010; *C. andersoni* Yang & Zheng, 2018; *C. dominici* Ziegler, Tran & Nguyen, 2019; *C. strigiventris* Poyarkov, Nguyen, Orlov & Vogel, 2019; *C. nebulosa* Lee, 2021; *C. arcana* Yeung, Lau & Yang, 2022; *C. jinggangensis* Cai, Jiang, Wu, Huang, Fei & Ding, 2023.

There were only three species of genus *Calamaria* recorded in China 26 years ago: *C. pavimentata*, *C. septentrionalis* and *C. yunnanensis* (Zhao et al. 1998). Recently, three more species were described: *C. andersoni*, *C. arcana*, *C. jinggangensis* (Yang and Zheng 2018; Yeung et al. 2022; Cai et al. 2023; Uetz et al. 2023). The species diversity of the genus in China is suggested to be underestimated, and those widely distributed species should be re-evaluated. For example, the widely recorded species *C. pavimentata* has a synonym, *C. berezowskii* Günther 1896, which was described based on two specimens from Lun-ngan-fu (龙安府 Long'an Fu, now 龙安镇 Long'an Town of 平武县 Pingwu County) of Sze-chuen (Sichuan Province of China) (Günther 1896).

During the scientific expeditions in the Gongga Mountains, Luding County, Sichuan Province, between 2017 and 2022, we collected three *Calamaria* specimens. Morphological and molecular phylogenetic analyses showed that these specimens represent a species that differs from all currently recognized congeners of the genus. However, the morphology of these specimens matches the original description of *C. berezowskii*. Besides, Luding County and Pingwu County both are located on the eastern slope of Qinghai-Tibet Plateau bordering the Sichuan Basin. Therefore, we identify the specimens as *C. berezowskii*, and the species is revalidated and redescribed here.

Materials and methods

Sampling

Three specimens of *Calamaria* were collected from eastern slope of Mt. Gongga, Moxi Town, Luding County, Ganzi Tibetan Autonomous Prefecture, Sichuan Province, China during 2017 to 2022 (Fig. 1). One adult female GXNU DLR195 (29.645105°N, 102.111076°E, 1736 m a.s.l.), one adult male GXNU DLR194 (29.615872°N, 102.109208°E, 1680 m a.s.l.), one juvenile female GXNU 20221215002 (29.641749°N, 102.110340°E, 1827 m a.s.l.), collected by Xu Zhang on 31 August 2018, Li Ding on 21 August 2017 and Congcong Du on 15 December 2022. The three specimens were fixed and stored in 80% ethanol and deposited at the School of Life Sciences, Guangxi Normal University.

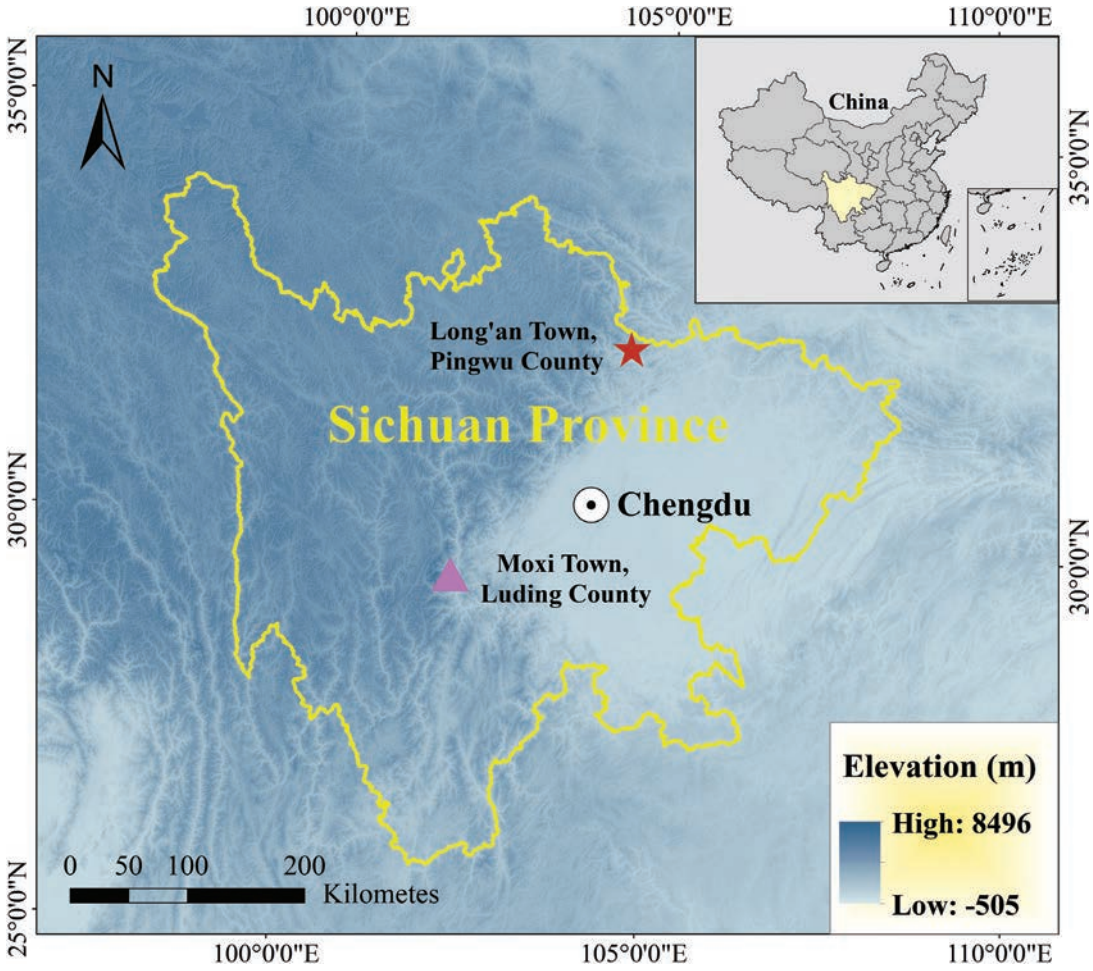

Figure 1. Distribution map of *Calamaria berezowskii*. Red star indicates the type locality, purple triangle indicates the distribution found in this study.

Molecular phylogenetic analysis

Genomic DNA was extracted from muscle or liver tissue taken from the collected specimens using the TIANamp Marine Animals DNA Kit (TIANGEN Biotech). We sequenced a fragment of the mitochondrial gene cytochrome *b* (Cyt *b*) using the primer pair L14910/H16064 (Burbrink et al. 2000). PCR amplification was performed in 25 µl reactions containing 12.5 µl 2× SanTaq PCR Master Mix (with Blue Dye), 10 µl ddH_2O, 1 µl F-primers, 1 µl R-primers and 0.5 µl DNA template. The PCR conditions were an initial denaturing step at 94 °C for 5 min, followed by 35 cycles: denaturing at 94 °C for 30 s, annealing at 48.5 °C for 45 s, an extension step at 72 °C for 35 s; and a final extension of 72 °C for 10 min. Finally, the PCR products were sent to Sangon Biotechnologies Co., Ltd. (Shanghai, China), where the purified PCR products were sequenced using the same forward and reverse primers. Sequences for comparison of available species were downloaded from GenBank (Table 1).

We evaluated and manually corrected the sequencing peak maps of the three sequences obtained, downloaded 29 Cyt *b* sequences of 12 species of the genus *Calamaria* that have been reported in Southeast Asia and China in GenBank, and selected three species *Elaphe quatuorlineata*, *Lycodon rufozonatus* and *Orientocoluber spinalis* as outgroups (Yang and Zheng 2018; Yeung et al. 2022), for a total of 35 sequences to be used for multiple sequence comparisons. All sequences were aligned with other retrieved sequences in the same gene loci by using software MEGA 11 (Kumar et al. 2018). Phylogenetic trees were constructed based on mitochondrial gene Cyt *b* using maximum likelihood (ML) and Bayesian inference (BI). Maximum likelihood analysis was conducted in RAxML v8.2.4 (Stamatakis 2014). Confidence intervals were determined with 1000 bootstrap replicates utilizing the rapid bootstrap option under the GTR+GAMMA substitution model. Bayesian inference analysis was conducted in MrBayes 3.2 (Ronquist et al. 2012). PartitionFinder 2.1.1 software was used to select the most suitable nucleotide substitution models for Cyt *b* sequence data based on the Bayesian information criterion (BIC): GTR+G, HKY+G and GTR+G (Lanfear et al. 2012; Lanfear et al. 2017). We ran our analyses for 20 million generations with the chains, sampling every 1000 generations using the Markov Chain Monte Carlo (MCMC). After removing outgroup taxa, MEGA11 (Kumar et al. 2018) was used to calculate uncorrected pairwise sequence divergence between the *Calamaria* species.

Table 1. DNA sequences used in this study.

No.	Taxa	Voucher	Locality	Cyt *b*	Reference
1	*C. septentrionalis*	HSR19100	Mt. Huangshan, Anhui, China	OQ354842	Cai et al. 2023
2	*C. septentrionalis*	HS11145	Mt. Nanling, Guangdong, China	OQ354840	Cai et al. 2023
3	*C. septentrionalis*	DL2021610-1	Huangsha, Guangxi, China	OQ354838	Cai et al. 2023
4	*C. septentrionalis*	KFBG14506	Hainan Island, China	MH445956	Yang and Zheng 2018
5	*C. septentrionalis*	ROM35605	Nguyên Bình, CaoBang, Vietnam	AF471081	Lawson et al. 2005
6	*C. septentrionalis*	ROM35597	Cao Bang, Vietnam	KX694890	Alencar et al. 2016
7	*C. pavimentata*	KFBG14507	Ningming, Guangxi, China	MH445957	Yang and Zheng 2018
8	*C. andersoni*	HSR20101	Dehong, Yunnan, China	OQ354844	Cai et al. 2023
9	*C. andersoni*	HSR20181	Tengchong, Yunnan, China	OQ354845	Cai et al. 2023
10	*C. andersoni*	SYSr001699	Yingjiang, Yunnan, China	MH445955	Yang and Zheng 2018
11	*C. yunnanensis*	ROM41547	Simao, Yunnan, China	KX694891	Zaher et al. 2009
12	*C. yunnanensis*	YPx503	Unknown	JQ598922	Grazziotin et al. 2012
13	*C. arcana*	HS17082	Mt. Dawu, Guangdong, China	OQ354835	Cai et al. 2023
14	*C. arcana*	KFBG14611	Mt. Dadongshan, Guangdong, China	ON482335	Yeung et al. 2022
15	*C. arcana*	GP9975	Yongxing, Hunan, China	OP980549	Cai et al. 2023
16	*C. arcana*	DLR199	Mt. Wuyi, Fujian, China	OQ354834	Cai et al. 2023
17	*C. jinggangensis*	DL20200725	Mt. Jinggangshan, Jiangxi, China	OQ354830	Cai et al. 2023
18	*C. jinggangensis*	DL20200625-2	Mt. Jinggangshan, Jiangxi, China	OQ354831	Cai et al. 2023
19	*C. jinggangensis*	DL20200625-3	Mt. Jinggangshan, Jiangxi, China	OQ354832	Cai et al. 2023
20	*C. jinggangensis*	DL20200625-4	Mt. Jinggangshan, Jiangxi, China	OQ354833	Cai et al. 2023
21	*C. muelleri*	RMB1283	Gowa, South Sulawesi, Indonesia	MT819391	Weinell et al. 2021
22	*C. muelleri*	TNHC58955	Gowa, South Sulawesi, Indonesia	MT819390	Weinell et al. 2021
23	*C. lumbricoidea*	USMHC1560	Penang, Peninsular, Malaysia	MN338526	Quah et al. 2019
24	*C. palavanensis*	KU311411	Mt. Mantalingahan, Palawan, Philippine	MT819387	Weinell et al. 2021
25	*C. palavanensis*	KU309445	Barangay Irawan, Palawan, Philippine	MT819386	Weinell et al. 2021
26	*C. gervaisii*	KU334485	Municipality, Ilocos Sur, Philippines	MT819385	Weinell et al. 2021
27	*C. gervaisii*	KU324661	Puguis, Benguet, Philippines	MT819384	Weinell et al. 2021
28	*C. schlegeli*	LSUHC10278	Perak, Peninsular, Malaysia	MN338525	Quah et al. 2019
29	*C. nebulosa*	FMNH258666	Phongsaly, Laos	MN338524	Quah et al. 2019
30	*C. berezowskii*	GXNU DLR194	Mt. Gongga, Sichuan, China	PP747047	This study
31	*C. berezowskii*	GXNU DLR195	Mt. Gongga, Sichuan, China	PP747048	This study
32	*C. berezowskii*	GXNU 20221215002	Mt. Gongga, Sichuan, China	PP747049	This study
33	*Elaphe quatuorlineata*	LSUMZ40626	Turkey, European Turkey	AY486931	Nagy et al. 2004
34	*Lycodon rufozonatus*	LSUMZ44977	Unknown	AF471063	Lawson et al. 2005
35	*Orientocoluber spinalis*	MVZ211019	Yinnan, Ningxia, China	AY486924	Nagy et al. 2004

Morphological analysis

Terminology and descriptions follow the views of Inger and Marx (1965) and Ziegler et al. (2008). Body and tail length were measured with a tape ruler to the nearest 1 mm: total length (**TL**), from the tip of snout to the tip of tail; snout-vent length (**SVL**), from the tip of snout to posterior margin of cloaca; tail length (**TaL**), from posterior margin of cloaca to the tip of tail. Other measurements were conducted with a digital caliper to the nearest 0.1 mm: head length (**HL**), from the snout tip to the posterior margin of the mandible; head width (**HW**), measured at the widest part of the head on posterior side; head height (**HH**), at the maximal highest part of the head; the eye horizontal diameter (**EyeD**); and eye-mouth distance (**Eye–Mouth D**), measured from the anterior point of the eye to the mouth gap. Ventral scales (**VEN**) were counted according to Dowling (1951). The enlarged shield(s) anterior to the first ventral were regarded as preventral(s). The number of dorsal scale rows (**DSR**) are given at one head length behind head, at midbody, and at one head length before vent, respectively. The tail tip was not included in the number of subcaudal scales (**SC**). Sex was determined by examining the presence or absence of hemipenis.

Type specimen (lectotype ZISP 8823) was examined for morphological comparisons. Relevant morphological data of other *Calamaria* species were obtained from examined specimens (Appendix 1) and literatures.

Institution acronyms

FMNH: Field Museum of Natural History, Chicago. **GXNU**: Guangxi Normal University. **KFBG**: Kadoorie Farm and Botanic Garden. **KU**: University of Kansas Biodiversity Institute. **LSUHC**: La Sierra University Herpetological Collections. **LSUMZ**: Louisiana State University Museum of Natural Science. **MVZ**: Museum of Vertebrate Zoology. **RMB**: Rafe M. Brown field tag (specimen deposited in Museum Zoologicum Bogoriense, Indonesia). **ROM**: Royal Ontario Museum, Canada. **SYS**: Biological Museum of Sun Yat-sen University, Guangzhou, China. **TNHC**: Texas Natural History Collections. **USMHC**: Universiti Sains Malaysia Herpetological Collection, Malaysia. **ZFMK**: Zoologisches Forschungsmuseum Alexander Koenig, Bonn, Germany. **ZISP**: Zoological Institute, Russian Academy of Sciences, St. Petersburg, Russia.

Molecular results

The DNA dataset contains 35 samples with a total of 1105 base pairs. The phylogenetic topologies that resulted from Bayesian Inference (BI) and Maximum likelihood analysis (ML) are generally consistent in phylogenetic structure (Fig. 2). Phylogenetically, the species *Calamaria* from Mt. Gongga strongly clustered into a single lineage with high nodal support (Fig. 2, BPP 1.00 / UFB 100). Subsequently, it clustered with *C. pavimentata* KFBG14507 from Ningming, Guangxi (BPP 0.96 / UFB 94), and was clustered into the same clade with *C. arcana*, *C. jinggangensis*, *C. septentrionalis*, *C. pavimentata*, *C. andersoni* and *C. yunnanensis*.

The uncorrected pairwise *p*-distances of Cyt *b* sequences between the specimen of Mt. Gongga and the other 12 congeners included in the study were 17.1–31.2%, with the minimum value observed in the comparison with sequences of *C. arcana* (*P* = 17.1%) (Table 2). This divergence is clearly among interspecies level since these levels of divergences are distinctly higher than those observed between two other well distinguished species of *C. andersoni* and *C. yunananensis* (*P* = 12.2–12.6%). The

Table 2. Uncorrected *p*-distances between *Calamaria* species based on 1105 base pairs from the mitochondrial genes Cyt *b*. The serial numbers in Table 2 are consistent with those in Table 1.

No.	Taxa	1–6	7	8–10	11–12	13–16	17–20	21–22	23	24–25	26–27	28	29	30–32
1–6	*C. septentrionalis*	0.000–0.038												
7	*C. pavimentata*	0.174–0.194												
8–10	*C. andersoni*	0.130–0.148	0.246	0–0.019										
11–12	*C. yunnanensis*	0.159–0.164	0.237	0.122–0.126	0.000									
13–16	*C. arcana*	0.090–0.116	0.179–0.199	0.181–0.206	0.183–0.209	0.007–0.034								
17–20	*C. jinggangensis*	0.095–0.103	0.180	0.161–0.171	0.158	0.062–0.074	0.000							
21–22	*C. muelleri*	0.202–0.223	0.266	0.228–0.238	0.261–0.273	0.178–0.198	0.169–0.178	0.007						
23	*C. lumbricoidea*	0.243–0.248	0.258	0.244–0.256	0.251	0.228–0.239	0.228	0.164						
24–25	*C. palavanensis*	0.187–0.222	0.231–0.242	0.227–0.243	0.254–0.266	0.207–0.229	0.173–0.192	0.167–0.182	0.166–0.181	0.022				
26–27	*C. gervaisii*	0.178–0.207	0.243–0.258	0.202–0.212	0.243–0.244	0.197–0.223	0.159–0.163	0.173–0.183	0.197–0.223	0.112–0.174	0.100			
28	*C. schlegeli*	0.232–0.243	0.263	0.258	0.271	0.217–0.228	0.217	0.182–0.192	0.205	0.170–0.175	0.186–0.218			
29	*C. nebulosa*	0.186–0.196	0.214	0.172	0.173	0.162–0.182	0.176	0.208–0.219	0.193	0.202–0.207	0.187–0.234	0.197		
30–32	*C. berezowskii*	**0.187–0.203**	**0.190**	**0.216–0.226**	**0.208**	**0.171–0.200**	**0.202**	**0.223–0.234**	**0.255**	**0.254–0.277**	**0.254–0.271**	**0.312**	**0.176**	**0.000**

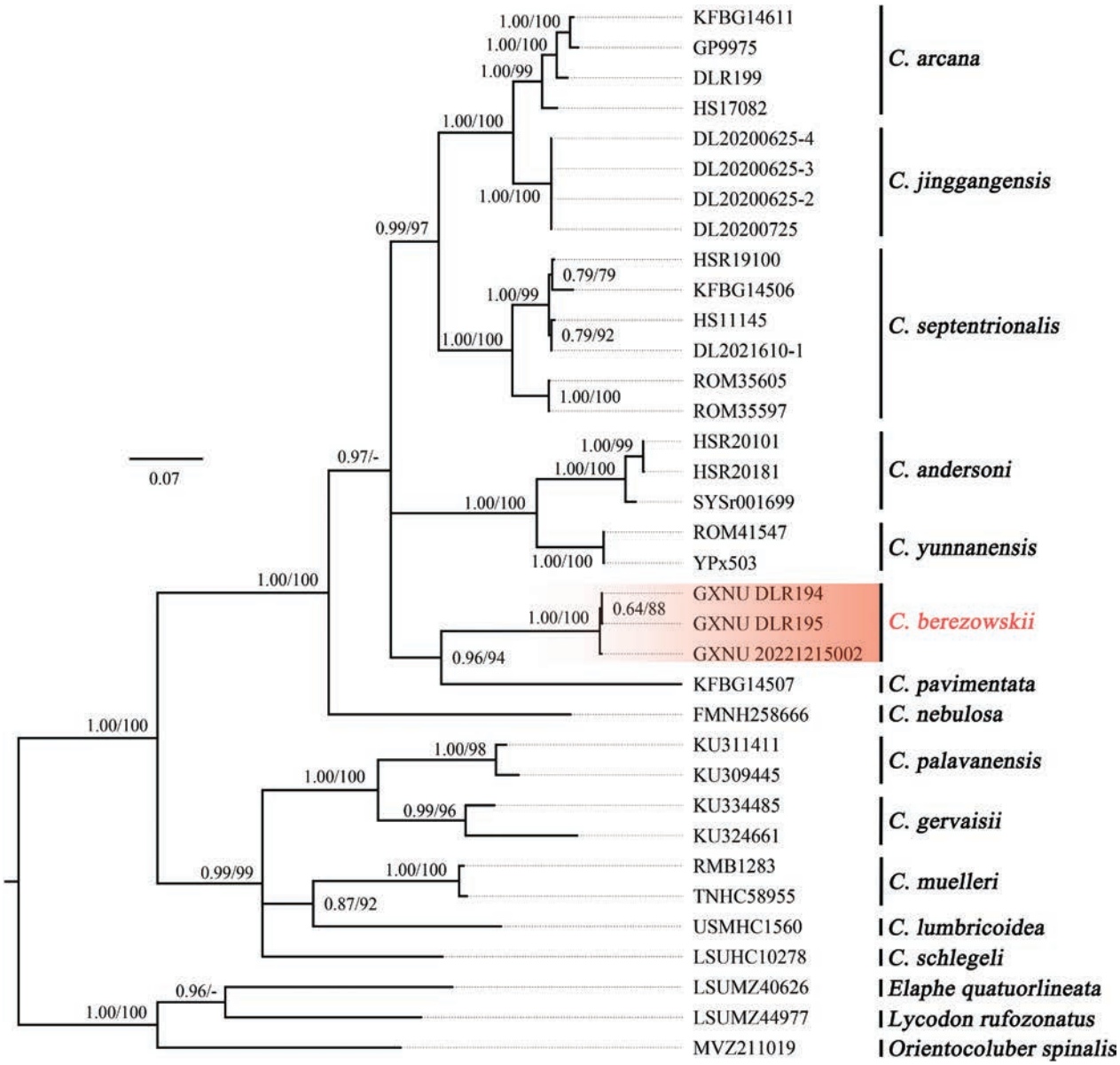

Figure 2. Phylogenetic relationships of *Calamaria* species based on Cyt *b*. Bayesian posterior probabilities (BPP) and Ultrafast bootstrap approximation (UFB) were denoted beside each node (those lower than 75/0.7 were denoted as "-").

Calamaria specimens from Mt. Gongga, Luding, Sichuan represent an evolutionary distinct lineage.

Morphological results

Morphology of the three *Calamaria* specimens from Luding County, Sichuan province matches the original description of *C. berezowskii* Günther 1896 and the morphological characters of lectotype ZISP 8823 (Figs 3, 4, 5, 6). They share the following characters: one preocular and one postocular; presence of a more or less distinct yellowish collar; similar number of ventral scales (149–165 vs 155–167) and subcaudal scales (16–25 vs 14–22); presence of a faint dark line on each side of the back; tail blunt and conical at the end. Besides, Luding County and the type locality Pingwu County are both located on the eastern slope of Qinghai-Tibet Plateau bordering the Sichuan Basin, with a geographic distance of about 350 km (Fig. 1). Hence, the Luding specimens were identified as conspecific with *C. berezowskii*.

Morphological comparisons based on some characters between *Calamaria berezowskii* and other known species of the genus from mainland Southeast Asia and China were listed in Table 3. It can be distinguished by a combination of the following characters: four supralabials; preocular present; rostral shield width greater than height; mental not touching anterior chin shields; eye diameter less than distance from eye to mouth edge; less than 1/2 of the posterior chin shield meets in the midline; dorsal scales reduced to six rows at tail; presence of indistinct light rings in the nuchal region or a more or less distinct yellowish collar; and the two outermost dorsal scale rows light khaki, with upper margins partly dark pigmented.

Table 3. Morphological comparisons of species of *Calamaria* from mainland Southeast Asia and China. "1+***" indicates preventrals + ventrals. Entries marked with '–' are not available.

Species	Comparison between rostral height and width	Comparison between eye diameter and eye-mouth distance	Number of scales surrounding paraparietal	Preocular: present (1) or absent (0)	Supralabials	Mental touching (1) or separated from (0) anterior chin shields	Posterior chin shields meeting in midline (1), diverging or meeting only in anteriorly (0)	End of tail	Modified maxillary teeth	Ventrals		Subcaudals		Dorsal scales reducing to four rows above position of subcaudal on tail	Total length	
										Male	Female	Male	Female		Male	Female
C. berezowskii	H < W	<	6	1	4	0	1	Obtuse point	–	2+149–155	153–2+165	22–25	16	Not reduced	248–290	123–305
C. pavimentata	H ≥ W	≥	5–6	1	–	0	1	Sharp point	8–9	125–168	137–206	3–33	8–20	Last–13th subcaudal	84–313	115–485
C. septentrionalis	H < W	≥	6	1	–	1	1	Broadly rounded	8–9	148–166	168–188	15–19	6–11	Not reduced	111–344	117–384
C. yunnanensis	H < W	–	6	0	4	0	–	Obtuse point	8–9	167–184	199	15–20	19	3rd–last subcaudal	245–300	516
C. andersoni	H < W	>	6	1	4	0	0	Obtuse point	9	171	–	23	–	2nd–last subcaudal	351.4	–
C. arcana	H < W	>	6	1	4	0	1	Obtuse point	10	170–176	192	20–22	12	Not reduced	144–303.2	36.5
C. jinggangensis	H < W	>	6	1	4	0	1	Obtuse point	9	159–160	179	20–22	12–14	Not reduced	314–353+	329–364
C. lumbricoidea	H < W / H >W	≥	4–5	1	5	1	1	Sharp point	9–11	144–196	137–229	17–27	13–21	Last–11th subcaudal	149–498	120–642
C. albiventer	H < W	>	5	1	5	1	1	Sharp point	9	143–144	147–162	21–22	15–19	5th–8th subcaudal	205	170–361
C. schlegeli	–	–	5–6	0–1	5	0	0–1	Blunt	9–10	129–161	136–180	25–44	19–37	3rd–25th subcaudal	–	
C. lovii gimletii	–	–	6	0	–	0	1	Blunt	8–9	161–202	215–249	14–20	10–12	Last–5th subcaudal	–	
C. prakkei	H = W	>	5	1	5	1	1	Sharp point	7–8	126–132	142–144	31–32	24–25	7th–15th subcaudal	172–245	230–256
C. buchi	H > W	≤	5	1	5	1	1	Obtuse point	9	–	221–236	–	13–14	3rd–4th subcaudal	–	389–466
C. thanhi	H < W	>	6–7	0	4	0	0	Gradually to a point	9	184	198	28	21	Not reduced	461	455
C. gialaiensis	H < W	>	5	1	4	1	0	Rounded	9	3+191	–	23	–	Last subcaudal	457	–
C. sangi	H < W	>	5–6	1	4	1	0	Obtuse point	9	2+190		19		Last–3rd subcaudal	373.3	
C. abramovi	H = W	<	6	1	4	0	0	Sharp point	8	159	174	26	20	Last subcaudal	–	482
C. concolor	H < W	<	5	1	5	1	1	Obtuse point	8	3+209	–	19	–	Last subcaudal	578	–
C. dominici	H < W	>	6	1	4–5	1	0	Obtuse point	9	–	1+174	–	17–18	5th–6th subcaudal	–	
C. strigiventris	H < W	<	6	1	4	0	0	Abruptly to point	9–11	130–157	158–180	29–33	20–30	Last–6th subcaudal	–	
C. nebulosa	H < W	>	6	0	4	0	0	Obtuse point	9	–	3+179	–	22	Last subcaudal	–	354

Taxonomy

Calamaria berezowskii Günther, 1896

Figs 3, 4, 5, 6

Calamaria pavimentata — populations in Sichuan of Zhao et al. (1998) and Zhao (2006); Zhao (2003). Synonym.

Description of lectotype ZISP 8823. Adult male, collected from Lun-ngan-fu (龙安府 Long'an Fu, now 龙安镇 Long'an Town of 平武县 Pingwu County) of Szechuen (Sichuan Province of China) (Günther 1896).

HL: 8.0 mm, 3.0% of SVL; HW: 5.0 mm, HW/HL: 62.5%; HH: 4.0 mm, HH/HL: 50.0%; EyeD: 0.7 mm, larger than eye-mouth distance 1.0 mm; EyeD 8.8% of HL.

SVL: 271 mm; TaL: 19 mm; TL: 290 mm; Tal/TL: 6.6%.

DSR: 13–13–13 scales; VEN: 155; SC: 22, divided, followed by a shield covering tail tip; anal scale single.

Rostral as broad as high; pupil rounded; preocular 1/1 (left/right, hereafter); postocular 1/1; supralabials 4/4, the second and third supralabials entering orbit, the fourth longest; infralabials 5/5. Visible yellowish collar on left and right sides of the neck present. Dorsal color brown, with a faint dark line along each side of the back; ventral surface uniform white. Tail rather obtuse, with a conical end. 2–3 pairs light color spots at the base of the tail.

Description of referred specimen GXNU DLR195. Adult female, collected from Mt. Gongga, Moxi Town, Luding County, Ganzi Tibetan Autonomous Prefecture, Sichuan Province, China (29.645105°N, 102.111076°E, 1736 m a.s.l.) collected by Xu Zhang on 31 August 2018.

Body elongated, cylindrical; head small, not distinct from nape; tail short, similar in form to head; tail not flattened, tapering and bluntly pointed at tip.

HL: 8.3 mm, 2.9% of SVL; HW: 3.9 mm, HW/HL: 47.0%; HH: 4.0 mm, HH/HL: 48.2%; EyeD: 0.7 mm, larger than eye-mouth distance 1.1 mm; EyeD 8.4% of HL.

SVL: 288 mm; TaL: 17 mm; TL: 305 mm; Tal/TL: 5.6%. Body thickness about 4.70 to 6.71 mm; base of tail 3.18 mm thick.

Table 3. Continued.

Species	TaL / TL ratio (given as %)		Coloration of dorsum	Coloration of venter	Dorsal scales with light spots present (1) or absent (0)	Dorsum with light nuchal collar (1) or absent (0)	Tail with light rings: present (1) or absent (0)	References
	Male	Female						
C. berezowskii	6.6–10.5	5.6–6.5	Blackish-brown or brown	Light khaki or white	0	1	0–1	Günther 1896; this study
C. pavimentata	6.9–16.9	3.7–8.5	Brown	Yellow	0	0–1	0–1	Inger and Marx 1965; Ziegler et al. 2008; Nguyen et al. 2009
C. septentrionalis	6.3–8.6	2.6–4.3	Dark brown to black	Yellow	1	1	1	Inger and Marx 1965; Ziegler et al. 2008; Poyarkov et al. 2019
C. yunnanensis	5.4–8.2	5	Bluish-grey or olive-brown	Red or yellow	0	0–1	1	Chernov 1962; Stuart and Heatwole 2008; Yang and Rao 2008; Lee 2021
C. andersoni	9.2	–	Brownish	Yellow	1	0	0	Yang and Zheng 2018
C. arcana	7.2–11.8	4.7	Grey-brown with somewhat iridescent (in life) or caramel-brown (in alcohol)	Orangish-red (in life) or light yellowish-beige (in alcohol)	0	0	1	Yeung et al. 2022; Zhang et al. 2023; Cai et al. 2023
C. jinggangensis	7.1–10.1	3.6–4.6	Brownish black with iridescent (in life) or brownish black (in alcohol)	Dark orange (in life) or light khaki (in alcohol)	0	0	0–1	Cai et al. 2023; this study
C. lumbricoidea	6.3–11.4	3.9–8.3	Dark brown to black	Yellow	0–1	0	0–1	Inger and Marx 1965; Weinell et al. 2021; Lee 2021
C. albiventer	8.8–9.3	4.7–8.8	Brown	Red	1	1	0	Inger and Marx 1965; Wallach et al. 2014; Lee 2021
C. schlegeli	11.1–21.3	7.3–14.4	Dark brown to black	White or yellow	0	0	0–1	Inger and Max 1965; Quah et al. 2018; Weinell et al. 2021
C. lovii gimletii	6.2–8.4	3.0–3.7	Dark brown	Yellow	0	0–1	0–1	Inger and Marx 1965; Quah et al. 2018; Grismer et al. 2004; Lee 2021
C. prakkei	16.5–16.7	9.6–10.5	Brown	Yellow	1	1	–	Inger and Marx 1965; Wallach et al. 2014
C. buchi	–	3.9–4.1	Black	Yellow	1	0	0	Inger and Marx 1965; Ziegler er al. 2008; Nguyen et al. 2009
C. thanhi	9.9	6.8	Dark blue to grey	Yellow	0	0	1	Ziegler and Quyet 2005; Ziegler et al. 2007; Ziegler et al. 2008; Nguyen et al. 2009; Wallach et al. 2014
C. gialaiensis	8.1	–	Grey-brown	Yellow	0	0	1	Ziegler et al. 2008; Wallach et al. 2014; Lee 2021
C. sangi	6.2		Greyish-brown	yellow	0	1	0	Nguyen et al. 2009; Wallach et al. 2014
C. abramovi	13.3	7.1	Black	Black and yellow	1	0	0	Orlov 2009; Wallach et al. 2014
C. concolor	7.3	–	Brown	Cream	0	0	0	Orlov et al. 2010; Wallach et al. 2014
C. dominici	_	6.2	Black	Yellow and black	0	0	0	Ziegler et al. 2019
C. strigiventris	13.8–17.9	8.4–11.5	Slate grey to grey-brown	Yellow and black	0	0	0	Poyarkov et al. 2019
C. nebulosa	–	7.9	Bluish-grey	Yellow	1	0	0	Lee 2021

VEN: 165 (+2 preventrals); SC: 16, all paired; anal shield entire, ventral scales immaculate.

DSR: 13–13–13 scales, dorsal scales smooth and immaculate.

Rostral shield width (2.22 mm) is larger than height (1.62 mm), internasals and prefrontals fused 2 scales; prefrontal length (2.28 mm) is less than frontal length (2.61 mm), not entering orbit, and touching first two supralabials; frontal hexagonal, longer (2.61 mm) than wide (2.50 mm); six paraparietals; parietal scales long, tangent to supraocular, postocular scales, supralabials; one preocular present; parietal broadly in contact with the last supralabials; pupil rounded; supralabials 4/4, second and third entering orbit, the fourth largest (length 2.34/2.32 mm) and tangent to the postoculars; mental not touching anterior chin shields; infralabials 5/5, first three touching anterior chin shields; anterior chin shields are slightly longer than posterior chin shields, presence of mental groove; less than 1/2 of the posterior chin shield meets in the midline; dorsal scales reduced to 6 rows above last subcaudal at tail; anal scale is complete and single.

Coloration in life. The dorsal color was blackish brown, with a faint dark line along each side of the back which is about 3 scales wide apart; the outermost corners of the ventral scales were brownish, and the ventral surface was lighter; presence of distinct yellowish collar; absence of light ring at the base of the tail.

Coloration in preservative. The specimen was preserved in alcohol. Dorsal body blackish brown, ventral surface light khaki. Dorsal head and neck coincide with the dorsal body, with a pair of light spots on each side of the neck and on the back of head; dorsum without distinct blotches; venter immaculate, without any dark stripes or scattered spots; ventral surface of tail with a dark longitudinal stripe and blotches; ventral scales with dark outermost corners.

Variations for population from Mt. Gongga, Luding County. Measurements of other specimens are given in Table 4. Male with relatively longer tail (TaL/TL are distinctly larger in the adult male). Adult female GXNU DLR194 displays many scattered brown spots on the venter, and with distinct light-yellow blotches on the left and right sides of the neck, but in adult male GXNU DLR195 the venter is immaculate without any dark spots. The population of Mt. Gongga, Luding County differs slightly from the type specimen in dorsal and ventral coloration (dorsal body blackish brown vs brown, ventral surface light khaki vs white), and differs from the lectotype ZISP 8823 in color spots at the base of the tail (absent vs present) (Figs 3, 4, 5).

Table 4. Main morphological characters of *Calamaria berezowskii*. Abbreviations are listed in the Materials and Methods. "–" indicates missing data. Data of lectotype and syntype of *C. berezowskii* by Günther 1896 and Nikolai Orlov.

Voucher No.	ZISP 8823	–	GXNU DLR194	GXNU DLR195	GXNU 20221215002
Type of specimen	Lectotype	Syntype	–	–	–
Sex	♂	–	♂	♀	♀
Ontogenetic	Adult	Adult	Adult	Adult	Juvenile
Preocular	1/1	1	1/1	1/1	–
Postocular	1/1	1	1/1	1/1	–
Supralabials	4/4	4	4/4	4/4	4/4
Infralabials	5/5	–	5/5	5/5	5/5
Dorsals	13–13–13	–	13–13–13	13–13–13	13–13–13
Ventrals	155	167	2+149	2+165	153
Subcaudals	22	14	25	16	16
Tailspot	2+1	–	Absent	Absent	Absent
TL (mm)	290	245	248	305	123
SVL (mm)	271	220	222	288	115
TaL (mm)	19	25	26	17	8
TaL/TL	0.066	0.102	0.105	0.056	0.065
HL (mm)	8.0	7.0	8.1	8.3	–
HW (mm)	5.0	–	4.1	3.9	–
HH (mm)	4.0	–	3.5	4.0	–
HW/HL	0.625	–	0.506	0.470	–
HH/HL	0.500	–	0.432	0.482	–
EyeD (mm)	0.7	–	0.6	0.7	–
Eye-MouthD (mm)	1.0	–	0.9	1.1	–

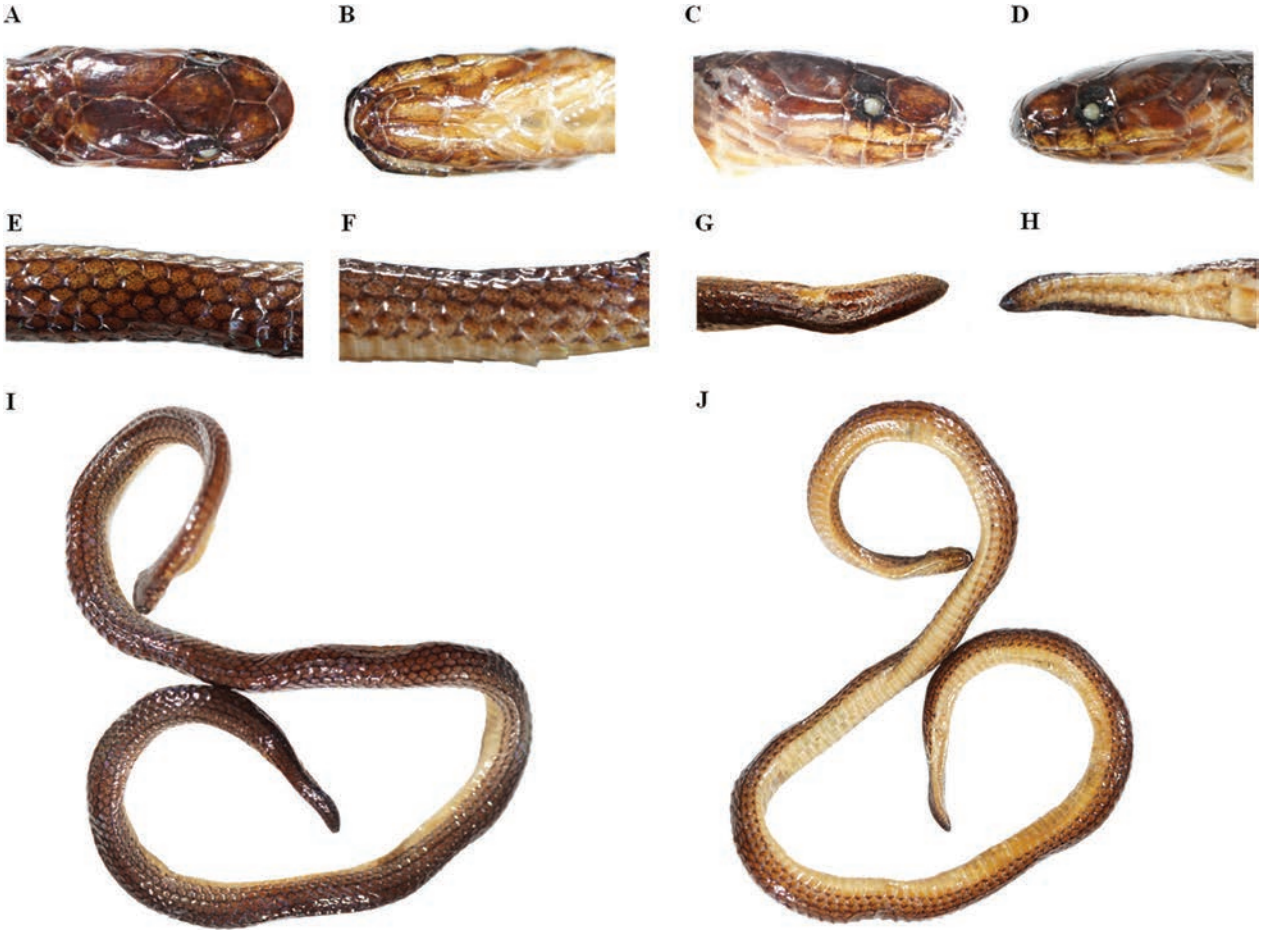

Figure 3. *Calamaria berezowskii* (GNXU DLR195): **A.** Dorsal head; **B.** Ventral head; **C.** Right view of head; **D.** Left view of head; **E.** Dorsal middle body; **F.** Lateral middle body; **G.** Dorsal tail; **H.** Ventral tail; **I.** Dorsal view; **J.** Ventral view.

Detailed morphological comparisons. Detailed morphological comparisons between *Calamaria berezowskii* and 20 congeners of the genus from China and mainland Southeast Asia are:

Calamaria berezowskii is distinguished from *C. albiventer*, *C. lumbricoidea*, *C. prakkei*, *C. schlegeli*, and *C. concolor* by having fewer supralabials (4 vs 5–6), and the 2nd and 3rd supralabials shields touching the orbit (vs.

Figure 4. *Calamaria berezowskii* (GXNU DLR194) in life.

3rd and 4th supralabials touching orbit), mental not touching anterior chin shields (vs. touching in *C. albiventer*, *C. lumbricoidea*, *C. prakkei* and *C. concolor*).

Calamaria berezowskii is distinguished with *C. lovii*, *C. nebulosa*, *C. thanhi* and *C. yunnanensis* by having presence of preocular scale (vs. absence of preocular scale), eye diameter less than distance from eye to mouth edge (vs. reverse condition in *C. thanhi* and *C. nebulosa*), fewer ventral scales in males (149–155 vs 161–202 in *C. lovii*, 149–155 vs 184 in *C. thanhi* and 149–155 vs 167–184 in *C. yunnanensis*), more subcaudal scale in males (22–25 vs 14–20 in *C. lovii*, 22–25 vs 15–20 in *C. yunnanensis*).

Calamaria berezowskii differs from *C. sangi*, *C. gialaiensis* and *C. buchi* by having mental not touching anterior chin shields (vs. touching), dorsal scales reduced to six rows at tail (vs. reduced to four rows), fewer ventral scales (149–167 vs 190 in *C. sangi*, 149–167 vs 191 in *C. gialaiensis*, 149–167 vs 221–236 in *C. buchi*).

Calamaria berezowskii is distinct from *C. arcana* and *C. jinggangensis* by having the eye diameter less than the distance from the eye to mouth edge (vs. reverse condition in *C. arcana* and *C. jinggangensis*), fewer ventral scales (149–167 vs 170–192 in *C. arcana* and *C. jinggangensis*), more subcaudals in females (16 vs 12–14 in *C. arcana* and *C. jinggangensis*), a distinctly different coloration (dark orange or orangish-red in fresh specimens in *C. arcana* and *C. jinggangensis*), presence of dark outermost corners on ventral scales (vs. absence in *C. arcana* and *C. jinggangensis*), a faint dark line along each side of the back present (vs. opposite condition in *C. arcana* and *C. jinggangensis*), a dark longitudinal line or scattered spots on the underside of tail present (vs. absent in *C. arcana* and *C. jinggangensis*).

Calamaria berezowskii differs from *C. abramovi* by having the rostral wider than high (vs. width equal to high in *C. abramovi*), fewer ventral scales in males (149–155 vs 159 in *C. abramovi*), dorsal scales reduced to six rows at tail (vs. reduced to four rows in *C. abramovi*), tail ends in obtuse point (vs. sharp point in the end of tail in *C. abramovi*), and a distinctly different coloration (body black with yellow-orange spots on venter in *C. abramovi*).

Calamaria berezowskii differs from *C. andersoni* by having eye diameter smaller than distance from eye to mouth edge (vs. reverse condition in *C. andersoni*), fewer ventral scales in males (149–155 vs 171 in *C. andersoni*), dorsal scales reduced to six rows at tail (vs. reduced to four rows in *C. andersoni*), light blotches on neck present (vs. absent in *C. andersoni*).

Calamaria berezowskii differs from *C. septentrionalis* by having eye diameter less than distance from eye to mouth edge (vs. reverse condition in *C. septentrionalis*),

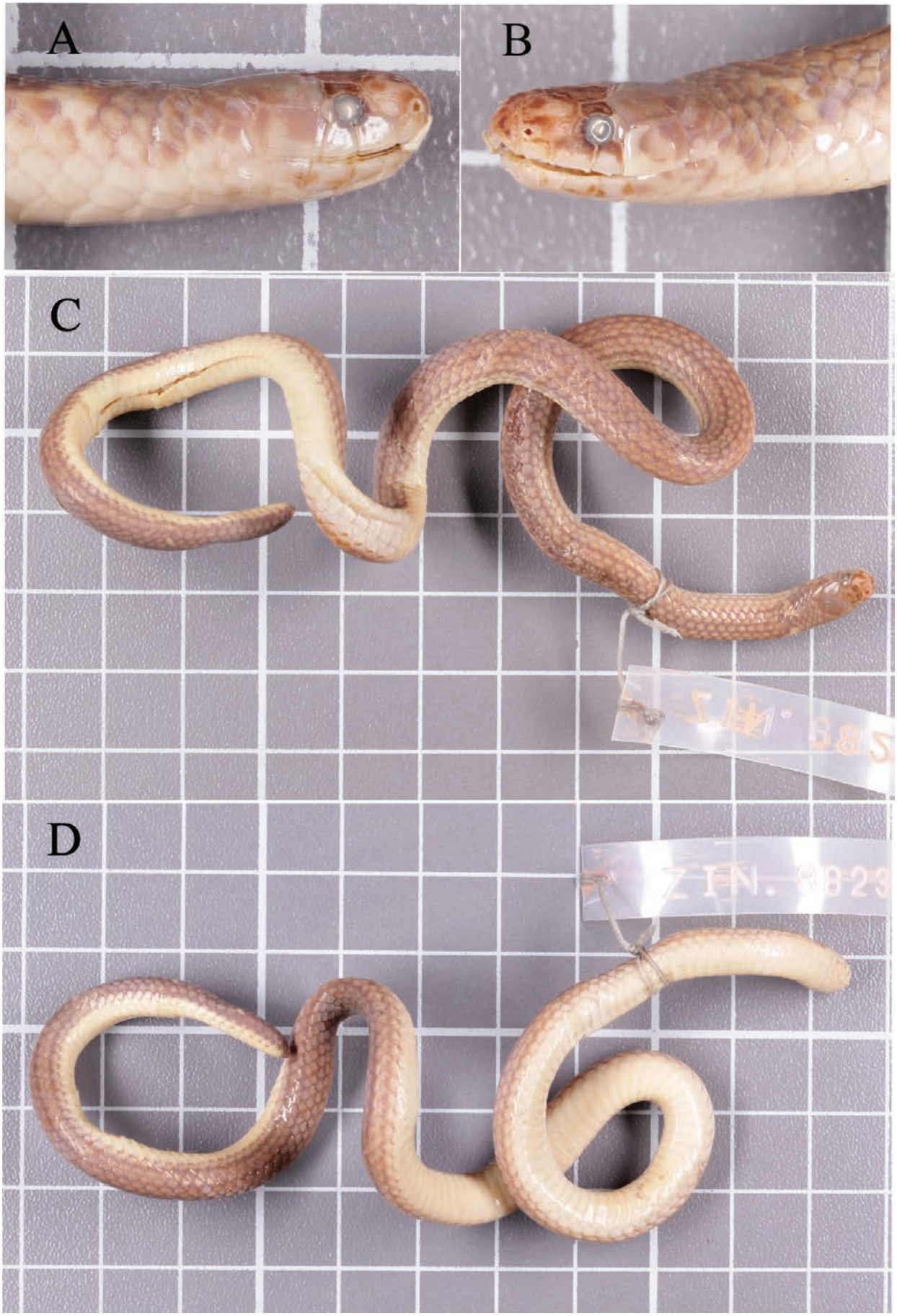

Figure 5. Lectotype ZISP 8823 of *Calamaria berezowskii*: **A.** Right view of head; **B.** Left view of head; **C.** Dorsal view; **D.** Ventral view.

A

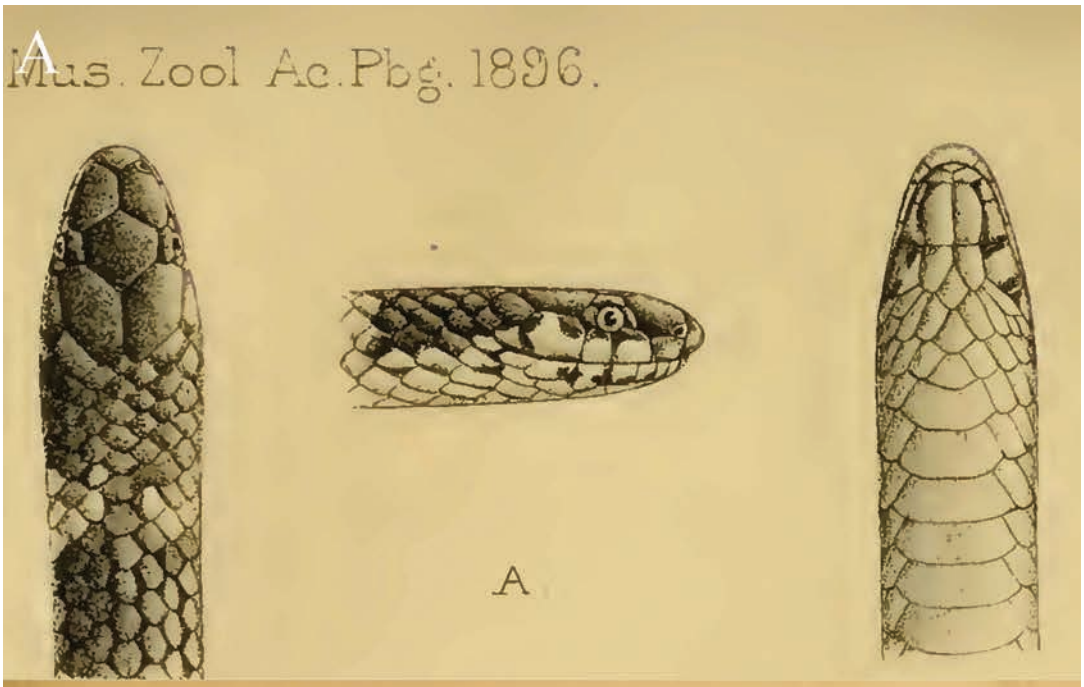

A

B

– 205 –

Calamaria berezowskii, sp. n.

(Pl. I, fig. A.)

Rostral shield reverted to, and distinctly visible on, the upper side of the head. Vertical as broad as long, about four times as wide as the supraocular; one ante-, and one post-ocular. Four upper labials; the first pair of lower labials meeting behind the symphysial. Two pairs of chin-shields, without a central shield between them, the anterior not much longer than the posterior. Orbit narrower than its distance from the labial margin. Ventrals 155, 167; subcaudals 22, 14. Tail rather obtuse, with a conical end. Upper parts brown, with a faint dark line along each side of the back, and another running along the meeting edges of the two outer series of scales. Lower parts, and the lower half of the outer-most row of scales uniform white. A more or less distinct yellowish collar, about five scales distant from the head. Two pairs of small white spots may be present or absent on the tail.

Total length	290 mill.	245 mill.
Length of head . . .	8 „	7 „
„ „ tail	18 „	25 „

Two specimens from Lun-ngan-fu (Berezowski, 1893).

This species is allied to its compatriot, *Calamaria septentrionalis*, but has an entirely different rostral shield. In this respect it comes nearer to *Calamaria siamensis*, which has a narrower vertical shield, and variegated abdomen.

Figure 6. Original description of *Calamaria berezowskii* Günther, 1896: **A.** Drawing; **B.** Description.

mental separated from anterior chin shields (vs. reverse condition in *C. septentrionalis*), not gradually tapering at tip (vs. tail tip broadly rounded in *C. septentrionalis*), higher number of subcaudals (22–25 vs 15–19 in males and 16 vs 6–11 in females), absence of black stripe on venter of tail (vs. venter of tail with broad and distinct median black stripe in *C. septentrionalis*).

Calamaria berezowskii differs from *C. pavimentata* by having the rostral shield width larger than high (vs. reverse condition in *C. pavimentata*), the eye diameter less than the distance from eye to mouth edge (vs. reverse condition in *C. pavimentata*), tail not tapering anteriorly and abruptly pointed at tip (vs. tail tapering gradually to a point in *C. pavimentata*), dorsal scales reduced to six rows at tail (vs. reduced to four rows in *C. pavimentata*), dorsum of body with two faint dark lines (vs. distinct narrow and dark longitudinal lines on dorsum in *C. pavimentata*).

Calamaria berezowskii differs from *C. dominici* by having eye diameter less than eye-mouth distance (vs. opposite situation in *C. dominici*), mental separated from anterior chin shields (vs. mental touching tip of right anterior chin shield in *C. dominici*), dorsal scales reduced to six rows at tail (vs. reduced to four rows in *C. dominici*), fewer ventral scales in females (153–165 vs 174 in *C. dominici*), absence of blotches on dorsum (vs. present irregular yellow blotches on dorsum in *C. dominici*), venter immaculate without dark stripes (vs. ventral side dark with yellow blotches and bands).

Calamaria berezowskii differs from *C. strigiventris* by having posterior chin shields meeting in midline (vs. diverging or meeting only in anteriorly in *C. strigiventris*), dorsal scales reduced to six rows at tail (vs. reduced to four rows in *C. strigiventris*), lower number of subcaudals (22–25 vs 29–33 in males and 16 vs 20–30 in females in *C. strigiventris*), venter immaculate (vs. presence of three interrupted longitudinal black stripes in *C. strigiventris*), tail not flattened, tapering and bluntly pointed at tip (vs. slowly tapering anteriorly, then abruptly tapering to a point in *C. strigiventris*).

Diagnosis. *Calamaria berezowskii* can be distinguished from all other congeneric species by having the following combination of morphological characters: 1) rostral shield width larger than high; 2) prefrontal shorter than frontal, touching the first and second supralabials; 3) frontal hexagonal, length longer than width; 4) mental not touching anterior chin shields; 5) two pairs of chinshields, the anterior not much longer than the posterior, less than 1/2 of the posterior chin shield meets in the midline; 6) eye diameter less than eye-mouth distance; 7) single preocular, single postocular; 8) four supralabials, second and third supralabials entering orbit; 9) five infralabials, first three touching anterior chin shields, first pair of supralabials touching each other; 10) six scales and shields surrounding the paraparietals; 11) dorsal scales smooth, DSR 13–13–13 (n = 4); 12) dorsal scales reduced to six rows above last subcaudal at tail; 13) 149 (+2 preventrals)–155 ventrals in the males (n = 2), 153–165 (+2 preventrals) in the females (n = 2); 14) 22–25 subcaudals in the males (n = 2), 16 in the females (n = 2), all paired; 15) anal plate single and intact; 16) dorsum of body and tail blackish-brown or brown, with a faint dark line along each side of the back; 17) a more or less distinct yellowish collar; 18) 2–3 pairs of small white spots may be present or absent on the tail; 19) ventral scales of body light khaki or white, with a dark longitudinal line or scattered spots on the underside of tail; 20) two outermost dorsal scale rows light khaki with upper margins partly dark pigmented; 21) tail relatively short (5.6–10.5% of the total length), not flattened, slowly tapering to obtuse, with a conical end.

Etymology. Named after collector of type specimen, Russian traveler and zoologist. Michael Berezowski. For common name, we suggest "川西两头蛇" (Chinese), "Berezowski's Reed Snake" (English).

Distribution and ecology. Terra typica of *Calamaria berezowskii* is Lun-ngan-fu (now Long'an Town of Pingwu County) (Günther 1896). It is known from western Sichuan Province, China, including Pingwu County, Shimian County, Baoxing County, Luding County, Mt. Emei and Pingshan County (Zhao et al. 1998; Zhao 2003; this study). These localities are all on the eastern edge of the Qinghai-Tibet Plateau bordering Sichuan Basin. In Luding County, it was found at an elevation of 1680–1827 meters, surrounded by mountainous evergreen broad-leaved forest belt and evergreen broad-leaved deciduous broad-leaved mixed forest belt (Fig. 7). It has a typical subtropical-based vertical natural belt spectrum, with big altitude differences, and abundant rare plant and animal resources (Wang et al. 2023).

Discussion

Morphologically, specimens of *C. berezowskii* collected in Luding County, Sichuan Province are a close match to the type specimens collected in Pingwu County, Mianyang City of Sichuan Province (Günther 1896). For example, there was no significant difference in the number of ventral and subcaudal scales; presence of a more or less distinct yellowish collar; one preocular and one postocular; presence of faint dark line along each side of the dorsum. Geographically, Luding County and Pingwu County are both located in the western region of the Sichuan Province, which lies on the eastern slope of the Qinghai-Tibet Plateau bordering the Sichuan Basin. Even though the samples of *Calamaria* used by this study do not originate from the type locality, the morphology of the voucher specimens matches the original description by Günther (1896), so we confirm that the *Calamaria* specimens collected in Luding County, Sichuan Province are *C. berezowskii* and recover the validity of *C. berezowskii*.

Due to their subterranean mode of life, digging behavior and mysterious habits, *Calamaria* species are not often encountered in the wild. However, in the last five years, five species of *Calamaria* were described, which

Figure 7. Macrohabitat of *Calamaria berezowskii* in Luding County, Sichuan Province, China.

once more shows that the diversity of the genus *Calamaria* is still highly underestimated. In addition, the formal redescription of *C. berezowskii* brings the total number of species of the genus *Calamaria* in China to seven, namely *C. pavimentata*, *C. septentrionalis*, *C. yunnanensis*, *C. andersoni*, *C. arcana*, *C. jinggangensis*, and *C. berezowskii* (Cai et al. 2023; Uetz et al. 2023). At the same time, finding additional specimens of *C. berezowskii* from the type locality and surrounding areas would allow for a greater understanding of its intraspecific variation.

C. berezowskii was found at an elevation of 1680–1827 meters, which is higher than the altitude of all previously known *Calamaria* in China (vs.175–1520 m a.s.l.). The discovery of this new species increases the elevation of all known *Calamaria* species in China and suggests that the actual habitat of *Calamaria* species may span a greater range of elevations. The Hengduan Mountains in southwest China are a biodiversity hot spot, harboring a high percentage of endemic biota (Hu et al. 2012; Wu et al. 2013; Sun et al. 2017; Qiao et al. 2022). For snakes, the high altitude, steep terrain and varying climatic conditions of the Hengduan Mountains are important factors limiting their distribution and are conducive to species migration and isolation, accelerating gene flow and promoting species adaptation to the environment and species formation. Therefore, studying this species is beneficial for understanding the influence of geographical factors and the ecological environment on species formation and evolution.

We update the key to *Calamaria* in China, which is based on Zhao (2006), Yeung et al. (2022) and Cai et al. (2023). The identification of this key is only for reference. Species should be identified by comparing more morphological characteristics or molecular sequences.

Key to the identification of the genus *Calamaria* from China

1	Preocular absent	*Calamaria yunnanensis*
–	Preocular present	2
2	Dorsal scales reduced to four rows on tail at last subcaudals	3
–	Dorsal scales reduced to more than four rows on tail at last subcaudals	5
3	Light rings/blotches on neck and tail absent	*Calamaria andersoni*
–	Presence of light rings/blotches on neck or tail	4
4	Tail tapering gradually to a point	*Calamaria pavimentata*
–	Tail not tapering, broadly rounded on tip	*Calamaria septentrionalis*

5 Most of the posterior chin shield meets in the midline, absence of collar or spots in nuchal region ..... *Calamaria jinggangensis*
– Less than 1/2 of the posterior chin shield meets in the midline, present indistinct light ring or one pair of spots in nuchal region 6
6 Ventral scales immaculate, without dark outermost corners and pigmentation anteriorly ..... *Calamaria arcana*
– Two outermost dorsal scale rows light khaki, with upper margins partly dark pigmented ..... *Calamaria berezowskii*

Acknowledgements

This study was supported by Science and Technology Programme Project of Guangxi, China (AD21220058), the National Natural Science Foundation of China (NSFC 32200379), the Natural Science Foundation of Guangxi, China (2023GXNSFBA026309), and Survey and Assessment of Priority Areas for Biodiversity Conservation in the Terrestrial Area of Guangxi, China (2022–2023). It is partly supported by the State Themes of ZISP 122031100282-2 and grant no.075-15-2021-1069 by the Ministry of Science and Higher Education of the Russian Federation.

We thank Xu Zhang and Congcong Du for providing specimens, and thanks to Konstantin Milto for the help with photographs of type specimens. We would also like to thank Xin Wang and the reviewers for their valuable comments on the manuscript.

References

Alencar LRV, Quental TB, Grazziotin FG, Alfaro ML, Martins M, Venzon M, Zaher H (2016) Diversification in vipers: Phylogenetic relationships, time of divergence and shifts in speciation rates. Molecular Phylogenetics and Evolution 105: 50–62. https://doi.org/10.1016/j.ympev.2016.07.029

Burbrink FT, Lawson R, Slowinski JB (2000) Mitochondrial DNA phylogeography of the polytypic North American rat snake (*Elaphe obsoleta*): A critique of the subspecies concept. Evolution 54(6): 2107–2118. https://doi.org/10.1111/j.0014-3820.2000.tb01253.x

Cai B, Jiang JP, Wu YY, Huang S, Fei DB, Ding L (2023) A new species of *Calamaria* (Reptilia: Serpentes: Colubridae) from Western Jiangxi Province, China. Russian Journal of Herpetology 30(2): 101–111. https://doi.org/10.30906/1026-2296-2023-30-2-101-111

Dowling HG (1951) A proposed standard system of counting ventrals in snakes. British Journal of Herpetology 1: 97–99.

Grazziotin FG, Zaher H, Murphy RW, Scrocchi G, Benavides MA, Zhang YP, Bonatto SL (2012) Molecular phylogeny of the new world Dipsadidae (Serpentes: Colubroidea): a reappraisal. Cladistics 28(5): 437–459. https://doi.org/10.1111/j.1096-0031.2012.00393.x

Grismer LL, Kaiser H, Yaakob NS (2004) A new species of reed snake of the genus *Calamaria* H. Boie, 1827, from Pulau Tioman, Pahang, West Malaysia. Hamadryad 28: 1–6.

Günther A (1896) Report on the collections of reptiles, batrachians and fishes made by Messrs Potanin and Berezowski in the Chinese provinces Kansu and Sze-chuen. Ezhegodnik. Zoologicheskogo Muzeya Akademii Nauk SSSR 1896: 199–219.

Hu JH, Li C, Xie F, Jiang JP (2012) Endemic amphibians and their distribution in China. Asian Herpetological Research 3(2): 163–171. https://doi.org/10.3724/SP.J.1245.2012.00163

Inger RF, Marx H (1965) The systematics and evolution of the oriental colubrid snakes of the genus *Calamaria.* Fieldiana. Zoology 49: 1–304.

Kumar S, Stecher G, Li M, Knyaz C, Tamura K (2018) MEGA X: Molecular evolutionary genetics analysis across computing platforms. Molecular Biology and Evolution 35(6): 1547–1549. https://doi.org/10.1093/molbev/msy096

Lanfear R, Calcott B, Ho SYW, Guindon S (2012) PartitionFinder: Combined selection of partitioning schemes and substitution models for phylogenetic analyses. Molecular Biology and Evolution 29(6): 1695–1701. https://doi.org/10.1093/molbev/mss020

Lanfear R, Frandsen PB, Wright AM, Senfeld T, Calcott B (2017) PartitionFinder 2: New methods for selecting partitioned models of evolution for molecular and morphological phylogenetic analyses. Molecular Biology and Evolution 34(3): 772–773. https://doi.org/10.1093/molbev/msw260

Lawson R, Slowinski JB, Crother BI, Burbrink FT (2005) Phylogeny of the Colubroidea (Serpentes): New evidence from mitochondrial and nuclear genes. Molecular Phylogenetics and Evolution 37(2): 581–601. https://doi.org/10.1016/j.ympev.2005.07.016

Lee JL (2021) Description of a new species of Southeast Asian reed snake from northern Laos (Squamata: Colubridae: Genus *Calamaria* F. Boie, 1827) with a revised diagnosis of *Calamaria yunnanensis* Chernov, 1962. Journal of Natural History 55(9–10): 531–560. https://doi.org/10.1080/00222933.2021.1909165

Nagy ZT, Lawson R, Joger U, Wink M (2004) Molecular systematics of racers, whipsnakes and relatives (Reptilia: Colubridae) using mitochondrial and nuclear markers. Journal of Zoological Systematics and Evolutionary Research 42(3): 223–233. https://doi.org/10.1111/j.1439-0469.2004.00249.x

Nguyen TQ, Koch A, Ziegler T (2009) A new species of reed snake, *Calamaria* Boie, 1827 (Squamata: Colubridae), from central Vietnam. Hamadryad 34(1): 1–8.

Orlov NL (2009) A new species of the genus *Calamaria* (Squamata: Ophidia: Colubridae) from the Central Highlands (Ngoc Linh Nature Reserve, Ngoc Linh Mountain, Kon Tum Province), Vietnam. Russian Journal of Herpetology 16(2): 146–154. https://doi.org/10.30906/1026-2296-2009-16-2-146-154

Orlov NL, Nguyen QT, Nguyen TT, Ananjeva NB, Ho TC (2010) A new species of the genus *Calamaria* (Squamata: Ophidia: Colubridae) from Thua Thien-Hue Province, Vietnam. Russian Journal of Herpetology 17(3): 236–242. https://doi.org/10.30906/1026-2296-2010-17-3-236-242

Poyarkov NA, Van Nguyen T, Orlov NL, Vogel G (2019) A new species of the genus *Calamaria* Boie, 1827 from the highlands of the Langbian Plateau, Southern Vietnam (Squamata: Colubridae). Russian Journal of Herpetology 26(6): 335–348. https://doi.org/10.30906/1026-2296-2019-26-6-335-348

Qiao J, Jia GQ, Zhou HM, Gong L, Jiang Y, Xiao NW, Gao XQ, Wen AX, Wang J (2022) Mammal and bird diversity recorded with camera traps in Gongga Mountain National Nature Reserve,

Sichuan, China. Shengwu Duoyangxing 30(2): 20395. https://doi.org/10.17520/biods.2020395

Quah RV, Tan YH, Mubarak NM, Khalid M, Abdullah EC, Nolasco-Hipolito C (2019) An overview of biodiesel production using recyclable biomass and non-biomass derived magnetic catalysts. Journal of Environmental Chemical Engineering 7(4): 103219. https://doi.org/10.1016/j.jece.2019.103219

Ronquist F, Teslenko M, Van Der Mark P, Ayres DL, Darling A, Höhna S, Larget B, Liu L, Suchard MA, Huelsenbeck JP (2012) MrBayes 3.2: Efficient Bayesian phylogenetic inference and model choice across a large model space. Systematic Biology 61(3): 539–542. https://doi.org/10.1093/sysbio/sys029

Stamatakis A (2014) RaxML version 8: A tool for phylogenetic analysis and post-analysis of large phylogenies. Bioinformatics 30(9): 1312–1313. https://doi.org/10.1093/bioinformatics/btu033

Stuart BL, Heatwole H (2008) Country records of snakes from Laos. Hamadryad 33(1): 97–106.

Sun H, Zhang JW, Deng T, Boufford DE (2017) Origins and evolution of plant diversity in the Hengduan Mountains, China. Plant Diversity 39(4): 161–166. https://doi.org/10.1016/j.pld.2017.09.004

Uetz P, Freed P, Hošek J (2023) The Reptile Database. http://www.reptile-database.org [Accessed on 9 May 2023]

Wallach V, Williams KL, Boundy J (2014) Snakes of the World: A Catalogue of Living and Extinct Species. CRC press, 1st edn., 1237. https://doi.org/10.1201/b16901

Wang XM, Li Y, Liao R, Liu YX, Zhang XA, Qiao J, Wang Y, Wang X, Liu SY (2023) Species diversity of small mammals on the north and south slopes of Gongga Mountain National Nature Reserve. Sichuan Linye Keji 44(6): 1–8. https://doi.org/10.12172/202307240001

Weinell J, Leviton AE, Brown RM (2021) A new species of reed snake, genus *Calamaria* (Colubridae: Calamariinae), from Mindoro Island, Philippines. Philippine Journal of Systematic Biology 14(2): 1–14. https://doi.org/10.26757/pjsb2020b14006

Wu YJ, Colwell RK, Rahbek C, Zhang CL, Quan Q, Wang CK, Lei FM (2013) Explaining the species richness of birds along a subtropical elevational gradient in the Hengduan Mountains. Journal of Biogeography 40(12): 2310–2323. https://doi.org/10.1111/jbi.12177

Yang DT, Rao DQ (2008) Amphibia and Reptilia of Yunnan. Kunming: Yunnan Science and Technology Press.

Yang JH, Zheng X (2018) A new species of the genus *Calamaria* (Squamata: Colubridae) from Yunnan Province, China. Copeia 106(3): 485–491. https://doi.org/10.1643/CH-17-663

Yeung HY, Lau MWN, Yang JH (2022) A new species of *Calamaria* (Squamata: Colubridae) from Guangdong Province, southern China. Vertebrate Zoology 72: 433–444. https://doi.org/10.3897/vz.72.e84516

Zaher H, Grazziotin FG, Cadle JE, Murphy RW, Moura-Leite JCD, Bonatto SL (2009) Molecular phylogeny of advanced snakes (Serpentes, Caenophidia) with an emphasis on South American Xenodontines: A revised classification and descriptions of new taxa. Papéis Avulsos de Zoologia 49(11): 115–153. https://doi.org/10.1590/S0031-10492009001100001

Zhang H, Fei DB, Zhao C, Liu S, Cai B, Guo P, Wu YY (2023) *Calamaria arcana* found in Chenzhou, Hunan. Chinese Journal of Zoology 58(4): 615–621. https://doi.org/10.13859/j.cjz.202304014

Zhao EM (2003) Coloured Atlas of Reptiles of Sichuan. China Forestry Press: Beijing, China.

Zhao EM (2006) Snakes of China. Hefei, China: Anhui Science and Technology Press.

Zhao EM, Huang MH, Zong Y (1998) Fauna Sinica Reptilia, Vol. 3: Squamata: Serpentes. Beijing. Science Press 1998(522): 1–8.

Ziegler T, Quyet LK (2005) A new species of reed snake, *Calamaria* (Squamata: Colubridae), from the Central Truong Son (Annamite Mountain range), Vietnam. Zootaxa 1042(1): 27–38. https://doi.org/10.11646/zootaxa.1042.1.2

Ziegler T, Hendrix R, Vu NT, Vogt M, Forster B, Dang NK (2007) The diversity of a snake community in a karst forest ecosystem in the central Truong Son, Vietnam, with an identification key. Zootaxa 1493(1): 1–40. https://doi.org/10.11646/zootaxa.1493.1.1

Ziegler T, Nguyen VS, Nguyen QT (2008) A new reed snake of the genus *Calamaria* Boie (Squamata: Colubridae) from Vietnam. Current Herpetology 27(2): 71–80. https://doi.org/10.3105/1881-1019-27.2.71

Ziegler T, Tran VA, Babb RD, Jones TR, Moler PE, Van Devender RW, Nguyen TQ (2019) A new species of reed snake, *Calamaria* Boie, 1827 from the Central Highlands of Vietnam (Squamata: Colubridae). Revue Suisse de Zoologie 126(1): 17–26. https://doi.org/10.5281/zenodo.2619512

Appendix 1

Examined specimens (n = 6)

Calamaria berezowskii (n = 4). China: Sze-chuen (now Sichuan Province): Lun-ngan-fu (Long'an Fu, now Long'an Town of Pingwu County): ZISP 8823 (lectotype, adult male); Sichuan: Mt. Gongga, Moxi Town, Luding County, Ganzi Tibetan Autonomous Prefecture: GXNU DLR195 (adult female); GXNU DLR194 (adult male); GXNU 20221215002 (juvenile female).

Calamaria jinggangensis (n = 2). China: Guangxi: Quanzhou County, Guilin: GXNU 20210909007 (adult male); Longsheng County, Guilin: GXNU 20220613012 (adult male).

Zoosyst. Evol. 100 (3) 2024, 913–922 | DOI 10.3897/zse.100.126340

PENSOFT

für Natur MUSEUM FÜR NATURKUNDE BERLIN

A new species of *Grandinenia* Minato & Chen, 1984 (Gastropoda, Stylommatophora, Clausiliidae, Garnieriinae) from Guangxi, China

Zhong-Guang Chen[1*], Jiao Jiang[2*], Ran-Xi Lin[3], Guang-Long Xie[4], Yu-Ting Dai[1], Xiao-Ping Wu[1], Shan Ouyang[1]

1 *School of Life Sciences, Nanchang University, Nanchang, Jiangxi 330031, China*

2 *Zhejiang Museum of Natural History, Hangzhou, Zhejiang 310012, China*

3 *State Key Laboratory for Conservation and Utilization of Subtropical Agro-Bioresources, Guangdong Laboratory for Lingnan Modern Agriculture, College of Agriculture, College of Life Sciences, South China Agricultural University, Guangzhou 510642, China*

4 *School of Life Sciences, Qufu Normal University, Qufu, Shandong 273165, China*

https://zoobank.org/CA2E9204-BB04-4AF9-964C-910DCFAE7A8D

Corresponding authors: Jiao Jiang (149152414@qq.com); Shan Ouyang (ouys1963@qq.com)

Academic editor: Frank Köhler ♦ **Received** 27 April 2024 ♦ **Accepted** 20 June 2024 ♦ **Published** 8 July 2024

Abstract

A molecular phylogenetic study was conducted on genus *Grandinenia*, based on *COI* and *16S* sequences. A total of eight out of 26 species in the genus, as well as three unidentified species were sequenced. Phylogenetic results supported the monophyly of *Grandinenia* and the validity of all sampled species and subspecies. A new species, *Grandinenia jiangjilini* Chen, Lin, Wu & Ouyang, **sp. nov.**, from Guangxi, southern China is identified and described, based on morphological comparison and molecular phylogeny. The discovery indicates that the inflated-fusiform shell is not isolated in genus *Grandinenia* and the species diversity of the genus still remains to be explored.

Key Words

Door snails, karst landscape, phylogeny, taxonomy

Introduction

The Guangxi Zhuang Autonomous Region is situated in southern China and is renowned for its distinctive landscape and rich biodiversity. The karst landscape in this region provide a suitable habitat for land snails. The well-developed and exposed limestone have nurtured diverse rock-dwelling gastropod groups, with genus *Grandinenia* Minato & Chen, 1984 of subfamily Garnieriinae Boettger, 1926 being the most diverse and widespread in the region (Nordsieck 2012a, 2012b, 2012c, 2016; Lin and Lin 2022).

The subfamily Garnieriinae Boettger, 1926 is a group of medium to large-sized door snails distributed from Myanmar to southern China. It is characterised by a furrowed neck, projected and unattached, so-called apostrophic peristome and a lunella-type lunellar region (Nordsieck 2007). There are few molecular phylogenetic studies on the Garnieriinae and the limited studies suggest its close relationship with Synprophyminae Nordsieck, 2007 and Phaedusinae Wagner, 1922 (Uit de Weerd and Gittenberger 2013; Mamos et al. 2021; Uit de Weerd et al. 2023). Currently, Garnieriinae consist of seven genera, three of which are recorded in China: *Garnieria*

* These authors contributed equally to this work.

Bourguignat, 1877, *Grandinenia* Minato & Chen, 1984 and *Tropidauchenia* Lindholm, 1924 (Nordsieck 2012a, 2012b, 2012c). The genus *Grandinenia* is defined by the furrowed neck, the distinctly expanded and unattached peristome, the lunella-type lunellar and the inferior lamella separated from the superior lamella (Nordsieck 2007, 2012a). It is distributed in Laos, Vietnam and southern China and consists of 26 known species (Nordsieck 2012a, 2012c, 2016; Grego et al. 2014; Lin and Lin 2022). Guangxi is the centre of diversity of the genus, with a total of 17 species recorded (Nordsieck 2012a, 2012c, 2016; Lin and Lin 2022). Most of these species were described in recent years, indicating that the species diversity has been poorly known in the past. Currently, the taxonomy of genus *Grandinenia* mainly rely on shell morphology, only two out of 26 species have been sequenced, but without detailed molecular phylogenetic studies.

In this study, we conducted the molecular phylogenetic analysis of genus *Grandinenia*, based on partial *COI* and *16S* sequences and described a new species with a peculiar morphology from Guangxi, southern China. The discovery of this new taxon further increases the species diversity of land snails in Chinese karst landforms.

Materials and methods

Samples were collected from Guangxi and Guangdong, China from 2022 to 2023. Living specimens were initially frozen at -20 °C for 12 hours and subsequently thawed at room temperature for 12 hours to extract the soft parts. The soft parts were then fixed in 70% ethanol. Empty shells were cleaned, dried and preserved at 4 °C. All specimens were deposited in the School of Life Sciences, Nanchang University (Nanchang, Jiangxi, China). Photographs were taken by a Sony® Alpha a6500 Digital Camera and edited in Adobe Photoshop CC 2015 (Adobe, San Jose, US). Maps were made in ArcGIS Pro (Esri, Redlands, US).

Genomic DNA was extracted from foot tissues preserved in 70% ethanol using a TIANamp Marine Animals DNA Kit (Tiangen Biotech, China). The quality and concentration of the DNA were checked on 1% agarose gel electrophoresis and NanoDrop 2000 (Thermo Scientific, USA). Partial cytochrome c oxidase subunit 1 (*COI*) and partial 16S ribosomal RNA (*16S*) gene segments were amplified and sequenced for molecular phylogenetic analyses. Polymerase chain reaction (PCR) systems, conditions and primer pairs are listed in Table 1. Sequences were aligned using MEGA v. 6.0 (Tamura et al. 2013) and checked manually. The accession numbers of newly-obtained sequences and other species are given in Table 2.

Phylogenies were reconstructed by the dataset combined *COI* and *16S* genes using Maximum Likelihood (ML) and Bayesian Inference (BI). Five clausiliid species were used as outgroups for rooting the tree. ML analyses were performed in IQ-TREE v. 1.6.12 (Minh et al. 2013) using the Ultrafast fast bootstrap approach (Minh et al. 2013) with 10000 reiterations. The most appropriate model of sequence evolution (GTR+I+G for *COI*, GTR+G for *16S*) was selected under PartitonFinder2 v. 1.1 (Robert et al. 2017). Bayesian Inference (BI) was conducted in MrBayes v. 3.2.6 (Ronquist et al. 2012). The most appropriate model of sequence evolution (GTR+I+G) was selected under ModelFinder (Subha et al. 2017). Four simultaneous runs with four independent Markov Chain Monte Carlo (MCMC) were implemented for 10 million generations and trees were sampled every 1000 generations with a burn-in of 25%. The convergence was checked with the average standard deviation of split frequencies < 0.01 and the potential scale reduction factor (PSRF) ~ 1. Trees were visualised in FigTree v.1.4.3.

Abbreviations

NCU_XPWU Laboratory of Xiao-Ping Wu, Nanchang University (Nanchang, Jiangxi, China); **cp** clausilium plate; **il** inferior lamella; **lu** lunella; **pp** principal plica; **sc** subcolumellar lamella; **sl** superior lamella; **sp** spiral lamella; **At** atrium; **BC** bursa copulatrix; **BCD** bursa copulatrix duct; **D** diverticulum; **Ep** epiphallus; **FO** free oviduct; **P** penis; **PC** penial caecum; **PR** penial retractor muscle; **V** vagina; **VD** vas deferens.

Results

Phylogenetic analyses

A dataset consisting of 39 *COI* and 42 *16S* sequences from 11 species of *Grandinenia*, along with five outgroup taxa, was employed for phylogenetic analyses (Table 2). The aligned lengths of *COI* and *16S* genes were 669 and 484 nucleotides. Within these sequences, 236 and 233 were revealed as variable sites, while 232 and 229 were designated as parsimony informative sites. Phylogenetic analyses generated ML and BI trees with congruent topologies (Fig. 1). Genus *Grandinenia* forms a monophyly and further clustered into 12 dis-

Table 1. Primer pairs and PCR conditions used in the analyses of the *COI* and *16S* rRNA genes of Grandinenia.

Genes	Primer pairs	Reaction systems	Cycling conditions	Reference
COI	LCO1490: GGTCAACAAATCATAAAGATATTGG HCO2198: TAAACTTCAGGGTGACCAAAAAATCA	12.5 µl 2 × Taq Plus Master Mix II (Vazyme, Nanjing, China), 1 µl template DNA, 1 µl of each pair of primers, 9.5 µl ddH_2O	94 °C: 2 min; 94 °C: 10 s, 50 °C: 60 s, 72 °C: 1 min, 35 cycles; 72 °C: 10 min	Folmer et al. (1994)
16S	16SA: CGGCCGCCTGTTTATCAAAAACAT 16SB: GGAGCTCCGGTTTGAACTCAGATC	12.5 µl 2 × Taq Plus Master Mix II (Vazyme, Nanjing, China), 1 µl template DNA, 1 µl of each pair of primers, 9.5 µl ddH_2O	94 °C: 2 min; 94 °C: 10 s, 50 °C: 60 s, 72 °C: 1 min, 35 cycles; 72 °C: 10 min	Páll-Gergely et al. (2019)

Table 2. GenBank accession numbers of the sequences for this study.

Species	Locality	CO1	16S	References
Grandinenia mirifica	Lianggu, Qintang, Guigang, Guangxi, China (type locality), 23°19'1"N, 109°14'34"E	PP473344	PP472576	This study
		PP473345	PP472577	This study
		PP473346	PP472578	This study
		PP473347	PP472579	This study
G. jiangjilini sp. nov.	Yao mountain, Binyang, Nanning, Guangxi, China, 23°26'12"N, 108°51'49"E	PP473375	PP472607	This study
		PP473376	PP472608	This study
		PP473377	PP472609	This study
		PP473378	PP472610	This study
		PP473379	PP472611	This study
		PP473380	PP472612	This study
		PP473381	PP472613	This study
		PP473382	PP472614	This study
		PP473383	PP472615	This study
		PP473384	PP472616	This study
G. ookuboi pulchricosta	Shanglin, Nanning, Guangxi, China, 23°27'9"N, 108°45'52"E	PP473369	PP472601	This study
		PP473370	PP472602	This study
		PP473371	PP472603	This study
G. rex	Chenghuang, Xingye, Yulin, Guangxi, China (type locality), 22°36'36"N, 109°46'19"E	PP473366	PP472598	This study
		PP473367	PP472599	This study
		PP473368	PP472600	This study
G. cf. *rutila*	Binyang, Nanning, Guangxi, China, 23°12'14"N, 109°8'16"E	PP473361	PP472593	This study
		PP473362	PP472594	This study
G. fuchsi	Guilin, Guangxi, China, 25°18'35"N, 110°16'19"E	PP473351	PP472583	This study
		PP473352	PP472584	This study
		PP473353	PP472585	This study
G. gastrum gastrum	Lianggu, Qintang, Guigang, Guangxi, China (type locality), 23°18'51"N, 109°15'49"E	PP473348	PP472580	This study
		PP473349	PP472581	This study
		PP473350	PP472582	This study
G. gastrum laticosta	Qintang, Guigang, Guangxi, China, 23°18'55"N, 109°16'30"E	PP473354	PP472586	This study
		PP473355	PP472587	This study
		PP473356	PP472588	This study
G. ignea	Zhongshan, Hezhou, Guangxi, China (type locality), 24°27'48"N, 111°10'35"E,		PP472617	This study
			PP472618	This study
			PP472619	This study
G. magnilabris	Guzhai, Mashan, Nanning, Guangxi China (type locality), 23°41'7"N, 108°19'11"E	PP473363	PP472595	This study
		PP473364	PP472596	This study
		PP473365	PP472597	This study
G. sp. 1	Shanglin, Nanning, Guangxi, China, 23°26'42"N, 108°44'33"E	PP473372	PP472604	This study
		PP473373	PP472605	This study
		PP473374	PP472606	This study
G. sp. 2	Menggong, Qintang, Guigang, Guangxi, China, 23°10'52"N, 109°22'11"E	PP473357	PP472589	This study
		PP473358	PP472590	This study
Tropidauchenia yanghaoi	Huaiji, Zhaoqing, Guangxi, China (type locality), 23°55'18"N, 112°9'59"E		PP472620	This study
			PP472621	This study
			PP472622	This study
T. orientalis	Chongzuo, Guangxi, China, 22°16'29"N, 107°4'14"E	PP473359	PP472591	This study
		PP473360	PP472592	This study
Agathylla goldi	Europe	KC756080	KF601271	Fehér et al. (2013b), Parmakelis et al. (2013)
Alopia mariae	Europe	JQ911821		Fehér et al. (2013a)
Isabellaria praestans	Europe	AY425575		Uit de Weerd et al. (2004)

tinct lineages. The phylogenetic relationships did not reflect a significant geographical correlation. *Grandinenia magnilabris* Nordsieck, 2012 from the middle northern Guangxi is the earliest diverging lineage. *Grandinenia jiangjilini* sp. nov. formed a distinct lineage, but its relationship within the genus was not well resolved (bootstrap supports = 55, posterior probabilities = 0.88). The genetic distances of *COI* sequences between *Grandinenia jiangjilini* sp. nov. and other congeneric species ranged from 9.1% to 19.3% (Table 3).

Taxonomy

Family Clausiliidae Gray, 1855
Subfamily Garnieriinae Boettger, 1926

Genus *Grandinenia* Minato & Chen, 1984

Type species. *Steatonenia mirifica* Chen & Gao, 1982, by original designation.

Table 3. Genetic distances of COI sequences computed by MEGA 6 of *Grandinenia*.

	1	2	3	4	5	6	7	8	9	10	11
1 *Grandinenia mirifica*	**0.006**										
2 *G. jiangjilini* sp. nov.	0.106	**0.001**									
3 *G. ookuboi pulchricosta*	0.103	0.100	**0**								
4 *G. rex*	0.097	0.091	0.087	**0.001**							
5 *G.* cf. *rutila*	0.116	0.101	0.083	0.079	**0.001**						
6 *G. fuchsi*	0.119	0.120	0.125	0.115	0.131	**0.003**					
7 *G. gastrum gastrum*	0.055	0.119	0.121	0.102	0.132	0.122	**0.003**				
8 *G. gastrum laticosta*	0.063	0.127	0.131	0.119	0.135	0.124	0.036	**0.004**			
9 *G. magnilabris*	0.198	0.193	0.212	0.183	0.207	0.216	0.207	0.209	**0.005**		
10 *G.* sp. 1	0.097	0.100	0.016	0.083	0.088	0.124	0.118	0.128	0.206	**0.001**	
11 *G.* sp. 2	0.118	0.142	0.130	0.115	0.130	0.145	0.127	0.145	0.200	0.130	**0.001**

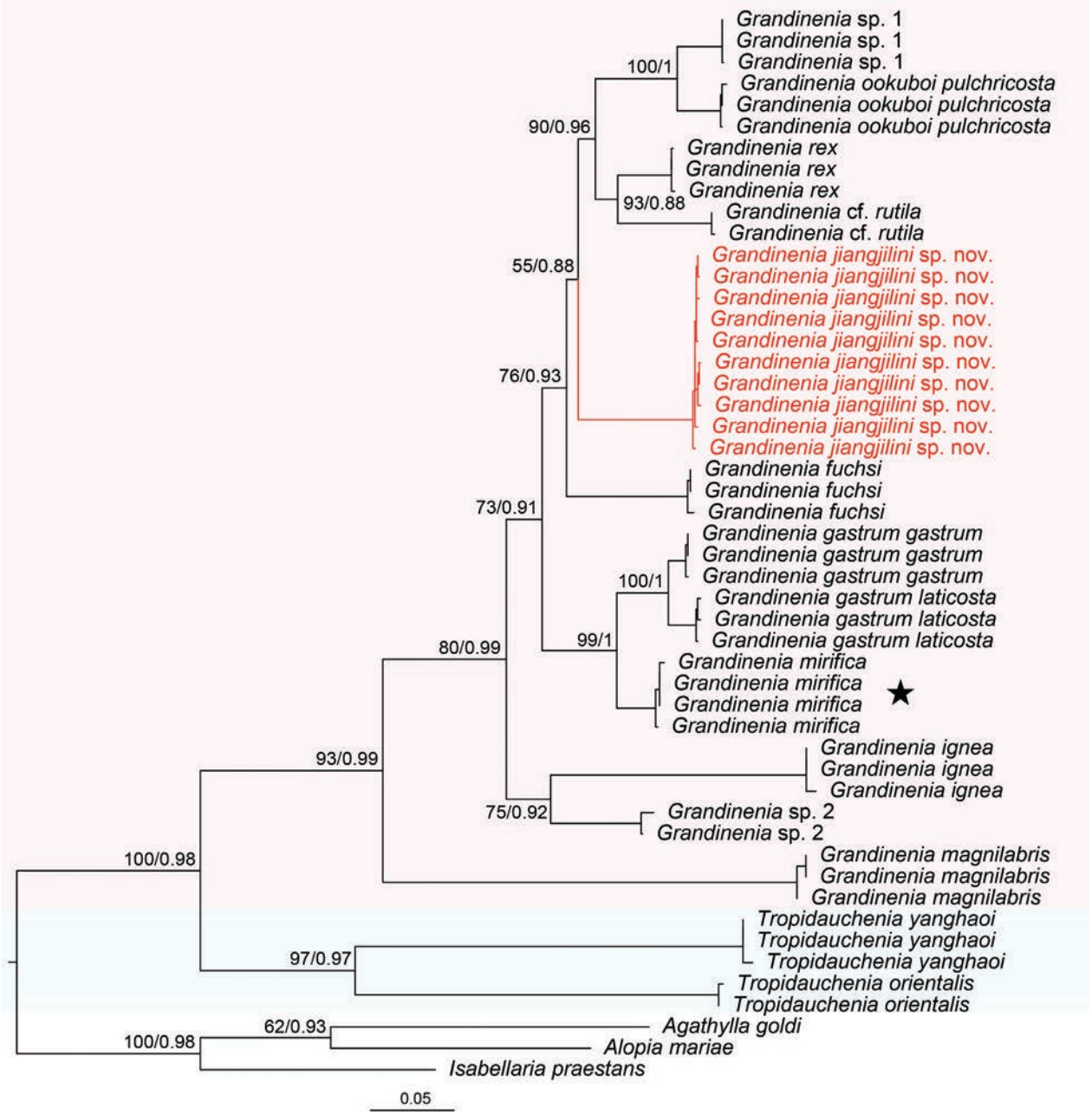

Figure 1. Maximum Likelihood tree and Bayesian Inference tree inferred from *COI* and *16S* gene sequences. Bootstrap supports/posterior probabilities are shown on the left/right of nodes. Star shows the type species of the genus.

***Grandinenia jiangjilini* Chen, Lin, Wu & Ouyang, sp. nov.**

https://zoobank.org/B234FD40-DDE4-4301-8724-E8FB819FCB81

Figs 2A, 3, 4A, B

Type material. *Holotype*. 23_NCU_XPWU_YG01, Yao Mountain [瑶山], Binyang County [宾阳县], Nanning City [南宁市], Guangxi Zhuang Autonomous Region [广西壮族自治区], China, 23°26'12"N, 108°51'49"E, leg. Zhong-Guang Chen, Ji-Lin Jiang & Guang-Long Xie, September 2023.

***Paratypes*.** 49 specimens, 23_NCU_XPWU_YG02–50, other information same as holotype.

Different diagnosis. Shell entire (vs. decollated in *G. ardouiniana* (Heude, 1885), *G. gabijakabi* Grego & Szekeres, 2014, *G. gastrum* (Nordsieck, 2005), *G. mirifica* (Chen & Gao, 1982), *G. pallidissima* Nordsieck, 2010, *G. pseudofuchsi* (Nordsieck, 2005), *G. rex* Nordsieck, 2007, *G. rutila* Nordsieck, 2016, *G. schomburgi* (Schmacker & Boettger, 1890), *G. takagii* (Chang, 2004), *G. umbra* (Chang, 2004)), hardly decollated, inflated-fusiform (vs. slender-fusiform in all other congeners, except *G. mirifica*), light yellowish-brown, semitranslucent; teleoconch with broad, blunt and sparse wrinkles (ribs) (vs. without or with thin and dense ribs in all other congeners); peristome not reflected; inferior lamella lower in front than within; penial caecum present (vs. absent in *G. fuchsi* (Gredler, 1883), *G. pseudofuchsi*, *G. takagii* and *G. mirifica*).

Description. Shell (Figs 2A, 3A, B, 4A, B) (n = 50). Entire, with 8.75–9.5 whorls, hardly decollated,

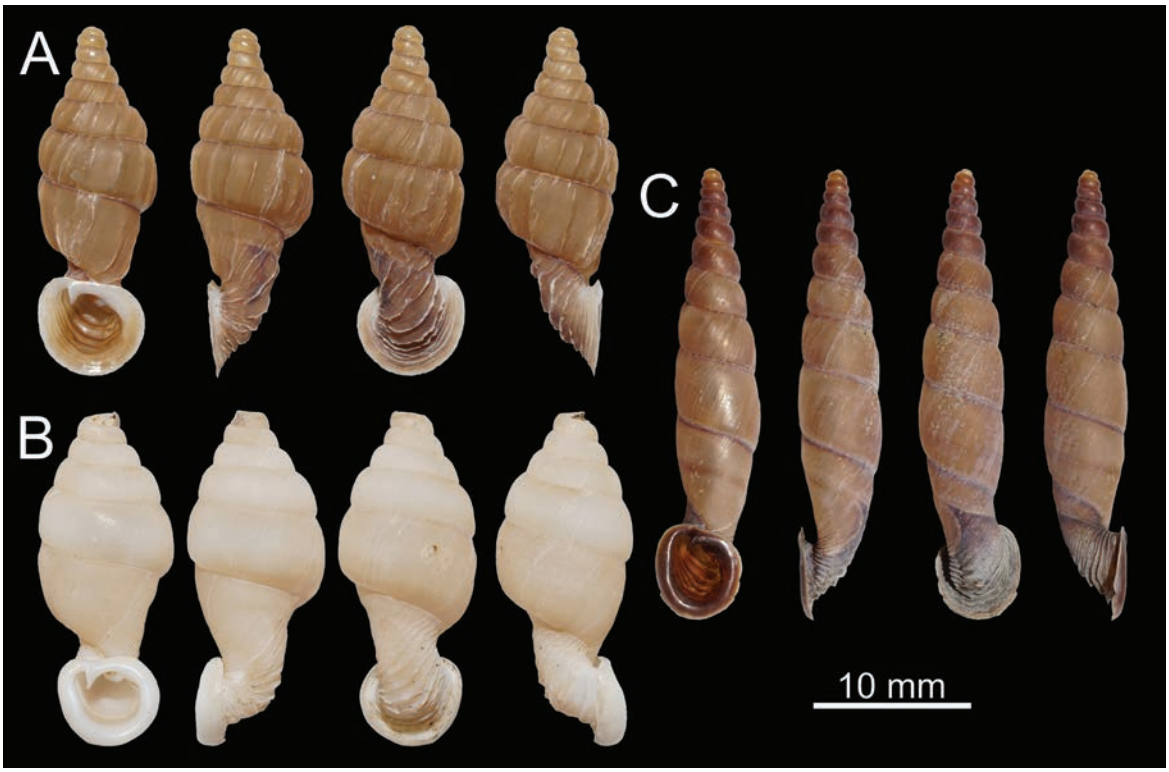

Figure 2. *Grandinenia jiangjilini* sp. nov. and two congeners. **A.** *Grandinenia jiangjilini* sp. nov., holotype (23_NCU_XPWU_YG01); **B.** *G. mirifica*; **C.** *G. ignea*.

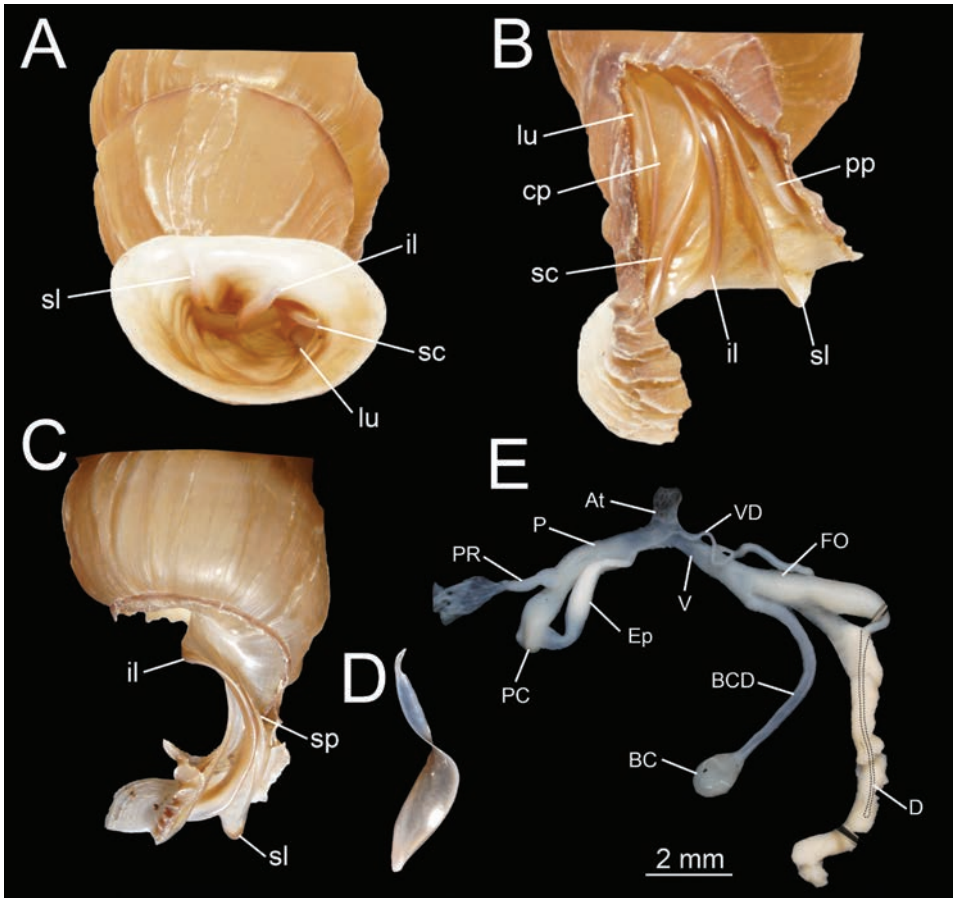

Figure 3. Detailed morphology of *Grandinenia jiangjilini* sp. nov. **A–C.** Shell morphology; **D.** Clausilium plate; **E.** Genital anatomy. Abbreviations: cp clausilium plate; il inferior lamella; lu lunella; pp principal plica; sc subcolumellar lamella; sl superior lamella; sp spiral lamella; At atrium; BC bursa copulatrix; BCD bursa copulatrix duct; D diverticulum; Ep epiphallus; FO free oviduct; P penis; PC penial caecum; PR penial retractor muscle; V vagina; VD vas deferens.

Figure 4. Living specimens of *Grandinenia*. **A, B.** *Grandinenia jiangjilini* sp. nov.; **C.** *G. gastrum*; **D.** *G. mirifica*.

inflated-fusiform, thin, fragile, semi-translucent, light yellowish-brown, with distinct darkish-red ribbon beneath the suture (fades quickly after fixing); dark seam along principal plica and lunella, body whorl in front of lunella darker; apical part conical to strongly attenuated. Suture deep. Protoconch smooth with 2.0–2.5 whorls. Wrinkles (ribs) on the teleoconch broad and blunt, most of them extending across the whole whorl, rather evenly distributed and widely spaced; on the neck, riblets white, thinner, stronger, more widely spaced and undulate. Aperture vastly extended, oval. Peristome expanded, not reflected. Superior lamella continuous with spiral lamella without a curve. Inferior lamella visible in front view of the aperture, steeply ascending, moderately low to high within, it ends deeper than the end of spiral lamella. Subcolumellar lamella strong, bent, visible or not in front view of the aperture, ending less deeply than the end of inferior lamella. Lunella vertical, in oblique view, partly visible through the aperture. Principal plica short, initiates ventrolaterally and extending laterally, not reaching peristome. Clausilium plate in oblique view nearly fully invisible, semi-translucent; overall slender; stalk thin; plate relatively broad.

Genitalia (Fig. 3C) (n = 10). Atrium short and relatively broad. Penis almost cylindrical and shortly narrower at transition to epiphallus. Penial caecum present. Epiphallus slender, shorter than penis and smaller diameter. Penial retractor relatively thick and short, inserted at the middle part of penis. Vas deferens relatively slender and short. Vagina thick, cylindrical, slightly longer than free oviduct. Basal part of diverticulum thick, rapid thinning to apical part and attached to spermoviduct. Spermoviduct thick and long. Pedunculus of bursa copulatrix slender and long. Bursa copulatrix large, oval.

Measurements. Holotype: shell height 24.5 mm, width 8.3 mm; aperture height 7.0 mm, width 7.7 mm. Paratypes: shell height 21.9–28.5 mm, width 7.4–8.4 mm; aperture height 5.9–7.3 mm, width 6.9–8.0 mm (n = 49).

Etymology. The species is named after Mr Ji-Lin Jiang who first discovered the new species and assisted in the field survey.

Vernacular name. 江氏斜管螺 (Pinyin: jiāng shì xié guǎn luó).

Distribution and ecology. *Grandinenia jiangjilini* sp. nov. is found from the Yao Mountain only (Figs 5–7). No other localities were found during the detailed survey conducted in 2022–2023 of the surrounding hills. It inhabits the vertical limestone cliff together with *Papilliphaedusa porphyrea* (Möllendorff, 1882) (Fig. 4A, B).

Discussion

The placement of the new species within *Grandinenia* is supported by both morphology (inferior lamella separated from superior lamella) and molecular phylogeny. The absence of a comprehensive description of the genitalia,

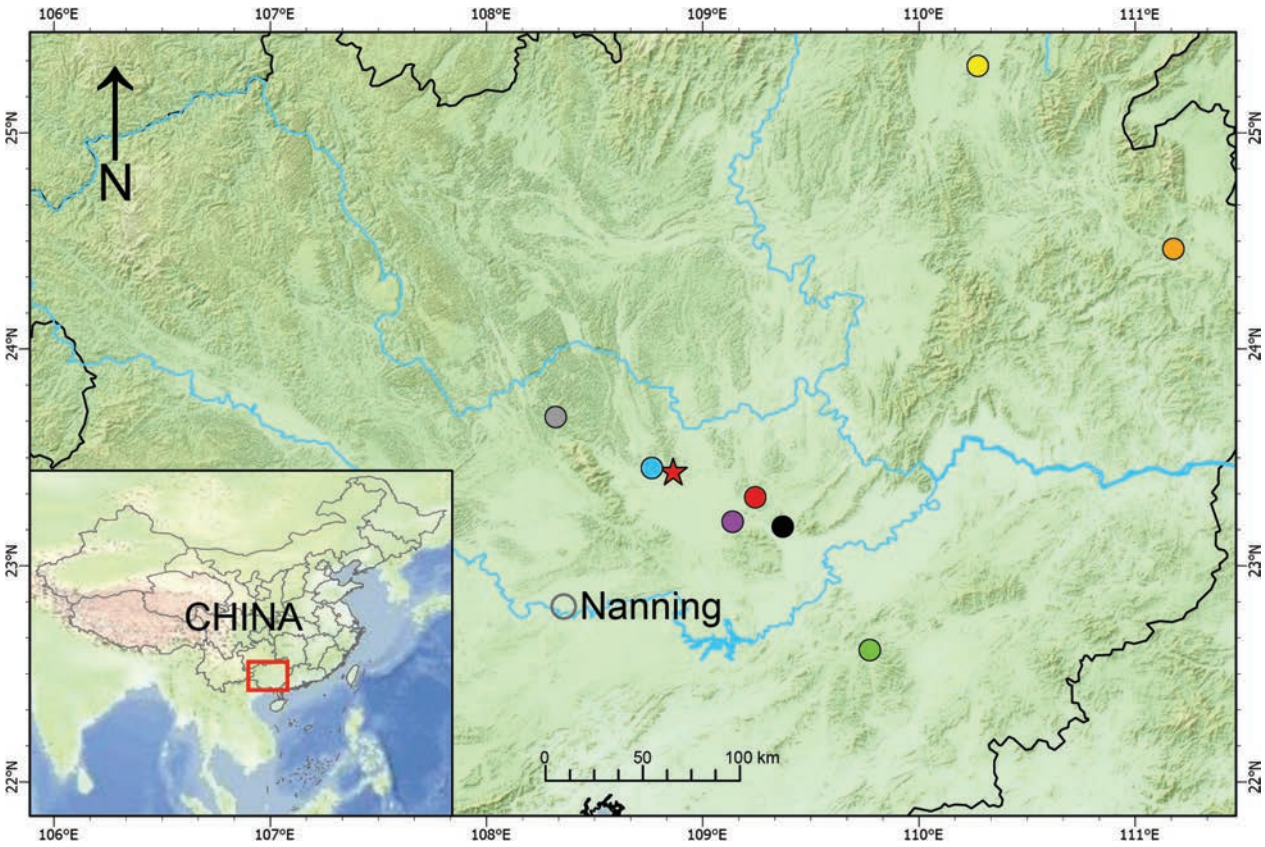

Figure 5. Sample localities of *Grandinenia* used in this study. **Star.** *Grandinenia jiangjilini* sp. nov.; **red point.** *G. mirifica*, *G. gastrum gastrum* and *G. gastrum laticosta*; **blue point.** *G. ookuboi pulchricosta* and *G.* sp. 1; **green point.** *G. rex*; **purple point.** *G.* cf. *rutila*; **yellow point.** *G. fuchsi*; **orange point.** *G. ignea*; **grey point.** *G. magnilabris*; **black point.** *G.* sp. 2.

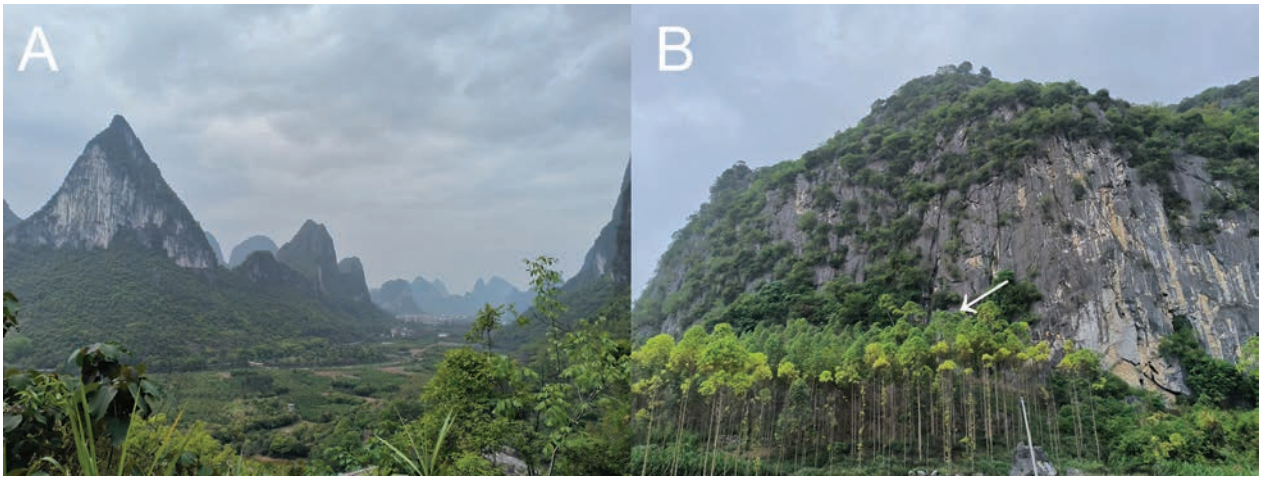

Figure 6. Sampling locality. **A.** Karst hills surrounding the type locality; **B.** Type locality of *Grandinenia jiangjilini* sp. nov. Arrow shows the sampling locality.

as well as the dearth of illustrations of lamellae and genitalia in the most original descriptions of *Grandinenia* species, precludes the possibility of detailed comparison of the new species with most other congeners for these two characters. The comparison of the shell morphology of the new species with that of eight congeners collected in this study revealed that the lamellae of them are highly similar. In contrast to *Tropidauchenia*, no variation in the fusion or separation of lamellae was identified between *Grandinenia* species. The new species is preliminarily distinguished from *G. fuchsi*, *G. pseudofuchsi*, *G. takagii* and *G. mirifica* by the presence of penial caecum. However, the shell appearance of the new species is sufficiently distinctive that it can be readily distinguished from all other congeners through a simple comparison. *Grandinenia jiangjilini* sp. nov. can be easily distinguished from all other congeners by the teleoconch with broad, blunt and sparse wrinkles (ribs) (vs. without or with thin and dense ribs).

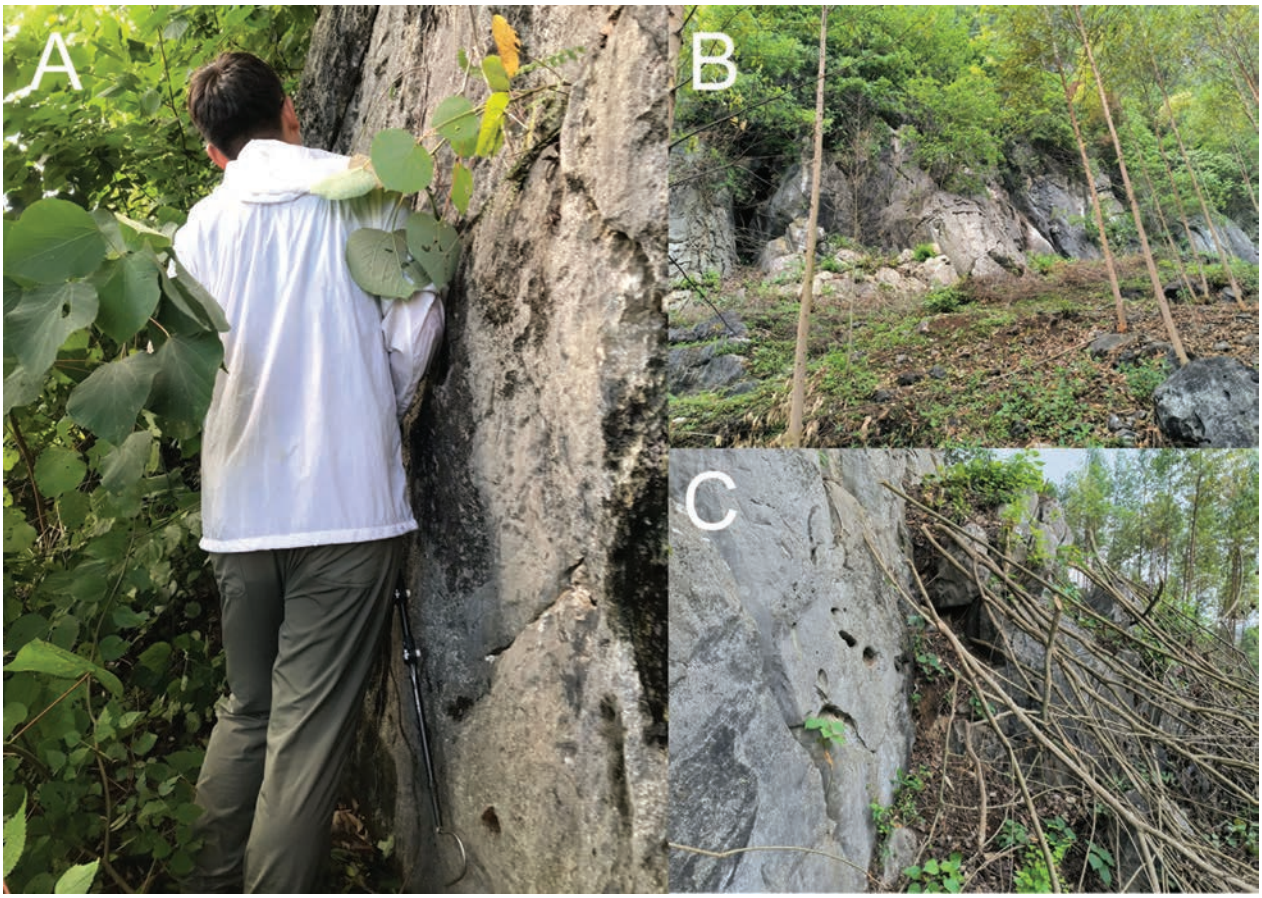

Figure 7. Comparison of type locality in 2023 and 2024. **A.** September 2023; **B, C.** April 2024.

Furthermore, except for *G. mirifica*, the remaining 25 species of *Grandinenia* exhibit a relatively slender shell (Fig. 2C). *Grandinenia jiangjilini* sp. nov. can be easily distinguished from them by the different shell shape (inflated-fusiform vs. slender-fusiform). *Grandinenia jiangjilini* sp. nov. is most similar to *G. mirifica* by similar inflated-fusiform shell (Fig. 2A, B), but differs by the broad and sparse wrinkles (ribs) on teleoconch (vs. thin and dense), peristome not reflected (vs. reflected), protoconch preserved (vs. decollated), shell semi-translucent and fragile (vs. opaque and solid) and the different shell colour (yellowish-brown vs. yellowish-white). *Grandinenia jiangjilini* sp. nov. is also somewhat similar to *G. dautzenbergi* (Morlet, 1892) and *G. yulinensis* Nordsieck, 2012, but differs by the more inflated shell, the stronger ribs on neck, the deeper suture, the thinner-walled and more fragile shell and the broad, blunt and sparse wrinkles (ribs) on teleoconch (vs. with very weak ribs to even smooth).

The validity of *Grandinenia jiangjilini* sp. nov. was also supported by the molecular phylogeny. It forms a distinct lineage and has a distant relationship with *G. mirifica*. The molecular phylogenetic relationships of genus *Grandinenia* do not correspond to the morphological similarities. The important characters of shell including shell shape, integrity, ribs, thickness and spiral ribbon, have homoplasiously evolved more than once. The species like *G. rex*, *G. fuchsi* and *G. ignea* with clearly similar smooth, thin, fragile and semi-translucent shells with spiral ribbons, do not form a monophyletic group. The same phenomenon also occurs in species with similar thick and ribbed shells. The result shows that the shell appearance of *Grandinenia* is an effective means of distinguishing species, but does not reflect the interspecies affinities. The phylogenetic relationship also did not demonstrate a clear geographical correlation overall. *Grandinenia magnilabris* from the middle northern Guangxi (the western-most distribution of the sampled species) is the earliest diverging lineage. *Grandinenia ignea* from north-eastern Guangxi sistered with *G.* sp. 2 from the central region. In addition, *G. fuchsi* from north-eastern Guangxi was sistered with the clade, which consists of four species from the central region and one from the south-eastern region. The distribution pattern may be attributed to multiple independent diffusions from west to east in history. Only two lineages exhibited a certain geographical correlation, *G.* sp. 1 and *G. ookuboi pulchricosta* from Shanglin and *G. mirifica*, *G. gastrum gastrum* and *G. gastrum laticosta* from Guigang, which formed monophyletic lineages, respectively. Due to the limited species included in this study, extensive and continuous sampling in future studies may help further analysis of the phylogeny and elucidation of the reasons for its distribution pattern formation.

The variation of shell morphology is frequently selected by environmental factors (Chiba 2004; Rolán-Alvarez 2007; Giokas et al. 2014). The shell characters of land snails play a pivotal role in regulating the water and

heat budget, thereby preventing desiccation (Cowie and Jones 1985; Pfenninger et al. 2005; Giokas et al. 2014). The discovery of the new species shows that the special inflated-fusiform shells are not isolated in genus *Grandinenia*. Phylogenetic result indicates that the new species and *G. mirifica* do not form a monophyletic group, suggesting that the similar shell shape between them may be the result of convergent evolution. Nordsieck (2012a) proposed that the inflated-fusiform shell of *G. mirifica* is an adaptation to a special habitat, but did not specify what this habitat is. For *Grandinenia*, it is probable that the inflated-fusiform shells have increased resistance to desiccation and ultraviolet radiation compared to the slender-fusiform shells, although the precise mechanism of action remains unclear. Through field observation, it was found that the two shell shapes of *Grandinenia* correspond to two life strategies. The majority of *Grandinenia* species with slender-fusiform shells burrow into crevices to hibernate during the dry season (Fig. 4C). It is challenging to find them during the dry season, but a considerable number of individuals can be observed during the rainy season in the same area. In contrast, the two species with inflated-fusiform shells primarily hibernate on rock surfaces which can be found throughout the year, regardless of precipitation patterns (Fig. 4A, B, D).

The discovery of new taxon or just new species indicates that the species diversity of *Grandinenia* in Guangxi still remains to be explored. Nine species of *Grandinenia* have been recoded within a few dozen kilometres of the new species' type locality (Nordsieck 2012a, 2012c, 2016; Lin and Lin 2022) and several specimens which may represent other undescribed species were found during the field survey. Extensive exploration of land snails in Guangxi should be strengthened in the future which may lead to the discovery of yet-to-be-described species. In addition, the protection of *Grandinenia* should be a priority. As a rock-dwelling land snail, the survival of *Grandinenia* depends on the exposed rock environment under the forest. Large-scale mining of limestone and agricultural reclamation in Guangxi pose a threat to it. It was even found that some peaks that used to be rich in *Grandinenia* have been completely blasted and disappeared. The field survey conducted in 2024 revealed that the native shrubs in the type locality of *Grandinenia jiangjilini* sp. nov. had been completely cut down (Fig. 7). This has resulted in the environment of the rock walls becoming more exposed and dry and has led to a significant reduction in the population size of *Grandinenia jiangjilini* sp. nov. It is imperative that further protection measures are implemented without delay, otherwise a significant number of unique species may be lost.

Acknowledgements

We thank Ji-Lin Jiang (Zhaoqing), Meng-Hua Li (Sichuan Agriculture University), Chen-Yu Fei (Guangzhou) and Shi-Yang Feng (Sichuan Agriculture University) for assistance in collecting specimens; Frank Köhler, Zhe-Yu Chen, Barna Páll-Gergely, Miklós Szekeres and Anna Sulikowska-Drozd for their valuable comments for the manuscript. This study was supported by the National Natural Science Foundation of China under Grant No.32360132, No.31772412, the research project of Zhejiang Natural History Museum under Grant No.2024001 and the Biodiversity Monitoring Project of Xixi National Wetland Park of Hangzhou.

References

Chiba S (2004) Ecological and morphological patterns in communities of land snails of the genus *Mandarina* from the Bonin Islands. Journal of Evolutionary Biology 17(1): 131–143. https://doi.org/10.1046/j.1420-9101.2004.00639.x

Cowie RH, Jones JS (1985) Climatic selection on body color in Cepaea. Heredity 55(2): 261–267. https://doi.org/10.1038/hdy.1985.100

Fehér Z, Németh L, Nicoară A, Szekeres M (2013a) Molecular phylogeny of the land snail genus *Alopia* (Gastropoda: Clausiliidae) reveals multiple inversions of chirality. Zoological Journal of the Linnean Society 167(2): 259–272. https://doi.org/10.1111/zoj.12002

Fehér Z, Parmakelis A, Koutalianou M, Mourikis T, Erőss ZP, Krízsik V (2013b) A contribution to the phylogeny of Albanian *Agathylla* (Gastropoda, Clausiliidae): Insights using morphological data and three mitochondrial markers. The Journal of Molluscan Studies 80(1): 24–34. https://doi.org/10.1093/mollus/eyt039

Folmer O, Black M, Hoeh W, Lutz R, Vrijenhoek R (1994) DNA primers for amplification of mitochondrial cytochrome c oxidase subunit I from diverse metazoan invertebrates. Molecular Marine Biology and Biotechnology 3: 294–299.

Giokas S, Páll-Gergely B, Mettouris O (2014) Nonrandom variation of morphological traits across environmental gradients in a land snail. Evolutionary Ecology 28(2): 323–340. https://doi.org/10.1007/s10682-013-9676-5

Grego J, Van Luong H, Van Pham S, Szekeres M (2014) Vietnamese clausiliidae (Gasropoda: Pulmonata): New taxa and novel distribution data. Journal of Conchology 41(6): 749–757.

Lin LW, Lin RX (2022) A review of subfamily Garnieriinae C. R. Boettger, 1926. [in Chinese] https://mp.weixin.qq.com/s?__biz=MzU2MzAyMTI2Mg==&mid=2247484089&idx=1&sn=202e28f8d489c9c3e7b92fb713ea0ce9&chksm=fc61d618cb165f0efad99983465336918e4a3124bfd14c2cd163061c745415e79f8d118eedea&mpshare=1&scene=23&srcid=03128t81MCrf5aG9Gl20jfjn&sharer_shareinfo=fd8f3a4ab07b45a317b71d8a05a3f78b&sharer_shareinfo_first=fd8f3a4ab07b45a317b71d8a05a3f78b#rd [access on April 21, 2024]

Mamos T, Uit de Weerd DR, von Oheimb PV, Sulikowska-Drozd A (2021) Evolution of reproductive strategies in the species-rich land snail subfamily Phaedusinae (Stylommatophora: Clausiliidae). Molecular Phylogenetics and Evolution 158: 107060. https://doi.org/10.1016/j.ympev.2020.107060

Minh BQ, Nguyen MAT, von Haeseler A (2013) Ultrafast approximation for phylogenetic bootstrap. Molecular Biology and Evolution 30(5): 1188–1195. https://doi.org/10.1093/molbev/mst024

Nordsieck H (2007) Worldwide Door Snails (Clausiliidae), recent and fossil. ConchBooks, Germany, 214 pp.

Nordsieck H (2012a) Clausiliidae of Guangxi, southern China (Gastropoda, Pulmonata, Stylommatophora). Acta Conchyliorum 12: 3–56.

Nordsieck H (2012b) Note on Garnieriini (Gastropoda, Stylommatophora, Clausiliidae, Garnieriinae). Acta Conchyliorum 12: 57–62.

Nordsieck H (2012c) Check-list of the Clausiliidae of mainland China (Gastropoda, Stylommatophora). Acta Conchyliorum 12: 63–73.

Nordsieck H (2016) New species taxa of Clausiliidae (Gastropoda, Stylommatophora) from China and Vietnam. Conchylia 47: 37–57.

Páll-Gergely B, Hunyadi A, Chen ZY, Lyu ZT (2019) A review of the genus *Coccoglypta* Pilsbry, 1895 (Gastropoda: Pulmonata: Camaenidae). Zoosystema 41(29): 595–608. https://doi.org/10.5252/zoosystema2019v41a29

Parmakelis A, Kotsakiozi P, Rand DM (2013) Animal Mitochondria, Positive Selection and Cyto-Nuclear Coevolution: Insights from Pulmonates. PLOS ONE 8(4): e61970. https://doi.org/10.1371/journal.pone.0061970

Pfenninger M, Hrabakova M, Steinke D, Depraz A (2005) Why do snails have hairs? A Bayesian inference of character evolution. BMC Evolutionary Biology 5(1): 59. https://doi.org/10.1186/1471-2148-5-59

Robert L, Paul BF, April MW, Tereza S, Brett C (2017) Partitionfinder 2: New methods for selecting partitioned models of evolution for molecular and morphological phylogenetic analyses. Molecular Biology and Evolution 34: 772–773. https://doi.org/10.1093/molbev/msw260

Rolán-Alvarez E (2007) Sympatric speciation as a by-product of ecological adaptation in the Galicia *Littorina saxatilis* hybrid zone. The Journal of Molluscan Studies 73(1): 1–10. https://doi.org/10.1093/mollus/eyl023

Ronquist F, Teslenko M, van der Mark P, Ayres DL, Darling A, Höhna S, Larget B, Liu L, Suchard MA, Huelsenbeck J (2012) Mrbayes 3.2: Efficient bayesian phylogenetic inference and model choice across a large model space. Systematic Biology 61(3): 539–542. https://doi.org/10.1093/sysbio/sys029

Subha K, Bui Quang M, Wong TKF (2017) Modelfinder: Fast model selection for accurate phylogenetic estimates. Nature Methods 14(6): 587–589. https://doi.org/10.1038/nmeth.4285

Tamura K, Stecher G, Peterson D, Filipski A, Kumar S (2013) MEGA6: Molecular evolutionary genetics analysis version 6.0. Molecular Biology and Evolution 30(12): 2725–2729. https://doi.org/10.1093/molbev/mst197

Uit de Weerd DR, Gittenberger E (2013) Phylogeny of the land snail family Clausiliidae (Gastropoda: Pulmonata). Molecular Phylogenetics and Evolution 67(1): 201–216. https://doi.org/10.1016/j.ympev.2013.01.011

Uit de Weerd DR, Piel WH, Gittenberger E (2004) Widespread polyphyly among Alopiinae snail genera: When phylogeny mirrors biogeography more closely than morphology. Molecular Phylogenetics and Evolution 33(3): 533–548. https://doi.org/10.1016/j.ympev.2004.07.010

Uit de Weerd DR, Gittenberger E, Mamos T, Sulikowska-Drozd A (2023) The phylogenetic position of *Synprosphyma* A.J. Wagner, 1920 within Clausiliidae: Biogeographic and taxonomic implications. Archiv für Molluskenkunde 152(2): 257–267. https://doi.org/10.1127/arch.moll/152/257-267

Zoosyst. Evol. 100 (3) 2024, 923–939 | DOI 10.3897/zse.100.116350

PENSOFT

für Natur MUSEUM FÜR NATURKUNDE BERLIN

A new glassfrog of the genus *Centrolene* (Amphibia, Centrolenidae) from the Subandean Kutukú Cordillera, eastern Ecuador

Santiago R. Ron[1], Dominike García[1], David Brito-Zapata[2], Carolina Reyes-Puig[2,3], Elías Figueroa-Coronel[2], Diego F. Cisneros-Heredia[2,3]

1 *Pontificia Universidad Católica del Ecuador, Escuela de Biología, Museo de Zoología, Quito, Ecuador*

2 *Universidad San Francisco de Quito USFQ, Colegio de Ciencias Biológicas y Ambientales, Instituto de Biodiversidad Tropical IBIOTROP, Laboratorio de Zoología Terrestre, Museo de Zoología, Quito 170901, Ecuador*

3 *Instituto Nacional de Biodiversidad, Quito, Ecuador*

https://zoobank.org/E07EDFEB-3798-490F-B676-C912AE951C92

Corresponding author: Diego F. Cisneros-Heredia (diego.cisnerosheredia@gmail.com)

Academic editor: Pedro Taucce ♦ **Received** 27 November 2023 ♦ **Accepted** 1 May 2024 ♦ **Published** 8 July 2024

Abstract

We describe a new species of *Centrolene* from the Subandean Cordillera of Kutukú in southeastern Ecuador. The new species differs from all other glassfrogs by the combination of the following characters: presence of processes of vomers but without vomerine teeth; humeral spines in males; dorsum green with light green dots and without dark marks; dorsal skin with abundant tubercles; all visceral peritonea translucent (except for pericardium); and small body size (snout-vent length 21.5–21.9 mm in adult males). The new species is sister to *Centrolene camposi* from the Western Cordillera of the Andes of southwestern Ecuador, and together they form a clade with *C. condor* from the Subandean Cóndor Cordillera in southeastern Ecuador. Our time tree suggests that the new species originated at the end of the Pliocene. In addition, we present new information for *C. zarza*, expanding its geographic range across the southeastern Andes and the Kutukú and Cóndor cordilleras, amending its definition and diagnosis, and offering new information on its natural history and extinction risk. We also discuss the taxonomic status of Ecuadorian populations reported as *C. huilensis* and conclude that they are *C. muelleri* based on their close phylogenetic relationships and morphological similarity to samples of *C. muelleri* from Peru. *Centrolene huilensis* is a valid species and not closely related to *C. muelleri*.

Resumen

Describimos una nueva especie de *Centrolene* de la cordillera subandina de Kutukú en el sureste de Ecuador. La nueva especie difiere de todas las demás ranas de cristal por la combinación de los siguientes caracteres: presencia de procesos vomerinos pero sin dientes vomerinos, espinas humerales en los machos, dorso verde con puntos verdes claros y sin marcas oscuras, piel dorsal con abundantes tubérculos, todos los peritoneos viscerales traslúcidos (excepto el pericardio) y un tamaño corporal pequeño (longitud rostro-cloacal de 21.5–21.9 mm en machos adultos). La nueva especie es hermana de *Centrolene camposi* de la Cordillera Occidental de los Andes del suroeste de Ecuador y juntas forman un clado con *C. condor* de la cordillera subandina del Cóndor en el sureste de Ecuador. Nuestro árbol de tiempo sugiere que la nueva especie se originó a finales del Plioceno. Adicionalmente, presentamos nueva información para *C. zarza*, expandiendo su rango geográfico a lo largo de los Andes del sureste y las cordilleras de Kutukú y Cóndor, modificando su definición y diagnóstico, y ofreciendo nueva información sobre su historia natural y riesgo de extinción. También discutimos el estado taxonómico de las poblaciones ecuatorianas reportadas como *C. huilensis* y concluimos que son *C. muelleri*, basados en sus estrechas relaciones filogenéticas y similitud morfológica con muestras de *C. muelleri* de Perú. *Centrolene huilensis* es una especie válida y no cercanamente relacionada con *C. muelleri*.

Key Words

Andes, Anura, *Centrolene kutuku* sp. nov., *Centrolene huilensis*, *Centrolene muelleri*, *Centrolene zarza*, Cóndor Cordillera, Kutukú Cordillera, new species, phylogenetic relationships, taxonomy

Palabras clave

Andes, Anura, *Centrolene kutuku* sp. nov., *Centrolene huilensis*, *Centrolene muelleri*, *Centrolene zarza*, Cordillera del Cóndor, Cordillera del Kutukú, nueva especie, relaciones filogenéticas, taxonomía

Introduction

The genus *Centrolene* Jiménez de la Espada, 1872 currently contains 33 described species of glassfrogs distributed across the Andes from Venezuela to Peru (AmphibiaWeb 2023; Cisneros-Heredia et al. 2023; Frost 2023). Frogs of the genus *Centrolene* are characterised by having humeral spines present in adult males (except *C. daidalea* Ruiz-Carranza & Lynch, 1991b, *C. savagei* Ruiz-Carranza & Lynch, 1991b, and *C. solitaria* Ruiz-Carranza & Lynch, 1991b), liver lobed and covered by a translucent hepatic peritoneum, ventral parietal peritoneum partially covered by iridophores, pericloacal warts enamelled, bones green in life, dorsal background lavender in preservative, and males with dorsal spicules during breeding season (Cisneros-Heredia and McDiarmid 2007; Guayasamin et al. 2009, 2020; Cisneros-Heredia et al. 2023). The monophyly of *Centrolene* has been supported by molecular evidence (Guayasamin et al. 2009; Twomey et al. 2014; Cisneros-Heredia et al. 2023), but the relationships of some species remain unexplored (Cisneros-Heredia and McDiarmid 2007; Guayasamin et al. 2020; Cisneros-Heredia et al. 2023).

Thirteen species of *Centrolene* are known in the Republic of Ecuador, all living in the Andes and adjacent Subandean Cordilleras (Lynch and Duellman 1973; Cisneros-Heredia and McDiarmid 2005, 2007; Guayasamin et al. 2006, 2020; Cisneros-Heredia 2007; Cisneros-Heredia and Yánez-Muñoz 2007; Cisneros-Heredia and Morales-Mite 2008; Almendáriz and Batallas 2012; Cisneros-Heredia et al. 2023; Székely et al. 2023). Four species of *Centrolene* are known to inhabit the Cóndor Cordillera: *C. charapita* Twomey, Delia, and Castroviejo-Fisher, 2014; *C. condor* Cisneros-Heredia and Morales-Mite, 2008; *C. sanchezi* Ruiz-Carranza & Lynch, 1991a; and *C. zarza* Székely, Córdova-Díaz, Hualpa-Vega, Hualpa-Vega & Székely, 2023, with *C. condor* and *C. zarza* being considered endemic to that cordillera (Cisneros-Heredia and Morales-Mite 2008; Guayasamin et al. 2020; Székely et al. 2023). However, there are no records of *Centrolene* in the Kutukú Cordillera.

During surveys in southeastern Ecuador, we found a new species of *Centrolene* at the Kutukú Cordillera, which we are pleased to describe herein based on morphological and molecular evidence. We also report new Subandean and Andean localities for *Centrolene zarza*, a recently described species known from a single locality at the Cóndor Cordillera. In addition, we discuss the status of the Ecuadorian population ascribed to *Centrolene huilensis* Ruiz-Carranza & Lynch, 1995.

Materials and methods

Ethics statement

Our study was authorised under research permits N° MAE-DNB-ARRGG-CM-2014-0002 (issued to PUCE), 003-17 IC-FAU-DNB/MA (PUCE), 011-2018-IC-FAU-DNB/MA (PUCE), and 028-2018-IC-FLO-FAU-DPAZCH-UPN-VS/MA (ZSFQ) and framework contracts for access to genetic resources MAE-DNB-CM-2015-0025 (PUCE) and MAE-DNB-CM-2018-0106 (USFQ) issued by the Ministerio del Ambiente, Agua y Transición Ecológica del Ecuador. We followed the standard guidelines for using live amphibians and reptiles in field research by Beaupre et al. (2004).

Species concept

We consider species as separately evolving metapopulation lineages, recognisable from an operational point of view to the extent that isolation from their putative sister lineages can be inferred (De Queiroz 2007).

Taxonomic sampling

Specimens from the following collections were examined: División de Herpetología, Instituto Nacional de Biodiversidad, Quito (DHMECN); Instituto de Ciencias Naturales, Universidad Nacional de Colombia, Bogotá (ICN); University of Kansas Natural History Museum,

Lawrence (KU); Museum of Comparative Zoology, Harvard University, Cambridge, MA (MCZ); Museo de Zoología, Pontificia Universidad Católica del Ecuador, Quito (QCAZ); National Museum of Natural History, Smithsonian Institution, Washington, D.C. (USNM); Museo de Zoología, Universidad San Francisco de Quito, Quito (ZSFQ).

The following specimens were examined for the diagnosis (H and P between square brackets stand for holotype and paratype, respectively): ***Centrolene camposi*** (2 specimens): ECUADOR: province of Azuay: La Enramada (DHMECN 11407 [H], DHMECN 11408 [P]). ***C. condor*** (7 specimens): ECUADOR: province of Zamora Chinchipe: Destacamento Militar Cóndor Mirador (QCAZ 37279 [H]), Paquisha Alto (DHMECN 11208–11210), Concesión Colibrí (DHMECN 12049), Concesión La Zarza (DHMECN 12053); province of Morona-Santiago: near Reserva Biológica El Quimi (QCAZ 72514). ***C. pipilata*** (3 specimens): ECUADOR: province of Napo: 14.7 km NE Salado River (ICN 23756 [P], USNM 286717, MCZ A-97803). ***C. sanchezi*** (15 specimens): COLOMBIA: department of Cauca: Guanacas River (ICN 11685 [H], ICN 11686 [H, *C. guanacarum*]); department of Caquetá: 3.1 km por carretera abajo del Alto Gabinete (ICN 24293 [H]); ECUADOR: province of Napo: Yanayacu Biological Station (QCAZ 16212, 17807, 22386–87); province of Morona-Santiago: 11.2 km WSW Plan de Milagro (KU 202803 [H, *C. bacata*], KU 202804, 202807-12 [P, *C. bacata*]). ***C. zarza***: (13 specimens): ECUADOR: province of Zamora Chinchipe: El Zarza (MUTPL-A 1051, 1022 [P]); Los Encuentros, Relaves, 3.7555°S, 78.4998°W, 1470 m (ZSFQ 2361–2363; ZSFQ 2361 tissue sample was sequenced under QCAZ 78311); Concesión Minera Kinross-Aurelian, Los Encuentros, 3.8121°S, 78.6147°W, 1530 m (DHMECN 10223); province of Morona Santiago: Sardinayacu, Parque Nacional Sangay, 2.0938°S, 78.1688°W, 1685 m (QCAZ 58685–88, 59066); Puchimi, Kutukú Cordillera, 2.7834°S, 78.1444°W, 1840 m (QCAZ 69116–18). Additional specimens examined during our studies in Centrolenidae are listed in Cisneros-Heredia & McDiarmid (2007), Guayasamin et al. (2020), and Cisneros-Heredia et al. (2023).

Fieldwork

Fieldwork was conducted at the following localities in Ecuador: province of Morona Santiago: Sardinayacu, Parque Nacional Sangay (2.0938°S, 78.1688°W, 1685 m elevation) in January 2015; Kutukú Cordillera, Puchimi, parish of San Francisco de Chinimbimi (2.7834°S, 78,1444°W, 1840 m) in September 2017 and January 2018, at both localities by expeditions of the Museo de Zoología, Pontificia Universidad Católica del Ecuador; and at the province of Zamora-Chinchipe, Los Encuentros, Relaves (3.7555°S, 78.4498°W, 1470 m) in February 2019 by an expedition affiliated to the Museo de Zoología, Universidad San Francisco de Quito. Specimens were found during visual encounter surveys for herpetological searches. Individuals were photographed alive and euthanised with benzocaine; a muscle tissue sample was extracted and preserved in 95% ethanol; and whole specimens were fixed in 10% formalin and preserved in 75% ethanol.

Morphology and colouration

Diagnosis, terminology, characters, and measurements follow the format and definitions proposed by Cisneros-Heredia & McDiarmid (2007) and Kok & Castroviejo-Fisher (2008) for fringes and folds. All characteristics reported in the description of the type series are from adult specimens. Sex and maturity were determined by directly examining gonads through dissections and noting the presence of secondary sexual characters (i.e., vocal slits and nuptial pads). All morphometric data were measured with a digital calliper (0.05 mm accuracy, rounded to the nearest 0.1 mm) under a stereomicroscope, reported as range (mean ± standard deviation), and included snout-vent length (SVL), head length (HL), head width (HW), interorbital distance (IOD), eye diameter (ED), internarial distance (IND), eye-nostril distance (EN), tympanum diameter (TD), tibia length (TL), foot length (FL), hand length (HAL), and Finger III disk width (F3DW). Digital X-ray images were obtained with the Thermo Kevex X-ray Imaging System at the QCAZ museum. Colour patterns are described based on photographs of live specimens taken in the field. The adjective "enamelled" describes the shiny white colouration produced by an accumulation of iridophores (Lynch and Duellman 1973; Cisneros-Heredia and McDiarmid 2007). Our species descriptions follow the recommendation by Vences (2020) to speed up species inventories by emphasising diagnosis over descriptions and images over words. To streamline the description of the new species, we present high-quality colour photographs of all relevant specimens instead of verbal descriptions, which have an inherently subjective component.

Phylogenetic analyses and genetic distances

We obtained DNA sequences for nuclear and mitochondrial genes to assess the phylogenetic relationships of the new species and additional populations of *C. zarza* within the genus *Centrolene*. DNA was extracted from muscle or liver tissue preserved in 95% ethanol or tissue storage buffer using standard phenol-chloroform extraction protocols (Sambrook et al. 1989). We used a polymerase chain reaction (PCR) to amplify DNA fragments for the mitochondrial genes 12S rRNA (12S), two overlapping fragments for the last ~320 bp of 16S rRNA (16S), NADH

dehydrogenase subunit 1 (ND1) and adjacent tRNAs ($tRNA^{Leu}$, $tRNA^{Ile}$, and $tRNA^{Gln}$), and the nuclear genes RAG1 and C-MYC 2. PCR amplification was performed under standard protocols and sequenced by the Macrogen Sequencing Team (Macrogen Inc., Seoul, Korea).

Our phylogeny also includes sequences from GenBank (Guayasamin et al. 2008, 2020; Castroviejo-Fisher et al. 2014; Twomey et al. 2014; Mendoza-Henao et al. 2023; Cisneros-Heredia et al. 2023). We obtained all available Genbank sequences of *Centrolene* and its sister clade, *Nymphargus*. We also included representative samples of *Allophryne*, *Celsiella*, *Chimerella*, *Cochranella*, *Espadarana*, *Hyalinobatrachium*, *Ikakogi*, *Rulyrana*, *Sachatamia*, *Teratohyla*, and *Vitreorana*. The phylogeny was rooted in *Allophryne ruthveni* (specimen MAD1857; outgroup choice based on Guayasamin et al. (2008, 2020) and Castroviejo-Fisher et al. (2014). Sample information for GenBank sequences is listed in the literature (Guayasamin et al. 2008; Castroviejo-Fisher et al. 2014; Mendoza-Henao et al. 2023; Cisneros-Heredia et al. 2023). GenBank accession numbers for newly generated sequences are listed in Table 1.

Table 1. Genbank accession numbers for DNA sequences included in the phylogenetic analysis.

Museum No.	Species	Genbank Accession No.				
		12S	16S	ND1	RAG1	C-MYC2
QCAZ 71386	*C. kutuku* sp. nov.	PP868294	PP868288	PP870124	–	–
DHMECN 10223 (QCAZ 59066)	*C. zarza*	PP868290	–	PP870119	PP886045	PP886042
QCAZ 58686	*C. zarza*	PP868291	PP868285	PP870120	PP886046	PP886043
QCAZ 58687	*C. zarza*	PP868292	PP868286	PP870121	PP886047	PP886044
QCAZ 58688	*C. zarza*	–	PP868287	PP870122	PP886048	–
QCAZ 69118	*C. zarza*	PP868293	–	PP870123	–	–
ZSFQ 2361 (QCAZ 78311)	*C. zarza*	–	PP868289	PP870125	–	–

We analysed the mitochondrial genes (12S rRNA, 16S rRNA, ND1) and the nuclear genes (BDNF, C-MYC 2, CXCR4, POMC, RAG1, SLC8A1, SLC8A3) for a total of 10 loci. The sequences were aligned in GeneiousPro 9.1.8 (Kearse et al. 2012) with the MAFFT plug-in (Katoh and Standley 2013). The alignment was manually corrected with Mesquite v.3.02 (Maddison and Maddison 2019). The aligned concatenated matrix had 6626 bp and 239 terminals (available at http://zenodo.org under doi: 10.5281/zenodo.11077755). Phylogenetic relationships were inferred for all genes concatenated using maximum likelihood (ML) as the optimality criterion. We partitioned the matrix by gene and codon position (the total number of partitions was 26). Each partition was analysed under model GTR + R + I in the software IQ-TREE multicore version 2.1.2 (Nguyen et al. 2015; Minh et al. 2020). We used the same software under default settings to find the best phylogeny. To estimate branch support, we made 1000 ultrafast non-parametric bootstrap searches (-bb 1000 command; Hoang et al. 2018) and 1000 replicates for the SH-like approximate likelihood ratio test with the -alrt 1000 command (Guindon et al. 2010). We considered that branches with bootstrap values > 94 and SH-aLRT values > 79 had strong support. We applied the least-squares dating method (To et al. 2016) to obtain a time tree in IQ-TREE. We used two calibration points based on the phylogeny of Hime et al. (2020): 23.1 Mya for the divergence between *Espadarana* and *Hyalinobatrachium* and 12.5 Mya for the divergence between *Espadarana* and *Teratohyla*. We prefer to rely on the estimates by Hime et al. (2020) because they were based on phylogenomic data instead of sequences from a few mitochondrial and nuclear genes, an improvement relative to previous time-tree estimates for Centrolenidae (e.g., Castroviejo-Fisher et al. 2014).

Extinction risk assessment

Extinction risk assessment was conducted following the system for classifying species at high risk of global extinction presented by the IUCN (2012) and the IUCN Standards and Petitions Committee (2022) guidelines. The extent of occurrence (EOO) and area of occupancy (AOO, with a cell size of 2 km) were calculated using GeoCAT (Bachman et al. 2011).

Nomenclatural acts

The electronic version of this article in Portable Document Format (PDF) will represent a published work according to the International Commission on Zoological Nomenclature (ICZN). Hence, the new names in the electronic version are effectively published under that code in the electronic edition alone. This published work and its nomenclatural acts have been registered in ZooBank, the online registration system for the ICZN. The ZooBank LSIDs (Life Science Identifiers) can be resolved, and the associated information can be viewed through any standard web browser by appending the LSID to the prefix http://zoobank.org/. The LSID for this publication is urn:lsid:zoobank.org:pub:E07EDFEB-3798-490F-B676-C912AE951C92. The online version of this work is archived and available from the following digital repositories: Zenodo, CLOCKSS , and other international archives.

Results

Phylogenetic analysis

According to our time tree, *Centrolene* diverged from its sister clade, *Nymphargus*, during the early Miocene (~18 Mya), a value similar to the ~17 Mya estimated by Castroviejo-Fisher et al. (2014). This similarity is remarkable because our secondary calibration points are from a time tree with taxon and gene sampling strategies (Hime et al. 2020) that are extremely different from those of Castroviejo-Fisher et al. (2014). Our phylogeny (Fig. 1) is similar to recent *Centrolene* phylogenies (Guayasamin et al. 2020; Cisneros-Heredia et al. 2023). Two notable exceptions are (1) *C. charapita* as a sister species of all other species of *Centrolene* (embedded within *Centrolene* in Guayasamin et al. 2020) and (2) the paraphyly of samples of *C. muelleri* Duellman & Schulte, 1993, from Peru relative to a specimen previously reported as *C. huilensis* from Ecuador (*C. muelleri* monophyletic and sister to *C. huilensis* from Ecuador in Guayasamin et al. 2020). Our estimate of time divergence between the Ecuadorian sample of *C. huilensis* and *C. muelleri* from Peru (CORBIDI 14667, collected 15 km from the type locality of *C. muelleri*) is 0.45 Mya, a value too low for sister species within *Centrolene* (see Fig. 1 for comparisons). In addition, their genetic distance is low (0.6% for gene 16S), and both specimens are very similar to each other morpho-

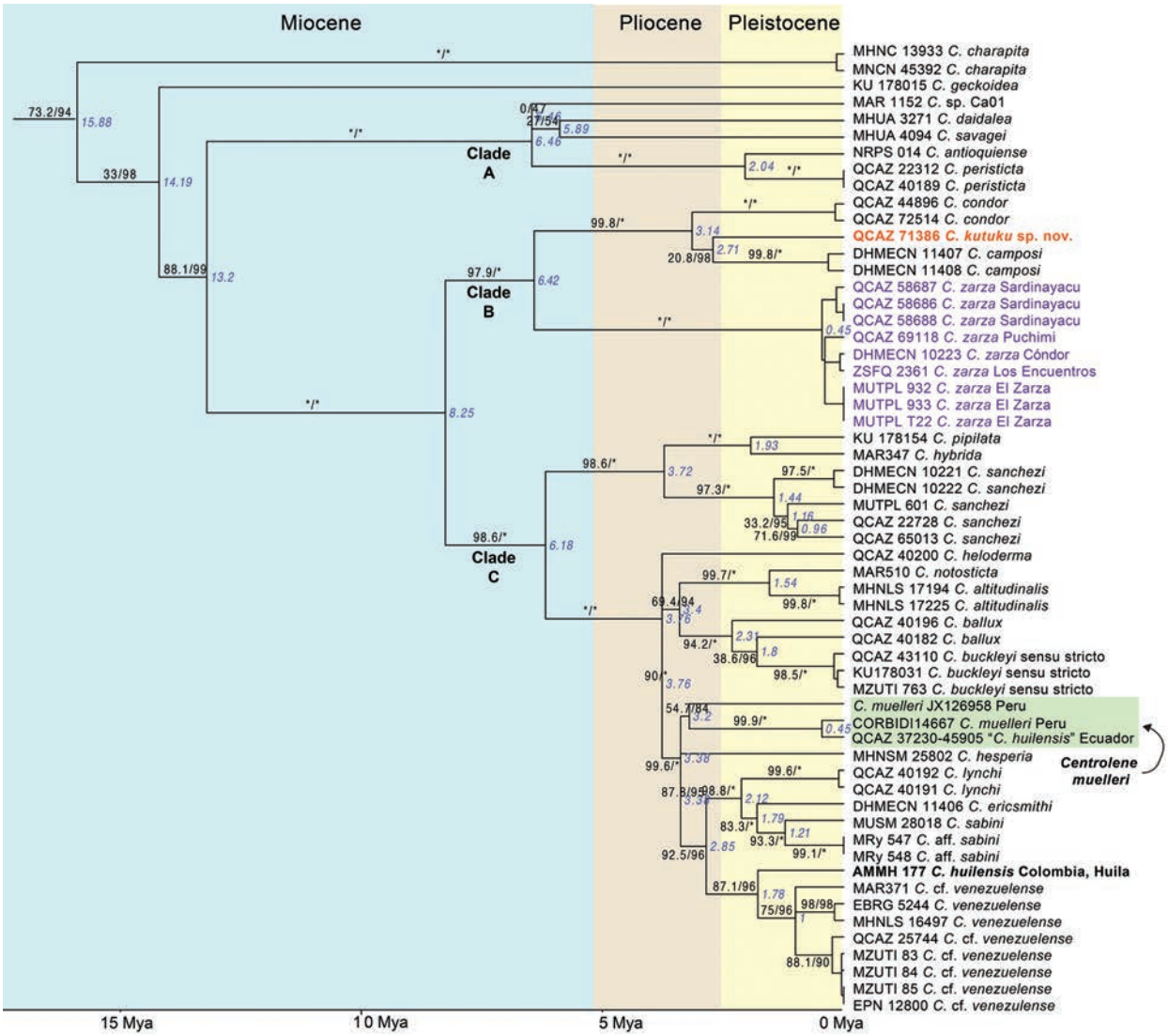

Figure 1. Maximum likelihood time-tree inferred from a partitioned analysis of 6626 aligned sites of the mitochondrial genes 12S rRNA, 16S rRNA, and ND1 and the nuclear genes BDNF, C-MYC 2, CXCR4, POMC, RAG1, SLC8A1, and SLC8A3 showing phylogenetic relationships of *Centrolene*. Support values are shown as percentages next to the branches: SH-aLRT before the slash and ultrafast bootstrap after. The "*" symbol indicates 100%. Node ages in Mya are shown in blue italics (ages lower than 0.5 Mya are not shown). Only the genus *Centrolene* is presented (a complete tree is available in the Suppl. material 1). Voucher catalogue numbers are displayed before species names. *Centrolene kutuku* sp. nov. and *C. zarza* are shown in orange and purple, respectively. The Colombian population of *C. huilensis* is shown in bold. The complete phylogeny is available as Suppl. material 1.

logically (Twomey et al. 2014). This evidence suggests that the identification of the Ecuadorian population as *C. huilensis* needs reconsideration. Moreover, the Colombian sample of *C. huilensis* (AMMH 177, from a locality 2 km N of the type locality of *C. huilensis*, Huila, Colombia) is not closely related to *C. muelleri* from Peru, nor to "*C. huilensis*" from Ecuador, but to the *C. venezuelense* species complex (see also Mendoza-Henao et al. 2023). The combined evidence allows us to confidently conclude that the Ecuadorian populations are not *C. huilensis*, but instead, they are *C. muelleri*.

Centrolene charapita and *C. geckoidea* Jiménez de la Espada, 1872 are unusual for having old divergence times (over 14 Mya; Fig. 1). The remaining species of *Centrolene* segregate into three younger and strongly supported clades (Clades A–C in Fig. 1). Clades A and B have few species (five and four, respectively) and are geographically restricted: Clade A in the Andes of northern Ecuador, Colombia, and western Venezuela; and Clade B in southern Ecuador. Clade C is more speciose, has younger species, and is geographically widespread. Within Clade B, a sample from the Kutukú Cordillera diverged from its closest relative, *C. camposi* Cisneros-Heredia, Yánez-Muñoz, Sánchez-Nivicela & Ron, 2023, approximately 2.7 Mya. Its time of divergence and morphological distinctiveness (see Systematic Account) indicate that it is a new species that we describe below. The uncorrected p-genetic distance, gene 12S, between the new species from Kutukú and *C. camposi* is 1.6%, and both are sister to specimens tentatively assigned to *C. condor*. The three species are sister to the recently described *C. zarza*, the oldest species of the clade (~6.4 Mya).

Samples previously ascribed to *C. buckleyi* (Boulenger, 1882) are non-monophyletic, as reported by Amador et al. (2018). Populations from the Eastern Cordillera of the Andes in northern Ecuador (e.g., MZUTI 83, QCAZ 25744) and Chingaza National Park in Colombia have a divergence time from *C. venezuelense* (Rivero, 1968) of ~ 1 Mya, suggesting they may be conspecific. We tentatively refer to them as "*C.* cf. *venezuelense*".

New data on *Centrolene zarza*

Centrolene zarza was recently described from a single locality, El Zarza Wildlife Refuge, in the Cóndor Cordillera (Székely et al. 2023). Samples collected during expeditions to the Subandean Cóndor and Kutukú cordilleras and the Sangay National Park in the Eastern Cordillera of the Andes allow us to add four new localities, increasing its known range 200 km to the north (Fig. 2). We examined two paratypes of *C. zarza*, an adult male (MUTPL-A 1022) and an adult female (MUTPL-A 1051), and eleven non-type specimens collected from these new localities. Contrary to what was reported in the original description, both paratypes have a thin layer of iridophores covering the pericardium (Fig. 3), slightly scalloped folds along the postaxial edge of Finger IV and Toe V, slightly scalloped metacarpal, ulnar, metatarsal, and tarsal folds, and abundant heel warts. To complement its original description, it can be mentioned that *C. zarza* has a distinct enamelled spot on the dorsal surfaces of upper arms and thighs; it shows abundant, elevated, rounded, enamelled warts on snout, infraocular and infratympanic areas, and flanks (sometimes low and flat due to preservation artefacts); the humeral spine is short, barely protruding through the skin; some specimens show a fairly distinct prepollex through the skin, giving the appearance of a slightly projecting prepollical spine; and adult males have nuptial excrescence Type VI (glandular clusters and individual glands distributed along the venter and flanks). Enamelled warts on infraocular and infratympanic areas are a characteristic otherwise present in five species not closely related to *C. zarza* or among themselves: *C. altitudinalis* (Rivero, 1968), *C. notosticta* Ruiz-Carranza & Lynch, 1991a, *C. pipilata* (Lynch & Duellman, 1973), *C. robledoi* Ruiz-Carranza & Lynch, 1995, and *C. sanchezi*. The presence of elevated warts on the snout of *C. zarza* is a distinctive condition, and few centrolenid frogs have dermal ornamentations on the snout (spiculated tubercles or warts, e.g., *Centrolene acanthidiocephalum* [Ruiz-Carranza & Lynch, 1989]).

Amended definition

We modified the definition of *C. zarza* as follows based on our findings (character states reported by Székely et al. are in square brackets and italics; character numbers follow Székely et al. 2023): **(2)** snout rounded with elevated warts at the tip in dorsal view and sloping in lateral view [snout rounded in dorsal view, sloping in profile]; **(4)** dorsal skin shagreen with scattered warts of varying size on head, dorsum, and limbs and abundant, elevated, enamelled warts on snout, infraocular and infratympanic areas, and flanks—reaching at least to the middle of flanks [dorsal skin shagreen with elevated, and some enamelled, warts corresponding to white spots]; **(6)** parietal peritoneum white—iridophores covering ½ of ventral parietal peritoneum (condition P3), pericardium covered by iridophores and all other visceral peritonea clear (condition V1, Fig. 3) [iridophores absent on all visceral peritonea, including pericardium, condition V0]; **(9)** absent or basal webbing between fingers I and II, II (2^{-}–2^{+}) –3^{-} III (2^{-}–2⅓) – (2^{-}–2^{+}) IV [webbing absent between Fingers I and II, basal between II and III, moderate between outer fingers: III 2^{+}–2 IV]; **(10)** toe webbing I (1^{-}–1 ½) – (2^{-}–2^{+}) II (1^{-}–1^{+}) – (2^{-}–2) III (1^{-}–1^{+}) – (1½–2) IV (1½–2) – (1–1^{+}) V [webbing between toes moderate: I 1−–2− II 1−–2 III 1−–2 IV 2–1+V]; **(11)** row of enamelled warts or scalloped dermal fringe along postaxial edge of Finger IV, enamelled metacarpal and ulnar folds, row of enamelled warts or scalloped dermal fringe along postaxial edge of Toe V, enamelled metatarsal and tarsal folds, and abundant enamelled heel warts [outer edge of forearms and tarsus with row of enamelled warts that often continue into the external edges of Finger IV and/or Toe V; fingers and toes with

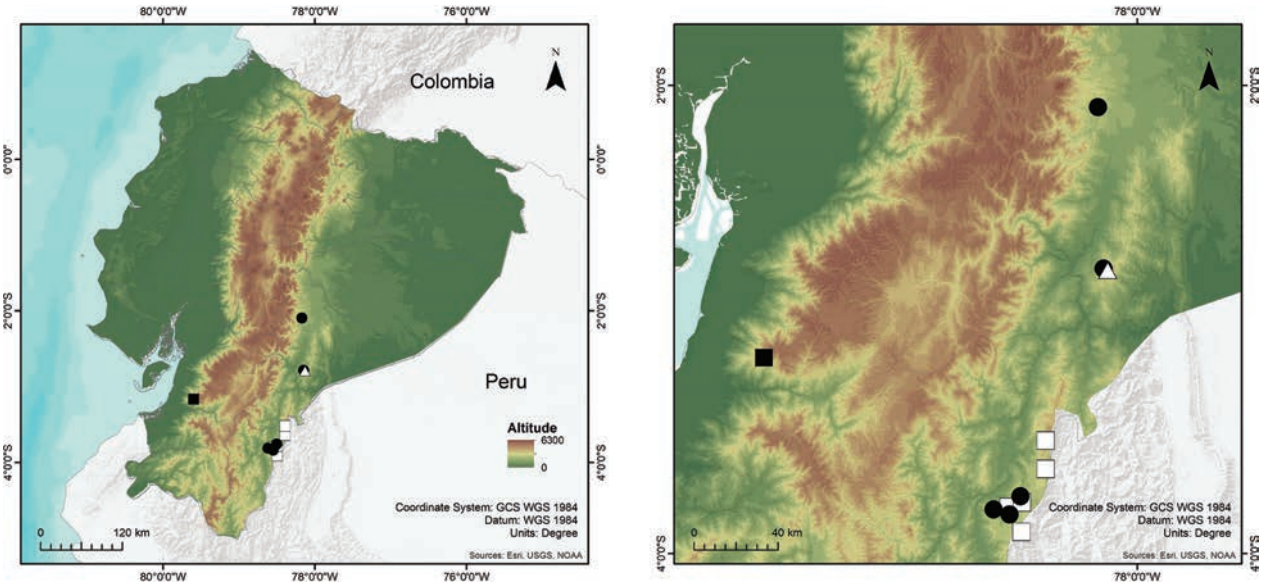

Figure 2. Map of Ecuador (left) and expanded area (right) showing known localities for *Centrolene camposi* (black square), *C. condor* (white square), *C. kutuku* sp. nov. (white triangle), and *C. zarza* (black circle) in southern Ecuador. Localities are based on specimens deposited at the DHMECN, QCAZ, and ZSFQ collections (see Materials and Methods for a list), Székely et al. (2023), and Cisneros-Heredia et al. (2023).

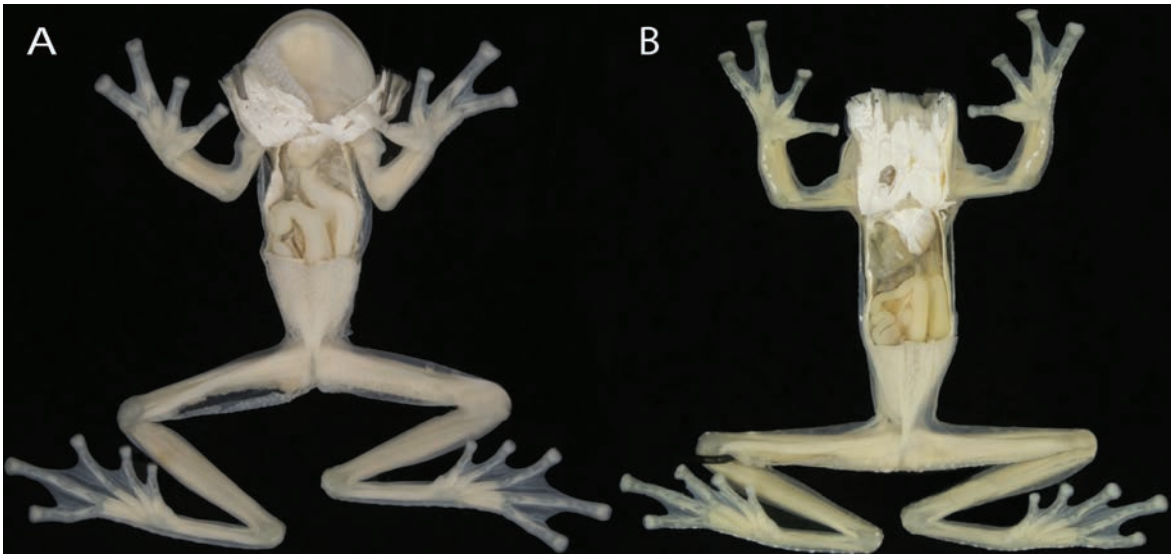

Figure 3. *Centrolene zarza* showing iridophores on the visceral peritonea, note pericardium covered by iridophores. **A.** MUTPL-A 1022 (paratype); **B.** QCAZ-A 58686.

broad lateral fringes]; **(12)** unpigmented nuptial pad Type I and Type VI; prepollex fairly distinct to concealed prepollex [unpigmented Type I nuptial pads present in males; concealed prepollex]; **(15)** color in life, all dorsal surfaces dark or light green with yellowish-green dots, enamelled warts on snout, infraocular and infratympanic areas, and flanks, a large enamelled spot on dorsal surfaces of each upper arm and thigh, enamelled flecks and dots on dorsal surfaces of hind and forelimbs, enamelled folds on hind and forelimbs, bones green (Fig. 4) [dorsum light green with many white or whitish, elevated, spots and flecks of various sizes; bones green]; **(16)** colour in preservative, dorsal surfaces dark grey to grey lavender with pale dots of varying size, enamelled warts on snout, infraocular and infratympanic areas, and flanks, a large enamelled spot on dorsal surfaces of each upper arm and thigh, enamelled flecks and dots on dorsal surfaces of hind and forelimbs, enamelled warts and folds on hind and forelimbs (Fig. 5) [dorsal surfaces greyish with white spots]; **(18)** abundant to scattered melanophores and small iridophore flecks present on Finger IV and towards the base of Finger III; abundant to scattered melanophores and small iridophore flecks on toes IV and V [fingers and toes yellowish, usually lacking melanophores except for Finger IV and Toes IV and V]; **(23)** SVL in adult females 25.5–30.0 [25.5–27.0 mm]. Differences are likely the result of interpopulation variation except for the presence of iridophores on the pericardium (verified in two paratypes of *C. zarza*, Fig. 3).

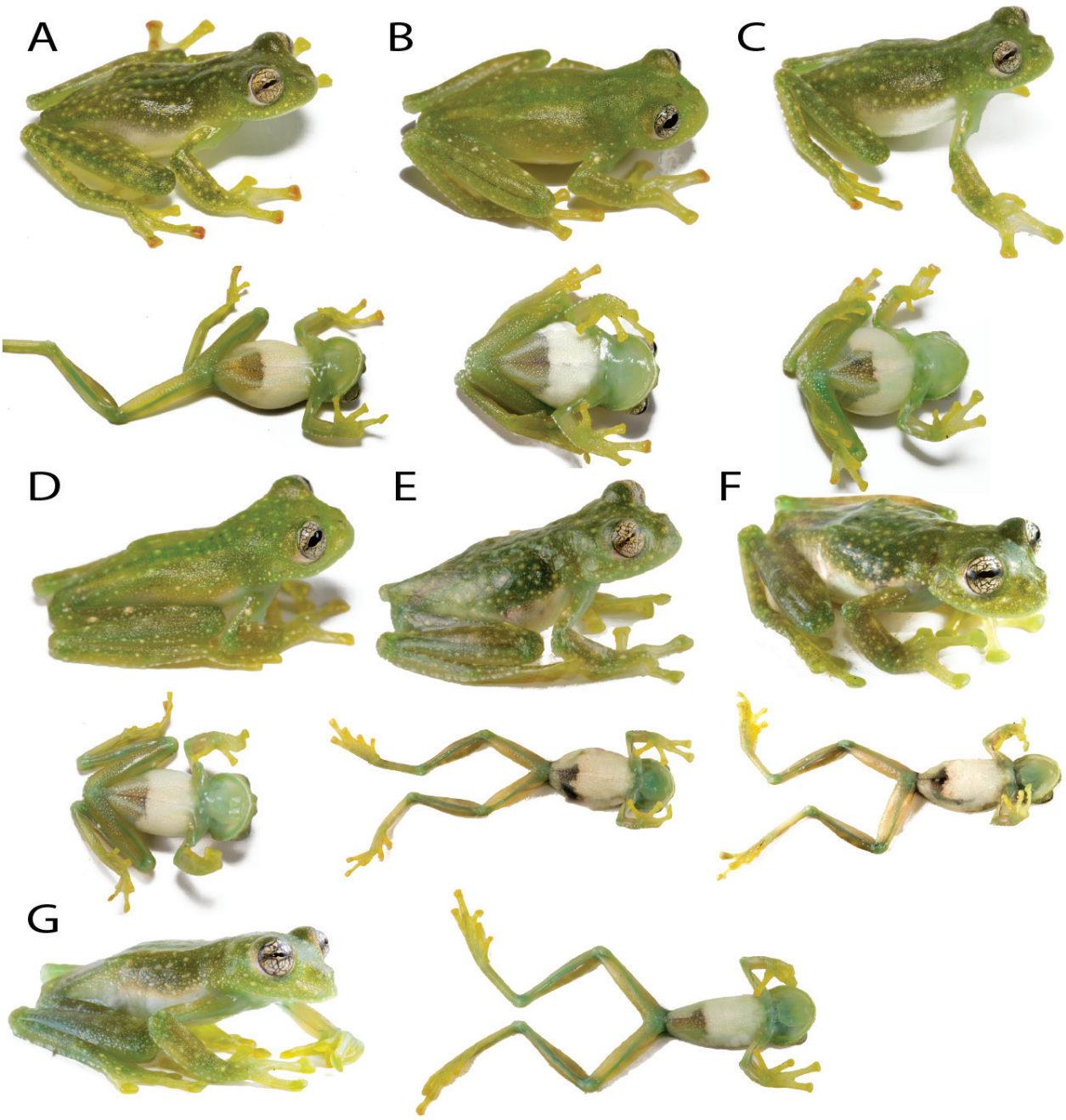

Figure 4. Dorsolateral and ventral views of live adult males of *Centrolene zarza*, corresponding to new records from Sardinayacu and Puchimi, Ecuador. **A.** QCAZ 58685, SVL = 23.8 mm; **B.** QCAZ 58688 (holotype), SVL = 23.8 mm; **C.** QCAZ 58687, SVL = 24.1 mm; **D.** QCAZ 58686, SVL = 23.9 mm; **E.** QCAZ 69116, SVL = 26.2 mm; **F.** QCAZ 69117, SVL = 29.4 mm; **G.** QCAZ 69118, SVL = 26.4 mm.

Distribution and Natural History

Centrolene zarza is now known from four localities in southeastern Ecuador: one on the eastern slopes of the Eastern Cordillera of the Andes at 1685 m elevation and three on the western slopes of the Subandean Cordilleras of Cóndor and Kutukú, between 1430–1905 m elevation (Fig. 2). The species inhabits Low Montane Evergreen Forest (Low Montane Evergreen Forest of the southern Eastern Cordillera of the Andes and Low Montane Evergreen Forest of the Cóndor-Kutukú Cordilleras, *sensu* MAE et al. 2013). All individuals have been found at night. At Sardinayacu, frogs were found next to a forested stream. All individuals were on the underside of leaves between 40 and 200 cm above the ground. At Puchimi, one adult male (QCAZ 69116) was calling 0.5 m above ground, next to a body of water at 20h59, and two individuals were found in an old-growth forest, 0.8–1.5 m above ground. At Los Encuentros, one individual was found on top of a leaf 0.5 m above ground, and two individuals were on top of leaves 0.3–2.8 m above a crystalline stream.

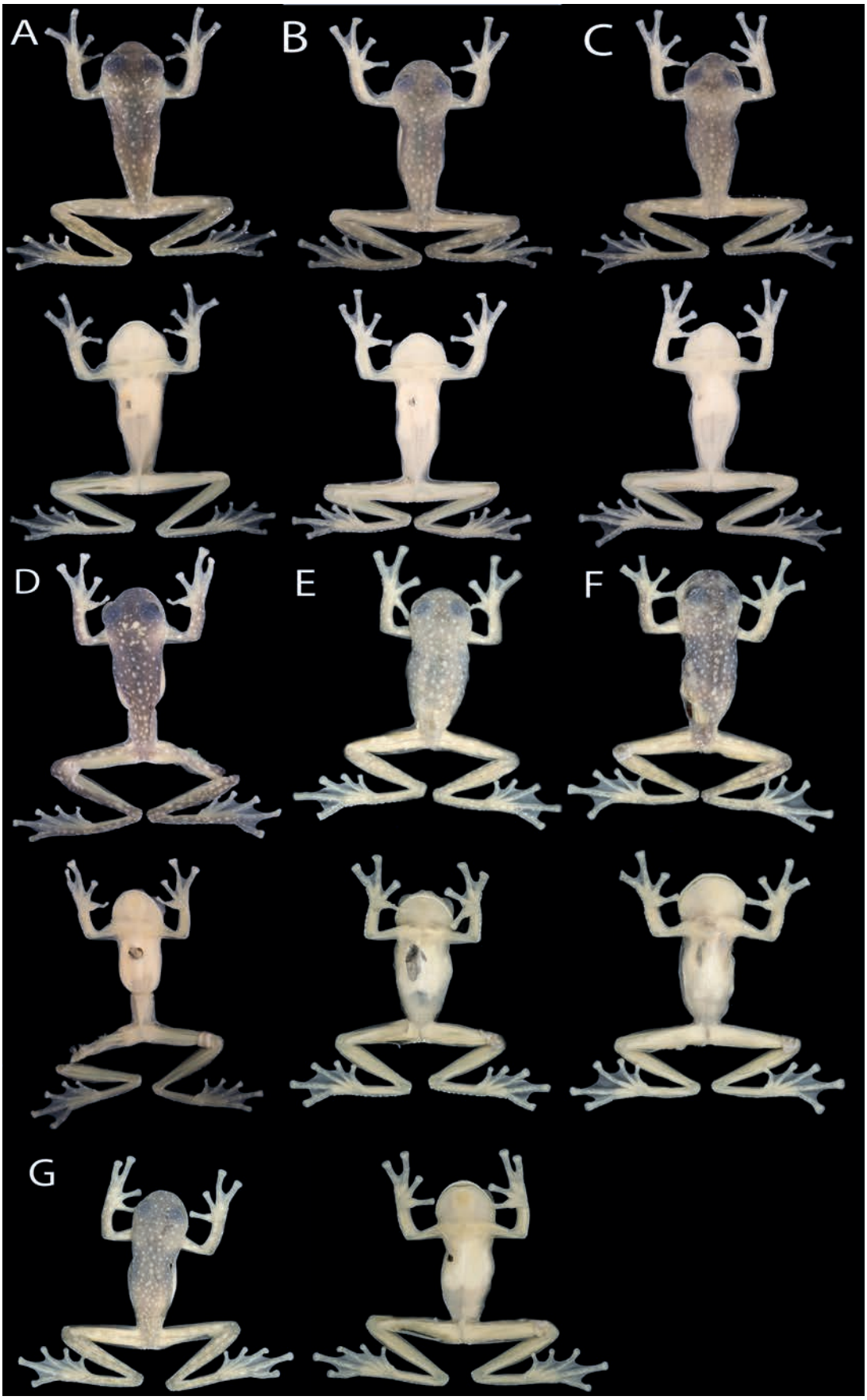

Figure 5. Dorsal and ventral views of preserved adult males of *Centrolene zarza* from Sardinayacu and Puchimi, Ecuador. **A.** QCAZ 58686, SVL = 23.9; **B.** QCAZ 58687, SVL = 24.1 mm; **C.** QCAZ 58688, SVL = 23.8 mm; **D.** QCAZ 58685, SVL = 23.8 mm; **E.** QCAZ 69116, SVL = 26.2; **F.** QCAZ 69117, SVL = 29.4; **G.** QCAZ 69118, SVL = 26.4 mm.

Conservation status

Székely et al. (2023) reported an extent of occurrence and area of occupancy for *C. zarza* of 7 km^2, based on a single known locality that could be affected by mining activities, thus categorising it as Critically Endangered [CR B1ab(i,ii,iii)+2ab(i,ii,iii)]. We increase the species' distribution range to four localities in three mountain ranges. Two localities are protected areas (Sangay National Park and La Zarza Wildlife Refuge), but localities at the Cóndor Cordillera are under intense mining pressure, and expansion of the agricultural frontier impacts the locality at the Kutukú Cordillera (Roy et al. 2018). The species has an extent of occurrence of 3026 km^2 and an area of occupancy of 24 km^2. We recommend categorising *C. zarza* as Endangered following the criteria B1ab(iii)+B2ab(iii).

***Centrolene kutuku* Ron, García, Brito-Zapata, Reyes-Puig, Figueroa-Coronel, & Cisneros-Heredia, sp. nov.**

https://zoobank.org/458CECC2-8C71-4390-8FD5-B4F1F6F42317

Proposed Spanish common name. Rana de Cristal de Kutukú.

Proposed English common name. Kutukú Glassfrog.

Type material. ***Holotype*.** (Figs 6–9) QCAZ-A 71386 (field number PUCE SC 61758), collected at República del Ecuador, provincia de Morona Santiago, cantón Santiago de Mendez, parroquia San Francisco de Chinimbimi, Cordillera del Kutukú, sector Puchimi, 22 km ESE Santiago de Mendez (2.7901°S, 78.1266°W, 2264 m elevation), by Diego Almeida, Diego Paucar, Darwin Núñez, Kunam Nusirquia, and Ricardo Gavilanes on 25 January 2018.

***Paratypes*.** (1 specimen) QCAZ-A 71400, adult male, collected near the type locality (2.7903°S, 78.1265°W, 2255 m elevation) on 27 January 2018, same collectors as holotype.

Definition. *Centrolene kutuku* sp. nov. is distinguished from all other Centrolenidae by the following combination of characters: (1) dentigerous process of vomer present, without vomerine teeth; (2) snout slightly subacuminate to round in dorsal view and sloping in lateral view; (3) tympanic annulus evident, almost completely visible except for upper most border, tympanic membrane coloured as surrounding skin, supratympanic fold present; (4) dorsal skin microspiculate with abundant tubercles on head and body; (5) ventral skin granular, subcloacal area with two large subcloacal warts; elevated, abundant, enamelled, pericloacal warts, other cloacal ornamentation absent; (6) parietal peritoneum white—iridophores covering ½ of ventral parietal peritoneum (condition P2), pericardium covered by iridophores and all other visceral peritonea translucent (condition V1); (7) liver lobed and hepatic peritoneum translucent (condition H0); (8) adult males with short humeral spines, barely protruding through skin (Fig. 9); (9) absent webbing between fingers I and II, II (2$^-$– 2$^+$) –3$^-$ III (2$^+$) – (2½$^-$2 ⅓) IV; (10) toe webbing I (1–1 ½) –(2–2$^+$) II (1$^-$–1$^+$–2$^-$) III (1$^+$–1½) IV (1½–1) V; (11) dermal fringe along postaxial edge of Finger IV and hand, slightly enamelled ulnar fold; dermal fringe along postaxial edge of Toe V, slightly enamelled metatarsal and tarsal folds, warts on heel absent; (12) unpigmented nuptial pad Type I; prepollex concealed; (13) Finger II slightly longer than Finger I, (14) eye diameter larger than width of disc on Finger III; (15) colour in life, all dorsal surfaces green with light green dots, bones green; (16) colour in preservative, dorsal surfaces lavender with lighter tubercles, white supralabial stripe, flanks with contrasting dorsal-ventral transition in colour, dorsal surfaces of limbs lavender clearer than body with slightly lighter dots; two white spots on arm near shoulder; (17) in life, iris cream with grey reticulations; (18) melanophores on Finger IV absent; scattered melanophores along toes IV and V; (19) calling site of males unknown; call undescribed; (20, 21, 22) fighting behaviour, egg clutches, and tadpoles unknown; (23) SVL in adult males 21.5–21.9 mm (n = 2); females unknown.

Diagnosis. *Centrolene kutuku* sp. nov. differs from all other glassfrogs, except *C. heloderma*, by having humeral spines in males, dorsum green with light dots and without dark marks, dorsum with abundant tubercles, and visceral peritonea translucent (except for pericardium). *Centrolene kutuku* sp. nov. is similar to *C. camposi*, *C. ericsmithi*, *C. heloderma*, and *C. zarza* in having humeral spines in males and elevated dermal ornamentations (i.e., dorsal tubercles or warts) and lacking dorsal dark-coloured marks. *Centrolene camposi* differs from *C. kutuku* sp. nov. by having (characters of *C. kutuku* sp. nov. in parentheses) sloping snout in lateral view (rounded), tympanic annulus barely visible (completely visible), colouration in life green dorsum with thick yellowish-white labial stripe continuing into a faint yellowish lateral line and yellowish green flanks (green dorsum with light green dots), and larger body size in males (SVL 29.1–31.2 mm in *C. camposi* vs. 21.5–21.9 mm in *C. kutuku* sp. nov.). *Centrolene ericsmithi* differs from *C. kutuku* sp. nov. by having tympanic annulus barely visible (almost completely visible), dorsal skin with dispersed spicules (with abundant tubercles), colouration in life green dorsum with thin yellowish labial stripe continuing into a row of white lateral tubercles and yellowish lateral line (green dorsum with light green dots), and larger body size in males (SVL 27.3 mm in *C. ericsmithi* vs. 21.5–21.9 mm in *C. kutuku* sp. nov.). *Centrolene heloderma* differs by having pustular dorsal skin (with abundant tubercles), grey lavender dorsum in preservative (lavender), and outer tarsal fold with low white tubercles (enamelled fold without tubercles). *Centrolene zarza* differs by having snout rounded with elevated warts at the tip in dorsal view and sloping in lateral view (round, without elevated warts at the tip in dorsal view and rounded in lateral view), dorsal skin shagreen with scattered warts of varying size and abundant, elevated, enamelled warts on head and flanks (abundant tubercles, lacking enamelled warts), dorsum green with yellowish-green dots and enamelled warts (green dorsum with light green dots), and larger body size in males (SVL 23.2–26.2 mm in *C. zarza* vs. 21.5–21.9 mm in *C. kutuku* sp. nov.).

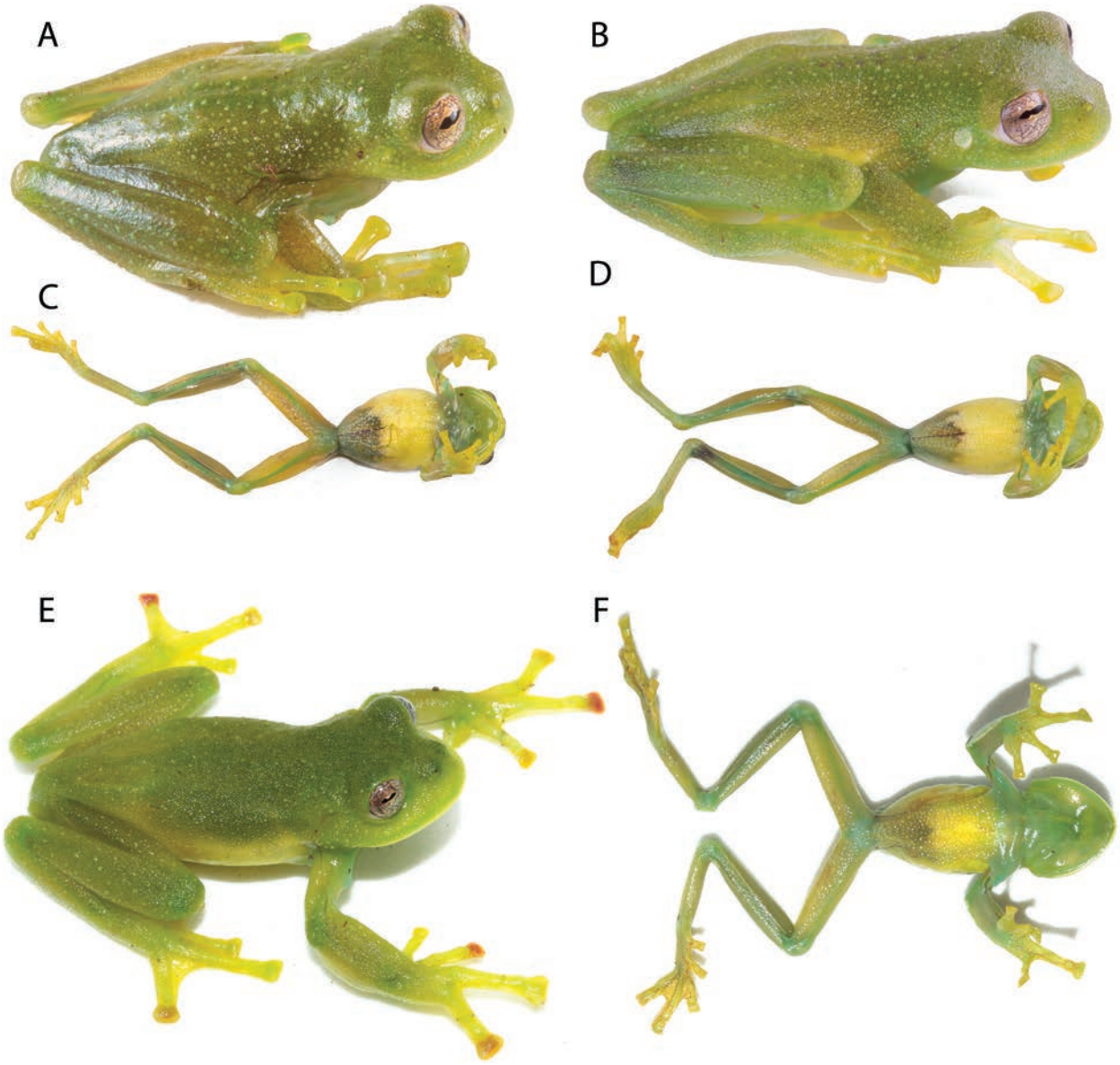

Figure 6. *Centrolene kutuku* sp. nov. and *C. camposi* in life. A, B, and E are dorsolateral views, and C, D, and F are ventral views. **A–C.** *Centrolene kutuku* sp. nov., holotype, male, QCAZ 71386, SVL = 21.9 mm; **B–D.** *C. kutuku* sp. nov., paratype, male, QCAZ 71400, SVL = 21.5 mm. **E–F.** *C. camposi*, holotype, DHMECN 11407, SVL = 29.1 mm. Photographs of *C. camposi* by Juan C. Sánchez-Nivicela.

Description of the holotype. (Figs 6–9) SVL = 21.9 mm, HW = 9.0, HL = 7.2, IOD = 4.1, ED = 2.8, EN = 1.4, IN = 1.9, TYD = 1.0, HAL = 8.6, FL = 10.8, TL = 13.2, F3DW = 1.5.

Adult male. Snout rounded in dorsal view, sloping in lateral view, EN/HL = 0.22; nostrils slightly elevated, producing a low depression in the internarial area, loreal region concave; canthus rostralis indistinct. Small-sized eyes, ED/HL = 0.38, directed anterolaterally at about 45° from midline, interorbital area wider than eye diameter, IOD/ED = 1.46, EN/ED = 0.59, EN/IOD = 0.34. Tympanic annulus evident and slightly oriented dorsolaterally, supratympanic fold above upper portion of tympanum and extending down to shoulder. Dentigerous processes of vomers present but vomerine teeth absent; choanae rounded, separated; tongue rounded; vocal slits present, extending from mid tongue to near jaw angle.

Skin of dorsal surfaces of body and limbs shagreen with scattered tubercles of varying size on head, dorsum and limbs. Skin of ventral surfaces of body granular. Cloacal opening directed posteriorly at upper level of thighs, no distinct cloacal sheath; subcloacal area coarsely granular with a pair of large, round, flat subcloacal warts on ventral surfaces of thighs below vent; pericloacal area with enamelled warts of similar size; other cloacal ornamentation absent.

Upper arm thinner than moderately robust forearm. Humeral spine present, short, and barely visible externally, not piercing the skin. Relative lengths of fingers III > IV > II > I; webbing formula between fingers absent

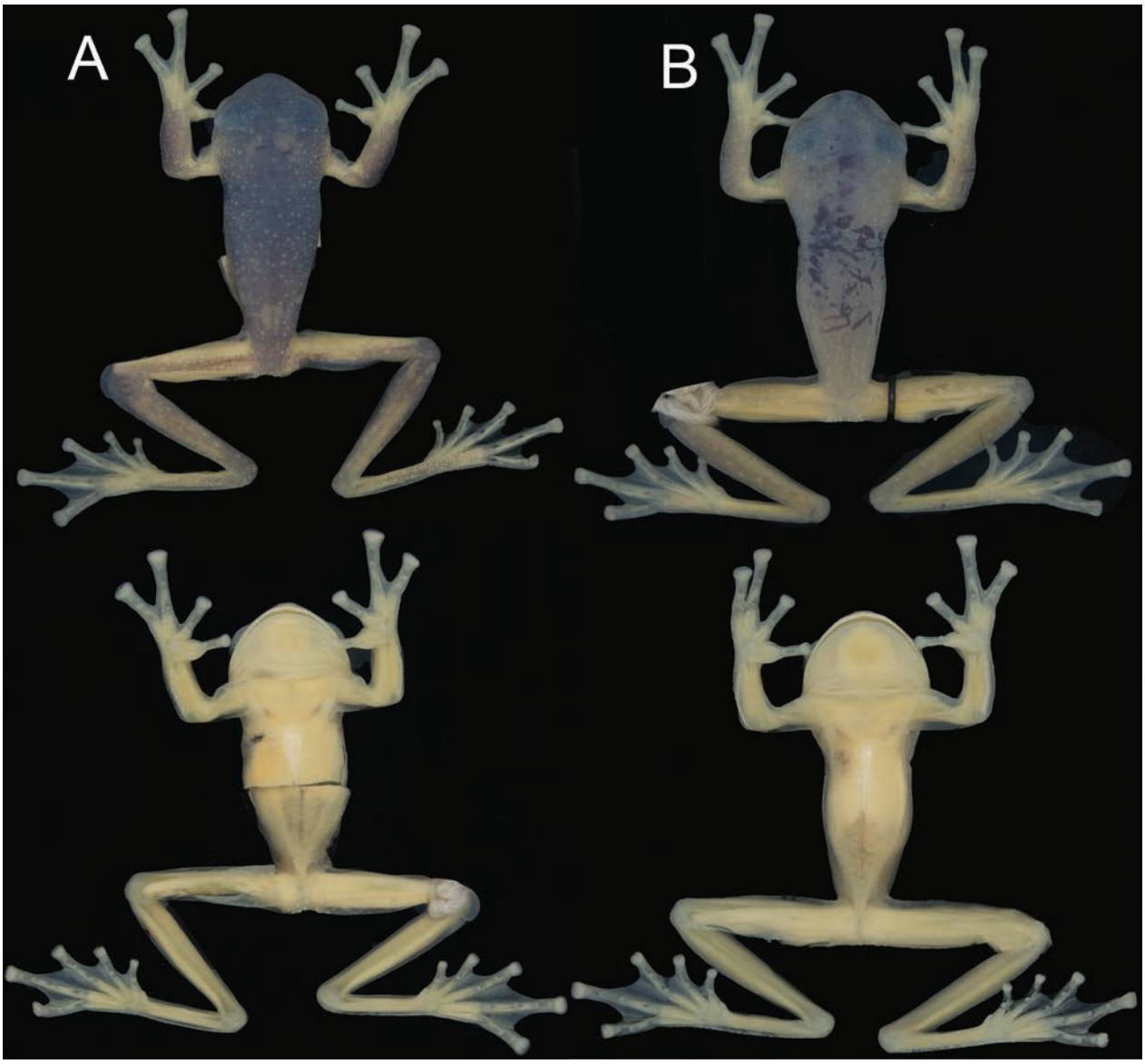

Figure 7. *Centrolene kutuku* sp. nov. in preservative. Upper row: dorsal view; lower row: ventral view. **A.** Holotype, male, QCAZ 71386, SVL = 21.9 mm; **B.** Paratype, male, QCAZ 71400, SVL = 21.5 mm.

between I and II, II basal III 2–2$^{1/3}$ IV; finger discs wider than the adjacent phalanx, nearly truncate; disc on third finger slightly larger than those on toes, ED/F3DW = 1.86; subarticular tubercles rounded and slightly elevated, supernumerary tubercles abundant and distinct; palmar tubercle prominent, rounded, elevated; thenar tubercle elliptic. Concealed prepollex, unpigmented nuptial excrescences present, Type I on dorsolateral side of thumbs.

Hind limbs slender; TL/SVL = 0.60, FL/SVL = 0.49. Inner metatarsal tubercle large and elliptical; outer metatarsal tubercle small and round. Subarticular tubercles rounded and low, supernumerary tubercles distinct but low. Webbing on feet I 1½–2 II 1–2 III 1–2 IV 2–1½ V; toe discs bluntly truncate. Papilla on tip of discs absent.

Colour of holotype. Colour in preservative is shown in Figs 7, 8. Pale dots on dorsum are of varying sizes. Iris silver with dark, fine reticulations. Parietal peritoneum white, iridophores covering 1/3 of ventral parietal peritoneum. Pericardium white (i.e., covered by iridophores), all other visceral peritonea translucent. Colour in life is shown in Fig. 6.

Variation. Measurements of QCAZ 71400 in mm: SVL = 21.5, HW = 8.5, HL = 7.0, IOD = 4.0, ED = 2.4, EN = 1.7, IN = 2.0, TYD = 0.9, HAL = 7.5, FL = 10.6, TL = 13.0, F3DW = 1.5. The single paratype differs from the holotype by having lower dorsal tubercles (wart-like), a dorsal lavender colour that is lighter, and more contrasting enamelled colouration on limbs.

Etymology. The specific name of this new taxon is a noun in apposition and refers to the Kutukú Cordillera, the Subandean Cordillera where the new species was discovered. The name originates from the Shuar language, meaning "paramo with stunted vegetation" (Pérez 1984).

Distribution and natural history. *Centrolene kutuku* sp. nov. is known from a single locality in southeastern

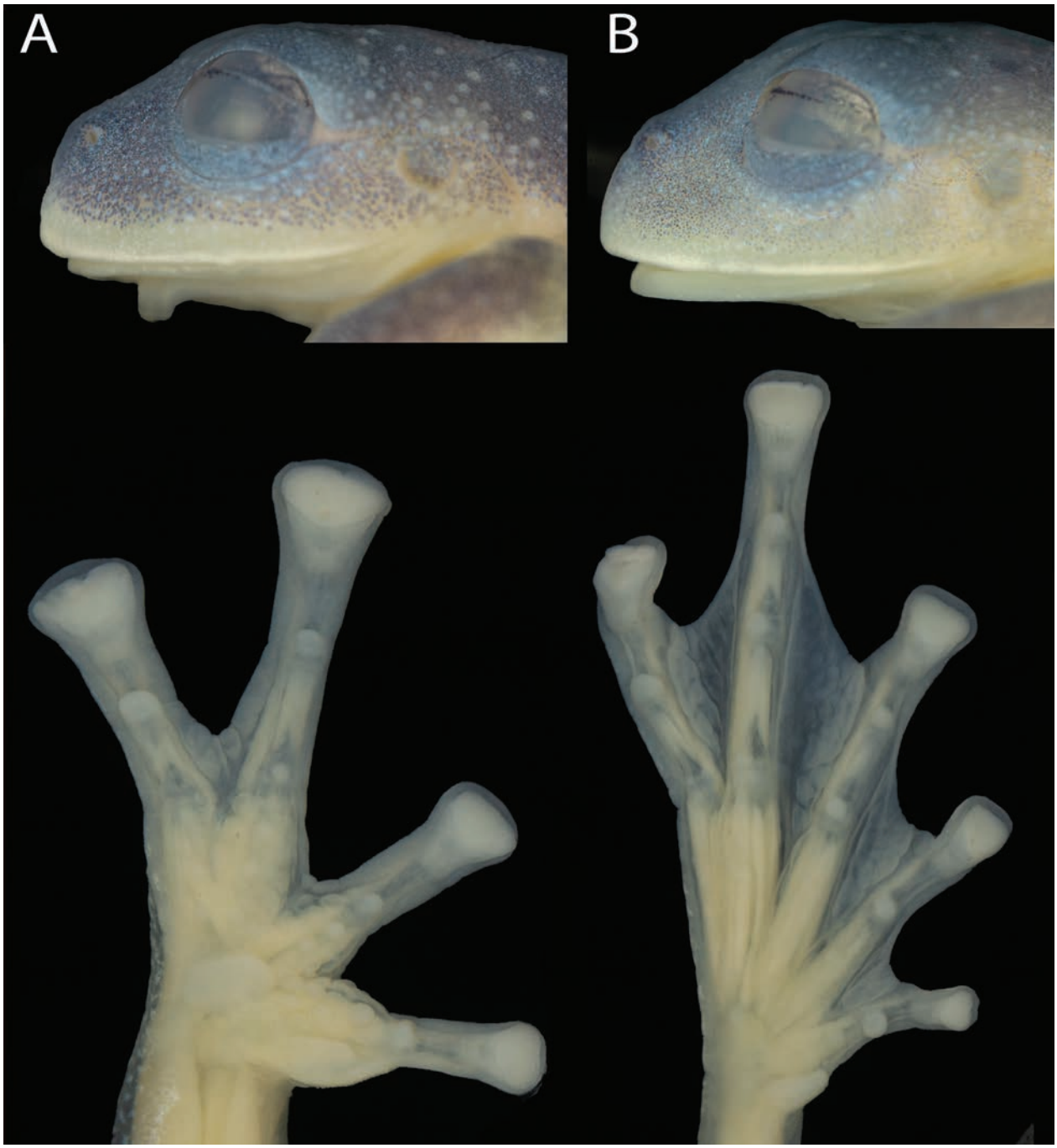

Figure 8. *Centrolene kutuku* sp. nov. head, hand, and foot in preservative. Upper row: lateral view of the head; lower row: ventral view of hand (left) and foot (right) of the holotype. **A.** Holotype, male, QCAZ 71386, SVL = 21.9 mm, head length = 7.2 mm; **B.** Paratype, male, QCAZ 71400, SVL = 21.5 mm, head length = 7.0 mm.

Ecuador, on the western slope of the Kutukú Subandean cordillera, between 2255–2264 m elevation (Fig. 2). The species inhabits Montane Evergreen Forest over the Sandstone Plateaus of the Cóndor-Kutukú Cordillera (*sensu* MAE et al. 2013). Sandstone plateaus in the Subandean Cordilleras have forest ground covered by mosses and roots, forming a false floor with large spaces between roots. The holotype was calling over a leaf 200 cm above the ground, on the edge of a small spring flowing into a black water ravine in a primary forest. The paratype was on a leaf, 300 cm above the ground, next to a black water stream. Both individuals were found in primary forest (QCAZ specimen database).

Conservation status. *Centrolene kutuku* sp. nov. is known from a single locality in the Kutukú cordillera, southeastern Ecuador. The locality is not in a protected area, and by 2020, there were agricultural lands at a distance of 2.7 km (MAATE 2022). Because collections in Kutukú have been limited, the distribution of the species is likely to be larger. The population status of this new species is unknown, and we recommend assigning it to the Data Deficient Red List category.

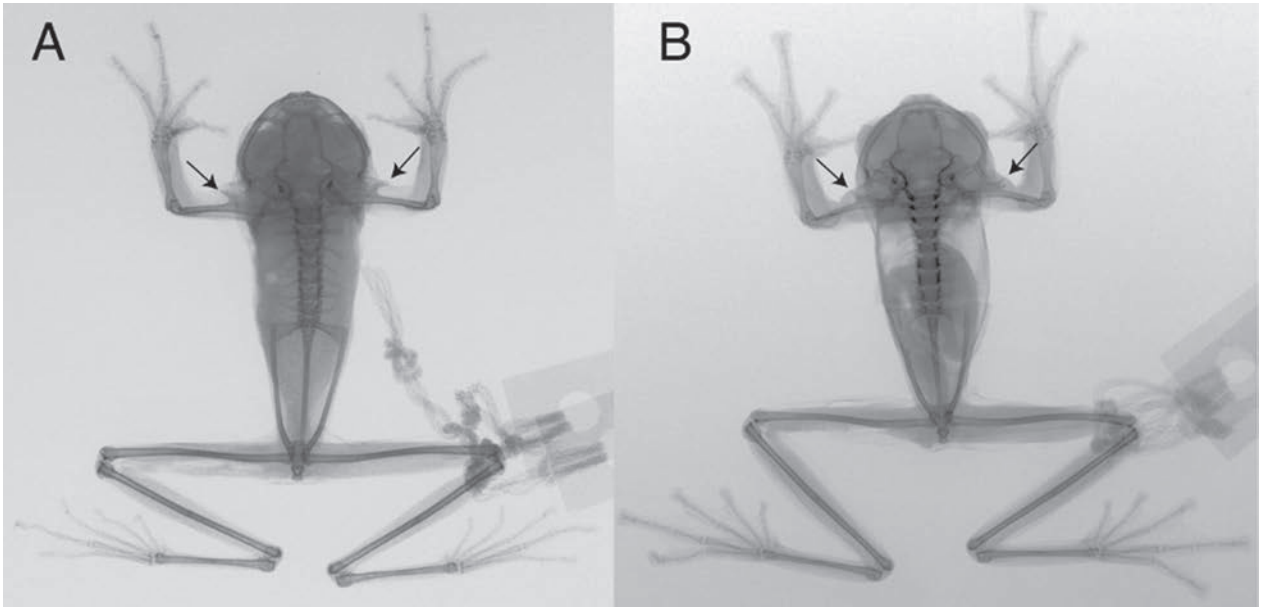

Figure 9. Dorsal X-ray views of *Centrolene zarza* and *Centrolene kutuku* sp. nov. **A.** *Centrolene zarza* QCAZ 58686, adult male, SVL = 23.9 mm; **B.** *Centrolene kutuku* sp. nov. QCAZ 71386, adult male (holotype), SVL = 21.9 mm. Black arrows point to humeral spines; notice the difference in angle orientation, curvature, and size.

Discussion

We present morphological and genetic evidence of the distinctiveness of *Centrolene kutuku* sp. nov., the 34th described species of *Centrolene* (AmphibiaWeb 2023). Of them, 29 have been included in molecular phylogenies (Fig. 1). The new species belongs to an old clade (origin ~8 Mya; clade B in Fig. 1) composed of four species, three of which have been described within the last two years (Cisneros-Heredia et al. 2023; Székely et al. 2023, and herein). Its sister clade (C in Fig. 1) has 15 species, almost four times more speciose. Because both clades have the same age, the diversification rate within clade C would appear much higher. However, we suspect this difference is partly a sampling artefact because clade B occurs in mountain regions of southern Ecuador and northern Peru, where amphibian inventories have been limited. Within the distribution range of clade B, the least sampled regions are the Subandean Cordilleras of Cóndor and Kutukú. *Centrolene kutuku* sp. nov. and *C. zarza* are the first *Centrolene* known from the Kutukú Cordillera. In addition to the Cóndor and Kutukú, the only other Subandean cordillera where species of *Centrolene* have been recorded is the Guacamayos Cordillera, with records of *Centrolene* cf. *venezuelense*, *C. muelleri*, and *C. sanchezi* (Guayasamin et al. 2020). Fieldwork in southwestern Ecuador and adjacent Peru should result in the discovery of additional species from that clade.

Centrolene kutuku sp. nov. is sister to *C. camposi*, a recently described species from the southwestern Andes of Ecuador (Cisneros-Heredia et al. 2023). This biogeographic pattern of sister species on opposite sides of the Andes is unusual, with only two other examples known in Centrolenidae: *Teratohyla amelie* (Cisneros-Heredia & Meza-Ramos, 2007)–*T. pulverata* (Peters, 1873) and *Cochranella granulosa* (Taylor, 1949)–*C. resplendens* (Lynch & Duellman, 1973) (Guayasamin et al. 2020). In both cases, divergence times are > 7 Mya, higher than the 2.7 Mya separating *C. camposi* and *C. kutuku* sp. nov. The topology and geographic distribution of Clade B suggest that its most recent common ancestor inhabited the Amazon basin of southern Ecuador. Therefore, *C. camposi* should result from recent dispersal across the Andes, from the Amazon basin to the Pacific basin, a putative example of peripatric speciation. Dispersal should have been possible due to the relatively low elevations of the Andes in southern Ecuador (Fig. 2). Cisneros-Heredia et al. (2023) discussed this pattern between *C. condor* and *C. camposi* because, at the time, they were considered sister species (*C. kutuku* sp. nov. was unknown).

Centrolene huilensis was described from the Huila department in southern Colombia and is currently known from a few localities in the southeastern slopes of the Central Cordillera of the Andes of Colombia (Ruiz-Carranza and Lynch 1995; Mendoza-Henao et al. 2020). It was reported from a single locality on the northeastern slopes of the Eastern Cordillera of the Andes of Ecuador, 320 km S of the type locality (Guayasamin et al. 2020). Our phylogeny shows that the Ecuadorian population is not closely related to *C. huilensis* from Colombia. Moreover, the Ecuadorian population has a low genetic distance from the Peruvian specimen of *C. muelleri* (CORBIDI 14667) collected near the species' type locality (0.6%, 16S gene). The colouration in life and external morphology of the Peruvian and Ecuadorian populations are very similar (see Fig. 9 in Twomey et al. 2014), reinforcing the hypothesis of conspecificity between them. The other Peruvian specimen (PV from

Gocta) probably represents a distinct species given its divergence time of 3.2 Mya relative to the other two populations. Our phylogeny and that of Twomey et al. (2014) are inconsistent with Guayasamin et al.'s (2020) phylogeny, which shows a monophyletic *C. muelleri* from Peru, sister to the Ecuadorian population. Our phylogeny shows, in contrast, that the Peruvian *C. muelleri* is paraphyletic relative to the Ecuadorian population (Fig. 1). This inconsistency is puzzling given that both topologies have strong support and, as far as we can tell, are based on the same set of sequences for both species. *Centrolene huilensis* and *C. muelleri* are morphologically very similar (Mendoza-Henao et al. 2020); nevertheless, both species are not closely related, indicating their phenotypic similarity is a remarkable case of morphological convergence within *Centrolene*.

Other samples with uncertain identification belong to populations of *Centrolene* from the eastern Andean slopes of Ecuador and Colombia (e.g., QCAZ 25744, MZUTI 85, MR371) that have been referred to either as "*C. buckleyi*" (e.g., Amador et al. 2018), "*C.* aff. *buckleyi*" (e.g., Castroviejo-Fisher et al. 2014), or "*Centrolene* sp." (Guayasamin et al. 2020). An additional closely related sample (QCAZ 47338) has been referred to as "*C. condor*" (e.g., Guayasamin et al. 2020; Székely et al. 2023). Our phylogeny indicates those samples are closely related to *C. venezuelense* (Fig. 1), with a divergence time of ~ 1 Mya. Because such a recent divergence is uncharacteristic for different species, we tentatively refer to them as "*C.* cf. *venezuelense*" until a thorough review is carried out for that clade. Similar to previous reviews (e.g., Castroviejo-Fisher et al. 2014; Cisneros-Heredia et al. 2023), we assign "*C. condor*" to a species belonging to clade B (Fig. 1) based on its resemblance to specimens of *C. condor* from the type locality.

Acknowledgements

We thank Diego Almeida, Andrea Correa, Ricardo Gavilanes, Francy Mora, Jefferson Mora, Darwin Núñez, Kunam Nusirquia, Diego Paucar, Javier Pinto, Juan Carlos Sanchez, David Velalcázar, and Juan Hurtado for collecting the specimens used in this study. Field and laboratory work by QCAZ was funded by the Secretaría Nacional de Educación Superior, Ciencia, Tecnología e Innovación del Ecuador SENESCYT (Arca de Noé initiative; SRR and Omar Torres principal investigators) and grants from the Pontificia Universidad Católica del Ecuador, Dirección General Académica. Universidad San Francisco de Quito USFQ funded lab work by ZSFQ through COCIBA research grants to DFCH and IBIOTROP operative funds. For their support during visits to their institutions, we thank Mario Yánez-Muñoz (INABIO); William E. Duellman, Linda Trueb, Juan M. Guayasamin, and Elisa Bonaccorso (KU); George Zug, Roy McDiarmid, Ron Heyer, Robert Reynolds, Kenneth A. Tighe, Steve W. Gotte, Carole C. Baldwin, and Mary Sangrey (USNM). Diego F. Cisneros-Heredia thanks María Elena Heredia, Laura Heredia, and Jonathan Guillemot for their constant support. We thank Juan C. Sánchez-Nivicela for providing photographs of *C. camposi*, and Mario Yánez-Muñoz and Juan M. Guayasamin for their comments on the manuscript as part of the peer-review process.

References

Almendáriz A, Batallas D (2012) Nuevos datos sobre la distribución, historia natural y el canto de *Centrolene condor* Cisneros-Heredia y Morales-Mite 2008 (Amphibia: Anura: Centrolenidae). Revista Politécnica 30: 42–53.

Amador L, Parada A, D'Elía G, Guayasamin JM (2018) Uncovering hidden specific diversity of Andean glassfrogs of the *Centrolene buckleyi* species complex (Anura: Centrolenidae). PeerJ 6: e5856. https://doi.org/10.7717/peerj.5856

AmphibiaWeb (2023) AmphibiaWeb. https://amphibiaweb.org/

Bachman S, Moat J, Hill A, de la Torre J, Scott B (2011) Supporting Red List threat assessments with GeoCAT: Geospatial conservation assessment tool. ZooKeys 150: 117–126. https://doi.org/10.3897/zookeys.150.2109

Beaupre SJ, Jacobson ER, Lillywhite HB, Zamudio KR (2004) Guidelines for use of live amphibians and reptiles in field and laboratory research. American Society of Ichthyologists and Herpetologists, 24 pp.

Boulenger GA (1882) Catalogue of the Batrachia Salientia s. Ecaudata in the Collection of the British Museum. 2nd edn. Taylor & Francis, London.

Castroviejo-Fisher S, Guayasamin JM, Gonzalez-Voyer A, Vila C (2014) Neotropical diversification seen through glassfrogs. Journal of Biogeography 41(1): 66–80. https://doi.org/10.1111/jbi.12208

Cisneros-Heredia DF (2007) A new species of glassfrog of the genus *Centrolene* from the foothills of Cordillera Oriental of Ecuador. Herpetozoa (Wien) 20: 27–34.

Cisneros-Heredia DF, McDiarmid RW (2005) Amphibia, Centrolenidae, *Centrolene peristictum*, *Centrolene prosoblepon*, *Cochranella cochranae*, *Cochranella midas*, *Cochranella resplendens*, *Cochranella spinosa*, *Hyalinobatrachium munozorum*: Range extensions and new provincial records. Check List 1(1): 18–22. https://doi.org/10.15560/1.1.18

Cisneros-Heredia DF, McDiarmid RW (2007) Revision of the characters of Centrolenidae (Amphibia: Anura: Athesphatanura), with comments on its taxonomy and the description of new taxa of glassfrogs. Zootaxa 1572(1): 1–82. https://doi.org/10.11646/zootaxa.1572.1.1

Cisneros-Heredia DF, Meza-Ramos P (2007) An enigmatic new species of glassfrog (Amphibia: Anura: Centrolenidae) from the Amazonian Andean slopes of Ecuador. Zootaxa 1485(1): 33–41. https://doi.org/10.11646/zootaxa.1485.1.3

Cisneros-Heredia DF, Morales-Mite M (2008) A new species of glassfrog from elfin forests of the Cordillera del Cóndor, southeastern Ecuador. Herpetozoa (Wien) 21: 49–56.

Cisneros-Heredia DF, Yánez-Muñoz MH (2007) Amphibia, Anura, Centrolenidae, *Centrolene balionotum*, *Centrolene geckoideum*, and *Cochranella cariticommata*: Distribution extension, new provincial records, Ecuador. Check List 3(1): 39–42. https://doi.org/10.15560/3.1.39

Cisneros-Heredia DF, Yánez-Muñoz MH, Sánchez-Nivicela JC, Ron SR (2023) Two new syntopic species of glassfrogs (Amphibia, Centrolenidae, *Centrolene*) from the southwestern Andes of Ecuador. PeerJ 11: e15195. https://doi.org/10.7717/peerj.15195

De Queiroz K (2007) Species concepts and species delimitation. Systematic Biology 56(6): 879–886. https://doi.org/10.1080/10635150701701083

Frost DR (2023) Centrolenidae Taylor, 1951 | Amphibian Species of the World. Amphibian Species of the World: an Online Reference. https://amphibiansoftheworld.amnh.org/Amphibia/Anura/Centrolenidae [January 31, 2022]

Guayasamin JM, Cisneros-Heredia DF, Yánez-Muñoz MH, Bustamante MR (2006) Amphibia, Centrolenidae, *Centrolene ilex*, *Centrolene litorale*, *Centrolene medemi*, *Cochranella albomaculata*, *Cochranella ametarsia*: Range extensions and new country records. Check List 2(1): 70. https://doi.org/10.15560/2.1.70

Guayasamin JM, Castroviejo F, Ayarzagüena J, Trueb L, Vilà C (2008) Phylogenetic relationships of glassfrogs (Family Centrolenidae) based on mitochondrial and nuclear genes. Molecular Phylogenetics and Evolution 48(2): 574–595. https://doi.org/10.1016/j.ympev.2008.04.012

Guayasamin JM, Castroviejo-Fisher S, Trueb L, Ayarzagüena J, Rada M, Vilà C (2009) Phylogenetic systematics of glassfrogs (Amphibia: Centrolenidae) and their sister taxon *Allophryne ruthveni*. Zootaxa 2100(1): 1–97. https://doi.org/10.11646/zootaxa.2100.1.1

Guayasamin JM, Cisneros-Heredia DF, McDiarmid RW, Peña P, Hutter CR (2020) Glassfrogs of Ecuador: Diversity, evolution, and conservation. Diversity 12(6): 222. https://doi.org/10.3390/d12060222

Guindon S, Dufayard JF, Lefort V, Anisimova M, Hordijk W, Gascuel O (2010) New algorithms and methods to estimate maximum-likelihood phylogenies: Assessing the performance of PhyML 3.0. Systematic Biology 59(3): 307–321. https://doi.org/10.1093/sysbio/syq010

Hime PM, Lemmon AR, Lemmon ECM, Prendini E, Brown JM, Thomson RC, Kratovil JD, Noonan BP, Pyron RA, Peloso PLV, Kortyna ML, Keogh JS, Donnellan SC, Mueller RL, Raxworthy CJ, Kunte K, Ron SR, Das S, Gaitonde N, Green DM, Labisko J, Che J, Weisrock DW (2020) Phylogenomics reveals ancient gene tree discordance in the Amphibian tree of life. Systematic Biology 70(1): 49–66. https://doi.org/10.1093/sysbio/syaa034

Hoang DT, Chernomor O, von Haeseler A, Minh BQ, Vinh LS (2018) UFBoot2: Improving the ultrafast bootstrap approximation. Molecular Biology and Evolution 35(2): 518–522. https://doi.org/10.1093/molbev/msx281

IUCN (2012) IUCN Red List Categories and Criteria: Version 3.1. Second edition. International Union for Conservation of Nature and Natural Resources IUCN, Gland, Switzerland and Cambridge, UK, 32 pp.

IUCN Standards and Petitions Committee (2022) Guidelines for using the IUCN Red List Categories and Criteria, version 15.1. IUCN.

Jiménez de la Espada M (1872) Nuevos batrácios americanos. Anales de la Sociedad Española de Historia Natural 1: 84–88.

Katoh K, Standley DM (2013) MAFFT multiple sequence alignment software version 7: Improvements in performance and usability. Molecular Biology and Evolution 30(4): 772–780. https://doi.org/10.1093/molbev/mst010

Kearse M, Moir R, Wilson A, Stones-Havas S, Cheung M, Sturrock S, Buxton S, Cooper A, Markowitz S, Duran C, Thierer T, Ashton B, Meintjes P, Drummond A (2012) Geneious Basic: An integrated and extendable desktop software platform for the organization and analysis of sequence data. Bioinformatics (Oxford, England) 28(12): 1647–1649. https://doi.org/10.1093/bioinformatics/bts199

Kok PJR, Castroviejo-Fisher S (2008) Glassfrogs (Anura: Centrolenidae) of Kaieteur National Park, Guyana, with notes on the distribution and taxonomy of some species of the family in the Guiana Shield. Zootaxa 1680(1): 25–53. https://doi.org/10.11646/zootaxa.1680.1.2

Lynch JD, Duellman WE (1973) A review of the Centrolenid frogs of Ecuador, with descriptions of new species. Occasional Papers of the Museum of Natural History, The University of Kansas 16: 1–66. https://doi.org/10.5962/bhl.part.29037

MAATE (2022) Mapa de Cobertura y Uso de la Tierra 2020. Ministerio del Ambiente, Agua y Transición Ecológica del Ecuador.

Maddison WP, Maddison DR (2019) Mesquite: a modular system for evolutionary analysis. Version 3.61. http://mesquiteproject.org

MAE, Galeas R, Guevara JE, Medina-Torres B, Chinchero MÁ, Herrera X (Eds) (2013) Sistema de Clasificación de Ecosistemas del Ecuador Continental. Ministerio del Ambiente del Ecuador MAE, Subsecretaría de Patrimonio Natural, Quito, 232 pp.

Mendoza-Henao AM, Basto-Riascos MC, Rada, M (2020) *Centrolene huilensis* Ruiz-Carranza y Lynch, 1995. Catálogo de anfibios y reptiles de Colombia 5: 18–23.

Mendoza-Henao AM, Zamudio KR, Guayasamin JM, Escalona M, Parra-Olea G (2023) Environment rather than character displacement explains call evolution in glassfrogs. Evolution; International Journal of Organic Evolution 77(2): 355–369. https://doi.org/10.1093/evolut/qpac041

Minh BQ, Schmidt HA, Chernomor O, Schrempf D, Woodhams MD, von Haeseler A, Lanfear R (2020) IQ-TREE 2: New Models and Efficient Methods for Phylogenetic Inference in the Genomic Era. Molecular Biology and Evolution 37(5): 1530–1534. https://doi.org/10.1093/molbev/msaa015

Nguyen LT, Schmidt HA, von Haeseler A, Minh BQ (2015) IQ-TREE: A fast and effective stochastic algorithm for estimating maximum-likelihood phylogenies. Molecular Biology and Evolution 32(1): 268–275. https://doi.org/10.1093/molbev/msu300

Pérez AR (1984) Significado de lugares geográficos y de poblaciones importantes para turistas nacionales y extranjeros. Cartilla de divulgación ecuatoriana 43: 1–15.

Peters WCH (1873) Über eine neue Schildkrötenart, *Cinosternon effeldtii* und einige andere neue oder weniger bekannte Amphibien. Monatsberichte der Königlichen Preussische Akademie des Wissenschaften zu Berlin 1873: 603–618. https://doi.org/10.5962/bhl.part.26974

Rivero JA (1968) Los centrolenidos de Venezuela (Amphibia, Salientia). Memorias de la Sociedad de Ciencias Naturales La Salle 28: 301–334.

Roy BA, Zorrilla M, Endara L, Thomas DC, Vandegrift R, Rubenstein JM, Policha T, Ríos-Touma B, Read M (2018) New Mining Concessions Could Severely Decrease Biodiversity and Ecosystem Services in Ecuador. Tropical Conservation Science 11: 194008291878042. https://doi.org/10.1177/1940082918780427

Ruiz-Carranza PM, Lynch JD 1989. Una nueva especie de *Centrolenella* Noble, 1920 (Amphibia: Anura: Centrolenidae) de la Cordillera Oriental de Colombia. Trianea. Bogotá 3: 67–75.

Ruiz-Carranza PM, Lynch JD (1991a) Ranas Centrolenidae de Colombia II. Nuevas especies de *Centrolene* de la Cordillera Oriental y Sierra Nevada de Santa Marta. Lozania 58: 1–26.

Ruiz-Carranza PM, Lynch JD (1991b) Ranas Centrolenidae de Colombia III: Nuevas especies de *Cochranella* del grupo *granulosa*. Lozania 59: 1–18.

Ruiz-Carranza PM, Lynch JD (1995) Ranas Centrolenidae de Colombia VIII. Cuatro nuevas especies de *Centrolene* de la Cordillera Central. Lozania 65: 1–16.

Sambrook J, Fritsch EF, Maniatis T (1989) Molecular Cloning: a Laboratory Manual. Cold Spring Harbor Laboratory Press, Cold Spring Harbor, 1546 pp.

Székely P, Córdova-Díaz M, Hualpa-Vega D, Hualpa-Vega S, Székely D (2023) A new glassfrog species of the genus *Centrolene* (Amphibia, Anura, Centrolenidae) from Cordillera del Cóndor, southern Ecuador. ZooKeys 1149: 53–84. https://doi.org/10.3897/zookeys.1149.96134

Taylor EH (1949) Costa Rican frogs of the genera *Centrolene* and *Centrolenella*. The University of Kansas Science Bulletin 33: 257–270. https://doi.org/10.5962/bhl.part.16128

To T-H, Jung M, Lycett S, Gascuel O (2016) Fast dating using least-squares criteria and algorithms. Systematic Biology 65(1): 82–97. https://doi.org/10.1093/sysbio/syv068

Twomey E, Delia J, Castroviejo-Fisher S (2014) A review of northern Peruvian glassfrogs (Centrolenidae), with the description of four new remarkable species. Zootaxa 3851(1): 1–87. https://doi.org/10.11646/zootaxa.3851.1.1

Vences M (2020) The promise of next generation taxonomy. Megataxa 1(1): 35–38. https://doi.org/10.11646/megataxa.1.1.6

Supplementary material 1

Maximum likelihood time-tree of Centrolenidae

Authors: Santiago R. Ron, Dominike García, David Brito-Zapata, Carolina Reyes-Puig, Elías Figueroa-Coronel, Diego F. Cisneros-Heredia

Data type: pdf

Explanation note: Maximum likelihood time-tree inferred from a partitioned analysis of 6626 aligned sites of the mitochondrial genes 12S rRNA, 16S rRNA, ND1 and the nuclear genes BDNF, C-MYC 2, CXCR4, POMC, RAG1, SLC8A1, SLC8A3 showing phylogenetic relationships of Centrolenidae.

Link: https://doi.org/10.3897/zse.100.116350.suppl1

Zoosyst. Evol. 100 (3) 2024, 941–963 | DOI 10.3897/zse.100.124370

PENSOFT

für Natur MUSEUM FÜR NATURKUNDE BERLIN

Taxonomic resolution of the hillstream suck-loach *Beaufortia pingi* species group (Cypriniformes, Gastromyzontidae) and two new species from Southwest China–*Beaufortia granulopinna* and *Beaufortia viridis*

Jing-Chen Chen[1,2], Jia-Jia Li[1,2], Wen-Qiao Tang[1,2], Xin-Rui Pu[3], Hao-Tian Lei[4]

1 *Shanghai Universities Key Laboratory of Marine Animal Taxonomy and Evolution, Shanghai Ocean University, Shanghai 201306, China*
2 *Key Laboratory of Exploration and Utilization of Aquatic Genetic Resources, Ministry of Education, Shanghai Ocean University, Shanghai 201306, China*
3 *International College, Yunnan Agricultural University, Kunming 650500, China*
4 *College of Plant protection, China Agricultural University, Beijing 100093, China*

https://zoobank.org/59836C29-33F6-40F1-A9EC-16D17086D820

Corresponding author: Wen-Qiao Tang (wqtang@shou.edu.cn)

Academic editor: Nicolas Hubert ♦ **Received** 1 April 2024 ♦ **Accepted** 31 May 2024 ♦ **Published** 9 July 2024

Abstract

Two new species, *Beaufortia granulopinna* and *Beaufortia viridis*, are described from the upper Pearl River system in southwest China. Both species share the characteristics of the *Beaufortia pingi* species group, including prominent vertical stripes on the lateral body and pinnate-type lower lips, distinguishing them from other *Beaufortia* species. *Beaufortia granulopinna* is differentiated from other species in the group by possessing a unique set of characteristics: the presence of well-developed prominent tubercles on the first 6–9 pectoral fin rays in adults; and a significant proportion (54.76%) of individuals experiencing blurriness or absence of vertical stripes in the mid-section of the lateral body upon reaching adulthood. The minimum interspecific genetic distance within the genus based on mitochondrial *cyt*b gene sequences is 10.80%. *Beaufortia viridis* is distinguished from other species in the group by consistently exhibiting vertical stripes of uniform length, width, and spacing across all stages of growth; the absence of tubercles on the branched rays of pectoral fins; and a body coloration of dark cyan to green. The minimum interspecific genetic distance within the genus based on mitochondrial *cyt*b gene sequences is 4.60%. Molecular phylogenetic results confirm that the *Beaufortia pingi* species group forms a monophyletic clade, which is congruent with morphological classification findings. This study also addresses and resolves the taxonomic ambiguity surrounding *Beaufortia pingi* and *Beaufortia zebroida*, providing a redescription of these taxa.

Key Words

Beaufortia pingi, *Beaufortia zebroida*, *Beaufortia*, morphology, molecular phylogeny, redescription

Introduction

The genus *Beaufortia*, belonging to the order Cypriniformes and family Gastromyzontidae, is distributed in the upper and middle reaches of the Yangtze River system, the Pearl River system, Hainan Island, and from Yunnan in China to the northern part of the Red River system in Vietnam (Kottelat 2012). This genus comprises small, benthic fish species that inhabit mountain streams. To adapt to fast-flowing environments, these rheophilic fish have undergone significant morphological specializations, including a compressed body, a flattened ventral surface, and greatly expanded paired fins forming a suction cup-like structure. These adaptations enable them to adhere to the rocky substrate, resisting the currents while feeding on algae and invertebrates.

In 1932, Hora established the genus *Beaufortia* for *Gastromyzon* species distributed in China, based on the absence of a continuous, elongated skin flap between the bases of the pectoral and ventral fins. Other characteristics of this genus as defined by Hora include small gill openings restricted to above the pectoral fins, the posterior edges of the ventral fins fused into a fin disk, a mouth slit smaller than 1/3 of the head width, and pectoral fins extending beyond the origin of the ventral fins (Hora 1932). These diagnostic features have been widely accepted over time, and several species have subsequently been discovered and classified within this genus.

At the onset of this study, the Catalog of Fishes had recorded 13 valid species within the genus, 12 of which were distributed in China (Frice et al. 2024). Among these, *Beaufortia yunnanensis* (Li, Lu & Mao, 1998) is particularly controversial. It was initially classified under the genus *Paraprotomyzon*, and its type specimen has been lost; it was later reassigned to the genus *Beaufortia* by Kottelat (Li et al. 1998; Kottelat 2012). *B. buas* (Mai, 1978) was deemed questionable due to unclear locality data, low identification clarity in hand-drawn illustrations, and rudimentary morphological information (Kottelat 2012). Historically, six other species have been included in the genus *Beaufortia* based on Vietnamese literature. Among these, *B. fasciolata* Nguyen, 2005; *B. multiocellata* Nguyen, 2005; and *B. triocellata* Nguyen, 2005 are now considered junior synonyms of *B. zebroida* (Fang, 1930) (Kottelat 2012). *Gastromyzon daon* Mai, 1978; *Gastromyzon elongata* Mai, 1978; and *Gastromyzon loos* Mai, 1978, which were described in the same publication as *Beaufortia buas*, also suffer from unclear locality data, low identification clarity in hand-drawn illustrations, and rudimentary morphological information and are currently regarded as species inquirenda and assigned to the genus *Pseudogastromyzon* (Kottelat 2012). Kottelat (2013) included them as species inquirenda within the genus *Beaufortia*. According to Chen et al. (2023), species of the genus *Pseudogastromyzon* are restricted to southeastern mainland China and do not extend to Vietnam. Therefore, the validity and taxonomic status of these species remain contentious.

Following extensive sampling of specimens from the genus *Beaufortia* and through morphological and phylogenetic analyses, we identified two new species: *Beaufortia granulopinna* Chen & Tang, 2024, sp. nov. and *Beaufortia viridis* Chen & Tang, 2024, sp. nov. Additionally, we addressed the taxonomic issues surrounding *Beaufortia pingi* and *Beaufortia zebroida*, providing redescriptions of these two species.

Materials and methods

Sample collection

Handheld dip nets were utilized as the primary tool for sample collection. According to documented literature, the distribution range of the *B. pingi* species group includes Lingyun County, Tian'e County, Tianlin County, and Longzhou County in Guangxi Province, and Guangnan County in Yunnan Province, where specimen collection was conducted (Fang 1930; Chen 1990; Chen and Tang 2000). Due to various natural and anthropogenic factors leading to habitat alterations, no specimens were collected in Tian'e County and Longzhou County. Extensive exploration of other potential distribution areas was conducted, leading to the discovery and collection of specimens in the Youjiang District of Baise City, Debao County, Xilin County, Napo County, and Wuming District of Nanning City in Guangxi Province, and Wenshan Zhuang and Miao Autonomous Prefecture in Yunnan Province. Additional collections of *B. szechuanensis* (Fang, 1930), *B. liui* Chang, 1944, *B. niulanensis* Chen, Huang & Yang, 2009, *B. polylepis* Chen, 1982, *B. kweichowensis* (Fang, 1931), and *B. leveretti* (Nichols & Pope, 1927) specimens were conducted from the middle and upper reaches of the Yangtze River in Sichuan Province, the Jinsha River basin and Nanpan River basin in Yunnan Province, the Li River basin in Guangxi Province, and the Duliu River basin in Guizhou Province, as well as from Hainan Province for comparative purposes. Following euthanasia, specimens were preserved in a 95% ethanol or 0.3% formalin solution, with 3–5 individuals randomly selected from each batch for mitochondrial cytb gene sequencing. Despite repeated attempts, no specimens of *B. yunnanensis*, *B. huangguoshuensis* Zheng & Zhang, 1987, *B. intermedia* Tang & Wang, 1997, and *B. cyclica* Chen, 1980 were obtained, and morphological data were cited from their original descriptions based on examination of their holotypes or paratypes. All fish collections followed the Law of the People's Republic of China on the Protection of Wildlife, and we strictly adhered to all applicable international, national, and institutional guidelines for the care and use of animals.

For other questionable species with unobtainable specimens and disputed taxonomic status, their original morphological descriptions were referenced.

Morphometric data measurement

Countable characteristics were examined using a stereoscopic microscope. The last branched anal-fin and dorsal-fin rays located on the last complex pterygiophore were counted as a single ray (Fig. 1). A considerable percentage of the population belonged to a phenotype characterized by attenuated and unbranched terminal fin rays in the paired fins. This specific anatomical feature was quantitatively assessed as equivalent to 0.5 of a standard branched fin ray. Following the photographic documentation of specimens in dorsal, lateral, and ventral views, measurements were conducted using TPSDIG2 software (Rohlf 2016), as depicted in Fig. 1. Statistical analyses of the measurable characteristics were conducted using SPSS v.26.0 (IBM Corp. 2020) to assess the significance of differences.

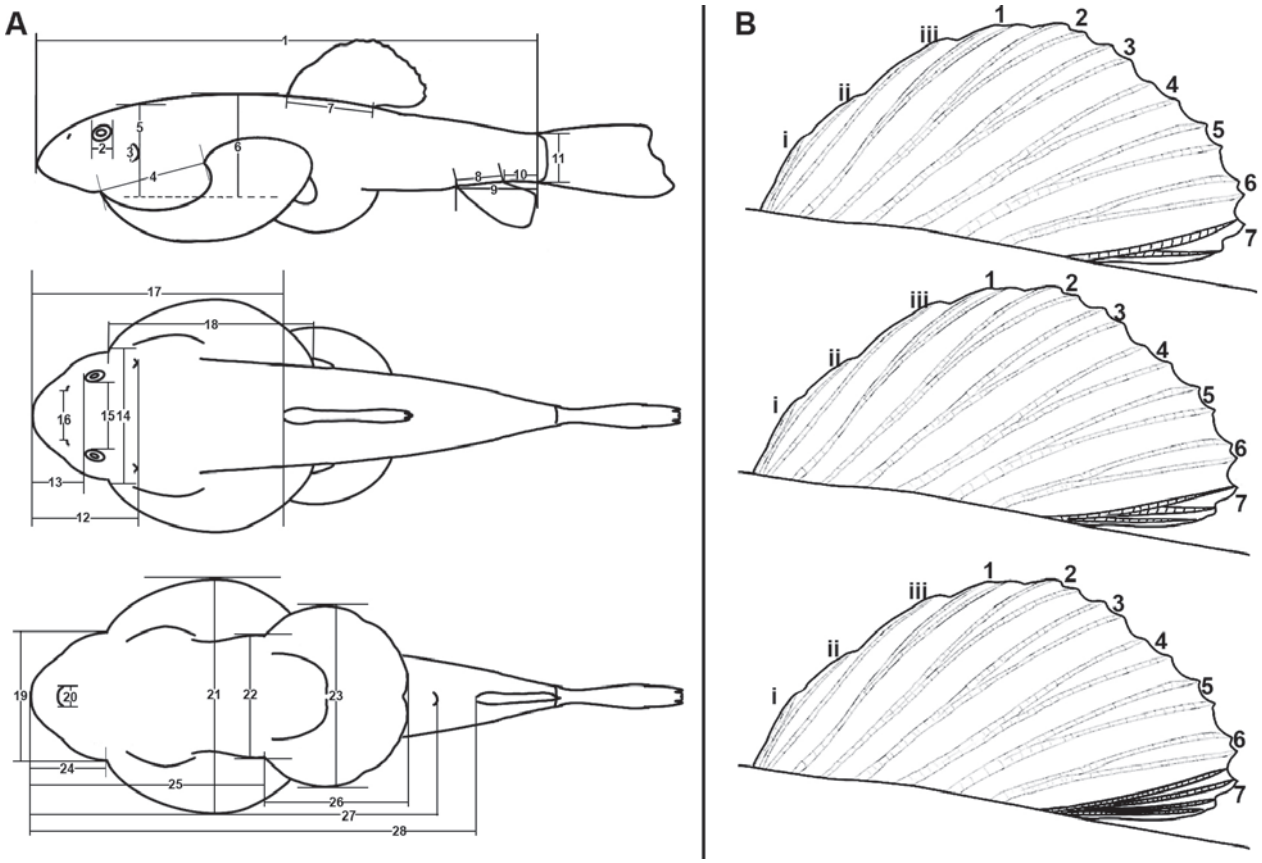

Figure 1. A. Morphometric measurement methodology for species within the genus *Beaufortia*: 1 - Standard length (SL); 2 - Eye diameter (ED); 3 - Gill slit length (GSL); 4 - Pectoral fin base length (PBL); 5 - Head length (HL); 6 - Body depth (BD); 7 - Dorsal fin base length (DBL); 8 - Anal fin base length (ABL); 9 - Post-anal fin length (PoAL); 10 - Caudal peduncle length (CL); 11 - Caudal peduncle depth (CD); 12 - Head length (HL); 13 - Snout Length (SnL); 14 – Head width (HW); 15 - Interorbital distance (IOD); 16 - Distance between nostrils (ND); 17 - Pre-dorsal Length (PrDL); 18 - Pectoral fin disc length (PL); 19 - Head width at pectoral fin origin (HWPO); 20 - Mouth slit width (MW); 21 - Pectoral fin disc width (PW); 22 - Body width (BW); 23 - Pelvic fin disc width (PvW); 24 – Pre-pectoral length (PrPL); 25 – Pre-pelvic length (PrPvL); 26 - Pelvic fin disc length (PvL); 27 - Pre-anal pore length (PrApL); 28 - Pre-anal fin length (PrAL); **B.** The last branched anal-fin and dorsal-fin rays located on the last complex pterygiophore were counted as a single ray.

Mitochondrial *cyt*b gene sequencing

DNA was extracted from the right pectoral fin rays using a kit produced by Sangon Biotech (Shanghai) Co., Ltd., following the protocol provided. Primers GAC TTG AAG AAC CAC CGT TGT TAT T 5'–3' and TCT TCG GAT TAC AAG ACC GAT GCT TT 5'–3' were employed to amplify the *cyt*b gene. The PCR mixture consisted of 1μL DNA template, 1μL of each primer (10 μM), 12.5μL Taq Mix (Sangon Biotech), and 9.5μL deionized water, totaling a reaction volume of 25μL. The PCR conditions included an initial denaturation at 95 °C for 3 minutes, followed by 35 cycles of 94 °C for 30 seconds, 55 °C for 45 seconds, and 72 °C for 60 seconds, with a final extension at 72 °C for 5 minutes and a hold at 4 °C. Amplified products were sequenced by Sangon Biotech, and the sequences were verified for accuracy before submission to the National Center for Biotechnology Information (NCBI). The collection sites for the molecular materials are listed in Table 1.

Phylogenetic analysis and genetic distance estimation

A total of 35 mitochondrial *cyt*b gene haplotypes were identified. The *cyt*b sequence of *Plesiomyzon baotingensis* (KF732713), retrieved from NCBI, was utilized as the outgroup, with a haplotype of *B. szechuanensis* (NC027291) included as additional material. Phylogenetic analyses were conducted using PHYLOSUITE (Zhang et al. 2020) with sequence alignment performed by MAFFT (Katoh and Standley 2013) set to automatic strategy and normal alignment mode. ModelFinder (Kalyaanamoorthy et al. 2017) was used to determine the best-fit models for both Maximum Likelihood (ML) and Bayesian Inference (BI) methods. The ML phylogenetic tree was constructed using IQ-TREE (Nguyen et al. 2015), with the best-fit model according to BIC being MGK+G4, and the outgroup set to *Plesiomyzon baotingensis*, with default parameters for other settings. The BI phylogenetic tree was constructed using MRBAYES 3.2.6 (Ronquist

Table 1. Collection localities and accession numbers of molecular samples.

Species	Specimen voucher	Sampling localities	River system	GenBank accession
Beaufortia granulopinna sp. nov.	SHOU20240103028	Tianlin County, Guangxi	Pearl River (upper reaches)	PP482589
	SHOU20240102801	Tianlin County, Guangxi		PP482590
	SHOU20240103650	Tianlin County, Guangxi		PP482592
	SHOU20240103652	Tianlin County, Guangxi		PP482593
	SHOU20240115013	Guangnan County, Yunnan		PP482591
Beaufortia viridis sp. nov.	SHOU20240103615	Nanning City, Guangxi		PP482580
	SHOU20240126801	Lingyun County, Guangxi		PP482581
	SHOU20240112104	Guangnan County, Yunnan		PP482578
	SHOU20240111616	Guangnan County, Yunnan		PP482579
	SHOU20240112103	Guangnan County, Yunnan		PP482582
Beaufortia pingi	SHOU20240102207	Lingyun County, Guangxi		PP482563
	SHOU20240102216	Lingyun County, Guangxi		PP482564
	SHOU20240102217	Lingyun County, Guangxi		PP482565
	SHOU20240102206	Lingyun County, Guangxi		PP482566
	SHOU20240102602	Lingyun County, Guangxi		PP482567
	SHOU20240126802	Baise City, Guangxi		PP482561
	SHOU20240102212	Baise City, Guangxi		PP482568
	SHOU20240103210	Debao County, Guangxi		PP482562
Beaufortia zebroida	SHOU20240111304	Guangnan County, Yunnan	Red River (lower reaches, North bank)	PP482585
	SHOU20240111302	Guangnan County, Yunnan		PP482588
	SHOU20240111313	Malipo County, Yunnan		PP482586
	SHOU20240111312	Funing County, Yunnan		PP482587
Beaufortia kweichowensis	SHOU20231212604	Congjiang County, Guangxi	Pearl River (upper reaches)	PP482574
	SHOU20231212645	Lingchuan County, Guangxi		PP482576
	SHOU20231212620	Huizhou City, Guangdong	Pearl River (lower reaches)	PP482575
Beaufortia leveretti	SHOU20231212641	Baisha County, Hainan	Nandu River	PP482577
Beaufortia szechuanensis	SHOU20231220642	Neijiang City, Sichuan	Yangtze River (upper reaches)	PP482569
Beaufortia niulanensis	SHOU20240120617	Qujing District, Yunnan		PP482583
	SHOU20240120616	Qujing District, Yunnan		PP482584
Beaufortia polylepis	SHOU20231220644	Kaiyuan City, Yunnan	Pearl River (upper reaches)	PP482570
	SHOU20231220619	Shizong County, Yunnan		PP482571
	SHOU20231220630	Luoping County, Yunnan		PP482572
	SHOU20231220636	Luoping County, Yunnan		PP482594
Beaufortia cf. *szechuanensis*	SHOU20231220611	Qijiang District, Chongqing	Yangtze River (upper reaches)	PP482573

et al. 2012), with the model set to HKY+F+G4 and the outgroup as *Plesiomyzon baotingensis*, maintaining default parameters for other settings. The resulting tree files were visualized and embellished using FIGTREE v1.4.4 (Rambaut 2018).

Genetic distances were calculated using MEGA11 (Tamura et al. 2021) with the Kimura 2-parameter model (rates among sites: G4), computing distances among all samples, average interspecific genetic distances, and average intraspecific genetic distances.

Results

Taxonomic account

Beaufortia granulopinna Chen & Tang, sp. nov.

https://zoobank.org/8A80A35D-C2A8-4B55-80D1-2BFDBA68B374
Figs 2–4

Gastromyzon pingi Fang, 1930: 35–36, No. 955, paratype, former Lingyun County, near the border of Yunnan.

Beaufortia pingi: Chen and Zhang (2006): 376–377, Tianlin County, Guangxi (fig. X98).

Type material. ***Holotype*.** SHOU20240103001, 72.48 mm total length (TL), 57.17 mm standard length (SL), adult (Fig. 2). Collected by Jing-Chen Chen and Qian-Yu Liang on 24 December 2023, from Lizhou River, a stream tributary of Bo′ai River of Pearl River basin, at Tianlin County, Guangxi Province, China (24°20.34'N, 106°21.624'E; c. 470m a.s.l.) (Fig. 5).

***Paratypes*.** 21 specimens from the same locality as holotype, SHOU20240103002-022, 21.41–54.00 mm SL, were collected by Qian-Yu Liang and Jing-Chen Chen on 24 December 2023; 12 specimens from Guangnan County, Wenshan Zhuang, and Miao Autonomous Prefecture, Yunnan Province, China, SHOU20240115001-012, 31.86–44.07 mm SL, were collected by Xinrui Pu and Jing-Chen Chen on 08 January 2024.

Additional materials. Seven specimens from the type locality, SHOU20240103023-29, were collected by Qian-Yu Liang from December 2022 to April 2023; one specimen from Guangnan County, Wenshan Zhuang, and Miao Autonomous Prefecture, Yunnan Province, China, SHOU20240115013 was collected by Lin Yang and Lao Xing in December 2022.

Diagnosis. *B. granulopinna* sp. nov. shares typical characteristics with members of the *B. pingi* species group,

Figure 2. Lateral (top), dorsal (middle), and ventral (bottom) views of *Beaufortia granulopinna* sp. nov., holotype, adult, SHOU20240103001, 57.17 mm SL; from Lizhou River, a stream tributary of Bo′ai River of the Pearl River basin, at Tianlin County, Guangxi Province, China.

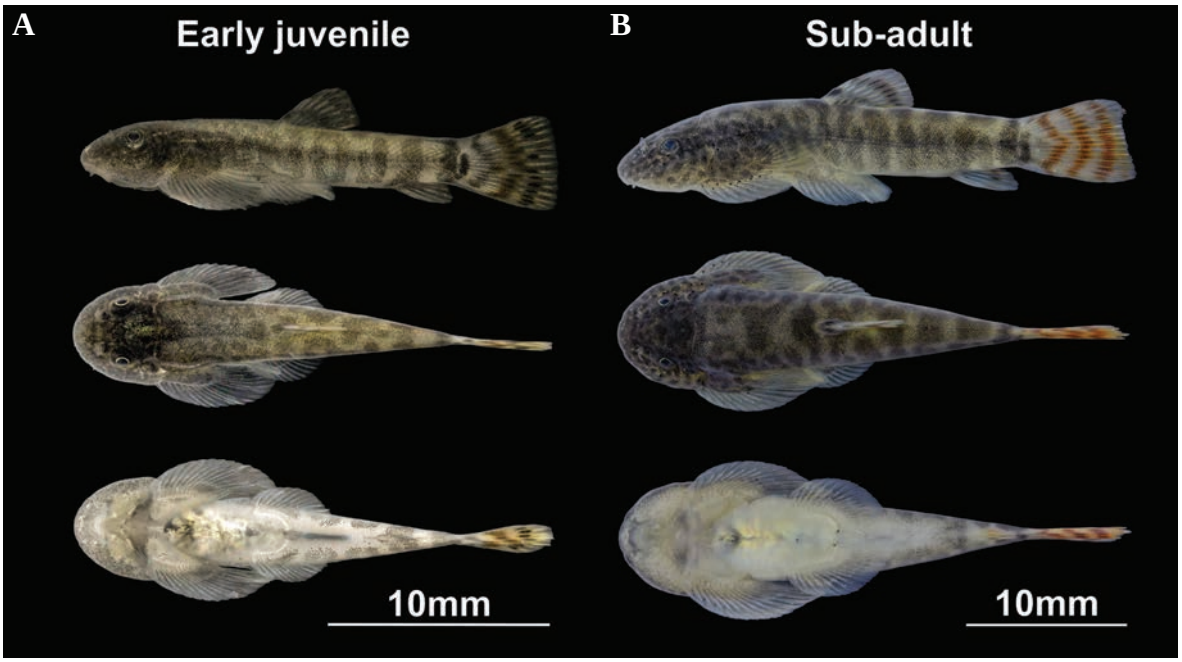

Figure 3. Lateral (top), dorsal (middle), and ventral (bottom) views of *Beaufortia granulopinna* sp. nov. during early juvenile and sub-adult stages. **A.** Early juvenile stage, SHOU20240103658, from type locality, 16.09 mm SL, pelvic fins completely separated; **B.** Sub-adult stage, SHOU20240103005, paratype, 24.21 mm SL.

with distinct vertical stripes on the flank, and a pinnate-type lower lip (vs. lacking prominent vertical stripes and having a dicot-type lower lip in other congeneric species apart from this group) (see Figs 6D, 7, Table 2). *B. granulopinna* can be clearly distinguished from *B. pingi*, *B. zebroida*, and *B. viridis* sp. nov. by the presence of well-developed tubercles on the anterior 6–9 pectoral fin rays (vs. absent or inconspicuous tubercles on pectoral fin rays). Moreover, *B. granulopinna* can be distinguished from *B. pingi* by generally fewer branched fin rays in the paired fins, with 18.5–22 (mean 20.11±0.77) in pectoral fins (vs. 21–24 (mean 22.19±0.78)) and 15–18 (mean 16.51±0.86) in pelvic fins (vs. 17–21 (mean 18.64±0.97)). It can be further differentiated from *B. viridis* sp. nov. and *B. zebroida* by a certain proportion (54.76%) of individuals exhibiting blurred or vanished vertical stripes in the mid-section of the lateral body in adulthood (vs. stable presence of vertical stripes at all growth stages).

Description. Dorsal iii-6–7(6.98±0.15), anal ii-4, pectoral i-18.5-22(20.11±0.77), pelvic i-15-18(16.51±0.86). Lateral-line canal pores and scales: 63–73 (68.76±2.5) (see Table 2).

Morphometric measurements for the specimens examined are given in Table 3. See Fig. 2 for lateral, dorsal, and ventral views of the body.

Head-thorax cylindrical, dorsal slightly humped medially, flattened ventrally, body compressed from pelvic fins to caudal peduncle. Head broad, blunt, length slightly less than width, more than depth, nuptial tubercles well-developed on lower half of head in mature individuals, snout rounded, length about half of head length. Mouth inferior, narrow, width about one-fifth head width, horseshoe-shaped, angle about 96° from midpoint to ends. Upper lip smooth, without distinct papillae; lower lip pinnate-type, slightly concave medially with multilobed sides; jaw edges slightly protrude. Shallow groove between upper lip and snout, extending to mouth corners. Lateral grooves shallow or indistinct. Two pairs of rostral barbels present, with outer pair slightly longer, space between rostral barbels with leaf-like folds, edges of which rounded and poor developed. One pair of maxillary barbels, length about equal to outer rostral barbels. Nostrils with tubular nasal flaps, distance between nostrils equals one-third head width. Eyes supralateral, medium-sized, eye diameter about one-quarter head length, interorbital space flat, width about half head width. Gill opening small, about equal to eye diameter, originated about vertically above the second branched pectoral fin ray, limited to dorsal side of head. Scales small, diameter smaller than pupil, dorsal surface of head, base of paired fins, and ventral area before pelvic fin bases nude. Lateral line complete, at midlateral.

Dorsal fin base about equal to pre-pectoral length, starting around midpoint from snout to caudal fin base, adpressed extending to about midway between dorsal fin origin and caudal fin base. Anal fin base length about half of that of dorsal fin base, adpressed extending slightly beyond caudal fin base. Paired fins extending outwards, forming disc-like structure with body. Pectoral fin base slightly longer than head length, starting at the posterior one-third point of head, pectoral fin length about twice head length, tips of which reaching pelvic fin base midpoint, pectoral disc width about 1.5 times head width at pectoral origin. Anterior 6–9 pectoral fin rays

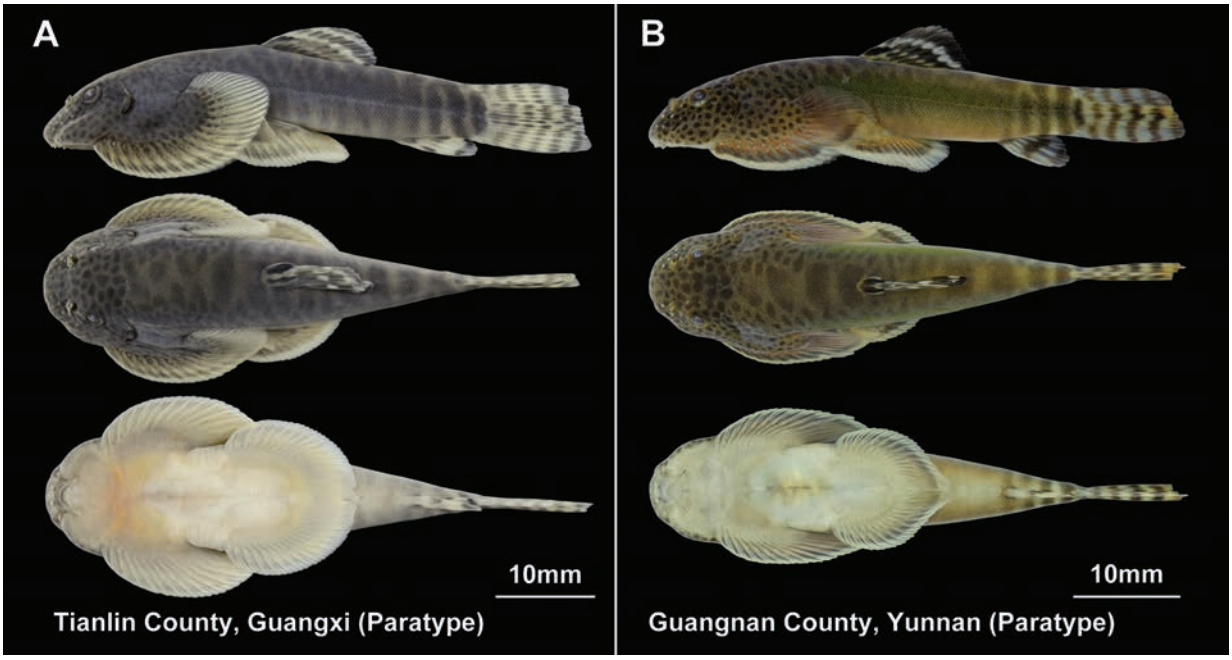

Figure 4. Lateral (top), dorsal (middle), and ventral (bottom) views of one common phenotypic variation of *Beaufortia granulopinna* sp. nov. and other regional phenotypes. **A.** Phenotype with persistent vertical stripe on lateral body, paratype, SHOU20240103003, 40.77 mm SL, from Tianlin County, Guangxi; **B.** Regional phenotype from Qingshui River, Guangnan County, Yunnan Province, paratype, SHOU20240115001, 39.01 mm SL.

Table 2. Key diagnostic features and countable characteristics of species within the genus *Beaufortia*.

Species	Vertical stripes on flank	Type of lower lip	Pectoral branch rays		Pelvic branch rays		Dorsal branch rays		Anal branch rays		Lateral-line canal-pores and scales		N
			Range	Mean ± SD	Range	Mean ± SD	Range	Mean ± SD	Range	Mean ± SD	Range	Mean ± SD	
***B. granulopinna* Chen & Tang 2024, sp. nov.**	present	pinnate	18.5–22	20.11 ± 0.77	15–18	16.51 ± 0.86	6–7	6.98 ± 0.15	4	4	63–73	68.76 ± 2.5	42
***B. viridis* Chen & Tang 2024, sp. nov.**	present	pinnate	19–23	21.09 ± 1.03	14.5–19	17.11 ± 1.02	7	7	4	4	65–83	73.51 ± 4.26	36
***B. pingi* (Fang, 1930)**	present	pinnate	21–24	22.19 ± 0.78	17–21	18.64 ± 0.97	7–8	7.08 ± 0.27	3–4	3.98 ± 0.14	68–92	75.28 ± 4.01	50
***B. zebroida* (Fang, 1930)**	present	pinnate	20–23	21.5 ± 0.73	16–19	17.53 ± 0.86	7	7	3–4	3.94 ± 0.24	70–84	75.12 ± 3.55	17
? *B. fasciolata* Nguyen, 2005	present	pinnate	21	21	16	16	7	7	5	5	87–88	–	2
? *B. triocellata* Nguyen, 2005	present	pinnate	21–22	–	16–17	–	7	7	5	5	86–96	–	3
? *B. multiocellata* Nguyen, 2005	present	pinnate	21–22	–	15–16	–	7	7	5	5	91–102	–	7
B. szechuanensis (Fang, 1930)	absent	Dicot	25–26.5	25.9 ± 0.55	18.5–20.5	19.6 ± 0.82	7	7	5	5	82–95	89.4 ± 5.32	5
B. liui Chang, 1944	absent	Dicot	21	21	17	17	7	7	5	5	92	92	1
B. huangguoshuensis Zheng & Zhang, 1987	absent	Dicot	27	27	19	17	6	6	5	5	84	84	1
B. polylepis Chen, 1982	absent	Dicot	26–27	26.5 ± 0.71	19–21	20 ± 1.41	6–7	6.5 ± 0.71	5	5	80–84	82 ± 2.83	2
B. intermedia Tang & Wang, 1997	absent	Dicot	25–28	–	24	–	7–8	–	5	5	81–86	–	9
B. niulanensis Chen, Huang & Yang, 2009	absent	Dicot	25.5–27.5	26.17 ± 1.15	20	20	7	7	5	5	78–90	84.33 ± 6.03	3
? *B. yunnanensis* (Li, Lu & Mao, 1998)	absent	Dicot	26	26	20	20	8	8	5	5	87	87	1
B. leveretti (Nichols & Pope, 1927)	absent	Dicot	23–25	24.4 ± 0.89	19.5–23.5	21.5 ± 1.77	8	8	4–5	4.4 ± 0.55	59–63	60.6 ± 1.82	5
B. kweichowensis (Fang, 1931)	absent	Dicot	24–25.5	24.9 ± 0.55	21.5–24.5	23 ± 1.22	8	8	4–5	4.4 ± 0.55	60–64	62.4 ± 1.52	5
B. cyclica Chen, 1980	absent	Dicot	30	30	20	20	7	7	5	5	72	72	1
? *B. buas* (Mai, 1978)	absent	–	24	24	19	19	8	8	5	5	55–65	–	–
? *B. daon* (Mai, 1978)	absent	–	25	25	19	19	9	9	5	5	75–85	–	–
? *B. elongata* (Mai, 1978)	absent	–	27	27	20	20	8	8	5	5	65	65	–
? *B. loos* (Mai, 1978)	absent	–	25	25	21	21	8	8	5	5	–	–	–

Species belonging to the *Beaufortia pingi* species group are highlighted in bold; a question mark "?" indicates substantial taxonomic controversy surrounding the species, and "-" stands for no corresponding data.

Figure 5. Collection site of the holotype (SHOU20240103001) of *Beaufortia granulopinna* sp. nov., from Lizhou River, a stream tributary of Bo′ai River of the Pearl River basin, Tianlin County, Guangxi Province, China. Photographed by Qian-Yu Liang on 24 December 2023.

Table 3. Morphometric results for species within the *Beaufortia pingi* group.

Characters	*B. granulopinna* sp. nov. (N=42)			*B. viridis* sp. nov. (N=36)			*B. pingi* (N=50)		*B. zebroida* (N=17)	
	Holotype	All materials		Holotype	All materials		Range	Mean ± SD	Range	Mean ± SD
		Range	Mean ± SD		Range	Mean ± SD				
Standard length (mm)	57.17	21.41–57.17	36.34±8.30	38.03	18.82–59.85	41.64±11.37	27.64–58.12	47.53±6.94	33.24–49.96	41.25±5.18
Vertical stripe blurring propotion	54.76% (N=23)			0			94.00% (N=47)		0	
Ratio of standard length to										
Body depth	3.97	3.97–6.27	**5.10±0.43***	5.36	4.25–6.11	5.31±0.54	3.91–6.48	**5.09±0.71***	4.90–5.98	5.47±0.33
Body width	3.93	3.92–5.34	4.61±0.35	4.54	3.79–5.46	4.43±0.41	3.65–4.88	**4.20±0.36***	3.93–5.19	4.62±0.37
Head length	4.94	4.19–5.05	4.63±0.21	4.40	3.91–4.98	4.45±0.24	4.42–5.32	**4.9±0.18***	4.28–5.06	4.61±0.19
Caudal peduncle length	17.17	10.42–21.40	14.38±2.61	13.11	9.72–17.16	12.53±1.78	10.85–17.99	13.77±1.57	9.62–16.94	12.37±1.85
Caudal peduncle depth	7.67	7.32–9.89	**8.36±0.52***	9.51	7.89–11.53	9.87±1.01	8.52–11.93	10.21±1.00	8.84–10.9	10.01±0.48
Predorsal length	2.03	1.88–2.11	1.97±0.06	1.99	1.81–2.14	1.98±0.07	1.95–2.21	2.04±0.06	1.90–2.47	2.01±0.13
Prepelvic length	2.40	2.14–2.40	2.29±0.06	2.34	2.07–2.52	2.28±0.08	2.19–2.49	2.36±0.08	2.15–2.38	2.28±0.06
Prepectoral length	7.36	5.70–7.73	6.72±0.51	6.83	5.54–7.51	6.71±0.41	6.60–8.24*	**7.42±0.39***	5.94–7.52	6.84±0.42
Pectoral base length	4.46	4.00–5.46	4.67±0.37	4.48	3.89–5.37	4.55±0.29	4.06–5.24	4.59±0.29	4.32–5.3	4.80±0.28
Pectoral length	2.56	2.44–3.56	2.63±0.19	2.47	2.37–2.84	2.55±0.12	2.43–2.84	2.63±0.09	1.94–2.73	2.50±0.18
Pectoral width	2.30	2.21–2.97	2.55±0.18	2.59	2.18–2.80	2.44±0.15	2.13–3.11	2.43±0.21	2.34–2.85	2.59±0.18
Pelvic length	3.27	3.03–3.88	3.46±0.20	3.30	2.97–4.04	3.33±0.23	2.94–3.67	3.26±0.18	3.29–3.65	3.44±0.11
Ratio of caudal peduncle length to										
Caudal peduncle depth	0.45	0.37–0.80	0.60±0.11	0.73	0.53–1.17	0.81±0.16	0.57–0.99	0.75±0.12	0.61–1.13	0.82±0.12
Ratio of head length to										
Head depth	1.05	1.01–1.66	1.27±0.12	1.54	1.19–1.72	1.41±0.13	1.05–1.58	1.26±0.13	1.13–1.72	1.35±0.15
Head width	0.71	0.71–0.91	0.82±0.05	0.87	0.70–0.97	0.84±0.06	0.65–0.88	0.77±0.06	0.78–1.07	0.88±0.06
Snout length	2.08	1.97–2.77	2.31±0.18	2.24	1.89–2.59	2.24±0.19	1.76–3.24	2.09±0.22	2.15–2.49	2.30±0.10
Eye diameter	5.15	3.37–5.23	4.30±0.50	4.41	3.51–6.95	4.59±0.76	3.86–5.58	4.53±0.41	3.62–5.35	4.36±0.47
Interorbital width	1.38	1.35–2.38	1.73±0.26	1.60	1.48–1.99	1.68±0.14	1.18–2.30	1.51±0.24	1.47–2.32	1.78±0.28
Prepectoral length	1.49	1.26–1.65	1.45±0.10	1.55	1.38–1.75	1.51±0.08	1.39–1.68	1.51±0.07	1.30–1.62	1.49±0.09
Ratio of head width to										
Mouth width	4.59	4.27–6.40	5.19±0.46	4.99	4.32–6.60	5.44±0.63	4.69–6.72	**5.79±0.50***	4.37–5.73	5.02±0.36
Internostril width	3.97	2.80–4.37	3.56±0.38	3.12	3.09–4.07	3.51±0.27	2.69–4.53	3.31±0.35	2.76–3.79	3.32±0.31
Ratio of postanal length to										
Caudal peduncle depth	1.21	1.06–1.49	**1.29±0.11***	1.67	1.17–2.08	1.61±0.22	1.29–1.86	1.55±0.15	1.38–1.86	1.66±0.15
Ratio of prepelvic length to										
Length of pelvic origin to anal origin	1.01	0.97–1.21	1.07±0.06	1.08	0.95–1.33	1.11±0.10	0.90–1.27	**1.00±0.07***	1.02–1.29	1.11±0.07

"*" denotes that, in a one-way ANOVA test, post-hoc comparisons reveal that the trait in question significantly differs from those of other species (without "*") ($p < 0.05$).

with nuptial tubercles in adults. Pelvic fin shorter than pectoral, well-developed fleshy flap at dorsal base, last 1–3 branched rays partially connected by fin membrane forming pelvic disc, connected part about two-thirds ray length, remaining parts separated, forming notch in middle rear edge, exposing anus. Pelvic disc width about equal to length. Anus at or near posterior edge of pelvic disc, distance to which less than to anal fin origin. Caudal fin length about equal to pelvic fin, slanted end, lower lobe slightly longer.

Coloration in preservation. Preserved specimens from sub-adult to adult stage, body dark brown to grey, white ventrally. Head with black spots or vermiculations dorsally, 2–5 larger black blotches along mid-dorsal body anterior to dorsal fin. Sides with 4–15 thick dark vertical stripes, stripes posterior to dorsal fin origin wider than intervals. In smaller individuals, stripes clear and distinguishable, in larger individuals, stripes anterior to caudal peduncle sometimes blur or disappear. Paired fin with white margin, black arc, or dotted-arc line inside white ring. Dorsal fin with alternating black, white stripes, anal fin hyaline with black stripes.

Coloration in live. In life, dorsal body dark brown to green. Mature individuals with metallic, green longitudinal band along lateral line, area below lateral line behind pelvic fins and base of paired fins sometimes light orange, more pronounced in Qing Shui River basin populations, Yunnan. Dorsal fin black pattern wider than white.

Juvenile morphology. Pelvic fins completely separated, dorsal body side gray-brown, few wider vertical dark stripes on flank, 2–3 vertical black stripes on caudal fin, other fins hyaline or with inconspicuous black lines (see Fig. 3).

Sexual dimorphism. In fully mature individuals, males slightly larger than females, with well-developed nuptial tubercles (see Fig. 8E, F).

Geographic variation. Qing Shui River basin populations, Yunnan, more pronounced orange color below lateral line behind pelvic fins, dorsal side of paired-fins base after sexual maturity compared to type locality Tianlin County populations (see Fig. 4B).

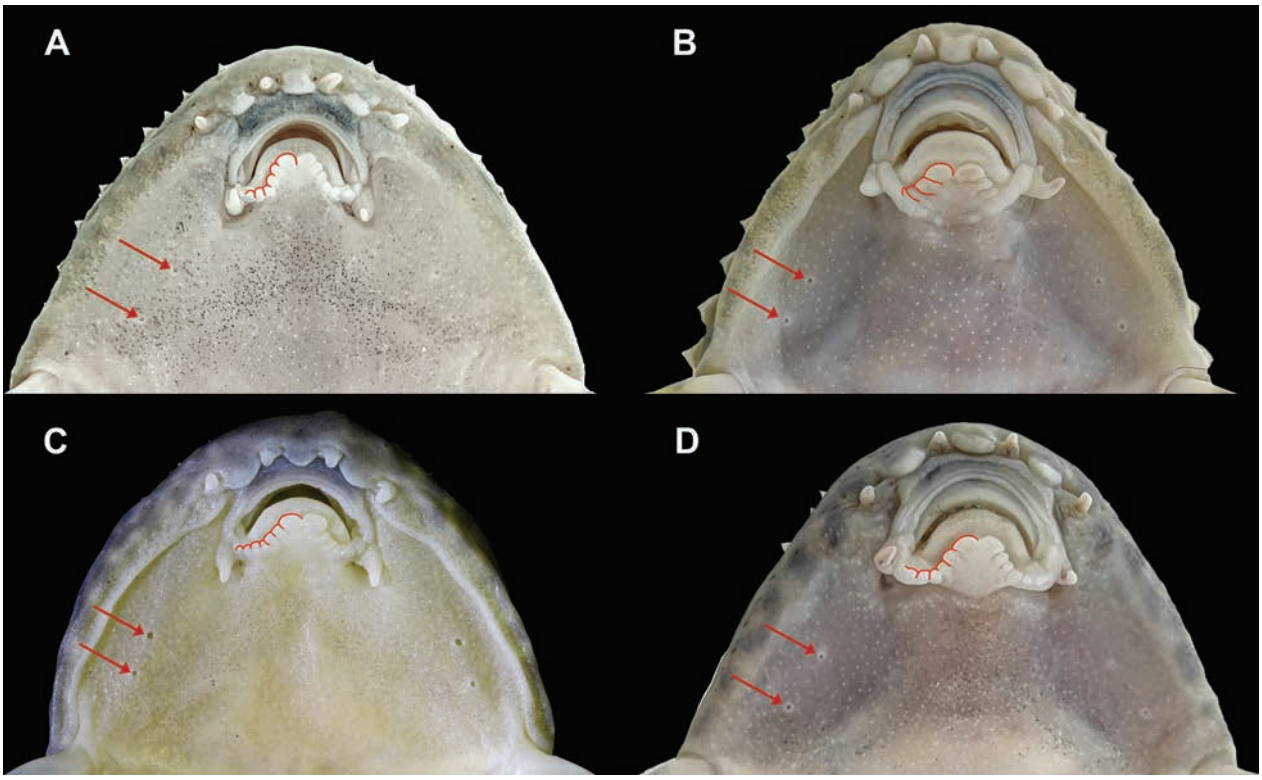

Figure 6. Pinnate-type lower lip of the *Beaufortia pingi* species group, elongated, with the lower lip on both sides being multilobed, typically comprising more than three lobes, with deep divisions; the extremities of the lower lip extend to the corners of the mouth, with several wart-like protrusions present on the extended parts. The red line outlines the left side of the lower lip contour; the red arrow indicates the position of the ventral head sensory canal-pores located anterior to the origin of the pectoral fins. **A.** *B. pingi*, from the type locality; **B.** *B. zebroida*, from Napo County, Guangxi Province; **C.** *B. viridis*, from the type locality; **D.** *B. granulopinna*, from the type locality.

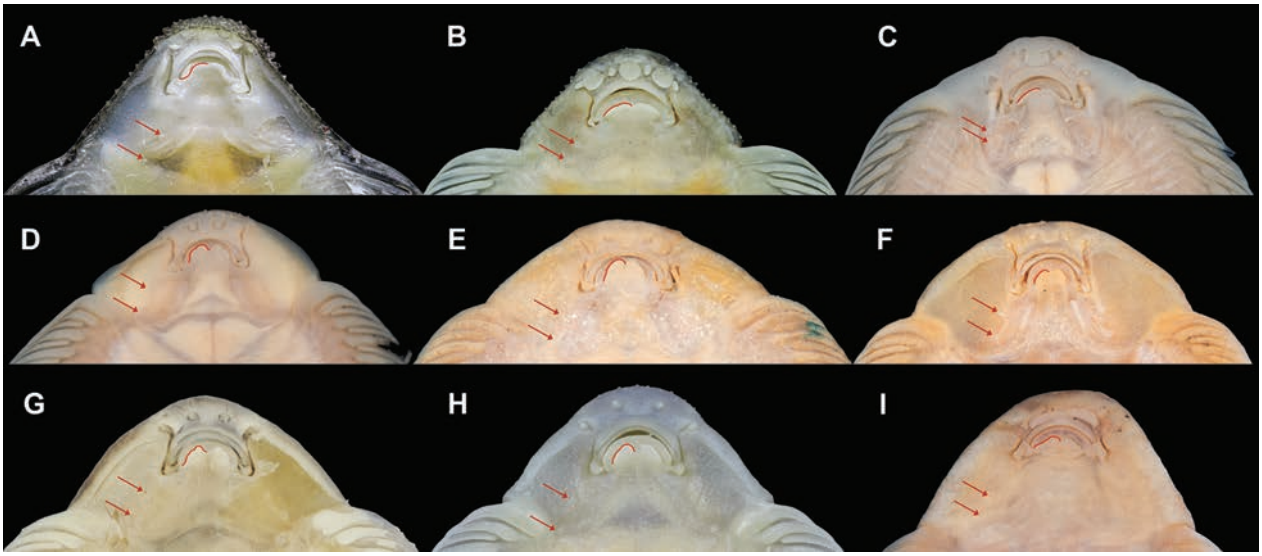

Figure 7. Dicot-type lower lip of species outside the *Beaufortia pingi* group, shorter, with the sides of the lower lip being smooth or featuring 1–2 shallow notches; the ends of the lower lip do not extend to the corners of the mouth, or the extension is poor-developed and lacks protrusions. The red line outlines the left side of the lower lip contour; the red arrow indicates the position of the ventral head sensory canal-pores, with the second pair of canal-pores located posterior to the origin of the pectoral fins in all species except *B. liui*. **A.** *B. leveretti*, from the type locality; **B.** *B. kweichowensis*, from Congjiang County, Guizhou Province, downstream near the type locality; **C.** *B. cyclica*, holotype; **D.** *B. intermedia*, paratype; **E.** *B. polylepis*, syntype; **F.** *B. huangguoshuensis*, syntype; **G.** *B. szechuanensis*, from Neijiang City, Sichuan Province; **H.** *B. niulanensis*, from the type locality; **I.** *B. liui*, syntype. (C-F and I were photographed by Yi-Yang Xu, Institute of Hydrobiology, Chinese Academy of Sciences.)

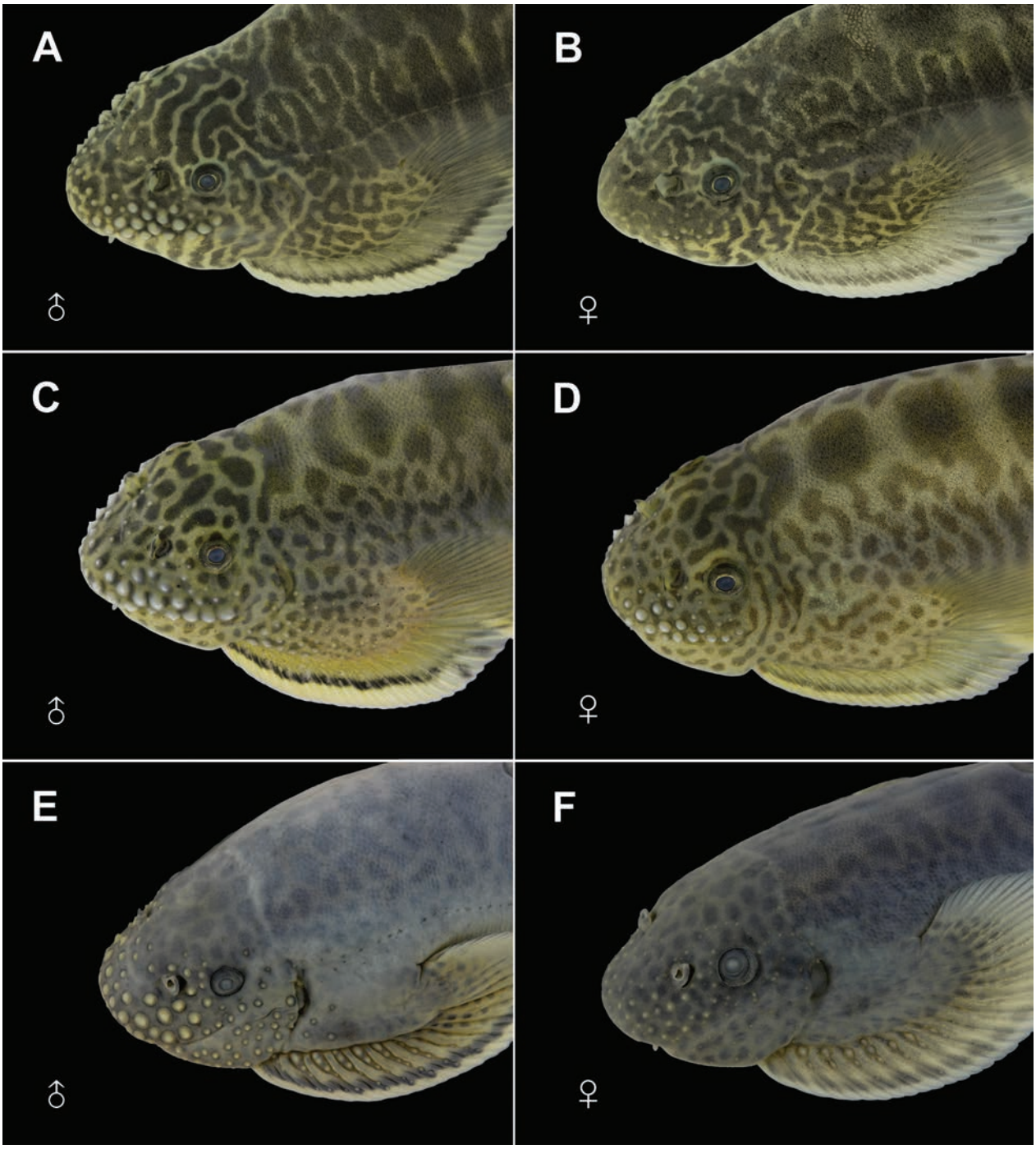

Figure 8. Sexual dimorphism within the *Beaufortia pingi* species group, with males exhibiting well-developed and numerous nuptial tubercles on the head compared to females. **A, B.** *B. viridis* sp. nov.; **C, D.** *B. pingi*; and **E, F.** *B. granulopinna* sp. nov.

Individual variation. Among the 42 specimens examined, one (SHOU20240103017) with six branched rays in dorsal fin.

Ethology. Inhabits shallow streams with rapid currents and smooth pebble substrates that adhere to crevices between stones. Feeds on algae and small invertebrates and consumes mucus from fresh fish carcasses. Exhibits strong territorial behavior and aggression; adults may head-butt and extend dorsal fins to drive away rivals.

Distribution. Found exclusively in the small tributaries of the Bo′ai River basin, ranging from the northwestern part of Guangxi to the eastern part of Yunnan in China, as well as in the small tributaries of the Qingshui River section and its downstream Nanpan River basin, upper reaches of the Pearl River system (see Fig. 9).

Etymology. The specific epithet *granulopinna* combines Latin "*granulo-*," meaning grainy, and "*-pinna*," meaning fin, referring to the well-developed tubercles on pectoral fins; the term is in the nominative masculine singular. We propose the Chinese common specific name "珠鳍爬岩鳅".

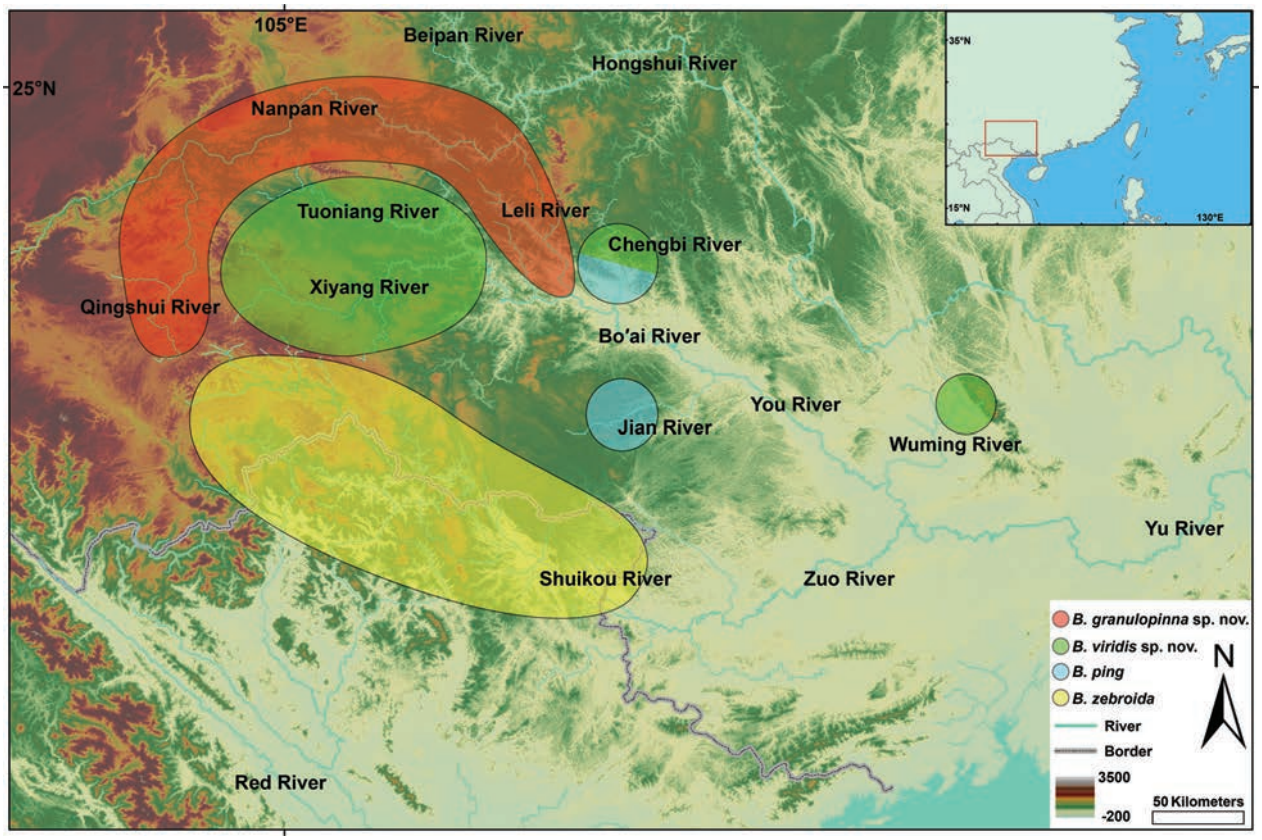

Figure 9. Distribution map of species within the *Beaufortia pingi* species group. Light red: *B. granulopinna* sp. nov.; light green: *B. viridis* sp. nov.; light blue: *B. pingi*; light yellow: *B. zebroida*. Rivers are labeled with their names in Chinese: Qingshui River (清水江), Nanpan River (南盘江), Beipan River (北盘江), Hongshui River (红水河), Tuoniang (驮娘江), Xiyang River (西洋江), Leli River (乐里河), Chengbi River (澄碧河), Bo'ai River (剥隘河), Jian River (鉴河), You River (右江), Wuming River (武鸣河), Yu River (郁江), Shuikou River (水口河, known as Sông Bằng in Vietnamese), and Red River (红河).

Beaufortia viridis Chen & Tang, sp. nov.

https://zoobank.org/268BD22A-C14B-4662-BFFC-A8C3369DACC7
Figs 10–12

Beaufortia pingi: Yue (1981): 170–172, Lingyun County, Guangxi, admixed within *B. pingi*. Zheng (1989): 257–258, Lingyun County, Guangxi, admixed within *B. pingi*.

Beaufortia pingi: Chen (1990): 85–87, Xiyang River, Guangnan County, Yunnan.

Beaufortia zebroidus: Chen and Tang (2000): 504–505, Tian'e County, Guangxi. Chen (2013): 292, Xiyang River, Yunnan.

Type material. ***Holotype*.** SHOU20240103101, 48.42 mm total length (TL), 38.03 mm standard length (SL), adult (Fig. 10). Collected by Jing-Chen Chen and Qian-Yu Liang on 27 December 2023, from Wuming River, a stream tributary to the You River of the Pearl River basin, at Wuming District, Nanning City, Guangxi Province, China (24°20.34'N, 106°21.624'E; c. 160 m a.s.l.) (Fig. 13).

***Paratypes*.** 15 specimens from the same locality as holotype, SHOU20240103102-116, 18.82–46.64 mm SL, were collected by Qian-Yu Liang and Jing-Chen Chen on 27 December 2023; eight specimens from Lingyun County, Baise City, Guangxi Province, China, SHOU20240126101-108, 50–59.85mm SL, were collected by Qian-Yu Liang and Jing-Chen Chen on 24 January 2024; five specimens from Guangnan County, Wenshan Zhuang, and Miao Autonomous Prefecture, Yunnan Province, China, SHOU20240109101-105, 36.23–54.20mm SL, were collected by Lao Xing on 28 December 2023.

Additional materials. Seven specimens from Guangnan County, Wenshan Zhuang, and Miao Autonomous Prefecture, Yunnan Province, China, SHOU20240112101-107, 39.97–48.64mm SL, were collected by Lin Yang and Lao Xing from December 2022 to February 2023.

Diagnosis. *B. viridis* sp. nov. shares the typical characteristics with members of the *B. pingi* species group, with distinct vertical stripes on lateral body and a pinnate-type lower lip (vs. lacking prominent vertical stripes and having a dicot-type lower lip in other congeneric species apart from this group) (see Figs 6C, 7, Table 2). *B. viridis* sp. nov. can be clearly distinguished from *B. granulopinna*, *B. pingi*, and *B. zebroida* by consistent vertical stripes with uniform length, width, and inter-spacing at all growth stages (stripes on mid-section lateral body occasionally shorten in individuals from the Xiayang and Tuoniang Rivers in Yunnan) (vs. a certain proportion (54.76%) of adults exhibit blurred or vanished vertical stripes on mid-section lateral body in *B. granulopinna*;

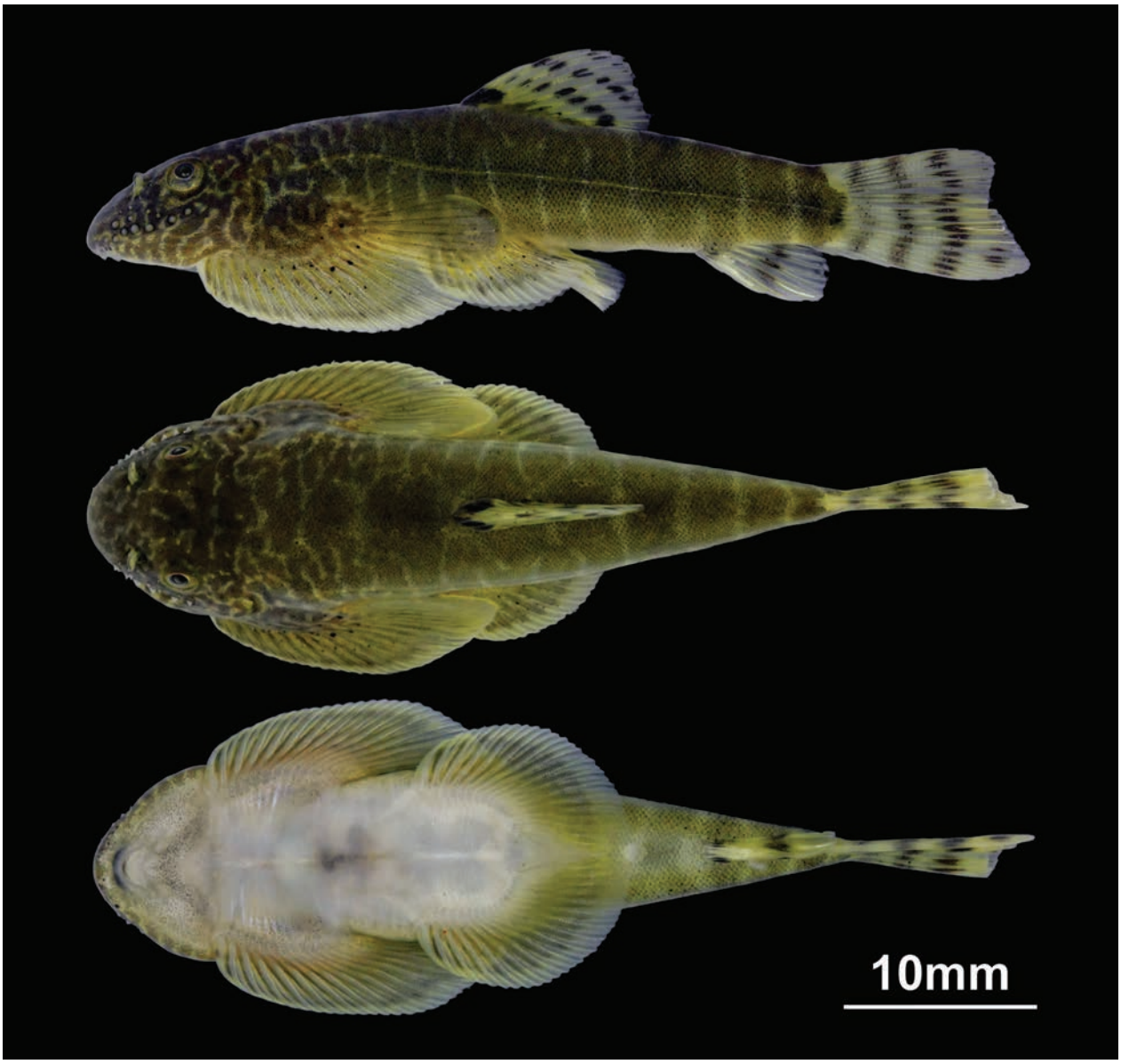

Figure 10. Lateral (top), dorsal (middle), and ventral (bottom) views of *Beaufortia viridis* sp. nov., holotype, adult, SHOU20240103101, 38.03mm SL; from Wuming River, a stream tributary to the You River of the Pearl River basin, at Wuming District, Nanning City, Guangxi Province, China.

stripe length and width uneven, with a high proportion (94.00%) of adults showing blurred or vanished mid-section vertical stripes in *B.pingi*; stripe length and width uneven, typically narrower than inter-spacing, sometimes reduced to dots in *B. zebroida*). *B. viridis* sp. nov. can be further distinguished from *B. granulopinna* sp. nov. by the lack of prominent tubercles on the branched rays of the pectoral fins (vs. well-developed tubercles on anterior 6–9 rays of the pectoral fins present). Moreover, *B. viridis* sp. nov. differs from *B. zebroida* by body dark cyan to green in dorsal profile (vs. brown yellow to golden).

Description. Dorsal iii-7, anal ii-4, pectoral i-19–23 (21.08±1.02), pelvic i-14.5–19 (17.11±1.01). Lateral-line canal pores and scales: 65–83 (73.47±4.21) (see Table 2).

Morphometric measurements for the specimens examined are given in Table 3. See Fig. 10 for lateral, dorsal, and ventral views of the body.

Head-thorax cylindrical, dorsal slightly humped medially, flattened ventrally, body compressed from pelvic fins to caudal peduncle. Head broad, blunt, length slightly less than width, more than depth, nuptial tubercles well-developed on lower half of head in mature individuals, snout rounded, length about half of head length. Mouth inferior, narrow, width about one-fifth head width, horseshoe-shaped, angle about 94° from midpoint to ends. Upper lip smooth, without distinct papillae; lower lip pinnate-type, slightly concave medially with multilobed sides; jaw edges slightly protrude. Shallow groove between upper lip and snout, extending to mouth corners. Lateral grooves shallow or indistinct. Two pairs of rostral barbels present, with outer pair slightly longer, space between rostral barbels with leaf-like folds, edges of which rounded and poor developed. One pair of maxillary barbels, length about equal to outer rostral barbels. Nostrils with tubu-

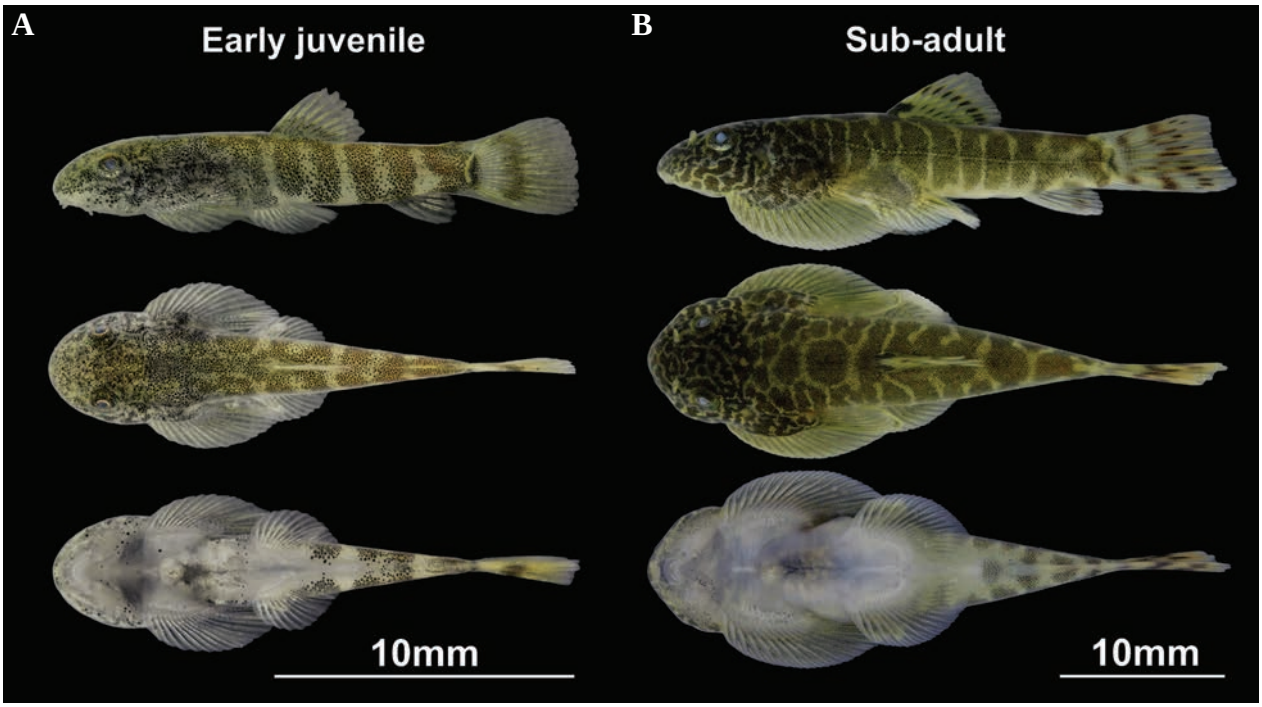

Figure 11. Lateral (top), dorsal (middle), and ventral (bottom) views of *Beaufortia viridis* sp. nov. during early juvenile and sub-adult stages. **A.** Early juvenile stage, SHOU20240103623, from type locality, 12.64 mm SL, pelvic fins completely separated; **B.** Sub-adult stage, SHOU20240103102, paratype, 25.81 mm SL.

lar nasal flaps, distance between nostrils equals one-third head width. Eyes supralateral, medium-sized, eye diameter about one-quarter head length, interorbital space flat, width about half head width. Gill opening small, about equal to eye diameter, originated about vertically above the second to third branched pectoral fin ray, limited to dorsal side of head. Scales small, diameter smaller than pupil, dorsal surface of head, base of paired fins, and ventral area before pelvic fin bases nude. Lateral line complete, at midlateral.

Dorsal fin base about equal to pre-pectoral length, starting around midpoint from snout to caudal fin base, adpressed extending to about midway between dorsal fin origin and caudal fin base. Anal fin base length about half of that of dorsal fin base, adpressed extending to slightly beyond caudal fin base. Paired fins extending outwards, forming disc-like structure with body. Pectoral fin base slightly longer than head length, starting at the posterior one-third point of head, pectoral fin length about twice to head length, tip of which reaching pelvic fin base midpoint, pectoral disc width about 1.5 times head width at pectoral origin, tubercles on rays absent. Pelvic fin shorter than pectoral, with well-developed fleshy flap at dorsal base, last 1–3 branched rays partially connected by fin membrane forming pelvic disc, connected part about two-thirds ray length, remaining parts separated, forming notch in middle rear edge, exposing anus. Pelvic disc width about equal to length. Anus at or near posterior edge of pelvic disc, distance to which less than to anal fin origin. Caudal fin length about equal to pelvic fin, slanted end, lower lobe slightly longer.

Coloration in preservation. Preserved specimen from sub-adult to adult stage, body dark green to grey, white ventrally. Head with black spots or vermiculation dorsally, 2–5 larger black blotches along mid-dorsal body anterior to dorsal fin. Sides with 9–15 thick dark vertical stripes, with uniform length, width, and inter-spacing, easily recognizable at all ages. Paired fin with pale-white or hyaline margin, inner edges with continuous or dotted black arc. Dorsal fin hyaline with black stripes, one black spot present on the root before the second branched ray.

Coloration in live. In life, sides of body dark cyan to green. After maturity, black stripes and spots on body turn metallic green, inter-spacing and hyaline fin membranes pale yellow.

Juvenile morphology. Pelvic fins completely separated, body dark green in dorsal profile, few wider vertical dark stripes on sides, 2–3 vertical black stripes on caudal fin, other fins hyaline or with inconspicuous black lines (see Fig. 11).

Sexual dimorphism. In fully mature individuals, males generally slightly larger than females, with well-developed tubercles (see Fig. 8A, B).

Geographic variation. From east to west, vertical stripes generally tend to become thinner. Specimens from type locality, inter-spacings narrower than dark stripes, sometimes appearing fissure-like (see Fig. 10). In contrast, Lingyun County populations typically exhibit broader and taller bodies, shorter and thicker caudal peduncles, longer snouts, and wider inter-spacings (see Fig. 12A, Table 4). In populations from the Xiyang River and Tuoniang River, vertical stripes vary greatly, sometimes becoming finer, inter-spacings wider than stripes, few individuals with shorter stripes before caudal peduncle (see Fig. 12B).

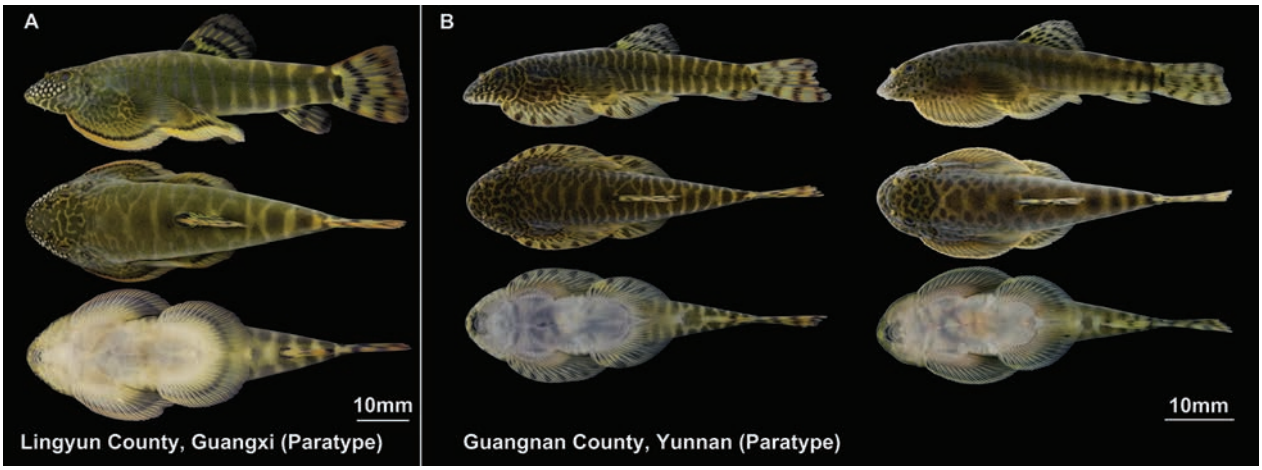

Figure 12. Lateral (top), dorsal (middle), and ventral (bottom) views of different regional phenotypes of *Beaufortia viridis* sp. nov. **A.** Regional phenotype from Lingyun County, Guangxi, SHOU20240126104, paratype, 58.71 mm SL; **B.** Regional phenotype from Tuoniang River, Guangnan County, Yunnan, SHOU20240109105, paratype, 40.15 mm SL (left); SHOU20240109103, paratype, 39.36 mm SL (right).

Table 4. Morphological variations among populations of *Beaufortia viridis* sp. nov. and *Beaufortia pingi* from different distribution areas.

***B. viridis* sp. nov.**	**Wuming County (N=16)**		**Linyun County (N=8)**		**Tuoniang River and Xiyang River (N=12)**	
Characters	Range	Mean ± SD	Range	Mean ± SD	Range	Mean ± SD
Pectoral branched rays	19–21	20.25±0.68	21–22	21.37±0.44	21–23	22±0.74
Pelvic branched rays	14.5–17	16.5±0.71	17–19	17.62±0.74	16–19	17.58±1.10
Ratio of prepelvic length to						
Head width	1.53–1.88	1.65±0.08	1.40–1.65	**1.53±0.08***	1.54–1.85	1.67±0.12
Pectoral width	1.01–1.30	1.11±0.07	0.94–1.03	**0.99±0.03***	0.96–1.19	1.08±0.07
Body width	1.79–2.63	2.04±0.22	1.62–1.82	**1.73±0.07***	1.79–2.29	1.97±0.15
Body depth	2.19–2.77	2.50±0.17	1.76–2.20	**1.98±0.15***	2.09–2.65	2.34±0.21
Head depth	2.53–3.27	2.89±0.22	2.30–2.67	**2.48±0.12***	2.40–3.14	2.79±0.25
Caudal peduncle depth	4.07–5.16	4.54±0.29	3.26–4.11	**3.59±0.28***	3.90–5.05	4.55±0.37
Pelvic width	1.31–2.02	1.43±0.17	1.15–1.30	**1.25±0.05***	1.21–1.74	1.44±0.17
Ratio of head length to						
Snout length	2.23–2.59	**2.40±0.11***	1.89–2.12	**2.01±0.08***	1.98–2.43	**2.19±0.12***
Ratio of postanal length to						
Caudal peduncle depth	1.48–2.08	1.10±0.16	1.17–1.39	**1.28±0.08***	1.37–1.94	1.70±0.15
Ratio of prepelvic length to						
Length of pelvic origin to anal origin	1.06–1.33	**1.19±0.74***	0.95–1.17	1.02±0.71	0.96–1.17	1.08±0.58
B. pingi	Linyun County & Youjiang County (N=38)		Debao County (N=12)			
Characters	Range	Mean ± SD	Range	Mean ± SD		
Pelvic branched rays	17.5–21	18.95±0.89	17–18.5	17.67±0.39		
Ratio of pectoral width to						
Body depth	1.67–2.50	2.02±0.21	1.92–2.49	**2.32±0.19****		
Ratio of postanal length to						
Caudal peduncle depth	1.29–1.77	1.50±0.13	1.58–1.86	**1.69±0.09****		
Ratio of prepelvic length to						
Length of pelvic origin to anal origin	0.90–1.27	**0.98±0.66****	0.97–1.14	1.07±0.52		

"*" indicates that, in a one-way ANOVA test, post-hoc comparisons show significant differences in the trait in question from populations in other regions ($p < 0.05$).
"**" indicates that, in an independent sample T-test, the trait in question significantly differs from populations in other regions ($p < 0.01$).

Individual variation. Two specimens, SHOU20240109101 and SHOU20240112102, from Tuoniang River, Guangnan County, Yunnan, vertical stripes notably shortened. One specimen, SHOU20240109701, from Chengbi River, Lingyun County, Guangxi, possesses completely separated pelvic fins.

Ethology. Inhabits shallow streams with rapid currents and smooth pebble substrates that adhere to crevices between stones. Feeds on algae and small invertebrates and consumes mucus from fresh fish carcasses. Exhibits territorial behavior.

Distribution. Found exclusively in small tributaries from the Tuoniang River, Xiyang River, Leli River, and Wuming River to the You River basin, the upper reaches of the Pearl River system, central Guangxi, and eastern Yunnan, China (see Fig. 9).

Etymology. Species epithet "*viridis*," from Latin, meaning "green," describes bright green coloration over dorsal body after sexual maturity, in nominative masculine. We propose the Chinese common specific name "绿斑爬岩鳅."

Figure 13. Collection site of the holotype (SHOU20240103101) of *Beaufortia viridis* sp. nov., from Wuming River, a stream tributary to the You River of the Pearl River basin, Wuming District, Nanning City, Guangxi Province, China. Photographed by Jing-Chen Chen on 27 December 2023.

Beaufortia pingi (Fang 1930)

Fig. 14

Gastromyzon pingi Fang, 1930: 31–34 (original description: former Lingyun County, near the border of Yunnan and Guangxi; Damaoping Village, Lingyun County, Guangxi). Nichols (1943): 231.

Beaufortia pingi: Hora (1932): 319.

Gastromyzon pingi: Nichols (1943): 231.

Beaufortia pingi: Chen (1980): 113–114 (Xi River, Guangxi).

Comparative materials. 23 specimens from type locality, SHOU20240102201-217, SHOU20240126201-206, 27.64–56.89 mm SL, were collected by Qian-Yu Liang and Jing-Chen Chen from December 2022 to January 2024; 15 specimens from Youjiang District, Baise City, Guangxi Province, China, SHOU20240110201-204, SHOU20240127201-211, 43.53–56.28 mm SL, were collected by Qian-Yu Liang and Jing-Chen Chen from December 2021 to January 2024; 12 specimens from Debao County, Baise City, Guangxi Province, China, SHOU20240112201-202, SHOU20240103201-210, 44.53–58.12 mm SL, were collected by Qian-Yu Liang from April 2023 to January 2024.

Diagnosis. *B. pingi* shares the typical characteristics with members of the *B. pingi* species group, with distinct vertical stripes on the flank and a pinnate-type lower lip (vs. lacking prominent vertical stripes and having a dicot-type lower lip in other congeneric species apart from this group) (see Figs 6A, 7, Table 2). *B. pingi* can be clearly distinguished from *B. granulopinna* sp. nov. by absent or inconspicuous tubercles on pectoral fin rays (vs. well-developed tubercles present on anterior 6–9 rays of pectoral fins); paired fins with more branched rays, with 21–24 (mean 22.19±0.78) in pectoral fins and 17–21 (mean 18.64±0.97) in pelvic fins (vs. 18.5–22 (mean 20.11±0.77) and 15–18 (mean 16.51±0.86)). *B. pingi* can be clearly distinguished from *B. viridis* sp. nov. by vertical stripes uneven in length and width and a significant proportion (94.00%) of adults displaying blurred or vanished stripes on the mid-section flank (vs. the stable presence of uniform vertical stripes in length, width, and inter-spacing at all growth stages). *B. pingi* differs from *B. zebroida* by having a larger proportion of adults with blurred or vanished mid-section vertical stripes (vs. stable presence of vertical stripes) and body dark brown to green in dorsal profile (vs. brown yellow to golden).

Redescription. Dorsal iii-7–8 (7.08±0.27), anal ii-3–4 (3.98±0.14); pectoral i-21–24 (22.19±0.78); pelvic i-17–21 (18.64±0.97). Lateral-line canal pores and scales: 68–92 (75.28±4.01).

Morphometric measurements for the specimens examined are given in Table 3. See Fig. 14 for lateral, dorsal, and ventral views of the body.

Body closely resembles *B. viridis* sp. nov. in general shape and structure but significantly different in stripes pattern and coloration. Tubercles on rays absent or poor developed, only faintly visible in large males.

Coloration in preservation. Preserved specimens from sub-adult to adult stage, body dark brown to grey, white ventrally. Head with black spots or vermiculation dorsally, 2–5 larger black blotches along mid-dorsal body anterior to dorsal fin. Sides of body with 4–15 vertical dark stripes, length and width of stripes uneven. In smaller individuals, stripes clear and distinguishable, in larger individuals, a significant proportion possesses a blur region before caudal peduncle, extending to dorsal fin origin at maximum, caudal peduncle with 2–5 distinct vertical stripes. Paired fin margins hyaline or pale white, inner edges with continuous or dotted black arc. Dorsal fin hyaline, with black stripes, one black spot on the root before the first branched ray.

Coloration in live. In life, dorsal body dark brown to green. Mature individuals with metallic green longitudinal band along lateral line, area below lateral line behind

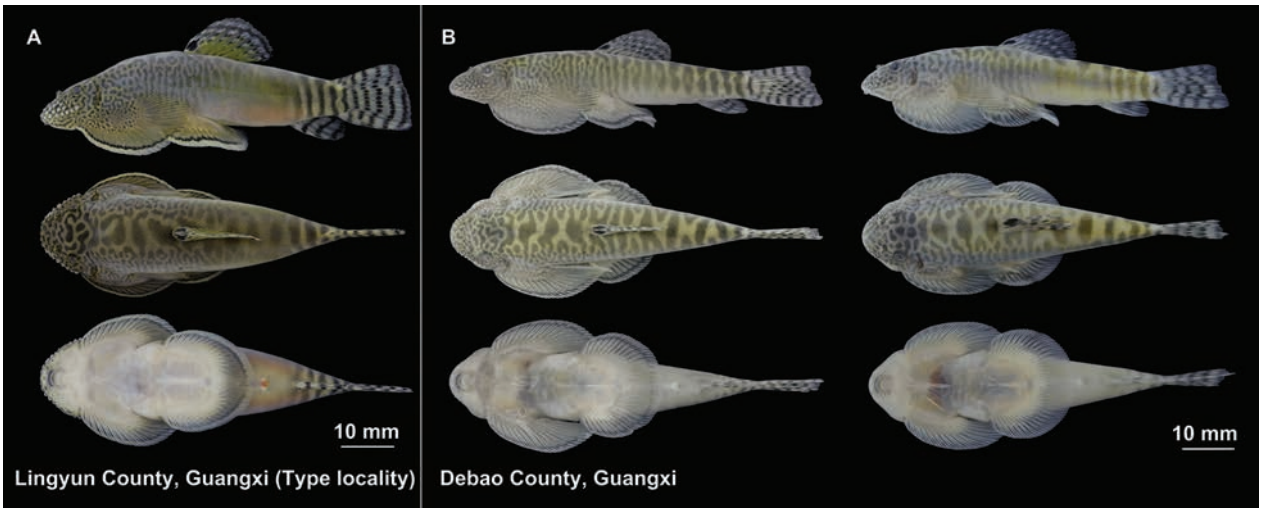

Figure 14. Lateral (top), dorsal (middle), and ventral (bottom) views of different regional phenotypes of *Beaufortia pingi*. **A.** Regional phenotype from Lingyun County, Guangxi, SHOU20240126202, from type locality, 56.89mm SL. **B.** Regional phenotype from Debao County, Guangxi, SHOU20240103203, 58.12 mm SL (left), with clearer vertical stripes; SHOU20240103204, 53.18 mm SL (right), with blurred vertical stripes.

pelvic fins and base of paired fins sometimes light orange, fin membranes pale green.

Sexual dimorphism. In fully mature individuals, males slightly larger than females, with well-developed nuptial tubercles (see Fig. 8C, D).

Geographic variation. Compared to type locality, Lingyun County, Guangxi, population in Debao County, Guangxi with more compressed body, and more elongated tail (see Fig. 14B, Table 4).

Individual variation. Among 50 specimens, four (SHOU20240102213, SHOU20240102215, SHOU20240126205, and SHOU20240127211) with eight dorsal fin-branched rays; one (SHOU20240127204) with three anal fin-branched rays.

Ethology. Inhabits shallow streams with rapid currents and smooth pebble substrates that adhere to crevices between stones. Feeds on algae and small invertebrates and consumes mucus from fresh fish carcasses. Exhibits territorial behavior and aggression; adults may head-butt and extend dorsal fins to drive away rivals.

Distribution. Found exclusively in the small tributaries of the Chengbi River and Jian River to the You River basin, upper reaches of the Pearl River system, Western Guangxi, China (see Fig. 9).

Beaufortia zebroida (Fang 1930)

Fig. 15

Gastromyzon pingi zebroidus Fang, 1930: 35 (original description: Donggui River, Longzhou County, Guangxi).
Beaufortia zebroidus: Hora (1932): 319.
Gastromyzon pingi zebroidus: Nichols (1943): 231.
Beaufortia pingi: Nguyen and Nguyen (2005): 282–283
Beaufortia fasciolata Nguyen & Nguyen, 2005: 588–590.
Beaufortia multiocellata Nguyen & Nguyen, 2005: 590–592.
Beaufortia triocellata Nguyen & Nguyen, 2005: 592–594.
Beaufortia zebroida: Kottelat (2012): 59–60.

Comparative materials. MMNHN1544, one specimen, holotype, not found yet, refers to the original description. SHOU20240111301-317, 33.24–49.96 mm SL, 17 specimens from Guangnan County, Xichou County, Malipo County, Funing County, Yunnan, and Napo County, Guangxi, SHOU20240111301-317, 33.24–49.96 mm SL, were collected by Lao Xing and Lin Yang from December 2021 to January 2024.

Diagnosis. *B. zebroida* shares the typical characteristics with members of the *B. pingi* species group, with distinct vertical stripes on lateral body and a pinnate-type lower lip (vs. lacking prominent vertical stripes and having a dicot-type lower lip in other congeneric species apart from this group) (see Figs 6B, 7, Table 2). *B. zebroida* can be clearly distinguished from *B. granulopinna* sp. nov. by the absence of prominent tubercles on the pectoral fin rays (vs. well-developed tubercles present on anterior 6–9 rays of pectoral fins); vertical stripes slender, narrower than inter-spacing, present consistently at all growth stages (vs. vertical stripes typically wider than inter-spacing, with a certain proportion (54.76%) of adults exhibiting blurred or vanished mid-section stripes). *B. zebroida* can be clearly distinguished from *B. viridis* sp. nov. by the vertical stripes present uneven in width and length, typically narrower than inter-spacing, sometimes reduced to dots (vs. stripes of consistent length, width, and inter-spacing); body brown yellow to golden in dorsal profile (vs. dark cyan to green). *B. zebroida* can be clearly distinguished from *B. pingi* by the stable presence of vertical stripes at all growth stages (vs. a large proportion (94.00%) of adults with blurred or vanished vertical stripes at mid-section of lateral body) and body brown yellow to golden in dorsal profile (vs. dark brown to green).

Redescription. Dorsal iii-7; anal ii-3–4 (3.98±0.14); pectoral i-20–23 (21.5±0.73); pelvic i-16–19 (17.53±0.86). Lateral-line canal pores and scales: 70–84 (75.12±3.55).

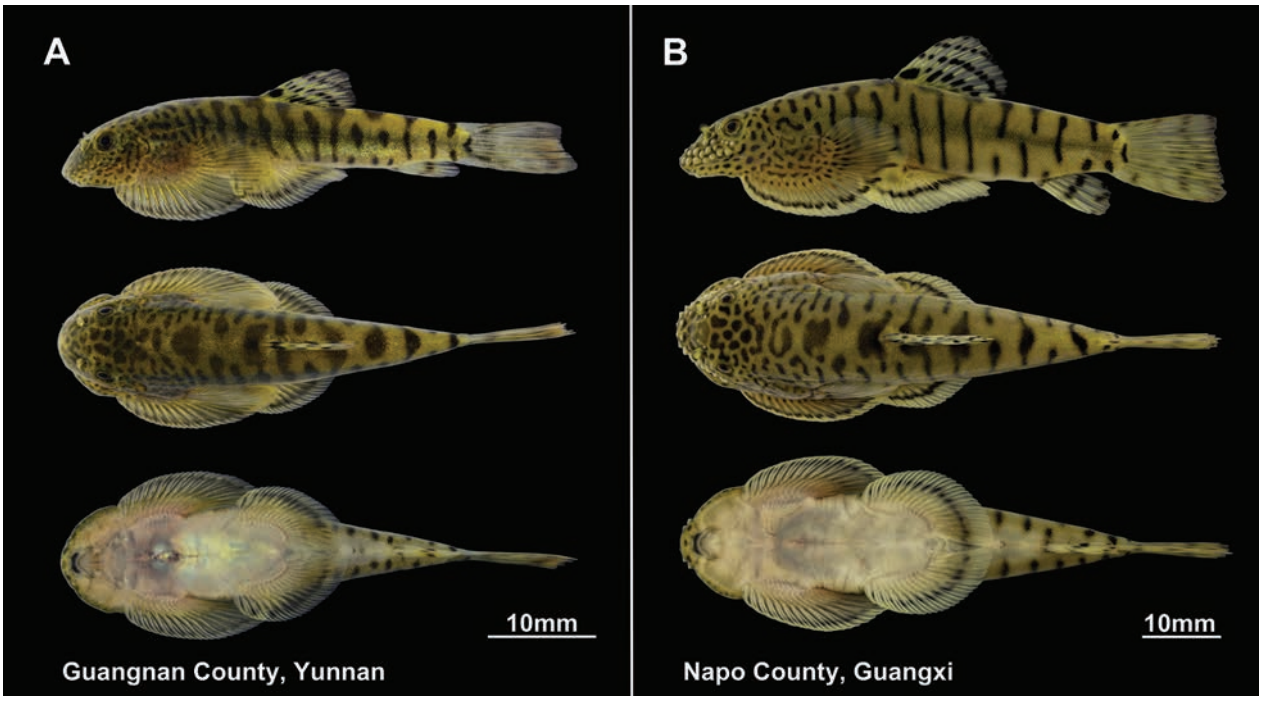

Figure 15. Lateral (top), dorsal (middle), and ventral (bottom) views of different regional phenotypes of *Beaufortia zebroida*. **A.** Regional phenotype from a stream tributary to the Red River, Guangnan County, Yunnan, SHOU20240111308, 36.64 mm SL; **B.** Regional phenotype from Napo County, Guangxi, SHOU20240316602, 56.12 mm SL, originating from upstream within the same basin as the type locality.

Morphometric measurements for the specimens examined are given in Table 3. See Fig. 15 for lateral, dorsal, and ventral views of the body.

Body closely resembles *B. viridis* sp. nov. in general shape and structure, but significantly different in stripes pattern and coloration.

Coloration in preservation. Preserved specimens from sub-adult to adult stage, body brown yellow to grey, white ventrally. Head with black spots or vermiculation dorsally, 2–5 larger black blotches along mid-dorsal body anterior to dorsal fin. Sides with 8–15 vertical dark stripes, varying greatly in length, which sometimes appearing as dots, stripe width narrower than inter-spacing, present at all growth stages. Paired fin margins hyaline or pale white, inner edges with continuous or dotted black arc. Dorsal fin hyaline, with black stripes, one black spot on the root before the second branched ray.

Coloration in live. In life, body brown yellow to golden in dorsal profile. Mature individuals with a more vivid golden coloration, and fin membranes pale yellow.

Individual variation. Among 17 specimens, one (SHOU20240111307) had three branched anal fin rays.

Ethology. Inhabits shallow streams with rapid currents and smooth pebble substrates that adhere to crevices between stones. Feeds on algae and small invertebrates and consumes mucus from fresh fish carcasses. Exhibits territorial behavior.

Distribution. Exclusively in small tributaries on the north bank of the mid-lower Red River system and the upper Shuikou River to Zuo River basin (upper Pearl River system), from Maguan County, Wenshan Zhuang, and Miao Autonomous Prefecture, Yunnan, to Longzhou County, Guangxi, near the China-Vietnam border, extending into northeastern Vietnam (see Fig. 9).

Genetic distances and phylogenetic analysis

A total of 35 mitochondrial *cyt*b gene haplotypes were obtained. The computed genetic distances revealed that *B. granulopinna* sp. nov. shared the smallest average genetic distance with *B. zebroida* at 10.80% (with the maximum interspecific genetic distance reaching 11.37%). Intraspecific genetic distances ranged from 0.26% to 5.12%, with an average of 3.63%, surpassing the average intraspecific genetic distances of all other species within the same genus. *B. viridis* sp. nov. exhibited a minimum average interspecific genetic distance with *B. pingi* of 4.60% (with a maximum interspecific genetic distance of 5.2%), significantly exceeding the current minimum intrageneric interspecific distance. Intraspecific genetic distances ranged from 0.09% to 2.80%, with an average of 1.47%, exceeding the average intraspecific genetic distances of all other congeneric species except for *B. granulopinna* sp. nov. *B. zebroida* had a minimum average genetic distance with *B. pingi* of 5.62% (with the maximum interspecific genetic distance at 5.88%), considerably above the current minimum intrageneric interspecific distance. The genetic distances between the aforementioned species and those within the *B. pingi* species group were smaller, indicating

their affiliation with the *B. pingi* species group, aligning with morphological classification results.

Notably, the genetic distance between *B. niulanensis* and *B. szechuanensis* was only 0.53%, whereas the *B.* cf. *szechuanensis* collected from Qijiang, Chongqing (a tributary on the southern bank of the upper Yangtze River) morphologically conformed to *B. szechuanensis* but exhibited a genetic distance of 2.30% from *B. szechuanensis*, exceeding the genetic distance between *B. polylepis* and *B. szechuanensis* (2.20%) (see Table 5).

Phylogenetic trees generated using maximum likelihood and Bayesian inference methods exhibited identical topological structures, with all nodes demonstrating high support values. All species within the *B. pingi* species group coalesced to form a single clade, with each species within this clade establishing distinct lineages. Among these, *B. pingi* and *B. viridis* sp. nov. were identified as sister taxa positioned at the derived end of the phylogenetic tree, followed by *B. zebroida* as a sister group to the aforementioned species. *B. granulopinna* sp. nov. was situated at the most basal position within the *B. pingi* species group clade, with a relatively longer branch length indicating an early divergence.

The remaining species formed another clade, distinctly divergent from the *B. pingi* species group, which aligns with the classification results based on morphological characteristics. Within this clade, two significantly divergent lineages were identified. One lineage was composed of all haplotypes of *B. kweichowensis* and *B. leveretti*. The other lineages included *B. szechuanensis*, *B. polylepis*, *B. niulanensis*, and *B.* cf. *szechuanensis*. (see Fig. 16).

Table 5. Inter-specific mean mitochondrial *cyt*b genetic distances, maximum genetic distances among species, and intra-specific genetic distances within the genus *Beaufortia* in Kimura 2-parameter genetic distance analysis.

	Species (haplotype count)	Between species mean distance (below diagonal) and maximum distance (above diagonal)) (%)										Within species distance (%)	
		1	2	3	4	5	6	7	8	9	10	Range	Mean
1	***B. viridis* sp. nov.** (5)		5.20	7.52	11.45	15.71	15.74	17.40	17.67	17.54	17..83	0.09–2.80	1.47
2	*B. pingi* (8)	4.60		5.88	11.46	15.70	16.33	17.37	17.77	17.26	17.93	0.09–0.89	0.50
3	*B. zebroida* (4)	7.07	5.62		11.37	16.29	15.56	16.27	16.66	16.04	16.31	0.09–0.53	0.28
4	***B. granulopinna* sp. nov.** (5)	10.86	11.15	10.80		16.43	16.97	17.78	17.51	17.18	17.67	0.26–5.12	3.63
5	*B. kweichowensis* (3)	15.31	15.53	15.68	16.13		3.86	14.22	14.00	14.24	14.02	0.09–2.06	1.37
6	*B. leveretti* (1)	15.51	16.19	15.50	16.25	3.44		13.64	13.65	13.89	13.80	–	–
7	*B. niulanensis* (2)	15.77	16.92	16.05	17.04	13.80	13.58		0.71	2.34	2.25	0.09	0.09
8	*B. szechuanensis* (2)	16.16	17.25	16.31	17.39	13.71	13.53	0.53		2.43	2.53	0.44	0.44
9	*B. polylepis* (4)	16.28	16.84	15.84	16.94	13.91	13.77	2.11	2.20		3.09	0.18–0.35	0.23
10	*B.* cf. *szechuanensis* (1)	16.44	17.54	16.16	17.37	13.82	13.80	2.20	2.30	2.90		–	–

"-" stands for no corresponding data.

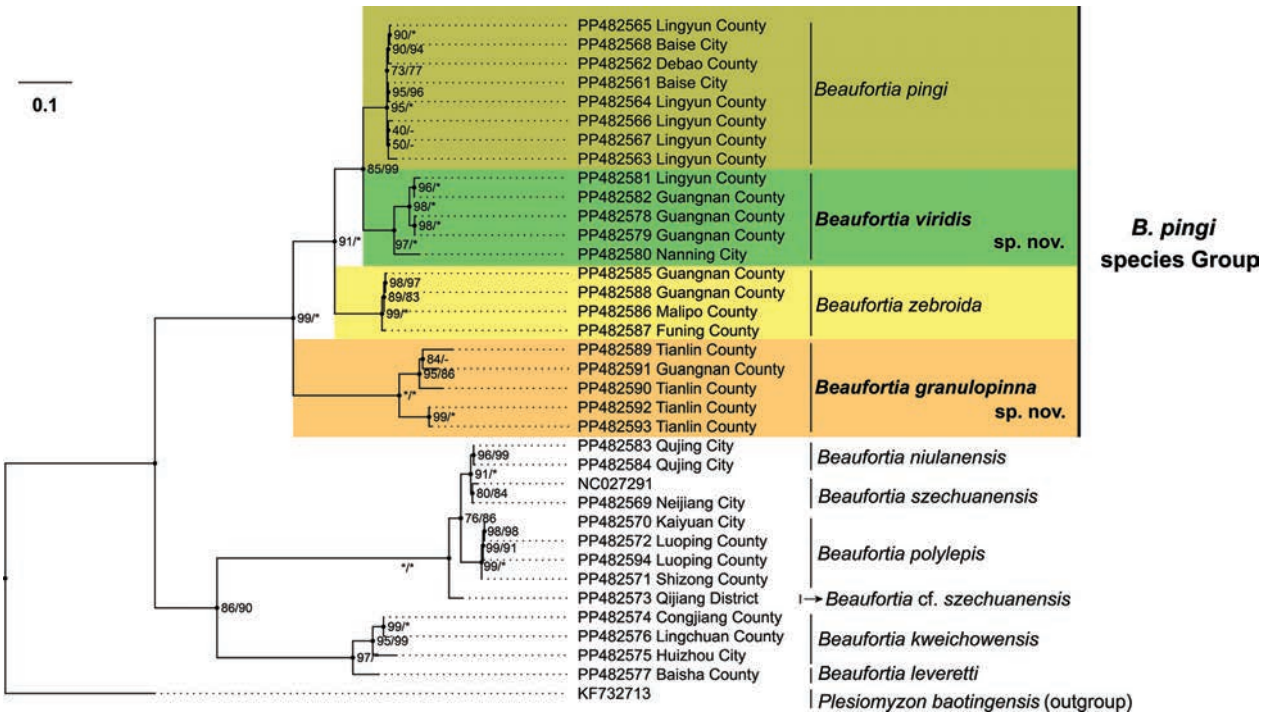

Figure 16. Phylogenetic tree of *Beaufortia* species based on haplotypes of mitochondrial *cyt*b genes, with the tree topology inferred through maximum likelihood (ML) and Bayesian inference (BI) methods. Support values for each branch are indicated at the nodes (ML/BI), with "*" denoting bootstrap values of 100% or posterior probabilities of 1, and "-" indicating insufficient genetic variation to display posterior probabilities.

Morphological characteristics of the *Beaufortia pingi* species group

The preceding phylogenetic results have confirmed that the *Beaufortia pingi* species group constitutes a monophyletic clade and exhibits significant genetic divergence from other *Beaufortia* species. Morphologically, this group is distinctly differentiated from other species. The lower lip of the species group can be represented by a pinnate-type appearance, being overall slender with a central indentation and multiple lobed sides. There is variation among individuals in the number of lobes and the depth of the clefts, with most specimens possessing no fewer than three lobes and the depth of clefts exceeding that found in species outside this group. The extremities of the lower lip extend to the corners of the mouth, with several wart-like protrusions present on the extended parts (Fig. 6). In contrast, species outside this group possess a dicot-type lower lip, which is broad and short with a central indentation, and sides that are not lobed but occasionally have 0–2 shallow notches. The ends of the lower lip do not extend to the corners of the mouth, or the extension is poorly developed and lacks protrusions (Fig. 7). Additionally, the *Beaufortia pingi* species group is characterized by distinct vertical stripes along the body sides, a feature absent in other *Beaufortia* species.

Morphometric variability within the *Beaufortia pingi* species group

B. pingi has more branched rays in its paired fins, with an average of 22.19±0.78 in pectoral fins and 18.64±0.97 in pelvic fins. In contrast, *B. granulopinna* sp. nov. exhibits fewer branched rays in its paired fins, averaging 20.11±0.77 in pectoral fins and 16.51±0.86 in pelvic fins.

Differences in morphometric proportions were observed among the four species within the *Beaufortia pingi* group. *B. granulopinna* sp. nov. and *B. pingi* have comparatively taller bodies, as reflected in lower mean SL/BD ratios (5.10±0.43 and 5.09±0.71, respectively) compared to those observed in *B. viridis* sp. nov. and *B. zebroida* (5.31±0.54 and 5.47±0.33, respectively). *B. pingi* is distinguished by a broader body, as evidenced by smaller mean ratios of SL/BW and SL/PW (4.2±0.36 and 7.42±0.39, respectively), a shorter head, indicated by a larger mean SL/HL (4.9±0.18), and a narrower mouth, denoted by a larger mean HW/MW (5.79±0.5). Compared to the other three species, *B. granulopinna* sp. nov. features a shorter and thicker caudal peduncle, as shown by the smaller mean SL/CD and PoAL/CD (8.36±0.52 and 1.29±0.11, respectively).

Variability in morphometric characteristics is observed within populations of *B. viridis* sp. nov. from different regions. Specimens from Lingyun County possess a more robust anterior body segment, with wider and taller heads and trunks (PrPvL/HW=1.53±0.08, PrPvL/PW=0.99±0.03, PrPvL/BW=1.73±0.07, PrPvL/BD=1.98±0.15, PrPvL/HD=2.48±0.12, PrPvL/PW=1.25±0.05), and a thicker caudal peduncle (PrPvL/CD=3.59±0.28). The population from the type locality, Wuming District, Nanning City, exhibits fewer branched rays in the paired fins (pectoral fins 20.25±0.68, pelvic fins 16.5±0.71).

Compared to the type locality, the population from Debao County is characterized by a broader and flatter body (PW/BD=2.32±0.19) and a thinner caudal part (PoAL/CD=1.69±0.09) (see Table 4).

It is noteworthy that, despite the statistically significant and visually discernible differences in measurable characteristics, the presence of overlap among different species precludes recommending these characteristics as reliable bases for species identification.

Discussion

Taxonomic clarification and redescription of *Beaufortia pingi*

In 1930, Fang described *Gastromyzon pingi* with the type locality specified as Lingyun County in 1928. He mentioned two collection sites, one near the boundary of Yunnan Province (type locality) and the other in Damaoping Village. At that time, the jurisdiction of Lingyun County was more extensive, bordering Yunnan and encompassing the current eastern area of Tianlin County. The county's watershed includes the Xiyang River, Bo′ai River, Jia River (currently Leli River), and Chengbi River. This broad and somewhat vague collection range coincides with the primary distribution area of the *Beaufortia pingi* species group. Given the relatively short geographical distances between distribution areas of different species within this region, it is highly probable that the type specimens could actually belong to different species. The paratype specimen NO. 955 exhibits a notably lower count of pectoral fin rays, a distinguishing characteristic of *B. granulopinna* sp. nov. from *B. pingi*. Excluding the lateral line scale count, the morphological features of the remaining specimens align with those of *B. pingi* specimens collected from the Chengbi River basin within the current boundaries of Lingyun County. The scales of the *B. pingi* species group are exceptionally fine, often less than 0.5 mm in diameter, suggesting that the original counts might have been inaccurately high due to the limitations of observation equipment.

Apart from the Chengbi River basin, *B. pingi* was also collected from the Jian River basin in Debao County. Compared to the holotype, these specimens have slightly fewer ventral fin rays and a somewhat broader and flatter body, but they share the main differential features of the species. The genetic distance of the mitochondrial *cyt*b gene is less than 1%, indicating minor genetic variation, and phylogenetically, these specimens cluster within the same lineage as *B. pingi*.

In summary, the species within the *Beaufortia pingi group* are geographically proximate and morphologically similar. The type locality of *B. pingi* is relatively indistinct, and the age of the specimens complicates identification. The inclusion of other species among the paratypes, the original vague description, and some inaccuracies in detail present challenges. Considering these issues, we have conducted a redescription of *B. pingi* based on extensive specimen collection, morphological comparisons, and molecular phylogenetic analysis.

Taxonomic clarification and redescription of *Beaufortia zebroida*

Gastromyzon pingi zebroidus was also described in the same article, in which Fang (1930) described *Gastromyzon pingi* with a single-type specimen collected from the Dongui River along the China-Vietnam border in Longzhou County, Guangxi Province. Since its publication, no further records of this species have been found in that basin. Despite multiple surveys in Longzhou County, the species was not rediscovered, and the local rivers, mostly altered by human activities and facing severe bioinvasions, significantly reduced the habitats suitable for gastromyzonids.

The limited information from a single specimen, coupled with the low distinctiveness of the illustrations and the relatively vague morphological description of *Gastromyzon pingi zebroidus*, has led to significant controversy over the identity of this species and multiple changes in its taxonomic status.

In the original description, Fang (1930) distinguished this subspecies by the anal pore's proximity to the posterior edge of the ventral fins and the presence of stripes along the entire flank (vs. the anal position being further from the posterior edge of the ventral disc and stripes being pronounced at the caudal peduncle in *Gastromyzon pingi*). Later, Hora (1932) elevated its taxonomic status to species level as *Beaufortia zebroidus* without providing justification. Nichols (1943) followed Fang's (1930) perspective, considering it a subspecies of *Gastromyzon pingi*.

Chen (1980), upon examination of two specimens from the Xijiang River (location unspecified), with total lengths of 29 mm and 52 mm, respectively, observed that both specimens exhibited pronounced or faint vertical stripes and noted the anal pore situated at a considerable distance from the ventral fins. Consequently, Chen tentatively synonymized *Beaufortia zebroidus* with *Beaufortia pingi*, pending further collection of specimens for a definitive conclusion. According to our observations, the vertical stripes on juvenile stages of *B. pingi* typically do not disappear, and the specimen measuring 29 mm in length is likely in a late juvenile stage. Therefore, the species in question is inferred to be *B. pingi*.

Yue (1981), upon examination of nine specimens from Lingyun County, Guangxi, identified them as *B. pingi* and noted the presence of 2–4 transverse vertical stripes on the caudal peduncle. The presence and clarity of stripes anterior to the caudal peduncle varied among individuals, with some exhibiting up to 10 distinct stripes. The anal pore was observed to be closer to the anal fins than to the posterior edge of the ventral fins, with distance varying across the specimens. Notably, one specimen, No.74664, possessed an anal pore precisely at the posterior edge of the ventral fins. Based on these findings, Yue proposed that *B. zebroidus* could be a synonym of *B. pingi* or not a valid subspecies. Zheng (1989) examined 15 specimens from Lingyun County, Guangxi, and Xingyi County, Guizhou, and identified them as *B. pingi*. Zheng observed the terminal rays of the ventral fins connecting medially on both sides, with a notch at the end (presumably a typographical error for "a pair of notches"), the posterior edges located near the anal pore or slightly distant, and 11–13 transverse bands across the dorsal midline accompanied by approximately 20 vertical stripes. The presence of unclear stripes, visible only at the caudal peduncle in some individuals, led Zheng to consider *B. zebroidus* a junior synonym of *B. pingi*. Both researchers examined the specimens from the type locality, and given that Lingyun County is habitat to both *B. pingi* and *B. viridis* sp. nov., the possibility of these specimens comprising two distinct species cannot be excluded.

Subsequently, Chen (1990) examined 21 specimens from the Xiyang River in Guangnan County, Yunnan, identifying them as *B. pingi*. The observations revealed that the tips of the pelvic fin rays were proximal to the anal pore in all specimens, with numerous dark and light stripes along the dorsal midline and flanks. Chen thus regarded *B. zebroidus* as a junior synonym of *B. pingi*. Our research indicates that the species distributed in the Xiyang River is *B. viridis* sp. nov., and given the consistent presence of vertical stripes in all specimens, the referenced species is likely *B. viridis* sp. nov.

Later, Chen and Tang (2000) measured three specimens from Tian'e, Guangxi, noting that the posterior edges of the pelvic fins were proximal to the anal pore. The dorsal and lateral sides exhibited approximately 20 black vertical stripes, with the pre-pelvic length significantly exceeding the distance from the pelvic fin origin to the anal fin origin. The branched ray count in the paired fins (pectoral 19, pelvic 15–16) was slightly lower than that observed in the specimens from the type locality of *B. pingi* (pectoral 21–23, pelvic 18–20), leading them to recognize *B. zebroidus* as a valid species. We noted that the branched ray counts in the paired fins of the specimens collected from Tian'e County fell within the variation range of the specimens from the type locality of *B. viridis* sp. nov., with the pre-pelvic length generally greater than the length from the pelvic origin to the anal origin (mean PrPvL/POAO=1.19±0.74), distinct from the specimens from the type locality of *B. pingi* (PrPvL/POAO=0.98±0.66). Hence, the specimens collected from Tian'e County are identified as *B. viridis* sp. nov.

Chen and Zhang (2006), after examining six specimens from Tianlin County and Lingyun County and referencing Chen and Tang (2000), encountered individuals exhibiting characteristics of both *B. pingi* and *B. zebroidus* (presence or absence of vertical stripes, count of branched rays in paired fins, PrPvL/POAO ratio), thereby considering *B. zebroidus* a synonym of *B. pingi*. Tianlin County serves as the type locality for *B. granulopinna* sp. nov. Our statistical analysis indicates that a certain proportion of vertical stripes disappear in the adult stages of both *B. granulopinna* sp. nov. and *B. pingi* (54.76% and 94.00%, respectively). The branched ray counts in the paired fins of *B. granulopinna* sp. nov. are also marginally less than those of *B. pingi*, and the PrPvL/POAO ratios for both species fluctuate around 100% (as shown in Table 3). Moreover, we observed that the photographs provided by the authors (original fig. X 98), which depicted *B. granulopinna* sp. nov., showed the first few rays of the pectoral fins exhibiting well-developed tubercles. Therefore, the batch of specimens actually represents a mix of *B. pingi* and *B. granulopinna* sp. nov. from their type localities.

Finally, Kottelat (2012) recognized *B. zebroidus* as a valid species, changing the suffix to -a, and synonymized *B. fasciolata*, *B. multiocellata*, and *B. triocellata*, collected from the China-Vietnam border, with *B. zebroida*.

After investigating all possible distribution areas and combining morphological analysis with mitochondrial *cyt*b gene phylogenetic analysis, we conclude the following:

The type locality of *B. zebroida* is the border river between China and Vietnam. Among all the literature records, the ones closest to the type locality are the collection sites of *B. fasciolata*, *B. multiocellata*, and *B. triocellata*. Although the type specimens of these three species are lost, their original descriptions and unclear illustrations still confirm that they belong to the same species as our specimens collected from the southeastern Yunnan Province to the western Guangxi border area with Vietnam. Fang (1930) mentioned the specimen color as pale fleshy, which aligns with the body color of the aforementioned populations but not with *B. pingi* and *B. viridis* sp. nov. Thus, we consider *B. zebroida* a species distributed from Maguan County in Yunnan Province to Longzhou County in Guangxi Province along the China-Vietnam border, as well as in northeastern Vietnam. The region contains small tributaries flowing to both the Red River and the Zuo River (Pearl River system), closely spaced due to the karst landscape, facilitating stream capture and exchange. The type locality, Longzhou County, represents the eastern boundary of the species' distribution, but due to habitat destruction and bioinvasions, no further records of this species have been found there. Besides this area, the species has been discovered in Maguan County, Guangnan County, Xichou County, Malipo County, Funing County, and Napo County (stream tributary to the upper reaches of the Shuikou River, same basin as the type locality) within China and northeastern Vietnam. Following the clarification of its taxonomic status, we have provided a redescription of *B. zebroida*.

Key to the *Beaufortia pingi* species group

1 Vertical black stripe on flank absent; lower lip dicot-type, sides not lobed or with 1–2 small notches...other *Beaufortia* species
– Flank with multiple vertical dark stripes; lower lip pinnate-type, sides multilobed 2
2 Adult pectoral fins with 6–9 rays bearing well-developed granular nuptial tubercles ..... *B. granulopinna*
– Nuptial tubercles on adult pectoral fin rays absent or indistinct 3
3 Vertical stripes in a large proportion (94.00%) of adults show blurred or vanished before caudal peduncle ..... *B. pingi*
– Vertical stripes consistently present at all developmental stages, not blurring or vanishing 4
4 Vertical stripes uniform in width and length, often wider than spacing; dorsal body dark cyan to green..... *B.viridis*
– Stripes uneven in width and length, often narrower than spacing, sometimes reduced to dots; body brown yellow to golden dorsally..... *B.zebroida*

Survival status and conservation recommendations for the *Beaufortia pingi* species group

The research on the Beaufortia *pingi* group is mostly in its initial stages; however, their situation is far from optimistic. These species have become popular ornamental fish in China. Aquarium trade operators reap substantial profits through the capture and sale of these fish from the wild, yet among them are those who act with disregard for sustainability; their harvesting practices are often destructive. Given their rheophilic nature, projects that obstruct rivers can easily lead to regional extinction. Their low pollution tolerance and sensitivity to changes in water quality also contribute to the significant reductions in population that many species are suffering. In the type locality of *B. viridis* sp. nov., Wuming District, Nanning City, most small tributaries have been modified into step-like reservoirs for water storage, and those near agricultural irrigation areas are polluted, rendering these areas unsuitable for their survival. Interestingly, a stable population was discovered inside a commercial eco-camping site. To satisfy consumers' pursuit of "pristine nature," contractors have left some river sections poor developed, providing a refuge for this species. We suggest that future efforts should focus on increasing attention to these species, conducting

fundamental research, and further exploring their scientific and economic potential. Simultaneously, it is crucial to enhance habitat conservation awareness, scientifically plan, and develop sustainably, ensuring harmonious coexistence between humans and nature.

Comparative materials

Beaufortia szechuanensis: SHOU20231220601, one specimen, 59.18 mm SL, from Wanzhou District, Chongqing, upper Yangtze River basin. SHOU20231220602, one specimen, 42.94 mm SL, from Qijiang District, Chongqing, upper Yangtze River basin. SHOU20231220640-642, three specimens, 46.17–54.93 mm SL, from Neijiang City, Sichuan, upper Yangtze River basin. Collected by Jing-Chen Chen and Hao-Tian Lei.

Beaufortia liui: SHOU20240225701, one specimen, 36.64 mm SL, from Huidong County, Sichuan, upper Yangtze River basin. Collected by Can Liu. IHASW83VI0424-425, two specimens, from Huidong County, Sichuan, upper Yangtze River basin, inspection only. IHW 2247, 2446, two specimens, syntype, inspection only.

Beaufortia niulanensis: SHOU20231220614-615, SHOU20231220617, three specimens, 41.38–43.66 mm SL, from type locality, Qujing City, Yunnan, upper Yangtze River basin. Yangtze River basin. Collected by Xin-Rui Pu, Lao Xing, and Lingzi.

Beaufortia polylepis: SHOU20231220643-644, two specimens, 40.06–41.02 mm SL, from downstream near the type locality, Kaiyuan City, Yunnan, upper Nanpan River (Pearl River system). Collected by Lin Yang. IHW 774330, one specimen, syntype, inspection only.

Beaufortia huangguoshuensis: IHASW83IV0049, one specimen, syntype, and fin rays were counted; the other data refers to Chen and Tang (2000).

Beaufortia intermedia: IHW 87IV516, one specimen, paratype, inspection only. Measurement data refers to Tang et al. (1997).

Beaufortia leveretti: SHOU20231212626-627, two specimens, 44.65–52.42 mm, from Fangchenggang City, Guangxi, collated by Qian-Yu Liang. SHOU20231212628-630, three specimens, 59.94–64.71 mm, from type locality, Baisha County, Hainan, collector unknown.

Beaufortia kweichowensis: SHOU20231212601-602, two specimens, 53.77–55.24 mm, from Congjiang County, Guizhou, Duliu River (Pearl River system). SHOU20231212614-616, three specimens, 44.38–47.77 mm, from Pingle County, Guangxi, Li River (Pearl River system). Collected by Jing-Chen Chen.

Beaufortia cyclica: IHASW75IV1417, one specimen, holotype, inspection only. Measurement data refers to the original description.

Beaufortia yunnanensis, *Beaufortia fasciolata*, *Beaufortia triocellata*, *Beaufortia multiocellata*, *Beaufortia buas*, *Beaufortia daon*, *Beaufortia elongata*, and *Beaufortia loos*: Referenced original descriptions (Li et al. 1998; Kottelat 2001; Nguyen and Nguyen 2005).

Contributions

Jing-Chen Chen conducted sample collection, specimen identification and measurement, photography, map drafting, molecular genetic analysis, and manuscript composition. Jia-Jia Li was responsible for specimen measurement, illustration of measurement methodologies, and molecular genetic experimentation. Wen-Qiao Tang provided guidance on research concepts as well as review and revision of the manuscript. Xin-Rui Pu participated in sample collection and specimen identification. Hao-Tian Lei carried out specimen collection and grammatical checks.

Acknowledgments

We sincerely thank the Institute of Hydrobiology, Chinese Academy of Sciences, for their assistance in the inspection of type specimens. Our deep appreciation goes to Mr. Jia-Jun Zhou, Mr. Qian-Yu Liang, Mr. Lao Xing, Mr. Lin Yang, Mr. Guo Yu, Mr. Xi-Xian Chen, and Mr. Can Liu for their invaluable support and assistance with sample collection. We also extend our thanks to Yi-Yang Xu and Hao-Yang Xie for their contributions to photographing the type specimens. Special thanks are due to Zhi-Xian Sun for his guidance and assistance with photography. We are grateful to the Library of Nha Trang University for providing the necessary reference materials. This work was supported by the National Natural Science Foundation of China (NSFC) (Grant No. 31093430) and the National Special Program for Basic Research Works in Science and Technology (2015FY110200).

References

Chen YY (1980) Systematic studies on the fishes of the family Homalopteridae of China II. Classification of the fishes of the subfamily Gastromyzoninae. Shui Sheng Sheng Wu Hsueh Bao 7: 95–120. https://doi.org/10.3724/issn1000-3207-1980-1-95-c

Chen YR (1990) *Beaufortia*. In: Zhe LX, Chen YR (Eds) The Fishes of Yunnan, China Part II Cyprinidae. Science Press, Beijing, 85–89.

Chen XY (2013) Checklist of Fishes of Yunnan. Zoological Research 34: 281–343.

Chen YY, Tang WQ (2000). Homalopteridae. In: Le PQ (Ed.) Fauna Sinica, Osteichthyes, Cypriniformes III. Science Press, Beijing 438–567.

Chen W, Zhang CG (2006) *Beaufortia*. In: Zhou J, Zhang CG (Eds) Freshwater fishes of Guangxi, China (Second Edition). People's Publishing House, Nanning, 376–381.

Chen JC, Chen YY, Tang WQ, Lei HT, Yang JQ, Song XJ (2023) Resolving phylogenetic relationships and taxonomic revision in the

Pseudogastromyzon (Cypriniformes, Gastromyzonidae) genus: Molecular and morphological evidence for a new genus, *Labigastromyzon*. Integrative Zoology 00: 1–22. https://doi.org/10.1111/1749-4877.12761

IBM Corp. (2020) IBM SPSS Statistics for Windows (Version 26.0).

Fang PW (1930) New homalopterin loaches from Kwangsi, China. Sinensia 1: 25–42.

Frice R, Eschmeyer WN, Van der Laan R (2024) Eschmeyer's catalog of fishes: genera, species, references. https://researcharchive.calacademy.org/research/ichthyology/catalog/fishcatmain.asp

Hora SL (1932) Classification, bionomics and evolution of homalopterid fishes. Memoirs of the Indian Museum 12: 263–330.

Kalyaanamoorthy S, Minh BQ, Wong TKF, von Haeseler A, Jermiin LS (2017) ModelFinder: Fast model selection for accurate phylogenetic estimates. Nature Methods 14(6): 587–589. https://doi.org/10.1038/nmeth.4285

Katoh K, Standley DM (2013) MAFFT multiple sequence alignment software version 7: Improvements in performance and usability. Molecular Biology and Evolution 30(4): 772–780. https://doi.org/10.1093/molbev/mst010

Kottelat M (2001) Freshwater fishes of northern Vietnam. World Bank, Washington.

Kottelat M (2012) Conspectus Cobitidum: An Inventory of the Loaches of the World (Teleostei: Cypriniformes: Cobitoidei). Raffles Bulletin of Zoology. National University of Singapore Press, Singapore.

Kottelat M (2013) The fishes of the inland waters of Southeast Asia: A catalogue and core bibliography of the fishes known to occur in freshwaters, mangroves and estuaries. The Raffles Bulletin of Zoology 27: 1–663.

Li WX, Mao WN, Lu ZM, Sun RF, Lu HS (1998) Two new species of Homalopteridae from Yunnan China. Chinese Journal of Fisheries 11(1): 1–6.

Mai D (1978) Identification of the Fresh-Water Fishes of North Vietnam. Scientific, Technology Publisher, Ha Noi.

Nguyen HD, Nguyen VH (2005) Ca Nuoc Ngot Viet Nam. Tap II. Nha Xuat Ban Nong Nghiep. Ha Noi 282–283: 588–593.

Nguyen LT, Schmidt HA, von Haeseler A, Minh BQ (2015) IQ-TREE: A fast and effective stochastic algorithm for estimating maximum-likelihood phylogenies. Molecular Biology and Evolution 32(1): 268–274. https://doi.org/10.1093/molbev/msu300

Nichols JT (1943) The fresh-water fishes of China. Natural history of Central Asia 9: 231. https://doi.org/10.5962/bhl.title.12103

Rambaut A (2018) FigTree v1.4.4. http://tree.bio.ed.ac.uk/software/figtree/

Rohlf FJ (2016) tpsDig2w64, digitize landmarks and outlines version 2.32. State University of New York at Stony Brook, New York.

Ronquist F, Teslenko M, van der Mark P, Ayres DL, Darling A, Höhna S, Larget B, Liu L, Suchard MA, Huelsenbeck JP (2012) MrBayes 3.2: Efficient Bayesian phylogenetic inference and model choice across a large model space. Systematic Biology 61(3): 539–542. https://doi.org/10.1093/sysbio/sys029

Tamura K, Stecher G, Kumar S (2021) MEGA11: Molecular evolutionary genetics analysis version 11. Molecular Biology and Evolution 38(7): 3022–3027. https://doi.org/10.1093/molbev/msab120

Tang WQ, Wang DZ, Yu T (1997) A new species of the genus *Beaufortia* from Guizhou Province, China (Cypriniformes: Homalopteridae). Zoological Research 18: 19–22.

Yue ZH (1981) Gastromyzonidae. In: Zheng BS (Ed.) Freshwater fishes of Guangxi, China. Guangxi People's Publishing House, Nanning, 166–175.

Zhang D, Gao F, Jakovlić I, Zou H, Zhang J, Li WX, Wang GT (2020) PhyloSuite: An integrated and scalable desktop platform for streamlined molecular sequence data management and evolutionary phylogenetics studies. Molecular Ecology Resources 20(1): 348–355. https://doi.org/10.1111/1755-0998.13096

Zheng CY (1989) The Fishes of Pearl River. Science Press, Beijing, 257–260.

Zoosyst. Evol. 100 (3) 2024, 965–987 | DOI 10.3897/zse.100.117859

PENSOFT

MUSEUM FÜR NATURKUNDE BERLIN

Morphological and molecular evidence for *Gothus teemo* gen. et sp. nov., a new xanthid crab (Crustacea, Brachyura, Xanthoidea) from coral reefs in the South China Sea, with a review of the taxonomy of *Actaeodes consobrinus* (A. Milne-Edwards, 1867)

Zi-Ming Yuan[1,2,3,4], Wei Jiang[1,2,3], Zhong-Li Sha[1,2,3]

1 *Department of Marine Organism Taxonomy and Phylogeny, Institute of Oceanology, Chinese Academy of Sciences, Qingdao 266071, China*
2 *Laoshan Laboratory, Qingdao 266237, China*
3 *Shandong Province Key Laboratory of Experimental Marine Biology, Institute of Oceanology, Chinese Academy of Sciences, Qingdao, China*
4 *College of Biological Sciences, University of Chinese Academy of Sciences, Beijing 100049, China*

https://zoobank.org/15CA9ED4-C24C-4AD7-81AC-F699FA953FE8

Corresponding author: Zhong-Li Sha (shazl@qdio.ac.cn)

Academic editor: M. Christodoulou ♦ **Received** 27 December 2023 ♦ **Accepted** 13 June 2024 ♦ **Published** 9 July 2024

Abstract

A new genus and species within the family Xanthidae MacLeay, 1838, are described from coral reefs in the South China Sea. The new genus, *Gothus*, with its type species *G. teemo* **sp. nov.**, is distinguishable from allied genera by characteristics of the carapace, chelipeds, and male pleon. Based on morphological evidence, we tentatively place this genus within the subfamily Euxanthinae Alcock, 1898. However, molecular systematic analysis based on COI, 12S, 16S, and H3 indicates that it does not form a stable monophyletic group with any related subfamily. Another species, *Actaeodes consobrinus* (A. Milne-Edwards, 1873), is also reclassified into this new genus, based on both morphological and molecular evidence.

Key Words

Euxanthinae, integrative taxonomy, Nansha Islands, Xanthidae, Xisha Islands

Introduction

Xanthidae MacLeay, 1838, is one of the most diverse families in Brachyura, comprising 639 species across 124 genera (updated from Ng et al. 2008). Recent molecular phylogenetic studies have gradually deciphered the complex internal systematic and evolutionary relationships within this large taxonomic group (Lai et al. 2011; Thoma et al. 2014; Mendoza et al. 2022). However, the morphological delineation of various clades still requires further investigation. Potentially undiscovered taxa may also offer novel insights into or challenge the classification system of this group.

During a recent biological research expedition to the coral reefs of the South China Sea, we discovered a small and distinctive species of Xanthidae in the Xisha Islands (Paracel Islands) and Nansha Islands (Spartly Islands), which we confirmed as a new genus and species. We discussed its taxonomic status within the family using an integrative taxonomic approach that combines morphological and molecular phylogenetics, with particular focus on its subfamily affiliation. Additionally, we revisited the taxonomic status of another common species of the South China Sea coral reefs, *Actaeodes consobrinus* (A. Milne-Edwards, 1873), reassigning it to the present new genus.

Materials and methods

Specimens were obtained during scuba diving at coral reefs in the South China Sea, subsequently photographed, and conserved in 70% ethyl alcohol. These specimens have been deposited at the Marine Biological Museum, Chinese Academy of Sciences in Qingdao, China (MBM). Morphology was observed using a ZEISS SteREO Discovery stereoscopic microscope. Photographs were captured using a Canon EOS 6D camera with a Canon MP-E 65 mm lens, a Nikon D800 camera with a Nikon AF-S 105 mm lens, or a ZEISS Axiocam 506 microscope camera.

The terminology used in this paper mainly follows that of Serène (1984) and Davie et al. (2015). The following abbreviations were used: **CW** = maximum carapace width; **CL** = median carapace length; **G1** = first gonopod of male; **G2** = second gonopod of male.

The molecular sequences used in this study were primarily obtained from NCBI, particularly from Lai et al. (2011) and Mendoza et al. (2022) (Table 1). The sequences acquired in this study were obtained through the following methods: DNA was extracted from muscle tissue using the OMEGA EZNA Tissue DNA Kit (USA). Molecular characters were derived from three mitochondrial and one nuclear markers: mitochondrial 12S rRNA (12S, approximately 363 bp), 16S rRNA (16S, approximately 521 bp), cytochrome oxidase I (COI, approximately 658 bp), and nuclear histone H3 (H3, approximately 328 bp). 44 species within the family Xanthidae and two outgroup taxa were encompassed in the phylogenetic analysis (Suppl. material 1). Amplification was carried out via polymerase chain reaction (PCR), employing primers 12sf and 12s1r for 12S (Buhay et al. 2007), 16Sar and 16Sbr for 16S (Palumbi, 1996), Hex-AF and Hex-AR for H3 (Svenson & Whiting, 2004), and either jgLCO1490 and jgHCO2198 (Geller et al. 2013) or Pano-F and Pano-R (Thoma et al. 2014) for COI. The amplification protocol was as follows: initial denaturation at 94 °C for 3 min, followed by 35 cycles of denaturation at 94 °C for 30 s, annealing at 60 °C for 12 s, 48 °C for 16 s, 48 °C for COI, 66 °C for H3 for 45 s each, extension at 72 °C for 45 s, and a final extension at 72 °C for 10 min.

The sequences obtained were aligned using MEGA 6 (Tamura et al. 2013) and concatenated using SequenceMatrix 1.8 (Vaidya et al. 2011), resulting in a combined sequence length of 2019 bp. Phylogenetic trees were constructed using the maximum likelihood (ML) method and Bayesian inference (BI). The optimal model of evolution for each dataset was determined using jModelTest 0.1.1 based on the Akaike information criterion (AIC) (Posada, 2008). Bayesian analyses were executed with MrBayes 3.2.7 (Huelsenbeck & Ronquist, 2001), employing a Markov Chain Monte Carlo (MCMC) algorithm with two runs, each consisting of four chains, for 1,000,000 generations and sampling trees every 500 generations, totaling 2,000 sampled trees. The initial 500 trees were discarded as burn-in, and posterior probabilities were calculated from the remaining trees. The ML analyses were conducted online using W-IQ-TREE (http://iqtree.cibiv.univie.ac.at/) (Jana et al. 2016), with clade support evaluated via 10,000 ML bootstrap replications.

Multiple species delimitation methods were utilized to assess the hypothesis that the specimen is a distinct species. The COI data, comprising 17 homologous sequences, were subjected to automated barcode gap discovery (ABGD) analysis using a web-based interface (https://bioinfo.mnhn.fr/abi/public/abgd/abgdweb.html), as described by Puillandre et al. (2012). The analysis was conducted using the Kimura 2-parameter substitution model (TS/TV = 2.0), with a prior range for maximum intraspecific divergence set between 0.001 and 0.1, encompassing 10 recursive steps, and a relative gap width (X) of 1.0. Additionally, Bayesian implementation of the Poisson tree processes (PTP) species delimitation model was employed as per Zhang et al. (2013), conducted on the web server of the Heidelberg Institute for Theoretical Studies, Germany (http://species.h-its.org/), using BI phylogenetic trees as the input data.

Results

Systematic account

Family Xanthidae MacLeay, 1838
Subfamily Euxanthinae Alcock, 1898

***Gothus* gen. nov.**

https://zoobank.org/240FAE30-235A-49A8-995D-6209A7F68991

Figs 1–5

Type species. *Gothus teemo* sp. nov., by present designation.

Diagnosis. Small species, CW under 10 mm. Carapace broader than long, dorsal surface bearing round granules, regions clearly defined; front wide, not protruding, divided into two slightly triangular lobes by a V-shaped notch; frontal lobes and dorsal inner orbital angle separated by shallow depression; eyestalks densely granulated; area beneath outer orbital angle slightly concave, not forming a subhepatic cavity; anterolateral margin with four teeth, first tooth flattened, sometimes completely reduced to appear as three teeth; posterolateral margin almost straight; subhepatic region densely granulated.

Epistome central region with low median projection on posterior margin. Maxilliped 3 granulated, anterior edge of merus indented, external terminal angle expanded. Antennule folding transversely; basal segment of antenna subrectangular; contacting ventral external frontal margin and ventral internal orbital angle; antennal flagellum filling orbital hiatus.

Chelipeds symmetrical, merus short; carpi robust, surface granulated, aggregated into nodules; outer and dorsal surfaces of palm densely granulated; fingers elongated, with triangular teeth; tips sharp, crossing at extremities when closed; dorsal surface of movable finger with three granulated ridges. Fingers brownish-black, coloration of immovable finger extending onto inner and outer surfaces of palm in male.

Table 1. Details of specimens and GenBank accession numbers used in this study.

Species	Locality	Voucher	COI	16S	12S	H3	Sources
Actaea pura Stimpson, 1858	Xiamen, Fujian, China	AP01	PP028728	PP024661	PP025373	PP001490	present study
Actaeodes hirsutissimus (Rüppell, 1830)	Milne Bay Province, Papua New Guinea	USNM:1467002	MZ560478	NA	NA	NA	Plaisance et al. 2021
Actaeodes hirsutissimus (Rüppell, 1830)	Pulau Bintan, Indonesia	ZRC 2008.1143	NA	HM798418	HM851287	HM798267	Lai et al. 2011
Actaeodes tomentosus (H. Milne-Edwards, 1834)	Pulau Sapi, Sabah, Malaysia	ZRC 2000.1673	HM750947	HM798420	HM851289	HM798269	Lai et al. 2011
Atergatis integerrimus (Lamarck, 1818)	Beting Bronok Reef, Singapore	ZRC 2007.0252	HM750950	HM798423	HM851292	HM798271	Lai et al. 2011
Banareia nobili (Odhner, 1925)	Bolod, Panglao Island, Philippines	ZRC 2010.0131	HM750954	HM798429	HM851299	HM798277	Lai et al. 2011
Chlorodiella nigra (Forskål, 1775)	Bar Al Hikman Peninsula, Oman	UF 17948	HM750961	HM798437	HM851307	HM798286	Lai et al. 2011
Cymo quadrilobatus Miers, 1884	NA	ZRC 2009.1173	HM750969	HM798443	HM851314	HM798292	Lai et al. 2011
Demania intermedia Guinot, 1969	Northwest coast of Panglao, Philippines	ZRC 2009.0187	HM750972	HM798448	HM851319	HM798297	Lai et al. 2011
Eriphia gonagra (Fabricius, 1781)	NA	ULLZ 5463	HM638035	HM637964	HM637933	HM596633	Direct Submission
Etisus anaglyptus H. Milne-Edwards, 1834	Paya Beach, Paya Beach, Malaysia	ZRC 1999.0931	HM750975	HM798451	HM851322	HM798300	Lai et al. 2011
Euxanthus exsculptus (Herbst, 1790)	Paya Beach, Pulau Tioman, Malaysia	ZRC 2002.0535	HM750983	HM798460	HM851332	HM798310	Lai et al. 2011
Euxanthus herdmani Laurie, 1906	Looc, Panglao Island, Philippines	NMCR 27334	HM750984	HM798461	HM851333	HM798311	Lai et al. 2011
Euxanthus huonii (Hombron & Jacquinot, 1846)	Pontod Isle, Panglao Island, Philippines	ZRC 2008.1376	HM750985	HM798462	HM851334	HM798312	Lai et al. 2011
Euxanthus ruali Guinot, 1971	E Aoré Island, Aimbué Bay, Vanuatu	ZRC 2009.1178	HM750986	HM798463	HM851335	HM798313	Lai et al. 2011
Forestiana depressa (White, 1848)	NA	ZRC1998.404	NA	MZ412992	NA	MZ823053	Mendoza et al. 2022
Gaillardiellus rueppelli (Krauss, 1843)	Weizhou Island, Guangxi, China	G02	PP028729	PP024662	PP025374	PP001491	present study
Gothus consobrinus comb. nov.	Yongshu Reef, Nansha Islands, China	NS-YS-2022-1336	PP028733	PP024664	PP025376	PP001493	present study
Gothus consobrinus comb. nov.	Meiji Reef, Nansha Islands, China	NS-MJ-2022-1438	PP028736	NA	NA	NA	present study
Gothus consobrinus comb. nov.	Qilianyu, Xisha Islands, China	XS-QL-2022-1014	PP028737	NA	NA	NA	present study
Gothus teemo sp. nov.	Meiji Reef, Nansha Islands, China	NS-MJ-2022-1287	PP028734	NA	NA	NA	present study
Gothus teemo sp. nov.	Meiji Reef, Nansha Islands, China	2304278486	NA	PP024665	PP025377	PP001494	present study
Hepatoporus orientalis (Sakai, 1935)	Off western coast ofBatangas, Philippines	ZRC 2008.1379	HM750994	HM798471	HM851343	HM798321	Lai et al. 2011
Hypocolpus abbotti (Rathbun, 1894)	NA	UF 14978	HM750995	HM798472	HM851344	HM798322	Lai et al. 2011
Hypocolpus diverticulatus (Strahl, 1861)	Northwest of Nosy Komba, Madagascar	UF 14076	HM750997	HM798474	HM851346	HM798324	Lai et al. 2011
Hypocolpus pararugosus Crosnier, 1996	Balicasag Island, Philippines	ZRC 2008.1389	HM750998	HM798475	HM851347	HM798325	Lai et al. 2011
Liagore rubromaculata (De Haan, 1835)	Cortes, Bohol Island, Philippines	ZRC 2010.0143	HM751006	HM798484	HM851356	HM798334	Lai et al. 2011
Liomera cinctimanus (White, 1847)	Apra harbour, Guam	ZRC 2000.0730	HM751008	HM798486	HM851358	HM798336	Lai et al. 2011
Lybia tessellata (Latreille in Milbert, 1812)	Southwest of Orote Peninsula, Guam	ZRC 2000.0710	HM751017	HM798497	HM851369	HM798346	Lai et al. 2011
Macromedaeus crassimanus H. Milne Edwards, 1834	Balicasag Island, Philippines	ZRC 2003.0369	HM751018	HM798498	HM851370	HM798347	Lai et al. 2011
Menippe rumphii (Fabricius, 1798)	Labrador Beach, Singapore	ZRC 2003.0211	HM638051	HM637976	HM637946	HM596626	Lai et al. 2011
Neoliomera striata Buitendijk, 1941	Yuzhuo Reef, Xisha Islands, China	TX02	PP028735	PP024666	NA	PP001495	present study
Neoxanthias michelae Serène & Vadon, 1981	Pichai fishing port, Phuket, Thailand	ZRC 1999.0516	HM751038	HM798522	HM851394	HM798371	Lai et al. 2011
Novactaea bella Guinot, 1976	Pulau Bintan, Indonesia	ZRC 1998.0981	HM751044	HM798529	HM851401	HM798378	Lai et al. 2011
Olenothus uogi Ng, 2002	Guam	ZRC 2002.0176	HM751046	HM798531	HM851403	HM798380	Lai et al. 2011
Paractaea rufopunctat(H. Milne Edwards, 1834)	Pago Bay, Guam	ZRC 2000.0718	HM751048	HM798535	HM851407	HM798383	Lai et al. 2011
Paractaeopsis quadriareolata (Takeda & Miyake, 1968)	NA	UF 16755	MZ400990	MZ413003	NA	MZ823064	Mendoza et al. 2022
Paratergatis longimanus Sakai, 1964	Tai-chi Port, Han county, Taiwan Island, China	ZRC 1998.0047	HM751051	HM798538	HM851410	NA	Lai et al. 2011

Species	Locality	Voucher	COI	16S	12S	H3	Sources
Platypodia pseudogranulosa Serène, 1984	Cyrene Reef, Singapore	ZRC 2008.0492	HM751058	HM798546	HM851418	HM798393	Lai et al. 2011
Psaumis cavipes (Dana, 1852)	Yongle blue hole, Xisha Islands, China	AOP03	PP028730	NA	NA	NA	present study
Psaumis cavipes (Dana, 1852)	Panglao Island, Sungcolan Bay, Philippines	ZRC 2010.0157	NA	HM798549	HM851421	HM798395	Lai et al. 2011
Pseudoliomera granosimana (A. Milne-Edwards, 1865)	NA	UF 10496	MZ400994	MZ413006	NA	MZ823067	Mendoza et al. 2022
Pseudoliomera speciosa (Dana, 1852)	Zhongsha Islands, China	ZS57	PP028732	PP024663	PP025375	PP001492	present study
*Pulcratis reticulatus*Ng & Huang, 1997	Ping-tung County, Taiwan Island, China	ZRC 1997.0402	HM751064	HM798553	HM851425	HM798399	Lai et al. 2011
Rizalthus anconis Mendoza & PKL Ng, 2008	Meiji Reef, Nansha Islands, China	NS-MJ-2022-1457	PP028731	NA	NA	NA	present study
Rizalthus anconis Mendoza & PKL Ng, 2008	Pontod lagoon, Panglao Island, Philippines	ZRC 2008.0215	NA	HM798555	HM851427	HM798401	Lai et al. 2011
Visayax osteodictyon Mendoza & Ng, 2008	Panglao Island, Philippines	ZRC 2008.0753	HM751070	HM798559	HM851432	HM798405	Lai et al. 2011
Xanthias canaliculatus Rathbun, 1906	Sodwana Bay, South Africa	ULLZ 4381	MZ400999	EU863382	EU863316	GU144502	Mendoza et al. 2022; Thoma et al. 2009; Felder and Thoma 2010
*Xanthias joanneae*Mendoza, 2013	NA	ZRC 2013.0435	MZ400998	MZ413008	NA	MZ955031	Mendoza et al. 2022
Xanthias latifrons (De Man, 1887)	Tepungan Channel, Guam	ZRC 2000.0728	HM751072	HM798561	HM851434	HM798407	Lai et al. 2011
Zalasius sakaii Balss, 1938	Mitou, Kaoshiung county, Taiwan,China	ZRC 1997.0399	HM751077	HM798566	HM851439	HM798413	Lai et al. 2011
Zosimus aeneus (Linnaeus, 1758)	Heng Chun Peninsula, Taiwan Island, China	ZRC 1998.0388	HM751078	HM798567	HM851440	HM798414	Lai et al. 2011

Ambulatory legs with meri flattened, granulated along anterior and posterior edges; dactyli elongated, margins with granules and setae, terminal end chitinous, sharp, slightly curved backward, dactylo-propodal lock present but underdeveloped.

Male thoracic sternum with sternites 1 and 2 completely fused, suture between sternites 2 and 3 straight, complete, sternites 3 and 4 mostly fused, suture between them visible only at margins, sternites 3 short, sternite 4 with central longitudinal groove, tubercle of sterno-pleonal lock located on posterior of sternite 5. Male pleon narrow, pleonites 3 to 5 completely fused, lateral margins of pleonite 6 slightly concave. Telson long, broad, truncated oval, base margin wider than terminal margin of pleonite 6.

G1 slender, curving slightly outward, distal lobe spoon-shaped, long setae on inner subdistal part, small spines on outer part. G2 not exceeding 1/6 length of G1, distal lobe elongated.

Etymology. The genus is named after the game of Go, alluding to the intermingled black and white patterns on the carapace, beneath which lie circular granules resembling the pieces of the game. "-thus" is a common suffix for species names within the Xanthidae family. Gender masculine.

Comparative material. ***Rizalthus anconis* Mendoza & PKL Ng, 2008** (Fig. 6A). China • 1 female; CW 4.2 mm, CL 2.7 mm; Meiji Reef, Nansha Islands; 9°52'38.19"N, 115°31'17.08"E; 8 m; 7 May 2022; Ziming Yuan, Yuli Sun, Shaobo Ma coll.; NS-MJ-2022-1457.

***Hypocolpus haanii* Rathbun, 1909** (Fig. 6B). China • 1 male; CW 45.3 mm, CL 34.2 mm; Lingao Cape, Hainan Island; 15–30 m; 20 Aug. 2018; Yunhao Pan coll.; MBM286755.

***Euxanthus exsculptus* (Herbst, 1790)** (Fig. 6C). China • 1 male; Wenchang, Hainan Island; 20 Dec. 2018; Yunhao Pan coll.; Xan016 • 1 male; Yongxing Island, Xisha Islands; 15–17 May 1957; MBM163793 • 2 males; Wood Island, Xisha Islands; 1957; MBM163791 • 1 male, 2 females; Wood Island, Xisha Islands; 15–17 May 1957; MBM163788 • 3 males, 3 females; East Island, Xisha Islands; 28–31 May 1980; MBM163785 • 1 female; Yongxing Island, Xisha Islands; 11–13 Jun. 1980; MBM163784 • 1 female; East Island, Xisha Islands; 12 Jun. 1975; Xianqiu Ren coll.; MBM163792. CW 15–52.8 mm, CL 9.7–33.2 mm.

***Euxanthus huonii* (Hombron & Jacquinot, 1846)** (Fig. 6D). China • 1 male; Dengqing Island, Xisha Islands; 11–17 Apr. 1958; MBM163762 • 1 female; Tree Island, Xisha Islands; 1 May 1958; MBM163761 • 1 female; Yongxing Island, Xisha Islands; 7 May 1980; MBM163780 • 2 females; Drummond Island, Xisha Islands; 1980; MBM163781 • 1 male; Meiji Reef, Nansha Islands; 9°53'30.84"N, 115°34'22.05"E; 10 m; 10 May 2022; Ziming Yuan, Yuli Sun, Shaobo Ma coll.; NS-MJ-2022-1734. CW 19.3–37.3 mm, CL 13.1–26.4 mm.

***Psaumis cavipes* (Dana, 1852)** (Fig. 6E). China • 1 female ovigerous; Xisha Islands, Jinqing Island; 10 Jul. 2019; azp01 • 1 male, 3 females; Sanya Station Front, Hainan; 30 Apr. 2021; Zhang Xu coll.; aop01 • 2 males; Xisha Islands, Yongle blue hole; 10 Jul. 2019; aop02 • 1 female ovigerous; Xisha Islands, Yongle blue hole; 10 Jul. 2019; aop03 • 1 male; Phoenix Island, Sanya, Hainan; Zhang Xu coll.; 2022010 • 1 juvenile; Xisha Islands, Yuzhuo Reef; 9 Jul. 2019; aop04 • 2 males; Hainan, subtidal 9–10 m; 21 Nov. 2016; Xan020-2. CW 5.1–17.4 mm, CL 3.3–10.6 mm

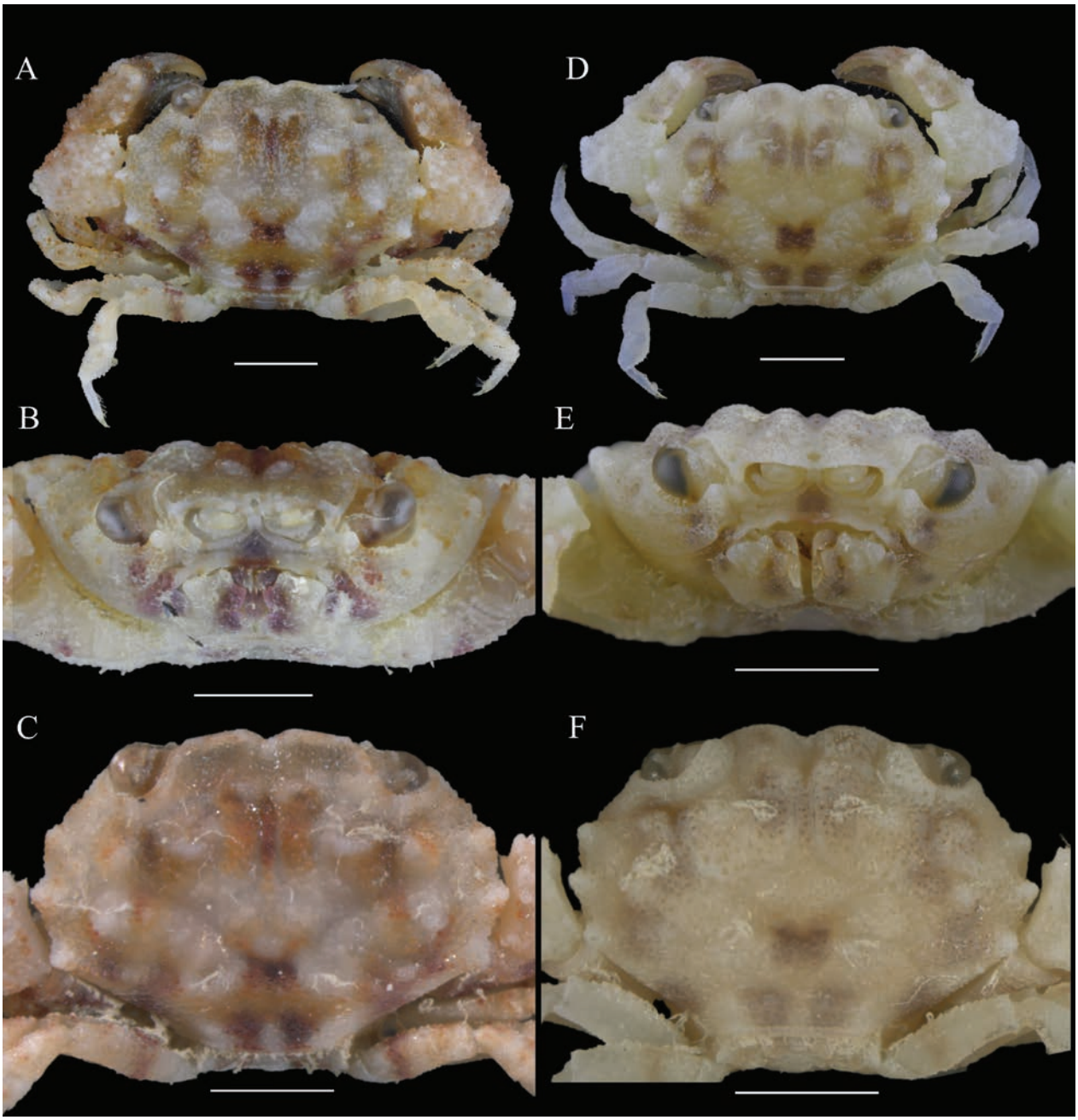

Figure 1. *Gothus teemo* sp. nov. **A–C.** Holotype, male, CW 3.7 mm, CL 2.6 mm, MBM287027; **D–F.** Paratype, CW 3.2 mm, CL 2.2 mm, MBM287026; **A, D.** Dorsal view; **B, E.** Frontal view; **C, F.** Carapace. Scale bar: 1 mm.

Remarks. *Gothus* gen. nov. exhibits the closest resemblance to the subfamily Euxanthinae, particularly to Eux 1, as defined and morphologically summarized in the molecular systematic study by Lai et al. (2011)., mainly considering its anterolateral margin of the carapace, which does not clearly meet the orbit but instead continues down to the subhepatic region, presenting an ambiguous starting point (Fig. 1B). Other characteristics justifying its inclusion are chelipeds almost completely symmetrical, which can be coapted against the carapace (Fig. 1A); male pleon long, with the telson reaching to the level above the coxo-sternal condyles of pereiopod 1, and base of somite 3 only slightly wider than tip of somite 5 (Figs 2F, 3F) (see also Serène, 1984; Lai et al. 2011). However, its ambulatory legs do not form a similar perfect coapted structure, especially since the corresponding posterolateral margin is nearly non-concave (Fig. 1A, C). Other features notably distinguishing it from any member of the subfamily Euxanthinae are its extremely narrow male pleon with a long and broad, overall truncated oval telson (Figs 2F, 3F), the base of which is wider than the width of the end of the sixth pleonite, the terminal end wide and rounded, with the lateral edges barely converging inward but rather forming two opposing arcs, unlike the typically triangular telson common in the Euxanthinae.

Gothus gen. nov. shares the closest similarities with the genus *Rizalthus* Mendoza & PKL Ng, 2008, due to both possessing a granule-covered carapace surface,

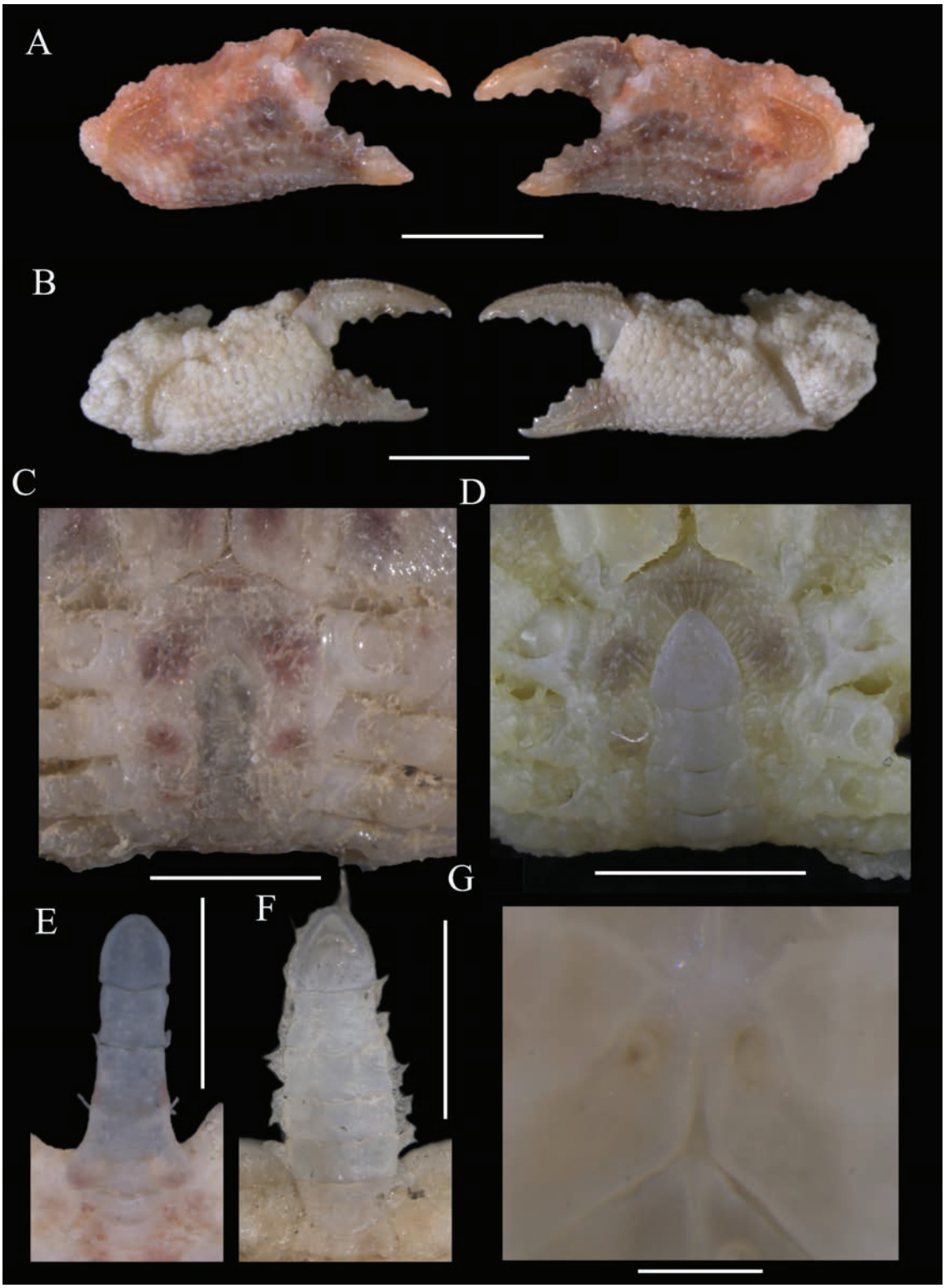

Figure 2. *Gothus teemo* sp. nov. **A, C, E.** Holotype, male, CW 3.7 mm, CL 2.6 mm, MBM287027; **B, D, F, G.** Paratype, female, CW 3.2 mm, CL 2.2 mm, MBM287026; **A.** Male chelipeds; **B.** Female chelipeds; **C.** Male thoracic sternites; **D.** Female thoracic sternites; **E.** Male pleon; **F.** Female pleon; **G.** Female vulva. Scale bar: 1 mm (**A–F**); 0.2 mm (**G**).

similar carapace outlines and front, developed cheliped carpus, and analogous G1 structures. However, *Gothus* can be easily distinguished from *Rizalthus* by several key characteristics: its anterolateral margin with four teeth, first tooth flattened, sometimes completely reduced to appear as three teeth (Figs 1A, C, 3A) (vs. no clearly defined teeth in *Rizalthus*; Fig. 6A; cf. Mendoza and Ng 2008: fig. 1A); absence of etched depressions on body (Fig. 1A) (vs. distinct etched depressions on thoracic sternum in *Rizalthus*; cf. Mendoza and Ng 2008: fig. 1C);

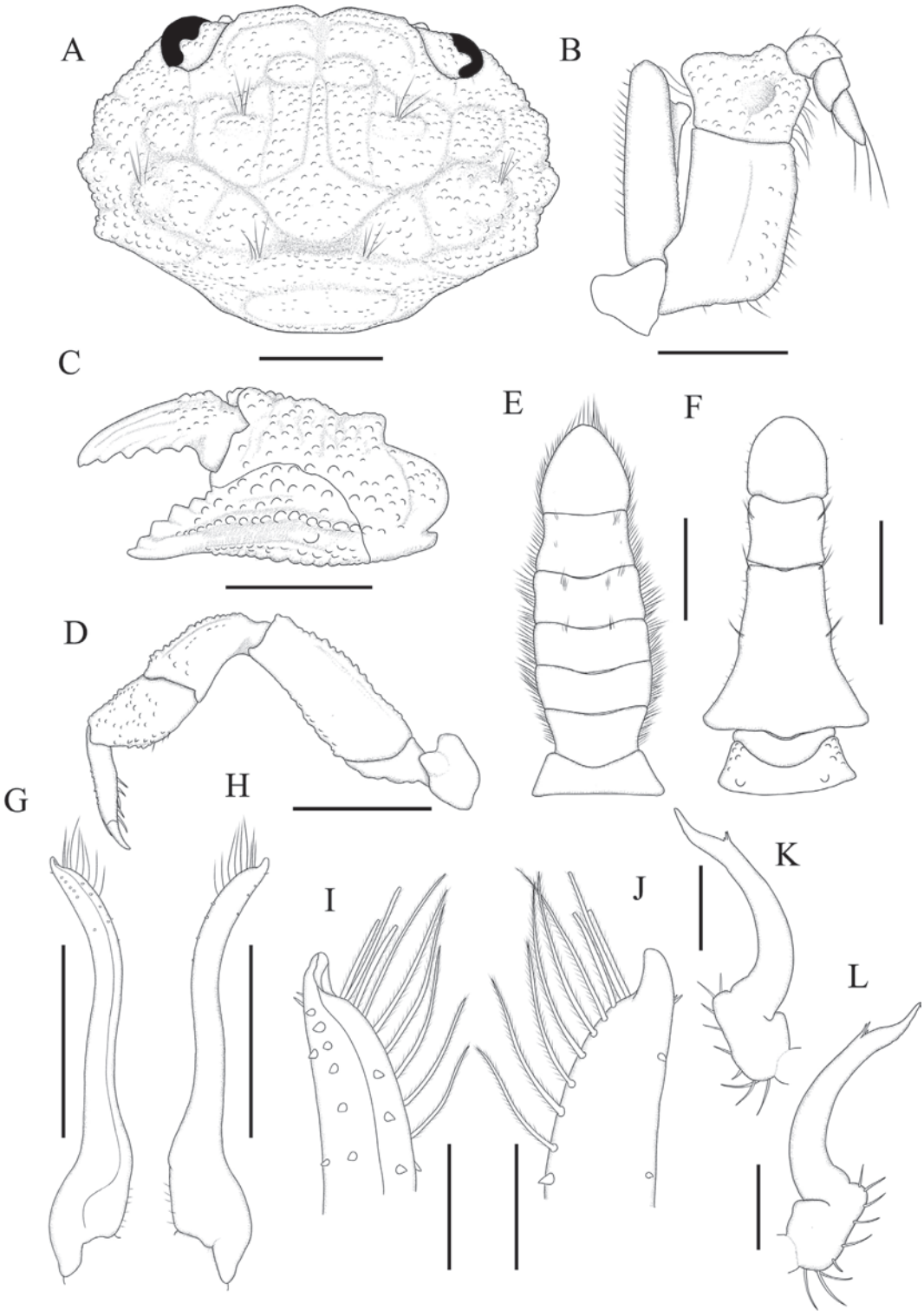

Figure 3. *Gothus teemo* sp. nov. **A–C, F, G–L.** Holotype, male, CW 3.7 mm, CL 2.6 mm, MBM287027; **D, E.** Paratype, female, CW 3.2 mm, CL 2.2 mm, MBM287026; **A.** Carapace; **B.** Maxilliped 3; **C.** Cheliped; **D.** Pereopod 5; **E.** Female pleon; **F.** Male pleon; **G.** right G1, ventral view; **H.** Same, dorsal view; **I.** Right G1, distal part, ventral view; **J.** Same, dorsal view; **K.** Right G2, ventral view; **L.** Same, dorsal view. Scale bar: 1 mm (**A, C, D**); 0.5 mm (**B, E, F, G, H**); 0.1 mm (**I–L**).

central part of epistome raised (Fig. 1B) (vs. central part of epistome not protruding in *Rizalthus*; cf. Mendoza and Ng 2008: fig. 1B); robust cheliped carpus, sometimes slightly expanded (Fig. 1A) (vs. strongly expanded and protruding in *Rizalthus*; Fig. 5A; cf. Mendoza and Ng 2008: fig. 1A); male pleon with a long, broad, truncated oval telson (Figs 2F, 3F) (vs. a smaller, triangular telson in *Rizalthus*; cf. Mendoza and Ng 2008: fig. 2C); G1 distal lobe curved inwards (Fig. 3G–J) (vs. nearly straight, not curved inwards in *Rizalthus*; cf. Mendoza and Ng

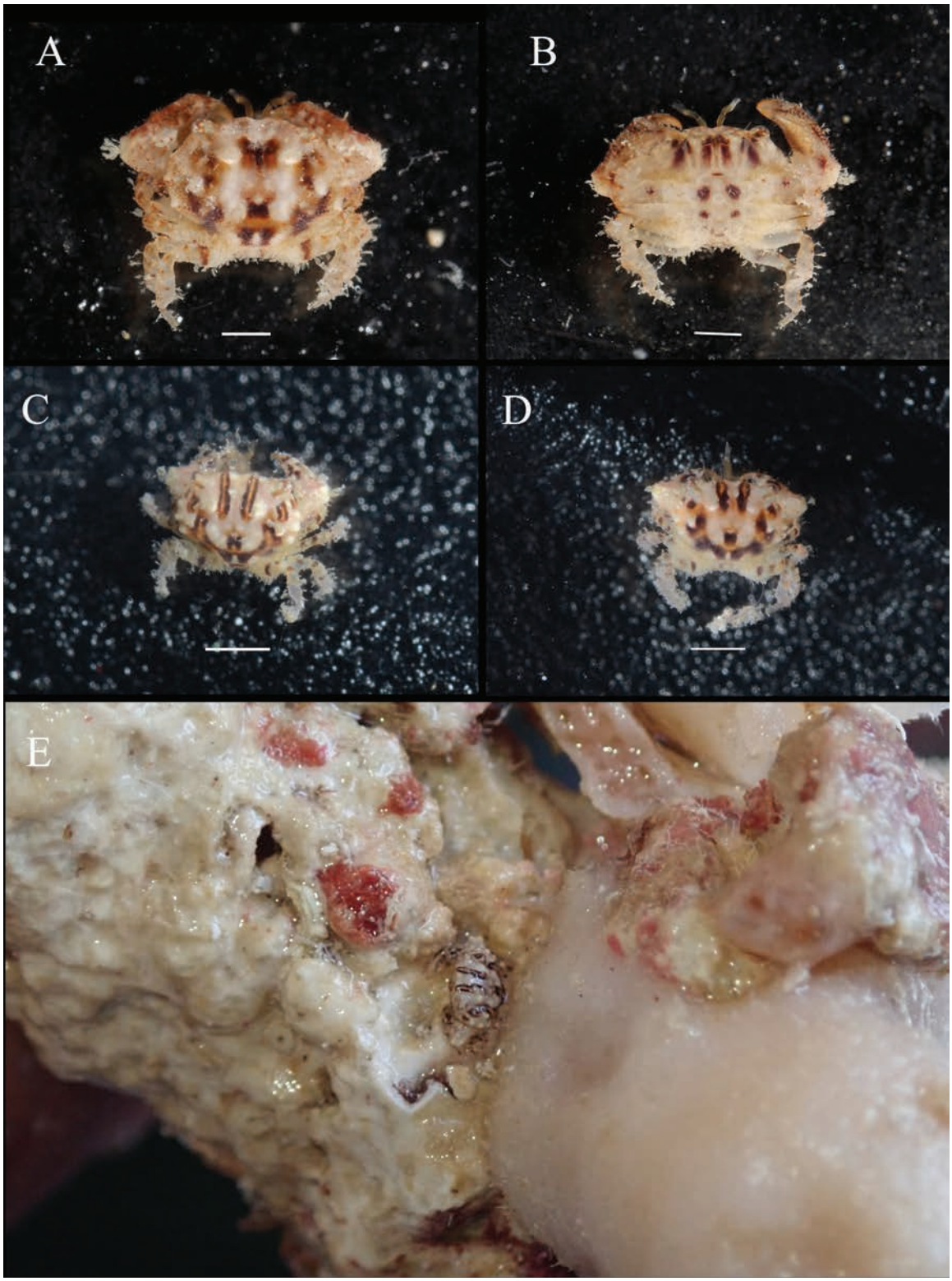

Figure 4. *Gothus teemo* sp. nov. **A, B.** Holotype, male, CW 3.7 mm, CL 2.6 mm, MBM287027; **C–E.** Paratypes, 2 juvenile, CW 1.8–2.2 mm, CL 1.3–1.5 mm, MBM287023; **A–D.** Live coloration; **E.** Habitat and substrate conditions. Scale bar: 1 mm.

2008: fig. 2F–H) and G2 with a longer, straighter distal lobe (Fig. 3K, L) (vs. shorter and curved in *Rizalthus*; cf. Mendoza and Ng 2008: fig. 2I).

Due to its similar carapace outline, particularly the less concave posterolateral margins, *Gothus* also resembles *Visayax* Mendoza & Ng, 2008. However, it can be easily differentiated by the following characteristics: *Gothus* lacks erosive depressions across body (Fig. 1A) (vs. chelipeds, ambulatory legs, carapace, and thoracic sternum with erosive depressions in *Visayax*; cf. Mendoza and Ng 2008: figs 3–6); carapace regions more flattened (Fig. 1A, C) (vs. carapace regions more pronounced in

Figure 5. *Gothus teemo* sp. nov., paratype, female, CW 3.2 mm, CL 2.2 mm, MBM287026, artistic illustration, displaying live coloration. Drawn by Fei Gao.

Visayax; cf. Mendoza and Ng 2008: figs 3A, C, 5A, C); posterior three teeth on anterolateral margin of carapace well-developed (Fig. 1A, C, 3A) (vs. absence of developed teeth on anterolateral margin in *Visayax*; cf. Mendoza and Ng 2008: figs 3A, 5A); male abdominal telson larger, truncated oval (Figs 2F, 3F) (vs. smaller, semi-circular in *Visayax*; cf. Mendoza and Ng 2008: figs 4E, 6D); G1 more slender (Fig. 3G–J) (vs. G1 more robust in *Visayax*; cf. Mendoza and Ng 2008: figs 4F, G, 6F, G).

The new genus exhibits a general morphological similarity to typical Euxanthinae members such as *Euxanthus* Dana, 1851, and *Hypocolpus* Rathbun, 1897. In addition to the existing comparative specimens, Guinot-Dumortier (1960) provided excellent descriptions and photographs of species from the above two genera. Subsequently published species also have relatively clear morphological descriptions and images available for comparison (cf. Guinot 1971b; Galil and Vannini 1990; Crosnier 1996). The new genus can be easily distinguished from *Euxanthus* by the following features: entire body covered with granules and short pubescence (Fig. 1A) (vs. relatively smooth in *Euxanthus*; Fig. 6C, D; cf. Guinot-Dumortier 1960: pl. VIII, figs 42, 44, 46, pl. IX, figs 48–52); carapace anterolateral margin with four teeth, first tooth flattened, sometimes completely reduced to appear as three teeth (Figs 1A, C, 3A) (vs. 4–6 teeth on anterolateral margin in *Euxanthus*; Fig. 6C, D; cf. Guinot-Dumortier 1960: pl. VIII, figs 42, 44, 46, pl. IX, figs 48–52); front not prominent, divided by a V-shaped notch (Figs 1C, 3A) (vs. more protruding, divided by a narrow fissure in *Euxanthus*; Fig. 6C, D; cf. Guinot-Dumortier 1960: pl. VIII, figs 42, 44, 46, pl. IX, figs 48–52); male abdominal telson large and truncated oval (Figs 2F, 3F) (vs. small and triangular in *Euxanthus*; cf. Guinot-Dumortier 1960: pl. VIII, fig. 47); G1 with a prominent, spoon-shaped distal lobe, and long setae on inner subdistal part (Fig. 3G–J) (vs. G1 with a short, non-protruding distal lobe, inwardly curved and encircling, with short setae on inner subdistal part in *Euxanthus*; cf. Guinot-Dumortier 1960: pl. VI, figs 36–39). Similarly, the new genus is easily distinguishable from *Hypocolpus* by the absence of a developed subhepatic cavity (Fig. 1B) (vs. a developed subhepatic cavity in *Hypocolpus*; cf. Guinot-Dumortier 1960: pl. II, figs 40–41); posterior three teeth on anterolateral margin well-developed (Figs 1C, 3A) (vs. underdeveloped teeth in *Hypocolpus*; Fig. 6B; cf. Guinot-Dumortier 1960: pl. VII, figs 40–41); front not prominent, divided by a V-shaped notch (Figs 1C, 3A) (vs. more protruding, divided by a narrow fissure in *Hypocolpus*; Fig. 6B; cf. Guinot-Dumortier 1960: pl. VII, figs 40–41); male abdominal telson large and truncated oval (Figs 2F, 3F) (vs. small and triangular in *Hypocolpus*; cf. Guinot-Dumortier 1960: pl. IX, fig. 53, pl. X, fig. 55); G1 with a prominent, spoon-shaped distal lobe (Fig. 3G–J) (vs. G1 with a short, non-protruding distal lobe, inwardly curved and encircling in *Hypocolpus*; cf. Guinot-Dumortier 1960: pl. VI, figs 32–35).

The new genus slightly resembles *Psaumis* Kossmann, 1877, and *Paractaeopsis* Serène, 1984, but can be readily distinguished. *Gothus* can be easily distinguished from *Psaumis* by lack of erosive depressions across body (Fig. 1A) (vs. chelipeds, ambulatory legs, carapace with strong erosive depressions in *Psaumis*; Fig. 6E; cf. Serène 1984: pl. XVIII, fig. E); front divided by a V-shaped notch (Figs 1C, 3A) (front divided by a narrow fissure in *Psaumis*; Fig. 6E; cf. Serène 1984: pl. XVIII, fig. E); anterolateral

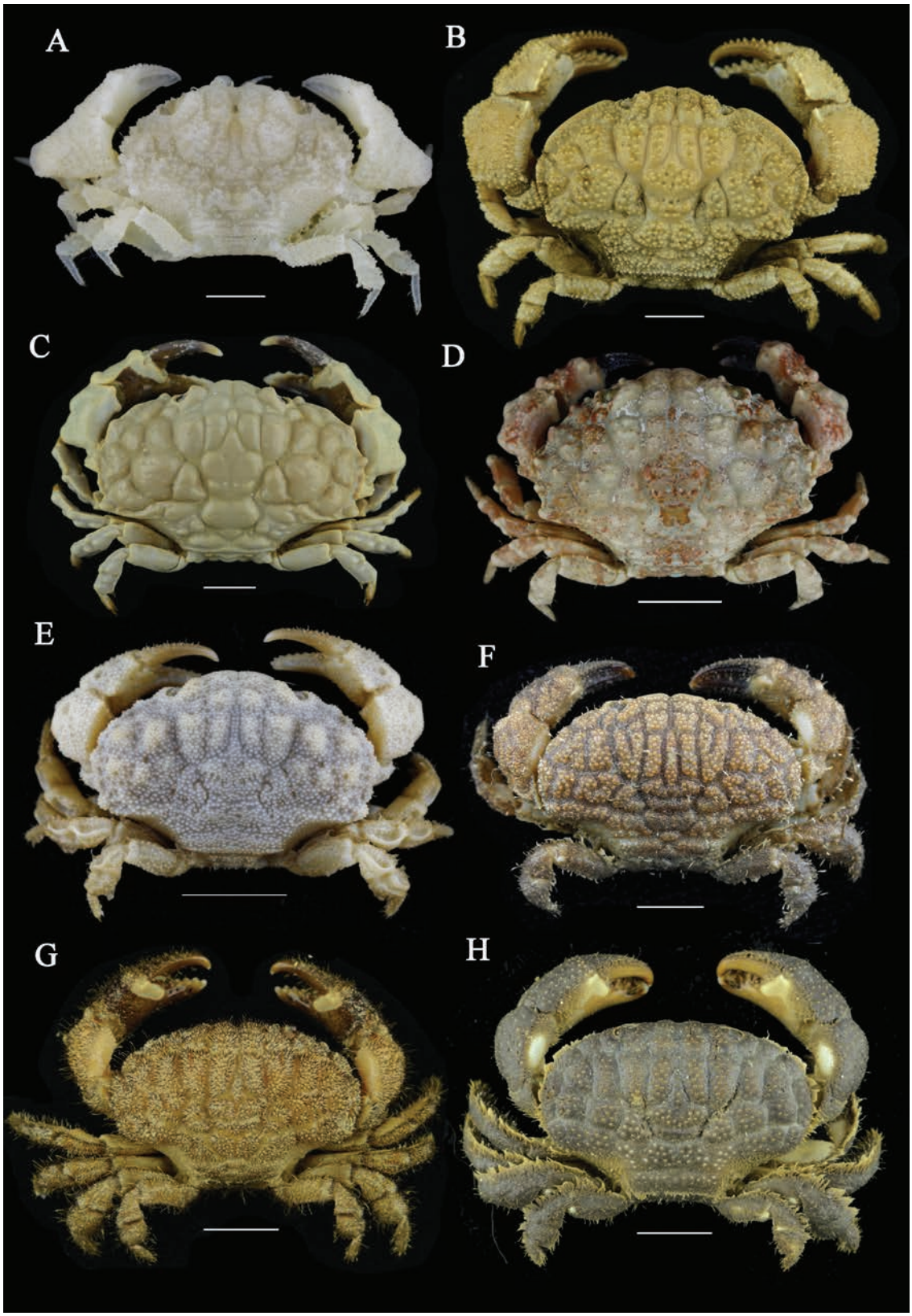

Figure 6. Euxanthinae and *Actaeodes* species in comparative material. **A.** *Rizalthus anconis* Mendoza & PKL Ng, 2008, female; CW 4.2 mm, CL 2.7 mm, NS-MJ-2022-1457; **B.** *Hypocolpus haanii* Rathbun, 1909, 1 male, CW 45.3 mm, CL 34.2 mm, MBM286755; **C.** *Euxanthus exsculptus* (Herbst, 1790), 1 male, CW 52.6, CL 33.2 mm, MBM163793; **D.** *Euxanthus huonii* (Hombron & Jacquinot, 1846), CW 34.0 mm, CL 24.0 mm, NS-MJ-2022-1734; **E.** *Psaumis cavipes* (Dana, 1852), 1 male, CW 13.8 mm, CL 8.6 mm, aop01; **F.** *Actaeodes mutatus* Guinot, 1976, 1 female, CW 20.8 mm, CL 12.5 mm, BF02; **G.** *Actaeodes hirsutissimus* (Rüppell, 1830), 1 male, CW 31.9 mm, CL 21.0 mm, MBM164298; **H.** *Actaeodes tomentosus* (H. Milne Edwards, 1834), 1 male, CW 35.8 mm, CL 22.5 mm, Xan041. Scale bar: 1 mm (**A**); 5 mm (**E, F**); 10 mm (**B–D, G, F**).

margin with four teeth, first tooth flattened, sometimes completely reduced to appear as three teeth (Figs 1A, C, 3A) (anterolateral margin with very flat teeth, except for fourth tooth at junction of anterior and posterior lateral margins, which is more prominent in *Psaumis*; Fig. 6E; cf. Serène 1984: pl. XVIII, fig. E). It can be distinguished from *Paractaeopsis* by anterolateral margin with four teeth, first tooth flattened, sometimes completely reduced to appear as three teeth (Figs 1A, C, 3A) (anterolateral margin with four well development teeth in *Paractaeopsis*; cf. Takeda and Miyake 1968: fig. 1a); carapace broad, approximately 1.5 times as wide as long, with a relatively flat dorsal surface (Figs 1A, C, 3A) (carapace narrower, with a width not exceeding 1.4 times the length, and dorsal surface convex both anteroposteriorly and laterally in *Paractaeopsis*; cf. Serène 1984: pl. XVII, fig. E); carapace 2M region divided into two lobes (Figs 1A, C, 3A) (carapace 2M region divided into four lobes in *Paractaeopsis*; cf. Takeda and Miyake 1968: fig. 1a); ambulatory legs comparatively slender (Figs 1A, 3D) (ambulatory legs very short and stout in *Paractaeopsis*; cf. Takeda and Miyake 1968: fig. 1c).

Given the above comparisons, the current species cannot be placed within any known genera, necessitating the establishment of a new genus. The main morphological characteristics comparing *Gothus* gen. nov. with closely related genera are listed in Table 2.

Gothus teemo sp. nov.

https://zoobank.org/9A4FA138-D3F0-4FC0-8687-844B52C5BA15

Figs 1–5

Type material. ***Holotype.*** China • 1 male; CW 3.7 mm, CL 2.6 mm; Triton Island, Xisha Islands; 15°46'52.61"N, 111°12'28.62"E; 5 m; 10 May. 2024; Ziming Yuan coll.; 2404189149; MBM287027.

Paratypes. China • 1 female; CW 3.2 mm, CL 2.2 mm; Meiji Reef, Nansha Islands; 9°52'57.47"N, 115°33'48.59"E; 27 Apr. 2023; Aiyang Wang, Bingqin Liu coll.; 2304278379; MBM287026 • 1 male (decalcified); CW 3.2 mm, CL 2.4 mm; Meiji Reef, Nansha Islands; 9°53'1.15"N, 115°33'37.42"E; 27 Apr. 2023; Aiyang Wang, Bingqin Liu coll.; 2304278461; MBM287024 • 1 male (partially crushed); CW 4 mm, CL 2.7 mm; Meiji Reef, Nansha Islands; 9°53'1.15"N, 115°33'37.42"E; 27 Apr. 2023; Aiyang Wang, Bingqin Liu coll.; 2304278486; MBM287025 • 2 juveniles; CW 1.8–2.2 mm, CL 1.3–1.5 mm; Meiji Reef, Nansha Islands; 9°54'25.75"N, 115°29'49.44"E; 3 m; 6 May 2022; Ziming Yuan, Yuli Sun, Shaobo Ma coll.; NS-MJ-2022-1287; MBM287023 • 1 juvenile; CW 2 mm, CL 1.3 mm; Meiji Reef, Nansha Islands; 9°53'30.84"N, 115°34'22.05"E; 5 m; 11 Apr. 2024; Ziming Yuan coll.; 2404188048; MBM287022.

Table 2. Comparison of the characters of *Gothus* gen. nov. and six related genera included in the subfamily Euxanthinae.

Character	*Gothus* gen. nov.	*Rizalthus*	*Visayax*	*Euxanthus*	*Hypocolpus*	*Psaumis*	*Paractaeopsis*
carapace dorsal surface	with round granules, with clustered long setae or scattered short setae	with large granules, surrounded by short setae basally	with distinct or faint reticulate pattern of fused granules	relatively smooth, without well-developed granules.	with granules and setae	densely covered with granules	with pearly granules, scattered long tubular setae
carapace anterolateral margin	with four anterolateral teeth, first tooth flattened, posterior three teeth well-developed	without clearly defined anterolateral teeth	absence of developed anterolateral teeth	with four to six anterolateral teeth	anterolateral teeth underdeveloped	with very flat anterolateral teeth, only fourth tooth prominent	with four developed anterolateral teeth
carapace posterolateral margin	non-concave	concave	concave	concave	concave	concave	non-concave
front	not protruding, divided by a V-shaped notch	not protruding, divided by a V-shaped notch	not protruding, divided by a V-shaped notch	protruding, divided by a narrow fissure	protruding, divided by a narrow fissure	not protruding, divided by a narrow fissure	protruding, divided by a V-shaped notch
epistome	central part protruding	central part not protruding	central part not protruding or slightly protruding	central part protruding	central part protruding	central part protruding	unknown
subhepatic cavity	absent	absent	absent	absent	present	absent	absent
etched depressions	absent	present on thoracic sternum	present on chelipeds, ambulatory legs, carapace, and thoracic sternum	absent	present on thoracic sternum	present on chelipeds, ambulatory legs and carapace	absent
male telson	broad, truncated oval	smaller, triangular	smaller, semi-circular	smaller, triangular	smaller, triangular	smaller, semi-circular	unknown
cheliped carpus	robust, sometimes slightly expanded	strongly expanded and protruding	robust	robust	robust	slightly robust	robust
ambulatory leg	comparatively slender	comparatively slender	comparatively slender	comparatively slender	comparatively slender	comparatively slender	very short and stout
male first gonopod	slender, distal lobe prominent, spoon-shaped, curved inwards, with long setae on inner subdistal part	slender, distal lobe prominent, spoon-shaped, nearly straight, with long setae on inner subdistal part	robust, distal lobe prominent, nearly straight, with long setae on inner subdistal part	slender, distal lobe non-protruding, inwardly curved and encircling, with short setae on inner subdistal part	slender, distal lobe non-protruding, inwardly curved and encircling, with long setae on inner subdistal part	slender, distal lobe prominent, spoon-shaped, nearly straight, with long setae on inner subdistal part	robust, distal lobe prominent, nearly straight, with long setae on inner subdistal part

Description. Carapace (Figs 1, 3A) broader than long, CW about 1.5 times the CL, dorsal surface bearing round granules, regions well defined, 1M separated from 2M by shallow transverse groove; 2M indistinct divided, lateral lobe with elevated pointed tuberosity; 3M distinct, undivided; 4M indistinct; 1L, 3L, 4L indistinct; 2L, 5l, 6L distinct, with elevated sharp tuberosity each on 2L, 5L; 1P distinct, 2P indistinct, flat; 2M, 5L, and 6L regions each with a tuft of setae; front wide, about 0.4 times CW, not protruding, divided into two slightly triangular lobes by a V-shaped notch, a small pore visible from front introduced from median notch (Fig. 1B), frontal lobes and dorsal inner orbital angle separated by shallow depression; eyestalks densely granulated; area behind outer orbital angle slightly concave, not forming a subhepatic cavity; anterolateral margin starting from subhepatic region; first tooth nearly completely reduced; subsequent three teeth developed; second and third teeth nearly equal; fourth tooth smaller; carapace widest at second tooth; posterolateral margin almost straight; subhepatic region densely granulated; posterior margin nearly straight.

Epistome (Fig. 1B, E) central region with short median projection on posterior margin pronounced; lateral regions with undulating posterior margins; maxilliped 3 (Figs 1B, E, 3B) granulated; ischium subrectangular; presenting submedian groove; merus subquadrate; anterior margin indented; external anteroexternal angle expanded. Antennule (Fig. 1B, E) folding transversely; basal segment of antenna subrectangular; contacting ventral external frontal margin and ventral internal orbital angle; antennal flagellum filling orbital hiatus.

Chelipeds (Figs 2A, B, 3C) symmetrical; meri short; carpi robust, with square-shaped outward expansion, surface granulated, aggregated into nodules; palms dorsally with three protuberances, outer and dorsal surfaces densely granulated; fingers elongated, with triangular teeth, tips sharp, crossing at extremities when closed; dorsal surface of movable finger with three granular ridges; outer surface of immovable finger with two granular ridges.

Ambulatory legs (Figs 1A, D, 3D) meri flattened, P5 merus length about 3.6 times width of distal end, granulated dorsally and along anterior and posterior edges; carpi granulated dorsally and along anterior edge, dorsal surface with a grooved indentation near anterior edge; propodi granulated dorsally and along edges; dactyli elongated, margins armed with granules and setae, terminal end chitinous, sharp, slightly curved backward, dactylo-propodal lock very weak and inconspicuous.

Male thoracic sternum (Fig. 2C) with sternites 1 and 2 completely fused, suture between sternites 2 and 3 straight, complete, sternites 3 and 4 mostly fused, suture between them visible only at margins, sternites 3 short, sternite 4 with central longitudinal groove, tubercle of sterno-pleonal lock (press-button mechanism) located on posterior of sternite 5. Male pleon (Figs 2C, E, 3F) narrow; pleonites 3 to 5 completely fused, lateral margins of pleonite 6 slightly concave, telson long and broad, width slightly greater than length, truncated oval, basal margin wider than terminal margin of pleonite 6; paired tufts of setae present on margins of middle part and terminal margin of pleonites 3–5 and terminal margin of pleonite 6. Female pleon (Figs 2D, F, 3E) oval-shaped, margins of pleonite 6 slightly concave; telson triangular; vulva longitudinally ovate, located at upper of sternite 6, occupying anteromedial half, near sternites 5/6 (Fig. 2G).

G1 (Fig. 3G, H, I, J) slender, distal lobe prominent but not excessively elongated, long setae on inner subdistal side, small spines on outer side. G2 (Fig. 3K, L) short, distal lobe elongated, slightly curved upwards.

Live coloration. Overall white to coral pink in coloration, carapace adorned with symmetrical black to brown stripes, ambulatory legs and chelipeds bearing stripes of similar coloration, anterior part of chelipeds carpus red (Figs 4, 5). Fingers brownish-black, the coloration of immovable finger extending onto the palm along both the inner and outer surfaces in male (Fig. 2A, B).

Etymology. The new species is named after Teemo, a character from the MOBA (Multiplayer Online Battle Arena) video game League of Legends. This character, modeled after a raccoon, has a fluffy, diminutive stature with a brown and white intermingled fur coat. This alludes to the new species' small size, densely covered short setae, and brown-striped coloration.

Distribution. Currently known from the type locality at Triton Island, Xisha Islands (Paracel Islands), and Meiji Reef (Mischief Reef), Nansha Islands (Spratly Islands), it inhabits crevices in shallow coral reefs.

Remarks. Apart from the members of the subfamily Euxanthinae already compared in the remarks of *Gothus* gen. nov., the species is most similar to *Actaeodes consobrinus* (A. Milne-Edwards, 1873). They share similarities in the carapace outline, the shape of the male pleon, and even in the pattern of the live coloration. However, *G. teemo* sp. nov. can be differentiated from *A. consobrinus* by the following features: the first tooth on the anterolateral margin of the carapace is completely reduced, almost invisible (Figs 1A, C, 3A) (vs. the first tooth low but still visible in *A. consobrinus*; Figs 7A, B, 8A, 9A, B); carapace regions more pronounced, with tufts of setae (Figs 1C, 3A) (vs. carapace regions flatter, without tufts of setae in *A. consobrinus*; Figs 7A, B, 8A, 9A, B); cheliped carpus with square-shaped outward expansion (Fig. 1A) (vs. cheliped carpus nearly spherical in *A. consobrinus*; Figs 7A, 8A, B); male pleon relatively broader, telson width slightly greater than length (Figs 2F, 3F) (vs. pleon very narrow, telson longer than wide in *A. consobrinus*; Figs 7D, 8E); G1 distal lobe shorter (Fig. 3G–J) (vs. G1 distal lobe significantly elongated in *A. consobrinus*; Fig. 8F–G).

Gothus consobrinus (A. Milne-Edwards, 1873), comb. nov.

Figs 7–10

Actaea consobrina A. Milne-Edwards, 1873: 255; de Man, 1896: 503; Odhner, 1925: 67, pl. 4, fig. 14; Ward, 1933: 246; Sakai, 1939: 491, pl. 94, fig. 2; Tweedie, 1950: 118; Serène & Lang, 1959: 291, fig. 2, A1-A3; Guinot, 1967a: 260

Actaea suffuscula Rathbun, 1911: 220, pl. 17, figs 10–11; Ward, 1934: 18; Estampador, 1959: 81.

Actaeodes consobrinus Guinot, 1967b: 561; Guinot, 1976: 246, pl. 15, fig. 5; Sakai, 1976: 448, pl. 158, fig. 3; Takeda & Miyake, 1976: 108; Serène, 1984: 133(key), 134(key), 135, pl. 18 C; Galil & Vannini, 1990: 37.

Actaeodes consobrina Guinot, 1971a: 1072.

Non *Actaea consobrina* Nobili, 1907: 390.

= *Pseudoliomera ruppellioides* (Odhner, 1925).

Material examined. China • 1 male; CW 3.0 mm, CL 1.9 mm; Yongshu Reef, Nansha Islands; 9°39'51.97"N, 113°0'52.98"E; 10 m; 6 May 2022; Ziming Yuan, Yuli Sun, Shaobo Ma coll.; NS-YS-2022-1226 • 1 male; CW 7.6 mm, CL 5.2 mm; same collection data as for preceding; 14 May 2022; NS-YS-2022-1227 • 2 juveniles; CW 2.1–2.2 mm, CL 1.5–1.6 mm; same collection data as for preceding; NS-YS-2022-1263 • 1 male; CW 6.7 mm, CL 4.4 mm; same collection data as for preceding; NS-YS-2022-1336 • 1 juvenile; CW 2.5 mm, CL 1.7 mm; Meiji Reef, Nansha Islands; 9°52'38.19"N, 115°31'17.08"E; 8 m; 7 May 2022; NS-MJ-2022-1438 • 1 juvenile; CW 2.2 mm, CL 1.5 mm; same collection data as for preceding but at 9°53'30.84"N, 115°34'22.05"E; 10 m; 10 May 2022; NS-MJ-2022-1789 • 1 female; CW 4.5 mm, CL 2.9 mm; Qilianyu, Xisha Islands; 16°58'04.2"N, 112°16'11.0"E; 10 m; 19 May 2022; XS-QL-2022-1014 • 1 juvenile; CW 2.9 mm, CL 2.0 mm; Bei Reef, Xisha Islands; 17°07'00.5"N 111°32'03.2"E; 8 May 2023; Aiyang Wang, Bingqin Liu coll.; 2305089358 • 1 male; not measured; Zhongsha Islands; 18–23 m; dead coral; 5 Jun. 2021; Geng Qin coll.; C13-5 • 1 male; not measured; same collection data as for preceding, 9 Jun. 2021; C57-3 • 1 male; CW 5.4 mm, CL 3.6 mm; Zhongsha Islands; 15°53'10.5"N, 114°47'29.76"E, 20 m; 26 Jun. 2020; Wei Jiang, Geng Qin coll.; ZS233C07.

Comparative material. ***Actaeodes mutatus*** **Guinot, 1976** (Fig. 6F). China • 1 male; Lingao, Hainan Island; 25 Nov. 2007; Xan074 • 1 female; Hainan Island; 2022; Xu Zhang coll.; BF01 • 1 female; Phoenix Island, Sanya, Hainan Island; 2021; Xu Zhang coll.; BF02. CW 14.8–20.8 mm, CL 8.6–12.5 mm.

Actaeodes hirsutissimus **(Rüppell, 1830)** (Fig. 6G). China • 3 males; Zhao Shu Island, Xisha Islands; 15 Apr. 1976; MBM164262 • 1 female; north of Dong Island, Xisha Islands; 9 Jun. 1975; MBM164166 • 2 males, 3 ovigerous females; Dong Island, Xisha Islands; 9 Jun. 1975; MBM164155 • 1 male, 1 female, 3 juveniles; Northeast of Dong Island, Xisha Islands; 10 Jun. 1975; MBM164148 • 4 males, 2 females; Rocky Island, Xisha Islands; 2–4 Jun. 1981; MBM164151 • 1 female; Dong Island, Xisha Islands; 28–30 May 1980; MBM164140 • 2 juveniles; Jinqing Island, Xisha Islands; 10 Jul. 2019; MF01 • 2 males; E Xuan Port, Danzhou, Hainan Island; 7 Nov. 2021; Xan179 • 1 male; Yuzhuo Reef, Xisha Islands; 9 Jul. 2019; MF02 • 9 males, 9 females; Rocky Island, Xisha Islands; 9 May 1975; Xianqiu Ren coll.; MBM164298 • 8 males, 5 females, 2 juveniles; Coral Island, Xisha Islands; 19–23 May 1980; MBM164189 • 2 males, 4 females, 1 juvenile; Jinqing Island, Xisha Islands; 9 May 1980; MBM164190 • 1 female; Xian'e Reef, Nansha Islands; 12 May 1989; MBM164196 • 2 males, 2 females; Jinyin Island, Xisha Islands; 14 May 1980; MBM164185 • 2 ovigerous females; Northeast of Dong Island, Xisha Islands; 10 Jun. 1975; MBM164261 • 5 males, 4 females; Jinqing Island, Xisha Islands; 19 May 1981; MBM164225. CW 7.7–34.2 mm, CL 5.2–22 mm.

Actaeodes tomentosus **(H. Milne Edwards, 1834)** (Fig. 6H). China • 1 male; Wenchang, Hainan Island; 24 Jul. 2021; RF01 • 1 male; Xincun, Hainan Island; 29 Mar. 2008; Ping Lan, Yongqiang Wang coll.; MBM282509 • 3 males; Xiaodonghai, Hainan Island; 23 Mar. 2008; MBM282414 • 4 males, 4 females; same collection data as for preceding; 25 Dec. 2007; MBM283216 • 9 males, 6 females; same collection data as for preceding; 24 Dec. 2007; Xan045, MBM283218 • 2 males, 1 female; same collection data as for preceding; 23 Mar. 2008; Wei Jiang coll.; Xan041 • 1 female; Langhua Reef, Xisha Islands; 11 May 2015; Xan126 • 1 male; Houhai, Sanya, Hainan Island; 22 Mar. 2018; Xan048 • 1 female; Dadonghai, Hainan Island; 2021; Xu Zhang coll.; RF03 • 1 male; Sanya, Hainan Island; 2022; Xu Zhang coll.; RF04 • 1 female; Sanya, Hainan Island; 20 Aug. 2019; Yunhao Pan coll.; RF05 • 1 male; Yuzhuo Reef, Xisha Islands; 9 Jul. 2019; RF06 • 1 male; Lingyang Reef, Xisha Islands; 11 Jul. 2019; RF07 • 1 male; Yongxing Island, Xisha Islands; 27 Mar. 1980; MBM164194 • 1 female; Sanya Bay, Hainan Island; 22 Nov. 1990; MBM164492. CW 11.2–37.4 mm, CL 7.4–24.9 mm.

Description. Carapace (Figs 7A, B, 8B, 9A, D, G) broader than long, CW about 1.5 times the CL, dorsal surface bearing round granules, granules interspersed with short pubescence; regions well defined, grooves wide and deep, 1M separated from 2M; 2M completely divided; 3M distinct, divided into three lobes; 4M distinct; 1L, 4L indistinct; 2L, 3L, 5l, 6L distinct, 5L, 6L partially divided; 1P, 2P distinct; front broad, about 0.3 times CW, not protruding, divided into two slightly triangular lobes by a wide and deep V-shaped notch, frontal lobes and dorsal inner orbital angle separated by shallow depression; eyestalks densely granulated; Anterolateral margin divided into four teeth by narrow but sometimes opened fissures; first tooth extremely flattened, second tooth broader, sometimes obtuse, third tooth prominent, fourth tooth slightly smaller than third; carapace widest at third tooth; posterolateral margin almost straight; subhepatic region densely granulated; Posterior margin nearly straight.

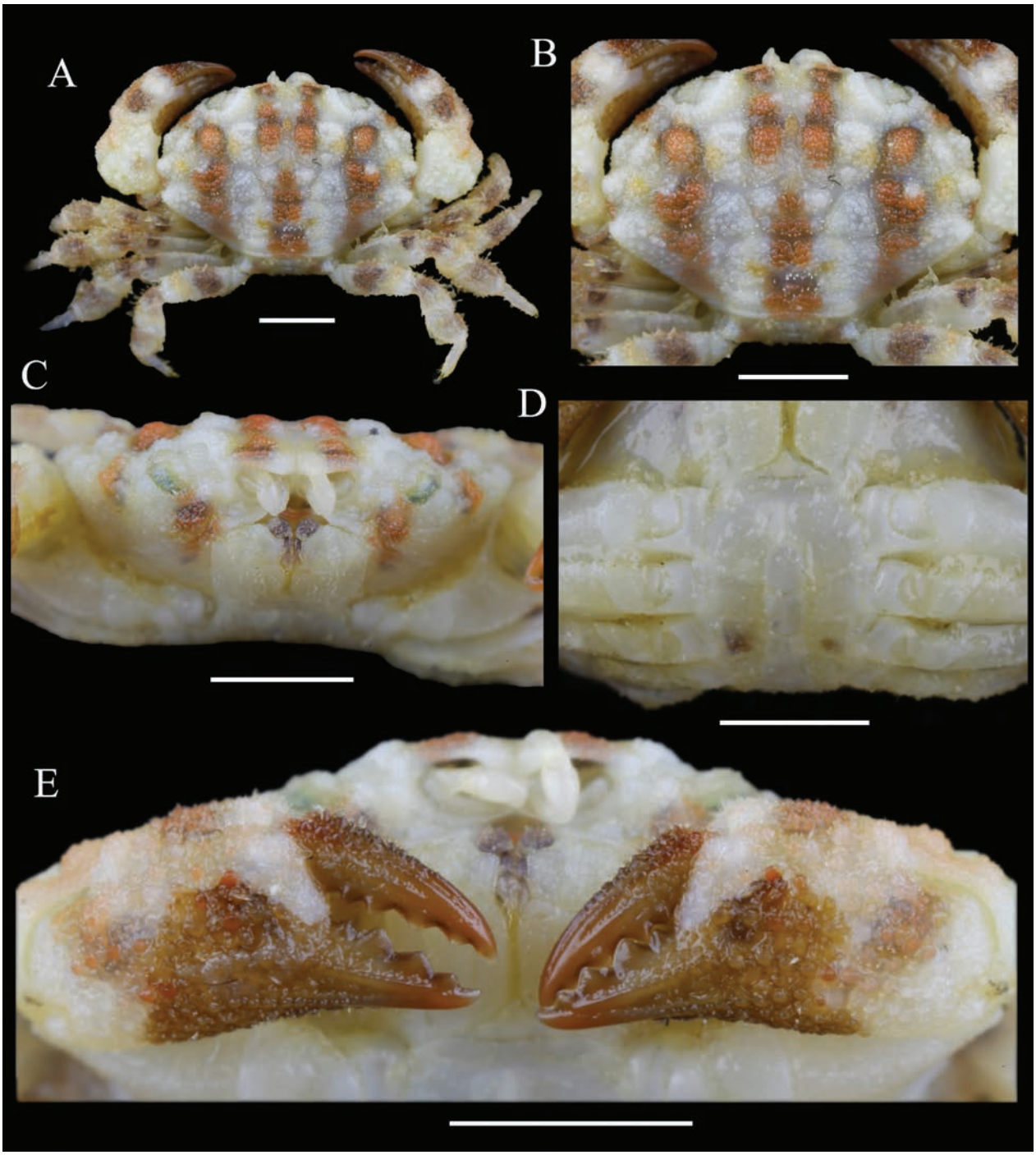

Figure 7. *Gothus consobrinus* (A. Milne-Edwards, 1873), male, CW 6.7 mm, CL 4.4 mm, NS-YS-2022-1336. **A.** Dorsal habitus; **B.** Carapace; **C.** Frontal view; **D.** Thoracic sternites and pleon; **E.** Chelipeds. Scale bar: 2 mm.

Epistome (Figs 7C, 9B, E, H) Central region with median projection on posterior margin; lateral regions with undulating posterior margins. Maxilliped 3 (Figs 7C, 8B) granulated, ischium subrectangular, presenting submedian groove; merus subquadrate; anterior margin indented; anteroexternal angle square-shaped expanded. Antennule (Fig. 7C, 9B, E, H) folding transversely; basal segment of antenna subrectangular; contacting ventral external frontal margin and ventral internal orbital angle; antennal flagellum filling orbital hiatus.

Chelipeds (Figs 7E, 8C) symmetrical, meri short; carpi robust, nearly spherical, surface granulated, aggregated into nodules; outer and dorsal surfaces of palms densely granulated; fingers elongated, with triangular teeth, tips sharp, crossing at extremities when closed; dorsal surface of movable finger with three granular ridges; outer surface of immovable finger with two ridges. Fingers brownish-black, coloration of immovable finger extending onto palm along both inner and outer surfaces in male.

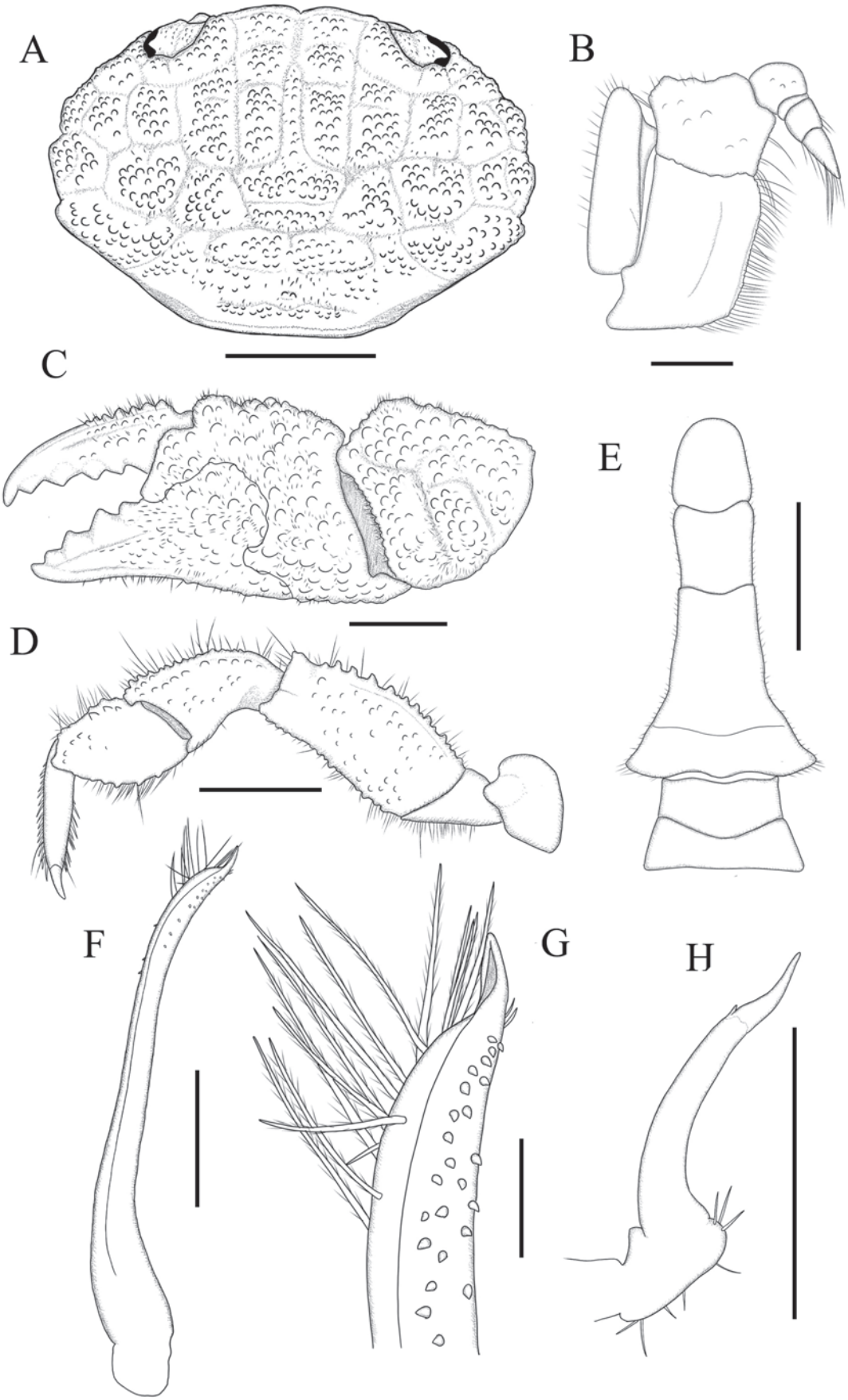

Figure 8. *Gothus consobrinus* (A. Milne-Edwards, 1873), male, CW 6.7 mm, CL 4.4 mm, NS-YS-2022-1336. **A.** Carapace; **B.** Maxilliped 3; **C.** Cheliped; **D.** Pereopod 5; **E.** Pleon; **F.** Left G1, ventral view; **G.** Left G1; **H.** Left G2, ventral view. Scale bar: 2 mm (**A**); 0.5 mm (**B, F, H**); 1 mm (**C, D, E**); 0.1 mm (**G**).

Ambulatory legs (Figs 7A, 8D) with meri flattened, P5 merus length about 3 times as wide as distal end, granulated dorsally and along anterior and posterior edges; carpi granulated dorsally and along anterior edge; dorsal surface with a grooved indentation near anterior edge; propodi granulated dorsally and along edges; dactyli elongated, margins armed with granules and setae, terminal end chitinous, sharp, slightly recurved, dactylo-propodal lock present.

Male thoracic sternum (Fig. 7D) with sternites 1 and 2 completely fused, suture between sternites 2 and 3 straight, complete, sternites 3 and 4 mostly fused, suture between them visible only at margins, sternites 3 short, sternite 4 with central longitudinal groove, tubercle of sterno-pleonal lock (press-button mechanism) located on posterior of sternite 5. Male pleon (Figs 7D, 8E) very narrow; pleonites 3 to 5 completely fused; lateral margins of pleonite 6 slightly concave; telson long, broad, longer than wide; truncated oval; basal margin wider than terminal margin of pleonite 6.

G1 (Fig. 8F–G) slender, distal lobe prominent, elongated, curved upwards, long setae on inner subdistal side, small spines on outer side. G2 (Fig. 8H) short, distal lobe elongated, slightly curved upwards.

Live coloration. Overall white to ivory-colored, carapace adorned with symmetrical black to brown stripes and orange spots, ambulatory legs and chelipeds bearing black to brown stripes, cheliped palm dorsal surface and anterior part of carpus sometimes coral pink (Fig. 10). Fingers brownish-black, coloration of immovable finger extending onto inner and outer surfaces of palm in male (Fig. 7E).

Distribution. Distributed in the Zhongsha (=Macclesfield Bank), Xisha (=Paracel Islands), and Nansha Islands (=Spratly Islands) of the China Sea; widely found in the Indo-West Pacific, with the type locality at Upolu Island, inhabiting crevices in shallow coral reefs.

Remarks. This report constitutes the first record of this species in the Chinese sea. Alphonse Milne-Edwards (1873: 255 [79]) briefly described "*Actaea consobrina*" from Upolu in present-day Samoa and provided the carapace measurements of one specimen (CW 10 mm, CL 7 mm), though they did not indicate the sex of the specimen nor how many other specimens they examined. This species remained in the genus *Actaea* until Guinot (1967b) transferred it to *Actaeodes*. As part of her revision of some Actaeinae genera, including *Actaeodes*, Guinot (1976: 246) examined two female specimens collected by A. Milne-Edwards and deposited in the MNHN (MP-B3885S from Upolu and a specimen without a collection number from "Samoa?"). She pointed out that based on the measurements (CW 10 mm, CL 7 mm), this specimen MP-B3885S could be the holotype of *Actaeodes consobrinus*. For the purposes of this study, we consider this specimen to be typical of *A. consobrinus* and use it for our comparisons (Fig. 9A–C). It exhibits a nearly truncated second anterolateral tooth with open fissures between the anterolateral teeth, which is also observed in some of the current specimens (Fig. 9G–I). Compared to the specimens from the China Sea, it has deeper grooves on the carapace, which may be attributed to growth-related differences considering its larger size. The other female individual (MNHN-IU-2024-3483) found together with this specimen is likely the one collected by A. Milne-Edwards that lacks a collection number (Guinot, 1976: 246; CW 8.5 mm, CL 6 mm), based on its measurements (CW 8.8 mm, CL 5.7 mm; Fig. 9D–F). This specimen possesses triangular anterior lateral teeth and shallower grooves on the carapace (Fig. 9D–F).

There are some issues regarding the classification of this species within its genus: Alphonse Milne-Edwards (1873) put the species in *Actaea* De Haan, 1833, and initially compared it with *Actaea hirsutissimus* (Rüppell, 1830) (presently known as *Actaeodes*) and *Actaea kraussi* (Heller, 1860) (presently known as *Banareia*) and primarily considered it similar to the former. Sakai (1939) considered the species to be close to *Paractaea tumulosa* (Odhner, 1925). Guinot (1967b, 1976) opposed the similarity to *P. tumulosa* but acknowledged its relationship with *Actaeodes*, and upon reviewing *Actaeodes*, *Actaea consobrina* was classified into the genus *Actaeodes* Dana, 1851, and supplemented its morphological characteristics.

In Guinot's review (1976), the definition of *Actaeodes* includes the following characteristics: 1) carapace wide to very wide; 2) long anterolateral margins curving back over branchial regions, divided into lobes by fissures that extend as grooves into the subhepatic region; 3) very short posterolateral margins with a strong concavity that coapted against the last three pairs of ambulatory legs; 4) developed areolation of the dorsal surface with granular and pilosity lobules; 5). The frontal edge slopes downward with a central notch leading to the anterior tip of the epistome; the frontal lobes barely form a canopy above the antennules; 6) orbits round and relatively small, with specific fissures on supraorbital and exorbital edges; no infraorbital fissure 7) Equal and short chelipeds, with fingers either ending in a spoon-shaped tip or crossing at tips; 8) antenna fitting between front and orbit or with a closed orbit in *Actaeodes semoni* (Ortmann, 1894); 9) small and slightly depressed epistome, with the anterior tip projecting forward to join the anterior median groove of the dorsal face; 10) short ambulatory legs; 11) sub-hepatic region grooved; 12) thoracic sternite 4 traversed by two transverse grooves and two oblique grooves, and with a very clear longitudinal groove, hidden by telson; a median line present at levels of sternites 6, 7, and 8; 13) male pleon with fused pleonites 3–5, elongated and projecting forward, featuring a median longitudinal swelling from 3 to 6 pleonites; 14) G1 with a tapered distal lobe adorned with relatively short bristles.

Actaeodes currently comprises six species, among which the type species *A. tomentosus*, *A. semoni* (Ortmann, 1894), *A. hirsutissimus* (Rüppell, 1830), and

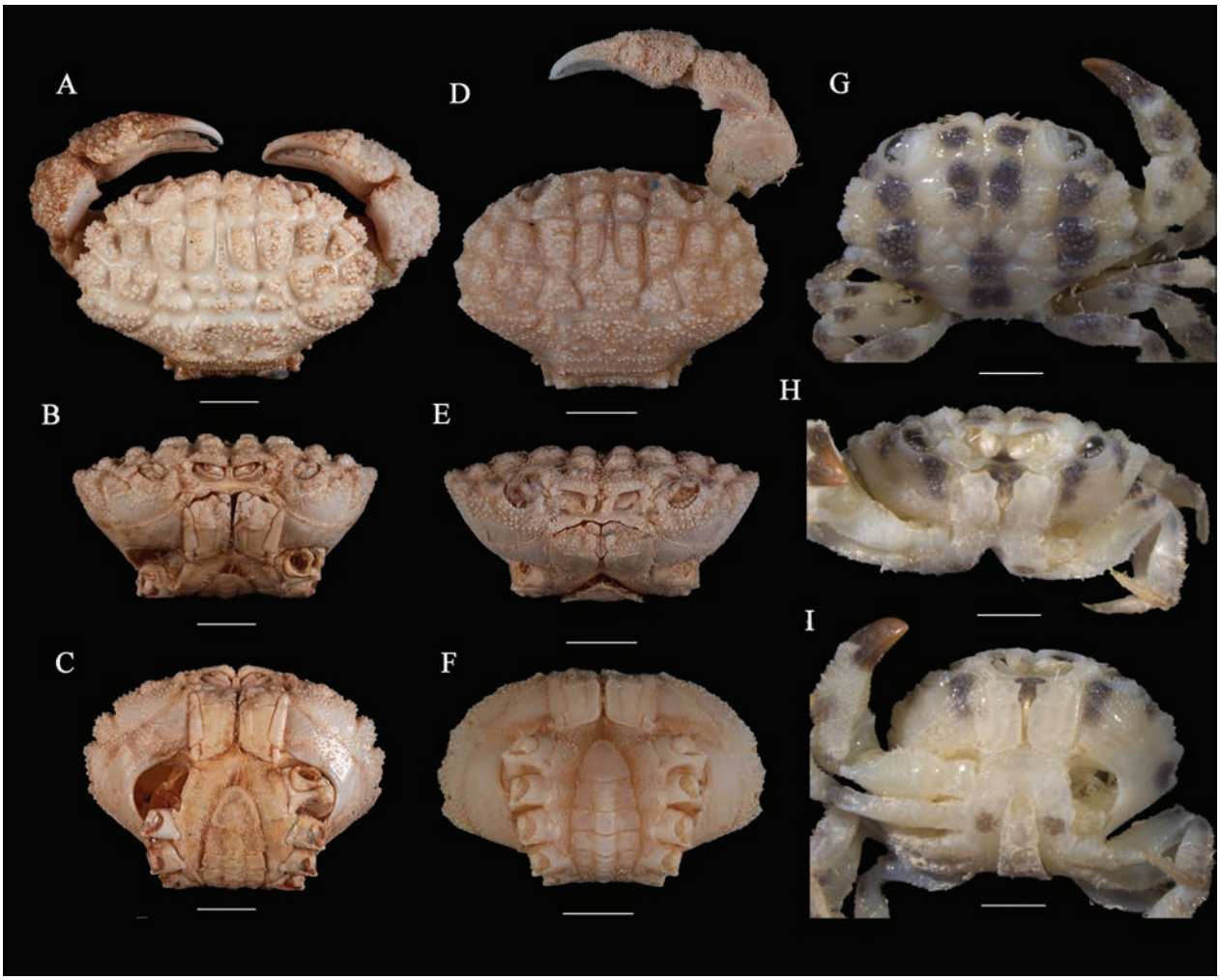

Figure 9. *Gothus consobrinus* (A. Milne-Edwards, 1873). **A–C.** Female, CW 10.5 mm, CL 6.8 mm, MNHN-IU-2000-3885 (=MP-B3885S); **D–F.** Female, CW 8.8 mm, CL 5.7 mm, MNHN-IU-2024-3483; photographed by Sébastien Soubzmaigne; **G–I.** Female, CW 4.5 mm, CL 2.9 mm, XS-QL-2022-1014. Scale bar: 2 mm (**A–F**); 1 mm (**G–I**).

A. mutatus Guinot, 1976 share a relatively similar appearance and match the description above. The most direct similarity is likely due to the very short posterolateral margins with a strong concavity that coapted against the last three pairs of ambulatory legs. However, *A. consobrinus* and *A. quinquelobatus* Garth & Kim, 1983 exhibit morphologies that differ significantly and may not fit well within the genus *Actaeodes*.

For the current species *A. consobrinus*, it indeed exhibits several features similar to typical *Actaeodes* species, which mainly include a carapace with developed dorsal areolation with granular and setae, longer anterolateral margins and shorter posterolateral margins, symmetrical chelipeds with sharply crossing tips, an elongated male pleon, and a G1 that is overall similar in morphology. However, this similarity is superficial, and there are some undeniable differences between *A. consobrinus* and typical *Actaeodes* species. A. Milne-Edwards, in the original description, compared *A. consobrinus* with *A. hirsutissimus*, noting the absence of a pronounced concavity in its posterior margin. In current observations, the posterior margin of this species is almost straight (Figs 7A, B, 8A, 9A, D, F), which significantly deviates from *Actaeodes* (Fig. 6F–H; cf. Guinot 1976: pl. XV, figs 1–4). Furthermore, the morphology of the thoracic sternum in the current species markedly differs from *Actaeodes*, with its third sternite being very short (Fig. 7D) (vs. elongated third sternite in *Actaeodes*; cf. Guinot 1976: fig. 41C) and the fourth sternite lacking oblique grooves (Fig. 7D) (fourth thoracic sternite of *Actaeodes* traversed by two transverse grooves and two oblique grooves; cf. Guinot 1976: fig. 41C). Other differences include *A. consobrinus* having an elongated pleon that barely extends beyond the coxo-sternal condyles of pereiopod 1 (Fig. 7D) (vs. pleon being significantly elongated, clearly surpassing the coxo-sternal condyles of pereiopod 1 in *Actaeodes*; cf. Guinot 1976: fig. 41C); like other species in *Actaeodes*, *A. consobrinus* has an elongated telson, but its overall shape is truncate-oval, with relatively arcuate lateral edges (Fig. 7D) (vs. triangular telson with converging lateral edges in *Actaeodes*; cf. Guinot 1976: fig. 41C); *A. consobrinus* has the first tooth flattened and the subse-

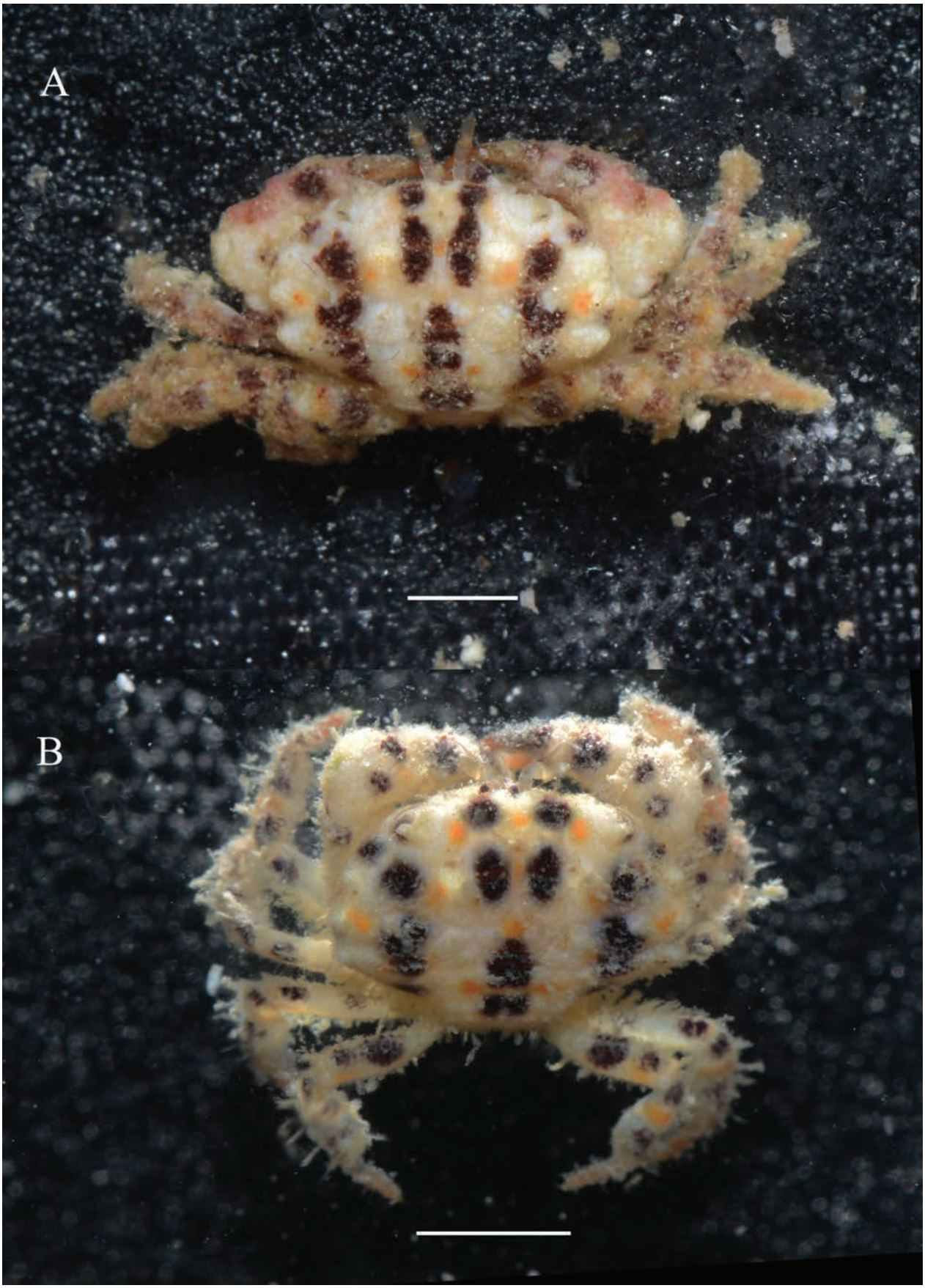

Figure 10. *Gothus consobrinus* (A. Milne-Edwards, 1873). **A.** Male, CW 6.7 mm, CL 4.4 mm, NS-YS-2022-1336; **B.** Female, CW 4.5 mm, CL 2.9 mm, XS-QL-2022-1014, displaying live coloration. Scale bar: 2 mm.

quent three teeth prominent (Figs 7A, B, 8A, 9A, D, F) (vs. anterolateral margin divided into four distinct but not very prominent lobes in *Actaeodes*; Fig. 6F–H; cf. Guinot 1976: pl. XV, figs 1–4); the cheliped carpus is more robust in *A. consobrinus* (Figs 7A, 9A, D, F) (vs. proportionally more slender carpus in *Actaeodes*; Fig. 6F–H; cf. Guinot 1976: pl. XV, figs 1–4). It is worth mentioning that although body color is generally not used as a basis for defining genera within the family Xanthidae, the vibrant and high-contrast living coloration of *A. consobrinus* is also quite unique in *Actaeodes* (Fig. 10). Based on the aforementioned reasons, *A. consobrinus* is not suitable for placement within the genus *Actaeodes*.

Another genus worth considering is *Meractaea* Serène, 1984, characterized by almost straight posterolateral margins, developed areolation on the dorsal surface of the carapace, and four underdeveloped small teeth on the anterolateral margins, all of which are similar to the current species. However, there are also differences between this genus and *A. consobrinus*, including an almost straight, quadrilobate frontal margin with a rounded central notch (cf. Serène 1984: pl. XIX, fig. C) (vs. front not very prominent but not straight, divided by a V-shaped notch into two inclined rounded lobes in *A. consobrinus*; Figs 7A, B, 8A, 9A, D, F); markedly slender ambulatory legs (cf. Serène 1984: pl. XIX, fig. C) (vs. flat and robust ambulatory legs in *A. consobrinus*; Figs 7A, 8D); a completely smooth dorsal surface of the carapace with irregularly sized granules, sometimes connected (cf. Serène 1984: pl. XIX, fig. C) (vs. carapace dorsal surface with setae, regularly sized granules, never connected in *A. consobrinus*; Figs 7A, B, 8A, 9A, D, F); G1 distal lobe slightly curved outward (cf. Serène 1984: fig. 63) (vs. G1 distal lobe curved inward in *A. consobrinus*; Fig. 8F–G). Considering these significant differences, *A. consobrinus* also cannot be placed within this genus.

Compared with the species of *Actaeodes* and *Meractaea*, *A. consobrinus* is actually more closely related to *G. teemo*. Beyond the most noticeable similarity in vibrant living coloration, both share similar carapace contours, flattened first anterolateral teeth, robust cheliped carpus, similar states of thoracic sternum, and special male abdominal morphology, particularly the truncate-oval telson (see the comparison in the remarks of *G. teemo*). We believe that placing this species into the current new genus and new combination is more appropriate.

Regarding the status of *A. quinquelobatus*, in the absence of specimens, we hereby present some limited queries. Similar to the new combination *G. consobrinus*, the morphology of *A. quinquelobatus* also appears to deviate from the definition of *Actaeodes* sensu stricto, featuring 5 instead of 4 anterolateral teeth and possessing non-concave posterior margins (cf. Garth and Kim 1983: fig. 5A). As Garth and Kim (1983) noted, *A. quinquelobatus* has carapace partitioning similar to *G. consobrinus*. However, current evidence does not affirm its placement within the genus *Gothus*, given it has 5 anterolateral teeth (cf. Garth and Kim 1983: fig. 5A) (vs. 3 or 4 in *Gothus*; Figs 1C, 7A), and the carapace and chelae exhibit a multitude of developed nodules (cf. Garth and Kim 1983: fig. 5A, B) (vs. surfaces have granules but lack nodules in *Gothus*; Figs 1A, 7A). Further examination is necessary to confirm its taxonomic status.

Molecular data analysis

To further confirm the taxonomic status of the new genus, new species, and new combination, we conducted molecular phylogenetic studies. The topologies of the ML and BI phylogenetic trees differed, yet both consistently supported the formation of a high-confidence clade comprising *G. teemo* and *G. consobrinus* (100/100), distinct from any related genera (Fig. 11). The species delimitation based on both ABGD and bPTP methods has validated the new species' legitimacy (Fig. 12).

In the previous study of Lai et al. (2011), the genera *Euxanthus*, *Hepatoporus* Serène, 1984, *Hypocolpus*, *Olenothus* Ng, 2002, *Rizalthus*, *Visayax*, and *Psaumis* were grouped into a monophyletic clade, referred to as Eux 1. Similar monophyletic clades were observed in the molecular systematic studies of the Xanthoidea by Mendoza et al. (2022), with the addition of the genus *Paractaeopsis*. This clade has been recognized as the Euxanthinae sensu stricto. However, in current research, neither phylogenetic tree supports the monophyly of Euxanthinae sensu stricto. In the ML tree, *Gothus* clustered with the subfamily Liomerinae Sakai, 1976, but with low bootstrap support (BS=67), and some species of the genus *Xanthias* Rathbun, 1897, disrupted the monophyly of Euxanthinae sensu stricto. In the BI tree, *Gothus*, certain species of *Xanthias*, and part of the Euxanthinae sensu stricto species clustered together with low posterior probability (PP=51), also disrupting the monophyly of the previous Euxanthinae sensu stricto species. In current research, the scope of Euxanthinae sensu stricto may need to be further narrowed, excluding *Rizalthus* and *Visayax*.

Discussion

The results of integrative taxonomy suggest that *G. teemo* and *G. consobrinus* together constitute a distinct genus within the family Xanthidae.

Despite molecular phylogenetic results indicating that *Gothus* does not form a stable monophyletic group with any related subfamily and is not well integrated into Euxanthinae sensu stricto, we have nonetheless decided to tentatively maintain its placement within Euxanthinae, albeit with reservations. This decision is based on the species' close morphological congruence with the traditional understanding of Euxanthinae, and molecular systematic studies have also shown it to have a closer phylogenetic relationship with Euxanthinae sensu stricto.

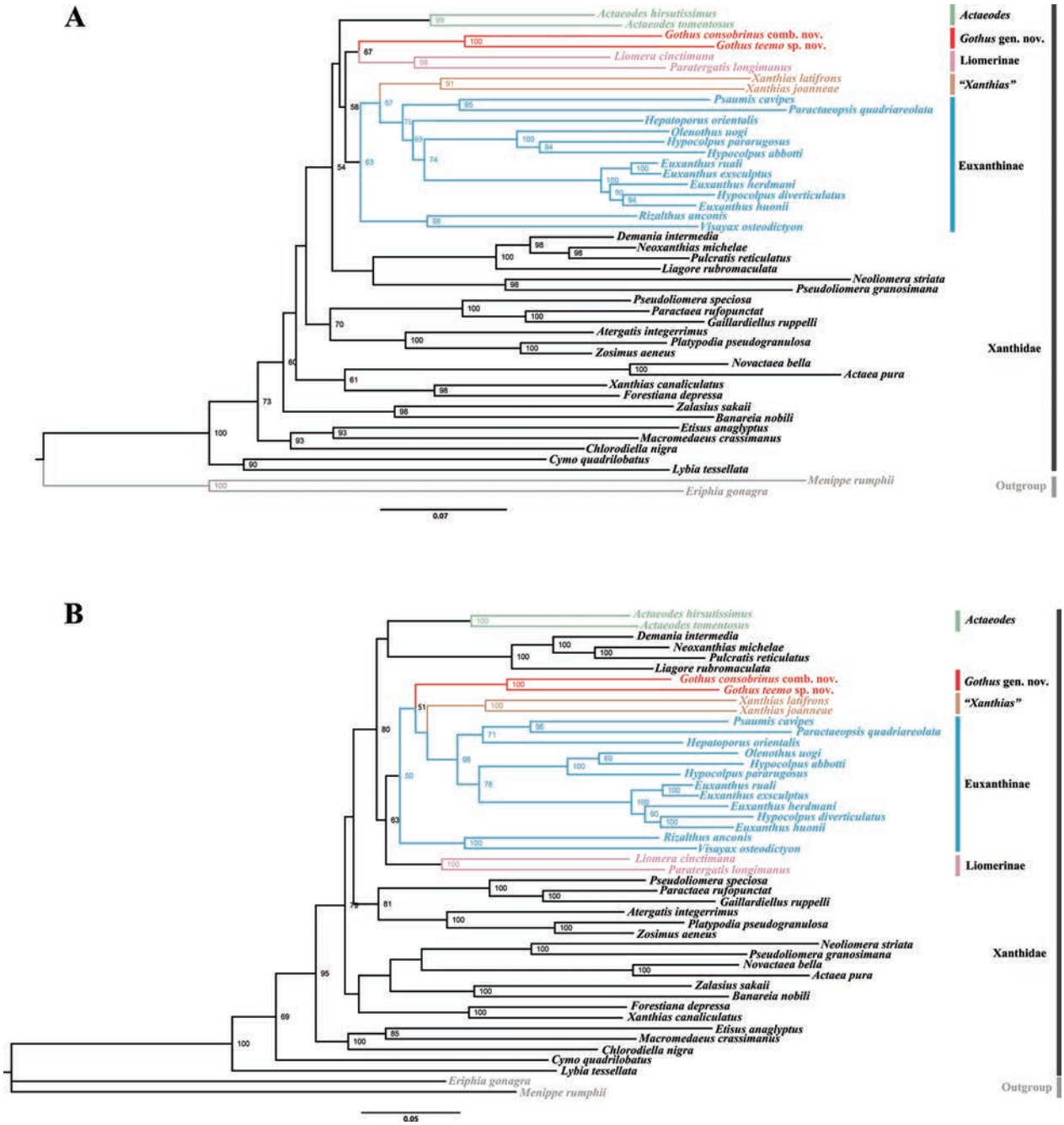

Figure 11. Phylogenetic relationships inferred from combined 12S, 16S, COI, and H3 sequences among *Gothus* gen. nov. and related species in Xanthidae, analyzed by Bayesian Inference (BI) and maximum likelihood (ML) analyses. **A.** BI tree, with posterior probabilities (PP) labeled; **B.** ML tree, with bootstrap replications (BS) labeled; values below 50 are hidden. Most data are derived from Lai et al. (2011) and Mendoza et al. (2022), as shown in Table 1.

Mendoza et al. (2022) had already pointed out the non-monophyly of the Euxanthinae subfamily. Our study also challenges the monophyly of the primary monophyletic group within the subfamily as identified in the previous research, or the previous Euxanthinae sensu stricto. Considering the limited number of molecular markers currently used, unaccounted species, and the potential impact of incomplete lineage sorting (ILS), the inclusion of additional taxa and data may further corroborate the taxonomic status of the new genus and the internal relationships within the subfamily Euxanthinae.

Current research suggests that for complex and diverse taxonomic groups like the family Xanthidae, potentially undiscovered taxa could offer new insights into their classification systems. The integration of morphological and molecular phylogenetic analyses may aid in further taxonomic revisions of these groups.

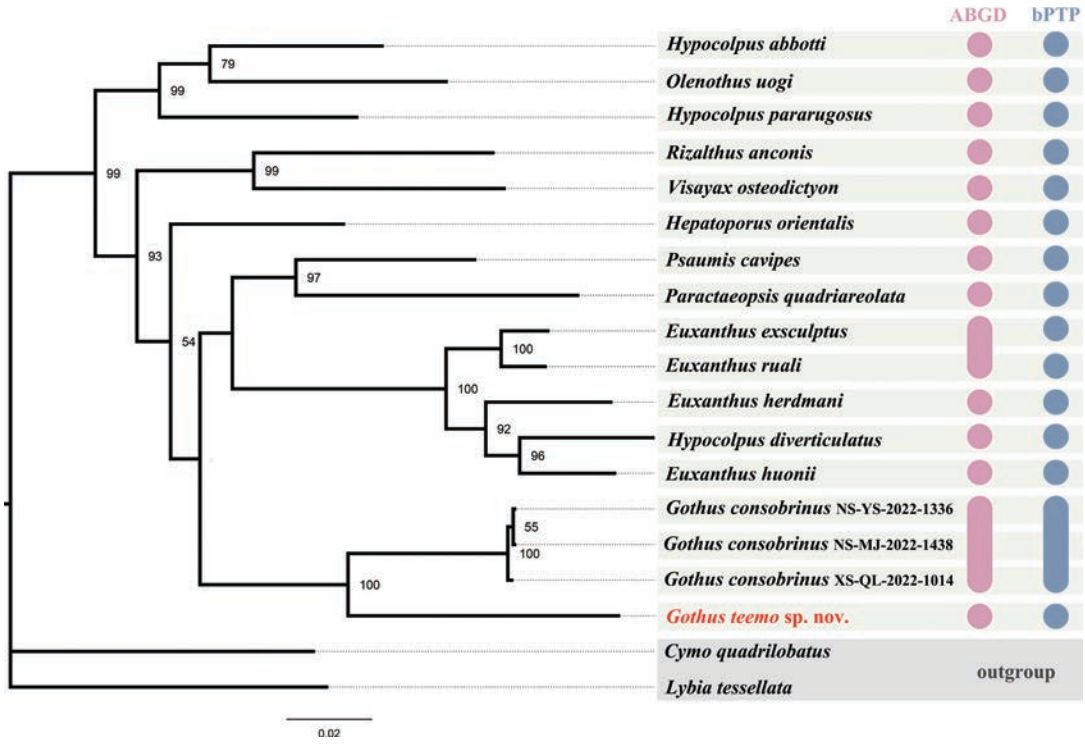

Figure 12. Bayesian inference (BI) phylogenic tree based on COI showing the phylogenetic relationship between *Gothus teemo* sp. nov., *G. consobrinus*, and related Euxanthinae species, with bootstrap replications (BS) labeled and values below 50 not shown. The results of automated barcode gap discovery (ABGD) and Bayesian implementation of the Poisson tree processes (BPTP) species delimitation methods are shown on the right of the figure; each circle or capsule shape represents one species.

Acknowledgements

The authors express their gratitude to Yuli Sun, Shaobo Ma, Aiyang Wang, and Bingqin Liu for their significant contributions to the sample collection. The authors would also like to thank Xu Zhang and Yunhao Pan for providing samples. The authors also wish to acknowledge and thank Fei Gao for the exquisite artistic illustrations provided for the new species. The authors extend their sincere gratitude to Sébastien Soubzmaigne (Muséum National d'Histoire Naturelle) for his assistance in locating and photographing the holotype specimen of G. consobrinus. Lastly, we would like to thank the editor and reviewers for their valuable comments and suggestions, which greatly improved the quality of this manuscript. This work was supported by the Ministry of Science and Technology of China (2021YFF0502801), the National Natural Science Foundation of China (42176138), Qingdao New Energy Shandong Laboratory Open Project (QNESL OP202306), and the National Key R&D Program of China (2022YFC3102403).

References

Alcock A (1898) Materials for a carcinological Fauna of India. No. 3. The Brachyura Cyclometopa. Part I. The family Xanthidae. Journal of the Asiatic Society of Bengal 67(2): 67–233.

Buhay JE, Moni G, Mann N, Crandall KA (2007) Molecular taxonomy in the Dark: Evolutionary history, phylogeography, and diversity of cave crayfish in the cubgenus *Aviticambarus*, genus *Cambarus*. Molecular Phylogenetics and Evolution 42(2): 435–438. https://doi.org/10.1016/j.ympev.2006.07.014

Crosnier A (1996) *Hypocolpus pararugosus*, espèce nouvelle de l'Indo-Ouest Pacifique (Crustacea, Decapoda, Brachyura, Xanthidae). Bulletin du Muséum National d'Histoire Naturelle 4, sec. A, 18(3–4): 557–564. https://doi.org/10.5962/p.290344

Dana JD (1851) On the Classification of the Cancroidea. The American Journal of Science and Arts 2 12(34): 121–131.

Davie PJF, Guinot D, Ng PKL (2015) Anatomy and functional morphology of Brachyura. In: Castro P, Davie PJF, Guinot D, Schram FR, von Vaupel Klein JC (Eds) Treatise on Zoology-Anatomy, Taxonomy, Biology-The Crustacea, Complementary to the Volumes Translated from the French of the Traité de Zoologie, 9(C)(I), Decapoda: Brachyura. Part 2. Brill, Leiden, 11–163. https://doi.org/10.1163/9789004190832_004

de Man JG (1896) Bericht über die von herrn schiffscapitän storm zu atjeh, an den westlichen küsten von Malakka, Borneo und Celebes sowie in der Java-See gesammelten Decapoden und Stomatopoden. Theil 4. Zoologische Jahrbucher. Abteilung fur Systematik, Geographie und Biologie der Tiere 9: 459–514. https://doi.org/10.5962/bhl.title.16084

Estampador EP (1959) Revised check list of Philippine crustacean decapods. Natural and Applied Science Bulletin 17(1): 1–127.

Felder DL, Thoma BP (2010) Description of *Etisus guinotae* n. sp., and discussion of its recent discovery in the Gulf of Mexico (Brachyura,

Decapoda, Xanthidae). In: Ng PKL, Castro P, Davie PJF, de Forges BR (Ed.) Studies on Brachyura: A Homage to Danièle Guinot. Brill, 117–138. https://doi.org/10.1163/ej.9789004170865.i-366.78

Galil BS, Vannini M (1990) Research on the coast of Somalia. Xanthidae, Trapeziidae, Carpiliidae, Menippidae (Crustacea, Brachyura). Tropical Zoology 3(1): 21–56. https://doi.org/10.1080/03946975.1990.10539447

Garth JS, Kim HS (1983) Crabs of the family Xanthidae (Crustacea, Brachyura) from the Philippine Islands and adjacent waters based largely on collections of the U.S. Fish Commission steamer Albatross in 1908–1909. Journal of Natural History 17(5): 663–729. https://doi.org/10.1080/00222938300770561

Geller J, Meyer C, Parker M, Hawk H (2013) Redesign of PCR primers for mitochondrial cytochrome c oxidase subunit I for marine invertebrates and application in all-taxa biotic surveys. Molecular Ecology Resources 13(5): 851–861. https://doi.org/10.1111/1755-0998.12138

Guinot D (1967a) La faune carcinologique (Crustacea, Brachyura) de l'Océan Indien Occidental et de la Mer Rouge: Catalogue, Remarques Biogéographiques et Bibliographiques. In: Réunion de Spécialistes C.S.A. sur les Crustacés, Zanzibar 1964. Mémoires de l'Institut Fondamental d'Afrique Noire, 77 (1966), 235–352. [pls 1–26, 1 table]

Guinot D (1967b) A propos des affinités des Genres *Dairoides* Stebbing et *Daira* de Haan. In: Recherches Préliminaires sur les Groupements Naturels chez les Crustacés, Décapodes, Brachyoures, III. Bulletin du Muséum National d'Histoire Naturelle, Paris 2 39(3): 540–563. [figs 1–36]

Guinot D (1971a) Recherches préliminaires sur les groupements naturels chez les Crustacés Decapodes Brachyoures. VIII. Synthèse et Bibliographie. Bulletin du Muséum National d'Histoire Naturelle 42(5): 1063–1090.

Guinot D (1971b) Un nouvel *Euxanthus* de Nouvelle-Calédonie; *E. ruali* sp. nov. Cahiers du Pacifique: 15: 19–21. [pl. 1–2]

Guinot D (1976) Constitution de quelques groupes naturels chez les Crustacés Décapodes Brachyoures. I. La Superfamille des Bellioidea Dana et Trois Sous-Familles de Xanthidae (Polydectinae Dana, Trichiinae de Haan, Actaeinae Alcock). Mémoires du Muséum National d'Histoire Naturelle, Paris: A, 97, 1–308. [figs 1–47, pls 1–19]

Guinot-Dumortier D. (1960) Révision des genres *Euxanthus* Dana et *Hypocolpus* Rathbun (Crustacea, Decapoda, Brachyura). Memoirs du Museum national d'Histoire naturelle, A (Zoology), nouvelle sèrie 20(2): 153–218.

Herbst JFW (1782–1790) Versuch einer naturgeschichte der krabben und krebse nebst einer systematischen beschreibung ihrer verschiedenen arten. Erster Band. Mit XXI Kupfer-Tafeln und Register. Krabben. Joh. Casper Fuessly, Zürich / Gottlieb August Lange, Berlin und Stralsund, iv + 274 pp. [21 pls] https://doi.org/10.5962/bhl.title.62813

Hombron JB, Jacquinot H (1842–1854) Crustacés. Atlas d'Histoire Naturelle. Zoologie. Voyage au Pôle Sud et dans l'Océanie sur les Corvettes l'Astrolabe et la Zélée Pendant les Années 1837–1838–1839–1840, Crustacés. [pls. 1–9]

Huelsenbeck JP, Ronquist F (2001) MRBAYES: Bayesian inference of phylogeny. Bioinformatics (Oxford, England) 17(8): 754–755. https://doi.org/10.1093/bioinformatics/17.8.754

Jana T, Lam-Tung N, Arndt VH, Quang MB (2016) W-iq-tree: A fast online phylogenetic tool for mmaximum likelihood analysis. Nucleic Acids Research 44(W1): W232–W235. https://doi.org/10.1093/nar/gkw256

Kossmann R (1877) Malacostraca (I. Theil, Brachyura). Zoologische ergebnisse einer im auftrage der königlichen academie der wissenschaften zu Berlin ausgeführten reise in die küstengebiete des Rothen Meeres. Wilhelm Engelmann, Leipzig, 66 pp. [3 pls] https://doi.org/10.5962/bhl.title.12140

Lai JCY, Mendoza JCE, Guinot D, Clark PF, Ng PKL (2011) Xanthidae MacLeay, 1838 (Decapoda, Brachyura, Xanthoidea) systematics: A multi-gene approach with support from adult and zoeal morphology. Zoologischer Anzeiger 250(4): 407–448. https://doi.org/10.1016/j.jcz.2011.07.002

MacLeay WS (1838) Illustrations of the Annulosa of South Africa. On the Brachyurous Decapod Crustacea. Brought from the Cape by Dr. Smith. In: Smith A (Eds) Illustrations of the Zoology of South Africa. London, pp. i–iv + 53–71. [pls. 2, 3]

Mendoza JCE, Ng PKL (2008) New genera and species of Euxanthine crabs (Crustacea, Decapoda, Brachyura, Xanthidae) from the Bohol Sea, the Philippines. The Raffles Bulletin of Zoology 56: 385–404.

Mendoza JCE, Chan KO, Lai JCY, Thoma BP, Clark PF, Guinot D, Felder DL, Ng PKL (2022) A comprehensive molecular phylogeny of the Brachyuran crab superfamily Xanthoidea provides novel insights into its systematics and evolutionary history. Molecular Phylogenetics and Evolution 177: 107627. https://doi.org/10.1016/j.ympev.2022.107627

Milne-Edwards A (1873) Description de Quelques Crustacés nouveaux ou peu connus provenant du musée de M. C. Godeffroy. Journal des Museum Godeffroy 1: 253–264. [pls. 12–13] https://doi.org/10.5962/bhl.title.10644

Ng PKL (2002) *Olenothus*, a new genus of Euxanthine crab (Crustacea: Decapoda: Brachyura: Xanthidae) from Guam. Micronesica 34(2): 201–208.

Ng PKL, Guinot D, Davie PJF (2008) Systema Brachyurorum: Part I. An Annotated Checklist of Extant Brachyuran Crabs of the World. The Raffles Bulletin of Zoology 17: 1–208.

Nobili MG (1907) Ricerche sui crostacei della Polinesia (Decapodi, Stomatopodi, Anisopodi e Isopodi). Memorie della reale accademia delle scienze di torino 57 (2): 351–430. [pls 1–3] https://doi.org/10.5962/bhl.title.53748

Odhner T (1925) Monographierte gattungen der krabben-familie Xanthidae. I. Göteborgs Kungliga Vetenskaps- och Vitterhets-Samhälles Handlingar (4) 29(1): 1–92. [figs 1–7, pls 1–5]

Palumbi SR (1996) Nucleic Acids II: The polymerase chain reaction. In: Hillis DM, Moritz C, Mable BK (Eds) Molecular Systematics. Sinauer Associates Inc, Sunderland, 205–247.

Plaisance L, Matterson K, Fabricius K, Drovetski S, Meyer C, Knowlton N (2021) Effects of low pH on the coral reef cryptic invertebrate communities near CO2 vents in Papua New Guinea. PLoS ONE 16(12): e0258725. https://doi.org/10.1371/journal.pone.0258725

Posada D (2008) jModelTest: Phylogenetic model averaging. Molecular Biology and Evolution 25(7): 1253–1256. https://doi.org/10.1093/molbev/msn083

Puillandre N, Lambert A, Brouillet S, Achaz G (2012) ABGD, automatic barcode gap discovery for primary species delimitation. Molecular Ecology 21(8): 1864–1877. https://doi.org/10.1111/j.1365-294X.2011.05239.x

Rathbun MJ (1897) A revision of the nomenclature of the Brachyura. Proceedings of the Biological Society of Washington 11: 153–167.

Rathbun MJ (1909) New crabs from the Gulf of Siam. Proceedings of the Biological Society of Washington 22: 107–114.

Rathbun MJ (1911) Marine Brachyura. In: The Percy Sladen Trust expedition to the Indian Ocean in 1905, under the leadership of Mr J. Stanley Gardiner. Vol. III, part II, No. XI. Transactions of the Linnean Society of London: (Zool.), (2) 14(2): 191–261. [figs 1–2, pls 15–20]

Rüppell E (1830) Beschreibung und abbildung von 24 arten kurzschwänzigen krabben, als beitrag zur naturgeschichte des rothen meeres. H.L. Brönner, Frankfurt am Main, 28 pp. [6 pls]

Sakai T (1939) Studies on the Crabs of Japan. IV. Brachygnatha, Brachyrhyncha. Yokendo Co., Tokyo, 365–741. [figs 1–129, pls 42–111, table 1]

Sakai T (1976) Crabs of Japan and the adjacent seas. Kodansha Ltd, Tokyo, pp. i–xxix, 1–773. [figs 1–379; pls 1–251; 1–461, figs 1–2, 3 maps]

Serène R (1984) Crustacés Décapodes Brachyoures de l'Océan Indien Occidental et de la Mer Rouge, Xanthoidea, Xanthidae et Trapeziidae. Faune Tropicale, no. XXIV, 1–349. [figs A–C + 1–243, pls 1–48]

Serène R, Lang BT (1959) Observations sur les premiers pléopodes mâles d'espèces d'Actea (Brachyures) du Viêt-Nam. Annales de la Faculté des Sciences: Saigon 43: 285–300.

Svenson GJ, Whiting MF (2004) Phylogeny of Mantodea based on molecular data: Evolution of a charismatic predator. Systematic Entomology 29(3): 359–370. https://doi.org/10.1111/j.0307-6970.2004.00240.x

Takeda M, Miyake S (1968) Two new xanthid crabs inhabiting coral reefs of the Ryukyu Islands. OHMU, Occasional Papers of the Zoological Laboratory, Faculty of Agriculture, Kyushu University 1(9): 183–189. [pl. 8]

Takeda M, Miyake S (1976) Crabs of the Ogasawara Island. Researches on Crustacea, Tokyo 7: 101–115. [fig. 1] https://doi.org/10.18353/rcustacea.7.0_101

Tamura K, Stecher G, Peterson D, Filipski A, Kumar S (2013) MEGA6: Molecular evolutionary genetics analysis version 6.0. Molecular Biology and Evolution 30(12): 2725–2729. https://doi.org/10.1093/molbev/mst197

Thoma BP, Schubart CD, Felder DL (2009) Molecular phylogeny of Western Atlantic representatives of the Genus *Hexapanopeus* (Decapoda: Brachyura: Panopeidae). In: Decapod Crustacean Phylogenetics, Crustacean Issues, CRC Press, Boca Raton, 551–565. https://doi.org/10.1201/9781420092592-c28

Thoma BP, Guinot D, Felder DL (2014) Evolutionary relationships among American mud crabs (Crustacea, Decapoda, Brachyura, Xanthoidea) inferred from nuclear and mitochondrial markers, with comments on adult morphology. Zoological Journal of the Linnean Society 1(1): 86–109. https://doi.org/10.1111/zoj.12093

Tweedie MWF (1950) The fauna of the Cocos-Keeling Islands. Brachyura and Stomatopoda. Bulletin of the Raffles Museum, Singapore 22: 105–148. [figs 1–4, pls 16–17]

Vaidya G, Lohman DJ, Meier R (2011) SequenceMatrix: Concatenation software for the fast assembly of Multi-Gene datasets with character set and codon information. Cladistics 27(2): 171–180. https://doi.org/10.1111/j.1096-0031.2010.00329.x

Ward M (1933) The true crabs of the Capricorn group, Queensland (Class Crustacea, Order Decapoda Brachyura). Part 1. Xanthidae. Australian Zoologist, Sydney 7(5): 237–255.

Ward M (1934) Notes on a collection of crabs from Christmas Island, Indian Ocean. Bulletin of the Raffles Museum, Singapore 9: 5–28. [pls 1–3]

Zhang J, Kapli P, Pavlidis P, Stamatakis A (2013) A general Species delimitation method with applications to phylogenetic placements. Bioinformatics (Oxford, England) 29(22): 2869–2876. https://doi.org/10.1093/bioinformatics/btt499

Zoosyst. Evol. 100 (3) 2024, 989–1004 | DOI 10.3897/zse.100.121692

PENSOFT

MUSEUM FÜR NATURKUNDE BERLIN

Gammarus sezgini sp. nov. (Arthropoda, Amphipoda, Gammaridae), a new amphipod species from the Eastern Black Sea region of Türkiye

Hazel Baytaşoğlu[1], İsmail Aksu[1], Murat Özbek[2]

1 *Recep Tayyip Erdogan University, Faculty of Fisheries and Aquatic Sciences, 53100 Rize, Turkiye*

2 *Ege University, Faculty of Fisheries, 35100 İzmir, Turkiye*

https://zoobank.org/8CF9597B-97B7-4E42-AE6A-55AD07C25878

Corresponding author: Hazel Baytaşoğlu (gokbuluthazel@gmail.com)

Academic editor: Luiz F. Andrade ♦ **Received** 25 March 2024 ♦ **Accepted** 17 June 2024 ♦ **Published** 11 July 2024

Abstract

A new amphipod species belonging to the genus *Gammarus* was identified in the rivers of the Eastern Black Sea Region of Türkiye: *G. sezgini* **sp. nov.** The authors described the new species using a taxonomic approach that combines morphological and molecular data. The newly identified species belongs to the *G. komareki* species complex because of the setation of antenna 2, pereopods 3 and 4, and the uropod 3. Some of its characteristic features are as follows: A medium-large species (holotype male, 9.8 mm). The body is yellowish; no dorsal keel or hump; eyes well developed, kidney-shaped; extremities not elongated; the second antenna bears numerous groups of long setae on the peduncle and flagellar segments; antennal gland cone long, not curved; the posterior margin of pereopod 3 is densely setose; the setae on the posterior edge of pereopod 4 are shorter and fewer in number; the anterior margins of pereopods 5 to 7 bear spines in the male; epimeral plates are not pointed. The newly identified species looks similar to *G. komareki* but differs from it by having a longer antennal gland cone, having fewer D-setae (33) in the third segment of the mandible palp, having shorter setae on the ventral part of the peduncular segment of the antenna 2, and having longer antenna 1, having fewer setae along the posterior margins of pereopods 3 and 4, and the absence of setae along the anterior margins of merus and carpus of pereopod 7. The new species is distinct from its relatives by high genetic distance (COI: 17.10% and 28S: 0.88%) and was resolved from them as an independent lineage with high support (ML: 78%, NJ: 70%, and BI: 1.0) in all phylogenetic results, based on the concatenated dataset (28S+COI). Additionally, species delimitation analyses (ASAP and PTP) based on the COI gene supported the conclusion that the new species constitutes an independent lineage. Detailed descriptions and drawings of the male holotype and the female allotype are given, and the morphology of the newly identified species is compared with that of its relatives.

Key Words

Eastern Black Sea, freshwater, identification, molecular analysis, taxonomy

Introduction

The order Amphipoda Latreille, 1816, is comprised of six suborders represented by approximately 11,000 species. The suborder Senticaudata Lowry & Myers, 2013, which also includes the family Gammaridae Latreille, 1802, encompasses around 6,000 species, hosting nearly all freshwater species and numerous marine benthic species. The genus *Gammarus* Fabricius, 1775, with approximately 200 described species, exhibits a wide distribution in the Holarctic region. Previous studies suggest that *Gammarus* originated from ancient Tethys and then diversified due to plate tectonic activities between Eurasia and Africa/India (Hou et al. 2011; Horton et al. 2024).

Studies on *Gammarus* species in Türkiye began in the early 20th century and have continued until the present day (Vavra 1905; Coifman 1938; Bacescu 1954; Özbek and Ustaoğlu 1998, 2001, 2005a, 2005b; Sarı et al. 2001; Balık et al. 2004; Özbek et al. 2004, 2007; Akbulut et al. 2009; Albayrak and Özuluğ 2016; Özbek and Özkan 2017; Baytaşoğlu and Gözler 2018). Especially in recent years, newly recorded species from the inland waters

of Türkiye have been evaluated not only based on their morphological characteristics but also through molecular analysis (Rewicz et al. 2016; Özbek et al. 2023a, 2023b). So far, 55 species belonging to the genus *Gammarus* have been identified in Turkish inland waters (İpek and Özbek 2022; Özbek et al. 2023a, 2023b).

The Eastern Black Sea Basin covers Artvin, Rize, Trabzon, Gümüşhane, Giresun, and Ordu provinces. The rivers of the area are mainly fed by precipitation and have a regular regime. The flow rate is normal during the summer months, while the flow rate increases with melting snow. Some of the rivers flow directly into the Black Sea after a short flow, and some of them originate in central Anatolia and reach the Black Sea by crossing the North Anatolian Mountains (Selim 2011). In previous studies conducted in this basin, six species [*G. balcanicus* Schäferna 1922, *G. birsteini* Karaman & Pinkster, 1977, *G. kischineffensis* Schellenberg 1937, *G. komareki* Schäferna 1923, *G. pulex pulex* (Linnaeus 1758), and *G. fossarum* Koch 1835] were reported (Karaman 2003). However, no detailed distribution data for these species has been presented to date.

This study aimed to investigate the amphipod samples collected from streams (Balat-Yeşildere-Taşlı) in the Eastern Black Sea Basin (Rize) of Türkiye both morphologically and genetically. As a result of the study, a new amphipod species was described, *Gammarus sezgini* sp. nov., detailed descriptions and drawings of the extremities of the male holotype and female allotype were given, and the morphology of the newly described species was compared with its relatives.

Materials and methods

Study area

Samplings were conducted in Balat Stream, Taşlı Stream, and Yeşildere Stream within the borders of Rize province, the northeastern part of Türkiye. Balat Stream is a tributary of the Büyük Stream, which flows from Rize/Çayeli district to the Black Sea. There are trout farming facilities on the stream. Yeşildere Stream is a tributary of the Taşlı Stream, flowing from Rize/Andon Hot Springs to the Black Sea. In these locations, there are trout farming facilities and tea collection centers. The map of the stations where the species was identified is given in Fig. 1. A map was created using the QGIS v.3.8.3-Zanzibar software available at http://diva-gis.org (Fig. 1).

Data collection and analysis

Samplings were carried out at three stations in October 2019 and September 2020. A 30×30 cm sized hand net (D-Frame net) with a 250 µ mesh size was used to collect the specimens. The collected samples were placed in plastic sample containers, and the labels on which the date, the name of the station, the coordinate, the altitude, and the name of the city where they are located are written both inside the container and on the outside. The first fixation of the samples was made with 96% alcohol in the field. The samples brought to the laboratory were cleared of their sludge under tap water with the help of sieves with a mesh size of 4 mm–63 µm. Each individual was examined under a Leica MC 170 HD brand stereomicroscope.

Morphological identification

One adult male and one female individual from the samples were selected as holotype and allotype individuals, respectively. Both selected individuals were kept in a lactic acid and 10% NaOH solution for 2 hours. The holotype male individual was photographed under a stereomicroscope before being dissected. After holotype and allotype individuals were dissected in a glycerin alcohol solution, permanent slides were prepared with a CMCP-10 high-viscosity mount. Detailed photographs of the extremities

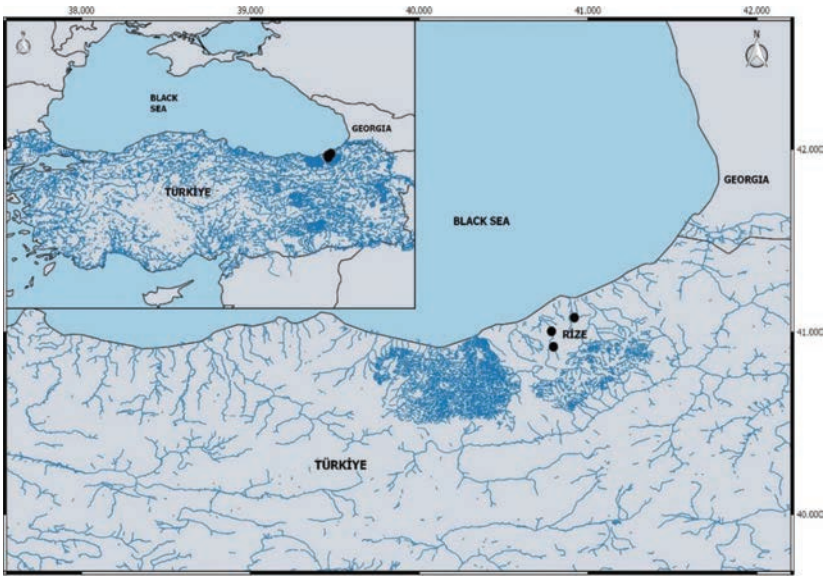

Figure 1. Map of the sampling area and the localities.

were taken with a 5-megapixel resolution digital camera mounted on an Olympus CKX-41 model binocular microscope. For detailed drawings of the extremities, a digitizer board (Wacom PTH-451) and a standard pen connected to the computer were used. Image processing programs were used in the drawings of the extremities, and the drawing techniques specified by Coleman (2003) were followed.

Molecular identification

Total DNA isolation, PCR amplification, and sequencing

The DNA of *Gammarus* specimens was extracted on the Qiacube Automated DNA Isolation Device (Qiagen, Valencia, CA) according to the DNeasy Blood & Tissue Kit (Qiagen, Hilden, Germany) protocol. The mitochondrial cytochrome c oxidase subunit I gene (COI) was amplified with the primers UCOIF (5'-TAWACTTCDGGRTGRCCRAAAAAYCA-3') and UCOIR (5'-ACWAAYCAYAAAGAYATYGG-3') as described by Costa et al. (2009), and cycle conditions were as follows: 3 min. first denaturation at 95 °C, followed by 35 cycles of denaturing for 30 sec. at 95 °C, annealing for 30 sec. at 47 °C, extension for 45 sec. at 72 °C, and final extension for 7 min. at 72 °C. The nuclear large subunit ribosomal RNA gene (28S) was amplified with the primers 28F (5'-TTAGTAGGGGCGACCGAACAGGGAT-3') and 28R (5'-GTCTTCGCCCCTATGCCCAACTGA-3') as described by Hou et al. (2007), and cycle conditions were as follows: 3 min. first denaturation at 95 °C, followed by 35 cycles of denaturing for 35 sec. at 95 °C, annealing for 30 sec. at 62 °C, extension for 1.15 min. at 72 °C, and final extension for 7 min. at 72 °C. The QIAquick PCR Purification Kit (Qiagen) was utilized to purify the amplified PCR products. Two-directional sequencing of PCR products was performed with an ABI PRISM 3730×1 Genetic Analyser using a BigDye Terminator 3.1 cycle sequencing ready reaction kit (Applied Biosystems) at Macrogen Europe.

Molecular data analysis

We carried out analyses to genetically compare the potential new species with its congeners and to generate its first molecular records. We sequenced the COI and 28S genes of a total of five specimens from three populations (Balat, Yeşildere, and Taşlı streams) of the new species (see "Genetic material" section). In addition, we downloaded the COI and 28S sequences of valid *Gammarus* species from GenBank. Detailed information on these species is available in Table 1.

The raw COI and 28S sequences of the new species were corrected by checking their chromatograms in the Bioedit 7.2.5 program (Hall 1999). All sequences were

Table 1. Information on sequences used in molecular analyses.

Species	Locality	28S	COI	References
G. sezgini sp. nov. (T)	Balat stream, Rize, Türkiye	PP456724	PP457381	This study
G. sezgini sp. nov. (T)	Balat stream, Rize, Türkiye	PP456725	PP457382	This study
G. sezgini sp. nov. (T)	Yeşildere stream, Rize, Türkiye	PP456726	PP457383	This study
G. sezgini sp. nov. (T)	Yeşildere stream, Rize, Türkiye	PP456727	PP457384	This study
G. sezgini sp. nov. (T)	Taşlı stream, Rize, Türkiye	PP456728	PP457385	This study
G. kunti (T)	Fakıllı Cave, Türkiye	OP650556	OP642558	Özbek et al. (2023a)
G. tumaf (T)	Gökgöl Cave, Türkiye	ON751931	ON749780	Özbek et al. (2023b)
G. baysali (T)	Cumayanı Cave, Türkiye	ON751932	ON749781	Özbek et al. (2023b)
G. kesslerianus (T)	Simferopol, Crimea, Ukraine	JF965721	JF965909	Hou et al. (2011)
G. komareki (T)	ca 200 km SE Sofia, Bulgaria	JF965725	JF965913	Hou et al. (2011)
G. komareki	Mazandaran, Iran	JF965723	JF965911	Hou et al. (2011)
G. rambouseki (T)	Bitola, Macedonia	JF965770	JF965946	Hou et al. (2011)
G. roeselii	Netherlands	JF965771	JF965947	Hou et al. (2011)
G. fossarum (T)	Regensburg, Germany	JF965696	JF965886	Hou et al. (2011)
G. plaitisi	Tinos, Komi, Greece	MT999102	MT999049	Hupało et al. (2020)
G. uludagi	Evia, Greece	JF965817	JF965986	Hou et al. (2011)
G. monspeliensis (T)	Montpellier, France	JF965738	JF965923	Hou et al. (2011)
G. ibericus	Lascaux, France	JF965713	JF965901	Hou et al. (2011)
G. pulex (T)	Slovenia	JF965767	JF965943	Hou et al. (2011)
G. lacustris	Bled, Slovenia	JF965728	JF965915	Hou et al. (2011)
G. italicus	Rieti, Lazio, Italy	JF965716	JF965904	Hou et al. (2011)
G. varsoviensis (T)	Secymin, Poland	JF965818	JF965987	Hou et al. (2011)
G. kischineffensis (T)	Targu Bujor, Romania	MG987529	MG987571	Copilaş-Ciocianu et al. (2018)
G. spelaeus (T)	Simferopol, Crimea, Ukraine	JF965801	JF965971	Hou et al. (2011)
G. balcanicus (T)	Kolašin, Montenegro	JF965640	JF965834	Hou et al. (2011)
G. bosniacus (T)	Sarajevo, Bosnia and Herzegovina	JF965680	JF965872	Hou et al. (2011)
G. leopoliensis (T)	Vistula, Poland	JF965734	JF965919	Hou et al. (2011)
G. stojicevici (T)	Bela Palanka, Serbia	JF965808	JF965978	Hou et al. (2011)
G. halilicae (T)	Lazaropole, Macedonia	JF965711	JF965900	Hou et al. (2011)
G. pljakici	Galicica planina, Macedonia	JF965758	JF965936	Hou et al. (2011)
G. stankokaramani (T)	Ohrid, Macedonia	JF965806	JF965976	Hou et al. (2011)
G. salemaai	Gradište, Macedonia	JF965780	JF965955	Hou et al. (2011)
Pontogammarus robustoides	Delta Volgi, Russia	JF965822	JF965990	Hou et al. (2011)

Note: (T) Topotype samples of nominal taxa.

then aligned with the Clustal W method (Thompson et al. 1994). The pairwise genetic distances were calculated for the COI and 28S genes according to the uncorrected *p*-distance in the MEGA X software (Kumar et al. 2018).

To reconstruct the phylogeny of the genus *Gammarus*, the COI and 28S sequences of all species were added end-to-end, resulting in a concatenated data set (28S+-COI) for each species. Phylogeny was estimated by using Neighbour-Joining (NJ; Saitou and Nei 1987), Maximum Likelihood (ML; Felsenstein 1981) methods in MEGA X software, and Bayesian inference (BI) in MrBayes v3.2.1 (Ronquist et al. 2012). The appropriate nucleotide substitution models were selected according to the Akaike Information Criterion (AIC) and Bayesian Information Criterion (BIC) in jModeltest 0.1.1 (Posada 2008). The NJ tree was constructed using the *p*-distance node support, which was calculated (Felsenstein 1985) using 1000 bootstrap pseudo-replicates. The ML tree was constructed using the Tamura-Nei model (TN93; Tamura and Nei 1993) with gamma-correction and invariant sites (G+I), and node support was calculated with 500 bootstrap pseudo-replicates. The BI tree was constructed using the TN93+G+I model. The analysis was run for 5 million generations with Metropolis-coupled Monte Carlo Markov Chains (MCMC) sampled every 1000 generations. As burn-in, the first 25% of generations were discarded. The convergence of the runs was confirmed using Tracer v1.7.1 (Rambaut et al. 2018). The iTOL (Interactive Tree of Life; https://itol.embl.de/), a web-based program, was used to visualize the BI tree. In all phylogenies, *Pontogammarus robustoides* (Sars, 1894) (Table 1) was chosen as the outgroup.

We applied one distance-based method, Assemble Species by Automatic Partitioning (ASAP; Puillandre et al. 2020), and one tree-based method, Poisson Tree Processes (PTP; Zhang et al. 2013), to identify the Molecular Operational Taxonomic Units (MOTUs) based on the COI dataset. To implement the ASAP method, we used the Kimura 2-parameter (K2P) distances and transition/transversion ratio (R:1.4) settings at the web address https://bioinfo.mnhn.fr/abi/public/asap/. The transition/transversion ratio (R) for the COI data was calculated in MEGA X software. PTP with a maximum likelihood solution was implemented via a web server (http://mptp.h-its.org/#/tree) (accessed on February 2, 2024).

Results

Gammarus sezgini sp. nov.

https://zoobank.org/BE51BA07-80D8-4832-96F3-594D0CD087FF

Figs 2–7

Material examined. ***Holotype*:** Türkiy • Male; 9.8 mm; Rize Province, Yeşildere stream/Balat stream/Taşlı Stream; coordinates: 40.9493°N, 40.5394°E / 41.0227°N, 40.7130°E / 40.8701°N, 40.5859°E. Specimens collected by Hazel BAYTAŞOĞLU; 16 October 2019 and 1 September 2020. Holotypes with paratypes are stored under catalog number RTEÜ-FFR200001; (GenBank accession numbers: PP457383, PP457384 for COI, and PP456726, PP456727 for 28S; PP457381, PP457382 for COI, and PP456724, PP456725 for 28S; PP457385 for COI and PP456728 for 28S).

***Paratypes*:** 38 males and 34 females, same data as the holotype.

Genetic material. RTEÜ-FFR-DNA K2, K4, Yeşildere stream, Rize Province, Türkiye, 40.9493°N, 40.5394°E (GenBank accession numbers: PP457383, PP457384 for COI, and PP456726, PP456727 for 28S) - RTEÜ-FFR-DNA K5, K8, Balat stream, Rize Province, Türkiye, 41.0227°N, 40.7130°E (GenBank accession numbers: PP457381, PP457382 for COI, and PP456724, PP456725 for 28S) - RTEÜ-FFR-DNA K9, Taşlı stream, Rize Province, Türkiye, 40.8701°N, 40.5859°E (GenBank accession numbers: PP457385 for COI and PP456728 for 28S).

Diagnosis. A medium-large species. The body is yellowish; no dorsal keel or hump; the eyes are well developed; kidney-shaped; the extremities are not elongated; the second antenna bears numerous groups of long setae on the peduncle and flagellar segments; the antennal gland cone is straight and reaches to the distal end of the third peduncular segment; posterior margin of pereopod 3 densely setose; the setae on the posterior edge of pereopod 4 are shorter and fewer in number; the anterior margins of pereopods 5 to 7 bear spines in the male, while they bear long setae along with the spines in females; epimeral plates are pointed; the inner ramus of uropod 3 is slightly longer than 0.8 of the outer one; each telson lobe bears a pair of spines distally and setae longer than the spines.

Description of male holotype. Head: Rostrum absent, inferior antennal sinus deep, rounded. Eyes kidney-shaped; length is slightly shorter than the diameter of the first peduncular segment of antenna 1 (Fig. 2).

Antennae: Antenna 1 (Fig. 4A) is half as long as the body length; the length ratio of the peduncular segments is 1:0.75:0.38; peduncle segments bear a few groups of minute setae; the length of the setae is much shorter than the segment where they are implanted; the main flagellum with 32 segments; each segment bears a few short setae in distal side; aesthetasc absent; accessory flagel-

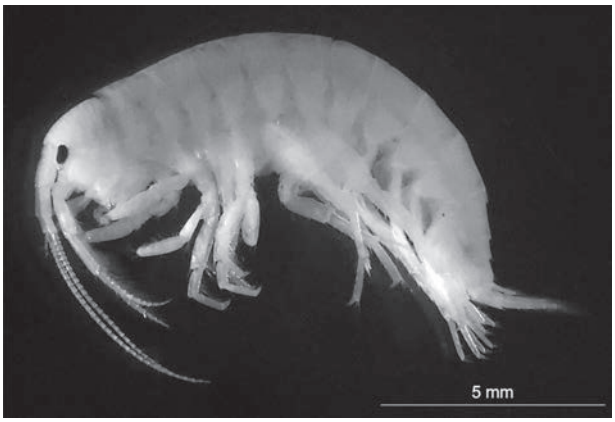

Figure 2. Habitus of the holotype male of *Gammarus sezgini* sp. nov.

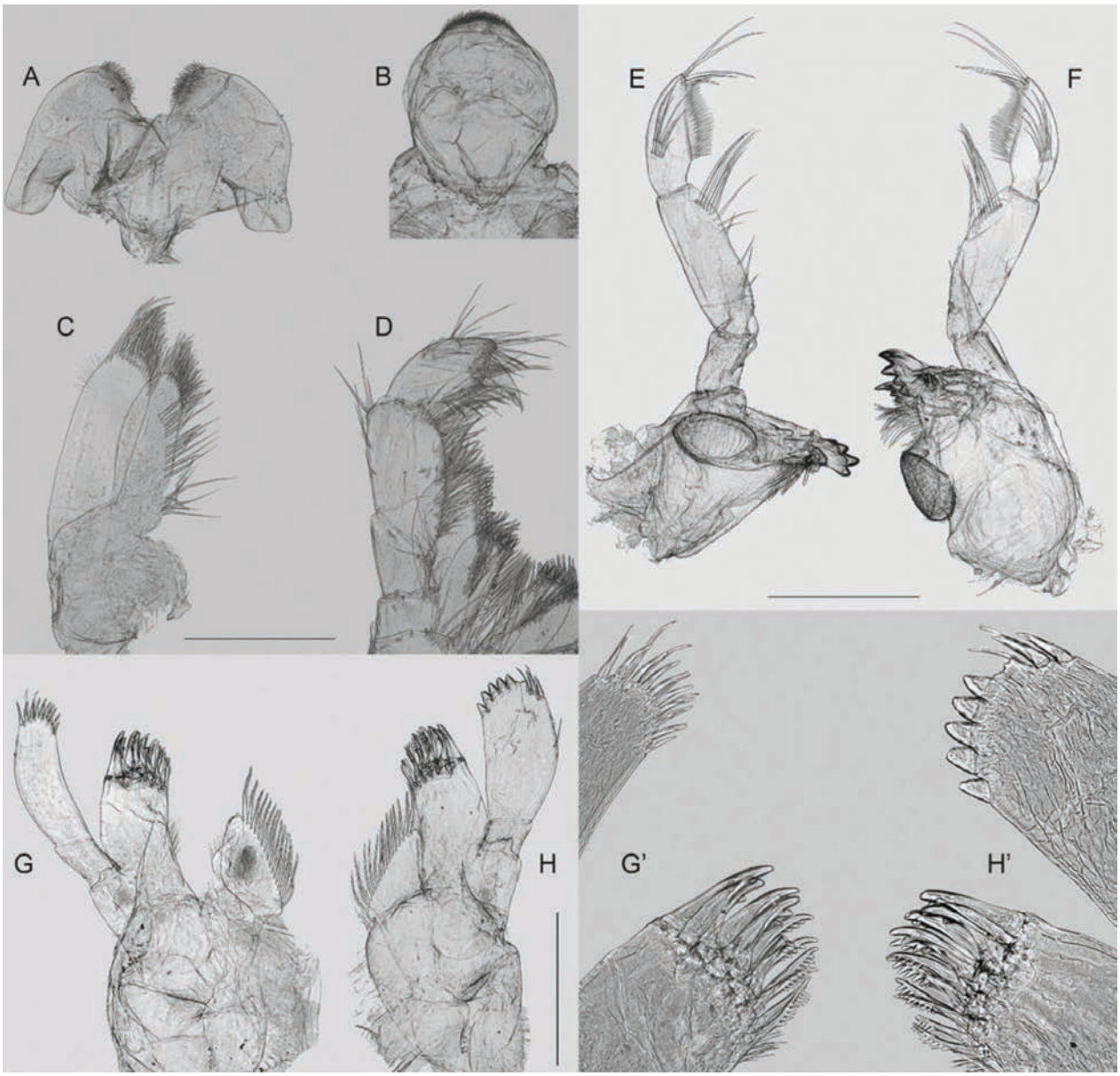

Figure 3. Mouthparts of the holotype male of *Gammarus sezgini* sp. nov. **A.** Lower lip; **B.** Upper lip; **C.** Maxilla 2; **D.** Maxilliped; **E.** Right mandible; **F.** Left mandible; **G.** Left maxilla 1; **H.** Right maxilla 1; **G', H'.** Detail of the left and right maxilla 1.

lum with five segments. Antenna 2 (Fig. 4B) is shorter than antenna 1 (ratio 1:0.7); the antennal gland cone is straight and reaches the distal end of the third peduncular segment; setation is rich both on peduncular and flagellar segments; peduncular segments 4 and 5 bear many groups of setae; the setae on the ventral part of the peduncle segments are shorter than the diameter of the segment but longer than those on the dorsal part; flagellum consists of 12 segments; flagellar segments are setose and swollen; each segment bears many long setae groups on both dorsal and ventral sides; calceoli absent.

Mouthparts: Upper lip (Fig. 3B) with numerous minute setules in the distal part.

Left mandible (Fig. 3F) with 4-toothed incisor, lacinia mobilis with 4 dentitions, molar triturative. The first article of palp without setae; the second one bears 14 setae; the setae become shorter from distal to proximal. The third segment has 33 D-setae, 4–5 E-setae, one group of A-setae, and one group of B-setae. C-setae absent.

Right mandible (Fig. 3E) has a 4-toothed incisor and bifurcate lacinia mobilis.

Right maxilla 1 (Fig. 3H, H') is asymmetric to the left; it has 16 plumose setae along the inner margin of the inner lobe. The outer lobe bears 11 distal stout serrate spines and some tiny setules on the inner margin. Palp of the outer lobe with no setae in the first segment and six stout spines (one of them lost) and three setae (two of them robust) on the distal part of the second segment, in addition to a marginal seta along the outer margin. The second article of left palp is elongated and bears 10 spines, five simple setae on its distal part, and no setae along the outer margin (Fig. 3G, G').

Lower lip (Fig. 3A) has no inner lobe and bears numerous small simple setae along the distal margins of both lobes.

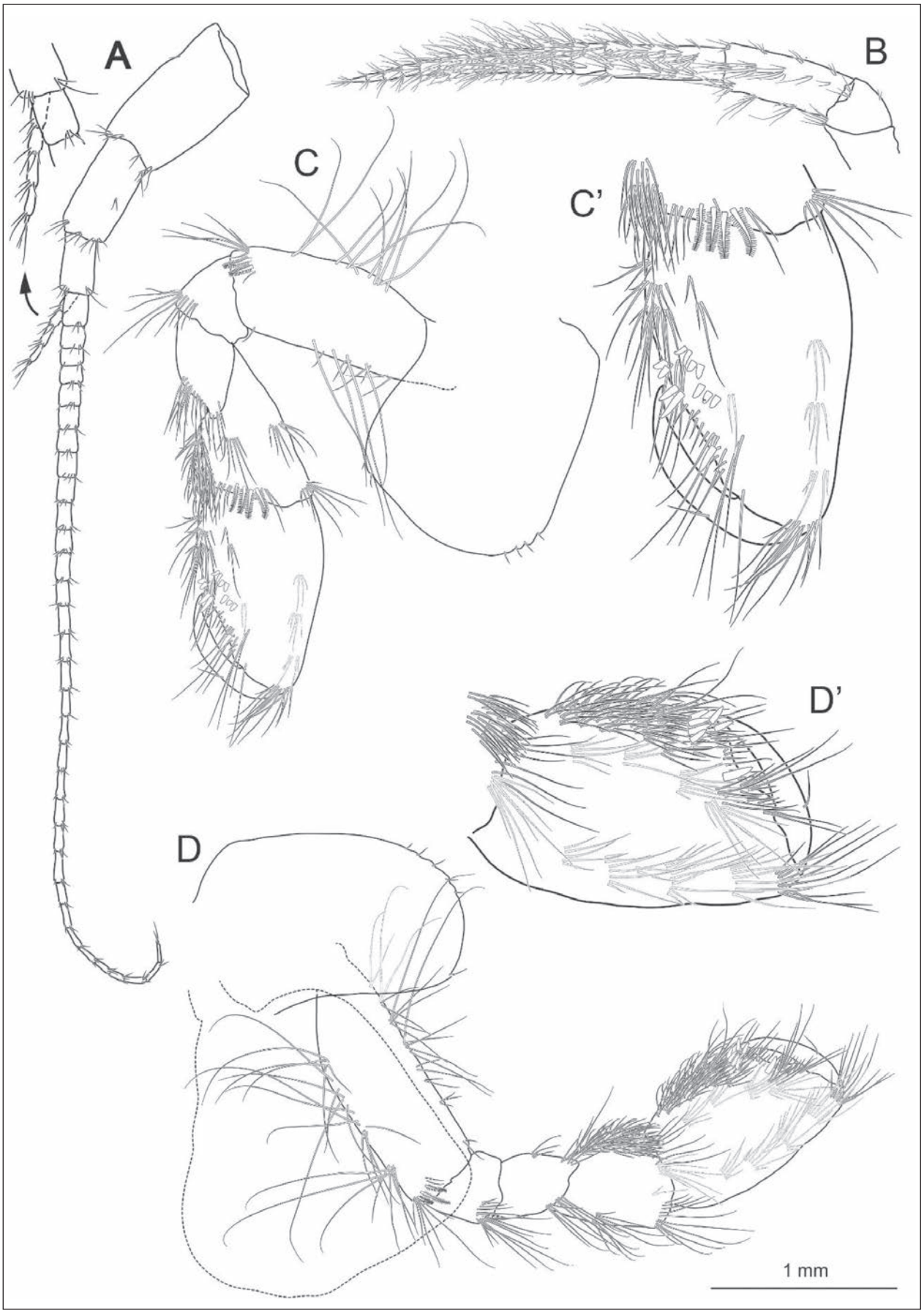

Figure 4. Extremities of the holotype male of *Gammarus sezgini* sp. nov. **A.** Antenna 1; **B.** Antenna 2; **C.** Gnathopod 1; **C'.** Palm of Gnathopod 1; **D.** Gnathopod 2; **D'.** Gnathopod 2.

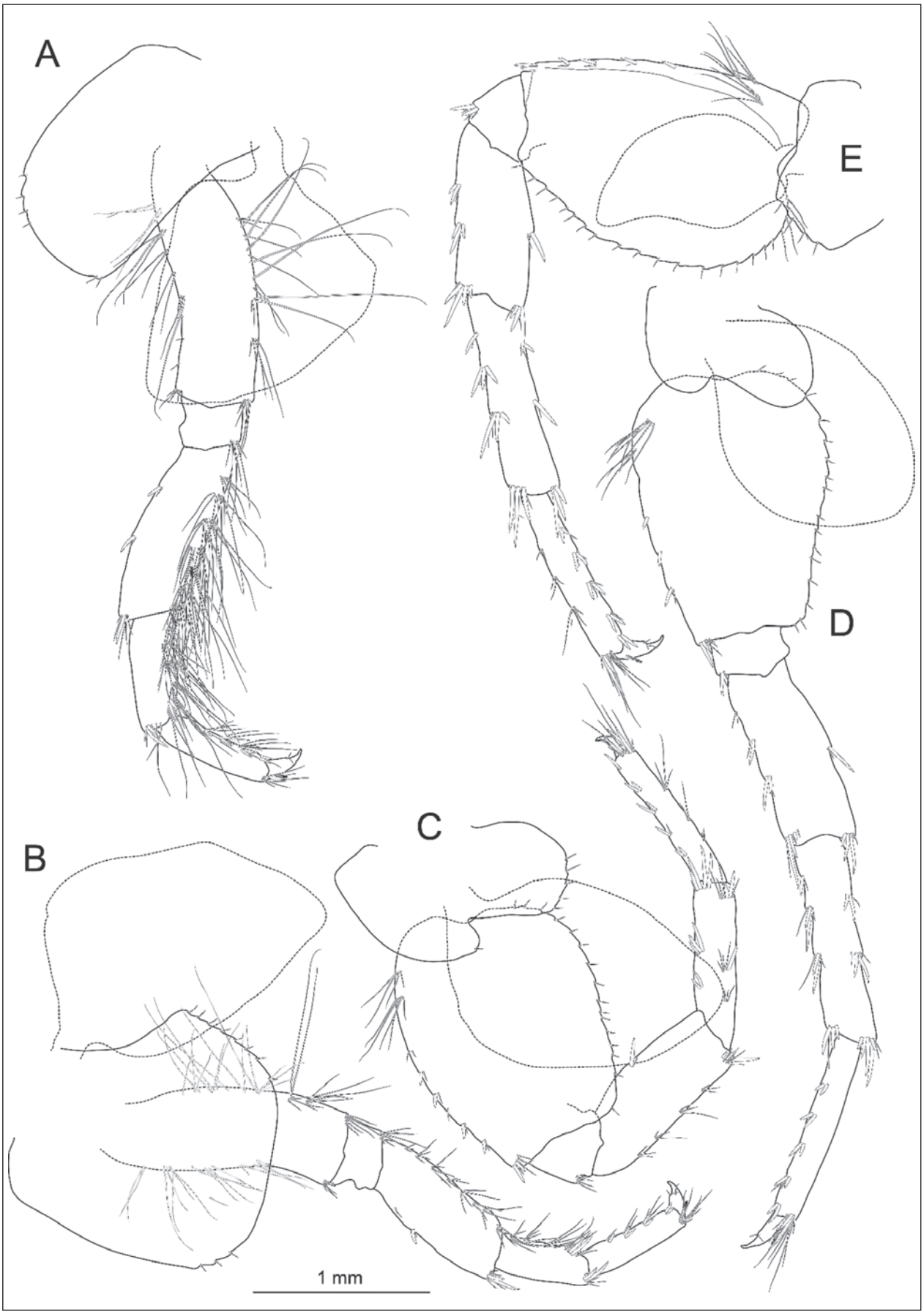

Figure 5. Pereopods of the holotype male of *Gammarus sezgini* sp. nov. **A.** Pereopod 3; **B.** Pereopod 4; **C.** Pereopod 5; **D.** Pereopod 6; **E.** Pereopod 7.

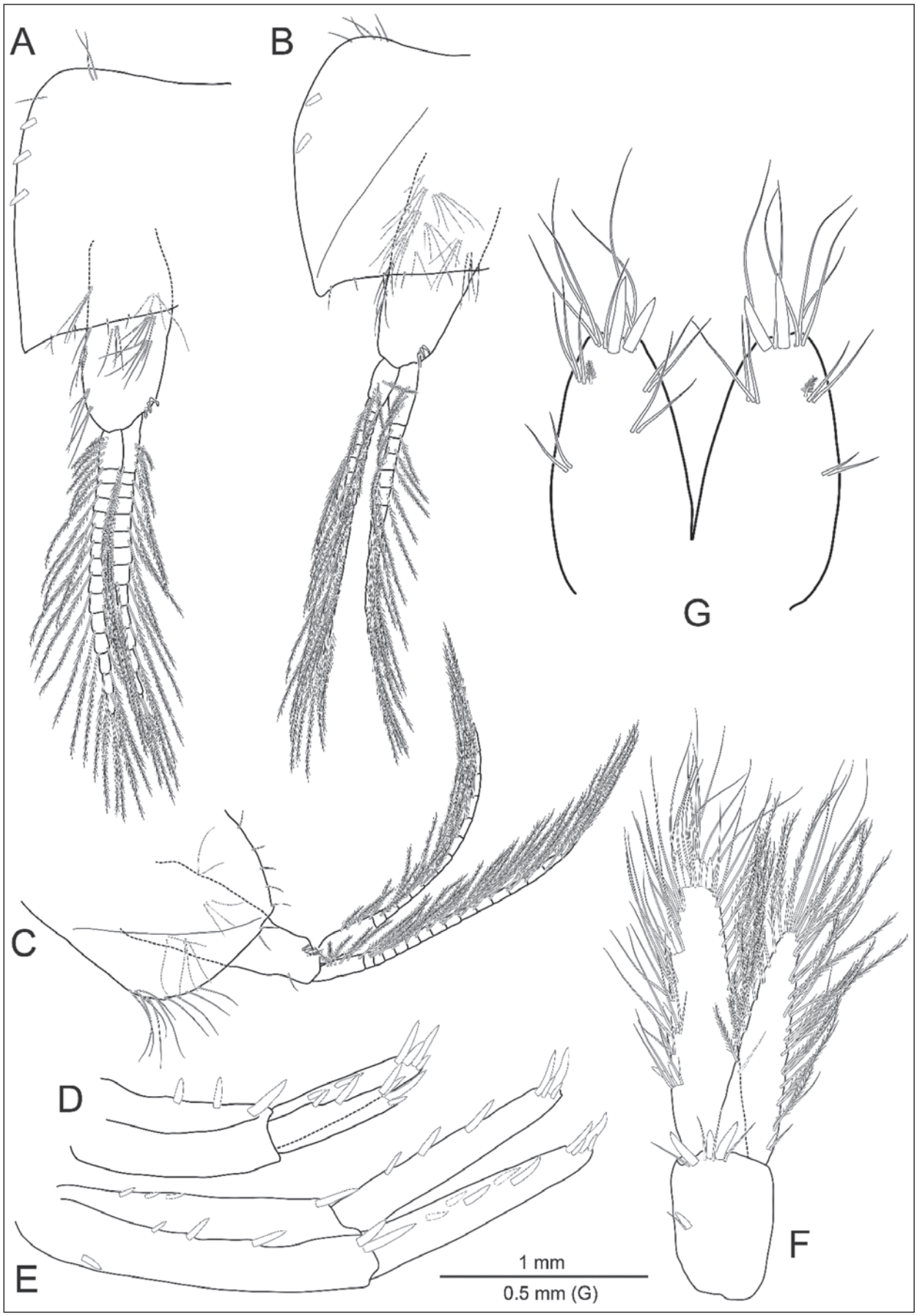

Figure 6. Extremities of the holotype male of *Gammarus sezgini* sp. nov. **A.** Pleopod 3 and Epimeral plate 3; **B.** Pleopod 2 and Epimeral plate 2; **C.** Pleopod 1 and Epimeral plate 1; **D.** Uropod 2; **E.** Uropod 1; **F.** Uropod 3; **G.** Telson.

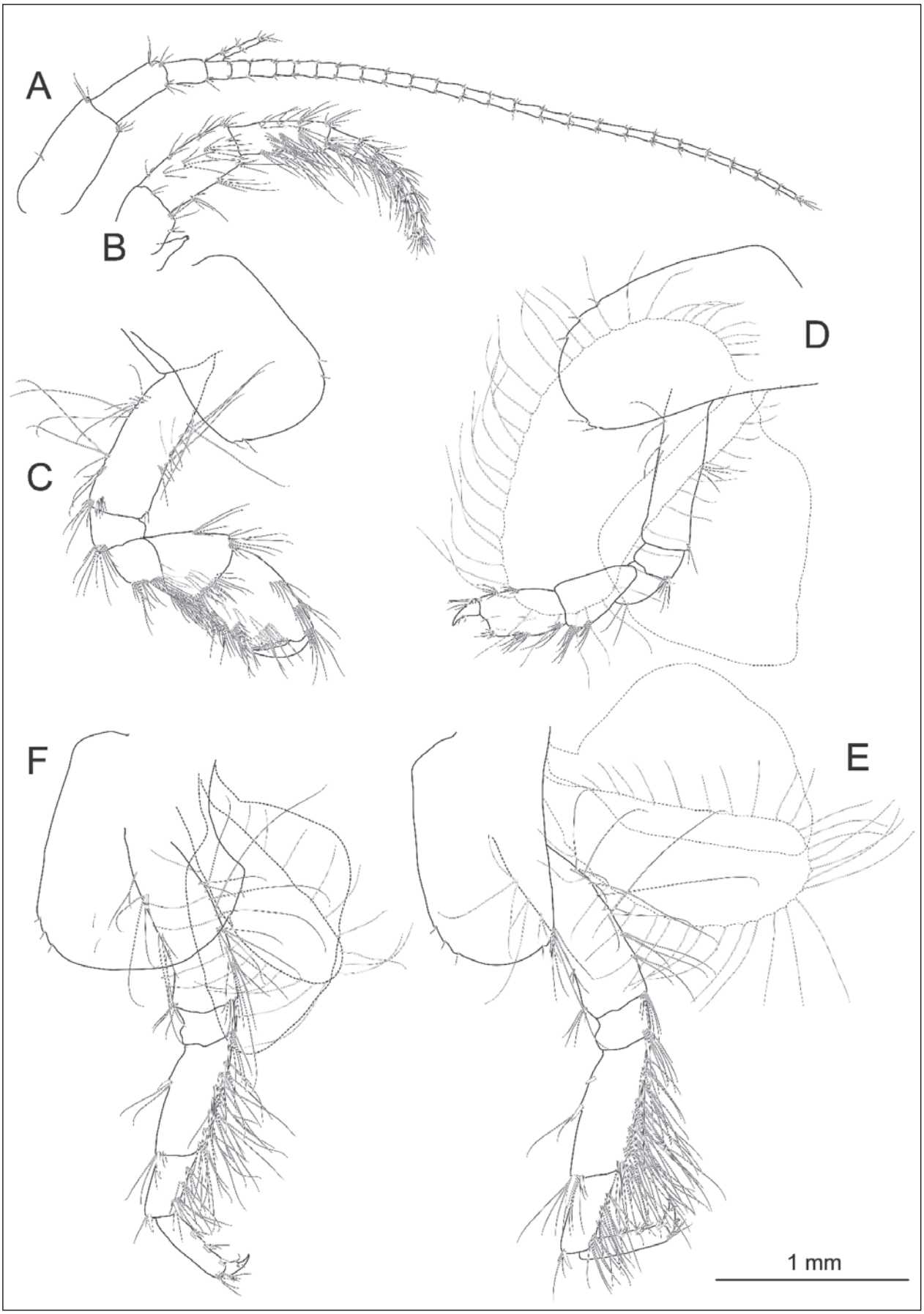

Figure 7. Appendages of the allotype female of *Gammarus sezgini* sp. nov. **A.** Antenna 1; **B.** Antenna 2; **C.** Gnathopod 1; **D.** Gnathopod 2; **E.** Pereopod 3; **F.** Pereopod 4.

Maxilla 2 (Fig. 3C) has 20–30 simple setae in the distal part of the outer lobe and a few tiny hairs along the outer margin. The inner lobe also has 10–15 simple setae in the distal part in addition to 14–15 (two of them lost) plumose setae located in a diagonal row along the inner margin. There are also a few tiny hairs on the proximal part of the inner margin of the lobe.

Maxilliped (Fig. 3D) inner plate has three tooth-like spines and a spine in the distal part and the distal corner, respectively. Additionally, there are 10 plumose setae along the inner margin of the lobe. Outer plate armed with 5–6 serrate stout setae in the distal part and 12 spines along its inner margin.

Coxal plates: Coxal plate 1 (Fig. 4C) is rectangular, the distal part slightly widened, the ventral margin slightly convex, and bears four antero-distal setae and two postero-distal setae. Coxal plate 2 (Fig. 4D) is in the shape of an elongated rectangle; distal part narrower than the proximal; the ventral margin is highly convex; anterodistal part with five setae; and postero-distal part with one seta. Coxal plate 3 (Fig. 5A) is similar to coxal plate 2 in shape, with four and two setae in the antero- and postero-distal ends, respectively. The ventral edge of the coxal plate 4 (Fig. 5B) is slightly convex and bears three and eight setae along the anteroventral and posterior margins, respectively. Coxal plate 5 (Fig. 5C) bilobate and has one and five setae in the anterior and posterior lobes, respectively. Coxal plate 6 (Fig. 5D) bilobate and has one seta in the posterior lobe. Coxal plate 7 (Fig. 5E) is characterized by the presence of four setae on the postero-ventral margin.

Gnathopods: Basal segment of gnathopod 1 (Fig. 4C, C') bears many long setae along both margins; the length of the setae can be longer than twice the diameter of the segment. Ischium bears a group of setae in postero-ventral corner. Merus is in diamond shape and bears some setae along its disto-posterior margin. Carpus is triangular and bears two groups of setae along the anterior margin, in addition to many setae groups on both ventral and posterior sides. Propodus pyriform, the length/width ratio is 1:0.60; anterior margin with four groups of setae; medial palmar spine is present; posterodistal corner armed with two strong spines in addition to some small spines; posterior margin bears 4–5 groups of setae. Dactylus reaches the postero-distal corner and bears a simple seta along the outer margin in addition to a small setule around the distal part of the inner margin.

The basis and ischium of gnathopod 2 (Fig. 4D, D') are similar to those of gnathopod 1 but have denser setae. Merus and carpus are more setose than those of gnathopod 1. Carpus is triangular, densely setose along the posterior margin, in addition to two groups of setae along the anterior margin. Propodus is densely setose and has a sub-rectangular shape; the length/width ratio is 1: 0.6; anterior margin bears six groups of setae; posterior margin with many groups of setae; medial palmar spine is present; the postero-distal corner is armed with six strong spines. Dactylus reaches the postero-distal corner and bears a simple seta along the outer margin in addition to a small setule around the distal part of the inner margin.

Pereopods: Anterior and posterior margins of the basal segment of pereopod 3 bear long setae; the setae along the posterior margin are longer than those in the anterior margin; posterior margins of the merus, carpus, and propodus bear long setae; the setae can be more than three times the diameter of the segment where they are implanted. Dactylus slim, a minute plumose seta occurs on the outer margin; the inner margin with two small setules (Fig. 5A).

The basal segment of pereopod 4 (Fig. 5B) has a similar setation to that of pereopod 3. Ischium, merus, carpus, and propodus have groups of setae along their posterior margins, but they are much shorter and less than those in pereopod 3. The length of the setae can be as long as (or slightly longer) than the diameter of the segment where they are implanted. Dactylus slim, a minute plumose seta, occurs on the outer margin; the inner margin with two small setules.

Posterior margins of the basal segments of pereopods 5 to 7 (Fig. 5C–E) are more or less convex and bear many short setae, anterior margins with 3–7 small spines, and no setae present on the inner surfaces of the basal segments; no spine exists in the postero-ventral corner of the basal segment of pereopod 7. Pereopod 7 bears no setae along the anterior margins of merus and carpus, while pereopods 5 and 6 have a few setae accompanying spines along with the mentioned segments. Propodus of pereopods 5 to 7 with 2–3 groups of long setae groups along their outer margins in addition to 5–6 groups of small spines along their inner margins. Dactylus slim, a minute plumose seta, occurs on the outer margin; the inner margin with two small setules.

Epimeral plates: They are slightly pointed. Epimeral plate 1 (Fig. 6C) bears 10 long setae along the anteroventral margin, and the postero-ventral corner is angular. Epimeral plate 2 (Fig. 6B) bears five setae in the anteroventral corner; the ventral margin is armed with two spines; the posterior margin with 4–5 setules; the postero-ventral corner is pointed. Epimeral plate 3 (Fig. 6A) is pointed; the anteroventral corner bears two setae; the ventral margin is armed with three spines in addition to a seta; the posterior margin bears 5–6 setules.

Urosomites: Not elevated (Fig. 2). Each segment bears a median and two dorsolateral groups of armaments; each of them consists of 1–2 spines and 3–4 accompanying setae.

Uropods: Uropod 1 (Fig. 6E) has a spine in the outer margin of the base; inner margins bear 4+5 spines; the peduncle is longer than rami; the length ratio is about 1:0.7. Peduncle with a spine in the outer margin of the proximal part in addition to three spines along the inner margin and three spines in the distal part. The inner ramus is slightly longer than the outer ramus and bears three spines along their inferior margin in addition to 4–5 distal spines. The outer ramus has two and three spines along the inferior and outer margins in addition to 4–5 distal spines, respectively.

Uropod 2 (Fig. 6D) is smaller than the first one; the length ratio is about 1:0.6; the peduncle segment is slightly longer than the rami and bears 2+1 spines along the inner margin and the distal part, respectively. The outer margin is bare. The length and armaments of both rami are similar to each other; they bear two spines along their

inner margins in addition to 4–5 longer spines on their distal tips.

Uropod 3 (Fig. 6F) is setose and bears both simple and plumose setae. The peduncle segment is much shorter than the outer ramus, and the length ratio is about 1:0.48. The outer ramus is two articulated and densely setose along both margins; the outer margin bears three groups of spines accompanied by groups of long simple setae; the inner margin with plumose setae; the second article is well developed and longer than the surrounding distal spines. The inner ramus is about 0.78 times the length of the outer ramus. It bears one spine in the proximal part of the outer margin in addition to groups of simple and plumose setae; the inner margin bears both simple and plumose setae.

Telson: Telson (Fig. 6G) lobes cleft; each lobe bears two spines and 5–6 simple setae in their distal parts. The setae are twice as long as the spines. There are 3–4 groups of short setae on the dorsal surface of the lobes in addition to two plumose setules. The length/width ratio of each lobe is about 1:0.5.

Description of females. Smaller than males. Except for the sexual dimorphism indicated for the genus *Gammarus*, females do not show obvious differences from males. At first glance, the morphological differences between the female allotype and the male holotype can be listed as follows: More setose antenna 2, less setose and small gnathopod 2, more setose pereopod 4; more setose anterior margins of pereopods 5 to 7 (Figs 7, 8).

Variability. Some of the paratypes are immature. The eyes are kidney-shaped, or elongated, and oval. The number of flagellar segments in antenna 1 varies between 26 and 29. Similarly, there are 10–11 flagellar segments in antenna 2.

Etymology. The species epithet is derived from the name of our dear friend Prof. Dr. Murat Sezgin (R.I.P.), who made valuable contributions to the marine amphipod species in Türkiye.

Results of molecular data analyses

We tested the new species with molecular methods as well as morphological characters. For this, firstly, the COI (573 bp.) and 28S (911 bp.) genes of the new species from type and paratypes were amplified and sequenced. The obtained sequences were deposited in Genbank with the corresponding accession numbers: PP457381–PP457385 for COI and PP456724–PP456728 for 28S. For molecular comparison, sequences of topotype samples of valid congeners of the new species or otherwise correct sequences of valid species were downloaded from GenBank (see Table 1) and used in all analyses.

The pairwise genetic distance amongst *Gammarus* species based on the COI was calculated to range from 5.24% (*G. stankokaramani* G. Karaman, 1976 - *G. salemaai* G. Karaman, 1985) to 28.97% (*G. sezgini* sp. nov. - *G. roeselii* Gervais, 1835). The species most closely related to *G. sezgini sp. nov.* is *G. tumaf* Özbek, Aksu & Baytaşoğlu, 2023, with 17.10%, approximately three times larger than the minimum genetic distance. The pairwise genetic distance amongst *Gammarus* species based on the 28S was calculated to range from 0.11% (*G. halilicae* G. Karaman, 1969 - *G. pljakici* G. Karaman, 1964) to 7.73% (*G. rambouseki* G. Karaman, 1931 - *G. stojicevici* (S. Karaman, 1929)). The species most closely related to *G. sezgini* sp. nov. is *G. kesslerianus* Martynov, 1931, with 0.88%, eight times larger than the minimum genetic distance. All pairwise genetic distance values calculated with the *p*-distance model based on COI and 28S genes amongst *Gammarus* species are given in Suppl. material 1.

Phylogenetic trees constructed with ML, NJ, and BI methods based on the concatenated dataset (28S+COI) showed similar topologies with a few exceptions and had high bootstrap (ML and NJ BP≥70%; Fig. 9) and posterior probability (BI PP≥0.7; Fig. 9) support for a large number of nodes. In the phylogenies constructed according to all three methods, the newly identified species, *G. sezgini* sp. nov., formed the sister clade of the *G. kunti* Özbek, Baytaşoğlu & Aksu, 2023, *G. tumaf*, and *G. baysali* Özbek, Yurga & Külköylüoğlu, 2013 (*G. sezgini* sp. nov., (*G. kunti*, (*G. tumaf* + *G. baysali*))) and was resolved from it with strong support (ML BP: 78%, NJ BP: 70%, and BI PP: 1.0; Fig. 9).

The species delimitation analysis we performed according to the ASAP method identified 27 MOTUs for 27 morphologically valid species (Fig. 9). The best ASAP score was 3.0 (p = 0.01) at a threshold distance of 0.079053. The analysis identified the species *G. stankokaramani* and *G. salemaai* as a single MOTU, while the Bulgarian and Iranian samples of *G. komareki* were identified as separate MOTUs. The PTP method identified 28 MOTUs for 27 species (Fig. 9). p=0.001, null-model score: 84.937039, best score for single coalescent rate: 95.647569. Similar to ASAP, Bulgarian and Iranian samples of *G. komareki* formed separate MOTUs, while unlike ASAP, *G. stankokaramani* and *G. salemaai* species also formed separate MOTUs. *Gammarus sezgini* sp. nov. formed a single MOTU independently of other species according to both methods (Fig. 9).

Discussion

The consensus of morphological and molecular findings has shown that the Balat, Taşlı, and Yeşildere streams at Rize province populations of *Gammarus* are distinct from their congeners and should be recognized as a separate species. *Gammarus sezgini* sp. nov. belongs to the *G. komareki*-group due to the characteristic setation of the posterior part of pereopod 3 and 4, the setation of antenna 2 and uropod 3 (Karaman and Pinkster 1977).

At first glance, the newly identified species looks similar to *G. komareki* by the setation of the antenna 2, pereopod 3, and uropod 3, by the presence and the shape of the eyes; but *G. sezgini* sp. nov. differs from *G. komareki* by having a longer antennal gland cone, having fewer D-setae (33) in the third segment of the mandible palp,

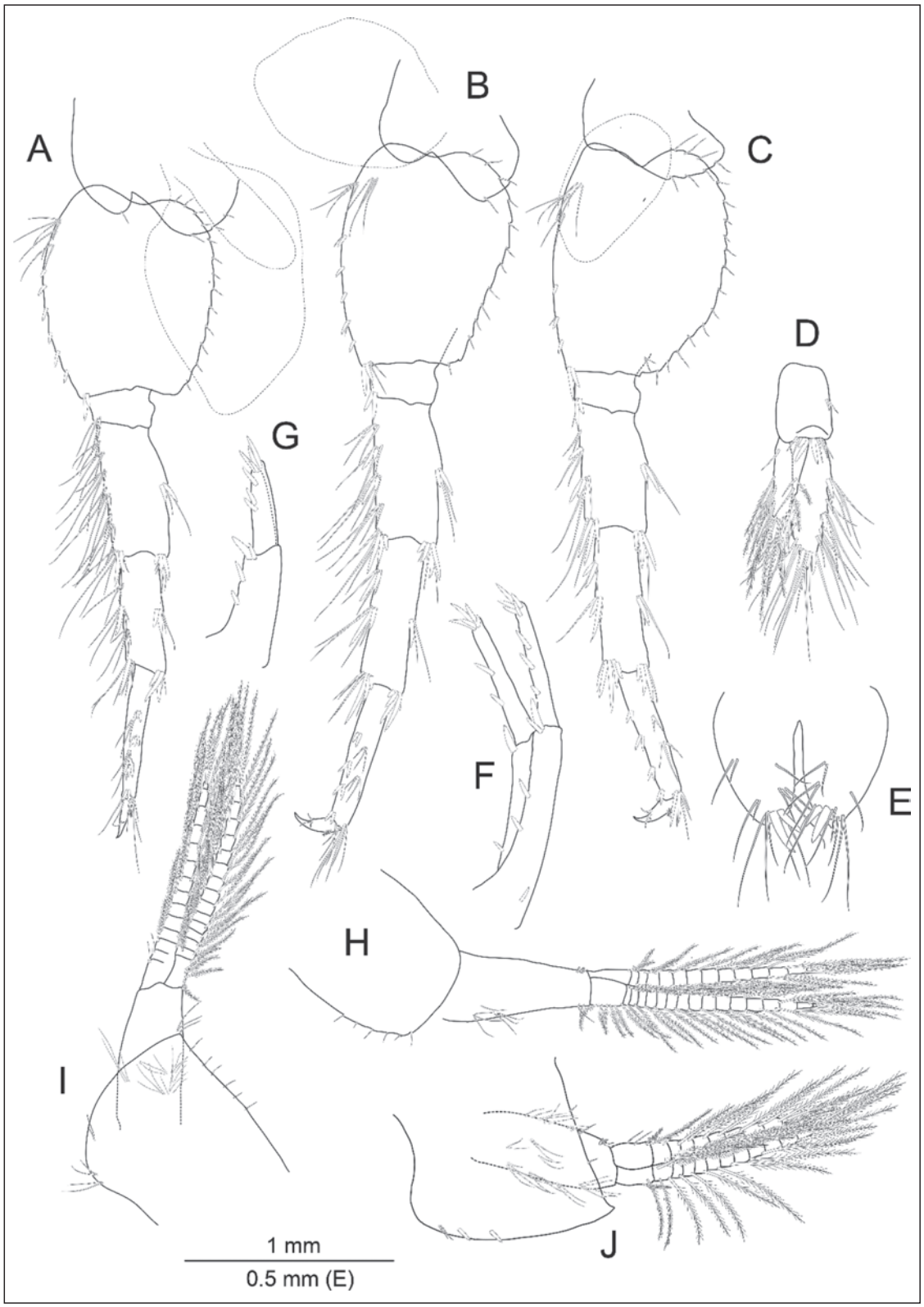

Figure 8. Appendages of the allotype female of *Gammarus sezgini* sp. nov. **A.** Pereopod 5; **B.** Pereopod 6; **C.** Pereopod 7; **D.** Uropod 3; **E.** Telson; **F.** Uropod 1; **G.** Uropod 2; **H.** Pleopod 1 and Epimeral Plate 1; **I.** Pleopod 2 and Epimeral Plate 2; **J.** Pleopod 3 and Epimeral Plate 3.

having shorter setae on the ventral part of the peduncular segment of the antenna 2, and having a longer antenna 1, having fewer setae along the posterior margins of pereopod 3 and 4, by the absence of setae along the anterior margins of merus and carpus of pereopod 7.

Gammarus komareki has been recorded from the Black Sea coasts, Eastern Europe, the Balkans, and Iran in previous studies (Copilaş-Ciocianu et al. 2014; Grabowski and Pešic 2007; Zamanpoore et al. 2011). The species was reported from the Zonguldak, Trabzon, Sinop, and

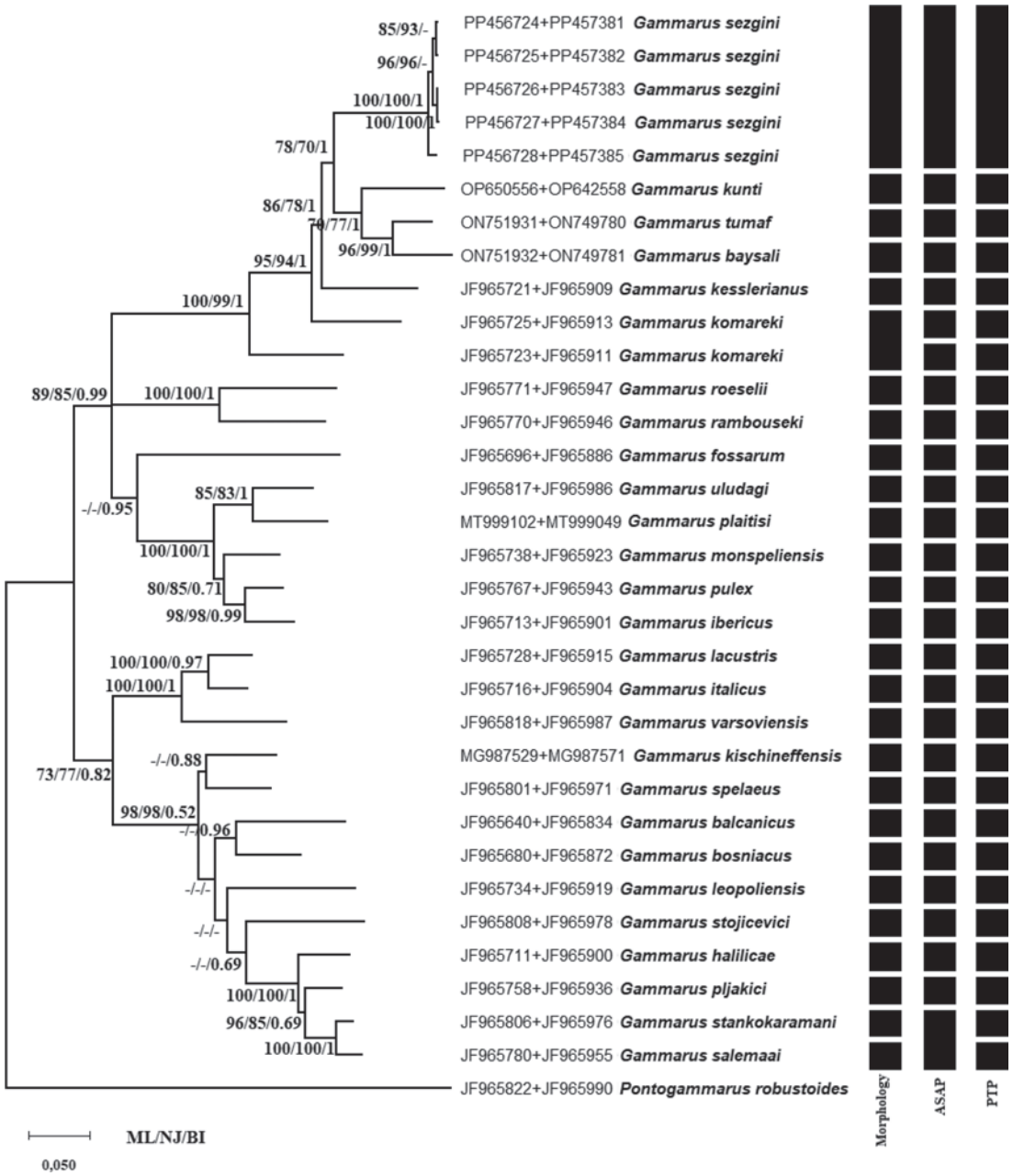

Figure 9. Phylogenetic relationships of *Gammarus* species reconstructed with the ML method based on the concatenated data set (28S+COI). Since the ML, NJ, and BI methods generally yield similar topologies, only the ML phylogeny is shown. The nodes (ML, NJ, and BI) show the Bayesian posterior probabilities and the bootstrap percentage. For the support values of the nodes, ML ≥ 70%, NJ ≥ 70%, and BI ≥ 0.70 are shown. Black bars indicate OTUs. The first column shows morphology-based results, the second column shows ASAP results, and the third column shows PTP results.

Rize provinces previously (Karaman 2003; Özbek 2011). Additionally, it was reported from the inland waters of Gökçeada Island (Özbek and Özkan 2017), from the lakes of the Western Black Sea Region and the Sakarya River Basin (Özbek 2008), from the inland waters of Sinop and Samsun provinces (Akbulut et al. 2009), and from the inland waters of Ordu (Ekinci and Miroğlu 2016).

Due to the lack of detailed sampling in the rivers in the Eastern Black Sea Basin, it is likely that the species *G. sezgini* sp. nov. has been diagnosed as *G. komareki* or has not been reached. The present study reveals the morphological and molecular differences between the two species in detail.

Gammarus obruki Özbek, 2012, *G. baysali*, *G. tumaf*, and *G. kunti* have been recently identified from four different caves (Inderesi Cave/Bartın province, Cumayanı Cave/Zonguldak province, Gökgöl Cave/Zonguldak province, and Fakıllı Cave/Düzce province, respectively) within the Western Black Sea Basin (Özbek 2012; Özbek et al. 2013; Özbek et al. 2023a, 2023b). They are the closest relatives of the newly described species due to their presence in geographically close localities and their morphological similarities. The four species mentioned above, including *Gammarus sezgini* sp. nov., are morphologically very similar to *G. komareki*, especially due to the dense setation on the flagellum and peduncle

segments of antenna 2. As a result of the study, morphological and genetic similarities and differences were defined in detail (Table 2, Fig. 9).

Gammarus sezgini sp. nov. is similar to *G. obruki* in that it has a yellowish body color, kidney-shaped eyes, and densely setose flagellum and peduncle segments of antenna 2. But the newly described species is almost half the size of *G. obruki*, has a much shorter antenna 1 (52 vs. 32 segments), and no elongated extremities. Additionally, the inner ramus of the uropod 3 is shorter in the newly identified species (Table 2).

Although the newly described species is similar to *G. baysali* in having setose antenna 2, it is quite different from it in terms of both morphological characters and habitat. *G. baysali*, like *G. obruki*, is a large species and is approximately 2 times larger than the newly described species. Additionally, *G. baysali* is a hypogean eyeless species and has elongated extremities. *Gammarus sezgini* sp. nov. is an epigean species with well-developed kidney-shaped eyes and does not have elongated extremities. Although there are spines and setae on the anterior margins of pereopods 6 and 7 in *G. baysali*, the newly described species has no setae along the mentioned margins. While the inner lobe/outer lobe length ratio is 0.9 in the third uropod of *G. baysali*, this ratio is 0.78 in *G. sezgini* sp. nov. (Table 2).

The newly described species is similar to *G. kunti* in having kidney-shaped eyes and setose antennae 1 and 2, but differs from it in the following features: Its body has a yellowish rather than whitish color; it bears one seta instead of two along the anterior margin of the inner lobe of the right maxilla 1; the inner lobe of the right maxilla bears more than 14 plumose setae. In addition, the 2nd and 3rd epimeral plates are more pointed, and the telson lobes bear more and longer setae on the dorsal surface and the distal part (Table 2).

Gammarus sezgini sp. nov. differs from *G. tumaf* by having kidney-shaped eyes, a less setose inner lobe of right maxilla 1 (16–17 vs. 20), the armaments of the palp of maxilla 1, having fewer plumose setae on maxilla 2 (14–15 vs. 20), and having more setose telson. Additionally, the newly identified species has 33 D-setae, while the number is 28 in *G. tumaf* (Table 2).

Although the newly described species is similar to *G. kesslerianus* in having a setose second antenna 2, *Gammarus sezgini* sp. nov. differs from it in having almost half a smaller body length (20 mm vs. 9.8 mm), a shorter flagellum of antenna 2 (13 vs. 17 segments), and a shorter inner lobe of uropod 3.

Anatolia is a peninsula very rich in biodiversity, as it is located at the intersection of three different biodiversity hot spots. The presence of several unique habitats is an important factor in increasing the number of endemic species on the peninsula. Türkiye's Black Sea region hosts fast-flowing streams that are generally fed by snow water. The authors believe that *G. komareki*, which is a typical species of these types of habitats, still contains many cryptic and undefined species and should be ex-

Table 2. Some morphological features of *Gammarus sezgini* sp. nov. and its sister species (*G. baysali*, *G. tumaf*, *G. kunti*) and *G. obruki* (reproduced from Özbek et al. 2023a).

Characters	*Gammarus sezgini* sp. nov.	*G. obruki*	*G. baysali*	*G. tumaf*	*G. kunti*	*G. komareki*
Body length	9.8 mm	21.0 mm	18.1 mm	12.6 mm	11.5 mm	15 mm
Eyes	kidney-shaped	kidney-shaped	eyeless	minute	kidney-shaped	reniform
Body color	yellowish	yellowish	colorless, whitish	whitish	whitish	
Antenna 1	32+5 flagellar segments	52+6 flagellar segments	41+6 flagellar segments	30+5 flagellar segments	32+6 flagellar segments	39+5 flagellar segments
Antenna 2	peduncular and flagellar segments densely setose; flagellum 12 segmented	fifth peduncular and flagellar segments densely setose; flagellum 17 segmented	peduncular and flagellar segments setose; flagellum 20 segmented	peduncular and flagellar segments densely setose; flagellum 13 segmented	peduncular and flagellar segments densely setose; flagellum 15 segmented	peduncular and flagellar segments densely setose; flagellum 13 segmented
Antennal gland cone	straight, reaches to the distal end of the third peduncular segment	straight, not reaches to the distal end of the third peduncular segment	straight, reaches to the distal end of the third peduncular segment	straight, reaches to the distal end of the third peduncular segment	straight, reaches to the distal end of the third peduncular segment	Short, about half as long as the third peduncle segment
Inner lobe of right maxilla 1	with 16 (17) plumose setae	with 18 plumose setae	with 19 plumose setae	with 20 plumose setae	with 14 plumose setae	No data in original description
Palp of right maxilla 1	6 stout spines, 1 seta along the anterior margin	6 stout spines, 3 setae along the anterior margin	6 stout spines, 4 setae along the anterior margin	5 stout spines, 2 setae along the anterior margin	6 stout spines, 2 setae along the anterior margin	No data in original description
Maxilla 2	inner lobe with 14–15 plumose setae	inner lobe with 21 plumose setae	inner lobe with 21 plumose setae	inner lobe with 20 plumose setae	inner lobe with 15 plumose setae	No data in original description
Number of D-setae	33	37	34	28	28	40
Pereopods	not elongated	slightly elongated	elongated	not elongated	not elongated	No data in original description
Pereopods 6–7	anterior margins without setae	anterior margins without setae	anterior margins with setae	anterior margins without setae	anterior margins without setae	anterior margins without setae
Uropod 3	setose, inner/outer lobe ratio: 0.78	setose, inner/outer lobe ratio: 0.9	setose, inner/outer lobe ratio: 0.9	setose, inner/outer lobe ratio: 0.75	setose, inner/outer lobe ratio: 0.77	setose, inner/outer lobe ratio: 0.75
Telson (each lobe)	with 2 distal spines and 5–6 longer setae; l/w ratio 1:0.5	with 1–2 distal spines and 3–4 longer setae; l/w ratio 1:0.5	with 2 distal spines and 4–5 longer setae; l/w ratio 1:0.5	with 2 distal spines and 3–4 longer setae; l/w ratio 1:0.5	with 2 distal spines and 3–4 longer setae; l/w ratio 1:0.5	with 2 distal spines and 3–4 longer setae; l/w ratio 1:0.5

amined in detail from both molecular and morphological perspectives. Such an integrative approach would help highlight the true biodiversity of gammarids in Anatolia.

Acknowledgments

This work was financially supported by TUBITAK (Project No. 119Y006). The authors would like to thank TUBITAK for their financial support.

References

Akbulut M, Ustaoğlu MR, Çelik EŞ (2009) Freshwater and Brackish Water Malacostraca (Crustacea-Arthropoda) Fauna of Sinop and Samsun and Their Ecology. Journal of the Black Sea/Mediterranean Environment 15: 47–60.

Albayrak E, Özuluğ O (2016) Danamandıra Gölü (Silivri-İstanbul) Bentik Makro Omurgasızları. Turkish Journal of Aquatic Science 31: 51–58. https://doi.org/10.18864/TJAS201606

Bacescu M (1954) Fauna Repulicii Populare Romine, Crustacea 4(3). Academia Republicii Populare Romine, 126 pp.

Balık S, Ustaoğlu MR, Özbek M, Taşdemir A, Yıldız S (2004) Buldan Baraj Gölü'nün (Denizli-Türkiye) Bentik Faunası. Ege Üniversitesi Su Ürünleri Dergisi 21: 139–141.

Baytaşoğlu H, Gözler AM (2018) Seasonal Changes of Malacostraca (Crustacea) Fauna of the Upper Çoruh River Basin (Bayburt Province, Turkey) and Its Ecological Characteristics. Turkish Journal of Fisheries and Aquatic Sciences 18(3): 367–375. https://doi.org/10.4194/1303-2712-v18_3_02

Coifman I (1938) Nota Sul Potamon Edule, Dell'anatolia. Bollettino di Zoologia 17(1): 223–225. https://doi.org/10.1080/11250003809437002

Coleman CO (2003) "Digital inking": How to make perfect line drawings on computers. Organisms Diversity & Evolution. Organisms, Diversity & Evolution 3(4, Supplement 14): 1–14. https://doi.org/10.1078/1439-6092-00081

Copilaş-Ciocianu D, Grabowski M, Parvulescu L, Petrusek A (2014) Zoogeography of Epigean freshwater Amphipoda (Crustacea) in Romania: Fragmented distributions and wide altitudinal variability. Zootaxa 2: 243–260. https://doi.org/10.11646/zootaxa.3893.2.5

Copilaş-Ciocianu D, Zimţa AA, Grabowski M, Petrusek A (2018) Survival in northern microrefugia in an endemic Carpathian gammarid (Crustacea: Amphipoda). Zoologica Scripta 47(3): 357–372. https://doi.org/10.1111/zsc.12285

Costa FO, Henzler CM, Lunt DH, Whiteley NM, Ock J (2009) Probing Marine *Gammarus* (Amphipoda) Taxonomy with DNA Barcodes. Systematics and Biodiversity 7(4): 365–379. https://doi.org/10.1017/S1477200009990120

Ekinci M, Miroğlu A (2016) Ordu İli (Türkiye) Tatlısu Gammaridea (Crustacea, Amphipoda) Üzerine Araştırma. Ordu Üniversitesi Bilim ve Teknoloji Dergisi 6: 158–169.

Felsenstein J (1981) Evolutionary trees from DNA sequences: A maximum likelihood approach. Journal of Molecular Evolution 17(6): 368–376. https://doi.org/10.1007/BF01734359

Felsenstein J (1985) Confidence Limits on Phylogenies: An Approach Using the Bootstrap. Evolution; International Journal of Organic Evolution 39(4): 783–791. https://doi.org/10.2307/2408678

Grabowski M, Pešıc V (2007) New Data on the Distribution and Checklist of Fresh- and Brackishwater Gammaridae, Pontogammaridae and Behningiellidae (Amphipoda) in Bulgaria. Lauterbornia 59: 53–62.

Hall TA (1999) BioEdit: A user–friendly biological sequence alignment editor and analysis program for Windows 95/98/NT. Nucleic Acids Symposium Series 41: 95–98.

Horton T, Lowry J, De Broyer C, Bellan-Santini D, Copilaş-Ciocianu D, Corbari L, Costello MJ, Daneliya M, Dauvin J-C, Fišer C, Gasca R, Grabowski M, Guerra-García JM, Hendrycks E, Hughes L, Jaume D, Jażdżewski K, Kim Y-H, King R, Krapp-Schickel T, LeCroy S, Lörz A-N, Mamos T, Senna AR, Serejo C, Souza-Filho JF, Tandberg AH, Thomas JD, Thurston M, Vader W, Väinölä R, Valls Domedel G, Vonk R, White K, Zeidler W (2024) World Amphipoda Database. Senticaudata. World Register of Marine Species. https://www.marinespecies.org/aphia.php?p=taxdetails&id=719424 [on 2024-03-12]

Hou Z, Fu J, Li S (2007) A molecular phylogeny of the genus *Gammarus* (Crustacea: Amphipoda) based on mitochondrial and nuclear gene sequences. Molecular Phylogenetics and Evolution 45(2): 596–611. https://doi.org/10.1016/j.ympev.2007.06.006

Hou Z, Sket B, Fiser C, Li S (2011) Eocene habitat shift from saline to freshwater promoted tethyan amphipod diversification. Proceedings of the National Academy of Sciences of the United States of America 108(35): 14533–14538. https://doi.org/10.1073/pnas.1104636108

Hupało K, Karaouzas I, Mamos T, Grabowski M (2020) Molecular data suggest multiple origins and diversification times of freshwater gammarids on the Aegean archipelago. Scientific Reports 10(1): 19813. https://doi.org/10.1038/s41598-020-75802-2

İpek M, Özbek M (2022) An updated and annotated checklist of the Malacostraca (Crustacea) species inhabited Turkish inland waters. Turkish Journal of Zoology 46(1): 14–66. https://doi.org/10.3906/zoo-2109-12

Karaman GS (2003) New Data on Some Gammaridean Amphipods (Amphipoda, Gammaridea) from Palearctic. (Contribution to the Knowledge of the Amphipoda 245). Glasnik Odjeljenja Prirodnih Nauka. Crnogorska Akademija Nauka Umjetnosti Podgorica 15: 21–37.

Karaman GS, Pinkster S (1977) Freshwater *Gammarus* species from Europe, North Africa and Adjacent Regions of Asia (Crustacea-Amphipoda), Part I *Gammarus pulex*-Group and related species. Bijdragen tot de Dierkunde 47(1): 1–97. https://doi.org/10.1163/26660644-04701001

Kumar S, Stecher G, Li M, Knyaz C, Tamura K (2018) MEGA X: Molecular Evolutionary Genetics Analysis Across Computing Platforms. Molecular Biology and Evolution 35(6): 1547–1549. https://doi.org/10.1093/molbev/msy096

Özbek M (2008) Malacostraca (Crustacea) Fauna of Some Lakes Western Black Sea Region. Ege Üniversitesi Su Ürünleri Dergisi 25: 311–314.

Özbek M (2011) An Oveview of the *Gammarus* Fabricius (Gammaridae: Amphipoda) Species of Turkey, With An Updated Checklist. Zoology in the Middle East 53(1): 71–78. https://doi.org/10.1080/09397140.2011.10648863

Özbek M (2012) A new freshwater amphipod species, *Gammarus obruki* sp. nov., from Turkey (Amphipoda: Gammaridae). Turkish Journal of Zoology 36(5): 567–575. https://doi.org/10.3906/zoo-1112-2

Özbek M, Özkan N (2017) Gökçeada içsularının Amphipoda (Crustacea: Malacostraca) faunası. Ege Journal of Fisheries and Aquatic Sciences 34: 63–67. https://doi.org/10.12714/egejfas.2017.34.1.09

Özbek M, Ustaoğlu MR (1998) Amphipoda (Crustacea-Arthropoda) Fauna of İzmir and Adjacent Areas Inland-Waters. Ege Üniversitesi Su Ürünleri Dergisi 15: 211–231.

Özbek M, Ustaoğlu MR (2001) İzmir İli ve Civarı Tatlısu Malacostraca (Crustacea) Faunası (Amphipoda Hariç). Anadolu Üniversitesi Bilim ve Teknik Dergisi 2: 19–25.

Özbek M, Ustaoğlu MR (2005a) Taxonomical Investigation of Lake District Waters Malacostraca (Crustacea-Arthropoda) Fauna. Ege University Journal of Fisheries and Aquatic Sciences 22: 357–362.

Özbek M, Ustaoğlu MR (2005b) Göller Bölgesi Içsularının Malacostraca (Crustacea-Arthropoda) Faunasının Taksonomik Açıdan Incelenmesi. Ege Üniversitesi Su Ürünleri Dergisi 22: 357–362.

Özbek M, Balık S, Ustaoğlu MR, Berber S, Topkara ET (2004) Apolyont ve İznik Gölleri'nin Malacostraca (Crustacea) Faunası. Anadolu Üniversitesi Bilim ve Teknoloji Dergisi 5: 291–295.

Özbek M, Balık S, Topkara E (2007) Türkiye Tatlı Su Amphipodlarının (Crustacea: Malacostraca) Dağılımları ve Ekolojilerine Katkılar. Fırat Üniversitesi Fen ve Mühendislik Bilimleri Dergisi 19: 455–461.

Özbek M, Yurga L, Külköylüoğlu O (2013) *Gammarus baysali* sp. nov., a new freshwater amphipod species from Turkey (Amphipoda: Gammaridae). Turkish Journal of Zoology 37(2): 163–171. https://doi.org/10.3906/zoo-1209-14

Özbek M, Baytaşoğlu H, Aksu İ (2023a) A new freshwater amphipod (Amphipoda, Gammaridae) from the Fakıllı Cave, Düzce Türkiye: *Gammarus kunti* sp. nov. Zoosystematics and Evolution 99(2): 473–487. https://doi.org/10.3897/zse.99.108048

Özbek M, Aksu İ, Baytaşoğlu H (2023b) A new freshwater amphipod (Amphipoda, Gammaridae), *Gammarus tumaf* sp. nov. from the Gökgöl Cave, Türkiye. Zoosystematics and Evolution 99(1): 15–27. https://doi.org/10.3897/zse.99.89957

Posada D (2008) jModelTest: Phylogenetic model averaging. Molecular Biology and Evolution 25(7): 1253–1256. https://doi.org/10.1093/molbev/msn083

Puillandre N, Brouille S, Achaz G (2020) ASAP: Assemble species by automatic partitioning. Molecular Ecology Resources 21(2): 609–620. https://doi.org/10.1111/1755-0998.13281

Rambaut A, Drummond AJ, Xie D, Baele G, Suchard MA (2018) Posterior Summarization in Bayesian Phylogenetics Using Tracer 1.7. Systematic Biology 67(5): 901–904. https://doi.org/10.1093/sysbio/syy032

Rewicz T, Konopacka A, Bącela-Spychalska K, Özbek M, Grabowski M (2016) First Records of Two Formerly Overlooked Ponto-Caspian Amphipods from Turkey, *Echinogammarus trichiatus* (Martynov, 1932) and *Dikerogammarus villosus* (Sovinsky, 1894). Turkish Journal of Zoology 40: 328–335. https://doi.org/10.3906/zoo-1505-31

Ronquist F, Teslenko M, van der Mark P, Ayres DL, Darling A, Höhna S, Larget B, Liu L, Suchard MA, Huelsenbeck JP (2012) MrBayes 3.2: Efficient Bayesian phylogenetic inference and model choice across a large model space. Systematic Biology 61(3): 539–542. https://doi.org/10.1093/sysbio/sys029

Saitou N, Nei M (1987) The neighbor-joining method: A new method for reconstructing phylogenetic trees. Molecular Biology and Evolution 4(4): 406–425. https://doi.org/10.1093/oxfordjournals.molbev.a040454

Sarı HM, Balık S, Özbek M, Aygen C (2001) Bafa Gölü'nün Makro ve Meiobentik Omurgasız Faunası. Anadolu Üniversitesi Bilim ve Teknoloji Dergisi 2: 285–291.

Selim S (2011) Akarsu Vadisindeki İnsan Kaynaklı Faaliyetlerin Ekosistem Bütünlüğüne Olası Etkileri: Çağlayan Örneği. Süleyman Demirel Üniversitesi Fen Bilimleri Enstitüsü Dergisi 15: 94–101. https://doi.org/10.19113/sdufbed.29642

Tamura K, Nei M (1993) Estimation of the number of nucleotide substitutions in the control region of mitochondrial DNA in humans and chimpanzees. Molecular Biology and Evolution 10(3): 512–526. https://doi.org/10.1093/oxfordjournals.molbev.a040023

Thompson JD, Higgins DG, Gibson TJ (1994) CLUSTAL W: Improving The Sensitivity of Progressive Multiple Sequence Alignment Through Sequence Weighting, Position-Specific Gap Penalties and Weight Matrix Choice. Nucleic Acids Research 22(22): 4673–4680. https://doi.org/10.1093/nar/22.22.4673

Vavra (1905) Rotatorien Und Crustaceen. Annalen des K. K. Naturhistorichen Hofmuseums in Wien 20: 106–113.

Zamanpoore M, Grabowski M, Poeckl M, Schiemer F (2011) Taxonomic review of freshwater *Gammarus* (Crustacea: Amphipoda) from Iran. Zootaxa 3140(1): 1–14. https://Doi.Org/10.11646/zootaxa.3140.1.1. https://doi.org/10.11646/zootaxa.3140.1.1

Zhang J, Kapli P, Pavlidis P, Stamatakis A (2013) A general species delimitation method with applications to phylogenetic placements. Bioinformatics 29(22): 2869–2876. https://doi.org/10.1093/bioinformatics/btt499

Supplementary material 1

The pairwise genetic distance values amongst the *Gammarus* species, based on the COI datasetand 28S dataset

Authors: Hazel Baytaşoğlu, İsmail Aksu, Murat Özbek
Data type: xlsx

Link: https://doi.org/10.3897/zse.100.121692.suppl1

Zoosyst. Evol. 100 (3) 2024, 1005–1015 | DOI 10.3897/zse.100.123331

PENSOFT

für Natur MUSEUM FÜR NATURKUNDE BERLIN

Pamirosa gen. nov., unexpected record of Artoriinae (Araneae, Lycosidae) from the rooftop of Pamir, Central Asia

Alexander A. Fomichev[1], Mikhail M. Omelko[2], Yuri M. Marusik[3,4]

1 *Altai State University, Lenina Pr., 61, Barnaul, RF-656049, Russia*

2 *Federal Scientific Center of East Asia Terrestrial Biodiversity, Far Eastern Branch, Russian Academy of Sciences, Vladivostok 690022, Russia*

3 *Institute of Biological Problems of the North, Far Eastern Branch, Russian Academy of Sciences, Portovaya Str., 18, Magadan 68500, Russia*

4 *Department of Zoology & Entomology, University of the Free State, Bloemfontein 9300, South Africa*

https://zoobank.org/FDF2CBE1-60D9-42B3-B33C-481C54B22712

Corresponding author: Alexander A. Fomichev (a.fomichov@mail.ru)

Academic editor: Danilo Harms ♦ **Received** 18 March 2024 ♦ **Accepted** 12 June 2024 ♦ **Published** 12 July 2024

Abstract

A new monotypic genus, *Pamirosa* **gen. nov.** with the type species *P. kudratbekovi* **sp. nov.** (♂♀), is described from Pamir Mountains in eastern Tajikistan. The new genus represents the first record of the mainly Australasian subfamily Artoriinae Framenau, 2007 in Central Asia. It differs from all known genera of Artoriinae, as well as from all other lycosids, by having a unique spiraled embolus and epigyne with screw-shaped membranous copulatory ducts unknown in other wolf spiders. The new species was collected among stone screes at an elevation of 4700 meters. Unlike all other Palaearctic lycosids inhabiting stony screes and possessing four or more pairs of ventral tibial spines on leg I, *Pamirosa* **gen. nov.** has only three pairs. Description, figures, diagnosis of the new species, and a photograph of its habitat are provided. Additionally, the distribution of scree-dwelling Lycosidae in Asia is discussed.

Key Words

Aranei, biodiversity, new genus, new species, Palaearctic, Pardosinae, spiny-legs Lycosidae

Introduction

Lycosidae Sundevall, 1833, commonly known as wolf spiders, is one of the largest spider families, currently encompassing 2476 extant species in 132 genera (WSC 2024). The family has worldwide distribution, ranging from Peary Land (82°30'N, Marusik et al. 2006) to Navarino Island (55°S: Tullgren 1901: 254). The altitudinal distribution of Lycosidae is also wide, from the shores of Dead Sea (–400 m, Armiach Steinpress et al. 2021) to the Himalayan glaciers (6100 m, Buchar 1976). Wolf spiders are common in all zoogeographical realms (WSC 2024). Spiders of this family are well represented in the Palaearctic: one third of all known lycosid genera (45), are known to occur in this region (WSC 2024). To date, 89 species of Lycosidae have been reported from the Mountains of Middle (=Central) Asia (Mikhailov 2021), with nearly a third of them being endemic. Notably, a single genus, *Dzhungarocosa* Fomichev & Marusik, 2017 (Fomichev and Marusik 2017), is known to be endemic to the mountains of Central Asia. Other genera, such as *Oculicosa* Zyuzin, 1993 and *Zyuzicosa* Logunov, 2010, restricted to Central Asia, dwell in low mountains or in plains (Logunov 2010; Fomichev 2020). Despite the substantial biodiversity, the spider fauna of Tajikistan is unevenly studied, with most papers focusing solely on the low southwestern part of this country (Zhang and Marusik 2016; Fomichev and Marusik 2021; Fomichev et al. 2023). The challenging-to-access Pamir Mountains have been largely neglected in these studies. According to Andreeva (1976), only ten species of Lycosidae have been reported or described from the Pamir Mountains. Recently, the first author had the opportunity to participate in an expedition to the Pamir Mountains, where he collected rich material on wolf spiders. A detailed study of this material revealed several undescribed taxa one of which belongs to an undescribed genus of Australasian subfamily Artoriinae Framenau, 2007. The goal of the present paper is to diagnose and to describe this new genus and to report Artoriinae in Central Asia for the first time.

Material and methods

Specimens were photographed by an Olympus DP74 camera attached to an Olympus SZX16 stereomicroscope at the Altai State University (Barnaul, Russia). Photographs were taken in dishes with white cotton at the bottom, filled with ethanol. Digital multifocus images were stacked by using "Zerene Stacker". SEM micrographs were produced using a Hitachi TM-1000 scanning microscope at the Institute of Systematics and Ecology of Animals SB RAS (Novosibirsk, Russia). The epigyne was cleared in KOH/water solution during the day and stained with methylene blue. The endogyne was photographed on a slide, submerged in glycerol, using Olympus XC50 camera attached to an Olympus BH-51 stereomicroscope (Altai State University, Barnaul, Russia). All measurements are in millimeters (mm). Lengths of leg segments were measured on the dorsal side. Data about spination of legs are based on examination of one side of the body. Apical spines on metatarsi were not counted. We followed the terminology of the parts of the copulatory organs and format of description as in Fomichev (2021) and Wang et al. (2021), with modifications and additions. The studied material is deposited in the Institute of Systematics and Ecology of Animals SB RAS (ISEA; curator G.N. Azarkina).

Abbreviations: **ALE** – anterior lateral eye, **AM** – accompanying membrane, **AME** – anterior median eye, **BA** – basoembolic apophysis, **CD** – copulatory duct, **Cn** – conductor, **CO** – copulatory opening, **d** – dorsal, **DE** – distal part of the embolus, **DP** – dorsal process of embolic division, **EP** – epigynal plate, **FD** – fertilization duct, **Fe** – femur, **Fo** – fovea, **Mt** – metatarsus, **p** – prolateral, **Pa** – patella, **PE** – proximal part of embolus, **PLE** – posterior lateral eye, **PME** – posterior median eye, **PO** – prolateral outgrowth, **PP** – prolateral process, **PS** – plumose seta, **r** – retrolateral, **Re** – receptacles, **RG** – rod-shaped gland, **RH** – head of receptacle, **RP** – retrolateral process, **RR** – retrolateral ridge, **SD** – sperm duct, **SS** – stick-like setae, **St** – subtegulum, **TA** – tegular apophysis, **TD** – threadlike denticles, **Te** – tegulum, **Ti** – tibia, **Tr** – terminal apophysis, **Ts** – tarsus, **TS** – stalk of tegular apophysis, **v** – ventral.

Result

Family Lycosidae Sundevall, 1833
Subfamily Artoriinae Framenau, 2007

Pamirosa gen. nov.

https://zoobank.org/5D29F6B9-9434-4663-B88E-6098477C12E1

Type species. *Pamirosa kudratbekovi* sp. nov.

Etymology. The generic name is derived from the type locality of the type species, Pamir Mountains, and end with –osa, typical ending for Lycosidae genera. The gender is feminine.

Diagnosis. The new genus differs from all known genera of Artoriinae by the helicoid tip of embolus in male (vs. straight or smoothly curved) and by screw-shaped membranous copulatory ducts in female. The presence of membranous copulatory ducts is a unique character for *Pamirosa* gen. nov. which is unknown in all other genera of Lycosidae.

Relationships. The new genus belongs to Artoriinae to judge from the following features: 1) small subtegulum located at retrolateral half of the bulb, 2) very complex tegular apophysis, 3) transversal course of the sperm duct, 4) absence of palea, 5) presence of tegular outgrowth prolaterally from the tegular apophysis, 6) presence of basoembolic apophysis, 7) lacking cymbial claws (modified macrosetae), 8) posteriorly opened epigynal fovea lacking any septum.

Description. See species description.

Composition. Only the type species.

Comments. Artoriinae are known to occur in the Indo-Malayan, Australasian, Pacific and Neotropical regions (Framenau 2007; Piacentini and Grismado 2009). The majority of taxa of Artoriinae are located in Australia and New Zealand (Framenau 2007). Among these are the following genera: *Anoteropsis* L. Koch, 1878; *Artoria* Thorell, 1877; *Artoriopsis* Framenau, 2007; *Diahogna* Roewer, 1960; *Kangarosa* Framenau, 2010; *Kochosa* Framenau et al., 2023; *Notocosa* Vink, 2002 and *Tetralycosa* Roewer, 1960 (WSC 2024). *Navira* and *Lobizon* are restricted to the south of the Neotropical Realm (Piacentini and Grismado 2009). One genus of Artoriinae, *Syroloma* Simon, 1900, is known to be endemic to the Hawaiian Islands (WSC 2024). Species from the poorly known genus *Lycosella* Thorell, 1890 were described by Simon (WSC 2024) and Thorell (WSC 2024) from Hawaiian Islands and from Sumatra Island. There are no published images and redescriptions of *Lycosella* species. Two species of *Artoria* described from southern Africa (Roewer 1960) are most likely misplaced. Several species from this genus are known from the Malay Archipelago, Malay Peninsula and southeast China (Framenau 2005; Wang et al. 2019; 2021). Finally, the genus *Sinartoria* Wang, Framenau & Zhang, 2021, comprising two species, was recently described from the Daming Mountain in the tropical part of China (Wang et al. 2021). Thus, *Pamirosa* gen. nov. extends the known range of Artoriinae about 6° to the North and 28° to the West and is the first record of the subfamily in Central Asia (Fig. 51). More reports of Artoriinae in Tibet, the Himalaya and the Karakoram can be expected.

Pamirosa kudratbekovi sp. nov.

https://zoobank.org/4C8B361F-07FA-4719-994F-680251B7DF42

Figs 1–38, 49–54

Types. ***Holotype*** ♂ (ISEA, 001.9080) and ***paratype*** 1♀ (ISEA, 001.9081) Tajikistan, Gorno-Badakhshan Region, Muzkol Mt Range, near Ak-Baital Mt Pass (38°32.871'N, 73°33.736'E), scree, 4700 m, 19 Jul. 2023, leg. A. A. Fomichev & Y. V. Dyachkov.

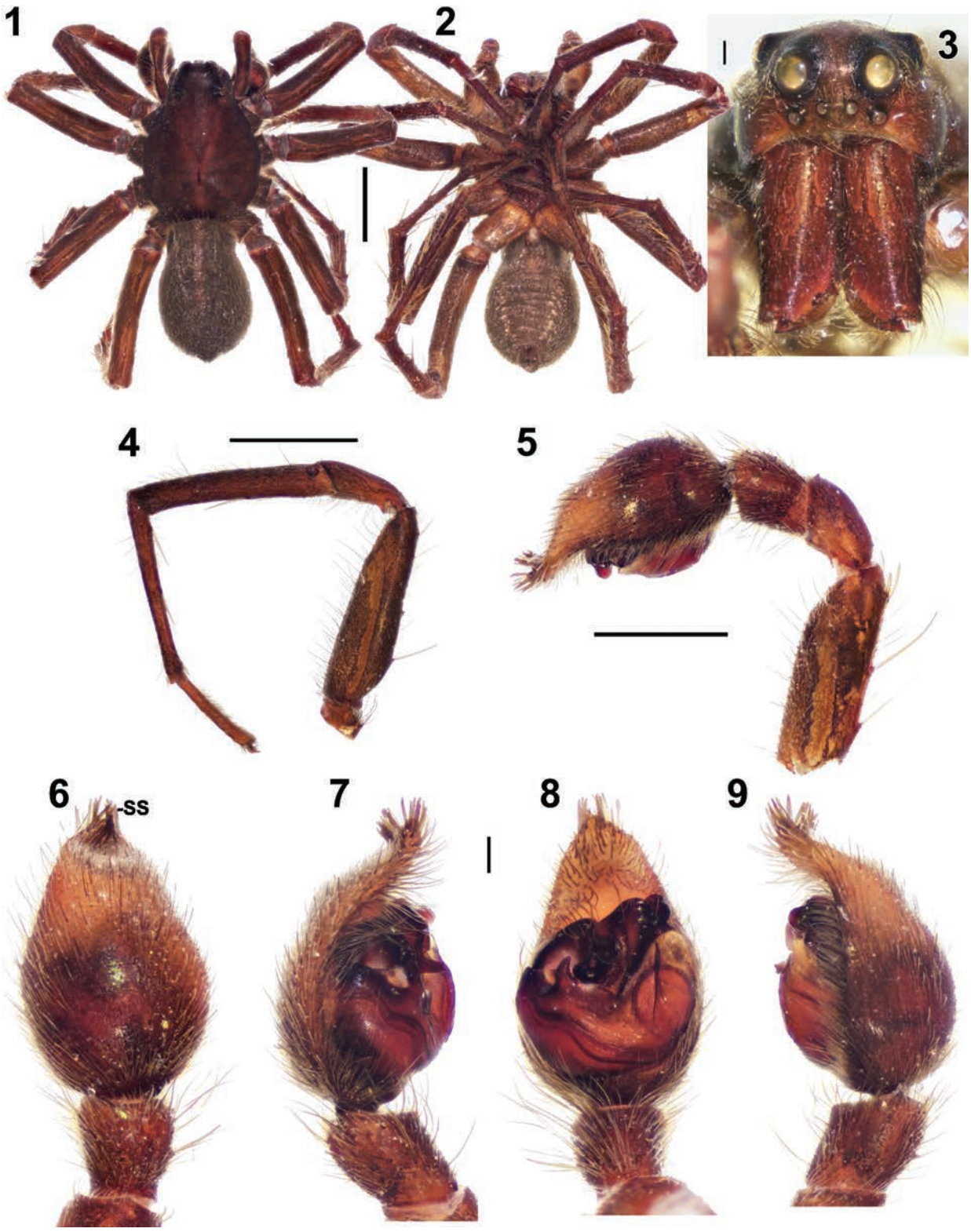

Figures 1–9. Male of *Pamirosa kudratbekovi* sp. nov. **1, 2.** Habitus; **3.** Cephalic part; **4.** Leg I; **5.** Whole palp; **6–9.** Distal part of the palp. **1, 6**. Dorsal; **2, 8**. Ventral; **3**. Anterior; **4–5, 9**. Retrolateral; **7.** Prolateral. Abbreviation: SS – stick-like seta. Scale bars: 2 mm (**1, 2**); 0.2 mm (**3–9**).

Diagnosis. See generic diagnosis.

Description. Male. Total length 8.2. Carapace: 4.35 long, 3.25 wide. Abdomen: 3.95 long, 2.6 wide. General appearance as in Figs 1, 2. Coloration. Carapace dark brown with brown, barely visible median band; lateral bands indistinct. Eye field almost black. Clypeus, chelicerae and labium dark brown. Endites and coxae yellow-brown. Sternum brown, darker at margins. Palps dark brown, distal part of cymbium yellow. Legs dark brown, without annulations. Abdomen gray, with dark

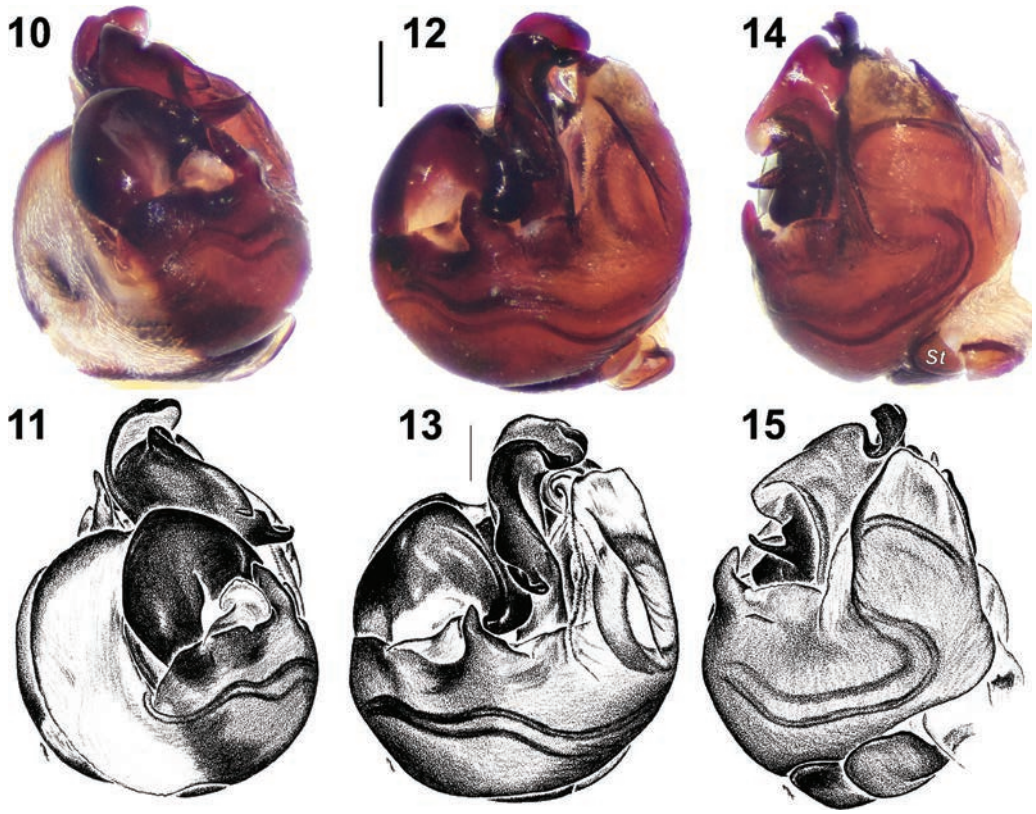

Figures 10–15. Bulb of *Pamirosa kudratbekovi* sp. nov. **10, 11.** Prolateral; **12, 13.** Ventral; **14, 15.** Retrolateral. Abbreviation: *St* – subtegulum. **11, 13, 15**. Courtesy of Galina N. Azarkina. Scale bars: 0.2 mm.

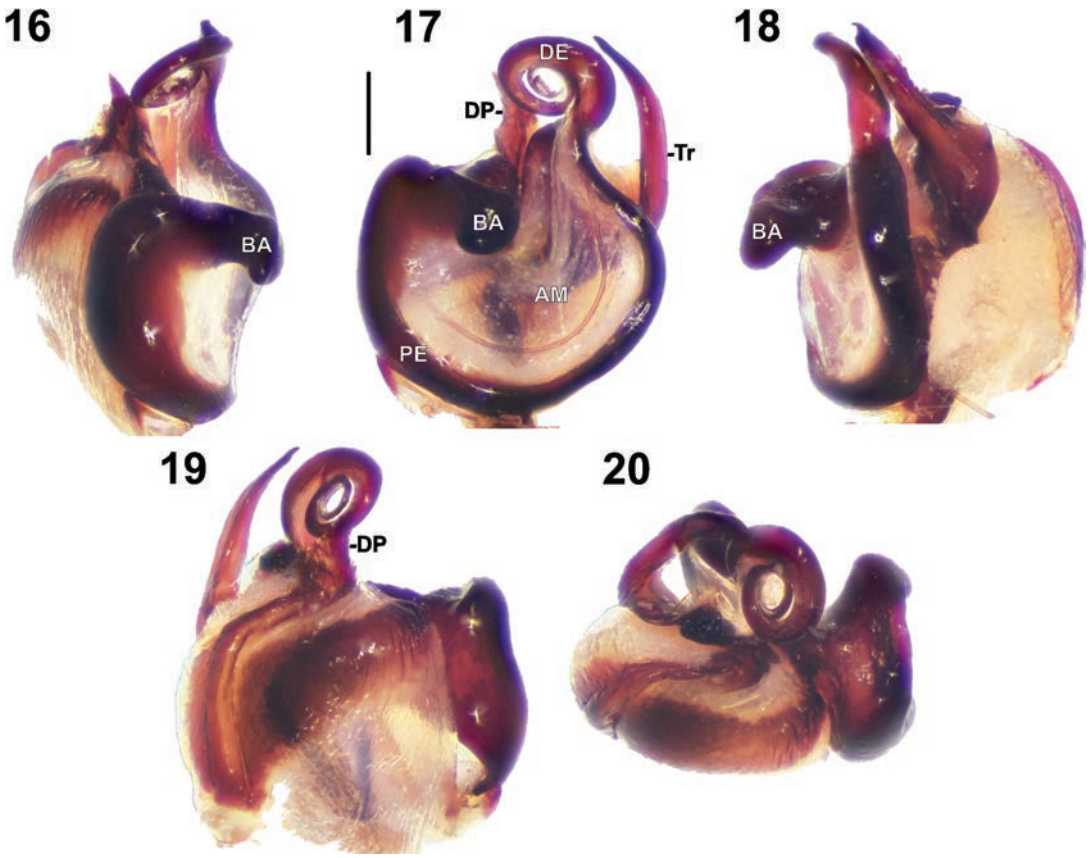

Figures 16–20. Embolic division of *Pamirosa kudratbekovi* sp. nov. **16**. Prolateral; **17**. Ventral; **18**. Retrolateral; **19**. Dorsal; **20**. Anterior. Abbreviations: AM – accompanying membrane, BA – basoembolic apophysis, DE – distal part of embolus, DP – dorsal process of embolic division, PE – proximal part of embolus, Tr – terminal apophysis. Scale bar: 0.2 mm.

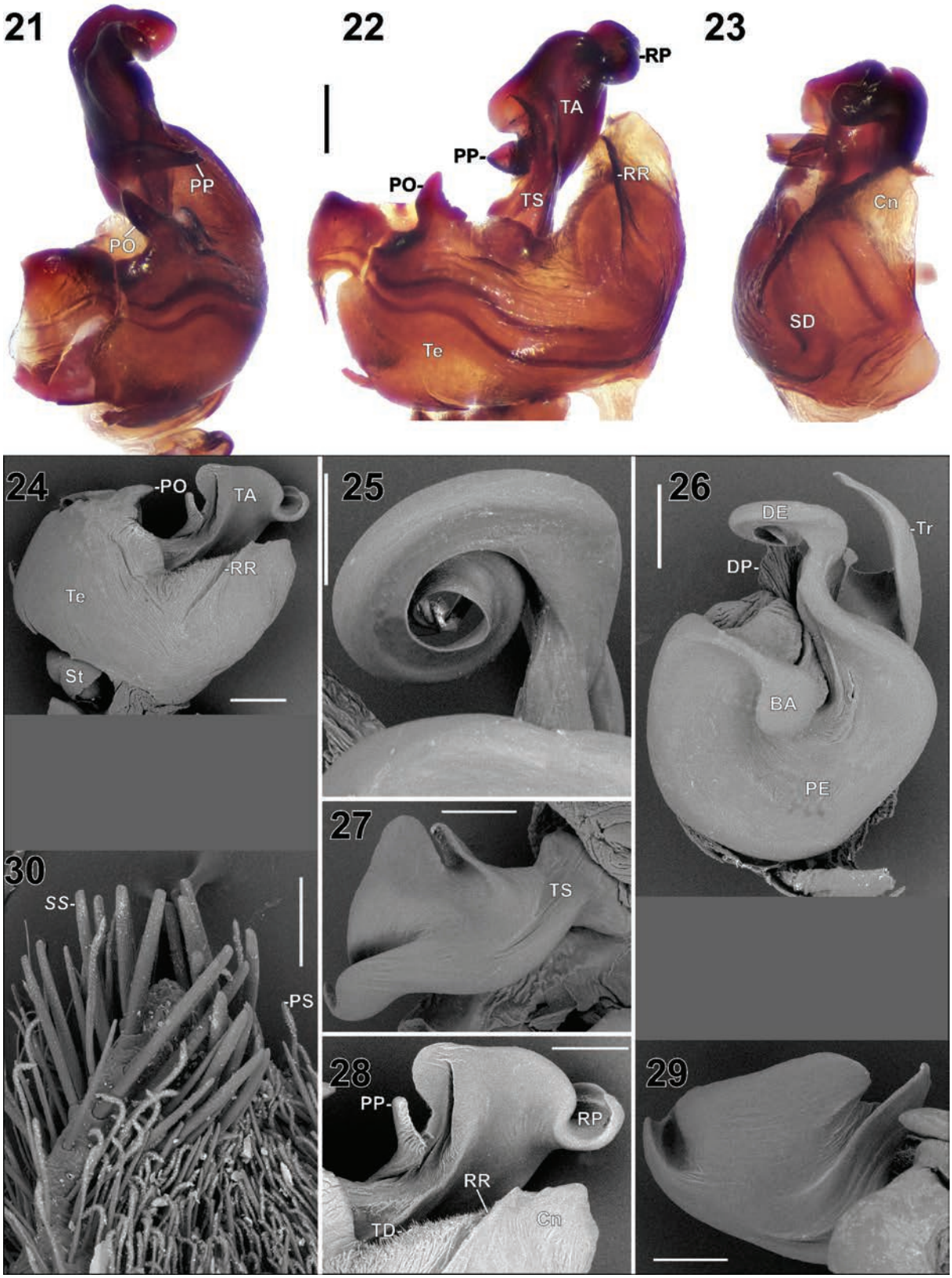

Figures 21–30. Male of *Pamirosa kudratbekovi* sp. nov. **21–24.** Tegulum; **25.** Embolus; **26.** Embolic division, **27–29.** Tegular apophysis; **30.** Tip of cymbium. **21, 29**. Prolateral; **22, 24, 26, 28**. Ventral; **23**. Retrolateral; **25**. Pro-ventral; **27, 30.** Dorsal. Abbreviations: BA – basoembolic apophysis, Cn – conductor, DE – distal part of embolus, DP – dorsal process of embolic division, PE – proximal part of embolus, PO – prolateral outgrowth of tegulum, PP – prolateral process of tegular apophysis, PS – plumose seta, RP – retrolateral process of tegular apophysis, RR – retrolateral ridge of tegulum, SD – sperm duct, SS – stick-like seta, St – subtegulum, TA – tegular apophysis, TD – threadlike denticles, Te – tegulum, Tr – terminal apophysis, TS – stalk of tegular apophysis. Scale bars: 0.2 mm (**21–24, 26**); 0.1 mm (**25**); 0.15 mm (**27–29**); 0.1 mm (**30**).

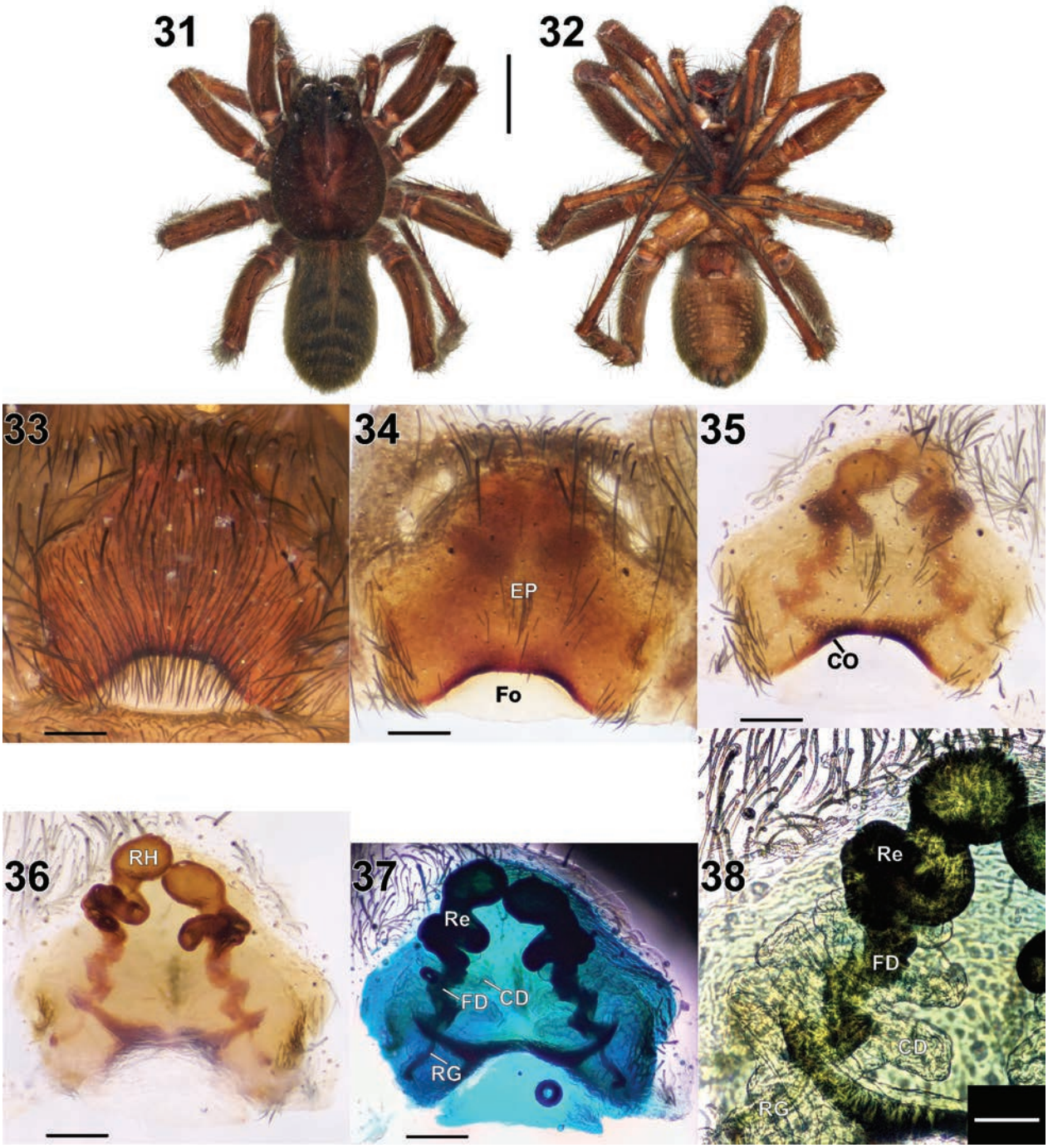

Figures 31–38. Female of *Pamirosa kudratbekovi* sp. nov. **31–32.** Habitus; **33–38.** Epigyne. **31**. Dorsal; **32**. Ventral; **33**. Intact, ventral; **34**. Dissected, ventral; **35**. Macerated, ventral; **36**. Macerated, dorsal; **37, 38**. Macerated and painted, dorsal. Abbreviations: CD – copulatory duct, CO – copulatory opening, EP – epigynal plate, FD – fertilization duct, Fo – fovea, Re – receptacle, RG – rod-shaped gland, RH – head of receptacle. Scale bars: 2 mm (**31, 32**); 0.2 mm (**33–37**); 0.1 mm (**38**).

brick red-colored cardiac mark. Spinnerets gray. Eye sizes and interdistances: AME 0.1, ALE 0.11, PME 0.41, PLE 0.3, AME–AME 0.16, AME–ALE 0.16, PME–PME 0.43, PLE – PLE 1.26. Width of anterior eye row 0.86, 2nd row 1.13, 3rd row 1.57. Clypeus height at AME 0.16. Chelicerae with 3 promarginal and 3 retromarginal teeth. For legs measurements see Table 1. For legs spination see Table 2.

Table 1. Legs' measurements of male of *Pamirosa kudratbekovi* sp. nov.

	Fe	Pa	Ti	Mt	Ts	Total
Leg I	3.3	1.65	3.0	2.95	1.45	12.35
Leg II	3.3	1.6	2.9	3.0	1.5	12.3
Leg III	3.25	1.4	2.6	3.4	1.45	12.1
Leg IV	3.8	1.45	3.4	4.8	1.8	15.25

Table 2. Legs' spination of male of *Pamirosa kudratbekovi* sp. nov.

	Fe	Pa	Ti	Mt
Leg I	d1-1-1 p0-0-1	p1 r1	p1-0-0 r1-0-1 v2-2-1-2	p1-1-0 r1-1-0 v2-1-0
Leg II	d1-1-1 p1-0-1 r1-0-0	p1 r1	p1-0-0 r1-0-1 v2-2-1-2	p1-1-0 r1-1-0 v2-2-0
Leg III	d1-1-1 p1-0-1 r1-0-1	p1 r2	d1-0-1 p1-0-1 r1-0-1 v2-2-2	d0-1-0 p1-1-0 r1-1-0 v2-2-0
Leg IV	d1-1-1 p2-0-1 r0-0-2	p1 r1	d1-1-1 p0-1-1 r0-2-1 v2-2-1-2	d1-1-0 p1-2-0 r1-1-0 v2-2-2

Male palp as shown in Figs 5–30. Femur 2.5 times longer than tibia, with 3 dorsal and 2 prolateral spines. Patella 1.4 times longer than tibia, with one prolateral spine. Tibia 2.9 times shorter than cymbium. Cymbium broad and rounded; length/width ratio 1.6. Tip of cymbium bent dorsally and equipped with stick-like (NS) and plumose setae (PS). Subtegulum (St) very small, oval located on retrolateral side of bulb. Tegulum (Te) circular, length/width ratio 0.74; anterior part with long and narrow retrolateral ridge (RR) on ventral margin of conductor (Cn) and triangular prolateral outgrowth (PO); conductor not tapering. Median sector of anterior edge of tegulum covered with number of short, thread-like denticles (TD). Sperm duct (SD) S-shaped in retrolateral view; tegular apophysis complex. Thin stalk of tegular apophysis (TS) starts from dorsal surface of tegulum. Tegular apophysis massive, hammer-shaped; prolateral process of tegular apophysis (PP) triangular; retrolateral process of tegular apophysis (RP) semicircular, with tip bent ventrally. Palea absent. Embolus large, coiled in 2 planes; proximal part (PE) with accompanying membrane (AM) forming loop ca 270°. Basoembolic apophysis (BA) circular in ventral view, strongly sclerotized, in intact bulb tightly fixed between prolateral outgrowth of tegulum (PO) and prolateral process of tegular apophysis (PP). Terminal apophysis (Tr) elongated, with sharply pointed tip. Embolic division with small, sharply pointed dorsal process (DP), partly hidden by embolus in ventral view. Distal part of embolus (DE) tightly twisted, making two complete loops (720°).

Female. Total length 8.0. Carapace: 4.1 long, 3.0 wide. Abdomen: 4.0 long, 2.45 wide. General appearance as in Figs 28, 29. Coloration as in male, but palps, legs, venter of the abdomen and spinnerets lighter. Dorsal surface of abdomen with blurred herringbone pattern. Eye sizes and interdistances: AME 0.1, ALE 0.13, PME 0.39, PLE 0.27, AME–AME 0.19, AME–ALE 0.16, PME–PME 0.36, PLE–PLE 1.07. Width of anterior eye row 0.87, second row 1.06, third row 1.46. Clypeus height at AME 0.19. Chelicerae as in male. For legs' measurements see Table 3. For legs' spination see Table 4.

Epigyne as shown in Figs 33–38. Epigynal plate trapezoidal, convex, with large trapezoidal fovea located posteriorly, septum absent. Fovea (Fo) ca. 3 times wider than long. Copulatory openings (CO) located at antero-lateral parts of fovea. Copulatory ducts (CD) membranous, corkscrew-shaped, form approximately 3 turns around fertilization ducts (FD). Receptacles (Re) screw-shaped, strongly sclerotized; heads (RH) touching each other. Fertilization ducts (FD) sinusoidal, strongly sclerotized. Rod-shaped glands (RG) located posterior to the copulatory openings.

Table 3. Legs' measurements of female of *Pamirosa kudratbekovi* sp. nov.

	Fe	Pa	Ti	Mt	Ts	Total
I	2.75	1.4	2.25	2.0	1.15	9.55
II	2.75	1.4	2.15	2.05	1.15	9.5
III	2.75	1.35	2.0	2.45	1.25	9.8
IV	3.15	1.45	2.8	3.8	1.6	12.8

Etymology. The specific name is a patronym in honour of Uvaido Kudratbekov (Porshinev, Tajikistan) who helped to organize an expedition to Pamir Mountains in which the types of this new species were collected.

Distribution. Known only from the type locality (Figs 51–54).

Note. Having only one female, we cannot cut the single epigyne to check the origin of membranous ducts in endogyne, which would allow us to perceive if they are copulatory or fertilization ducts. Membranous parts of the endogyne are unknown in other lycosids occurring in the Holarctic.

Habitat. The specimens were collected among stone screes (Fig. 51) on elevations about 4700 m.

Comments. Among the genera of alpine Lycosidae inhabiting stone screes in the Palearctic are the following: *Acantholycosa* Dahl, 1908; *Dzhungarocosa*; *Evippa* Simon, 1882; *Gulocosa* Marusik et al. 2015; *Mongolicosa* Marusik et al. 2004 and *Sibirocosa* Marusik et al. 2004 (see Table 5). Species from all of these genera share one common character: they have more than three pairs of ventral spines on tibia I. This is true for the widespread *Acantholycosa* complex (group of genera) and in genera not related to *Acantholycosa* Dahl, 1908 (Marusik et al. 2015; Fomichev and Marusik 2017; Fomichev 2022). Unlike all other scree-dwelling wolf-spiders, *P. kudratbekovi* sp. nov. has only three pairs of ventral tibial spines on leg I, as in many non- scree dwelling Pardosinae spiders (cf. Figs 49, 50, 39–48).

Table 4. Legs' spination of female of *Pamirosa kudratbekovi* sp. nov.

	Fe	Pa	Ti	Mt
I	d1-1-1 p0-0-1	0	p1-0-0 r0-0-1 v2-2-2	p1-1-0 r1-1-0 v2-2-0
II	d1-1-1 p1-0-1 r0-1-0	p1	p1-0-1 r1-0-1 v2-2-2	p1-1-0 r1-1-0 v2-2-0
III	d1-1-1 p0-1-1 r0-1-1	p1 r1	d1-1-0 p1-0-1 r1-0-1 v2-2-2	p1-1-0 r1-1-0 v2-2-0
IV	d1-1-1 p1-0-1 r0-0-1	p1 r1	d1-0-1 p1-0-1 r1-0-1 v2-2-2	d0-1-0 p1-1-0 r1-1-0 v2-1-2

Table 5. Distribution of the genera of alpine scree-dwelling Lycosidae in mountain systems of Asia. * – our unpublished data.

	Pardosinae						*Artoriinae*	*Evippinae*
	Acantholycosa-complex							
	Acantholycosa	*Gulocosa*	*Mongolicosa*	*Sibirocosa*	*Dzhungarocosa*	*Pardosa*	*Pamirosa*	*Evippa*
Putorana Plateau	-	-	-	+	-	-	-	-
Mts. of North-Eastern Siberia	+	-	-	+	-	-	-	-
Mts. of South Siberia and Mongolia	+	-	+	+	-	-	-	-
Sikhote-Alin	+	+	-	+	-	+	-	-
Tarbagatai	+	-	-	-	-	-	-	-
Dzhungarian Alatau	-	-	-	-	+	-	-	-
Tian Shan	-	-	+	-	-	+	-	-
Pamir	-	-	-	-	-	+	+	+*
Hindu Kush	-	-	-	-	-	-	-	+
Tibetan Plateau	-	-	-	-	-	+	-	+
Himalayas	-	-	-	-	-	+	-	+
Main references	Zyuzin and Marusik 1988; Marusik et al. 2004; Marusik and Logunov 2011; Marusik and Omelko 2011	Marusik et al. 2015	Marusik et al. 2004	Omelko and Marusik 2013	Fomichev and Marusik 2017	Kononenko 1978; Buchar 1984; Hu 2001; Omelko, 2009; Marusik et al. 2013	Present data	Miller and Buchar 1972; Sankaran and Caleb 2023; present data

Figures 39–50. Retro-ventral view of the tibia I. **39, 40.** *Acantholycosa sayanensis* from South Siberia; **41, 42.** *Dzhungarocosa omelkoi* from Kazakhstan; **43, 44.** *Mongolicosa glupovi* from South Siberia; **45, 46.** *Sibirocosa arsenyevi* from Far East of Russia; **47, 48.** *Evippa* sp. from Pamir Mountains; **49, 50.** *Pamirosa kudratbekovi* sp. nov. **39, 41, 43, 45, 47, 49.** Male; **40, 42, 44, 46, 48, 50**. Female. Arrows indicate ventral spines (some spines are broken). Scale bar: 1 mm.

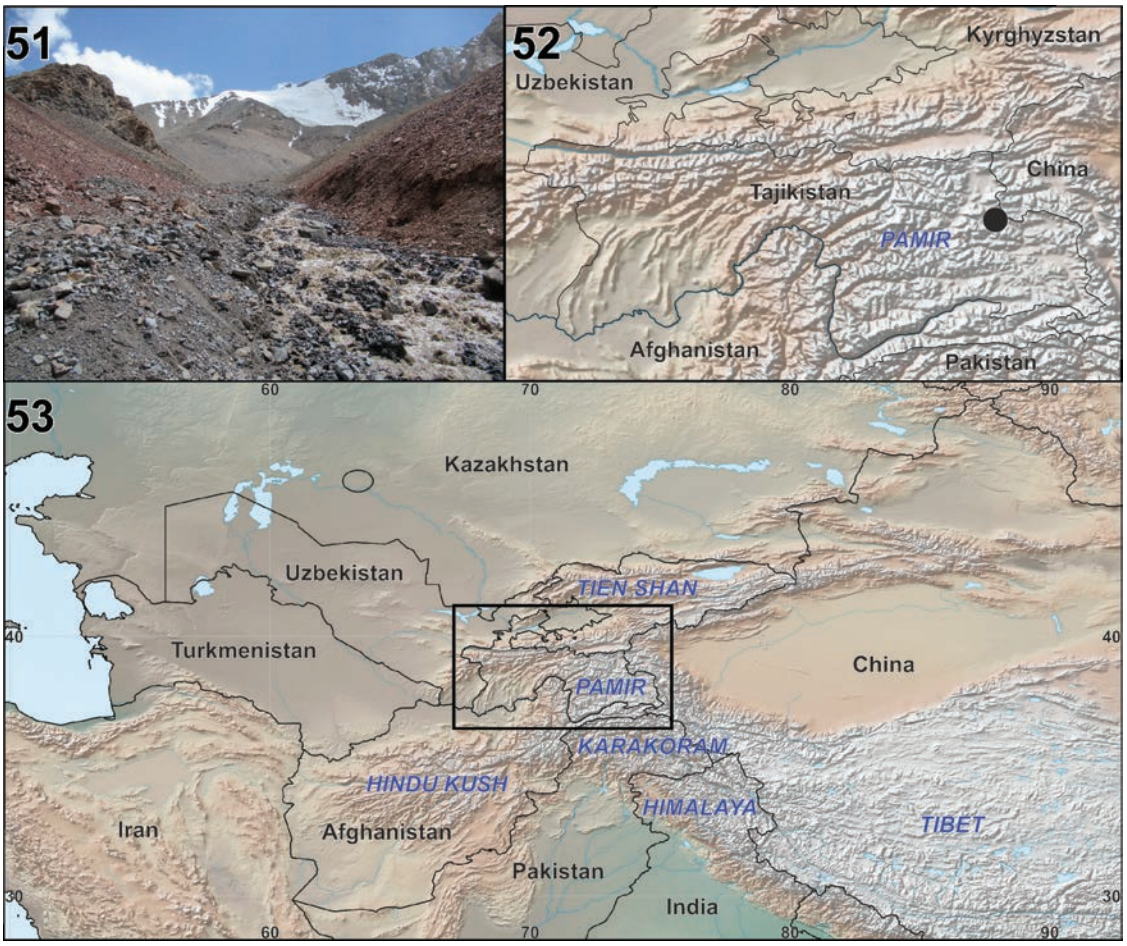

Figures 51–53. *Pamirosa kudratbekovi* sp. nov. **51.** Habitat; **52, 53.** Collecting locality. The frame on Fig. 53 refers to the content of Fig. 52. The country names are written in black font. The names of mountain systems are written in dark blue font.

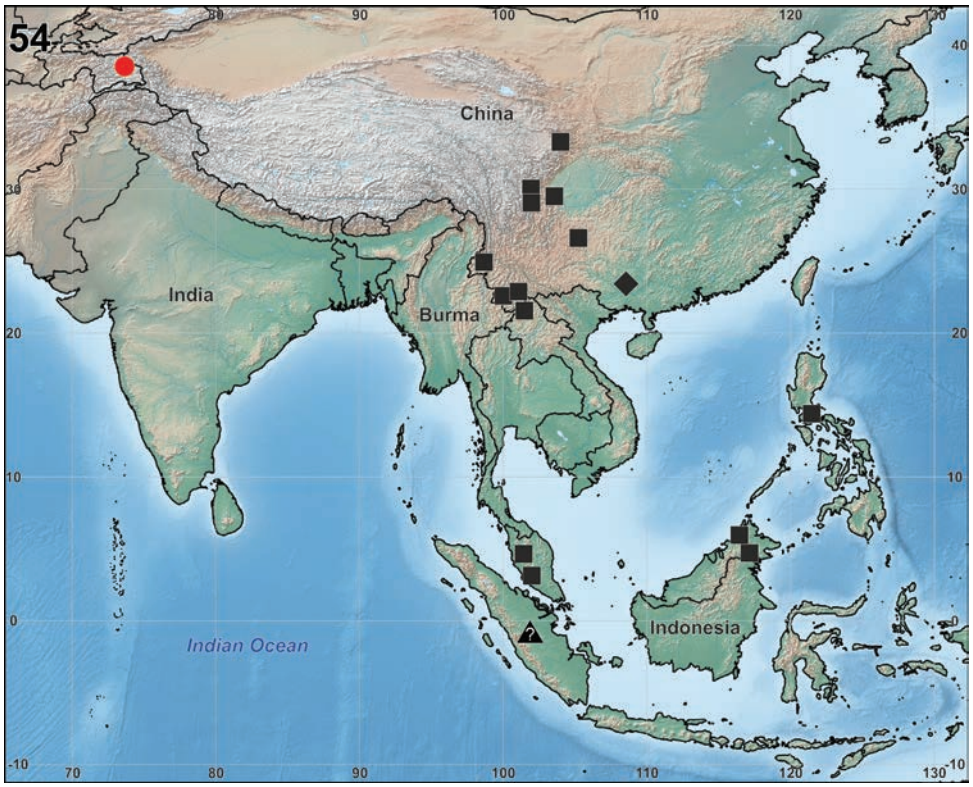

Figure 54. Collecting localities of Artoriinae in Palaearctic and Indo-Malayan Realm. Circle – *Pamirosa kudratbekovi* sp. nov.; square – *Artoria* spp.; diamond – *Sinartoria* spp.; triangle – *Lycosella* spp. ? – record without precise location.

Discussion

Lycosidae is one of the dominant spider families in the highlands of the Palaearctic and in the Arctic (Buchar and Thaler 1998; Marusik and Koponen 2002). Within the highlands, these spiders primarily inhabit stony screes (Marusik et al. 2004). Most wolf spiders inhabiting the highlands of Asia belong to the so-called *Acantholycosa* complex (= group of genera) placed within Pardosinae (cf. Marusik et al. 2015). A great number of species with ranges restricted to a single mountain range or even one mountain are known among alpine Lycosidae (Table 5). Several genera of alpine wolf spiders are known to be endemic to a specific mountain system. Examples of such genera are: *Gulocosa* for Sikhote-Alin Mt. range (south part of the Russian Far East), *Melecosa* Marusik, Omelko & Koponen, 2015 for Tian Shan, *Dzhungarocosa* for Dzhungarian Alatau and *Pamirosa* gen. nov. for Pamir Mountains (Marusik et al. 2004; Fomichev 2021; Marusik et al. 2015; Fomichev and Marusik 2017; present data). The most common genus of alpine Lycosidae is *Acantholycosa* Dahl, 1908. This genus is widespread in many mountain systems from Fennoscandia and North-Eastern Siberia to the Tarbagatai Mt. Range in Kazakhstan (Marusik et al. 2004; Marusik and Logunov 2011). The greatest diversity of scree-dwelling alpine wolf spiders is observed in the mountains of Southwest Siberia and Mongolia (Marusik et al. 2004; Fomichev and Marusik 2018; Fomichev 2021), due to representatives of three genera, *Acantholycosa*, *Mongolicosa* and *Sibirocosa*. Despite the large number of species, there are no endemic genera among scree-dwelling Lycosidae in the mountains of South Siberia (Fomichev 2021). Endemic genera are restricted to lower latitudes. It is worth noting that some of these endemic genera, such as *Dzhungarocosa* and *Pamirosa* gen. nov., do not belong to the *Acantholycosa* complex, which is common in Siberia. Thus, for high-altitude wolf spiders, there is an increase in the level of endemism from north to south, accompanied by a simultaneous decrease in the role of the *Acantholycosa* complex, due to other genera with similar lifestyles that are not part of it. In the future, the discovery of additional new genera of scree-dwelling alpine wolf spiders, not belonging to the *Acantholycosa* complex, is very likely. Perhaps these undescribed genera will turn out to be as peculiar as *Pamirosa* gen. nov. In this regard, the most promising territories are Hindu Kush (Afghanistan, Pakistan), Karakorum (Pakistan, India, China), Himalaya (India, Nepal, Bhutan, China) and Tibet (China). For details on the distribution of the genera of alpine wolf spiders in mountain systems of Asia, see Table 5.

Acknowledgements

We thank Roman V. Yakovlev (Altai State University), Uvaido Kudratbekov (Porshinev, Tajikistan) and Vyacheslav V. Doroshkin (Chelyabinsk, Russia) for organizing and undertaking an expedition to Pamir, in which the material treated in this paper was collected. Special thanks go to Yuri V. Dyachkov (Altai State University) for being a great help in field work and collecting. We also wish to thank Galina N. Azarkina (ISEA) for preparing drawings of the bulb and helping with producing scanning electron micrographs and Natalya Y. Speranskaya (Altai State University) for providing institutional facilities. We are grateful to Dmitri V. Logunov (Manchester, UK) for commenting on an early draft of the manuscript and Lu-Yu Wang (Chongqing, China) for the help in recognizing the subfamily to which the new genus belongs. The English in the final draft was kindly edited by Danniella Sherwood (London, UK). The work of Alexander A. Fomichev was funded by the state assignment of the Ministry of Science and Higher Education of the Russian Federation (project FZMW-2023-0006 “Endemic, local and invasive arthropods (Arthropoda) of the mountains of South Siberia and Central Asia: a unique gene pool of a biodiversity hotspot”. The work by Mikhail M. Omelko was carried out within the state assignment of the Ministry of Science and Higher Education of the Russian Federation (theme No. 124012200183-8). Finally, we thank the editor and reviewers Francesco Ballarin (Tokyo, Japan), Luis Piacentini (Buenos Aires, Argentina) and Luis C. Crespo (Lisboa, Portugal) for their critical comments which helped to improve the manuscript.

References

Andreeva EM (1976) Pauki Tadzhikistana [Spiders of Tajikistan]. Dushanbe, 196 pp. [in Russian]

Armiach Steinpress I, Alderweireldt M, Cohen M, Chipman A, Gavish-Regev E (2021) Synopsis of the Evippinae (Araneae, Lycosidae) of Israel, with description of a new species. European Journal of Taxonomy 733: 87–124. https://doi.org/10.5852/ejt.2021.733.1225

Buchar J (1976) Über einige Lycosiden (Araneae) aus Nepal. Ergebnisse des Forschungsunternehmens Nepal Himalaya 5: 201–227.

Buchar J (1984) Lycosidae aus dem Nepal-Himalaya. III. Die *Pardosa ricta*- und *P. lapponica*-Gruppe (Araneae: Lycosidae: Pardosinae). Senckenbergiana Biologica 64(4/6): 381–391.

Buchar J, Thaler K (1998) Lycosidae from the high alpine zone of the Caucasus range, with comparative remarks on the fauna of the Alps (Arachnida: Araneae). Linzer Biologische Beiträge 30: 705–717.

Fomichev AA (2020) New observations on *Oculicosa supermirabilis* Zyuzin 1993 (Araneae: Lycosidae) in south-western Kazakhstan. Acta Arachnologica 69(2): 71–74. https://doi.org/10.2476/asjaa.69.71

Fomichev AA (2021) New data on the wolf spiders from the *Acantholycosa*-complex (Araneae: Lycosidae) from the South Siberia. Zootaxa 5026(4): 567–585. https://doi.org/10.11646/zootaxa.5026.4.7

Fomichev AA (2022) A new species of *Pardosa* C. L. Koch 1847 (Araneae: Lycosidae) from the highlands of Tian Shan Mountains (southern Kazakhstan). Acta Arachnologica 71(1): 1–4. https://doi.org/10.2476/asjaa.71.1

Fomichev AA, Marusik YM (2017) A survey of East Palaearctic Lycosidae (Araneae). 13. A new genus of spiny-legs Pardosinae from Eastern Kazakhstan. Zootaxa 4320(2): 339–350. https://doi.org/10.11646/zootaxa.4320.2.8

Fomichev AA, Marusik YM (2018) Five new species of the *Acantholycosa*-complex (Araneae: Lycosidae) from Mongolia. Zootaxa 4497(2): 271–284. https://doi.org/10.11646/zootaxa.4497.2.7

Fomichev AA, Marusik YM (2021) A survey of East Palaearctic Gnaphosidae (Araneae). 11. New data on Gnaphosidae (Araneae) from Tajikistan. Zootaxa 4966(4): 443–457. https://doi.org/10.11646/zootaxa.4966.4.3

Fomichev AA, Marusik YM, Zonstein S (2023) New and poorly known species of *Palpimanus* Dufour, 1820 (Araneae, Palpimanidae) from Uzbekistan and Tajikistan. Zootaxa 5339(3): 256–272. https://doi.org/10.11646/zootaxa.5339.3.3

Framenau VW (2005) The wolf spider genus *Artoria* Thorell in Australia: New synonymies and generic transfers (Araneae, Lycosidae). Records of the Western Australian Museum 22(4): 265–292. https://doi.org/10.18195/issn.0312-3162.22(4).2005.265-292

Framenau VW (2007) Revision of the new Australian genus *Artoriopsis* in a new subfamily of wolf spiders, Artoriinae (Araneae: Lycosidae). Zootaxa 1391(1): 1–34. https://doi.org/10.11646/zootaxa.1391.1.1

Hu JL (2001) Spiders in Qinghai-Tibet Plateau of China. Henan Science and Technology Publishing House, 658 pp.

Kononenko AP (1978). Doklady Akademii Nauk Tadzhikistan SSR 21(3): 65–66. [*Pardosa muzkolica* (Aranei: Lycosidae) – new species of spider from eastern Pamir] [in Russian]

Logunov DV (2010) On new central Asian genus and species of wolf spiders (Araneae: Lycosidae) exhibiting a pronounced sexual size dimorphism. Trudy Zoologicheskogo Instituta 314(3): 233–263. https://doi.org/10.31610/trudyzin/2010.314.3.233

Marusik YM, Böcher J, Koponen S (2006) The collection of Greenland spiders (Aranei) kept in the Zoological Museum, University of Copenhagen. Arthropoda Selecta 15(1): 59–80.

Marusik YM, Koponen S (2002) Diversity of spiders in boreal and arctic zones. The Journal of Arachnology 30(2): 205–210. https://doi.org/10.1636/0161-8202(2002)030[0205:DOSIBA]2.0.CO;2

Marusik YM, Logunov DV (2011) New faunistic records of spiders from East Kazakhstan (Arachnida: Aranei). Arthropoda Selecta 20(1): 57–63. https://doi.org/10.15298/arthsel.20.1.04

Marusik YM, Omelko MM (2011) A survey of East Palaearctic Lycosidae (Araneae). 7. A new species of *Acantholycosa* Dahl, 1908 from the Russian Far East. ZooKeys 79: 1–10. https://doi.org/10.3897/zookeys.79.945

Marusik YM, Azarkina GN, Koponen S (2004) A survey of east Palearctic Lycosidae (Aranei). II. Genus *Acantholycosa* F. Dahl, 1908 and related new genera. Arthropoda Selecta 12 (2, 2003): 101–148.

Marusik YM, Nadolny AA, Omelko MM (2013) A survey of east Palearctic Lycosidae (Araneae). 10. Three new *Pardosa* species from the mountains of Central Asia. Zootaxa 3722(2): 204–218. https://doi.org/10.11646/zootaxa.3722.2.5

Marusik YM, Omelko MM, Koponen S (2015) A survey of East Palaearctic Lycosidae (Araneae). 11. Two new genera from the *Acantholycosa* complex. Zootaxa 3985(2): 252–264. https://doi.org/10.11646/zootaxa.3985.2.4

Mikhailov KG (2021) Advances in the study of the spider fauna (Aranei) of Russia and adjacent regions: a 2017 update. Invertebrate Zoology 18 (1): 25–35. [Supplements 1.01–1.15, 2.01–2.24] https://doi.org/10.15298/invertzool.18.1.03

Miller F, Buchar J (1972) Einige neue Spinnenarten (Araneae) aus dem Hindukusch. Acta Universitatis Carolinae Biologica (Biol.) 1970: 383–398.

Omelko MM (2009) Altitudinal distribution of the ground dwelling spider (Arachnida, Aranei) in Oblachnaya Mountain, South Primorye. Chteniya Pamyati Alekseya Ivanovicha Kurencova 20: 138–146. [in Russian]

Omelko MM, Marusik YM (2013) A survey of east Palearctic Lycosidae (Araneae). 9. A review of *Sibirocosa* with a descriptions of three new species. Zootaxa 3666(3): 319–330. https://doi.org/10.11646/zootaxa.3666.3.2

Piacentini LN, Grismado CJ (2009) *Lobizon* and *Navira*, two new genera of wolf spiders from Argentina (Araneae: Lycosidae). Zootaxa 2195(1): 1–33. https://doi.org/10.11646/zootaxa.2195.1.1

Roewer CF (1960) Araneae Lycosaeformia II (Lycosidae) (Fortsetzung und Schluss). Exploration du Parc National de l'Upemba, Mission G. F. de Witte 55: 519–1040.

Sankaran PM, Caleb JTD (2023) Notes on Indian wolf spiders: III. Genera *Acantholycosa* Dahl, 1908, *Evippomma* Roewer, 1959, *Hippasosa* Roewer, 1960 and *Trochosa* C.L. Koch, 1847 (Araneae: Lycosidae). Zootaxa 5369(4): 533–552. https://doi.org/10.11646/zootaxa.5369.4.4

Tullgren A (1901) Contribution to the knowledge of the spider fauna of the Magellan Territories. In: Svenska Expeditionen till Magellansländerna 2(10): 181–263.

Wang LY, Zhang ZS, Peng XJ (2019) First record of *Artoria* Thorell, 1877 (Araneae: Lycosidae) from Malaysia, with the description of a new species. Zootaxa 4657(2): 392–396. https://doi.org/10.11646/zootaxa.4657.2.12

Wang LY, Framenau VW, Zhang ZS (2021) A further study on the wolf spider subfamily Artoriinae from China (Araneae: Lycosidae). Zootaxa 4964(3): 571–584. https://doi.org/10.11646/zootaxa.4964.3.8

WSC (2024) World Spider Catalog. Natural History Museum Bern. Version 24.5 http://wsc.nmbe.ch [Accessed 10 January 2024]. https://doi.org/10.24436/2

Zhang XQ, Marusik YM (2016) A survey of *Pireneitega* from Tajikistan (Agelenidae, Coelotinae). ZooKeys 635: 89–107. https://doi.org/10.3897/zookeys.635.10487

Zyuzin AA, Marusik YM (1988) A new species of spiders of the genus *Acantholycosa* (Aranei, Lycosidae) from the East Siberia. Zoologicheskiy Jurnal 67(7): 1083–1085. [in Russian]

Zoosyst. Evol. 100 (3) 2024, 1017–1028 | DOI 10.3897/zse.100.125826

PENSOFT

für Natur MUSEUM FÜR NATURKUNDE BERLIN

On the identity and placement of *Xysticus lendli* Kulczyński, 1897 (Araneae, Thomisidae): an integrative approach

Nikolett Gallé-Szpisjak[1], Róbert Gallé[1,2], Krisztián Szabó[3], Tamás Szűts[3]

1 *HUN-REN, CER, IEB "Lendület" Landscape and Conservation Ecology Research Group, H-2163 Alkotmány road 2-4, Vácrátót, Hungary*

2 *Department of Ecology, University of Szeged, H-6726, Közép fasor 52., Szeged, Hungary*

3 *Molecular Ecology Research group, Department of Zoology, University of Veterinary Medicine Budapest, Rottenbiller u. 50., Budapest, H-1077, Hungary*

https://zoobank.org/B38CF174-7F50-41FC-B520-2217BE1665D6

Corresponding author: Nikolett Gallé-Szpisjak (szpisjak.nikolett@ecolres.hu)

Academic editor: Danilo Harms ♦ **Received** 20 April 2024 ♦ **Accepted** 9 June 2024 ♦ **Published** 25 July 2024

Abstract

The species *Xysticus lendli* is known only from its original description of a single male and one doubtful record so far. Here, we illustrate and redescribe the species based on 34 specimens in total and describe its female for the first time. We illustrated the male palp via compound micrographs and scanning electron micrographs. We generated a DNA barcode and placed it into a current phylogenetic scaffold to confirm the species' placement of *Spiracme*, a long-debated sister- or subgroup of *Xysticus*; hence, a new combination of *Spiracme lendli* (Kulczyński, 1897), **comb. nov.** is proposed. We illustrated the visually similar *Xysticus mongolicus* and the type species of *Spiracme*, *S. striatipes*, and compared them to *S. lendli* to aid future distinctions between those species.

Key Words

Central Europe, crab spiders, new combination, redescription, *Spiracme*

Introduction

Hungary has a rich arachnofauna, which has been well studied for a long time. Due to its unique location, glaciation history, and topological arrangement (the Carpathian Basin), numerous species have been described in this region. The Pannonian biogeographic region lies on a unique meeting point of various other biogeographic regions (Molnár et al. 2008; Fekete et al. 2016); for instance, the Eurasian steppe/forest steppe zone's westernmost part is located here (Bátori et al. 2018). On the eastern part of Hungary, the forest steppe biome is present in the Kiskunság National Park, offering a unique opportunity to study the forest steppe biota (Gallé et al. 2022a) (Fig. 1A). The arachnofauna of Kiskunság National Park has been intensively studied due to the increased interest of ecologists and conservation biologists, who have conducted frequent studies in the last few decades (Gallé et al. 2022a, 2022b, 2022c, and references therein). During these studies, several new species have been discovered (*Parasyrisca arrabonica* Szinetár & Eichard, 2009; *Sernokorba betyar* Gallé-Szpisjak et al., 2023), and a few other "forgotten" taxa have been rediscovered as well. One of these taxa is *Xysticus lendli* Kulczyński, 1897, an enigmatic thomisid that was known by a single male specimen and did not have a verified record besides its original description more than a century ago.

Xysticus has been the subject of several classification attempts in the past 50 or so years (see Lehtinen 2002; Jantscher 2002; and Breitling 2019 for details). Almost all of these papers used morphological data, whereas the last treatment by Breitling (2019) used the phylogeny of barcode sequences alone. One main result of the latter was the resurrection of the genus *Spiracme* Menge, 1876, with the type species *Spiracme striatipes* (L. Koch, 1870) and including nine other species: *Spiracme baltistana* (Caporiacco, 1935), *Spiracme dura* (Sørensen, 1898), *Spiracme keyserlingi* (Bryant, 1930), *Spiracme lehtineni*

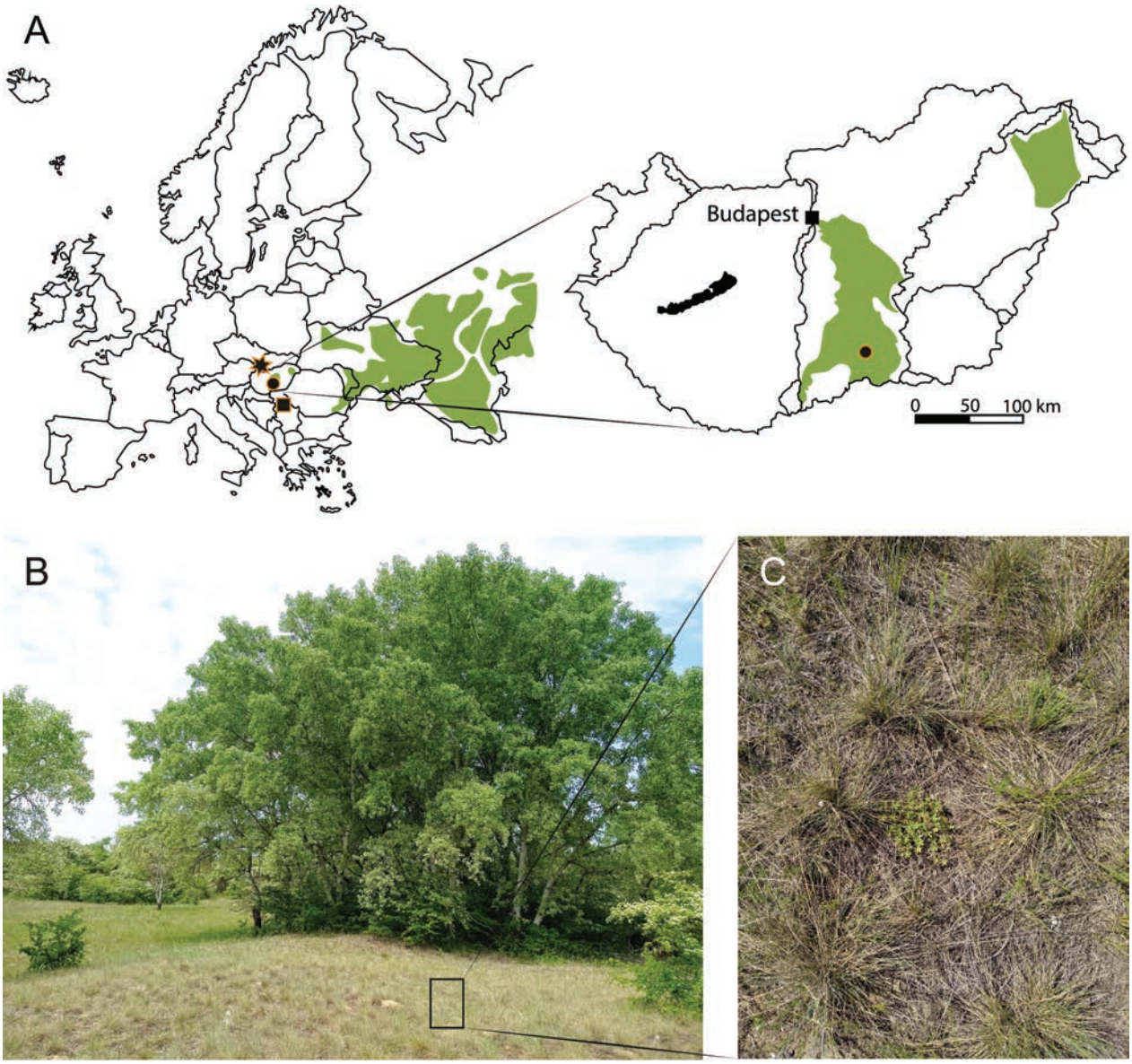

Figure 1. A. Map of Europe and Hungary with the forest-steppe zone (green patches), the Hungarian sampling site (black circle), the Slovakian sampling site (black star, Purgat et al. 2021), and the Serbian sampling site (black square, Grbić et al. 2019); **B.** Forest-steppe patch; **C.** Open sand grassland.

(Fomichev, Marusik & Koponen, 2014), *Spiracme nigromaculata* (Keyserling, 1884), *Spiracme quadrata* (Tang & Song, 1988), *Spiracme triangulosa* (Emerton, 1894), *Spiracme vachoni* (Schenkel, 1963). Later, Purgat et al. (2021) added *Spiracme mongolica* (Schenkel, 1963) to the genus.

While identifying our specimens, we noticed that the palp shows a high overall similarity to that of *S. mongolica*, as illustrated by Purgat et al. (2021). Still, at the same time, significant differences could be observed between the illustrations of the original description of Schenkel (1963) and the specimen identified and pictured by Fomichev (2015).

The aims of this paper are to provide illustrations and a description for *Xysticus lendli* Kulczyński, 1897, based on freshly collected material, describe the hitherto unknown female of the species, and reevaluate current faunistic records that may involve this species. We provide a DNA barcode for the species and test its phylogenetic position by reanalysing the matrix of Breitling (2019) with this new sequence added, and we discuss the accompanying results using a comparison with the type species of *Spiracme*.

Materials and methods

Specimens were collected in the Kiskunság region, Hungary, in 2017, 2018, and 2021 by sweep net from semi-natural sandy forest steppe patches (Fig. 1B, C). The specimens were photographed with a Nikon D300S camera attached to a Nikon S800 stereomicroscope and a Tucsen

Truechrome Metrics camera attached to an Eclipse E200 compound microscope. Multifocal images were compiled using HeliconFocus. The female vulva and palps in Fig. 5 were illustrated while immersed in methyl salicylate. Scanning electron micrographs were made in a low vacuum on a Hitachi SV1000 FlexSEM scanning electron microscope in the Plant Protection Institute (NÖVI) HUN-REN Centre for Agricultural Research. Drawings were made by the first author using a fineliner and 80 g/m^2 of printing paper. The maps were made using Adobe Illustrator CS6 software. All measurements are given in millimetres. The material is deposited in the Museum of Natural History, Budapest (MNHB) and the first author's personal collection in Szeged.

Whole genomic DNA was extracted from one leg using standard extraction kits. For the barcoding, the LCO1940/HCO2198 primers (Folmer et al. 1994) were used. PCR has been carried out in the Department of Zoology of the University of Veterinary Medicine Budapest, and capillary electrophoresis has been done at Commercial Biomi Services (Gödöllő, Hungary). Sequences were edited using Gap4 of the Staden Packge (Staden et al. 2000) and deposited in GenBank with the accession number PP545308. Phylogenetic relationships were inferred via both maximum likelihood and Bayesian methods based on the dataset that has been published so far (Breitling 2019). MAFFT v.7.450 online (https://mafft.cbrc.jp/alignment/server/) was used with default settings to align the sequences. A maximum likelihood phylogram was constructed using IQ-TREE (Nguyen et al. 2015) under the GTR+F+I+G model, performing 1000 ultrafast bootstrap replicates. Bayesian inference was performed using MrBayes v. 3.2.6 (Ronquist and Huelsenbeck 2003), using the GTR+I+G model of sequence evolution. Analyses consisted of two independent runs with one cold chain and five hot chains from random starting trees, run for 10 million generations, and sampled every 1000 generations. Convergence was assessed through examination of the standard deviation of split frequencies, which was well below recommended thresholds (0.01). The two MrBayes runs were combined after the deletion of burn-in generations (25%), and a majority-rule consensus phylogram was created. The resulting phylograms were edited and visualised with FigTree v.1.4 (Rambaut 2014).

Abbreviations

ALE — Anterior lateral eyes; **AME** — Anterior median eyes; **Fe** — Femur; **MOA-WA** — width of anterior median ocular area; **MOA-L** — median ocular area length; **MOA-WA** — width of anterior median ocular area; **MOA-WP** — width of posterior median ocular area; **Mt** — Metatarsus; **PLE** — Posterior lateral eyes; **PME** — Posterior median eyes; **RTA** — Retrolateral tibial apophysis; **Ta** — Tarsus; **tb** — tegular bump; **Ti** — tibia; **tut** — tutaculum; **VTA** — Ventral tibial apophysis.

Results

Taxonomy

Spiracme Menge, 1876

Figs 2, 3A–C, G–I, 4A–C, 5A, B, 6–8

Type species. *Spiracme striata* Menge, 1864. *Xysticus striata* Menge, 1876, by monotypy.

Note. Breitling (2019) revalidated the genus *Spiracme*, but he did not provide any diagnosis or any diagnostic features. As delimited by Breitling (2019), it is impossible to give a precise diagnosis for the genus, including all and only those species. Hence, it should be subject to future revision or reconsideration.

Diagnosis. Males can be recognised by the bulb lacking apophyses (Fig. 6A, D) or tegular apophysis (Gertsch 1953; Menge 1876; Lehtinen 2002). The tutaculum is triangle-shaped in this type of species. Tibia with two or three apophyses; VTA is simple and rounded; and RTA has a distinct pointed hook (Lehtinen 2002). Females can be recognised by the prominent septum (but can be absent; see Gertsch 1953). Both sex lateral eyes are 1.5 times larger than the median eyes and have light elevation (Menge 1876).

Composition. Currently 10 species have been added to this genus (WSC 2024): *S. striatipes* (L. Koch, 1870), *S. baltistana* (Caporiacco, 1935), *S. dura* (Sørensen, 1898), *S. keyserlingi* (Bryant, 1930), *S. lehtineni* (Fomichev, Marusik & Koponen, 2014), *S. nigromaculata* (Keyserling, 1884), *S. quadrata* (Tang & Song, 1988), *S. triangulosa* (Emerton, 1894), *S. vachoni* (Schenkel, 1963).

Description. see Menge (1876) and Lehtinen (2002).

Distribution. Holarctic.

Spiracme lendli (Kulczyński, 1897), comb. nov.

Figs 2, 3A–C, 4A–C, 5A, B, 6A–C, 7, 8

Xysticus lendli Kulczyński, 1897: Chyzer and Kulczyński 1897: 301, Tab X, fig. 64 (♂).

Spiracme mongolica: Purgat et al. 2021: fig. 6 (misidentification).

Xysticus cf. lendli: Ponomarev and Shmatko 2021: 217, fig. 16.

Type material. ***Holotype male*:** Hungary Örkény (thoroughly searched for in the collection of the Hungarian Natural History Museum, without any success, likely lost).

Material examined. Hungary • 1 male; Szank; forest steppe; 46.602°N, 19.571°E; 11 Sep. 2017; N. Gallé-Szpisjak and R. Gallé leg.; sweep net; (HNHM Araneae-11039) • 1 female; Zsana; forest steppe; 46.415°N, 19.621°E; 11 Sep. 2017; N. Gallé-Szpisjak and R. Gallé leg.; sweep net; (HNHM Araneae-10719) • 1 male; Harkakötöny; forest steppe, 46.507°N, 19.568°E; 11 Sep. 2017; N. Gallé-Szpisjak and R. Gallé leg.; sweep net • 2 males; Kiskunhalas; forest steppe; 46.477°N, 19.432°E; 11 Sep. 2017;

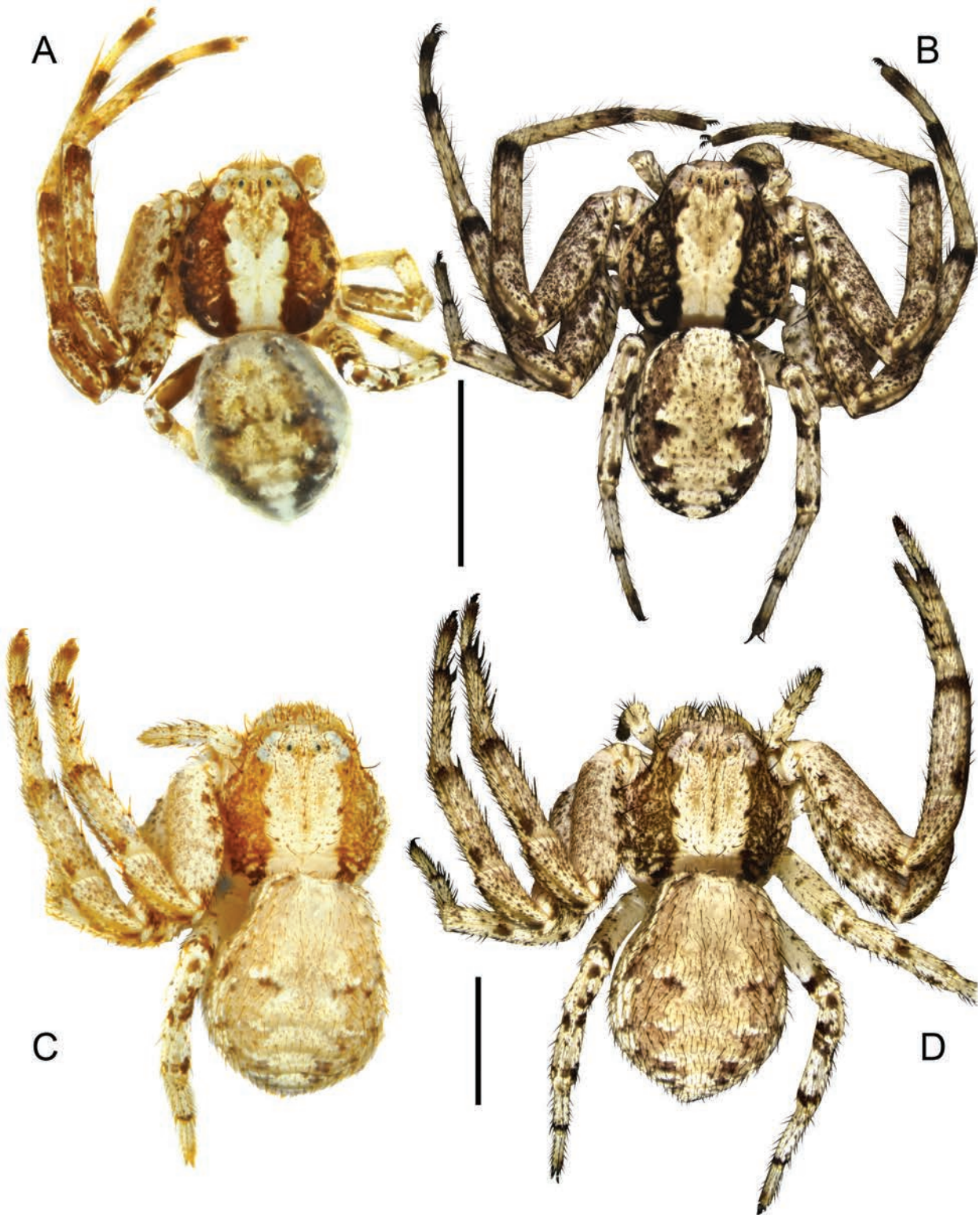

Figure 2. Habitus of *Spiracme lendli*: **A, B.** Male; **C, D.** Female; **A, C.** Specimen in alcohol, bleached out; **B, D.** Fresh specimens; Scale bar: 2.0 mm.

N. Gallé-Szpisjak and R. Gallé leg.; sweep net • 3 males; Kiskunhalas; forest steppe; 46.483°N, 19.452°E; 09 Sep. 2018; N. Gallé-Szpisjak and R. Gallé leg.; sweep net • 2 males; Kiskunhalas; forest steppe; 46.493°N, 19.415°E; 21 Sep. 2018; N. Gallé-Szpisjak and R. Gallé leg.; sweep net • 1 male; Soltvadkert; forest steppe; 46.536°N, 19.384°E; 11 Sep. 2017; N. Gallé-Szpisjak and R. Gallé leg.; sweep net • 1 male; Soltvadkert; forest steppe; 46.527°N, 19.374°E; 11. Sep. 2017, N. Gallé-Szpisjak and R. Gallé leg.; sweep net • 3 males; Soltvadkert; forest steppe; 46.530°N, 19.401°E; 11. Sep. 2017, N. Gallé-Szpisjak and R. Gallé leg.; sweep net • 3 males;

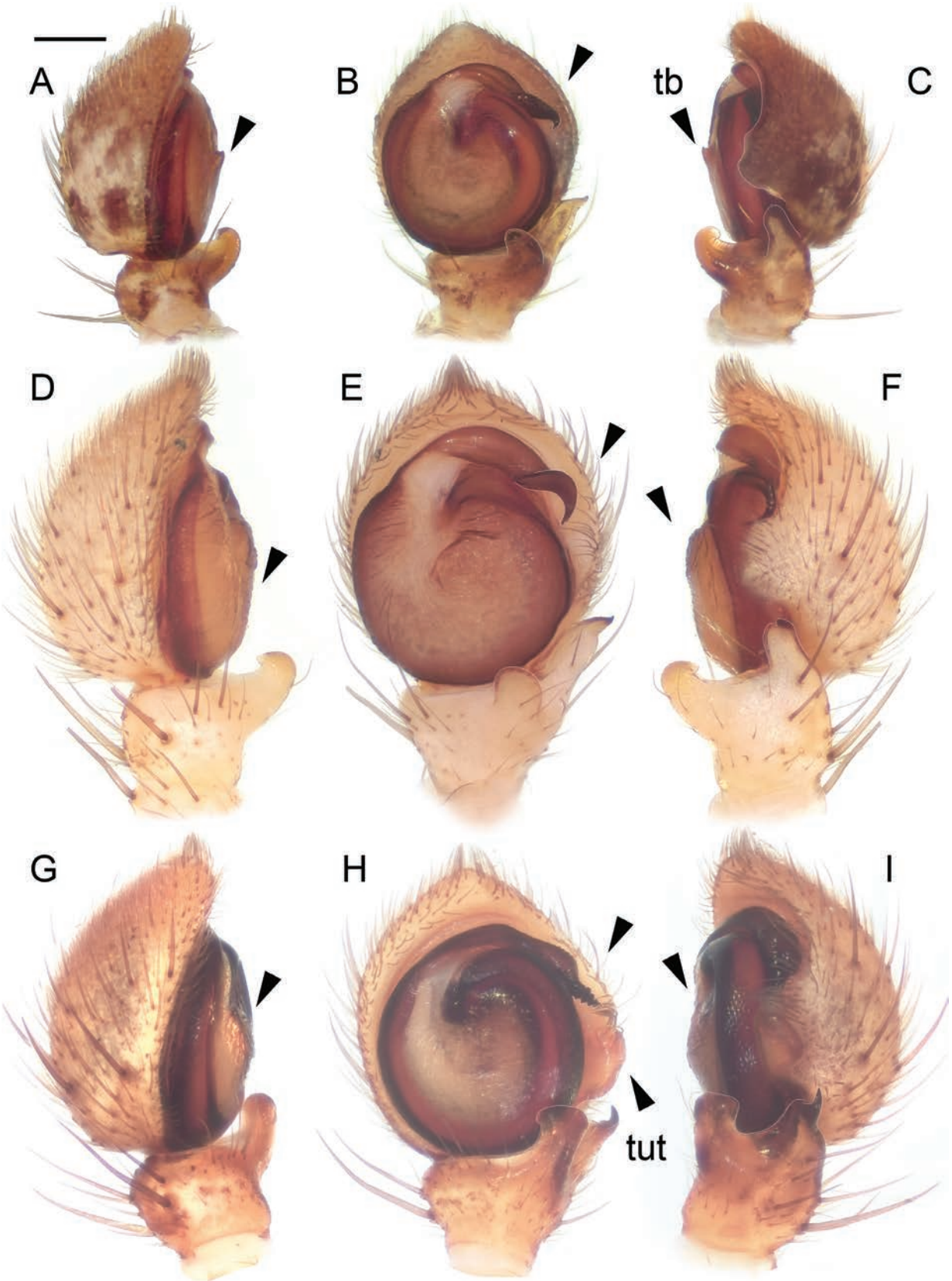

Figure 3. Male palps: **A–C.** *Spiracme lendli*; **D–F.** *Xysticus mongolicus*; **G–I.** *S. striatipes*; **A, D, G.** Prolateral view; **B, E, H.** Ventral view; **C, F, I.** Retrolateral view. Scale bar: 0.2 mm. Abbreviations: tb — tegular bump; tut — tutaculum.

Soltvadkert; forest steppe; 46.532°N, 19.385°E; 21. Sep. 2018, N. Gallé-Szpisjak and R. Gallé leg.; sweep net • 1 male; Zsana; forest steppe; 46.409°N, 19.621°E; 11. Sep. 2017, N. Gallé-Szpisjak and R. Gallé leg.; sweep net • 3 males; Zsana; forest steppe; 46.415°N, 19.621°E; 09. Sep. 2018, N. Gallé-Szpisjak and R. Gallé leg.; sweep net

• 3 males; Zsana; forest steppe; 46.396°N, 19.647°E; 09. Sep. 2018, N. Gallé-Szpisjak and R. Gallé leg.; sweep net • 2 males; Imrehegy; forest steppe; 46.446°N, 19.318°E; 11. Sep. 2017, N. Gallé-Szpisjak and R. Gallé leg.; sweep net • 1 male; Pirtó; forest steppe; 46.493°N, 19.415°E; 20. Sep.–05. Oct. 2018, N. Gallé-Szpisjak and R. Gallé leg.; pitfall trap • 1 male; Pirtó; forest steppe; 46.472°N, 19.436°E; 09. Sep. 2018, N. Gallé-Szpisjak and R. Gallé leg.; sweep net • 4 males; Pirtó; forest steppe; 46.496°N, 19.421°E; 05. Oct. 2018, N. Gallé-Szpisjak and R. Gallé leg.; sweep net • 2 males; Bócsa; forest steppe; 46.614°N, 19.464°E; 07. Sep. 2021, N. Gallé-Szpisjak and R. Gallé leg.; sweep net.

Comparative material. *S. striatipes* Hungary • 2 males, 2 females; Csengőd; mesic grassland; 46.722°N, 19.350°E; 15 Jun. 2018; N. Gallé-Szpisjak and R. Gallé leg.; sweep net.

Diagnosis. Males of this species can be readily distinguished from congeners by the thick and bent embolus, with transverse ridges (pine cone-like pattern in Fig. 5A–B) near the tip. The thick embolus makes it similar to that of *S. striatipes* but differs by the bent embolus (straight in *S. striatipes*; see Figs 3, 4), the less pronounced indentations (deep indentations in *S. striatipes*; see Fig. 6), the absence of the large triangular-shaped tutaculum (present in *S. striatipes*; see Fig. 6), and the slightly pointing outward RTA (curved towards the cymbium in *S. striatipes*; see Figs 3, 4) as seen from the ventral side (compare Fig. 6A vs. Fig. 6D). The bent embolus is present in *Xysticus mongolicus*, and the bulb shows an overall similarity. However, the indentations (absent in *X. mongolicus*), the tegular bump Fig. 3C (absent in *X. mongolicus*; see Fig. 3F), and the twisted embolus as seen from the side (strongly bent in *X. mongolicus*) separate *S. lendli* from *X. mongolicus*. Female epigyne of *S. lendli* with an upside-down heart-shaped median septum (see Fig. 8B), which is seemingly a plate with a pronounced anterior border (Fig. 8A, C) with a clear indention on the posterior margin (Fig. 8B, C, F), probably to accommodate the thin tip of the RTA (Figs 3C, 7A).

Description. Male. Total length 3.88. Carapace: 1.84 long, 1.79 wide. Abdomen: 2.17 long, 1.71 wide. Clypeus 0.16 high, chelicera 0.70 long. Eye sizes and inter-distances: MOA-WA 0.22, MOA-WP 0.23, MOA-L 0.23, AME 0.07, ALE 0.10, PME 0.06, PLE 0.09, AME-AME 0.20, AME-ALE 0.13, PME-PME 0.23, PME-PLE 0.29.

Colouration (on a freshly collected specimen, Fig. 2B): Carapace dark brown sides with median, longitudinal, beige-coloured, wide stripe. Ocular area white. Abdomen dark brown with mottled black spots and median folium-shaped light stripe. Around folium's lobe, three pairs of white and black spots present (Fig. 2A, B). These spots can be seen on bleached specimen as well, where the dark brown coloured areas became light brown. Chelicera, gnathocoxae, labium, and sternum sand-yellow with small dark brown spots.

Legs: sand-yellow with mottled dark brown dots (uneven in size). Tibiae I–II, metatarsi I–II, and tarsi I–II with dark brown/blackish rings on the distal end of the segment. Hindlegs light in colour, almost white, with black dots mottled on the appendage. The proximal end of tibia IV and the distal end of the femur, patella, tibia, and metatarsus IV with dark rings. Leg segments: I: 7.05 (2.04+0.96+1.6+1.6+0.85); II: 6.67 (1.95+0.88+1.45+1.48+0.91); III: 3.87 (1.19+0.58+0.83+0.67+0.6); IV: 4.51 (1.4+0.58+0.92+0.89+0.72).

Palpal femur, patella tibia, and cymbium with sand-coloured background mottled with dark brown dots and patches. Bulb without significant appendages, but tegular ledge or bump present (Figs 3C, 4C, 7A). Embolus originates on prolateral part of the bulb at 11 o'clock position, twisted as seen from the side (Fig. 7) and bent as seen from the venter (Figs 3A–C, 4A–C, 5A, B), with indentations on the distal third of embolus (Figs 5A, B, 6A, B), making it pine cone-like.

Female. Total length: 5.99. Carapace: 2.66 long, 2.89 wide. Abdomen: 3.68 long, 2.92 wide.

Clypeus 0.24 high, chelicera 1.01 long. Eye sizes and inter-distances: MOA-WA 0.58, MOA-WP 0.53, MOA-L 0.40, AME 0.11, ALE 0.16, PME 0.09, PLE 0.12, AME-AME 0.40, AME-ALE 0.21, PME-PME 0.37, and PME-PLE 0.45. Leg segments: I: 8.49 (2.61+1.34+1.87+1.7+0.97); II: 8.49 (2.65+1.24+1.84+1.77+0.99); III: 5.53 (1.76+0.91+0.93+1.05+0.88); IV: 6.16 (1.94+0.88+1.44+1.07+0.83).

Colouration lighter than in males, carapace and abdomen patterns similar as in males (Fig. 2C, D), but with less contrast on the pattern. Leg colouration and pattern also similar to males, but overall lighter in colour.

Distribution. Pannonian: Hungary, Serbia, Slovakia.

Habitat. Specimens were collected in habitats characterised by sandy soil, covered with open dry grassland, and small forest patches (forest steppe, Fig. 1B, C). The grassland consists of drought-tolerant plant species (e.g., *Alkanna tictoria*, *Festuca vaginata*, and *Stipa borysthenica*). The main tree species of the forest patches are *Poplus alba*, and the bush layer includes *Juniperus communis* and *Crataegus monogyna* (see further details in Gallé et al. 2022a).

Biology and phenology. Adult specimens were collected in September and October. We used a sweep net to collect *S. lendli* specimens very close to the ground surface in the herb layer. Life history remains mainly unknown. Noteworthy, females were very rarely found, so far only one. The overall ratio of the sexes was 33:1.

Xysticus mongolicus Schenkel, 1963, comb. rev.

Figs 3D–F, 4D–F, 5C, D

Xysticus mongolicus Schenkel, 1963: Schenkel 1963: 227, fig. 127a–c (♂).

X. mongolicus Song, Yu & Yang, 1982: 210 (♂♀); Song 1987: 284, fig. 241a–d (♂♀); Song and Zhu 1997: 95, fig. 62a–d (♂♀); Utochkin 1995: 67, fig. 1a–g (♂♀); Zhao 1993: 388, fig. 193a–b (♂♀); Marusik and Logunov 1990: 47, figs 48–49 (♂); Fomichev 2015: 97, figs 13–15 (♂).

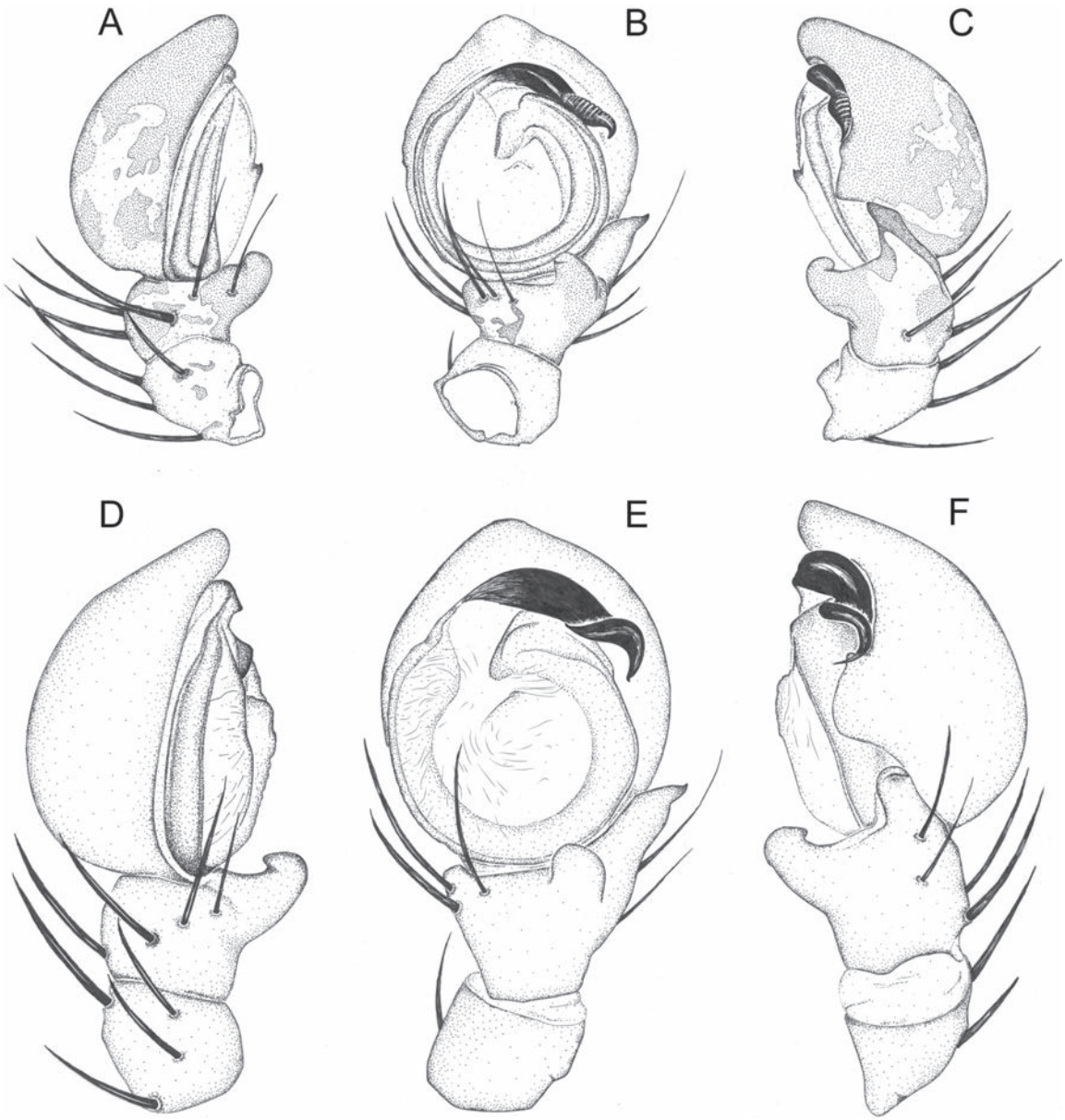

Figure 4. Distinguishing characters of *Spiracme lendli* (**A–C**) and *Xysticus mongolicus*: (**D–F**); **D.** Prolateral view; **B, E.** Ventral view; **C, F.** Retrolateral view. Scale bar: 0.2 mm.

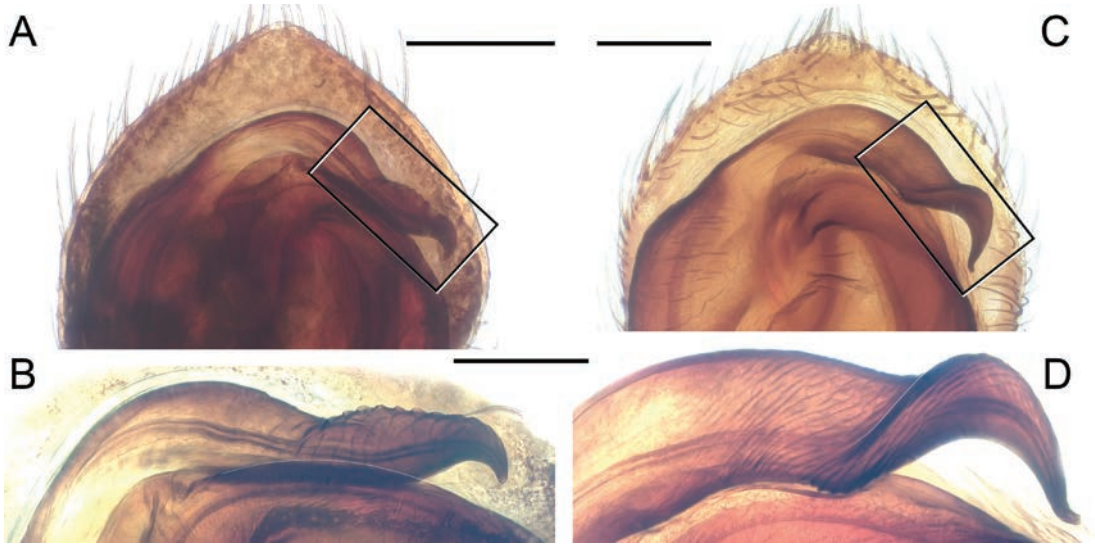

Figure 5. Comparison of male emboluses: *Spiracme lendli* (**A, B**) and *Xysticus mongolicus* (**C, D**). Scale bars: 0.2 mm.

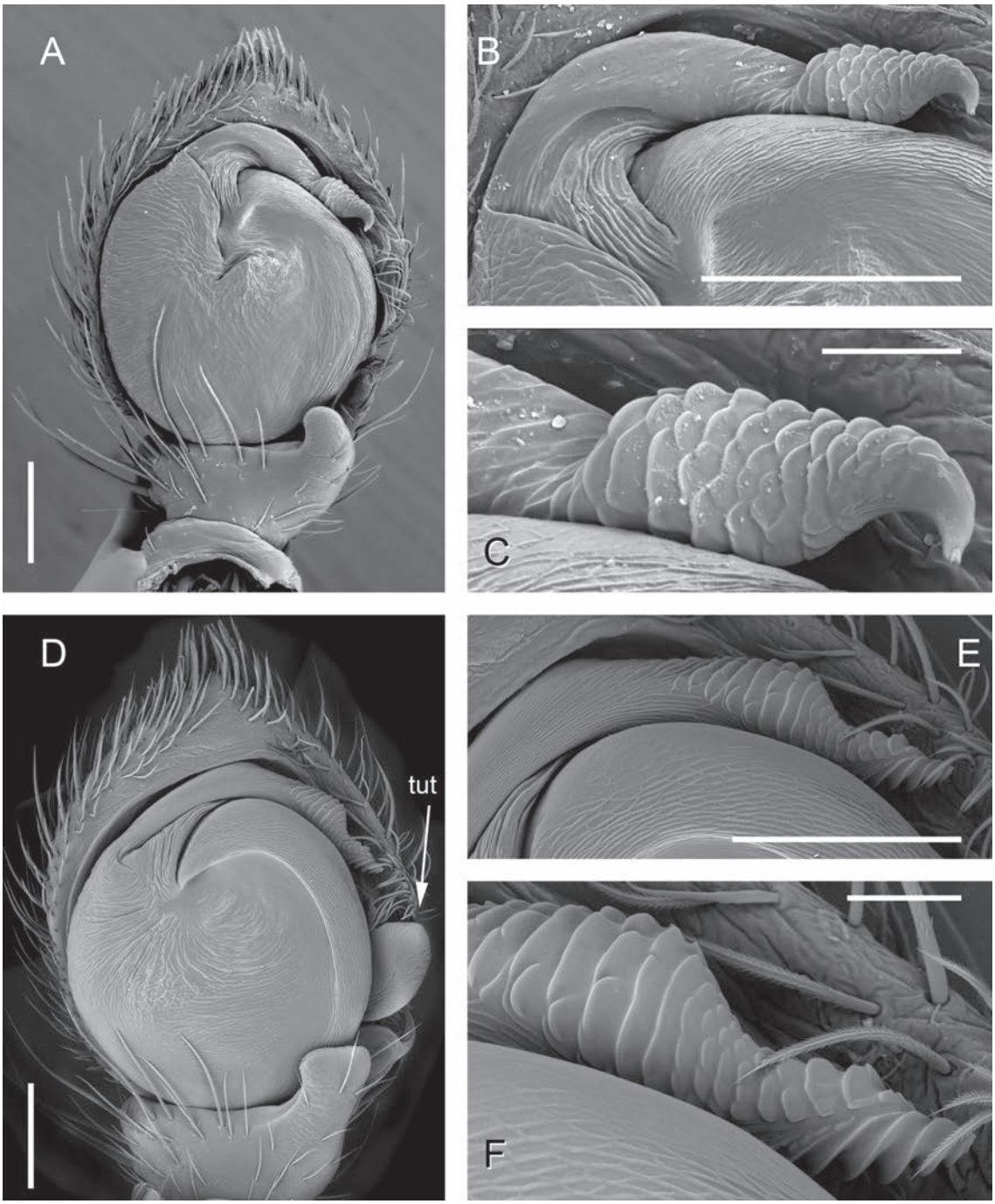

Figure 6. *Spiracme* spp. Male palps scanning micrographs *Spiracme lendli*: (**A–C**) *Spiracme striatipes*: (**D–F**); **A.** Bulb, ventral view; **B, C.** Closeup of the embolus, ventral view; **D.** Bulb, ventral view; **E, F.** Closeup of the embolus, ventral view. Scale bar: 0.2 mm (**A–B, D–E**); 0.05 mm (**C, F**). Abbreviation: tut — tutaculum.

Note. Because Purgat et al. 2021 (fig. 6) based their proposal of the new combination on a misidentified *S. lendli* specimen, we reinstate its original combination.

Material examinded. Russia • 1 male (ISEA, 001.7306), Russia, Altai Republic, 6 km SE of Chagan-Uzun Vill., 26.07.2021. 50.066667°N, 88.433333°E, 1900 m asl., stony semi-desert steppe, leg. & det. A.A. Fomichev.: Altai Republic,

Diagnosis. The male can be identified by the spiral-shaped and bare embolus with fine tip. *X. mongolicus* has no tegular ridge.

Description. See Fomichev, 2015.

Distribution. Nentwig et al. (2024) report this species from Europe to Central Asia. So far, all Central European records have turned out to be *S. lendli*. We could not examine the specimens used for the Ukrainian records by Polchaninova N., Prokopenko E. (2019), or the Russian records (Ponomarev 2022).

Both ML and BI phylogenetic trees (Fig. 9, Suppl. material 1, respectively) place Spiracme lendli grouping with the type species of the genus, *S. striatipes*. In that group, *S. triangulosus* is a sister. We were unable

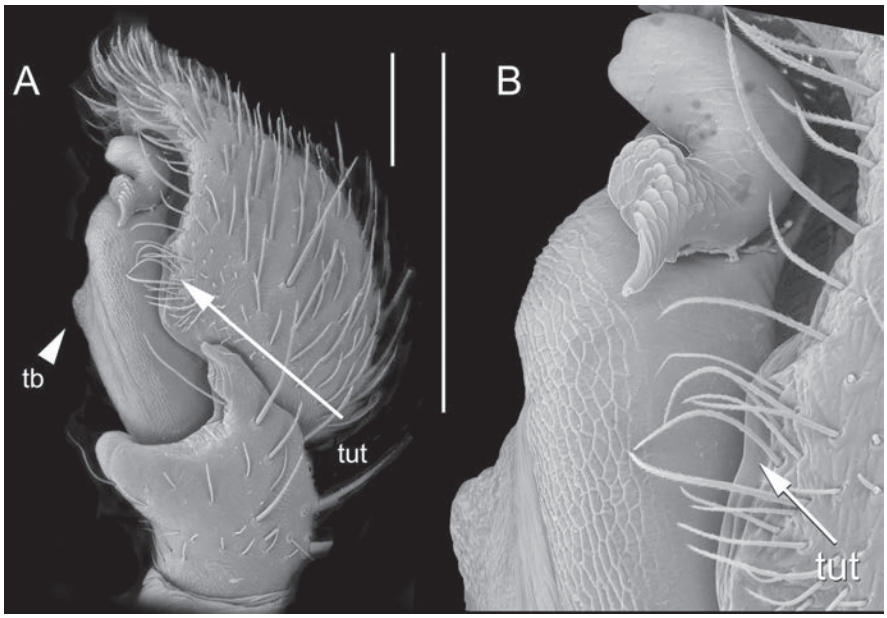

Figure 7. *Spiracme lendli*, male palps scanning micrographs: **A.** Entire palp retrolateral view. male; **B.** Bulb closeup, showing the embolus, the tegular bump, and the tutaculum. Scale bars: 0.2 mm. Abbreviations: tb — tegular bump; tut — tutaculum.

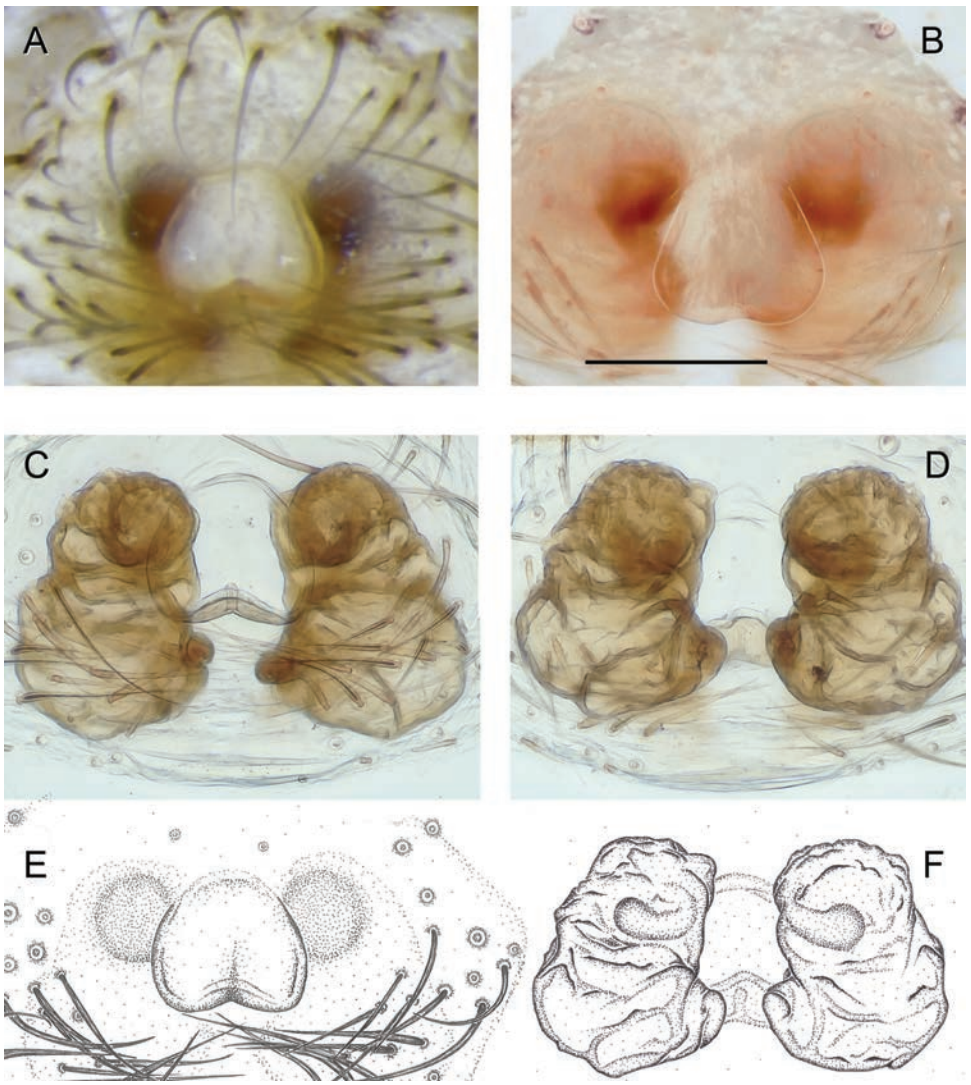

Figure 8. *Spiracme lendli* epigyne **A.** Fresh specimen, intact epigyne, ventral view; **B.** Prepared epigyne, ventral view; **C.** Same, in wintergreen oil; **D.** Vulva, dorsal view; **E.** Epigyne, ventral view; **F.** Vulva, dorsal view. Scale bar: 0.2 mm.

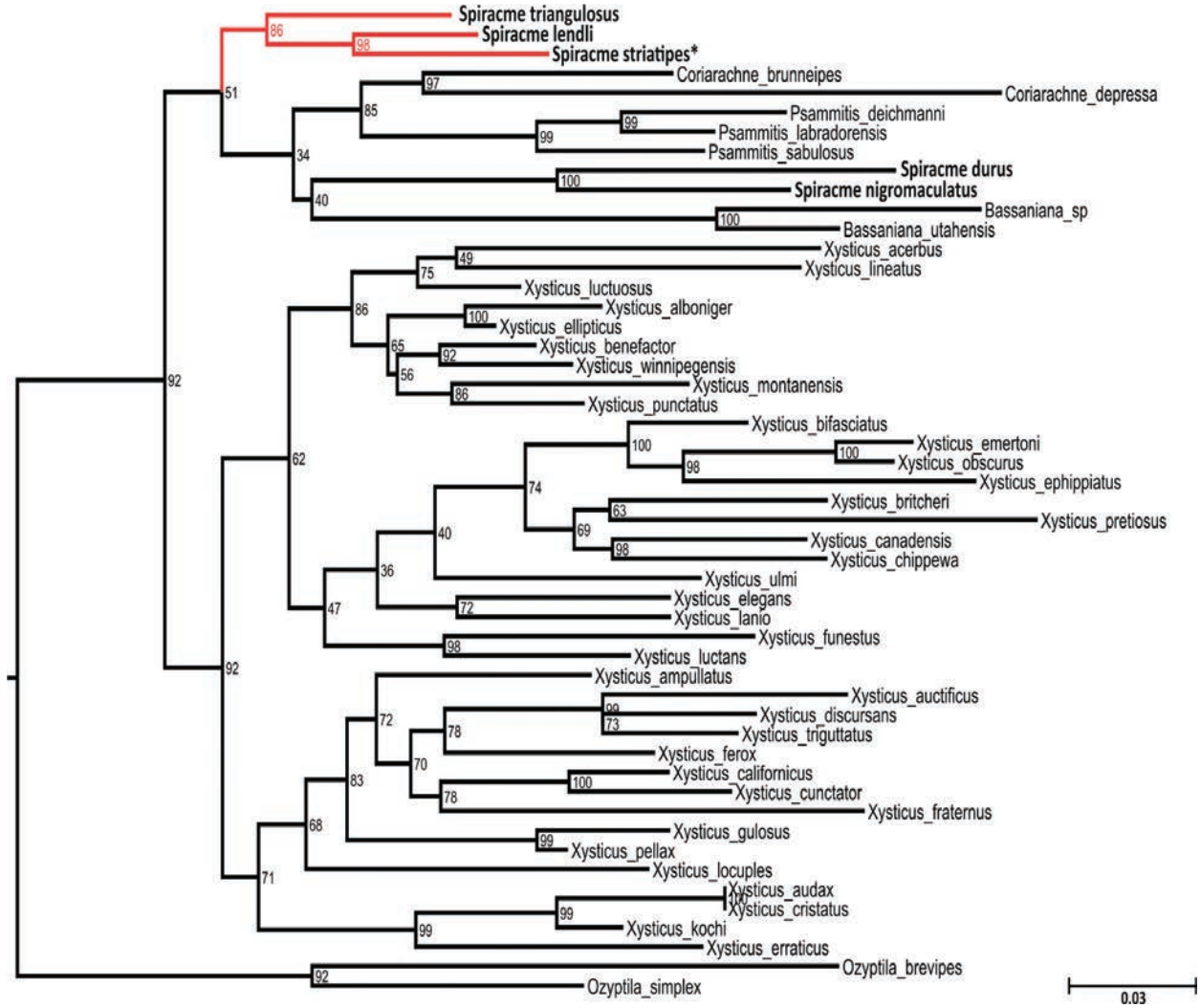

Figure 9. Maximum likehood tree based on the DNA barcode data (658 nt of the mitochondrial COX1 gene), inferred with IQ-TREE.

to recover a monophyletic *Spiracme*, as *S. durus* and *S. nigromaculatus* grouped together but not with the type species. Given the limited use of a single mitochondrial gene in systematics and the low support values on the tree, we would not draw further conclusions regarding the genus limits.

Discussion

With the revalidation of *Spiracme*, perhaps Pandora's box has been opened. As it stands, the genus contains other species groups (*durus* and *nigromaculatus*). From the original description of the genus erected for *S. striatipes* (L. Koch, 1870) by Menge (1876), it is now clear that he not only specifically listed the unique shape of the embolus of the type species ("*spitze schraubenförmig gewundenen eindringer*" [=embolus spirally twisted]) as diagnostic, but the etymology is also based on the spirally twisted embolus ("*spira and cuspis... Von der schraubenfürmigen spitze des eindringers*") as well. We assume that the genus concept of the auctor was to include species with spirally twisted emboli on top of an anapophysate tegulum. In the genus, as delimited currently by Breitling (2019), most of the species have filiform emboli and various tegular outgrowths. Considering all available information, including any species with filiform embolus in the genus *Spiracme*, on the basis of DNA barcode data alone might have been premature.

Menge erected another genus, *Psammitis* Menge, 1876, of which at least the type species, *Psammitis sabulosus* (Hahn, 1832), has a similar indentation on the embolus (Jantscher 2001). There is little to no consensus among the plethora of opinions regarding the limits and placement of *Spiracme* or *Psammitis*. However, placing *Spiracme lendli* based on morphology alone provides a challenge. It does not have a prominent tutaculum (Figs 3, 4, 7) versus *Spiracme striatipes*, which has a large, prominent triangular one (Figs 3H, 4H), and the tutaculum of *Psammitis* species is thin and points upward. *Spiracme lendli* has indentations on the bent embolus (Figs 5–7), *S. striatipes* has deeper indentations and a straight embolus; *P. sabulosus has* weaker indentations and a *bent* embolus; and finally, *S. lendli* has a tegular pocket similar to *P. sabulosus*, which is absent in *S. striatipes* (Figs 3I, 4I). Due to the inconsistent distribution of the

morphological characters used to place species into these genera, we decided to use the grouping with the type species of *Spiracme* and place *Xysticus lendli* Kulczyński, 1897, to *Spiracme* Menge, 1876.

Acknowledgements

We are thankful to Peter Batáry for his support and the free use of the equipment for identification. This work was supported by the Hungarian Research and Developmental Fund (Grant ID: NKFIH FK 142926). Barna Páll-Gergely and Jenő Kontschán have granted us access to their scanning electron microscope in the Plant Protection Institute (NÖVI) HUN-REN Centre for Agricultural Research, which is highly appreciated. We are especially grateful to Galina Azarkina and Alexander A. Fomichev in the Institute for Systematics and Ecology of Animals, Siberian Branch of the Russian Academy of Sciences, for giving us access to the *Xysticus mongolicus* specimen. We are indebted to Gordana Grbić, Ambros Hänggi, and Nina Polchaninova for their efforts and help to confirm their identification. Ábris Tóth kindly translated the Latin original description of *Xysticus lendli*, which is highly appreciated. We are grateful to Eszter Lazányi for facilitating several opportunities to revise and search through the whole *Xysticus* material in the Hungarian Natural History Museum's collection to find the type specimen. We would like to thank Suresh Benjamin and Yura Marusik for their reviews of an earlier version of the manuscript. Grant McDonald has helped with the English grammar, which is highly appreciated.

References

Bátori Z, Erdős L, Kelemen A, Deák B, Valkó O, Gallé R, Bragina TM, Kiss PJ, Kröel-Dulay G, Tölgyesi C (2018) Diversity patterns in sandy forest-steppes: A comparative study from the western and central Palaearctic. Biodiversity and Conservation 27(4): 1011–1030. https://doi.org/10.1007/s10531-017-1477-7

Breitling R (2019) A barcode-based phylogenetic scaffold for *Xysticus* and its relatives (Araneae: Thomisidae: Coriarachnini). Ecologica Montenegrina 20: 198–206. https://doi.org/10.37828/em.2019.20.16

Chyzer C, Kulczyński W (1897) Araneae Hungariae. Tomus II. Academia Scientarum Hungaricae, Budapest, 147–366. [Pl. VI–X]

Fekete G, Király G, Molnár Z (2016) Delineation of the Pannonian vegetation region. Community Ecology 17(1): 114–124. https://doi.org/10.1556/168.2016.17.1.14

Folmer O, Black M, Hoeh W, Lutz R, Vrijenhoek R (1994) DNA primers for amplification of mitochondrial cytochrome c oxidase subunit I from diverse metazoan invertebrates. Molecular Marine Biology and Biotechnology 3(5): 294–299.

Fomichev AA (2015) New data on the crab spider genus *Xysticus* C.L. Koch, 1835 from the Altai, South Siberia (Aranei: Thomisidae). Arthropoda Selecta 24(1): 91–97. https://doi.org/10.15298/arthsel.24.1.05

Gallé R, Tölgyesi C, Császár P, Bátori Z, Gallé-Szpisjak N, Kaur H, Maák I, Torma A, Batáry P (2022b) Landscape structure is a major driver of plant and arthropod diversity in natural European forest fragments. Ecosphere 13(1): e3905. https://doi.org/10.1002/ecs2.3905

Gallé R, Tölgyesi C, Torma A, Bátori Z, Lörinczi G, Szilassi P, Gallé-Szpisjak N, Kaur H, Makra T, Módra G, Batáry P (2022a) Matrix quality and habitat type drive the diversity pattern of forest steppe fragments. Perspectives in Ecology and Conservation 20(1): 60–68. https://doi.org/10.1016/j.pecon.2021.11.004

Gallé R, Korányi D, Tölgyesi C, Lakatos T, Marcolin F, Török E, Révész K, Szabó ÁR, Torma A, Gallé-Szpisjak N, Marja R, Szitár K, Deák B, Batáry P (2022c) Landscape-scale connectivity and fragment size determine species composition of grassland fragments. Basic and Applied Ecology 65: 39–49. https://doi.org/10.1016/j.baae.2022.10.001

Gertsch WJ (1953) The spider genera *Xysticus*, *Coriarachne*, and *Oxyptila* (Thomisidae, Misumeninae) in North America. Bulletin of the AMNH, American Museum of Natural History, New York, 417–482.

Grbić G, Hänggi A, Gajić I, Vaselek S, Ivković S (2019) Spiders (Araneae) of the Deliblato Sands (Serbia). Acta Entomologica Serbica 24: 79–93. https://doi.org/10.5281/zenodo.3249916

Jantscher E (2001) Revision der Krabbenspinnengattung *Xysticus* C.L. Koch, 1835 (Araneae, Thomisidae) in Zentraleuropa. Dissertation, Univ. Graz, 328 pp. [81 pls]

Jantscher E (2002) The significance of male pedipalpal characters for the higher systematics of the crab spider genus Xysticus CL Koch, 1835 (Araneae: Thomisidae). In European Arachnology 2000: Proceedings of the 19th European Colloquium of Arachnology. Aarhus University Press, Aarhus, 329–336.

Lehtinen PT (2002) Generic revision of some thomisids related to Xysticus CL Koch, 1835 and Ozyptila Simon, 1864. In European Arachnology 2000: Proceedings of the 19th European Colloquium of Arachnology. Aarhus Univ. Press, Aarhus, 315–327.

Marusik YM, Logunov DV (1990) The crab spiders of Middle Asia, USSR (Aranei, Thomisidae). 1. Descriptions and notes on distribution of some species. Korean Arachnology 6: 31–62.

Menge A (1876) Preussische Spinnen. VIII. Fortsetzung. Schriften der Naturforschenden Gesellschaft in Danzig (N. F.) 3: 423–454.

Molnár C, Molnár Zs, Barina Z, Bauer N, Biró M, Bodonczi L, Csathó AI, Csiky J, Deák JÁ, Fekete G, Harmos K, Horváth A, Isépy I, Mesterházy A, Molnár A, Nagy J, Óvári M, Purger D, Schmidt D, Sramkó G, Szénási V, Szmorad F (2008) Vegetation-based landscape regions of Hungary. Acta Botanica Hungarica 50(1): 47–58. https://doi.org/10.1556/ABot.50.2008.Suppl.4

Nentwig W, Blick T, Bosmans R, Gloor D, Hänggi A, Kropf C (2024) Spiders of Europe. Version 03.2024. [https://www.araneae.nmbe.ch, accessed on 21.03.2024] https://doi.org/10.24436/1

Nguyen LT, Schmidt HA, Von Haeseler A, Minh BQ (2015) IQ-TREE: A fast and effective stochastic algorithm for estimating maximum-likelihood phylogenies. Molecular Biology and Evolution 32(1): 268–274. https://doi.org/10.1093/molbev/msu300

Polchaninova N, Prokopenko E (2019) An updated checklist of spiders (Arachnida: Araneae) of Left-Bank Ukraine. Arachnologische Mitteilungen. Arachnologische Mitteilungen 57(1): 60–64. https://doi.org/10.30963/aramit5711

Ponomarev AV (2022) Spiders (Arachnida: Araneae) of the southeast of the Russian Plain: catalogue, the fauna specific features. SSC RAS Publishers, Rostov-on-Don, 640 pp.

Ponomarev AV, Shmatko VY (2021) New data on the fauna and taxonomy of spiders (Aranei) in southern Russia.

Caucasian Entomological Bulletin 17(1): 211–218. https://doi.org/10.23885/181433262021171-211218

Purgat P, Gajdoš P, Purkart A, Hurajtová N, Volnár Ľ, Krajčovičová K (2021) *Walckenaeria stylifrons* and *Spiracme mongolica* (Araneae, Linyphiidae, Thomisidae), two new species to Slovakia. Check List 17(6): 1601–1608. https://doi.org/10.15560/17.6.1601

Rambaut A (2014) FigTree vi. 4.2. released 2014-07-09. http://tree.bio.ed.ac.uk/software/figtree

Ronquist F, Huelsenbeck JP (2003) MrBayes 3: Bayesian Phylogenetic Inference under Mixed Models. Bioinformatics 19(12): 1572–1574. https://doi.org/10.1093/bioinformatics/btg180

Schenkel E (1963) Ostasiatische Spinnen aus dem Muséum d'Histoire naturelle de Paris. Mémoires du Muséum National d'Histoire Naturelle de Paris A. Zool 25: 1–481.

Song DX (1987) Spiders from agricultural regions of China (Arachnida: Araneae). Agriculture Publishing House, Beijing, 376 pp.

Song DX, Zhu MS (1997) Fauna Sinica: Arachnida: Araneae: Thomisidae, Philodromidae. Science Press, Beijing, 259 pp.

Song DX, Yu SY, Yang HF (1982) A supplement note on some species of spiders from China. Acta Scientiarum Naturalium Universitatis Intramongolicae 13: 209–213.

Staden R, Beal KF, Bonfield JK (2000) The Staden package, 1998. In: Misener S, Krawetz SA (Eds) Bionformatics Methods and Prtocolls. Methods in Molecular Biology 132. Humana Press, Clifton, New Jersey, 115–130. https://doi.org/10.1385/1-59259-192-2:115

Utotchkin AS (1995) Review of the spider genus Xysticus CL Koch, 1935 (Arachnida, Aranei, Thomisidae) in the East Kazakhstan Area. Arthropoda Selecta 4: 65–69.

WSC (2024) World Spider Catalog. Version 25.0. Natural History Museum Bern. [http://wsc.nmbe.ch, accessed on 21.02.2024] https://doi.org/10.24436/2

Zhao JZ (1993) Spiders in the cotton fields in China. Wuhan Publishing House, Wuhan, China, 552 pp.

Supplementary material 1

BI phylogram based on the barcode COI dataset (657 bp), inferred with MrBayes 3.2

Authors: Nikolett Gallé-Szpisjak, Róbert Gallé, Krisztián Szabó, Tamás Szűts

Data type: jpg

Link: https://doi.org/10.3897/zse.100.125826.suppl1

Zoosyst. Evol. 100 (3) 2024, 1029–1039 | DOI 10.3897/zse.100.128096

PENSOFT

für Natur MUSEUM FÜR NATURKUNDE BERLIN

Oleaxonchium olearum gen. et sp. nov. (Nematoda, Dorylaimida) associated with an olive grove in the southern Iberian Peninsula, and new insights into the evolutionary relationships within Belondiridae

Reyes Peña-Santiago[1], Miriam García-Ruiz[1], Alba N. Ruiz-Cuenca[1], Joaquín Abolafia[1]

1 *Departamento de Biología Animal, Biología Vegetal y Ecología, Universidad de Jaén, Campus "Las Lagunillas" s/n, 23071, Jaén, Spain*

https://zoobank.org/B08F64F7-9C46-4F05-A836-76A41117CE73

Corresponding author: Reyes Peña-Santiago (rpena@ujaen.es)

Academic editor: A. Schmidt-Rhaesa ♦ **Received** 22 May 2024 ♦ **Accepted** 25 June 2024 ♦ **Published** 25 July 2024

Abstract

A new belondirid, dorylaimid taxon, *Oleaxonchium olearum* **gen. et sp. nov.**, collected from an olive grove in the Andalusia region of Spain, is characterised, including its morphological description, morphometrics, SEM study, and molecular (18S-, 28S-rDNA) analyses. The new genus displays a unique combination of traits that distinguishes it from its closest genera: a rectangular lip region with sclerotized margins when observed in lateral view and visibly hexagonal in face view under SEM; a comparatively long cheilostom with thickened walls at its anterior part; a short isthmus-like section separating both pharyngeal regions; a mono-opistho-ovarian didelphic female genital system without *pars refringens vaginae*; and a short and rounded tail. The new species is characterised by its 2.44–2.87 mm long body, lip region 7–7.5 µm wide, odontostyle 10–10.5 µm long, neck 723–973 µm long, pharyngeal expansion occupying 63–72% of the total neck length, female anterior genital branch 4–6% of body length, tripartite posterior uterus 1.9–2.6 body diameters long, with a short intermediate section bearing sclerotized elements, vulva (V = 58–61) a transverse slit, caudal region 29–35 µm long (c = 74–89, c' = 0.9–1.1), and male unknown. As derived from an integrative approach combining morphological and molecular data, the new genus is close to *Metaxonchium*, the polyphyly of Belondiridae is confirmed, and support is provided in favour of the monophyly of Axonchiinae.

Key Words

morphology, new taxa, phylogeny, SEM, taxonomy, 18S-, 28S-rDNA

Introduction

Dorylaims, the members of the order Dorylaimida, are probably the most diverse nematode taxon. Being present in any continental (soil and freshwater) habitat and exploiting a wide spectrum of feeding resources, they are regarded as good bioindicators of environmental health (Peña-Santiago 2021). With 36 valid genera and 242 valid species, the family Belondiridae Thorne, 1939 represents almost 10 percent of all the dorylaims (Andrássy 2009). This family currently includes three subfamilies, one of which, Belondirinae Thorne, 1939, is less diverse and more frequent in temperate areas.

The free-living dorylaimid fauna of olive groves is poorly explored in spite of the fact that this culture is the most prominent and most socioeconomically important fruit tree in Europe, especially across the Mediterranean Basin (Vilar and Pereira 2018). Actually, at present, only eight species, eight genera, and six families were previously found in dwelling olive orchards (unpublished data). Representatives of Belondirinae are scarce in the Iberian fauna, with four species hitherto recorded, mainly in natural areas (Jiménez-Guirado et al. 2007).

A belondirid population was collected in the course of a nematological survey conducted to study the free-living fauna inhabiting olive soils in the framework of the

project Soil O-Live (EU Horizon Programme Grant No. 101091255). Its morphological and molecular study revealed that it represented a new generic taxon. Thus, this contribution aims to describe its morphological pattern, obtain its molecular characterization, and discuss its evolutionary relationships.

Materials and methods

Nematodes and their morphological and morphometrical study

A total of 12 female specimens, found in the soils of an olive grove named "La Capilla" (Spain, Málaga province, Antequera municipality), were available to study. Nematodes were extracted by centrifugation (CDFA 2015; based on Jenkins 1964) and/or with Baermann's funnels following the protocol by Flegg (1967), somewhat modified, killed by heat, fixed in 4% formaldehyde, preserved in anhydrous glycerin according to Siddiqi's (1964) method, mounted on permanent glass slides that were sealed with paraffin, and measured and photographed using an Eclipse 80i microscope (Nikon) equipped with differential interference contrast optics, a drawing tube (*camera lucida*), and a DS digital camera. Morphometrics include Demanian indices and other measurements and ratios; some of them are presented in a separate table, while others form part of the literal description of species. Two specimens preserved in glycerin were selected for observation with a SEM, according to Abolafia (2015). The nematodes were hydrated in distilled water, dehydrated in a graded ethanol-acetone series, critical point dried, coated with gold, and observed with a Zeiss Merlin microscope (5 kV).

Molecular study

For molecular analyses, single specimens were temporarily mounted in a drop of 1 M sodium chloride containing glass beads. This was followed by DNA extraction from single individuals, as described by Archidona-Yuste et al. (2016). The D2–D3 domains were amplified using the D2A (5′−ACAAGTACCGTGAGGGAAAGTTG−3′) and D3B (5′−TCGGAAGGAACCAGCTACTA−3′) primers (De Ley et al. 1999). The portion of 18S rRNA was amplified using primers 988F (5′−CTCAAAGATTAAGCCATGC−3′), 1912R (5′−TTTACGGTCAGAACTAGGG−3′), 1813F (5′−CTGCGTGAGAGGTGAAAT−3′), and 2646R (5′−GCTACCTTGTTACGACTTTT−3′) (Holterman et al. 2006). All polymerase chain reaction (PCR) assays were done according to the conditions described by Archidona-Yuste et al. (op. cit.). The amplified PCR products were purified using ExoSAP-IT (Affimetrix, USB products) and used for direct sequencing on a DNA multicapillary sequencer (Model 3130XL genetic analyser; Applied Biosystems, Foster City, CA, USA), using the BigDye Terminator Sequencing Kit V.3.1 (Applied Biosystems, Foster City, CA, USA), at the StabVida sequencing facilities (Caparica, Portugal). The newly obtained sequences were submitted to the GenBank database under the accession numbers indicated on the phylogenetic trees.

Phylogenetic analyses

For phylogenetic relationships, analysis was based on 18S and 28S rDNA fragments. The obtained sequences were manually edited using Chromas 2.6.6 (Technelysium) and aligned with other rDNA sequences available in GenBank using the ClustalW alignment tool implemented in MEGA7 (Kumar et al. 2016). Poorly aligned regions at extremes were removed from the alignments using MEGA7. The best-fit model of nucleotide substitution used for the phylogenetic analysis was statistically selected using jModelTest 2.1.10 (Darriba et al. 2012). The phylogenetic tree was generated with the Bayesian inference method using MrBayes 3.2.6 (Ronquist et al. 2012). The analysis under the general time reversible plus invariant sites plus gamma distribution (GTR + I + G) model was initiated with a random starting tree and run with the Markov chain Monte Carlo (MCMC) (Larget and Simon 1999) for 1×10^6 generations. The tree was visualised and saved with FigTree 1.4.4 (Rambaut 2018).

Results

Description of new taxa

***Oleaxonchium* gen. nov.**

https://zoobank.org/D5B8C148-9476-4684-AC45-255492E8F9A6

Diagnosis. Belondiridae, Belondirinae. Medium-sized nematodes, 2.44–2.87 mm long. Cuticle dorylaimid, thick, two-layered. Body pores button-like. Lip region narrower than the adjoining body, rectangular in lateral view, with distinctly sclerotized margins, totally fused lips, and simple, pore-like cephalic papillae. Amphid cup-like, with large aperture. Cheilostom a relatively long truncate cone with thickened walls at its anterior (perioral) part. Odontostyle small, robust, slightly fusiform, with short aperture, up to one-third of its length. Guiding ring simple, refractive. Odontophore linear, lacking any differentiation. Pharynx entirely muscular, with both regions separated by a short, isthmus-like narrowing; basal expansion occupying *ca* two-thirds of the total neck length, surrounded by a conspicuous muscular sheath. Female genital system mono-opistho-ovarian, didelphic, without *pars refringens vaginae*, well-developed *pars distalis vaginae*, and transverse vulva. Caudal region short and rounded. Male unknown.

Type and only species. *Oleaxonchium olearum* sp. nov.

Etymology. The genus name is derived from *Olea europaea* L., the scientific name of olive, as the type species was found associated with this typical Mediterranean fruit tree, and *Axonchium*, a very close taxon.

***Oleaxonchium olearum* gen. et sp. nov.**

https://zoobank.org/244ABA7C-4365-4FE8-9340-F765726A3811

Figs 1–4

Material examined. Twelve females from one location are in good condition for preservation.

Morphometrics. See Table 1.

Table 1. Main morphometrics of *Oleaxonchium olearum* gen. et sp. nov. from Spain. Measurements in µm except L in mm are in the form of average ± sd (range).

Character n	Holotype	Paratypes
	♀	**11**♀♀
L	2.87	2.61 ± 0.12 (2.44–2.87)
a	60	56.6 ± 3.3 (53–64)
b	2.9	3.1 ± 0.3 (2.6–3.5)
c	84	81.8 ± 5.4 (74–89)
V	59	58.6 ± 0.7 (58–61)
c'	1.0	1.0 ± 0.1 (0.9–1.1)
Lip region diameter	7.5	7.03 ± 0.3 (7.0–7.5)
Odontostyle length	10	10.1 ± 0.2 (10–10.5)
Odontophore length	16	15.7 ± 0.4 (15–16)
Neck length	973	894 ± 86 (723–973)
Pharyngeal expansion length	670	566 ± 79 (458–679)
Body diameter at neck base	47	44.5 ± 1.7 (42–47)
mid-body	48	46.2 ± 1.6 (44–48)
anus	34	33.6 ± 0.9 (32–35)
Distance vulva – anterior end	1680	1530 ± 79 (1419–1680)
Prerectum length	392	361 ± 25 (326–392)
Rectum length	35	33.4 ± 2.4 (29–37)
Tail length	34	32 ± 1.9 (29–35)

Description. Female. Very slender and medium-sized nematodes. Body cylindrical, conspicuously tapering towards the anterior end, much less so towards the posterior one as the tail is short and rounded. Upon fixation, habitus curved ventrad to a more or less open C shape. Cuticle smooth, two-layered, 0.5–1 µm thick at anterior region, 2.5–4 µm in mid-body, and 8–11 µm on tail, consisting of a thinner outer layer and a much thicker inner layer bearing radial striation, especially appreciable at caudal region. Large cervical lacunae are present. Lateral chord very narrow, 4–10 µm wide, occupying up to one-fifth (9–21%) of midbody diameter, bearing abundant elliptical gland bodies, more perceptible at posterior body region. Lateral pores button-like, when observed with SEM. Lip region almost rectangular in lateral view, visibly narrower than the adjoining body, 1.8–2.1 times wider than high, and *ca* one-sixth (15–17%) of body diameter at neck base, its anterior and lateral margins sclerotized and somewhat refractive, with hardly visible labial and cephalic papillae. SEM observations: lip region almost octogonal when observed in face view, with totally fused lips; its margin slightly elevated, marking off a somewhat sunken area; oral field comparatively small as inner labial papillae are almost equidistant between the oral aperture and the marging, far from the outer labial papillae; labial papillae button-like, delimited by a small circular incisure, with a distinct pore at their center, cephallic papillae unusually simple, small pore-like. Amphid fovea cup-like, its aperture 6.5–7.5 µm long, almost equal (0.9–1.1 times) to the lip region width. Cheilostom a truncate cone 11.5–12 µm long, 1.6–1.7 times as long as the lip region width, with thin walls that distinctly thicken at its anterior (perioral) end. Odontostyle slightly fusiform, 5–7 times as long as wide, longer (1.3–1.5 times) than lip region width, 0.35–0.42% of body length, its aperture 2–3 µm or less than one-third (20–30%) of total length. Guiding ring simple, distinct. Odontophore rod-like, 1.4–1.6 times the odontostyle, bearing very weak thickenings at its base. Pharynx very long, consisting of a slender anterior region, a very short narrower (isthmus-like) intermediate section, and a large, strongly muscular posterior expansion 18–38 times as long as wide, 10–15 times longer than body diameter at neck base, which occupies *ca* two−thirds (63–72%) of the total neck length, and appears enveloped by a strong spiral muscular sheath with almost strait bands; gland nuclei obscure in the specimens examined. Nerve ring situated at 147–178 µm, or 17–22% of the total neck length from the anterior end. Pharyngo-intestinal junction consisting of a cylindrical, tongue-like, 20–27 × 6.5–11 µm cardia, almost totally surrounded by intestinal tissue. Genital system mono-opistho-ovarian, didelphic: anterior branch reduced, 102–165 µm long or 4–6% of body length, consisting of a tube-like uterus, a narrowing, probably a very weak sphincter, and a distal cell mass 20–24 µm long, certainly representing a vestigial oviduct and/or ovary; posterior branch well-developed, 190–303 µm long or 8–11% of body length, with a variably large ovary 56–146 µm long, often not reaching the sphincter, bearing oocytes first in several rows and then in a single row, oviduct 72–116 µm long or 1.6–2.6 body diameters that consists of a slender distal region made of prismatic cells and a proximal *pars dilatata* with visible lumen inside, sphincter present but not especially distinct between oviduct and uterus, uterus 87–122 µm long or 1.9–2.6 body diameters (its length however should be taken with caution as it always appears convoluted), tripartite as it consists of a longer proximal region with wider lumen, a shorter intermediate section that bears refractive elements (Z-like structure), and a dilate, almost spherical, distal part. Vagina 22–27 µm long, extending inwards to often more than one-half (48–60%) of body diameter: *pars proximalis* 11–16 × 8–17 µm and encircled by moderately developed musculature, *pars distalis* 9–12 µm long. Vulva a transverse slit *ca* 10 µm long. Prerectum 9.6–12.2, rectum 0.9–1.1 anal body diameters long. Anus a visibly arched transverse slit *ca* 4 µm long. Caudal region short and rounded, its inner core reaching 61–77% of tail length, caudal pores two pairs, sublateral, at the middle of tail.

Male. Unknown.

Molecular characterization. After sequencing and editing, ten sequences of type specimens were obtained for phylogenetic analyses. Six 18S rDNA sequences, which were 1653, 1696, 1705, and 1709 (three sequences) bp length (acc. PP956610–PP956615, respectively), presented 1651 bp in common, and a Blast search showed that they were 98.97% similar to those of *Axonchium* sp. (acc. MG921264 and OQ946544). Four 28S rDNA sequences, which were 728, 739, 742, and 745 bp length (acc. PP956616–PP956619, respectively), presented 720 bp in common, and a Blast search showed that they were 93.34%

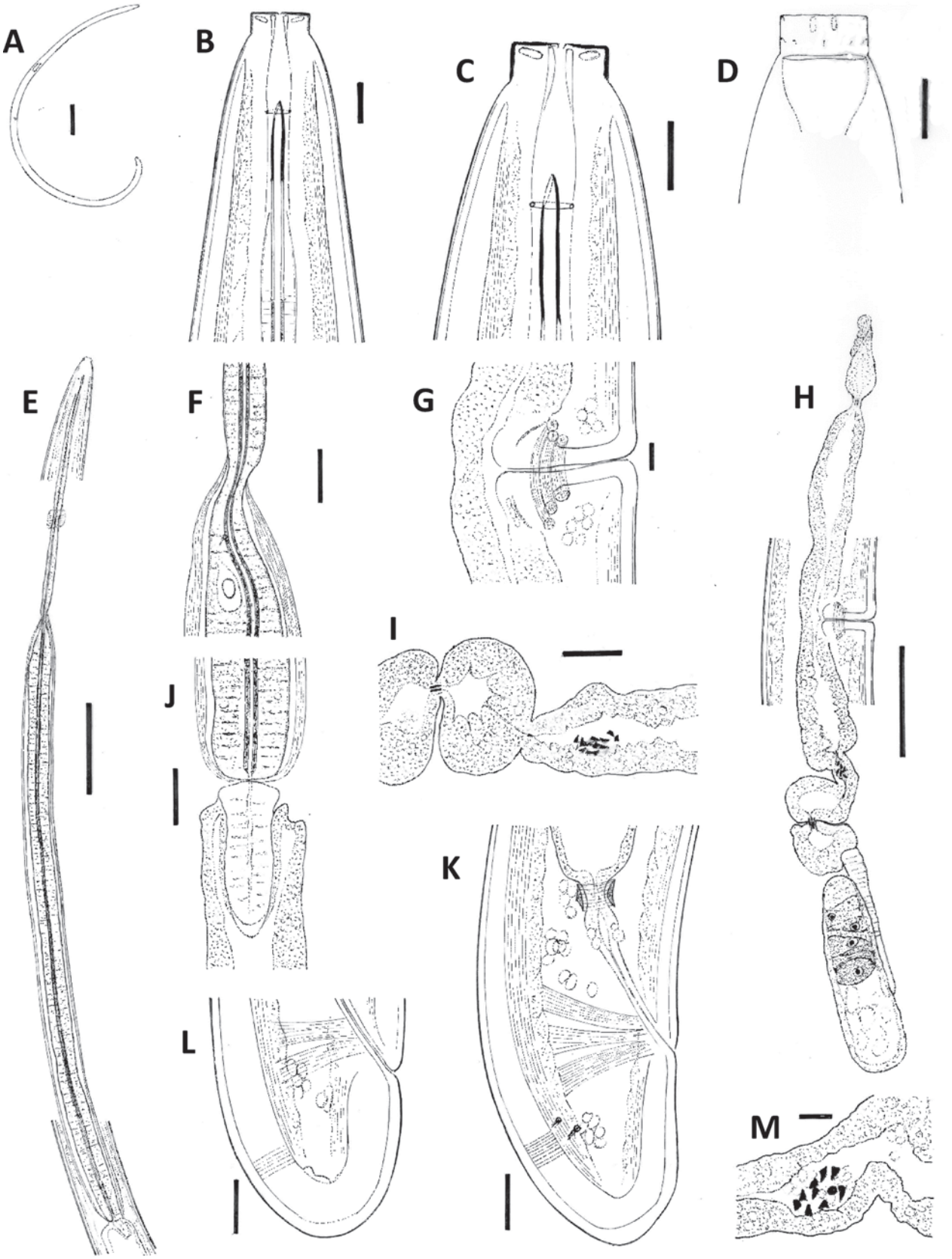

Figure 1. *Oleaxonchium olearum* gen. et sp. nov. (female). **A.** Entire; **B-D.** Anterior body region in lateral median (**B, C**) and lateral surface (**D**) views; **E.** Neck region; **F.** Isthmus-like narrowing between both pharyngeal sections; **G.** Vagina; **H.** Genital system; **I.** Oviduct-uterus junction; **J.** Pharyngo-intestinal junction; **K, L.** Caudal region; **M.** Detail of uterine Z-like sructure Scale bars: 200 µm (**A**); 5 µm (**B–D, G, M**); 100 µm (**E**); 10 µm (**F, I–L**). 50 µm (**H**).

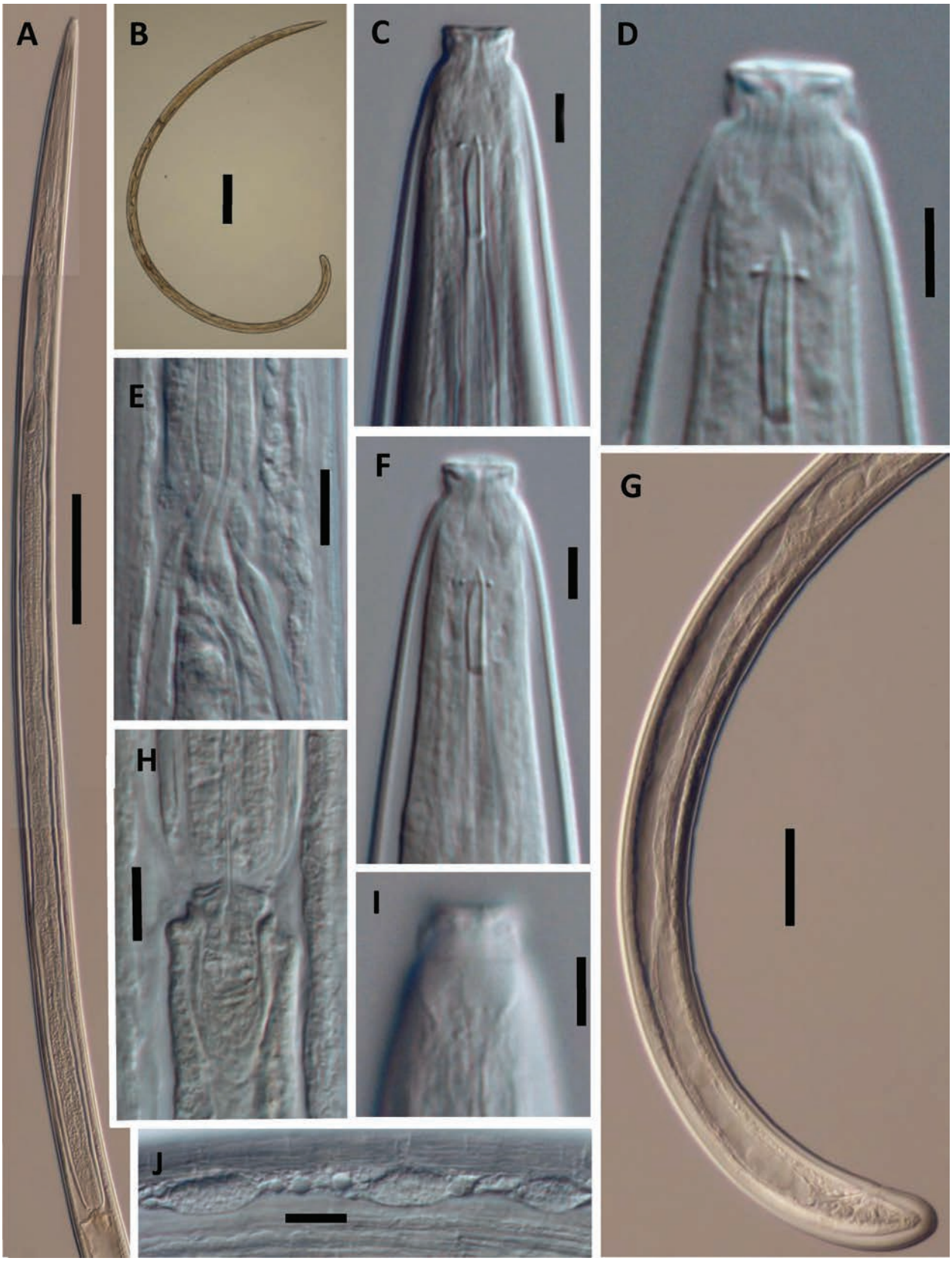

Figure 2. *Oleaxonchium olearum* gen. et sp. nov. (female, general morphology, LM). **A.** Neck region; **B.** Entire; **C, D, F, I.** Anterior body region in lateral median (**C, D, F**) and lateral surface (**I**) views; **E.** Isthmus-like narrowing between both pharyngeal sections; **G.** Posterior body region; **H.** Pharyngo-intestinal junction; **J.** Gland-like bodies at the lateral chord. Scale bars: 100 µm (**A**); 200 µm (**B**); 5 µm (**C, D, F, I**); 50 µm (**G**); 10 µm (**E**, **H, J**).

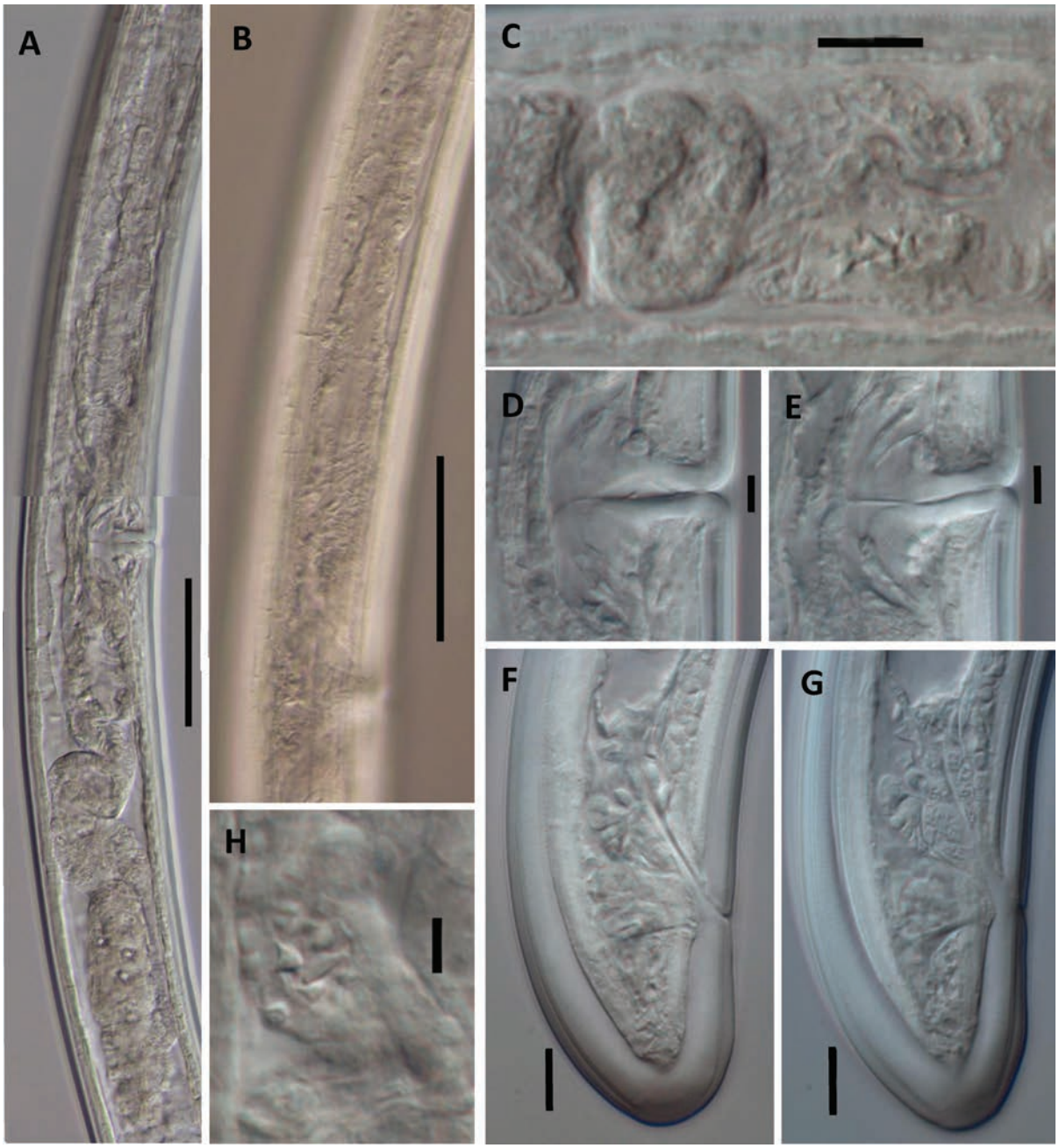

Figure 3. *Oleaxonchium olearum* gen. et sp. nov. (female, genital system, and caudal region, LM). **A.** Genital system; **B.** Anterior genital branch; **C.** Oviduct-uterus junction; **D, E.** Vagina; **F, G.** Rectum and caudal region; **H.** Detail of uterine Z-like structure. Scale bars: 50 µm (**A, B**); 10 µm (**C, F, G**); 5 µm (**D, E, H**).

similar to those of *Metaxonchium giennense* (acc. OQ473053–OQ473054), 91.14% to those of *Metaxonchium magnum* (OQ099691, OQ099693), and 88.86% to that of *Axonchium* sp. (ON927906).

Diagnosis. The new species is characterised by its 2.44–2.87 mm long body, lip region 7–7.5 µm wide, odontostyle 10–10.5 µm long, neck 723–973 µm long, pharyngeal expansion occupying 63–72% of the total neck length, female genital system mono-opisthoovarian, didelphic, with anterior branch occupying 4–6% of body length, posterior uterus 87–122 µm long or 1.9–2.6 body diameters and tripartite, with a short intermediate section bearing refractive elements, vulva (*V* = 58–61) a transverse slit, caudal region short and rounded (29–35 µm, *c* = 74–89, *c'* = 0.9–1.1), and male unknown.

Type locality and habitat. Spain, Málaga province, Antequera municipality, "La Capilla" farm (37.198283, -4.543868, elevation 491 m), where the new species was collected in an olive grove with intensive tillage.

Type material. Female holotype and nine female paratypes were deposited in the nematode collection of the University of Jaén, Spain. Two female paratypes were deposited with the United States Department of Agriculture Nematode Collection (USDANC) at Beltsville, MD, USA.

Etymology. The species epithet is the Latin term *olearum* = belonging to or corresponding to olives, as type material was found in an olive grove.

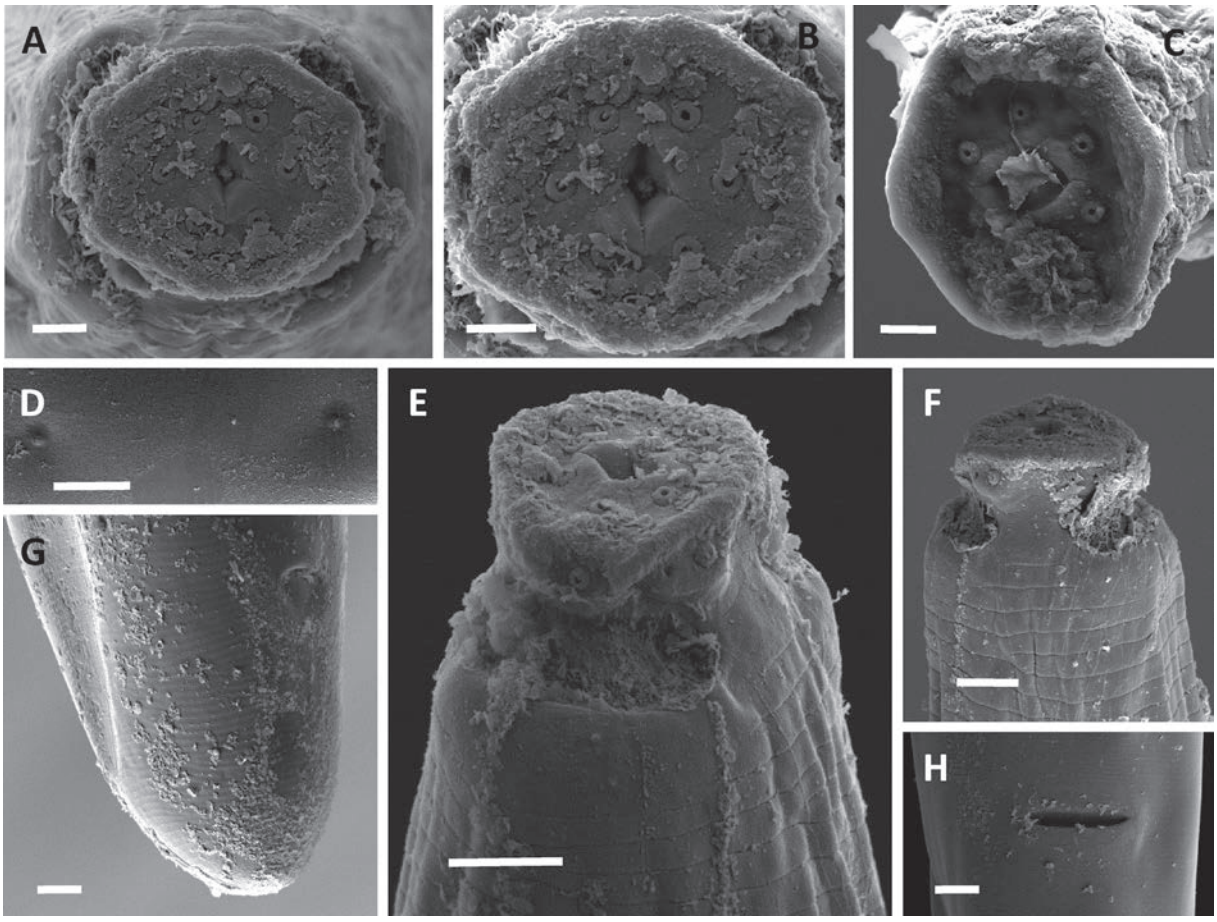

Figure 4. *Oleaxonchium olearum* gen. et sp. nov. (female, SEM). **A–C.** Lip region, in face view; **D.** Lateral pores; **E.** Anterior body region, lateral view; **F.** Anterior body region, ventral view; **G.** Caudal region, sublateral view; **H.** Vulva, ventral view. Scale bars: 1 µm (**A–C**); 5 µm (**D**); 2 µm (**E, F**); 4 µm (**G, H**).

Evolutionary relationships of the new taxon

As derived from morphological data

The general appearance of the new genus is very similar to that found in representatives of the *Axonchium*-like pattern, including comparatively short and slightly fusiform odontostyle, simple odontophore, both pharyngeal sections distinctly separated, very long pharyngeal expansion, mono-opistho-ovarian, didelphic female genital system, and a short and rounded tail (cf. Coomans and Nair 1975). Some of these traits should be interpreted as relevant apomorphies (fusiform odontostyle, very long pharyngeal expansion, mono-opistho-ovarian female genital system), if not autapomorphies (separation of both pharyngeal sections) within the family Belondiridae (cf. Peña-Santiago and Abolafia 2023). Nevertheless, *Oleaxonchium* gen. nov. is easily distinguishable from other *Axonchium*-like genera in the unique aspect of its lip region (rectangular in lateral view, plane and almost octagonal in face view, and with sclerotized margins vs. typically cap-like and without sclerotized margins), which is herein interpreted as an outstanding autapomorphy. The very small cephalic papillae (simple pores) observed in the type species, as well as its button-like lateral pores, represent apomorphic (if not autapomorphic) features too. Besides, the cheilostom, comparatively long and with thickened walls at its anterior, perioral part, is an apomorphic condition, never recorded in other genera that bear shorter and thin-walled cheilostoms.

In having a short, narrower (isthmus-like) section between both pharyngeal sections, the new genus is close to *Metaxonchium* Coomans & Nair, 1975, but, leaving aside the lip region, both taxa differ in the shape of the vagina, which lacks (vs. bears) *pars refringens* and presents very well-developed (vs. very short) *pars distalis*, respectively. In the absence of *pars refringens vaginae*, *Oleaxonchium* gen. nov. also resembles the genera *Axonchium* Cobb, 1920, and *Syncheilaxonchium* Coomans & Nair, 1975, differing from them in the nature of their pharynx: a slender anterior region separated from the posterior expansion by a short isthmus-like section vs. a well-muscular anterior region separated from the posterior one by a marked constriction (abutting).

As derived from molecular analyses

The results of the analyses of six 18S rDNA and four 28S rDNA sequences (see above) are presented in the trees of Fig. 5 (18S) and Fig. 6 (28S). In both trees, the sequences of the new taxon form maximally supported clades, confirming their identity. Nevertheless,

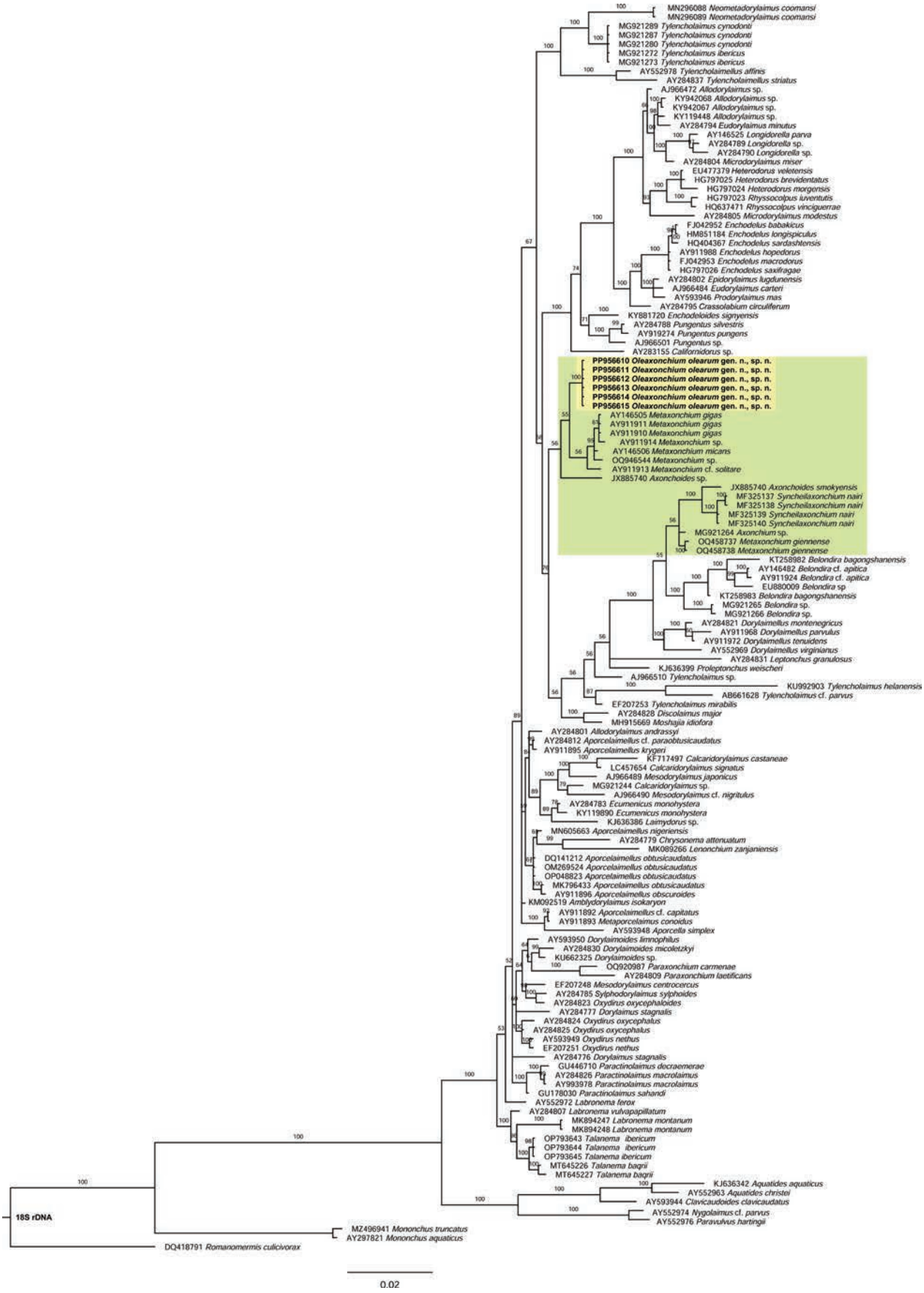

Figure 5. Bayesian inference tree from the newly sequenced *Oleaxonchium olearum* gen. et sp. nov. based on sequences of the 18S rDNA region. Bayesian posterior probabilities (%) are given for each clade. The scale bar shows the number of substitutions per site.

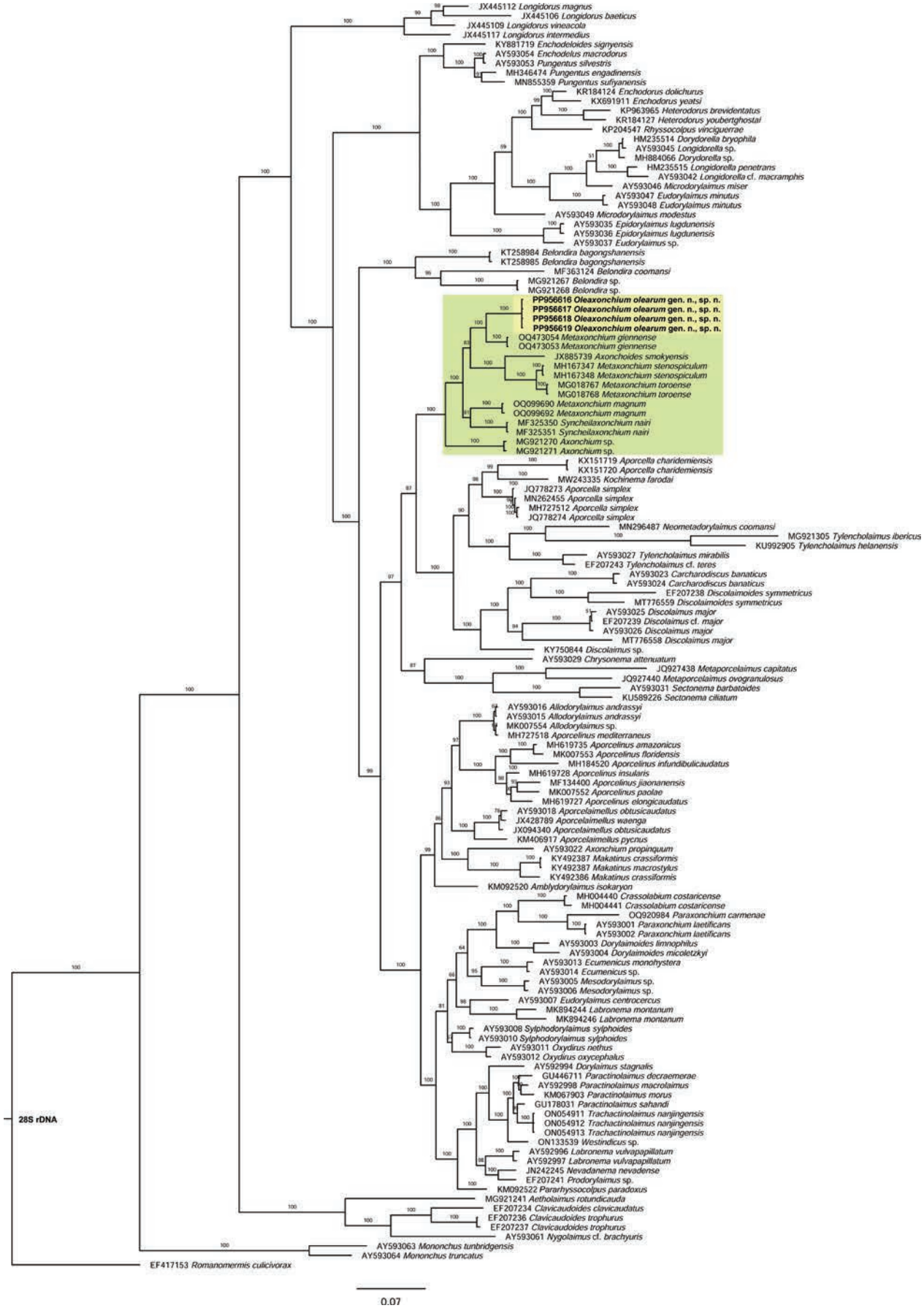

Figure 6. Bayesian inference tree from the newly sequenced *Oleaxonchium olearum* gen. et sp. nov. based on sequences of the 28S rDNA region. Bayesian posterior probabilities (%) are given for each clade. The scale bar shows the number of substitutions per site.

other aspects of its evolutionary relationships significantly differ when the trees are compared.

The 18S tree provides very unsatisfactory branching resolution. On the one hand, the *Oleaxonchium* gen. nov. clade forms part of a very lowly (55%) supported clade, where it appears as the sister group of an also lowly (56%) supported subclade that includes sequences of several *Metaxonchium* species. On the other hand, sequences of *Axonchium*-like genera (*Axonchium*, *Axonchoides*, and *Syncheilaxonchium*) and *M. giennensis* (all of them highlighted in green in the tree) form part of a maximally supported clade with sequences of the genera *Belondira* and *Dorylaimellus.*

The 28S tree offers better resolution as all *Axonchium*-like sequences form a maximally supported clade. Nevertheless, some uncertainties persist about the internal relationships within this clade, mainly due to the apparent polyphyly of *Metaxonchium*, whose sequences form part of three different subclades, namely (new taxon + *M. giennense*), (*Axonchoides smokyensis* + (*M. stenospiculum* + *M. toroense*)), and (*M. magnum* + *Syncheilaxonchium nairi*). Besides, the *Axonchium*-like clade is included in a much larger clade, with *Belondira* sequences not forming part of it.

An integrative approach and general discussion

The singularity of the lip region of *Oleaxonchium* gen. nov., unique within Belondiridae and probably in Dorylaimida, and a recognisable autopomorphy, supports its separation from its closest relatives. The peculiar shape of its body pores and cephalic papillae also represent remarkable differences with other axonchiid genera. Molecular analyses based on both 18S and 28S genes coincide when indicating that there is a closer evolutionary relationship between the new taxon and *Metaxonchium* representatives, but the results significantly differ in the nature and robustness of this relationship when the respective molecular trees are compared. Anyway, *Metaxonchium* is a rather homogeneous genus with a recognisable morphological pattern (Peña-Santiago and Abolafia 2023), easily distinguishable from *Oleaxonchium* gen. nov. (see above).

Present results confirm that the internal evolutionary relationships of Belondiridae remain unsatisfactorily resolved, with morphological and molecular data not always in agreement. First, the polyphyly of the family is once again noted in both 18S and 28S trees, as *Oxydirus* (subfamily Swangeriinae) sequences appear in a separate clade, far from those including other representatives of the group. Second, morphological features and 28S analysis support the validity of Axonchiinae Thorne, 1964, as a monophyletic taxon that should be reinstaurated (cf. Andrássy 2009). Third, relationships between *Belondira* (subfamily Belondirinae) and axonchiid genera remain obscure, as 18S and 28S analyses did not provide comparable evidence. Once more, further research should be accomplished to clarify these issues.

Acknowledgments

This contribution derives from the project Soil O-Live. This project has received funding from the European Union's Horizon Europe research and innovation programme under grant agreement No. 101091255 (Soil Deal for Europe - HORIZON-MISS-2021-SOIL-02-03). The authors thank Dr. Pablo Castillo (IAS, Córdoba, Spain) for his collaboration in molecular analyses and are grateful for the SEM pictures obtained with the assistance of technical staff (Amparo Martínez-Morales) and equipment belonging to the Centro de Instrumentación Científico-Técnica (CICT) of the University of Jaén. A.N. Ruiz-Cuenca is a recipient of a postdoctoral grant for the requalification of the Spanish University System 2021–2023 (modality "Margarita Salas"), financed by Next Generation EU (NGEU) funding through the Spanish Ministry of Universities.

References

Abolafia J (2015) A low-cost technique to manufacture a container to process meiofauna for scanning electron microscopy. Microscopy Research and Technique 78(9): 771–776. https://doi.org/10.1002/jemt.22538

Andrássy I (2009) Free-living nematodes of Hungary III (*Nematoda errantia*). Pedozoologica Hungarica No. 5 (Series Csuzdi C. and Mahunka S). Hungarian Natural History Museum and Systematic Zoology Research Group of the Hungarian Academy of Sciences, Budapest, Hungary, 608 pp.

Archidona-Yuste A, Navas-Cortés JA, Cantalapiedra-Navarrete C, Palomares-Rius JE, Castillo P (2016) Unravelling the biodiversity and molecular phylogeny of needle nematodes of the genus *Longidorus* (Nematoda: Longidoridae) in olive and a description of six new species. PLOS ONE 11(1): e0147689. https://doi.org/10.1371/journal.pone.0147689

CDFA (2015) Protocol for extraction of plant parasitic nematodes from samples. https://www.cdfa.ca.gov/plant/ppd/nematode_extraction.html

Cobb NA (1920) One hundred new nemas. (Type species of 100 new genera). Contributions to Science Nematology 9: 217–243.

Coomans A, Nair P (1975) The genus *Axonchium* (Nematoda: Belondiridae). VI. Atypical species, keys, subgenera and conclusions. Nematologica 21(3): 296–332. https://doi.org/10.1163/187529275X00059

Darriba D, Taboada GL, Doallo R, Posada D (2012) jModelTest 2: More models, new heuristics and parallel computing. Nature Methods 9(8): 772. https://doi.org/10.1038/nmeth.2109

De Ley P, Felix AM, Frisse LM, Nadler SA, Sternberg PW, Thomas WK (1999) Molecular and morphological characterization of two reproductively isolated species with mirror−image anatomy (Nematoda: Cephalobidae). Nematology 1(6): 591–612. https://doi.org/10.1163/156854199508559

Flegg JJM (1967) Extraction of *Xiphinema* and *Longidorus* species from soil by a modification of Cobb's decanting and sieving technique. Annals of Applied Biology 60(3): 423–437. https://doi.org/10.1111/j.1744-7348.1967.tb04497.x

Holterman M, van derWurff A, van den Elsen S, vanMegen H, Bongers T, Holovachov O, Bakker J, Helder J (2006) Phylum-wide analysis

of SSU rDNA reveals Deep phylogenetic relationships among nematodes and accelerated evolution toward crown clades. Molecular Biology and Evolution 23(9): 1792–1800. https://doi.org/10.1093/molbev/msl044

Jenkins WR (1964) A rapid centrifugal-flotation technique for separating nematodes from soil. The Plant Disease Reporter 48: 692.

Jiménez-Guirado D, Peralta M, Peña-Santiago R (2007) Nematoda, Mononchida, Dorylaimida I. In: Ramos MA et al. (Eds) Fauna Ibérica, 30. Museo Nacional de Ciencias Naturales, CSIC, Madrid, 325 pp.

Kumar S, Stecher G, Tamura K (2016) MEGA7: Molecular evolutionary genetics analysis version 7.0 for bigger datasets. Molecular Biology and Evolution 33(7): 1870–1874. https://doi.org/10.1093/molbev/msw054

Larget B, Simon DL (1999) Markov chain Monte Carlo algorithms for the Bayesian analysis of phylogenetic trees. Molecular Biology and Evolution 16(6): 750–759. https://doi.org/10.1093/oxfordjournals.molbev.a026160

Peña-Santiago R (2021) Morphology and bionomics of dorylaims (Nematoda: Dorylaimida). Nematology Monographs and Perspectives 13 (Series Editors: Cook R and Hunt DJ). Brill, Leiden, The Netherlands, 278 pp.

Peña-Santiago R, Abolafia J (2023) General morphology, taxonomy and phylogeny of the genus *Metaxonchium* Coomans & Nair, 1975 (Nematoda: Dorylaimida: Belondiridae). Zoologischer Anzeiger 304: 32–48. https://doi.org/10.1016/j.jcz.2023.03.002

Rambaut A (2018) Figtree, a graphical viewer of phylogenetic trees. https://github.com/rambaut/figtree/releases/tag/v1.4.4

Ronquist F, Teslenko M, van der Mark P, Ayres DL, Darling A, Höhna S, Larget B, Liu L, Suchard MA, Huelsenbeck JP (2012) MrBayes 3.2: Efficient Bayesian phylogenetic inference and model choice across a large model space. Systematic Biology 61(3): 539–542. https://doi.org/10.1093/sysbio/sys029

Siddiqi MR (1964) Studies on *Discolaimus* spp. (Nematoda: Dorylaimidae) from India. Journal of Zoological Systematics and Evolutionary Research 2(1–3): 174–184. https://doi.org/10.1111/j.1439-0469.1964.tb00720.x

Thorne G (1939) A monograph of the nematodes of the superfamily Dorylaimoidea. Capita Zoologica 8: 1–261.

Thorne G (1964) Nematodes of Puerto Rico: Belondiroidea, new superfamily, Leptonchidae Thorne, 1935, and Belonenchinae new family (Nematoda, Adenophorea, Dorylaimida). University of Puerto Rico Agricultural Experiment Station Technical Paper 39: 1–51.

Vilar J, Pereira JE [Eds] (2018) International olive growing − Worldwide analysis and summary. Fundación Caja Rural de Jaén. Gráficas La Paz, Torredonjimeno, Jaén, Spain, 149 pp.

Zoosyst. Evol. 100 (3) 2024, 1041–1052 | DOI 10.3897/zse.100.127635

PENSOFT

MUSEUM FÜR NATURKUNDE BERLIN

A field survey on the genus *Xenophrys* (Amphibia, Megophryidae) confirms underestimated diversity in the Gaoligong Mountains, with the description of a new species

Yun-He Wu[1,2*], Zhong-Bin Yu[1,2*], Jin-Min Chen[1], Felista Kasyoka Kilunda[1,3], Ding-Can Zhang[4], Chang-Sheng Zuo[4], An-Ru Zuo[4], Zheng-Pan Duan[4], Jing Che[1,2]

1 *Key Laboratory of Genetic Evolution and Animal Models, and Yunnan Key Laboratory of Biodiversity and Ecological Conservation of Gaoligong Mountain, Kunming Institute of Zoology, Chinese Academy of Sciences, 650223, Kunming, Yunnan, China*

2 *Southeast Asia Biodiversity Research Institute, Chinese Academy of Sciences, 05282, Yezin, Nay Pyi Taw, Myanmar*

3 *Kunming College of Life Science, University of the Chinese Academy of Sciences, 650204, Kunming, Yunnan, China*

4 *Administrative Bureau of Tongbiguan Provincial Nature Reserve, 679300, Dehong, Yunnan, China*

https://zoobank.org/0ADBE147-7D99-45EC-A77D-9520BB1B7A9A

Corresponding author: Jing Che (chej@mail.kiz.ac.cn)

Academic editor: Umilaela Arifin ♦ **Received** 16 May 2024 ♦ **Accepted** 9 July 2024 ♦ **Published** 25 July 2024

Abstract

The Gaoligong Mountains, located in the western part of China's Yunnan Province adjoining northern Myanmar, harbor a striking diversity of species and endemism. Previous studies have shown that amphibian diversity in this region remains underestimated. A field survey carried out in 2023 oversaw a collection of eight *Xenophrys* specimens from the Tongbiguan Provincial Nature Reserve, Yunnan Province, China. Subsequent molecular analyses revealed two distinct and previously undescribed lineages. Based on morphological evidence, we formally describe one of the lineages as a new species and tentatively assign the other lineage to *X.* sp. due to the absence of adult specimens for examination. Our results bring the total number of *Xenophrys* species to 29 and the number of *Xenophrys* species known to occur in China to 11. Furthermore, our study reveals that five species and putative species of *Xenophrys* (*X. dehongensis*, *X. glandulosa*, *X. periosa*, *X. yingjiangensis* **sp. nov.**, and *X.* sp.) exhibit sympatric distribution. These findings highlight the need for future research to investigate the mechanisms of sympatric coexistence in *Xenophrys*. In addition, our study confirms that the amphibian diversity of the Gaoligong Mountains is undoubtedly underestimated. As a result, continued exploration of amphibians in the future is necessary to obtain a clearer understanding of the overall biodiversity in this region.

Key Words

Biodiversity, cryptic species, frog, sympatric distribution, Tongbiguan Provincial Nature Reserve, *Xenophrys yingjiangensis* sp. nov.

Introduction

The Asian horned toads of the subfamily Megophryinae (Bonaparte, 1850) are widely distributed in tropical Asia, from India and Bhutan to China and south to the Sundas and the Philippines (Frost 2024). It currently includes 136 recognized species, with more than half of the species described in the last 10 years (Frost 2024). As a consequence of both morphological similarity among species and the complex patterns of genetic divergence, the generic classification of the subfamily Megophryinae has been constantly under debate (e.g., Delorme et al. 2006; Fei et al. 2009; Chen et al. 2017; Mahony et al. 2017; Lyu et al. 2023). In this study, we followed the classification

* These authors contributed equally to this work.

system outlined in Frost (2024) and Lyu et al. (2023), in which Megophryidae was divided into 10 genera for the convenience of our comparisons.

The genus *Xenophrys* Günther, 1864, of the subfamily Megophryinae is distributed widely throughout southern China to the Indochina Peninsula and currently includes 28 recognized species (Frost 2024). These species inhabit primarily montane forests. To date, 10 species have been recorded in China (Frost 2024), with nearly half of the recognized species described in the last 10 years (e.g., Mahony et al. 2018; Lyu et al. 2023; Shu et al. 2023). Moreover, five species of *Xenophrys* have been recorded in Yunnan (AmphibiaChina 2024; Frost 2024).

The Gaoligong Mountains, located in the western part of China's Yunnan Province bordering northern Myanmar, form a long, narrow mountain range. It stretches 600 km from the Tibetan Plateau to Myanmar across a 5° latitude with a large elevation range of 210 m to 5000 m. Renowned as one of the world's most significant biodiversity hotspots outside of the tropics, its complex geography, hydrology, and climate have fostered many distinct habitat types that support diverse biotic components (Chaplin 2005). Several cryptic and novel amphibian species have been described from this mountain ecosystem in recent years (AmphibiaChina 2024), indicating that amphibian diversity in the region may still be diverse and largely underestimated.

A recent herpetological survey conducted at the Gaoligong Mountains, Yunnan Province, China, saw a collection of some *Xenophrys* specimens. Subsequent studies, including molecular data and morphological comparisons, revealed that these specimens represent five distinct evolutionary lineages, two of which could not be assigned to any known *Xenophrys* species. Therefore, we herein describe one of the two lineages as a new species.

Materials and methods

Sampling

Field surveys were conducted in August 2023. A total of eight *Xenophrys* specimens were collected in Tongbiguan Town, Yingjiang County, Yunnan, China (Fig. 1). After taking photographs, the toads were euthanized using benzocaine. Liver tissue was taken from the specimens and preserved in 95% ethanol at -80 °C. The specimens were then fixed in 10% formalin and subsequently stored in 75% ethanol after 24 hours. All the newly collected specimens were deposited in the herpetological collection of the Museum of the Kunming Institute of Zoology (KIZ), Chinese Academy of Sciences (CAS).

Molecular data and phylogenetic analyses

Total genomic DNA was extracted using the standard phenol-chloroform extraction protocol (Sambrook et al. 1989). The mitochondrial fragment 16S ribosomal RNA gene (16S rRNA) was amplified and sequenced using the primer pairs (5'–3') 16SAR (CGCCTGTTTAYCAAAAACAT) and 16SBR (CCGGTYTGAACTCAGATCAYGT) (Kocher et al. 1989). The polymerase chain reaction (PCR) was performed in a 25 µl volume reaction with the following conditions: an initial denaturing step at 94 °C for 4 min; 35 cycles of denaturing at 94 °C for 40 s; annealing at 55 °C for 40 s; and extending at 72 °C for 1 min; and a final extending step of 72 °C for 10 min. PCR products were sequenced using the same forward and reverse primers as those used in PCR. Sequencing was conducted using an ABI 3730xl DNA automated sequencer (Applied Biosystems, UK). All sequences were assembled from forward and reverse reads

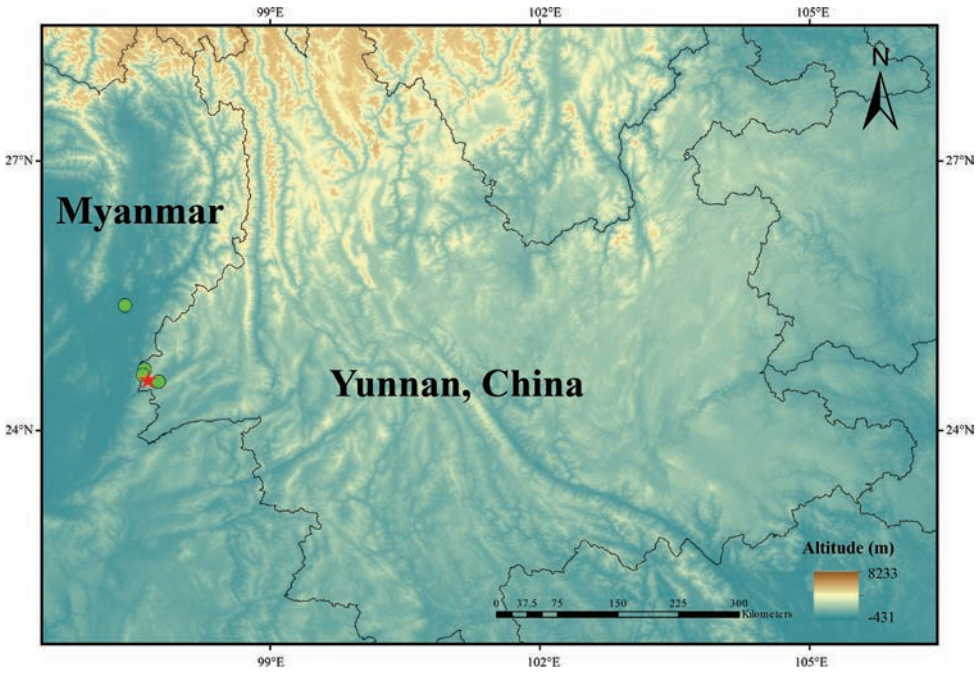

Figure 1. Known distribution of *Xenophrys yingjiangensis* sp. nov. The red pentagram indicates the type locality of *Xenophrys yingjiangensis* sp. nov.

and edited manually using DNASTAR LASERGENE 7.1. New sequences were deposited in GenBank (Table 1).

Maximum likelihood (ML) and Bayesian inference (BI) were used to infer phylogenetic trees. Fifty-eight homologous sequences of *Xenophrys* and representative outgroups (*Brachytarsophrys feae*, *Leptobrachella ventripunctata*, and *Leptobrachium huashen*) were downloaded from the GenBank (Table 1). The dataset was aligned using MUSCLE v3.8 (Edgar 2004), checked by eye, and trimmed to minimize missing characters in MEGA v6.0.6 (Tamura et al. 2013). BI and ML analyses were performed on the CIPRES web server (Miller et al. 2010) using MrBayes v3.2.4 (Ronquist et al. 2012). For BI analyses, the best-fit model of evolution was determined using the Bayesian information criterion (BIC; Posada 2008) implemented in jModelTest 2.1.7 (Darriba et al. 2012). GTR+G was the best-fit model of evolution for 16S rRNA. The Monte Carlo Markov chain length was run for 10 million generations and sampled every 1000 generations, with a burn-in of 25%. Convergence was assessed by the average standard deviation of split frequencies (below 0.01) and ESS values (greater than or equal to 200) in TRACER 1.6 (Rambaut et al. 2014). ML analyses were performed using RAxML-HPC BlackBox 8.2.10 (Stamatakis 2014) with 1,000 bootstrap replicates and using the standard bootstrap search (random seed value 12,345) under the GTR+gamma nucleotide substitution model. Mean genetic distances between and within species were calculated using uncorrected pairwise distances (*p*-distance) by 16S rRNA implemented in MEGA v6.0.6, with complete deletion of missing data and gaps (Tamura et al. 2013).

Table 1. Localities, voucher information, and Genbank accession numbers for all specimens used in this study.

Species	Voucher	Locality	Accession No.	Reference
Xenophrys ancrae	SDBDU 2009.727	India, Arunachal, Changlang	KY022318	Mahony et al. 2018
Xenophrys ancrae	ZSI A 11606	India, Arunachal, Changlang	MN734391	Mahony et al. 2020
Xenophrys auralensis	NCSM 79599	Cambodia, Kampong Speu, Aural	KX811807	Chen et al. 2017
Xenophrys awuh	SDBDU 2007.192	India, Nagaland state, Kohima district, above New Ministers' Hill, Aradurah Forest	MN734399	Mahony et al. 2020
Xenophrys awuh	MZUHC 314	India, Mizoram	MT793046	Lalronunga et al. 2020
Xenophrys dehongensis	SYS a005823	China, Yunnan, Yingjiang	OQ180993	Lyu et al. 2023
Xenophrys dehongensis	KIZ 053847	China, Yunnan, Tongbiguan	PP989323	This study
Xenophrys dzukou	SDBDU 2007.106	India, Nagaland, Kohima	KY022324	Mahony et al. 2017
Xenophrys flavipunctata	SDBDU 2009.298	India, East Khasi Hills district, Meghalaya	MH647517	Mahony et al. 2018
Xenophrys flavipunctata	SDBDU 2007.134	India, Kohima district, Nagaland	MH647518	Mahony et al. 2018
Xenophrys glandulosa	KIZ 013609	China, Yunnan, Wenlong	KX811761	Chen et al. 2017
Xenophrys glandulosa	SYS a003757	China, Yunnan, Mt Gaoligong	MH406754	Liu et al. 2018
Xenophrys glandulosa	KIZ 053845	China, Yunnan, Tongbiguan	PP989322	This study
Xenophrys himalayana	SDBDU 2009.1227	India, West Kameng district, Arunachal Pradesh	MH647526	Mahony et al. 2018
Xenophrys himalayana	SDBDU 2009.1206	India, West Kameng district, Arunachal Pradesh	MH647527	Mahony et al. 2018
Xenophrys lancangica	SYS a007794	China, Yunnan, Simao	OQ180994	Lyu et al. 2023
Xenophrys lancangica	SYS a007825	China, Yunnan, Jinghong	OQ180997	Lyu et al. 2023
Xenophrys lekaguli	FMNH 265955	Thailand, Sa Kaeo, Mueang Sa Kaeo	KY022214	Mahony et al. 2017
Xenophrys major	RGK 0089	India, Manipur,Tamenglong	KY022308	Mahony et al. 2017
Xenophrys major	SDBDU 2007.229	India, Nagaland, Kohima	MH647514	Mahony et al. 2018
Xenophrys mangshanensis	KIZ 021786	China, Guangdong, Mt Nanling	KX811790	Chen et al. 2017
Xenophrys mangshanensis	SYS a002177	China, Guangdong, Huaiji	MH406666	Liu et al. 2018
Xenophrys maosonensis	KIZ 016045	China, Yunnan, Xichou	KX811780	Chen et al. 2017
Xenophrys maosonensis	SYS a008748	China, Guangxi, Mt Shiwandashan	OQ181000	Lyu et al. 2023
Xenophrys maosonensis	SYS a008766	China, Guangxi, Mt Shiwandashan	OQ181002	Lyu et al. 2023
Xenophrys medogensis	KIZ 06657	China, Xizang, Beibeng	KX811768	Chen et al. 2017
Xenophrys medogensis	SYS a002932	China, Xizang, Medog	MH406725	Liu et al. 2018
Xenophrys megacephala	ZSI A 11213	India, Meghalaya, Ri Bhoi	KY022315	Mahony et al. 2018
Xenophrys montana	SDBDU 2011.1047	India, West Bengal, Darjeeling	KY022312	Mahony et al. 2017
Xenophrys montana	SDBDU 2011.1049	India, West Bengal, Darjeeling	MH647506	Mahony et al. 2018
Xenophrys numhbumaeng	SDBDU 2007.041	India, Manipur, Tamenglong	KY022316	Mahony et al. 2017
Xenophrys numhbumaeng	BNHS 6076	India, Manipur, Tamenglong	MN734393	Mahony et al. 2020
Xenophrys oreocrypta	SDBDU 2008.1400	India, West Garo Hills district, Meghalaya	MH647520	Mahony et al. 2018
Xenophrys oreocrypta	SDBDU 2009.1108	India, West Garo Hills district, Meghalaya	MH647521	Mahony et al. 2018
Xenophrys oropedion	ZSI A 11601	India, Meghalaya state, East Khasi Hills district, Shillong, Malki Forest	MN734394	Mahony et al. 2020
Xenophrys oropedion	ZSI A 11603	India, Meghalaya state, East Khasi Hills district, Shillong, Malki Forest	MN734395	Mahony et al. 2020
Xenophrys pangdaensis	YBU 21248	China, Xizang, Yadong County, Pangda Village	OR026569	Shu et al. 2023
Xenophrys pangdaensis	YBU 21261	China, Xizang, Yadong County, Pangda Village	OR026572	Shu et al. 2023
Xenophrys periosa	SDBDU 2009.793	India, East Siang district, Arunachal Pradesh	MH647522	Mahony et al. 2018
Xenophrys periosa	SDBDU 2009.1285	India, West Kameng district, Arunachal Pradesh	MH647524	Mahony et al. 2018
Xenophrys periosa	CIB YN201909160	China, Yunnan, Gongshan, Dulongjiang	MT225581	Shi et al. 2020
Xenophrys periosa	KIZ 053849	China, Yunnan, Tongbiguan	PP989324	This study
Xenophrys robusta	K5207/ZSI11404	India, Sikkim, North Sikkim	KX894674	Deuti et al. 2017
Xenophrys robusta	SDBDU 2011.1057	India, West Bengal, Darjeeling	KY022314	Mahony et al. 2018
Xenophrys serchhipii	SDBDU 2009.612	India, Tripura, North Tripura	KY022323	Mahony et al. 2018
Xenophrys serchhipii	SDBDU 2008.1492	India, Manipur, Tamenglong	MN734405	Mahony et al. 2020
Xenophrys "sp.17"	KIZ 011940	Myanmar, Myitkyina	KX811792	Chen et al. 2017
Xenophrys "sp.17"	KIZ 048503	China, Yunnan, Tongbiguan Provincial Nature Reserve	KX811793	Chen et al. 2017

Species	Voucher	Locality	Accession No.	Reference
Xenophrys "sp.17"	KIZ 048504	China, Yunnan, Tongbiguan Provincial Nature Reserve	KX811794	Chen et al. 2017
Xenophrys "sp.17"	KIZ 048505	China, Yunnan, Tongbiguan Provincial Nature Reserve	KX811795	Chen et al. 2017
Xenophrys yingjiangensis sp. nov.	KIZ 053814	China, Yunnan, Tongbiguan Provincial Nature Reserve	PP989318	This study
Xenophrys yingjiangensis sp. nov.	KIZ 053815	China, Yunnan, Tongbiguan Provincial Nature Reserve	PP989320	This study
Xenophrys yingjiangensis sp. nov.	KIZ 053828	China, Yunnan, Tongbiguan Provincial Nature Reserve	PP989319	This study
Xenophrys yingjiangensis sp. nov.	KIZ 053848	China, Yunnan, Tongbiguan Provincial Nature Reserve	PP989317	This study
Xenophrys sp.	KIZ 053846	China, Yunnan, Tongbiguan Provincial Nature Reserve	PP989321	This study
Xenophrys takensis	FMNH 261711	Thailand, Kampaeng, Khlong Lan	KY022215	Mahony et al. 2017
Xenophrys truongsonensis	IEBRA 4943	Vietnam, Dak Lak	ON146200	Luong et al. 2022
Xenophrys truongsonensis	IEBRA 4948	Vietnam, Lam Dong	ON146201	Luong et al. 2022
Xenophrys truongsonensis	IEBRA 4952	Vietnam, Ninh Thuan	ON146202	Luong et al. 2022
Xenophrys zhangi	KIZ 014278	China, Xizang, Nyalam	KX811765	Chen et al. 2017
Xenophrys zhangi	SYS a008204	China, Xizang, Nyalam	OQ180998	Lyu et al. 2023
Xenophrys zunhebotoensis	RGK41	India, Nagaland, Zunheboto	KY022322	Mahony et al. 2017
Xenophrys zunhebotoensis	SDBDU 2009.374	India, Nagaland, Kohima	MN734418	Mahony et al. 2020
Outgroups				
Brachytarsophrys feae	KIZ YN070570	China, Yunnan, Longchuan	KX811809	Chen et al. 2017
Leptobrachella ventripunctata	KIZ 046940	China, Yunnan, Wenlong	KX811929	Chen et al. 2017
Leptobrachium huashen	KIZ 049025	China, Yunnan, Mengyang	KX811931	Chen et al. 2017

Morphology and morphometrics

All the measurements were recorded with digital calipers to the nearest 0.1 mm. Morphological terminology followed Fei et al. (2009). Twenty-five measurements included the following: **SVL**: snout-vent length (measured from tip of snout to vent); **HDL**: head length (measured from tip of snout to rear of jaw); **HDW**: maximum head width (measured width of head at its widest point); **SNT**: snout length (measured from tip of snout to anterior corner of ocular aperture); **ED**: eye diameter (diameter of exposed portion of eyeball); **UEW**: width of upper eyelid (maximum width of upper eyelid); **TD**: tympanum diameter (measured as maximal diameter of tympanum); **DNE**: distance from nostril to eye (distance from the front of the eye to the center of the nostril); **SN**: distance from the center of the nostril to the tip of the snout; **IND**: internarial distance (distance between nares); **TEY**: distance from anterior edge of tympanum to posterior corner of eye; **IOD**: interorbital distance (measured at narrowest point between eyes on top of the head); **FAL**: forearm length (measured from the elbow to the wrist); **LAD**: (diameter of lower arm); **FHL**: forearm and hand length (distance from elbow to the tip of the third finger); **TL**: tibia length (distance from knee to heel); **HL**: hand length (distance from the posterior end of the inner metacarpal tubercle to tip of third finger); **HLL**: hindlimb length; **FL**: foot length (distance from the proximal end of inner metatarsal tubercle to the tip of fourth toe); **THL**: thigh length (from the cloaca to the knee); **TAL**: tarsus length (measured as the distance from knee to heel); **FLI-IV**: first to fourth finger length.

Results

The aligned sequence matrix of the 16S gene contained 490 bp, among which 215 sites were variable and 159 were parsimony-informative (including outgroups). Both BI and ML trees had almost identical topologies with relatively robust support for most nodes, differing mainly at terminal nodes identified as weakly supported or collapsed. The genus *Xenophrys* was recovered as monophyletic with strong support from both analyses (BPP=1; BS=96; Fig. 2). The newly collected sympatric samples from Tongbiguan Nature Reserve, Yunnan, China, were divided into five highly divergent clades with strong nodal supports: three were nested within a clade containing recognized species, while the other two formed their own previously unknown lineages (Fig. 2).

The newly collected specimen (KIZ 053849) and *X. periosa* (including the type specimens) nested into a single clade with strong support (BPP=1; BS=81; clade A), and the within-group mean genetic *p*-distance was 1.7% (0%–3.4%, Suppl. material 1). The newly collected specimen (KIZ 053845) strongly clustered with *X. glandulosa* (BPP=1; BS=100; clade B), with maximal uncorrected pairwise 16S distances of merely 0.0%. The newly collected specimen (KIZ 053847) formed a monophyletic clade with *X. dehongensis* from the paratype (BPP=1; BS=99; clade E), with shallow within-group genetic differentiation (0.7%, Suppl. material 1).

For the two new distinct clades, the newly collected samples and samples proposed as *Megophrys* sp. 17 in Chen et al. (2017) clustered into a monophyletic clade with a strong nodal support (BPP=1; BS=99; clade D). This clade was recovered as a sister taxon to *X. dehongensis*. In addition, the remaining sample (KIZ 053846) formed an independent monophyletic clade, which clustered with *X. awuh*, *X. zunhebotoensis*, *X. serchhipii*, *X. numhbumaeng*, *X. oropedion*, *X. ancrae*, *X. megacephala*, and *X. dzukou* with moderate support (BPP=0.96; BS=81; clade C). The two putative new species showed obvious genetic divergence from the other congeners. The genetic distance between the new populations and the other congeneric species ranged from 5.3% (with *X. megacephala*) to 12.0% (with *X. lancangica*) for clade D, 7.1% (with *X. ancrae*), and 12.2% (with *X. robusta*) for clade C (Suppl. material 1). It is comparable to the divergences among the nearest neighbor genetic distances of the described *Xenophrys* species, which ranged from 2.1% (*X. mangshanensis* and *X. maosonensis*) to 15.7% (*X. dzukou* and *R. awuh*). In addition, these levels

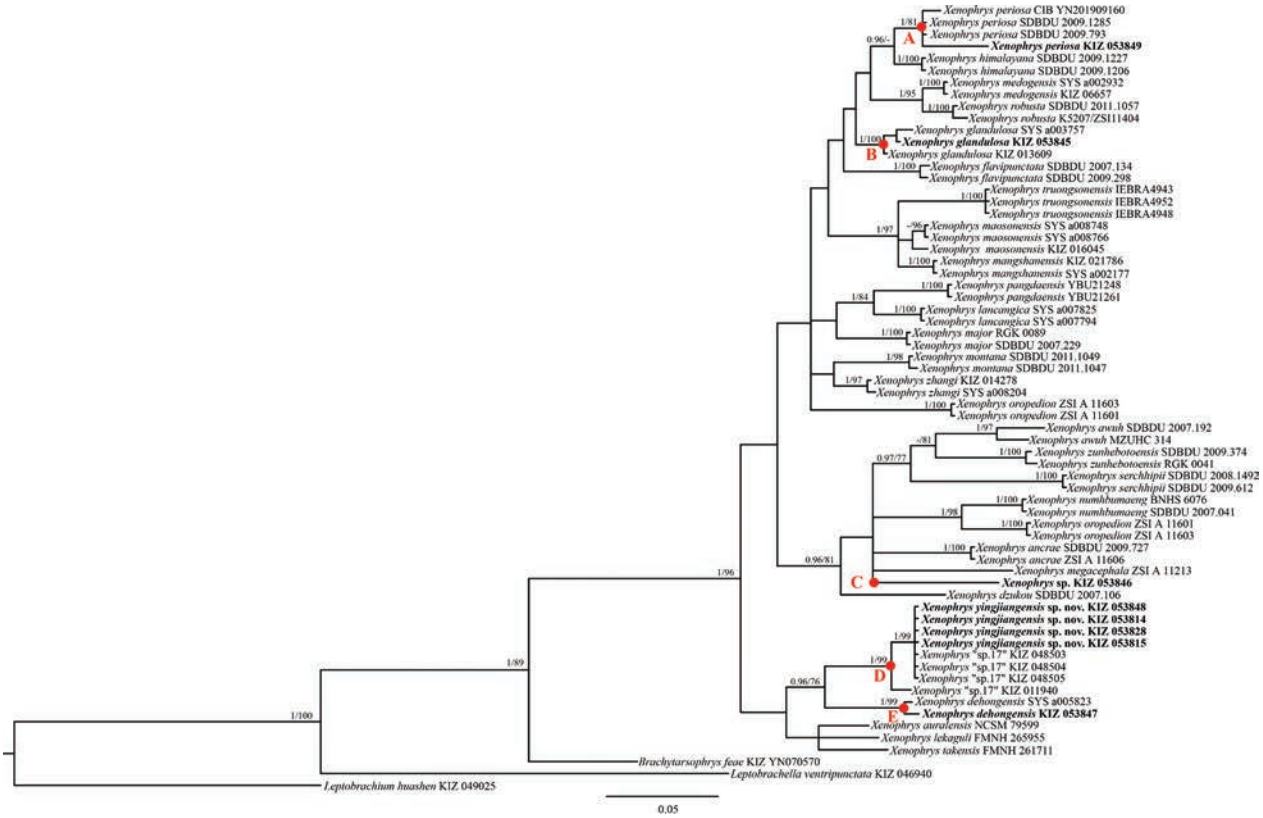

Figure 2. Phylogram of *Xenophrys* based on the mitochondrial 16S rRNA gene. Node values with Bayesian posterior probabilities (BPP) < 0.95 and Bootstrap support (BS) < 70 are not shown. A "-" denotes Bayesian posterior probabilities (BPP) < 0.95 and bootstrap support (BS) < 70. New samples for the present study are indicated in bold font.

of pairwise divergence of the 16S rRNA gene exceeded the acceptable threshold (3%) of species-level genetic divergence in anurans (Vences et al. 2005).

Morphologically, these specimens from Clade D differed from recognized congeners; therefore, we formally describe them as new. However, Clade C contains only one subadult specimen, and further surveys are needed to retrieve adult specimens.

Taxonomic account

***Xenophrys yingjiangensis* Wu, Yu, Chen & Che, sp. nov.**

https://zoobank.org/C2E61BB7-426B-448F-8A9C-66B993E7201A

Figs 3, 4, Table 2

Chresonymy. *Megophrys* sp17., Chen et al. 2017.

Type material. *Holotype*: KIZ 053848, an adult male collected from Tongbiguan Provincial Nature Reserve, Yingjiang County, Yunnan, China (24.563°N, 97.639°E; elevation 1478 m a.s.l.), collected by Zhong-Bin Yu, Dong An, Tian-En Chen, and Xian-Kun Huang on 12 August 2023.

***Paratypes*:** KIZ 048503–KIZ 048505, three adult males, from Tongbiguan Provincial Nature Reserve, Yingjiang County, Yunnan, China (24.546°N, 97.759°E; elevation 809 m a.s.l.), collected by Jin-Min Chen and Mian Hou on 11 August 2013; KIZ 053828, one adult male, collected at the same locality and with the same collection information as the holotype.

Etymology. The specific epithet "yingjiang" is a Latinized adjective derived from the name of Yingjiang County, Yunnan Province, China, where the new species occurs. We propose the English common name "Yingjiang horned toad" and the Chinese common name "Yíng Jiāng Jiǎo Chán (盈江角蟾)".

Diagnosis. *Xenophrys yingjiangensis* sp. nov. differs from its congeners by a combination of the following morphological characters: (1) medium adult size, adult male SVL 44.6–49.8 mm (N=5); (2) head slightly longer than wide; (3) tympanum distinct, narrow anteriorly, slightly widening posteriorly; (4) pupil vertically elliptical; (5) vomerine ridges and vomerine teeth present; (6) tongue large, oval-shaped, feebly notched posteriorly; (7) relative finger lengths: II < IV < I < III; (8) the heels slightly overlapping when the tibias are positioned at right angles to the body axis; (9) tibio-tarsal articulation of straightened limb reaching the nostril; (10) lateral dermal fringes on toes distinct, narrow; (11) toes with rudimentary webbing; (12) inner metatarsal tubercle large, elongate; (13) a distinct narrow '\ /'-shaped parietoscapular ridge present; (14) flesh pink ventral surface of thighs.

Description of the holotype (measurements in Table 2). KIZ 053848, mature male, sized medium body (SVL 45.0 mm); head moderate (HDL/SVL 39.6%, HDW/SVL 38.9%), slightly longer than wide (HDW/HDL 98.3%); snout obtusely rounded in dorsal view, obtusely projecting beyond the lower jaw in profile, without rostral appendage; triangular in dorsal view; top of head flat; loreal

Figure 3. Views of the Holotype KIZ 053848 in life. **A.** Lateral view; **B.** Lateral view of head; **C.** Dorsal view of hindlimbs; **D.** Ventral view; **E.** Ventral view of hand, and **F.** Ventral view of foot. Photos by Zhong-Bin Yu.

region vertical and concave; canthus rostralis angular; eyes large (ED/HDL 31.5%); eye less than twice as long as maximum tympanum diameter (ED/TD 207.4%) and shorter than snout length (SNT 6.8 mm, ED/SNT 82.4%); tympanum distinct, circular in shape, relatively small (TD/HDL 15.2%), with upper border concealed by supratympanic ridge; eye-tympanum distance (TYE 3.3 mm) longer than tympanum diameter (TD 2.7 mm); nostril rounded, laterally positioned, nostril closer to the tip of snout than to the anterior corner of the eye (SN/DNE 81.6%); internarial distance greater than interorbital distance (IND/IOD 109.4%) and width of upper eyelid (IND/UEW 126.1%); pineal ocellus absent; vomerine teeth in two oblique series, positioned between choanae, separated from each other by distance equal to distance from choanae; maxillary teeth present; choanae oval; tongue large, oval-shaped, feebly notched posteriorly; single internal vocal sac, with a sac slit opening on floor of mouth at each corner; pupil vertically elliptical (Fig. 3B).

Forelimbs moderately long and thin; forearm not enlarged relative to the upper arm, its length shorter than the hand length (FAL/HL 86.4%); fingers long and narrow, lateral fringes on fingers absent, relative finger lengths: II < IV < I < III; tips of all fingers rounded, slightly expanded relative to digit widths, with subcircular pads, terminal grooves absent; no webbing between fingers; subarticular tubercle absent; supernumerary tubercle absent; metacarpal tubercle absent (Fig. 3E).

Hindlimbs relatively long and thin, thigh length (THL 22.3 mm) shorter than the tibia length (TL 23.8 mm) but slightly longer than the foot length (FL 21.4 mm); the heels slightly overlapping when the tibias are positioned at right angles to the body axis; tibio-tarsal articulation of straightened limb reaching the nostril; toes long and thin, relative toe lengths: I < II < V < III < IV; tips of all toes rounded, slightly dilated, terminal grooves absent; notably expanded relative to digit widths forming circular

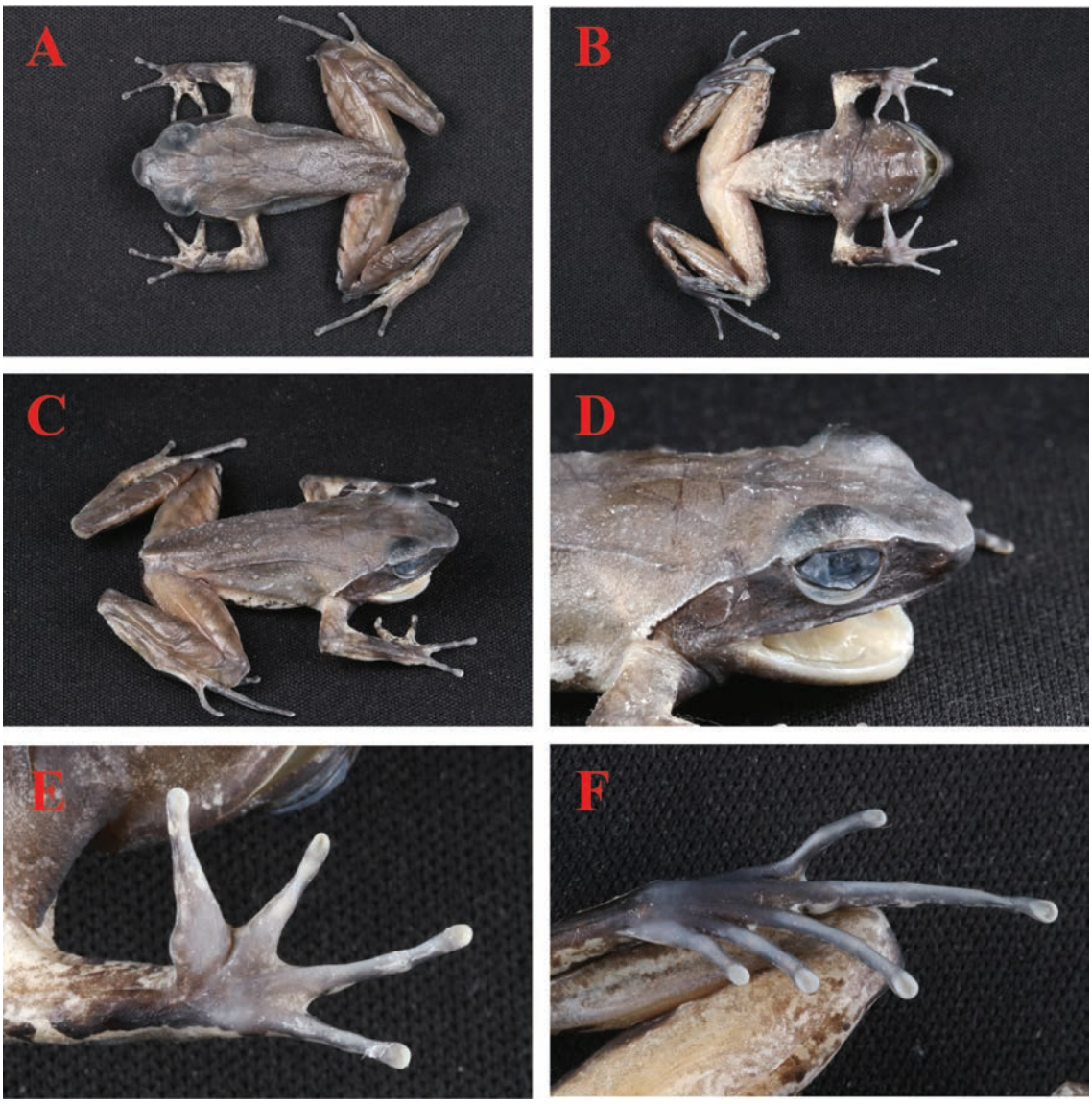

Figure 4. Views of the Holotype KIZ 053848 in preservative. **A.** Dorsal view; **B.** Ventral view; **C.** Lateral view; **D.** Lateral view of head; **E.** Ventral view of hand, and **F.** Ventral view of foot. Photos by Zhong-Bin Yu.

pads; lateral dermal fringes on toes distinct, narrow; toes with rudimentary webbing; tarsal fold absent; subarticular tubercle, supernumerary tubercle, and outer metatarsal tubercle absent; inner metatarsal tubercle large, elongate, ca. one and a half times longer than wide (Fig. 3F).

Skin of dorsal surfaces of head, body and limbs relatively smooth, with very small granules; posterior back densely-distributed with numerous small to medium sized granules and tubercles; flanks with small scattered tubercles (Fig. 3A); supratympanic fold distinct, narrow anteriorly, slightly widening posteriorly, extending from the posterior corner of the eye to a level above the insertion of the arm; tympanum skin smooth, tympanic rim slightly elevated relative to skin of temporal region (Fig. 3B); two opposing "V"-shaped parietoscapular ridge present on dorsum joined by a ca. 10 mm long dorsomedial fold in a hourglass-shape; dorsolateral fold absent; a distinct narrow '\ /'-shaped parietoscapular ridge present, its two sides extending posteriorly from above tympanum, terminating beyond level of axilla; dorsal surface of thighs, shanks and upper forearms with distinct transverse ridges (Fig. 3A, C); ventral surfaces of limbs, throat, chest, and abdomen smooth; pectoral glands small, rounded, slightly raised, closer to the axilla than to the mid-ventral line; femoral gland distinct, extend longitudinally, positioned equidistant from the knee and cloacal opening on rear of each thigh.

Coloration in life. For the coloration of the holotype in life, see Fig. 3. Dorsal surface reddish brown, with a complete inverted triangle bordered with a light edge present between eyes; lateral surface of trunk of body and anterior surface of the thighs near the groin pinkish; throat purplish grey with white flecking; chest and anterior half of abdomen purplish grey with yellowish flecking and grey-brown blotches; posterior half of abdomen white with irregular lighter greyish blotches; ventral surface of thighs pinkish; ventral surface of feet and shanks brown-black; brown nuptial pads present on the base of first and second finger; supratympanic fold, light colored, bordered by a black lower margin; iris copper-brown, with tiny dark

Table 2. Measurements (in mm) of the type series of *Xenophrys yingjiangensis* sp. nov. Bold font and an asterisk (*) indicate the holotype.

	KIZ 053848*	KIZ 053828	KIZ 048503	KIZ 048504	KIZ 048505
Sex	♂	♂	♂	♂	♂
SVL	**45.0**	49.8	46.8	44.6	47.9
HDL	**17.8**	17.6	17.9	18.4	18.2
HDW	**17.5**	17.5	16.4	17.3	17.4
SNT	**6.8**	7.0	6.5	7.0	7.1
ED	**5.6**	5.7	5.2	6.0	5.8
IOD	**5.3**	4.7	5.3	5.3	4.9
UEW	**4.6**	5.2	4.5	4.9	5.2
IND	**5.8**	6.1	5.7	5.6	5.8
DNE	**3.8**	3.2	3.4	3.4	3.4
SN	**3.1**	2.9	3.0	3.1	3.5
TD	**2.7**	3.2	4.3	3.3	3.3
TYE	**3.3**	3.0	3.1	2.6	3.1
FHL	**23.3**	23.5	22.8	22.5	21.8
FAL	**10.8**	10.9	10.0	10.0	9.9
HL	**12.5**	12.6	12.8	12.5	12.0
LAD	**4.3**	4.6	4.3	4.1	3.9
FLI	**5.9**	6.1	3.8	3.8	4.1
FLII	**4.5**	5.0	3.7	3.1	3.8
FLIII	**8.6**	8.2	6.1	5.9	6.0
FLIV	**5.2**	5.4	4.6	4.6	4.0
HLL	**75.9**	80.4	76.0	78.7	72.6
THL	**22.3**	25.1	23.9	23.0	20.7
TL	**23.8**	24.8	24.0	25.7	24.0
TAL	**32.7**	34.3	12.3	12.9	12.9
FL	**21.4**	21.6	20.7	21.2	20.4

reticulations spreading from pupil; pectoral and femoral glands creamy white; inner metatarsal tubercle off-white.

Coloration in preservative. For coloration of the holotype in preservative, see Fig. 4. After eight months of storage in ethanol, dorsal and lateral surfaces of head and body fading to greyish-brown; slightly darker brown triangular marking between the eyes; two opposing "V"-shaped parietoscapular ridges present on two sides of dorsum becoming less distinct; the '\ /'-shaped parietoscapular ridge present dorsum still clear; lateral surfaces of head below supratympanic ridges and canthus rostralis dark brown; supratympanic ridges whitish-cream; dorsal surfaces of forelimbs and hindlimbs primarily light greyish-brown; granules and tubercles on posterior half of back and flanks more distinct; throat and chest faded greyish-brown with several scattered white dots; ventral thighs and shank faded to pale yellow, with several dark brown blotches on the anterior thigh and shank; pectoral and femoral glands white; inner metatarsal tubercle still off-white.

Sexual dimorphism. All adult males with nuptial pads covering most of the dorsal surface of the bases of fingers I and II; male with single internal vocal sac (Fig. 5), with a sac slit opening on floor of mouth at each corner.

Distribution and ecology. *Xenophrys yingjiangensis* sp. nov. is only known from the Tongbiguan Provincial Nature Reserve, Tongbiguan Town, Yingjiang County, Yunnan, China, and Myitkyina, Myanmar (Fig. 1). All individuals were discovered in a mountainous area surrounded by shrubland at elevations of approximately 800–1200 m (Fig. 6). This species is in sympatric distribution with *X. periosa*, *X. dehongensis*, *X. glandulosa*, and *Xenophrys* sp. of congeners. In addition, other frog species also found at the site include *Leptobrachella yingjingensis*, *Jingophrys feii*, and *Kurixalus yangi*.

Comparison. We compared *Xenophrys yingjiangensis* sp. nov. with other congeneric species (Ohler et al. 2002; Stuart et al. 2006; Mahony 2011; Mahony et al. 2011; Mahony et al. 2013, 2018; 2020; Che et al. 2020; Luong et al. 2022; Lyu et al. 2023; Shu et al. 2023).

Xenophrys yingjiangensis sp. nov. is obviously different from its four most phylogenetically close congeners (*X. dehongensis*, *X. auralensis*, *X. lekaguli*, and *X. takensis*). It differs from *X. dehongensis* by adult male SVL 44.6–49.8 mm, n = 5 (vs. adult male SVL 34.8–36.7 mm, n = 5), metacarpal tubercle absent (vs. two metacarpal tubercles indistinct), tibio-tarsal articulation of straightened limb reaching the nostril (vs. tibio-tarsal articulation reaching posterior corner of eye), inner metatarsal tubercle large, elongate, ca. one and a half times longer than wide (vs. inner metatarsal tubercle indistinct), relative finger lengths: II < IV < I < III (vs. II < I < IV < III); from *X. auralensis* by medium adult size, adult male SVL 44.6–49.8 mm, n = 5 (vs. large sized species, adult male SVL 71.0–76.9 mm, n = 9), head longer than wide (vs. head wider than long), internarial distance greater than interorbital distance and width of upper eyelid (vs. interorbital distance larger than internarial distance and width of upper eyelid), relative finger lengths: II < IV < I < III (vs. II < I < IV < III), transverse crossbar in hindlimbs absent (vs. forelimb, dorsal parts of thigh, tibia and foot greyish brown with darker brown bands); from *X. lekaguli* by adult male SVL 44.6–49.8 mm, n = 5 (vs. adult male SVL 55.6–66.6 mm, n = 8), head longer than wide (vs. head slightly wider than long), relative finger lengths: II < IV < I < III (vs. IV < II < I < III); tongue feebly notched posteriorly (vs. tongue unnotched), vertical bar below eye absent (vs. wide, dark vertical bar below eye), transverse crossbar in limbs absent (vs. limbs with narrow dark brown crossbars); from *X. takensis* by head longer than wide (vs head wider than long), tongue large, oval-shaped, feebly notched posteriorly (vs. tongue oval, not notched posteriorly), relative finger lengths: II < IV < I < III (vs. IV ≤ II < I < III or IV = I < II < III), lateral dermal fringes on toes distinct, narrow (vs. absent).

Xenophrys yingjiangensis sp. nov. is different from other congeneric species. The new species differs from *X. ancrae* by inner metatarsal tubercle large, elongate, ca. one and a half times longer than wide (vs. inner metatarsal tubercle very weak), pupil horizontally orientated (vs. pupil vertically elliptical), relative finger lengths: II < IV < I < III (vs. I < II < IV < III), lateral dermal fringes on toes distinct, narrow (vs. absent); from *X. awuh* by adult male SVL 44.6–49.8 mm, n = 5 (vs. adult male SVL 35.7–41.1 mm, n = 4), nostril closer to the tip of snout than to the anterior corner of the eye (vs. nostril closer to eye than to snout), vomerine teeth present (vs. absent), inner metatarsal tubercle large, elongate, ca. one and a half times longer than wide (vs. inner metatarsal tubercle indistinct), lateral dermal fringes on toes distinct, narrow (vs. absent); from *X. damrei* by adult male SVL 44.6–49.8 mm, n = 5 (vs. adult male SVL 57.1 mm, n = 1), head longer than wide (vs head wider than long), nostril

Figure 5. Advertisement calls for Paratype KIZ 048505. Photo by Jin-Min Chen.

Figure 6. Habitat of *Xenophrys yingjiangensis* sp. nov. at the type locality in Tongbiguan Provincial Nature Reserve, Yingjiang County, Yunnan, China. Photo by Zhong-Bin Yu.

closer to the tip of snout than to the anterior corner of the eye (vs. nostril closer to eye than snout), lateral dermal fringes on toes distinct, narrow (vs. absent), male with single internal vocal sac (vs. external vocal sac indistinct); from *X. dzukou* by adult male SVL 44.6–49.8 mm, n = 5 (vs. adult male SVL 34.2–35.3 mm, n = 4), nostril closer to the tip of snout than to the anterior corner of the eye (vs. nostril closer to eye than snout), inner metatarsal tubercle large, elongate, ca. one and a half times longer than wide (vs. inner metatarsal tubercle indistinct), toes with rudimentary webbing (vs. webbing absent); from *X. flavipunctata* by adult male SVL 44.6–49.8 mm, n = 5 (vs. adult male SVL 56.9–68.4 mm, n = 4), head longer than wide (vs head wider than long), tongue large, oval-shaped, feebly notched posteriorly (vs. tongue moderately large, deeply notched posteriorly), inner metatarsal tubercle large, elongate, ca. one and a half times longer than wide (vs. inner metatarsal tubercle indistinct), transverse crossbar in hindlimbs absent (vs. dorsal surfaces of hindlimbs with distinct mid brown transverse crossbars); from *X. himalayana* by adult male SVL 44.6–49.8 mm, n = 5 (vs. adult male SVL 68.0–73.5 mm, n = 6), lateral dermal fringes on toes distinct, narrow (vs. absent), outer metacarpal tubercle absent (vs. outer metacarpal tubercle weakly developed), transverse crossbar in hindlimbs absent (vs. dorsal surfaces of thighs and shanks with distinct dark brown transverse crossbars); from *X. megacephala* by the heels slightly overlapping when the tibias positioned at right angles to the body axis (vs. not meeting), inner metatarsal tubercle large, elongate, ca. one and a half times longer than wide (vs. inner metatarsal tubercle indistinct), relative finger lengths: II < IV < I < III (vs. IV < II < I< III); dorsal surface of thighs, shanks and upper forearms with distinct transverse ridges (vs. absent), transverse crossbar in limbs absent (vs. dorsal surface of the fore and hind limbs with faint dark cross bars); from *X. numhbumaeng* by adult male SVL 44.6–49.8 mm, n = 5 (vs. adult male SVL 33.8–34.6 mm, n = 2), pupil vertically elliptical (vs. pupil horizontally orientated), inner metatarsal tubercle large, elongate, ca. one and a half times longer than wide (vs. inner metatarsal tubercle weak), lateral dermal fringes on toes distinct, narrow (vs. absent); from *X. oreocrypta* by lateral dermal fringes on toes distinct, narrow (vs. absent), pupil vertically elliptical (vs. pupil horizontally orientated), inner metatarsal tubercle large, elongate, ca. one and a half times longer than wide (vs. inner metatarsal tubercle very weak), relative finger lengths: II < IV < I < III (vs. I < II < IV < III); from *X. oropedion* by adult male SVL 44.6–49.8 mm, n = 5 (vs. adult male SVL 32.8–39.6 mm, n = 7), lateral dermal fringes on toes distinct, narrow (vs. absent), inner metatarsal tubercle large, elongate, ca. one and a half times longer than wide (vs. inner metatarsal tubercle indistinct); from *X. pangdaensis* by adult male SVL 44.6–49.8 mm, n = 5 (vs. adult male SVL 17.9–22.2 mm, n = 6), tympanum distinct (vs. indistinct), inner metatarsal tubercle large, elongate, ca. one and a half times longer than wide (vs. inner metatarsal tubercle indistinct), transverse crossbar in limbs absent (vs. two dark transverse bands on each forearm, three dark transverse bands on anterior surface of thigh and shank), iris copper-brown (vs. iris orange-red); from *X. periosa* by medium adult size, adult male SVL 44.6–49.8 mm, n = 5 (vs. medium adult size, adult male SVL 71.3–93.8 mm, n = 12), outer metacarpal tubercle absent (vs. outer metacarpal tubercle weakly developed), inner metatarsal tubercle large, elongate, ca. one and a half times longer than wide (vs. inner metatarsal tubercle weakly defined), iris copper-brown (vs. iris very dark orange), transverse crossbar in hindlimbs absent (vs. hindlimbs with distinct transverse crossbars); from *X. truongsonensis* by adult male SVL 44.6–49.8 mm, n = 5 (vs. adult male SVL 58.8–71.4 mm, n = 14), internarial distance greater than interorbital distance and width of upper eyelid (vs. internarial distance narrower than interorbital distance but wider than upper eyelid), external vocal sac indistinct (vs. absent), upper lip dark brown (vs. upper lip with a continuous white stripe, running from the nostril to shoulder), hindlimbs (vs. dorsal surface of fore and hind limbs reddish brown with dark crossbars); from *X. lancangica* by adult male SVL 44.6–49.8 mm, n = 5 (vs. adult male SVL 64.0–65.4 mm, n = 3), metacarpal tubercle absent (vs. two metacarpal tubercles indistinct), tibio-tarsal articulation of straightened limb reaching the nostril (vs. tibiotarsal articulation reaching region between nostril and tip of snout), inner metatarsal tubercle large, elongate, ca. one and a half times longer than wide (vs. inner metatarsal tubercle indistinct), transverse crossbar in limbs absent (vs. dorsal limbs with transverse bands), relative finger lengths: II < IV

< I < III (vs. II < IV < I < III); from *X. glandulosa* by adult male SVL 44.6–49.8 mm, n = 5 (vs. adult male SVL 77.0–81.0 mm, n = 3), head longer than wide (vs head wider than long), tongue large, feebly notched posteriorly (vs. tongue distinctly notched posteriorly), lateral dermal fringes on toes distinct, narrow (vs. moderately wide lateral fringes present on all toes), transverse crossbar in limbs absent in preservative (vs. dorsal surfaces of hindlimbs with distinct brown transverse crossbars in preservative), sides of head smooth (vs. sides of head finely granular); from *X. monticola* by vomerine teeth present (vs. vomerine teeth absent), inner metatarsal tubercle large, elongate, ca. one and a half times longer than wide (vs. inner metatarsal tubercle indistinct), toes with rudimentary webbing (vs. absent), lateral dermal fringes on toes distinct, narrow (vs. absent), pupil vertically elliptical (vs. pupil horizontally orientated), tongue large, feebly notched posteriorly (vs. tongue large, appears rounded posteriorly without notch); from *X. robusta* by adult male SVL 44.6–49.8 mm, n = 5 (vs. adult male SVL 73.5–83.1 mm, n = 6), head longer than wide (vs head wider than long), vomerine teeth present (vs. absent), lateral dermal fringes on toes distinct, narrow (vs. absent); from *X. medogensis* by inner metacarpal tubercle absent (vs. distinct), toes with rudimentary webbing (vs. absent), lateral dermal fringes on toes distinct, narrow (vs. absent), relative finger lengths: II < IV < I < III (vs. I < II < IV < III); dark brown stripe in lower margin of the supratympanic folds absent (vs. lower margin of the supratympanic folds with dark brown stripe); from *X. major* by medium adult size, adult male SVL 44.6–49.8 mm, n = 5 (vs. large sized species, adult male SVL 75.0–87.5 mm, n = 12), throat purplish grey with white flecking; chest and anterior half of abdomen purplish grey with yellowish flecking and grey-brown blotches (vs. light-edged wide dark brown stripe extending from posterior edge of mandible onto base of forearms), dorsolateral surface of forearms without blotch (vs. three dark brown blotches on dorsolateral surface of forearms); from *X. maosonensis* by adult male SVL 44.6–49.8 mm, n = 5 (vs. adult male SVL 66.2 mm, n = 1), metacarpal tubercle absent (vs. two metacarpal tubercles indistinct), relative finger lengths: II < IV < I < III (vs. I < II < IV < III), tibio-tarsal articulation of straightened limb reaching the nostril (vs. tibio-tarsal articulation reaching center of eye), inner metatarsal tubercle large, elongate, ca. one and a half times longer than wide (vs. inner metatarsal tubercle indistinct); from *X. mangshanensis* by adult male SVL 44.6–49.8 mm, n = 5 (vs. adult male SVL 60.4–71.6 mm, n = 10), metacarpal tubercle absent (vs. two metacarpal tubercles indistinct), relative finger lengths: II < IV < I < III (vs. II < I < IV < IIII), tibio-tarsal articulation of straightened limb reaching the nostril (vs. tibio-tarsal articulation reaching center of eye), lateral dermal fringes on toes distinct, narrow (vs. absent), toes with rudimentary webbing (vs. absent), inner metatarsal tubercle large, elongate, ca. one and a half times longer than wide (vs. inner metatarsal tubercle indistinct); from *X. zhangi* by adult male SVL 44.6–49.8 mm, n = 5 (vs. adult male SVL 32.5–40.0 mm, n = 7), metacarpal tubercle absent (vs. two metacarpal tubercles indistinct), relative finger lengths: II < IV < I < III (vs. I < II < IV < III), tibio-tarsal articulation of straightened limb reaching the nostril (vs. tibio-tarsal articulation reaching anterior corner of eye), toes with rudimentary webbing (vs. absent); from *X. zunhebotoensis* by adult male SVL 44.6–49.8 mm, n = 5 (vs. adult male SVL 28.4–33.9 mm, n = 23), vomerine teeth present (vs. absent), lateral dermal fringes on toes distinct, narrow (vs. absent), toes with rudimentary webbing (vs. absent), the heels slightly overlapping when the tibias positioned at right angles to the body axis (vs. meeting); absent (vs. dense orange speckling on chest and anterior abdomen); from *X. serchhipii* by lateral dermal fringes on toes distinct, narrow (vs. absent), relative finger lengths: II < IV < I < III (vs. IV < I = II < III), two opposing "V"-shaped parietoscapular ridge present on dorsum joined by a ca. 10 mm long dorsomedial fold in a hourglass-shape (vs. unconnected inverted "V"-shaped sacral ridge).

Discussion

Our study demonstrates that species diversity within the genus *Xenophrys* remains largely underestimated. Recent phylogenetic analysis has revealed multiple genetic lineages of *Xenophrys* that may represent new species (Chen et al. 2017). Among these, *X. yingjiangensis* sp. nov. was previously suggested to be a putative new species based on molecular phylogenetic analysis. In our present study, we combined morphological and molecular lines of evidence to confirm its species status and formally describe it. Our results bring the total number of *Xenophrys* to 29, and the number of *Xenophrys* known from China to 12. In addition to the new taxon described herein, the following species of *Xenophrys* are known from China: *X. dehongensis*, *X. glandulosa*, *X. himalayana*, *X. lancangica*, *X. mangshanensis*, *X. maosonensis*, *X. medogensis*, *X. pangdaensis*, *X. parva*, *X. periosa*, and *X. zhangi* (Frost 2024). Furthermore, our study also reveals a new distinct lineage from Tongbiguan Provincial Nature Reserve that we consider a putative species. However, at present, we only have one subadult specimen. Further fieldwork is needed to collect more adult specimens and compare their morphological characteristics to determine their taxonomic status.

During our field work in the Tongbiguan Provincial Nature Reserve, adults and subadults of five species and putative species of *Xenophrys* (*X. dehongensis*, *X. glandulosa*, *X. periosa*, *X. yingjiangensis* sp. nov., and *X.* sp.) were found at the same site at the same time. A sympatric distribution pattern has been observed in other amphibians, such as *L. flaviglandulosa*, *L. nyx*, *L. feii*, and *L. bourreti*, in the Xiaoqiaogou Nature Reserve (Chen et al. 2020). However, research on the mechanism of sympatric distribution in amphibians is not well understood. Further evolutionary studies that integrate life history (e.g., advertisement call and breeding season) with genome data will be critical in the future to explore the mechanisms of sympatric coexistence among multiple lineages in *Xenophrys*.

The Gaoligong Mountains may harbor more hidden amphibian diversity than previously postulated. Recent

intensive surveys have significantly enhanced our understanding of the amphibian diversity of the Gaoligong Mountains, with discoveries of multiple new species, new national record species, and a series of new regional record species (e.g., Liu et al. 2021; Zhang et al. 2022; Hou et al. 2023; Wu et al. 2024, 2021). Our new findings of *X. yingjiangensis* sp. nov. and putative species further confirm that amphibian diversity in this mountain ecosystem is undoubtedly underestimated. Future amphibian exploration will hopefully continue to discover more new taxa in the region. In addition, the classification and diversity of some species distributed in the Gaoligong Mountains have long been disputed, such as *Amolops bellulus* (Liu et al. 2000; Wu et al. 2020) and *Nanorana arnoldi* (AmphibiaChina 2024). Considering that the Gaoligong mountains are located at the China-Myanmar border, future international collaborations between herpetologists from both countries are necessary to clarify the distribution and classification of these species.

Acknowledgments

This work was supported by the National Key R & D Program of China (2022YFC2602500), the Second Tibetan Plateau Scientific Expedition and Research (STEP) program (Grant No. 2019QZKK0501), Science and Technology Basic Resources Investigation Program of China (Grant No. 2021FY100200); National Natural Science Foundation of China (NSFC 32100371); Yunnan Applied Basic Research Projects (No. 202301AT070312, 202301AT070431), Major Science and Technique Program (202102AA310055) and Key R & D program (202103AC100003, 202301AT070431) in Yunnan Province; China's Biodiversity Observation Network (Sino-BON), and the Animal Branch of the Germplasm Bank of Wild Species, CAS (Large Research Infrastructure Funding). We thank Mian Hou, Xian-Kun Huang, Dong An, and Tian-En Chen for their help in the field. We thank the Tongbiguan Provincial Nature Reserve for their support in undertaking field surveys and specimen collections.

References

AmphibiaChina (2024) The Database of Chinese Amphibians. Kunming Institute of Zoology (CAS), Kunming, Yunnan, China. Electronic Database. http://www.amphibiachina.org [accessed 15 April 2024]

Chaplin G (2005) Physical geography of the Gaoligong Shan area of southwest China in relation to biodiversity. Proceedings of the California Academy of Sciences 56(28): 527–556.

Che J, Jiang K, Yan F, Zhang YP (2020) Amphibians and Reptiles of Tibet – Diversity and Evolution. Science Press, Beijing. [In Chinese]

Chen JM, Zhou WW, Poyarkov Jr NA, Stuart BL, Brown RM, Lathrop A, Wang YY, Yuan ZY, Jiang K, Hou M, Chen HM, Suwannapoom C, Nguyen SN, Duong TV, Papenfuss TJ, Murphy RW, Zhang YP, Che J (2017) A novel multilocus phylogenetic estimation reveals unrecognized diversity in Asian horned toads, genus *Megophrys* sensu lato (Anura: Megophryidae). Molecular Phylogenetics and Evolution 106: 28–43. https://doi.org/10.1016/j.ympev.2016.09.004

Chen JM, Xu K, Poyarkov NA, Wang K, Yuan ZY, Hou M, Suwannapoom C, Wang J, Che J (2020) How little is known about "the little brown frogs": description of three new species of the genus *Leptobrachella* (Anura: Megophryidae) from Yunnan Province, China. Zoological Research 41(3): 292–313. https://doi.org/10.24272/j.issn.2095-8137.2020.036

Darriba D, Taboada GL, Doallo R, Posada D (2012) jModelTest 2: More models, new heuristics and parallel computing. Nature Methods 9(8): 772–772. https://doi.org/10.1038/nmeth.2109

Delorme M, Dubois A, Grosjean S, Ohler A (2006) Une nouvelle ergotaxinomie des Megophryidae (Amphibia, Anura). Alytes 24: 6–21.

Edgar RC (2004) MUSCLE: Multiple sequence alignment with high accuracy and high throughput. Nucleic Acids Research 32(5): 1792–1797. https://doi.org/10.1093/nar/gkh340

Fei L, Hu SQ, Ye CY, Huang YZ (2009) Fauna Sinica. Amphibia Vol. 2 Anura. Science Press, Beijing. [In Chinese]

Frost DR (2024) Amphibian Species of the World: An Online Reference. Version 6.1. https://amphibiansoftheworld.amnh.org/ [accessed 15 April 2023]

Hou M, Yu GH, Liu XL, Liu S, Wang B, Li PP, Orlov NL (2023) New records of *Amolops kaulbacki* specimens from Yunnan Province, China with discussion on species distribution. Russian Journal of Herpetology 30(3): 144–166. https://doi.org/10.30906/1026-2296-0-0-0-23

Kocher TD, Thomas WK, Meyer A, Edwards SV, Pääbo S, Villablanca FX, Wilson AC (1989) Dynamics of mitochondrial DNA evolution in animals: Amplification and sequencing with conserved primers. Proceedings of the National Academy of Sciences of the United States of America 86(16): 6196–6200. https://doi.org/10.1073/pnas.86.16.6196

Lalronunga S, Zosangliana I, Lalhmangaiha K, Lalhmingliani E (2020) First record of the Naga Hills Horned Frog, *Megophrys awuh* Mahony, Kamei, Teeling, and Biju (Anura: Megophryidae: Megophryinae), from Mizoram, India. Reptiles & Amphibians : Conservation and Natural History 27(3): 472–473. https://doi.org/10.17161/randa.v27i3.14884

Liu W, Yang D, Ferraris C, Matsui M (2000) *Amolops bellulus*: A new species of stream-breeding frog from western Yunnan, China (Anura: Ranidae). Copeia 2000(2): 536–541. https://doi.org/10.1643/0045-8511(2000)000[0536:ABANSO]2.0.CO;2

Liu Z, Chen G, Zhu T, Zeng Z, Lyu Z, Wang J, Messenger K, Greenberg AJ, Guo Z, Yang Z, Shi S, Wang Y (2018) Prevalence of cryptic species in morphologically uniform taxa–Fast speciation and evolutionary radiation in Asian frogs. Molecular Phylogenetics and Evolution 127: 723–731. https://doi.org/10.1016/j.ympev.2018.06.020

Liu X, He YH, Wang Y, Beukema W, Hou S, Li Y, Che J, Yuan ZY (2021) A new frog species of the genus *Odorrana* (Anura: Ranidae) from Yunnan, China. Zootaxa 4908(2): 263–275. https://doi.org/10.11646/zootaxa.4908.2.7

Luong AM, Pham CT, Nguyen TT, Orlov N, Ziegler T, Nguyen TQ (2022) A new species of *Xenophrys* (Amphibia: Anura: Megophryidae) from Truong Son Range, Vietnam. Zootaxa 5150(3): 333–356. https://doi.org/10.11646/zootaxa.5150.3.2

Lyu ZT, Qi S, Wang J, Zhang SY, Zhao J, Zeng ZC, Wang H, Yang JH, Mo YM, Wang YY (2023) Generic classification of Asian horned toads (Anura: Megophryidae: Megophryinae) and monograph of Chinese species. Zoological Research 44(2): 380–450. https://doi.org/10.24272/j.issn.2095-8137.2022.372

Mahony S (2011) Two new species of *Megophrys* Kuhl & van Hasselt (Amphibia: Megophryidae), from western Thailand and southern Cambodia. Zootaxa 2734(1): 23–39. https://doi.org/10.11646/zootaxa.2734.1.2

Mahony S, Sengupta S, Kamei RG, Biju SD (2011) A new low altitude species of *Megophrys* Kuhl and van Hasselt (Amphibia: Megophryidae), from Assam, Northeast India. Zootaxa 3059(1): 36–46. https://doi.org/10.11646/zootaxa.3059.1.2

Mahony S, Teeling EC, Biju SD (2013) Three new species of horned frogs, *Megophrys* (Amphibia: Megophryidae), from northeast India, with a resolution to the identity of *Megophrys boettgeri* populations reported from the region. Zootaxa 3722(2): 143–169. https://doi.org/10.11646/zootaxa.3722.2.2

Mahony S, Foley NM, Biju SD, Teeling EC (2017) Evolutionary history of the Asian Horned Frogs (Megophryinae): Integrative approaches to timetree dating in the absence of a fossil record. Molecular Biology and Evolution 34(3): 744–771. https://doi.org/10.1093/molbev/msw267

Mahony S, Kamei RG, Teeling EC, Biju SD (2018) Cryptic diversity within the *Megophrys major* species group (Amphibia: Megophryidae) of the Asian Horned Frogs: Phylogenetic perspectives and a taxonomic revision of South Asian taxa, with descriptions of four new species. Zootaxa 4523(1): 1–96. https://doi.org/10.11646/zootaxa.4523.1.1

Mahony S, Kamei RG, Teeling EC, Biju SD (2020) Taxonomic review of the Asian Horned Frogs (Amphibia: *Megophrys* Kuhl & Van Hasselt) of Northeast India and Bangladesh previously misidentified as *M. parva* (Boulenger), with descriptions of three new species. Journal of Natural History 54(1–4): 119–194. https://doi.org/10.1080/00222933.2020.1736679

Miller MA, Pfeiffer W, Schwartz T (2010) Creating the CIPRES Science Gateway for inference of large phylogenetic trees. Gateway Computing Environments Workshop (GCE), 2010: 1–8. https://doi.org/10.1109/GCE.2010.5676129

Ohler A, Swan SR, Daltry JC (2002) A recent survey of the amphibian fauna of the Cardomom Mountains, Southwest Cambodia with descriptions of three new species. The Raffles Bulletin of Zoology 50(2): 465–482.

Posada D (2008) jModelTest: Phylogenetic model averaging. Molecular Biology and Evolution 25(7): 1253–1256. https://doi.org/10.1093/molbev/msn083

Rambaut A, Suchard MA, Xie D, Drummond AJ (2014) Tracer v1.6. http://beast.bio.ed.ac.uk/Tracer [accessed 15 April 2024]

Ronquist F, Teslenko M, Paul VDM, Ayres DL, Darling A, Höhna S, Larget B, Liu L, Suchard MA, Huelsenbeck JP (2012) MrBayes 3.2: Efficient Bayesian phylogenetic inference and model choice across a large model space. Systematic Biology 61(3): 539–542. https://doi.org/10.1093/sysbio/sys029

Sambrook J, Fritsch EF, Maniatis T (1989) Molecular Cloning: A Laboratory Manual. 2nd edn. Cold Spring Harbor Laboratory Press, Cold Spring Habor, NY.

Shi SC, Wang B, Zhu WB, Fu L, Jiang W, Li DH, Jiang JP (2020) *Megophrys periosa* (Mahony, Kamei, Teeling, and Biju 2018) was first recorded in Yunnan province, China with description of its tadpole. Dongwuxue Zazhi 55(6): 730–740.

Shu G, Li K, Wu Y, Liu Q, He Z, Li L, Zhang H, Guo P (2023) A new species of *Xenophrys* (Amphibia, Anura, Megophryidae) from southern Tibet, China. ZooKeys 1182: 307–329. https://doi.org/10.3897/zookeys.1182.106828

Stamatakis A (2014) RAxML version 8: A tool for phylogenetic analysis and post-analysis of large phylogenies. Bioinformatics (Oxford, England) 30(9): 1312–1313. https://doi.org/10.1093/bioinformatics/btu033

Stuart BL, Chuaynkern Y, Chan-ard T, Inger RF (2006) Three new species of frogs and a new tadpole from eastern Thailand. Fieldiana. Zoology 2006(111): 1–19. https://doi.org/10.3158/0015-0754(2006)187[1:TNSOFA]2.0.CO;2

Tamura K, Stecher G, Peterson D, Filipski A, Kumar S (2013) MEGA6: Molecular evolutionary genetics analysis version 6.0. Molecular Biology and Evolution 30(12): 2725–2729. https://doi.org/10.1093/molbev/mst197

Vences M, Thomas M, Van der Meijden A, Chiari Y, Vieites DR (2005) Comparative performance of the 16S rRNA gene in DNA barcoding of amphibians. Frontiers in Zoology 2(1): 1–12. https://doi.org/10.1186/1742-9994-2-5

Wu YH, Yan F, Stuart BL, Prendini E, Suwannapoom C, Dahn HA, Zhang BL, Cai HX, Xu YB, Jiang K, Chen HM, Lemmon AR, Lemmon EM, Raxworthy CJ, Orlov NL, Murphy RW, Che J (2020) A combined approach of mitochondrial DNA and anchored nuclear phylogenomics sheds light on unrecognized diversity, phylogeny, and historical biogeography of the torrent frogs, genus *Amolops* (Anura: Ranidae). Molecular Phylogenetics and Evolution 148: 106789. https://doi.org/10.1016/j.ympev.2020.106789

Wu YH, Liu XL, Gao W, Wang YF, Li YC, Zhou WW, Yuan ZY, Che J (2021) Description of a new species of Bush frog (Anura: Rhacophoridae: *Raorchestes*) from northwestern Yunnan, China. Zootaxa 4941(2): 239–258. https://doi.org/10.11646/zootaxa.4941.2.5

Wu YH, Yu ZB, Lu CQ, Zhang YP, Dong WJ, Liu XL, Kilunda FK, Xiong Y, Jiang YF, Ouyang H, Fu ZX, He YB, Yuan ZY, Che J (2024) A new species of the genus *Amolops* (Amphibia: Ranidae) and the first national record of *Amolops vitreus* from China. Vertebrate Zoology 74: 343–357. https://doi.org/10.3897/vz.74.e108013

Zhang YP, Liu XL, Stuart BL, Wu DY, Wang YF, Che J, Yuan ZY (2022) *Amolops putaoensis* Gan, Qin, Lwin, Li, Quan, Liu & Yu, 2020, a newly recorded torrent frog for China. Herpetozoa (Wien) 35: 231–237. https://doi.org/10.3897/herpetozoa.35.e94745

Supplementary material 1

Average uncorrected p-distances (percentage) among *Xenophrys* species calculated from 16S rRNA gene sequences (below the diagonal) and standard error estimates (above the diagonal)

Authors: Yun-He Wu, Zhong-Bin Yu, Jin-Min Chen, Felista Kasyoka Kilunda, Ding-Can Zhang, Chang-Sheng Zuo, An-Ru Zuo, Zheng-Pan Duan, Jing Che

Data type: xls

Explanation note: The ingroup mean uncorrected p-distances are shown on the diagonal.

Link: https://doi.org/10.3897/zse.100.127635.suppl1

Zoosyst. Evol. 100 (3) 2024, 1053–1060 | DOI 10.3897/zse.100.123213

PENSOFT

MUSEUM FÜR NATURKUNDE BERLIN

The pseudoscorpion genus *Nipponogarypus* (Pseudoscorpiones, Olpiidae) found in seashore habitats in Japan and Korea

Kyung-Hoon Jeong[1,2,3,4], Danilo Harms[5,6,7], Jung-Sun Yoo[2]

1 *Seoul National University, 1, Gwanak-ro, Gwanak-gu, Seoul, 08826, Republic of Korea*
2 *National Institute of Biological Resources, Species Diversity Research Division, Environmental Research Complex, Hwangyeong-ro 42, Seo-gu, Incheon, 22689 Republic of Korea*
3 *Department of Agricultural Convergence Technology, Jeonbuk National University, Jeonju, Republic of Korea*
4 *Lab of Insect Phylogenetics & Evolution, Department of Plant Protection & Quarantine, Jeonbuk National University, Jeonju, Republic of Korea*
5 *Museum of Nature Hamburg – Zoology, Leibniz Institute for the Analysis of Biodiversity Change, Martin-Luther-King-Platz 3, Hamburg, 20146, Germany*
6 *Harry Butler Institute, Murdoch University, Murdoch, Australia*
7 *Australian Museum Research Institute, Australian Museum, Sydney, Australia*

https://zoobank.org/CF91D7F2-FC99-431C-AD78-6C5CB1DB1E9D

Corresponding author: Kyung-Hoon Jeong (ds16203@snu.ac.kr)

Academic editor: Martin Husemann ♦ **Received** 16 March 2024 ♦ **Accepted** 13 June 2024 ♦ **Published** 25 July 2024

Abstract

Some pseudoscorpions (Arachnida: Pseudoscorpions) occur in seashore habitats where they are typically found under driftwood or rocks. Here we review the genus *Nipponogarypus* Morikawa, 1955 from littoral habitats in Japan and South Korea and describe a new species, *Nipponogarypus seosanensis* **sp. nov.**, from the Korean Peninsula. We also elevate two former subspecies to species rank: *N. enoshimaensis enoshimaensis* Morikawa, 1960 = *N. enoshimaensis* Morikawa, 1955, and *N. enoshimaensis okinoerabensis* Morikawa, 1960 = *N. okinoerabensis* Morikawa, 1960, **stat. nov.** The distribution of all *Nipponogarypus* species is mapped, and an identification key for the species is provided.

Key Words

False scorpions, morphology, South Korea, systematics, taxonomy

Introduction

Most arachnids are strictly terrestrial, but some lineages occur in seashore habitats or even under water. Some pseudoscorpions (Arachnida, Pseudoscorpiones) have also adapted to littoral or coastal habitats, and these include members of diverse families such as the Garypidae (Harvey et al. 2020), Parahypidae (Harvey et al. 2007), Neobisiidae (e.g., Glynne-Williams and Hobart 1952), and some species in the Olpiidae (Beier 1932; Sato 1994). The family Olpiidae, with its 24 genera and 211 described species (World Pseudoscorpiones Catalog 2022), is most diverse in xeric environments such as semideserts and deserts (Harvey and Leng 2008). However, in 1955, Japanese zoologist Kuniyasu Morikawa discovered several small blackish olpiid pseudoscorpions between rock crevices near the seashore on Enoshima Island (Kanagawa-ken, Honshū) in Japan. These specimens differed from all other Olpiidae genera and were described as a new monotypic genus, *Nipponogarypus*. In a subsequent publication, Morikawa (1960) split his nominate species, *N. enoshimaensis*, into two subspecies: *N. enoshimaensis enoshimaensis* Morikawa, 1955, originally described from Enoshima Island near Honshu, and *N. enoshimaensis okinoerabensis* Morikawa, 1960, originally described from Okinoerabu-jima in the Satsunan Islands. At least *N. enoshimaensis* seems to be widespread in supralittoral habitats, and Morikawa (1960) listed additional

records from middle and southern Japan, but always in supralittoral habitats (Fig. 1). Nothing else has been published on this interesting genus ever since, and these two subspecies remain valid until today.

In this paper, we establish the first record of *Nipponogarypus* on the Korean Peninsula and describe a new species, *Nipponogarypus seosanensis* sp. nov., from South Korea. We also provide adequate illustrations and images for the first time since the original description of this genus, which is now outdated, and diagnose the genus within a modern taxonomic concept for the order Pseudoscorpiones. We also take the liberty to elevate Morikawa's original subspecies to species status because they are clearly diagnosable under the morphospecies concept. With this step, we recognize three species within *Nipponogarypus* and clarify the distribution of this genus in eastern Asia.

Materials and methods

All specimens used for this study are deposited in the National Institute for Biological Resources (NIBR) and were collected in Ganwoldo, Seosan-si, Chungcheongnam-Province, South Korea by the primary author. All specimens were preserved in 100% ethanol and examined using a Leica MSV266. Images were taken using a Leica Z16 AP0 attached to a Leica MSV266, and illustrations were created by hand, which were then enhanced using Adobe Illustrator 2023 and Adobe Photoshop 2023 (Adobe Inc.). Scanning electron micrographs were obtained using a Hitachi TM4000Plus scanning electron micrograph (SEM) system. Measurements and terminology follow Chamberlin (1931), Harvey (1992), Judson (2007), and Harvey et al. (2012). The distribution map was created using QGIS 3.22.10 (OGSeo). Abbreviations of chelal trichobothria: *b* – basal, *sb* – subbasal, *st* – subterminal, *t* – terminal, *ib* – internal basal, *isb* – internal subbasal, *eb* – external basal, *esb* – external subbasal, *it* – internal terminal, *ist* – internal subterminal, *et* – external terminal, *est* – external subterminal.

Systematics

Family Olpiidae Banks, 1895

Genus *Nipponogarypus* Morikawa, 1955

Type species. *Nipponogarypus enoshimaensis* Morikawa, 1955, by original designation.

Diagnosis. *Nipponogarypus* can be distinguished from other olpiid genera known to occur in East Asia as follows: from *Beierolpium* Heurtault, 1977, by trichobothrium *st* positioned distal to *sb* in *Nipponogarypus* and dorsal to *sb* in *Beierolpium* (Harvey 1988; Harvey and Leng 2008); from *Euryolpium* Redikorzev, 1938, by trichobothria *it*, *isb*, *esb*, and *eb* not clustered in *Nipponogarypus* but clustered in the latter. *Nipponogarypus* also shows similar characteristics to *Olpium* Koch, 1873, and *Indolpium* Hoff, 1945. However, *Nipponogarypus* can be distinguished from *Indolpium* by the position of trichobothria *st* and *isb*. In *Indolpium*, trichobothrium *isb* is situated proximally to trichobohtorium *st* (Murthy and Ananthakrishnan 1977). However, in *Nipponogarypus*, trichobothrium *isb* is situated distally from *st*. Furthermore, *Nipponogarypus* an easily be distinguised from *Olpium* by the length of its venom ducts. *Olpium* has long venom ducts that extend to trichobothrium *t*, whereas *Nipponogarypus*' venom ducts only extend to half of trichobothrium *t* (Mahnert 1991; Nassirkhani 2015). *Nipponogarypus* is morphologically most similar to *Olpiolum* Beier, 1931, and both have trichobothrium *est* positioned in the middle of the fixed finger; *ist* positioned between *est* and *isb*; *isb*, *esb*, and *eb* grouped together; and *sb* positioned closer to *b* than *st*. However, *Nipponogarypus* differs from *Olpiolum* by tergal chaetotaxy (four to six setae on the middle tergites in *Nipponogarypus*, always six setae on the middle tergites in *Olpiolum*) and the number of pseudotactile seta (two setae present in *Nipponogarypus*, one seta in *Olpiolum*) (Muchmore 1986).

Remarks. Subspecies are a rare concept in pseudoscorpion taxonomy since recognizable morphological divergences between populations are usually associated with morphological species. Unfortunately, Morikawa had the habit of designating subspecies (and subgenera) when morphological divergences were seen by him as too minor to warrant species- or genus status for any given taxon (e.g., Morikawa 1960). Pseudoscorpion taxonomy has advanced significantly in the past decades, and we are now aware that minor morphological divergences in cryptic lineages such as pseudoscorpions are generally indicative of species status (e.g., Hlebec et al. 2024; Muster et al. 2024). Following the recent example set by You et al. (2022), who elevated all subterranean subspecies of the genus *Spelaeochthonius* (family Pseudotyrannochthoniidae) in Japan and Korea to species status, we also elevate Morikawa's subspecies of *Nipponogarypus enoshimaensis* to species rank. Unfortunately, this taxonomic act needs to be done without reexamining the primary types that are held at Ehime University but are difficult to access and in poor condition (slide-mounted specimens in dried and contracted Hoyer's solution; see You et al. 2022). However, Morikawa's diagnoses are clear and reiterated here: *N. enoshimaensis okinoerabensis* is elevated to species rank as *N. okinoerabensis* **stat. nov**., and this name refers to specimens from the Ryuku and Satsunan Islands that have relatively short body appendages (pedipalpal femur length 0.48 mm, pedipalpal patella length 0.45 mm) and two pseudotacticle hairs that are equal in size on the palpal femur. The subspecies *N. enoshimaensis enoshimaensis* sensu Morikawa (1960) actually refers to *N. enoshimaensis* sensu Morikawa (1955) and is here recognized in its original form, *N. enoshimaensis*. This is a rather widespread morphospecies with records from Honshu and Shikoku (Fig. 1) that has slightly longer body appendages than *N. okinoerabensis* (pedipalpal

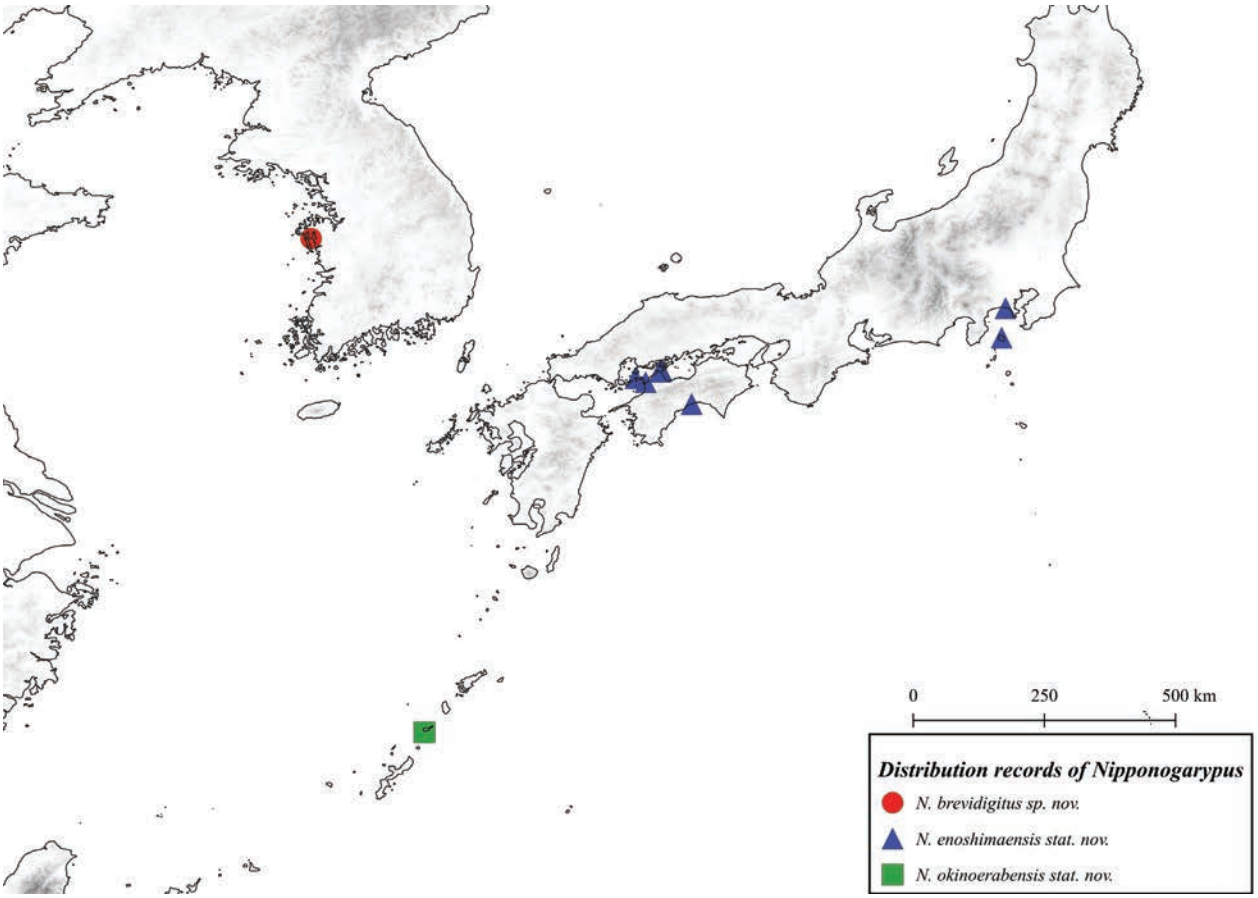

Figure 1. Distribution of the genus *Nipponogarypus* (Olpiidae) in Japan and Korea.

femur length 0.52–0.59 mm, pedipalpal patella length 0.57 mm) and unequal pseudotactile hairs (proximal hair smaller than distal hairs). A full description of both species is available in Morikawa (1960). Following this taxonomic act, the genus *Nipponogarypus* now contains three morphospecies that are found along the coastlines of the Korean Peninsula and Japan.

Nipponogarypus seosanensis Jeong & Harms, sp. nov.

https://zoobank.org/2CFFDE30-7D05-4E5B-9006-E57EE69E780F

Typematerial.*Holotype*. Female (NUHGIV0000001225). Korea: Chungcheongnam-province: Ganwoldo 1–gil, Buseok-myeon, Seosan-si, 36°36'5.56"N, 128°10'28.54"E, 03, Jul 2022, KH Jeong leg.

***Paratypes*:** One female and two males (NUHGIV0000001228), same data as holotype.

Etymology. This species is named after the type locality, Seosan-si, Chungcheongnam-do, in South Korea.

Habitat. This species was collected from cracks and fissures of moist rocks in the supralittoral zone, right next to the shoreline (Fig. 2).

Diagnosis. This species is most similar to *N. enoshimaensis* by having similar L/W ratios in the pedipalpal femur (0.56–0.61/0.18–0.20 mm in *N. seosanensis* sp. nov. and 0.52–0.59/0.18 mm in *N. enoshimaensis*) and pedipalpal patella (0.53–0.59/0.21–0.23 mm in *N. seosanensis* sp. nov. and 0.57/0.22 mm in *N. enoshimaensis*). Both species can easily be distinguished by the number of marginal teeth on the fixed chelal finger (40–43 in *N. seosanensis* sp. nov., 50 in *N. enoshimaensis*). *N. seosanensis* sp. nov. can further be distinguished from *N. okinoerabensis* stat. nov. by having a longer pedipalpal femur (0.56–0.61 mm in *N. seosanensis* sp. nov. and 0.48 mm in *N. okinoerabensis* stat. nov.) and patella (0.53–0.59 mm in *N. seosanensis* sp. nov. and 0.45 mm in *N. okinoerabensis* stat. nov.).

Description. Female, adult (holotype) (Fig. 3A, B).

Color. Blackish-brown, glossy; the ventral surface darker than the end of the body appendages; the coxal region reddish-orange.

Cephalothorax (Fig. 4A, H). Carapace 1.18 times longer than the broad; carapace sub-rectangular; four conspicuous eyes; two transverse furrows on the carapace; ten lyrifissures; first furrow situated in medial position on the carapace, second furrow near the posterior margin of the carapace; carapacal chaetotaxy 4–2: 22; setae short and acuminate. Pedipalpal coxa with 10 setae; coxal chaetotaxy 5: 5: 6: 13; one lyrifissure on coxa I–III, two lyrifissures on coxa IV.

Chelicera (Figs 4C, 5A). Cheliceral margin smooth; five setae on the cheliceral hand, one seta on the movable finger; galea long and shortly three-branched at the tip in

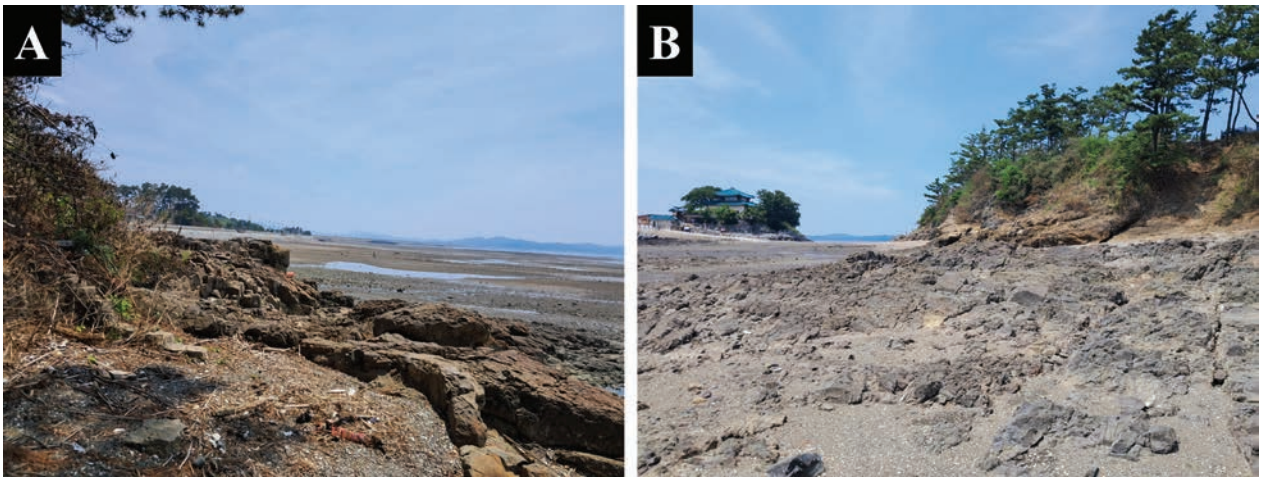

Figure 2. Habitat of *Nipponogarypus seosanensis* sp. nov. in the littoral zone of Seosan-si, Chungcheongnam-do, South Korea.

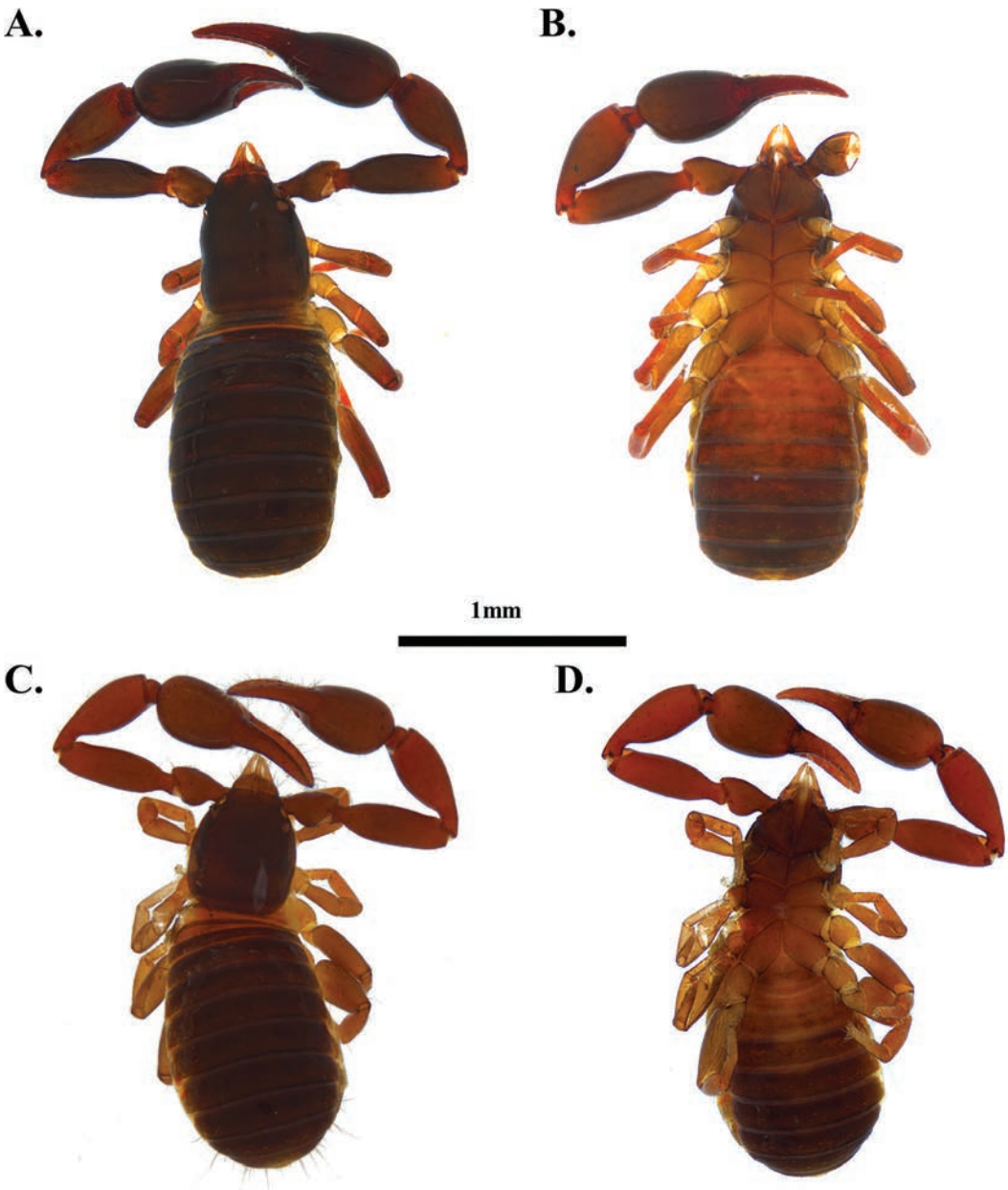

Figure 3. Habitus of *Nipponogarypus seosanensis* sp. nov. **A.** Female holotype, dorsal view; **B.** Female holotype, ventral view; **C.** Male paratype, dorsal view; **D.** Male paratype, ventral view.

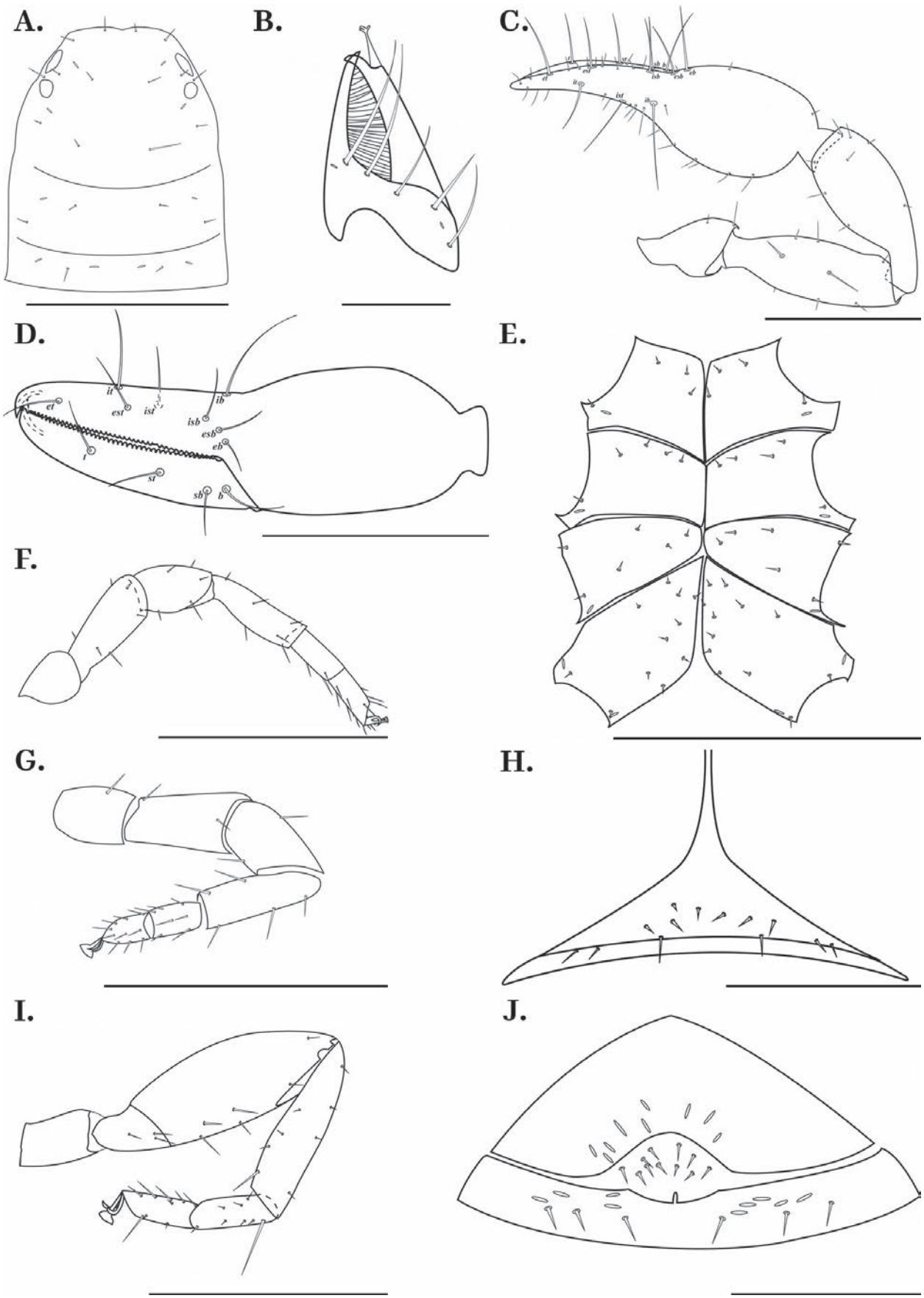

Figure 4. Appendages of *Nipponogarypus seosanensis* sp. nov., holotype female. **A.** Carapace; **B.** Chelicera in dorsal view; **C.** Left pedipalp in dorsal view; **D.** Right chela from lateral view; **E.** Coxa; **F.** Right leg I; **G.** Right leg II; **H.** Female genital sternites; **I.** Right leg IV; **J.** Male genital sternites. Scale bars: 0.5 mm (**A, C**–**G, I**); 0.2 mm (**H, J**); 0.1 mm (**B**).

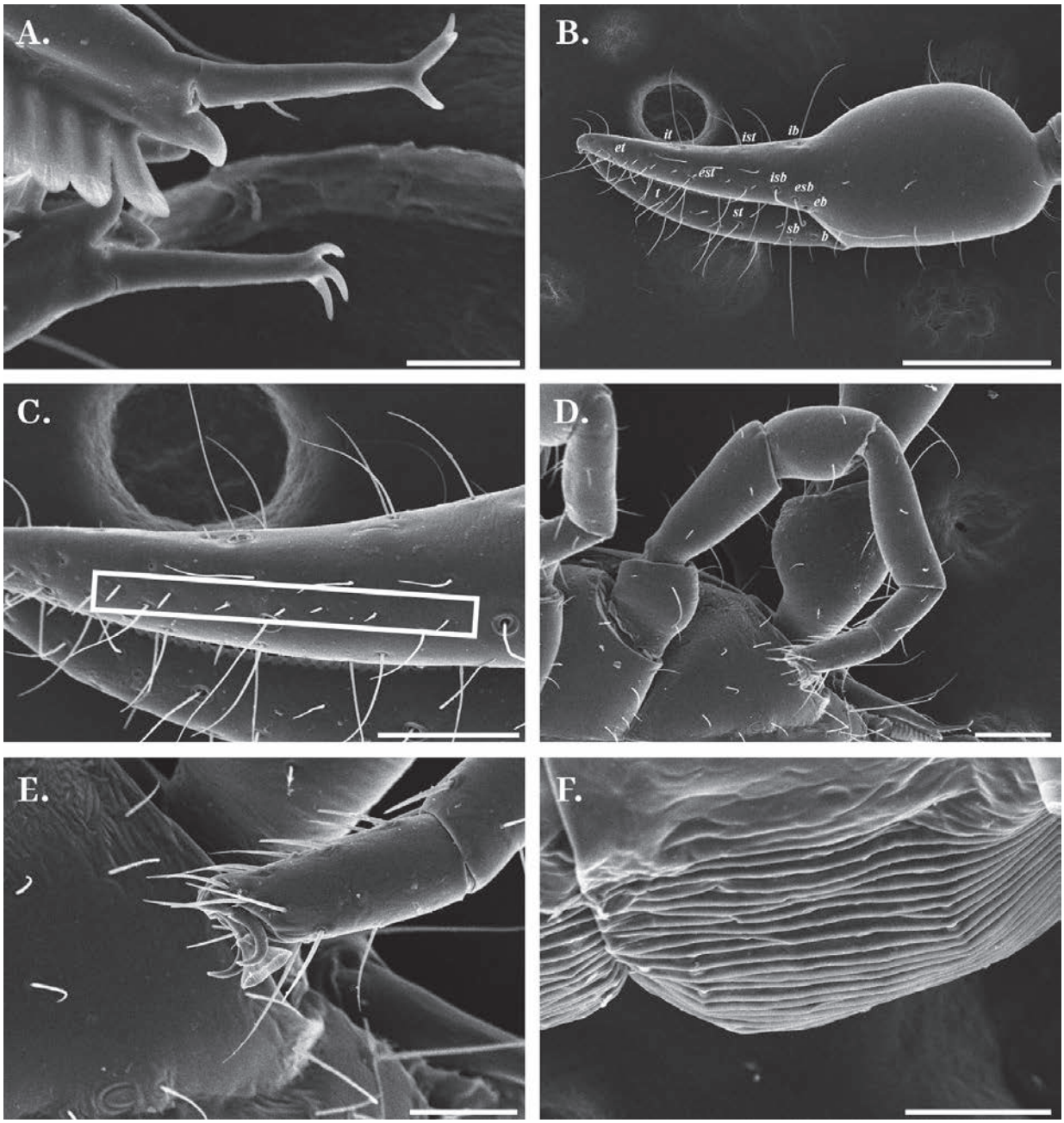

Figure 5. Appendages of *Nipponogarypus seosanensis* sp. nov., paratype female. **A.** Galea; **B.** Left chela, lateral view; **C.** Left chelal fingers, lateral view, sensory setae in the white box; **D.** Right leg I; **E.** Claws and arolium of right leg I; **F.** Pleural membrane. Scale bars: 0.02 mm (**A**); 0.3 mm (**B**); 0.1 mm (**C**, **D**, **F**); 0.05 mm (**E**).

both sexes; serrula exterior with 19 blades, rallum with three blades. Two lyrifissures on the hand.

Pedipalp (Figs 4B, 5B, C). Trochanter 1.60, femur 2.95, patella 2.46, chela 3.24 times longer than the broad, movable finger 0.99 times longer than the hand. Two pseudotactile setae on the femur. Sensory setae present between *et* and *isb*. *b* and *sb* on the basal of the finger; *st* on the middle of the *t* and *b*. *ib*, *esb*, and *eb* grouped at the base of the finger; *est* on the middle of *et* and *esb*; *it* and *ib* on the dorsal surface of the fixed finger, *it* on the middle of the finger, and *ib* on the basal of the finger; *ist* on the paraxial surface of the chela, between *isb* and *est*, but closer to *isb*; short venom ducts in both fingers, not extending past trichobothrium *et*.

Marginal teeth small and contiguous; triangular teeth on both fingers; fixed finger with 40, movable finger with 43 marginal teeth.

Legs (Figs 4D, E, 5D). Leg I: trochanter 1.56, femur 2.51, patella 1.80, tibia 3.06, metatarsus 2.08, tarsus 2.33 times longer than the broad; leg IV: trochanter 1.40, femur + patella 3.26, tibia 3.93, metatarsus 2.69, tarsus 2.98 times longer than the broad. Typical for the genus: femur and patella of leg I freely mobile; metatarsus of leg IV shorter than the tarsus; metatarsus of leg I longer than the tarsus; one each pseudotactile seta in the distal position

of the tarsus; basal position of the metatarsus; arolium undivided, longer than claws, and simple.

Abdomen (Fig. 5F). Pleural membrane striate; all tergites and sternites both undivided; all setae short and acuminate; tergal chaetotaxy 2: 4: 4: 4: 4: 4: 6: 5: 6: 4: 4: 2. Sternal chaetotaxy 10: 4: 6: 8: 6: 4: 6: 6: 4: 4: 2.

Dimensions (in mm). Body length: 1.93 cephalothorax: carapace 0.63/0.54, anterior eye 0.07, posterior eye 0.05; chelicera: total 0.22/0.12, movable finger 0.16; pedipalp: trochanter 0.31/0.19, femur 0.59/0.20, patella 0.58/0.23, chela 1.08/0.33, movable finger 0.53, hand 0.54; leg I: trochanter 0.15/0.10, femur 0.23/0.09, patella 0.18/0.10, tibia 0.21/0.07, metatarsus 0.10/0.05, tarsus 0.11/0.05; leg IV: trochanter 0.16/0.11, femur + patella 0.55/0.17, tibia 0.38/0.10, metatarsus 0.17/0.06, tarsus 0.16/0.05.

Variation (one female, paratype)

Cephalothorax. Carapace 1.16 times longer than broad.

Pedipalp. Trochanter 1.65, femur 3.13, patella 2.64, chela 3.29 times longer than broad, movable finger 0.88 times longer than hand. Fixed finger with 42, movable finger with 43 marginal teeth.

Legs. Leg I: trochanter 1.28, femur 3.29, tibia 3.34, metatarsus 2.38, tarsus 2.89 times longer than broad; leg IV: trochanter 1.50, femur + patella 3.06, tibia 3.08, metatarsus 2.25, tarsus 2.82 times longer than broad.

Abdomen. Tergal chaetotaxy 2: 4: 4: 4: 4: 6: 6: 6: 4: 2: 2. Sternal chaetotaxy 8: 4: 6: 6: 6: 6: 6: 4: 4: 4: 2.

Dimensions (in mm). Body length 1.90; cephalothorax: carapace 0.58/0.50, anterior eye 0.06, posterior eye 0.05; chelicera: total 0.20/0.12, movable finger 0.16; pedipalp: trochanter 0.33/0.20, femur 0.61/0.20, patella 0.59/0.22, chela 1.04/0.32, movable finger 0.49, hand 0.56; leg I: trochanter 0.14/0.11, femur 0.24/0.10, patella 0.19/0.10, tibia 0.25/0.08, metatarsus 0.12/0.05, tarsus 0.13/0.05; leg IV: trochanter 0.19/0.13, femur + patella 0.60/0.20, tibia 0.34/0.11, metatarsus 0.15/0.07, tarsus 0.18/0.06.

Variation (two males, paratype)

Cephalothorax. Carapace 1.20–1.23 times longer than broad.

Pedipalp. Trochanter 1.34–1.59, femur 3.07–3.13, patella 2.6, chela 3.05–3.21 times longer than the broad, movable finger 0.81–0.89 times longer than the hand. Fixed finger with 40–41, movable finger with 41–43 marginal teeth.

Legs. Leg I: trochanter 1.20–1.67, femur 2.08–2.45, patella 1.66–1.70, tibia 2.67–3.22, metatarsus 2.62–2.67, tarsus 2.86–3 times longer than broad; leg IV: trochanter 1.25–1.39, femur + patella 2.67–2.74, tibia 3.54–3.63, metatarsus 2.77–3.16, tarsus 2.5–2.7 times longer than broad.

Abdomen. Tergal chaetotaxy 2: 4: 4: 4: 4: 6: 6: 6: 6: 4: 4: 2. Sternal chaetotaxy 11: 6: 4: 6: 6: 6: 6: 5: 4: 4: 2.

Male genital sternites (Fig. 4G). Nine lyrifissures on sternites II and III; 11 setae on the genital opening area; six setae on the sternite III.

Dimensions (in mm). Body length: 1.83–1.84; cephalothorax: carapace 0.61/0.50–0.51, anterior eye 0.06, posterior eye: 0.04–0.05; chelicera: total 0.20/0.10–0.11 movable finger 0.14; pedipalp: trochanter 0.25–0.32/0.19–0.20, femur 0.56–0.60/0.18–0.19, patella 0.53–0.57/0.21–0.22, chela 0.91–0.92/0.21–0.29, movable finger 0.41–0.43, z 0.49–0.50; leg I: trochanter 0.12/0.07–0.10, femur 0.18–0.24/0.09–0.10, patella 0.15–0.16/0.09–0.10, tibia 0.17–0.23/0.06–0.07, metatarsus 0.12–0.13/0.05, tarsus 0.13/0.04; leg IV: trochanter 0.17–0.18/0.13, femur + patella 0.51/0.19, tibia 0.37/0.10, metatarsus 0.15–0.16/0.05, tarsus 0.12–0.16/0.05–0.06.

Key to the species of *Nipponogarypus*

1 Length of pedipalpal femur and patella more than 0.5 mm 2
– Length of pedipalpal femur and patella less than 0.5 mm ..... *Nipponogarypus okinoerabensis* stat. nov.
2 Fixed chelal finger with more than 45 marginal teeth ..... *N. enoshimaensis*
– Fixed chelal finger with less than 45 marginal teeth ..... *N. seosanensis* sp. nov.

Acknowledgements

KHJ would like to thank Mark Harvey (Western Australian Museum) for sending valuable reference papers and Sora Kim (Jeonbuk National University) for accessing the microscope and camera systems at Jeonbuk National University. This work has been supported by a grant from the National Institute of Biological Resources (NIBR), funded by the Ministry of Environment (MOE) of the Republic of Korea (NIBR202304103).

References

Beier M (1932) Pseudoscorpionidea I. Subord. Chthoniinea et Neobisiinea. Tierreich 57: 1–258. https://doi.org/10.1515/9783111435107.1

Chamberlin JC (1931) The arachnid order Chelonethida. Stanford University Publications, University Series (Biological Sciences) 7(1): 1–284.

Glynne-Williams J, Hobart J (1952) Studies on the crevice fauna of a selected shore in Anglesey. Proceedings of the Zoological Society of London, Wiley Online Library 122(3): 797–824. https://doi.org/10.1111/j.1096-3642.1952.tb00249.x

Harvey MS (1988) Pseudoscorpions from the Krakatau Islands and adjacent regions, Indonesia (Chelicerata, Pseudoscorpionida). Memoirs of the Museum of Victoria 49(2): 309–353. https://doi.org/10.24199/j.mmv.1988.49.13

Harvey MS (1992) The phylogeny and classification of the Pseudoscorpionida (Chelicerata: Arachnida). Invertebrate Systematics 6(6): 1373–1435. https://doi.org/10.1071/IT9921373

Harvey MS, Leng MC (2008) The first troglomorphic pseudoscorpion of the family Olpiidae (Pseudoscorpiones), with remarks on

the composition of the family. Records of the Western Australian Museum 24(4): 387–394. https://doi.org/10.18195/issn.0312-3162.24(4).2008.387-394

Harvey MS, Waldock J, Teale RJ, Webber J (2007) New distribution records of the intertidal pseudoscorpion *Parahya submersa* (Pseudoscorpiones, Parahyidae). Records of the Western Australian Museum 23(4): 393. https://doi.org/10.18195/issn.0312-3162.23(4).2007.393-395

Harvey MS, Ratnaweera PB, Udagama PV, Wijesinghe MR (2012) A new species of the pseudoscorpion genus *Megachernes* (Pseudoscorpiones, Chernetidae) associated with a threatened Sri Lankan rainforest rodent, with a review of host associations of *Megachernes*. Journal of Natural History 46(41–42): 2519–2535. https://doi.org/10.1080/00222933.2012.707251

Harvey MS, Hillyer MJ, Carvajal JI, Huey JA (2020) Supralittoral pseudoscorpions of the genus *Garypus* (Pseudoscorpiones, Garypidae) from the Indo-West Pacific region, with a review of the subfamily classification of Garypidae. Invertebrate Systematics 34(1): 34–87. https://doi.org/10.1071/IS19029

Hlebec D, Harms D, Kučinić M, Harvey MS (2024) Integrative taxonomy of the pseudoscorpion family Chernetidae (Pseudoscorpiones, Cheliferoidea): Evidence for new range-restricted species in the Dinaric Karst. Zoological Journal of the Linnean Society 200(3): 644–669. https://doi.org/10.1093/zoolinnean/zlad083

Judson ML (2007) A new and endangered species of the pseudoscorpion genus *Lagynochthonius* from a cave in Vietnam, with notes on chelal morphology and the composition of the *Tyrannochthoniini* (Arachnida, Chelonethi, Chthoniidae). Zootaxa 1627(1): 53–68. https://doi.org/10.11646/zootaxa.1627.1.4

Mahnert V (1991) Pseudoscorpions (Arachnida) from the Arabian Peninsula. Fauna of Saudi Arabia 12: 171–199.

Morikawa K (1955) On a new Garypidae (Pseudoscorp.) from Japan. Zoological Magazine, Tokyo 64: 225–228.

Morikawa K (1960) Systematic studies of Japanese pseudoscorpions. Memoir of Ehime University 4(2B): 85–172.

Muchmore WB (1986) Redefinition of the genus *Olpiolum* and description of a new genus Banksolpium (Pseudoscorpionida, Olpiidae). The Journal of Arachnology 14: 83–92.

Murthy VA, Ananthakrishnan TN (1977) Indian Chelonethi. Oriental Insects Monograph 4: 1–210.

Muster C, Korba J, Bogusch P, Heneberg P, Šťáhlavský F (2024) And Yet They Differ: Reconsiderations of Diversity within *Dactylochelifer latreillii* (Arachnida, Pseudoscorpiones). Diversity 16(3): 137. https://doi.org/10.3390/d16030137

Nassirkhani M (2015) Notes on Olpiidae (Arachnida, Pseudoscorpiones) from Iran: Description of *Cardiolpium bisetosum* sp. nov. and redescription of *Olpium omanense*. Arachnologische Mitteilungen 50: 1–10. https://doi.org/10.5431/aramit5001

Sato H (1994) Pseudoscorpions from the Northern Mariana Islands, Micronesia. Natural History Museum and Institute Chiba 1: 173–174.

World Pseudoscorpion Catalog (2022) World Pseudoscorpiones Catalog. Natural History Museum Bern. http://wac.nmbe.ch [Accessed 28 June 2024]

You JY, Yoo JS, Harvey MS, Harms D (2022) Some cryptic Korean karst creatures: Revalidation of the pseudoscorpion genus *Spelaeochthonius* (Pseudoscorpiones, Pseudotyrannochthoniidae) and description of two new species from Korea. The Journal of Arachnology 50(2): 135–157. https://doi.org/10.1636/JoA-S-21-025

Zoosyst. Evol. 100 (3) 2024, 1061–1073 | DOI 10.3897/zse.100.119292

PENSOFT

MUSEUM FÜR NATURKUNDE BERLIN

Distribution and systematics of the cosmopolitan *Amynthas carnosus* complex (Crassiclitellata, Megascolecidae) from eastern Asia

Anne Charis N. Han[1,2], Yufeng Zhang[2], Pu Miao[3], Shaolong Wu[4], Nengwen Xiao[5], Mingyan Qin[1,2], Huifeng Zhao[2,6], Donghui Wu[1,6], Nonillon M. Aspe[7]

1 *State Environmental Protection Key Laboratory of Wetland Ecology and Vegetation Restoration, School of Environment, Northeast Normal University, Changchun 130117, China*
2 *Hebei Key Laboratory of Animal Diversity, College of Life Science, Langfang Normal University, Langfang 065000, China*
3 *Henan Province Tobacco Company, Luoyang 471000, China*
4 *Hunan Province Tobacco Company, Changsha 410004, China*
5 *State Key Laboratory of Environmental Criteria and Risk Assessment, Chinese Research Academy of Environmental Sciences, Beijing 100012, China*
6 *Key Laboratory of Wetland Ecology and Environment, State Key Laboratory of Black Soils Conservation and Utilization, Northeast Institute of Geography and Agroecology, Chinese Academy of Sciences, Changchun 130102, China*
7 *College of Marine and Allied Sciences, Mindanao State University at Naawan, Naawan 9023, Misamis Oriental, Philippines*

https://zoobank.org/541660A7-7B6A-4432-AEF5-C689737C0A3C

Corresponding authors: Huifeng Zhao (zhaohf@lfnu.edu.cn); Donghui Wu (wudonghui@iga.ac.cn)

Academic editor: Pavel Stoev ♦ **Received** 23 January 2024 ♦ **Accepted** 17 June 2024 ♦ **Published** 1 August 2024

Abstract

Pheretimoid earthworms, *Amynthas carnosus*, were collected from Northeast and North China. An update on the distribution and systematics of the *A. carnosus* complex in eastern Asia using both morphological and molecular data is provided. Three subspecies, *A. carnosus carnosus*, *A. carnosus naribunji*, and *A. carnosus roki*, are confirmed. Comparisons of morphological characters between the subspecies of *A. carnosus* are provided. Our results support the subspecies assignment with an intraspecific K2P genetic distance of not greater than 10% using the mitochondrial cytochrome c oxidase subunit I (COI). In addition, a re-description of the morphology of *A. carnosus naribunji* is presented here.

Key Words

DNA barcoding, earthworm, morphological characters, K2P, Megascolecidae

Introduction

Pheretimoids are a group of earthworms belonging to the family Megascolecidae (Oligochaeta) characterized by having a perichaetine setal arrangement, a meronephridial excretory system, a single gizzard around segment VIII, a pair of racemose prostates opening through male pores in XVIII, and testes contained within testis sacs (Aspe 2016). They are known to be widely distributed and predominantly occur in East and Southeast Asia. *Amynthas* and *Metaphire*, two of the most speciose pheretimoid genera, have species with a wider range of distribution and have become well established outside their native ranges (McCay et al. 2020; Chang et al. 2021). In China, *Amynthas*, with around 450 species, and *Metaphire*, with around 130 species, account for 88.9% of the total number of earthworm species in the country (Aspe 2016; Jiang and Qiu 2018).

Amynthas carnosus Goto & Hatai, 1899 is known to be one of the cosmopolitan pheretimoid species (Blakemore 2009). They are characterized by four pairs of obvious spermathecal pores in segments 5/6–8/9, or occasionally three pairs in segments 6/7–8/9, with genital markings typically closely paired mid-ventral and presetal in VIII–

IX and often also in XVIII–XIX (Chen 1933; Blakemore 2012). Its distribution has been reported in Japan, from Kyushu to Tohoku and Hokkaido (Goto and Hatai 1899; Kobayashi 1936; Ohfuchi 1937; Easton 1981), in Nara and Hikone (Blakemore 2013a), and in South Korea, including Jeju Island and Dagelet Island (Ulleung-do) (Kobayashi 1938; Blakemore 2013b, c). In China, the species has been reported in several provinces (Xiao 2019), but such claims are deemed questionable because of the lack of information about where the specimens were collected. So far, the published record of *A. carnosus* in China is in Hainan (Sun 2013) and Shanghai (Zhang et al. 2016), which only provided molecular data. In the USA, the species was reported near Manhattan in Kansas (Carrera-Martínez and Snyder 2016). Therefore, the known distribution of this species is in South Korea, Japan, China, and North America.

There has been an underlying confusion regarding *A. carnosus* morphology in the past due to its poor original account and successive misdescriptions. The problem with the original description by Goto and Hatai (1899) was that there were three pairs of spermathecal pores in 5/6/7/8, but the spermathecae were stated to be in 7, 8, and 9, suggesting they exited in 6/7/8/9 with the possibility of missing a pair. Nevertheless, Ohfuchi (1937), in a more detailed account, showed the species to have four pairs of spermathecal pores in 5/6/7/8/9. This then caused other character traits (e.g., dorsal pores, genital markings, segment count, and so on) to be misnumbered as well (Blakemore 2012). Not to mention that the species synonymy was caused by the erroneous assignment of names, which has added to the complexity of this species' identity. Further information about *A. carnosus'* provisional synonyms is listed and discussed by Blakemore (2012).

Amynthas pingi was previously considered a questionable synonym of *A. carnosus*, "as it is, on average, a larger worm with several other differences that presently exclude it from *A. carnosus*" (Blakemore 2012). However, Blakemore (2013a) re-examined the London type mature *A. pingi* specimen labeled as "*Pheretima pingi* 1924.11.29.5 HOLOTYPE (sic) Nanking, China Don. Prof. C. Ping" and refuted those differences (e.g., the supposed larger size in *A. pingi*, now known to be false as the type is only 132 mm long, and a later onset of intestine origin and septal glands, now also proven false). There, he also pointed out errors in Gates (1939) redefinition of *Pheretima pingi*, such as having "lower setal counts, mistaken septa, hearts, and spermathecal pores that he insisted were posterior in segments 5–8 (but that are now shown to be in the intersegmental furrows of 5/6/7/8/9 in the types of both *A. pingi* and *A. carnosus*). Moreover, the assumption that the 'characteristic' tubercles were nephridial (Goto and Hatai 1899) was more likely due to Monocystis infestation, as indicated by both Gates (1939) and Blakemore (2013a), hence dismissing the possible justification of retaining *A. pingi* as a separate species from *A. carnosus*. In which case, *A. carnosus* would likely suggest prevalence in China, from which *A. pingi* (= *A. carnosus*) was reported to have been abundantly distributed in Nanking (Stephenson 1931). Given this and with the incorporation of the new investigation of *A. carnosus* specimens in Northeast and North China (reported here), it may further support a possible indication of the prevalent range of *A. carnosus* in the country, as was suggested by Chen (1936) and concluded by Kobayashi (1936).

Preliminary attempts at using the DNA barcodes of *A. carnosus* specimens from Japan and South Korea were carried out (Blakemore 2013b). Two new subspecies have been established, namely, *A. carnosus naribunji* Blakemore 2013 from Naribunji, Ulleung-do (Dagelet Island, South Korea), and *A. carnosus roki* Blakemore and Lee 2013 from Incheon (South Korea). Preliminary DNA data for taxon identification and phylogenetic relationships were also explored, yet a rather deficient description of *A. carnosus naribunji*'s morphological characters by Blakemore (2013a) was presented, which then makes it more of a molecular taxon.

This paper provides an update on the taxonomic status of the *A. carnosus* complex in East Asia using both morphological and molecular data, as well as a report on the present distribution of this species in China. In addition, an update on the morphological diagnosis of *A. carnosus carnosus* and a re-description of *A. carnosus naribunji* are presented.

Materials and methods

Sampling

Earthworm specimens were collected during the summer of 2022 and 2023, around the months of May and July, in Northeast China and the neighboring provinces. The collection sites chosen were mainly based on three habitat types, including forests, farmlands, and urban parks (Table 1). Earthworm samples were also collected in a nature reserve area on Changbai Mountain. Earthworms were collected through digging and hand sorting. Collections near the sites with surface castings were also taken into account. The earthworms collected were preserved and stored in 100% ethanol.

DNA extraction, amplification, and sequencing

Total genomic DNA was extracted from the muscle tissue of the posterior part using the TIANGEN Genomic DNA Kit (China) following the manufacturer's instructions. Regions of the cytochrome c oxidase subunit I (COI) were amplified using the polymerase chain reaction (PCR). The mixture (total volume 25 µl) contained 1 µl DNA and 17.25 µl sterile ddH_2O, 2.0 µl of dNTP, 2.5 µl of buffer, 0.25 µl TransGen EasyTaq-polymerase and 1.0 µl of Primer HCO1490 (5-GGTCAACAAATCATAAAGATATTGG-3) (Folmer et al. 1994), and 1.0 µl of Primer COIE (5-TATACTTCTGGGTGTC-

Table 1. Collection information for sampling areas and specimens.

Sampling ID	Location	Latitude, Longitude	Specimen number
362R	Liaoning Prov., Jinzhou Pref., Nanshan Park	41.0718°N, 121.1479°E	8
533R	Liaoning Prov., Dandong Pref., Jinjiang Mt. Park	40.1312°N, 124.3746°E	12
534R	Liaoning Prov., Dandong Pref., Kundian County, Beishan Park	40.7319°N, 124.7780°E	10
551R	Liaoning Prov., Huludao City, Longwan Park	40.7143°N, 120.8415°E	10
LFXH	Hebei Prov., Xianghe County, Zhuti Park	39.7774°N, 116.9816°E	7
LFSF	Hebei Prov., Langfang Pref., Anci Dist., Langfang Normal University	39.5222°N, 116.6654°E	1
E28, E29	Tianjin Municipality, Dongli Dist., Anonymous Park	39.0836°N, 117.3125°E	2
BJCY	Beijing Municipality, Chaoyang Dist., Lvfeng Park	39.8760°N, 116.5800°E	1
BJTZ	Beijing Municipality, Tongzhou Dist.,	39.8760°N, 116.7250°E	1
HNLNR2, HNLNGR, HNLNNG	Henan Prov., Luoyang Pref., Luoning County	34.4363°N, 111.6398°E	4
HNSQ	Henan Prov., Shangqiu Pref., Liangyuan Dist.	34.4291°N, 115.6183°E	3

CGAAGAATCA-3) (Bely and Wray 2004). The cycling profile was as follows: firstly, initial denaturation for 5 min at 95 °C; secondly, denaturation for 30 sec at 95 °C, annealing for 30 sec at 51 °C, and extension for 45 sec at 72 °C for 35 cycles; thirdly, final extension for 5 min at 72 °C. PCR amplifications were confirmed by electrophoresis in 1% agarose gel, which were visualized by SAGECREATION Gel Documentation and Image Analysis System Equipment, and Sage software was used for capturing the image. DNA samples were sent to Tianyi Huiyuan Biotechnology Co., Ltd. (Beijing) for Sanger sequencing using an ABI 3730 automated sequencer.

Data analysis

The raw data were corrected manually in BioEdit (Hall 1999), and the exported fasta files were aligned using Clustal W (Thompson et al. 1994). COI sequences from Genbank labeled as *A. carnosus* have also been included in the analysis (Suppl. material 1: table S1). A phylogenetic tree was constructed using the maximum likelihood method (ML) performed in RAxML 8.0 (Stamatakis 2014), using the default rapid hill-climbing algorithm and the GTRGAMMA model to search for the best tree. Clade support was assessed using 1,000 rapid bootstrap replicates. The tree was rooted using *Pontodrilus litoralis* as an outgroup. Pairwise distance analysis among *A. carnosus* subspecies and between COI sequences of the other 10 *Amynthas* species downloaded from GenBank was conducted using MEGA5 (Tamura et al. 2011) with the Kimura-2 parameter model (Kimura 1980).

Morphological examination and identification

Fixed specimens were brought to the laboratory for external and internal examination using a stereomicroscope (ZEISS) and ZEN 3.3. Pro software was used for image capture and to aid in identifying and measuring small organs and other characters. The generic diagnoses and taxonomic assignments to the subspecies level follow Blakemore (2012, 2013b) and Blakemore and Lee (2013).

References to figures from the cited papers are listed in lowercase (fig. or figs), and figures in this paper are noted with an initial capital (Fig. or Figs). The following abbreviations are used:

Ag accessory gland;
mp male pore;
re receptacle;
Amp ampula;
P prostomium;
sp spermathecal pore;
Gm genital marking;
prg prostate gland;
sv seminal vesicles.

Results and discussion

Molecular characterization

A total of 66 COI sequences had been sequenced and submitted to Genbank (Accession numbers: PP067669–PP067734). Results of the K2P analysis using COI show that the three intraspecific taxa of *A. carnosus* have inter-subspecific genetic distances that are between 7% and 10% (Table 2). Meanwhile, the genetic distance between *A. carnosus* and other species in the same genus is greater than 16% (16–22%). A study by Dong et al. (2019) revealed a genetic distance of 10.7–11.4% between two subspecies of *Amynthas shengtangmontis*: *A. s. shengtangmontis* and *A. s. minusculus*, which showed to be more than 1% and less than 15%. The intra-specific pairwise distances of subspecies *A. c. naribunji* and *A. c. roki* from *A. c. carnosus* are 7–8% and 9–10%, respectively (Table 2). In other studies, the interspecific distances in the same genus ranged between 17–23% (Sun 2013), 16–23% (Huang et al. 2007), 15–16% (Admassu et al. 2006), 16–22% (Novo et al. 2009), 15–28% (Chang et al. 2008), and 14.7–25% (Dong et al. 2019), which are all in agreement with our results.

Also, a specimen identified as "*A. carnosus carnosus*" in Hainan (China) by Sun (2013) (cf. Dong et al. 2019; KF205962) is seen to have diverged greatly from the *A. carnosus* taxa (Fig. 1), having a pairwise distance to the remaining *A. carnosus* taxa of 22–24% (Table 1), which could possibly suggest a misidentification of this species or subspecies.

Table 2. Percentage of K2P distance of the three subspecies of *A. carnosus* with inclusion of other pheretimoid species (values in %).

Species		1	2	3	4	5	6	7	8	9	10	11	12	13
1	*A. carnosus carnosus*	0–1												
2	*A. carnosus naribunji*	7–8	0–1											
3	*A. carnosus roki*	9–10	8	0										
4	*A. carnosus carnosus* (KF205962)	23–24	22–23	24	0									
5	*A. daeari*	20	19	20	22	0								
6	*A. gageodo*	17–18	19–20	18–19	21	21	0							
7	*A. gracilis*	19	19–20	20–21	19	18–19	21	0						
8	*A. corticis*	16–20	17–19	19–20	19	18–19	18–20	18–20	0–7					
9	*A. fuscatus*	17–20	17–22	18–22	19–20	18–20	20–23	18–21	17–20	0–15				
10	*A. tokioensis*	20–21	19–21	22–23	23	16	20–21	20–21	18–21	18–22	0–1			
11	*A. maximus*	19	19	20	20	18	18	22	17–18	16–19	20–21	0		
12	*A. shengtangmontis*	20–21	19	20	21	20	20	20–21	18–19	19–21	22–23	23	0	
13	*A. robustus*	20–22	21–22	21–23	17–22	21–22	22–23	20	17–21	17–21	23–24	24	19–22	0–21

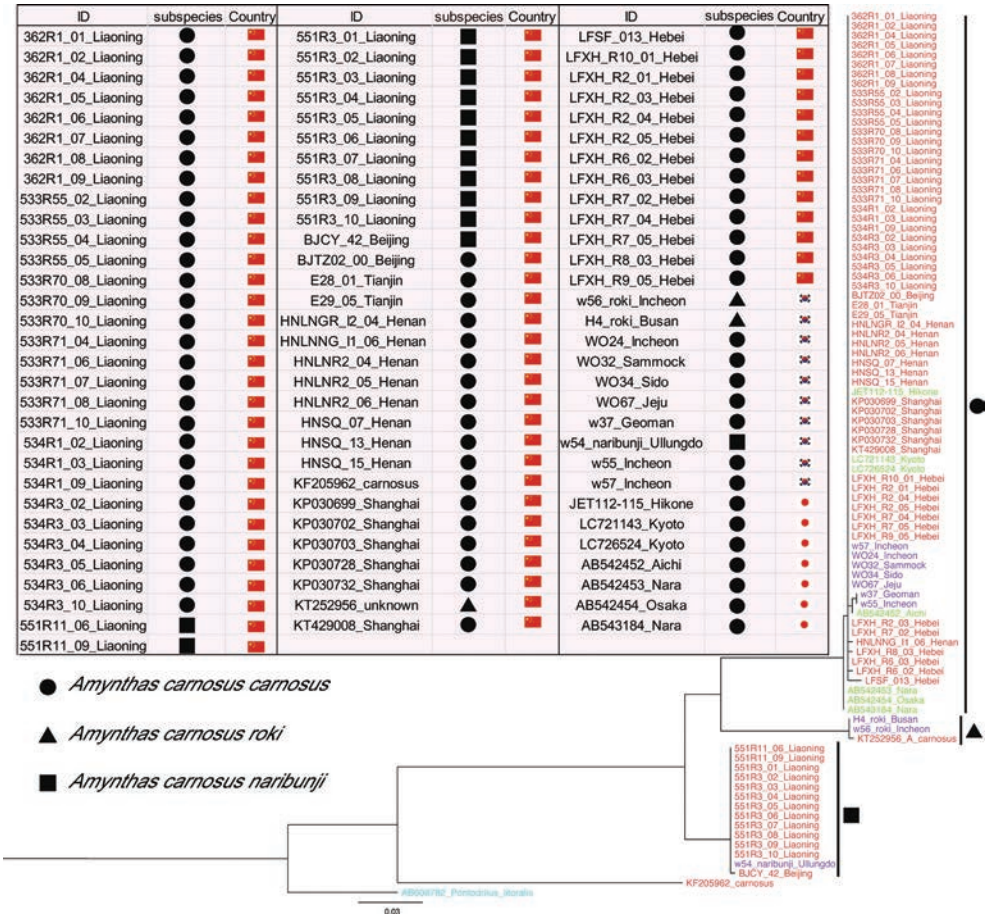

Figure 1. The geographical distribution of the *A. carnosus* complex in eastern Asia and its corresponding phylogenetic tree based on COI using the maximum likelihood method. Color coding: red for China, purple for South Korea, and green for Japan.

Molecular data show a divergence among the subspecies of *A. carnosus* (Fig. 1), which comprise the DNA samples provided from China, Japan, and South Korea. It also shows little genetic variation of *A. c. carnosus*, as shown by the absence or having of very short branches within the clade that is composed of the three countries. The same is observed in the other two subspecies that occur in China and South Korea. Here, the geographic representation shows a wide distribution of the species in eastern China (Fig. 1).

On the one hand, *A. c. naribunji*'s current distribution pattern has been expanded because of its new record in northern China (Beijing and Liaoning). Still, future investigations and additional sampling sites must be explored to be able to have a thorough understanding of the origin of this species and its migration pattern across countries.

Moreover, the specimen of *A. c. roki* (NIBR-IV0000261264 providing DNA w56) from Incheon Great Park (Blakemore and Lee 2013) has inter-subspecific distance values of 8.1–10% from *A. c. carnosus* and

7.2–7.5% from *A. c. naribunji*, respectively. Alternatively, a specimen labeled "*A. carnosus*" from China (KT252956; the detailed location is unknown) was grouped with the *A. c. roki* specimens from South Korea, with a 100% bootstrap value. Intersubspecific distances among *A. c. carnosus* and *A. c. naribunji* are 9–10% and 8%, respectively. As no data on the exact location and morphological descriptions of *A. c. roki* in China have been reported, further sampling of *A. c. roki* needs to be done in the future.

Morphological characterization

Family Megascolecidae Rosa, 1891
Genus *Amynthas* Kinberg, 1867

Amynthas carnosus carnosus Goto & Hatai, 1899

Perichaeta carnosa Goto & Haitai, 1899: 15.

Pheretima carnosa – Kobayashi 1936: 115.

Amynthas carnosus – Sims and Easton 1972: 235. Blakemore 2012: 36; 2013a: 58; 2013c: 101. Carrera-Martínez and Snyder 2016: 297. Chang et al. 2016: 505.

Amynthas pingi (Stephenson, 1925) – Sims and Easton 1972: 235. Blakemore 2013c: 112.

Material examined. Specimen IDs: 362R1_01, 02, 04, 05, 06, 07, 09, seven matures from Nanshan Park, Jinzhou, Liaoning; 533R70_08, 09, 10, three matures from Jinjiang Mt. Park, Dandong, Liaoning; LFXHR7_02, 04, 05, three matures from Zhuti Park, Xianghe County, Langfang, Hebei; LFSF_013, one mature from Langfang Normal University, Anci District Langfang, Hebei; E29_05, one mature from an anonymous park in Dongli District, Tianjin Municipality; HNLNR2_04, 05, 06, three matures from the tobacco field in Xiaojie Town, Luoning County, Luoyang, Henan; HNSQ_07, 13, 15, three matures under the bushes in Shangqiu Normal University, Liangyuan District, Shangqiu, Henan.

Diagnosis. Length 105–210 mm. Spermathecal pores having four pairs in 5/6/7/8/9, rarely 3 pairs in 6/7/8/9, with pre-intersegmental hemispherical arc (spermathecal papillae). Dorsal pores typically from 12/13. Pre-clitellar genital markings typically with two pairs, pre-setal in VIII and IX; these genital markings paired either widely or closely apart (B1 and B2, Fig. 3); Post-clitellar genital markings prominent, up to three pairs median to male pores; first pair pre-setal on XVIII, slightly median to male pores; second pair post-setal and more medial than the first; third pair pre-setal in XIX (Fig. 4). Male pores superficially paired in XVIII close to the lateral margin on round or elliptical porophores (Fig. 4). Ampulla ovate to narrowly ovate (Fig. 2D–F). Intestinal caeca simple at XXVII.

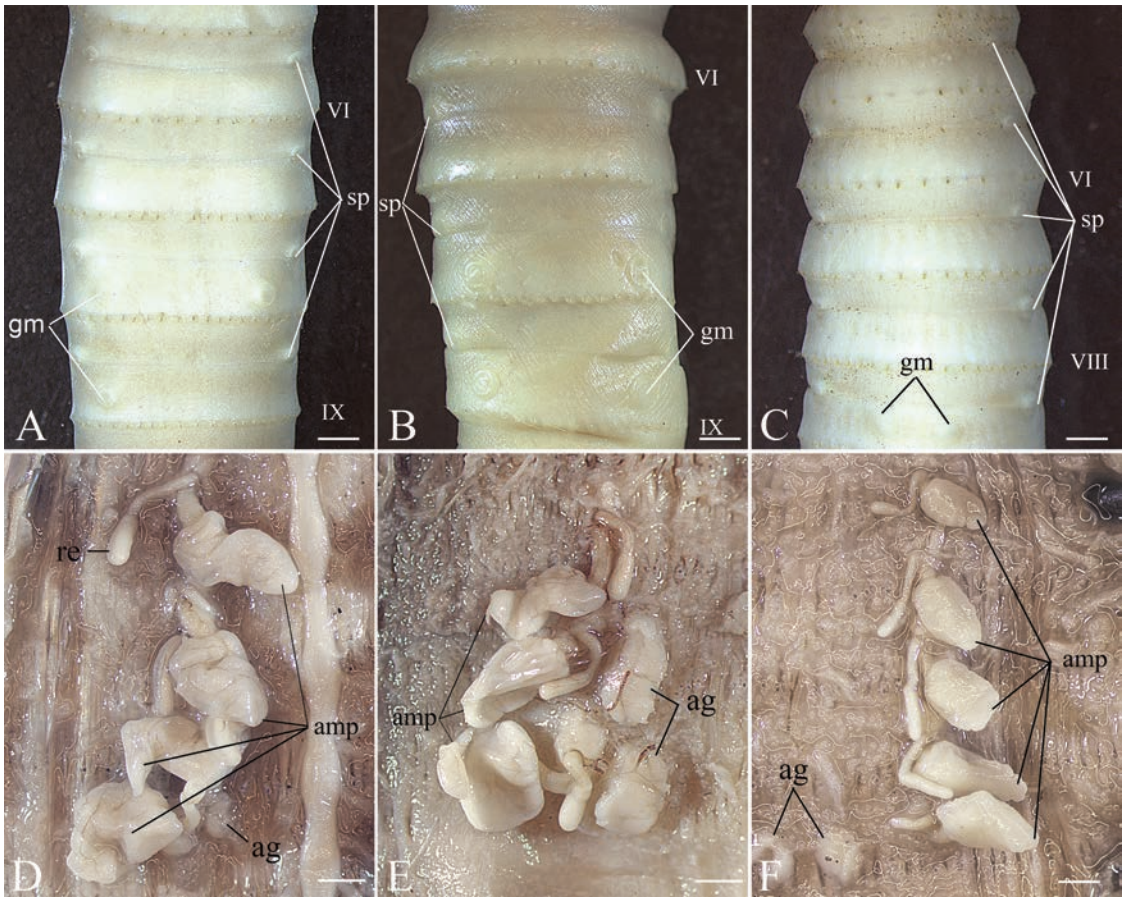

Figure 2. *Amynthas carnosus carnosus* variations on the number of spermathecal pores and spermathecae: four pairs (**A, D**) (specimen ID 362R1_06), three pairs (**B, E**) (specimen ID LFXHR7_05), five pairs (**C, F**) (specimen ID HNLNR2_05). Scale bars: 1 mm.

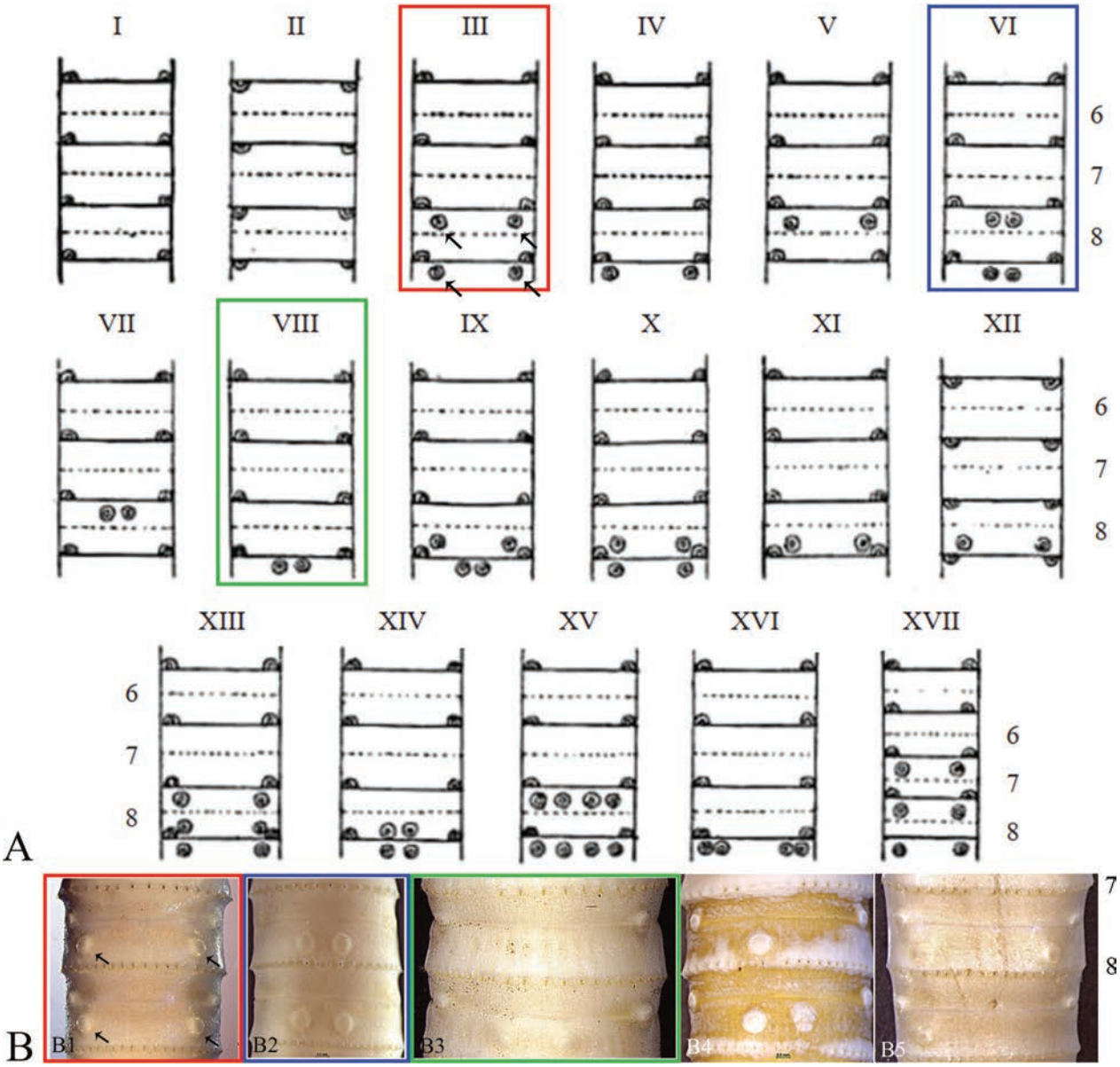

Figure 3. Pre-clitellar genital marking (arrows) variations of *Amynthas carnosus*. **A.** Modified fig. 1 of the variations of pre-clitellar genital markings from Kobayashi (1936); **B.** This study. **B1.** (specimen ID 362R1_01); **B2.** (specimen ID 533R70_09), and **B3.** (specimen ID HNLNR2_05) comply with the "permissible variations" [termed by Blakemore (2012)] of Kobayashi's (1936) Type III (red), VI (blue), and VIII (green).

Variations. For the *A. c. carnosus* from China, the number of spermathecal pores and spermathecae are variable: 14 out of 16 specimens typically have four pairs in 5/6/7/8/9, one specimen has three pairs in 6/7/8/9 (LFXHR7_05), and another one has five pairs in 4/5/6/7/8/9 (HNLNR2_05) (Fig. 2). However, despite these variations, molecular analyses have shown them to belong in the same clade with little genetic divergence within the clade (Table 2, Fig. 1). Two specimens from South Korea and one specimen from the USA have three pairs of spermathecal pores in 6/7/8/9 (Kobayashi 1936; Carrera-Martínez and Snyder 2016). However, prior to this study, no other specimen with five pairs was recorded elsewhere.

Distribution. China (Liaoning, Beijing, Tianjin, Hebei, Henan, and Shanghai), Japan (Kyushu, Honshu, and Hokkaido), and South Korea (Incheon, Jeju Island).

Remarks. Detailed descriptions of *A. carnosus* were reported by Kobayashi (1936), Ohfuchi (1937), and Blakemore (2012, 2013a, c). Rather than typical closely spaced mid-ventral pre-clitellar genital markings (Blakemore 2012), widely spaced ones are mostly observed with the *A. carnosus* specimen from China, which resembles those Hikone specimens from Japan (Tokyo An-460-DNA JET-112) [cf. fig. 3 by Blakemore (2013a)]. In contrast, the closely spaced pre-clitellar genital markings of the Liaoning specimens (Dandong, DNA 533R) match those of the South Korean specimen from Geoman

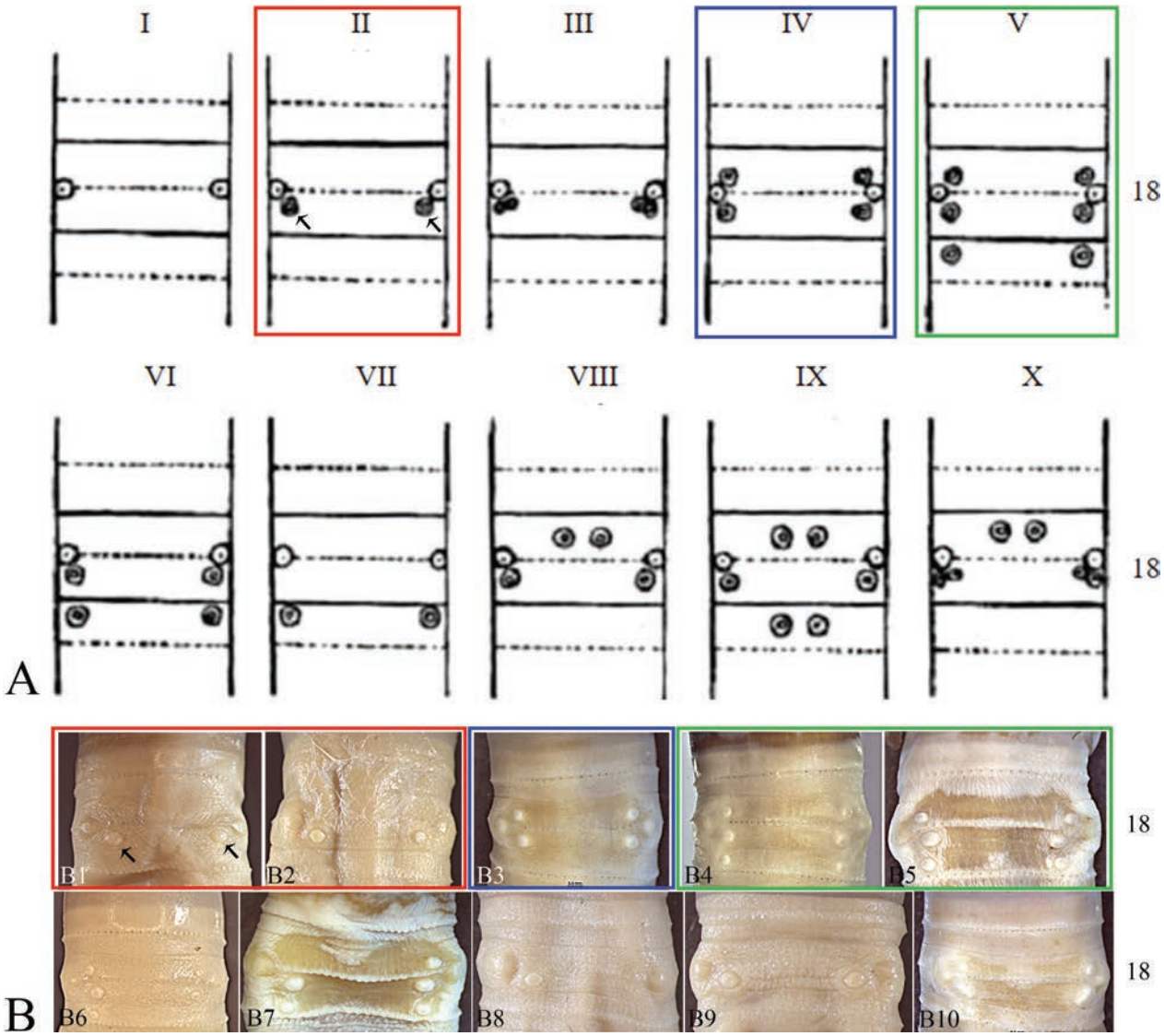

Figure 4. Post-clitellar genital marking (arrows) variations of *Amynthas carnosus*. **A.** Modified fig. 2 of the variations of post-clitellar genital markings from Kobayashi (1936); **B.** This study. **B1, B2. (**specimen IDs 362R1_07 and HNLNR2_04); **B3** (specimen ID 362R1_04); **B4, B5. (**specimen IDs 362R1_01 and 533R70_10) comply with the "permissible variations" [termed by Blakemore (2012)] of Kobayashi's (1936) Type II (red), IV (blue), and V (green).

(NIBR IV261234-DNA w37) and the Japanese neotype of *A. carnosus* (Tokyo An435) [cf. fig. 2 by Blakemore (2013a)].

A comparison of characters from the specimens of China, Japan (a neotype NSMT An435 from the Tokyo Museum) (Blakemore 2012), and the USA (Kansas) (Chang et al. 2016) is presented in Suppl. material 1: table S2. External characters such as the number of spermathecal pores and segment locations of pre-clitellar genital markings match among specimens from different countries. However, internal character variations are observed in the position of the intestinal caeca, which was reported to begin at XXVII and extend to XXIII or XXIV (Blakemore, 2012; 2013b; 2013c; Chang et al. 2016), while the intestinal caeca in the Chinese specimens extends up to XX, XXI (or XXIII) (Fig. 5), 2–3 segments more anterior than those from the two previous accounts. Moreover, some character measurements that were not presented in the other two accounts, such as the ventral distances between male pores (0.25–0.29 mm), spermathecal pores (0.28–0.30 mm), and genital markings (latero-ventrally with 0.21–0.29 mm distance apart or mid-ventrally with 0.08 mm distance apart), were added to further aid species identification.

Kobayashi (1936), in his thorough investigation of *A. carnosus*, presented "permissible" variations on the pre-clitellar and post-clitellar genital markings [text-figs. 1–2 in Kobayashi (1936)]. The pre-clitellar genital making variations in the *A. c. carnosus* from China comply with Kobayashi's Types IIII, VI, and VIII (see Fig. 3), while the post-clitellar genital marking variations comply with Kobayashi's Types II, IV, and V (see Fig. 4). It is important to take note that genital marking patterns can also be considered a distinctive character for species identification (e.g., Nguyen et al. 2020; Aspe et al. 2021).

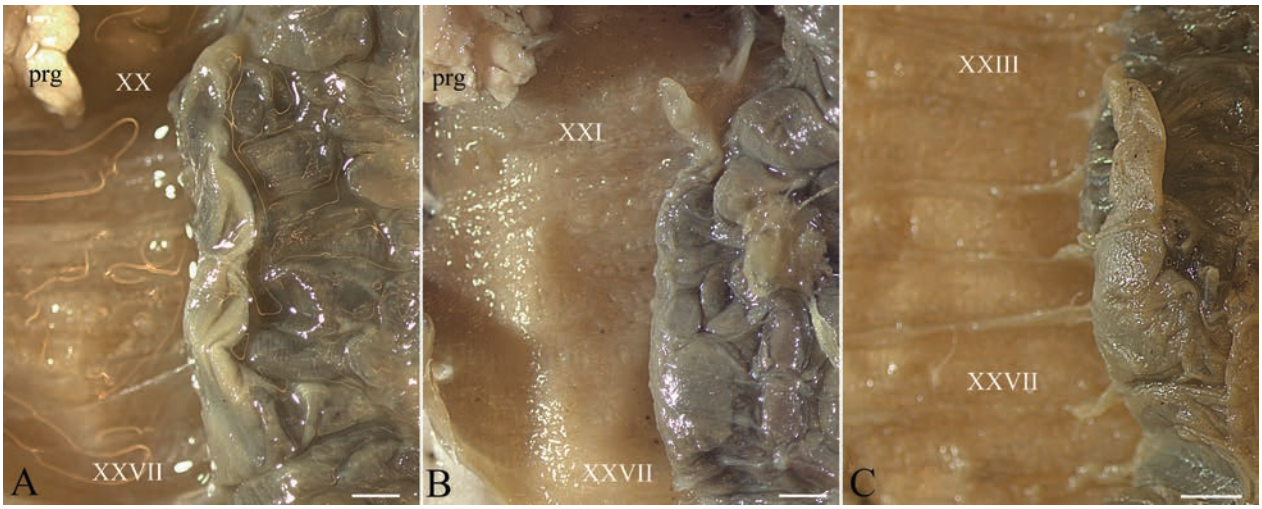

Figure 5. *Amynthas carnosus carnosus* intestinal caeca showing the segment length variations: **A.** (specimen ID 533R70_10); **B.** (specimen ID 362R1_05), and **C.** (specimen ID HNLNR2_05). Scale bars: 1 mm.

Amynthas carnosus naribunji Blakemore, 2013

Amynthas pingi: Blakemore 2013a: 60, figs 4, 5.

Material examined. Specimen IDs: 551R3 (01–10), 10 adults from Longwan Park, Huludao Pref., Liaoning Prov. One specimen from Beijing is a juvenile and was poorly preserved. Thus, its morphological examination was not performed. However, the molecular data is presented (DNA ID: BJCY_42, Fig. 1).

Diagnosis. Spermathecal pores four pairs in 5/6/7/8/9, located latero-ventrally (0.29–0.30 mm), each with pre-intersegmental hemispherical arc (spermathecal papillae) anterior to intersegments **(**Fig. 6). Pre-clitellar genital markings absent (complying with Kobayashi Type I in Blakemore 2013a); if present, one to three pairs; pre-setal in VIII and IX when one or two pairs and having a post-setal pair in VIII when three pairs (complying with Kobayashi's Types III, IV, and VIII); asymmetrical patterns also present (Fig. 7). Male pores superficial in XVIII having "disc-like" genital markings paired posterio-median to male pores (Fig. 8).

Description. Length 185–228 mm. Color of preserved specimens may have varying shades of brown but dorsum generally dark brown in pre-clitellar region to brown in post-clitellar region, fading to lighter brown towards posterior end with darker clitellum, while ventrum part is paler/fleshy color. Clitellum width 5.8–8.3 mm. Segments 115–137. Prostomium epilobous. First dorsal pore on 12/13. Clitellum annular at XIV–XVI without setae or dorsal pores. Setal arrangement perichaetine, setae between male pore 18–19. Female pore single and circular, midventral at XIV.

Spermathecal pores large, having four pairs in 5/6/7/8/9 and widely-spaced, latero-ventral (0.29–0.30 mm) in pre-intersegmental hemispherical arc (spermathecal papillae). Pre-clitellar genital markings circular in shape, latero-ventral (0.25–0.29 mm), randomly located in pairs (three pairs/two pairs/one pair, a total of 2–6 genital markings), or asymmetrically located on one side (1–2 genital markings), about 0.38–0.59 mm in diameter.

Male pores superficially paired in XVIII close to lateral margin (with ventral distance 0.26–0.29 mm) on large circular porophores. Post-clitellar genital markings distinguishably paired, post-setally in XVIII, mid-ventral to male pore, 0.42–0.69 mm in diameter.

Septa 4/5–7/8 and 10/11–14/15 thickened, 8/9/10 absent. Esophageal gizzard within VIII−X. Intestinal origin at XV (or XIV). Intestinal caeca simple, paired in XXVII, extending anteriorly to XXII. Last hearts in XIII.

Four pairs of spermathecae in VI−IX. Ampulla ovate, wrinkled; ducts short and stout. Diverticula reaching one-third to half of ampulla with a slender stalk and a wider seminal chamber; seminal chamber elongated or botuliform. Accessory glands sessile and round.

Seminal vesicles paired in XI and XII, large, smooth, yellowish, posterior pair larger but not as obvious compared to *A. c. carnosus*, each with a dorsal lobe. Ovaries present. Prostate glands paired in XVIII, large, lobulated, covering XVI−XX; ducts thick and large, U-shaped. Accessory glands round, sessile, or slightly lobed, corresponding to each genital marking around male pore area.

Distribution. Northern China (Liaoning, Beijing) and South Korea (Ulleung Island).

Remarks. There is not much of a thorough morphological description of *A. carnosus naribunji* in the original account of Blakemore (2013a) (see Suppl. material 1: table S3) aside from its single illustration of paired post-clitellar genital markings in the male pore area and a spermathecal pore with corresponding spermathecae shown in fig. 4 by Blakemore (2013c).

Notable features of *A. c. naribunji* in comparison with *A. c. carnosus* were its slightly larger size with lengths of 185–228 mm, typically wide-spaced pre-clitellar genital markings with a maximum number of six (three pairs) to at least three genital markings; pre-setal/post-setal in VIII and pre-setal in IX. In contrast, *A. c. carnosus* is

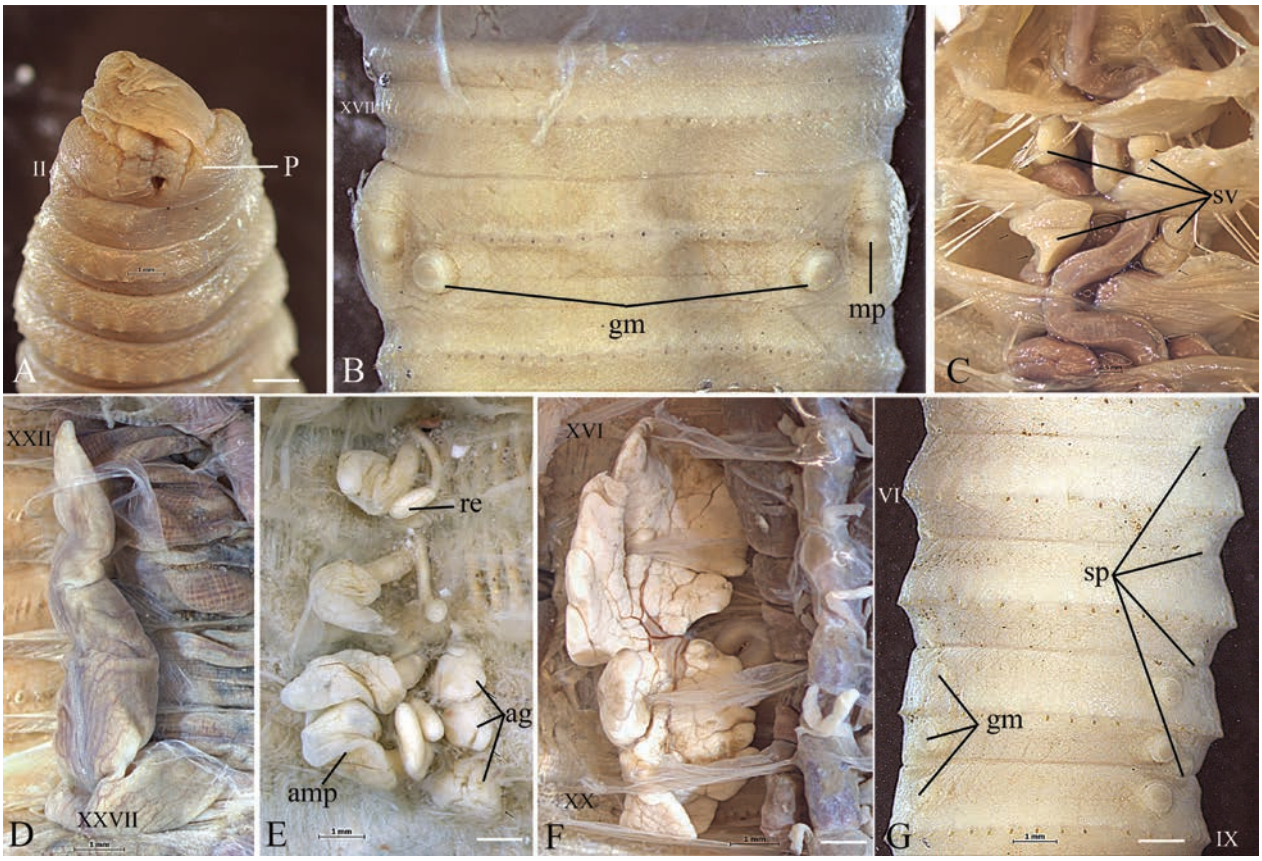

Figure 6. *A. carnosus naribunji* (specimen ID 551R3_01): Prostomium (**A**); Male pore with posterio-median paired genital marking (**B**); Seminal vesicles (**C**); Intestinal caeca (**D**); spermathecae (**E**); Prostate gland with U-shaped think duct (**F**); and Spermathecal pores with three pairs of pre-clitellar genital markings (**G**). Scale bars: 1 mm.

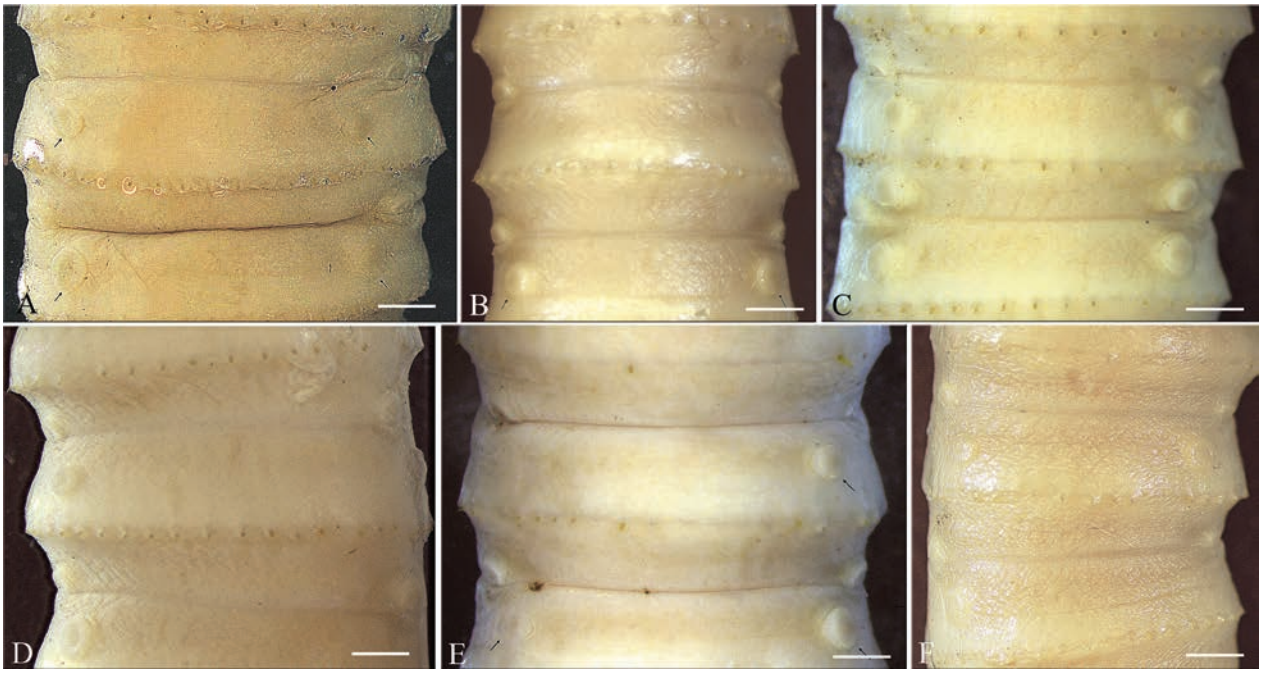

Figure 7. *A. carnosus naribunji* pre-clitellar genital marking variations; **A–C.** Complying with Kobayashi's (1936) Types III, IV, and VIII, respectively; **D–F.** Displays asymmetrical patterns. Scale bars: 1 mm.

typically medium to smaller size, with mostly only four genital markings (two pairs) or less, either wide or closely-spaced pre-clitellar (Table 3).

The distinctive character of having "a pair of genital markings posterio-median to male pores" in *A. c. naribunji* may distinguish it from those of *A. c. carnosus*

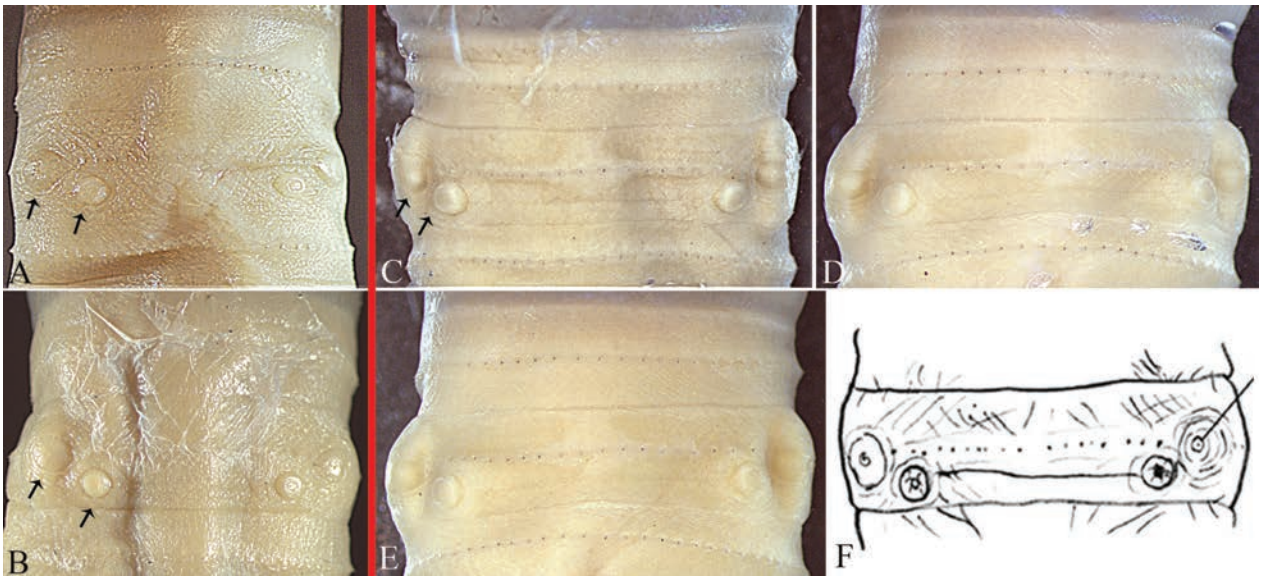

Figure 8. Image comparison of male pore porophores and paired posterio-median genital markings between *A. carnosus carnosus*. **A, B.** (specimen IDs 362R1_07 and HNLNR2_04) and *A. carnosus naribunji* from Liaoning; **C–E.** (specimen IDs 551R3_01, 551R3_09, and 551R3_06) and Ulleungdo, **F.** (specimen ID w54).

Table 3. Character comparison among *A. c. carnosus*, *A. c. naribunji*, and *A. c. roki*. The asterisk stands for the figure in Blakemore and Lee 2013a, p. 131, yet there is no definite description.

Characters	*A. carnosus carnosus*	*A. carnosus naribunji*	*A. carnosus roki*
Length	105–340 mm	185–228 mm	175–300 mm
No. of segments	96–179	121–137	136
No. of setae between mp	16–20	17–20	14
Male pore	round or elliptical porophores	on large circular porophores,	superficial on small mounds within concentric rings
Distance between Male pores (circumference apart)	0.25–0.29	0.26–0.29	0.30
Spermathecal pore	6/7/8/9 (three pairs, rarely); 5/6/7/8/9 (four pairs); 4/5/6/7/8/9 (five pairs, rarely); with pre-intersegmental spemathecal papillae	5/6/7/8/9 (four pairs) with pre-intersegmental spermathecal papillae	post-intersegmental pores 5/6/7/8/9 (four pairs) with post-intersegmental spermathecal papillae
Distance between spermathecal pores (circumference apart)	0.28–0.30	0.29–0.30	NA
Pre-clitellar gm (circumference apart)	closely paired or widely spaced pre-setal in VIII and IX, mid-ventral (mostly two pairs, total of 1–4 GMs)	widely spaced, randomly located in pairs (three pairs or two pairs or one pair, a total of 2–6 GMs)	absent
Post-clitellar gm (circumference apart)	up to three pairs of genital markings near male pores, pre-/post-setal in VXIII and pre-setal in XIX. Second pair, post-setal more medial than the first	distinguishably paired, post-setal in XVIII, mid-ventral to male pore	absent
Spermathecae (circumference apart)	typically four pairs in VI–IX, first pair often slightly smaller; or three pairs in VII–IX or five in IV–IX	four pairs in VI–IX	four pairs in VI–IX
Ampulla and Duct (circumference apart)	Wrinkled; Ovate to narrowly ovate	Wrinkled; Ovate to narrowly ovate	Narrowly ovate*
Prostate gland (circumference apart)	racemose at XVIII, covering XV (or XVI)–XX	racemose at XVIII, covering XVI–XX	racemose in XVIII
Intestinal caeca (circumference apart)	paired in XXVII, simple, extending to XX, or XI, or XIII	paired in XXVII, simple, extending to XXII	Simple from XXVII
Gizzard (circumference apart)	VIII–X	VIII–X	NA
Intestine	XV (or XIV)	XV	NA

(Blakemore, 2013a). However, it is now undeniable that this seemingly "distinctive character" was likewise observed in the *A. c. carnosus* specimens from Liaoning and Henan (Fig. 8). Here, we dismiss the former notion of Blakemore (2013a) "to consider for exclusion Kobayashi's Types I and II markings" as a distinctive character for the *A. c. carnosus* subspecies, *A. c. naribunji*. Although this might be the case, one cannot ignore the certain degree of dissimilarity between the two subspecies' morphological characters (e.g., the shape of male pore porophore and the distinct shape of the genital markings in *A. c. naribunji*, described as "disc-like" by Blakemore). As such, applications of state-of-the-art methodologies such as high-throughput sequencing or geometric morphometric (Marchán et al. 2020) may be adopted that go beyond traditional methods of taxonomic diagnosis

(which in this case is rather insufficient to "quantify" the degree of variations). Nevertheless, the incorporation of genetic data such as DNA barcoding and calculating K2P intraspecific distances (as conducted in this study) may aid in suggesting subspecies delineation.

***Amynthas carnosus roki* Blakemore & Lee, 2013**

Material examined. In China, only molecular data is available in the Genbank (Accession No. KT252956).

Description. See Blakemore and Lee 2013: 129–132.

Distribution. South Korea, China.

Morphological comparison among the subspecies of *A. carnosus*

A list of character comparisons between *A. c. carnosus*, *A. c. naribunji*, and *A. c. roki* is summarized in Table 3. Most of the distinctive characters for *A. c. carnosus* and *A. c. naribunji* are discussed above. As for *A. c. roki*, "distinctive characters are the tendency to have large size (175–300 mm) post-intersegmental spermathecal pores with U-shaped spermathecal papillae. Obvious distinctive character accounts for the lack of genital markings, thereby complying with Kobayashi's Types II and I" (Blakemore and Lee 2013). Blakemore and Lee (2013) added further: "On these characters, the present subspecies appears to differ from the nominal taxon's neotype and from other synonyms in Blakemore." Aside from the external morphological differences, slight internal character differences were also observed (Table 3).

According to Blakemore (2012), "the genital marking variation in *A. carnosus* allowed for by Kobayashi in his detailed and most thorough account is excessive, rather representing a congery of morphs, if not separate species'', this can be said out from the preliminary DNA results forming new taxa as *A. c. naribunji* and *A. c. roki* (Blakemore 2013a; Blakemore and Lee 2013). Genital marking variations as observed in our specimens here did appear to have variations exceeding that of Kobayashi's permissible" genital marking variations (with asymmetrical GMs also observed).

Conclusion

Our results agree with Blakemore's subspecies assignment of *A. c. naribunji* and *A. c. roki* (additional molecular data only). Furthermore, the attempt to justify the presumed "distinctive character" of having a pair of genital markings posterio-median to male pores in *A. c. naribunji*, which is distinct from the *A. c. carnosus* as noted by Blakemore (2013a, c), has now been invalidated, given that both *A. c. naribunji* and *A. c. carnosus* specimens in China possess this same character. Here, a pairwise distance for the *A. carnosus* subspecies was shown to be 10% and below. With new occurrences of *A. carnosus* in China, patterns of morphological as well as genetic variations in different geographical occurrences of this species can be further elucidated. Still, a more thorough investigation should be carried out by conducting a broader sampling collection in the country, which may contribute to new distribution records. Moreover, with the updated and detailed morphological descriptions of *A. c. naribunji* provided here, elaborate data can now be used to clarify morphological distinctions. Thus, similar specimens from any region may now be compared genetically to an increasingly refined formulation of *A. carnosus*, its subspecies, and even synonymous species.

Acknowledgments

We thank the reviewer, Parin Jirapatrasilp, for his valuable suggestions. This study was supported by the National Natural Sciences Foundation of China (42071059); the Northeast Asia Biodiversity Research Center (2572022DS09); by the China National Tobacco Corporation of Science and Technology Major Projects (110202201018 [LS-02]); by the "One Belt, One Road" international scholarship from the Ministry of Science and Technology of China (DL2023130001L); and by the President's International Fellowship Initiative from the Chinese Academy of Sciences (2024VCA0009); the National Science and Technology Fundamental Resources Investigation Program of China (2018FY100301).

References

Admassu B, Juen A, Traugott M (2006) Earthworm primers for DNA-based gut content analysis and their cross-reactivity in a multi-species system. Soil Biology & Biochemistry 38(6): 1308–1315. https://doi.org/10.1016/j.soilbio.2005.08.019

Aspe NM (2016) The geographic distribution of the genera in the *Pheretima* complex (Megascolecidae) in eastern Asia and the Pacific region. Kaiyo Monthly 48: 39–45.

Aspe NM, Manasan RE, Manlavi AB, Ma. Patiluna LE, Sebido MA, Obusan MCM, Simbahan JF, James SW (2021) The earthworm fauna of Palawan, Philippines with description of nineteen new pheretimoid species (Clitellata, Megascolecidae). Journal of Natural History 55(11–12): 11–12, 733–779. https://doi.org/10.1080/00222933.2021.1923849

Bely AE, Wray GA (2004) Molecular phylogeny of naidid worms (Annelida, Clitellata) based on cytochrome oxidase I. Molecular Phylogenetics and Evolution 30(1): 50–63. https://doi.org/10.1016/S1055-7903(03)00180-5

Blakemore R (2009) Cosmopolitan Earthworms–A Global and Historical Perspective. 257–283. https://doi.org/10.1002/9780470455203.ch14

Blakemore R (2012) *Amynthas carnosus* (Goto & Hatai, 1899) redescribed on its neotype (Oligochaeta, Megadrilacea, Megascolecidae). Journal of Species Research 1(1): 35–46. https://doi.org/10.12651/JSR.2012.1.1.035

Blakemore R (2013a) *Megascolex* (*Perichaeta*) *diffringens* Baird, 1869 and *Pheretima pingi* Stephenson, 1925 types compared to the *Amynthas corticis* (Kinberg, 1867) and *A. carnosus* (Goto & Hatai, 1899) species-groups (Oligochaeta, Megadrilacea, Megascolecidae).

Journal of Species Research 2(2): 99–126. https://doi.org/10.12651/JSR.2013.2.2.099

Blakemore R (2013b) Jeju-do earthworms (Oligochaeta, Megadrilacea)-Quelpart Island revisited. Journal of Species Research 2(1): 15–54. https://doi.org/10.12651/JSR.2013.2.1.015

Blakemore R (2013c) Ulleung-do earthworms - Dagelet Island revisited. Journal of Species Research 2(1): 55–68. https://doi.org/10.12651/JSR.2013.2.1.055

Blakemore R, Lee W (2013) Survey of Busan Oligochaeta earthworms supported by DNA barcodes. Journal of Species Research 2(2): 127–144. https://doi.org/10.12651/JSR.2013.2.2.127

Carrera-Martínez R, Snyder B (2016) First report of *Amynthas carnosus* (Goto & Hatai, 1899) (Oligochaeta, Megascolecidae) in the Western Hemisphere. Zootaxa 4111(3): 297–300. https://doi.org/10.11646/zootaxa.4111.3.7

Chang C-H, Lin S-M, Chen J-H (2008) Molecular systematics and phylogeography of the gigantic earthworms of the Metaphire formosae species group (Clitellata, Megascolecidae). Molecular Phylogenetics and Evolution 49(3): 958–968. https://doi.org/10.1016/j.ympev.2008.08.025

Chang C-H, Snyder B, Szlávecz K (2016) Asian pheretimoid earthworms in North America north of Mexico: An illustrated key to the genera *Amynthas*, *Metaphire*, *Pithemera*, and *Polypheretima* (Clitellata, Megascolecidae). Zootaxa 4179(3): 495–529. https://doi.org/10.11646/zootaxa.4179.3.7

Chang C-H, Bartz M, Brown G, Callaham M, Cameron E, Davalos A, Dobson A, Gorres J, Herrick B, Ikeda H, James S, Johnston M, McCay T, McHugh D, Minamiya Y, Nouri Aiin M, Novo M, Ortiz-Pachar J, Pinder R, Szlávecz K (2021) The second wave of earthworm invasions in North America: Biology, environmental impacts, management and control of invasive jumping worms. Biological Invasions 23(11): 1–32. https://doi.org/10.1007/s10530-021-02598-1

Chen Y (1933) A preliminary survey of the earthworms of the Lower Yangtze Valley. Contributions from the Biological Laboratory of the Science Society of China 9: 177–296.

Chen Y (1936) On the terrestrial Oligochaeta from Szechuan II with the notes on Gates' types. Contributions of Biological Laboratory of Science Society of China. Zoology 11: 269–306.

Dong Y, Law MMS, Jiang J, Qiu J (2019) Three new species and one subspecies of the *Amynthas corticis*-group from Guangxi Zhuang Autonomous Region, China (Oligochaeta, Megascolecidae). ZooKeys 884: 23–42. https://doi.org/10.3897/zookeys.884.30988

Easton EG (1981) Japanese earthworms: A synopsis of the Megadrile species (Oligochaeta). Bulletin of the British Museum (Natural History). Zoology : Analysis of Complex Systems, ZACS 40: 33–65.

Folmer O, Black M, Hoeh W, Lutz R, Vrijenhoek R (1994) DNA primers for amplification of mitochondrial cytochrome c oxidase subunit I from diverse metazoan invertebrates. Molecular Marine Biology and Biotechnology 3: 294–299.

Gates GE (1939) On some species of Chinese earthworms with special reference to specimens collected in Szechuan by Dr. D.C. Graham. Proceedings of the United States National Museum 85: 405–507. https://doi.org/10.5479/si.00963801.3040.405

Goto S, Hatai S (1899) New or imperfectly known species of earthworms. No. 2. Annotationes Zoologicae Japonenses 3: 13–24.

Hall TA (1999) BioEdit: A user-friendly biological sequence alignment editor and analysis program for Windows 95/98/NT. Nucleic Acids Symposium Series 41: 95–98. https://doi.org/10.14601/phytopathol_mediterr-14998u1.29

Huang J, Xu Q, Sun Z, Tang G, Su Z (2007) Identifying earthworms through DNA barcodes. Pedobiologia 51(4): 301–309. https://doi.org/10.1016/j.pedobi.2007.05.003

Jiang J, Qiu J (2018) Origin and evolution of earthworms belonging to the family Megascolecidae in China. Shengwu Duoyangxing 26(10): 1074–1082. https://doi.org/10.17520/biods.2018105

Kimura M (1980) A simple method for estimating evolutionary rates of base substitutions through comparative studies of nucleotide sequences. Journal of Molecular Evolution 16(2): 111–120. https://doi.org/10.1007/BF01731581

Kobayashi S (1936) Distribution and some external characteristics of *Pheretima* (*Ph.*) *carnosa* (Goto et Hatai) from Korea. Science Report of the Tohoku Imperial University 11: 115–138.

Kobayashi S (1938) Earthworms of Korea I. Science Report of the Tohoku Imperial University 13: 89–170.

Marchán DF, Novo M, Sánchez N, Domínguez J, Díaz Cosín DJ, Fernández R (2020) Local adaptation fuels cryptic speciation in terrestrial annelids. Molecular Phylogenetics and Evolution 146: 106767. https://doi.org/10.1016/j.ympev.2020.106767

McCay TS, Brown G, Callaham Jr MA, Chang C-H, Dávalos A, Dobson A, Görres JH, Herrick BM, James SW, Johnston MR, McHugh D, Minteer T, Moore J-D, Nouri-Aiin M, Novo M, Ortiz-Pachar J, Pinder RA, Richardson JB, Snyder BA, Szlavecz K (2020) Tools for monitoring and study of peregrine pheretimoid earthworms (Megascolecidae). Pedobiologia 83: 150669. https://doi.org/10.1016/j.pedobi.2020.150669

Nguyen TT, Nguyen NQ, Lam DH, Nguyen AD (2020) Six new species of the genus *Metaphire* Sims & Easton, 1972 (Annelida, Oligochaeta, Megascolecidae) from southeastern Vietnam. The Raffles Bulletin of Zoology 68: 220–236. https://doi.org/10.26107/RBZ-2020-0019

Novo M, Almodóvar A, Diaz Cosin DJ (2009) High genetic divergence of hormogastrid earthworms (Annelida, Oligochaeta) in the central Iberian Peninsula: Evolutionary and demographic implications. Zoologica Scripta 38(5): 537–552. https://doi.org/10.1111/j.1463-6409.2009.00389.x

Ohfuchi S (1937) On the species possessing four pairs of spermathecae in the genus *Pheretima*, together with the variability of some external and internal characteristics. Saito Ho-On Kai Museum Research Bulletin: 31–136.

Sims RW, Easton EG (1972) A numerical revision of the earthworm genus *Pheretima* auct. (Megascolecidae, Oligochaeta) with the recognition of new genera and an appendix on the earthworms collected by the Royal Society North Borneo Expedition. Biological Journal of the Linnean Society, Linnean Society of London 4(3): 169–268. https://doi.org/10.1111/j.1095-8312.1972.tb00694.x

Stamatakis A (2014) RAxML version 8: A tool for phylogenetic analysis and post-analysis of large phylogenies. Bioinformatics 30(9): 1312–1313. https://doi.org/10.1093/bioinformatics/btu033

Stephenson J (1925) Oligochaeta from various regions, including those collected by the Mount Everest Expedition 1924. Proceedings of the Zoological Society of London 95: 879–907. https://doi.org/10.1111/j.1469-7998.1925.tb07109.x

Stephenson J (1931) Oligochaeta from Burma, Kenya and other parts of the world. Proceedings of the Zoological Society of London 101: 33–92. https://doi.org/10.1111/j.1469-7998.1931.tb06185.x

Sun J (2013) Taxonomy and Molecular Phylogeny of *Amynthas* Earthworms from China. Shanghai: Shanghai Jiao Tong University.

Tamura K, Peterson D, Peterson N, Stecher G, Nei M, Sudhir K (2011) MEGA5: Molecular evolutionary genetics analysis using maximum likelihood, evolutionary distance, and maximum parsimony methods. Molecular Biology and Evolution 28(10): 2731–2739. https://doi.org/10.1093/molbev/msr121

Thompson JD, Higgins DG, Gibson TJ (1994) CLUSTAL W: Improving the sensitivity of progressive multiple sequence alignment through sequence weighting, position-specific gap penalties and weight matrix choice. Nucleic Acids Research 22(22): 4673–4680. https://doi.org/10.1093/nar/22.22.4673

Xiao N (2019) Terrestrial Earthworms (Oligochaeta, Opisthopora) of China. Elsevier Inc, China, 395 pp. https://doi.org/10.1016/B978-0-12-815587-5.09986-8

Zhang L, Sechi P, Yuan M-L, Jiang J, Dong Y, Qiu J (2016) Fifteen new earthworm mitogenomes shed new light on phylogeny within the *Pheretima* complex. Scientific Reports 6(1): 20096. https://doi.org/10.1038/srep20096

Supplementary material 1

Taxa list with the accession numbers and comparison of morphological characters

Authors: Anne Charis N. Han, Yufeng Zhang, Pu Miao, Shaolong Wu, Nengwen Xiao, Mingyan Qin, Donghui Wu, Huifeng Zhao, Nonillon M. Aspe

Data type: docx

Link: https://doi.org/10.3897/zse.100.119292.suppl1

Zoosyst. Evol. 100 (3) 2024, 1075–1084 | DOI 10.3897/zse.100.130661

PENSOFT

MUSEUM FÜR NATURKUNDE BERLIN

A new species of *Tropidauchenia* Lindholm, 1924 (Gastropoda, Stylommatophora, Clausiliidae, Garnieriinae) from Guangdong, China

Zhong-Guang Chen[1], Zhe-Yu Chen[2], Ran-Xi Lin[3], Yu-Ting Dai[1], Xiao-Ping Wu[1], Jiao Jiang[4], Shan Ouyang[1]

1 *School of Life Sciences, Nanchang University, Nanchang, Jiangxi 330031, China*

2 *Parasitology research group, Department of Veterinary Biosciences, Faculty of Science, The University of Melbourne, Parkville VIC 3010, Australia*

3 *State Key Laboratory for Conservation and Utilization of Subtropical Agro-Bioresources, Guangdong Laboratory for Lingnan Modern Agriculture, College of Agriculture, College of Life Sciences, South China Agricultural University, Guangzhou 510642, China*

4 *Zhejiang Museum of Natural History, Hangzhou, Zhejiang 310012, China*

https://zoobank.org/BBA9A2D1-3E5D-4F42-9BA3-456957BA0706

Corresponding authors: Jiao Jiang (149152414@qq.com); Shan Ouyang (ouys1963@qq.com)

Academic editor: Frank Köhler ♦ **Received** 27 June 2024 ♦ **Accepted** 17 July 2024 ♦ **Published** 1 August 2024

Abstract

A molecular phylogenetic study was conducted on genus *Tropidauchenia*, based on *COI* and *16S* sequences. A total of six out of 18 species in the genus, as well as three species of *Grandinenia* and eight species of subfamily Synprosphyminae and Phaedusinae were sequenced. The phylogenetic results supported the monophyly of three Clausiliid subfamilies distributed in East Asia and demonstrated that *Tropidauchenia* was divided into two clades that corresponded to its two main distribution areas. A new species, *Tropidauchenia jiangjilini* Z.-G. Chen, Z.-Y. Chen & R.-X. Lin, **sp. nov.**, from Guangdong, southern China, has been identified and described based on morphological comparison and molecular phylogeny. The discovery expanded the distribution range of *Tropidauchenia* and revealed the potential species diversity of land snails in the karst region of Guangdong.

Key Words

Door snails, karst landscape, phylogeny, taxonomy

Introduction

Clausiliidae Gray, 1855 is a group of small to large-sized land snails with nearly global distribution (Nordsieck 2007a). A total of three subfamilies of it have been recorded in East Asia: Phaedusinae Wagner, 1922, Garnieriinae Boettger, 1926 and Synprosphyminae Nordsieck, 2007 (Nordsieck 2007a, 2007b, 2012a, 2012b, 2012c; Uit de Weerd et al. 2023). Among the three subfamily, Garnieriinae has a relatively low species diversity and the narrowest distribution. It is relatively narrowly distributed from Myanmar to southern China and consists of seven genera, three of which are recorded in China: *Garnieria* Bourguignat, 1877, *Grandinenia* Minato & Chen, 1984 and *Tropidauchenia* Lindholm, 1924 (Nordsieck 2012a, 2012b, 2012c). The genus *Tropidauchenia* is a group of medium to large-sized door snails distributed from southern China to central Vietnam (Nordsieck 2007a, 2007b, 2012a, 2012b, 2012c; Grego and Szekeres 2017; Qiu 2021) and defined by a furrowed neck, projected and unattached, so-called apostrophic peristome, a lunella-type lunellar region, and the inferior lamella near to or fused with superior lamella (Nordsieck 2007a, b, 2012a). Currently, it consists of 18 species, 12 of which are recorded in China: *T. orientalis* (Mabille, 1887), *T. dorri* (Bavay & Dautzenberg, 1899), *T. hitomiae* Nordsieck, 2007, *T. lucida* Nordsieck, 2007, *T. nakaharai* Nordsieck, 2007, *T. napoensis* Nordsieck, 2007, *T. ootanii* Nordsieck, 2007, *T. mengyuanensis* Chen, Tian & Fan, 2016, *T. sulcicollis* Grego & Szekeres, 2017, *T. yanghaoi* Grego

& Szekeres, 2017, *T. danjuan* Qiu, 2021 and *T. parasulcicollis* Qiu, 2021 (Nordsieck 2007b, 2012c; Chen, Tian and Fan 2016; Grego and Szekeres 2017; Qiu 2021; Lin and Lin 2022). These species are mainly distributed in the west Guangxi, with only three species being recorded in Yunnan and Guangdong.

Guangdong is situated in southern China and adjacent to Guangxi. In contrast to Guangxi, which is renowned for its karst landscape and high diversity of land snails, Guangdong is relatively understudied and lacks an understanding of its land snail fauna. Only one recently described species of *Tropidauchenia*, namely *T. yanghaoi*, has been recorded in Guangdong (Grego and Szekeres 2017). The distribution of this species is significantly far from that of all its congeners, suggesting the potential existence of additional yet-to-be-described species. Based on the land snails' survey conducted in April to May 2024, it has been discovered that the *Tropidauchenia* specimens with a ribbed shell from Luoding of Guangdong represent an undescribed species. In this study, we conducted the molecular phylogenetic analysis of three subfamilies of Clausiliidae distributed in China based on partial *COI* and *16S* sequences, and described a new species of *Tropidauchenia*. The discovery of the new taxon has expanded the distribution range of *Tropidauchenia* and confirmed the existence of yet-to-be-described species in the distribution gap.

Materials and methods

Samples were collected from Sichuan, Chongqing, Yunnan, Guangxi and Guangdong, China in 2023–2024. Living specimens were initially frozen at -20 °C for 12 hours and subsequently thawed at room temperature for 12 hours to extract the soft parts. The soft parts were then fixed in 70% ethanol. Empty shells were cleaned, dried, and preserved at 4 °C. All specimens were deposited in the School of Life Sciences, Nanchang University (Nanchang, Jiangxi, China) and the mollusc collection of Museum of Hebei University (Hebei, China). Photographs were taken by Sony® Alpha a6500 Digital Camer and edited in Adobe Photoshop CC 2015 (Adobe, San Jose, US). Maps were made in ArcGIS Pro (Esri, Redlands, US).

Genomic DNA was extracted from foot tissues preserved in 70% ethanol using a TIANamp Marine Animals DNA Kit (Tiangen Biotech, China). The quality and concentration of the DNA were checked on 1% agarose gel electrophoresis and NanoDrop 2000 (Thermo Scientific, USA). Partial cytochrome c oxidase subunit 1 (*COI*) and partial 16S ribosomal RNA (*16S*) gene segments were amplified and sequenced for molecular phylogenetic analyses. Polymerase chain reaction (PCR) systems, conditions and primer pairs are listed in Table 1. Sequences were aligned using MEGA v. 6.0 (Tamura et al. 2013) and checked manually. The accession numbers of newly obtained sequences and other species are given in Table 2.

Phylogenies were reconstructed by the dataset combined two genes using maximum likelihood (ML) and Bayesian inference (BI). Seventeen species of three subfamilies distributed in east Asia were included. Three species of subfamily Alopiinae Wagner, 1913 were used as outgroups for rooting the tree. ML analyses were performed in IQ-TREE v. 1.6.12 (Minh et al. 2013) using Ultrafast fast bootstrap approach (Minh et al. 2013) with 10000 reiterations. The most appropriate model of sequence evolution (GTR+I+G) was selected under PartitionFinder2 v. 1.1 (Lanfear et al. 2017). Bayesian inference (BI) was conducted in MrBayes v. 3.2.6 (Ronquist et al. 2012). The most appropriate model of sequence evolution (GTR+I+G) was selected under ModelFinder (Kalyaanamoorthy et al. 2017). Four simultaneous runs with four independent Markov Chain Monte Carlo (MCMC) were implemented for 10 million generations, and trees were sampled every 1000 generations with a burn-in of 25%. The convergence was checked with the average standard deviation of split frequencies <0.01 and the potential scale reduction factor (PSRF) ~1. Trees were visualised in FigTree v.1.4.3.

Abbreviations. **NCU_XPWU** Laboratory of Xiao-Ping Wu, Nanchang University (Nanchang, Jiangxi, China); **HBUMM** mollusc collection of Museum of Hebei University, Hebei, China; **cp** clausilium plate; **il** inferior lamella; **lu** lunella; **pp** principal plica; **sc** subcolumellar lamella; **sl** superior lamella; **sp** spiral lamella; **At** atrium; **BC** bursa copulatrix; **BCD** bursa copulatrix duct; **D** diverticulum; **Ep** epiphallus; **P** penis; **PR** penial retractor muscle; **V** vagina; **VD** vas deferens.

Results

Phylogenetic analyses

A dataset consisting of 44 *COI* and 47 *16S* sequences from 17 species, along with three outgroup taxa, was employed for phylogenetic analyses (Table 2). The *COI* sequence of *T. yanghaoi* was unable to be amplified by the several universal primers employed. The aligned lengths of *COI* and *16S* genes were 669 and 492 nucleotides. Within these sequences, 330 and 266 were revealed as variable sites, while 325 and 255 were designated as parsimony informative sites. Phylogenetic analyses generated ML and BI trees with congruent topologies (Fig. 1). The results supported the monophyly of three subfamilies of Clausiliidae Gray, 1855 distributed in China. It demonstrated a phylogenetic relationship of Garnieriinae + (Synprosphyminae + Phaedusinae). The genus *Excussispira* Lindholm, 1925, which has an undetermined systematic position, has been confirmed as belonging to Synprosphyminae. The monophyly of Garnieriinae is supported but with relatively low nodal support (bootstrap support = 66, posterior probability = 0.70). Genus *Tropidauchenia* form a monophyly and further clustered into two clades, consisted of the species from Guangdong and Guangxi respectively. *Tropidauchenia jiangjilini* sp. nov. was sistered with *T. yanghaoi* (bootstrap support =99, posterior probability = 1) and the genetic distances of *16S* sequences between them is 8.6%.

Table 1. Primer pairs and PCR conditions used in the analyses of the *COI* and *16S* rRNA genes.

Genes	Primer pairs	Reaction systems	Cycling conditions	Reference
COI	LCO1490: GGTCAACAAATCATAAAGATATTGG HCO2198: TAAACTTCAGGGTGACCAAAAAATCA	12.5 μl 2× Taq Plus Master Mix II (Vazyme, Nanjing, China), 1 μl template DNA, 1 μl of each pair of primers, 9.5 μl ddH2O	94 °C: 2 min; 94 °C: 10s, 50 °C: 60s, 72 °C: 1 min, 35 cycles; 72 °C: 10 min	Folmer et al. 1994
16S	16SA: CGGCCGCCTGTTTATCAAAAACAT 16SB: GGAGCTCCGGTTTGAACTCAGATC	12.5 μl 2× Taq Plus Master Mix II (Vazyme, Nanjing, China), 1 μl template DNA, 1 μl of each pair of primers, 9.5 μl ddH2O	94 °C: 2 min; 94 °C: 10s, 50 °C: 60s, 72 °C: 1 min, 35 cycles; 72 °C: 10 min	Páll-Gergely et al. 2019

Table 2. GenBank accession numbers of the sequences for this study.

Species	Locality	CO1	16S	References
Tropidauchenia jiangjilini sp. nov.	Pingtang, Luoding, Guangdong, China, 22°43'26"N, 111°44'56"E	PP945861	PP956568	This study
		PP945862	PP956569	This study
		PP945863	PP956570	This study
		PP945864	PP956571	This study
		PP945865	PP956572	This study
		PP945866	PP956573	This study
T. danjuan	Maan, Jiangzhou, Chongzuo, Guangxi, China (type locality), 22°27'16"N, 107°19'56"E	PP945851	PP956558	This study
		PP945852	PP956559	This study
	Baoan, Jiangzhou, Chongzuo, Guangxi, China, 22°17'50"N, 107°21'24"E	PP945853	PP956560	This study
		PP945854	PP956561	This study
T. parasulcicollis	Daxin, Chongzuo, China (type locality), 22°42'41"N, 107°11'55"E	PP945855	PP956562	This study
		PP945856	PP956563	This study
		PP945857	PP956564	This study
		PP945858	PP956565	This study
T. cf. *lucida*	Chongzuo, Guangxi, China, 22°8'15"N, 106°46'41"E	PP945859	PP956566	This study
		PP945859	PP956567	This study
T. yanghaoi	Huaiji, Zhaoqing, Guangxi, China (type locality), 23°55'18"N, 112°9'59"E		PP472620	Unpublished
			PP472621	Unpublished
			PP472622	Unpublished
T. orientalis	Chongzuo, Guangxi, China, 22°16'29"N, 107°4'14"E	PP473359	PP472591	Unpublished
		PP473360	PP472592	Unpublished
Grandinenia mirifica	Lianggu, Qintang, Guigang, Guangxi, China (type locality), 23°19'1"N, 109°14'34"E	PP473344	PP472576	Unpublished
		PP473345	PP472577	Unpublished
		PP473346	PP472578	Unpublished
G. gastrum	Lianggu, Qintang, Guigang, Guangxi, China (type locality), 23°18'51"N, 109°15'49"E	PP473348	PP472580	Unpublished
		PP473349	PP472581	Unpublished
		PP473350	PP472582	Unpublished
G. fuchsi	Guilin, Guangxi, China, 25°18'35"N, 110°16'19"E	PP473351	PP472583	Unpublished
		PP473352	PP472584	Unpublished
		PP473353	PP472585	Unpublished
Excussispira fargesiana	Sichuan, China (type locality), 32°5'2"N, 108°3'12"E	PP945871	PP956578	This study
		PP945872	PP956579	This study
		PP945873	PP956580	This study
E. lunatica	Chengkou, Chongqing, China (type locality), 31°57'34"N, 108°38'31"E	PP945867	PP956574	This study
		PP945868	PP956575	This study
		PP945869	PP956576	This study
		PP945870	PP956577	
Synprosphyma suilla	Honghe, Yunnan, China, 29°56'39"N, 103°02'35"E	PP945876	PP956583	This study
S. basilissa	Chengdu, Sichuan, China, 30°55'26"N, 103°29'23"E	PP945874	PP956581	This study
		PP945875	PP956582	This study
Miraphaedusa takagii	Guilin, Guangxi, China (type locality), 25°18'35"N, 110°16'19"E	PP945877	PP956584	This study
		PP945878	PP956585	This study
Serriphaedusa zhengpingi	Yaan, Sichuan, China (type locality), 29°37'28"N, 102°53'18"E	PP945879	PP956586	This study
		PP945880	PP956587	This study
Paraformosana indurata	Wushan, Chongqing, China, 31°19'2"N, 109°47'53"E	PP945881	PP956588	This study
		PP945882	PP956589	This study
Cirrophaedusa plicilabris	Beibei, Chongqing, China (type locality), 30°1'47"N, 106°37'24"E	PP945883	PP956590	This study
Agathylla goldi	Europe	KC756080	KF601271	Fehér et al. (2013b), Parmakelis et al. (2013)
Alopia mariae	Europe	JQ911821		Fehér et al. (2013a)
Isabellaria praestans	Europe	AY425575		Uit de Weerd et al. (2004)

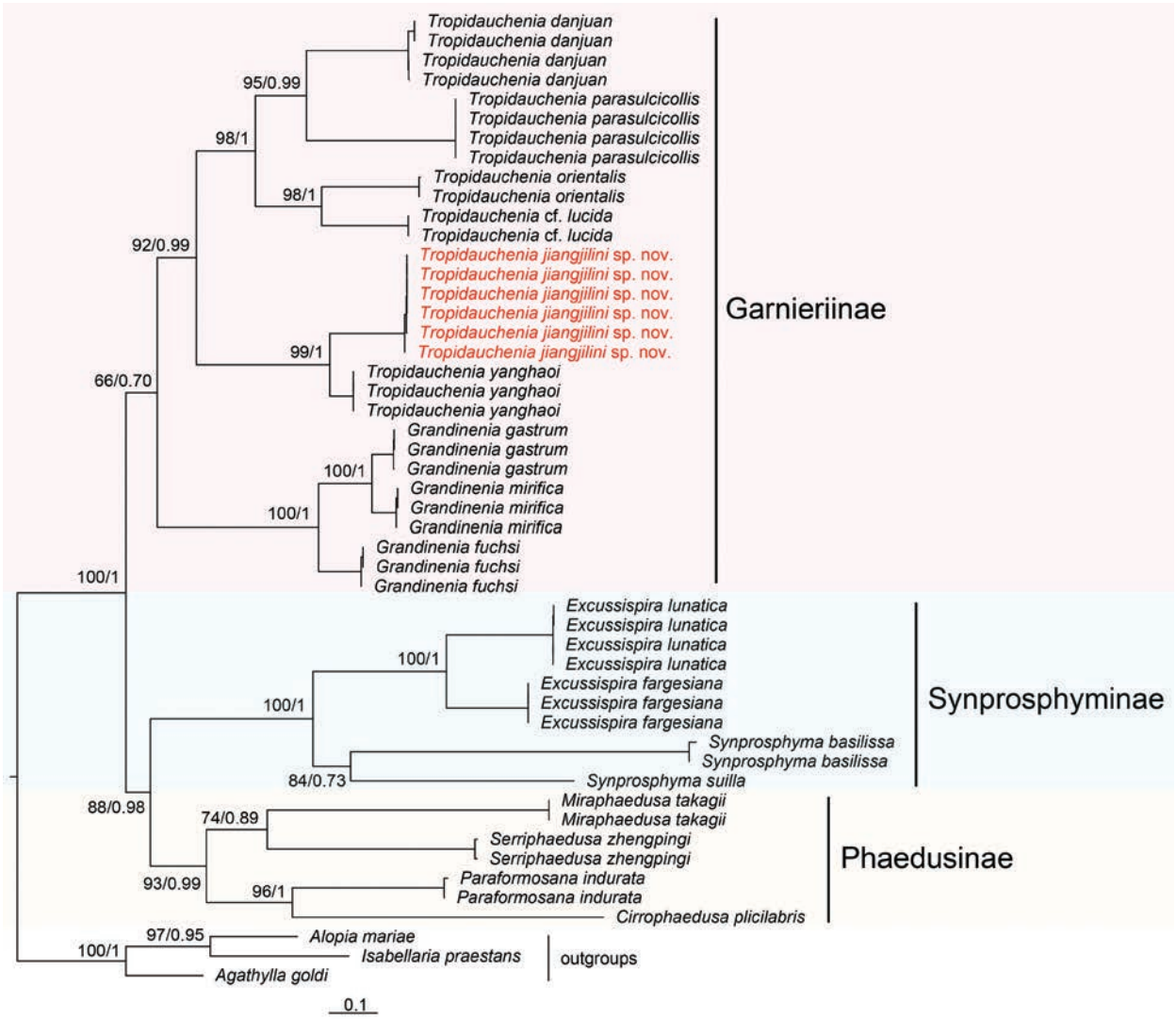

Figure 1. Maximum likelihood tree and Bayesian inference tree inferred from *COI* and *16S* gene sequences. Bootstrap supports/posterior probabilities are shown on the left/right of nodes.

Taxonomy

Family Clausiliidae Gray, 1855
Subfamily Garnieriinae Boettger, 1926

Genus *Tropidauchenia* Lindholm, 1924

Type species. *Clausilia bavayi* Lindholm, 1924, by original designation.

***Tropidauchenia jiangjilini* Z.-G. Chen, Z.-Y. Chen & R.-X. Lin, sp. nov.**

https://zoobank.org/0421ED62-C136-4882-AF91-544D7B15821C

Figs 2A, 3, 4A, B, 5B–D

Type material. *Holotype*. 24_NCU_XPWU_YG01, Julongdong Scenic Spot [聚龙洞风景区], Pingtang Town [苹塘镇], Luoding City [罗定市], Guangdong Province [广东省], China, 22°43'26"N, 111°44'56"E, leg. Ji-Lin Jiang, May 2024.

***Paratypes*.** 11 specimens. 24_NCU_XPWU_YG02–09, HBUMN 10073–74, other information same as holotype; 24_NCU_XPWU_YG10, Longji village [龙吉村], Luoding City [罗定市], Guangdong Province, China, 22°44'40"N, 111°48'01"E, leg. Ji-Lin Jiang & Ran-Xi Lin, May 2024.

Diagnosis. Shell entire (vs. decollated or fragile to almost decollated in *T. bavayi*, *T. dorri*, *T. donggiaensis* Nordsieck, 2002, *T. giardi* and *T. proc*tostoma (Mabille, 1889)), slender-fusiform (vs. broader in *T. danjuan*, *T. hitomiae*, *T. lucida*, *T. mengyuanensis*, *T. messageri* (Bavay & Dautzenberg, 1899), *T. nakaharai*, *T. napoensis*, *T. orientalis*, *T. palatalis*, *T. parasulcicollis* and *T. sulcicollis*), fragile; teleoconch with very thin and dense ribs (vs. smooth in *T. yanghaoi*; ribs stronger but sparser in *T. danjuan*, *T. messageri*, *T. orientalis*, *T. ootanii*, *T. parasulcicollis* and *T. sulcicollis*; ribs weaker and sparser in *T. hitomiae*, *T. lucida*, *T. mengyuanensis*, *T. nakaharai*, *T. napoensis* and *T. palatalis*); aperture colored, lower part reddish-brown; penial pilasters transversal, relatively sparse, irregular zigzag.

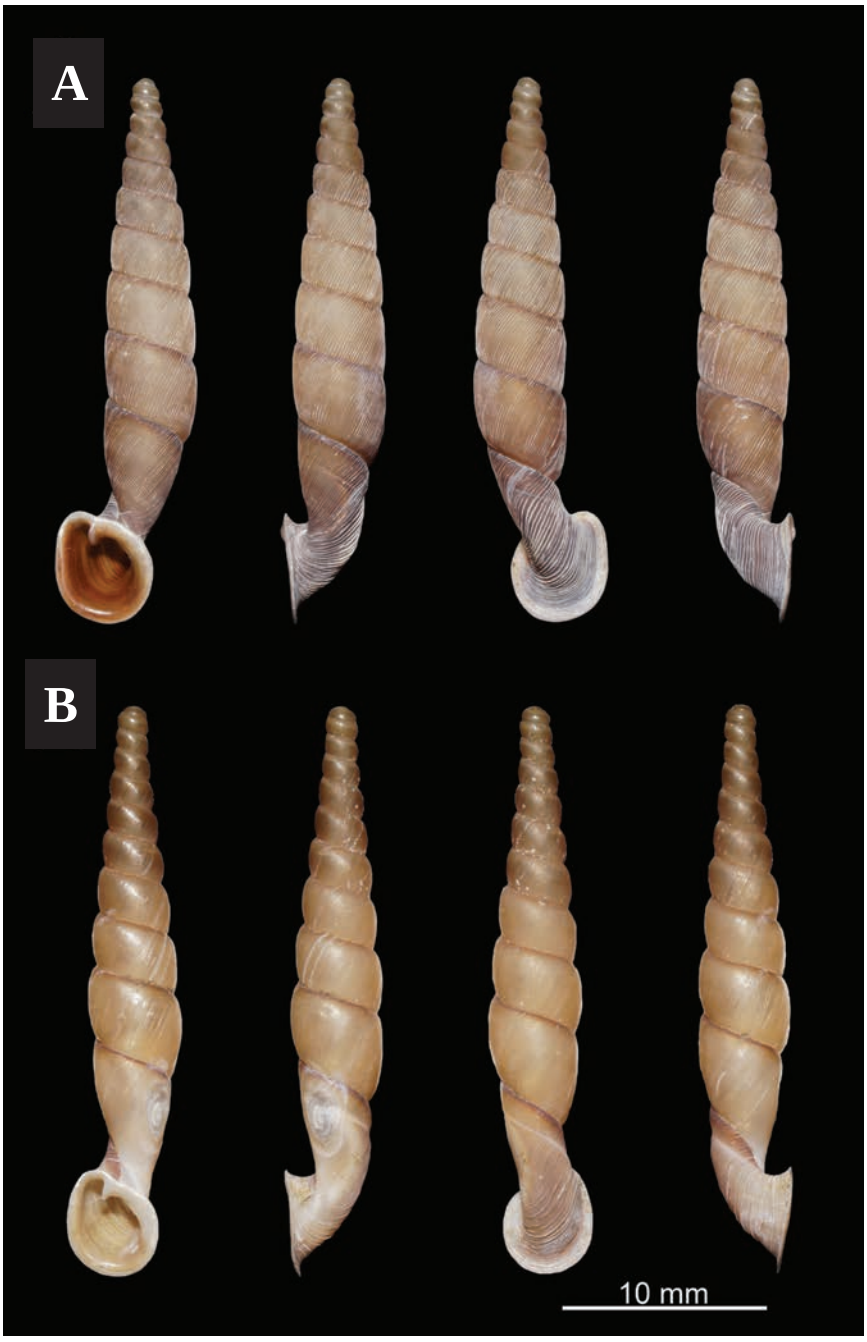

Figure 2. *Tropidauchenia jiangjilini* sp. nov. and its most similar congener. **A.** *Tropidauchenia jiangjilini* sp. nov., holotype (24_NCU_XPWU_YG01); **B.** *T. yanghaoi*.

Description. Shell (n=12). Entire, with 10.5–11.5 whorls, hardly decollated, slender-fusiform, thin, fragile, semitranslucent, light brown, with indistinct darkish-red ribbon beneath the suture; body whorl in front of lunella darker; apical part conical to slowly attenuated. Suture shallow. Protoconch smooth with 2.5–3.0 whorls. Ribs on the teleoconch very thin and dense, extending across the whole whorl, rather evenly distributed and narrowly spaced; on the neck riblets white, broader, stronger, more widely spaced and undulate. Aperture vastly extended, oval. Peristome expanded, thickened, slightly reflected, lower part reddish-brown. Only the superior lamella visible through aperture. Superior lamella bent, fused with inferior lamella but separated with spiral lamell. The end of superior lamella longer than that of spiral lamella. Subcolumellar lamella invisible in oblique view, strong, bent, its end shorter than the end of superior lamella. Lunella invisible in oblique view, vertical. Principal plica short, initiates ventrolaterally and extending laterally, not reaching peristome. Clausilium plate invisible in oblique view, semitranslucent; overall slender; stalk thin; plate relatively broad.

Genitalia (n=4). Atrium short and relatively narrow. Penis relatively slender, almost cylindrical. Penial pilasters transversal, relatively sparse, irregular zigzag. Penial caecum strong, long, tubular. Epiphallus slender,

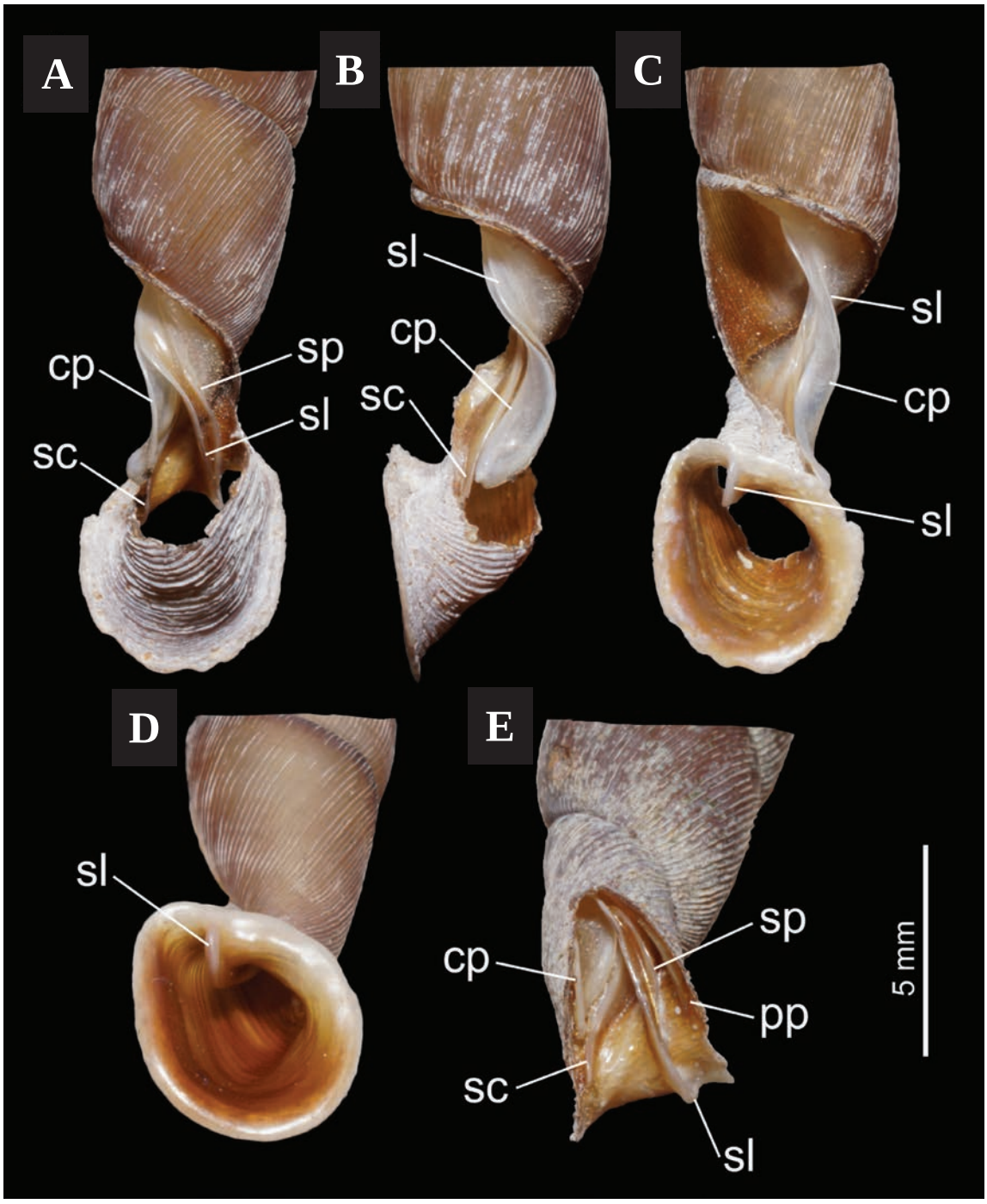

Figure 3. Detailed shell morphology of *Tropidauchenia jiangjilini* sp. nov. Abbreviations: cp clausilium plate; il inferior lamella; lu lunella; pp principal plica; sc subcolumellar lamella; sl superior lamella; sp spiral lamella.

shorter and thinner than penis. Penial retractor relatively thick and long, inserted at the middle part of penis. Vas deferens relatively slender and short. Vagina relatively slender, cylindrical. Diverticulum slender, unexpanded. Bursa copulatrix duct slender and long. Bursa copulatrix small, oval.

***Measurements*.** Holotype: shell height 27.7 mm, width 5.0 mm; aperture height 5.6 mm, width 5.3 mm. Paratypes: shell height 23.6–28.8 mm, width 4.6–5.2 mm; aperture height 4.9–5.9 mm, width 4.6–5.2 mm (n = 11).

Etymology. The species is named after Ji-Lin Jiang who first discovered the new species and assisted with the field survey.

Vernacular name. 江氏伞管螺 (Pinyin: jiāng shì sǎn guǎn luó).

Distribution and ecology. *Tropidauchenia jiangjilini* sp. nov. is found from two adjacent hills in Luoding (Figs 6, 7). Other surrounding hills are also potential distributions but require further survey. It inhabits the vertical limestone cliff together with *Gyliotrachela* sp. (Figs 5B–D).

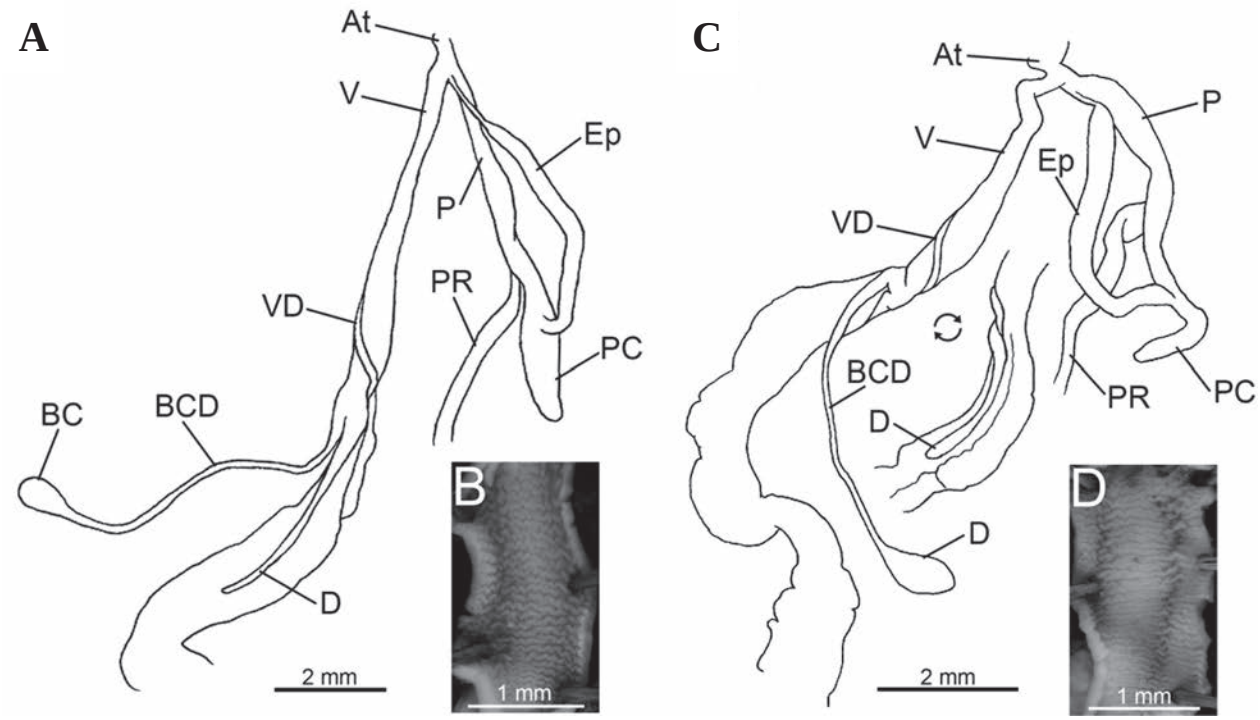

Figure 4. Genital anatomy. **A.** *Tropidauchenia jiangjilini* sp. nov., **B.** Penial pilasters of *Tropidauchenia jiangjilini* sp. nov., **C.** *T. yanghaoi*, **D.** Penial pilasters of *T. yanghaoi*. Abbreviations: At atrium; BC bursa copulatrix; BCD bursa copulatrix duct; D diverticulum; Ep epiphallus; P penis; PR penial retractor muscle; V vagina; VD vas deferens.

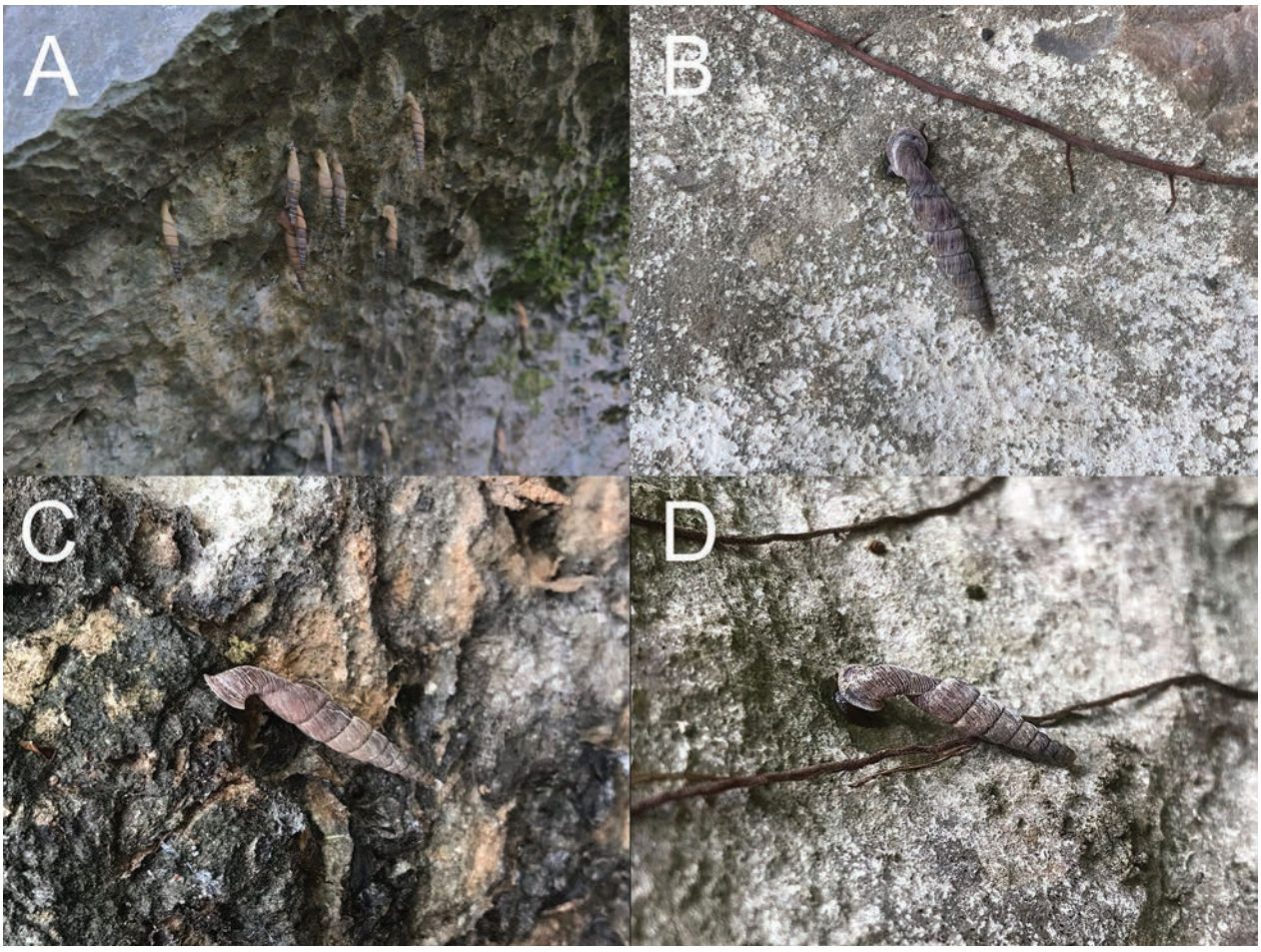

Figure 5. Living specimens. **A.** *T. yanghaoi*; **B–D.** *Tropidauchenia jiangjilini* sp. nov.

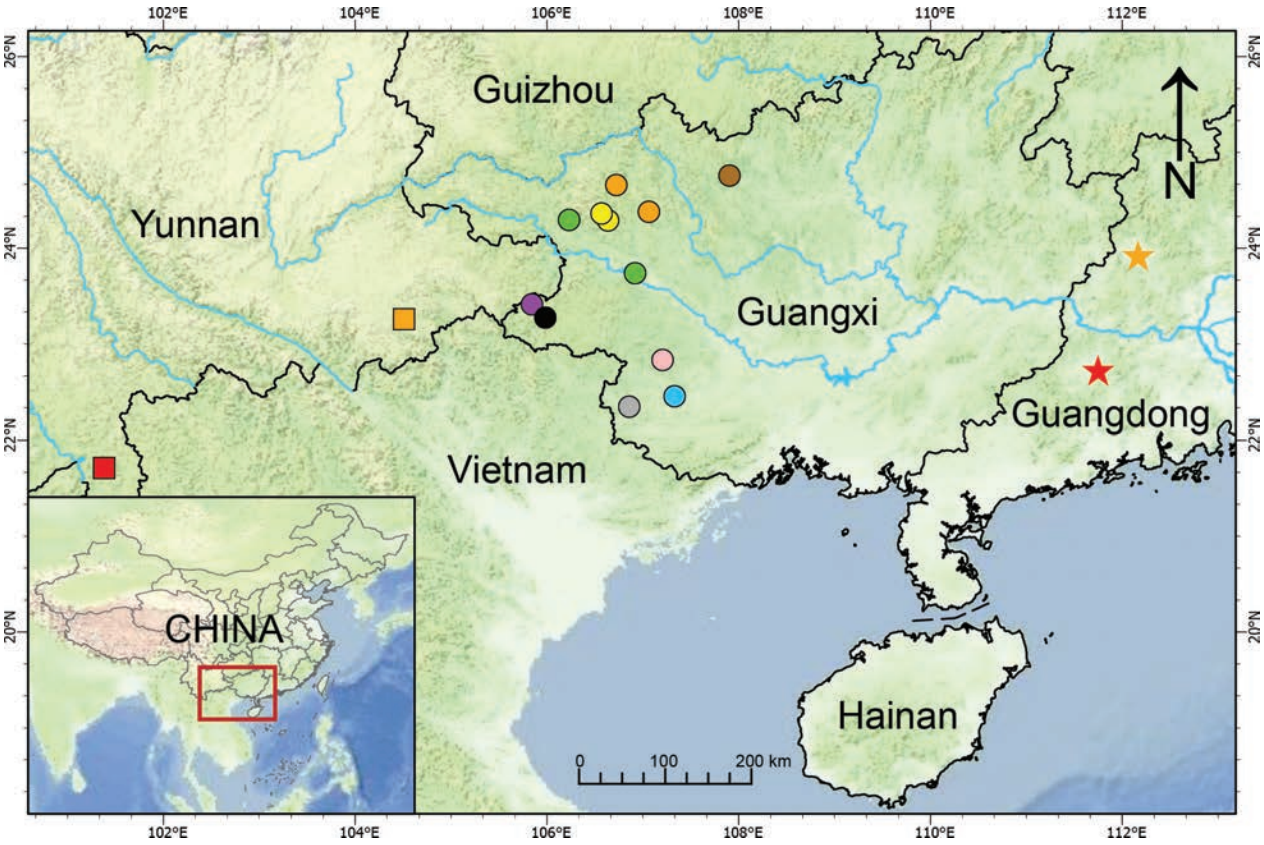

Figure 6. Distribution of *Tropidauchenia* in China. **Red star.** *Tropidauchenia jiangjilini* sp. nov., **orange star.** *T. yanghaoi*, **red square.** *T. mengyuanensis*, **orange square.** *T. ootanii*, **purple dot.** *T. napoensis*, **black dot.** *T. nakaharai*, **green dot.** *T. dorri*, **yellow dot.** *T. hitomiae*, **orange dot.** *T. lucida*, **brown dot.** *T. sulcicollis*, **pink dot.** *T. parasulcicollis*, **blue dot.** *T. danjuan*, **grey dot.** *T. orientalis*.

Figure 7. Type locality of *Tropidauchenia jiangjilini* sp. nov. **A.** overall environment; **B.** sampling locality.

Discussion

It is possible that different environmental choices may promote the differentiation of the Clausiliidae in East Asia. Although the three subfamilies are to some extent sympatric in the region, they display different microenvironmental preferences. Phaedusinae exhibits the widest adaptability to the environment, with a preference for well-ventilated and relatively humid habitats. Synprosphyminae inhabits the extremely humid environments at relatively high altitudes. It is highly dependent on the extremely humid and low temperature, with the

majority of species being found in the seepage points of groundwater or even by the river. Some species of it have evolved specialized respiration channels to facilitate survival in frequently inundated habitats. Garnieriinae is a strict rock-dwelling group and rarely descends to the ground except for spawning and dormancy. Within the subfamily, the genera *Grandinenia* and *Tropidauchenia* may demonstrate differential environmental selectivity. It has been observed that *Tropidauchenia* is predominantly found on the shaded, humid rock walls of dense forests, whereas *Grandinenia* is more commonly encountered in the more exposed and drier environment.

The placement of the new species within *Tropidauchenia* is supported by both morphology (inferior lamella fused with superior lamella) and molecular phylogeny. The absence of description of the genitalia, as well as the dearth of illustrations of lamellae and genitalia in the most original descriptions of *Tropidauchenia* species, precludes the possibility of a detailed comparison of the new species with most other congeners for these two characters. However, the distinctive shell morphology can distinguish it from all its congeners. *Tropidauchenia jiangjilini* sp. nov. can be easily distinguished from *T. bavayi*, *T. dorri*, *T. donggiaensis*, *T. giardi* and *T. proc*tostoma by the protoconch solid and preserve (vs. decollated or fragile to almost decollated) and the thinner shell. *Tropidauchenia jiangjilini* sp. nov. is similar to *T. danjuan*, *T. hitomiae*, *T. lucida*, *T. mengyuanensis*, *T. messageri*, *T. nakaharai*, *T. napoensis*, *T. orientalis*, *T. palatalis*, *T. parasulcicollis* and *T. sulcicollis* in its entire shell, but differs from them by the more slender shell. It is further distinguished from *T. danjuan*, *T. messageri*, *T. orientalis*, *T. parasulcicollis* and *T. sulcicollis* by the weaker but denser ribs on teleoconch, from *T. hitomiae*, *T. lucida*, *T. mengyuanensis*, *T. nakaharai*, *T. napoensis* and *T. palatalis* by the stronger and denser ribs on teleoconch. *Tropidauchenia jiangjilini* sp. nov. is relatively similar to *T. ootanii* by the similar slender and ribbed shell, but differs by the weaker but denser ribs on teleoconch, the ribs' uniform thickness and height (vs. ribs beneath the suture stronger) and the thicker and darker colored shell. The unique and distant distribution can also distinguish the new species from all the above congeners (Guangdong vs. Guangxi or Yunnan). *Tropidauchenia jiangjilini* sp. nov. is most similar with *T. yanghaoi* by the similar slender shell and the near distribution, but differs by the ribbed teleoconch (vs. smooth), the stronger and denser ribs on neck, the thinner diverticulum, the stronger penial caecum and the thinner and sparser penial pilasters. The new species and *T. yanghaoi* presence of a very long and strong penial caecum, while the known penial caecum in *Grandinenia* species are very small. For a long time, *Tropidauchenia* and *Grandinenia* can only distinguished by the lamella, the difference in penial caecum may be a diagnostic character of the two genera. However, due to the lack of information on the genitalia of most *Tropidauchenia* and *Grandinenia* species, the speculation remain further study and verification. The validity of *Tropidauchenia jiangjilini* sp. nov. was also supported by the molecular phylogeny. It was sistered with *T. yanghaoi* and forms a monophyly with the species from Guangxi.

The discovery of new species indicates that the species diversity of Garnieriinae in western Guangdong remains to be fully explored. As a group of rock-dwelling land snails, the species diversity of Garnieriinae is particularly high in the karst region. In comparison to the diverse species found in Guangxi, the known species of Garnieriinae in the karst region of Guangdong remain relatively few. Further comprehensive surveys in the future may reveal additional yet-to-be-described species.

Acknowledgments

We thank Ji-Lin Jiang (Zhaoqing), Meng-Hua Li (Sichuan Agriculture University), Chen-Yu Fei (Guangzhou) and Shi-Yang Feng (Sichuan Agriculture University) for assistance in collecting specimens, Frank Köhler for assistance in processing the manuscript, Chih-Wei Huang for reviewing the manuscript. This study was supported by the National Natural Science Foundation of China under Grant No.32360132, No.31772412, research grants from the Malacological Society of London, the Melbourne Research Scholarship for ZYC, the research project of Zhejiang Natural History Museum under Grant No.2024001 and the Biodiversity Monitoring Project of Xixi National Wetland Park of Hangzhou.

References

Chen YX, Tian M, Fan B (2016) Terrestrial molluscs in Yunnan. Science Press, China, 259 pp.

Fehér Z, Németh L, Nicoară A, Szekeres M (2013a) Molecular phylogeny of the land snail genus *Alopia* (Gastropoda: Clausiliidae) reveals multiple inversions of chirality. Zoological Journal of the Linnean Society 167(2): 259–272. https://doi.org/10.1111/zoj.12002

Fehér Z, Parmakelis A, Koutalianou M, Mourikis T, Erőss ZP, Krízsik V (2013b) A contribution to the phylogeny of Albanian *Agathylla* (Gastropoda, Clausiliidae): Insights using morphological data and three mitochondrial markers. The Journal of Molluscan Studies 80(1): 24–34. https://doi.org/10.1093/mollus/eyt039

Folmer O, Black M, Hoeh W, Lutz R, Vrijenhoek R (1994) DNA primers for amplification of mitochondrial cytochrome c oxidase subunit I from diverse metazoan invertebrates. Molecular Marine Biology and Biotechnology 3: 294–299.

Grego J, Szekeres M (2017) New Clausiliidae (Mollusca: Gastropoda) from China. Visaya 4(6): 79–93.

Kalyaanamoorthy S, Minh BQ, Wong TKF, von Haeseler A, Jermiin LS (2017) Modelfinder: Fast model selection for accurate phylogenetic estimates. Nature Methods 14(6): 587–589. https://doi.org/10.1038/nmeth.4285

Lanfear R, Frandsen PB, Wright AM, Senfeld T, Calcott B (2017) Partitionfinder 2: New methods for selecting partitioned models of evolution for molecular and morphological phylogenetic analyses. Molecular Biology and Evolution 34: 772–773. https://doi.org/10.1093/molbev/msw260

Lin LW, Lin RX (2022) A review of subfamily Garnieriinae C. R. Boettger, 1926. [in Chinese] https://mp.weixin.qq.com/s?__biz=MzU2MzAyMTI2Mg==&mid=2247484089&idx=1&sn=202e28f8d489c9c3e7b92fb713ea0ce9&chksm=fc61d618cb165f0efad999834653369 18e4a3124bfd14c2cd163061c745415e79f8d118eedea&mpshare=1&scene=23&srcid=03128t81MCrf5aG9Gl20jfjn&sharer_shareinfo=fd8f3a4ab07b45a317b71d8a05a3f78b&sharer_shareinfo_first=fd8f3a4ab07b45a317b71d8a05a3f78b#rd [access on April 21, 2024]

Minh BQ, Nguyen MAT, von Haeseler A (2013) Ultrafast approximation for phylogenetic bootstrap. Molecular Biology and Evolution 30(5): 1188–1195. https://doi.org/10.1093/molbev/mst024

Nordsieck H (2007a) Worldwide Door Snails (Clausiliidae), recent and fossil. ConchBooks, Germany, 214 pp.

Nordsieck H (2007b) New taxa of Phaedusinae and Garnieriinae from southern China (Gastropoda: Stylommatophora: Clausiliidae). Archiv für Molluskenkunde der Senckenbergischen Naturforschenden Gesellschaft 136(2): 217–243. https://doi.org/10.1127/arch.moll/0003-9284/136/217-243

Nordsieck H (2012a) Clausiliidae of Guangxi, southern China (Gastropoda, Pulmonata, Stylommatophora). Acta Conchyliorum 12: 3–56.

Nordsieck H (2012b) Note on Garnieriini (Gastropoda, Stylommatophora, Clausiliidae, Garnieriinae). Acta Conchyliorum 12: 57–62.

Nordsieck H (2012c) Check-list of the Clausiliidae of mainland China (Gastropoda, Stylommatophora). Acta Conchyliorum 12: 63–73.

Páll-Gergely B, Hunyadi A, Chen ZY, Lyu ZT (2019) A review of the genus *Coccoglypta* Pilsbry, 1895 (Gastropoda: Pulmonata: Camaenidae). Zoosystema 41(29): 595–608. https://doi.org/10.5252/zoosystema2019v41a29

Parmakelis A, Kotsakiozi P, Rand DM (2013) Animal Mitochondria, Positive Selection and Cyto-Nuclear Coevolution: Insights from Pulmonates. PLoS ONE 8(4): e61970. https://doi.org/10.1371/journal.pone.0061970

Qiu L (2021) Two new *Tropidauchenia* species (Gastropoda: Clausiliidae: Garnieriinae) from Guangxi, China. Folia Malacologica 29(3): 147–152. https://doi.org/10.12657/folmal.029.016

Ronquist F, Teslenko M, van der Mark P, Ayres DL, Darling A, Höhna S, Larget B, Liu L, Suchard MA, Huelsenbeck J (2012) Mrbayes 3.2: Efficient bayesian phylogenetic inference and model choice across a large model space. Systematic Biology 61(3): 539–542. https://doi.org/10.1093/sysbio/sys029

Tamura K, Stecher G, Peterson D, Filipski A, Kumar S (2013) MEGA6: Molecular evolutionary genetics analysis version 6.0. Molecular Biology and Evolution 30(12): 2725–2729. https://doi.org/10.1093/molbev/mst197

Uit de Weerd DR, Piel WH, Gittenberger E (2004) Widespread polyphyly among Alopiinae snail genera: When phylogeny mirrors biogeography more closely than morphology. Molecular Phylogenetics and Evolution 33(3): 533–548. https://doi.org/10.1016/j.ympev.2004.07.010

Uit de Weerd DR, Gittenberger E, Mamos T, Sulikowska-Drozd A (2023) The phylogenetic position of *Synprosphyma* A.J. Wagner, 1920 within Clausiliidae: Biogeographic and taxonomic implications. Archiv für Molluskenkunde 152(2): 257–267. https://doi.org/10.1127/arch.moll/152/257-267

Zoosyst. Evol. 100 (3) 2024, 1085–1097 | DOI 10.3897/zse.100.121396

PENSOFT

MUSEUM FÜR NATURKUNDE BERLIN

Re-description of *Xyliphius barbatus* (Siluriformes, Aspredinidae), with comments on osteology and distribution

Guillermo E. Terán[1*], Alejandro Méndez-López[1*], Mauricio F. Benitez[2], Wilson S. Serra[3,4], Sergio Bogan[5], Gastón Aguilera[1]

1 *Fundación Miguel Lillo – Unidad Ejecutora Lillo FML-UEL-CONICET, (4000), Miguel Lillo 251, San Miguel de Tucumán PC 4000, Tucumán, Argentina*

2 *Instituto de Biología Subtropical (UNaM-CONICET), Félix de Azara 1552, Posadas, Misiones, Argentina*

3 *Sección Ictiología, Departamento de Zoología, Museo Nacional de Historia Natural, Montevideo, Uruguay*

4 *Centro Universitario Regional del Este (CURE) Sede Rocha, Rocha, Uruguay*

5 *Division Ictiología, Museo Argentino de Ciencias Naturales "Bernardino Rivadavia", Av. Ángel Gallardo 470, C1405DJR, Buenos Aires, Argentina*

https://zoobank.org/64E8D409-0377-4629-90DC-946A2CB4BE61

Corresponding author: Gastón Aguilera (gaguilera@lillo.org.ar)

Academic editor: Nicolas Hubert ♦ **Received** 22 February 2024 ♦ **Accepted** 15 July 2024 ♦ **Published** 1 August 2024

Abstract

The banjo catfish, *Xyliphius barbatus*, belongs to the Aspredinidae family and typically inhabits the main channels of medium to large rivers in the La Plata River basin. The mimetic coloration with the substrate and the benthic lifestyle likely contribute to the challenge of sampling this species, resulting in its underrepresentation in museums and ichthyological collections. In fact, the original description of *X. barbatus* was based solely on two specimens. Consequently, little is known about its osteology, distribution, and phylogenetic relations. In this work, these information gaps are filled and the distributional range for *X. barbatus* is extended to northwestern Argentina.

Key Words

Banjo catfish, fossorial fishes, La Plata River basin, morphology, osteology

Introduction

The family Aspredinidae is composed of 13 genera and 49 valid species (Fricke et al. 2023a), among which the genus *Xyliphius* Eigenmann, 1912, include seven species (Fricke et al. 2023b). According to Friel (1994) the genus is distinguishable from all other aspredinids by the following combination of characters: eyes highly reduced, premaxillary toothless and displaced lateral to mesethmoid, a row of fleshy papillae on lower lip, *unculi* and *unculiferous* tubercles flattened, lamina of pterotic rounded, and lateral end of posterohyal expanded. Members of this genus are distributed in different basins in South America: *X. sofiae* Sabaj Pérez, Carvalho & Reis, 2017 in the Amazon River basin in Peru, *X. melanopterus* Orcés, 1962 and *X. lepturus* Orcés, 1962 in the upper Amazon and Orinoco River basins, *X. kryptos* Taphorn & Lilyestrom, 1983 in the Maracaibo basin, *X. anachoretes* Figueiredo & Britto, 2010 in the Tocantins River basin, *X. magdalenae* Eigenmann, 1912 in the Magdalena River basin, and *X. barbatus* Alonso de Arámburu & Arámburu, 1962 from La Plata River basin.

* These authors contributed equality.

Except for *Xyliphius lepturus*, all the species of the genus were described based on one to three specimens (*X. lombarderoi*, *X. melanopterus*, *X. magdalenae* and *X. sofiae* based on a single specimen; *X. barbatus* and *X. anachoretes* on two specimens; and *X. kryptos* on three specimens). These fishes are rare in inventories of fish fauna and consequently in museum collections. This sparse representation is due to several factors, including their mimetic coloration with the substrate, their benthic lifestyle, the infaunal habits of many species, and, most importantly, their specific habitat preferences. Indeed, these species live in the main channels of medium to large rivers, where sampling is difficult (Carvalho et al. 2017). *Xyliphius barbatus*, originally described from the Paraná River in Rosario (Alonso de Arámburu and Arámburu 1962), has a few records along the La Plata River basin: Paraná River in Misiones, Santa Fe (García 1992; Calviño and Castello 2008) and Chaco provinces (type locality of *Xyliphius lombarderoi* Risso & Risso, 1964, a synonym of *Xyliphius barbatus*) (Risso and de Risso, 1964); in the Uruguay River in Uruguay (Loureiro et al. 2013) and, more recently, in the Paraguay River basin, Pantanal, Brazil (Gimênes Junior and Rech 2022).

In Argentina, other aspedinids have been recorded: *Amaralia oviraptor* Friel & Carvalho, 2016, *Bunocephalus doriae* Boulenger, 1902, *Pseudobunocephalus iheringii* (Boulenger, 1891), *Pseudobunocephalus rugosus* (Eigenmann & Kennedy, 1903), and *Pterobunocephalus depressus* (Haseman, 1911). Although the upper section of the Bermejo River basin has many endemisms (e.g., Mirande et al. 2004a, b, 2006; Casciotta and Almirón 2004; Terán et al. 2016a, 2019; Alonso et al. 2018; Aguilera et al. 2019), it shares elements with the Paraguay-Paraná River basin (Alonso et al. 2016; Terán et al. 2016b, 2016c; Vanegas-Ríos et al. 2019), and the Amazon River basins (Littmann et al. 2015; Aguilera et al. 2022). The only record of aspredinids in this area is *Bunocephalus doriae* Aguilera et al. (2016).

New inventories made in the Bermejo River basin have revealed the presence of *Xyliphius barbatus*, a species not previously recorded for the area. This record is the largest known batch regarding the species. The aim of this contribution, is to provide an accurate re-description of *X. barbatus.*

Materials and methods

Specimens were collected by electrofishing and hand nets, euthanized by immersion in tricaine methanesulfonate (MS222), fixed in 10% formalin solution, and transferred to individual batches in a 70% alcohol solution. The material was deposited in ichthyological collections. In some fresh individuals, a small tissue sample was taken and immediately preserved in absolute ethanol for genetic analysis. The tissue aliquots were deposited in the tissue collection of CIT-FML. The study complied with the animal welfare laws, guidelines, and policies of the Comité Nacional de Ética en la Ciencia y Tecnología, Argentina. Collection permits were granted by the Ministerio de Ambiente of Jujuy. (permits' numbers: 1103-306-M/2016, Res. N° 137/2016-MA).

Point to point measurements were taken with a digital caliper to the nearest 0.1 mm and expressed as percentage of the standard length (SL), except for subunits of head, expressed as percent of the head length (HL) (see Table 1). Measurements follow Friel (1995) and Cardoso (2010), with the modifications proposed by Carvalho et al. (2017). Nomenclature of anatomical structures follows that used by the three mentioned authors and Dahdul et al. (2010), included in the Teleost Anatomy Ontology of Uberon Ontology Documentation (Mungall et al. 2012, http://obophenotype.github.io/uberon/). Specimens were cleared and stained (C&S) following Taylor and Van Dyke (1985). An asterisk (*) indicates holotype counts. Vertebral counts included the Weberian Complex (5 vertebrae) plus all free vertebrae and the compound caudal centrum (PU1 +U1) counted as one element.

Total genomic DNA was extracted from ethanol-preserved muscle tissue of specimen CI-FML 7944 (tissue collection number: CIT-FML 00169), using a salt-based protocol (Aljanabi and Martinez 1997). A 651pb fragment of mitochondrial gene Cytochrome oxidase subunit I (COI) was amplified by Polymerase Chain Reaction (PCR) using the cocktail primers proposed by Ivanova et al. (2007). The PCR protocol was the implemented by Ward et al. (2005). PCR-amplified product was purified with 20% PEG . The product was sequenced with automated sequencer (Macrogen, Korea) in both directions to check for potential errors. The Chromatogram was processed and edited using Geneious (Technelysium Pty Ltd) and deposited in GenBank under the accession number OQ539436. COI sequences of different *Xyliphius* species from GenBank (http://www.ncbi.nlm.nih.gov/Genbank) were used to assess the relationships between *X. barbatus* and the remaining species of the genus, providing a preliminary phylogenetic hypothesis. GeneBank codes and references for the employed sequences are shown in Table 2. Pairwise genetic distances with K2P model and UPGMA analysis were performed for 651 -pb fragments using MEGA11 (Tamura et al. 2021). The Maximum likelihood tree was estimated employing RAxML (Randomized Axelerated Maximum Likelihood) under GTR+FO+G4m model and 100 bootstrap replicates.

Collection's acronyms: **MACN-Ict** Museo Argentino de Ciencias Naturales, Buenos Aires, Argentina, **MG-ZV-P** Museo Provincial de Ciencias Naturales "Dr. Ángel Gallardo", Rosario, Argentina, **MLP-Ict** Museo de la Plata, La Plata, Argentina, **CFA-IC** Fundación de Historia Natural Félix de Azara, Buenos Aires, Argentina, **CI-FML** Fundación Miguel Lillo, San Miguel de Tucumán, Argentina.

Table 1. Morphometric data of *Xyliphius barbatus*. SD= standard deviation. Holotype (MLP 6798), Paratype (MLP 2799), Paraná River (MACN-Ict 6791. 5 ex.) Bermejo River specimens (CI-FML7944 and CFA-IC-12742 34 ex.).

	Holotype	Paratype	Bermejo River (N= 20)			Paraná River (N= 5)		
			mean	range	SD	mean	range	SD
Standard length	90.3	87.2	91.3	79.6 – 111.3	8.3	66.2	44.6 – 93.6	17.6
Percentage of SL								
Body depth at dorsal – fin origin	15.9	14.1	14.9	12.3 – 16.9	1.2	17.2	15.6 – 19.9	1.7
predorsal length	42.6	40.4	40.4	38.3 – 45.2	1.4	41.7	40.0 – 43.0	1.1
prepectoral length	26.6	25.6	25.8	23.6 – 28.4	1.1	27.2	25.8 – 28.9	1.2
prepelvic length	47.3	45.8	44.0	41.0 – 49.1	1.7	45.9	43.2 – 51.8	3.5
preanal length	63.9	63.2	60.3	58.2 – 64.1	1.4	60.9	58.0 – 63.9	2.4
caudal peduncle length	26.2	23.2	27.7	25.0 – 31.1	1.8	26.6	24.4 – 29.6	2.0
caudal peduncle depth	7.3	8.1	7.4	6.8 – 8.1	0.3	8.2	8.0 – 8.6	0.2
pelvic fin length	14.9	12.6	14.1	12.6 – 15.2	0.8	15.5	13.3 – 16.6	1.3
anal – fin base	13.3	11.6	14.3	12.7 – 16.6	1	13.2	11.6 – 15.5	1.5
caudal-fin length	23.3	17.2	20.3	18.1 – 22.2	1.2	20.0	17.1 – 22.2	1.9
pectoral spine length	16.8	16.6	15.5	13.8 – 17.2	0.9	17.2	15.0 – 19.5	2.0
humeral process length	10.6	11.1	9.8	8.2 – 12.4	1.1	8.0	5.5 – 11.6	2.2
posterior process of coracoid length	10.4	9.5	9.8	8.3 – 11.1	0.8	10.5	9.6 – 11.7	0.9
head length	28	28.5	28.2	26.0 – 31.0	1.4	34.9	33.4 – 35.4	0.8
width at pectoral – fin insertion	27.5	27.7	24.7	23.3 – 27.4	0.9	27.4	26.8 – 28.2	0.6
Percentage of HL								
maximum head depth	51.4	51.5	46.9	42.2 – 51.8	2.7	41.4	36.9 – 44.5	3.1
snout length	35.4	25.9	33.0	29.7 – 39.9	2.4	25.1	21.8 – 29.2	2.8
eye diameter	3.7	3.5	3.5	2.3 – 5.8	0.9	4.0	3.0 – 5.4	1.0
interorbital width	30.1	24.9	30.6	27.3 – 35.8	2.2	21.7	19.7 – 23.8	1.8
maxillary barbel	95.2	94.9	86.9	71.6 – 105.1	7.7	68.0	60.7 – 76.8	5.9
anterior to posterior nares distance	11.2	8.4	10.7	7.6 – 16.5	2.1	11.3	7.3 – 14.3	3.4
posterior nare to orbit	7.2	5.4	7.3	5.8 – 9.9	1.0	4.8	4.1 – 6.4	0.9
anterior internareal distance	20.7	13.8	16.6	13.8 – 22.1	1.9	15.0	14.0 – 15.9	0.7
posterior internareal distance	30.7	25.7	28.8	26.2 – 31	1.6	25.7	22.8 – 30.2	3.2

Table 2. List of sequences, with accessions and vouchers employed for molecular analysis.

Species	GenBank ID	Catalog	Basin
Xyliphius barbatus	OQ539436	CI-FML 7944	Bermejo River. Argentina
Xyliphius barbatus	KU288948	MG ZV-P 355	Paraná River. Argentina
Xyliphius lepturus	MF489386	AUM46757	Amazon River, Peru
Xyliphius magdalenae	MF489382	ANSP192845	Magdalena River, Colombia
Xyliphius melanopterus	MF489383	MUSM36715_AP12	Amazon River, Peru
Xyliphius melanopterus	MF489384	MUSM36715_AP28	Amazon River, Peru
Xyliphius melanopterus	MF489385	STRI01784	Amazon River, Peru
Xyliphius sofiae	KU736764	ANSP 182322	Amazon River, Peru

Results

Xyliphius barbatus Alonso de Arámburu & Arámburu, 1962

Figs 1–6

Material examined. All from Argentina: **MLP 6798.** Holotype. 90.3 mm SL. Paraná River at Rosario, Santa Fe province. Col. C. Vidal. **MLP 2799**. Paratype. 87.2 mm SL. Paraná River at Rosario, Santa Fe province. Col. R. Ringuelet. **MACN 6791.** 5 ex, 44.6–93.6 mm SL. Paraná River near Curtiembre, border between Santa Fe and Entre Rios provinces. 31°27'18.34"S, 60°10'11.95"W. 35–45 m depth 1961–1962 Col. N. Bellisio. **MG-ZV-P 355** (LAR-254). 1 ex, 99.1 mm SL. Paraná River in front of Rosario, Entre Rios province, Argentina. 32°55'58.8"S, 60°37'58.8"W. 6 m depth. 04/03/2013 Col. Julián Aguilar. **CI-FML 7944.** 29 ex (3 C&S), 79.6–111.3 mm SL. **CFA-IC-12742**, 5 ex. 79,7–99,2 mm SL. San Francisco River, Bermejo River basin, Jujuy province; 23°50'27.08"S, 64°37'24.70"W, ca. 370 m asl. 1–2 m depth. 30 Sep 2016. G.E. Terán, G. Aguilera and D. Delgado.

Diagnosis. *Xyliphius barbatus* is distinguishable from the remaining species of genus by the following combination of characters: (1) seven to 11 retrorse dentations on posterior margin of pectoral-fin spine (*vs.* six in *X. anachoretes* and four or five in *X. magdalenae*); (2) 24 to 30 dendriform papillae on inferior lip (*vs.* 20–22 in *X. magdalenae*, 30 in *X. sofiae*, and 22 to 27 triangular papillae, with only the lateral ones branched in

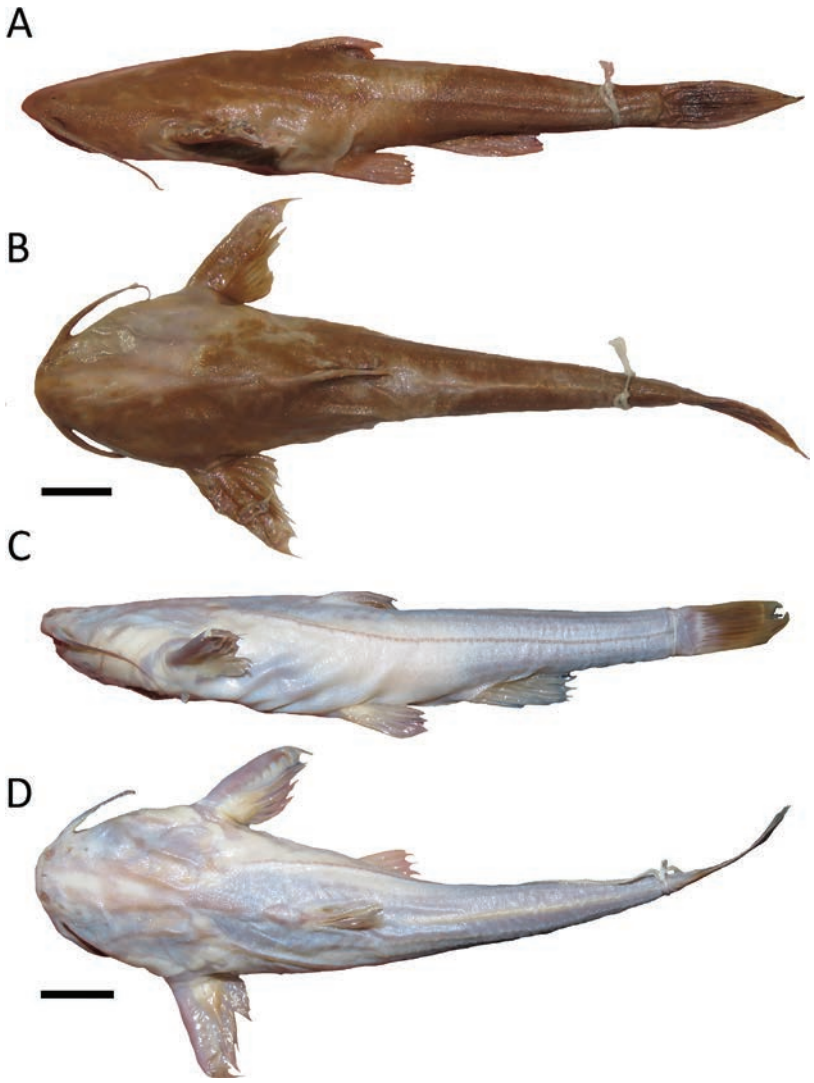

Figure 1. A, B. Holotype MLP 6798 of *Xyliphius barbatus*. 90.3 mm SL. C-D Paratype MLP 2799. 87.2 mm SL. Paraná River at Rosario, Santa Fe province, Argentina. Scale bar: 10 mm.

X. kryptos); (3) I,3 or I,4 dorsal-fin rays (*vs.* I,5 in *X. lepturus* and *X. melanopterus*); (4) absence of dorsal pale band from snout tip to caudal-fin origin (*vs.* presence in *X. anachoretes*, *X. magdalenae* and *X. melanopterus*); (5) absence of a latero-dorsal band following the second row of tubercles on anterior part of body (*vs.* present in *X. magdalenae* and *X. melanopterus*); (6) eyes present and reduced (*vs.* absent in *X. sofiae*); (7) five to eight anal-fin rays (*vs.* nine in *X. lepturus*).

The additional characters that distinguish *Xyliphius barbatus* from the remaining species of the genus are: papillae dendriform on lower lip with large branches (*vs.* papillae with minute branches on *X. anachoretes*); three dorsal procurrent rays (*vs.* two in *X. anachoretes*, four to five in *X. lepturus*, and four in *X. magdalenae*); pelvic fin not reaching anal-fin origin (*vs.* just reaching in *X. magdalenae*); maxillary barbel surpassing pectoral-fin spine insertion (*vs.* not quite reaching pectoral in *X. magdalenae*); four branchiostegal rays (*vs.* five in *X. sofiae*); and two ossified proximal radials on pectoral fin (*vs.* one in *X. sofiae*).

Morphological description. Morphometric data is summarized in Table 1. Head and anterior part of body depressed, compressed from dorsal-fin origin to caudal-fin insertion. Maximum depth at dorsal-fin origin. Dorsal profile straight from snout tip to dorsal-fin origin, relatively depressed along dorsal-fin base, and relatively straight from this point to caudal-fin origin. Ventral profile of body, straight from lower-jaw to pectoral-fin origin, convex to pelvic-fin origin with the lowest point at the origin of the pelvic bone, then slanted dorsally to anal-fin origin and relatively straight form this point to caudal-fin base. Greatest width just anterior to pectoral-fin origin.

Head triangular with a rounded snout. Eyes reduced (Fig. 3), located closer to snout tip than to supraoccipital protuberance, and covered with skin less pigmented than surroundings areas. Two nares, anterior nostril tubular, posterior one smaller and located closer to eyes than to anterior nostril. Maxillary barbel on side of snout, inserted just above rictus. Maxillary barbel reaching pectoral-fin base. Two pairs of mental barbels smaller than maxillary ones and located close to the mouth gape.

Figure 2. Lateral, dorsal and ventral views of *Xyliphius barbatus*. CI-FML 7944. San Francisco River, Bermejo River basin, Jujuy province. Scale bar: 10 mm.

The external one just before the vertical line through eye, reaching mouth gape when adpressed; inner mental barbels smaller, reaching outer barbels origin, surpassing the lower lip and reaching end of papillae when adpressed. Mouth subterminal, much wider than snout, with 20 to 30 dendritic papillae. Anterior margin of snout with a groove at middle line in dorsal view. Gill slits small, located ventrally on head, before pectoral-fin origin; gill membranes united to isthmus. Small genital papillae just posterior to anus.

Head, trunk, and fins are all covered by thick skin, while the skin in the ventral area and at the fin insertions is thinner. Trunk covered by unculiferus tubercles, which are more concentrated in the head. Five lateral rows of large tubercles extending from post-cephalic region to caudal-fin base, and concentrated in mid-dorsal line.

Dorsal-fin I,2,i (1) or I,3,i (33*), spine feeble. Dorsal-fin insertion on anterior half of body, closer to snout tip than to caudal-fin insertion, anterior to pelvic-fin insertion; shape triangular, rays elongated beyond the membrane. Anal fin i,3,i(1), ii,3,i(6), iii-3,i(7), ii-4,i(16*), iii-4,i(1), ii-5,i(3), ovoid, first branched anal-fin ray longest. Anal-fin insertion on the posterior half of body, closer to caudal-fin insertion than to snout tip. Pectoral-fin I,4,i (34*), its origin almost at half way between snout tip and dorsal-fin origin, and its distal tip reaching pelvic-fin origin. Distal tips of branched rays elongated beyond membrane. Pectoral spines thick, with seven to 11 developed retrorse serrae along posterior margin; spine capped by a fleshy elongation. Pelvic fin i,3,i (1) or i,4,i (33*), origin just posterior to vertical through dorsal-fin origin. The tip of pelvic-fin rays elongated throughout the membrane. Caudal fin i,4/4,i (34*), The ventral-most three branched caudal-fin rays longer.

Osteology (Figs 4–6).

Mesethmoid deep, slightly longer (anteroposteriorly) than wide, with an anterior notch separating two anterior wings. Premaxillae articulating on a ventrolateral concavity of mesethmoid, not visible in dorsal view due to a dorsal lamina. Two diverging laminae articulating dorsally with frontals by interdigitations. Lateral ethmoids articulate with frontals through a dorsal interdigitated

Figure 3. Head detail of *Xyliphius barbatus*. CI-FML 7944. San Francisco River, Bermejo River basin, Jujuy province. Scale bar: 5 mm.

process and medially with orbitosphenoid by cartilage; the latter covered ventrally by a laminar extension of the same bone articulating with parasphenoid; projecting lateral process joined to autopalatine at its middle length; ventrally flattened and extensively articulating with parasphenoid posteromedially. Frontals about 3.5 times longer than wide, their posterior wing articulating with supraoccipital, and lateral posterior margins enclosed by anterior extension of sphenotic. Anterior fontanel about 1.4 times larger than posterior one, synchondral articulation between lateral ethmoids and mesethmoid completely visible through fontanel. Supraoccipital enclosing almost half of posterior fontanel. Epiphyseal bar with a strong suture, its length equal to or greater than that of posterior fontanel. Supraoccipital a little longer than wide, extensively articulating with pterotic laterally, and with epioccipital posterolaterally; a notch in posterior region receiving the ascending process of posttemporal-supracleithrum; posterior process wide and short, in contact with dorsal portion of complex vertebrae. Sphenotic pitted; ventral surface with greater pores, sutured to pterotic laterally, leaving a posterior space with same bone in ventral view, with extensive anterior synchondral articulation with hyomandibula, sutured medially to parasphenoid and posteriorly to anterior lamina of prootic. Dorsal prootic covering lateral surface of frontals and with posterior articulation with supraoccipital. Pterotic with anterior lamina sutured to sphenotic, a concavity after its contact with suprapreopercle, and a lateral rounded expansion reaching opercle ventrally; contacting posttemporal-supracleithrum lateral arm at its posteriormost region. Epioccipital articulating anterolaterally with pterotic, medially with supraoccipital and dorsally with posttemporal-supracleithrum. The latter bone with dorsal process reaching lateral surface of supraoccipital over epioccipital; a ventral pointed process contacting posterior expansion of pterotic and posterior arm of the bone sutured to complex vertebra. Wider portion of parasphenoid at its articulation with sphenotic, extended to middle bassioccipital at its posterior end. Prootic visible only in ventral view, anterior lamina over sphenotic cartilage, extensively contacting parasphenoid medially,

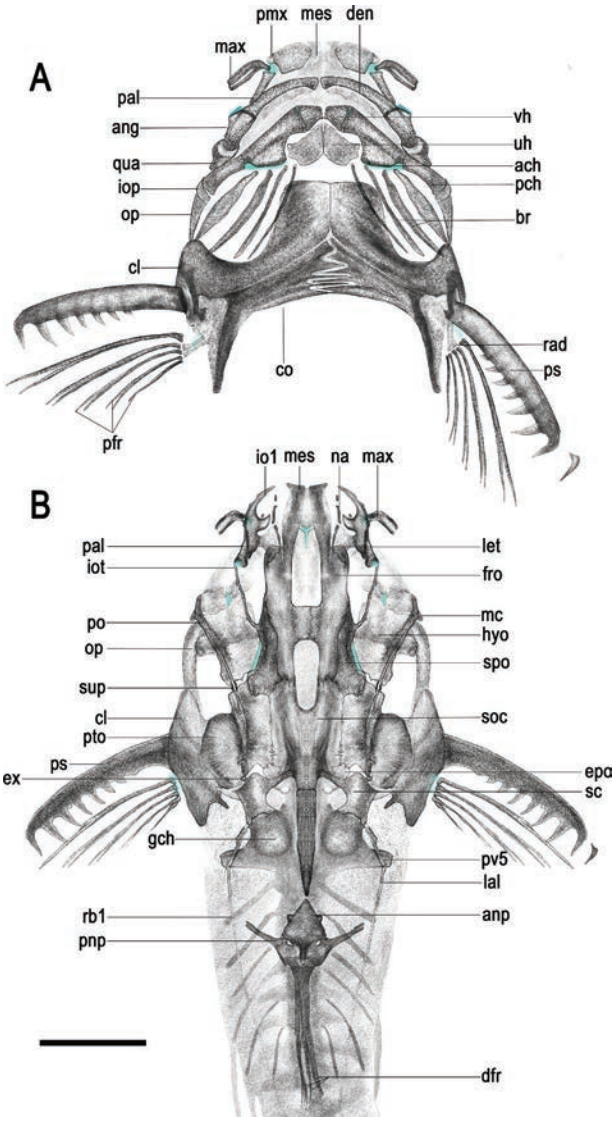

Figure 4. Skull of *Xyliphius barbatus* CI-FML 7944. **A**. Ventral view; **B**. Dorsal view. ach: anterior ceratohyal; ang: anguloarticular; anp: anterior nuchal plate; br: branchiostegal rays; cl: cleithrum; co: scapulocoracoid; den: dentary; dfr: dorsal fin rays; epo: epioccipital; ex: extrascapular; fro: frontal; gch: gas bladder chamber; hyo: hyomandibula; io1: infraorbital 1; iop: interopercle; iot: infraorbital tubules; lal: lateral line tubules; let: lateral ethmoid; mc: mandibular canal tubules; mes: mesethmoid; max: maxilla; na: nasal; op: opercle; pal: autopalatine; pch: posterior ceratohyal; pfr: pectoral-fin rays; pmx: premaxilla; pnp: posterior nuchal plate; po: preopercle; ps:pectoral-fin spine; pto: pterotic; pv5: parapophysis of vertebra five; qua: quadrate; rad: pectoral-fin radial; rb1: first rib; soc: supraoccipital; sc: posttemporal-supracleithrum; spo: sphenotic; sup: suprapreopercle; uh:urohyal; vh: ventral hypohyal. Scale bar: 1 mm.

and sutured to pterotic posterolaterally, leaving to an anterior space with the same bone. Exoccipital bearing two projections enclosing posterior parasphenoid, strongly sutured to posteromedial edge of prootic, to exoccipital laterally and with complex vertebra by interdigitations. Basioccipital sub triangular, with a large foramen on its posterior half, a conspicuous pore anteromedially and additional ones laterally.

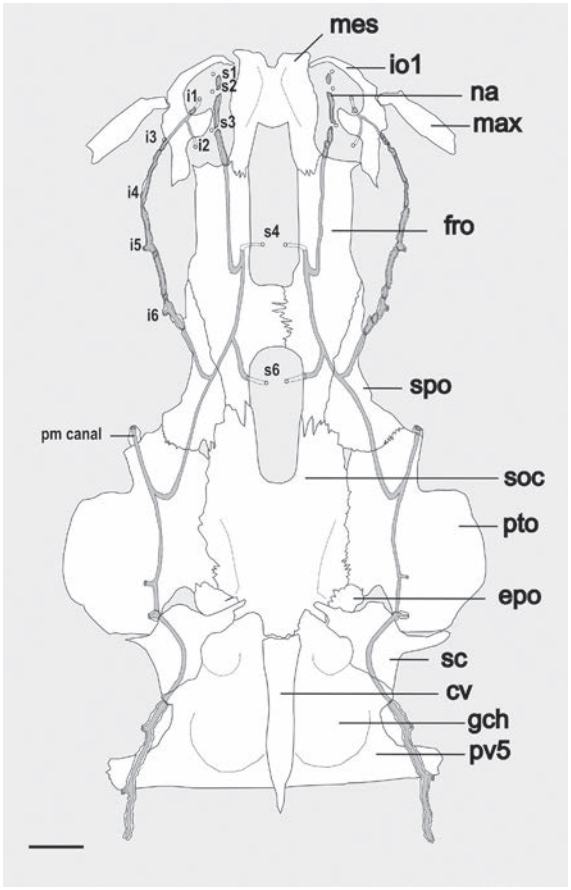

Figure 5. Dorsal view of the neurocranium of *Xyliphius barbatus* CI-FML 7944. mes: mesethmoid; io1: infraorbital 1; na: nasal; max: maxilla; fro: frontal; spo: sphenotic; soc: supraoccipital; pto: pterotic; epo: epioccipital; sc: supracleithrum; cv: weber camara; gch: gas bladder chamber; pv5: parapophysis of vertebra five. Pores of the cephalic sensory lateral system s1 to s6 represent the pores from the supraorbital canal and i1 to i6 from the infraorbital canal. Scale bar: 2 mm.

Premaxillaries dorsomedially flattened and oval, in contact with ventrolateral notches of mesethmoid and separated by the latter. Premaxillary teeth absent. Maxillary tubular, with furrowlike opening on ventral surface; its condyle attached to anterior palatine cartilage. Dentary long and slender, laminar posterior region overlapping anterior face of angular; teeth conical and pointed inwards, arranged in two rows, the outer one with 3 to 5 teeth near the symphysis, and the inner row with 11–12 teeth; coronomeckelian absent. Meckel's cartilage somewhat conical, wider laterally from its origin at angular, and slender medially at its joining with the dentary, which is located ventral to (or a little displaced medially) dentary dorsolateral notch.

Hyomandibula in dorsoventrally oblique position with respect to neurocranium; dorsalmost edge under anterior extension of sphenotic, followed by a synchondral articulation with the same bone; anterior cartilage contacting quadrate and extended to lateral portion of metapterygoid. Preopercle on lateral portion of hyomandibula, sutured to quadrate on its synchondral articulation with the same bone. Quadrate condyle anteroventrally oriented, to anguloarticular. Metapterygoid square, a little larger than endopterygoid, with a posterior concavity for the anterior lamina of hyomandibula. Endopterygoid ventral to posterior third of autopalatines, at posteroventral concavity of lateral ethmoids after its projecting lateral process, bearing a lateral pointed projection reaching autopalatine middle cartilage.

Autopalatines with expanded anterior and posterior edges, its narrower portion anterior to lateral ethmoids cartilage. Opercle medially articulated with lateral arm of hyomandibula, anteriorly expanded and sutured with interopercle; posterior pointed projection reaching ventral expansion of pterotic. Interopercle accompanying ventralmost edge of opercle, its anterior pointed projection over posterior ceratohyal, covering the interhyal articulation from lateral view.

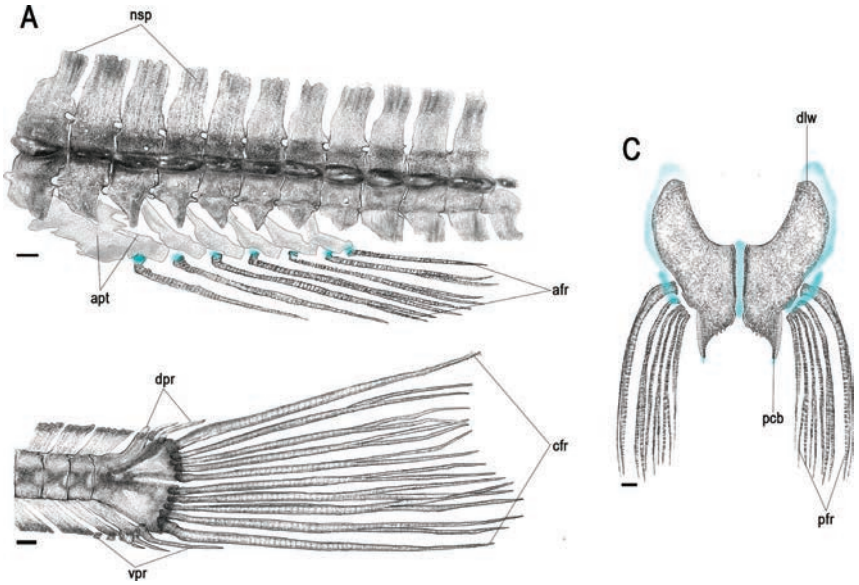

Figure 6. Anal, caudal and pelvic fins of *Xyliphius barbatus* CI-FML 7944. **A.** Anal-fin and pterygiophores; **B.** Caudal complex and fin; **C.** basipterygium. afr: anal-fin rays; apt: anal-fin pterygiophores; cfr: caudal-fin rays; dlw: dorsolateral wing of basipterygium; dpr: dorsal procurrent rays; nsp: neural spines of vertebrae 15 to 18; pcb: posterior cartilage of basipterygium; pfr: pelvic-fin rays; vpr: ventral procurrent rays. Scale bar: 1 mm.

Urohyal subtriangular, with a medial longitudinal cleft on anterior corner and posterolateral developed wings. Two basibranchials, the anterior one about twice larger, contacting first hypobranchial anteriorly and second hypobranchial cartilage posterolaterally; posterior one reached by third hypobranchial. Only the first hypobranchial ossified with wider distal portion. Hypohyals squarish, narrow in its proximal region, and articulated to ceratohyal synchondrally. Ceratohyals with posteroventrally expanded lamina at the articulation with banchiostegal rays; dorsal and ventral extensions over cartilage with posterior ceratohyal sutured to anterior extensions of same bone. Posterior ceratohyal rectangular, with a notch anterior to posterodorsal corner at the articulation with interhyal. Branchiostegal rays four, lateral ones thicker and with more developed lamina, first one (medial) between posterior urohyal and lateral to corner of ceratohyal expanded lamina, the remaining ones associated with anterior ceratohyal cartilage, lateral-most at the articulation cartilage of ceratohyals. Interhyal present, articulated to posterodorsal ceratohyal, with lateral portion of hyomandibular and quadrate.

Ceratobranchials five, first two and last one (fifth) with a single series of small gill rakers, third and fourth with two series; fifth ceratobranchial bearing a dorsal drop-shaped plate with conical teeth, posterior portion long and slender, with four or five gill rakers. Five gill rakers on the anterior border of first and second ceratobranchials, one in the cartilage with first epibranchial; only epibranchials one to three with gill rakers, first with single row and the remaining two with double row of one or two gill rakers restricted to proximal portion. Epibranchials four, an uncinated process on the third one. Third pharyngobranchial thicker at its articulation with cartilage of third epibranchial; fourth pharyngobranchial about half of the latter and located dorsal to an oval tooth plate.

Nasal separated in two tubular ossifications by supraorbital sensory pore s2, posterior tubular ossifications of the supraorbital canal enters frontal just lateral to its articulation with mesethmoid posterior projection. Antorbital present, small, its canal piercing base of dorsal projection of infraorbital 1 and exiting posteriorly. First infraorbital over anterior cartilage of autopalatine, with notch bordering maxillary condyle; anteromedial projection pointed and curved, limiting the anterolateral portion of nares. Posterior infraorbitals as a small series of ossicles entering sphenotic canal laterally; ventral branches of i5 and i6 ossified.

Supraorbital sensory canal with pores s1-s2 and s2-s3 separating nasal in two tubular ossifications. Pore S4 opening at anterior frontal fontanel, s5 is missing and s6 opening at posterior frontal fontanel. Infraorbital sensory canal composed of six pores, the first and second ones opening at inner margin of infraorbital 1, and the third at outer margin. Pores i4 to i6 arranged in an arch reaching up close to anterior half of sphenotic.

Tubular series of preopercle mandibular canal initiating below posterior portion of dentary and separated by those joined to preopercle by a gap just lateral to quadrate condyle. Suprapreopercle as a small tubular canal between hyomandibula and pterotic, with dorsal and ventral laminae present. Extrascapular present. Lateral line complete, beginning at posterolateral exit of posttemporal-supracleithrum canal.

Dorsal lamina of Weber apparatus reaching dorsal surface, with flattened and slender process almost reaching nuchal plate posteriorly. The latter rhomboid in dorsal view, with a ventral lamina reaching neural processes of sixth vertebra. Posterior nuchal plate with two slender and pointed anterolateral projections joined to first rib by a ligament, ventrally contacting anterior plate. Gas bladder chamber evident from dorsal view, posteroventral portion partially enclosed by an anteriorly directed ventral lamina. Parapophyses of fifth vertebra reaching lateral wall of body, continuous with posterolateral edge of cleithrum; extensively joined to posterior region of complex vertebrae and covering its lateral border. Ribs six, first pair on sixth vertebra. Vertebrae 35, fist 30 or 31 bearing transversal lateral processes.

Pectoral spine retrorse serrations larger distally; first branched ray reaching end of spine or slightly beyond. Two proximal radials associated with the three proximal most rays; first branched ray associated with scapulocoracoid cartilage. Cleithrum dorsomedial pointed projection entering cavity formed by ventral posttemporal-supracleithrum and lateral lamina of complex vertebra; dorsolateral arm with a proximal pointed projection lateral to posttemporal-supracleithrum and rounded edge; medial arm anteriorly concave, bearing an extensive contact scapulocoracoid posteriorly, and sutured to contralateral cleithrum in larger C&S specimen (102.58 mm SL). Coracoids strongly interdigitated medially, their posterior processes passing base of last pectoral-fin rays and reaching vertical through dorsolateral arm of cleithrum. Pelvic fins not reaching anal-fin origin. Basipterygia with developed dorsolateral wings and lateral cartilage present; medial cartilage not reaching posterior medial margin of bone, which bear jagged borders; posterior cartilage short. First anal-fin pterygiophore reaching posterior portion of vertebra 15 and posterior anal-fin pterygiophore at posterior portion of vertebra 21. Caudal fin with five principal rays on both lobes, three dorsal and four or five ventral procurrent rays.

Coloration (Fig. 7).

Ground of body dark brown to black, head light brown, pectoral region lighter than dorsal region. A barely evident light brown middorsal stripe on head from snout tip to the middle of caudal peduncle, interrupted at dorsal-fin base. Lateral rows of tubercles brown, lighter than the background. Maxillary barbels dark brown with lighter tips; the remaining barbels light brown. Pectoral fins black with whitish tips; anal fin black with distal half whitish; all the other fins black with the distal third whitish. After the fixation process, the color tends to become paler brown, and the white portions on the fins are less noticeable (Figs 1–3).

Figure 7. CI-FML 7944. *Xyliphius barbatus*. Live specimen, 92.4 mm SL. San Francisco River, Bermejo River basin, Jujuy. Scale bar: 10 mm.

Molecular analysis. Molecular comparison employing the COI sequence (see Table 2) shows no difference between *Xyliphius barbatus* specimen from lot CI-FML 7944 and *Xyliphius* sp. reported by Díaz et al. (2016) from Paraná River Basin in Rosario, Argentina, herein identified as *Xyliphius barbatus*. The estimated evolutionary divergence (number of base substitutions per site from between sequences) is quite small (D≥0.0031) between *X. barbatus* and *X. melanopterus*, but greater with specimens of *X. magdalenae*, *X. sofiae* and *X. lepturus* (D=0.1092; 0.1414 and 0.1558). Comparisons with *X. anachoretes* and *X. kryptos* were not possible due the lack of available COI sequences for these species. Moreover, the tree topology for UPGMA and Maximum Likelihood analysis was similar (Fig. 8).

Distribution. Including the new record from the San Francisco River, upper Bermejo River basin, Jujuy province and the previous records from the Paraná River, in Rosario (Santa Fe province), and in Chaco province (locality of *X. lombarderoi*), together with the records from the Paraguay River basin in Paraguay reported by Carvalho et al. (2017) and from the Pantanal in Brazil (Gimênes Junior and Rech 2022), the species exhibit a broad distribution in the Parana-Paraguay system. The new record of specimens from the San Francisco River, Upper Bermejo River basin, Jujuy province, is approximately 750 km in a straight line from the closest record in Tragadero River, Paraná River basin in Chaco Province (Fig. 9).

Ecological notes. Most of the records of this species are from the main channel of big rivers and were collected by trawl nets from the bottom of Parana River at 35–40 m depth (MACN 6791). The specimens from the San Francisco River (Fig. 10) were collected (1 to 4 m depth) using cast nets, and hand nets. Other informal captures made by anglers, supported by photographical evidence (see Suppl. material 1), include one record from the Paraná River in Misiones province (6 to 8 m depth), and another record in Misión, in the Bermejo River, Salta province (about 4 m depth). In both cases, captures were made using earthworm as bait (Julio Endler and Roberto Toval), see appendix 1. Although speculative, based on available records, this species seems to exhibit fossorial habits, regardless of the substrate depth.

Conservation status. The global conservation status of *Xyliphius barbatus* was evaluated in 2021, being considered as Near Threatened under criteria B2a by the IUCN

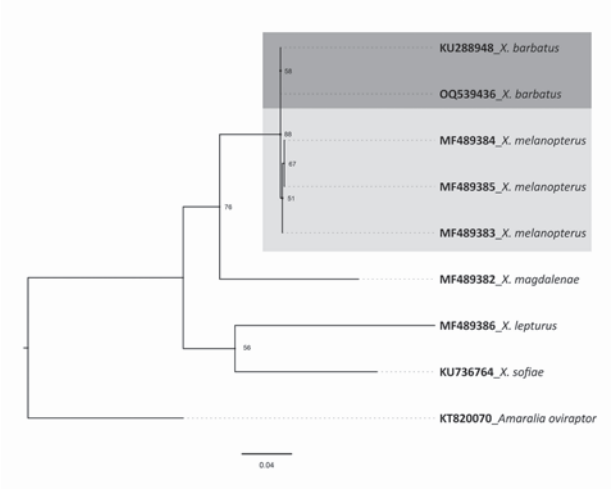

Figure 8. Maximum likelihood tree based on available COI sequences. Bootstrap values are shown next to each node. The boxes highlight the close relation between *X. barbatus* and *X. melanopterus*.

Red List of Threatened Species (Vera-Alcaraz 2023). When the species was evaluated, there was registers for only three specific locations at the Paraná and Paraguay rivers, with an estimate of the Extent Of Occurrence (EOO) of 21,366 to 143,190 km^2, and an estimate of Area Of Occupancy (AOO) between 48 km^2 and 1,999 km^2. According to these values, the species belongs to threat categories (criterion B2), but without meeting sufficient conditions to be considered as a species threatened with extinction. Since its evaluation, four new localities have been found, three in Mato Grosso de Sul, almost 600 km farther north from the nearest locality (Gimênes Junior and Rech 2022), and the locality reported in the present work, more than 650 km to the west of the nearest locality, which significantly expands the known distribution of the species. A preliminary exploration of the data indicates an EOO of about 600,000 km^2, which greatly exceeds previous estimates. A detailed reassessment of the species' threat status under IUCN criteria is necessary, which will likely result in a recategorization to Least Concern (LC).

However, evaluations for this species should be made with caution because it has relatively few records and inhabits areas that are difficult to sample. Additionally, there is no information available on its population structure or density throughout its range.

Comparative material examined. See Suppl. material 2.

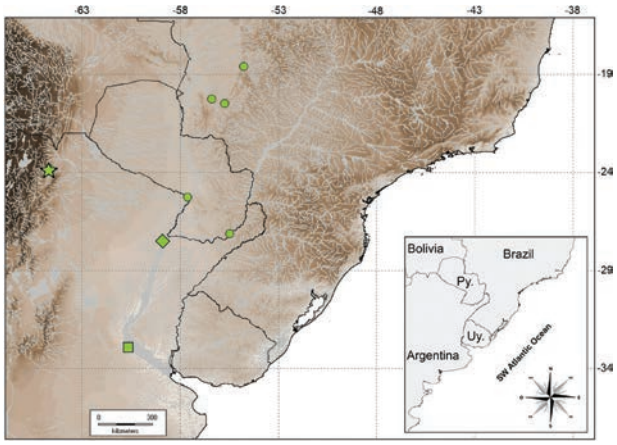

Figure 9. Geographical distribution of *Xyliphius barbatus*. Square: type locality of *Xyliphius barbatus*; rhombus: type locality of *Xyliphius lombarderoi*, Circules: other published records; star: new record from Bermejo River.

Figure 10. San Francisco River, Jujuy province at 23°50'27.08"S, 64°37'24.70"W.

Discussion

In this contribution we report the northwesternmost record of *Xyliphius barbatus* in Argentina, more than 750 km from the previously distribution record of the species. According to Carvalho et al. (2017) species of *Xyliphius* are commonly found in the main channel of large rivers and most records are restricted to the upland portions of Andean piedmont rivers. Conversely *X. barbatus* and *X. sofiae* occur in relatively lowland stretches. Records of these species and their presence in museum collections are scarce, mainly due to the depth at which they occur, making them difficult to sample. Additionally, their fossorial habits and mimetic coloration contribute to this scarcity. *Xyliphius barbatus* was also recorded in the Uruguay River basin by Loureiro et al. (2013), but this record is indeed a miss-identification of *Bunocephalus doriae* (Loureiro Pers. Comm., 2022). García (1992) includes *X. barbatus* in a list of species from the Paraná River basin in Misiones, but the accuracy of this record cannot be confirmed because the reference specimen is missing; in addition, this record is part of the environmental impact report and is not a formal publication. Nevertheless, the information provided by García (1992) was subsequently repeated (Liotta 2006; Calviño and Castello 2008; Rosso and Liotta 2021).

The scarcity of material has led to biased descriptions, since variations in morphology and meristic counts have not been considered, making it difficult to establish comparisons among species. This situation was also highlighted by Figuereido and Britto (2010) in the description of *Xyliphius anachoretes*; the authors considered that any inferences concerning the direction of change in the number of papillae from lower-lip is speculative and premature due to the absence of comparative material.

The specimens of *Xyliphius barbatus* collected in the upper Bermejo River represent the largest known batch for the species and one of the largest for the genus. Other numerous collections of aspredinids were made under special conditions. For example, when a river section was dried 70 exemplars of *Hoplomyzon sexpapilostoma* Taphorn and Marrero 1990 were collected, and when a dam was closed more than 100 exemplars of *Xyliphius* cf. *lepturus* were collected (Taphorn and Marrero 1990). This suggests the low efficacy of conventional fishing methods due to the distinct habitat use by members of the genus (Carvalho et al. 2017). The new *Xyliphius barbatus* material obtained has allowed us to make an accurate re-description for a species which, despite its wide distribution in the Paraná-Paraguay River basins, is poorly represented in fish collections in museums. The inclusion of new material for the re-description of *Xyliphius barbatus* has led to an objective assessment of inter-specific variation of characters useful for distinguishing the species from the remaining members of the genus. Among these characters, we found that the lower limit of papillae on lower lip ranges from 24 to 30 instead of the previously reported 28 to 30; the anal-fin rays now range from 5 to 8 instead of 6 to 8; the number of retrorse serrae along the posterior border of the pectoral-fin spine now ranges from 6 to 11 instead of 6 to 8; and the extension of lower limit range of vertebral count to 35.

From a genetic perspective, maximum likelihood analysis identified two main groups: one comprising *Xyliphius lepturus* and *X. sofiae*, and the other including *X. magdalenae*, *X. barbatus*, and *X. melanopterus*. This tree topology aligns with the morphological inferences made by Carvalho et al. (2017). They suggested that *X. sofiae* and *X. lepturus* shared enough features to support a sister-group relationship. These characters include snout morphology, lack of median notch, fifth ceratobranchial morphology, branchial apertures separation, anal-fin rays' modal number; and lateral line extension. Carvalho et al. (2017) also proposed a close relationship between *X. anachoretes*, *X. barbatus*, and *X. melanopterus* who share a relatively long and narrow fourth parapophysis and fifth parapophysis deflected anteriorly (*vs*. short and broad fourth parapophysis and fifth directed laterally in the remaining species of *Xyliphius*). Despite the lack of

X. anachoretes sequences, our ML tree recovers a very close relationship between *X. barbatus* and *X. melanopterus.* The low genetic distance between *Xyliphius barbatus* and *X. melanopterus* is noteworthy, since the distance to other species and between the other species is almost 50 times that value. In fact, one of the sequences of *X. melanopterus* (MF489383) differs only in 1 nucleotide from the *X. barbatus* sequence. It is evident that this comparison (based in one mitochondrial marker and a few sequences) is not enough to make inferences about the taxonomy of these two species (which have morphological differences, such as ray counts and coloration, and inhabit different basins), but it highlights the need for a complete morphological and molecular revision of the group in order to complement its definition and species diagnosis.

Additional similarities in the complex vertebra between *Xyliphius melanopterus* and *X. barbatus* were previously indicated by Carvalho et al. (2017); a narrow and long fourth parapophyses vertebra (observed in examined specimens), and anteriorly deflected fifth parapohyses, perpendicular in the examined *X. barbatus*. The same authors discuss the possible independent acquisition of gas bladder encapsulation in *Xyliphius* due to its absence in *X. magdalenae* and *X. kryptos* (see also Carvalho et al. 2018, Fig. 3), and the presence in the remaining congeners (with the polymorphism in *X. lepturus*). Our results also suggest the reduction of this feature in *X. magdalenae* instead of two independent events of gas bladder encapsulation (Fig. 6A). Nonetheless, these characters must be tested and optimized in a morphological analysis to support any conclusive hypothesis.

Neither Friel (1994) nor Cardoso (2008) included specimens of *Xyliphius barbatus* in their works. *Xyliphius barbatus* bears the eight synapomorphies proposed by the former author and the additional six synapomorphies for the subfamily Xyliphiinae proposed by the latter author: (1) lateral surface of frontal lacking orbital concavity; (2) antero-dorsal process of lacrimal-antorbital (first infraorbital) developed; (3) supra-preopercle present Friel (1994: Ch.28); (4) expanded proximal margin of posterior ceratohyal (Friel 1994: Ch.34); (5) more than 30 gill filaments on first epibranchial and ceratobranchial (Britto 2002: Ch. 126); (6) four to eight dorsal plus ventral procurrent rays on caudal-fin. We also observed the bony bulge on ventral surface lateral ethmoid possibly housing the olfactory bulb as suggested by Carvalho et al. (2017), as an additional synapomorphy of the genus.

Conclusions

In this work, an accurate re-description of *Xyliphius barbatus* based on osteological observations, morphometry, meristic counts and molecular data is provided. The distributional range of this species is widened to the upper Bermejo River basin in northwestern Argentina, more than 750 km in straight line from the previously known record of the species in the country. A provisional phylogenetic molecular hypothesis is provided in which the close relation with *X. melanopterus* is observed.

Acknowledgements

We extend our gratitude to Tiago Carvalho for reviewing the manuscript and making invaluable comments on *Xyliphius* species, which significantly enhanced the quality and accuracy of this paper. Pablo Pereyra (FML) made figures 4 and 6. We thank Gustavo Chiaramonte (MACN), James Anyelo Vanegas-Rios (MLP), Diego Nadalin (MLP), Germán Saigo (MG), Eugenia Montani (MG) and Adrián Giacchino (CFA, UMAI) for the support provided and for making available the ichthyological collections of the respective institutions. GET and GA thank Diego Delgado for help in sampling trips. Julio Endler and Roberto Toval, for the photograph of specimens (Suppl. material 1). We thank Jorgelina Brasca for english review and Florencia Brancolini, Pablo Calviño, Miguel Angel Cortés Hernández for valuable comments. Felipe Alonso and Marcos Mirande for permanent support. This manuscript benefited from the comments and revisions of Nicolas Hubert, Lucas Medeiros, and two anonymous reviewers

References

Aguilera G, Terán GE, Alonso F, Mirande JM (2016) First record of the banjo catfish *Bunocephalus doriae* Boulenger, 1902 (Siluriformes: Aspredinidae) in the Bermejo River Basin, Salta, Argentina. Check List 12(3): 1888. https://doi.org/10.15560/12.3.1888

Aguilera G, Terán GE, Mirande JM, Alonso F, Rometsch S, Meyer A, Torres-Dowdall J (2019) Molecular and morphological convergence to sulfide-tolerant fishes in a new species of *Jenynsia* (Cyprinodontiformes: Anablepidae), the first extremophile member of the family. PLoS ONE 14(7): e0218810. https://doi.org/10.1371/journal.pone.0218810

Aguilera G, Terán GE, Mirande JM, Alonso F, Chumacero GM, Cardoso Y, Bogan S, Faustino-Fuster DR (2022) An integrative approach method reveals the presence of a previously unreported species of *Imparfinis* Eigenmann and Norris 1900 (Siluriformes: Heptapteridae) in Argentina. Journal of Fish Biology 101(5): 1248–1261. https://doi.org/10.1111/jfb.15197

Aljanabi SM, Martinez I (1997) Universal and rapid salt-extraction of high quality genomic DNA for PCR-based techniques. Nucleic Acids Research 25(22): 4692–4693. https://doi.org/10.1093/nar/25.22.4692

Alonso F, Terán GE, Aguilera G, Mirande JM (2016) First record of *Hypostomus boulengeri* (Siluriformes: Loricariidae) from Bermejo River basin. Revista Del Museo Argentino de Ciencias Naturales. Nueva Serie 18(1): 85–88. https://doi.org/10.22179/REVMACN.18.440

Alonso F, Terán GE, Calviño P, García I, Cardoso Y, García G (2018) An endangered new species of seasonal killifish of the genus *Austrolebias* (cyprinodontiformes: Aplocheiloidei) from the Bermejo

River basin in the western chacoan region. PLoS ONE 13(5): e0196261. https://doi.org/10.1371/journal.pone.0196261

Alonso de Arámburu AS, Arámburu RH (1962) Una nueva especie de *Xyliphius* de la Argentina (Siluriformes, Bunocephalidae). Physis (Buenos Aires) 23(65): 219–222.

Britto MR (2002) Análise filogenética da ordem Siluriformes com ênfase nas relações da superfamília Loricarioidea (Teleostei: Ostariophysi). Tese de doutorado, Universidade de São Paulo, São Paulo. 512 pp.

Calviño PA, Castello HP (2008) Sobre um bagre ciego del río Paraná medio, *Xyliphius barbatus* Arámburu y Arámburu, 1962 (Siluriformes: Aspredinidae) una nueva cita en la Argentina y comentarios adicionales. Las Ciencias. Revista de la Universidad Maimónides 1: 55–59.

Cardoso AR (2008) Filogenia da família Aspredinidae Adams, 1854 e revisão taxonômica de Bunocephalinae Eigenmann & Eigenmann, 1888 (Teleostei: Siluriformes: Aspredinidae)). Tese de doutorado. Pontifícia Universidade Católica do Rio Grande do Sul. 259 pp.

Cardoso AR (2010) *Bunocephalus erondinae*, a new species of banjo catfish from southern brazil (siluriformes: Aspredinidae). Neotropical Ichthyology 8(3): 607–613. https://doi.org/10.1590/S1679-62252010000300005

Carvalho TP, Reis RE, Sabaj MH (2017) Description of a new blind and rare species of *Xyliphius* (Siluriformes: Aspredinidae) from the amazon basin using high-resolution computed tomography. Copeia 105(1): 14–28. https://doi.org/10.1643/CI-16-456

Carvalho TP, Arce MH, Reis RE, Sabaj Pérez MH (2018) Molecular phylogeny of banjo catfishes (Ostaryophisi: Siluriformes: Aspredinidae): a continental radiation in South American freshwaters. Molecular Phylogenetics and Evolution 127: 459–467. https://doi.org/10.1016/j.ympev.2018.04.039

Casciotta JR, Almirón AE (2004) *Astyanax chico* sp. n. a new species from the río San Francisco basin, northwest of Argentina (Teleostei: Characiformes: Characidae). Zoologische Abhandlungen / Staatliches Museum fur Tierkunde in Dresden 54: 11–17.

Dahdul WM, Lundberg JG, Midford PE, Balhoff JP, Lapp H, Vision TJ, Haendel MA, Westerfield M, Mabee PM (2010) The teleost anatomy ontology: Anatomical representation for the genomics age. Systematic Biology 59(4): 369–383. https://doi.org/10.1093/sysbio/syq013

Díaz J, Villanova GV, Brancolini F, del Pazo F, Posner VM, Grimberg A, Arranz SE (2016) First DNA barcode reference library for the identification of south American freshwater fish from the lower Paraná River. PLoS ONE 11(7): e0157419. https://doi.org/10.1371/journal.pone.0157419

Eigenmann CH (1912) Some results from an ichthyological reconnaissance of Colombia, South America. Part I (Contrib. Zool. Lab. Ind. Univ. No. 127.). Indiana University Studies 16(8): 1–27.

Figueiredo CA, Britto MR (2010) A new species of *Xyliphius*, a rarely sampled banjo catfish (Siluriformes: Aspredinidae) from the rio Tocantins-Araguaia system. Neotropical Ichthyology 8(1): 105–112. https://doi.org/10.1590/S1679-62252010000100013

Fricke R, Eschmeyer WN, Fong JD (2023a) Eschmeyer's catalog of fishes: genera/species by family/subfamily. California Academy of Sciences, San Francisco, CA. http://researcharchive.calacademy.org/research/ichthyology/catalog/SpeciesByFamily.asp [accessed 21March 2023].

Fricke R, Eschmeyer WN Van der Laan R (Eds) (2023b) Eschmeyer's catalog of fishes: genera, species, references. California Academy of Sciences, San Francisco, CA. http://researcharchive.calacademy.org/research/ichthyology/catalog/fishcatmain.asp [accessed 21March 2023].

Friel J (1994) A phylogenetic study of the Neotropical banjo catfishes (Teleostei: Siluriformes: Aspredinidae) Ph.D. thesis, Duke University, North Carolina, United States of America.

Friel J (1995) *Acanthobunocephalus nicoi*, a new genus and species of miniature banjo catfish from the upper Orinoco and Casiquiare Rivers, Venezuela (Siluriformes: Aspredinidae). Ichthyological Exploration of Freshwaters 6(1): 89–95.

García JO (1992) Lista de peces de la cuenca del alto Paraná misionero. Programa de Estudios Ecológicos Regionales, Universidad Nacional de Misiones. Serie de Informes Técnicos 1(1): 1–15.

Gimênes Junior H, Rech R (org.) (2022) Guia ilustrado dos peixes do Pantanal e entorno. MS: Julien Design Campo Grande, Brazil.

Ivanova N, Zemlak TS, Hanner RH, Hebert PDN (2007) Universal primer cocktails for fish DNA barcoding. Molecular Ecology Notes 7(4): 544–548. https://doi.org/10.1111/j.1471-8286.2007.01748.x

Liotta J (2006) Distribución geográfica de los peces de aguas continentales de la República Argentina. Primera edición de la Secr. Agric, Gan, Pesca y Alimentos, año 2005. ProBiota, FCNyM, UNLP, La Plata, Argentina. Serie Documentos (3): 654.

Littmann MW, Azpelicueta MDLM, Vanegas-Rios JA, Lundberg JG (2015) Holotype-based validation, redescription and continental-scale range extension of the South American catfish species *Hypophthalmus oremaculatus* Nani & Fuster, 1947, with additional information on *Hypophthalmus edentatus* Spix & Agassiz, 1829 (Siluriformes, Pimelodidae). Proceedings. Academy of Natural Sciences of Philadelphia 164(1): 159–176. https://doi.org/10.1635/053.164.0115

Loureiro M, Zarucki M, González I, Vidal N, Fabiano G (2013) Peces continentales. In: Especies prioritarias para la conservación en Uruguay. Vertebrados, moluscos continentales y plantas vasculares. Soutullo A, Clavijo, C, and Martínez-Lanfranco, J.A (Eds) SNAP/DINAMA/MVOTMA y DiCyT/MEC, Montevideo, Uruguay, 91–112

Mirande JM, Aguilera G, Azpelicueta MDLM (2004a) A new genus and species of small characid (Ostariophysi, Characidae) from the upper río Bermejo basin, northwestern Argentina. Revue Suisse de Zoologie 111(4): 715–728. https://doi.org/10.5962/bhl.part.80265

Mirande JM, Aguilera G, Azpelicueta MDLM (2004b) A new species of *Astyanax* (Characiformes, Characidae) from the upper río Bermejo basin, Salta, Argentina. Revue Suisse de Zoologie 111(1): 213–223. https://doi.org/10.5962/bhl.part.80235

Mirande JM, Aguilera G, Azpelicueta MDLM (2006) *Astyanax endy* (Characiformes: Characidae), a new fish species from the upper Río Bermejo basin, northwestern Argentina. Zootaxa 1286(1): 57-6. https://doi.org/10.11646/zootaxa.1286.1.6

Mungall CJ, Torniai C, Gkoutos GV, Lewis SE, Haendel MA (2012) Uberon, an integrative multi-species anatomy ontology. Genome Biology 13(1): R5. https://doi.org/10.1186/gb-2012-13-1-r5

Orcés VG (1962) Dos nuevos peces del género *Xyliphius*. Ciencia y Naturaleza (Quito) 5(2): 50–54.

Risso FJJ, de Risso ENP (1964) Hallazgo de una nueva especie de *Xyliphius* en el Paraná (Pisces - Aspredinidae). Notas del Museo de Ciencias Naturales del Chaco 1: 11–16.

Rosso JJ, Liotta J (2021) Peces Continentales. In: Inventario Biológico Argentino.Vertebrados. Bauni, V, Bertonatti, C, and Giacchino,

A (Eds) Fundación de Historia Natural Félix de Azara, Ciudad Autónoma de Buenos Aires, Argentina, 135–198.

Tamura K, Stecher G, Kumar S (2021) MEGA11: Molecular Evolutionary Genetics Analysis Version 11. Molecular Biology and Evolution 38(7): 3022–3027. https://doi.org/10.1093/molbev/msab120

Taphorn DC, Marrero C (1990) *Hoplomyzon sexpapilostoma*, a new species of Venezuelan catfish (Pisces, Aspredinidae): With comments on the Hoplomyzontini. Fieldiana. Zoology 61: 1–9. https://doi.org/10.5962/bhl.title.3099 [New Series]

Taylor WR, Van Dyke GC (1985) Revised procedure for staining and clearing small fishes and other vertebrates for bone and cartilage study. Cybium 9: 107–119.

Terán GE, Alonso F, Aguilera G, Mirande JM (2016b) First record of *Aphyocharax anisitsi* Eigenmann & Kennedy, 1903 in the upper Bermejo River basin, northwestern Argentina. Ichthyological Contributions of PecesCriollos 44: 1–4.

Terán GE, Alonso F, Aguilera G, Mirande JM (2016c) Range extension of *Hypostomus cochliodon* Kner, 1854 (Siluriformes: Loricariidae) in Bermejo River, Salta, Argentina. Check List 12(4): 1953. https://doi.org/10.15560/12.4.1953

Terán GE, Jarduli LR, Alonso F, Mirande JM, Shibatta OA (2016a) *Microglanis nigrolineatus*, a new species from northwestern Argentina (Ostariophysi: Pseudopimelodidae). Ichthyological Exploration of Freshwaters 27(3): 193–202.

Terán GE, Ballen GA, Alonso F, Aguilera G, Mirande JM (2019) A new species of *Farlowella* (Siluriformes: Loricariidae) from the upper Bermejo River, La Plata River basin, northwestern Argentina. Neotropical Ichthyology 17(2): 1–7. https://doi.org/10.1590/1982-0224-20180114

Vanegas-Ríos JA, Britzke R, Mirande JM (2019) Geographic variation of *Moenkhausia bonita* (Characiformes: Characidae) in the rio de la Plata basin, with distributional comments on M. intermedia. Neotropical Ichthyology 17(1): e170123. https://doi.org/10.1590/1982-0224-20170123

Vera-Alcaraz HS (2023) *Xyliphius barbatus*. The IUCN Red List of Threatened Species 2023: e.T176402183A176402187. https://doi.org/10.2305/IUCN.UK.2023-1.RLTS.T176402183A176402187.en [Accessed on 06 June 2024]

Ward RD, Zemlak TS, Innes BH, Last PR, Hebert PDN (2005) DNA barcoding Australia's fish species. Philosophical Transactions of the Royal Society of London. Series B, Biological Sciences 360(1462): 1847–1857. https://doi.org/10.1098/rstb.2005.1716

Supplementary material 1

Informal records by anglers, with photograph evidence. Speciemens colleced with earthworm bait

Authors: Guillermo E. Terán, Alejandro Méndez-López, Mauricio F. Benitez, Wilson S. Serra, Sergio Bogan, Gastón Aguilera

Data type: docx

Explanation note: The information provided here represent records of *Xyliphius barbatus* capture by anglers in two localities algon the Paraná river, also including a map of these localities.

Link: https://doi.org/10.3897/zse.100.121396.suppl1

Supplementary material 2

Comparative material examined

Authors: Guillermo E. Terán, Alejandro Méndez-López, Mauricio F. Benitez, Wilson S. Serra, Sergio Bogan, Gastón Aguilera

Data type: docx

Explanation note: In this file all reference material consulted in this work is listed.

Link: https://doi.org/10.3897/zse.100.121396.suppl2

Zoosyst. Evol. 100 (3) 2024, 1099–1106 | DOI 10.3897/zse.100.127612

PENSOFT

für Natur MUSEUM FÜR NATURKUNDE BERLIN

First record of the genus *Falconina* (Araneae, Corinnidae) from Mexico, with a description of a new species and observations on its interactions with ants

Guillermo Ibarra-Núñez[1], Linda Marín[2]

1 *El Colegio de la Frontera, Sur. Carretera Antiguo Aeropuerto km 2.5, Tapachula, Chiapas, C: P. 30700, Mexico*

2 *Instituto de Investigaciones Forestales, Universidad Veracruzana, Parque El Haya, Carretera Antigua a Coatepec, Xalapa, Veracruz, C. P 91070, Mexico*

https://zoobank.org/C271E63A-0E30-452A-855A-BF028E691880

Corresponding authors: Linda Marín (lemarinsky@gmail.com); Guillermo Ibarra-Núñez (gibarra@ecosur.mx)

Academic editor: Danilo Harms ♦ **Received** 15 May 2024 ♦ **Accepted** 13 July 2024 ♦ **Published** 1 August 2024

Abstract

Falconina cafetera **sp. nov.** (Araneae, Corinnidae) is described based on specimens of both sexes. Specimens were collected in shaded coffee agro-ecosystems and in a suburban cacao orchard in Chiapas, Mexico. This new species is the first *Falconina* recorded from Mexico and the northernmost species of the genus in continental America, with the exception of *F. gracilis* (Keyserling, 1891) introduced to the USA and Cuba. *F. cafetera* **sp. nov.** differs from all other *Falconina* species by having most of its opisthosoma light-colored with some dark patches and by the characteristics of the male palp and female epigynum. Observations are included about one sclerite found in the male palp of this species, not mentioned for other species in this genus. The key of *Falconina* species by García and Bonaldo (2023) is modified to include this species. Furthermore, field observations and laboratory rearing of juveniles indicate that *F. cafetera* **sp. nov.** spiders are able to feed on ants.

Key Words

Coffee agroecosystems, Chiapas, North America, male palpal structure

Introduction

The taxonomic history of the genus *Falconina* Brignoli, 1985 (Corinnidae) has been summarized by García and Bonaldo (2023) in a review of this genus. Currently, *Falconina* includes 10 species: nine from South America and one from Central America (World Spider Catalog 2024). It should be noted that *F. gracilis* (Keyserling, 1891), originally recorded from South America, has recently been introduced into the United States of America (Valle et al. 2013; Ubick and Richman 2017) and Cuba (García and Bonaldo 2023). Here we describe *Falconina cafetera* sp. nov., the first species of this genus recorded from Mexico. We include observations on its palpal morphology, including the origin of one bulbar sclerite, not mentioned previously for other species in this genus, and present observations on interactions of this species with ants. Moreover, we propose a modification to the key of *Falconina* species by García and Bonaldo (2023) to include *F. cafetera* sp. nov.

Methods

The examined specimens are deposited in the following institutions (acronyms and curators in parenthesis): American Museum of Natural History, New York, USA (AMNH, L. Prendini); Colección Nacional de Arácnidos, Instituto de Biología, UNAM, México (CNAN, E. González-Santillán); Colección de Arácnidos del Sureste de México, El Colegio de la Frontera Sur (ECOSUR), Tapachula, Chiapas, México (ECOTAAR, G. Ibarra-Núñez); Museum of Comparative Zoology, Cambridge,

MA., USA (MCZ, G. Giribet). Specimens were measured and photographed with an Olympus SZX16 microscope provided with an ocular reticle and a Sony SLT-A58 digital camera. All measurements are in millimeters (mm). Leg measurements are noted as total length (femur, patella, tibia, metatarsus, and tarsus). Images from multiple focal planes were assembled with ZERENE STACKER (version 1.04) image stacking software. Drawings were made with INKSCAPE (version 1.3) drawing software. Color descriptions are for live specimens, with notes on color changes in ethanol. Male palp was expanded in KOH 10% for 15 minutes, then transferred to distilled water, and after expansion, returned to ethanol 80%. Female genitalia were dissected and cleaned with a solution made with an eye lens cleaner (half a tablet of AMO Ultrazyme with Subtilisin A, diluted in 1 ml of distilled water) and cleared with methyl salicylate. Spination follows Petrunkevitch (1925). The format of descriptions follows García and Bonaldo (2023) with modifications.

Abbreviations

Female structures*: AEP**, anterior epigynal plate; **CD**, copulatory duct; **CO**, copulatory opening; **ExPVP**, extension of posterior vulvar plate; **FD**, fertilization duct; **PmEP**, posterior margin of the epigynal plate; **PVP**, posterior vulvar plate; **S1**, primary spermatheca; **S2**, secondary spermatheca. ***Male structures, **AS**, apical spur of RTA; **C**, conductor; **Cb**, cymbium; **CRP**, cymbial retrolateral basal process; **E**, embolus; **EB**, embolar base; **H**, hematodocha; **ML**, median lobe of RTA; **Pe**, petiole; **PTA**, prolateral tibial apophysis; **RPE**, retrolateral process of embolar base; **RTA**, retrolateral tibial apophysis; **Sp**, spermophore; **ST**, subtegulum; **T**, tegulum; **TP**, tegular process; **TPlss**, less sclerotized stripe on tegular process; **VL**, ventral lobe of RTA; **VPE**, ventral process of embolar base.

Results

Taxonomy

Family Corinnidae Karsch, 1880
Genus *Falconina* Brignoli, 1985

***Falconina cafetera* sp. nov.**

https://zoobank.org/D7235B0F-5DD5-46A8-8873-BF1910BABA9F

Figs 1–23

Type material. Mexico • 1 ♂ ***holotype***; Chiapas, Municipio de Tapachula, Finca Santa Anita; 15.1579°N, 92.3438°W; 980 m a.s.l.; 24 Oct. 2012; L. Marín leg.; in soil of coffee orchard, kept alive, became adult 7 Dec. 2012 (ECOTAAR-011484).

Paratypes. Mexico • 1 ♀ (***allotype***); Chiapas, Municipio de Tapachula, Finca Irlanda; 15.1697°N, 92.3400°W; 1070 m a.s.l.; 20 Jul. 2012; L. Marín leg.; in soil of coffee orchard (ECOTAAR-011485) • 1 ♂; same data as for holotype; became adult 10 Dec. 2012 (CNAN) • 1 ♂; same data as for holotype; became adult 11 Dec. 2012 (MCZ) • 1 ♂; same data as for holotype; became adult 12 Dec. 2012 (AMNH) • 1 ♂; same data as for holotype; became adult 14 Dec. 2012 (ECOTAAR-11489) • 1 ♀; same data as for holotype; 15.1554°N, 92.3403°W; 830 m a.s.l.; 31 Jul. 2011; (CNAN) • 1 ♀; same data as for preceding; (ECOTAAR-11491) • 1 ♂; same data as for allotype; (ECOTAAR-11492) • 1 ♂; Chiapas, Municipio de Tapachula, Camino a Raymundo Enríquez; 14.8738°N, 92.3096°W; 100 m a.s.l.; 15 Oct. 2015; E. Chamé-Vázquez leg.; in suburban cacao orchard (ECOTAAR-011498).

Etymology. The specific name is an arbitrary combination of letters derived from the Spanish word for coffee plantation, "finca cafetalera," where this species was first collected.

Differential diagnosis. Males and females differ from all other species by having most of their opisthosoma light in color with some dark patches (Figs 1–4, 21), while in all other species it is mostly dark with some light patches. Males of *Falconina cafetera* sp. nov. are similar to *F. albomaculosa* by sharing a long apical spur, by having only two lobes (ventral and median) on the retrolateral tibial apophysis, and by having a lighter, less sclerotized, longitudinal stripe (TPlss) on the sclerotized tegular process (Figs 5–16; figs 13A, 14A in García and Bonaldo 2023). Males of *F. cafetera* sp. nov. differ from *F. albomaculosa* by having a prominent prolateral tibial apophysis (small in *F. albomaculosa*), a relatively longer tibia, with the length of the prolateral margin of the tibia (including PTA) about two thirds the cymbium length on its prolateral margin (about half the cymbium length in *F. albomaculosa*), a massive cymbial retrolateral basal process (smaller in *F. albomaculosa*) (Fig. 6; fig. 13A in García and Bonaldo 2023); the apical spur slender (thicker in *F. albomaculosa*); and the median lobe of the RTA subtriangular (squared in *F. albomaculosa*) (Fig. 7; fig. 13B in García and Bonaldo 2023). The epigynum of *F. cafetera* sp. nov. females is similar to that of *F. albomaculosa* in having the posterior margin of the anterior epigynal plate procurved and close to the posterior margin of epigynum, PVP slightly projected posteriorly (Fig. 17; fig. 14C in García and Bonaldo 2023), and dorsally by having copulatory ducts in heavily sclerotized, wide chambers (Fig. 18; fig. 14D in García and Bonaldo 2023); *F. cafetera* sp. nov. females differ from *F. albomaculosa* in having the posterior margin of the anterior epigynal plate with a shallow notch (notch pronounced in *F. albomaculosa*), the posterior margin of the posterior vulvar plate almost straight (procurved in *F. albomaculosa*) (Fig. 17; fig. 14C in García and Bonaldo 2023), in dorsal view the posterior vulvar plate wider than long (about as wide as long in *F. albomaculosa*), with its anterior margin straight (procurved in *F. albomaculosa*), primary spermathecae separated by about four times their own diameter (separated by less than three diameters in *F. albomaculosa*), and by having secondary spermathecae inserted anteriorly in relation to primary spermathecae (secondary spermathecae inserted medially in *F. albomaculosa*) (Fig. 18; fig. 14D in García and Bonaldo 2023).

Figures 1–4. Habitus of *Falconina cafetera* sp. nov. **1, 2.** male; **3, 4.** female; **1, 3.** dorsal view; **2, 4.** ventral view. Scale bars: 1 mm (**1–4**).

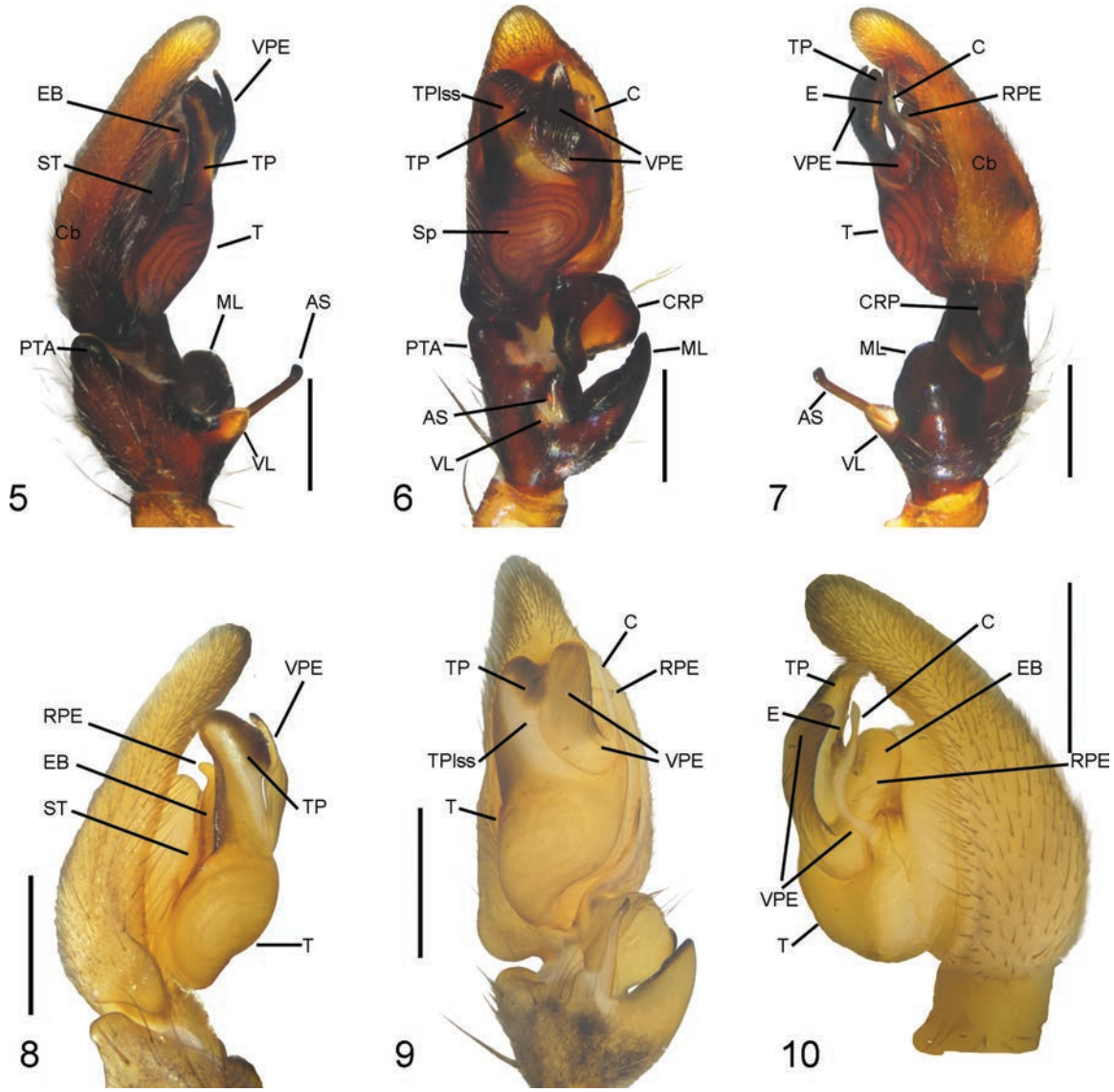

Figures 5–10. Male palp of *Falconina cafetera* sp. nov. **5–7.** Field-collected specimen (ECOTAAR-011492); **8–10.** Laboratory-reared specimen recently molted (ECOTAAR-011489); **5, 8**. Prolateral view; **6, 9.** Ventral view; **7, 10.** Retrolateral view; **AS**—apical spur of RTA; **C**—conductor; **Cb**—cymbium; **CRP**—cymbial retrolateral basal process; **E**—embolus; **EB**—embolar base; **ML**—median lobe of RTA; **PTA**—prolateral tibial apophysis; **RPE**—retrolateral process of embolar base; **Sp**—spermophore; **ST**—subtegulum; **T**—tegulum; **TP**—tegular process; **VL**—ventral lobe of RTA; **VPE**—ventral process of embolar base. Scale bars: 0.5 mm (**5–10**).

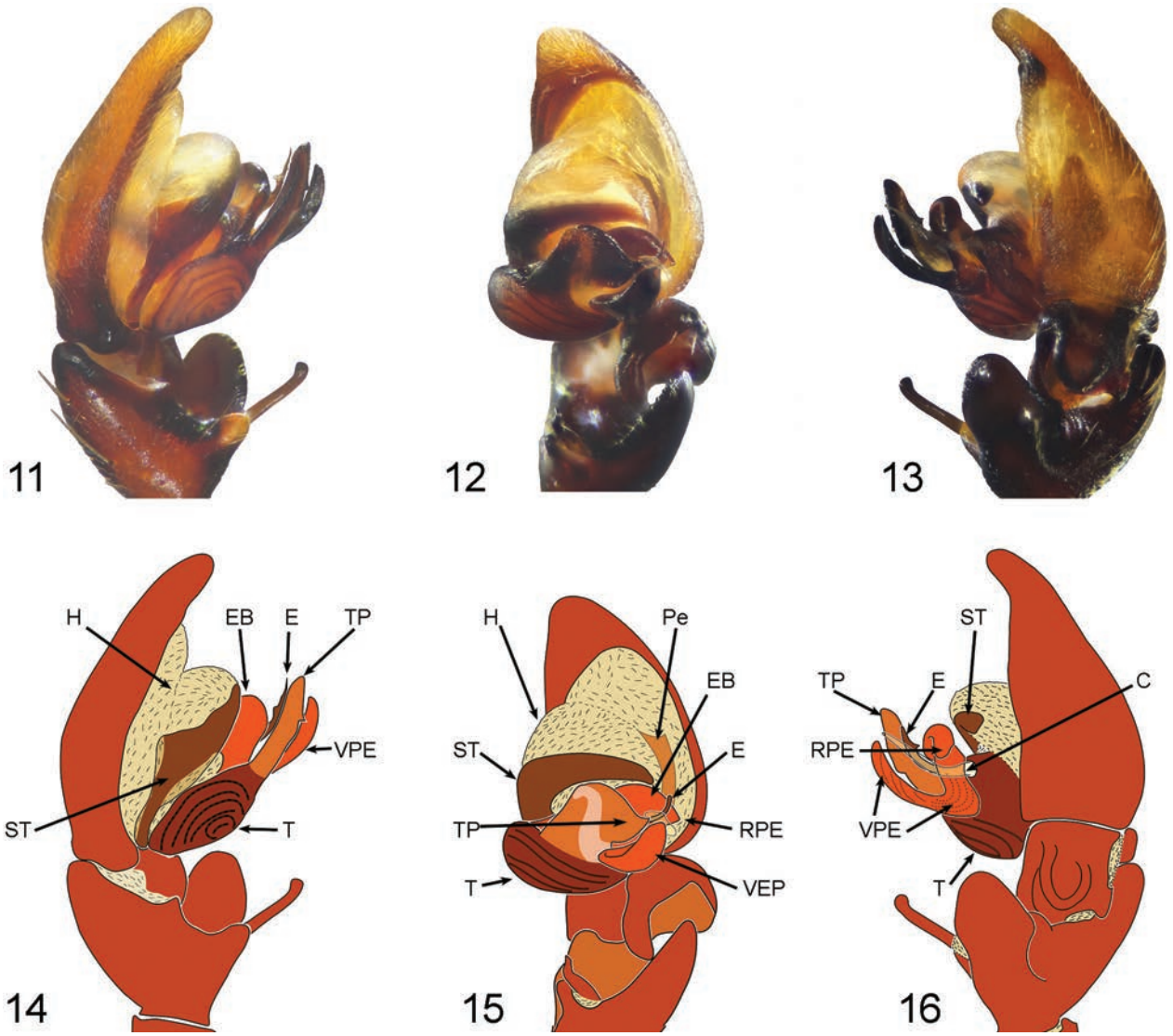

Figures 11–16. Expanded male palp of *Falconina cafetera* sp. nov. **11–13**. Field-collected specimen (ECOTAAR-011492); **14–16.** Drawings based on figures **11–13**; **11, 14.** Prolateral view; **12, 15.** Ventral view; **13, 16.** Retrolateral view; **C**—conductor; **E**—embolus; **EB**—embolar base; **H**—hematodocha; **Pe**—petiole; **RPE**—retrolateral process of embolar base; **ST**—subtegulum; **T**—tegulum; **TP**—tegular process; **VPE**—ventral process of embolar base.

Description. Male (holotype). ***Color pattern and habitus.*** Carapace dark brown, pars thoracica lighter, eyes surrounded by narrow black rings; chelicerae dark brown, labium and endites brown, distal margins of endites white; sternum light brown with brown margin; palpal trochanter to patella light brown, tibia dark brown, cymbium brown; legs: coxa, trochanter yellowish brown, femur to metatarsus dark brown, with dorsal lighter patches, tarsus light brown; opisthosoma orange (light yellow in ethanol), with two small oval black patches at the sides of anterior half, a thick, transversal black band at posterior half, with a thin, transverse orange (light-yellow in ethanol) line near its posterior margin, the thick black band continues to the sides, narrowing, posteriorly directed, surrounding the spinnerets, dorsum with an orange (yellow in ethanol), narrow, coriaceous dorsal scutum on the anterior two thirds (Figs 1–2, 21). Carapace mostly glabrous, with very short, sparse, translucid setae, with a few sparse long setae on the ocular area; fovea longitudinal; chelicera geniculate, with prominent cheliceral boss, anterior face with abundant small tubercles supporting small erect setae and a few sparse long setae, promargin of cheliceral furrow with rows of long bristles, with three teeth (second tooth largest), retromargin with four teeth; sternum with scattered small tubercles and a few long, scattered setae. Dorsum of opisthosoma covered with abundant, small, translucid setae, darker over and around the black patches, with scattered long setae, venter with abundant, small, gray setae (Figs 1–2). Metatarsi III–IV with dense preening brush. ***Measurements.*** Total length 5.94; carapace length 2.81, width 2.25, sternum length 1.45, width 1.40; opisthosoma length 3.05, width 2.16. Anterior, posterior eye rows procurved; anterior median eyes largest, separated by a little less their diameter; anterior eye row width 0.76, posterior eye row width 0.90; median ocular quadrangle length 0.40, anterior width

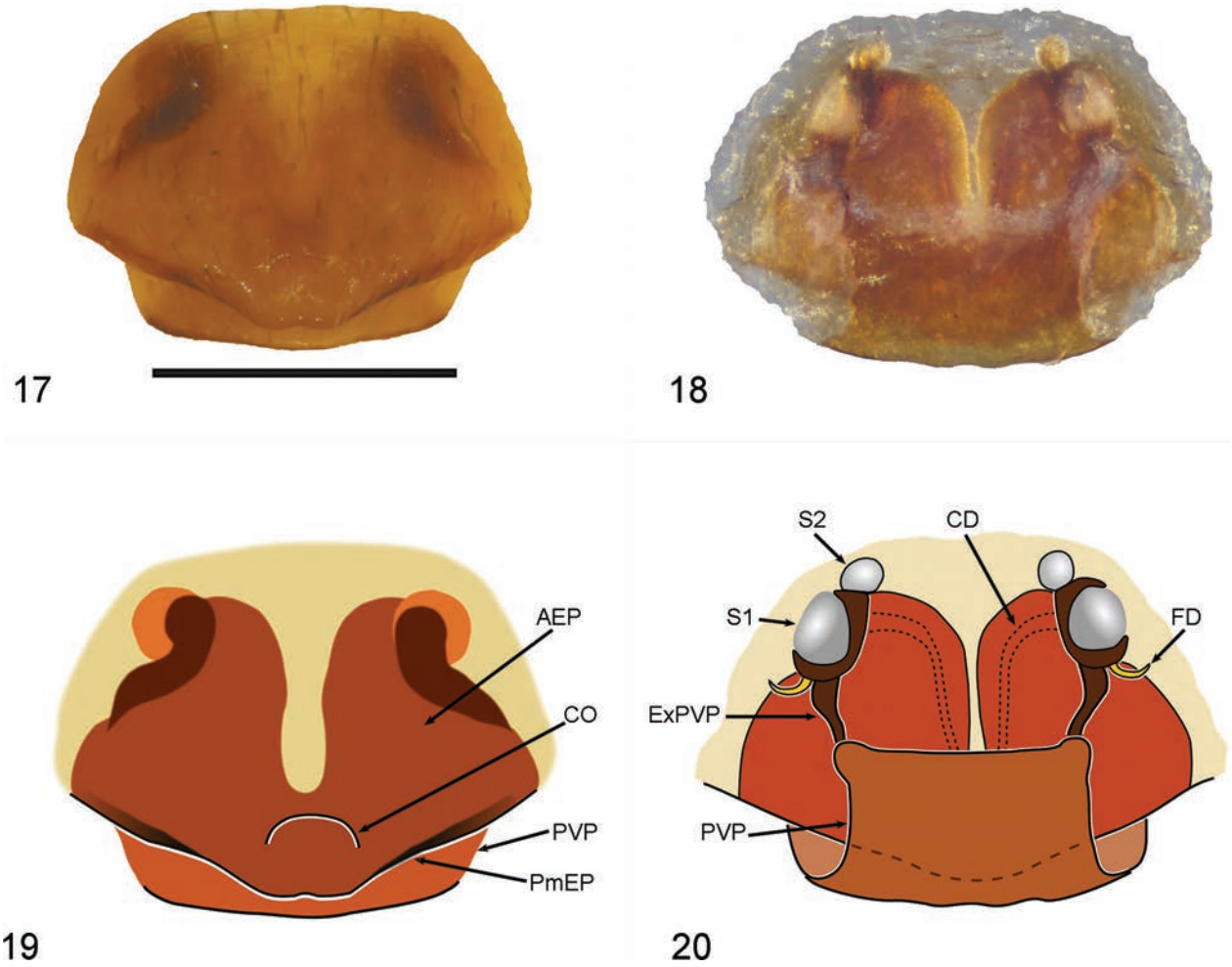

Figures 17–20. Female epigynum of *Falconina cafetera* sp. nov. **17–18.** Field-collected specimen (ECOTAAR-011491); **19–20.** Drawings based on figures **17–18**; **17, 19.** Ventral view; **18, 20.** Dorsal view (cleared); **AEP**—anterior epigynal plate; **CD**—copulatory duct; **CO**—copulatory opening; **ExPVP**—extension of posterior vulvar plate; **FD**—fertilization duct; **PmEP**—posterior margin of the epigynal plate; **PVP**—posterior vulvar plate; **S1**—primary spermatheca; **S2**—secondary spermatheca. Scale bar: 0.5 mm (**17**).

0.46, posterior width 0.44; clypeus height 0.28. ***Legs measurements*.** I total 9.04 (femur 2.40/ patella 1.00/ tibia 2.20/ metatarsus 1.84/ tarsus 1.60); II 8.04 (2.32/ 0.92/ 1.84/ 1.76/ 1.20); III 7.57 (2.06/ 0.76/ 1.55/ 1.84/ 1.36); IV 9.97 (2.60/ 0.91/ 2.12/ 2.76/ 1.58). Leg formula 4123. ***Legs spination*.** Femora: I d1-1, p0-0-1; II d1-1, p0-0-2; III–IV d1-1-1, p0-1-1, r0-0-1; tibiae: I v4-4-4; II v4-4, p1; III–IV d0-0-1, p1-0-1, r1-0-1, v2-2-2; metatarsi: I–II v2-2; III–IV p1-1, r1-1, v2-2-2. ***Male Palp*.** Tibia heavily sclerotized, conoid, wider than long, its length about two thirds the cymbium length, with a rounded, prolateral apophysis (PTA) conspicuous, distally oriented, RTA bilobed, with a massive, subtriangular, median lobe (ML) projected retrodistally, concave on its inner face, and with a smaller ventral lobe (VL) with conical base, its retrolateral face membranous, where arises a long, straight, thin apical spur (AS) pointing ventrodistally, its tip slightly sinuous (Figs 5–7). Cymbium (Cb) about twice as long as wide, with a heavily sclerotized, wide, squared, prolateral basal process, having a shallow grove facing the PTA (Figs 5–6, 8–9); with a massive, heavily sclerotized cymbial retrolateral basal process (CRP) much extended proximally, opposite to ML, subquadrate, somewhat ear-like in ventral view (Figs 6, 7, 9), its dorsal face convex, its ventral face concave (Figs 6, 9). Bulb structures heavily sclerotized, subtegulum (ST) long, partially visible on prolateral view (Figs 5, 8), completely visible in the expanded bulb (Figs 11–16), in which is also visible the petiole (Pe), as a slightly sclerotized rectangular plate at the dorsal part of alveolus, united to the basal hematodocha (Fig. 12, 15). The spermophore (Sp) occupies the basal half of bulb; tegulum (T) convex, occupying almost all width of alveolus, narrowed on its proximal margin (Figs 5–10), prolonged distally as a prolateral, laminar tegular process (TP), longer than wide, subrectangular, slightly convex, with a longitudinal, lighter, less sclerotized stripe (TPlss), its distal prolateral corner rounded, its distal retrolateral corner pointed, its retrolateral margin (next to the less sclerotized stripe) hidden by the ventral process of the embolar base (VPE) (Figs 5, 6, 8, 9); embolar base (EB) rounded, heavily sclerotized, arising on the dorsal, distal tegulum, in ventral view hidden by the tegular process, in prolateral view between subtegulum and tegular process (Figs 5, 8); embolus (E) starting

Figures 21–23. Live specimens of *Falconina cafetera* sp. nov. **21.** Pair of *Falconina cafetera* sp. nov. collected to be used in feeding trials, showing color pattern of living specimens; **22, 23.** Male and female living specimens of *Falconina cafetera* sp. nov. each feeding on an *Azteca sericeasur* ant; **22.** Male; **23.** Female.

on the ventral side of EB, spine-like, angled at mid length (Figs 7, 10, 11–16), embolar base with two processes beyond embolus, a short, blunt retrolateral process (RPE) (Figs 6, 7, 9, 10, 12, 13, 15, 16), and a greatly developed U-shaped ventral process (VPE) issuing from EB, proximally directed, overlapping the distal-retrolateral area of the tegulum, then making an U-twist (Figs 7, 10, 13, 16), widening to form a heavily sclerotized, convex, subtriangular plate distally oriented, adjacent and overlapping the retrolateral margin of TP, in ventral view hiding the E and part of the EB (Figs 5–16); conductor (C) membranous, slender, sinuous, arising from the distal, retrolateral corner of T, flattened and slightly widened distally, ending in front of embolus tip (Figs 6, 7, 9, 10, 13, 16).

Female (allotype). Color pattern as in male, except palpal tibia, tarsus brown, tip of tarsi light brown; opisthosoma without dorsal scutum, posterior thick transversal black band with two middle, orange (light yellow in ethanol), threadlike chevrons (Figs 3–4). ***Measurements*.** Total length 5.32; carapace length 2.40, width 1.90, sternum length 1.27, width 1.20; opisthosoma length 2.92, width 2.20. Anterior eye row width 0.68, posterior eye row width 0.78; median ocular quadrangle length 0.34, anterior width 0.36, posterior width 0.38; clypeus height 0.18. ***Legs measurements*.** I total 6.20+ (2.10/ 0.84/ 1.80/ 1.46/ lacking); II 7.03 (1.98/ 0.78/ 1.61/ 1.40/ 1.26); III 6.45 (1.80/ 0.61/ 1.43/ 1.65/ 0.96); IV 8.74 (2.28/ 0.79/ 1.91/ 2.44/ 1.32). ***Leg spination*.** As in male, except femora: II d1-1, p0-0-1; IV d1-1-1, p1-0-1, r0-0-1; tibiae: II v4-4, p2; IV p1-0-1, r1-0-1, v2-2-2; metatarsus: III p1-1-1, r1-1-1, v2-2-1r. ***Female genitalia*.** Epigynum heavily sclerotized, wider than long, maximum width at posterior half; anterior plate (AEP) occupying about nine-tenths of epigynum length, posterior margin (PmEP) procurved, close to posterior margin of posterior vulvar plate (PVP), with a median, small, copulatory opening (CO) partially covered by a shallow hood (Figs 17, 19); with posterior margin of PVP almost straight, slightly projected over epigastric furrow, occupying about four-fifths of epigynum width (Figs 17, 19); dorsally, vulva with a wider than long, subrectangular PVP occupying the posterior two-fifths of epigynum, having anterolateral sclerotized extensions (ExPVP) joined to primary spermathecae (S1) (Figs 18, 20); copulatory ducts (CD) visible in the cleared epigynum, long, slender, widening distally, ducts inside heavily sclerotized wide chambers, about half as long as epigynum, almost contiguous, ending at about one-tenth of anterior epigynum margin, where emerges on each, an anteriorly, small, globular secondary spermatheca (S2), separated one from the other by about five diameters, followed posteriorly by an elliptic, disk-like S1, just lateral and closely joined to the anterior end of each wide chamber, separated one from the other by about three diameters, its width about two diameters that of S2; fertilization duct (FD) short, arc-shaped, sclerotized, originating on the posterior margin of each S1, lateral to the point where extensions of PVP join to S1 (Figs 18, 20).

Variation. ***Males*** (n = 7): total body length 4.88–6.60; carapace length 2.42–3.00; carapace width 2.08–2.38; leg I: femur 2.30–2.63, patella 0.90–1.06, tibia 2.05–2.44, metatarsus 1.78–1.97, tarsus 1.49–1.90; leg IV: femur 2.48–2.78, patella 0.85–1.03, tibia 2.02–2.28, metatarsus 2.65–3.04, tarsus 1.49–1.70. ***Females*** (n = 3): total body length 5.22–5.76; carapace length 2.30–2.44; carapace width 1.77–1.96; leg I: femur 1.95–2.10, patella 0.71–0.84, tibia 1.67–1.80, metatarsus 1.37–1.46, tarsus 1.24–1.25; leg IV: femur 1.96–2.28, patella 0.72–0.79, tibia 1.64–1.91, metatarsus 2.20–2.44, tarsus 1.21–1.32.

Distribution. Known only from the collection localities in Chiapas, México. This is the first record for a *Falconina* species in Mexico and the northernmost native species of this genus in continental America.

Field observations and rearing trials. In the coffee plantations, specimens of *F. cafetera* sp. nov. were observed wandering in tree trunks with *Azteca sericeasur* Longino, 2007 (Formicidae: Dolichoderinae) nests (at heights between 1 and 1.6 m above the ground) or in the soil leaf litter accumulated at the base of those trees, but rarely far away from trees with ant nests. In order to corroborate that *F. cafetera* sp. nov. lives in close proximity with *A. sericeasur* ants, nests of these ants were disturbed by stirring a fine stick into them. After the disturbance, ac-

tive *F. cafetera* sp. nov. spiders were observed coming out of the nests along with some excited ants; however, when ants were very close to spiders, these tended to evade them. In order to test whether *F. cafetera* sp. nov. consumed *A. sericeasur* individuals, feeding trials were carried out at Finca Irlanda. For these trials, 18 spiders were captured alive (Fig. 21), and each spider was put into a 1-liter plastic container with approximately 25 *A. sericeasur* ants. After 24 hours, we found 11 ants dead, and two spiders were observed with an ant on their chelicerae (Fig. 22–23). However, we do not know if the spiders preyed on alive, healthy ants or consumed dead or injured ants. Additionally, six juvenile spiders were collected alive and reared at the Colección de Arácnidos del Sureste de México (32 km away from the coffee plantations, without the availability of *Azteca* ants). These juveniles were offered two types of prey. For the first two weeks, each juvenile received two *Camponotus* sp. Mayr, 1861 ants (Formicidae: Formicinae). Every two days, the spiders accepted the *Camponotus* ants as prey. Later, in lack of ants, one *Anastrepha* sp. Schiner, 1868 fruit fly (Diptera, Tephritidae) was offered to each of these juveniles every three days; all flies were accepted as prey. All laboratory-reared individuals (except one that escaped its cage) reached adulthood.

Proposed addition to the key to the species of *Falconina* by García and Bonaldo (2023)

1A Opisthosoma mostly dark in color with some light patches 1
– Opisthosoma mostly light in color with some dark patches (Figs 1–4, 21) ..... *Falconina cafetera* sp. nov.

Discussion

The previously known species of *Falconina* were found only in South and Central America, with one species introduced in the USA and Cuba (Valle et al. 2013; Ubick and Richman 2017; García and Bonaldo 2023). *Falconina cafetera* sp. nov. is the first species of this genus from Mexico and extends the natural distribution of the genus *Falconina* to North America. *Falconina cafetera* sp. nov. is one additional example of spider genera that were previously found only in South America and are now found in Chiapas, Mexico, as is the case of the genera *Josa* (Ibarra-Núñez et al. 2011), *Taczanowskia* (Ibarra-Núñez 2013), and *Wirada* (Campuzano and Ibarra-Núñez 2018).

This is the first *Falconina* species in which the ventral process of the embolar base (VPE) has been observed. This is an unusual sclerite; no record has been made for other species in this genus, nor seemingly for any other species of the subfamily Corinninae. In this subfamily, the bulb structures are usually strongly sclerotized (except the conductor), which makes it difficult to study them with an optical microscope since the boundaries between sclerites are difficult to discern. However, the observation of a recently molted adult male of *Falconina cafetera* sp. nov., with the bulb structures slightly sclerotized (Figs 8–10), and the expansion of the bulb in other specimens (Figs 11–16) facilitated the observation of the VPE as a sclerite developed from the embolar base, not as a bifurcation of the tegular process. In *Falconina cafetera* sp. nov., there are two structures issued from the embolar base: 1) the retrolateral process of the embolar base (RPE), corresponding to the "embolar process, developed retrolaterally" of García and Bonaldo (2023, page 203), and 2) the greatly developed VPE. In ventral view, the VPE shows a rounded proximal, prolateral edge, where it overlaps the TP. This seems to be indicative of the U-shaped fold of this sclerite. This same rounded edge seems to be present in the palps of some other *Falconina* species, as figured in *F. adriki* (fig. 15A in García and Bonaldo 2023), *F. albomaculosa* (fig. 13A in García and Bonaldo 2023), and *F. melloi* (figs 6–7 in Müller and Heimer 1988; fig. 211 in Bonaldo 2000; fig. 12B in García and Bonaldo 2023). It is possible that those species have a palp configuration like that of *F. cafetera* sp. nov. concerning the presence of a VPE, but which until now has not been observed due to intense sclerotization and tight overlap of VPE over TP. Submitting the palp of those species to expansion or examination at the scanning electronic microscope can help to clarify this issue.

Among the *Falconina* species, only *F. gracilis* has been previously observed having interactions with ants (Fowler 1984; Ubick and Richman 2017; García and Bonaldo 2023). Cushing (1997, 2012) defined three types of associations between spiders and ants: myrmecomorphy (mimicry), myrmecophily, and myrmecophagy. Myrmecomorph spiders have a modified body and/or color pattern that "gives the illusion that the spider has more than two body parts" and a way of moving that mimics that of ants. In addition, myrmecomorph spiders are normally active during the day, like the ants they mimic (Cushing 2012). *Falconina gracilis* (cited as its junior synonym *Corina vertebrata* Mello-Leitão, 1939) has been considered an apparent myrmecomorph of *Acromyrmex landolti* (Forel, 1885) (Myrmicinae) because the "spider resembled the worker ant, both in size and form" (Fowler 1984). The bright orange hue of the opisthosoma of live *F. cafetera* sp. nov. individuals (Fig. 21) is like that of the abdomen of *Azteca sericeasur* ants, but the shape and size of the spiders (being clearly bigger than the ants, Figs 22, 23) are not visually close to those of these ants, indicating the spider does not have the characteristics of a myrmecomorph (Cushing 2012).

Myrmecophile spiders have adaptations to live alongside the ants or within the ant colonies, such as a small size, chemical mimicry, and mechanisms to mislead or appease the ant hosts (Cushing 2012). *Falconina gracilis*

individuals have been observed entering and leaving nests of *Acromyrmex landolti* (Fowler 1984) and *Atta* spp. (Myrmicinae) (García and Bonaldo 2023). Fowler (1984) observed that "when touched by an ant in the foraging column, the spider momentarily accelerates…" indicating a refusal to be contacted by ants. Ubick and Richman (2017) cite that *F. gracilis* has been associated with nests of *Solenopsis invicta* Buren, 1972 (Myrmicinae) in Texas, where both ant and spider are considered introduced species. However, Ubick and Richman did not mention the type of association that was observed between spiders and ants. Some *F. cafetera* sp. nov. individuals were observed coming out of ant nests. Nevertheless, individual spiders are about one-third to one-half longer than *Azteca sericeasur* workers (Figs 22, 23), and the observation of *F. cafetera* sp. nov. individuals evading contact with groups of *Azteca sericeasur* suggests that these spiders lack mechanisms to pass unnoticed when meeting ants, so it could not be a myrmecophile.

Contrary to most spiders, myrmecophage spiders can take ants as prey. Some species of myrmecophage spiders use several mechanisms to reduce or inhibit the aggression of ants (Cushing 2012). *Falconina gracilis* individuals have been observed preying on the ants *Acromyrmex landolti* (Fowler 1984) and *Atta* spp. (García and Bonaldo 2023). Individuals of *F. cafetera* sp. nov. were observed eating *Azteca sericeasur* and *Camponotus* sp. ants but also accepted non-ant prey in laboratory trials. The fact that practically all the laboratory-reared juveniles reached adulthood on a mixed diet of ants and dipterans suggests this spider is a generalist predator, but in contrast to many other spider species, *F. cafetera* sp. nov. can capture and eat ants. However, more studies are needed to elucidate accurately this spider´s relationships with ants.

Acknowledgments

Thanks are due to Cristian López and Gabriel Domíguez for their help with field work, to Zach Hajian Fooroshani for his collaboration at the beginning of this work, and to Ivette Perfecto for her comments on preliminary findings. Specimens were collected under permit SGPA/DGVS/03998/11 issued by Mexico´s Secretaria de Medio Ambiente y Recursos Naturales (SEMARNAT). The authors thank the reviewers, N. Dupérré and I. Magalhães, for their helpful and insightful suggestions. This work was supported by a doctoral Conacyt fellowship granted to L. M. The Universidad Veracruzana and El Colegio de la Frontera Sur supported the writing process.

References

Bonaldo AB (2000) Taxonomia da subfamília Corinninae (Araneae, Corinnidae) nas regioes Neotropica e Neárctica. Iheringia. Série Zoologia 89(89): 3–148. https://doi.org/10.1590/S0073-47212000000200001

Brignoli PM (1985) On some generic homonymies in spiders (Araneae). Bulletin - British Arachnological Society 6(9): 380. https://britishspiders.org.uk/system/files/library/060906.pdf

Campuzano EF, Ibarra-Núñez G (2018) A new species of the spider genus *Wirada* (Araneae, Theridiidae) from Mexico, with taxonomic notes on the genus and a key to the species. Zootaxa 4457(3): 495–500. https://doi.org/10.11646/zootaxa.4457.3.13

Cushing P (1997) Myrmecomorphy and myrmecophily in spiders: A review. The Florida Entomologist 80(2): 165–193. https://doi.org/10.2307/3495552

Cushing P (2012) Spider-ant associations: An updated review of myrmecomorphy, myrmecophily, and myrmecophagy in spiders. Psyche 2012, article ID 151989: 1–23. https://doi.org/10.1155/2012/151989

Fowler H (1984) Note on a clubionid spider associated with Attine ants. The Journal of Arachnology 12(1): 117–118. https://www.americanarachnology.org/journal-joa/joa-all-volumes/detail/volume/104/

García F, Bonaldo AB (2023) Taxonomic revision of the soldier spider genus *Falconina* Brignoli, 1985 (Araneae, Corinnidae, Corininae). Zootaxa 5343(3): 201–242. https://doi.org/10.11646/zootaxa.5343.3.1

Ibarra-Núñez G (2013) A new species of the spider genus *Taczanowskia* (Araneae, Araneidae) from Mexico. Zootaxa 3664(1): 57–62. https://doi.org/10.11646/zootaxa.3664.1.3

Ibarra-Núñez G, Maya-Morales J, Chamé-Vázquez D (2011) Las arañas del bosque mesófilo de montaña de la Reserva de la Biosfera Volcán Tacaná, Chiapas, México. Revista Mexicana de Biodiversidad 82(4): 1183–1193. https://doi.org/10.22201/ib.20078706e.2011.4.736

Keyserling E (1891) Die Spinnen Amerikas. Brasilianische Spinnen. Bauer & Raspe. Nürnberg 3: 1–278. https://doi.org/10.5962/bhl.title.64832

Müller HG, Heimer S (1988) Spiders from Colombia, report X. Redescription of *Corinna meloi* (Schenkel, 1953) (=*FALCONIA*) (Araneae, Clubionidae). Bulletin Zoölogisch Museum Universiteit van Amsterdam 11(19): 153–156. https://repository.naturalis.nl/pub/505434/BULL1988011019001.pdf

Petrunkevitch A (1925) Arachnida from Panama. Transactions of the Connecticut Academy of Arts and Sciences 27: 51–248.

Ubick D, Richman D (2017) Corinnidae. In: Ubick D, Paquin P, Cushing P, Roth V (Eds) Spiders of North America: an identification manual. American Arachnological Society, Keene, 91–93.

Valle S, Keiser C, Vincent L, Vetter R (2013) A South American spider, *Falconina gracilis* (Keyserling 1891) (Araneae, Corinnidae), newly established in southern California. The Pan-Pacific Entomologist 89(4): 259–263. https://doi.org/10.3956/2013-23.1

World Spider Catalog (2024) World Spider Catalog. Version 25.0. Natural History Museum Bern, Bern. https://doi.org/10.24436/2 [accessed February 1st, 2024]

Zoosyst. Evol. 100 (3) 2024, 1107–1120 | DOI 10.3897/zse.100.119662

One hundred years of solitude: The rediscovery of *Pristimantis ruidus* (Anura, Strabomantidae) in the southern Andes, Ecuador and its phylogenetic relationships

Juan C. Sánchez-Nivicela[1,2,3,4], Diana Székely[5,6,7], Luis A. Salagaje M.[8], Nicolás Astudillo-Abad[8], Jaime Culebras[8,9], Ernesto Arbeláez Ortiz[4,8], Paul Székely[5,6,7]

1 *Universidad Nacional de Colombia, Facultad de Ciencias, Grupo de Investigación Evolución y Ecología de Fauna Neotropical, Bogotá, D.C., Colombia*
2 *Universidad San Francisco de Quito USFQ, Colegio de Ciencias Biológicas y Ambientales COCIBA, Laboratorio de Zoología Terrestre y Museo de Zoología, Campus Cumbayá, Quito 170901, Ecuador*
3 *Instituto Nacional de Biodiversidad del Ecuador, calle Rumipamba 341 y Av. de los Shyris, Casilla 17-07-8976, Quito, Ecuador*
4 *Fundación y Bioparque AMARU, Cuenca, Ecuador*
5 *Museo de Zoología, Universidad Técnica Particular de Loja, San Cayetano Alto, calle París s/n, 110107, Loja, Ecuador*
6 *Laboratorio de Ecología Tropical y Servicios Ecosistémicos (EcoSs-Lab), Facultad de Ciencias Exactas y Naturales, Departamento de Ciencias Biológicas y Agropecuarias, Universidad Técnica Particular de Loja, San Cayetano Alto s/n, 110107, Loja, Ecuador*
7 *Research Center of the Department of Natural Sciences, Faculty of Natural and Agricultural Sciences, Ovidius University Constanța, Al. Universității no.1, 900470, Constanța, Romania*
8 *Fundación Cóndor Andino, Quito, Ecuador*
9 *Photo Wildlife Tours, Quito, Ecuador*

https://zoobank.org/38565FEC-15BA-4832-8DC5-875963431C79

Corresponding author: Juan C. Sánchez-Nivicela (juan.sanchezn13@gmail.com)

Academic editor: Pedro Taucce ♦ **Received** 27 January 2024 ♦ **Accepted** 16 July 2024 ♦ **Published** 13 August 2024

Abstract

We report the rediscovery, a century after its last record, of two specimens of *Pristimantis ruidus* from approximately 6 km northeast of its type locality, in a montane forest from the western Andes of southern Ecuador. This species, described by John D. Lynch in 1979, based on specimens collected in 1922 by George H. Tate, was previously known only from the type series, all specimens originating from a single locality (Molleturo, Provincia Azuay, Ecuador, 2317 m elev.). The rediscovery occurred in November 2022 in the Reserva de Conservación Quitahuaycu, Molleturo Parish, Azuay Province. The two specimens, both females, are characterised by rough skin with numerous rounded low warts and tubercles on their dorsum, a W-shaped occipital fold, tympanum and tympanic ring not externally visible and by the lack of cranial crests, characters that correspond with the description of the holotype. We evaluate the phylogenetic relationships, based on two mitochondrial genes (*12S* and *16S* rRNA) and one nuclear gene (*RAG-1*). These analyses reveal *Pristimantis ruidus* as a member of the subgenus *Huicundomantis*, being most closely related to *P. philipi*, a species with a distribution restricted to the paramo of the same mountain region (Macizo del Cajas). *Pristimantis ruidus* co-exists with *Pristimantis jimenezi*, three additional species of *Pristimantis* and one *Noblella* with uncertain taxonomic status. This rediscovery underscores the urgency of implementing effective conservation and monitoring measures for the few remnants of the original ecosystems from western Ecuador, which face ongoing anthropogenic threats and harbour a diversity that remains insufficiently studied.

Resumen

Reportamos el redescubrimiento, un siglo después de su último registro, de dos especímenes de *Pristimantis ruidus* en aproximadamente 6 km al noreste de su localidad tipo, en un bosque montano en los Andes occidentales del sur de Ecuador. Esta especie, descrita por John D. Lynch en 1979, con base en especímenes recolectados en 1922 por George H. Tate, se conocía solo por la serie tipo con todos los especímenes originarios de la misma localidad (Molleturo, Provincia Azuay, Ecuador, 2317 m.). El redescubrimiento ocurrió en noviembre de 2022 en la Reserva de Conservación Quitahuaycu, parroquia Molleturo, provincia de Azuay. Los dos ejemplares son hembras y se caracterizan por presentar una piel rugosa con numerosas verrugas bajas y tubérculos redondeados

en su textura dérmica dorsal, un pliegue occipital en forma de W, tímpano y anillo timpánico no visibles externamente y carecen de crestas craneales, caracteres que concuerdan con el holotipo. Evaluamos relaciones filogenéticas basadas en dos genes mitocondriales (*12S* y *16S* rRNA) y un gen nuclear (*RAG-1*). Estos análisis revelan a *Pristimantis ruidus* como miembro del subgénero *Huicundomantis*, estando más estrechamente relacionado con *P. philipi*, especie de distribución restringida que habita el páramo de la misma región montañosa (Macizo del Cajas). *Pristimantis ruidus* coexiste con *Pristimantis jimenezi*, tres especies adicionales de *Pristimantis* y una *Noblella* con estatus taxonómico incierto. Este redescubrimiento subraya la urgencia de implementar planes efectivos de conservación y monitoreo para todos los remanentes de los ecosistemas del oeste de Ecuador, que enfrentan amenazas antropogénicas continuas y albergan una diversidad que aún no está suficientemente estudiada.

Key Words

Amphibia, biodiversity, conservation, *Huicundomantis*, molecular genetics, morphology, new record, phylogeny, systematics, taxonomy

Palabras clave

Anfibios, biodiversidad, conservación, filogenia, genética molecular, *Huicundomantis*, morfología, nuevo registro, sistemática, taxonomía

Introduction

The direct-developing frogs of the genus *Pristimantis* Jiménez de la Espada, 1870 are the most species-rich group of all amphibians, with more than 600 formally recognised species (Frost 2023). The high diversity of the genus is also accompanied by exceptional levels of ecological specialisation, many species presenting small ranges of distribution, especially at higher elevations in the Andes (Ron et al. 2022). With respect to southern Ecuador, numerous studies of the *Pristimantis* have revealed an extraordinary diversity and endemism, but also massive threats (Lynch 1979; Lynch and Duellman 1997; Urgiles et al. 2014, 2017, 2019; Yánez-Muñoz et al. 2016, 2019; Sánchez-Nivicela et al. 2018, 2021; Székely et al. 2018, 2020, 2021; Páez and Ron 2019; Ortega-Andrade et al. 2021).

Pristimantis ruidus (Lynch, 1979) has eluded field researchers for over a hundred years. The 16 known specimens used in the description were collected by the naturalist George Henry Hamilton Tate (1894–1953) during his 1922 expedition for the American Museum of Natural History. The specimens were collected in south-western Ecuador, in Molleturo, Azuay Province, on the Pacific slopes of the Cordillera Occidental, at an elevation of 2317 m (Lynch 1979; Lynch and Duellman 1997).

In 2022, during an expedition to the Reserva de Conservación Quitahuaycu, led by Fundación y Bioparque AMARU, members of the exploration team collected two specimens of *Pristimantis*, which, after comparison with the original description and holotype photographs, were identified as *P. ruidus*. Based on the newly-acquired specimens, we present a re-description of this species, provide for the first time images of living specimens, as well as a genetic assessment and evaluation of phylogenetic relationships of *P. ruidus*.

Methods

Specimen collection and study site

Fieldwork was carried out at Reserva de Conservación Quitahuaycu (-2.74047, -79.33532 [WGS84]), Molleturo Parish, Azuay Province, Ecuador (Fig. 1). The study area is a montane forest, situated at an elevation between 2400 and 2900 m, approximately 6 km southwest from the type locality of *P. ruidus*. For the species habitat description, we follow the ecosystem classification system proposed by the Ministerio del Ambiente del Ecuador (MAE 2012).

We used the complete species inventory methodology (Angulo et al. 2006), with diurnal and nocturnal samplings, visits being conducted in November 2022. The collected specimens were deposited at the División de Herpetología (DHMECN) of the Instituto Nacional de Biodiversidad (INABIO), Quito, Ecuador and Museo de Zoología, Universidad Técnica Particular de Loja (MUTPL), Loja, Ecuador. Specimens were manipulated in accordance with Beaupre et al. (2004), photographed alive and euthanised with a 5% Roxicain solution. Liver tissue samples were extracted and preserved in 90% ethanol, after which the specimens were fixed with 10% formalin and preserved in 70% ethanol, following the methods proposed by Heyer et al. (2001) and Simmons and Muñoz-Saba (2005). Research permits were issued by the Ecuadorian Ministry of Environment (019-2018-IC-FAU-DNB/MAE, MAE-DNB-CM-2018-0106 and MAATE-DBI-CM-2021-0181).

Morphological analysis

The collected specimens were identified, based on the original description (Lynch 1979) and compared with photographs of the holotype AMNH 17590 (**AMNH** = American Museum of Natural History). The definition follows the

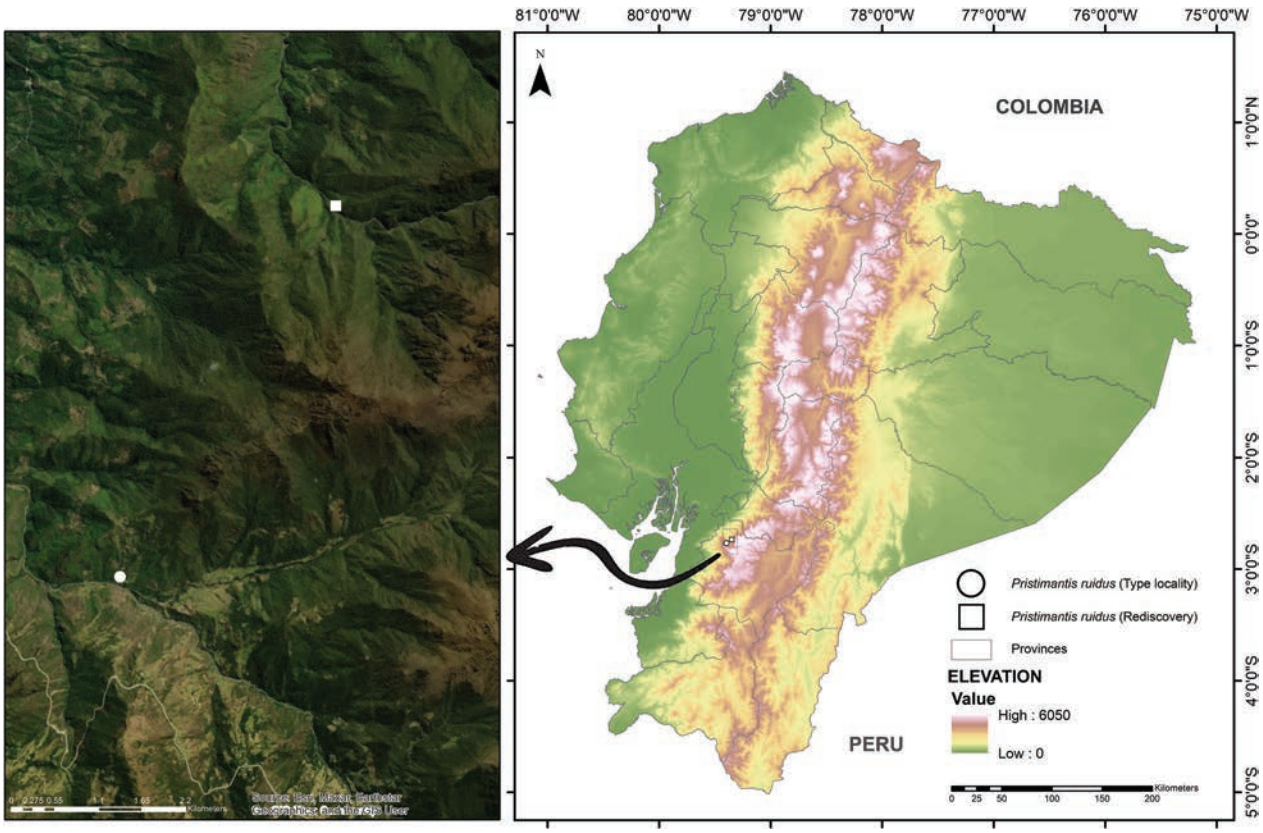

Figure 1. Map of Ecuador showing the distribution of *Pristimantis ruidus* in Azuay Province, Ecuador. On the left, an enlarged view of the area. Source: Esri, Maxar, Earthstar geographics and the GIS User Community.

characters and diagnostic terms proposed by Duellman and Lehr (2009). The sex and maturity of the specimens were determined by inspecting the sexual organs through a dorsolateral incision and the external characteristics. Fingers and Toes are numbered pre-axially to postaxially from I to IV and I to V, respectively. The relative lengths of Toes III and V were determined by adpressing them against Toe IV and Fingers I and II were compared by adpressing them against each other.

Morphological measurements were taken with a precision caliper and rounded to the nearest 0.1 mm. The abbreviations used follow the format of Duellman and Lehr (2009): **SVL** = Snout-vent length (distance from the tip of snout to the vent); **TL** = Tibia length (distance from the knee to the distal tibia end); **FL** = Foot length (distance from the proximal margin of inner metatarsal tubercle to tip of Toe IV); **HL** = Head length (distance from angle of the jaw to the tip of the snout); **HW** = Head width (distance between the angle of the jaws); **IOD** = Interorbital distance (between the orbits); **EW** = Width of upper eyelid (perpendicular distance to the outer edge of the upper eyelid); **IND** = Internarial distance (distance between the inner edges of the narial openings); **EN** = Eye-nostril distance (between the anterior corner of orbit and posterior margin of the narial opening); **ED** = Eye diameter (horizontal length of the orbit).

Colour patterns in life and other important external characteristics were based on field notes and photographs taken in the field and laboratory. The colour identification in life follows Köhler (2012). The photographs were taken by Ernesto Arbeláez, Jaime Culebras and Juan Sánchez.

Molecular analysis

Genomic extraction, amplification and sequencing were done as described in Székely et al. (2020); the six newly-generated DNA sequences were deposited in GenBank (Appendix 1). We analysed the molecular data by using sequences of two mitochondrial genes (*12S* and *16S* rRNA) and one nuclear gene (*RAG-1*) from 61 specimens (60 from Ecuador and one from Peru) of 35 species or candidate species available in GenBank, representing all the currently confirmed species of the subgenus *Huicundomantis* of *Pristimantis* (*sensu* Ortega et al. (2022)). As outgroups, we used the species from Székely et al. (2021): *Pristimantis unistrigatus* (Günther, 1859), *P. ceuthospilus* (Duellman & Wild, 1993), *P. imitatrix* (Duellman, 1978), *P. diadematus* (Jiménez de la Espada, 1875), *P. rhodoplichus* (Duellman & Wild, 1993), *P. melanogaster* (Duellman & Pramuk, 1999), *P. wiensi* (Duellman & Wild, 1993), *P. simonsii* (Boulenger, 1900), *P. orestes* (Lynch, 1979), *P. colodactylus* (Lynch, 1979) and *P. orcesi* (Lynch, 1972), the trees being rooted with *P. galdi* Jiménez de la Espada, 1870. We conducted BLAST searches to identify similar *12S*, *16S* and *RAG-1* sequences in GenBank and used FastTree v.2.1 (Price et al. 2010), implemented in the programme Geneious Prime (v.2023.1.2, Biomatters Ltd., Auckland, New Zealand) to build an exploratory tree with most of the available Ecuadorian *Pristimantis* sequences in order to determine the identity and relationships of our species.

The sequences were edited, assembled and aligned (MAFFT algorithm with the G-INS-i iterative refinement

method; Katoh and Standley (2013) in Geneious Prime; the *12S*, *16S* and *RAG-1* aligned sequences were visually inspected to correct alignment errors in PhyDE (Müller et al. 2010), concatenated into a single matrix and then used for the phylogenetic analyses. The analyses were based on a 2413-base pair (bp) dataset (924 bp for *12S*, 877 bp for *16S* and 612 bp for *RAG-1*); the matrix is available at https://doi.org/10.5281/zenodo.11099783.

Phylogenetic relationships were inferred using both Bayesian Inference (BI) and Maximum Likelihood (ML). We used PartitionFinder v. 2.1.1 (Lanfear et al. 2017) to select the best partition scheme with the Bayesian Information Criterion (BIC) as a model of selection; PartitionFinder identified three partition schemes (best model in parentheses): *12S* and *16S* (GTR+I+G), *RAG-1* 1st position (K80+G) and *RAG-1* 2nd and 3rd position (F81+I+G). The BI analysis was implemented in MrBayes v.3.2.6 (Ronquist et al. 2012), the Markov Chain Monte Carlo runs being performed twice, independently, for 40 million generations, with trees sampled every 1,000 generations; convergence of the runs was assessed from the average split frequency of standard deviations ($p < 0.001$) and by checking the potential scale reduction factors (PSRF ~ 1.0) for all model parameters; consensus trees were summarised after discarding the initial 25% as burn-in. The ML analyses were conducted in IQ-TREE 2 (Minh et al. 2020). We performed four different runs, in order to test the tree's topologies: one with IQ-TREE's default settings, in which the programme determined the best-fit model for our alignment (TIM2+F+I+R4 under BIC), with 100,000 bootstrap replicates for the SH-like approximate likelihood ratio branch test (SH-aLRT; Guindon et al. (2010)) and with 100,000 ultrafast bootstrap replicates (UFBoot; Hoang et al. (2018)) to assess the branch support; a second run with the three partition schemes identified by PartitionFinder and with the same number of SH-aLRT and UFBoot replicates (100,000); a third run with the default settings, but with the -bnni option (optimised, hill-climbing nearest neighbour interchange, NNI, search) in order to reduce the risk of overestimating the branch supports of the UFBoot, with 10,000 replicates for both SH-aLRT and UFBoot; and finally, a fourth run with the default settings, but the branch support evaluated with 500 standard non-parametric bootstrap (Boot; Felsenstein (1985)) searches. The phylograms were visualised and edited with FigTree (Rambaut 2014) and the uncorrected genetic p-distances were calculated for *16S* with MEGA6 (Tamura et al. 2013).

Results

Morphological identification of *Pristimantis ruidus*

Using the diagnosis and description from Lynch (1979), the two specimens (DHMECN 19106 and MUTPL 1613) were recognised as *P. ruidus*, based on the following characters: dorsal skin warty, W-shaped ridge on occiput; some larger warts on flanks; no dorsolateral folds; venter coarsely areolate without discoidal folds; head wider than body, wider than long; tympanum, tympanic membrane and annulus absent; two large postrictal tubercles; snout rounded in dorsal and lateral view; cranial crest absent; vomerine odontophores triangular in contour; canthus rostralis rounded; loreal region concave, sloping to non-flared lips; upper eyelid warty (not bearing enlarged tubercles); supratympanic fold prominent, extending from corner of eye to base of arm; Finger I shorter than Finger II, digits bearing broad discs on dilated pads; fingers with lateral fringes; non-conical tubercles on heel; inner tarsal fold present; two metatarsal tubercles, inner oval, twice the size of round outer; supernumerary plantar tubercles only at bases of Toes II–IV; toes with lateral fringes, internal toe pads smaller than those of outer fingers (Figs 2–5).

Additionally, the photographs of holotype (AMNH 17590, Fig. 6) show that *P. ruidus* has a little tubercle in the interorbital space; digital discs are elliptical; ulnar tubercles are present, low, and rounded, present on the outer border of the forearm; basal web between toes is absent, the membrane appearance corresponds to dilated lateral fringes (all these characteristics being present also in the specimens DHMECN 19106 and MUTPL 1613).

Phylogeny

The Bayesian Inference and the four Maximum Likelihood phylogenetic trees showed almost the same topology, with only minor differences in the position of some of the unresolved branches; the BI tree presented fewer unresolved branches and relatively higher branch support (Fig. 7). In the case of the four ML trees, values of the branch support differed slightly between the runs; the non-parametric bootstrap run (fourth run) proved to be the most conservative (having overall the smallest support values), followed by the NNI tree (third run).

Similar to Ortega et al. (2022), we recovered the subgenus *Huicundomantis* of *Pristimantis* as monophyletic, with strong support (SH-aLRT = 99.8–99.9%; UFBoot = 100%; Boot = 97%; posterior probabilities (PP) = 1). However, in our tree (Fig. 7), the basal terminals are those represented by *P. philipi* (Lynch & Duellman, 1995) and *P. ruidus* and not the samples including *P. miktos* Ortego-Andrade & Venegas, 2014 (Ortega et al. 2022), although with strong support only in the BI and the SH-like approximate likelihood ratio branch test (SH-aLRT = 80.4–85.5%; UFBoot = 81–93%; Boot = 69%; PP = 0.98); this difference is most likely a consequence of the different gene sampling scheme and further analyses (with matrices that contain longer sequences and more genes) are needed to clarify the relationships of the species in this subgenus. However, our tree has a topology very similar to the one presented in Székely et al. (2021).

The initial exploratory FastTree, as well as the BI and ML phylogenetic trees, recovered *P. ruidus* as a species in the subgenus *Huicundomantis*. *Pristimantis ruidus* is revealed as the sister species of *P. philipi* and both together

form a basal group in *Huicundomantis* (Fig. 7). Uncorrected genetic p-distances for the *16S* gene between *P. ruidus* and its sister species, *P. philipi*, range from 4.1% to 5.3% and between them and the other species of the subgenus *Huicundomantis* from 4.6% to 11.4%.

Taxonomy

Pristimantis ruidus (Lynch, 1979)

Figs 2–6

Common English name: Molleturo Robber Frog

Common Spanish name: Cutín de Molleturo

Etymology. Latin, meaning rough, in reference to the skin texture (Lynch 1979).

Types and type locality. ***Holotype*** (AMNH 17590), adult female obtained at Molleturo, Provincia Azuay, Ecuador, 2317 m elev., on 5–19 June 1922 by G. H. Tate. Paratypes (AMNH 17588, 89, 17591–96, 17598–601, 17603), topoparatypes (Lynch 1979).

Newly-collected material. Two females: DHMECN 19106 (field series: JCS-2081) and MUTPL 1613 (field series: JCS-2084). The first individual was found amongst the remains of a felled tree (75 cm from the ground), along a stream edge (-2.73185, -79.34213, elevation 2677 m); the second individual, was on the leaf of a low shrub (40 cm from the ground), also by a stream edge (-2.73387, -79.34182, elevation 2525 m); both specimens were collected in the Reserva de Conservación Quitahuaycu, Molleturo Parish, Azuay Province, Ecuador, by Luis Salagaje, Ernesto Arbeláez, Jaime Culebras and Nicolás Astudillo, on 27 November 2022 (Fig. 1).

Definition. A moderate-sized species of *Pristimantis* in the subgenus *Huicundomantis* as inferred from molecular phylogenetic relationships, characterised by the following combination of traits: (1) skin on head, dorsum, flanks and extremities shagreen with scattered tubercles, pustules and W-shaped scapular fold; venter coarsely areolate; discoidal fold absent; ventral texture of thighs areolate; (2) tympanic membrane and tympanic annulus absent; (3) snout rounded in dorsal and profile views; (4) upper eyelid with small rounded tubercles, 85.2% of the IOD; interocular space with rounded tubercle; cranial crests absent; (5) dentigerous processes of vomers rounded, with four and five teeth each, triangular in contour; (6) males lacking vocal sac and slits; (7) Finger I shorter than Finger II; disc expanded, elliptical; (8) fingers with narrow lateral fringes; (9) ulnar tubercles present, rounded, on the outer border of the forearm; (10) heel with several small rounded tubercles; tarsal tubercles rounded; inner tarsal fold present; (11) inner metatarsal tubercle oval, twice the size of round outer metatarsal tubercle; supernumerary plantar tubercles few in number; (12) toes with narrow lateral fringes; webbing absent; Toe V longer than Toe III; discs slightly shorter in size than those on outer fingers; (13) dorsum dark olive or brown with dark brown spots; dark W-shaped mark in scapular region, with orange spots in the higher portions; interorbital blotch, post ocular stripe and labial bars dark brown; venter dusty brown with white spots; (14) SVL females 20.1 and 30.0 mm (type series: males = 25.8–31.1 mm, females = 37.1–39.8 mm).

Diagnosis. *Pristimantis ruidus* is distinguished from its congeners in the subgenus *Huicundomantis* by lacking a tympanic membrane and a tympanic annulus, head wider than long, short snout, cranial crest absent, thick supratympanic fold and by the presence of subacuminated postrictal tubercles. *Pristimantis philipi* is the only species lacking the middle ear and vocal apparatus and cranial crests (Lynch and Duellman 1997). *Pristimantis ruidus* differs from *P. philipi* by the broadly expanded discs of the digits (discs barely expanded in *P. philipi*), the evident scapular fold (lack of scapular fold in *P. philipi*) and the colouration pattern composed by dark olive or brown with dark brown spots, dark W-shaped marks in the scapular region, with orange spots in the higher portions (two colour patterns in dorsum, black and pale yellow blotches or irregular flecks and blotches green, black, yellowish-green and grey in *P. philipi*).

Description of female DHMECN 19106. Head wider than long, short snout (HL = 33% of SVL), rounded in dorsal and lateral profile, nostrils orientated posterodorsally; *canthus rostralis* concave; cranial crest absent; one rounded interocular tubercle; upper eyelid with rounded tubercles (three and four each) and few lower; supratympanic fold thick and discontinuous; four large subacuminated postrictal tubercles; tympanic annulus and membrane absent; few small and subconical maxillary tubercles; choana barely visible in the palatal shelf, posteriorly to level of choana and broadly separated, dentigerous process of vomers conspicuous, triangular, with four and five vomerine teeth each; tongue wider than long, 30% adhering to the floor mouth; scapular fold W-shaped. Dorsum skin shagreen with numerous low warts; dorsolateral and medial fold absent; flanks shagreen with low warts and scarcely subconical and low tubercles; venter areolate with large and scattered warts; discoidal and pectoral fold absent; cloacal vent with rounded warts. Arms with low and oblique ridges and small subconical tubercles; subconical ulnar tubercles; U-shaped palmar tubercle, same length to thenar tubercle; thenar tubercle oval; low and few palmar supernumerary tubercles; subarticular tubercles rounded; fingers with lateral fringes, without interdigital membranes; Finger I shorter than Finger II; all digits with ventral pads, narrow and rounded in Finger I, barely expanded and elliptical in Finger II, expanded and elliptical in Fingers III and IV; discs in Fingers II and IV with circumferential grooves. Legs with low and oblique ridges, more noticeable in hind limbs and foot and small rounded tubercles; TL = 51% of SVL; heel and tarsus with subconical tubercles; inner tarsal fold low and extending along the tarsus; inner metatarsal tubercle oval, three times larger than external which is round; few low plantar supernumerary tubercles; subarticular tubercles rounded; toes with lateral fringes, without interdigital membranes; all digits with ventral pads and circumferential grooves,

barely expanded and elliptical in Toes I–V; relative length of Toes I < II < III < V < IV (Figs 2–5).

In preservative, dorsum brown with dark brown blotches, interocular bar dark brown, scapular fold dark brown with yellowish-cream blotches in the higher portions. Flanks greyish-cream with white spots in tubercles tip or warts, postocular stripe black, labial bars dark brown with thin white lines or blotches. Venter yellowish-cream with white spots in warts. Extremities yellowish-cream in concealed surfaces, dorsally brown with diagonal dark brown bars with white spots in tubercles tip, ventrally yellowish-cream with some ash shading and white spots in tip tubercles or warts (Fig. 4).

In life, dorsally Olive Clay Colour (85), with Verona Brown (37) blotches including scapular fold, and diagonal bars in extremities; snout Olive Sulphur Yellow (90), tip of snout and upper eyelids Lime Green (105); tip of tubercles in scapular fold Brunt Orange (10). In lateral view, flanks Olive Clay Colour (85) with Russet (44) botches in the upper middle portion, change to Medium Greenish-Yellow (88) and ashen Ferruginous (35) in the lower middle portion; russet labial bars, canthal blotch and postocular stripe; Smoky White (261) blotches and lines in labials. Ventrally, ashen Cream Colour (12) with Smoky White (261) spots. Interior surfaces of digits, Spectrum Yellow (79) with Verona Brown (37) splashes. Iris Light Chrome Orange (76) with black reticulations and sclera (Figs 2, 3).

Variation. In the case of the MUTPL 1613 specimen, the Olive Clay Colour (85) of the dorsum and other olive or green colour tones are replaced with Salmon Colour (83) (Fig. 2). The two female specimens (MUTPL 1613 and DHMECN 19106) are smaller in size (SVL 20.1 and 30.0 mm, respectively) than the females of the type series (37.1–39.8 mm), reported by Lynch (1979). Morphometric variation is presented in Table 1.

Distribution and natural history. *Pristimantis ruidus* was known only from its type locality Molleturo (Lynch 1979). The new record is approximately 6 km from the town of Molleturo, from the Western Andean montane evergreen forest (MAE 2012), on the same western slope of the Macizo del Cajas (Fig. 1).

Both individuals were found during the night, with full moon lighting (21:58 h–00:09 h), close to the ground (< 70 cm), in forested areas with abundant shrubby and herbaceous vegetation, soil covered by leaf litter and close to streams (Fig. 8). *Pristimantis ruidus* was observed in sympatry with *P. jimenezi* Páez & Ron, 2019 and three additional *Pristimantis* species and one *Noblella* Barbour, 1930 species with uncertain taxonomic status.

Conservation status. Currently, the forests on the Andean foothills in western Ecuador, which include the Molleturo Forest, retain only 30% of their original extent, this being one of the most degraded and fragmented ecosystems in Ecuador (Sierra et al. 2021). Molleturo is part of the Área de Vegetación y Bosques Protectores (AVBP) Molleturo-Mollepungo, a form of community reserve that covers over 140,000 hectares; however, currently it does not have a management plan and is not included in the National Environmental Protection Policy (Política Ambiental Nacional del Ecuador); this makes the entire area highly vulnerable to loss and destruction of natural vegetation cover.

Various significant threats have been identified in the region, mostly linked to activities of anthropogenic origin, such as deforestation for the expansion of grazing areas and the extraction of wood for fire. The situation is aggravated by the presence of numerous mining concessions throughout the area, as well as the proliferation of illegal mining. The Molleturo Parish has one of the highest rates of poverty and inequality in the country (Molina et al. 2015), making the area even more susceptible to rapid destruction and consequent loss of environmental quality.

The Reserva de Conservación Quitahuaycu comprises approximately 900 hectares (0.6% of the total area of Molleturo-Mollepungo AVBP), protecting ecosystems of high montane and montane evergreen forests of the western mountain of the Andean cordillera (0.14%) and the Páramo grassland (0.02%) (MAE 2012). This Reserve is the result of conservation efforts made by the community coalition of Arquillo, San José de Huigra, San Antonio and Migüir, together with the Fundación y Bioparque AMARU, aiming to preserve threatened species of amphibians which are present here, such as *Atelopus nanay* Coloma, 2002 (CR), *Pristimantis verrucolatus* Páez & Ron, 2019 (CR), *Pristimantis jimenezi* (CR), in addition to species with taxonomic uncertainty that are probably new species to science.

Pristimantis ruidus has a very low detectability. Despite intense search efforts carried out by different research groups in the area, its presence was missed over the last century and we were only able to encounter two individuals. We suspect that it only inhabits densely-forested areas with ravines and humid areas, so that the species is restricted to the best conserved parts of the ecosystem, Bosque siempreverde montano de Cordillera Occidental de Los Andes (MAE 2012), between elevations of 2317 and 2677 m.

Pristimantis ruidus is categorised as "Critically Endangered (Possibly Extinct) D" according to a recent assessment, because "given survey efforts and lack of records since 1922, it was inferred that it is either extinct or if there is still an extant population, that it is very small (< 50 mature individuals)" (IUCN SSC Amphibian Specialist Group 2023). We consider the Critically Endangered status to be

Table 1. Morphological measurements (in mm) of the two newly-collected *Pristimantis ruidus* specimens and for the holotype as provided by Lynch (1979). Abbreviations: SVL = Snout-vent length, TL = Tibia length, FL = Foot length, HL = Head length, HW = Head width, IOD = Interorbital distance, EW = Width of upper eyelid, IND = Internarial distance, EN = Eye-nostril distance, ED = Eye diameter.

Museum Code	SVL	TL	FL	HL	HW	IOD	EW	IND	EN	ED	Sex	State
DHMECN 19106	30.0	15.5	15.3	10.0	10.9	3.0	2.6	2.5	2.6	3.3	Female	adult
MUTPL 1613	20.1	10.2	9.6	6.7	7.5	2.0	1.8	1.7	1.6	2.3	Female	adult
AMNH 17590 (Holotype)	38.4	16.3	–	11.4	13.4	2.9	3.6	–	3.2	4.5	Female	adult

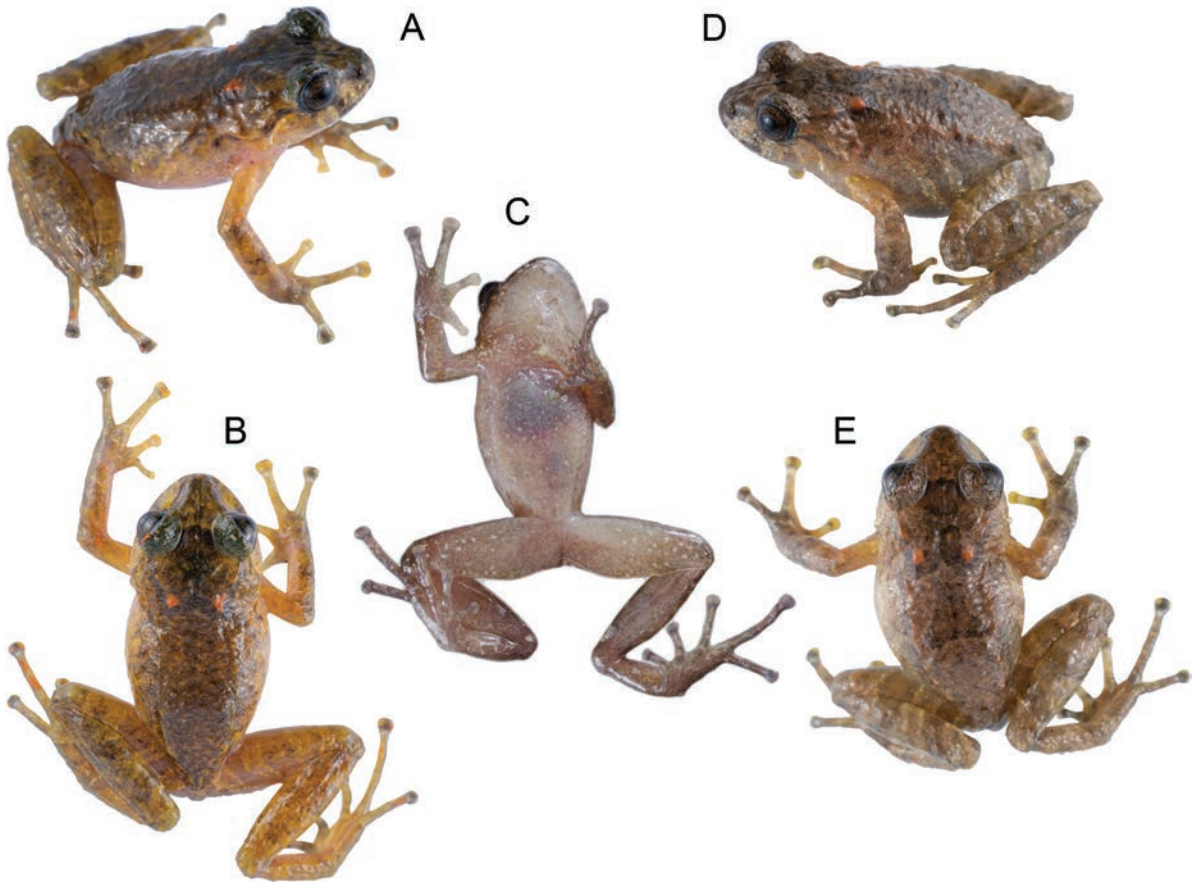

Figure 2. *Pristimantis ruidus* in life. Female DHMECN 19106: **A.** Dorso-lateral view; **B.** Dorsal view; **C.** Ventral view; SVL = 30.0 mm. Female MUTPL 1613; **D.** Dorso-lateral view; **E.** Dorsal view; SVL = 20.1 mm. Photographs: Jaime Culebras, Juan Sánchez.

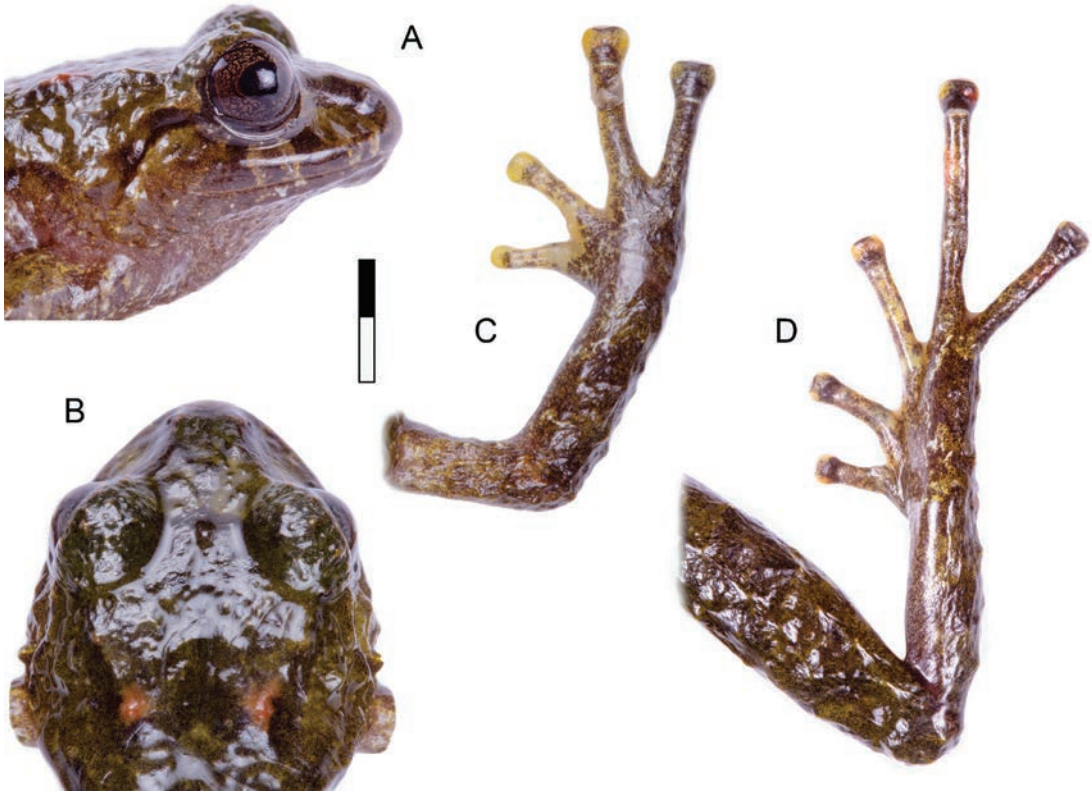

Figure 3. *Pristimantis ruidus*, adult female DHMECN 19106 in life: **A.** Lateral view of head; **B.** Dorsal view of head; **C.** Dorsal view of hand; **D.** Dorsal view of foot. Scale bar: 4 mm. Photographs: Juan Sánchez.

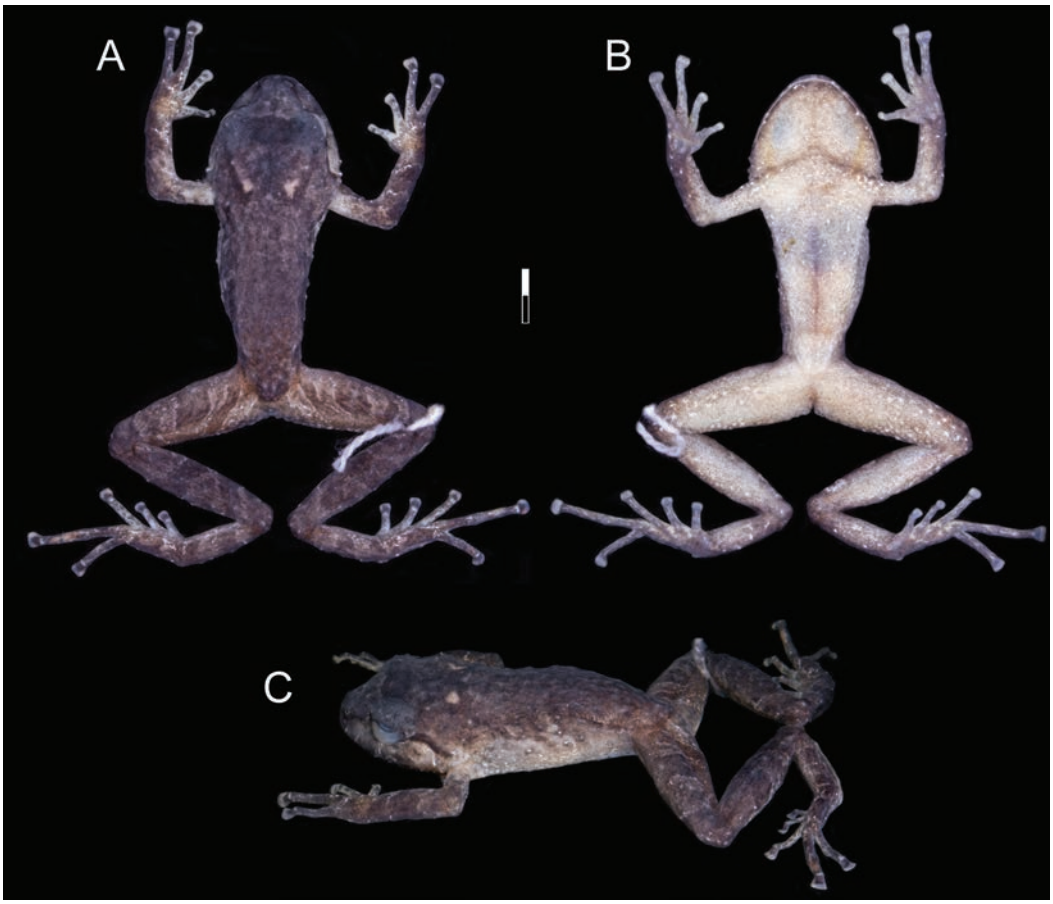

Figure 4. *Pristimantis ruidus*, adult female DHMECN 19106 in preservative: **A.** Dorsal view; **B.** Ventral view; **C.** Lateral view. Scale bar: 4 mm. Photographs: Juan Sánchez.

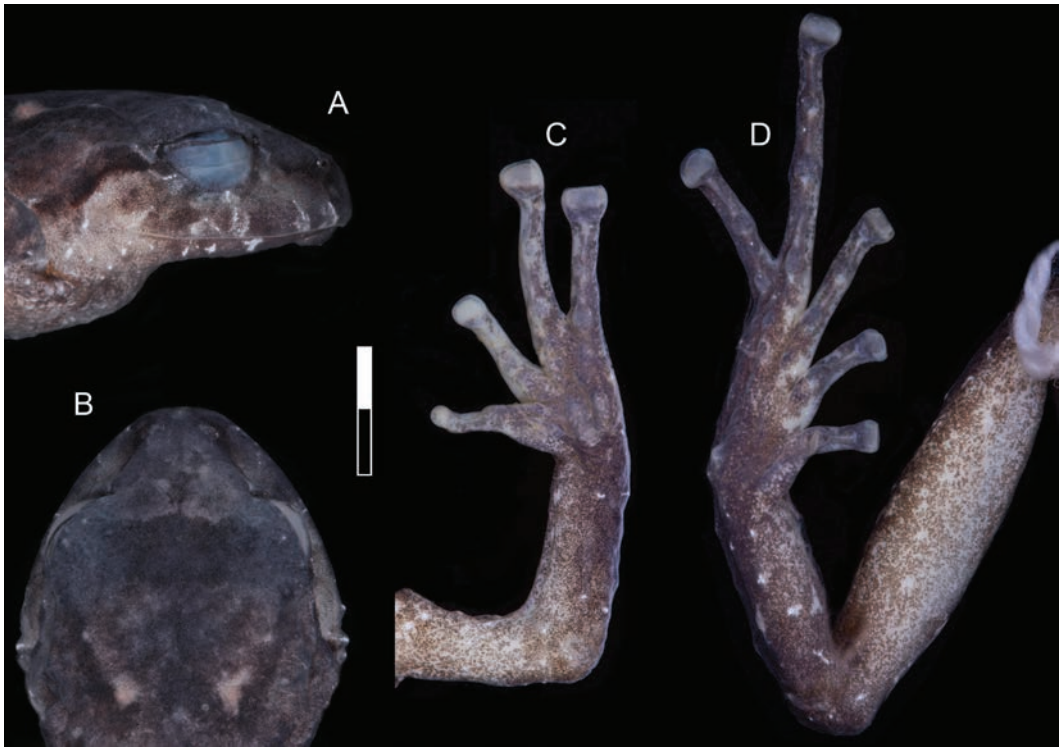

Figure 5. *Pristimantis ruidus*, adult female DHMECN 19106, details in preservative: **A.** Lateral view of head; **B.** Dorsal view of head; **C.** Ventral view of hand; **D.** Ventral view of foot. Scale bar: 4 mm. Photographs: Juan Sánchez.

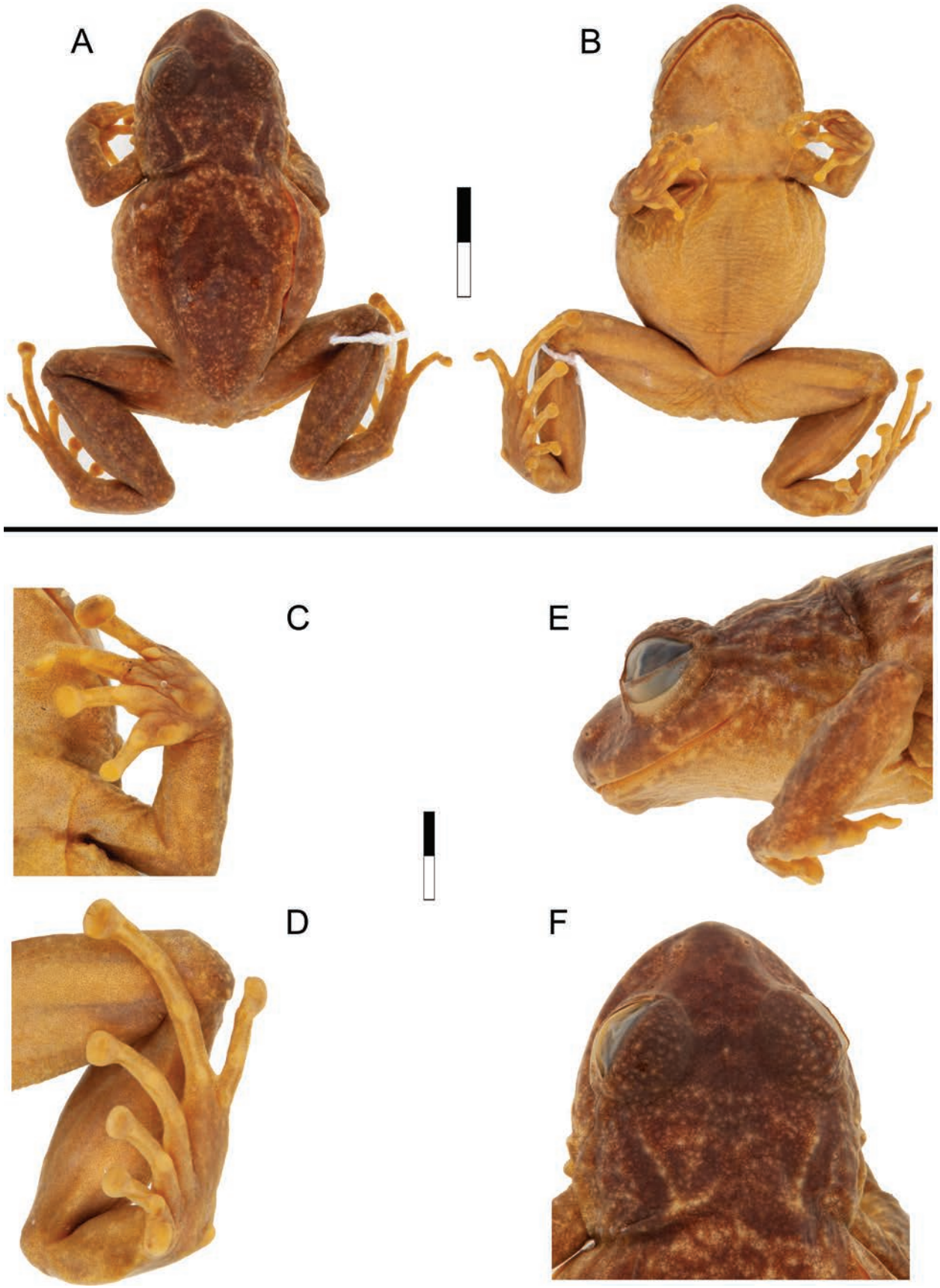

Figure 6. Holotype of *Pristimantis ruidus* AMNH 17590: **A.** Dorsal view; **B.** Ventral view; **C.** Ventral view of hand; **D.** Ventral view of foot; **E.** Lateral view of head **F.** Dorsal view of head; SVL = 38.4 mm. Scale bar: 10 mm (Above the black line); 4 mm (Below the black line). Photographs: Lauren Vonnahme.

Figure 7. Bayesian phylogenetic tree of the *Huicundomantis* subgenus of *Pristimantis*. The analysis is based on 2413 base-pairs of concatenated mitochondrial DNA from *12S* and *16S* and nuclear DNA *RAG-1* gene fragments. Outgroup is not shown. The catalogue number, species name, province and short locality name of the vouchers (in the case of Ecuadorian specimens) are shown next to each terminal (associated data are listed in Appendix 1). Abbreviations: SH-aLRT = SH-like approximate likelihood ratio branch test, UFBoot = ultrafast bootstrap, Boot = standard non-parametric bootstrap, PP = Bayesian posterior probabilities.

accurate, as the Extent of Occurrence (EOO) is less than 20 km^2, the Area of Occupancy (AOO) is less than 10 km^2, probably only one viable population and a low number of individuals. However, the complement "Possibly Extinct" should be removed from the IUCN assessment.

Remarks. We identified contradictions between the *Diagnosis* and *Description* sections from Lynch (1979), as well as characteristics that could have been lost due to the preservation of the original specimens and which are easily recognisable by examining the living specimens and recently preserved specimens. In the case of the condition of digits without rounded pads, we recognised them as elliptical. The interorbital space originally described as flat, but without mention of the presence of the one evident rounded tubercle, as it is noticeable in the photographs of the holotype and the fig. 18 in Lynch (1979). The discoidal fold is absent in our

Figure 8. Above: Panoramic view of Reserva de Conservación Quitahuaycu (Amaru Foundation). Below: Montane evergreen forest habitat of *Pristimantis ruidus*. Photographs: Ernesto Arbeláez.

specimens and the holotype photographs in concordance with *Diagnosis* (Lynch 1979) but differs from the *Description* in the same publication and is misidentified as relatively prominent. In Lynch and Duellman (1997), the authors mentioned that Toe V was much longer than Toe III; however, when examining the holotype photographs, we can observe that, in reality, the size relationship between Toe V and Toe III is similar to that of our specimens (Toe V extends slightly beyond subarticular tubercle II and Toe III does not exceed subarticular tubercle II) (Fig. 6). According to Lynch (1979), AMNH 17597 (SVL = 29.0 mm) is not a mature female, having moderate convolutions and small eggs. However, our specimen DHMECN 19106 (SVL = 30.0 mm) is an adult female because it has developed ovaries.

Discussion

The rediscovery of *P. ruidus* after one hundred years shows that there still exist montane forests that preserve conditions suitable for the survival of rare and threatened species. Despite several unsuccessful efforts to record the species in the type locality, leading to an evaluation of possibly extinct (IUCN 2023), we found that a population still persists in the area, emphasising the importance of conserving this habitat, one of the last remnants of West Andean Montane Forest in southern Ecuador (Sierra et al. 2021). For any effective conservation measures, efforts should focus on the protection and monitoring of montane forests and paramos in the region, along with the collection of basic ecological data, as well as intensive searches for additional populations.

In the original description of this species, Lynch (1979) reports that the specimens were found under rocks. This might be because, in the past, most searches for amphibians were done during the day, due to complicated logistics of night-time fieldwork. In several species of *Pristimantis* whose activity is nocturnal, they take refuge on the ground, under rocks or logs during the day (Arroyo et al. 2008). Based on our observations, *P. ruidus* similarly displays nocturnal activity. Additionally, both specimens of *P. ruidus* were found on shrubs or vegetation at the edge of streams, a microhabitat preference which we have also noticed in other *Pristimantis* species that lack an external tympanum, such as *P. philipi* and *P. cryophilius* (personal observation).

The phylogenetic closeness between *P. ruidus* and *P. philipi* and their basal position within the entire clade of the subgenus *Huicundomantis* (Páez and Ron 2019) implies an allopatric speciation process associated with the Macizo del Cajas. This region is isolated due to its high mountain ecosystems (Barnett 1999) and houses endemic species of amphibians, such as *Atelopus nanay*, *Atelopus onorei* Coloma, Lötters, Duellman & Miranda-Leiva, 2007, *P. erythros* Sánchez-Nivicela, Celi-Piedra, Posse-Sarmiento, Urgilés, Yánez-Muñoz & Cisneros-Heredia, 2018, *P. philipi* and *P. ruidus* (Lynch 1979; Lynch and Duellman 1997; Coloma 2002; Coloma et al. 2007; Sánchez-Nivicela et al. 2018).

Our comprehensive description of the morphological characters of *P. ruidus*, along with the additional information regarding its phylogenetic position, distribution and natural history, enhances our understanding of a species that has eluded researchers for decades. This will enable future taxonomic and systematic research of this group of frogs and assist in conservation efforts for a threatened fauna.

Acknowledgements

We express our gratitude to the colleagues and partners of the Fundación Cóndor Andino for being a part of the field exploration team. Additionally, we extend our thanks to the friends and associates from Fundación y Bioparque AMARU for their invaluable assistance during research field trips and collaboration for the development of this research. Likewise, we are indebted to the Instituto de Biodiversidad del Ecuador (INABIO) for accepting the valuable specimen in their collections. The phylogenetic work was partially funded by Universidad Técnica Particular de Loja, through the project "Descripción de nuevas especies de anfibios y reptiles del sur de Ecuador a partir de las colecciones del Museo de Zoología, UTPL" (PROY_INV_CCBIO_2020_2794), Rainforest Trust and Naturaleza y Cultura Internacional through the "Investigación científica, para la protección y monitoreo de especies de anfibios en el Área Clave de Biodiversidad Abra de Zamora" project (PROY_INV_BA_2022_3502 PY3502). We are kindly grateful to David A. Kizirian, Lauren Vonnahme and Jesse Delia of the American Museum of Natural History for the holotype photographs. The financial support and advice of Byron Swift from ReWild and Fabián Rodas from Naturaleza y Cultura Internacional were essential to promote conservation and biodiversity research of Reserva de Conservación Quitahuaycu.

References

Angulo A, Rueda-Almonacid JV, Rodríguez-Mahecha JV, La Marca E (2006) Técnicas de inventario y monitoreo para los anfibios de la región tropical andina. Conservación Internacional, Bogotá-Colombia, 290 pp.

Arroyo SB, Serrano-Cardozo VH, Ramírez-Pinilla MP (2008) Diet, microhabitat and time of activity in a *Pristimantis* (Anura, Strabomantidae) assemblage. Phyllomedusa 7(2): 109–119. https://doi.org/10.11606/issn.2316-9079.v7i2p109-119

Barnett A (1999) Small mammals of the Cajas Plateau, southern Ecuador: Ecology and natural history. Bulletin of the Florida State Museum Biological Sciences 42(4): 161–217. https://doi.org/10.58782/flmnh.ihkc6085

Beaupre SJ, Jacobson ER, Lillywhite HB, Zamudio K (2004) Guidelines for use of live amphibians and reptiles in field and laboratory research. Second Edition. Herpetological Animal Care and Use Committee (HACC) of the American Society of Ichthyologists and Herpetologists, Glen Allen, VA, 43 pp.

Coloma LA (2002) Two new species of *Atelopus* (Anura, Bufonidae) from Ecuador. Herpetologica 58(2): 229–252. https://doi.org/10.1655/0018-0831(2002)058[0229:TNSOAA]2.0.CO;2

Coloma LA, Lötters S, Duellman WE, Miranda-Leiva A (2007) A taxonomic revision of *Atelopus pachydermus*, and description of two new (extinct?) species of *Atelopus* from Ecuador (Anura: Bufonidae). Zootaxa 1557(1): 1–32. https://doi.org/10.11646/zootaxa.1557.1.1

Duellman WE, Lehr E (2009) Terrestrial-breeding frogs (Strabomantidae) in Peru. Natur und Tier Verlag, Münster, Germany, 384 pp.

Felsenstein J (1985) Confidence limits on phylogenies: An approach using the bootstrap. Evolution 39(4): 783–791. https://doi.org/10.2307/2408678

Frost DR (2023) Amphibian Species of the World: an Online Reference. Version 6.2. Electronic Database. American Museum of Natural History, New York, USA. https://doi.org/10.5531/db.vz.0001

Guindon S, Dufayard JF, Lefort V, Anisimova M, Hordijk W, Gascuel O (2010) New algorithms and methods to estimate maximum-likelihood phylogenies: Assessing the performance of PhyML 3.0. Systematic Biology 59(3): 307–321. https://doi.org/10.1093/sysbio/syq010

Heyer R, Donnelly MA, McDiarmid RW, Hayek LAC (2001) Medición y monitoreo de la diversidad biológica: métodos estandarizados para anfibios (No. Gn3150). Editorial Universitaria de la Patagonia, Chubut, Argentina, 349 pp.

Hoang DT, Chernomor O, von Haeseler A, Minh BQ, Vinh LS (2018) UFBoot2: Improving the ultrafast bootstrap approximation. Molecular Biology and Evolution 35(2): 518–522. https://doi.org/10.1093/molbev/msx281

IUCN SSC Amphibian Specialist Group (2023) *Pristimantis ruidus*. The IUCN Red List of Threatened Species 2023: e. T56935A98653456. https://doi.org/10.2305/IUCN.UK.2023-1.RLTS.T56935A98653456.en

Jiménez de la Espada M (1870) Fauna neotropicalis species quaedam nondum cognitae. Jornal de Sciências, Mathemáticas, Physicas e Naturaes. Lisboa 3: 57–65. https://biostor.org/reference/100700

Katoh K, Standley DM (2013) MAFFT multiple sequence alignment software version 7: Improvements in performance and usability. Molecular Biology and Evolution 30(4): 772–780. https://doi.org/10.1093/molbev/mst010

Köhler G (2012) Color Catalogue for Field Biologist. Herpeton, Offenbach, Germany, 49 pp.

Lanfear R, Frandsen PB, Wright AM, Senfeld T, Calcott B (2017) PartitionFinder 2: New methods for selecting partitioned models of evolution for molecular and morphological phylogenetic analyses. Molecular Biology and Evolution 34: 772–773. https://doi.org/10.1093/molbev/msw260

Lynch JD (1979) Leptodactylid frogs of the genus *Eleutherodactylus* from the Andes of southern Ecuador. University of Kansas Natural History Museum Miscellaneous Publication 66: 1–62. https://doi.org/10.5962/bhl.title.16268

Lynch JD, Duellman WE (1997) Frogs of the genus *Eleutherodactylus* (Leptodactylidae) in western Ecuador: systematic, ecology, and biogeography. Natural History Museum, University of Kansas, Lawrence, KS, 236 pp. https://doi.org/10.5962/bhl.title.7951

MAE (Ministerio del Ambiente del Ecuador) (2012) Sistema de clasificación de los ecosistemas del Ecuador continental. Subsecretaría de Patrimonio Natural. Quito, Ecuador, 136 pp.

Minh BQ, Schmidt HA, Chernomor O, Schrempf D, Woodhams MD, von Haeseler A, Lanfear R (2020) IQ-TREE 2: New models and efficient methods for phylogenetic inference in the genomic era. Molecular Biology and Evolution 37(5): 1530–1534. https://doi.org/10.1093/molbev/msaa015

Molina A, Cabrera E, Moreno L, Sharman MA, Cuevas F (2015) Mapa de Pobreza y Desigualdad por consumo Ecuador 2014. Instituto Nacional de Estadística y Censos y Banco Mundial (INEC-BM). Quito-Ecuador, 281 pp.

Müller J, Müller K, Neinhuis C, Quandt D (2010) PhyDe. Phylogenetic Data Editor versión 0.9971. http://www.phyde.de

Ortega JA, Brito J, Ron SR (2022) Six new species of *Pristimantis* (Anura, Strabomantidae) from Llanganates National Park and Sangay National Park in Amazonian cloud forests of Ecuador. PeerJ 10: e13761. https://doi.org/10.7717/peerj.13761

Ortega-Andrade HM, Rodes Blanco M, Cisneros-Heredia DF, Guerra Arévalo N, López de Vargas-Machuca KG, Sánchez-Nivicela JC, Armijos-Ojeda D, Cáceres Andrade JF, Reyes-Puig C, Quezada Riera AB, Székely P, Rojas Soto OR, Székely D, Guayasamin JM, Siavichay Pesántez FR, Amador L, Betancourt R, Ramírez-Jaramillo SM, Timbe-Borja B, Gómez Laporta M, Webster Bernal JF, Oyagata Cachimuel LA, Chávez Jácome D, Posse V, Valle-Piñuela C, Padilla Jiménez D, Reyes-Puig JP, Terán-Valdez A, Coloma LA, Pérez Lara MB, Carvajal-Endara S, Urgilés M, Yánez-Muñoz MH (2021) Red List assessment of amphibian species of Ecuador: A multidimensional approach for their conservation. PLoS ONE 16(5): e0251027. https://doi.org/10.1371/journal.pone.0251027

Páez NB, Ron SR (2019) Systematics of *Huicundomantis*, a new subgenus of *Pristimantis* (Anura, Strabomantidae) with extraordinary cryptic diversity and eleven new species. ZooKeys 868: 1–112. https://doi.org/10.3897/zookeys.868.26766

Price MN, Dehal PS, Arkin AP (2010) FastTree 2—Approximately maximum-likelihood trees for large alignments. PLoS ONE 5(3): e9490. https://doi.org/10.1371/journal.pone.0009490

Rambaut A (2014) FigTree, Tree Figure Drawing Tool. v. 1.4.2. http://tree.bio.ed.ac.uk/software/figtree

Ron SR, Merino-Viteri A, Ortiz DA (2022) Anfibios del Ecuador. Versión 2022.0. Museo de Zoología, Pontificia Universidad Católica del Ecuador. https://bioweb.bio/faunaweb/amphibiaweb

Ronquist F, Teslenko M, Van Der Mark P, Ayres DL, Darling A, Höhna S, Larget B, Liu L, Suchard MA, Huelsenbeck JP (2012) MrBayes 3.2: Efficient Bayesian phylogenetic inference and model choice across a large model space. Systematic Biology 61(3): 539–542. https://doi.org/10.1093/sysbio/sys029

Sánchez-Nivicela JC, Celi-Piedra E, Posse-Sarmiento V, Urgiles VL, Yánez-Muñoz M, Cisneros-Heredia DF (2018) A new species of *Pristimantis* (Anura, Craugastoridae) from the Cajas Massif, southern Ecuador. ZooKeys 751: 113–128. https://doi.org/10.3897/zookeys.751.20541

Sánchez-Nivicela JC, Toral-Contreras E, Urgiles VL (2021) Una nueva especie de *Pristimantis* (Anura, Strabomantidae) de la provincia del Azuay, Andes sur de Ecuador. Neotropical Biodiversity 8(1): 305–322. https://doi.org/10.1080/23766808.2022.2123731

Sierra R, Calva O, Guevara A (2021) La Deforestación en el Ecuador, 1990–2018. Factores promotores y tendencias recientes. Ministerio de Ambiente y Agua del Ecuador, Ministerio de Agricultura del Ecuador, Quito, Ecuador, 216 pp.

Simmons JE, Muñoz-Saba Y (2005) Cuidado, manejo y conservación de las colecciones biológicas. Conservación Internacional, Serie Manuales para la conservación. Conservación Internacional Colombia, Bogotá, 288 pp.

Székely P, Eguiguren JS, Székely D, Ordóñez-Delgado L, Armijos-Ojeda D, Riofrío-Guamán ML, Cogălniceanu D (2018) A new minute *Pristimantis* (Amphibia: Anura: Strabomantidae) from the Andes of southern Ecuador. PLoS ONE 13(8): e0202332. https://doi.org/10.1371/journal.pone.0202332

Székely P, Eguiguren JS, Ordóñez-Delgado L, Armijos-Ojeda D, Székely D (2020) Fifty years after: A taxonomic revision of the amphibian species from the Ecuadorian biodiversity hotspot Abra de Zamora, with description of two new *Pristimantis* species. PLoS ONE 15(9): e0238306. https://doi.org/10.1371/journal.pone.0238306

Székely P, Székely D, Ordóñez-Delgado L, Armijos-Ojeda D, Vörös J (2021) Our unknown neighbor: A new species of rain frog of the genus *Pristimantis* (Amphibia, Anura, Strabomantidae) from the city of Loja, southern Ecuador. PLoS One 16(10): e0258454. https://doi.org/10.1371/journal.pone.0258454

Tamura K, Stecher G, Peterson D, Filipski A, Kumar S (2013) MEGA6: Molecular Evolutionary Genetics Analysis Version 6.0. Molecular Biology and Evolution 30(12): 2725–2729. https://doi.org/10.1093/molbev/mst197

Urgiles VL, Sánchez-Nivicela JC, Nieves C, Yánez-Muñoz MH (2014) Ranas terrestres en los ecosistemas surandinos de Ecuador I: Dos nuevas especies de *Pristimantis* (Anura, Craugastoridae) de la ladera oriental. ACI Avances en Ciencias e Ingenierías 6(1): B51–B59. https://doi.org/10.18272/aci.v6i1.159

Urgiles VL, Posse V, Timbe BA, Astudillo PX, Sánchez-Nivicela JC (2017) A new terrestrial frog (Anura, Craugastoridae) from the montane cloud forests of the southeastern Ecuadorian Andes. Zootaxa 4318(3): 520–530. https://doi.org/10.11646/zootaxa.4318.3.5

Urgiles VL, Székely P, Székely D, Christodoulides N, Sánchez-Nivicela JC, Savage AE (2019) Genetic delimitation of *Pristimantis orestes* (Lynch, 1979) and *P. saturninoi* Brito et al., 2017 and description of two new terrestrial frogs from the *Pristimantis orestes* species group (Anura, Strabomantidae). ZooKeys 864: 111–146. https://doi.org/10.3897/zookeys.864.35102

Yánez-Muñoz MH, Sánchez-Nivicela JC, Reyes-Puig C (2016) Tres nuevas especies de ranas terrestres *Pristimantis* (Anura, Craugastoridae) de la Provincia de El Oro, Ecuador. ACI Avances en Ciencias e Ingenierías 8(1): 5–25. https://doi.org/10.18272/aci.v8i14.455

Yánez-Muñoz MH, Veintimilla-Yánez D, Batallas D, Cisneros-Heredia DF (2019) A new giant *Pristimantis* (Anura, Craugastoridae) from the paramos of the Podocarpus National Park, southern Ecuador. ZooKeys 852: 137–156. https://doi.org/10.3897/zookeys.852.24557

Appendix 1

Table A1. Voucher number, GenBank accession number and locality for the *Pristimantis* (*Huicundomantis*) specimens used in the phylogenetic analysis. Bold letters mark the sequences generated by the present study.

Species	Voucher number	GenBank accession no.			Locality
		12S	***16S***	***RAG1***	
Pristimantis andinogigas	MUTPL359	MT764339	MT756022	MT810305	Ecuador: Loja, Parque Nacional Podocarpus, Cajanuma
Pristimantis atillo	QCAZ42488	-	MK881440	MK881340	Ecuador: Morona Santiago, Parque Nacional Sangay, Lagunas de Atillo
Pristimantis atillo	QCAZ42498	-	MK881444	MK881344	Ecuador: Morona Santiago, Parque Nacional Sangay
Pristimantis atratus	QCAZ45580	-	MK881471	MK881364	Ecuador: Loja, Cajanuma
Pristimantis atratus	QCAZ45645	-	MK881473	MK881366	Ecuador: Loja, Parque Nacional Podocarpus, Cajanuma
Pristimantis balionotus	MUTPL180	MT778069	MT756023	MT810306	Ecuador: Loja, Reserva Madrigal del Podocarpus
Pristimantis balionotus	MUTPL392	MT778071	MT756025	MT810308	Ecuador: Loja, Abra de Zamora
Pristimantis ceuthospilus	KU212216	EF493520	EF493520	-	Peru: Cajamarca, Chota, 12 km W Llama
Pristimantis chomskyi	MUTPL524	MZ678943	MZ678934	MZ700220	Ecuador: Loja, Parque Nacional Podocarpus, Cerro Toledo
Pristimantis chomskyi	QCAZ45666	-	MK881476	MK881369	Ecuador: Zamora Chinchipe, Reserva Tapichalaca
Pristimantis colodactylus	MUTPL388	MT778072	MT762200	MT810310	Loja, Abra de Zamora
Pristimantis cryptomelas	MUTPL135	MT778073	MT756026	MT810311	Ecuador: Loja, Abra de Zamora
Pristimantis cryptomelas	MUTPL168	MT778075	MT756028	MT810313	Ecuador: Loja, Bosque Protector Washapamba
Pristimantis diadematus	KU221999	EU186668	EU186668	-	Peru: Loreto, Teniente Lopez
Pristimantis gagliardoi	QCAZ42575	-	MK881456	MK881355	Ecuador: Morona Santiago, Parque Nacional Sangay, Ranger Station, Tinguichaca river
Pristimantis gagliardoi	QCAZ46738	-	MK881480	MK881372	Ecuador: Cañar, Reserva Mazar
Pristimantis galdi	QCAZ32368	EU186670	EU186670	EU186746	Ecuador: Zamora Chinchipe, El Pangui
Pristimantis gloria	KU218035	EF493348	EF493348	-	Ecuador: Azuay, 8.1 km W Morona Santiago border, Gualaceo-Limón road
Pristimantis gloria	MUTPL223	MT778079	MT756032	MT810317	Ecuador: Loja, 21 km E Urdaneta
Pristimantis gloria	QCAZ16448	-	MK881402	MK881316	Ecuador: Azuay, Gualaceo-Macas road
Pristimantis hampatusami	QCAZ58042	-	MK881504	MK881387	Ecuador: El Oro, Reserva Buenaventura
Pristimantis hampatusami	QCAZ58044	-	KX525478	KX525472	Ecuador: El Oro, Reserva Buenaventura

Species	Voucher number	GenBank accession no.			Locality
		12S	*16S*	*RAG1*	
Pristimantis imitatrix	KU215476	EF493824	EF493667	-	Peru: Madre de Dios, Cuzco Amazonico, 15 km E Puerto Maldonado
Pristimantis jimenezi	QCAZ45178	-	MK881468	MK881362	Ecuador: Azuay, San Antonio, Parque Nacional Cajas border
Pristimantis jimenezi	QCAZ46978	-	MK881482	MK881374	Ecuador: Azuay, Molleturo, Zadracay river
Pristimantis lojanus	MUTPL178	MZ678945	MZ678936	MZ700222	Ecuador: Loja, Loja, Quebrada San Simon
Pristimantis lojanus	MUTPL191	MZ678946	MZ678937	MZ700223	Ecuador: Loja, Cristal
Pristimantis lutzae	QCAZ32785	-	MK881421	MK881326	Ecuador: Azuay, Bosque Protector Yanuncay-Irquis, Páramo de Quimsacocha
Pristimantis lutzae	QCAZ53728	-	MK881495	-	Ecuador: Azuay, Parque Nacional Cajas, El Capo, Laguna Toreadora
Pristimantis mallii	QCAZ45744	MZ330729	MZ241492	-	Ecuador: Pastaza, Reserva Comunitaria Ankaku
Pristimantis melanogaster	MHNSM56846	EF493826	EF493664	-	Peru: Amazonas, N. Slobe Abra Barro Negro, 28 km SSW Leimebambe
Pristimantis mallii	QCAZ45770	MZ330730	MZ241496	MZ332932	Ecuador: Pastaza, Reserva Comunitaria Ankaku
Pristimantis miktos	GGU807	-	KP064151	-	Peru: Loreto, Nanay, Lote 123
Pristimantis miktos	QCAZ55445	-	MZ241510	MK391383	Ecuador: Orellana, Parque Nacional Yasuní, Tambococha
Pristimantis multicolor	QCAZ47213	-	MK881488	-	Ecuador: Loja, Parque Nacional Yacuri, Laguna Negra
Pristimantis multicolor	QCAZ47214	-	MK881489	-	Ecuador: Loja, Parque Nacional Yacuri, Laguna Negra
Pristimantis muscosus	QCAZ54857	-	MK881501	MK881386	Ecuador: Zamora Chinchipe, Reserva Tapichalaca
Pristimantis nangaritza	QCAZ41710	-	MK881436	MK881336	Ecuador: Zamora Chinchipe, Alto Nangaritza PF, Las Orquídeas, Tepuy forest
Pristimantis orcesi	KU218021	EF493679	EF493679	-	Ecuador: Pichincha, Bosque de Pasochoa
Pristimantis orestes	MUTPL242	MT778087	MK604538	MK602185	Ecuador: Loja, 11 km NE Urdaneta
Pristimantis percultus	MUTPL810	MT778088	MT756034	MT810325	Ecuador: Loja, Parque Nacional Podocarpus, Cajanuma
Pristimantis percultus	MUTPL812	MT778089	MT756035	MT810326	Ecuador: Loja, Parque Nacional Podocarpus, Cajanuma
Pristimantis philipi	KU217863	EF493672	EF493672	-	Ecuador: Azuay, 4 km W Laguna Toreadora, nearby Parque Nacional Cajas
Pristimantis philipi	QCAZ37537	-	MK881426	MK881331	Ecuador: Azuay, Parque Nacional Cajas
Pristimantis phoxocephalus	QCAZ58463	-	MK881507	MK881390	Ecuador: Cotopaxi, Pilaló surroundings
Pristimantis rhodoplichus	KU219788	EF493674	EF493674	-	Peru: Piura, El Tambo
Pristimantis ruidus	DHMECN19106	**PP725379**	**PP723736**	**PP731015**	Ecuador: Azuay, Quitahuaycu reserve
Pristimantis ruidus	MUTPL1613	**PP725380**	**PP723737**	**PP731016**	Ecuador: Azuay, Quitahuaycu reserve
Pristimantis simonsii	KU212350	EU186665	EU186665	-	Peru: Cajamarca, S slope Abra Quilsh, 28 km NNW Cajamarca
Pristimantis spinosus	KU218052	EF493673	EF493673	-	Ecuador: Morona Santiago, 10.6 km W Plan de Milagro
Pristimantis tamia	QCAZ59630	MZ330735	MZ241526	MZ332958	Ecuador: Pastaza, Parque Nacional Llanganates, Comunidad Zarentza
Pristimantis tamia	QCAZ59643	MZ330736	MZ241528	MZ332960	Ecuador: Pastaza, Parque Nacional Llanganates, Comunidad Zarentza
Pristimantis teslai	QCAZ46213	-	MK881478	-	Ecuador: Tungurahua, Llanganatillo, Parque Nacional Llanganates border
Pristimantis tinguichaca	QCAZ31945	-	MK881418	MK881323	Ecuador: Morona Santiago, Parque Nacional Sangay, San Vicente
Pristimantis tinguichaca	QCAZ40582	-	MK881433	MK881334	Ecuador: Morona Santiago, Parque Nacional Sangay, Lagunas de Atillo
Pristimantis torresi	MUTPL996	MZ678947	MZ678938	MZ700224	Ecuador: Loja, Guachanamá, El Apretadero
Pristimantis torresi	QCAZ47397	-	MK881492	MK881380	Ecuador: Loja, Celica-Alamor road
Pristimantis totoroi	KU218025	EF493349	EF493349	-	Ecuador: Chimborazo, 70 km W Riobamba via Pallatanga
Pristimantis totoroi	QCAZ58425	-	MK881505	MK881388	Ecuador: Cotopaxi, Pilaló surroundings
Pristimantis unistrigatus	KU218057	EF493387	EF493387	EF493444	Ecuador: Imbabura, 35 km E Pquela
Pristimantis verrucolatus	QCAZ46982	-	MK881483	MK881375	Ecuador: Azuay, Yumate, Shoupshe
Pristimantis verrucolatus	QCAZ46993	-	MK881485	MK881377	Ecuador: Azuay, Cochapamba
Pristimantis versicolor	KU218096	EF493389	EF493389	EF493431	Ecuador: Loja, Abra de Zamora
Pristimantis versicolor	MUTPL494	MT778095	MT756038	MT810332	Ecuador: Loja, Reserva Madrigal del Podocarpus
Pristimantis wiensi	KU219796	EF493377	EF493668	-	Peru: Piura, 12.7 km E Canchaque
Pristimantis sp.	QCAZ26642	-	MK881409	-	Ecuador: Azuay, San Antonio de Chaucha
Pristimantis sp.	QCAZ32790	-	MK881423	MK881328	Ecuador: Azuay, Bosque Protector Yanuncay-Irquis, Páramo de Quimsacocha
Pristimantis sp.	QCAZ45029	-	MK881461	-	Ecuador: Morona Santiago, Parque Nacional Sangay, Etén, Rio Culebrillas
Pristimantis sp.	QCAZ45129	-	MK881462	MK881358	Ecuador: El Oro, Chillacocha
Pristimantis sp.	QCAZ45720	-	MZ241490	MZ332927	Ecuador: Pastaza, Reserva Comunitaria Ankaku
Pristimantis sp.	QCAZ45945	-	MZ241502	MZ332938	Ecuador: Pastaza, Reserva Comunitaria Ankaku
Pristimantis sp.	QCAZ53999	-	MK881496	-	Ecuador: Zamora Chinchipe, Yacuambi, Romerillos
Pristimantis sp.	QCAZ58855	-	MZ241514	MZ332949	Ecuador: Morona Santiago, Parque Nacional Sangay, Sardinayacu

Zoosyst. Evol. 100 (3) 2024, 1121–1134 | DOI 10.3897/zse.100.127268

PENSOFT

MUSEUM FÜR NATURKUNDE BERLIN

Taxonomic determination of *Hypselotriton* populations distributed in eastern Guangdong, China (Caudata, Salamandridae), with description of a new species and a new subgenus

Jian Wang[1,2], Zhao-Chi Zeng[1,2], Tian-Li Wei[1], Zhi-Tong Lyu[2,3]

1 *Guangdong Polytechnic of Environmental Protection Engineering, Foshan 528216, Guangdong, China*

2 *The Museum of Biology, School of Life Sciences, Sun Yat-sen University, Guangzhou 510275, Guangdong, China*

3 *CAS Key Laboratory of Mountain Ecological Restoration and Bioresource Utilization, Ecological Restoration and Biodiversity Conservation Key Laboratory of Sichuan Province, Chengdu Institute of Biology, Chinese Academy of Sciences, Chengdu 610040, Sichuan, China*

https://zoobank.org/7720F592-80B8-417D-AB7F-EF28AE0B91B4

Corresponding authors: Jian Wang (wangj-1994@outlook.com); Zhi-Tong Lyu (lvzt@foxmail.com)

Academic editor: Umilaela Arifin ♦ **Received** 10 May 2024 ♦ **Accepted** 22 July 2024 ♦ **Published** 14 August 2024

Abstract

In this work, the *Hypselotriton* populations distributed in eastern Guangdong, China are studied in detail to clarify their taxonomic status. Based on morphological comparison and phylogenetic analysis, *H. glaucus* **syn. nov.** is synonymised with *H. orphicus*. *Hypselotriton* (*Cynotriton*) *oolong* **sp. nov.** from Mt Fenghuang in Chaozhou which used to be misidentified as *H. orphicus*, is revealed to be an independent lineage of subgenus *Cynotriton* and can be distinguished from all known congeners in morphology. By contrast, *H. orphicus* did not cluster within *Cynotriton*, but gathered with *H. jiaoren* **comb. nov.** to form a distinct unnamed clade within the genus. We therefore re-delimitate the intrageneric classification of the genus and a new subgenus *Hakkatriton* **subgen. nov.** is erected, corresponding to this unnamed clade. The Chinese Fire-bellied Newt genus *Hypselotriton* currently contains three subgenera and about ten known species. Identified keys to the subgenera and related congeners of genus *Hypselotriton* are further provided.

Key Words

Chaozhou, *Cynops*, *Hakkatriton* subgen. nov., *Hypselotriton* (*Cynotriton*) *oolong* sp. nov., Jiexi

Introduction

The Fire-bellied Newts contain about 18 species distributed in China and Japan in East Asia (Raffaëlli 2022; Lyu et al. 2023a). In traditional configuration, these species were provisionally placed in a single genus *Cynops* Tschudi, 1838, in spite of several controversies (Zhao and Hu 1984; Zhao et al. 1988; Lyu et al. 2023a). However, recent phylogenetic studies suggested the Chinese and Japanese congeners are paraphyletic from each other (Rancilhac et al. 2021; Yuan et al. 2022). In the phylogenetic analysis, the Fire-bellied Newt species distributed in Japanese Archipelago are revealed to be the basal lineage of the Modern Asian Newts. Compared with the insular species, the Fire-bellied Newt species occurring in mainland China are phylogenetically closer to other newt genera from mainland China and Indochina, i.e. *Pachytriton* Boulenger, 1878, *Paramesotriton* Chang, 1935 and *Laotriton* Dubois & Raffaëlli, 2009 (Rancilhac et al. 2021; Yuan et al. 2022). Thus, Raffaëlli (2022) partitioned these species into two independent genera, *Cynops* for the Japanese Fire-bellied Newts and *Hypselotriton* Wolterstorff, 1934 for the Chinese Fire-bellied Newts and which was followed in this work. Particularly, a recent work has described two new species of Chinese Fire-bellied Newts (Lyu et al. 2023a), but did not adopt the latest taxonomic proposal by Raffaëlli (2022) in a timely manner, resulting in two new nomenclature combinations in this work, *H. jiaoren* (Lyu, Qi & Wang, 2023), comb. nov. and *H. maguae* (Lyu, Qi & Wang, 2023), comb. nov.

Within the genus *Hypselotriton*, Dubois and Raffaëlli (2011) classified the congeners into two subgenera, based on morphological and geographical characteristics, *Hypselotriton* and *Cynotriton* Dubois & Raffaëlli, 2011, corresponding to the former *Cynops wolterstorffi* and *Cynops orientalis* groups, respectively (Zhao et al. 1988; Raffaëlli 2022). Nonetheless, phylogenetic analysis has suggested three distinct and divergent clades within the genus, indicating that the intrageneric classification of this genus requires re-delimitation (Lyu et al. 2023a).

The species diversity of Fire-bellied Newts was considered underestimated. Tominaga et al. (2013, 2015) have revealed multiple distinct lineages within *Cynops pyrrhogaster* (Boie, 1826). Compared with the traditional recognition of two known species for Japanese Fire-bellied Newts, Raffaëlli (2022) documented four nominated species and four unnamed species within the insular genus *Cynops*. Meanwhile, four new species of *Hypselotriton* have been described from Southeast Chinese Hilly Area since 2010, dramatically raising the diversity of this mainland genus (Wu et al. 2010; Yuan et al. 2013; Lyu et al. 2023a). However, the taxonomic status for several *Hypselotriton* species remains unresolved. Lyu et al. (2023a) have discussed the taxonomic confusion on the congeners from Yunnan-Guizhou Plateau in southwestern China that still require further studies. During our fieldwork and study on the *Hypselotriton* populations from Guangdong in southeastern China, we have found that the recognition on *H. orphicus* (Risch, 1983) is also with confusion, especially for its delimitation from another congener in eastern Guangdong, *H. glaucus* (Yuan, Jiang, Ding, Zhang & Che, 2013).

Hypselotriton orphicus was nominated by Risch (1983), based on specimens collected and primarily described by Gressitt (1941) from "Dayang (Tai-Yong), Shantou Region [now belonging to Jiexi County, Jieyang City], 23°35'N, 115°51'E [= 23.58°N, 115.85°E], altitude 640 m" (Fig. 1, sites 2–3). *Hypselotriton glaucus* was described, based on specimens collected from "Meiguang Village (23.67°N, 115.80°E; elevation 742 m), in Mt Lianhua, Wuhua County, Meizhou" (Fig. 1, site 9) (Yuan et al. 2013), where it is in close proximity to the type locality of *H. orphicus*. When proposing *H. glaucus*, the data from Jiexi County were not mentioned. Instead, two separate populations collected from Mt Fenghuang of Guangdong and Mt Daiyun of Fujian were recorded as *H. orphicus* and used for comparison (Yuan et al. 2013). Morphologically, the diagnostic characters of *H. glaucus* almost match the description of *H. orphicus* in Risch (1983), except for the irregular greyish-blue patches on the dorsum of *H. glaucus*. Such colour pattern was not described by Gressitt (1941) based on living or freshly-preserved specimens and would fade after preservation. Particularly, Risch (1983) has mentioned that the type series of *H. orphicus* are morphologically different from the population from central Fujian. Thus, the employment of specimens from Mt Daiyun, central Fujian (as well as those from Mt Fenghuang, eastern Guangdong) as *H. orphicus* might be problematic, which further adds to the confusion on the proposal of *H. glaucus*.

In this work, we perform morphological comparisons and molecular analyses on the topotypical population of *Hypselotriton orphicus* and *H. glaucus*, as well as on the *Hypselotriton* population from Mt Fenghuang (Fig. 1, site 1). The results suggest that *H. glaucus* is conspecific with *H. orphicus*, while the population from Mt Fenghuang represents an unnamed lineage of genus *Hypselotriton* that is described hereby. The taxonomic status for the population from central Fujian is also discussed. Furthermore, we re-delimitate the intrageneric classification of the genus, as well as proposing a new subgenus for the clade comprised of *H. orphicus* and *H. jiaoren* comb. nov.

Materials and methods

Specimens and morphological analyses

A series of museum specimens of the genus *Hypselotriton* from eastern Guangdong were examined. Detailed information for these specimens is presented in related species accounts below. Abbreviations for museums and institutes include: **GEP** (Guangdong Polytechnic of Environmental Protection Engineering, Foshan, China), **CIB** (Herpetological Museum, Chengdu Institute of Biology, the Chinese Academy of Sciences, Chengdu, China), **SYS** (The Museum of Biology, Sun Yat-sen University, Guangzhou, China), **MVZ** (Museum of Vertebrate Zoology, University of California, Berkeley, USA), **MNHN** (Museum national d'Histoire naturelle, Paris, France), **AMNH** (American Museum of Natural History, New York, USA) and **CAS** (California Academy of Sciences, San Francisco, USA).

External measurements were made for the unnamed specimens with digital calipers (Neiko 01407A Stainless Steel 6-Inch Digital Caliper) to the nearest 0.1 mm. These measurements are as follows: total length (**TOL**) from tip of snout to tip of tail; snout–vent length (**SVL**) from tip of snout to posterior edge of vent; tail length (**TAL**) from posterior edge of vent to tip of tail; maximum tail depth (**TAD**); head length (**HL**) from tip of snout to the posterior edge of the parotoid gland; maximum head width (**HW**); snout length (**SL**) from tip of snout to the anterior corner of eye; eye diameter (**ED**) from the anterior corner to the posterior corner of the eye; interorbital distance (**IOD**) between the anterior corner of each eye; eye–nostril length (**EN**) from the anterior corner of the eye to the nostril; internasal distance (**IND**) between the external nares; axilla–groin length (**AG**) between the axilla and the groin along the body; fore-limb length (**FLL**) from elbow to tip of finger III; and hind-limb length (**HLL**) from knee to tip of toe III.

The morphological comparisons for known *Hypselotriton* congeners were attained from literature of the original and subsequently supplemental descriptions (David 1873; Boulenger 1905; Gressitt 1941; Liu et al. 1962; Kou and Xing 1983; Risch 1983; Yang 1983; Fei and Ye 1983, 2016; Fei et al. 2006; Wu et al. 2010; Yuan et al. 2013; Raffaëlli 2022; Lyu et al. 2023a).

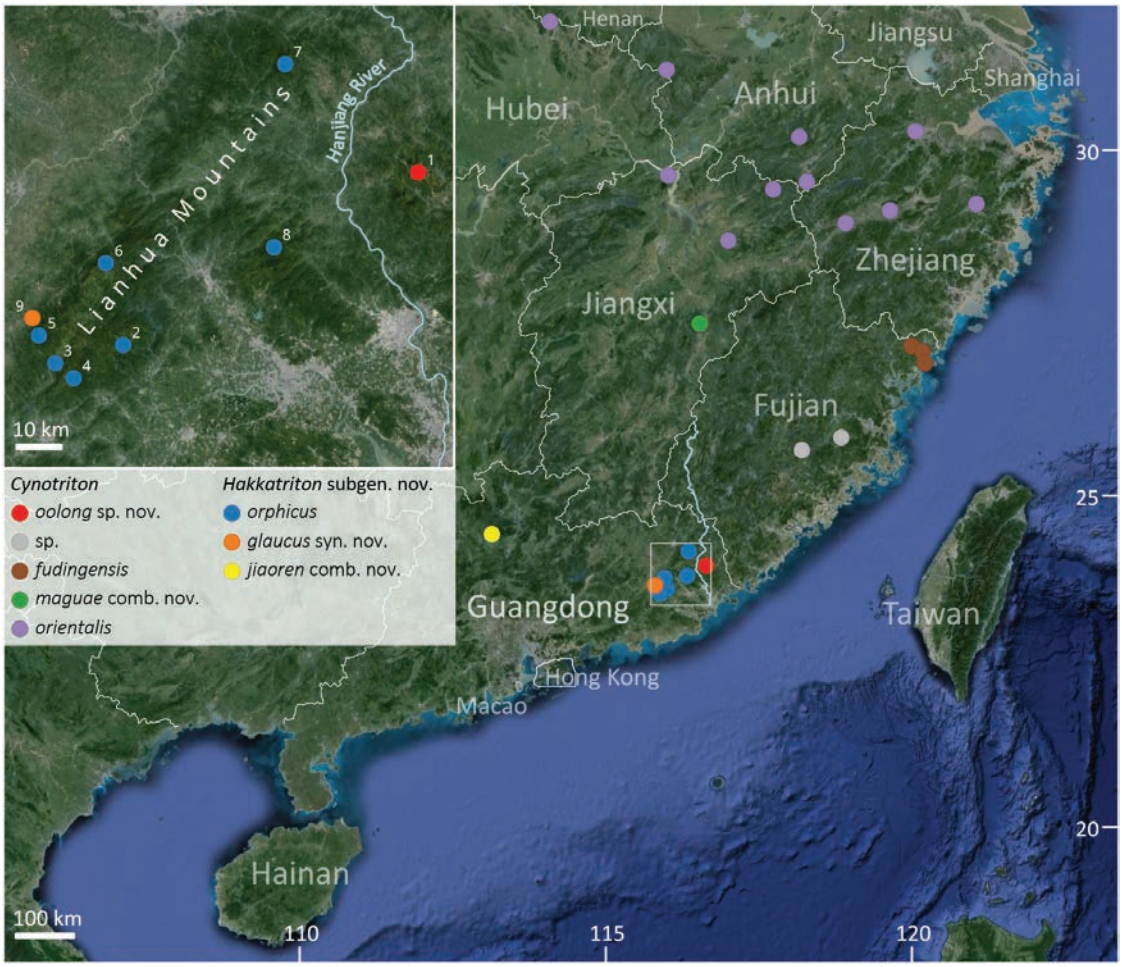

Figure 1. Map showing the localities for congeners of genus *Hypselotriton* from Southeast Chinese Hilly Area. Inset map on top left zooms in eastern Guangdong Province, showing the localities for *H.* (*Cynotriton*) *oolong* sp. nov. and *H.* (*Hakkatriton*) *orphicus*: **1.** Mt Fenghuang, Chao'an District, Chaozhou City (type locality of *H. oolong* sp. nov.); **2.** Dayang Township, Jiexi County, Jieyang City (purported type locality of *H. orphicus*; see Remarks in the species account for locality delimitation); **3.** Liangtian Township, Jiexi County (type locality of *H. orphicus* according to the original coordinate); **4.** Mt Dabei, Jiexi County; **5.** Mt Liwangzhang, Jiexi County; **6.** Mt Hongtuzhang, Fengshun County, Meizhou City; **7.** Mt Tongguzhang, Fengshun County; **8.** Mt Shijiadong, Fengshun County; **9.** Meiguang Village, Mt Lianhua, Wuhua County, Meizhou City (type locality of *H. glaucus* syn. nov.). The map is derived from Tianditu (www.tianditu.gov.cn).

Phylogenetic analyses

In total, 76 samples were used for phylogenetic analyses, encompassing 11 newly-sequenced individuals (three of the *Hypselotriton* population from Mt Fenghuang, four of *H. orphicus* from Jiexi County and two from Fengshun County in Guangdong and two of *H. yunnanensis* from Honghe County in Yunnan) and others obtained from GenBank.

Genomic DNA was extracted, using a DNA extraction kit from Tiangen Biotech (Beijing) Co., Ltd. Two mitochondrion genes, namely NADH dehydrogenase subunit 2 (*ND2*) and Cytochrome b (*cytb*) were amplified for phylogenetic analyses. Primers for *ND2* were L4437 (5'-AAGCTTTCGGGCCCATACC-3') and 5081R (5'-GTCGTAGGGTCAAAGCCTGC-3') and, for *cytb*, these were 14052F (5'-CCTGGGCTCTAACCAAGACC-3') and 15293R (5'-TCGGCTTACAAGACCGATGT-3'). PCR amplifications were processed with the cycling conditions of: initial denaturing step at 95 °C for 4 min, 35 cycles of denaturing at 95 °C for 40 s, annealing at 53 °C for 34 s and extension at 72 °C for 60 s and a final extension step at 72 °C for 10 min. PCR products were purified with spin columns and then sequenced with both forward and reverse primers using BigDye Terminator Cycle Sequencing Kit from Applied Biosystems, on an ABI Prism 3730 automated DNA sequencer by Guangzhou Jierui Biotechnology Co., Ltd. All sequences were deposited in GenBank (Table 1).

For phylogenetic analyses, DNA sequences were aligned by the Clustal W algorithm with default parameters (Thompson et al. 1997). PartitionFinder2 was used to test the best partitioning scheme and jModelTest v.2.1.2 was used to test the best fitting nucleotide substitution model. Bayesian Inference (BI) in MrBayes 3.2.4 (Ronquist et al. 2012) and Maximum Likelihood (ML) in RAxML GUI (Silvestro and Michalak 2012) were used to conduct phylogenetic analyses. For the ML analysis, an optimal tree was obtained and branch supports were evaluated with 1000 rapid bootstrapping replicates.

Table 1. Localities, voucher information and GenBank accession numbers for all samples used in this study.

ID	Genus / Species	Voucher	Locality	ND2	Cytb
1	*Hypselotriton oolong* sp. nov.	CIB 121429	China: Guangdong: Chaozhou: Mt Fenghuang	PP987004	PP987015
2	*Hypselotriton oolong* sp. nov.	CIB 121430	China: Guangdong: Chaozhou: Mt Fenghuang	PP987005	PP987016
3	*Hypselotriton oolong* sp. nov.	SYS a009274	China: Guangdong: Chaozhou: Mt Fenghuang	PP987003	PP987014
4	*Hypselotriton oolong* sp. nov.	KIZ 09816	China: Guangdong: Chaozhou: Mt Fenghuang	ON793719	ON793672
5	*Hypselotriton oolong* sp. nov.	KIZ 09819	China: Guangdong: Chaozhou: Mt Fenghuang	ON793720	ON793673
6	*Hypselotriton oolong* sp. nov.	KIZ 09820	China: Guangdong: Chaozhou: Mt Fenghuang	ON793721	ON793674
7	*Hypselotriton oolong* sp. nov.	KIZ 09821	China: Guangdong: Chaozhou: Mt Fenghuang	ON793722	ON793675
8	*Hypselotriton* sp.	KIZ 09839	China: Fujian: Dehua: Mt Daiyun	ON793723	ON793676
9	*Hypselotriton* sp.	KIZ 09843	China: Fujian: Dehua: Mt Daiyun	ON793725	ON793678
10	*Hypselotriton* sp.	KIZ 09905	China: Fujian: Yongtai	ON793728	ON793681
11	*Hypselotriton* sp.	KIZ 09908	China: Fujian: Yongtai	ON793730	ON793683
12	*Hypselotriton orphicus*	GEP a008	China: Guangdong: Jiexi: Mt Dabei	PP986999	PP987010
13	*Hypselotriton orphicus*	GEP a009	China: Guangdong: Jiexi: Mt Dabei	PP987000	PP987011
14	*Hypselotriton orphicus*	GEP a010	China: Guangdong: Jiexi: Mt Dabei	PP987001	PP987012
15	*Hypselotriton orphicus*	GEP a011	China: Guangdong: Jiexi: Mt Dabei	PP987002	PP987013
16	*Hypselotriton orphicus*	GEP a314	China: Guangdong: Fengshun: Mt Shijiadong	PP987008	PP987019
17	*Hypselotriton orphicus*	GEP a315	China: Guangdong: Fengshun: Mt Shijiadong	PP987009	PP987020
18	*Hypselotriton glaucus* syn. nov.	KIZ 09793	China: Guangdong: Wuhua: Mianyang	ON793715	ON793668
19	*Hypselotriton glaucus* syn. nov.	KIZ 09799	China: Guangdong: Wuhua: Mianyang	ON793716	ON793669
20	*Hypselotriton cyanurus*	KIZ 02330	China: Guizhou: Shuicheng	/	ON793711
21	*Hypselotriton cyanurus*	KIZ 02331	China: Guizhou: Shuicheng	ON793754	ON793712
22	*Hypselotriton cyanurus*	KIZ 02332	China: Guizhou: Shuicheng	ON793755	ON793713
23	*Hypselotriton fudingensis*	KIZ 012918	China: Fujian: Zherong	ON793745	ON793698
24	*Hypselotriton fudingensis*	KIZ 012214	China: Fujian: Ningde: Qingyu	ON793743	ON793696
25	*Hypselotriton fudingensis*	KIZ 012217	China: Fujian: Ningde: Qingyu	ON793744	ON793697
26	*Hypselotriton jiaoren* comb. nov.	SYS a008787	China: Guangdong: Yingde	OQ116680	/
27	*Hypselotriton jiaoren* comb. nov.	SYS a008788	China: Guangdong: Yingde	OQ116681	/
28	*Hypselotriton jiaoren* comb. nov.	SYS a008789	China: Guangdong: Yingde	OQ116682	/
29	*Hypselotriton maguae* comb. nov.	CIB 118535	China: Jiangxi: Nancheng: Mt Magu	OQ116685	/
30	*Hypselotriton maguae* comb. nov.	SYS a007032	China: Jiangxi: Nancheng: Mt Magu	OQ116686	/
31	*Hypselotriton orientalis*	KIZ 06358	China: Zhejiang: Jinhua	ON793718	ON793671
32	*Hypselotriton orientalis*	CIB 97919	China: Zhejiang: Quzhou	GU301790	/
33	*Hypselotriton orientalis*	KIZ 012940	China: Zhejiang: Tiantai	ON793731	ON793684
34	*Hypselotriton orientalis*	MVZ 230345	China: Zhejiang: Hanzhou	EU880311	EU880311
35	*Hypselotriton orientalis*	CIB 97867	China: Jiangxi: Wannian	GU301788	/
36	*Hypselotriton orientalis*	KIZ 013017	China: Henan: Xinyang: Mt Jigong	ON793734	ON793687
37	*Hypselotriton orientalis*	YPX25002	China: Jiangxi: Wuyuan	ON793740	ON793694
38	*Hypselotriton orientalis*	KIZ 020536	China: Jiangxi: Jiujiang	ON793738	ON793692
39	*Hypselotriton orientalis*	KIZ 021962	China: Anhui: Xiuning	ON793737	ON793691
40	*Hypselotriton orientalis*	KIZ 021844	China: Anhui: Huoshan	ON793742	ON793695
41	*Hypselotriton yunnanensis*	CIB 121432	China: Yunnan: Honghe	PP987006	PP987017
42	*Hypselotriton yunnanensis*	CIB 121433	China: Yunnan: Honghe	PP987007	PP987018
43	*Hypselotriton yunnanensis*	SYS a007780	China: Yunnan: Shiping	OQ116687	/
44	*Hypselotriton yunnanensis*	KIZ 01445	China: Yunnan: Ning'er	ON793756	ON793714
45	*Hypselotriton yunnanensis*	KIZ 021922	China: Yunnan: Chuxiong: Zijing	ON793749	ON793706
46	*Hypselotriton yunnanensis*	KIZ 022157	China: Yunnan: Kunming: Huahongdong	ON793751	ON793708
47	*Hypselotriton yunnanensis*	KIZ 022161	China: Yunnan: Kunming: Gulu	ON793753	ON793710
48	*Cynops pyrrhogaster*	KIZ 09755	Japan	/	ON793699
49	*Cynops pyrrhogaster*	KIZ 09757	Japan	/	ON793701
50	*Cynops pyrrhogaster*	MVZ 263718	Japan	EU880313	EU880313
51	*Laotriton laoensis*	FMNH 255452	Laos	EU880328	EU880328
52	*Pachytriton airobranchiatus*	SWUF YZY0301	China: Guangdong: Huizhou: Mt Lianhua	MG732934	MG732932
53	*Pachytriton archospotus*	CIB 95950	China: Jiangxi: Ganzhou: Mt Qiyun	GQ303629	GQ303666
54	*Pachytriton brevipes*	KIZ 08926	China: Fujian: Nanping: Mt Wuyi	ON793903	ON793838
55	*Pachytriton feii*	KIZ 04228	China: Anhui: Huangshan: Mt Huangshan	ON793879	ON793813
56	*Pachytriton granulosus*	KIZ 012977	China: Zhejiang: Taizhou: Tiantai	ON793920	ON793856
57	*Pachytriton inexpectatus*	KIZ 05203	China: Guangxi: Laibin: Mt Dayao	ON793885	ON793819
58	*Pachytriton moi*	KIZ 07767	China: Guangxi: Guilin: Mt Mao'er	ON793895	ON793830
59	*Pachytriton wuguanfui*	KIZ 08756	China: Guangxi: Hezhou	ON793901	ON793836
60	*Pachytriton xanthospilos*	KIZ 06750	China: Hunan: Chenzhou: Mt Mangshan	ON793907	ON793842
61	*Paramesotriton aurantius*	KIZ 012879	China: Fujian: Ningde: Zherong	ON794099	ON794033
62	*Paramesotriton caudopunctatus*	KIZ 03903	China: Guizhou: Qiandongnan: Mt Leigong	ON794069	ON794003
63	*Paramesotriton chinensis*	KIZ 013010	China: Zhejiang: Ningbo: Baixi	ON794108	ON794042

ID	Genus / Species	Voucher	Locality	ND2	Cytb
64	*Paramesotriton deloustali*	MVZ 223629	Vietnam: Tam Dao: Yinh Yen	FJ744600	GQ303669
65	*Paramesotriton fuzhongensis*	KIZ 08568	China: Guangxi: Hezhou: Chaodong	ON794073	ON794007
66	*Paramesotriton guangxiensis*	KIZ 09285	China: Guangxi: Chongzuo: Ningming	ON794071	ON794005
67	*Paramesotriton hongkongensis*	KIZ 01577	China: Hong Kong: Tai Mo Shan	ON794111	ON794045
68	*Paramesotriton labiatus*	KIZ 08769	China: Guangxi: Laibin: Mt Dayao	ON794077	ON794011
69	*Paramesotriton longliensis*	KIZ 03343	China: Guizhou: Qiannan: Longli	ON794064	ON793998
70	*Paramesotriton maolanensis*	GZNU 2006030004	China: Guizhou: Qiannan: Libo	JF438993	JX480887
71	*Paramesotriton qixilingensis*	KIZ 022289	China: Jiangxi: Ji'an: Mt Qixiling	ON794120	ON794055
72	*Paramesotriton wulingensis*	KIZ 03102	China: Chongqing: Youyang	ON794123	ON794058
73	*Paramesotriton yunwuensis*	KIZ 09676	China: Guangdong: Yunfu: Luoding	ON794086	ON794020
74	*Paramesotriton zhijinensis*	KIZ YPX6178	China: Guizhou: Bijie: Zhijing	ON794067	ON794001
75	*Calotriton asper*	Vieites 01	NA	EU880307	EU880307
76	*Euproctus platycephalus*	DBW-MVZ 01	NA	EU880317	EU880317

For the BI analysis, two independent runs with four Markov Chain Monte Carlo simulations were performed for ten million iterations and sampled every 1000 iterations. The first 25% of the samples were discarded as burn-in after the standard deviation of split frequencies of the two runs was less than a value of 0.01. The remaining trees were used to create a consensus tree.

Results

The BI and ML analyses resulted in identical topologies (Fig. 2). Most major nodes were well supported with the Bayesian posterior probabilities (BPP) > 0.95 and the ML bootstrap supports (BS) > 70. All samples of *Hypselotriton* formed a monophyletic group, as the sister taxon to the monophyletic group including *Paramesotriton*, *Pachytriton* and *Laotriton*, but paraphyletic with *Cynops*. This is corresponding to previous studies (Rancilhac et al. 2021; Yuan et al. 2022), supporting the resurrection of *Hypselotriton* as a distinct genus.

Within *Hypselotriton*, three distinct and divergent clades were revealed, as those recovered in Lyu et al. (2023a). Morphological comparisons further sustained the differences amongst these clades (present below), which are treated as representing three subgenera. The clade involving *H. orientalis* has been proposed as subgenus *Cynotriton* and the clade involving *H. cyanurus* is considered to represent the nominotypical subgenus *Hypselotriton* (Dubois and Raffaëlli 2011; Raffaëlli 2022). A new subgenus is nominated in this work to accommodate species within the remaining unnamed clade.

As shown in the tree, the *Hypselotriton* populations distributed in eastern Guangdong have been separated into two distinct and distant lineages. Topotypical samples of *H. orphicus* from Jiexi were clustered with samples of type series of *H. glaucus* in a lineage and almost without genetic divergences, indicating these samples should be conspecific. Morphological examination further confirmed such insight (present below). This lineage was the sister taxon to *H. jiaoren* comb. nov. from northern Guangdong and collectively constituted the new subgenus as mentioned above.

Samples of *Hypselotriton* population from Mt Fenghuang, which was employed as *H. orphicus* (Yuan et al. 2013, 2022; Lyu et al. 2023a), formed an independent lineage within the subgenus *Cynotriton*, representing the southernmost lineage of this subgenus (Fig. 1). Specimens of this lineage showed distinct differences in morphology that can be distinguished from *H. orphicus*, as well as all known congeners of *Hypselotriton*. Thus, this lineage represents an unnamed species that is described in this work. Moreover, the samples of *Hypselotriton* population from central Fujian, which was also employed as *H. orphicus* (Yuan et al. 2013, 2022; Lyu et al. 2023a), formed a distinct lineage as the sister taxon to the Mt Fenghuang lineage, with small genetic divergence. The taxonomic status of this lineage is further remarked below.

Systematics

Genus *Hypselotriton* Wolterstorff, 1934

Type species. *Molge wolterstorffi* Boulenger, 1905, by original designation.

Common name. Chinese Fire-bellied Newts (in English) / diān yuán shǔ (滇螈属 in Chinese).

Distribution. Endemic in mainland China.

Remark. In spite of the paraphyletic relationships and distinct geographical isolation, species of the mainland genus *Hypselotriton* are very similar to those of insular genus *Cynops* in morphology, resulting in the prolonged categorising of these Fire-bellied Newts in a single genus. *Hypselotriton* can be distinguished from *Cynops* by the inconspicuous parotoid gland (vs. well developed) and smooth or slightly granular skin (vs. distinctly granular).

Key to subgenus within *Hypselotriton*

1 Distinct orange-red spot behind the eye present; blue lateral stripe on tail in breeding males present ..... *Hypselotriton*
– Distinct orange-red spot behind the eye absent; blue lateral stripe on tail in breeding males absent 2

2 Mid-dorsal vertebral ridge continuous; irregular greyish-blue patches on dorsum and lateral tail in breeding males and females present ..... *Hakkatriton* subgen. nov.
– Mid-dorsal vertebral ridge interrupted; irregular greyish-blue patches on dorsum and lateral tail in breeding males and females absent..... *Cynotriton*

Subgenus *Hypselotriton* Wolterstorff, 1934

Type species. *Molge wolterstorffi* Boulenger, 1905, by original designation.

Diagnosis. (1) small to large size; (2) gular fold present; (3) mid-dorsal vertebral ridge continuous; (4) metacarpal and metatarsal tubercles on external side of hands and feet present; (5) postocular orange spot present; (6) blue lateral stripe on tail in breeding males present.

Content and remarks. This subgenus includes all known Fire-bellied Newts populations distributed in the Yunnan-Guizhou Plateau in southwestern China. Currently, four nomenclatures have been provisionally documented, i.e. *H.* (*Hy.*) *chenggongensis* (Kou & Xing, 1983), *H.* (*Hy.*) *cyanurus* (Liu, Hu & Yang, 1962), *H.* (*Hy.*) *wolterstorffi* (Boulenger, 1905) and *H.* (*Hy.*) *yunnanensis* (Yang, 1979) (Lyu et al. 2023a). However, the exact taxonomic status for these populations/species is still unresolved (Raffaëlli 2022; Lyu et al. 2023a). Thus, it is improper to present a key to these nomenclatures before a comprehensive study to precisely delimitate their taxonomic placements.

Subgenus *Hakkatriton* subgen. nov.

https://zoobank.org/504DCCDF-32D2-4894-AFBA-5766752AD418

Type species. *Cynops orphicus* Risch, 1983, by present designation.

Etymology. The nomen of *Hakkatriton* subgen. nov. is derived from Hakka, referring to its distribution in northern and eastern Guangdong where is the settlement of Hakka people and generic nomen *Triton* Laurenti, 1768.

Diagnosis. (1) small size; (2) gular fold absent; (3) mid-dorsal vertebral ridge continuous; (4) metacarpal and metatarsal tubercles on external side of hands and feet absent; (5) postocular orange spot absent; (6) blue lateral stripe on tail in breeding males absent; (7) irregular greyish-blue patches on dorsum and lateral tail in breeding males and females present.

Content. Two species distributed in isolated regions in northern and eastern Guangdong in southern China, respectively (Fig. 1).

Key to species of the subgenus *Hakkatriton* subgen. nov.

1 Ventral forearms and shanks uniformly dark brown; tail uniformly coloured ..... *H.* (*Ha.*) *jiaoren*
– Ventral forearms and shanks with bright orange patches; tail with irregular black spots ..... *H.* (*Ha.*) *orphicus*

***Hypselotriton* (*Hakkatriton*) *orphicus* (Risch, 1983)**

Pachytriton brevipes (Sauvage, 1876) – Pope and Boring (1940); Gressitt (1941)
Cynops shataukokensis Freytag & Eberhardt, 1977 – Freytag (1979)
Cynops orphicus Risch, 1983 – Risch (1983); Fei et al. (2006, 2012); Fei and Ye (2016)
Hypselotriton (*Pingia*) *orphicus* – Dubois and Raffaëlli (2009)
Hypselotriton (*Cynotriton*) *orphicus* – Dubois and Raffaëlli (2011)
Cynops glaucus Yuan, Jiang, Ding, Zhang & Che, 2013 syn. nov. – Yuan et al. (2013, 2022); Fei and Ye (2016); Lyu et al. (2023a)
Hypselotriton (*Cynotriton*) *glaucus* – Raffaëlli (2022)

Type. ***Holotype.*** China • ♂; Guangdong Province, Shantou Region [now belonging to Jieyang City, Jiexi County], Tai-Yong [Dayang Township]; 23°35'N, 115°51'E [=23.58°N, 115.85°E; located in Liangtian Township, see remarks below], 640 m elev.; 4 Aug. 1936; JL Gressitt leg.; MVZ 22474.

Paratypes. China • 97 adult specimens; same data as for holotype; MVZ 22416–73, 22475–506 [90 specimens], MNHN 1980.4096–4098 [3 specimens, formerly MVZ 24134–36], AMNH 46174, CAS 78704, 2 unnumbered specimens in the Department of Biology, Yenching University [probably lost according to Risch (1983)].

Examined specimens. China • 4♂♂; Guangdong Province, Jieyang City, Jiexi County, Mt Dabei; 23.55°N, 115.89°E, ca. 490 m elev.; GEP a008, 010–011, CIB 121434 • 2♀♀; same data as for preceding; GEP a009, CIB 121435 • 2♂♂; Guangdong Province, Meizhou City, Fengshun County, Mt Hongtuzhang; 23.78°N, 115.96°E, ca. 1200 m elev.; GEP a263–264 • 3♂♂; Guangdong Province, Meizhou City, Fengshun County, Mt Shijiadong; 23.81°N, 116.33°E, ca. 1140 m elev.; GEP a314–316 • 3♀♀; same data as for preceding; GEP a317–319.

Referred specimens. Seven specimens labelled as "*Cynops glaucus*" in Lyu et al. (2023a). China • 2♀♀; Guangdong Province, Jieyang City, Jiexi County, Mt Dabei; SYS a000729, 8511 • 1♂; Guangdong Province, Jieyang City, Jiexi County, Mt. Liwangzhang; 23.64°N, 115.81°E, ca. 990 m elev.; SYS a008602 • 1♀; same data as for preceding; SYS a008601 • 2♀♀; Guangdong Province, Meizhou City, Fengshun County, Mt. Tongguzhang; 24.18°N, 116.35°E, ca. 1500 m elev.; SYS a000730, 4743 • 1♀; same data as for preceding; SYS a000731.

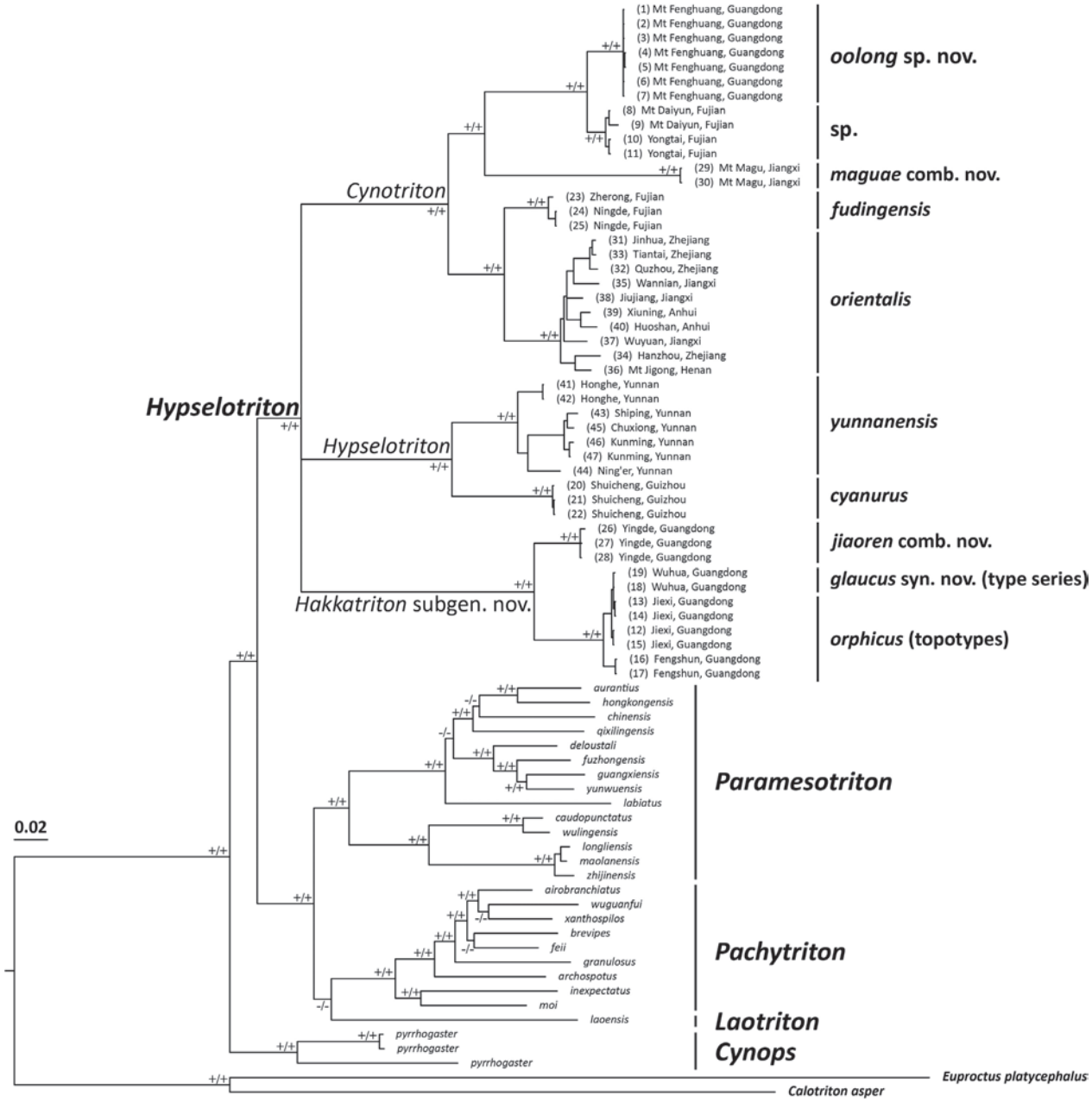

Figure 2. Bayesian Inference and Maximum-Likelihood phylogenies, based on mitochondrial *ND2* and *cytb* genes. Bayesian posterior probabilities (BPP) > 0.95 and the bootstrap supports (BS) > 70 are labelled with "+" and otherwise labelled with "-".

Etymology. The specific name *orphicus* is derived from the Greek legendary musician and poet Orpheus, in memory of several people who passed away in 1982 (Risch 1983).

Common name. Dayang Fire-bellied Newt (in English) / cháo shàn róng yuán (潮汕蝾螈 in Chinese).

Revised diagnosis. (1) small body size, TOL 68.5–77.0 mm in adult males, 85.1–99.7 mm in adult females; (2) parotoid gland inconspicuous; (3) postocular orange spot absent; (4) surface smooth, finely granulated, gular fold absent; (5) continuous vertebral ridge weak and inconspicuous; (6) fingers and toes overlapping when fore-limb and hind-limb adpressed towards each other along body; (7) ground colour dark brown to olive brown, with irregular greyish-blue patches on dorsum and lateral tail in breeding males and females; (8) lateral tail with black spots; (9) ground colour of venter dark brown with irregular bright orange patches, bright orange blotches on chin, ventral limbs and cloaca; (10) ventral tail with a bright orange stripe.

Description of new specimens. Body slender and small-sized, TOL 68.5–77.0 mm in adult males, 85.1–99.7 mm in adult females, with detailed measurements listed in Table 2. Head oval in dorsal view; snout truncate, projecting slightly beyond mandible; nostril small, but conspicuous; labial fold developed on posterior part of upper jaw; tongue elongate, enlarged anteriorly, with free lateral margin; vomerine tooth patch "^"-shaped; eye small, not extending beyond lateral margins of head; an inconspicuous longitudinal ridge found posterior to each eye; parotoid gland inconspicuous, gill remnants absent; gular fold absent.

Table 2. Measurements (in mm) of *Hypselotriton* (*Hakkatriton*) *orphicus* and *H.* (*Cynotriton*) *oolong* sp. nov.

Voucher	Sex	TOL	SVL	TAL	TAD	HL	HW	SL	ED	IOD	EN	IND	AG	FLL	HLL
Hypselotriton (*Hakkatriton*) *orphicus*															
GEP a008	M	73.5	41.9	29.1	6.1	13.1	8.8	4.5	2.6	4.1	2.8	2.9	20.6	10.6	12.1
GEP a010	M	73.5	43.3	32.3	5.0	12.5	8.8	4.2	2.5	4.1	2.7	2.9	20.8	8.8	9.4
GEP a011	M	77.0	44.2	32.8	6.5	12.8	9.7	4.2	2.7	4.7	2.8	3.2	19.5	10.6	11.5
GEP a263	M	75.6	44.3	31.3	4.8	10.0	8.6	4.3	2.8	4.4	3.0	3.1	18.8	8.7	10.3
GEP a264	M	75.9	43.0	32.9	4.9	12.6	8.7	4.4	2.6	4.5	3.1	3.2	18.8	9.2	10.6
GEP a314	M	72.1	42.3	29.8	6.6	12.5	10.0	4.4	2.6	5.1	3.0	3.1	18.9	10.4	11.2
GEP a315	M	70.7	40.8	29.9	6.4	11.8	9.4	3.9	2.8	4.4	2.6	2.9	18.0	9.6	9.8
GEP a316	M	74.5	42.2	32.3	6.2	12.2	9.3	4.3	2.9	4.9	2.7	2.9	18.2	8.8	10.2
CIB 121434	M	68.5	41.3	27.2	5.7	11.9	8.7	4.2	2.7	4.2	2.8	3.0	18.4	9.2	9.8
SYS a000730	M	70.7	43.4	27.3	6.8	12.2	9.2	4.7	2.4	5.6	2.9	3.2	18.6	8.6	8.8
SYS a004743	M	79.8	49.9	29.9	6.8	12.2	10.4	4.7	2.5	6.1	3.0	3.6	19.8	10.4	10.6
SYS a008602	M	73.5	43.5	30.0	6.4	12.5	10.0	4.8	2.5	5.7	2.9	3.3	19.4	9.1	10.1
GEP a009	F	85.1	48.7	36.4	6.6	14.1	9.9	4.5	2.8	5.2	3.4	3.2	22.2	10.0	11.0
GEP a317	F	86.1	48.1	38.1	6.1	13.6	10.8	4.6	2.8	5.2	3.6	3.7	24.0	10.1	10.3
GEP a318	F	91.2	50.3	40.9	7.4	14.6	10.8	4.9	2.9	5.4	3.5	3.2	23.9	10.5	10.7
GEP a319	F	91.0	50.6	40.4	6.3	14.2	10.7	4.6	2.9	5.0	3.6	3.3	25.4	9.7	10.6
CIB 121435	F	88.9	48.6	40.3	5.7	13.5	10.3	4.7	2.8	4.9	2.8	3.0	22.3	11.0	11.4
SYS a000729	F	87.5	50.2	37.3	5.9	13.7	10.1	4.5	2.5	6.0	2.8	3.4	23.6	10.3	10.6
SYS a000731	F	88.6	49.6	39.0	6.9	14.1	11.4	4.9	2.5	6.5	3.0	3.6	21.4	10.2	11.2
SYS a008511	F	90.2	50.6	39.6	5.7	13.7	10.5	4.8	2.6	5.8	3.0	3.6	23.5	10.6	11.0
SYS a008601	F	99.7	55.6	44.1	7.5	14.8	11.6	5.8	2.7	6.6	3.8	3.9	25.3	11.7	11.9
Hypselotriton (*Cynotriton*) *oolong* sp. nov.															
CIB 121430	M	70.7	45.2	25.5	6.1	12.5	9.1	4.1	2.9	4.5	2.8	2.5	22.7	9.5	10.4
CIB 121429	M	69.9	43.0	26.9	5.2	12.4	8.6	4.1	2.8	4.5	3.3	2.5	21.0	9.2	9.6
SYS a009274	M	70.0	43.5	26.5	5.0	11.6	8.4	4.1	2.6	4.5	2.9	2.6	20.0	9.2	9.6

Surface smooth, finely granular; a few inconspicuous longitudinal wrinkles present on chin; continuous vertebral ridge weak and inconspicuous; cloacal opening oval, slightly protruding.

Limbs slender, fingers and toes overlapping when forelimb and hind-limb adpressed towards each other along body; four fingers and five toes, slender and elongated, lack webbing; relative length of fingers I < IV < II < III; relative length of toes I < V < II < IV < III. Tail laterally compressed, tapering posteriorly; caudal fin distinct; tail tip bluntly pointed.

Colouration of new specimens. In life, ground colour dark brown to olive brown, with irregular greyish-blue patches on dorsum and lateral tail; lateral tail with black spots; a single bright orange dot on insertion of upper forearm; tips of digits light yellow to bright orange; ground colour of venter dark brown with irregular bright orange patches, bright orange blotches on chin, ventral limbs and cloaca; ventral tail with a bright orange stripe (Fig. 3).

In preservation, ground colour dark brown, irregular greyish-blue patches on dorsum and lateral tail faded and almost invisible; black spots on lateral tail and bright orange dot on insertion of upper forearm faded; bright orange blotches on ventral trunk and tail, bright orange blotches on chin, ventral limbs and cloaca slightly faded, dark patches more distinct.

Variations. For measurements, see Table 2. Larger body size in females; cloaca wider and more swollen in males than in females; tail proportionally shorter and wider in males than in females; variable greyish-blue patches on dorsum and lateral tail in both breeding males and females.

Distribution and natural history. This species is known from multiple localities at elevations of 490–1500 m in the Lianhua Mountains and on the west of the Hanjiang River in eastern Guangdong (Fig. 1).

Adults are observed in wetlands, seasonal ponds, cultivated valleys and small lakes surrounded by forests from March to September. The breeding season is spring to summer. When breeding, a large number of individuals gather in the lentic water area. Males chase the females and show their courtship willingness by wagging their tails. Females lay eggs with jelly coating on tips of the leaves of aquatic plants. Eggs develop into larvae after about half a month and larvae develop into adults after about six to eight months. The newts feed on a variety of food sources, mainly small molluscs and arthropods in their habitat. Risch (1983) surmises that the newt might inhabit water all year round; however, adults leave the water from late September to early March to live on land until the next spring rains arrive.

Remarks. The type specimens of this species were reported to be collected from Tai-yong (Gressitt 1937, 1941; Fig. 1, site 2). When describing them as a new species, Risch (1983) provided the type locality from traditional transliteration “Tai-yong” to current Pinyin as “Dayang”. Risch (1983) further provided the coordinates for this locality as “23°35'N, 115°51'E [= 23.58°N, 115.85°E]”; however, this coordinate is located in Liangtian Township

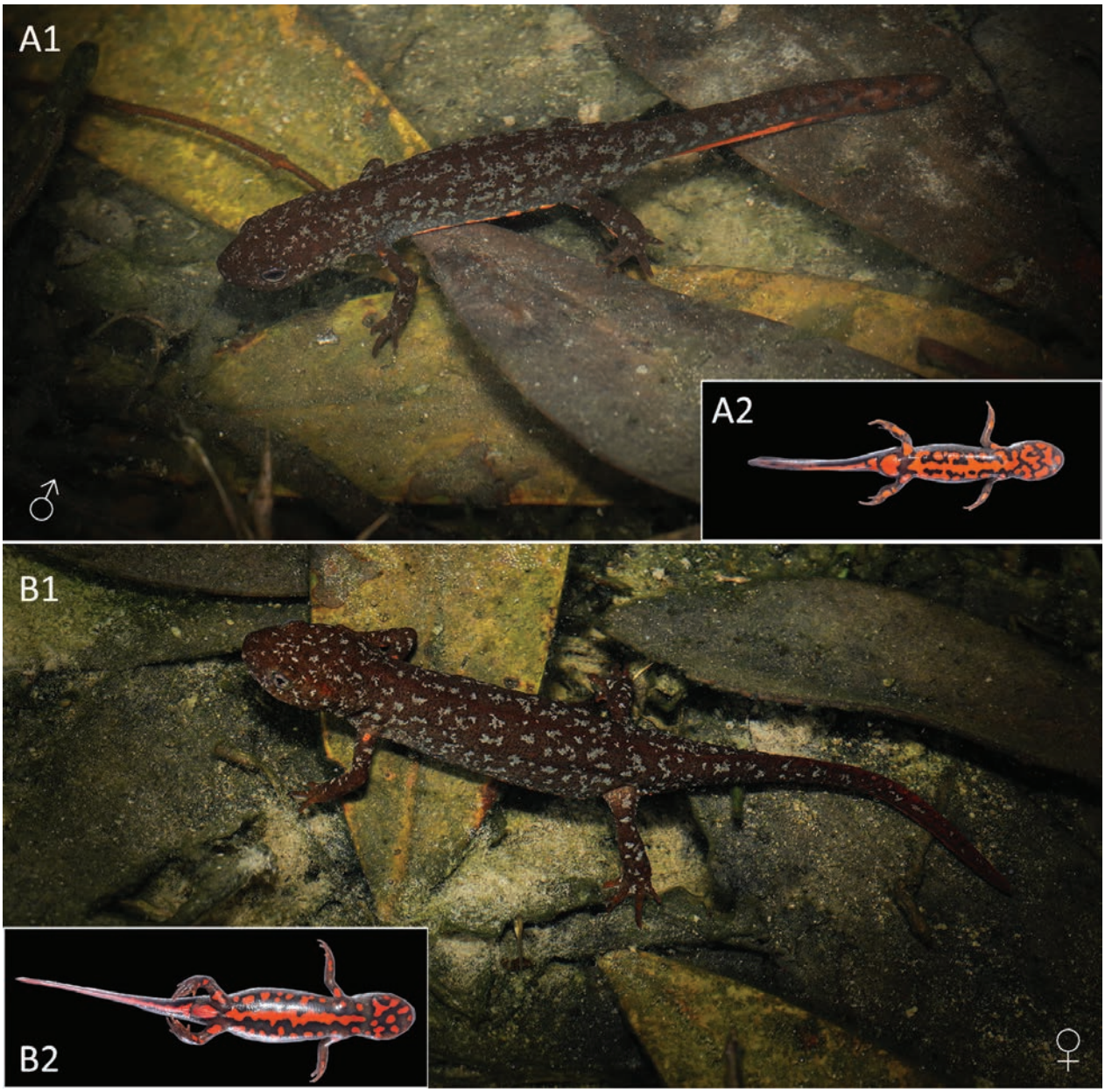

Figure 3. *Hypselotriton* (*Hakkatriton*) *orphicus* in life. **A.** CIB 121434, adult male; **B.** CIB 121435, adult female; **1.** Dorsal view in situ; **2.** Ventral view.

(Fig. 1, site 3) which is ca. 15 km from Dayang Township. During the surveys across the region in Jiexi and Fengshun counties encompassing these two localities, we failed to observed *Hypselotriton* populations from the vicinity of both sites 2 and 3, possibly due to the development of urbanisation. Nonetheless, morphological characters of the specimens from neighbouring Mt Dabei, Mt Liwangzhang, Mt Hongtuzhang, Mt Tongguzhang and Mt Shijiadong (Fig. 1, sites 4–8) all match the original description of *H. orphicus*.

According to the original descriptions of *Hypselotriton glaucus* syn. nov. and *H.* (*Ha.*) *orphicus*, the only difference between them is the irregular greyish-blue patches on dorsum. Such colour pattern just occurs in the breeding living individuals and will fade after preservation according to our examinations. Thus, based on the morphological and phylogenetic results, we synonymised *H. glaucus* syn. nov. with *H.* (*Ha.*) *orphicus*.

Subgenus *Cynotriton* Dubois & Raffaëlli, 2011

Type species. *Triton* (*Cynops*) *orientalis* David, 1875, by original designation.

Diagnosis. (1) small size; (2) gular fold present or absent; (3) mid-dorsal vertebral ridge interrupted; (4) metacarpal and metatarsal tubercles on external side of hands and feet absent; (5) postocular orange spot absent; (6) blue lateral stripe on tail in breeding males absent; (7) irregular greyish-blue patches on dorsum and lateral tail in breeding males and females absent.

Content. Four recognised species distributed in eastern China (Fig. 1).

Key to species of the subgenus *Cynotriton*

1 Gular fold absent ..... *H.* (*C.*) *maguae*
– Gular fold present 2
2 Mid-dorsal vertebral ridge weak; dorsal skin smooth ..... *H.* (*C.*) *orientalis*
– Mid-dorsal vertebral ridge bulged; dorsal skin relatively granular 3
3 Ventral surface almost entirely bright orange ..... *H.* (*C.*) *fudingensis*
– Ground colour of venter dark brown with irregular bright orange patches ..... *H.* (*C.*) *oolong* sp. nov.

***Hypselotriton* (*Cynotriton*) *oolong* sp. nov.**

https://zoobank.org/7E9557A2-9C78-4227-B7C1-07ED6930D045

Cynops orphicus Risch, 1983 – Fei et al. (2006, 2012); Yuan et al. (2013, 2022); Sparreboom (2014); Fei and Ye (2016); Lyu et al. (2023a)
Hypselotriton (*Cynotriton*) *orphicus* – Raffaëlli (2022)

Type. ***Holotype.*** China • ♂; Guangdong Province, Chaozhou City, Chao'an District, Mt Fenghuang, Peak Wudongding, Tianchi Lake; 23.96°N, 116.64°E, ca. 1320 m elev.; 21 Sep. 2019; Tian-Li Wei leg.; CIB 121430 [field number GEP a192] (Fig. 4).

Paratypes. China • 2♂♂; same data as for holotype; CIB 121429 [field number GEP a191], SYS a009274 [field number GEP a190].

Etymology. The specific name *oolong* is used as a noun in apposition, derived from oolong tea. The type locality of this species, Mt Fenghuang, is famous for the cultivation and production of the Phoenix Oolong Tea. Yet, the developments of tea cultivation have affected and threatened the habitats of this species. We name this new species after the most famous local economic output in the hope that it would bring attention on the green and sustainable development as well as the harmonious co-existence between humanity and nature. This species name is also in memory of the Japanese manga artist Akira Toriyama (1955–2024). His most famous work, *Dragon Ball*, was originally inspired by Chinese culture and one of the characters is named as Oolong who makes the first shown wish with the Dragon Balls.

Common name. Oolong Fire-bellied Newt (in English) / wū lóng róng yuán (乌龙蝾螈 in Chinese).

Diagnosis. (1) small body size, TOL 69.9–70.7 mm in adult males; (2) parotoid gland inconspicuous; (3) postocular orange spot absent; (4) surface rough and granulated, gular fold present; (5) interrupted vertebral ridge conspicuous and bulged; (6) fingers and toes overlapping when fore-limb and hind-limb adpressed towards each other along body; (7) ground colour dark brown to olive brown with black spots; (8) lateral tail with black spots; (9) ground colour of venter dark brown with irregular bright orange patches, bright orange blotches on chin, base of ventral limbs and anterior half of cloaca; (10) ventral tail with a bright orange stripe.

Description of the holotype. Body slender and small-sized, TOL 70.7 mm. Head oval in dorsal view; snout truncate, projecting slightly beyond mandible; nostril small, but conspicuous; labial fold well developed on posterior part of upper jaw; tongue elongate, enlarged anteriorly, with free lateral margin; vomerine tooth patch "^"-shaped; eye small, not extending beyond lateral margins of head; a conspicuous longitudinal ridge found posterior to each eye; parotoid gland inconspicuous, gill remnants absent; gular fold present.

Surface rough, dense tapered granules and tiny spines on dorsum, flanks, limbs and tail; dense granules and inconspicuous wrinkles on venter; interrupted vertebral ridge conspicuous and bulged; cloacal opening oval, slightly protruding.

Limbs slender, fingers and toes overlapping when fore-limb and hind-limb adpressed towards each other along body; four fingers and five toes, slender and elongated, lack webbing; relative length of fingers I < IV < II < III; relative length of toes I < V < II < IV < III. Tail laterally compressed, tapers posteriorly; caudal fin distinct; tail tip bluntly pointed.

Colouration of the holotype. In life, ground colour dark brown with black spots; vertebral ridge and upper margin of tail yellowish-brown; lateral tail with black spots; tips of digits light yellow; irregular bright orange stripe bordering dark patches on ventral trunk, bright orange blotches on chin, base of ventral limbs and anterior half of cloaca; ventral tail with a bright orange stripe.

In preservation, ground colour faded, greyish, black spots absent; vertebral ridge, upper margin of tail and digits dark grey; black spots on lateral tail indistinct; bright orange stripe on ventral trunk and tail, bright orange blotches on chin, ventral limbs and anterior half of cloaca slightly faded, dark patches more distinct.

Variations. Measurements of the type series are given in Table 2. All male specimens are similar in body proportions; however, the number, shape and position of ventral orange blotches vary amongst individuals.

Distribution and natural history. This species is known only from Tianchi Lake and surrounding streams of Mt Fenghuang at elevations of ca. 1300 m. This locality is situated on the east of the Hanjiang River in eastern Guangdong, while the populations of *H.* (*Ha.*) *orphicus* were all discovered from the west of the Hanjiang River (Fig. 1).

The adult individuals inhabit puddles and slow streams that are surrounded by bushes and weeds. Fei et al. (2006) reported that 26 adults were observed from Mt Fenghuang during a survey in July 2002. However, only nine adults were observed in September 2019. The type locality is being threatened by the developments of tourism and tea planting, which might cause negative effects on this species.

Remarks. The *Hypselotriton* populations from central Fujian were originally reported as *Cynops orientalis* (Hu

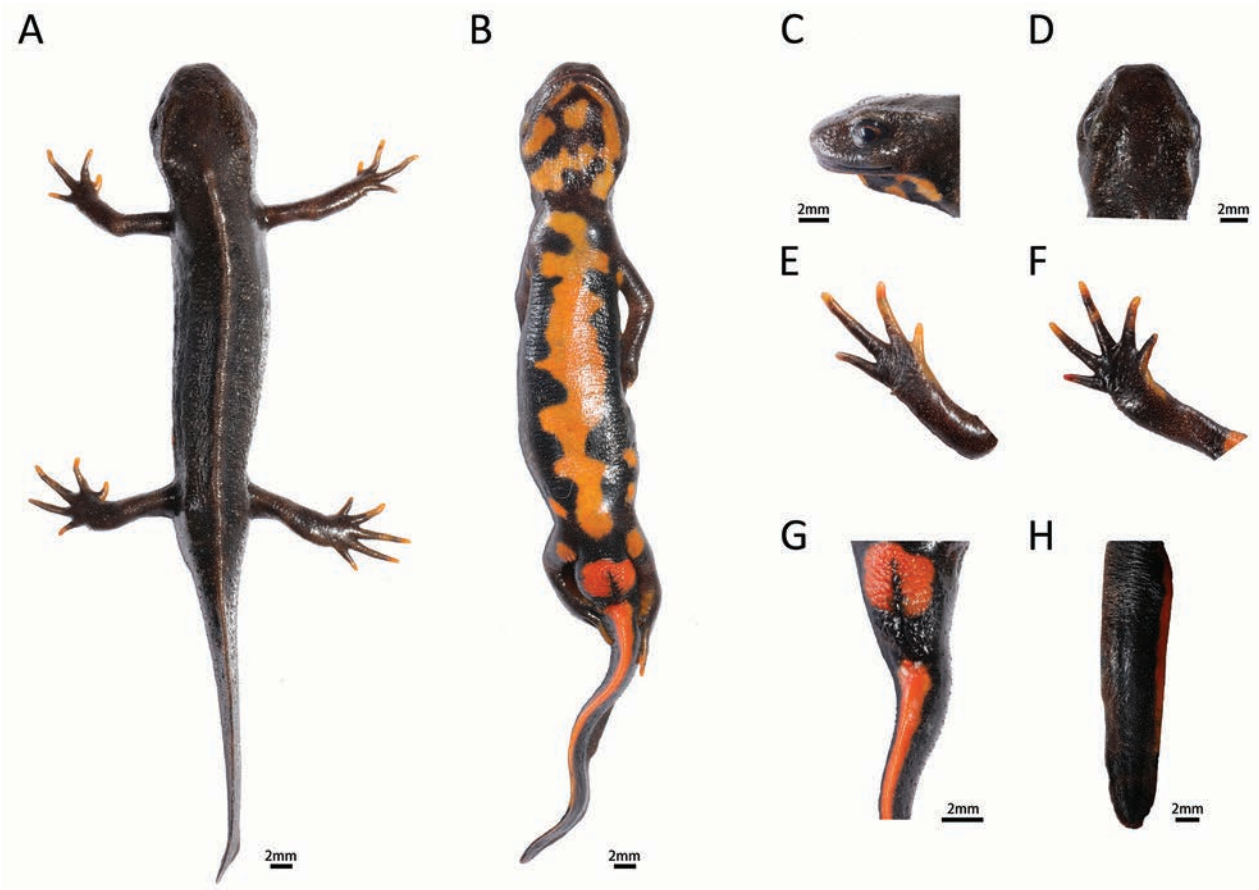

Figure 4. The holotype CIB 121430 of *Hypselotriton* (*Cynotriton*) *oolong* sp. nov. in life. **A.** Dorsal view; **B.** Ventral view; **C.** Lateral view of head; **D.** Dorsal view of head; **E.** Ventral view of hand; **F.** Ventral view of foot; **G.** Cloaca slit; **H.** Lateral view of tail.

et al. 1978; Risch 1983). Fei et al. (2006) re-identified the specimens from Mt Daiyun as *C. orphicus*, based on the ventral colouration that is similar to the paratypes of *C. orphicus* preserved in MNHN. However, our morphological examinations found that such colouration could not be a distinguished character between the two species, which led to the misidentification. The phylogenetic analysis revealed close relationships between the central Fujian populations and the new species, however, with distinct genetic divergences. Their distribution areas are also distantly isolated (Fig. 1). As there is a lack of detailed morphological data of the Fujian populations for accurate identification, we prudently label them as *Hypselotriton* sp. in this work provisionally.

Discussion

For the intrageneric classification in zoology, subgenus and species group are usually employed.

Several recent works have referred to the usage of these ranks in particular groups (e.g. Lyu et al. (2021, 2023b)). Subgenus is more official as it is regulated by the International Code of Zoological Nomenclature (the Code; available on https://www.iczn.org/the-code/the-codeonline/) in which a series of articles is formulated. For example, one of the requirements for the availability of a new subgenus is to provide a description or definition to differentiate the taxon (Article 13.1.1 of the Code). The species group is relatively flexible without clear rules, which was usually simply proposed for distinct phylogenetic clades and morphological definition is not mandatory (e.g. *Boulenophrys omeimontis* group in Lyu et al. (2023b)). In some cases, especially in the large genus containing numerous congeners, the subgenus and species group can be used simultaneously, while subgenus is always at the higher rank than species group indicating the subgenus possesses more distinct differences and divergences than the species group. Regardless, there are no strict standards on when to adopt subgenus or species group for classification and it usually depends on custom or subject tendencies. In the taxonomy of newt groups, subgenus is more welcome and widely used than species group. In a recent case for the intrageneric division of another newt genus *Tylototriton* Anderson, 1871, Lyu et al. (2021) suggested to partition the genus into three species groups while Raffaëlli (2022) replaced them with three subgenera that were previously nominated. Another newt genus *Echinotriton* Nussbaum & Brodie, 1982 has recently been partitioned into two subgenera(Dufresnes and Hernandez 2022).

The intrageneric classification of genus *Hypselotriton* is suggested for re-delimitation, as the result of a recent phylogenetic analysis (Lyu et al. 2023a). In this work, we

further perform the morphological comparison amongst the three distinct lineages of the genus, which sustains the phylogenetic insights. Since two clades have been previously nominated, we provided a new subgenus for the third clade as *Hakkatriton* subgen. nov. (Fig. 2). Geographically, the subgenus *Hypselotriton* is endemic in Yunnan-Guizhou Plateau in southwestern China that is distinctly isolated from the other two subgenera. *Cynotriton* is primarily distributed in eastern China. The basal lineage of *Cynotriton* including *H.* (*C.*) *orientalis* and *H.* (*C.*) *fudingensis* occurs in the relatively northern area, while the southern members *H.* (*C.*) *oolong* sp. nov. and *Hypselotriton* sp. from Fujian are revealed to be relatively terminal in phylogeny, suggesting the subgenus immigrated and separated from north to south. *Hakkatriton* subgen. nov. is primarily distributed in southern China. *Hypselotriton* (*Ha.*) *orphicus* and *H.* (*C.*) *oolong* sp. nov. both occur in neighbouring areas of eastern Guangdong and Hanjiang River might act as an isolation barrier between them (Fig. 1).

During the reviewing stage, an anonymous reviewer has raised an important issue which requires the skeletal data for the subgeneric comparisons. We appreciate this comment very much, even though we have different considerations. Indeed, we would like to include the skeletal data when we initially proposed the new subgenus. Nonetheless, when we reviewed the literature, the published skeletal data is very inadequate for comprehensive comparison. Based on the limited skeletal data, Fei et al. (2006) and Fei and Ye (2016) compared *Hypselotriton* (*Cynotriton*) *orientalis* (as *Cynops orientalis orientalis* and *Cynops orientalis qianshan* Fei, Ye & Jiang, 2012), *H.* (*Hy.*) *cyanurus* (as *Cynops cyanurus cyanurus*), *H.* (*Hy.*) *yunnanensis* (as *Cynops cyanurus chuxiongensis* Fei & Ye, 1983), *H.* (*Hy.*) *wolterstorffi* and *Cynops ensicauda* (Hallowell, 1861). Their results showed that *H.* (*Hy.*) *wolterstorffi* possesses relatively different skeletal characters while those amongst other species are very similar. Thus, we consider that, in this newt group, the skeletal characters are not suitable to be used for subgeneric diagnosis, as it might vary within a subgenus such as *H.* (*Hy.*) *wolterstorffi* vs. *H.* (*Hy.*) *yunnanensis*, while it may be with little differences amongst subgenera or genera, such as *H.* (*Hy.*) *cyanurus* vs. *H.* (*C.*) *orientalis* vs. *Cynops ensicauda*. Besides, when Dubois and Raffaëlli (2011) erected the subgenus *Cynotriton*, the skeletal data were also excluded. The recognition of this subgenus has been steadily supported by both genetic relationship and external morphology. Furthermore, as the developments of new biotechnology, more and more higher ranks of amphibian groups are erected without skeletal data, but are supported by multiple series of molecular and external morphological evidences, such as the anuran genera *Ghatixalus* Biju, Roelants & Bossuyt, 2008, *Sumaterana* Arifin, Smart, Hertwig, Smith, Iskandar & 2018, *Jingophrys* Lyu & Wang, 2023 and the newt genus *Laotriton* Dubois & Raffaëlli, 2009 and subgenera *Hightonia* Vieites, Nieto-Román, Wake & Wake, 2011 and *Sinotriton* Hernandez & Dufresnes, 2022. The recognition of these ranks is not seriously affected despite the absence of skeletal data.

Acknowledgements

We thank Bin-Bin Zhan, Wei-Wen Xiao and Hou-Hua Huang for their help in the fieldwork. We thank Ying-Yong Wang and Ke Jiang for their help on this work. We thank the editor Umilaela Arifin and two reviewers for their kind comments on the original manuscript. This work was supported by DFGP Project of Fauna of Guangdong-202115 and the National Animal Collection Resource Center, China.

References

Arifin U, Smart U, Hertwig ST, Smith EN, Iskandar DT, Haas A (2018) Molecular phylogenetic analysis of a taxonomically unstable ranid from Sumatra, Indonesia, reveals a new genus with gastromyzophorous tadpoles and two new species. Zoosystematics and Evolution 94(1): 163–193. https://doi.org/10.3897/zse.94.22120

Biju SD, Roelants K, Bossuyt F (2008) Phylogenetic position of the montane treefrog *Polypedates variabilis* Jerdon, 1853 (Anura: Rhacophoridae), and description of a related species. Organisms, Diversity & Evolution 8(4): 267–276. https://doi.org/10.1016/j.ode.2007.11.004

Boulenger GA (1905) Description of a new newt from Yunnan. Proceedings of the Zoological Society of London 1905: 277.

David A (1873) Quelques renseignements sur l'histoire naturelle de la Chine septentrionale et occidentale. Journal of the North-China Branch of the Royal Asiatic Society. New Series 7: 205–234.

Dubois A, Raffaëlli J (2009) A new ergotaxonomy of the family Salamandridae Goldfuss, 1820 (Amphibia, Urodela). Alytes 26: 1–85.

Dubois A, Raffaëlli J (2011) Subgeneric taxonomy and nomenclature of the genus *Hypselotriton* Wolterstorff, 1934 (Amphibia, Urodela). Alytes 27: 151–153.

Dufresnes C, Hernandez A (2022) Towards completing the Crocodile Newts' puzzle with all-inclusive phylogeographic resources. Zoological Journal of the Linnean Society 197(3): 620–640. https://doi.org/10.1093/zoolinnean/zlac038

Fei L, Ye CY (1983) A new subspecies of *Cynops cyanurus* from Chuxiong, Yunnan (Caudata: Salamandridae). Acta Herpetologica Sinica. New Series 2: 55–58.

Fei L, Ye CY (2016) Amphibians of China (Vol. 1). Beijing, China: Science Press.

Fei L, Hu SQ, Ye CY, Huang YZ (2006) Fauna Sinica. Amphibia. Volume 1. General Accounts of Gymnophiona and Urodela. Beijing, China: Science Press.

Fei L, Ye CY, Jiang JP (2012) Colored Atlas of Chinese Amphibians and Their Distributions. Chengdu, China: Sichuan Publishing House of Science & Technology.

Freytag GE (1979) Röntgenanatomische Befunde am Schädel von *Cynops shataukokensis* nebst Bemerkungen über Arten und Unterarten der Gattung *Cynops* Tschudi, 1838 (Amphibia: Urodela: Salamandridae). Sitzungsberichte der Gesellschaft Naturforschender Freunde zu Berlin 19: 70–80.

Gressitt JL (1937) Note on a collecting trip in southeastern China. Lingnan Science Journal 16: 439–444. https://doi.org/10.2307/1437386

Gressitt JL (1941) Amphibians and reptiles from southeastern China. Philippine Journal of Science 75: 1–59.

Hallowell E (1861) Report upon the Reptilia of the North Pacific Exploring Expedition, under command of Capt. John Rogers, U.S. N. Proceedings. Academy of Natural Sciences of Philadelphia 12: 480–510.

Hu SQ, Fei L, Ye CY (1978) Investigation report of amphibians in Fujian. Materials of Herpetological Research 4: 22–29.

Kou ZT, Xing YL (1983) A new species of *Cynops* from Yunnan. Acta Herpetologica Sinica. New Series 2: 51–54.

Liu CC, Hu SQ, Yang FH (1962) Preliminary report of Amphibia from western Kweichow. Dong Wu Xue Bao 14: 381–392.

Lyu ZT, Wang J, Zeng ZC, Zhou JJ, Qi S, Wan H, Li YY, Wang YY (2021) A new species of the genus *Tylototriton* (Caudata, Salamandridae) from Guangdong, southern China, with discussion on the subgenera and species groups within the genus. Vertebrate Zoology 71: 697–710. https://doi.org/10.3897/vz.71.e73563

Lyu ZT, Qi S, Zhang SY, Dai KY, Wang YY (2023a) Two new species of fire-bellied newts (Caudata, Salamandridae, *Cynops*) from southeastern China. Asian Herpetological Research 14: 41–53. https://doi.org/10.16373/j.cnki.ahr.220059

Lyu ZT, Qi S, Wang J, Zhang SY, Zhao J, Zeng ZC, Wan H, Yang JH, Mo YM, Wang YY (2023b) Generic classification of Asian horned toads (Anura: Megophryidae: Megophryinae) and monograph of Chinese species. Zoological Research 44(2): 380–450. https://doi.org/10.24272/j.issn.2095-8137.2022.372

Pope CH, Boring AM (1940) A survey of Chinese amphibia. Peking Natural History Bulletin 15: 13–86.

Raffaëlli J (2022) Salamanders & Newts of the World. Plumelec, France: Penclen Édition.

Rancilhac L, Irisarri I, Angelini C, Arntzen JW, Babik W, Bossuyt F, Künzel S, Lüddecke T, Pasmans F, Sanchez E, Weisrock DE, Veith M, Wielstra B, Steinfartz S, Hofreiter M, Philippe H, Vences M (2021) Phylotranscriptomic evidence for pervasive ancient hybridization among Old World salamanders. Molecular Phylogenetics and Evolution 155: 1–14. https://doi.org/10.1016/j.ympev.2020.106967

Risch JP (1983) *Cynops orphicus*, a new salamander from Guangdong Province, South China (Amphibia, Caudata, Salamandridae). Alytes 2: 45–52.

Ronquist F, Teslenko M, Van Der Mark P, Ayres DL, Darling A, Höhna S, Larget B, Liu L, Suchard MA, Huelsenbeck JP (2012) MrBayes 3.2: Efficient Bayesian phylogenetic inference and model choice across a large model space. Systematic Biology 61(3): 539–542. https://doi.org/10.1093/sysbio/sys029

Silvestro D, Michalak I (2012) RaxmlGUI: A graphical front-end for RAxML. Organisms, Diversity & Evolution 12(4): 335–337. https://doi.org/10.1007/s13127-011-0056-0

Sparreboom M (2014) Salamanders of the Old World. The Salamanders of Europe, Asia and Northern Africa. Zeist, Netherlands: KNNV Publishing. https://doi.org/10.1163/9789004285620

Thompson JD, Gibson TJ, Plewniak F, Jeanmougin F, Higgins DG (1997) The CLUSTAL_X windows interface: Flexible strategies for multiple sequence alignment aided by quality analysis tools. Nucleic Acids Research 25(24): 4876–4882. https://doi.org/10.1093/nar/25.24.4876

Tominaga A, Matsui M, Yoshikawa N, Nishikawa K, Hayashi T, Misawa Y, Tanabe S, Ota H (2013) Phylogeny and historical demography of *Cynops pyrrhogaster* (Amphibia: Urodela): taxonomic relationships and distributional changes associated with climatic oscillations. Molecular Phylogenetics and Evolution 66(3): 654–667. https://doi.org/10.1016/j.ympev.2012.10.015

Tominaga A, Matsui M, Kokuryo Y (2015) Occurrence and evolutionary history of two *Cynops pyrrhogaster* lineages on the Izu Peninsula. Current Herpetology 34(1): 19–27. https://doi.org/10.5358/hsj.34.19

Vieites DR, Nieto Román S, Wake MH, Wake DB (2011) A multigenicperspective on phylogenetic relationships in the largest family of salamanders,the Plethodontidae. Molecular Phylogenetics and Evolution 59(3): 623–635. https://doi.org/10.1016/j.ympev.2011.03.012

Wu Y, Wang Y, Jiang K, Hanken J (2010) A new newt of the genus *Cynops* (Caudata: Salamandridae) from Fujian Province, southeastern China. Zootaxa 2346(1): 42–52. https://doi.org/10.11646/zootaxa.2346.1.4

Yang DT (1983) A new subspecies of *Cynops cyanurus* in Yunnan (Caudata: Salamandridae). Zoological Research 4: 124.

Yuan ZY, Jiang K, Ding L, Zhang L, Che J (2013) A new newt of the genus *Cynops* (Caudata: Salamandridae) from Guangdong, China. Asian Herpetological Research 4(2): 116–123. https://doi.org/10.3724/SP.J.1245.2013.00116

Yuan ZY, Wu YK, Yan F, Murphy RW, Papenfuss TJ, Wake DB, Zhang YP, Che J (2022) Comparative multi-locus assessment of modern Asian newts (*Cynops*, *Paramesotriton*, and *Pachytriton*: Salamandridae) in southern China suggests a shared biogeographic history. Zoological Research 43: 706–718. https://doi.org/10.24272/j.issn.2095-8137.2022.080

Zhao EM, Hu QX (1984) Studies on Chinese Tailed Amphibians. Chengdu, China: Sichuan Scientific and Technical Publishing House.

Zhao EM, Hu QX, Jiang YM, Yang YH (1988) Studies on Chinese Salamanders. Oxford, USA: Society for the Study of Amphibians and Reptiles.

Zoosyst. Evol. 100 (3) 2024, 1135–1154 | DOI 10.3897/zse.100.129455

PENSOFT

für Natur MUSEUM FÜR NATURKUNDE BERLIN

Reassessment and phylogenetic position of the overlooked limacoid land snail *Trochomorpha sculpticarina* Martens, 1883 (Eupulmonata, Ariophantidae), with the description of a new genus

Arthit Pholyotha[1], Chirasak Sutcharit[1], Somsak Panha[1,2], Piyoros Tongkerd[1]

1 *Animal Systematics Research Unit, Department of Biology, Faculty of Science, Chulalongkorn University, Bangkok 10330, Thailand*

2 *Academy of Science, The Royal Society of Thailand, Bangkok 10300, Thailand*

https://zoobank.org/11F9B5B3-CEF8-4C81-943D-E23C9FF823FB

Corresponding author: Piyoros Tongkerd (piyorose@hotmail.com)

Academic editor: Frank Köhler ♦ **Received** 11 June 2024 ♦ **Accepted** 17 July 2024 ♦ **Published** 14 August 2024

Abstract

The Malay Peninsula has traditionally been considered to harbour a diverse land-snail fauna, both in terms of a high species richness and a wide variety of conchological traits, especially within the limacoid land snails. A recent survey along the Malay Peninsula of southern Thailand discovered an overlooked limacoid taxon "*Trochomorpha*" *sculpticarina* Martens, 1883, previously assigned to genus *Trochomorpha* of the Trochomorphidae. This genus is herein described as *Janbinmorpha* **gen. nov.** based on comparative studies of shell morphology, external features, genital anatomy and radular morphology, as well as analyses of partial sequences of two mitochondrial markers, COI and 16S rRNA, and of one nuclear marker, 28S rRNA. This new genus is characterised by a combination of distinct morphological and anatomical features. The most distinguishing features are a depressed trochiform shell with a keeled last whorl, gametolytic organ without a duct, gametolytic sac with two lobes, and proximal epiphallus encircled with a thick sheath and attached by the penial retractor muscle. In addition, an analysis of the differentiation in mitochondrial and nuclear markers confirmed that this new genus, first recognised by morphology, is also genetically distinct. The molecular data also confirm that *J. sculpticarina* **comb. nov.** is a member of the Ariophantidae and has a close evolutionary relationship to *Hemiplecta* and *Maelamaodiscus*.

Key Words

Helicarionoidea, land snails, Malay Peninsula, phylogeny, systematics, taxonomy

Introduction

The Malay Peninsula, located in the Indo-Burma biodiversity hotspot in tropical Asia, is a significant hotspot of diversity and endemism of malacofauna, with various distribution patterns and speciation mechanisms (Myers et al. 2000; Clements et al. 2006; Foon et al. 2017; Pholyotha et al. 2021c). Southern Thailand is a part of the Malay Peninsula, representing 14% of the total land area of the country (Gardner et al. 2015). This region has a high species diversity and is also uniquely biologically complex, requiring further research to fully understand. The high species richness is associated with a variety of different factors. High relative humidity, a short dry season, a great amount of rainfall, and extensive ranges of limestone karsts and outcrops scattered along this area together with the impact of Quaternary climatic oscillations have significantly influenced the land snail diversification and speciation in this region (Gupta 2005; Clements et al. 2006; Naggs et al. 2006; Ridd et al. 2011; Gardner et al. 2015; Pholyotha et al. 2021c).

Basic data on land snail biodiversity in the southern peninsula of Thailand have been continuously collected and studied. However, information beyond the original description of many land-snail taxa is scarce. "*Trochomorpha*" *sculpticarina* Martens, 1883 is one such group

of overlooked species in this region, and only a few taxonomic documents have mentioned this species. For example, in the comprehensive land snail checklists by Panha (1996) and Hemmen and Hemmen (2001), there is no record of this species from Thailand. Originally, Martens (1883) described this species based on specimens from Phuket Province in the South of Thailand and assigned it to *Trochomorpha* Albers, 1850 in the Trochomorphidae Möllendorff, 1890 because it has a depressed trochiform shell with a developed peripheral keel. Later, Maassen (2001) reported this species from Peninsular Malaysia under the trochomorphid genus *Videna* Adams & Adams, 1855. However, as known from several cases of conservatism and/or convergence in shell form, the general usefulness of the shell features as diagnostic characters has been challenged by studies of genital anatomy and molecular phylogeny (Hyman and Ponder 2010; Köhler and Shea 2012; Jirapatrasilp et al. 2021; Pholyotha et al. 2021a, b, 2022a; Sutcharit et al. 2021; Köhler et al. 2024).

During our field survey, many specimens identical to "*Trochomorpha*" *sculpticarina* were collected from southern Thailand and Myanmar. Its shell traits are similar to *Trochomorpha* or *Videna*, but the living snails resemble several species of the ariophantid genus *Hemiplecta* Albers, 1850. Moreover, its genital anatomy cannot be assigned to any known limacoid genera. Thus, we herein propose it as a new genus, *Janbinmorpha* gen. nov. for "*Trochomorpha*" *sculpticarina*. For proper taxonomic classification of this new genus, modern systematic study is needed. To ensure an accurate taxonomic assessment, we have generated DNA sequence data of this species for both mitochondrial and nuclear markers based on newly-collected samples and have analysed it with the current knowledge of the Asian limacoid snails (Jirapatrasilp et al. 2021; Bhosale et al. 2021; Pholyotha et al. 2021a, c, 2022a, 2023a; Sutcharit et al. 2021). The aims of the present study are to describe the new genus, *Janbinmorpha* gen. nov., based on a combination of morphological, anatomical and molecular information, and to understand the systematic position of the new genus within the limacoid clade.

Materials and methods

Preparation of specimens, species identification, and morphological studies

This study is based on dry shells and ethanol-preserved samples collected from Thailand since 2007 that are now deposited in the Malacological collections of the Chulalongkorn University Museum of Zoology (**CUMZ**), Bangkok, Thailand. Additional specimens from Myanmar were collected during the Myanmar land snail survey of the Forest Department, Ministry of Natural Resources and Environmental Conservation and Forestry, Myanmar, the Fauna & Flora International (**FFI**), and the Animal Systematics Research Unit, Department of Biology, Faculty of Science, Chulalongkorn University, Thailand (**ASRU**) in years 2016 and 2017. For the newly collected specimens, the animal use protocol was approved by the Chulalongkorn University Animal Care and Use Committee (**CU-ACUC**) under approval number 2123023. Before preservation, photographs of several living individuals were taken using a Nikon camera (DSLR D850) with a Nikon 105 Macro lens (AF-S VR Micro-Nikkor 105mm f/2.8G IF-ED). All living specimens were euthanised following the standard protocols for animal euthanasia (American Veterinary Medical Association 2020), and were subsequently preserved in 95% (v/v) ethanol for anatomical studies and DNA analyses.

Specimens were initially identified based on the literature describing Asian land snail taxonomy (e.g., Martens 1883; Blanford and Godwin-Austen 1908; Solem 1966; Schileyko 2002a, b, 2003; Liew et al. 2009; Pholyotha et al. 2023a; Inkhavilay et al. 2019; Jirapatrasilp et al. 2021; Sutcharit et al. 2021) and compared to the reference collections deposited in the Natural History Museum, London, UK (**NHM**; **NHMUK** when citing specimens deposited in the NHM), Forschungsinstitut und Naturmuseum Senckenberg, Frankfurt am Main, Germany (**SMF**), and Museum für Naturkunde, Humboldt University, Berlin, Germany (**ZMB**).

Adult shells were used to measure the shell height and shell width using a Vernier caliper, and to count the number of whorls. Photographs of shells were taken using a Nikon camera (DSLR D850) with Nikon 105 Macro lens. The shell sculpture was imaged by scanning electron microscopy (SEM; JEOL, JSM-6610 LV). Preserved snails were dissected using an Olympus SZX2-TR30 stereoscopic light microscope and were photographed using the Nikon camera (DSLR D850) with Nikon 105 Macro lens. The inner sculpture of genitalia was imaged by a stereo micro-scope with the Cell'D Imaging Software. Radulae were extracted with 10% (w/v) sodium hydroxide solution, cleaned with distilled water, and imaged by scanning electron microscopy (SEM; JEOL, JSM-6610 LV).

List of abbreviations used in the figures: **at** (atrium), **da** (dart apparatus), **e** (epiphallus), **ec** (epiphallic caecum), **es** (epiphallic sheath), **fo** (free oviduct), **gs** (gametolytic sac), **p** (penis), **prm** (penial retractor muscle), **v** (vagina), **vd** (vas deferens).

Molecular studies

We extracted genomic DNA from small pieces of foot muscle by use of a NucleoSpin DNA extraction kit (Macherey- Nagel, Germany) for animal tissue following the standard procedure of the manual. Fragments of two mitochondrial genes, cytochrome c oxidase subunit 1 (COI) and 16S rRNA (16S), and of one nuclear gene, 28S rRNA (28S) were amplified by PCR using the universal primer pair LCO1490 and HCO2198 (Folmer et al. 1994), the primer pair 16Sar and 16Sbr (Palumbi et al. 1991), and the primer pair LSU2 and LSU4 (Wade

and Mordan 2000), respectively. The PCR thermal cycling conditions for COI, 16S, and 28S were as follows: an initial cycle at 94 °C for 1 min; followed by 40 cycles of 10 s at 98 °C, 30 s at 51 °C for COI, 50 °C for 16S and 60 °C for 28S, and 2 min at 72 °C; and followed by a final extension step at 72 °C for 5 min. The amplified products were then sent for commercial sequencing at Bioneer Corporation, South Korea. Chromatograms were manually corrected for misreads, and forward and reverse strands were merged into one sequence file using MEGA v. 7.0 (Kumar et al. 2016). Sequences obtained in this study have been deposited in GenBank under accession numbers: PQ008991–PQ008998, PQ032739–PQ032747, and PQ032728–PQ032738 (Table 1).

Information regarding all sequences used in our molecular phylogenetic analyses is provided in Table 1. Sequence alignments of each gene fragment were generated separately using MAFFT v. 7 in the MAFFT online service (https://mafft.cbrc.jp/alignment/server/) with the default settings (Katoh et al. 2017). Uncorrected pairwise genetic distances (*P*-distances) were calculated using MEGA v. 7.0 (Kumar et al. 2016) under the option 'pairwise deletion of gaps'.

For phylogenetic analyses, sequences of the three genes were concatenated into one partitioned dataset and the best-fit model of nucleotide substitution was identified for each gene partition by means of the Bayesian Information Criterion using the program Kakusan4 (Tanabe 2011). As suggested by the program Kakusan4, the concatenated dataset was divided into five partitions; the Felsenstein 1981 model with a gamma distribution was chosen for the first codon positions of COI, the Hasegawa, Kishino and Yano 1985 model with a gamma distribution was chosen for the second codon positions of COI, and the general time-reversible model with a gamma distribution was chosen for the third codon positions of COI, 16S and 28S. Phylogenetic relationships were estimated by employing the Maximum Likelihood (ML) and the Bayesian Inference (BI) methods through the online CIPRES Science Gateway (Miller et al. 2010). The ML analyses were performed by applying the GTRCAT model to the entire dataset at the default settings of RAxML-HPC2 on ACCESS v. 8.2.12 (Stamatakis 2014), as the program used did not allow for data partitioning. Branch support was estimated using 1000 bootstrap (BS) replicates. The BI analyses were performed by running 50 million generations of Markov Chain Monte Carlo (MCMC) methods (two simultaneous runs, each with four chains, of which one was heated), as implemented by MrBayes on XSEDE v.3.2.7 (Ronquist et al. 2012). The sampling rate of the trees was 1000 generations, with the first 25% of obtained trees being discarded as burn-in. A branch/clade was considered to be strongly/well supported or statistically significant if the BI posterior probabilities (PP) were ≥ 0.95 and the ML bootstrap (BS) support values were ≥70% (Hillis and Bull 1993; Felsenstein 2004; Huelsenbeck and Rannala 2004; Mauro and Agorreta 2010).

Table 1. Information of specimens used in the molecular studies with species name, specimen codes, locality name, museum registration numbers, GenBank accession numbers, and references.

Taxa	Specimen Codes	Locality name	Museum registration number	GenBank accession numbers			References
				COI	16S	28S	
Infraorder Limacoidei							
Superfamily Helicarionoidea Bourguignat, 1877							
Family Ariophantidae Godwin-Austen, 1883							
Subfamily Ariophantinae Godwin-Austen, 1883							
Janbinmorpha sculpticarina (Martens, 1883), comb. nov.	S163-1	Anurak Community Lodge, Phanom, Surat Thani, Thailand	CUMZ 15076	–	PQ032739	PQ032728	This study
Janbinmorpha sculpticarina (Martens, 1883), comb. nov.	S163-2	Area near Anurak Community Lodge, Phanom, Surat Thani, Thailand	CUMZ 15076	PQ008991	PQ032740	PQ032729	This study
Janbinmorpha sculpticarina (Martens, 1883), comb. nov.	S208-2	Bang Pae Waterfall, Thalang, Phuket, Thailand	CUMZ 15077	PQ008992	–	–	This study
Janbinmorpha sculpticarina (Martens, 1883), comb. nov.	–	Tanintharyi, Myanmar	FLMNH 494197	MF983690	–	–	Slapcinsky and Mulcahy (Unpublished)
Janbinmorpha sculpticarina (Martens, 1883), comb. nov.	–	Tanintharyi, Myanmar	FLMNH 494198	MF983691	–	–	Slapcinsky and Mulcahy (Unpublished)
Ariophanta belangeri (Deshayes, 1832)	–	Kagal, Kolhapur, Maharashtra, India	BNHS GAS 73	–	–	MW583023	Bhosale et al. (2021)
Ariophanta intumescens (Blanford, 1866)	–	Mhalunge, Kolhapur, Maharashtra, India	BNHS GAS 74	–	–	MW583024	Bhosale et al. (2021)
Cryptozona bistrialis (Beck, 1837)	–	Nellore, Andhra Pradesh, India	–	KX514442	KT716352	KX378390	Ayyagari and Sreerama (2020)
Euplecta gardeneri (Pfeiffer, 1848)	–	Sri Lanka	–	–	–	AY841311	Wade et al. (2006)
Hemiplecta distincta (Pfeiffer, 1850)	H54	Tad Pha Suam, Paksong, Champasak, Laos	CUMZ 5267	MT654617	MT651533	MT651588	Sutcharit et al. (2021)
Hemiplecta humphreysiana (Lea, 1840)	H7	Botanic Garden, Singapore	CUMZ 5158	MT364994	MT365775	MT365719	Pholyotha et al. (2021c)
Hemiplecta pluto (Pfeiffer, 1863)	H63	Wat Pa Pha, Khamkeut, Bolikhamxay, Laos	CUMZ 5266	MT364995	MT365776	MT365720	Pholyotha et al. (2021c)
Khasiella pingoungensis (Godwin-Austen, 1888)	MY51-1	Pyinyaung, Mandalay, Myanmar	CUMZ 14560	PQ008993	PQ032741	PQ032730	This study

Taxa	Specimen Codes	Locality name	Museum registration number	GenBank accession numbers			References
				COI	16S	28S	
Khasiella pingoungensis (Godwin-Austen, 1888)	MY51-2	Pyinyaung, Mandalay, Myanmar	CUMZ 14560	PQ008994	PQ032742	PQ032731	This study
Mariaella dussumieri Pfeiffer, 1855	–	Ramling Temple, Kolhapur, Maharashtra, India	ZSI Moll 1789	–	–	MW583030	Bhosale et al. (2021)
Maelamaodiscus somsakpanhai Sutcharit & Pholyotha, 2023	W93-2	Phra Wor Shine, Mae Sod, Tak, Thailand	CUMZ 14295	–	–	PQ032732	This study
Maelamaodiscus somsakpanhai Sutcharit & Pholyotha, 2023	W109	Wat Phothikun, Mae Sod, Tak, Thailand	CUMZ 14296	–	–	PQ032733	This study
Megaustenia praestans Gould, 1843)	MY47	Golden valley near Bat Cave, Hpa-An, Myanmar (Burma)	CUMZ 14638	PQ008995	PQ032743	PQ032734	This study
***Megaustenia* sp.**	C19	Pa Ma-muang Bureau of Monks, Noen Maprang, Phitsanulok, Thailand	CUMZ 7241	MT364990	MT365778	MT365722	Pholyotha et al. (2021d)
***Ratnadvipia* sp.**	–	Sri Lanka	–	–	–	AY841312	Wade et al. (2006)
Subfamily Macrochlamydinae Godwin-Austen, 1888							
Macrochlamys aspides (Benson, 1863)	MY8	Lun Nya Mountain, Hpa An, Kayin, Myanmar	CUMZ 7135	MT364986	MT365761	MT365705	Pholyotha et al. (2021c)
Macrochlamys pedina (Benson, 1865)	–	Khandala,Maharashtra, India	BNHS GAS 146	–	–	MW583026	Bhosale et al. (2021)
Macrochlamys indica Godwin-Austen, 1883	–	Shivaji University, Kolhapur,Maharashtra, India	BNHS GAS 82	–	–	MW583025	Bhosale et al. (2021)
***Macrochlamys* sp.1**	L1	Laos	CUMZ 15262	PQ008996	PQ032744	PQ032735	This study
***Macrochlamys* sp.2**	MY4	Myanmar	CUMZ 15263	PQ008997	PQ032745	PQ032736	This study
Sarika resplendens (Philippi, 1847)	W4	Khao Cha Ngum, Photharam, Ratchaburi, Thailand	CUMZ 7234	MT364982	MT365763	MT365707	Pholyotha et al. (2021c)
Sarika obesior (Martens, 1867)	W65	Wat Nong Phlap, Hua Hin, Prachuap Khiri Khan, Thailand	CUMZ 7233	MT364977	MT365768	MT365712	Pholyotha et al. (2021c)
Taphrenalla diadema (Dall, 1897)	S46	Wat Tham Sumano, Srinagarindra, Phatthalung, Thailand	CUMZ 7175	MT364940	MT365729	MT365673	Pholyotha et al. (2021c)
Taphrenalla incilis Pholyotha & Panha, 2021	S69	Tham Khao Ting, Palian, Trang, Thailand	CUMZ 7209	MT364963	MT365746	MT365690	Pholyotha et al. (2021c)
Varadia amboliensis Bhosale, Thackeray, Muley & Raheem, 2021	–	Amboli, Maharashtra, India	BNHS GAS 129	–	–	MW583027	Bhosale et al. (2021)
Subfamily Ostracolethinae Simroth, 1901							
Parmarion martensi Simroth, 1893	NE100	Wat Tham Pha Khao, Si Wilai, Bueng Kan, Thailand	CUMZ 15264	PQ008998	PQ032746	PQ032737	This study
Family Helicarionidae Bourguignat, 1877							
Aenigmatoconcha clivicola Tumpeesuwan & Tumpeesuwan, 2017	NE68	Wat Tham Pha Lom, Mueang, Loei, Thailand	CUMZ 7929	MW703614	PQ032747	PQ032738	This study; Pholyotha et al. (2021d)
Chalepotaxis infantilis (Gredler, 1881)	Cha-inf-2	Guanyindong, Zhangjiajie Shi, Hunan, China	NHMW 111548	KX027275	–	KX027276	Pall-Gergely et al. (2016)
***Durgella* sp.**	N15	Tham Lom Tham Wang, Si Samrong, Sukhothai, Thailand	CUMZ 7242	MT364991	MT365777	MT365721	Pholyotha et al. (2021c)
Eurychlamys platychlamys (Blanford, 1880)	–	Sagar Upavan, Mumbai, Maharashtra, India	BNHS GAS 10	–	–	MW583029	Bhosale et al. (2021)
Fastosarion brazieri (Cox, 1873)	–	Mossman, Queensland, Australia	–	–	–	AY014099	Wade et al. (2001)
***Satiella* sp.**	–	Jawali, Kolhapur, Maharashtra, India	BNHS GAS 69	–	–	MW583028	Bhosale et al. (2021)
Sophina schistostelis (Benson, 1859)	MY24	Sanbel Cave, Mawlamyine, Mon, Myanmar	CUMZ 5195	MN897023	MN888602	MN892653	Sutcharit et al. (2020a)
Superfamily Trochomorphoidea Mörch, 1864							
Family Dyakiidae Gude & Woodward, 1921							
***Trochomorpha* sp.1**	NE74	Tham Khao Chakan, Khao Chakan, Sa Kaeo, Thailand	CUMZ 14870	OR075932	OR076723	OR076740	Pholyotha et al. (2023a)
***Trochomorpha* sp.2**	NE80	Wat Tham Pha Lom, Mueang, Loei, Thailand	CUMZ 14871	OR075933	OR076724	OR076741	Pholyotha et al. (2023a)
***Trochomorpha* sp.3**	S185-2	Talod Cave, Thung Song, Nakhon Si Thammarat, Thailand	CUMZ 14873	OR075934	OR076725	OR076742	Pholyotha et al. (2023a)
Trochomorpha froggatti (Iredale, 1941)	–	Batangan, Kinabatangan, Sabah, Malaysia	RMNH. 5005011.01	MK851194	MK851432	MK851503	Hendriks (2020)
Videna metcalfei (Pfeiffer, 1845)	–	Batangan, Kinabatangan, Sabah, Malaysia	RMNH. 5005031.01	MK851205	MK851445	MK851515	Hendriks (2020)
Family Geotrochidae Schileyko, 2002							
Geotrochus rhysa (Tillier & Bouchet, 1989)	–	Mount Kinabalu, Sabah, Malaysia	BORMOL 6347	MK779474	MK334188	OR076749	Chang and Liew (2021), Pholyotha et al. (2023a)
Geotrochus kitteli Vermeulen, Liew & Schilthuizen, 2015	–	Mount Kinabalu, Sabah, Malaysia	BORMOL 6406	MK779460	MK334194	OR076744	Chang and Liew (2021), Pholyotha et al. (2023a)

Taxa	Specimen Codes	Locality name	Museum registration number	GenBank accession numbers			References
				COI	16S	28S	
Family Euconulidae Baker, 1928							
Siamoconus geotrochoides Pholyotha, 2023	NE46-1	Wat Tham Pha Lom, Mueang, Loei, Thailand	CUMZ 14298	OR075923	OR076716	OR076735	Pholyotha et al. (2023a)
Siamoconus boreas Pholyotha, 2023	N70-3	Ban Tha Si, Mae Mo, Lampang, Thailand	CUMZ 14310	OR075905	OR076701	OR076726	Pholyotha et al. (2023a)
Superfamily Gastrodontoidea Tryon, 1866							
Family Oxychilidae Hesse, 1927							
Oxychilus alliarius (Miller, 1822)	–	Deepdale, Derbyshire, UK	–	MN022739	–	MN022673	Saadi and Wade (2019)
Superfamily Limacoidea Batsch, 1789							
Family Vitrinidae Fitzinger, 1833							
Vitrina pellucida (Müller, 1774)	–	Kirkdale, Derbyshire, UK	–	MN022738	–	MN022672	Saadi and Wade (2019)
Infraorder Arionoidei Gray, 1840							
Superfamily Arionoidea Gray, 1840							
Family Philomycidae Gray, 1847							
Meghimatium bilineatum (Benson, 1842)	–	Mauritius	–	MN022745	–	MN022678	Saadi and Wade (2019)
Family Arionidae Gray, 1840							
Arion hortensis Férussac, 1819	–	Kirkdale, Derbyshire, UK	–	MN022744	–	KU341315	Saadi and Wade (2019)

Results

Molecular phylogeny

Molecular phylogenetic trees were reconstructed based on the concatenated mitochondrial COI and 16S sequences, and nuclear 28S sequences obtained from 53 individuals, including 31 ariophantids, 7 helicarionids, 5 trochomorphids, 2 dyakiids, 2 geotrochids, 2 euconulids, 1 oxychilid, and 1 vitrinid together with 2 species of arionoideans for the more distantly related outgroups to root the phylogenetic tree. The suitable outgroups in this study were selected based on the recent phylogenetic trees presented by Bhosale et al. (2021) and Pholyotha et al. (2023a). The final concatenated mtDNA + nDNA dataset contained 39 COI sequences, with an alignment length of 691 sites (377 conserved sites, 260 parsimony informative sites, and 305 variable sites), 32 sequences of 16S, with an alignment length of 522 sites (215 conserved sites, 204 parsimony informative sites, and 249 variable sites), and 50 sequences of 28S, with an alignment length of 557 sites (387 conserved sites, 117 parsimony informative sites, and 164 variable sites).

In this study, both Maximum Likelihood (ML) and Bayesian Inference (BI) analyses produced trees with identical topologies; therefore, only the tree topology from the ML analysis is presented in Fig. 1. Analyses of the combined COI + 16S + 28S dataset of about 31 sequences of at least 24 species representing all known ariophantid genera that have available DNA information from Asia have confirmed the monophyly of the *Janbinmorpha* gen. nov. as delineated herein. However, our results indicated that the phylogenetic relationships within the Limacoidei are still unresolved, especially a clade of the Helicarionoidea (including Ariophantidae and Helicarionidae; Fig. 1).

Although the phylogeny is not fully resolved, it highlights or identifies the phylogenetic positions of *Janbinmorpha* gen. nov. and some ariophantid genera (such as *Megaustenia*, *Khasiella*, *Parmarion*, and *Maelamaodiscus*) for the first time. The new genus was grouped together with the *Maelamaodiscus* + *Hemiplecta* clade with high support by BI (BS = 62%, PP = 0.97). However, the phylogenetic relationships within the *Janbinmorpha* + *Maelamaodiscus* + *Hemiplecta* clade could not be resolved in this study (Fig. 1). This clade was retrieved as the sister clade to the *Khasiella* + *Macrochlamys aspides* + *Sarika* + *Taphrenalla* clade with good support (BS = 71%, PP = 1). Relationships within the latter clade were resolved in this study (Fig. 1).

Pairwise comparisons of COI sequences showed that conspecific specimens of *Janbinmorpha sculpticarina* comb. nov. were differentiated by means of 0% to 4.4% uncorrected *p*-distances (Table 2), whereas 16S and 28S sequences of conspecific specimens differed by 0%. Comparing *Janbinmorpha* gen. nov. and other ariophantid genera, the uncorrected *p*-distances of the COI, 16S and 28S sequences ranged from 12.2% (between the new genus and *Taphrenalla*) to 14.8% (between the new genus and *Parmarion*) for COI (Table 3), from 11.8% (between the new genus and *Hemiplecta*) to 17.8% (between the new genus and *Cryptozona*) for 16S (Table 4), and from 2.7% (between the new genus and *Hemiplecta*) to 6.0% (between the new genus and *Cryptozona*) for 28S (Table 5).

Taxonomy and systematics

Superfamily Helicarionoidea Bourguignat, 1877
Family Ariophantidae Godwin-Austen, 1883
Subfamily Ariophantinae Godwin-Austen, 1883

Janbinmorpha Pholyotha & Panha, gen. nov.

https://zoobank.org/953A9F87-2E64-4A11-AFD6-061303E94409

Type species. *Trochomorpha sculpticarina* Martens, 1883; here designated.

Etymology. The name combines "*Janbin*" in reference to the shape of an unidentified flying object (UFO) in the Thai language, and similar to the shell shape of

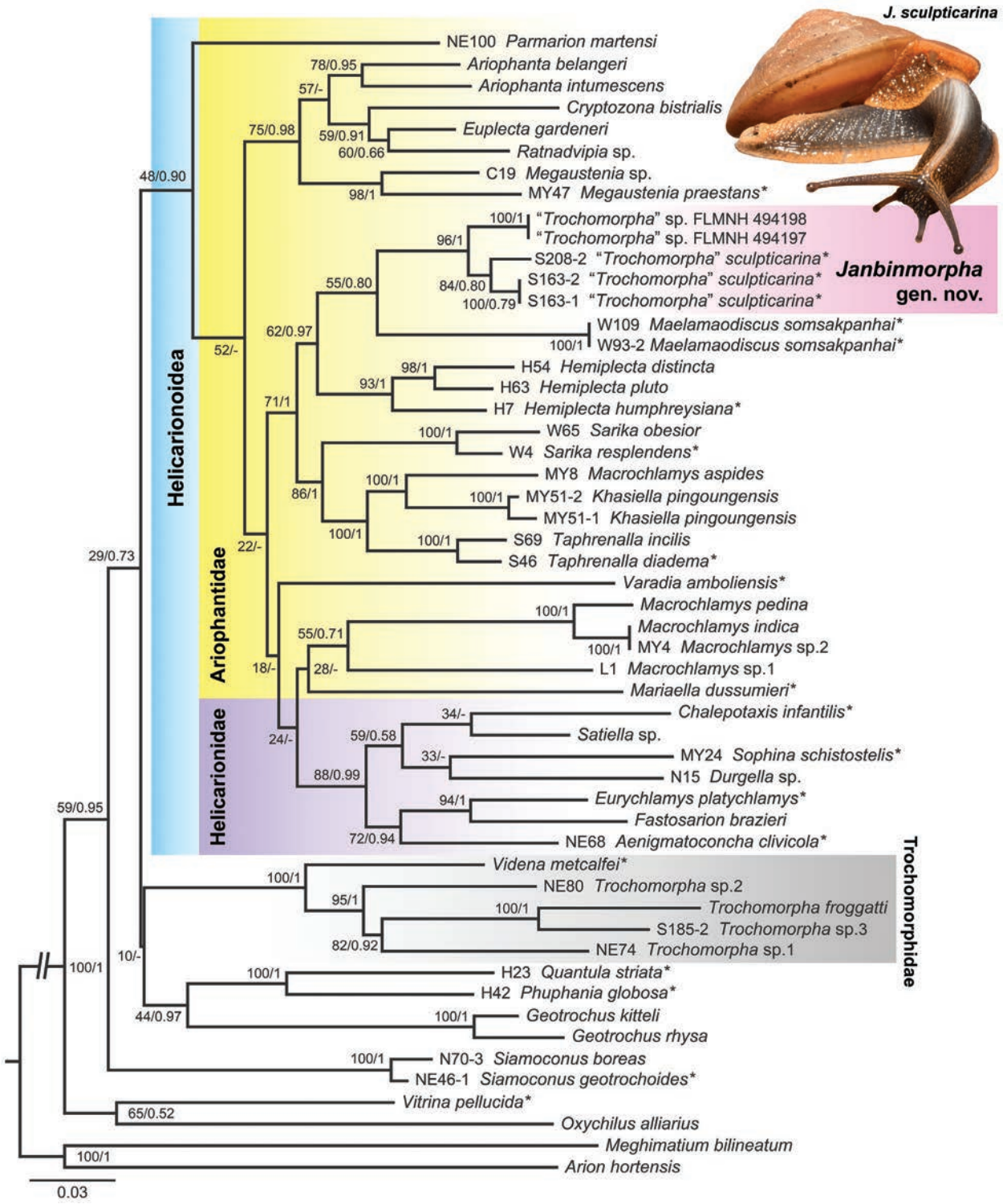

Figure 1. Maximum likelihood phylogram based on analyses of concatenated COI, 16S, and 28S sequences. Numbers on branches indicate nodal support by ML bootstrap (BS) and Bayesian posterior probabilities (PP) analyses. Asterisk indicates the type species of its corresponding genus. The sample code in front of species name indicates voucher samples as shown in Table 1. Living specimen of *Janbinmorpha sculpticarina* (Martens, 1883), comb. nov. from Phang-nga Province, not to scale.

this new genus, and "*morpha*" in reference to the similarity of shell morphology between this new genus and the genus *Trochomorpha*.

Diagnosis. Shell dextral, umbilicated, depressed, lenticular, ribbed, with keeled last whorl. Animal with three dorsal lobes; foot tripartite; caudal foss present; caudal horn very reduced. Genitalia having epiphallic caecum, flagellum and dart apparatus; proximal epiphallus encircled with thickened muscular epiphallic sheath; gametolytic organ without duct and gametolytic sac consisting of two bulbs. Radula with tricuspid central tooth; unicuspid or bicuspid lateral teeth; unicuspid marginal teeth.

Table 2. Estimates of cytochrome c oxidase I (COI) sequence divergence (uncorrected *p*-distances) within *Janbinmorpha sculpticarina* comb. nov.

Sequences of *Janbinmorpha sculpticarina*	*J. sculpticarina* S163-2	*J. sculpticarina* S208-2	*J. sculpticarina* FLMNH 494197	*J. sculpticarina* FLMNH 494198
***J. sculpticarina* S163-2**				
***J. sculpticarina* S208-2**	0.027			
***J. sculpticarina* FLMNH 494197**	0.044	0.043		
***J. sculpticarina* FLMNH 494198**	0.044	0.043	0.000	

Description. See below under the type species.

Constituent species. This new genus contains only the type species, *J. sculpticarina* comb. nov.

Distribution. Currently known only from the Malay Peninsula.

Remarks. *Janbinmorpha* gen. nov. is clearly discriminated from all other Southeast Asian limacoid genera (e.g., *Hemiplecta*, *Holkeion* Godwin-Austen, 1908, *Siamoconus* Pholyotha in Pholyotha et al. 2023a, *Videna* and *Trochomorpha*) by the shape of the gametolytic sac and by the attachment of the penial retractor muscle. This new genus has no gametolytic duct and the gametolytic sac is divided into two lobes, while the gametolytic sac of all other limacoid genera is not divided into two lobes and most of them have a gametolytic duct. The penial retractor muscle of this new genus is attached to two regions (epiphallic caecum and epiphallic sheath), while all other limacoid genera have the retractor muscle attached to either the epiphallic caecum or epiphallus (Blanford and Godwin-Austen 1908; Solem 1966; Schileyko 2002a, b, 2003; Sutcharit et al. 2020a, 2021; Sutcharit and Panha 2021; Pholyotha et al. 2021b, c, 2022a, b, 2023b, c).

Janbinmorpha gen. nov. also differs from *Videna* in having a long dart apparatus and the position of gametolytic organ on female side, while the latter genus has no dart apparatus and gametolytic duct opening into the base of the penis (Schileyko 2002a).

Janbinmorpha gen. nov. is conchologically very similar to the Indian helicarionoidean genus *Sivella* Blanford, 1863. However, this new genus differs by having a long dart apparatus, a straight epiphallic caecum, and no gametolytic duct. In comparison, *Sivella* has a relatively short gametolytic duct and a subglobular gametolytic sac, and does not have a dart apparatus or epiphallic caecum (Godwin-Austen 1918; Schileyko 2003).

In addition, the molecular phylogeny (Fig. 1) supports a distinct lineage of the monotypic *Janbinmorpha* gen. nov. from genera *Hemiplecta*, *Siamoconus*, *Videna* and *Trochomorpha*. Currently, genetic sequences of *Holkeion* and *Sivella* are not available in the online GenBank sequence database for phylogenetic analysis.

Janbinmorpha sculpticarina (Martens, 1883), comb. nov.

Figs 1–5, 6A

Trochomorpha sculpticarina Martens, 1883: 136, pl. 25, figs 13–16. Type locality: "insulam Salanga" [Phuket Province, Thailand].

Videna sculpticarina–Basch and Solem 1971: 95. Maassen 2001: 116.

Type material examined. Syntype ZMB/Moll 58132 (1 shell; Fig. 2A) ex. Paetel collection from Salanga [Phuket Province, Thailand]. Syntypes ZMB/Moll 34164 (2 shells; Fig. 2B) ex. Weber collection from Salanga [Phuket Province, Thailand].

Other material examined. Myanmar-Southern. Buddha Cave, Lenya City, Tanintharyi Region, 11°13'46.2"N, 99°10'34.3"E: CUMZ 15254 (1 preserved specimen). **Thailand. Salanga** [Phuket Province, Thailand]: ZMB/Moll 75765 (1 shell) ex. Webb collection, ZMB/Moll 88249 (1 shell) ex. Kammaun collection, SMF 179828/2 (2 shells; Fig. 2C), SMF 179829/2 (2 shells) ex. Möllendorff collection, NHMUK 1883.3.27.4 (1 shell). **Phuket:** Bang Pae Waterfall, Thalang District, 8°02'21.9"N, 98°23'27.8"E: CUMZ 15077 (4 shells and 4 preserved specimens; Fig. 2D), 15161 (3 shells). **Chumphon:** Tham Nam Lod Thepnimit Bureau of Monks, Sawi District, 10°22'37.8"N, 99°00'41.2"E: CUMZ 15157 (2 shells). Wat Tham Sanook, Mueang District, 10°28'51.4"N, 99°04'28.3"E: CUMZ 15156 (1 shell). Area in Pak Song, Phato District, 9°46'10.8"N, 98°40'42.9"E: CUMZ 15255 (1 preserved specimen). **Ranong:** Near Wat Pa Thung Rong, Kapoe District, 9°37'00.2"N, 98°37'52.3"E: CUMZ 15256 (2 preserved specimens). **Phang-nga:** Wat Khiriwong (Tham Kob), Thap Put District, 8°31'55.9"N, 98°34'38.4"E: CUMZ 15163 (1 shell). Wat Pa Dok Daeng, Takua Pa District, 8°44'28.6"N, 98°18'24.3"E: CUMZ 15151 (3 shells and 3 preserved specimens; Fig. 2F). Ton Phrai Waterfall, Thai Mueang District, 8°26'10.4"N, 98°18'33.3"E: CUMZ 15150 (1 shell and 2 preserved specimens). Nature study route 1 in Ko Surin Nuea, Khura Buri District, 9°27'01.1"N, 97°52'39.1"E: CUMZ 15164 (1 shell). Nature study route 4 in Ko Surin Nuea, Khura Buri District, 9°25'46.3"N, 97°52'14.0"E: CUMZ 15152 (2 preserved specimens). Nature study route 3 in Ko Surin Tai, Khura Buri District, 9°23'48.2"N, 97°52'02.8"E: CUMZ 15162 (2 shells). **Surat Thani:** Nature trail at Ratchaprapha Dam, Ban Ta Khun District, 8°58'19.1"N, 98°48'16.7"E: CUMZ 15154 (29 shells). Area in Khiri Rat Nikhom District, 9°04'13.1"N, 98°59'45.6"E: CUMZ 15153 (8 shells; Fig. 2E). Area near Anurak Community Lodge, Klong Sok, Phanom District, 8°53'05.6"N, 98°41'12.6"E: CUMZ 15076 (2 preserved specimens). **Nakhon Si Thammarat:** Area in Khao Noi, Sichon District, 8°56'17.3"N, 99°48'54.7"E: CUMZ 15155 (1 shell). **Krabi:** Toh Chong Toh Yuan Shrine, Ao Luek District, 8°22'25.5"N, 98°44'09.7"E: CUMZ 15160 (1 shell). **Trang:** Khao Ting Cave, Palian District, 7°09'32.3"N, 99°48'10.3"E: CUMZ 15158 (1 shell).

Table 3. Estimates of evolutionary divergence between *Janbinmorpha* gen. nov. and other genera based on uncorrected *p*-distance of COI gene fragment sequences.

Genera	01	02	03	04	05	06	07	08	09	10	11	12	13	14	15	16	17	18	19	20	21	22	23
01 *Janbinmorpha*	–																						
02 *Cryptozona*	0.138	–																					
03 *Hemiplecta*	0.126	0.118	0.080																				
04 *Megaustenia*	0.145	0.124	0.136	0.098																			
05 *khasiella*	0.128	0.115	0.112	0.133	–																		
06 *Macrochlamys*	0.141	0.129	0.131	0.136	0.113	0.133																	
07 *Sarika*	0.130	0.134	0.122	0.137	0.102	0.121	0.05																
08 *Taphrenalla*	0.122	0.116	0.110	0.134	0.094	0.118	0.116	0.05															
09 *Parmarion*	0.148	0.146	0.136	0.142	0.123	0.135	0.128	0.124	–														
10 *Aenigmatoconcha*	0.131	0.128	0.139	0.143	0.130	0.133	0.124	0.125	0.139	–													
11 *Chalepotaxis*	0.156	0.148	0.150	0.159	0.118	0.145	0.145	0.144	0.145	0.127	–												
12 *Durgella*	0.148	0.161	0.134	0.159	0.131	0.138	0.133	0.136	0.142	0.147	0.157	–											
13 *Sophina*	0.157	0.141	0.139	0.155	0.126	0.153	0.132	0.137	0.127	0.142	0.142	0.144	-										
14 *Quantula*	0.147	0.141	0.137	0.138	0.140	0.144	0.147	0.133	0.137	0.145	0.150	0.157	0.150	–									
15 *Phuphania*	0.144	0.144	0.134	0.143	0.133	0.141	0.136	0.133	0.142	0.145	0.147	0.140	0.166	0.125	–								
16 *Geotrochus*	0.170	0.172	0.167	0.179	0.159	0.170	0.156	0.161	0.171	0.143	0.165	0.163	0.165	0.185	0.179	0.049							
17 *Siamoconus*	0.129	0.124	0.134	0.139	0.134	0.137	0.143	0.126	0.134	0.131	0.147	0.143	0.163	0.146	0.150	0.147	0.031						
18 *Trochomorpha*	0.168	0.161	0.151	0.151	0.146	0.155	0.152	0.146	0.152	0.154	0.149	0.159	0.174	0.161	0.157	0.171	0.136	0.128					
19 *Videna*	0.153	0.140	0.131	0.135	0.124	0.133	0.129	0.118	0.151	0.141	0.135	0.153	0.157	0.138	0.138	0.174	0.135	0.121	–				
20 *Oxychilus*	0.173	0.146	0.155	0.167	0.159	0.175	0.169	0.153	0.156	0.157	0.171	0.171	0.151	0.168	0.174	0.195	0.175	0.173	0.171	–			
21 *Vitrina*	0.160	0.149	0.151	0.158	0.144	0.168	0.147	0.148	0.153	0.144	0.166	0.151	0.153	0.166	0.160	0.173	0.151	0.162	0.168	0.156	–		
22 *Meghimatium*	0.215	0.218	0.202	0.215	0.202	0.217	0.195	0.205	0.214	0.189	0.221	0.214	0.214	0.232	0.208	0.210	0.203	0.218	0.225	0.214	0.191	–	
23 *Arion*	0.223	0.205	0.219	0.222	0.205	0.207	0.185	0.202	0.215	0.194	0.211	0.203	0.198	0.218	0.212	0.199	0.208	0.207	0.214	0.234	0.224	0.214	–

Table 4. Estimates of evolutionary divergence between *Janbinmorpha* gen. nov. and other genera based on uncorrected *p*-distance of 16S gene fragment sequences.

Genera	01	02	03	04	05	06	07	08	09	10	11	12	13	14	15	16	17	18
01 ***Janbinmorpha***	–																	
02 ***Cryptozona***	0.178	–																
03 ***Hemiplecta***	0.118	0.164	0.068															
04 ***Megaustenia***	0.140	0.176	0.136	0.089														
05 ***khasiella***	0.126	0.193	0.139	0.156	–													
06 ***Macrochlamys***	0.153	0.188	0.158	0.173	0.149	0.167												
07 ***Sarika***	0.145	0.199	0.136	0.132	0.141	0.166	0.069											
08 ***Taphrenalla***	0.132	0.171	0.127	0.168	0.123	0.151	0.138	0.026										
09 ***Parmarion***	0.149	0.184	0.165	0.173	0.192	0.187	0.165	0.173	–									
10 ***Aenigmatoconcha***	0.126	0.183	0.146	0.142	0.149	0.159	0.155	0.162	0.175	–								
11 ***Durgella***	0.177	0.201	0.156	0.165	0.185	0.189	0.161	0.197	0.187	0.163	–							
12 ***Sophina***	0.184	0.202	0.155	0.165	0.176	0.197	0.171	0.196	0.182	0.145	0.122	–						
13 ***Quantula***	0.183	0.180	0.170	0.206	0.183	0.209	0.206	0.169	0.170	0.208	0.211	0.208	–					
14 ***Phuphania***	0.187	0.162	0.182	0.206	0.187	0.190	0.207	0.184	0.178	0.203	0.234	0.206	0.128	–				
15 ***Geotrochus***	0.191	0.227	0.200	0.207	0.218	0.206	0.208	0.201	0.210	0.200	0.249	0.225	0.189	0.176	0.082			
16 ***Siamoconus***	0.216	0.218	0.232	0.227	0.227	0.222	0.225	0.223	0.211	0.216	0.228	0.236	0.188	0.206	0.217	0.024		
17 ***Trochomorpha***	0.240	0.272	0.242	0.250	0.247	0.242	0.245	0.231	0.249	0.249	0.268	0.256	0.258	0.236	0.212	0.252	0.179	
18 ***Videna***	0.196	0.223	0.207	0.222	0.209	0.215	0.219	0.204	0.222	0.222	0.255	0.237	0.189	0.174	0.201	0.206	0.212	–

Table 5. Estimates of evolutionary divergence between *Janbinmorpha* gen. nov. and other genera based on uncorrected *p*-distance of 28S gene fragment sequences.

Genera	01	02	03	04	05	06	07	08	09	10	11	12	13	14	15	16
01 ***Janbinmorpha***	–															
02 ***Ariophanta***	0.041	0.022														
03 ***Cryptozona***	0.060	0.048	–													
04 ***Euplecta***	0.044	0.027	0.034	–												
05 ***Hemiplecta***	0.027	0.053	0.070	0.059	0.005											
06 ***Maelamaodiscus***	0.030	0.046	0.065	0.054	0.042	–										
07 ***Mariaella***	0.058	0.057	0.068	0.057	0.061	0.061	–									
08 ***Megaustenia***	0.040	0.031	0.047	0.028	0.049	0.046	0.053	0.006								
09 ***Ratnadvipia***	0.047	0.030	0.038	0.021	0.058	0.051	0.053	0.029	–							
10 ***khasiella***	0.047	0.053	0.064	0.055	0.056	0.045	0.064	0.046	0.058	-						
11 ***Macrochlamys***	0.057	0.061	0.073	0.064	0.071	0.058	0.067	0.056	0.065	0.059	0.049					
12 ***Sarika***	0.038	0.055	0.069	0.058	0.045	0.046	0.063	0.051	0.057	0.036	0.058	0.002				
13 ***Taphrenalla***	0.033	0.042	0.055	0.047	0.040	0.041	0.056	0.034	0.048	0.018	0.050	0.032	0.006			
14 ***Varadia***	0.051	0.053	0.060	0.057	0.056	0.054	0.062	0.053	0.058	0.066	0.065	0.063	0.055	–		
15 ***Parmarion***	0.041	0.050	0.062	0.050	0.042	0.053	0.049	0.046	0.052	0.054	0.062	0.044	0.042	0.056	–	
16 ***Aenigmatoconcha***	0.060	0.058	0.076	0.061	0.074	0.061	0.058	0.055	0.058	0.058	0.059	0.059	0.053	0.066	0.054	–
17 ***Chalepotaxis***	0.060	0.059	0.064	0.053	0.072	0.057	0.051	0.052	0.043	0.064	0.061	0.065	0.057	0.056	0.060	0.036
18 ***Durgella***	0.047	0.044	0.056	0.044	0.063	0.049	0.053	0.035	0.041	0.051	0.064	0.059	0.046	0.051	0.054	0.038
19 ***Eurychlamys***	0.058	0.062	0.072	0.057	0.063	0.061	0.058	0.055	0.058	0.060	0.069	0.067	0.057	0.066	0.054	0.038
20 ***Fastosarion***	0.062	0.069	0.082	0.069	0.075	0.067	0.060	0.061	0.062	0.068	0.067	0.068	0.059	0.073	0.053	0.039
21 ***Satiella***	0.054	0.053	0.060	0.048	0.061	0.049	0.051	0.042	0.049	0.053	0.056	0.057	0.050	0.051	0.053	0.034
22 ***Sophina***	0.047	0.048	0.052	0.044	0.058	0.049	0.062	0.042	0.045	0.049	0.058	0.053	0.044	0.047	0.054	0.039
23 ***Quantula***	0.082	0.077	0.103	0.084	0.082	0.093	0.094	0.078	0.084	0.082	0.098	0.090	0.076	0.091	0.083	0.087
24 ***Phuphania***	0.075	0.075	0.087	0.076	0.077	0.080	0.087	0.075	0.082	0.072	0.090	0.071	0.061	0.082	0.071	0.084
25 ***Geotrochus***	0.054	0.062	0.078	0.059	0.075	0.068	0.077	0.063	0.067	0.069	0.082	0.067	0.057	0.073	0.056	0.081
26 ***Siamoconus***	0.054	0.049	0.066	0.040	0.068	0.067	0.060	0.048	0.049	0.056	0.069	0.061	0.053	0.069	0.050	0.068
27 ***Trochomorpha***	0.064	0.063	0.073	0.058	0.089	0.076	0.079	0.056	0.064	0.073	0.084	0.071	0.069	0.070	0.070	0.078
28 ***Videna***	0.074	0.074	0.084	0.063	0.084	0.088	0.095	0.058	0.074	0.086	0.100	0.087	0.080	0.084	0.085	0.096
29 ***Oxychilus***	0.058	0.060	0.076	0.059	0.075	0.056	0.075	0.055	0.060	0.066	0.069	0.065	0.057	0.069	0.060	0.077
30 ***Vitrina***	0.060	0.051	0.058	0.044	0.075	0.069	0.065	0.057	0.056	0.069	0.075	0.070	0.061	0.064	0.054	0.073
31 ***Meghimatium***	0.086	0.077	0.094	0.084	0.106	0.099	0.090	0.089	0.088	0.092	0.101	0.093	0.088	0.083	0.088	0.105
32 ***Arion***	0.064	0.073	0.082	0.071	0.080	0.079	0.083	0.068	0.077	0.072	0.085	0.069	0.071	0.070	0.080	0.092

Table 5. Continued.

Genera	17	18	19	20	21	22	23	24	25	26	27	28	29	30	31	32
01 ***Janbinmorpha***																
02 ***Ariophanta***																
03 ***Cryptozona***																
04 ***Euplecta***																
05 ***Hemiplecta***																
06 ***Maelamaodiscus***																
07 ***Mariaella***																
08 ***Megaustenia***																
09 ***Ratnadvipia***																
10 ***khasiella***																
11 ***Macrochlamys***																
12 ***Sarika***																
13 ***Taphrenalla***																
14 ***Varadia***																
15 ***Parmarion***																
16 ***Aenigmatoconcha***																
17 ***Chalepotaxis***	–															
18 ***Durgella***	0.028	–														
19 ***Eurychlamys***	0.047	0.043	–													
20 ***Fastosarion***	0.045	0.051	0.032	–												
21 ***Satiella***	0.026	0.026	0.039	0.045	–											
22 ***Sophina***	0.038	0.034	0.043	0.049	0.030	–										
23 ***Quantula***	0.094	0.089	0.104	0.099	0.082	0.087	–									
24 ***Phuphania***	0.084	0.084	0.099	0.092	0.084	0.077	0.043	–								
25 ***Geotrochus***	0.081	0.075	0.083	0.077	0.073	0.077	0.061	0.057	0							
26 ***Siamoconus***	0.069	0.062	0.069	0.073	0.064	0.068	0.093	0.084	0.071	0						
27 ***Trochomorpha***	0.073	0.063	0.081	0.082	0.070	0.080	0.105	0.095	0.074	0.066	0.026					
28 ***Videna***	0.089	0.079	0.098	0.100	0.084	0.093	0.093	0.088	0.087	0.078	0.036	–				
29 ***Oxychilus***	0.073	0.064	0.077	0.081	0.071	0.062	0.091	0.077	0.071	0.064	0.078	0.093	–			
30 ***Vitrina***	0.071	0.064	0.066	0.079	0.064	0.054	0.098	0.094	0.069	0.065	0.083	0.097	0.064	–		
31 ***Meghimatium***	0.100	0.092	0.100	0.103	0.100	0.094	0.139	0.124	0.099	0.089	0.102	0.116	0.099	0.077	–	
32 ***Arion***	0.085	0.079	0.085	0.089	0.085	0.073	0.121	0.107	0.085	0.076	0.088	0.102	0.079	0.071	0.063	–

Diagnosis. Shell depressed and lenticular; body whorl keeled on periphery; surface with prominent radial ribs and reticulated microsculptures; whorls 6 and increasing regularly; aperture obliquely crescent-shaped with simple peristome; umbilicus open and funnel shaped. Animal dark gray with pigmentation of yellow to orange dots or patches; one stripe at middle of body running from anterior to posterior; three dorsal lobes present; foot tripartite; caudal foss present; caudal horn very reduced. Genitalia having very short flagellum; two bundles of penial retractor muscle; epiphallic sheath thickened and entirely covering proximal epiphallus; gametolytic duct absent; gametolytic sac having two lobes; dart apparatus present.

Description. ***Shell*** (Figs 2, 3A–D). Shell dextral, depressed, lenticular, medium-sized (shell width up to 19.8 mm, shell height up to 9.3 mm), thickened, rather opaque, yellowish brown to dark brownish. Embryonic shell about 2½ whorls, with raised growth lines forming riblet-like textures (Fig. 3A, B). Whorls 6, convex, regularly increasing, separated by shallow suture. Later

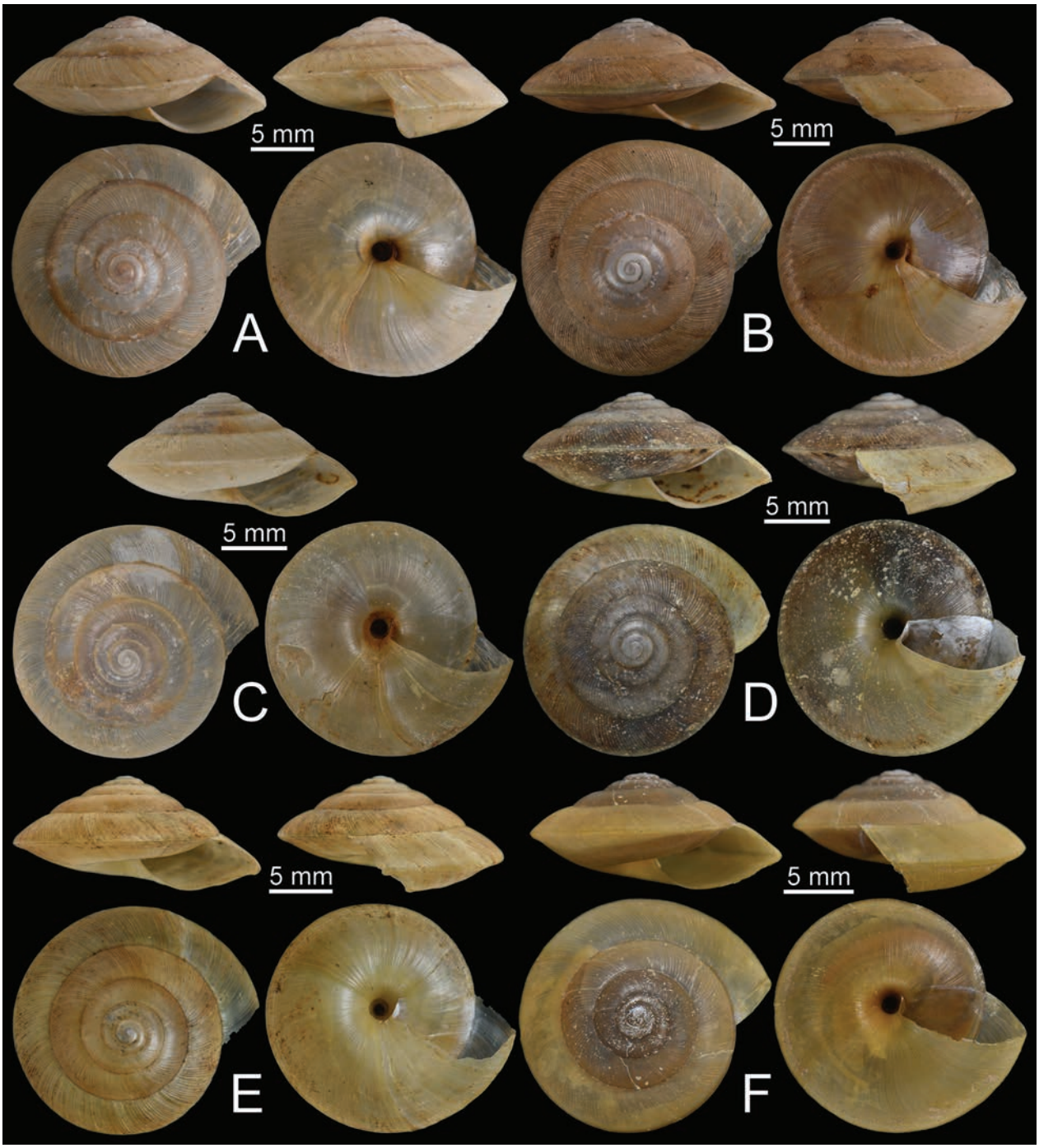

Figure 2. Shell of *Janbinmorpha sculpticarina* (Martens, 1883), comb. nov. **A.** Syntype from Salanga [Phuket Province]: ZMB/Moll 58132; **B.** Syntypes from Salanga [Phuket Province]: ZMB/Moll 34164; **C.** Specimen from Salanga I., Malaysia [Phuket Island, Phuket Province, Thailand]: NHMUK 1888.3.27.4; **D.** Specimen from Phuket Province: CUMZ 15077; **E.** Specimen from Surat Thani Province: CUMZ 15153; **F.** Specimen from Phang-nga Province: CUMZ 15151 using for SEM imaging.

whorls distinct, regular, curved radial ribs, with fine, widely regularly spaced radial ribs, with reticulated microsculptures; and 4–5 distinct spiral threads close to the periphery, positioned above the radial ribs (Fig. 3C, D). Last whorl distinctly angular, compressed at periphery, and moderately convex below periphery. Spire rather elevated. Aperture obliquely crescent-shaped; peristome simple; columellar margin simple and slightly reflected near umbilicus. Umbilicus opened, deep, slightly less than one-third the width of the last whorl from the bottom view of the shell.

Genitalia (Fig. 4). Atrium (at) enlarged and short. Penis (p) enlarged and short cylindrical. Inner wall sculptured with small, curly and closely packed oblique penial pilasters extending through entire penis chamber; penial verge absent; junction between penis and epiphallus thickened (Fig. 4B). Epiphallus (e) long cylindrical tube: proximal epiphallus longer than penis and vagi-

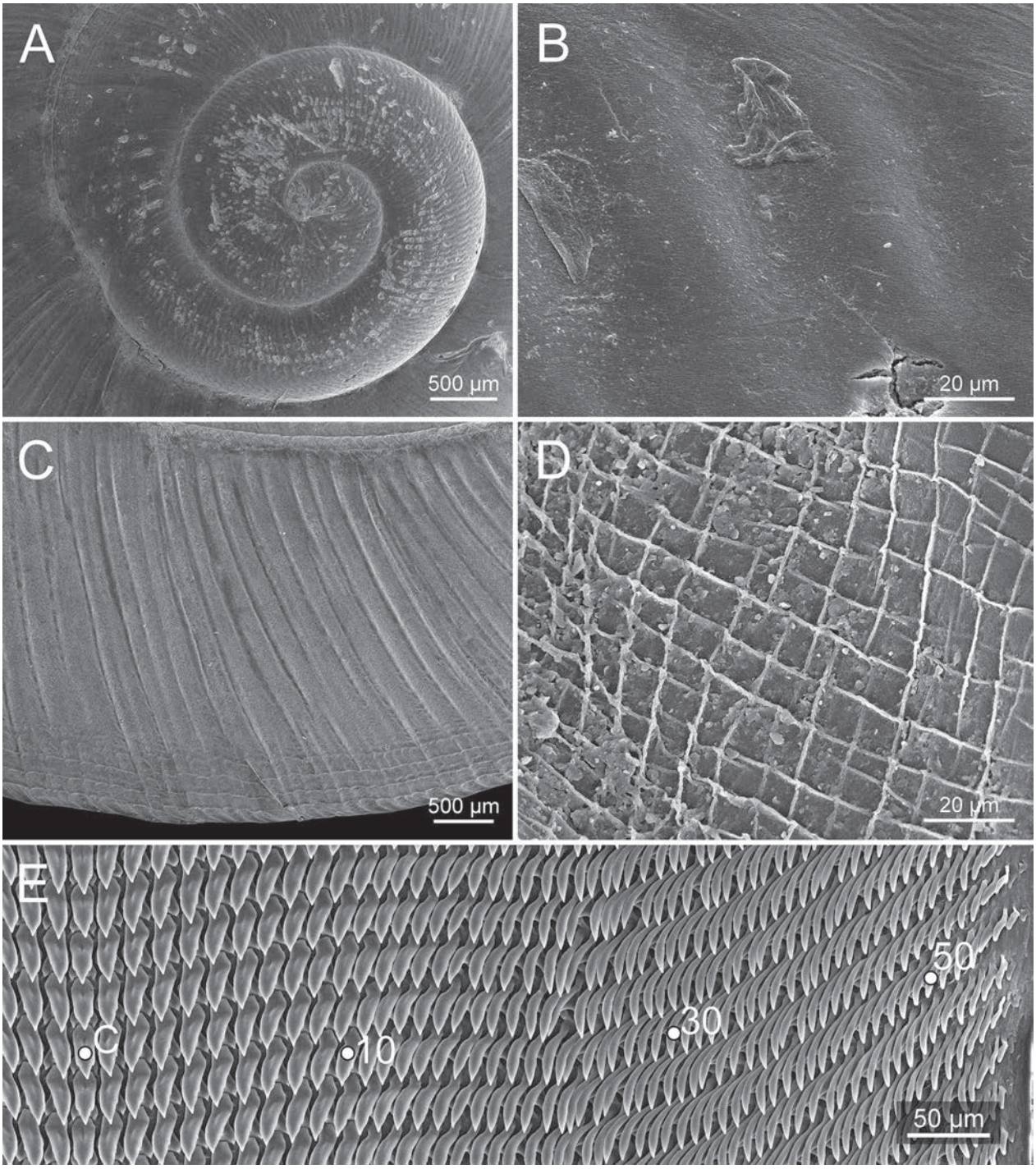

Figure 3. Scanning electron microscope (SEM) images of shell surface and radula of *Janbinmorpha sculpticarina* (Martens, 1883), comb. nov. **A–D.** Specimen CUMZ 15151, showing shell surface; **A.** Protoconch viewed from above; **B.** Zoomed-in view of protoconch; **C.** Body whorl viewed from above; **D.** Zoomed-in view of body whorl; **E.** Specimen CUMZ 15077, showing radula; central tooth indicated by 'C'.

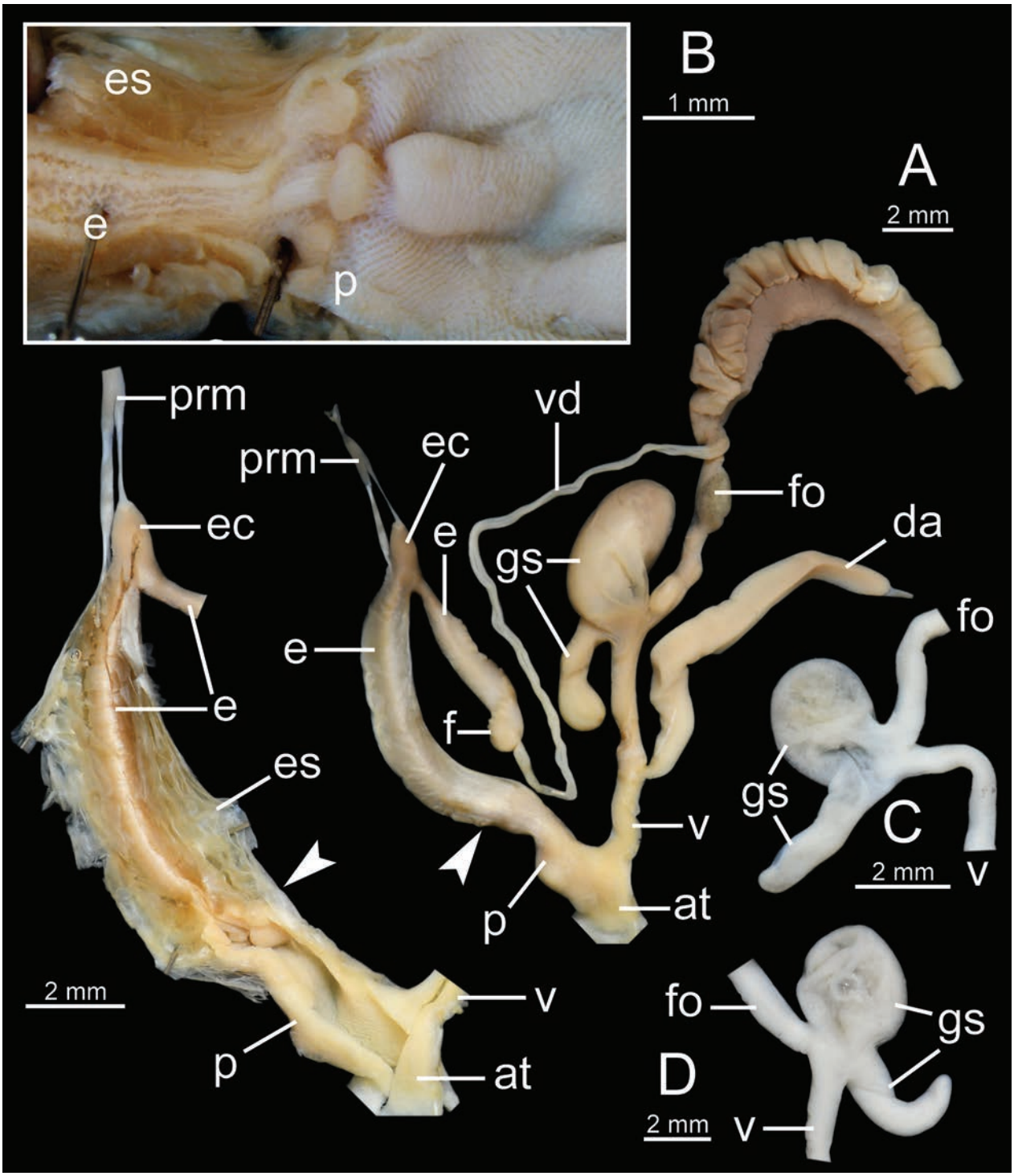

Figure 4. Genitalia of *Janbinmorpha sculpticarina* (Martens, 1883), comb. nov. **A.** Specimen from Surat Thani Province: CUMZ 15076, showing general view of genital system; **B.** Specimen from Phang-nga Province: CUMZ 15150, showing internal structure of penis and epiphallus; **C.** Specimen from Phuket Province: CUMZ 15077, showing gametolytic organ; **D.** Specimen from Phang-nga Province: CUMZ 15150, showing gametolytic organ. White arrowhead indicates the end of the penis.

na, and encircled with thickened epiphallic sheath (es); distal epiphallus smaller diameter than proximal part. Epiphallic caecum (ec) large, straight, and located near middle of epiphallus. Penial retractor muscle (prm) rather thickened and divided into two bundles: one bundle attached to tip of epiphallic caecum and another bundle attached to distal end of epiphallic sheath (Fig. 4A). Flagellum (f) very short or nearly absent. Vas deferens (vd) small tube continuing from free oviduct to near distal tip of epiphallus.

Vagina (v) long cylindrical tube, about two times penis length. Dart apparatus slender, long and located on mid-vaginal length. Gametolytic organ with undistinguished duct; gametolytic sac (gs) divided into two lobes separated at base: one large and bulbous shape, and another small and long-slender tube (Fig. 4A, C, D). Free

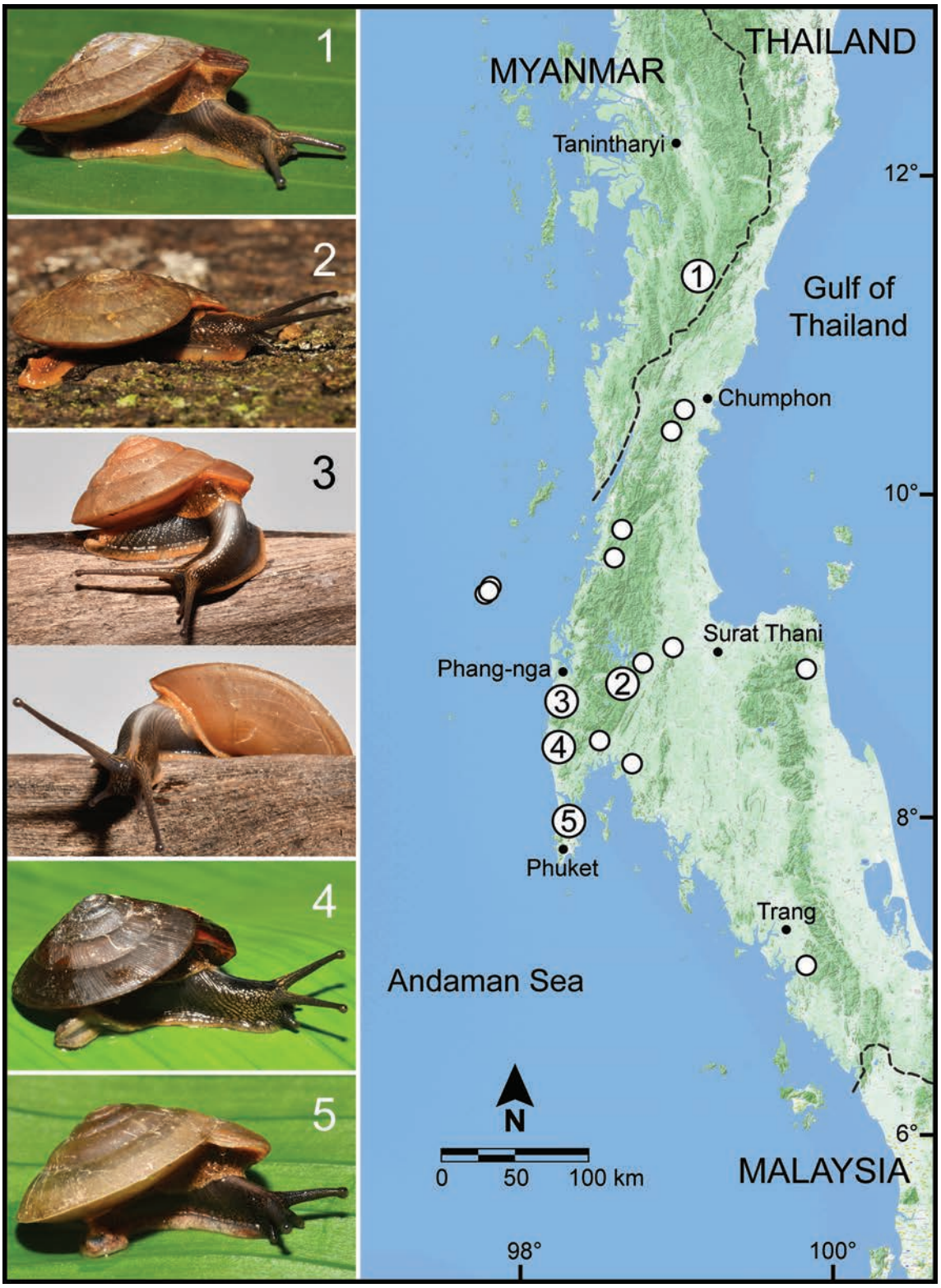

Figure 5. Map of the Malay Peninsula in southern Thailand and the southernmost tip of Myanmar showing the sampling sites. Localities where the living specimens were collected are indicated by numbers on map, not to scale.

oviduct (fo) long cylindrical, approximately as long as vagina length. Oviduct enlarged with lobules; prostate gland bound to oviduct.

Radula (Fig. 3E). Teeth arranged in a wide-angle U-shape with half-row formula: 1–(11–15)–56. Central tooth relatively symmetrical tricuspid; mesocone large and triangular shape with pointed cusp; ectocones very small with dull cusp. Lateral teeth unicuspid or asymmetrical bicuspid with mesocone large with pointed cusp and ectocone nearly wanting with dull cusp. Lateral teeth larger than marginal teeth. Marginal teeth starting at approximately row number 11 to 15 with obliquely elongate unicuspid form; outermost teeth narrower and shorter than inner teeth.

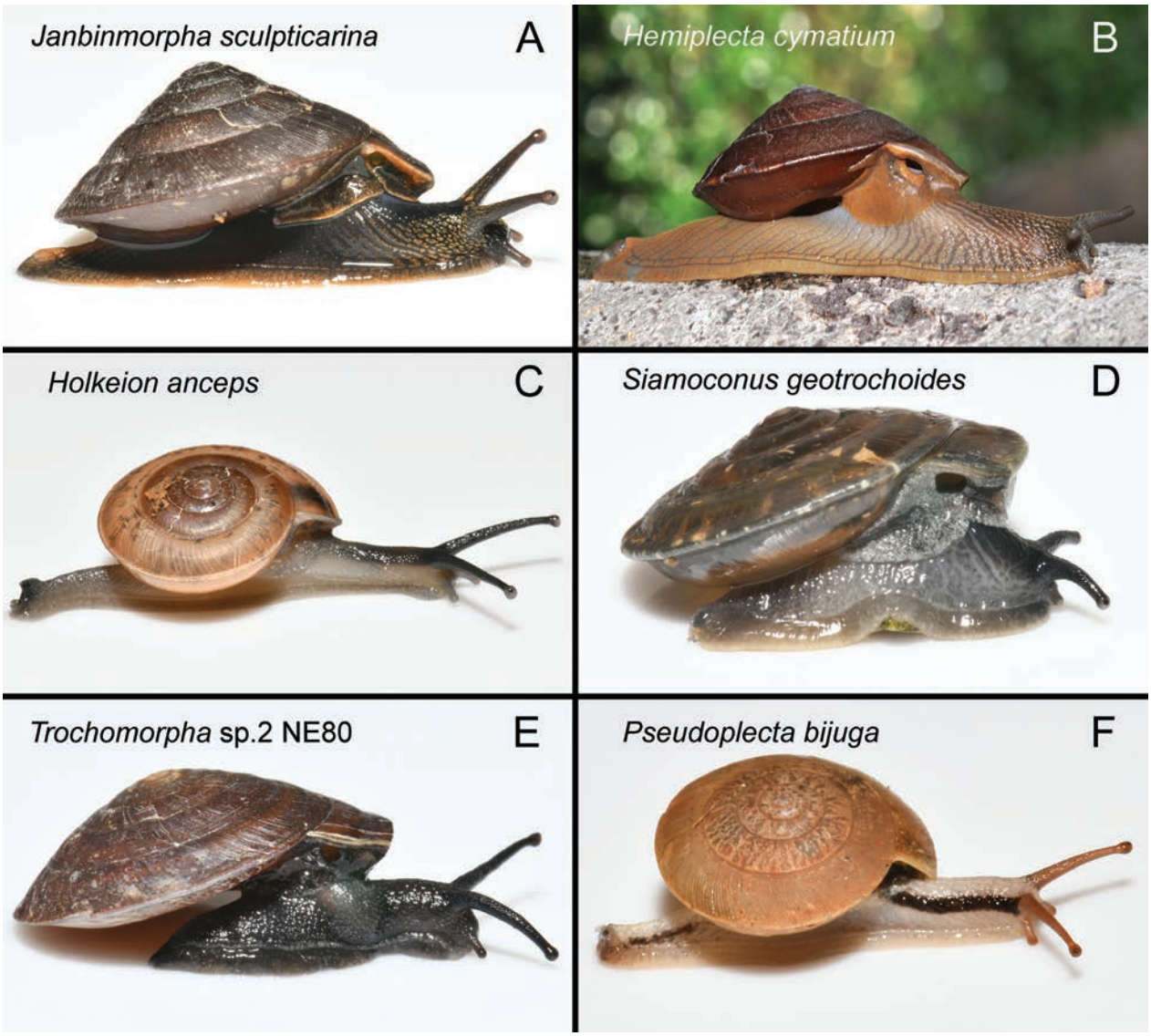

Figure 6. Representative living limacoid snails with a depressed trochiform shell from Thailand and the Malay Peninsula. **A.** *Janbinmorpha sculpticarina* (Martens, 1883), comb. nov. in the Ariophantidae; **B.** *Hemiplecta cymatium* (Pfeiffer, 1856) in the Ariophantidae; **C.** *Holkeion anceps* (Gould, 1843) in the Ariophantidae; **D.** *Siamoconus geotrochoides* Pholyotha, 2023 in the Euconulidae; **E.** *Trochomorpha* sp.2 in the Trochomorphidae; **F.** *Pseudoplecta bijuga* (Stoliczka, 1873) in the Dyakiidae.

External features (Figs 1, 5, 6A). Living snails with dark gray body and more or less distinct pale milky or yellow to orange stripe running from head to caudal horn; entire animal with pigmentation of yellow to orange dots or patches. Eye stalks long and pale blackish; lower tentacles shorter and paler in colour. Mantle lobes or mantle extensions well developed, crescent-shaped, yellow to orange, divided into three dorsal lobes, and somewhat thickened near their margins. Right dorsal lobe prominent, broadly crescent-shaped, and larger than both anterior and posterior left dorsal lobes. Anterior left dorsal lobe broadly crescent-shaped; posterior left dorsal lobe relatively long crescent-shaped. Sole evenly tripartite, pedal groove very strong. Foot margin yellow to orange. Caudal foss cup-shaped; caudal horn very reduced, short, not overhung, and yellow to orange.

Distribution. (Fig. 5). This species is apparently restricted to the southern peninsula of Thailand. Major populations of *J. sculpticarina* comb. nov. occur in the Phuket Range, while a few populations can be found in Nakhon Si Thammarat and the southern part of the Tenasserim ranges. This species was also recorded from the Pulau Aur Island, Malaysia (Basch and Solem 1971), but this record needs to be confirmed with the newly collected specimens.

Remarks. According to the limacoid snails with a depressed trochiform shell from Thailand and the Malay Peninsula, *Janbinmorpha sculpticarina* comb. nov. (Fig. 6A) is conchologically similar to some helicarionoidean species, for example *Hemiplecta cymatium* (Pfeiffer, 1856) (Fig. 6B) and *Holkeion anceps* (Gould, 1843) (Fig. 6C), and is also similar to some trochomorphoidean species, such as *Siamoconus geotrochoides* Pholyotha in Pholyotha et al. 2023a (Fig. 6D), *Trochomorpha* sp.2 (Fig. 6E), and *Pseudoplecta bijuga* (Stoliczka, 1873) (Fig. 6F). However, *J. sculpticarina* comb. nov. can be distinguished by its

genitalia in having two lobes of the gametolytic sac, no gametolytic duct, and a penial retractor muscle attached to the epiphallic caecum and epiphallic sheath. In comparison, *Hemiplecta cymatium* possesses a bulbous gametolytic sac, no gametolytic duct, and a penial retractor muscle attached to epiphallic caecum only (Sutcharit and Panha, unpublished data), while *Holkeion anceps* has an elongate gametolytic duct and a penial retractor muscle attached to the epiphallic caecum (Pholyotha et al. 2023b). The trochomorphoideans, *S. geotrochoides* and *Trochomorpha* sp.2 differ by having a long gametolytic duct and a penial retractor muscle attached to the epiphallus (Pholyotha et al. 2023a; Pholyotha and Panha, unpublished data). In addition, *P. bijuga* possesses a gametolytic organ located on the amatorial organ and a penial retractor muscle attached to the epiphallus (Jirapatrasilp et al. 2021).

Compared with other taxa having a depressed trochiform shell, and regardless of genitalia data, *J. sculpticarina* comb. nov. differs from *Trochomorpha* species and *Videna* species recorded from mainland Southeast Asia by a combination of no spiral band, larger shell size, relatively narrower umbilicus, and strong radial striations with reticulated microsculptures (Möllendorff 1902; Preece et al. 2022; Inkhavilay et al. 2023).

Trochomorpha benigna (Pfeiffer, 1863), *T. vinhensis* Thach, 2018 and *T. buotia* Inkhavilay et al., 2023 are very similar to *J. sculpticarina* comb. nov. in terms of shell shape and size. For comparison, *J. sculpticarina* comb. nov. has a narrower funnel-shaped umbilicus, while *T. benigna* and *T. vinhensis* have a wider funnel-shaped umbilicus and showing all preceding whorls (Inkhavilay et al. 2023). Compared with *T. buotia*, *J. sculpticarina* comb. nov. has radial striations and reticulated microsculptures on shell surface, depressed shell, a strong peripheral keel, and last whorl convex below periphery, while *T. buotia* has radial and spiral striations on the shell surface, a dome-shaped shell, distinctly sharpened peripheral keel, and last whorl flattened below periphery (Inkhavilay et al. 2023).

Discussion

Mainland Southeast Asia harbours a taxonomically diverse, overwhelmingly endemic fauna of limacoid snails, especially in the Helicarionoidea (e.g., Ariophantidae and Helicarionidae) and Trochomorphoidea (e.g., Dyakiidae, Euconulidae, and Trochomorphidae). Confusion in classification and identification of these limacoid snails has happened multiple times because there is a morphological convergence of shell shape; previously, most taxonomists or other researchers based their decisions only on shell morphology (Panha 1996; Hemmen and Hemmen 2001; Maassen 2001; Inkhavilay et al. 2019; Pholyotha et al. 2020, 2021a, c, 2022a, 2023c; Sutcharit et al. 2020b; Sutcharit and Panha 2021). The present study is an example of the long-standing taxonomic confusion that has existed since the works of Martens (1883) and Maassen (2001) were published. Prior to this study, *J. sculpticarina* comb. nov. had been assigned to either *Trochomorpha* or *Videna* in the Trochomorphidae. However, in this study, we have considered that general characters of *J. sculpticarina* comb. nov. are similar to those of *Hemiplecta* species in the Ariophantidae. The similarities include shell with an opened and deep umbilicus, animal with a reduced caudal horn and no shell lobe, genitalia with an absence of gametolytic duct and the presence of long dart apparatus and short flagellum (Sutcharit and Panha 2021).

The close relationship of *Janbinmorpha* gen. nov. and *Hemiplecta* is not only evident from their closely similar body features and reproductive anatomy, but also is evident from the molecular data. However, the significant differences in some genital traits and the amount of genetic variation among mitochondrial and nuclear gene sequences are indicative of the distinct lineages within the Ariophantidae. Our molecular phylogenetic analysis confirms that *Janbinmorpha* gen. nov. is a genetically well-supported clade that is grouped together with the ariophantid genera *Hemiplecta* and *Maelamaodiscus*, but the relationships among them remain only partially resolved. However, the genitalia of *Maelamaodiscus* are rather distinct from *Janbinmorpha* gen. nov. and *Hemiplecta* by the presence of a long flagellum and long gametolytic duct (Sutcharit and Pholyotha 2023). Although the relationships within the limacoid snails, especially the Ariophantidae, are not resolved, *Janbinmorpha* gen. nov. is not grouped with the Trochomorphidae. In this study, the monophyly of the Trochomorphidae is confirmed and includes both genera *Trochomorpha* and *Videna*. Therefore, we conclude that molecular and morphological data support *J. sculpticarina* comb. nov. as a member of the Ariophantidae instead of the Trochomorphidae.

Regarding the helicarionoidean snails, we also have pointed out unresolved aspects of molecular phylogenetics of the mainland Southeast Asian taxa, which are currently being studied and will continue as a goal moving forward. Our molecular phylogeny reveals that although the phylogenetic relationships within the Helicarionoidea are not resolved, all taxa assigned to the Helicarionidae always form a monophyletic clade. For the ariophantid lineages, despite the completely unresolved evolutionary relationships, we have found that there are at least two major clades of the Ariophantidae. The first major group includes the Indian taxa of *Ariophanta*, *Cryptozona*, *Euplecta*, *Ratnadvipia* and the Southeast Asian taxa of *Megaustenia*, while the second major group includes the Southeast Asian taxa of *Sarika*, *Khasiella*, *Taphrenalla*, *Macrochlamys*, *Hemiplecta*, *Maelamaodiscus*, and *Janbinmorpha* gen. nov. However, understanding phylogenetic relationships within this group is beyond the scope of this paper, and we suggest that more molecular data, especially the data of the type taxa of each genus from Asia as well as Australia and Africa, are needed to resolve the relationships within the Helicarionoidea.

Acknowledgements

We owe a debt of gratitude to all members of the Animal Systematics Research Unit, Chulalongkorn University for their kind help during field trips and technical support, and Ministry of Natural Resources and Environmental Conservation Forest Department, Myanmar and the Fauna & Flora International (FFI) for providing the study material. We thank J. Ablett, F. Naggs, and T. White (NHM, London), R. Janssen, J. Sigwart, and S. Hof (SMF, Frankfurt a.M.), and T. von Rintelen (ZMB, Berlin), for allowing the authors to examine the collections and photographs. This research is funded by the NSRF via the Program Management Unit for Human Resources & Institutional Development, Research and Innovation (grant number B42G670038), Ratchadapiseksompotch Fund Chulalongkorn University, and the Thailand Science Research and Innovation Fund Chulalongkorn University. In addition, we express our gratitude to D.J. Anderson for grammar checking, and to anonymous reviewers for helpful comments on this manuscript.

References

American Veterinary Medical Association (2020) AVMA Guidelines for the Euthanasia of Animals: 2020 Edition. https://www.avma.org/sites/default/files/2020-01/2020-Euthanasia-Final-1-17-20.pdf [accessed 12 Feb 2020]

Ayyagari VS, Sreerama K (2020) Molecular phylogeny and evolution of Pulmonata (Mollusca: Gastropoda) on the basis of mitochondrial (16S, COI) and nuclear markers (18S, 28S): an overview. Journal of Genetics 99(1): 17. https://doi.org/10.1007/s12041-020-1177-z

Basch PF, Solem A (1971) Notes on a collection of nonmarine Mollusca from Pulau Aur, an island off the east coast of Malaya. Federation Museums Journal 16: 91–95.

Bhosale AR, Saadi AJ, Wade CM, Thackeray TU, Tamboli AS, Kadam SK, Muley DV, Raheem DC (2021) *Varadia*, a new helicarionoidean semi-slug genus from India's Western Ghats (Stylommatophora: Helicarionoidea). European Journal of Taxonomy 757: 50–79. https://doi.org/10.5852/ejt.2021.757.1413

Blanford WT, Godwin-Austen HH (1908) The Fauna of British India. Mollusca. Testacellidae and Zonitidae. Taylor and Francis, London, UK. https://doi.org/10.5962/bhl.title.13103

Chang Z-Y, Liew T-S (2021) A molecular phylogeny of *Geotrochus* and *Trochomorpha* species (Gastropoda: Trochomorphidae) in Sabah, Malaysia reveals convergent evolution of shell morphology driven by environmental influences. PeerJ 9: e10526. https://doi.org/10.7717/peerj.10526

Clements R, Sodhi NS, Schilthuizen M, Ng PKL (2006) Limestone karsts of Southeast Asia: Imperiled arks of biodiversity. Bioscience 56(9): 733–742. https://doi.org/10.1641/0006-3568(2006)56[733:LKOSAI]2.0.CO;2

Felsenstein J (2004) Inferring phylogenies. Sinauer Associates, Massachusetts, Sunderland.

Folmer O, Black M, Hoeh W, Lutz R, Vrijenhoek R (1994) DNA primers for amplification of mitochondrial cytochrome c oxidase subunit I from diverse metazoan invertebrates. Molecular Marine Biology and Biotechnology 3: 294–299.

Foon JK, Clements GR, Liew T-S (2017) Diversity and biogeography of land snails (Mollusca, Gastropoda) in the limestone hills of Perak, Peninsular Malaysia. ZooKeys 682: 1–94. https://doi.org/10.3897/zookeys.682.12999

Gardner S, Sidisunthorn P, Chayamarit K (2015) Forest Trees of Southern Thailand Volume 1 (Acanthaceae to Escalloniaceae). Kobfai Publishing Project, Bangkok.

Godwin-Austen HH (1918) Zoological results of the Abor Expedition, 1911–1912. XLIX. Mollusca, IX. Records of the Indian Museum 8(12): 601–621. https://doi.org/10.26515/rzsi/v8/i12/1918/163139

Gupta A (2005) Landforms of Southeast Asia. In: Gupta A (Ed.) The Physical Geography of Southeast Asia. Oxford University Press, New York. https://doi.org/10.1093/oso/9780199248025.003.0013

Hemmen J, Hemmen C (2001) Aktualisierte Liste der terrestrischen Gastropoden Thailands. Schriften zur Malakozoologie 18: 35–70.

Hendriks KP (2020) On the origin of species assemblages of Bornean microsnails. Unpublished PhD Thesis, University of Groningen. https://doi.org/10.33612/diss.124819761

Hillis DM, Bull JJ (1993) An empirical test of bootstrapping as a method for assessing confidence in phylogenetic analysis. Systematic Biology 42(2): 182–192. https://doi.org/10.1093/sysbio/42.2.182

Huelsenbeck JP, Rannala B (2004) Frequentist properties of Bayesian posterior probabilities of phylogenetic trees under simple and complex substitution models. Systematic Biology 53(6): 904–913. https://doi.org/10.1080/10635150490522629

Hyman IT, Ponder WF (2010) A morphological phylogenetic analysis and generic revision of Australian Helicarionidae (Gastropoda: Pulmonata: Stylommatophora), and an assessment of the relationships of the family. Zootaxa 2462(1): 1–148. https://doi.org/10.11646/zootaxa.2462.1.1

Inkhavilay K, Sutcharit C, Bantaowong U, Chanabun R, Siriwut W, Srisonchai R, Pholyotha A, Jirapatrasilp P, Panha S (2019) Annotated checklist of the terrestrial molluscs from Laos (Mollusca, Gastropoda). ZooKeys 834: 1–166. https://doi.org/10.3897/zookeys.834.28800

Inkhavilay K, Sutcharit C, Pholyotha A (2023) Exploring the almost unknown *Trochomorpha* (Eupulmonata: Trochomorphidae) from Laos, with description of three new species. Tropical Natural History (Supplement 7): 93–106.

Jirapatrasilp P, Tongkerd P, Jeratthitikul E, Liew T-S, Pholyotha A, Sutcharit C, Panha S (2021) Molecular phylogeny of the limacoid snail family Dyakiidae in Southeast Asia, with the description of a new genus and species. Zoological Journal of the Linnean Society 193(1): 250–280. https://doi.org/10.1093/zoolinnean/zlaa129

Katoh K, Rozewicki J, Yamada KD (2017) MAFFT online service: Multiple sequence alignment, interactive sequence choice and visualization. Briefings in Bioinformatics 20(4): 1160–1166. https://doi.org/10.1093/bib/bbx108

Köhler F, Shea M (2012) *Youwanjela*, a new genus of land snail from the Kimberley, Western Australia (Eupulmonata, Camaenidae). Zoosystematics and Evolution 88(1): 25–31. https://doi.org/10.1002/zoos.201200004

Köhler F, Willan RC, Bourke AJ, Barden P, Shea M (2024) A new species of land snail, *Xanthomelon amurndamilumila*, from the North East Isles off Groote Eylandt (= Ayangkidarrba), Gulf of Carpentaria, Australia (Stylommatophora, Camaenidae). Zoosystematics and Evolution 100(1): 61–68. https://doi.org/10.3897/zse.100.113243

Kumar S, Stecher G, Tamura K (2016) MEGA7: Molecular Evolutionary Genetics Analysis version 7.0 for bigger datasets. Molecular

Biology and Evolution 33(7): 1870–1874. https://doi.org/10.1093/molbev/msw054

Liew T-S, Schilthuizen M, Vermeulen JJ (2009) Systematic revision of the genus *Everettia* Godwin-Austen, 1891 (Mollusca: Gastropoda: Dyakiidae) in Sabah, northern Borneo. Zoological Journal of the Linnean Society 157(3): 515–550. https://doi.org/10.1111/j.1096-3642.2009.00526.x

Maassen WJM (2001) A preliminary checklist of the nonmarine molluscs of West-Malaysia, "a handlist". De Kreukel (Supplement): 1–155.

Martens von E (1883) Conchylien von Salanga. Conchologische Mittheilungen 2: 129–138. https://www.biodiversitylibrary.org/page/15865880

Mauro DS, Agorreta A (2010) Molecular systematics: A synthesis of the common methods and the state of knowledge. Cellular & Molecular Biology Letters 15(2): 311–341. https://doi.org/10.2478/s11658-010-0010-8

Miller MA, Pfeiffer W, Schwartz T (2010) Creating the CIPRES Science Gateway for inference of large phylogenetic trees. Proceedings of the Gateway Computing Environments Workshop (GCE), 14 Nov. 2010, New Orleans, LA, 1–8. https://doi.org/10.1109/GCE.2010.5676129

Möllendorff von OF (1902) Binnenmollusken aus Hinterindien. 1. Landschnecken von Kelantan, Ostküste der Halbinsel Malacca. Nachrichtsblatt der Deutschen Malakozoologischen Gesellschaft 34: 135–149. https://www.biodiversitylibrary.org/page/15598858

Myers N, Mittermeier RA, Mittermeier CG, da Fonseca GAB, Kent J (2000) Biodiversity hotspots for conservation priorities. Nature 403(6772): 853–858. https://doi.org/10.1038/35002501

Naggs F, Panha S, Raheem D (2006) Developing land snail expertise in South and Southeast Asia, a new Darwin Initiative Project. The Natural History Journal of Chulalongkorn University 6: 43–46.

Pall-Gergely B, Fehér Z, Otani JU, Asami T (2016) An integrative taxonomic approach to infer the systematic position of *Chalepotaxis* Ancey, 1887 (Gastropoda: Stylommatophora: Helicarionidae). Molluscan Research 37(2): 113–119. https://doi.org/10.1080/13235818.2016.1234996

Palumbi S, Martin A, Romano S, McMillan WO, Stice L, Grabowwski G (1991) The simple fool's guide to PCR. Department of Zoology, University of Hawaii, Honolulu.

Panha S (1996) A checklist and classification of the land terrestrial pulmonate snail in Thailand. Walkerana 8: 31–40.

Pholyotha A, Sutcharit C, Tongkerd P, Panha S (2020) Integrative taxonomic revision of the land snail genus *Sarika* Godwin-Austen, 1907 in Thailand, with descriptions of nine new species (Eupulmonata, Ariophantidae). ZooKeys 976: 1–100. https://doi.org/10.3897/zookeys.976.53859

Pholyotha A, Sutcharit C, Jirapatrasilp P, Ngor PB, Oba Y, Panha S (2021a) Molecular phylogenetic and morphological evidence reveal a rare limacoid snail genus, *Khmerquantula* gen. nov. (Eupulmonata: Dyakiidae) from Cambodia. Systematics and Biodiversity 19(8): 1049–1061. https://doi.org/10.1080/14772000.2021.1970045

Pholyotha A, Sutcharit C, Panha S (2021b) Rediscovering the dancing semislug genus *Cryptosemelus* Collinge, 1902 (Eupulmonata, Ariophantidae) from Thailand with description of two new species. ZooKeys 1076: 43–65. https://doi.org/10.3897/zookeys.1076.75576

Pholyotha A, Sutcharit C, Tongkerd P, Jeratthitikul E, Panha S (2021c) Integrative systematics reveals the new land-snail genus *Taphrenalla* (Eupulmonata: Ariophantidae) with a description of nine new species from Thailand. Contributions to Zoology (Amsterdam, Netherlands) 90(1): 21–69. https://doi.org/10.1163/18759866-BJA10013

Pholyotha A, Sutcharit C, Tongkerd P, Panha S (2021d) Systematic revision of the limestone karst-restricted land snail genus *Aenigmatoconcha* (Eupulmonata: Helicarionidae), with description of a new species. European Journal of Taxonomy 767: 55–82. https://doi.org/10.5852/ejt.2021.767.1487

Pholyotha A, Sutcharit C, Lin A, Panha S (2022a) Multigene phylogeny reveals the ribbed shell morphotypes in the land snail genus *Sarika* (Eupulmonata: Ariophantidae), with description of two new species from Thailand and Myanmar. Contributions to Zoology (Amsterdam, Netherlands) 91(2): 97–132. https://doi.org/10.1163/18759866-bja10027

Pholyotha A, Sutcharit C, Lin A, Panha S (2022b) Uncovering local endemism from southeastern Myanmar: Description of the new karst-associated terrestrial snail genus *Burmochlamys* (Eupulmonata, Helicarionidae). ZooKeys 1110: 1–37. https://doi.org/10.3897/zookeys.1110.82461

Pholyotha A, Panha S, Sutcharit C, Jirapatrasilp P, Seesamut T, Liew T-S, Tongkerd P (2023a) Molecular phylogeny of the land snail family Euconulidae in Thailand and its position in the superfamily Trochomorphoidea (Stylommatophora: Limacoidei), with description of a new genus. Invertebrate Systematics 37(8): 571–605. https://doi.org/10.1071/IS23012

Pholyotha A, Sutcharit C, Panha S (2023b) Taxonomic revision of the land-snail genus *Holkeion* Godwin-Austen, 1908 (Eupulmonata: Ariophantidae), with a description of a new species, *H. nordsiecki*. Archiv für Molluskenkunde 152(2): 269–280. https://doi.org/10.1127/arch.moll/152/269-280

Pholyotha A, Tongkerd P, Sutcharit C (2023c) *Siamochlamys panhai*, a new limestone karst-restricted terrestrial snail from Thailand (Eupulmonata: Helicarionidae). Tropical Natural History (Supplement 7): 41–50.

Preece RC, White TS, Raheem DC, Ketchum H, Ablett J, Taylor H, Webb K, Naggs F (2022) William Benson and the golden age of malacology in British India: Biography, illustrated catalogue and evaluation of his molluscan types. Tropical Natural History (Supplement 6): 1–434.

Ridd MF, Barber AJ, Crow MJ (2011) Introduction to the geology of Thailand. In: Ridd MF, Barber AJ, Crow MJ (Eds) The Geology of Thailand. Geological Society, London. https://doi.org/10.1144/GOTH

Ronquist F, Teslenko M, van der Mark P, Ayres DL, Darling A, Höhna S, Larget B, Liu L, Suchard MA, Huelsenbeck JP (2012) MrBayes 3.2: Efficient Bayesian phylogenetic inference and model choice across a large model space. Systematic Biology 61(3): 539–542. https://doi.org/10.1093/sysbio/sys029

Saadi AJ, Wade CM (2019) Resolving the basal divisions in the stylommatophoran land snails and slugs with special emphasis on the position of the Scolodontidae. Molecular Phylogenetics and Evolution 139: 106529. https://doi.org/10.1016/j.ympev.2019.106529

Schileyko AA (2002a) Treatise on recent terrestrial pulmonate molluscs. Part 8. Punctidae, Helicodiscidae, Discidae, Cystopeltidae, Euconulidae, Trochomorphidae. Ruthenica (Supplement 2): 1035–1166.

Schileyko AA (2002b) Treatise on recent terrestrial pulmonate molluscs. Part 9. Helicarionidae, Gymnarionidae, Rhysotinidae, Ariophantidae. Ruthenica (Supplement 2): 1167–1307.

Schileyko AA (2003) Treatise on recent terrestrial pulmonate mollusks. Part 10. Ariophantidae, Ostracolethaidae, Ryssotidae, Milacidae, Dyakiidae, Staffordiidae, Gastrodontidae, Zonitidae, Daudebardiidae, Parmacellidae. Ruthenica (Supplement 2): 1309–1466.

Solem A (1966) Some non-marine mollusks from Thailand, with notes on classification of the Helicarionidae. Spolia Zoologica Musei Hauniensis 24: 1–110.

Stamatakis A (2014) RAxML version 8: A tool for phylogenetic analysis and post-analysis of large phylogenies. Bioinformatics (Oxford, England) 30(9): 1312–1313. https://doi.org/10.1093/bioinformatics/btu033

Sutcharit C, Panha S (2021) Systematic review of the dextral *Hemiplecta* Albers, 1850 (Eupulmonata, Ariophantidae) from Thailand with description of a new species and list of all the Indochinese species. ZooKeys 1047: 101–154. https://doi.org/10.3897/zookeys.1047.65735

Sutcharit C, Pholyotha A (2023) Hidden lineages in the mountains: The genus *Glyptaulax* Gude, 1914 and *Maelamaodiscus* gen. nov. (Heterobranchia: Stylommatophora: Charopidae and Ariophantidae) with description of two new species from Western Thailand. Tropical Natural History (Supplement 7): 123–138.

Sutcharit C, Jeratthitikul E, Pholyotha A, Lin A, Panha S (2020a) Molecular phylogeny reveals high diversity and endemism in the limestone karst-restricted land snail genus *Sophina* Benson, 1859 from Myanmar (Eupulmonata: Helicarionidae), with description of four new species. Journal of Zoological Systematics and Evolutionary Research 58(4): 957–981. https://doi.org/10.1111/jzs.12420

Sutcharit C, Thach P, Chhuoy S, Ngor PB, Jeratthitikul E, Siriwut W, Srisonchai R, Ng TH, Pholyotha A, Jirapatrasilp P, Panha S (2020b) Annotated checklist of the land snail fauna from southern Cambodia (Mollusca, Gastropoda). ZooKeys 948: 1–46. https://doi.org/10.3897/zookeys.948.51671

Sutcharit C, Jeratthitikul E, Tongkerd P, Panha S (2021) Reassessment and systematic position of the sinistral snails of genus *Hemiplecta* from Thailand (Eupulmonata: Ariophantidae), with description of two new species. Contributions to Zoology (Amsterdam, Netherlands) 90(2): 183–215. https://doi.org/10.1163/18759866-BJA10016

Tanabe AS (2011) Kakusan4 and Aminosan: Two programs for comparing nonpartitioned, proportional and separate models for combined molecular phylogenetic analyses of multilocus sequence data. Molecular Ecology Resources 11(5): 914–921. https://doi.org/10.1111/j.1755-0998.2011.03021.x

Wade CM, Mordan PB (2000) Evolution within the gastropod molluscs; using the ribosomal RNA gene-cluster as an indicator of phylogenetic relationships. Journal Molluscan Studies 66: 565–570. https://doi.org/10.1093/mollus/66.4.565

Wade CM, Mordan PB, Clarke B (2001) A phylogeny of the land snails (Gastropoda: Pulmonata). Proceedings of the Royal Society of London. Series B, Biological Sciences 268(1465): 413–422. https://doi.org/10.1098/rspb.2000.1372

Wade CM, Mordan PB, Naggs F (2006) Evolutionary relationships among the pulmonate land snails and slugs (Pulmonata, Stylommatophora). Biological Journal of the Linnean Society. Linnean Society of London 87(4): 593–610. https://doi.org/10.1111/j.1095-8312.2006.00596.x

Zoosyst. Evol. 100 (3) 2024, 1155–1173 | DOI 10.3897/zse.100.126702

PENSOFT

für Natur MUSEUM FÜR NATURKUNDE BERLIN

Forgotten for two centuries: redescription of *Phoxinus isetensis* (Georgi, 1775) (Cypriniformes, Leuciscidae) – the most widespread minnow in Europe

Oleg N. Artaev[1], Aleksey A. Bolotovskiy[1], Ilya S. Turbanov[1,2,3], Alexander A. Gandlin[1,2], Aleksey V. Kutuzov[1], Marina A. Levina[1,2,3], Danila A. Melentev[4,5], Ivan V. Pozdeev[6], Mikhail Ya. Borisov[7], Boris A. Levin[1,2,8]

1 *Papanin Institute for Biology of Inland Waters Russian Academy of Sciences, Borok, Russia*
2 *Severtsov Institute of Ecology and Evolution of the Russian Academy of Sciences, Moscow, Russia*
3 *Cherepovets State University, Cherepovets, Russia*
4 *Zoological Institute of the Russian Academy of Sciences, Saint Petersburg, Russia*
5 *Saint Petersburg University, Saint Petersburg, Russia*
6 *Saint Peterburg Scientific Center of the Russian Academy of Sciences, Saint Petersburg, Russia*
7 *Vologda branch of the Federal State Budget Scientific Institution "Russian Federal Research Institute of Fisheries and oceanography", Vologda, Russia*
8 *Laboratory of Molecular Genetics, Russian Federal Research Institute of Fisheries and Oceanography, 105187 Moscow, Russia*

https://zoobank.org/D0F79AB6-6FEB-4F39-AA08-FA2A57B1B913

Corresponding authors: Oleg N. Artaev (artaev@gmail.com); Boris A. Levin (borislyovin@gmail.com)

Academic editor: Nicolas Hubert ♦ **Received** 2 May 2024 ♦ **Accepted** 15 July 2024 ♦ **Published** 22 August 2024

Abstract

The morphology, phylogenetic position, and distribution of a recently revalidated species of leuciscid minnow, *Phoxinus isetensis*, were substantially clarified. The species was described in the late 18th century from the Middle Urals but later synonymized with *Phoxinus phoxinus*. As believed, *P. isetensis* is distributed in the Arctic Ocean catchment from the Murman coast via West and East Siberia until the Pacific Ocean catchment in Far East and Northeastern Asia. Our study, with the use of mtDNA markers coupled with extensive morphological data, showed that the distribution of *P. isetensis* is greatly different. Currently, this is the most widespread *Phoxinus* species in Europe, distributed in Northern and Eastern Europe and on the western edge of Siberia (Iset and Ural basins). In particular, *P. isetensis* inhabits the basins of the Caspian, Baltic, White, Barents, and Kara seas, possibly occurring in the North Sea basin. The species was redescribed, and the type locality and neotype were designated. The main morphological difference from other *Phoxinus* spp. is the large total number of vertebrae (39–43, mode 41) due to an increase in the number of caudal vertebrae (16–21, mode 19). Phylogenetically, *P. isetensis* is a sister to the Caucasian species *P. colchicus* (*p*-distance = 5%). The wide distribution of *P. isetensis* within the area of the Last Glacial Maximum suggests rapid colonization of deglaciated regions, probably due to its adaptation to a cold climate.

Key Words

DNA barcoding, Europe-Siberia corridor, freshwater fish, postglacial expansion, taxonomy

Introduction

Minnows of the genus *Phoxinus* Rafinesque, 1820, are predominantly rheophilic small freshwater fish of the family Leuciscidae Bonaparte, 1835, widespread in northern Eurasia from the Pyrenees to the Pacific coast. Initially, the morphology-based taxonomy of the genus *Phoxinus* was controversial due to the complex variability

of morphological features and their large overlap. In early comprehensive publications, all *Phoxinus* diversity was reduced either to one species with a number of subspecies (Berg 1949) or to several species (Kottelat and Freyhof 2007). The use of molecular genetic methods has shown a greatly underestimated species diversity in Europe (Palandačić et al. 2015, 2017, 2020), which suggested a new look at the taxonomy of the genus *Phoxinus*. Only two species (*P. bigerri* Kottelat, 2007 and *P. colchicus* Berg, 1910) were supported by morphological and genetic (mitochondrial) data, and six (*P. phoxinus* (Linnaeus, 1758), *P. lumaireul* (Schinz, 1840), *P. karsticus* Bianco & De Bonis, 2015, *P. septimanae* Kottelat, 2007, *P. marsilii* Heckel, 1836, and *P. csikii* Hankó, 1922) were supported by mitochondrial but limitedly corroborated by nuclear data (Palandačić et al. 2017). Then several new species were described using an integrative taxonomy approach: *P. krkae* Bogutskaya, Jelić, Vucić, Jelić, Diripasko, Stefanov & Klobučar, 2019 (Bogutskaya et al. 2019), *P. dragarum* Denys, Dettaï, Persat, Daszkiewicz, Hautecoeur & Keith, 2020, *P. fayollarum* Denys, Dettaï, Persat, Daszkiewicz, Hautecoeur & Keith, 2020 (Denys et al. 2020), *P. abanticus* Turan, Bayçelebi, Özuluğ, Gaygusuz & Aksu, 2023 (Turan et al. 2023), *P. radeki* Bayçelebi, Aksu & Turan, 2024 (Bayçelebi et al. 2024), and *P. adagumicus* Artaev, Turbanov, Bolotovskiy, Gandlin & Levin, 2024 (Artaev et al. 2024).

Along with the productive revision of the taxonomic and genetic diversity of species distributed in Western and Central Europe, the remaining part of the range, including Eastern Europe, was almost unexplored. For instance, taxonomic identification of northern and eastern European minnows with the largest range in Europe was problematic; those were assigned to mitochondrial Clade 17 without species naming (Palandačić at al. 2017, 2020). Our genetic data showed that unnamed *Phoxinus* sp. Clade 17 is conspecific to recently revalidated *Phoxinus isetensis* (Georgi, 1775) (Dyldin et al. 2023) described from the Middle Urals. This study aimed to make taxonomic redescription using the integrative (morphology and genetics) approach, to outline geographic distribution, and to clarify the phylogeny of *P. isetensis*.

Materials and methods

Sampling

Materials for morphological studies and partially for genetic studies were collected by the authors. Fish were caught using a frame net and seine net with a mesh size of 6–8 mm. Fish were euthanized in a solution of clove oil and photographed in an aquarium with artificial lighting using a Nikon D5300 camera (Nikon Corporation, Tokyo, Japan) with a Nikkor 60 mm f/2.8G lens (Nikon Corporation, Tokyo, Japan) using a physical white swatch for color correction. Fin clips (pectoral or pelvic) were taken from some specimens (DNA vouchers) and placed in 96% ethanol for subsequent DNA extraction in the laboratory. Then most fish were preserved in 10% formalin (form.), while some samples (usually small-sized specimens) were preserved in 96% ethanol for molecular analysis. Subsequently, formalin-fixed specimens were washed out in running water and transferred to 70% ethanol for long-term storage.

Neotype and additional material were deposited at the Fish Collection of the Papanin Institute for Biology of Inland Waters of the Russian Academy of Sciences, Borok, Russia (IBIW_FS).

Morphological studies

Morphological material on *Phoxinus* sp. (Clade 17) from seventeen localities (n=272, Fig. 1, Suppl. material 1) was examined. In studying the morphology of *Phoxinus*, we follow Bogutskaya et al. (2019, 2023) and Artaev et al. (2024). In particular, 42 morphometric (Suppl. materials 2, 3), 17 meristic, and two qualitative characters (Suppl. materials 2, 4) were processed. Abbreviations of morphometric characters are seen in Suppl. material 3. Morphometric measurements were taken from the left side of the body using a digital caliper to the nearest 0.1 mm by one operator for the purposes of consistency as recommended by Mina et al. (2005). Meristics (except for axial skeleton) and type of breast scalation (Bogutskaya et al. 2019) were assessed using material stained in an ethanol solution of alizarin red S (Taylor and Van Dyke 1985 with modifications), followed by short exposure to 1–2% potassium hydroxide and preservation in 70% ethanol.

Sex was determined by the shape and size of the pectoral fins, their rays, and the length of the pelvic fins (Frost 1943; Berg 1949; Chen 1996; Bogutskaya et al. 2019). External meristics were counted on the left side. Standard length (SL) was measured from the tip of the upper lip to the end of the hypural complex. The total number of pectoral and pelvic-fin rays was counted on the left fins. The last two branched rays articulated on a single pterygiophore in the dorsal and anal fins are counted as one. Scales above the lateral line were counted between the lateral line and base of the first unbranched ray in the dorsal fin; scales below the lateral line were between the lateral line and base of the first unbranched ray in the anal fin. In both cases, lateral line scales were not taken into account. The number of anterior gill rakers of the first gill arch was counted on the left and right sides of the specimens. Number lines on the scales were counted on the left and right breast patches, and an average value was taken. The counts of meristic characters (except for the axial skeleton) and assessment of qualitative characters were done using the stereomicroscope MC-2-ZOOM (Micromed, Saint Petersburg, Russia). Vertebrae and pterygiophores were counted following Naseka (1996) and Bogutskaya et al. (2019) using radiographs made by X-ray equipment PRDU II (ELTECH-Med, Saint Petersburg, Russia). Images of pharyngeal teeth were obtained

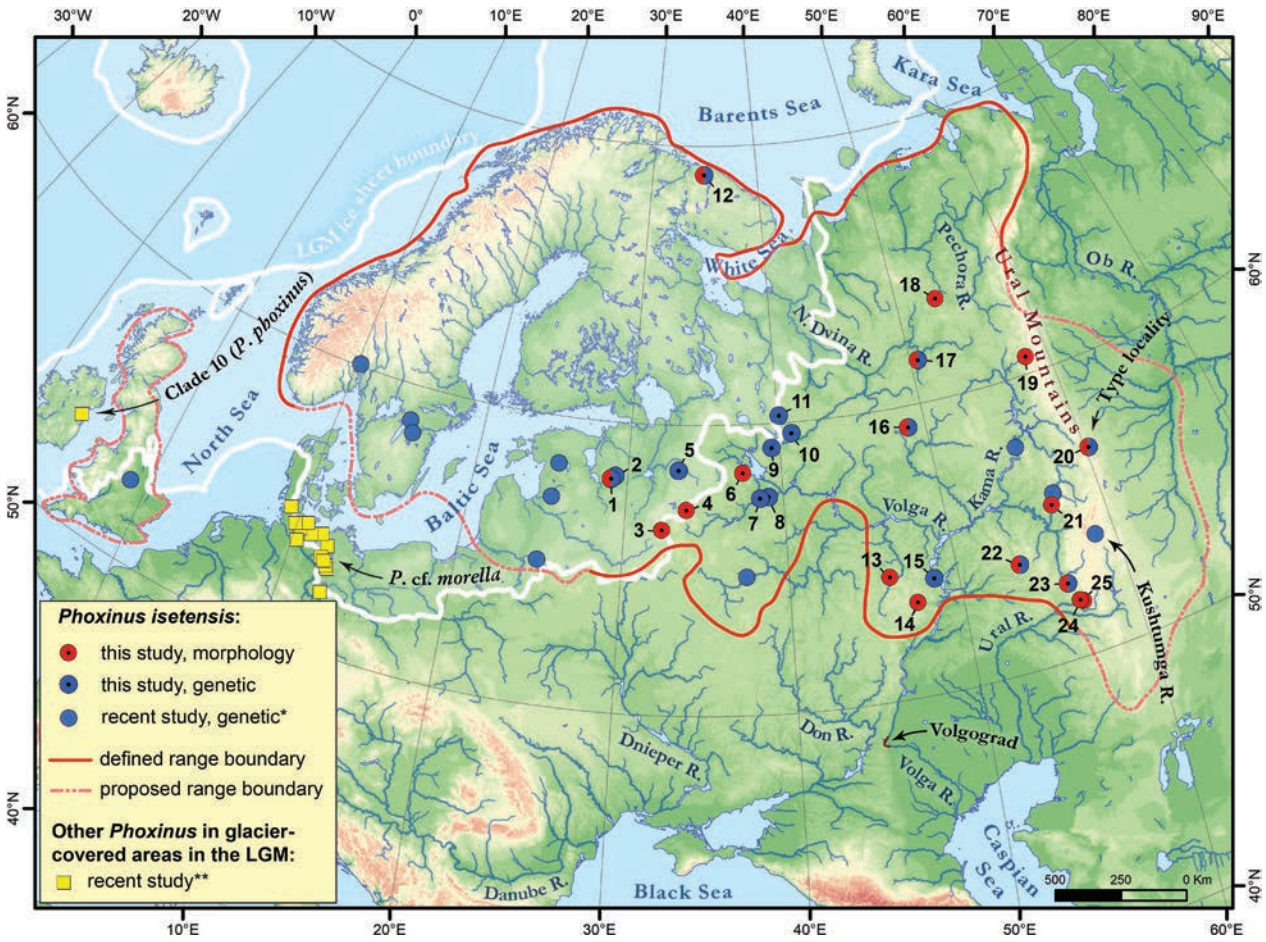

Figure 1. Distribution map and range boundaries of *Phoxinus isetensis* confirmed by morphological and genetic data along with other confirmed *Phoxinus* spp., whose distributions are partially within the glacier-covered area of the last glacial maximum. Locality numbers are designated in Suppl. materials 1, 5. * – by Palandačić et al. (2020); ** – by Palandačić et al. (2020) and Rothe et al. (2019).

using a JEOL JSM-6510LV scanning electron microscope (Jeol, Tokyo, Japan).

Measurement indexes were statistically processed in Microsoft Excel. Comparison of multiple samples was carried out using the Kruskal-Wallis test followed by Dunn's post hoc test with Bonferroni correction [*rstatix* (Kassambara 2020) and *tidyverse* (Wickham et al. 2019) packages in R version 4.3.1 (Ihaka and Gentleman 1996)]. Principal component analysis (PCA) was performed using the *ggfortify* (Tang et al. 2016) package in R. Differences between sexes were tested using the Mann-Whitney U test in Past 4.13 (Hammer and Harper 2001).

Phylogenetic placement and genetic distance.

DNA was isolated by salt extraction (Aljanabi and Martinez 1997) from ethanol-fixed tissues. Two mitochondrial markers were analyzed. The mitochondrial cytochrome *c* oxidase subunit I (COI) barcode region was amplified using the M13-tailed primer cocktail: FishF2_t1: 5′-TGT AAA ACG ACG GCC AGT CGA CTA ATC ATA AAG ATA TCG GCA C-3′, FishR2_t1: 5′-CAG GAA ACA GCT ATG ACA CTT CAG GGT GAC CGA AGA ATC AGA A-3′, VF2_t1: 5′-TGT AAA ACG ACG GCC AGT CAA CCA ACC ACA AAG ACA TTG GCA C-3′, and FR1d_t1: 5′-CAG GAA ACA GCT ATG ACA CCT CAG GGT GTC CGA ARA AYC ARA A-3′ (Ivanova et al. 2007). PCR conditions for COI followed protocols from Ivanova et al. (2007). In addition, the cytochrome *b* (cyt*b*) fragment was amplified by PCR using the following primers: GluF: 5′-AACCACCGTTGTATTCAACTACAA-3′ and ThrR: 5′-ACCTCCGATCTTCGGATTACAAGACCG-3′ (Machordom and Doadrio 2001). PCR amplifications were performed using Evrogen ScreenMix-HS under conditions described by Levin et al. (2017).

Sequencing of the PCR products, purified by ethanol and ammonium acetate (3 M) precipitation, was conducted using the Applied Biosystems 3500 DNA sequencer (Thermo Fisher Scientific, USA), with primers M13F 5′-GTA AAA CGA CGG CCA GT-3′ M13R-pUC 5′-CAG GAA ACA GCT ATG AC-3′ (Geiger et al. 2014) for COI and primers GluF: 5′-AACCACCGTTGTATTCAACTACAA-3′ and ThrR: 5′-ACCTCCGATCTTCGGATTACAAGACCG-3′ (Machordom and Doadrio 2001) for cyt*b*.

DNA chromatograms were checked for errors in FinchTV 1.4.0 (Rothgänger et al. 2006), and the DNA sequences were aligned using the ClustalW algorithm in MEGA7 (Kumar et al. 2016). Phylogenetic analysis was performed on COI (567 bp) and cyt*b* (1089 bp)

concatenated sequences. In addition to the 29 newly determined COI and cyt*b* sequences in this study, 294 concatenated sequences of all available *Phoxinus* spp. were mined from the GenBank (derived from the studies of Imoto et al. 2013; Xu et al. 2014; Palandačić et al. 2015, 2017, 2020; Ramler et al. 2016; Xie et al. 2016; Schönhuth et al. 2018; and unpublished works). Three outgroups representing the genera *Pseudaspius* Dybowski, 1869, *Rhynchocypris* Günther, 1889, and *Oreoleuciscus* Warpachowski, 1889, were selected according to the previous phylogenetic studies (Palandačić et al. 2015, 2020) (Suppl. material 5). Only unique haplotypes were used in downstream phylogenetic analyses.

The Bayesian phylogenetic analysis was performed in a Bayesian statistical framework implemented in BEAST v.1.10.4. (Hill and Baele 2019) with 2×10^7 MCMC generations (10% burn-in) and parameters sampled every 2000 steps. The substitution models by codon position for Bayesian analysis were selected in PartitionFinder v.2.1.1 (Lanfear et al. 2016) with the greedy algorithm (Lanfear et al. 2012) (Suppl. material 6).

Maximum likelihood phylogenies were inferred using IQ-TREE v.2.2.0 (Nguyen et al. 2015) in PhyloSuite v.1.2.3 (Zhang et al. 2020; Xiang et al. 2023) under the edgelinked partition model for 1000 ultrafast (Minh et al. 2013) bootstrapping. ModelFinder v.2.2.0 (Kalyaanamoorthy et al. 2017) in PhyloSuite v.1.2.3 was used to select the best-fit partition model (edge-linked) using the AICc criterion (Suppl. material 6).

The average intra-group as well as the average pairwise intergroup *p*-distances using the concatenated COI+cyt*b* sequences data set were calculated using the MEGA7 program (Kumar et al. 2016) with 1000 bootstrap replicas.

Map visualization

The map was created using the QGIS software, v.3.34. Digital elevation model visualized based on GMTED2010, 30 sec. resolution (Danielson and Gesch 2011); river systems – HydroATLAS v.1.0 (Linke et al. 2019); LGM ice sheet boundary according to Batchelor et al. (2019).

Results

Phylogenetic placement and genetic distance

The phylogenetic Bayesian tree of the genus *Phoxinus* shows that *P. isetensis* has its own lineage, being sister to *P. colchicus* distributed in the eastern Black Sea basin and the Kuban system in the Sea of Azov basin (*p*-distance = 0.050±0.005) with a high support in both BI (Fig. 2) and ML (Suppl. material 7) analyses. Three species combined together (*P. isetensis*, *P. colchicus*, and *P. chrysoprasius*) are early branching in the *Phoxinus* tree and represent a sister class to all other European *Phoxinus* spp. apart from *P. adagumicus*, although this was weakly supported. Intraspecies divergence of *P. isetensis* is moderate (0.005) despite its wide distributional range (Suppl. material 8).

Systematics

Class Actinopterygii Klein, 1885
Order Cypriniformes Bleeker, 1859
Family Leuciscidae Bonaparte, 1835
Genus *Phoxinus* Rafinesque, 1820

Phoxinus isetensis (Georgi, 1775)

Figs 3, 4

English name: Northern Minnow; Russian name: Северный гольян

Cyprinus phoxinus – Linnaeus 1758: 322 (Europa (part)); Falk 1786: 432 (Volga, Tsaritsa, Elshanka, Sarpa, etc.); Fischer 1791: 258 (Livonia); Hupel 1777: 467 (Liffland and Estonia).

Cyprinus aphya – Linnaeus 1758: 323 (European rivers (part)); Fischer 1791: 258 (Livonia); Georgi 1775: 881 (Sukhona River); Falk 1786: 429 (Kama R. and its tributaries).

Cyprinus (without Latin species name) – Lepechin 1771: 491 (circa Catharinopolin).

"Галїанъ" or "солдатъ" (without Latin species name) – Lepechin 1772: 309 (upstreams of the Isset, Chusovaya, and Tura rivers).

Cyprinus, "Krasnosobik" or "Soldat" (without Latin species name)– Georgi 1775: 550 (Iset River).

Cyprinus isetensis Georgi 1775: 621 (Chusovaya River).

Cyprinus galian Gmelin 1789: 1421 (vicinities of Yekaterinburg).

Phoxinus rivularis – Wałecki 1864: 50 (Neman River).

Phoxinus laevis – Kessler 1864: 124 (Neva River); Kessler 1870: 268 (Volga, Samara basins, Khmelevka creek near Vasilsursk); Warpachowski 1889: 61 (Volga R. system in Nizhny Novgorod province); Sabaneev 1892: 423 (Yaroslavl and Perm province, near Moscow: rivers Lichoborka and Sinichka (trib. of Jausa R.), Moskva R. at Kamenny most); Dybowski 1862: 105 (Livonia).

Tinca phoxinus – Plater 1861: 37, 63 (Daugava River).

Phoxinus phoxinus – Berg 1912: 260 (Finland, Kola region, European rivers of the Arctic Ocean basin); Berg 1923: 166 (in Russia all over); Berg 1932: 368 (in Arctic Ocean basin from Murmansk eastward, Volga basin upstream Syzran (include Kama and Oka rivers), possible in Ural River); Berg 1949: 588 (same place); Reshetnikov et al. 2003: 301 (widespread in Europe (part)); Kottelat and Freyhof 2007: 228 (Scandinavia and Russia's northernmost extremity; Upper and middle Volga, Ural).

Phoxinus isetensis – Dyldin et al. 2023: 36 (Arctic Ocean basin, from Murman coast to East Siberian Sea basin (part)).

Phoxinus sp. – Dyldin et al. 2023: 37 (Europe, in North Sea, Baltic Sea basins (including Gulf of Finland and Neva River), and northern Caspian Sea basin (Upper Volga River, including Kama and Oka rivers, probably in Ural River)).

Type material. Neotype, female (SL 63.9 mm, IBIW_FS_422, Genbank Accession numbers PP538745–COI, PP548200–cyt*b*), Russia, Sverdlovsk Region, Ob River basin, Severka River (Tobol River basin) upstream Severka village near Yekaterinburg, 56.8830°N, 60.2716°E,

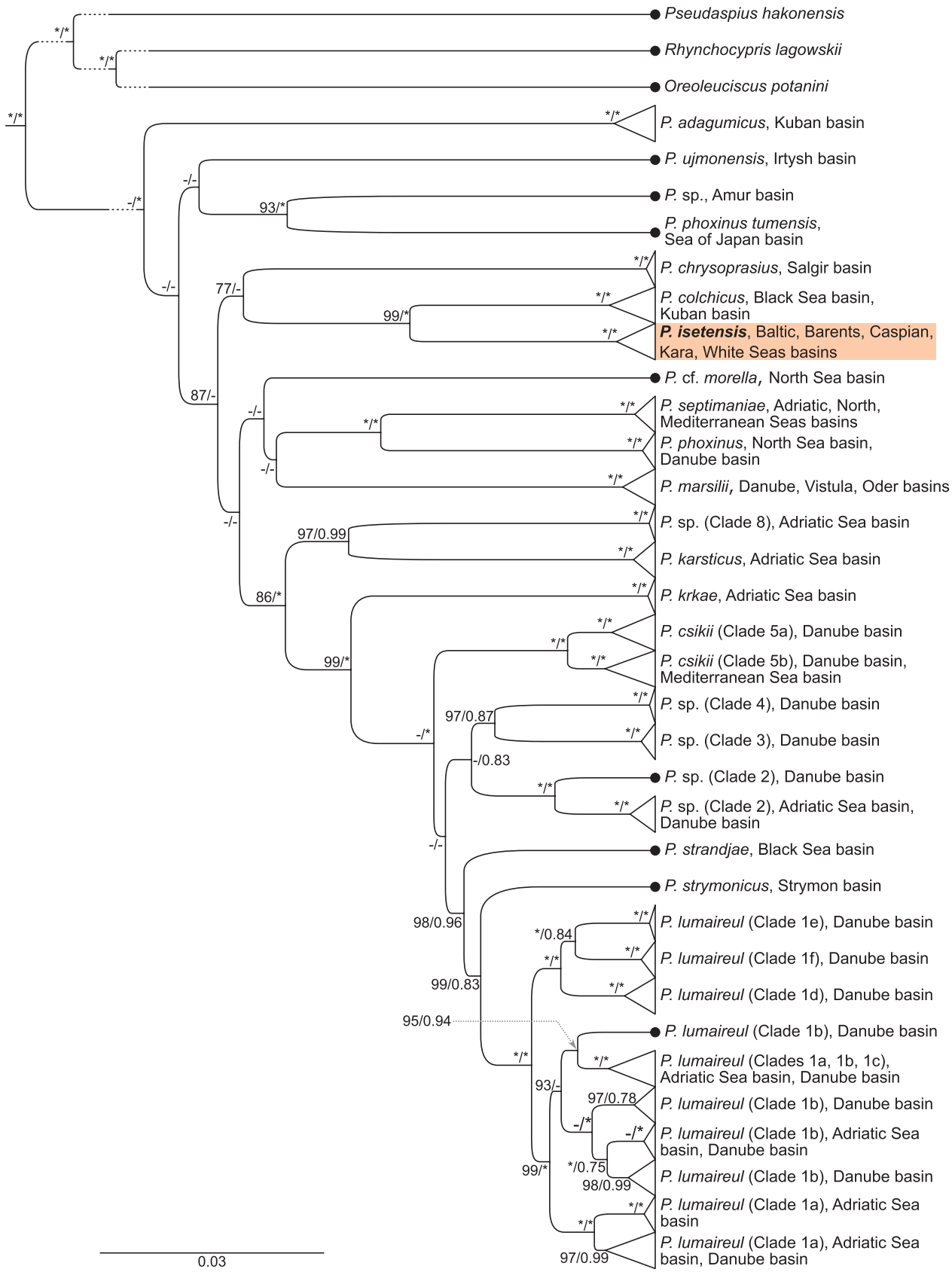

Figure 2. BI consensus tree of concatenated COI and cyt*b* mtDNA sequences representing available *Phoxinus* species in the NCBI data base combined with our data set. The numbers of some yet-unnamed clades are given according to the study of Palandačić et al. (2020). *Phoxinus isetensis* is highlighted with color. Bootstrap values/posterior probabilities above 70/0.7 are shown; asterisks represent 100/1 bootstrap/posterior probabilities values. The scale bar represents the expected substitutions per site. The nodes with multiple specimens were collapsed into a triangle, with the horizontal depth indicating the level of divergence within the node.

Figure 3. Neotype of *Phoxinus isetensis* (SL 63.9 mm, IBIW_FS_422, female). **A.** Live appearance; **B.** General appearance of the preserved specimen; **C.** Radiograph.

21 June 2023, O.N. Artaev, I.S. Turbanov, A.A. Bolotovskiy leg.

Additional material. see Suppl. material 1.

Comparative material. see Suppl. material 1.

Etymology. Since Lepechin (1771: 491) described species from the vicinity of Yekaterinburg, it can be assumed that Georgi (1775: 621) (see taxonomic remarks) gave its name to the Iset River, flowing through Yekaterinburg.

Diagnosis. *Phoxinus isetensis* is distinguished from other European minnows (*P. adagumicus*, *P. chrysoprasius*, *P. colchicus*, *P. csikii*, *P. krkae*, *P. lumaireul* (Clade 1a and Clade 1b), *P. marsilii*, *P. septimaniae*, *P. strandjae*, and *Phoxinus* sp. (Clade 2) by having a number of total vertebrae (39–43, mean 41.0, mode 41) and a number of caudal vertebrae (16–21, mean 18.9, mode 19).

Phoxinus isetensis is further distinguished from minnows from Eastern Europe (*P. adagumicus*, *P. chrysoprasius*, and *P. colchicus*) by a longer caudal peduncle (caudal peduncle length 2.5–3.7, mean 3.1 times caudal peduncle depth); fewer circumpeduncular scales (28–45, mean 35.3); fewer scale rows above the lateral line (10–21, mean 15.1); and a combination of characters, none of which is unique, as follows: eye horizontal diameter 5.9–8.8% SL, mean 7.2 and eye horizontal diameter 23.4–33.8% HL, mean 28.1; depth of caudal peduncle 6.6–9.0% SL, mean 7.7 in females and 7.2–9.5, mean 8.2 in males; caudal peduncle length 20.5–26.9% SL, mean 23.9 in females and 22.9–27.7 mean 25.1 in males; 8–16 scale rows below lateral line (mean 11.2, mode 11) (Suppl. materials 3, 4).

Description. The live and preserved appearance as well as radiograph of neotype is shown on Fig. 3, general appearance of live specimens of *Phoxinus isetensis* from different basins is shown on Fig. 4, morphometrics of neotype and additional material from the type locality with level of significance of sex-related differences are given in Table 1, meristic and qualitative characters for specimens from the type locality are given in Table 2, and primary morphological data for specimens from the type locality (neotype and additional material) are given in Suppl. material 2, the meristic and qualitative characters of *P. isetensis* and *Phoxinus* spp. are given in Suppl. material 4, the morphometrics of *P. isetensis*, *P. adagumicus*, *P. chrysoprasius*, and *P. colchicus* and their comparison are given in Suppl. material 3.

Figure 4. Live appearance of *Phoxinus isetensis* from different basins. **A.** Male in pre-spawning coloration, SL 48.5 mm, Nataleyka R. (Middle Volga basin), 53.9781°N, 45.6530°E, 05 May 2022; **B.** Female in pre-spawning coloration, SL 48.8 mm, same location and date; **C.** Female, SL 64.3 mm, Okhomlya R. (Baltic Sea basin), 58.7078°N, 33.5199°E, 12 September 2021; **D.** Female, SL 62.4 mm, Kyltymyu River (Northern Dvina basin), 61.4981°N, 50.5831°E, 21 September 2022; **E.** Male, SL 59.5 mm, Marat Bai River (Ural basin), 54.0668°N, 58.8038°E, 4 June 2023; **F.** Female, SL 63.6 mm, Karnasyavryok River (Barents Sea basin), 68.9314°N, 34.9318°E, 27 May 2023.

Table 1. Morphometrics of *Phoxinus isetensis* from the type locality (Severka River) (mean±SD - bold, and ranges - narrow) with level of significance of sex-related differences (primary data see in Suppl. material 2). * Difference between females and males, Mann-Whitney U test: ns ($p > 0.05$), + ($p < 0.05$), ++ ($p < 0.01$).

Morphometric characters	Neotype (female)	females, n=11	males, n=9	p*
SL	63.9	**56.5±3.7** 50.9–63.9	**50.5±2.7** 46.2–54.9	
In percentage of standard length (% SL)				
Body depth at dorsal-fin origin	18.0	**18.3±1.4** 15.9–20.2	**18.7±1.0** 16.7–20.0	ns
Body width at dorsal-fin origin	12.6	**13.4±0.8** 11.8–14.4	**12.6±1.2** 11.1–14.8	ns
Minimum depth of caudal peduncle	6.9	**7.7±0.4** 6.9–8.3	**8.3±0.4** 7.7–8.8	ns
Caudal peduncle width	8.7	**9.0±0.4** 8.3–9.6	**9.1±0.6** 7.5–9.7	+
Predorsal length	56.2	**56.5±0.7** 55.5–58.3	**55.6±1.3** 54.3–58.7	+
Postdorsal length	34.2	**33.8±1.3** 32.1–36.2	**34.2±0.9** 32.7–35.7	ns
Prepelvic length	47.8	**48.6±1.2** 47.1–51.1	**47.5±0.8** 46.1–48.4	ns
Preanal length	64.6	**65.0±1.5** 62.1–67.7	**63.4±0.9** 62.0–65.2	ns
Pectoral – pelvic-fin origin length	23.6	**24.8±1.2** 23.2–26.7	**23.0±1.1** 21.3–25.0	++
Pelvic – anal-fin origin length	17.7	**17.8±0.7** 16.5–18.9	**17.6±0.8** 16.6–19.0	ns
Caudal peduncle length	24.1	**23.9±1.0** 22.0–25.1	**25.3±0.8** 24.1–26.4	ns
Dorsal-fin base length	11.0	**11.1±0.6** 10.4–12.5	**11.6±0.6** 10.7–12.5	ns
Dorsal-fin depth	18.6	**18.9±0.7** 17.8–20.1	**20.8±1.0** 18.9–21.9	+
Anal-fin base length	11.4	**10.6±0.5** 9.7–11.4	**10.8±0.6** 10.0–11.6	ns
Anal-fin depth	18.6	**18.7±0.7** 17.5–19.9	**19.8±0.8** 18.7–21.1	++
Pectoral-fin length	17.1	**17.6±1.1** 16.3–20.1	**19.8±0.9** 18.1–20.7	+
Pelvic-fin length	13.2	**13.7±0.7** 12.9–15.4	**15.8±0.8** 14.7–17.1	+
Head length	25.6	**25.2±0.5** 24.4–25.8	**26.0±0.7** 24.8–27.5	ns
Head depth at nape	15.5	**15.5±0.5** 14.4–16.4	**16.4±0.4** 15.7–16.9	ns
Maximum head width	13.9	**13.6±0.5** 12.7–14.4	**13.6±0.6** 12.4–14.5	ns
Snout length	7.3	**7.6±0.3** 7.2–8.1	**7.8±0.3** 7.5–8.4	ns
Eye horizontal diameter	6.7	**6.9±0.3** 6.5–7.4	**7.1±0.3** 6.6–7.6	+
Interorbital width	8.5	**8.8±0.5** 8.2–9.7	**8.7±0.6** 7.6–9.6	ns
In percentage of head length (% HL)				
Maximum head width	54.3	**54.0±1.6** 51.5–56.0	**52.5±2.8** 47.7–55.9	ns
Snout length	28.4	**30.1±1.1** 28.4–31.6	**30.1±1.3** 28.3–32.6	ns
Head depth at nape	60.4	**61.3±1.8** 58.6–64.4	**63.2±1.8** 60.6–65.3	ns
Head depth through eye	48.3	**48.7±1.0** 47.4–50.8	**49.9±1.5** 48.1–52.2	ns
Eye horizontal diameter	26.2	**27.4±0.8** 26.2–28.8	**27.4±1.3** 25.3–29.6	++

Morphometric characters	Neotype (female)	females, n=11	males, n=9	p*
Postorbital distance	45.6	**44.5±1.1** 42.4–45.9	**44.8±2.1** 41.9–47.6	+
Interorbital width	33.4	**34.9±2.0** 31.7–38.6	**33.6±1.9** 29.5–35.4	ns
In percentage of caudal peduncle length				
Minimum depth of caudal peduncle	28.7	**32.4±2.0** 28.7–35.0	**32.8±2.2** 29.4–36.5	ns
In percentage of body depth				
Head length	142.5	**138.3±10.6** 127.1–159.6	**139.5±8.9** 129.6–155.2	+
In percentage of interorbital width				
Eye horizontal diameter	78.4	**79.0±5.2** 72.4–91.0	**81.8±4.1** 75.5–85.8	+
Ratios:				
Interorbital width/eye horizontal diameter	1.3	**1.3±0.1** 1.1–1.4	**1.2±0.1** 1.2–1.3	+
Snout length/eye horizontal diameter	1.1	**1.1±0.0** 1.0–1.2	**1.1±0.1** 1.0–1.2	ns
Head depth at nape/eye horizontal diameter	2.3	**2.2±0.1** 2.0–2.4	**2.3±0.1** 2.2–2.4	++
Head length/caudal peduncle depth	3.7	**3.3±0.2** 3.1–3.7	**3.1±0.2** 2.9–3.4	+
Length of caudal peduncle/caudal peduncle depth	3.5	**3.1±0.2** 2.9–3.5	**3.1±0.2** 2.7–3.4	ns
Pectoral fin length/pectoral – pelvic-fin origin distance	0.7	**0.7±0.1** 0.7–0.9	**0.9±0.1** 0.7–0.9	++
Predorsal length/head length	2.2	**2.2±0.0** 2.2–2.3	**2.1±0.1** 2.0–2.3	++
Body width at dorsal-fin origin/Caudal peduncle depth	1.8	**1.7±0.1** 1.6–1.8	**1.5±0.1** 1.4–1.7	+

Morphometrics (Table 1, Suppl. material 3). The maximum size among studied specimens 76.3 mm SL. The species has a slender and elongated caudal peduncle. The caudal peduncle depth 6.9% SL in neotype, 6.9–8.8% SL in additional material from type locality, and 6.6–9.5% SL in other additional materials (here and further – from basins of Caspian, Baltic, Barents, and Kara seas); caudal peduncle depth 28.7% in caudal peduncle length in neotype, 28.7–36.5 in additional material from type locality, and 26.9–40.6 in other additional material; caudal peduncle depth 3.5 times the caudal peduncle length in neotype, 2.9–3.4 in additional material from type locality, and 2.5–3.7 in other additional material. The species has a slender body, body depth at dorsal-fin origin 18.0% SL in neotype, 15.9–20.0 in additional material from type locality, and 14.7–21.6 in other additional material. Eyes larger (horizontal eye diameter: 26.2% HL in neotype, 25.3–29.6 in additional materials from type locality, 23.4–33.8 in other additional).

Meristics (Table 2, Suppl. material 4). Dorsal fin with 3 (very rarely 2) unbranched and (8) 7½ (6) branched rays. Anal fin with 3 unbranched and (6) 7½ (8) branched rays. Pectoral fin with 14–20, commonly 16–18 rays. Pelvic fin with (7) 8 (9) rays. Caudal fin with (18) 19 (20) rays.

Among 135 individuals, the most common pharyngeal teeth formula is classic for the genus 2.5–4.2 (n=102) (Fig. 5A; Suppl. material 4). Other variants are 2.5–4.1 (n=10), 2.4–4.2 (n=8), 1.5–4.2 (n=4), 2.5–5.2 (n=3), 1.5–4.1 (n=2), 2.4–4.1 (n=2), 2.3–4.2 (n=1), 2.5–4.3 (n=1), 2.3.5–4.3.2 (n=1). Among those one is exceptionally rare for phoxinin fishes – three-rowed formula 2.3.5–4.3.2 that was recorded in an individual from the Tsna R., Baltic Sea basin.

Forty-two total vertebrae in neotype, 40–42 in additional material from type locality, and 39–43 in other additional material from basins of Baltic and Barents seas, Volga and Ob rivers, commonly 41 vertebrae. Twenty-one abdominal vertebrae in neotype, 21–23 in additional material from type locality, and 21–24 in other additional material from basins of Baltic and Barents seas, Volga and Ob rivers, commonly 21–23 vertebrae. Twenty-one caudal vertebrae in neotype, 17–21 in additional material from type locality, and 16–21 in other additional material from basins of Baltic and Barents seas, Volga and Ob rivers, commonly 18–20 vertebrae. Fourteen predorsal vertebrae in neotype, 14–16 in additional material from type locality, and 13–16 for other additional material from basins of Baltic and Barents seas, Volga and Ob rivers, commonly 14–15 vertebrae. Three anal-fin pterygiophores in front of the first caudal vertebrae in neotype, 3–6 in additional material from type locality, and 3–7 in other additional material from basins of Baltic and Barents seas, Volga and Ob rivers, commonly 4–6 pterygiophores. Difference between numbers of abdominal and caudal vertebrae zero in neotype, zero to 6 in additional material from type locality, and zero to 7 for other additional material from basins of Baltic and Barents seas, Volga and Ob rivers, commonly 2–5.

Table 2. Meristic characters of *Phoxinus isetensis* from the type locality (Severka River) (primary data see in Suppl. material 2).

Characters	Mean±SD (or mode) range	n
Total number of scales in lateral series (sql)	**86.1±4.4** 80–93	10
Total number of lateral-line (pored) scales (llt)	**50.8±15.1** 23–66	10
Number of pored scales in first complete (non-interrupted) section of lateral line (llcs)	**20.8±12.7** 1–45	10
Relative number of total lateral-line scales, quotient llt: sql (lltr)	**0.60±0.19** 0.26–0.83	10
Mean number of scale rows on left and right breast patches (BrPScale)	**8.4±1.0** 7.5–10.5	8
Number of circumpeduncular scales (cps)	**35.2±1.6** 33–39	10
Scales above lateral line (between lateral line and base of first unbranched ray in D) (all)	**15.4±1.3** 14–18	10
Scales below lateral line (between lateral line and base of first unbranched ray in A) (bll)	**11.4±1.6** 9–14	10
Pattern of scalation on the breast and anterior belly (cstyp)	4 4–6	8
Total number of pectoral-fin rays (P)left	**16.4±0.8** 15–18	10
Total number of pelvic-fin rays (V)	**8.0±0.5** 7–9	10
Number of branched dorsal-fin rays (D)	**7.0±0.0** 7–7	10
Number of branched anal-fin rays) (A)	**7.0±0.0** 7–7	10
Number of rays in caudal fin (C)	**18.7±0.5** 18–19	10
Total number of vertebrae (tv)	**40.9±0.6** 40–42	30
Number of abdominal vertebrae (abdv)	**21.9±0.7** 21–23	30
Number of caudal vertebrae (caudv)	**19.0±0.9** 17–21	30
Number of predorsal abdominal vertebrae (preDv)	**14.7±0.5** 14–16	30
Number of anal-fin pterygiophores in front of the first caudal vertebrae (preAp)	**4.9±0.9** 3–6	30
Difference between numbers of abdominal and caudal vertebrae (dac)	**2.9±1.5** 0–6	30
Gill rakers in first arch	**8.5±0.8** 7–10	10

Seventy-one to 103 (mean 85.7) total number of scales in the lateral series. Lateral line incomplete and interrupted. The relative number of total lateral-line (pored) scales varies greatly from 12% to 99%, mean 61%. Five to 11 (commonly 6–9) scale rows on breast patches. 28–45 (mean 35.2) circumpeduncular scales. Ten to 21 (mean 15.1) scale rows above lateral line. Eight to 14 (16), mean 11.2 scale rows below lateral line.

Seven to 10 (mode 8) gill rakers (in series from type locality) on first arch.

Qualitative characters. Pectoral fins do not reach the beginning of pelvic fins in females and most of the males (ca. 75%). In the most specimens (ca. 85%) tip of the upper lip above horizontal level of lowest point of the eye and in about 5% of specimens – at this level. Origin of anal fin is mainly ahead or at vertical level of posterior insertion of the dorsal fin (ca. 45% for each form), rarely behind (ca. 8%). Free margin of the dorsal fin is mainly straight or slightly convex, rarely slightly concave; anal fin most often slightly concave and straight, rarely slightly convex. 3rd–6th type of breast scalation (mode 4th type, often 3th type, 5th and 6th type are less common) (Fig. 5B, Suppl. material 4).

Coloration. Males and females outside of spawning have predominantly brown coloring of the upper half of the body and light lower part in males and white in females (Fig. 4). Juveniles often show a large contrast: the black horizontal stripe and the white belly. During spawning, color of both sexes becomes much brighter, the color of the sides is dominated by green (many males become dark green, almost black), in front, it is mixed with golden, less often purple and red. In males, as well as some females, the lips and lower jaw, as well as body at the bases of the pectoral, pelvic, and anal fins, become red. The operculum is blue and the suboperculum is yellow in both sexes, but coloration is much more pronounced in males. In both sexes, the bases of ventral and anal fins are light blue. The specimens preserved in formalin had a yellowish color, which is somewhat darker with a brown tint in the upper parts.

Sexual dimorphism. Significant differences are observed in 18 out of 41 morphometric characters (Table 1). In general, females have smaller relative anal (anal-fin depth), dorsal (dorsal-fin depth), pelvic (pelvic-fin length), and pectoral fins (pectoral-fin length), a greater predorsal length, and pectoral – pelvic-fin origin length. In females, the pectoral fins never reach the pelvic fins, while in ca. 25% of males, reach.

Taxonomic remarks. According to the early literary sources reviewed in Berg (1912), the first name within the range of species is *Cyprinus isetensis*, given by Georgi (1775: 621), which lists species (without description) for the Chusovaya River with reference to Lepechin (1771: 491). Lepechin gives a description of the species but does not give the species name, designated as "CYPRINVS" with the type locality "circa Catharinopolin" (now Yekaterinburg). Although Georgi does not provide a description of species when mentioning the name *isetensis*, he makes a reference to the description of this species in Lepechin's study, which makes this name valid since it complies with Art. 12.1 and 12.2 of the International Code of Zoological Nomenclature (ICZN 1999).

Type locality. The type locality from the original description (Lepechin 1771: 493) is "… habitat in rivis scopulosus circa Catharinopolin," which means "… lives in the rocky streams around Catharinopolin (now Yekaterinburg)." Probably Lepechin meant the upper reaches of the Iset, Chusovaya, and Tura rivers, which were specified in further publication (Lepechin 1772: 311).

Type locality for the neotype: Severka River (56.8830°N, 60.2716°E) upstream of Severka village near Yekaterinburg, Sverdlovsk Oblast, Russia (Fig. 6). A tributary of the Reshotka River → Iset River → Tobol River → Irtysh River → Ob River → Kara Sea.

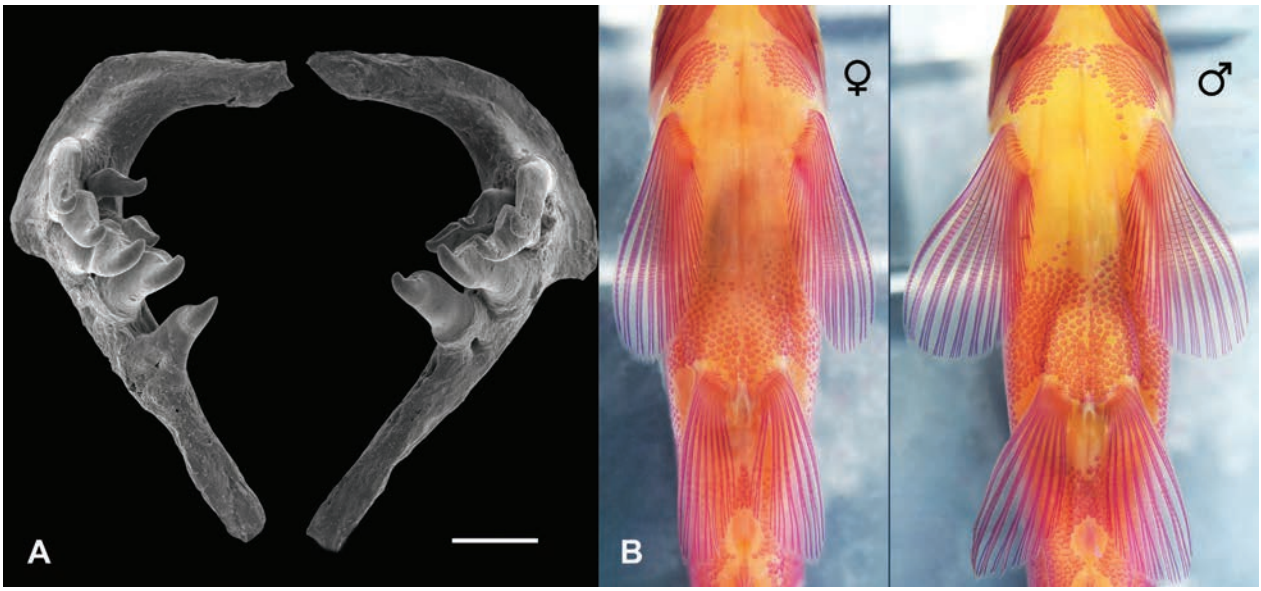

Figure 5. Morphological features of *Phoxinus isetensis*. **A.** Most frequent variant of the formula of pharyngeal bones: double-rowed formula 2.5–4.2, scale bar 0.5 mm; **B.** Ventral view of alizarin-stained female and male from the Bekshanka River (Volga basin). Female had 5th type scalation on breast and belly, male had 6th type.

Figure 6. Example of habitat in the Severka River, type locality for *Phoxinus isetensis*, 21 June 2023.

Nomenclatural and taxonomic actions. The need to designate a neotype for *P. isetensis* is determined by the following considerations: first, our attempts to find a type specimen at the Zoological Institute of the Russian Academy of Sciences, Saint Petersburg, Russia (ZISP), where the largest and oldest ichthyological collection in Russia is stored, were unsuccessful. At the end of the 18th century, at the time of the description of *P. isetensis*, it was the only scientific organization in Russia where type specimens were deposited. The type specimens of *P. isetensis* were absent in the ZISP already at the beginning of the 20th century (Berg 1912). Second, no type specimens for all the fish species described by the naturalist and explorer Johann Gottlieb Georgi (1729–1802) were designated

(Fricke et al. 2024). Thus, we conclude that Georgi did not designate a type series for this species. Third, in addition to *P. isetensis*, at least one more species of this genus inhabits the Ob River basin—*P. ujmonensis* Kashchenko, 1899 (see Discussion), and their possible sympatric co-occurrence requires further clarification.

Thus, based on the above-mentioned circumstances and in accordance with Article 75 of the ICZN, we designate a neotype for *P. isetensis*. Our nomenclatural actions do not contradict the statements of Article 75.3 (qualifying conditions), and the designation of a nomenclatural type (neotype) for *P. isetensis*, as a widespread species living in Europe and Asia, will make it possible to clearly describe both morphological and genetic differences from other species of the genus *Phoxinus* (Articles 75.3.1 and 75.3.2).

Distribution and habitat. Widespread in northern and eastern Europe and in the western edge of Siberia (Iset and partially Ural basin). *Phoxinus isetensis* inhabits the basins of the Caspian, Baltic, White, Barents, and Kara seas, possibly occurring in the North Sea basin. In the Caspian Sea basin, it is widely distributed in the upper and middle Volga, Kama, in the mountainous part of the Ural basin. In the Baltic Sea basin, it is widespread in the northern and eastern parts. In the Kara Sea basin, it is known in the Iset basin (Ob basin). According to Palandačić et al. (2017, 2020), mtDNA of this species (Clade 17) was detected in Scandinavia and the British Isles, suggesting that minnows from these areas also belong to the species *P. isetensis*.

Dyldin et al. (2023: 671) pointed out the distributional range of *P. isetensis* as "Arctic Ocean basin, from Murman coast to East Siberian Sea basin (Kolyma basin); rivers of northern and western Sea of Okhotsk basin (Ola and Uda rivers); rivers of Peter the Great Bay drainage, probably Amur River basin, and northwestern Sakhalin Island." This data only partially corresponds to the above-mentioned range. See further explanations in the discussion.

Phoxinus isetensis prefers rivers with fast-flowing water that are rheophilic. In the northern regions, it also inhabits riverbeds of large rivers, lakes, and brackish waters (Berg 1949: 590; Tsvelev 2007: 277; our data).

Morphology comparison. PCA of 41 morphometric characters shows differences between *P. isetensis* and *P. adagumicus*, *P. chrysoprasius*, and *P. colchicus* from the Crimean Peninsula and the Caucasus (Fig. 7). The greatest difference is from *P. colchicus* (no overlap), while the remarkable overlap with the other two species (*P. adagumicus* and *P. chrysoprasius*) is noted.

Compared to *P. abanticus* from the Lake Abant basin in Türkiye (Turan et al. 2023), *P. isetensis* has scales on the breasts in both sexes (vs. absence of scales on the breast in males); 18–20 rays in the caudal fin (vs. 15–16 rays); and a more slender caudal peduncle (6.6–9.5, mean 8.0 vs. 11.0–12.7, mean 12.0).

Compared to *P. adagumicus* from the Kuban basin (Artaev et al. 2024), *P. isetensis* has fewer scale rows above the lateral line (10–21, mean 15.1, vs. 15–24, mean 18.4); more total vertebrae (39–43, mean 41.0, mode 41, vs. 39–42, mean 40.4, mode 40); more caudal vertebrae (16–21, mean 18.9, mode 19, vs. 16–19, mean 18.0, mode 18); double-row pharyngeal teeth with modal formula 2.5–4.2 (vs. single-row pharyngeal teeth with modal formula 5–4) (Suppl. material 4).

Compared to *P. bigerri* from the Adour and Ebro basins in France and Spain (Kottelat 2007), *P. isetensis* has fewer scale rows above the lateral line (10–21, mean 15.1, vs. 19–23).

Compared to *P. chrysoprasius* from the rivers of the Crimean Peninsula (Artaev et al. 2024; Bogutskaya et al. 2023), *P. isetensis* has a slightly selender caudal peduncle (minimum depth of caudal peduncle (6.6–9.0% SL, mean 7.7 in females and 7.2–9.5, mean 8.2 in males (vs. 8.4–9.9, mean 9.1 in females and 8.1–11, mean 9.9 in males); slightly fewer circumpeduncular scales–28–45, mean 35.3 (vs. 41–55, mean 46.2); more total number of vertebrae–39–43, mean 41.0, mode 41 (vs. 38–42, mean 40.4, mode 40); more number of caudal vertebrae–16–21, mean 18.9, mode 19 (vs. 16–20, mean 18.0, mode 18) (Suppl. material 4).

Compared to *P. colchicus* from the Black Sea coast of the Caucasus and Kuban basin (Artaev et al. 2024; Bogutskaya et al. 2023), *P. isetensis* in both sexes have a slenderer caudal peduncle (minimum depth of caudal peduncle in percentage of caudal peduncle length 26.9–40.6, mean 32.5; vs. 42.0–58.6, mean 49.5); (Suppl. material 3); less number of circumpeduncular scales – 28–45, mean 35.3 (vs. 36–48, mean 40.9); less number of scales above lateral line – 10–21, mean 15.1 (vs. 16–23, mean 18.8); fewer scale rows below lateral line – 8–16, mean 11.2 (vs. 11–17, mean 13.4); different patterns of scalation on the breast and anterior belly – 3rd –6th types, mode 4th (vs. 3rd–10th, 13th and 14th, modal 6th); more total number of vertebrae – 39–43, mean 41.0, mode 41 (vs. 39–42, mean 40.1, mode 40); more number of caudal vertebrae – 16–21, mean 18.9, mode 19 (vs. 16–19, mean 17.6, mode 18) (Suppl. material 4).

Compared to *P. csikii* from the Danube River basin, Montenegro, and Bulgaria (Bogutskaya et al. 2019, 2023), *P. isetensis* has a different pattern of scalation on the breast and anterior belly–3rd–6th types, mode 4th (vs. 3rd–9th types, 11th, mode 7th); more total number of vertebrae–39–43, mean 41.0, mode 41 (vs. 38–42, mean 40.1, mode 40); more number of caudal vertebrae–16–21, mean 18.9, mode 19 (vs. 15–19, mean 17.4, mode 17); smaller difference between numbers of abdominal and caudal vertebrae–0–7, mean 3.2 (vs. 2–9, mean 5.4) (Suppl. material 4).

Compared to *P. krkae* from the Krka River, Croatia (Bogutskaya et al. 2019), *P. isetensis* has a greater number of lateral-line scales (pored) 12–94, mean 53.7 (vs. 11–54, mean 32.6); different pattern of scalation on the breast and anterior belly–3rd–6th types, mode 4th (vs. 3rd–7th types, mode 6th); more total number of vertebrae–39–43, mean 41.0, mode 41 (vs. 37–40, mean 38.4, mode 39); more number of caudal vertebrae–16–21, mean 18.9, mode 19 (vs. 15–18, mean 16.8, mode 17) (Suppl. material 4).

Compared to *P. lumaireul* Clades 1a and 1b from rivers in Adriatic and Black Sea basins in Italy, Slovenia, and Croatia (Bogutskaya et al. 2019), *P. isetensis* has a

Figure 7. PCA based on 41 morphometric characters for *Phoxinus* spp. – *P. isetensis*, *P. chrysoprasius* from the Crimean Peninsula, *P. colchicus*, and *P. adagumicus* from the Caucasus – and loading plot showing how strongly each character influences principal components. Samples of *P. isetensis* from the type locality (Severka River) are encircled by black.

different pattern of scalation on the breast and anterior belly–3rd–6th types, mode 4th (vs. 2nd–7th types, mode 3rd); more total number of vertebrae–39–43, mean 41.0, mode 41 (vs. 37–41, mean 39.3, mode 39); more number of caudal vertebrae–16–21, mean 18.9, mode 19 (vs. 16–19, mean 17.5, mode 18) (Suppl. material 4).

Compared to *P. marsilii* from the Danube River basin, Austria, and Croatia (Bogutskaya et al. 2019, 2023), *P. isetensis* has a different pattern of scalation on the breast and anterior belly–3rd–6th types, mode 4th (vs. 3rd–8th types, mode 6th); more total number of vertebrae–39–43, mean 41.0, mode 41 (vs. 38–42, mean 40.1, mode 40) (Suppl. material 4).

Compared to *P. radeki* from the Ergene River (Aegean Sea basin) in Türkiye (Bayçelebi et al. 2024), *P. isetensis* has a higher number of scales above the lateral line-10–21 (vs. 9–15) and below the lateral line–8–16 (vs. 6–9).

Compared to *P. septimaniae* from the Herault River, France (Bogutskaya et al. 2019), *P. isetensis* has a different pattern of scalation on the breast and anterior belly–3rd–6th types, mode 4th (vs. 12th–14th types, mode 14th); a greater total number of vertebrae–39–43, mean 41.0, mode 41 (vs. 37–41, mean 39.3, mode 39); a greater number of caudal vertebrae–16–21, mean 18.9, mode 19 (vs. 16–19, 21, mean 17.6, mode 18) (Suppl. material 4).

Compared to *P. strandjae* from the rivers of the Black Sea basin, Bulgaria, and the rivers of the Marmara Sea, Türkiye (Bogutskaya et al. 2019, 2023), *P. isetensis* has a different pattern of scalation on the breast and anterior belly–3rd–6th types, mode 4th (vs. 3rd–12th types, mode 11th); a greater total number of vertebrae–39–43, mean 41.0, mode 41 (vs. 38–42, mean 39.8, modal 40); a greater number of caudal vertebrae–16–21, mean 18.9, mode 19 (vs. 16–19, mean 17.7, mode 18) (Suppl. material 4).

Compared to *P. strymonicus* from the Strymon basin in Greece and Macedonia (Kottelat, 2007), *P. isetensis* has a smaller number of scales above the lateral line: 10–21 (vs. 21–24).

Compared to *P.* cf. *ujmonensis* from the Mundybash River in Altai part of the Ob basin (Suppl. material 4), *P. isetensis* has a smaller number of scales above the lateral line: 10–21, mean 15.1 (vs. 15–19, mean 17.3); and a number of scales below the lateral line: 8–16, mean 11.2 (vs. 12–15, mean 12.9).

Discussion

Our study recognized the unnamed *Phoxinus* sp. with the largest range in Europe (Clade 17 sensu Palandačić et al. 2017) as *P. isetensis*, the species that was described from the upper reach of the Chusovaya River (Kama-Volga basin) and the Iset River basin (Ob basin) in the Middle Urals. We redescribed the morphology and significantly clarified the distributional range of this species. According to our results, *P. isetensis* can be distinguished from other neighbor species by the large total number of vertebrae – 39–43 (mode 41) (vs. 37–42), primarily due to an increase in the number of caudal vertebrae – 16–21 (mode 19) (frequency distribution see in Suppl. material 4) and in sequences of COI mtDNA (minimal *p*-distance = 0.05 to closely related *P. colchicus*). Remarkably, there is some discrepancy between the genetic and morphological similarities of *P. isetensis*. Being close genetically to *P. colchicus* from the West Caucasus, it has more significant morphological differences with this species compared to other phylogenetically more distant species, *P. adagumicus* and *P. chrysoprasius* (Figs 2, 7). In particular, these species are more similar to *P. isetensis* in total number of vertebrae and number of caudal vertebrae (Suppl. material 4). Of the eighteen populations of *P. isetensis*, seventeen had modes of 41 or 42 vertebrae, and only one population from the Baltic Sea basin had 40 vertebrae. This main morphological difference – an increased number of vertebrae and northernmost range relative to other European *Phoxinus* – is consistent with Jordan's rule (vertebral number in fish increases with latitude) (McDowall 2008). However, it is noteworthy that within the species range extended in the latitudinal direction for more than 2000 km within 51–69 northern latitudes, there was no correlation.

Phoxinus isetensis redescribed in this study was recently revalidated in Dyldin et al. (2023), but the authors outlined its range mistakenly for the whole of West and East Siberia as well as for Northeast Asia and the Far East due to the absence of genetic and morphological data. According to our genetic results, the *P. isetensis* described from the rivers near Yekaterinburg belonging to both the upper stream of left tributaries of the Ob River and the Chusovaya River itself (Kama-Volga basin) are identical or very similar (conspecific) to other samples from the Volga basin, the Ural basin, and the remaining range as outlined for Clade 17 sensu Palandačić et al. (2017). Therefore, *P. isetensis* has a huge range in northern and eastern Europe, extending approximately 3.800 km from west to east and 2.000 km from north to south. Its range in Europe includes the basins of the Caspian, Baltic, White, Barents, and North Seas. In the Caspian Sea basin, it is widespread in the Upper and Middle Volga and Kama basins. In the Baltic Sea basin, it is widespread in the northern and eastern parts. In the North Sea basin, it is noted for Scandinavia and the British Isles (Palandačić et al. 2017).

To the best of our knowledge, the occurrence of *P. isetensis* in Asia is restricted to the Ural basin (Caspian Sea basin) and the Iset basin (Tobol River → Irtysh River → Ob River, which flows into the Kara Sea). The Ural Mountains are a well-known biogeographic barrier between Europe and Asia (Abell et al. 2008), which, however, is characterized by the corridor linking Europe and Asia in the Middle Ural via the Chusovaya River Valley. It was assumed this corridor might facilitate aquatic fauna exchange between Siberia (Ob basin) and European Russia (Volga basin) (Kostarev 1973; Makhrov et al. 2021). The Chusovaya River belongs to the Kama-Volga basin, but its upper reaches are located in Siberia – eastward the main Ural ridge and sharing a watershed with the Ob basin through the Iset river basin. We have to note that in the upper reaches of the Chusovaya River, there are a number of man-made reservoirs. One of those, the Volchikha Reservoir, has a connection through a small artificial canal to the Ob basin via the Reshotka River, a tributary of the Iset River. The reservoir and canal are dated to the mid-1940s (Korlyakov and Nohrin 2014). Although it can be assumed that an artificial canal could facilitate the dispersal of *P. isetensis* from the Kama-Volga system to the Ob basin, populations of minnow, at least in the Iset basin, apparently colonized the Ob basin rather earlier. First, it is supported by early evidence of the presence of conspecific populations in both the Ob and Chusovaya basins by Lepechin (1772) and Georgi (1775). This is further supported by the fact that not only the Severka (type locality), but other rivers in the Iset basin, inhabited just one species of minnow, *P. isetensis* – for instance, in the Kushtumga River (genetic data), which is located ca. 750 km along the riverbed from the canal connecting the Volga and Ob basins near Yekaterinburg (Fig. 1).

Our finding in the distributional pattern of *P. isetensis* is additional evidence of faunal exchange between Siberia and Europe via the Chusovaya River Valley. Contrary to previous observations and suggestions on fish migrations from Siberia to Europe (Kostarev 1973; Marić et al. 2014; Perdices et al. 2015; Levin et al. 2017; Zinoviev and Bogdanov 2017; Vinarski et al. 2021), the case of *P. isetensis* suggests that fish migrations took place in the reverse direction too. Remarkably, the eastward direction of the recent (seemingly postglacial) colonization pattern of *P. isetensis* is also corroborated by its presence in the Upper and Middle Ural systems.

Noteworthy, one more *Phoxinus* species inhabits the Ob basin – *P. ujmonensis*, described from the upper tributaries of the Ob in the Altai Mountains. This species is genetically distant from *P. isetensis* (Fig. 2, Suppl. material 7). Our unpublished molecular data indicate that the distribution of *P. ujmonensis* in the Ob basin is not restricted by the Altai Mountains. The distribution of both species in the Ob basin needs further clarification.

Based on the current distribution of *P. isetensis* (Fig. 1), this species might rapidly colonize large northern areas following the deglaciation of the last Pleistocene glaciers. This is in line with the previously proposed hypothesis about the colonization of Scandinavia by freshwater fish from the southeast (Museth et al. 2007). Within the boundaries of the Last Glacial Maximum (LGM), the habitation of two other *Phoxinus* species (clades) is confirmed – *P.* cf. *morella* and Clade 10 (*P. phoxinus*) from Ireland, with an unknown origin of population that might

be introduced – Denys et al. (2020) (Fig. 1). However, northern populations of those species are located on the southern periphery of the LGM, while *P. isetensis* inhabits most of the deglaciated region. One may suggest that during the colonization of new habitats after LGM, *P. isetensis* could hybridize with other minnow species. This hypothesis may be supported by a decrease in the total number of vertebrae (mean 40.5 vs. 41.1 in the rest of the range, Suppl. material 4) in the potential contact zone – the east of the Baltic Sea basin—and it should be tested in the future. It is noteworthy that in northern Norway, the *Phoxinus* minnow has been a significant expansion of the range as a result of introductions since the 1900s (Museth et al. 2007); its ancient DNA was not found in the sediments dating to 5.6–13 thousand years ago from the Storsteinhola cave, while the ancient DNA of species currently sharing biotopes with *Phoxinus* (*Barbatula* sp. and *Gobio gobio*) was found (Boilard et al. 2024). Seemingly, along with the post-glacial expansion of *P. isetensis* northward, a shrinking of the range from the south can be suggested. For example, Falk (1786: 432) recorded *Cyprinus phoxinus* for the Volga and small rivers ("Zariza, Jelschanka. Sarpa u. f.") near Volgograd city in Russia (Fig. 1). This is > 450 km southward from the most southern contemporary records in the upper reaches of the Tereshka (Artemyeva and Selishchev 2005) and Sura basins within the Volga system. Although the right drainage of the Volga north of Volgograd is steep and rich in small tributaries with fast-flowing water, minnows were not recorded in this region. Probably populations in these small rivers were extinct, being vulnerable to changes in the environment, including general climate warming.

Acknowledgements

The authors are very grateful to taxonomist Boris Kataev for his valuable advice on zoological taxonomy and nomenclature. We are very thankful to Alexandra Komarova, who helped with sampling. This study was supported by the Russian Science Foundation, grant no. 24-44-20019, "Fishes of the Caspian Sea basin: genetic diversity, evolution, and biogeography".

References

Abell R, Thieme ML, Revenga C, Bryer M, Kottelat M, Bogutskaya N, Coad B, Mandrak N, Balderas SC, Bussing W, Stiassny M, Skelton P, Allen GR, Unmack P, Naseka A, Ng R, Sindorf N, Robertson J, Armijo E, Higgins JV, Heibel TJ, Wikramanayake E, Olson D, López HL, Reis RE, Lundberg JG, Sabaj PMH, Petry P (2008) Freshwater ecoregions of the world: A new map of biogeographic units for freshwater biodiversity conservation. Bioscience 58(5): 403–414. https://doi.org/10.1641/B580507

Aljanabi SM, Martinez I (1997) Universal and rapid salt-extraction of high quality genomic DNA for PCR-based techniques. Nucleic Acids Research 25(22): 4692–4693. https://doi.org/10.1093/nar/25.22.4692

Artaev ON, Turbanov IS, Bolotovskiy AA, Gandlin AA, Levin BA (2024) Taxonomic revision of *Phoxinus* minnows (Leuciscidae) from Caucasus, with description of a new narrow-ranged endemic species. Zoosystematics and Evolution 100(1): 291–308. https://doi.org/10.3897/zse.100.115696

Artemyeva EA, Selishchev VI (2005) Biomonitoring of the Tereshka River basin. Nature of Simbirsk Volga Area 6: 19–25. [In Russian]

Batchelor CL, Margold M, Krapp M, Murton DK, Dalton AS, Gibbard PL, Stokes CR, Murton JB, Manica A (2019) The configuration of Northern Hemisphere ice sheets through the Quaternary. Nature Communications 10(1): 3713. https://doi.org/10.1038/s41467-019-11601-2

Bayçelebi E, Aksu İ, Turan D (2024) Description of a new species of *Phoxinus* from the Ergene River (Aegean Sea Basin) in Türkiye (Actinopterygii, Leuciscidae). Zoosystematics and Evolution 100(1): 101–110. https://doi.org/10.3897/zse.100.113467

Berg LS (1912) Fauna of Russia and neighboring countries based mainly on the collections of the Zoological Museum of the Imperial Academy of Sciences in St. Petersburg. Fish (Marsipobranchii and Pisces). Vol. III, Part 1. Ostariophysi. Saint Petersburg, Izdatelstvo Imperatorskoj Akademii Nauk, 336 pp. [In Russian]

Berg LS (1923) Freshwater fish of Russia. Second edition. Moscow, Gosudarstvennoe Izdatelstvo, 535 pp. [In Russian]

Berg LS (1932) Freshwater fish of the U.S.S.R. and adjacent countries. Part 1. Vsesojuznyi Institut Ozernogo i Rechnogo Rybnogo Khozyaistva, Leningrad, 543 pp. [In Russian]

Berg LS (1949) Freshwater fishes of the U.S.S.R. and adjacent countries. Part 2. Izdatelstvo Akademii Nauk SSSR, Leningrad, 456 pp. [In Russian]

Bogutskaya N, Jelić D, Vucić M, Jelić M, Diripasko O, Stefanov T, Klobučar G (2019) Description of a new species of *Phoxinus* from the upper Krka River (Adriatic Basin) in Croatia (Actinopterygii, Leuciscidae), first discovered as a molecular clade. Journal of Fish Biology 96(2): 378–393. https://doi.org/10.1111/jfb.14210

Bogutskaya NG, Diripasko OA, Palandačić A (2023) Novel data support validity of *Phoxinus chrysoprasius* (Pallas, 1814) (Actinopterygii, Leuciscidae). European Journal of Taxonomy 861: 1–20. https://doi.org/10.5852/ejt.2023.861.2061

Boilard A, Walker SJ, Lødøen TK, Henriksen M, Takken Beijersbergen LMT, Star B, Robu M, Tøssebro C, Albrektsen CM, Soleng Y, Aksnes S, Jørgensen R, Hufthammer AK, van Kolfschoten T, Lauritzen S-E, Boessenkool S (2024) Ancient DNA and osteological analyses of a unique paleo-archive reveal Early Holocene faunal expansion into the Scandinavian Arctic. Science Advances 10(13): eadk3032. https://doi.org/10.1126/sciadv.adk3032

Chen XYu (1996) Morphology, phylogeny, biogeography and systematics of *Phoxinus* (Pisces, Cyprinidae). Zoologisches Forschungsinstitut und Museum Alexander Koenig, Bonn, 227 pp. [ISBN 3-925382-42-9]

Danielson JJ, Gesch DB (2011) Global multi-resolution terrain elevation data 2010 (GMTED2010). US Geological Survey Open-File Report 2011-1073. https://doi.org/10.3133/ofr20111073

Denys GP, Dettai A, Persat H, Daszkiewicz P, Hautecoeur M, Keith P (2020) Revision of *Phoxinus* in France with the description of two new species (Teleostei, Leuciscidae). Cybium. Revue Internationale d'Ichtyologie 44(3): 205–237. https://doi.org/10.26028/cybium/2020-443-003

Dybowski BT (1862) Versuch einer Monographie der Cyprinoiden Livlands: nebst einer synoptischen Aufzählung der europäischen Arten dieser Familie. H. Laakmann, Dorpat, 215 pp. https://doi.org/10.5962/bhl.title.14430

Dyldin YV, Orlov AM, Hanel L, Romanov VI, Fricke R, Vasil'eva ED (2023) Ichthyofauna of the Fresh and Brackish Waters of Russia and Adjacent Areas: Annotated List with Taxonomic Comments. 2. Order Cypriniformes, Suborders Catostomoidei, Cobitoidei and Cyprinoidei. Journal of Ichthyology 63(4): 636–686. https://doi.org/10.1134/S0032945223040045

Falk IP (1786) Beytrage zur topographischen Kenntniss der Russischen Reichs. Academy of Sciences, St. Petersburg, 282 pp.

Fischer JB (1791) Versuch einer Naturgeschichte von Livland. bey F. Nicolovius, Königsberg, 826 pp. https://doi.org/10.5962/bhl.title.37356

Fricke R, Eschmeyer WN, Van der Laan R [Eds] (2024) Eschmeyer's Catalog of Fishes: Genera, Species, References. http://researcharchive.calacademy.org/research/ichthyology/catalog/fishcatmain.asp [Electronic version accessed 06.02.2024]

Frost WE (1943) The natural history of the minnow, *Phoxinus phoxinus*. Journal of Animal Ecology 12(2): 139–162. https://doi.org/10.2307/1374

Geiger MF, Herder F, Monaghan MT, Almada V, Barbieri R, Bariche M, Berrebi P, Bohlen J, Casal-Lopez M, Delmastro GB, Denys GPJ, Dettai A, Doadrio I, Kalogianni E, Kärst H, Kottelat M, Kovačić M, Laporte M, Lorenzoni M, Marčić Z, Özuluğ M, Perdices A, Perea S, Persat H, Porcelotti S, Puzzi C, Robalo J, Šanda R, Schneider M, Šlechtová V, Stoumboudi M, Walter S, Freyhof J (2014) Spatial heterogeneity in the Mediterranean Biodiversity Hotspot affects barcoding accuracy of its freshwater fishes. Molecular Ecology Resources 14(6): 1210–1221. https://doi.org/10.1111/1755-0998.12257

Georgi JG (1775) Bemerkungen einer Reise im Russischen Reich im Jahre 1772. Academie der Wissenschaften, St. Petersburg, 506 pp.

Gmelin JG (1789) Caroli a Linné. Systema Naturae per regna tria naturae, secundum classes, ordines, genera, species; cum characteribus, differentiis, synonymis, locis. Vol. 1(3). Lipsiae, 1033–1516 pp.

Hammer Ø, Harper DA (2001) Past: Paleontological statistics software package for educaton and data anlysis. Palaeontologia Electronica 4(1): 1–9.

Hill V, Baele G (2019) Bayesian estimation of past population dynamics in BEAST 1.10 using the Skygrid coalescent model. Molecular Biology and Evolution 36(11): 2620–2628. https://doi.org/10.1093/molbev/msz172

Hupel AW (1777) Topographische Nachrichten von Lief-und Ehstland (Vol. 2). Zweyter Band, Riga. ICZN (1999) International Code of Zoological Nomenclature. 4th edn. International Trust for Zoological Nomenclature, London. https://www.iczn.org/the-code/the-code-online/

Ihaka R, Gentleman R (1996) R: a language for data analysis and graphics. Journal of Computational and Graphical Statistics 5(3): 299–314. https://doi.org/10.1080/10618600.1996.10474713

Imoto JM, Saitoh K, Sasaki T, Yonezawa T, Adachi J, Kartavtsev YP, Miya M, Nishida M, Hanzawa N (2013) Phylogeny and biogeography of highly diverged freshwater fish species (Leuciscinae, Cyprinidae, Teleostei) inferred from mitochondrial genome analysis. Gene 514(2): 112–124. https://doi.org/10.1016/j.gene.2012.10.019

Ivanova NV, Zemlak TS, Hanner RH, Hebert PD (2007) Universal primer cocktails for fish DNA barcoding. Molecular Ecology Notes 7(4): 544–548. https://doi.org/10.1111/j.1471-8286.2007.01748.x

Kalyaanamoorthy S, Minh BQ, Wong TK, Von Haeseler A, Jermiin LS (2017) ModelFinder: Fast model selection for accurate phylogenetic estimates. Nature Methods 14(6): 587–589. https://doi.org/10.1038/nmeth.4285

Kassambara A (2020) rstatix: Pipe-friendly framework for basic statistical tests. R package version 0.6. 0. https://doi.org/10.32614/CRAN.package.rstatix

Kessler KF (1864) Descriptions of the fish which are found in the waters of St. Petersburg Province. In: Natural and Historical Researches in St. Petersburg Province Performed by the Members of Entomological Society in St. Petersburg. Vol. 1: Zoological Studies. Russ. Entomol. O-vo, St. Petersburg, 240 pp. [In Russian]

Kessler KF (1870) Ichthyofauna of the Volga River, Trudy S.-. Peterb. Obschestva Estestvoispytateley 1(2): 236–311.

Korlyakov KA, Nohrin DY (2014) Tendencies of occurrence invasion of the corridor Volga-Ob. Bulletin of the Council of Young Scientists and Specialists of the Chelyabinsk Region 2: 19–38. [In Russian]

Kostarev GF (1973) On the genesis of the ichthyofauna of the Chusovaya River. Voprosy Ikhtiologii 13(4): 611–617.

Kottelat M (2007) Three new species of *Phoxinus* from Greece and southern France (Teleostei, Cyprinidae). Ichthyological Exploration of Freshwaters 18(2): 145.

Kottelat M, Freyhof J (2007). Handbook of European Freshwater Fishes. Kottelat, Cornol, Switzerland and Freyhof, Berlin, 646–646.

Kumar S, Stecher G, Tamura K (2016) MEGA7: Molecular evolutionary genetics analysis version 7.0 for bigger datasets. Molecular Biology and Evolution 33(7): 1870–1874. https://doi.org/10.1093/molbev/msw054

Lanfear R, Calcott B, Ho SY, Guindon S (2012) PartitionFinder: Combined selection of partitioning schemes and substitution models for phylogenetic analyses. Molecular Biology and Evolution 29(6): 1695–1701. https://doi.org/10.1093/molbev/mss020

Lanfear R, Frandsen PB, Wright AM, Senfeld T, Calcott B (2016) PartitionFinder 2: New methods for selecting partitioned models of evolution formolecular and morphological phylogenetic analyses. Molecular Biology and Evolution, msw260. https://doi.org/10.1093/molbev/msw260

Lepechin II (1771) Descriptiones avium. Novi Commentarii Academiae Scientiarum Imperialis Petropolitanae, 15. 1770 (1771), 485–493.

Lepechin II (1772) Continuation of the day's notes of the traveler academician and medicine doctor Ivan Lepekhin in different provinces of the Russian state in 1770. Pri Imperatorskoi Akademii Nauk, Saint Petersburg, 338 pp. [In Russian]

Levin BA, Simonov EP, Ermakov OA, Levina MA, Interesova EA, Kovalchuk OM, Malinina YA, Mamilov NS, Mustafayev NJ, Pilin DV, Pozdeev IV, Prostakov NI, Roubenyan HR, Titov SV, Vekhov DA (2017) Phylogeny and phylogeography of the roaches, genus *Rutilus* (Cyprinidae), at the Eastern part of its range as inferred from mtDNA analysis. Hydrobiologia 788(1): 33–46. https://doi.org/10.1007/s10750-016-2984-3

Linke S, Lehner B, Dallaire CO, Ariwi J, Grill G, Anand M, Beames P, Burchard-Levine V, Maxwell S, Moidu H, Tan F, Thieme M (2019) Global hydro-environmental sub-basin and river reach characteristics at high spatial resolution. Scientific Data 6(283): 283. https://doi.org/10.1038/s41597-019-0300-6

Linnaeus C (1758) Systema naturae. Vol. 1(1). Laurentii Salvii, Stockholm, 532 pp.

Machordom A, Doadrio I (2001) Evidence of a Cenozoic Betic-Kabilian connection based on freshwater fish phylogeography (*Luciobarbus*, Cyprinidae). Molecular Phylogenetics and Evolution 18(2): 252–263. https://doi.org/10.1006/mpev.2000.0876

Makhrov AA, Vinarski MV, Gofarov MY, Dvoryankin GA, Novoselov AP, Bolotov IN (2021) Faunal exchanges between the basins of the Arctic Ocean and the Caspian Sea: Their history and current processes. Biology Bulletin of the Russian Academy of Sciences 48(7): 892–906. https://doi.org/10.1134/S1062359021070190

Marić S, Alekseyev S, Snoj A, Askeyev O, Askeyev I, Weiss S (2014) First mtDNA sequencing of Volga and Ob basin taimen *Hucho taimen*: Eu-

ropean populations stem from a late Pleistocene expansion of *H. taimen* out of western Siberia and are not intermediate to *Hucho hucho*. Journal of Fish Biology 85(2): 530–539. https://doi.org/10.1111/jfb.12428

McDowall RM (2008) Jordan's and other ecogeographical rules, and the vertebral number in fishes. Journal of Biogeography 35(3): 501–508. https://doi.org/10.1111/j.1365-2699.2007.01823.x

Mina MV, Levin BA, Mironovsky AN (2005) On the possibility of using character estimates obtained by different operators in morphometric studies of fish. Journal of Ichthyology 45(4): 284–294.

Minh BQ, Nguyen MA, von Haeseler A (2013) Ultrafast approximation for phylogenetic bootstrap. Molecular Biology and Evolution 30(5): 1188–1195. https://doi.org/10.1093/molbev/mst024

Museth J, Hesthagen T, Sandlund OT, Thorstad EB, Ugedal O (2007) The history of the minnow *Phoxinus phoxinus* (L.) in Norway: from harmless species to pest. Journal of Fish Biology 717: 184–195. https://doi.org/10.1111/j.1095-8649.2007.01673.x

Naseka AM (1996) Comparative study on the vertebral column in the Gobioninae (Cyprinidae, Pisces) with special reference to its systematics. Publicaciones Especiales Instituto Espanol de Oceanografia 21: 149–167.

Nguyen LT, Schmidt HA, von Haeseler A, Minh BQ (2015) IQ-TREE: a fast and effective stochastic algorithm for estimating maximum-likelihood phylogenies. Molecular Biology and Evolution 32: 268–274. Otrishko MP, Emtyl MKh (2013a) History of the formation of the ichthyofauna of the Kuban River basin. Science Prospects 9(48): 19–21. https://doi.org/10.1093/molbev/msu300 [In Russian]

Palandačić A, Bravničar J, Zupančič P, Šanda R, Snoj A (2015) Molecular data suggest a multispecies complex of *Phoxinus* (Cyprinidae) in the Western Balkan Peninsula. Molecular Phylogenetics and Evolution 92: 118–123. https://doi.org/10.1016/j.ympev.2015.05.024

Palandačić A, Naseka A, Ramler D, Ahnelt H (2017) Contrasting morphology with molecular data: An approach to revision of species complexes based on the example of European *Phoxinus* (Cyprinidae). BMC Evolutionary Biology 17(1): 1–17. https://doi.org/10.1186/s12862-017-1032-x

Palandačić A, Kruckenhauser L, Ahnelt H, Mikschi E (2020) European minnows through time: museum collections aid genetic assessment of species introductions in freshwater fishes (Cyprinidae: *Phoxinus* species complex). Heredity 124(3): 410–422. https://doi.org/10.1038/s41437-019-0292-1

Perdices A, Vasil'eva E, Vasil'ev V (2015) From Asia to Europe across Siberia: Phylogeography of the Siberian spined loach (Teleostei, Cobitidae). Zoologica Scripta 44(1): 29–40. https://doi.org/10.1111/zsc.12085

Plater A (1861) Opisanie hydrograficzno-statystyczne Dźwiny zachodniéj, oraz ryb w niéj żyjących. W diukarni A. K. Kirkora, Wilno, 72 pp.

Ramler D, Palandačić A, Delmastro GB, Wanzenböck J, Ahnelt H (2016) Morphological divergence of lake and stream *Phoxinus* of Northern Italy and the Danube basin based on geometric morphometric analysis. Ecology and Evolution 7(2): 572–584. https://doi.org/10.1002/ece3.2648

Reshetnikov YuS, Popova OA, Sokolov LI, Tsepkin EA, Sideleva VG, Dorofeeva EA, Chereshnev IA, Moskvalkova KI, Dgebuadze YuYu, Ruban GI, Korolev VV (2003) Atlas of freshwater fishes of Russia in 2 volumes. Vol.1. Nauka, Moscow, 379 pp. [In Russian]

Rothe U, Weiß JD, Geiger M, Martinez N, Pfaender J (2019) *Phoxinus morella* a cryptic Species. In: Kottelat M (Ed.) Frontiers in Marine Science 6. XVI European Congress of Ichthyology, Lausanne (Switzerland). https://doi.org/10.3389/conf.fmars.2019.07.00127

Rothgänger J, Weniger M, Weniger T, Mellmann A, Harmsen D (2006) Ridom TraceEdit: A DNA trace editor and viewer. Bioinformatics 22(4): 493–494. https://doi.org/10.1093/bioinformatics/btk002

Sabaneev LP (1892) Pisces of Russia. Life and catching (fishing) of our freshwater fish. Vol. 2. Izdatelstvo A.A. Kartseva, Moscow, 423 pp. [In Russian]

Schönhuth S, Vukić J, Šanda R, Yang L, Mayden RL (2018) Phylogenetic relationships and classification of the Holarctic family Leuciscidae (Cypriniformes, Cyprinoidei). Molecular Phylogenetics and Evolution 127: 781–799. https://doi.org/10.1016/j.ympev.2018.06.026

Tang Y, Horikoshi M, Li W (2016) ggfortify: Unified interface to visualize statistical results of popular R packages. The R Journal 8(2): 474–485. https://doi.org/10.32614/RJ-2016-060

Taylor WR, Van Dyke GC (1985) Revised procedures for staining and clearing small fishes and other vertebrates for bone and cartilage study. Cybium 9: 107–109. https://doi.org/10.26028/cybium/1985-92-001

Tsvelev NN (2007) Environment and biological diversity of Berezovye Islands archipelago (the Gulf of Finland). Saint Petersburg, 368 pp. [In Russian]

Turan D, Bayçelebi E, Özuluğ M, Gaygusuz Ö, Aksu İ (2023) *Phoxinus abanticus*, a new species from the Lake Abant drainage in Türkiye (Teleostei, Leuciscidae). Journal of Fish Biology 102(5): 1157–1167. https://doi.org/10.1111/jfb.15371

Vinarski MV, Bolotov IN, Aksenova OV, Babushkin ES, Bespalaya YV, Makhrov AA, Nekhaev IO, Vikhrev IV (2021) Freshwater Mollusca of the Circumpolar Arctic: A review on their taxonomy, diversity and biogeography. Hydrobiologia 848(12–13): 2891–2918. https://doi.org/10.1007/s10750-020-04270-6

Wałecki A (1864) Systematyczny przegląd ryb krajowych. Drukarnia Gazety Polskiej, Warszawa, 93–94 pp.

Warpachowski NA (1889) A key to the fishes of the Volga Basin (description of the fishes of Nizhegorodskaya District). Imperial Academy of Sciences, St Petersburg, 113 pp. [In Russian.]

Wickham H, Averick M, Bryan J, Chang W, McGowan LDA, François R, Grolemund G, Hayes A, Henry L, Hester J, Kuhn M, Pedersen TL, Miller E, Milton Bache S, Müller K, Ooms J, Robinson D, Paige Seidel D, Spinu V, Takahashi K, Vaughan D, Wilke C, Woo K, Yutani H (2019) Welcome to the Tidyverse. Journal of Open Source Software 4(43): 1686. https://doi.org/10.21105/joss.01686

Xiang CY, Gao F, Jakovlić I, Lei HP, Hu Y, Zhang H, Zou H, Wang GT, Zhang D (2023) Using PhyloSuite for molecular phylogeny and tree-based analyses. iMeta 87(1): e87. https://doi.org/10.1002/imt2.87

Xie P, Ao M, Liu C, Zhang Z, Zhang Y, Niu J, Karjan A, Ma X (2016) The complete mitochondrial genome of *Phoxinus phoxinus ujmonensis* (Cypriniformes, Cyprinidae). Mitochondrial DNA. Part A, DNA Mapping, Sequencing, and Analysis 27(1): 212–213. https://doi.org/10.3109/19401736.2014.880893

Xu W, Chen A, Xia R, Fu C (2014) Complete mitochondrial genome of *Phoxinus tumensis* (Cypriniformes, Cyprinidae). Mitochondrial DNA 25(5): 368–369. https://doi.org/10.3109/19401736.2013.803096

Zhang D, Gao F, Jakovlić I, Zou H, Zhang J, Li WX, Wang GT (2020) PhyloSuite: An integrated and scalable desktop platform for streamlined molecular sequence data management and evolutionary phylogenetics studies. Molecular Ecology Resources 20(1): 348–355. https://doi.org/10.1111/1755-0998.13096

Zinoviev EA, Bogdanov VD (2017) On the possibility of the presence of Siberian fish forms in the Kama basin. Fauna of Ural and Siberia 2: 62–68. [In Russian]

Supplementary material 1

Additional and comparative materials

Authors: Oleg N. Artaev, Aleksey A. Bolotovskiy, Ilya S. Turbanov, Alexander A. Gandlin, Aleksey V. Kutuzov, Marina A. Levina, Danila A. Melentev, Ivan V. Pozdeev, Mikhail Ya. Borisov, Boris A. Levin

Data type: docx

Explanation note: Additional material on *Phoxinus isetensis* and comparative material on *P. adagumicus*, *P. chrysoprasius* and *P. colchicus*.

Link: https://doi.org/10.3897/zse.100.126702.suppl1

Supplementary material 2

Primary morphological data from type locality

Authors: Oleg N. Artaev, Aleksey A. Bolotovskiy, Ilya S. Turbanov, Alexander A. Gandlin, Aleksey V. Kutuzov, Marina A. Levina, Danila A. Melentev, Ivan V. Pozdeev, Mikhail Ya. Borisov, Boris A. Levin

Data type: xlsx

Explanation note: Primary morphological data of *Phoxinus isetensis* from type locality (Severka River).

Link: https://doi.org/10.3897/zse.100.126702.suppl2

Supplementary material 3

Comparsion of morphometrics

Authors: Oleg N. Artaev, Aleksey A. Bolotovskiy, Ilya S. Turbanov, Alexander A. Gandlin, Aleksey V. Kutuzov, Marina A. Levina, Danila A. Melentev, Ivan V. Pozdeev, Mikhail Ya. Borisov, Boris A. Levin

Data type: xlsx

Explanation note: Morphometrics of *Phoxinus isetensis*, *P. adagumicus*, *P. chrysoprasius*, *P. colchicus* and its comparison.

Link: https://doi.org/10.3897/zse.100.126702.suppl3

Supplementary material 4

Meristic and qualitative characters

Authors: Oleg N. Artaev, Aleksey A. Bolotovskiy, Ilya S. Turbanov, Alexander A. Gandlin, Aleksey V. Kutuzov, Marina A. Levina, Danila A. Melentev, Ivan V. Pozdeev, Mikhail Ya. Borisov, Boris A. Levin

Data type: xlsx

Explanation note: Meristic and qualitative characters of *Phoxinus isetensis* and other *Phoxinus* species published in the literature.

Link: https://doi.org/10.3897/zse.100.126702.suppl4

Supplementary material 5

Material for genetic studies

Authors: Oleg N. Artaev, Aleksey A. Bolotovskiy, Ilya S. Turbanov, Alexander A. Gandlin, Aleksey V. Kutuzov, Marina A. Levina, Danila A. Melentev, Ivan V. Pozdeev, Mikhail Ya. Borisov, Boris A. Levin

Data type: xlsx

Link: https://doi.org/10.3897/zse.100.126702.suppl5

Supplementary material 6

Best partition schemes

Authors: Oleg N. Artaev, Aleksey A. Bolotovskiy, Ilya S. Turbanov, Alexander A. Gandlin, Aleksey V. Kutuzov, Marina A. Levina, Danila A. Melentev, Ivan V. Pozdeev, Mikhail Ya. Borisov, Boris A. Levin

Data type: docx

Explanation note: The best partition schemes generated by ModelFinder v.2.2.0 (ML) and PartitionFinder v.2.1.1 (BI).

Link: https://doi.org/10.3897/zse.100.126702.suppl6

Supplementary material 7

ML tree

Authors: Oleg N. Artaev, Aleksey A. Bolotovskiy, Ilya S. Turbanov, Alexander A. Gandlin, Aleksey V. Kutuzov, Marina A. Levina, Danila A. Melentev, Ivan V. Pozdeev, Mikhail Ya. Borisov, Boris A. Levin

Data type: docx

Explanation note: ML phylogenetic tree of concatenated COI and cyt*b* mtDNA sequences.

Link: https://doi.org/10.3897/zse.100.126702.suppl7

Supplementary material 8

Genetic *p*-distances

Authors: Oleg N. Artaev, Aleksey A. Bolotovskiy, Ilya S. Turbanov, Alexander A. Gandlin, Aleksey V. Kutuzov, Marina A. Levina, Danila A. Melentev, Ivan V. Pozdeev, Mikhail Ya. Borisov, Boris A. Levin

Data type: xls

Explanation note: estimates of average evolutionary divergence over sequence pairs within and between *Phoxinus* species and clades.

Link: https://doi.org/10.3897/zse.100.126702.suppl8

Zoosyst. Evol. 100 (3) 2024, 1175–1190 | DOI 10.3897/zse.100.129009

PENSOFT

für Natur MUSEUM FÜR NATURKUNDE BERLIN

Another new ring nematode, *Xenocriconemella andreae* sp. nov. (Nematoda, Criconematidae), from the Iberian Peninsula

Carolina Cantalapiedra-Navarrete[1], Ilenia Clavero-Camacho[1], Inmaculada Criado-Navarro[1], Rosana Salazar-García[1], Ana García-Velázquez[1], Juan E. Palomares-Rius[1], Pablo Castillo[1], Antonio Archidona-Yuste[1]

1 *Instituto de Agricultura Sostenible, Departamento de Protección de Cultivos, Avenida Menén-dez Pidal s/n, 14004 Córdoba, Campus de Excelencia Internacional Agroalimentario, ceiA3, Spain*

https://zoobank.org/E691CFAF-0825-43EA-8756-952C32174072

Corresponding author: Antonio Archidona-Yuste (antonio.archidona@ias.csic.es)

Academic editor: A. Schmidt-Rhaesa ♦ **Received** 4 June 2024 ♦ **Accepted** 9 July 2024 ♦ **Published** 23 August 2024

Abstract

Nematode surveys in natural environments in the Iberian Peninsula detected three unidentified *Xenocriconemella* populations that closely resembled the *X. macrodora*-species complex, but utilization of integrative taxonomy confirmed that they comprised a new taxon described in this paper as *X. andreae* **sp. nov.** Only females were detected in the new species (considered parthenogenetic) and delineated with a bare body (274–353 µm); lip region with two annuli, continuous with body delineation; second lip annulus enclosed by the first one. Flexible and thin stylet (88.0–99.0 µm), representing 30.4–47.8% of total body length. The excretory pore is positioned 2–3 annuli posterior to the level of stylet knobs, at 101.5 (87–107) µm from the lip region. Female genital tract: monodelphic, prodelphic, large, and representing 34.4–52.4% of the body length; vagina slightly ventrally curved. The anus is located at (6–9) annuli from the rear end. Tail short, conoid, and blunt round terminus. Ribosomal and mitochondrial markers (D2-D3 expansion domains of 28S, ITS, partial 18S rRNA, and COI), as well as molecular phylogenetic analyses of sequences, confirmed this new taxon, and it was clearly delineated from *X. macrodora* and species within the species complex (*X. costaricense*, *X. iberica*, *X. paraiberica*, and *X. pradense*).

Key Words

COI, description, D2-D3, integrative taxonomy, ITS, 18S, morphometry

Introduction

The ring nematode genus *Xenocriconemella* De Grisse & Loof, 1965 (De Grisse and Loof 1965) includes small ringed ectoparasite nematodes with a stylet *ca.* 40% of their body length. This species has become a topic of scientific attention in recent years. Particularly relevant is the novel incorporation of integrative taxonomy studies in deciphering populations within this genus (Archidona-Yuste et al. 2024; Peraza-Padilla et al. 2024). This unlocked the long-established assumption that *Xenocriconemella macrodora* (Taylor 1936; De Grisse and Loof 1965) was the unique valid species within the genus. That is, recent integrative taxonomic studies added taxa within the genus *Xenocriconemella*, including the three new species described in the Iberian Peninsula (*X. iberica* Archidona-Yuste et al. 2024, *X. paraiberica* Archidona-Yuste et al. 2024, and *X. pradense* Archidona-Yuste et al. 2024) and the new one from Costa Rica (*X. costaricense* Peraza-Padilla et al. 2024). Undoubtedly, this has allowed us to support the validity and monophyly of this genus and has also confirmed the already reported strong association with forest and shrub ecosystems dominated mainly by *Quercus* trees (Bello et al. 1986; Gómez-Barcina et al. 1989; Escuer et al. 1999).

In Nematoda, and especially in plant-parasitic nematodes, it is quite typical that molecular differences are not manifested in variations in morphology among species (i.e., the occurrence of cryptic species complexes; Cantalapiedra-Navarrete et al. 2013; Archidona-Yuste et al. 2016, 2020; Cai et al. 2020; Clavero-Camacho et al. 2021). The integration and complementarity of different perspectives and methods of taxonomy is an imperative need for rigorous species delimitation within a cryptic complex (Proudlove and Wood 2003; Dayrat 2005; Fišer and Koselj 2022). Over the last 15 years, much research has been conducted on soil nematodes in this direction (particularly in plant-parasitic species; e.g., Gutiérrez-Gutiérrez et al. 2010; Barsi et al. 2017; Decraemer et al. 2024). The genus *Xenocriconemella* is a recent example where the transition from traditional to integrative taxonomy has unraveled a model cryptic complex of species (Archidona-Yuste et al. 2024). Indeed, molecular taxonomy together with in-depth morphological and morphometrical analyses defined the *X. macrodora*-species complex (*X. macrodora*, *X. iberica*, *X. paraiberica*, and *X. pradense*) from nematode populations widely distributed in the Iberian Peninsula (Archidona-Yuste et al. 2024). Furthermore, several studies have revealed a wide number of cryptic species complexes within a large functional variability of plant-parasitic nematodes in the Iberian Peninsula (e.g., Gutiérrez-Gutiérrez et al. 2010; Cantalapiedra-Navarrete et al. 2013; Archidona-Yuste et al. 2016, 2020; Cai et al. 2020; Archidona-Yuste et al. 2024; Decraemer et al. 2024; among others). Although it is well known that the Iberian Peninsula stands out as one of the most biodiverse regions on the planet (Myers et al. 2000), this great diversity detected in this area could also be due to the notable scientific effort in discovering the diversity of soil nematodes in this area developed in the last few years.

Here, to enhance soil nematode records and advance the understanding of taxonomy, morphology, and molecular data within the genus *Xenocriconemella*, we carried out a further sampling campaign on the *Quercus*-dominated natural areas of the Iberian Peninsula. In this nematode survey, we detected several unknown populations based on the available information (that is, morphological and molecular data) of *Xenocriconemella* species from the USA (Powers et al. 2021), Italy (Subbotin et al. 2005), Costa Rica (Peraza-Padilla et al. 2024), and the Iberian Peninsula (Archidona-Yuste et al. 2024). The original objective of this research was therefore to explore the morphological-morphometrical and molecular diversity of these unresolved *Xenocriconemella* populations in the Iberian Peninsula genus and to compare them with the available morphometrical and molecular data by Archidona-Yuste et al. (2024). The key goals of this research were to (i) describe the three newly discovered Iberian Peninsula species both morphologically and morphometrically and compare them with other *Xenocriconemella* species in the *X. macrodora*-species complex; (ii) obtain molecular information about these *Xenocriconemella* populations using ribosomal (D2-D3 expansion domains of 28S rRNA, ITS region, partial 18S rRNA) and COI markers; and (iii) review the phylogenetic relationships of *Xenocriconemella andreae* sp. nov. within Criconematidae spp. and the *X. macrodora*-species complex.

Materials and methods

Nematode isolation and morphometrical characterization

Continuing the nematode surveys for deciphering the molecular and morphological diversity of *Xenocriconemella* isolates in the natural environments of the Iberian Peninsula started by Archidona-Yuste et al. (2024), three additional samples were collected in the autumn of 2023 containing an unidentified *Xenocriconemella* species (Table 1). Samples were taken from the rhizospheric soil of the selected plants and mixed to establish a single sample from each sample point. The soil samples were taken from a depth of 5 to 40 cm. Afterward, nematode specimens were isolated from a 500 cm^3 soil sub-sample using the centrifugal-flotation method (Coolen 1979).

Materials and methods used for light microscopy (LM) and morphometric studies followed the same protocols described by Archidona-Yuste et al. (2024) and other researchers (Seinhorst 1966; De Grisse, 1969). The following abbreviations (i.e., measurements and ratios) are used in the morphological descriptions, data analyses, and figures: **L** (total body length); **a** = body length/maximal body width; **b** = body length/pharyngeal length; **c** = body length/tail length; **c'** = tail length/body width at anus; **O** = distance between stylet base and orifice of dorsal pharyngeal gland as a percentage of stylet length; **R** = total number of body annuli; **Roes** = number of annuli in the pharyngeal region; **Rex** = number of annuli between the anterior end of the body and the excretory

Table 1. Host-plant species and localities of the analyzed populations of *Xenocriconemella andreae* sp. nov. inside the *Xenocriconemella macrodora* (Taylor, 1936) De Grisse and Loof 1965 species-complex from the Iberian Peninsula in this study.

Nematode species	Code	Host-plant species	Locality, province, Country	Abundance	NCBI Accessions			
				(Nem/500 cm^3 soil)	D2-D3	ITS	18S	COI
Xenocriconemella andreae **sp. nov.**	SIN03	*Pistacia lentiscus* L.	Linhó, Sintra, Portugal (type)	103	PP833567–PP833569	PP833563-PP833564	PP833577–PP833579	PP831172–PP831174
Xenocriconemella andreae **sp. nov.**	HUA03	*Quercus suber* L.	Aroche, Huelva, Spain	13	PP833570	-	-	PP831175–PP831176
Xenocriconemella andreae **sp. nov.**	LEO02	*Castanea sativa* Mill.	Trabadelo, León, Spain	552	PP833571–PP833576	PP833565-PP833566	PP833580–PP833582	PP831177

pore; **Rst** = number of body annuli between labial disc and stylet knobs; **RV** = number of annuli between posterior end of body and vulva; **Rvan** = number of annuli between vulva and anus; **Ran** = number of annuli on tail; **V** = (distance from anterior end to vulva/body length) × 100; **VL/VB** = distance between vulva and posterior end of body divided by body width at vulva; **T** = (distance from cloacal aperture to anterior end of testis/body length) × 100 (Archidona-Yuste et al. 2023; 2024). The raw photographs were edited using Adobe Photoshop v. 22.5.2 (San Francisco, CA, USA).

Molecular analyses

Total genomic DNA was extracted from single nematode specimens as previously described by Archidona-Yuste et al. (2023, 2024). As in previous studies, all four molecular markers for each *Xenocriconemella* isolate were obtained from the same PCR tube from a single individual without any exception.

Similarly to other studies, primers for ribosomal (D2-D3 expansion domains of 28S rRNA, internal transcribed pacer region (ITS) rRNA, and the partial 18S rRNA) and mitochondrial (COI) markers were the same as those specified in previous papers (De Ley et al. 1999; Subbotin et al. 2001; Hu et al. 2002; Derycke et al. 2005; Holterman et al. 2006). The PCR cycling conditions were also as described in previous papers (De Ley et al. 1999; Subbotin et al. 2005; Holterman et al. 2006; Powers et al. 2021). The PCR products were treated and sequenced at the Stab Vida sequencing facility (Caparica, Portugal) (see Archidona-Yuste et al. 2024 for details). The sequence chromatograms of all markers were analyzed with DNASTAR LASERGENE SeqMan v. 7.1.0. The species identity of the DNA sequences obtained in this study was confirmed by the basic local alignment search tool (BLAST) at the National Center for Biotechnology Information (NCBI) (Altschul et al. 1990). The accomplished sequences were delivered to the GenBank database under accession numbers specified on the phylogenetic trees and in Table 1.

Species delineation analyses

We used two independent approaches to species delineation to resolve the species boundaries within the *X. macrodora* species complex, counting morphometric and molecular data.

First, we conducted a principal component analysis (PCA) to delimit species using morphometric data (Legendre and Legendre 2012). We established the species delimitation amongst the new *Xenocriconemella* populations found in the Iberian Peninsula and other species recently described within this genus, and we further evaluated the relationships between these new isolates and those previously designated within *Xenocriconemella*. PCA was constructed upon the following morphological characters: L, stylet length, R, Rst, Roes, Rex, RV, Rvan, Ran, and the ratios a, b, c, V, VL/VB (Archidona-Yuste et al. 2024). For this analysis, we chose 25 *X. macrodora* s.l. populations previously characterized and recorded from numerous countries (Archidona-Yuste et al. 2024), as well as 28 Iberian populations previously studied under an integrative taxonomical approach, including 13 belonging to *X. iberica*, 12 belonging to *X. paraiberica*, 3 belonging to *X. pradense*, and 1 belonging to *X. costaricense* from Costa Rica (Archidona-Yuste et al. 2024; Peraza-Padilla et al. 2024). After data standardization (Zuur et al. 2010), the diagnostic character-data set was tested for collinearity using the values of the variance inflation factor (VIF) as recommended by Montgomery et al. (2012). PCA was carried out by means of the PCA function supplied in the software package 'FactoMineR' (Lê et al. 2008). All data analyses were performed with R version 4.2.2 (R Core Team 2022; https://www.R-project.org).

Species delimitation with molecular data and to compute intra- and inter-species disparity was performed by the P ID liberal and Rosenberg's PAB value using the species delimitation plugin implemented in the software Geneious Prime v2022.1.1. (Geneious, Auckland, New Zealand) (Masters et al. 2011). Genetic distance was calculated based on intra- and interspecies molecular variations established by determining the ratio between the average genetic distance between specimens within a species and the average genetic distance between specimens belonging to sister species; if the ratio is less than 0.10, the probability of species identification is high (Masters et al. 2011). The P ID (liberal) value (Ross et al. 2008) means the likelihood that a correct species identification would be carried out using the closest genetic distance or placement on a tree (falling within or being sister to a monophyletic species clade). Taxa with a P ID (liberal) ≥ 0.93 were considered to be satisfactorily demarcated (Hamilton et al. 2014). Rosenberg's P_{AB} means the likelihood that the monophyly of a group of sequences is the result of random branching; significant values were <0.05 (Rosenberg 2007).

Phylogenetic analyses

Methods and software programs for aligning, sequence edition, and phylogenetic analyses were performed following the same procedures already specified in previous papers, including outgroup selection and tree visualization (Hall 1999; Ronquist and Huelsenbeck 2003; Darriba et al. 2012; Tan et al. 2015; Rambaut, 2018; Katoh et al. 2019; Etongwe et al. 2020; Nguyen et al. 2022; Archidona-Yuste et al. 2024). The best-fit models for each marker were: the transitional model with invariable sites and a gamma-shaped distribution (TIM3 + I + G) for the D2-D3 expansion domains of 28S rRNA; the general time-reversible model with invariable sites and a gamma-shaped distribution (GTR + I + G) for ITS and the partial 18S rRNA gene; and the 3-parameter model with invariable sites and a gamma-shaped distribution (TPM3uf + I + G) for the COI gene.

Results

Low to moderate densities (312, 13, -552 nematodes/500 cm^3 of soil) of the currently characterized isolates of *Xenocriconemella* were determined in the soil samples collected from the rhizosphere of mastic tree, cork oak, and chestnut Linhó, Sintra region, Portugal, Aroche, Huelva province, Spain, and Trabadelo, Leon province, Spain, respectively. Comprehensive morphological, morphometric, and molecular data about this species are supplied below, confirming its identification as a new taxon within the *Xenocriconemella macrodora*-species complex.

Species delineation using morphometry

Our PCA results showed a wide intraspecific variation amongst the specimens of *Xenocriconemella* spp., especially for *X. iberica* and *X. paraiberica*, based on the wide morphometric variation in the following features: R, Rv, Roes, Rst, Rex, Stylet, V, and (VL/VB), confirming that previously described by Archidona-Yuste et al. (2024) (Fig. 1). As anticipated, we confirmed the high morphological variation displayed by *X. macrodora* (Archidona-Yuste et al. 2024). PCA clearly distinguished between almost all the individuals of *X. andreae* sp. nov., *X. pradense*, and *X. costaricense*, as well as those identified within *X. iberica* and *X. paraiberica*. However, this spatial separation occurred to a lower degree between *X. pradense* and *X. iberica*, where some individuals were found close to each other (Fig. 1). This species segregation was mostly observed along the first and second dimensions (Dim 1 and Dim2; 38.57 and 21.9% of the total variance, respectively). Dim1 was largely dominated by R, Rv, Roes, Rst, Rex, stylet length, and VL/VB (Fig. 1). On the other hand, Dim2 was mainly dominated by the Rvan and c ratio, thereby relating this dimension to the posterior part of the nematode. Except in specific cases, the delimitation of species boundaries provided by the PCA occurs through a linear combination of multiple diagnostic characters (Archidona-Yuste et al. 2016, 2024). Thus, we detected that species separations were mainly based on a combination of the following diagnostic characters: R, Roes, Rst, Rex, Rv, Rvan, c ratio, and stylet length. More explicitly, individuals with higher values in R, Rv, Roes, Rst, Rex, and Rv and longer stylet length were located on the right (i.e., *X. pradense* and *X. costaricense*), and those with lower values for these characters were located on the left side along Dim1 (i.e., *X. paraiberica and X. andreae* sp. nov.). Likewise, specimens with higher values of Rvan and c ratio (that is, longer length in the posterior part of the body) were located at the top (i.e., *X. costaricense* and *X. andreae* sp. nov.), and those with lower values for these characters were located at the bottom side along the Dim2 (i.e., *X. pradense*). Ultimately, we could conclude that Roes, Rst, Rex, and Rv were the most useful morphometrics for separating species within this cryptic complex in the genus *Xenocriconemella*. However, most of the specimens of *X. iberica* and *X. paraiberica* were located overlying each other, given their similar values for traits associated with Dim 1 and Dim2 (Fig. 1). Thus, we confirmed that both species are strictly related morphologically. Additionally, we found an analogous arrangement for individuals (i.e., mean values of isolates) of *X. macrodora* as described by Archidona-Yuste et al. (2024). Definitively, our data confirmed the idea that these already described species (i.e., *X. iberica*, *X. paraiberica*, and *X. pradense*) encompass a model complex of cryptic species (i.e., the *X. macrodora* species complex). However, PCA allowed us to separate the new taxa *X. andreae* sp. nov. and the already described species (*X. costaricense*) from this species cryptic complex.

Species delineation using ribosomal and mitochondrial DNA

Species delineation using ribosomal and mitochondrial markers proved that *X. andreae* sp. nov., *X. iberica*, *X. paraiberica*, *X. pradense*, and *X. costaricense* were undoubtedly distinguished among them, as were *X. macrodora* from the USA and Italy. The ratio between intra- and inter-species molecular variation for the D2–D3 expansion domains of 28S rRNA and the ITS region of all four Iberian Peninsula species was very low (0.01–0.08). In contrast, COI variation was higher in *X. macrodora* (0.33), followed by *X. iberica* (0.18). *X. paraiberica* (0.18), *X. andreae* sp. nov. (0.15), *X. pradense* (0.09), and *X. costaricense* (0.03), confirming that COI is more diversified in the USA than in the Iberian Peninsula and Costa Rica populations (Table 2). However, for all five species, the D2-D3 expansion domains of 28S rRNA and ITS genes undoubtedly displayed intra- and inter-species molecular variation (Table 2), signifying that the likelihood of species separation with these loci was high (Ross et al. 2008). Similarly, the P ID (liberal) values for all six species and loci were > 0.93 (the probability for P ID (liberal) to be considered adequately delimited in the species delimitation is $P \geq 0.93$), signifying that the six *Xenocriconemella* species can be adequately separated (Ross et al. 2008; Hamilton et al. 2014). The P ID (liberal) value (Ross et al. 2008) reveals the likelihood that a precise species identification would be completed using BLAST, the closest genetic distance, or placement on a tree. Species with a P ID (liberal) ≥ 0.93 were considered to be adequately delimited (Hamilton et al. 2014). Additionally, all clades were well-supported (PP = 1.00) in the phylogenetic trees for the three loci, and Rosenberg's PAB values also supported the monophyly (Rosenberg's significant values = $P < 0.05$) of the six species distinctly (Rosenberg 2007).

Ribosomal and mitochondrial DNA characterization

Xenocriconemella andreae sp. nov. was molecularly characterized by the sequences of three ribosomal genes, D2-D3 expansion domains of 28S rRNA, ITS rRNA,

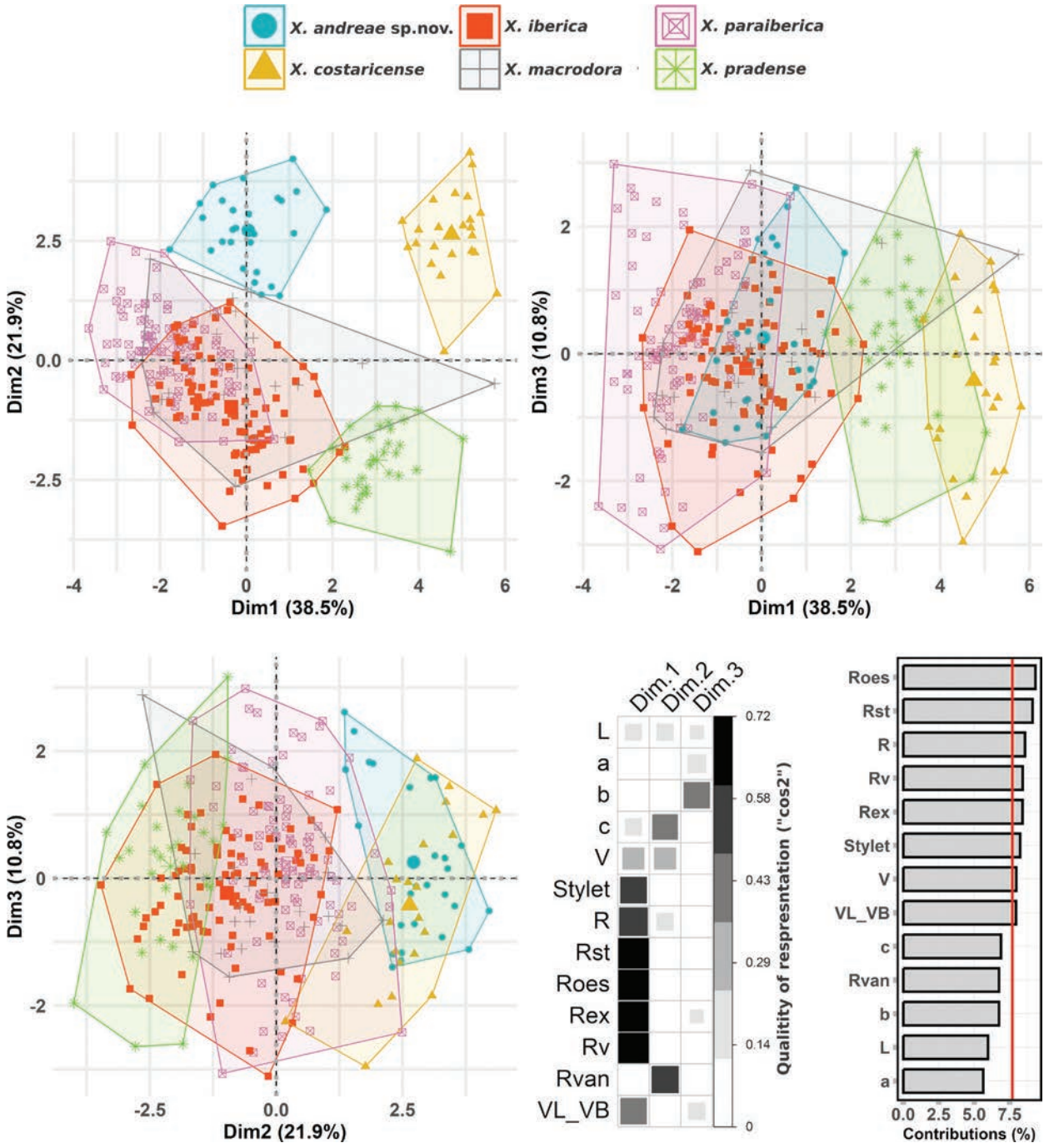

Figure 1. Principal component of the *Xenocriconemella macrodora* species complex. Projections of species on the plane of dimensions 1 and 2, 1 and 3, and 2 and 3. Correlation plot between dimensions and qualities of representation of the morphometric characters ("square cosine" (cos2)). Barplot showing the standardized contribution (%) of morphometric variables for the three dimensions retained by the PCA (only dimensions with sum of squares (SS) loadings > 1 were extracted). A reference soil (red) line is also shown on the barplot. This reference line corresponds to the expected value if the contribution were uniform. For a given dimension, any row or column with a contribution above the reference line could be considered important in contributing to the dimension.

and partial 18S rRNA, and the mitochondrial gene COI. The amplification of these regions yielded single fragments of approximately 800, 800, 1600, and 400 bp, respectively, based on gel electrophoresis. Ten D2-D3 expansion domains of 28S rRNA sequences from 676 to 714 bp (PP833567–PP833576), four ITS rRNA sequences from 677 to 830 bp (PP833563–PP833566), six 18S rRNA sequences from 1681 to 1708 bp (PP833577–PP833582), and six COI sequences from 368 to 385 bp (PP831172–PP831177) were generated for this new species. Intraspecific sequence variations in ribosomal and mitochondrial markers were low in D2-D3 expansion domains of 28S rRNA (99.5–100.0%, 1–3 bp and 0 indel), in the ITS region (99.1–100.0%, 0–6 bp and 0–3 indels),

Table 2. Parameters evaluating *Xenocriconemella macrodora* species-complex delimitation based on two rRNA genes (D2-D3 expansion segments of the 28S rRNA, ITS) and one mtDNA barcoding locus, COI, for six *Xenocriconemella* species of the complex.

Species	Gene	Intra/Inter [a]	P ID (Liberal) [b]	Clade Support [c]	Rosenberg's P_{AB} [d]
Xenocriconemella macrodora	D2-D3	-	-	-	-
	ITS	-	-	-	-
	COI	0.33	**0.97 (0.94, 0.99)** [e]	**1.00**	**1.2×10^{-31}**
Xenocriconemella andreae **sp. nov.**	D2-D3	0.08	**0.98 (0.93, 1.0)**	**1.00**	**5.6×10^{-7}**
	ITS	0.04	**0.97 (0.86, 1.0)**	**1.00**	**1.1×10^{-3}**
	COI	0.15	**0.96 (0.86, 1.0)**	**1.00**	**1.1×10^{-9}**
Xenocriconemella iberica	D2-D3	0.04	**0.98 (0.87, 1.0)**	**1.00**	**9.7×10^{-5}**
	ITS	0.02	**0.98 (0.87, 1.0)**	**1.00**	**4.1×10^{-3}**
	COI	0.18	**0.98 (0.95, 1.0)**	**1.00**	**1.1×10^{-9}**
Xenocriconemella paraiberica	D2-D3	0.05	**0.97 (0.87, 1.0)**	**1.00**	**1.1×10^{-3}**
	ITS	0.03	**0.97 (0.86, 1.0)**	**1.00**	**1.1×10^{-3}**
	COI	0.18	**0.98 (0.95, 1.0)**	**1.00**	**4.9×10^{-7}**
Xenocriconemella pradense	D2-D3	0.03	**0.98 (0.87, 1.0)**	**1.00**	**0.04**
	ITS	0.01	**0.98 (0.87, 1.0)**	**1.00**	**4.1×10^{-3}**
	COI	0.09	**0.98 (0.93, 1.0)**	**1.00**	**0.00**
Xenocriconemella costaricense	D2-D3	0.04	**0.97 (0.86, 1.0)**	**1.00**	**1.1×10^{-3}**
	ITS	0.02	**0.97 (0.82, 1.0)**	**1.00**	**4.9×10^{-3}**
	COI	0.03	**0.97 (0.86, 1.0)**	**1.00**	**4.9×10^{-7}**

[a] Intra-species variation relative to inter-species variation. [b] The P ID (liberal) value represents the probability (with the 95% confidence interval) for making a correct identification of an unknown specimen of the focal species using DNA barcoding (closest genetic distance). P ID (liberal) values ≥ 0.93 were considered to be significantly delimited (Hamilton et al. 2014). Numbers in bold represent significant values. [c] Clade support: posterior probabilities from Bayesian trees. [d] Rosenberg's P_{AB} value is the probability that the monophyly of a group of sequences is the result of random branching; Rosenberg's significant values = $P < 0.05$. [e] Significant results are indicated in bold. (-) Not obtained or performed because only a single sequence of D2-D3 or ITS for this species is available in NCBI.

in 18S rRNA (99.8–100.0%, 0–3 bp and 0 indel), and in COI (97.8–100.0%, 0–8 bp and 0–1 indel). D2-D3 expansion domains of 28S rRNA of *X. andreae* sp. nov. (PP833567–PP833576) were 95.0–94.6% similar (differing by 33–41 bp, 2–4 indels) to *X. paraiberica* from Spain (OR880152–OR880200), 93.3–93.5% similar (differing by 33–44 bp, 0 indels) to *X. costaricense* from Costa Rica (PP209388–PP209391), 92.3–92.7% similar (differing by 49–50 bp, 3 indels) to *X. iberica* from Spain and Portugal (OR880112–OR880149), 91.0–91.3% similar (differing by 58 bp, 1 indel) to *X. pradense* from Spain (OR880203–OR880217), and 91.4–91.2% similar (differing by 47–48 bp, 1 indel) to *X. macrodora* from Italy (AY780960). ITS of *X. andreae* sp. nov. (PP833563–PP833566) was 82.7% similar (differing by 138 bp, 51 indels) to *X. costaricense* from Costa Rica (PP209397, PP209398), 80.9–81.1% similar (differing by 165–167 bp, 102–103 indels) to *X. paraiberica* from Spain (OR878338–OR878349), 80.8% similar (differing by 161 bp, 49 indels) to *X. pradense* (OR878350), 79.5% similar (differing by 173–174 bp, 76–77 indels) to *X. iberica* (OR878332–OR878336), and 78.2–78.6% similar (differing by 64–65 bp, 33–34 indels) to *X. macrodora* from USA (JQ708139), but with a low coverage (50–59%). Partial 18S rRNA of *X. andreae* sp. nov. (PP833577–PP833582) was 98.8% similar (differing by 20 bp, 5 indels) to *X. paraiberica* (OR878358), 98.6–98.7% similar (differing by 23–24 bp, 3–4 indels) to *X. macrodora* (MF094906, MF094973, MF095001), 98.2–98.5% similar (differing by 25–30 bp, 3 indels) to *X. costaricense* (PP209396), 97.9–98.1% similar (differing by 32–35 bp, 5 indels) to *X. pradense* (OR878360–OR878361), and 97.8% similar (differing by 37 bp, 5 indels) to *X. iberica* (OR878356). Finally, COI of *X. andreae* sp. nov. (PP831172–PP831177) was 92.5–93.4% similar (differing by 23–27 bp, 0–1 indel) to *X. iberica* from Spain and Portugal (OR885936–OR885976), 90.3–92.0% similar (differing by 28–36 bp, 0–1 indel) to *X. paraiberica* from Spain (OR885983–OR886017), 89.1% similar (differing by 41–36 bp, 1 indel) to *X. costaricense* from Costa Rica (PP210897–PP210900), 89.0–91.7% similar (differing by 37–46 bp, 1 indel) to *X. macrodora* from USA (MF770894–MF770950, MN711386–MN711444), and 89.8–90.2% similar (differing by 31–32 bp, 1 indel) to *X. pradense* from Spain (OR886020–OR886029).

Phylogenetic analysis

Phylogenetic analysis among *Xenocriconemella* species, based on the D2–D3 expansion domains of 28S, ITS, the partial 18S rRNA, and the partial COI mtDNA gene sequences, was carried out using BI (Figs 2, 3, 4, 5, respectively). The phylogenetic trees created with the ribosomal and mitochondrial DNA markers included 78, 61, 94, and 171 sequences, and their alignment had 702, 728, 1694, and 360 characters, respectively. The Bayesian 50% majority rule consensus tree inferred from the D2-D3 expansion domains of the 28S rRNA alignment is given in Fig. 2. For this ribosomal marker, all six species belonging to the genus *Xenocriconemella* clustered together in a well-supported clade (PP = 1.00), clearly separated from all other genera within Criconematidae (Fig. 2). The *Xenocriconemella* clade was subdivided into four subclades; one of them (PP = 1.00) comprises all the sequences for *X. andreae* sp. nov. (PP833567–PP833576), followed by another one (PP = 0.96) including *X. paraiberica* (OR880152–OR880202) and *X. costaricense* (PP209388–PP209391), the third one (PP = 0.99) comprises *X. pradense* (OR880203–OR880218) and the single sequence for *X. macrodora* from Italy (AY780960), and the fourth subclades include *X. iberica* (OR880107–OR880151).

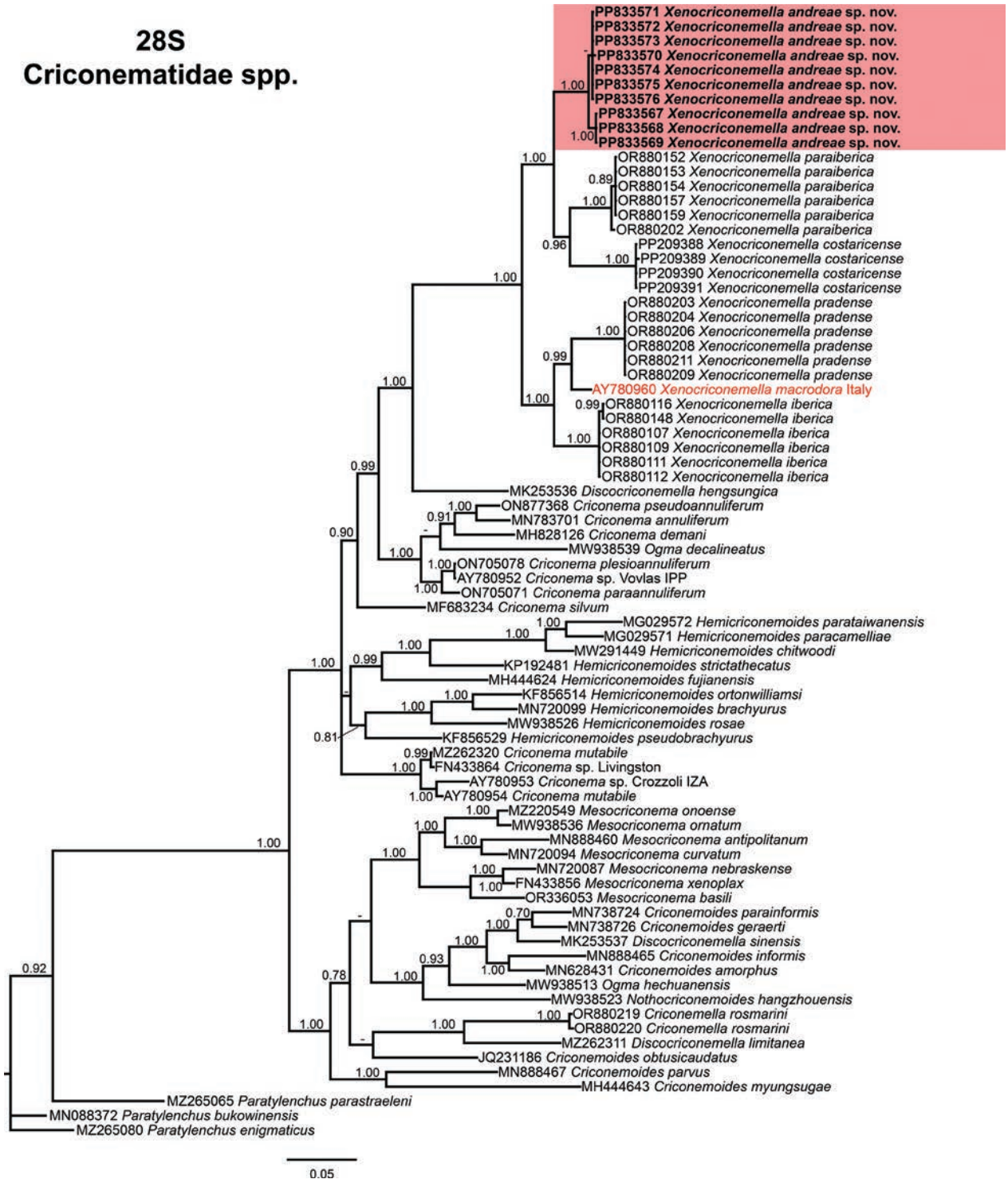

Figure 2. Phylogenetic relationships of *Xenocriconemella andreae* sp. nov. with Criconematidae spp. Bayesian 50% majority rule consensus tree as inferred from D2 and D3 expansion domains of 28S rRNA sequence alignment under the TIM3 + I + G model (−lnL = 8665.6142; AIC = 17655.228420; freqA = 0.1888; freqC = 0.2391; freqG = 0.3304; freqT = 0.2418; R(a) = 0.4795; R(b) = 1.6113; R(c) = 1.0000; R(d) = 0.4795; R(e) = 4.0922; R(f) = 1.0000; Pinva = 0.4170; and Shape = 0.9390). Posterior probabilities greater than 0.70 are given for appropriate classes. The newly obtained sequences in this study are shown in bold, and colored boxes indicate the clade association of the new species. Scale bar: expected changes per site.

In the ITS region tree (Fig. 3), phylogenetic relationships showed all *Xenocriconemella* species, except for *X. macrodora* from the USA (JQ708139), within a well-supported clade (PP = 1.00), undoubtedly separated from all other genera of Criconematidae. This clade was subdivided into two subclades, one of them (PP = 1.00), comprising all the sequences for *X. andreae* sp. nov. (PP833563–PP833566), *X. paraiberica* (OR878338–

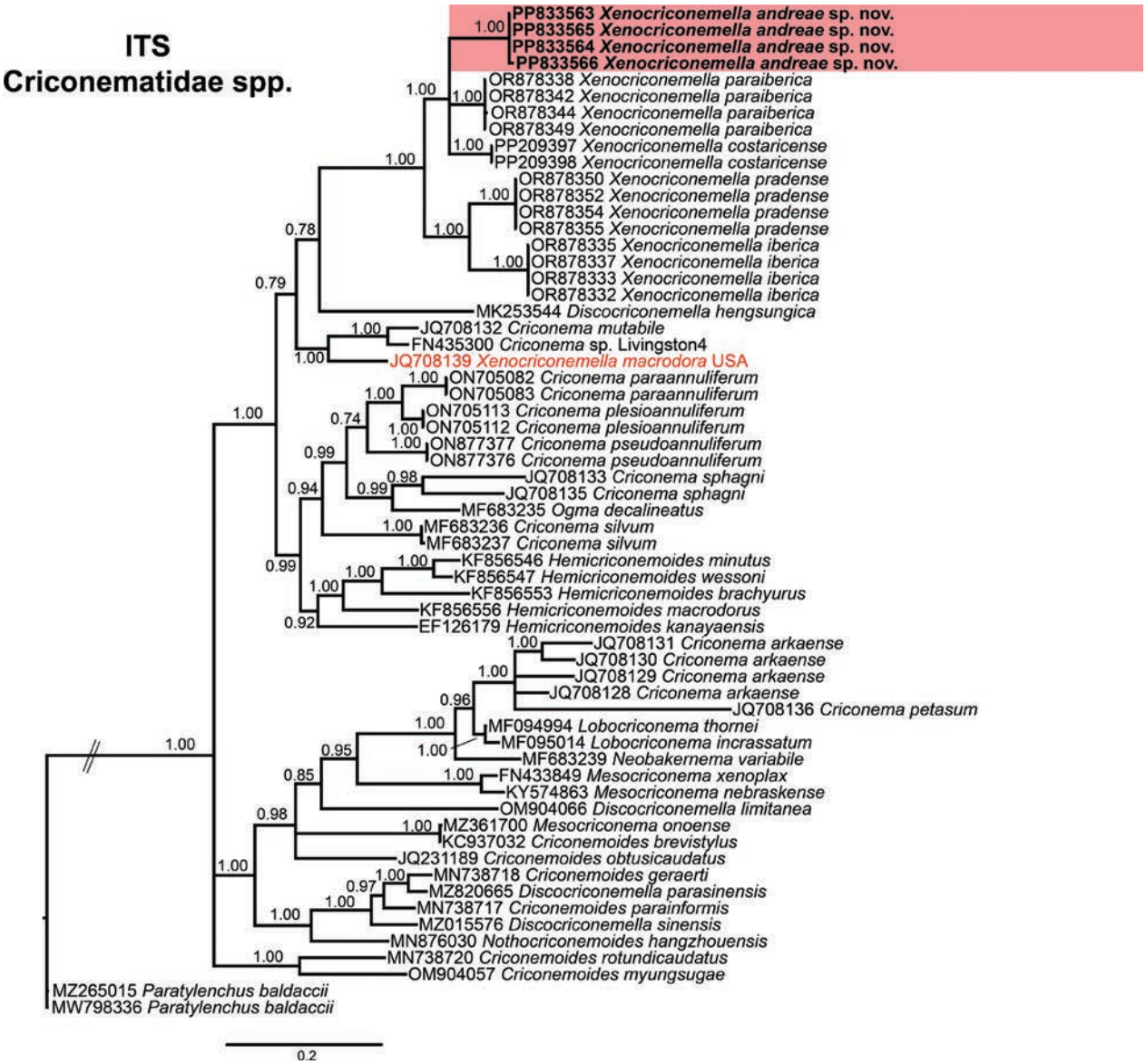

Figure 3. Phylogenetic relationships of *Xenocriconemella andreae* sp. nov. with Criconematidae spp. Bayesian 50% majority rule consensus tree as inferred from ITS rRNA sequence alignment under the GTR + I + G model (−lnL = 11773.3526; AIC = 23086.70524; freqA = 0.2179; freqC = 0.2568; freqG = 0.2584; freqT = 0.2669; R(a) = 1.3037; R(b) = 2.5717; R(c) = 1.7862; R(d) = 06486; R(e) = 2.8826; R(f) = 1.0000; Pinva = 0.1410; and Shape = 0.8680). Posterior probabilities greater than 0.70 are given for appropriate classes. The newly obtained sequences in this study are shown in bold, and colored boxes indicate the clade association of the new species. Scale bar: expected changes per site.

OR878349), and *X. costaricense* (PP209397–PP209398), and the second one (PP = 1.00), comprising sequences from *X. pradense* and *X. iberica*. *Xenocriconemella macrodora* from the USA (JQ708139) clustered with a low support (PP = 0.79) from the rest of *Xenocriconemella* spp. (and also with *Discocriconemella hengsungica*, MK253544), establishing a well-supported subclade with *Criconema mutabile* (JQ708132) and *Criconema* sp. 4 Livingston (FN435300).

In 18S rRNA phylogeny (Fig. 4), all the sequences included in the genus *Xenocriconemella* clustered in a well-supported clade (PP = 1.00), situated at the top of the tree (Fig. 4). This clade was subdivided into six subclades, each one separating a different *Xenocriconemella* species, including *X. costaricense* (PP209392–PP209396), *X. macrodora* (MF095001, MF094973, MF094906, and JF972482), *X. iberica* (OR878356–OR878357), *X. pradense* (OR878360–OR878361), *X. paraiberica* (OR878358–OR878359), *X. andreae* sp. nov. (PP833577–PP833582), and *X. macrodora* from Portugal (MT229843) (Fig. 4).

Lastly, using COI gene sequences, the phylogenetic position of *X. andreae* sp. nov. (PP831172–PP831177) and all other *Xenocriconemella* species was shown in Fig. 5. The phylogenetic position of *X. andreae* sp. nov. was well separated from other species of the genus (PP = 1.00),

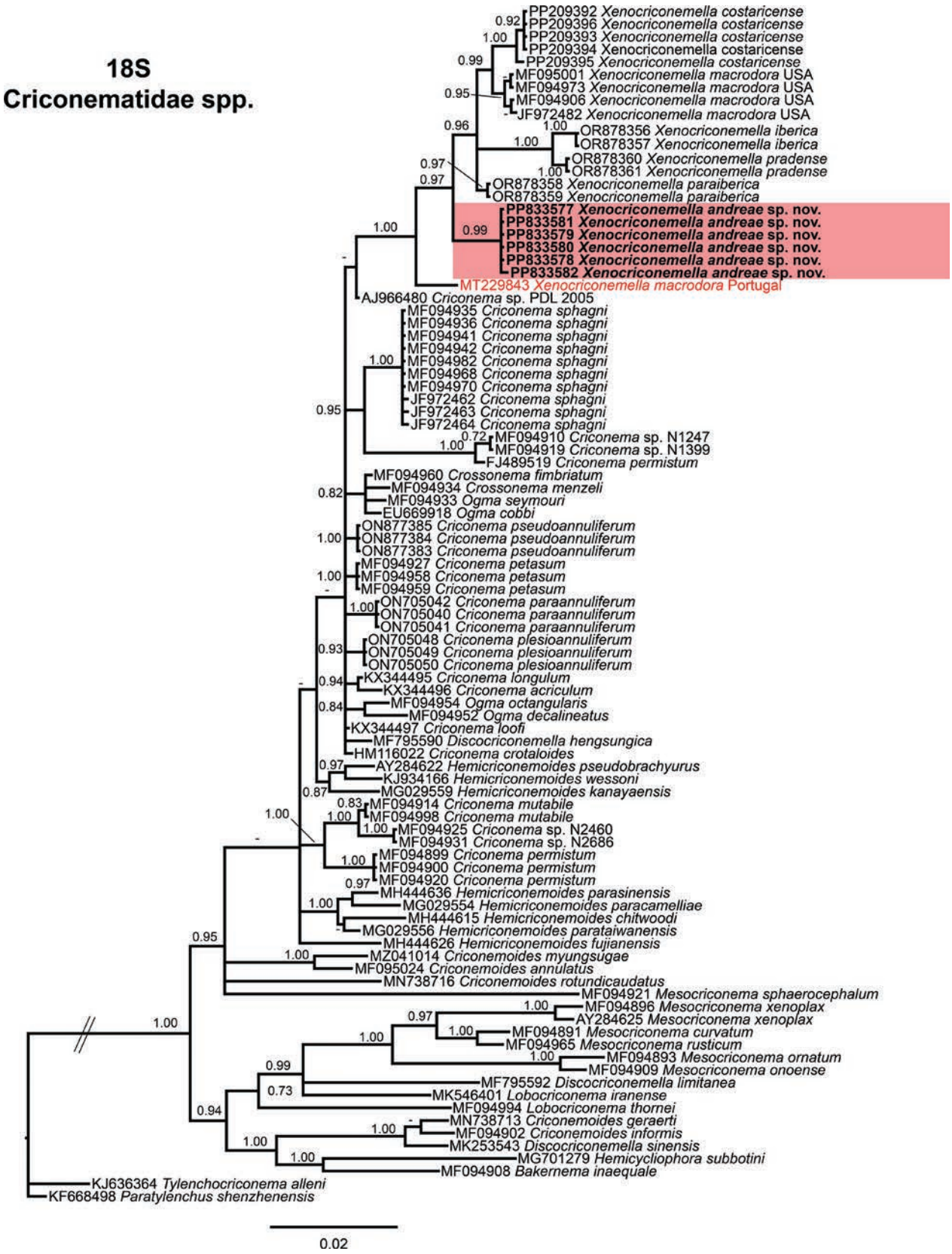

Figure 4. Phylogenetic relationships of *Xenocriconemella andreae* sp. nov. with Criconematidae spp. Bayesian 50% majority rule consensus tree as inferred from 18S rRNA sequence alignment under the GTR + I + G model (−lnL = 7859.2560; AIC = 16114.51198; freqA = 0.2451; freqC = 0.2388; freqG = 0.2784; freqT = 0.2378; R(a) = 1.4017; R(b) = 2.0249; R(c) = 1.0058; R(d) = 0.6630; R(e) = 5.7196; R(f) = 1.0000; Pinva = 0.6610; and Shape = 0.5740). Posterior probabilities greater than 0.70 are given for appropriate classes. The newly obtained sequences in this study are shown in bold, and colored boxes indicate the clade association of the new species. Scale bar: expected changes per site.

Figure 5. Phylogenetic relationships of *Xenocriconemella andreae* sp. nov. with other *Xenocriconemella* spp. Bayesian 50% majority-rule consensus trees as inferred from cytochrome c oxidase subunit I (COI) mtDNA gene sequence alignments under the TPM3uf + I + G model (−lnL = 2464.7614; AIC = 5639.5228; freqA = 0.3727; freqC = 0.0511; freqG = 0.0810; freqT = 0.4953; R(a) = 1.7003; R(b) = 9.5660; R(c) = 1.0000; R(d) = 1.7003; R(e) = 9.5660; R(f) = 1.0000; Pinva = 0.3460; and Shape = 0.4040). Posterior probabilities greater than 0.70 are given for appropriate classes. The newly obtained sequences in this study are shown in bold, and colored boxes indicate the clade association of the new species. Scale bar = expected changes per site.

but the phylogenetic relationship with them was not well resolved (Fig. 5). Sequences from *X. macrodora* from the USA appeared together in a well-supported (PP = 1.00) subclade.

Taxonomy

Phylum: Nematoda Rudolphi, 1808
Class: Chromadorea Inglis, 1983
Order: Rhabditida Chitwood, 1933
Suborder: Tylenchina Chitwood, 1950
Superfamily: Criconematoidea Khan & Ahmad, 1975
Family: Criconematidae Taylor, 1936
Genus: *Xenocriconemella* De Grisse & Loof, 1965

***Xenocriconemella andreae* sp. nov.**
https://zoobank.org/1A7BEE7F-3C2A-4E9F-8031-F5AD3C1300E2

Description. Females. Body ventrally arcuate to straight, slightly narrowing anteriorly and posteriorly. Body annuli smooth and retrorse 2.6 (2.5–3.0) µm wide, without anastomosis (Fig. 6). Lip region with two annuli, not offset, not separated from body contour; first lip annulus partially covering the second lip annulus (Fig. 6); second lip annulus retrorse and slightly wider than first annulus 9.1 (8.0–10.0) µm wide. Stylet thin, long, and flexible (Figs 6, 7, Table 3), occupying 31 (27.2–-35.0)% of the body length, with short basal portion 7.2 (7.0–8.0) µm long and knobs slightly rounded 5.1 (5.0–6.0) µm wide. Pharynx typical criconematoid, with a cylindroid procorpus widening to a large muscular oval median bulb containing well-developed valves (8.0–9.5 µm long), istmus slender, and amalgamated with basal bulb. Excretory pore located from two to three annuli posterior to level of stylet knobs, at 102 (87.0–107.0) µm from anterior end. Nerve ring located at the level of istmus, 116 (103–124) µm from the anterior end. Vagina ventrally curved (14.0–17.0 µm long). Female genital tract monodelphic, prodelphic, outstretched, and occupying 43 (34.4–52.4)% of the body length; spermatheca almost hemispherical (11.0–14.0 × 12.5–18.0) µm, sperm absent. Anus located at 7.7 (6–9) annuli from the terminus. Tail short, conoid, and bluntly rounded terminus.

Males. Not found.

Juveniles. Body similar to females, including tail shape, but shorter. Edge of body annuli without appendages, marked with delicate irregular punctations.

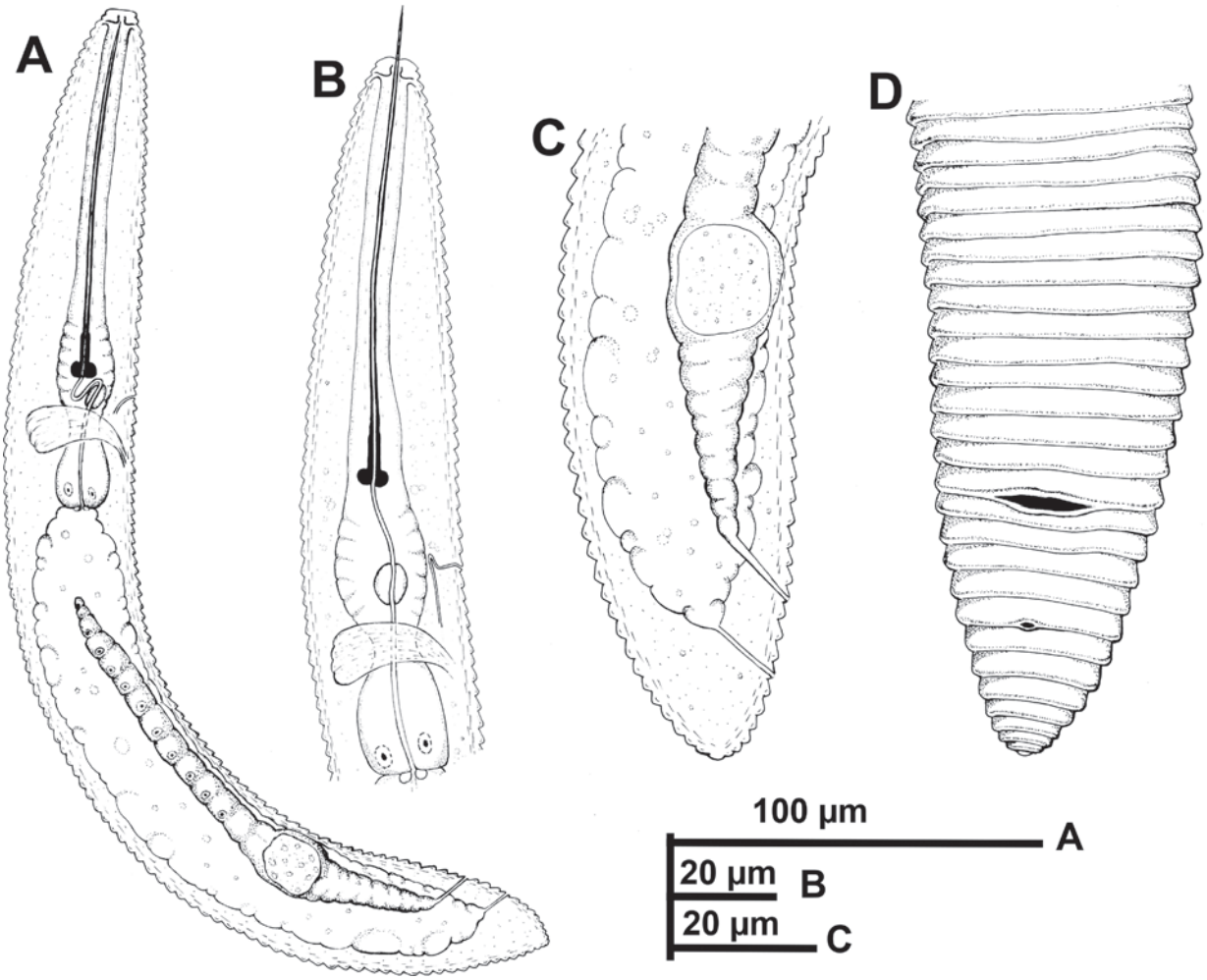

Figure 6. *Xenocriconemella andreae* sp. nov. (drawings). **A.** Entire female; **B.** Female anterior region; **C, D.** Detail of female posterior region showing vulva and anus.

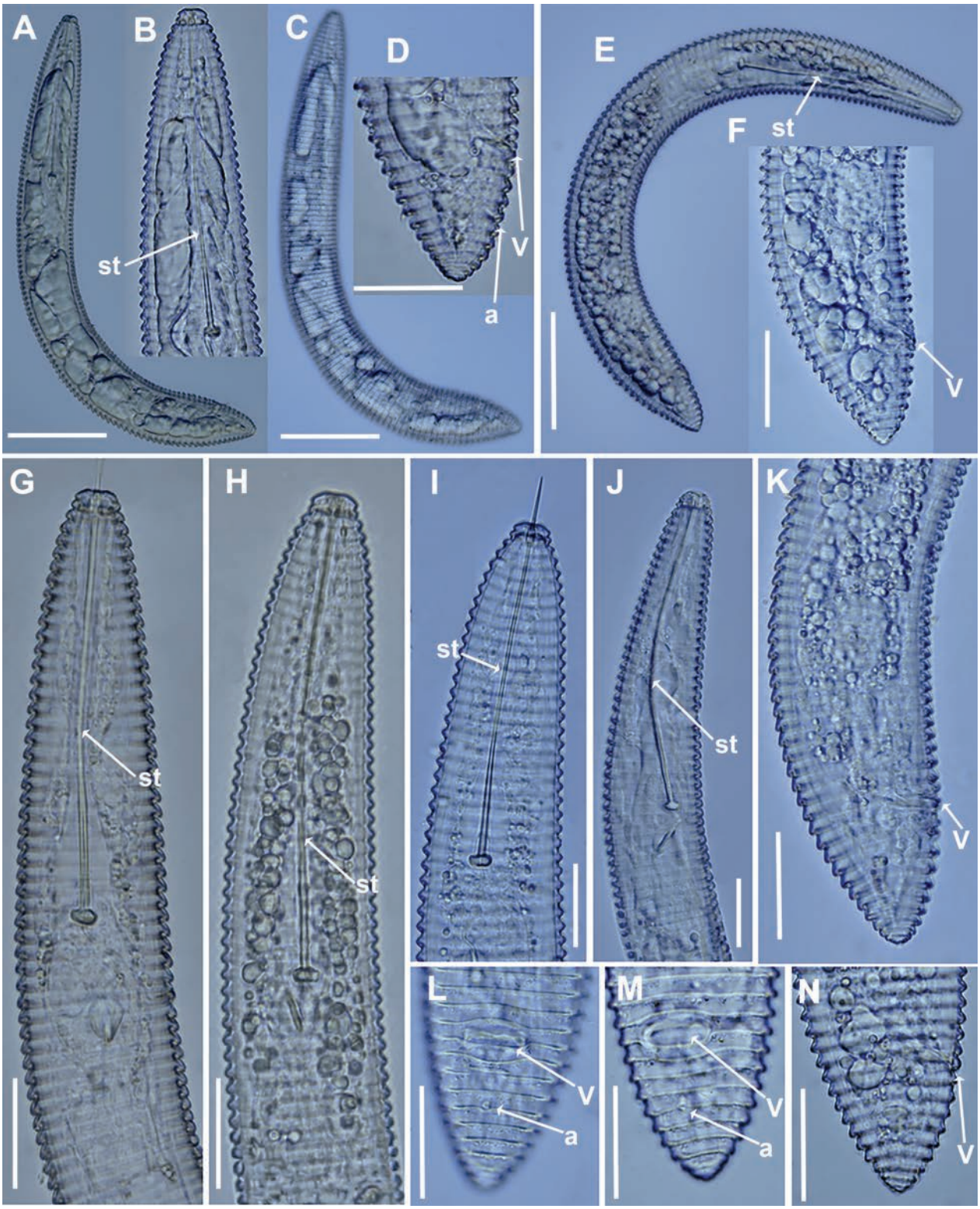

Figure 7. Light micrographs of *Xenocriconemella andreae* sp. nov. **A, E.** Entire female; **C.** Entire female showing body annuli without anastomosis; **B, G–J.** Female anterior body region showing stylet (arrowed); **D, F, K–N.** Vulval region showing vulva and anus (arrowed). Abbreviations: a = anus; st = stylet; V = vulva. Scale bars: 50 µm (**A, C, E**); 20 µm (**B, D, F–N**).

Diagnosis and relationships. *Xenocriconemella andreae* sp. nov. is characterized by the following measurements and ratios: a short-sized female body 307 (274–353) µm, a long and flexible stylet = 94.6 (88.0–99.0) µm long, V = 92 (90.2–92.5), a = 10.2 (8.4–12.2), b = 2.3 (2.1–2.6), c = 26.3 (21.9–32.5), c' = 0.7 (0.6–0.8), R = 113 (105–119), RV = 10.7 (9–12), Ran = 7.7 (6–9), VL/VB = 1.0 (0.8–1.1). Morphologically and morphometrically,

Table 3. Morphometrics of *Xenocriconemella andreae* sp. nov. from the rhizosphere of mastic tree, cork oak, and chestnut from Linhó, Sintra region, Portugal; Aroche, Huelva province, Spain; and Trabadelo, León province, Spain [1].

Character[1]	Portugal		Spain	
	Holotype	Paratype Females	Aroche, Huelva province	Trabadelo, León province
n	1	20	3	4
L	302	307.2 ± 21.0 (274–353)	331.3 ± 24.7 (303–348)	341.3 ± 12.9 (323–353)
R	114	112.5 ± 4.1 (105–119)	110.7 ± 2.9 (109–114)	114.3 ± 2.9 (111–118)
Rst	35	36.0 ± 2.4 (31–40)	34.7 ± 0.6 (34–35)	34.5 ± 1.3 (33–36)
Roes	47	47.7 ± 2.6 (42–52)	45.3 ± 1.2 (44–46)	46.0 ± 1.4 (45–48)
Rex	38	38.5 ± 2.6 (33–43)	37.0 ± 1.0 (36–38)	36.8 ± 1.0 (36–38)
RV	10	10.7 ± 0.8 (9–12)	12.3 ± 0.6 (12–13)	11.3 ± 1.0 (10–12)
Rvan	3	3.0 ± 0.0 (3–3)	3.0 ± 0.0 (3–3)	3.0 ± 0.0 (3–3)
Ran	7	7.7 ± 0.7 (6–9)	9.3 ± 0.6 (9–10)	8.3 ± 1.0 (7–9)
O	0.9	8.2 ± 0.4 (7.4–8.9)	7.6 ± 0.5 (7.4–8.2)	7.5 ± 0.5 (7.1–8.2)
A	8.9	10.2 ± 1.1 (8.4–12.2)	11.6 ± 0.6 (11.2–12.3)	11.5 ± 0.6 (10.7–11.9)
B	2.2	2.3 ± 0.1 (2.1–2.6)	2.5 ± 0.1 (2.4–2.5)	2.6 ± 0.1 (2.5–2.7)
C	22.4	26.3 ± 3.4 (21.9–32.5)	18.7 ± 0.8 (17.8–19.3)	20.2 ± 1.5 (18.7–22.3)
c'	0.6	0.7 ± 0.05 (0.6–0.8)	0.8 ± 0.03 (0.8–0.9)	0.8 ± 0.04 (0.7–0.9)
V	91.1	91.5 ± 0.7 (90.2–92.5)	90.8 ± 0.8 (90.2–91.7)	90.9 ± 0.7 (90.4–92.0)
VL/VB	0.9	1.0 ± 0.1 (0.8–1.1)	1.2 ± 0.06 (1.2–1.3)	1.1 ± 0.05 (1.1–1.2)
Stylet	95.0	94.6 ± 2.9 (88.0–99.0)	96.0 ± 1.7 (95.0–98.0)	96.3 ± 1.5 (95.0–98.0)
Pharynx	135	132.5 ± 5.1 (122–140)	133.3 ± 5.7 (127–138)	133.3 ± 6.1 (127–139)
Max. body width	34	30.5 ± 3.3 (24.0–37.0)	28.7 ± 2.1 (27.0–31.0)	29.8 ± 2.2 (28.0–33.0)
Anal body width	21	17.6 ± 1.9 (14.5–21.0)	20.8 ± 1.0 (20.0–22.0)	21.1 ± 1.7 (19.5–23.0)
Vulva to anus distance	14	12.7 ± 1.8 (10.0–16.0)	13.2 ± 1.0 (12.0–14.0)	13.3 ± 2.0 (11.5–16.0)
Tail	13.5	11.9 ± 1.5 (10.0–14.0)	17.7 ± 0.6 (17.0–18.0)	17.0 ± 1.8 (14.5–18.5)

[1]All measurements are in µm and in the form: mean ± s.d. (range).

X. andreae sp. nov. resembles members of the *X. macrodora*-species complex (including *X. macrodora*, *X. iberica*, *X. paraiberica*, *X. pradense*, and *X. costaricense*), from which it can be separated by several morphometric traits and ratios. From *X. macrodora*, it is almost undistinguishable but mainly differs by a slightly higher c ratio 26.3 (21.9–32.5) *vs.* 19.6 (12.8–25.3). From *X. iberica*, it is also almost undistinguishable, but differs by a slightly shorter tail length 11.9 (10.0–14.0) µm *vs.* 16.4 (11.0–24.5) µm and a slightly higher c ratio 26.3 (21.9–32.5) *vs.* 18.3 (12.1–27.3). From *X. paraiberica*, it is also almost undistinguishable, but mainly differs by a slightly longer stylet length 94.6 (88.0–99.0) µm *vs.* 89.6 (80.0–100.0) µm, a higher number of body annuli (R) 112.5 (105–119) *vs.* 104 (95–116), and a slightly higher c ratio 26.3 (21.9–32.5) *vs.* 20.2 (13.0–28.6). From *X. pradense*, it mainly differs by a slightly lower VL/VB ratio 1.0 (0.8–1.1) *vs.* 1.4 (1.1–1.5), a lower number of body annuli from vulva to posterior end (RV) 10.7 (9–12) *vs.* 16 (14–18), a slightly shorter tail length 11.9 (10.0–14.0) µm *vs.* 20.2 (15.5–25.0) µm, a higher c ratio 26.3 (21.9–32.5) *vs.* 16.6 (13.7–21.3), and a lower c' ratio 0.7 (0.6–0.8) *vs.* 0.9 (0.8–1.2). Finally, *X. andreae* sp. nov. clearly differs from *X. costaricense* by a shorter body length 307.2 (274–353) µm *vs.* 349 (276–404) µm, a shorter stylet length 94.6 (88.0–99.0) µm *vs.* 125 (113.0–133.0) µm, a slightly higher number of body annuli (R) 112.5 (105–119) *vs.* 124 (117–130), a slightly higher c ratio 26.3 (21.9–32.5) *vs.* 22.8 (16.0–28.8), and a slightly lower VL/VB ratio 1.0 (0.8–1.1) *vs.* 1.1 (0.9–1.3).

Etymology. The species epithet refers to the name of the daughter of the last author, Miss. Andrea Archidona Rosales, who helped to take the sample of the type population.

Type host and locality. The new species was recovered from the rhizosphere of a mastic tree (*Pistacia lentiscus* L.) at Linhó, Sintra region, Portugal (coordinates 38°46'07.78"N, 9°23'41.96"W). Additional specimens were detected from the rhizosphere of cork oak (*Quercus suber* L.) and chestnut (*Castanea sativa* Mill.) at Aroche, Huelva province, Spain (coordinates 37°54'13.06"N, 6°37'02.95"W), and Trabadelo, León province, Spain (coordinates 42°38'38.3"N, 6°52'14.0"W), respectively.

Type material. Holotype female and 16 female paratypes deposited at the nematode collection of the institute for sustainable agriculture (IAS) of the Spanish National Research Council (CSIC; collection nos. XEN-AND-01/XEN-AND-16), Córdoba, Spain; and two females at the USDA Nematode Collection (T-8065p).

Discussion

Late studies based on integrative taxonomy on profuse *X. macrodora*-species complex populations from the Iberian Peninsula and a population from Costa Rica clearly demonstrate that the cosmopolitan species *X. macrodora* need to be considered a species complex including at least five species, *viz. X. iberica*, *X. macrodora*, *X. paraiberica*, *X. pradense*, and *X. costaricense*, and probably comprising additional new cryptic species all over the world (Archidona-Yuste et al. 2024; Peraza-Padilla et al. 2024). Because of their basic morphology and a wide morphometric range of populations all over the world (Archidona-Yuste et al. 2024), accurate species identification within the genus *Xenocriconemella* has only been possible after applying integrative taxonomical studies,

allowing to decipher the presence of cryptic species (Archidona-Yuste et al. 2024; Peraza-Padilla et al. 2024). The main goal here was to describe and identify morphologically and molecularly the three new populations of *Xenocriconemella* found in natural environments on the Iberian Peninsula, as well as clarify phylogenetic relationships within this genus. Our results corroborate that the three new *Xenocriconemella* populations studied here are morphologically and morphometrically related to the *X. macrodora*-species complex, except for some minor morphometric features. Nevertheless, all the molecular markers certainly delineated the three new Iberian Peninsula populations from all other species within this genus, confirming that they comprise a new valid species within the genus *Xenocriconemella*. These data provide a clear indication that the global biodiversity of this genus is much greater than previously suspected, as has been suggested recently by Archidona-Yuste et al. (2024) and Peraza-Padilla et al. (2024). Certainly, although more studies are required to confirm this assumption on a global scale, the present results indicate that additional new taxa can be detected within the widely reported populations of *X. macrodora* s.l. in those regions of the Iberian Peninsula where the species complex has been reported (Archidona-Yuste et al. 2024).

Ribosomal and mitochondrial markers (D2-D3 expansion domains of the 28S and ITS rRNA and the mtDNA gene COI) are again demonstrated to be important tools for the accurate identification of *Xenocriconemella* spp. and other Criconematidae (Subbotin et al. 2005; Etongwe et al. 2020; Powers et al. 2021; Nguyen et al. 2022; Archidona-Yuste et al. 2024). In our studies on the molecular diversity of Xenocriconemella spp. in the Iberian Peninsula, ribosomal markers looked like the best molecular tools for identifying Xenocriconemella species since they showed the lowest intraspecific variability. Phylogenetic analyses based on D2-D3, ITS, 18S, and COI genes using BI mostly clearly demonstrated the monophyly of the genus *Xenocriconemella*, were consistent with those given by previous phylogenetic analyses (Subbotin et al. 2005; Etongwe et al. 2020; Nguyen et al. 2022; Archidona-Yuste et al. 2024; Peraza-Padilla et al. 2024), and confirmed the validity of *Xenocriconemella* within Criconematidae. Our data also suggest that the 18S rRNA accession of *X. macrodora* from Portugal (MT229843, differing by 12 bp from *X. andreae* sp. nov.) was most likely misidentified as hypothesized by Archidona-Yuste et al. (2024). Unfortunately, no additional molecular data were available in GenBank from this population, and further studies will be needed to clarify this identification, linking morphological and molecular data through integrative taxonomy. Similarly, the high diversity (up to 25%, 101–115 bp and 40–45 indels) among ITS sequences of *Xenocriconemella* spp. from the Iberian Peninsula and Costa Rica with the sequence of *X. macrodora* from the USA (JQ708139) suggests a misidentification that should be confirmed with additional studies since no other molecular markers of this population are available (Cordero et al. 2012).

Conclusions

This study expands our understanding of the biodiversity of the genus *Xenocriconemella* in the Iberian Peninsula. It also confirms the effectiveness of using an integrative approach that combines morphometric and morphological characteristics with the genotyping of rRNA and mtDNA markers for accurate species identification among *Xenocriconemella* species. Additionally, the study highlights the need for ongoing nematode surveys in natural habitats to uncover the uncharted biodiversity of this genus globally.

Acknowledgements

This work was supported by the Consejería de Universidad, Investigación e Innovación-Junta de Andalucia, Qualifica Project (QUAL21_023 IAS). A. Archidona-Yuste is funded by the Ramón y Cajal program (RYC2021-031108-I), and I. Criado-Navarro is funded by the Juan de la Cierva programs (JDC2022-048855-I), funded by MCIN/AEI/10.13039/501100011033 and UE "Next Generation EU/PRTR." The authors thank Gracia Liébanas and Maria Rodriguez Santamaria for their help with sampling. In addition, the authors thank Jorge Martin Barbarroja (IAS-CSIC), Guillermo León-Ropero (IASCSIC), and Inmaculada Casero Godoy for their excellent technical assistance.

References

Altschul SF, Gish W, Miller W, Myers EW, Lipman DJ (1990) Basic local alignment search tool. Journal of Molecular Biology 215(3): 403–410. https://doi.org/10.1016/S0022-2836(05)80360-2

Archidona-Yuste A, Navas-Cortes JA, Cantalapiedra-Navarrete C, Palomares-rius JE, Castillo P (2016) Cryptic divesrity and species delimitation in the *Xiphinema americanum*-group complex (Nematoda, Longidoridae) as inferred from morphometrics and molecular markers. Zoological Journal of the Linnean Society 176(2): 231–265. https://doi.org/10.1111/zoj.12316

Archidona-Yuste A, Cai R, Cantalapiedra-Navarrete C, Carreira JA, Rey A, Viñegla B, Liebanas G, Palomares-Rius JE, Castillo P (2020) Morphostatic speciation within the dagger nematode *Xiphinema hispanum*-complex species (Nematoda, Longidoridae). Plants 9(12): 1649. https://doi.org/10.3390/plants9121649

Archidona-Yuste A, Palomares-Rius JE, Clavero-Camacho I, Cantalapiedra-Navarrete C, Liébanas G, Castillo P (2023) A blind-identification test on *Criconema annuliferum* (de Man, 1921) Micoletzky, 1925 species complex corroborate the hyper-cryptic species diversity using integrative taxonomy. Plants 12(5): 1044. https://doi.org/10.3390/plants12051044

Archidona-Yuste A, Clavero-Camacho I, Ruiz-Cuenca AN, Cantalapiedra-Navarrete C, Liebanas G, Castillo P, Palomares-Rius JE (2024) The more we search, the more we find: Discovering and expanding the biodiversity in the ring nematode genus *Xenocriconemella* De Grisse and Loof, 1965 (Nematoda, Criconematidae). Zoological Letters 10(1): 8. https://doi.org/10.1186/s40851-024-00230-3

Barsi L, Fanelli E, De Luca F (2017) A new record of *Xiphinema dentatum* Sturhan, 1978 and description of *X. paradentatum* sp. n. (Nematoda, Dorylaimida) from Serbia. Nematology 19(8): 925–949. https://doi.org/10.1163/15685411-00003098

Bello A, Boag B, Thopham PB, Ibánez J (1986) Geographical distribution of *Xenocriconemella macrodora* (Nematoda, Criconematidae). Nematologia Mediterranea 14: 223–229.

Cai R, Archidona-Yuste A, Cantalapiedra-Navarrete C, Palomares-Rius JE, Castillo P (2020) New evidence of cryptic speciation in the family Longidoridae (Nematoda, Dorylaimida). Journal of Zoological Systematics and Evolutionary Research 58(4): 869–899. https://doi.org/10.1111/jzs.12393

Cantalapiedra-Navarrete C, Navas-Cortés JA, Liébanas G, Vovlas N, Subbotin SA, Palomares-Rius JE, Castillo P (2013) Comparative molecular and morphological characterisations in the nematode genus *Rotylenchus*: *Rotylenchus paravitis* n. sp., an example of cryptic speciation. Zoologischer Anzeiger 252(2): 246–268. https://doi.org/10.1016/j.jcz.2012.08.002

Clavero-Camacho I, Palomares-Rius JE, Cantalapiedra-Navarrete C, León-Ropero G, Martín-Barbarroja J, Archidona-Yuste A, Castillo P (2021) Integrative taxonomy reveals hidden cryptic diversity within Pin nematodes of the genus *Paratylenchus* (Nematoda, Tylenchulidae). Plants 10(7): 1454. https://doi.org/10.3390/plants10071454

Coolen W (1979) Methods for the extraction of *Meloidogyne* spp. and other nematodes from roots and soil. In: Lamberti F, Taylor CE (Eds) Root-knot nematodes (Meloidogyne species); systematics, biology and control. Academic Press, New York, USA, 317–329.

Cordero MA, Robbins RT, Szalanski AL (2012) Taxonomic and molecular identification of *Bakernema*, *Criconema*, *Hemicriconemoides*, *Ogma* and *Xenocriconemella* species (Nematoda, Criconematidae). Journal of Nematology 44: 427–446.

Darriba D, Taboada GL, Doallo R, Posada D (2012) jModelTest 2: More models, new heuristics and parallel computing. Nature Methods 9(8): 772–772. https://doi.org/10.1038/nmeth.2109

Dayrat B (2005) Towards integrative taxonomy. Biological Journal of the Linnean Society. Linnean Society of London 85(3): 407–415. https://doi.org/10.1111/j.1095-8312.2005.00503.x

De Grisse AT (1969) Redescription ou modifications de quelques techniques utilisées dans l'étude de nématodes phytoparasitaires. Mededelingen Rijksfaculteit Landbouwwetenschappen Gent 34: 315–359.

De Grisse A, Loof PAA (1965) Revision of the genus *Criconemoides* (Nematoda). Mededelingen van de Landbouwhogeschool en der opzoekingsstations van den Staat te Gent 30: 577–603.

De Ley P, Felix MA, Frisse L, Nadler S, Sternberg P, Thomas WK (1999) Molecular and morphological characterisation of two reproductively isolated species with mirror-image anatomy (Nematoda, Cephalobidae). Nematology 1(6): 591–612. https://doi.org/10.1163/156854199508559

Decraemer W, Archidona-Yuste A, Clavero-Camacho I, Vovlas A, Cantalapiedra-Navarrete C, Ruiz-Cuenca AN, Castillo P, Palomares-Rius JE (2024) Unravelling cryptic diversity in the *Paratrichodorus allius*-group species complex to resolve eight new species of the genus and new insights on the molecular phylogeny (Nematoda, Trichodoridae). Zoological Journal of the Linnean Society zlad194. https://doi.org/10.1093/zoolinnean/zlad194

Derycke S, Remerie T, Vierstraete A, Backeljau T, Vanfleteren J, Vincx M, Moens T (2005) Mitochondrial DNA variation and cryptic speciation within the free-living marine nematode Pellioditis marina. Marine Ecology Progress Series 300: 91–103. https://doi.org/10.3354/meps300091

Escuer M, Lara MP, Bello A (1999) Distribution of the Criconematidae in Peninsular Spain and Balearic Islands. International Journal of Nematology 9: 47–67.

Etongwe C, Singh R, Bert W, Subbotin S (2020) Molecular characterisation of some plant-parasitic nematodes (Nematoda, Tylenchida) from Belgium. Russian Journal of Nematology 28: 1–28. https://doi.org/10.24411/0869-6918-2020-10001

Fišer C, Koselj K (2022) Coexisting cryptic species as a model system in integrative taxonomy. In: Monro AK, Mayo SJ (Eds) Cryptic Species: Morphological Stasis, Circumscription, and Hidden Diversity. Cambridge University Press, Cambridge, 169–196. https://doi.org/10.1017/9781009070553.007

Gómez-Barcina A, Castillo P, González-País MA (1989) Nematodos fitoparásitos de la subfamilia Criconematinae Taylor, 1936 en la Sierra de Cazorla. Revista Iberica de Parasitologia 49: 241–255.

Gutiérrez-Gutiérrez C, Palomares-Rius JE, Cantalapiedra-Navarrete C, Landa BB, Esmenjaud D, Castillo P (2010) Molecular analysis and comparative morphology to resolve a complex of cryptic *Xiphinema* species. Zoologica Scripta 39(5): 483–498. https://doi.org/10.1111/j.1463-6409.2010.00437.x

Hall TA (1999) BioEdit: A user-friendly biological sequence alignment editor and analysis program for windows 95/98/NT. Nucleic Acids Symposium Series 41: 95–98.

Hamilton CA, Hendrixson BE, Brewer MS, Bond JE (2014) An evaluation of sampling effects on multiple DNA barcoding methods leads to an integrative approach for delimiting species: A case study of the North American tarantula genus *Aphonopelma* (Araneae, Mygalomorphae, Theraphosidae). Molecular Phylogenetics and Evolution 71: 79–93. https://doi.org/10.1016/j.ympev.2013.11.007

Holterman M, van der Wurff A, van den Elsen S, van Megen H, Bongers T, Holovachov O, Bakker J, Helder J (2006) Phylum-wide analysis of SSU rDNA reveals deep phylogenetic relationships among nematodes and accelerated evolution toward crown clades. Molecular Biology and Evolution 23(9): 1792–1800. https://doi.org/10.1093/molbev/msl044

Hu M, Chilton NB, Zhu X, Gasser RB (2002) Single-strand conformation polymorphism-based analysis of mitochondrial cytochrome c oxidase subunit 1 reveals significant substructuring in hookworm populations. Electrophoresis 23(1): 27–34. https://doi.org/10.1002/1522-2683(200201)23:1<27::AID-ELPS27>3.0.CO;2-7

Katoh K, Rozewicki J, Yamada KD (2019) MAFFT online service: multiple sequence alignment, interactive sequence choice and visualization. Briefings in bioinformatcis 20: 1160–1166. https://doi.org/10.1093/bib/bbx108

Lê S, Josse J, Husson F (2008) FactoMineR: An r package for multivariate analysis. Journal of Statistical Software 25(1): 1–18. https://doi.org/10.18637/jss.v025.i01

Legendre P, Legendre L (2012) Numerical Ecology. 3rd edn. Elsevier, Amsterdam, The Netherlands, 990 pp.

Masters BC, Fan V, Ross HA (2011) Species Delimitation - a Geneious plugin for the exploration of species boundaries. Molecular Ecology Resources 11(1): 154–157. https://doi.org/10.1111/j.1755-0998.2010.02896.x

Montgomery DC, Peck EA, Vining GG (2012) Introduction to linear regression analysis. John Wiley & Sons, Hoboken, New Jersey, 821 pp.

Myers N, Mittermeier RA, Mittermeier CG, da Fonseca GAB, Kent J (2000) Biodiversity hotspots for conservation priorities. Nature 403(6772): 853–858. https://doi.org/10.1038/35002501

Nguyen HT, Nguyen TD, Le TML, Trinh QP, Bert W (2022) Remarks on phylogeny and molecular variations of criconematid species (Nematoda, Criconematidae) with case studies from Vietnam. Scientific Reports 12(1): 14832. https://doi.org/10.1038/s41598-022-18004-2

Peraza-Padilla W, Aráuz-Badilla J, Cantalapiedra-Navarrete C, Palomares-Rius JE, Archidona-Yuste A, Castillo P (2024) A new ring nematode, *Xenocriconemella costaricense* sp. nov., (Nematoda, Criconematidae) from Costa Rica. Journal of Helminthology 98: e39. https://doi.org/10.1017/S0022149X24000294

Powers TO, Harris TS, Higgins RS, Mullin PG, Powers KS (2021) Nematode biodiversity assessments need vouchered databases: A BOLD reference library for plant-parasitic nematodes in the superfamily Criconematoidea. Genome 64: 232–241. https://doi.org/10.1139/gen-2019-0196

Proudlove G, Wood PJ (2003) The blind leading the blind: Cryptic subterranean species and DNA taxonomy. Trends in Ecology & Evolution 18(6): 272–273. https://doi.org/10.1016/S0169-5347(03)00095-8

R Core Team (2022) A language and environment for statistical computing. R Foundation for Statistical Computing, Vienna, Austria. https://www.R-project.org/

Rambaut A (2018) Rambaut A (2018) FigTree v1.4.4, A graphical viewer of phylogenetic trees. http://tree.bio.ed.ac.uk/software/figtree/

Ronquist F, Huelsenbeck JP (2003) MrBayes 3: Bayesian phylogenetic inference under mixed models. Bioinformatics 19(12): 1572–1574. https://doi.org/10.1093/bioinformatics/btg180

Rosenberg NA (2007) Statistical tests for taxonomic distinctiveness from observations of monophyly. Evolution; International Journal of Organic Evolution 61(2): 317–323. https://doi.org/10.1111/j.1558-5646.2007.00023.x

Ross HA, Murugan S, Li WL (2008) Testing the reliability of genetic methods of species identification via simulation. Systematic Biology 57(2): 216–230. https://doi.org/10.1080/10635150802032990

Seinhorst JW (1966) Killing nematodes for taxonomic study with hot F.A. 4:1. Nematologica 12(1): 178–178a. https://doi.org/10.1163/187529266X00239

Subbotin SA, Vierstraete A, De Ley P, Rowe J, Waeyenberge L, Moens M, Vanfleteren JR (2001) Phylogenetic relationships within the cyst-forming nematodes (Nematoda, Heteroderidae) based on analysis of sequences from the ITS regions of ribosomal DNA. Molecular Phylogenetics and Evolution 21(1): 1–16. https://doi.org/10.1006/mpev.2001.0998

Subbotin SA, Vovlas N, Crozzoli R, Sturhan D, Lamberti F, Moens M, Baldwin JG (2005) Phylogeny of *Criconematina* Siddiqi, 1980 (Nematoda, Tylenchida) based on morphology and D2-D3 expansion segments of the 28S-rRNA gene sequences with application of a secondary structure model. Nematology 7(6): 927–944. https://doi.org/10.1163/156854105776186307

Tan G, Muffato M, Ledergerber C, Herrero J, Goldman N, Gil M, Dessimoz C (2015) Current methods for automated filtering of multiple sequence alignments frequently worsen single-gene phylogenetic inference. Systematic Biology 64(5): 778–791. https://doi.org/10.1093/sysbio/syv033

Taylor AL (1936) The genera and species of the Criconematinae, a sub-family of the Anguillulinidae (Nematoda). Transactions of the American Microscopical Society 55(4): 391–421. https://doi.org/10.2307/3222522

Zuur AF, Ieno EN, Elphick CS (2010) A protocol for data exploration to avoid common statistical problems. Methods in Ecology and Evolution 1(1): 3–14. https://doi.org/10.1111/j.2041-210X.2009.00001.x